IMPROVEMENT FOR QUALITY AND SAFETY TRAITS IN HORTICULTURAL PLANTS

EDITED BY: Pei Xu, Xinchao Wang and Ferdinando Branca

PUBLISHED IN: Frontiers in Plant Science



frontiers Research Topics

Frontiers eBook Copyright Statement

The copyright in the text of individual articles in this eBook is the property of their respective authors or their respective institutions or funders. The copyright in graphics and images within each article may be subject to copyright of other parties. In both cases this is subject to a license granted to Frontiers.

The compilation of articles constituting this eBook is the property of Frontiers.

Each article within this eBook, and the eBook itself, are published under the most recent version of the Creative Commons CC-BY licence. The version current at the date of publication of this eBook is CC-BY 4.0. If the CC-BY licence is updated, the licence granted by Frontiers is automatically updated to the new version.

When exercising any right under the CC-BY licence, Frontiers must be attributed as the original publisher of the article or eBook, as applicable.

Authors have the responsibility of ensuring that any graphics or other materials which are the property of others may be included in the CC-BY licence, but this should be checked before relying on the CC-BY licence to reproduce those materials. Any copyright notices relating to those materials must be complied with.

Copyright and source acknowledgement notices may not be removed and must be displayed in any copy, derivative work or partial copy which includes the elements in question.

All copyright, and all rights therein, are protected by national and international copyright laws. The above represents a summary only. For further information please read Frontiers' Conditions for Website Use and Copyright Statement, and the applicable CC-BY licence.

ISSN 1664-8714
ISBN 978-2-88976-408-2
DOI 10.3389/978-2-88976-408-2

About Frontiers

Frontiers is more than just an open-access publisher of scholarly articles: it is a pioneering approach to the world of academia, radically improving the way scholarly research is managed. The grand vision of Frontiers is a world where all people have an equal opportunity to seek, share and generate knowledge. Frontiers provides immediate and permanent online open access to all its publications, but this alone is not enough to realize our grand goals.

Frontiers Journal Series

The Frontiers Journal Series is a multi-tier and interdisciplinary set of open-access, online journals, promising a paradigm shift from the current review, selection and dissemination processes in academic publishing. All Frontiers journals are driven by researchers for researchers; therefore, they constitute a service to the scholarly community. At the same time, the Frontiers Journal Series operates on a revolutionary invention, the tiered publishing system, initially addressing specific communities of scholars, and gradually climbing up to broader public understanding, thus serving the interests of the lay society, too.

Dedication to Quality

Each Frontiers article is a landmark of the highest quality, thanks to genuinely collaborative interactions between authors and review editors, who include some of the world's best academicians. Research must be certified by peers before entering a stream of knowledge that may eventually reach the public - and shape society; therefore, Frontiers only applies the most rigorous and unbiased reviews.
Frontiers revolutionizes research publishing by freely delivering the most outstanding research, evaluated with no bias from both the academic and social point of view. By applying the most advanced information technologies, Frontiers is catapulting scholarly publishing into a new generation.

What are Frontiers Research Topics?

Frontiers Research Topics are very popular trademarks of the Frontiers Journals Series: they are collections of at least ten articles, all centered on a particular subject. With their unique mix of varied contributions from Original Research to Review Articles, Frontiers Research Topics unify the most influential researchers, the latest key findings and historical advances in a hot research area! Find out more on how to host your own Frontiers Research Topic or contribute to one as an author by contacting the Frontiers Editorial Office: frontiersin.org/about/contact

IMPROVEMENT FOR QUALITY AND SAFETY TRAITS IN HORTICULTURAL PLANTS

Topic Editors:
Pei Xu, China Jiliang University, China
Xinchao Wang, Tea Research Institute, Chinese Academy of Agricultural Sciences (CAAS), China
Ferdinando Branca, University of Catania, Italy

Citation: Xu, P., Wang, X., Branca, F., eds. (2022). Improvement for Quality and Safety Traits in Horticultural Plants. Lausanne: Frontiers Media SA.
doi: 10.3389/978-2-88976-408-2

Table of Contents

06 ***Editorial: Improvement for Quality and Safety Traits in Horticultural Plants***
Xinyang Wu, Pingping Fang, Peipei Zhang, Ting Sun, Xinchao Wang, Ferdinando Branca and Pei Xu

10 ***Exogenous Application of 5-Aminolevulinic Acid Promotes Coloration and Improves the Quality of Tomato Fruit by Regulating Carotenoid Metabolism***
Junwen Wang, Jing Zhang, Jing Li, Mohammed Mujitaba Dawuda, Basharat Ali, Yue Wu, Jihua Yu, Zhongqi Tang, Jian Lyu, Xuemei Xiao, Linli Hu and Jianming Xie

26 ***Genome-Wide Investigation of N6-Methyladenosine Regulatory Genes and Their Roles in Tea (*Camellia sinensis*) Leaves During Withering Process***
Chen Zhu, Shuting Zhang, Chengzhe Zhou, Siyi Xie, Guangwu Chen, Caiyun Tian, Kai Xu, Yuling Lin, Zhongxiong Lai and Yuqiong Guo

47 ***Effects of Soil Type on Trace Element Absorption and Fruit Quality of Pepper***
Zhoubin Liu, Yu Huang, Fangjun Tan, Wenchao Chen and Lijun Ou

57 ***The Formation of Fruit Quality in* Cucumis sativus *L.***
Juping Zhang, Shengjun Feng, Jing Yuan, Chen Wang, Tao Lu, Huasen Wang and Chao Yu

67 ***Anthocyanin Genes Involved in the Flower Coloration Mechanisms of* Cymbidium kanran**
Zhuang Zhou, Zhen Ying, Zhigang Wu, Yanping Yang, Shuangbin Fu, Wan Xu, Lijuan Yao, Aiping Zeng, Jian Huang, Siren Lan, Xiaole Wang and Zhongjian Liu

81 ***Benzothiazole Treatment Regulates the Reactive Oxygen Species Metabolism and Phenylpropanoid Pathway of* Rosa roxburghii *Fruit to Delay Senescence During Low Temperature Storage***
Boyu Dong, Hongmin Tang, Dequan Zhu, Qiuping Yao, Hongqiang Han, Kequn He and Xiaochun Ding

92 ***Genetic Mapping and Identification of the Candidate Genes for Mottled Rind in* Cucumis melo *L.***
Jia Shen, Xinyang Xu, Yuejian Zhang, Xiaowei Niu and Weisong Shou

101 ***Genome-Wide Identification and Expression Analysis of Terpene Synthase Genes in* Cymbidium faberi**
Qian-Qian Wang, Meng-Jia Zhu, Xia Yu, Yuan-Yang Bi, Zhuang Zhou, Ming-Kun Chen, Jiating Chen, Diyang Zhang, Ye Ai, Zhong-Jian Liu and Siren Lan

115 ***S1-bZIP Transcription Factors Play Important Roles in the Regulation of Fruit Quality and Stress Response***
Hong Wang, Yunting Zhang, Ayla Norris and Cai-Zhong Jiang

128 ***Evolutionary Origin of the Carotenoid Cleavage Oxygenase Family in Plants and Expression of Pepper Genes in Response to Abiotic Stresses***
Yixiu Yao, Li Jia, Yuan Cheng, Meiying Ruan, Qingjing Ye, Rongqing Wang, Zhuping Yao, Guozhi Zhou, Jia Liu, Jiahong Yu, Peng Zhang, Yuhe Yin, Weiping Diao and Hongjian Wan

143 ***Genome-Wide Identification of the* PMEI *Gene Family in Tea Plant and Functional Analysis of* CsPMEI2 *and* CsPMEI4 *Through Ectopic Overexpression***
Bo Li, Huan Wang, Shan He, Zhaotang Ding, Yu Wang, Nana Li, Xinyuan Hao, Lu Wang, Yajun Yang and Wenjun Qian

162 ***Melatonin Treatment Delays Senescence and Maintains the Postharvest Quality of Baby Mustard (*Brassica juncea *var.* gemmifera*)***
Hongmei Di, Zhiqing Li, Yating Wang, Yi Zhang, Jinlin Bian, Jingyi Xu, Yangxia Zheng, Ronggao Gong, Huanxiu Li, Fen Zhang and Bo Sun

172 ***Practice in Nursery Weed Control—Review and Meta-Analysis***
Ping Yu and Stephen Christopher Marble

187 ***Genome-Wide Identification and Expression Profiling of CONSTANS-Like Genes in Pepper (*Capsicum annuum*): Gaining an Insight to Their Phylogenetic Evolution and Stress-Specific Roles***
Zhinan Huang, Xueying Bai, Weike Duan, Boqing Chen, Guodong Chen, Binghua Xu, Rui Cheng and Jizhong Wang

201 ***Overview of Witloof Chicory (*Cichorium intybus *L.) Discolorations and Their Underlying Physiological and Biochemical Causes***
Isabel De Jaegere, Yannah Cornelis, Tim De Clercq, Alain Goossens and Bram Van de Poel

212 ***Integrative Transcriptome and Proteome Analysis Reveals the Absorption and Metabolism of Selenium in Tea Plants [*Camellia sinensis *(L.) O. Kuntze]***
Hengze Ren, Xiaoman Li, Lina Guo, Lu Wang, Xinyuan Hao and Jianming Zeng

226 ***Ethylene-Inducible AP2/ERF Transcription Factor Involved in the Capsaicinoid Biosynthesis in* Capsicum**
Jinfen Wen, Junheng Lv, Kai Zhao, Xiang Zhang, Zuosen Li, Hong Zhang, Jinlong Huo, Hongjian Wan, Ziran Wang, Haishan Zhu and Minghua Deng

238 ***Advances in Understanding and Harnessing the Molecular Regulatory Mechanisms of Vegetable Quality***
Luyao Gao, Ning Hao, Tao Wu and Jiajian Cao

251 ***The Effect of Anti-browning Agent Activated Carbon and Polyvinyl Pyrrolidone on the Rooting of Embryo Seedlings of "FengDan" and Its Transcriptome Analysis***
Xia Chen, Chao Yu, Jingtao Nie, Hongmin Yang, Wen Ji, Gangwei Xu, Huijun Zhu, Songheng Jin and Xiangtao Zhu

264 ***Identification of Candidate Chromosome Region Related to Melon (*Cucumis melo *L.) Fruit Surface Groove Trait Through Biparental Genetic Mapping and Genome-Wide Association Study***
Xin Du, Hongyu Liu, Zicheng Zhu, Shusen Liu, Zhengfeng Song, Lianqin Xia, Jingchao Zhao, Feishi Luan and Shi Liu

275 ***Quantitative Extraction and Evaluation of Tomato Fruit Phenotypes Based on Image Recognition***
Yihang Zhu, Qing Gu, Yiying Zhao, Hongjian Wan, Rongqing Wang, Xiaobin Zhang and Yuan Cheng

287 ***Deep Learning and Hyperspectral Images Based Tomato Soluble Solids Content and Firmness Estimation***
Yun Xiang, Qijun Chen, Zhongjing Su, Lu Zhang, Zuohui Chen, Guozhi Zhou, Zhuping Yao, Qi Xuan and Yuan Cheng

298 ***Genetic Mapping and QTL Analysis of Stigma Color in Melon (*Cucumis melo *L.)***
Yuanzuo Lv, Peng Gao, Shi Liu, Xufeng Fang, Taifeng Zhang, Tai Liu, Sikandar Amanullah, Xinying Wang and Feishi Luan

309 ***Research Advances in Genetic Mechanisms of Major Cucumber Diseases Resistance***
Yujin He, Mingming Wei, Yanyan Yan, Chao Yu, Siqi Cheng, Yihan Sun, Xiangtao Zhu, Lingling Wei, Huasen Wang and Li Miao

frontiers | Frontiers in Plant Science

EDITORIAL
published: 31 May 2022
doi: 10.3389/fpls.2022.927779

Editorial: Improvement for Quality and Safety Traits in Horticultural Plants

Xinyang Wu[1,2], *Pingping Fang*[1], *Peipei Zhang*[1], *Ting Sun*[1], *Xinchao Wang*[3,4], *Ferdinando Branca*[5] *and Pei Xu*[1,2]*

[1] College of Life Sciences, China Jiliang University, Hangzhou, China, [2] Key Laboratory of Specialty Agri-Product Quality and Hazard Controlling Technology of Zhejiang, Hangzhou, China, [3] National Center for Tea Improvement, Tea Research Institute, Chinese Academy of Agricultural Sciences, Hangzhou, China, [4] Key Laboratory of Biology, Genetics and Breeding of Special Economic Animals and Plants, Ministry of Agriculture and Rural Affairs, Hangzhou, China, [5] Departments of Agriculture, Food, and Environment, University of Catania, Catania, Italy

Keywords: quality, safety, horticultural plants, phenotyping, genetics, integrative biology quality

Editorial on the Research Topics

Improvement for Quality and Safety Traits in Horticultural Plants

As the living standard of people rises, quality and safety traits of agricultural plants have received growing attentions by consumers and breeders alike. Quality traits are known as traits that offer better appearance, flavor, taste, nutrition, longer shelf life and less damage to plant products, while safety traits can be defined as plant traits that are directly or indirectly linked to human health, such as the content of antioxidant compounds in horticultural products. Typical quality and safety traits include, but are not limited to, appearance, texture, taste, flavor and aroma of plant products; nutritional, anti-nutritional or allergic component contents; uptake, accumulation and degradation of exogenous toxic substances by plants; synthesis and transformation of endogenous harmful substances in plants; post-harvest quality change and shelf life. Some quality and safety traits are more closely related to the environment or human activities, such as the accumulation of heavy metals, antibiotic residues and the novel artificial nanoparticles in plants. Tremendous efforts are being put into breeding programs to synergistically improve quality and safety traits, which, however, are in some cases impeded by the trade-offs among target traits. For example, plants may contain certain components, for instance, stone cells, anti-nutritional factors and allergens, which are beneficial to their own but unfavorable for human consumption or detrimental to health (Aranzana et al., 2019; Lin et al., 2022).

QUALITY AND SAFETY TRAITS ARE RECEIVING MORE ATTENTIONS IN HORTICULTURAL PLANTS

Horticultural crops generally refer to fruits, vegetables, floral and tea plants. Fresh fruits and vegetables are important parts of human diets because they are essential sources of nutrients (e.g. carbohydrates, minerals, vitamins) and dietary fiber. Tea plant has huge health benefits and economic values. Tea contains many secondary metabolites such as flavonoids, theanine and alkaloids, which play many health benefits in human body (Yang et al., 2009; Bag et al., 2021). Floral plants, by their decorative function and cultural value, are an indispensable component for quality life and gaining more importance in modern agriculture. Collectively, horticultural crops are playing versatile roles in meeting the diversified needs of people and the rapidly upgrading life quality. As such, compared to staple food crops, for which yield-related traits are more

OPEN ACCESS

Edited and reviewed by:
Leo Marcelis, Wageningen University and Research, Netherlands

***Correspondence:**
Pei Xu
peixu@cjlu.edu.cn

Specialty section:
This article was submitted to Crop and Product Physiology, a section of the journal Frontiers in Plant Science

Received: *25 April 2022*
Accepted: *09 May 2022*
Published: *31 May 2022*

Citation:
Wu X, Fang P, Zhang P, Sun T, Wang X, Branca F and Xu P (2022) Editorial: Improvement for Quality and Safety Traits in Horticultural Plants. Front. Plant Sci. 13:927779. doi: 10.3389/fpls.2022.927779

critical, quality and safety traits are of particular importance for horticultural plants. Driven by the increasing demand of high-end horticultural products, quality and safety traits are receiving unprecedently intense attentions around the globe and have become a research hotpot. This Research Topic presents 24 articles that report the recent progresses in various subjects of research on quality and safety traits in vegetable, fruit, beverage and floral plants. In this editorial article, we briefly summarize the recent progresses and provide prospective views of the future directions in this specific area.

PROGRESS IN PHENOTYPING OF QUALITY AND SAFETY TRAITS IN HORTICULTURAL PLANTS

Accurate acquisition of the phenotypic data is prerequisite for trait improvement. The past decades have witnessed big progress in phenotyping techniques and methods, covering a wide range of traits from morphological, biochemical to the physiological levels. For example, advanced mathematical algorithm such as Elliptic Fourier equation was employed in precise and comprehensive quantification of fruit shape in cucurbit crops (Xu et al., 2021). Recently, the Tomato Analyzer image toolkit provides quantitative and objective description for morphological traits of fruits, which are fundamental for the characterization, selection and breeding of cultivars with desired fruit appearances (Brewer et al., 2006; Hurtado et al., 2013). Similarly, Zhu et al. developed an automated method for measuring color and size indicators of tomato fruits by incorporating a deep learning model. Various phenotypes such as fruit color, horizontal and vertical diameters, top and navel angles, locule number, pericarp thickness can be extracted, providing an effective and accurate means of fruit phenotyping. The same research group also developed a method for measurement of soluble solids content (SSC) and fruit firmness based on hyperspectral images and deep learning regression, which offers a new solution for non-destructive assessment of cherry tomato fruit quality (Xiang et al.).

Phenomics, an emerging discipline that provides high-throughput quantification of traits, has exhibited unique advantages in characterizing traits of horticultural plants (Li et al., 2021; Pandey et al., 2021). Current phenomics techniques are able to capture the dynamic process of plant growth and responses to the environment. For example, non-destructive plant imaging combined with destructive leaf sampling allowed deep analysis of salt resistance (Berger et al., 2012). By employing non-destructive physiology-based phenomics assay, drought responses such as stomatal closure of tomato, cowpea and pepper were precisely and continuously phenotyped (Berger et al., 2010; Xu et al., 2015; Halperin et al., 2017; Dalal et al., 2019; Wu et al., 2021). Even though the phenomics characterization of quality and safety traits in horticultural crops has still been rare to date, a wave of phenomics-based technological revolution on phenotyping of these traits is expected to come soon in the near future.

PROGRESS IN GENETIC STUDIES OF QUALITY AND SAFETY TRAITS IN HORTICULTURAL PLANTS

As the genomic technologies burst in the recent decades, genetic dissection of a large number of quality and safety traits have become feasible in many horticultural plants, which solidifies the basis of genetic improvement of the traits. Particularly, pedigree-based genetic mapping using bi-parental populations such as second filial generation (F_2), recombinant inbred lines (RILs) or double haploids (DHs); genome-wide association studies (GWAS) based on natural populations; and faster approaches using bulked-segregant analysis sequencing (BSA-seq) or quantitative trait locus sequencing (QTL-seq) have been mostly applied. For example, a locus strongly associated with firmness and harvest date of fruit was identified in apple by GWAS and the causal gene was found to encode the transcription factor *NAC18.1*. Single nucleotide polymorphisms (SNPs) were found in both the CDS and promoter regions of *NAC18.1*, leading to the differential ripening programs among the apple accessions (Migicovsky et al., 2021). Another interesting example reported the identification of a non-bitter allele fixed in *C. lanatus* by genome resequencing, which helped understand the domestication history of watermelons and their improvement (Guo et al., 2019). Shen et al. identified the melon gene *MELO3C026282* involved in the development of chloroplast to be a candidate gene controlling the mottled rind trait. Another gene, *MELO3C019694*, which encodes a MADS-box transcription factor, was characterized as a recessive candidate gene governing melon fruit surface groove by Du et al. using GWAS and BSA-seq. By genetic analysis of F_2 and $F_{2:3}$ populations derived from the cross of "MR-1" (green stigma) and "M4-7" (yellow stigma), Lv et al. detected two stable QTLs (SC2.1 and SC8.1) related to stigma color. Apart from melon, the formation mechanism and determinants of fruit quality in cucumber was reviewed by Zhang et al. highlighting the importance of integrating the methods of traditional breeding, molecular markers and bio-technologies. Other than quality traits, studies on diseases resistances of cucumber were summarized by Miao et al., where recent discoveries on the inheritance, molecular markers and QTL mapping of various diseases were reviewed, which sheds lights on the strategy for resistance breeding in this crop.

The completeness of genome sequencing in many horticultural plants have allowed genome-wide identification of genes involve in quality and safety traits. Zhu et al. identify 34 *N6-methyladenosine* regulatory genes and Li et al. characterize 51 *pectin methylesterase inhibitor* (*PMEI*) genes in tea. In pepper, 158 *carotenoid cleavage oxygenase* (*CCO*) genes were identified by Yao et al. and 10 *CONSTANS-like* (*COL*) genes were characteized by Huang et al. and Wang et al. reported the identification of 32 *terpene synthases* (*TPS*) genes in *Cymbidium faberi*. In short, the elucidation of genetic architectures of many important quality and safety traits and the systemic identification of gene families responsible for the trait regulation have laid a foundation for breeding-by-molecular-design.

INTEGRATIVE BIOLOGY APPROACHES FOR THE STUDY OF QUALITY AND SAFETY TRAITS IN HORTICULTURAL PLANTS

Integrative biology features the integration and intersection of multiple disciplines to study the laws of living organisms at the systems level (Pazhamala et al., 2021). In particular, genomics, phenomics, transcriptomics and proteomics, along with state-of-the-art gene manipulation and synthetic biology technologies, have driven the studies of quality and safety traits into the systematic era.

A typical example of integrative biological study of quality and safety traits in horticultural plants is the dissection and manipulation of the bitterness trait in cucumber. Through large-scale phenotyping and genetic mapping, genomic regions governing fruit and leaf bitterness were delimited. Further facilitated by biochemical and molecular approaches, nine genes involved in the cucurbitacin C biosynthesis pathway were identified, and two transcription factors, Bl and Bt, were ultimately determined as the causal gene of leaf and fruit bitterness, respectively (Shang et al., 2014). Through a comparative genomic approach, Zhou et al. unveiled the conserved mechanism and syntenic loci governing bitterness trait in the related cucurbit species including melon and watermelon. Based on genetic and metabolic analyses, it is revealed that the phytochemicals (phenolics, ascorbic acid, glucosinolate, anthocyanin, carotenoids) have great diversity among populations of Brassica wild species (Branca et al., 2018; Picchi et al., 2020). Ren et al. elucidated the mechanisms underlying selenium absorption and assimilation in tea by a combinatory use of transcriptomic and proteomic approaches. They found that the predominant forms of bioavailable Se were selenite (SeO_3^{2-}) and selenate (SeO_4^{2-}). Certain phosphate transporter (*PHT3;1a*, *PHT1;3b*, and *PHT1;8*) and aquaporin (*NIP2;1*) genes were upregulated by selenite while transporter genes *SULTR1;1* and *SULTR2;1* were responsive to selenate. Using tissue culture and transcriptomic profiling, Chen et al. showed that activated carbon promoted the development of peony roots into seedlings by stimulating the processes of phenylpropanoid biosynthesis and biosynthesis of stratum cutin and suberin. In addition to omics, research paradigm integrating physiological, biochemical and molecular biological methods are also widely used. For example, exogenous application of 5-Aminolevulinic acid and melatonin enhanced the nutritional quality and changed mature period in tomato (Wang et al.) and baby mustard (Di et al.), respectively. Zhu et al. employed high-performance liquid chromatography (HPLC) analysis, comparative transcriptome sequencing and transient expression assay to investigate the regulation of floral pigmentation in orchids. *CkCHS-1*, *CkDFR*, and *CkANS* were identified as putative key genes regulating floral coloration. Another study by Wen et al. analyzed CcERF2, an ethylene-inducible transcription factor that preferentially expressed in the placenta of pepper fruit. Silencing *CcERF2* reduced the content of capsaicinoids in pepper, suggesting that the gene involved in the regulation of capsaicinoids biosynthetic pathway. In a review article, Wang et al. summarized the recent research on the evolution and biological functions of the S1-bZIP transcription factors in plants, highlighting their role as signaling hubs through dimerization with cofactors to coordinate the expression of downstream genes. Undoubtedly, integrative biology approaches have been critical for understanding how the many quality and safety traits are determined in horticultural plants.

OUTLOOK

Despite a rapid advancement in the studies of quality and safety traits in horticultural plants over the past decades, improvement of these traits has still been lagging behind other essential traits, especially yield- and stress-related traits. Two main reasons are considered to be underpinning this fact: (1) phenotyping of quality and safety traits is generally more difficult; and (2) many of these traits are governed by multiple genes that are more prone to be affected by the environment. In order to accelerate the improvement of these traits, the research community may need to first fully digest and utilize the recent fundamental discoveries in the biology of quality and safety traits in horticultural plants. Particular attentions may be paid to latest research progresses in the innovative phenotyping techniques, exploration of genetic variations, important genes/QTLs that were identified as controlling the interested traits, molecular markers that were developed to tag the target traits, and the gene regulatory mechanisms underlying traits formation. In addition, Gao et al. emphasized the necessity and importance of establishing efficient genetic transformation methods and the use of gene-editing technology. These biotechnologies will help verify the functions of the determinant genes/QTLs.

In summary, the series of researches here describe the latest progresses on quality and safety traits studies in horticultural crops and highlight the combination of phenotyping and genetic methods in this field. In the future, researches on plant quality and safety traits will benefit more from integrative or systems biology strategies to achieve the goal of comprehensively understanding the gene-gene network and the gene-environment interaction. More specifically, focuses will be on: (1) unifying phenomics and genomics to identify the genes controlling traits of interest, which can manifest the power of both high-throughput phenotyping and genotyping technologies; (2) unifying bioinformatics, bioengineering and synthetic biology to design new routes for genetic manipulation; (3) combining traditional and modernized breeding techniques such as marker-assisted backcrossing (MAB), marker-assisted recurrent selection (MARC) and genomic selection (GS) for more efficient and precise development of new varieties with desired traits. Such multi-dimensional efforts are expected to solidify the theoretical foundation as well as provide rich genetic resources for the improvement of quality and safety traits in horticultural plants.

AUTHOR CONTRIBUTIONS

All authors listed have made a substantial, direct, and intellectual contribution to the work and approved it for publication.

ACKNOWLEDGMENTS

We thank the supports of National Key Research & Development Program of China (2021YFE19800), Key Research Program of Zhejiang Province (2021C02041), the Major Science and Technology Special Project of Variety Breeding of Zhejiang Province (2021C02067-7-3 and 2021C02066-5-4), and the Natural Science Foundation of Zhejiang Province (LQ21C150004).

REFERENCES

Aranzana, M. J., Decroocq, V., Dirlewanger, E., Eduardo, I., Gao, Z. S., Gasic, K., et al. (2019). Prunus genetics and applications after de novo genome sequencing: achievements and prospects. *Hortic Res.* 6, 58. doi: 10.1038/s41438-019-0140-8

Bag, S., Mondal, A., Majumder, A., and Banik, A. (2021). Tea and its phytochemicals: Hidden health benefits and modulation of signaling cascade by phytochemicals. *Food Chem.* 371, 131098. doi: 10.1016/j.foodchem.2021.131098

Berger, B., de Regt, B., and Tester, M. (2012). Trait dissection of salinity tolerance with plant phenomics. *Methods Mol. Biol.* 913, 399–413. doi: 10.1007/978-1-61779-986-0_27

Berger, B., Parent, B., and Tester, M. (2010). High-throughput shoot imaging to study drought responses. *J. Exp. Bot.* 61, 3519–3528. doi: 10.1093/jxb/erq201

Branca, F., Chiarenza, G. L., Cavallaro, C., Gu, H., Zhao, Z., and Tribulato, A. (2018). Diversity of Sicilian broccoli (*Brassica oleracea var. italica*) and cauliflower (*Brassica oleracea var. botrytis*) landraces and their distinctive bio-morphological, antioxidant, and genetic traits. *Genet. Resour. Crop. Evol.* 65, 485–502. doi: 10.1007/s10722-017-0547-8

Brewer, M. T., Lang, L., Fujimura, K., Dujmovic, N., and Gray, S., et al. (2006). Development of a controlled vocabulary and software application to analyze fruit shape variation in tomato and other plant species. *Plant Physiol.* 141, 15–25. doi: 10.1104/pp.106.077867

Dalal, A., Bourstein, R., Haish, N., Shenhar, I., and Wallach, R., et al. (2019). Dynamic physiological phenotyping of Drought-Stressed pepper plants treated with "Productivity-Enhancing" and "Survivability-Enhancing" biostimulants. *Front. Plant Sci.* 10, 905. doi: 10.3389/fpls.2019.00905

Guo, S., Zhao, S., Sun, H., Wang, X., and Wu, S., et al. (2019). Resequencing of 414 cultivated and wild watermelon accessions identifies selection for fruit quality traits. *Nat. Genet.* 51, 1616–1623. doi: 10.1038/s41588-019-0518-4

Halperin, O., Gebremedhin, A., Wallach, R., and Moshelion, M. (2017). High-throughput physiological phenotyping and screening system for the characterization of plant-environment interactions. *Plant J.* 89, 839–850. doi: 10.1111/tpj.13425

Hurtado, M., Vilanova, S., Plazas, M., Gramazio, P., and Herraiz, F. J., et al. (2013). Phenomics of fruit shape in eggplant (*Solanum melongena* L.) using Tomato Analyzer software. *Sci. Hortic.* 164, 625–632. doi: 10.1016/j.scienta.2013.10.028

Li, Y., Wu, X., Xu, W., Sun, Y., and Wang, Y., et al. (2021). High-Throughput physiology-based stress response phenotyping: Advantages, applications and prospective in horticultural plants. *Hortic. Plant J.* 7, 181–187. doi: 10.1016/j.hpj.2020.09.004

Lin, S., Lin, D., Wu, B., Ma, S., Sun, S., Zhang, T., et al. (2022). Morphological and developmental features of stone cells in eriobotrya fruits. *Front. Plant Sci.* 13, 823993. doi: 10.3389/fpls.2022.823993

Migicovsky, Z., Yeats, T. H., Watts, S., Song, J., and Forney, C. F., et al. (2021). Apple ripening is controlled by a NAC transcription factor. *Front. Genet.* 12, 671300. doi: 10.3389/fgene.2021.671300

Pandey, A. K., Jiang L., Moshelion, M., Gosa, S. C., Sun T., Lin, Q., et al. (2021). Functional physiological phenotyping with functional mapping: a general framework to bridge the phenotype-genotype gap in plant physiology. *iScience*. 24, s102846. doi: 10.1016/j.isci.2021.102846

Pazhamala, L. T., Kudapa, H., Weckwerth, W., Millar, A. H., and Varshney, R. K. (2021). Systems biology for crop improvement. *Plant Genome.* 14, e20098. doi: 10.1002/tpg2.20098

Picchi, V., Lo Scalzo, R., Tava, A., Doria, F., Argento, S., Toscano, S., et al. (2020). Phytochemical characterization and in vitro antioxidant properties of four brassica wild species from Italy. *Molecules.* 25, 3495. doi: 10.3390/molecules25153495

Shang, Y., Ma, Y., Zhou, Y., Zhang, H., and Duan, L., et al. (2014). Plant science. Biosynthesis, regulation, and domestication of bitterness in cucumber. *Science* 346, 1084–1088. doi: 10.1126/science.1259215

Wu, X., Sun, T., Xu, W., Sun, Y., Wang, B., Wang, Y., et al. (2021). Unraveling the genetic architecture of two complex, stomata-related drought-responsive traits by high-throughput physiological phenotyping and gwas in cowpea (*Vigna.* unguiculata L. Walp). *Front. Genet.* 12, 743758. doi: 10.3389/fgene.2021.743758

Xu, P., Moshelion, M., Wu, X., Halperin, O., Wang, B., Luo, J., et al. (2015). Natural variation and gene regulatory basis for the responses of asparagus beans to soil drought. *Front. Plant Sci.* 6, 891. doi: 10.3389/fpls.2015.00891

Xu, P., Wang, Y., Sun, F., Wu, R., Du, H., Wang, Y., et al. (2021). Long-read genome assembly and genetic architecture of fruit shape in the bottle gourd. *Plant J.* 107, 956–968. doi: 10.1111/tpj.15358

Yang, C. S., Wang, X., Lu, G., and Picinich, S. C. (2009). Cancer prevention by tea: Animal studies, molecular mechanisms and human relevance. *Nat. Rev. Cancer* 9, 429–439. doi: 10.1038/nrc2641

Conflict of Interest: The authors declare that the research was conducted in the absence of any commercial or financial relationships that could be construed as a potential conflict of interest.

Publisher's Note: All claims expressed in this article are solely those of the authors and do not necessarily represent those of their affiliated organizations, or those of the publisher, the editors and the reviewers. Any product that may be evaluated in this article, or claim that may be made by its manufacturer, is not guaranteed or endorsed by the publisher.

Copyright © 2022 Wu, Fang, Zhang, Sun, Wang, Branca and Xu. This is an open-access article distributed under the terms of the Creative Commons Attribution License (CC BY). The use, distribution or reproduction in other forums is permitted, provided the original author(s) and the copyright owner(s) are credited and that the original publication in this journal is cited, in accordance with accepted academic practice. No use, distribution or reproduction is permitted which does not comply with these terms.

frontiers in Plant Science

ORIGINAL RESEARCH
published: 09 June 2021
doi: 10.3389/fpls.2021.683868

Exogenous Application of 5-Aminolevulinic Acid Promotes Coloration and Improves the Quality of Tomato Fruit by Regulating Carotenoid Metabolism

Junwen Wang[1], Jing Zhang[1], Jing Li[1], Mohammed Mujitaba Dawuda[2], Basharat Ali[3], Yue Wu[1], Jihua Yu[1,4]*, Zhongqi Tang[1], Jian Lyu[1], Xuemei Xiao[1], Linli Hu[1] and Jianming Xie[1]*

[1] College of Horticulture, Gansu Agricultural University, Lanzhou, China, [2] Department of Horticulture, FoA, University for Development Studies, Tamale, Ghana, [3] Department of Agronomy, University of Agriculture, Faisalabad, Pakistan, [4] Gansu Provincial Key Laboratory of Aridland Crop Science, Lanzhou, China

OPEN ACCESS

Edited by:
Xinchao Wang, Tea Research Institute, Chinese Academy of Agricultural Sciences (CAAS), China

Reviewed by:
Yuhua Wang, Nanjing Agricultural University, China
Catello Di Martino, University of Molise, Italy

***Correspondence:**
Yue Wu
wuyue_gsau@163.com
Jihua Yu
yujihuagg@163.com

Specialty section:
This article was submitted to Crop and Product Physiology, a section of the journal Frontiers in Plant Science

Received: *22 March 2021*
Accepted: *06 May 2021*
Published: *09 June 2021*

Citation:
Wang J, Zhang J, Li J, Dawuda MM, Ali B, Wu Y, Yu J, Tang Z, Lyu J, Xiao X, Hu L and Xie J (2021) Exogenous Application of 5-Aminolevulinic Acid Promotes Coloration and Improves the Quality of Tomato Fruit by Regulating Carotenoid Metabolism. Front. Plant Sci. 12:683868. doi: 10.3389/fpls.2021.683868

5-Aminolevulinic acid (ALA) plays an important role in plant growth and development. It can also be used to enhance crop resistance to environmental stresses and improve the color and internal quality of fruits. However, there are limited reports regarding the effects of ALA on tomato fruit color and its regulatory mechanisms. Therefore, in this study, the effects of exogenous ALA on the quality and coloration of tomato fruits were examined. Tomato (*Solanum lycopersicum* "Yuanwei No. 1") fruit surfaces were treated with different concentrations of ALA (0, 100, and 200 mg·L^{-1}) on the 24th day after fruit setting (mature green fruit stage), and the content of soluble sugar, titratable acid, soluble protein, vitamin C, and total free amino acids, as well as amino acid components, intermediates of lycopene synthetic and metabolic pathways, and ALA metabolic pathway derivatives were determined during fruit ripening. The relative expression levels of genes involved in lycopene synthesis and metabolism and those involved in ALA metabolism were also analyzed. The results indicated that exogenous ALA (200 mg·L^{-1}) increased the contents of soluble sugars, soluble proteins, total free amino acids, and vitamin C as well as 11 kinds of amino acid components in tomato fruits and reduced the content of titratable acids, thus improving the quality of tomato fruits harvested 4 days earlier than those of the control plants. In addition, exogenous ALA markedly improved carotenoid biosynthesis by upregulating the gene expression levels of geranylgeranyl diphosphate synthase, phytoene synthase 1, phytoene desaturase, and lycopene β-cyclase. Furthermore, exogenous ALA inhibited chlorophyll synthesis by downregulating the genes expression levels of Mg-chelatase and protochlorophyllide oxidoreductase. These findings suggest that supplementation with 200 mg·L^{-1} ALA not only enhances the nutritional quality and color of the fruit but also promotes early fruit maturation in tomato.

Keywords: 5-aminolevulinic acid, tomato fruit, internal quality, coloration, lycopene synthesis

INTRODUCTION

Fruit quality is determined by visual attributes, including size and color, as well as non-visual attributes, such as fruit taste and nutritional value (Nour et al., 2010). In recent years, consumer pursuit of tomato fruit qualities, such as appearance, flavor, and internal nutrition, has increased. Consumers equate the visual appearance of fresh fruits with their internal qualities (Saltveit, 1999), which jointly determines their preferences and purchase desires (Hadi et al., 2013). In fresh fruits, the internal qualities of fruit mainly refer to soluble sugars, organic acids, vitamin C, and other nutrients (Hecke et al., 2006). Moreover, the most important external quality is color, which is one of the critical factors determining consumer acceptance (Yu et al., 2016). Thus, improvement of the external qualities of fruits has become an important research area (Ye et al., 2017).

Tomato (*Solanum lycopersicum*) is one of the most widely produced and consumed fruits worldwide (Zhu et al., 2018). The fruit is rich in nutrients, such as minerals, vitamin C, and lycopene, which are good dietary antioxidants (Perveen et al., 2015; Xie et al., 2019) with the potential to delay aging and inhibit cancer cell proliferation (Buyuklu et al., 2015; Ye et al., 2016). Tomato fruits of different colors contain various pigments, such as carotenoids and anthocyanins (Borghesi et al., 2016). The red, pink, and orange coloration of tomato fruits is mainly attributed to carotenoid accumulation (Yu et al., 2016) and lycopene is the primary carotenoid in ripe tomato fruits (Ip et al., 2013). Lycopene is derived from the 5-carbon compound isopentenyl diphosphate (IPP) in plastids (Hirschberg, 2001). The addition of three IPP molecules to dimethylallyl diphosphate is catalyzed by geranylgeranyl diphosphate synthase (GGPPS) to produce geranylgeranyl diphosphate (GGPP) (Okada et al., 2000). The condensation of two GGPP molecules into phytoene is catalyzed by phytoene synthase (PSY), which is the first step in synthesizing carotenoids in mature tomato fruits (Fraser et al., 2002). Subsequently, phytoene and ζ-carotene undergo desaturation reactions that are catalyzed by phytoene desaturase (PDS) and ζ-carotene desaturase (ZDS) (Fraser et al., 2002). All-*trans*-lycopene is produced by isomerization catalyzed by carotene isomerase (CRTISO); when CRTISO is mutated, the fruit color is orange, and the carotenoids downstream of lycopene are significantly reduced (Isaacson et al., 2002; Fantini et al., 2013).

Multiple strategies for improving fruit coloration have also been reported. For example, lycopene content in tomato fruit can be increased by covering greenhouses with double-layer polyethylene films, thus promoting tomato coloration (Jarquín-Enríquez et al., 2013). Supplementation with red light can stimulate carotenoid accumulation (Dorais et al., 2008). Moreover, use of arbuscular mycorrhizal inoculum of *Funelliformis mosseae* in P-limited soil could improve tomato fruit color and nutritional quality (Palumbo et al., 2020). However, these methods increase the cost of tomato production under greenhouse conditions. Application of plant growth regulators is a convenient and economically viable method for improving plant growth and fruit ripening (Ali et al., 2015; Feng et al., 2016; Xie et al., 2019). For instance, in mango, the climacteric peak and skin coloration are promoted by ethylene application (Mohamed and Abu-Goukh, 2003). Conversely, in tomato fruit, downregulation of key genes in the ethylene biosynthetic pathway, *ACO* or *ACS*, leads to a reduction in lycopene content (Yokotani et al., 2004; Ito et al., 2017). However, exogenous application of ABA promotes carotenoid accumulation and accelerates fruit reddening in mature green tomatoes (Mou et al., 2016). During fruit ripening, brassinolide application effectively induced tomato fruit ripening and increased the lycopene content (Zhu et al., 2015). Among plant growth regulators, 5-aminolevulinic acid (ALA) is an essential biosynthetic precursor of all tetrapyrrole compounds (chlorophyll, heme, and vitamin B_{12}) (Senge et al., 2014), which have promotive effects on plant growth and stress resistance, such as seed germination (Korkmaz and Korkmaz, 2009; Fu et al., 2014), plant biomass (Xu et al., 2015), salinity tolerance (Ahmad et al., 2012; Naeem et al., 2012), drought (Li et al., 2011; Liu et al., 2013), and heavy metals (Ali et al., 2013a,b; Gill et al., 2015). In the ALA metabolic pathway, higher-plant chlorophyll has several precursors, including protoporphyrin IX (Proto IX), Mg-protoporphyrin IX (Mg-Proto IX), and protochlorophyllide (Pchlide) (Chen, 2014; Sobotka, 2014; Nguyen et al., 2015).

Several studies have reported that ALA is involved in the regulation of crop nutrient quality and fruit coloration. For example, exogenous application of ALA has been found to increase vitamin C and soluble sugar contents, reduce nitrate and crude fiber contents, and lead to better quality and taste in lettuce (Xu et al., 2012). Application of ALA significantly increased the soluble solid and soluble protein content by 20.9 and 31.4%, respectively, and decreased titratable acid content, thus promote the quality of tomato fruit (Wang et al., 2008). Rhizospheric application of ALA increased contents of ascorbic acid, soluble proteins, soluble solids, and soluble sugars of apple fruit, and decreased titratable acid content, thus improves interior qualities (Zheng et al., 2017). In addition, anthocyanin accumulation was increased in peach skin through the application of exogenous ALA, which upregulated the expression levels of *CHS*, *CHI*, *F3H*, *DFR*, *LDOX*, and *UFGT*, resulting in improved peach coloration (Ye et al., 2017). Another study showed that after ALA treatment, the content of heme (metabolic derivatives of ALA) increased, which may act as a transcription factor, up-regulating the gene expressions of *MYB*, *bHLH*, and *WD40*, the latter in turn up-regulate the expression of the structural genes such as *PAL*, *CHS*, and *UFGT*, thus, anthocyanin was synthesized *de novo* in apple skins (Xie et al., 2013). The expression of *MdMADS1*, a developmental transcription regulator of fruit ripening, was positively correlated with expression of anthocyanin biosynthetic genes (*MdCHS*, *MdDFR*, *MdLDOX*, and *MdUFGT*) in apple skin under ALA treatment, synergistic or additive responses between ALA and *MdMADS1* exists for regulation of apple skin anthocyanin accumulation (Feng et al., 2016). These results indicate that ALA can significantly promote anthocyanin accumulation and fruit coloration. However, the regulative role of ALA on carotenoid pigments biosynthesis, fruit coloration and its mechanisms have not been elucidated yet. Therefore, in the present study, red fruit tomato was used as the experimental material, and the positive effects of exogenous ALA application

on the coloration and nutrient quality of tomato fruits during ripening were investigated. Moreover, the relative expression levels of key genes involved in lycopene anabolism were assessed to understand the molecular mechanisms underlying ALA-induced lycopene accumulation.

MATERIALS AND METHODS

Plant Materials and Experimental Design

Tomato (*Solanum lycopersicum* "Yuanwei No. 1") plants were used in this study and grown in a solar greenhouse in Lanzhou City, China (35.87°N, 104.09°E).

Experiment I, the first fruit clusters (the growth position of the first inflorescence from bottom to top on tomato plants) were used to select the appropriate ALA concentration on fruit coloration and quality. The concentrations of ALA (Sigma-Aldrich, St. Louis, MO, United States) were 0, 50, 100, 200, and 300 mg L^{-1}. Tomato fruit were treated at the mature green stage (24 days after fruit setting). Fully expanded fruits with uniform sizes (diameters around 4 cm) were selected and treated at 3-days interval until the fruit matured. These fruit surfaces were evenly daubed with ALA solution containing 0.01% Tween-20. During fruit maturity, the contents of soluble sugar, soluble solids, and fruit firmness were determined to select the appropriate ALA treatment.

Experiment II, the third fruit clusters (the growth position of the third inflorescence from bottom to top on tomato plants) were selected for further test. During experimental treatment, 10 healthy tomato plants with same growth vigor were marked in each treatment, repeated three times. In order to ensure the same fruit maturity of each treatments, 2–3 fruits with the same pollination date were selected as the treatment target on the third fruit clusters. In total, there were about 90 fruits in each treatment. Tomato fruit were treated at the mature green stage (24 days after fruit setting). Fully expanded fruits and fruits of uniform sizes (diameters around 4 cm) were selected and treated at 3-days interval until the fruit matured. The most effective ALA (Sigma-Aldrich, United States) solution containing 0.01% Tween-20 as the surfactant. Three replications were carried out for each treatment, and each replicate included 10 tomato plants. Fruit samples were taken at 3-days interval during the treatment period until the fruits were mature. The tomato fruit was considered mature when 90% of its surface was red. During sampling, five tomato fruits were randomly selected for each treatment, and the treatment was repeated three times. Tomato fruits treated with exogenous ALA and those in the control group matured by the 40th and 44th days after fruit setting, respectively.

Tomato Fruit Morphology and Skin Color Parameters

After exogenous ALA application, the fruits were photographed at each sampling time point. The skin color of the fruit was measured using a colorimeter (CR-10 Plus, Konica Minolta, Inc., Tokyo, Japan), which provided color surface coordinates L^*, a^*, and b^* (L^* indicates lightness; a^* indicates a range between green and red; and b^* indicates a range between blue and yellow). The a^* and b^* values were processed to obtain the hue angle (hue angle value is a comprehensive indicator of color change, which is inversely proportional to a^* and directly proportional to b^*). The hue angle (in degrees) was calculated according to the following equation (Sagar et al., 2013):

$$\text{Hue} = \tan^{-1}(\text{b}^*/\text{a}^*),\ \text{ifa}^* > 0;\ \text{otherwise},$$

$$\text{Hue} = 180 + \tan^{-1}(\text{b}^*/\text{a}^*),\ \text{ifa}^* < 0$$

Each sample consisting of three fruits was randomly selected, and measurements were performed at the shoulder, at a point parallel to the equatorial plane, and on the top of each fruit.

Determination of the Nutrient Quality of Tomato Fruits

The fruit firmness was measured by GY-4-J firmness tester (Top Cloud-agri Technology Co., Ltd., Hangzhou, China). The soluble solids were determined by PAL-1 refractometer (ATAGO Co., Ltd., Japan). Soluble protein content was determined using Coomassie brilliant blue G250 staining (Sedmak and Grossberg, 1977) with some modifications. Fresh tomato fruit samples (0.5 g) were ground, transferred to a centrifuge tube, and deionized water was added to a volume of 10 mL. The extract was centrifuged at 5,000×g for 10 min at 4°C, and the supernatant was collected. The soluble protein content was determined at a wavelength of 595 nm. The vitamin C content was determined using an ascorbic acid content detection kit (Solarbio Life Science, Beijing, China) following the manufacturer's protocol. Total free amino acid content was determined using the ninhydrin assay (Sorrequieta et al., 2010) with some modifications. Briefly, fresh tomato fruit samples (0.25 g) were ground to a fine paste and placed in a volumetric flask. Then, deionized water was added to a volume of 100 mL; the mixture was filtered, and the filtrate was collected. The total free amino acid content was determined at a wavelength of 500 nm.

The soluble sugar content was determined using the method of Grandy et al.'s (2000) with some modifications. Fresh tomato fruit samples (0.2 g) were ground to a fine paste and placed in a sterile test tube to which 5 mL of deionized water was added, and the sample was mixed. This step was repeated twice, and the supernatant was collected after 30 min incubation in a water bath at 100°C. Deionized water was added to a volume of 25 mL. The soluble sugar content was determined using the anthrone method at a wavelength of 620 nm. The titratable acid content of tomato fruits was determined using the method described by Wang et al.'s (2013). Fresh tomato fruit samples (5 g) were ground to a fine paste and placed in an Erlenmeyer flask. Deionized water was then added to a volume of 50 mL, and the mixture was filtered. The filtrate then underwent titration with 0.1 mol·L^{-1} sodium hydroxide (containing two drops of 1% phenolphthalein), resulting in a faint pink color, which was used as an indicator. Mean values were calculated from three independent sample replicates.

The sample preparation and LC–MS analysis of amino acid components were according to the method described by Nimbalkar et al.'s (2012) with slight modifications. 0.5 g dried sample was weighed into sample container containing 20 mL of

0.1% (v/v) hydrochloric acid. Ultrasonic extraction for 15 min, followed by centrifugation at 4°C at 10,000 rpm for 5 min. The supernatant was passed through 0.2 μm nylon membrane filter and 5 μL of sample was injected to LC-MS (Agilent 1290-6460, CA, United States) analysis.

Determination of the Contents of Intermediates of the Lycopene Synthetic and Metabolic Pathways

Carotenoids were isolated according to the method described by Kang et al.'s (2010) with slight modifications. The tomato fruits were dried using a freeze dryer (LyoQuest-85, Telstar Technologies, Barcelona, Spain) and then ground into powder using a grinder (TissueLyser II; QIAGEN, Hilden, Germany). Sample powder (0.5 g) was added to a 30 mL solution (petroleum ether and acetone, 2:1 v/v) and then extracted at 30°C for 40 min by sonication (SB-800 DT, NingBo Scientz Biotechnology Co., Ltd., NingBo, China). After the aqueous phase was removed, the petroleum ether extract was poured into a round-bottom flask, dried by rotary evaporation at 40°C, and then dissolved in 25 mL of a mixture of acetonitrile, dichloromethane, and methanol (55:20:25, v/v/v). The mixture was then filtered through a 0.22 μm organic filter membrane and finally analyzed by high-performance liquid chromatography (HPLC) using a Symmetry C18 column (250 mm × 4.6 mm, 5 μm, Waters Corp., Milford, MA, United States). The flow rate was 1.2 mL·min^{-1}; the mobile phase was methanol, acetonitrile, and dichloromethane (25:55:20, v/v/v); and the column temperature was maintained at 30°C.

Compounds were detected at 450 nm (β-carotene and lutein), 470 nm (lycopene), and 286 nm (phytoene). The compounds were identified according to the retention times of standards (lycopene, β-carotene, and lutein obtained from YuanYe Biotechnology Co., Ltd., Shanghai, China, and phytoene obtained from Sigma–Aldrich) and quantified according to standard curves. Data were analyzed using Empower Software (Waters Corp.).

Determination of the Contents of Metabolic Derivatives of the ALA Metabolic Pathway

5-Aminolevulinic acid was determined according to the method described by Wu et al.'s (2018). Briefly, 5 g of fresh tomato fruit sample was ground with 6 mL acetate buffer (pH 4.6) on an ice bath, centrifuged at 5,000×*g* for 15 min at 4°C, and the supernatant collected. The absorbance was measured at 554 nm. The calculation of endogenous ALA concentration is based on the protein concentration of samples as reference (μmol·mg^{-1} Prot).

To determine the chlorophyll content of fresh tomato fruit samples, 2 g samples were extracted with 80% buffered aqueous acetone (Porra et al., 1989). The absorbance of the supernatant was determined at 646 and 663 nm. The chlorophyll content (Chl *a* and *b*) was calculated using the following formulas described by Lichtenthaler and Wellburn (1983). *V* values indicate the dissolved volume of the determined solution; FW values indicate the fresh weight of the sample.

$$\text{Chl a } \left(\text{mg g}^{-1}\text{ FW}\right) = (12.21 \times \text{OD}_{663} - 2.81 \times \text{OD}_{646}) \times V/\text{FW}$$

$$\text{Chl b } \left(\text{mg g}^{-1}\text{ FW}\right) = (20.13 \times \text{OD}_{646} - 5.03 \times \text{OD}_{663}) \times V/\text{FW}$$

Proto IX, Mg-Proto IX, and Pchlide were determined according to the methods described by Wu et al.'s (2018) with some modifications. Briefly, 1 g of fresh tomato fruit sample was homogenized with 2 mL 80% alkaline acetone, placed in a sterile test tube, and then 80% alkaline acetone was added to a volume of 25 mL. The homogenate was incubated under dark conditions until the sample was bleached. The homogenate was centrifuged at 1,500×*g* for 10 min, and the supernatant was collected. The absorbance of the supernatant was determined at 575, 590, and 628 nm. The results were calculated as described by Liu et al.'s (2015) with some modifications. The calculation of metabolic derivatives concentrations are based on the protein concentration of samples as reference (μmol·g^{-1} Prot). V1 values indicate the dissolved volume of the of the sample; V2 values indicate the determined volume of the sample; Cpr values indicate the protein concentration of the sample.

$$\text{Proto IX } \left(\mu\text{ mol g}^{-1}\text{ Prot}\right) = (0.18016 \times \text{OD}_{575} - 0.04036 \times \text{OD}_{628} - 0.0451 \times \text{OD}_{590}) \times \text{V1}/\left(\text{V2} \times \text{Cpr}\right)$$

$$\text{Mg} - \text{Proto IX } \left(\mu\text{ mol g}^{-1}\text{ Prot}\right) = (0.06077 \times \text{OD}_{590} - 0.01937 \times \text{OD}_{575} - 0.003423 \times \text{OD}_{628}) \times \text{V1}/\left(\text{V2} \times \text{Cpr}\right)$$

$$\text{Pchlide } \left(\mu\text{ mol g}^{-1}\text{ Prot}\right) = (0.03563 \times \text{OD}_{628} + 0.007225 \times \text{OD}_{590} - 0.02955 \times \text{OD}_{575}) \times \text{V1}/\left(\text{V2} \times \text{Cpr}\right)$$

Total RNA Extraction and Relative Gene Expression Analysis

Total RNA was extracted using the RNAprep Pure Plant Plus Kit (Tiangen Biotech, Beijing, China) according to the manufacturer's protocol, which included a genomic DNA elimination step. RNA quality and concentration were checked on a DS-11+ spectrophotometer (DeNovix Inc., Wilmington, DE, United States), and samples were stored at −80°C until further use. cDNA synthesis was performed using a FastKing RT Kit (Tiangen Biotech) according to the manufacturer's protocol. The tomato actin gene was used as an internal control. The GenBank accession numbers of the sequences used to design the primers are listed in **Table 1**. Finally, 1 μL of cDNA was used for quantitative real-time PCR (qRT-PCR) analysis in a real-time PCR detection system (QuantStudio 5 Real-Time PCR System; Thermo Fisher Scientific, Waltham, MA, United States). The reaction mixture included the following: 1 μL cDNA template, 10 μL of 2× Talent qPCR PreMix (Tiangen Biotech), 0.4 μL of 50×

TABLE 1 | Primer sequences and GenBank accession numbers of the geranylgeranyl diphosphate synthase (*GGPPS*), *PSY1*, phytoene desaturase (*PDS*), lycopene β-cyclase (*LCY-B*), *CHLH*, *POR*, and *ACTIN* gene sequences.

Gene symbol	Accession number	Forward primer 5′–3′	Reverse primer 5′–3′
GGPPS	NM_001366706.1	CTGCCTGTGCCTTAGAGATGGTTC	CCTCGTCGAGTTGTGTCATCATCC
PSY1	NM_001247883.2	GCTGGAAGGGTGACCGATAAATGG	GTCACGCCTTTCTCTGCCTCATC
PDS	NM_001247166.2	CGAGGTCGTCTTCTTTGGGAACTG	CAATCTTCTGGTCGTGGCATGGG
LCY-B	NM_001247297.2	GAGTCGTTGGAATCGGTGGTACAG	CAACAGGAGCCGCAGCTAGTG
CHLH	XM_004236562.4	GTGCTGGCATGATGGAGAAGAGG	GAGGTTCTGAACGAGGTTGGTTGG
POR	NM_001317974.1	TGGACCTCGCCTCTCTTGACAG	CAGCAGCATTAGCAACCAACACG
ACTIN	NM_001330119.1	TTGTGTTGGACTCTGGTGATGGTG	GACGGAGAATGGCATGTGGAAGG

ROX Reference Dye$^{\Delta}$ (Tiangen Biotech), 0.6 μL forward primer, 0.6 μL reverse primer, and RNase-Free ddH_2O to a final volume of 20 μL. For each sample, there were three wells for the target gene and three wells for the negative control (all components of the reaction mix, except for template cDNA replaced by RNase-free ddH_2O) on the plate. The two-step amplification procedure consisted of one cycle of pre denaturation at 95°C for 3 min, followed by 40 cycles of denaturation at 95°C for 5 s, annealing and extension at 60°C for 15 s. Each qPCR assay was repeated three times. Quantification analysis was performed using the comparative CT method (Livak and Schmittgen, 2001). The CT value of actin was subtracted from that of the target gene to obtain the ΔCT value. The average CT value of the control sample was subtracted from the ΔCT value to obtain the ΔΔCT value. For each sample, the expression level relative to the control was expressed as $2^{-\Delta\Delta CT}$.

Statistical Analysis

All experiments were performed in triplicate, and data from all experiments were expressed as means ± SE. Data were analyzed by analysis of variance (ANOVA) in SPSS version 23.0 (IBM Corp., Armonk, NY, United States), and treatment means were compared using Tukey's honest significant difference test at a 0.05 level of probability (P-value < 0.05). All figures were prepared using OriginPro 8.5.0 (OriginLab Corporation, Northampton, MA, United States).

RESULTS

Effects of Different Concentrations of Exogenous ALA on Soluble Sugar, Soluble Solids Content, and Firmness of Tomato Fruit

As shown in **Figure 1A**, at 36th day after fruit setting, the soluble sugar content of tomato fruit treated with 200 mg·L^{-1} ALA was significantly higher than those of other treatments. When 100 and 200 mg·L^{-1} ALA treatments reached maturity (40th day after fruit setting), the soluble sugar content was significantly higher than other treatments. The soluble solids content increased during fruit ripening (**Figure 1B**), at 36th day after fruit setting, 100 and 200 mg·L^{-1} ALA treatments was significantly higher than those in other treatments. At 40th day after fruit setting, 200 mg·L^{-1} ALA treatment reached the maximum and was significantly higher than other treatments. As shown in **Figure 1C**, at 40th day after fruit setting, the fruit firmness of 100–300 mg·L^{-1} ALA treatments were significantly lower than that of the control. At 40th day after fruit setting, 100 and 200 mg·L^{-1} ALA treatments were significantly lower than the control. Based on the effects of the various ALA concentrations on soluble sugar, soluble solids content and firmness of tomato fruit, we considered the 100 and 200 mg·L^{-1} ALA treatments were more effective to increase the content of soluble sugar and soluble solid and reduce fruit firmness. The 100 and 200 mg·L^{-1} ALA treatments were employed in the further experiment.

Protective Effects of ALA on Morphology and Skin Color Parameters of Tomato Fruits

During tomato ripening, i.e., coloration changes from green to red (**Figure 2A**), ALA treatment resulted in faded green areas on the fruit surface by the 32nd day after fruit setting. On the 36th day after fruit setting, fruits treated with 100 and 200 mg·L^{-1} ALA were at the pink stage when the fruit of the control group was at the color break stage. The ALA-treated fruits reached maturity 4 days earlier than the control fruits. The color difference of fruits in each treatment group was compared by measuring the values of a^*, b^*, and L^* and calculating the hue angle. The a^* value, which indicates colors ranging from green to red, gradually increased with tomato fruit development in each treatment (**Figure 2B**). In contrast, the b^* (**Figure 2C**), L^* (**Figure 2D**), and hue angle (**Figure 2E**) values showed an overall decreasing trend. In particular, 36–40 days after fruit setting, the a^* value of the 200 mg·L^{-1} ALA-treated fruit was significantly higher than that of the control. In addition, the values of b^* and L^*, and the hue angle values of the ALA treatment group were significantly lower than those of the control group. Hence, after exogenous ALA treatment, the green fading of the fruit skin was accelerated.

Exogenous Application of ALA Modulates the Nutrient Quality of Tomato Fruits

As shown in **Table 2**, the different exogenous ALA concentrations affected the quality indices of tomato fruits. The soluble sugar content of tomato fruit increased continuously, whereas the

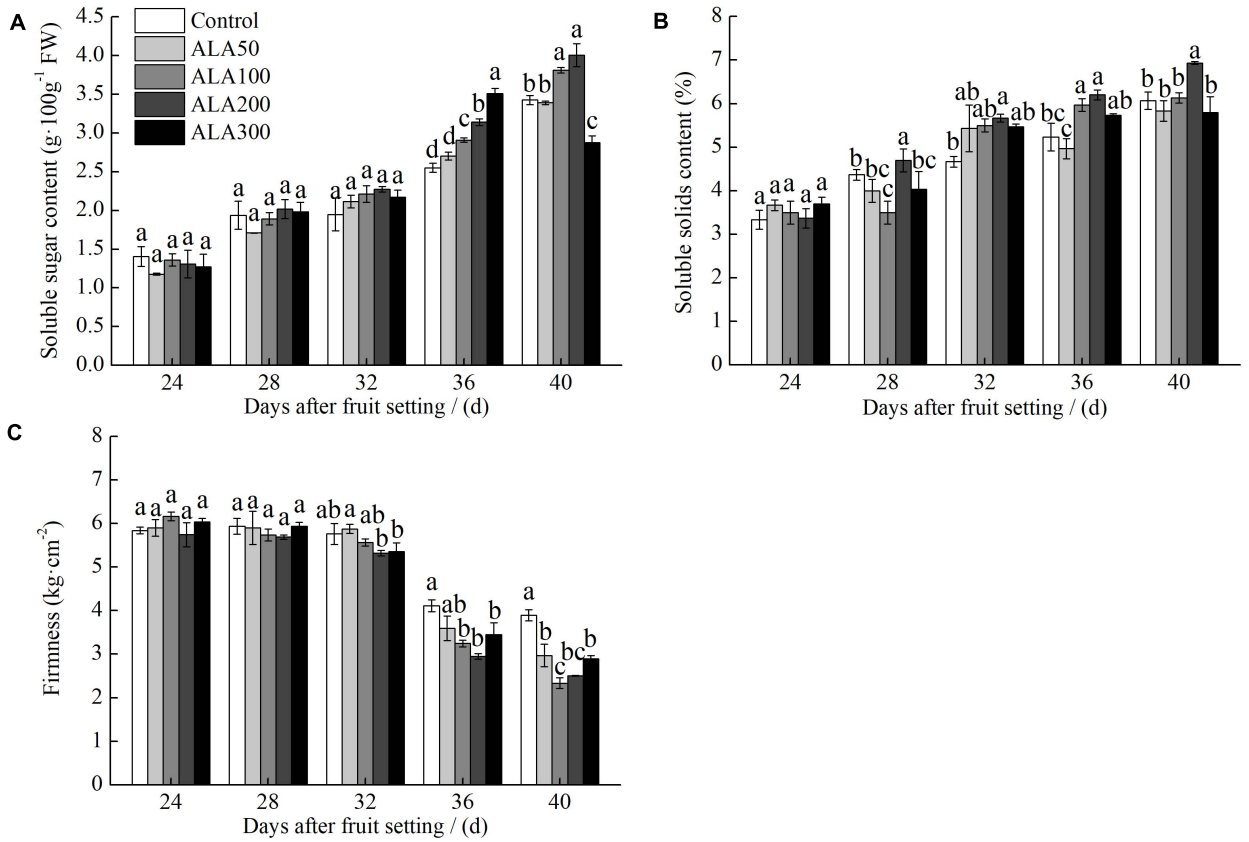


FIGURE 1 | The effects different concentrations of 5-aminolevulinic acid (ALA) on the soluble sugar, soluble solid content, and firmness of tomato fruit. **(A)** Soluble sugar content; **(B)** Soluble solid content; and **(C)** Firmness of tomato fruits at 24th–40th day after fruit setting under different treatments. Vertical bars represent mean ± SE from three independent replicates and the different letters denote significant differences ($p < 0.05$).

titratable acid first increased and then decreased. The soluble sugar content of fruit treated with 200 mg·L^{-1} ALA was significantly higher than that of the control, 28–40 days after fruit setting. When the fruit of the control group reached maturity (44 days after fruit setting), the soluble sugar content was significantly lower than that of the fruit treated with 200 mg·L^{-1} ALA on the 40th day after fruit setting. By day 24–32 after fruit setting, there was no significant effect on titratable acid content among the treatments. The titratable acid content in fruit treated with exogenous ALA decreased by the 36th day after fruit setting, whereas it decreased by the 40th day after fruit setting in the control group. The soluble protein content increased gradually during fruit ripening. Compared with the control group, exogenous ALA treatment significantly increased the soluble protein content in tomato fruit. When the fruits in the control group reached maturity (44 days after fruit setting), there was no significant difference in soluble protein content compared with the ALA treatments by the 40th day after fruit setting. The total free amino acid and soluble protein content showed a similar trend under ALA treatment. Both attained their highest levels under 200 mg·L^{-1} ALA treatment on the 40th day after fruit setting. The vitamin C content in tomato fruits increased with fruit development. Compared with the control group, both 100 and 200 mg·L^{-1} ALA treatments significantly increased the vitamin C content in tomato fruit. By 36–40 days after fruit setting, 200 mg·L^{-1} ALA treatment showed a stronger effect than 100 mg·L^{-1} ALA treatment (**Table 2**).

The 44th day after fruit setting data of the control group and the 40th day after fruit setting data of other treatments were analyzed by ANOVA to separate its significance. Each value represents mean ± SE from three independent replicates and the different letters denote significant differences ($p < 0.05$).

Effects of Exogenous ALA on Amino Acid Components of Tomato Fruit

As shown in **Figure 3**, the different exogenous ALA treatments affected the amino acid components of tomato fruits. The contents of threonine, phenylalanine, tryptophan, leucine, isoleucine, methionine, tyrosine, valine, alanine, glycine, and arginine of fruit treated with 200 mg·L^{-1} ALA was significantly higher than that of the control, at 40 days after fruit setting. During 24–32 day after fruit setting, there was no significant effect on alanine content among the treatments. However, the alanine content treated with 200 mg·L^{-1} ALA increased by the 36th day after fruit setting, it was significantly higher than that

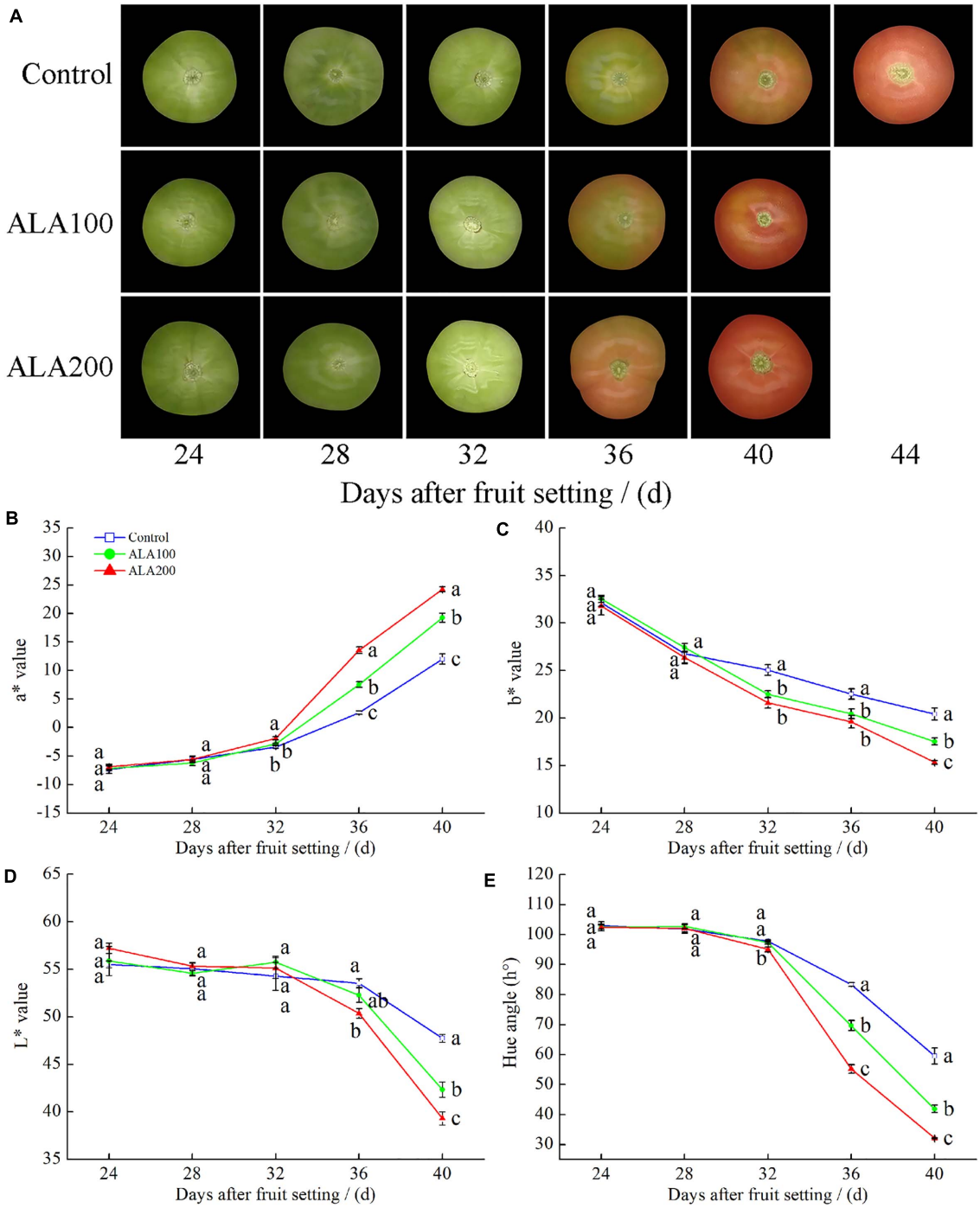


FIGURE 2 | The effects of ALA on morphology and skin color parameters of tomato fruits. **(A)** The fruit morphology; **(B)** the a^* value; **(C)** the b^* value; **(D)** the lightness; and **(E)** the hue angle of tomato fruits skin at 24th–40th day after fruit setting under different treatments. The data presented represent mean ± SE from three independent replicates and the different letters denote significant differences ($p < 0.05$).

of the control. The glutamic acid content of each treatment reached the maximum by the 36th days after fruit setting, and 200 mg·L^{-1} ALA treatment was significantly higher than that of the control. Then, glutamate content decreased markedly, and ALA treatment was significantly lower than the control. Similarly, glutamine and glutamic acid have similar trends. On the 40th day after fruit setting, ALA treatment was significantly lower than the control, and the effect of 200 mg·L^{-1} ALA treatment was more significant. Data of amino acid component contents were revealed in **Supplementary Table 1**.

TABLE 2 | Effects of ALA on the soluble sugar, titratable acid, soluble protein, total free amino acid, and vitamin C contents of tomato fruits.

Variables	Treatments	Days after fruit setting / (day)					
		24	28	32	36	40	44
Soluble sugar (g·100 g^{-1} FW)	Control	2.27 ± 0.07 a	2.54 ± 0.09 b	3.15 ± 0.03 c	3.93 ± 0.09 c	4.35 ± 0.04 b	4.50 ± 0.09 b
	ALA100	2.39 ± 0.05 a	2.89 ± 0.10 a	3.39 ± 0.05 b	4.20 ± 0.05 b	4.57 ± 0.03 b	
	ALA200	2.35 ± 0.06 a	3.05 ± 0.11 a	3.68 ± 0.09 a	4.47 ± 0.05 a	4.92 ± 0.10 a	
Titratable acid (g·100 g^{-1} FW)	Control	1.10 ± 0.05 a	1.02 ± 0.04 a	1.19 ± 0.02 a	1.33 ± 0.04 a	1.20 ± 0.01 a	1.04 ± 0.03 b
	ALA100	1.05 ± 0.01 a	0.99 ± 0.03 a	1.15 ± 0.04 a	1.25 ± 0.00 ab	1.10 ± 0.02 ab	
	ALA200	1.09 ± 0.04 a	1.04 ± 0.03 a	1.16 ± 0.02 a	1.19 ± 0.02 b	0.98 ± 0.05 b	
Soluble protein (mg·g^{-1} FW)	Control	0.16 ± 0.008 a	0.20 ± 0.008 b	0.49 ± 0.01 c	0.68 ± 0.015 c	0.91 ± 0.03 b	1.15 ± 0.028 a
	ALA100	0.17 ± 0.012 a	0.22 ± 0.007 b	0.60 ± 0.014 b	0.75 ± 0.016 b	1.14 ± 0.015 a	
	ALA200	0.16 ± 0.011 a	0.27 ± 0.011 a	0.70 ± 0.011 a	0.90 ± 0.014 a	1.22 ± 0.025 a	
Total free amino acid (mg·100 g^{-1} FW)	Control	12.44 ± 0.25 a	12.66 ± 0.56 b	14.64 ± 0.20 c	19.36 ± 0.42 b	21.56 ± 0.45 c	23.43 ± 0.31 b
	ALA100	12.71 ± 0.15 a	14.86 ± 0.38 a	17.11 ± 0.33 b	20.35 ± 0.44 b	23.10 ± 0.36 b	
	ALA200	12.49 ± 0.67 a	14.91 ± 0.29 a	18.21 ± 0.34 a	21.89 ± 0.24 a	25.74 ± 0.57 a	
Vitamin C (mg·100 g^{-1} FW)	Control	5.54 ± 0.26 a	6.34 ± 0.32 b	7.10 ± 0.26 b	7.94 ± 0.29 b	9.95 ± 0.44 c	11.37 ± 0.25 b
	ALA100	5.82 ± 0.47 a	7.11 ± 0.23 ab	8.07 ± 0.25 a	8.71 ± 0.34 b	11.74 ± 0.36 b	
	ALA200	6.12 ± 0.34 a	7.58 ± 0.05 a	8.37 ± 0.12 a	10.44 ± 0.28 a	13.02 ± 0.13 a	

The 44th day after fruit setting data of the control group and the 40th day after fruit setting data of other treatments were analyzed by ANOVA to separate its significance. Each value represents mean ± SE from three independent replicates and the different letters denote significant differences ($p < 0.05$).

Ameliorative Role of ALA in the Lycopene Synthetic and Metabolic Pathways

We determined the lycopene, phytoene, β-carotene, and lutein contents of tomato fruits 24–44 days after fruit setting. The lycopene content increased as the fruits ripened (**Figure 4A**). Lycopene was not detected in either control or ALA-treated fruits 24–28 days after fruit setting. On the 32nd day after fruit setting, a small amount of lycopene was detected but only in the 200 mg·L^{-1} ALA-treated fruit. By day 36–40 after fruit setting, the lycopene content of ALA-treated fruit was significantly higher than that of the control fruit, and lycopene levels were highest after 200 mg·L^{-1} ALA treatment 40 days after fruit setting. However, when the control group reached maturity (44 days after fruit setting), the lycopene content was significantly lower than that of mature fruits treated with 200 mg·L^{-1} ALA (40 days after fruit setting). Phytoene content first increased and then decreased with fruit ripening (**Figure 4B**). Phytoene content in fruits treated with ALA was significantly higher than that of the control by 28–36 days after fruit setting but decreased on the 40th day after fruit setting. During the ripening process, the β-carotene content continuously increased (**Figure 4C**). The β-carotene content was higher in ALA-treated fruits than in the controls. The lutein content initially decreased and then increased during the ripening process of tomato fruit (**Figure 4D**). However, it remained at a similarly low level in ALA-treated fruits. On the 32nd, 36th, and 40th day after fruit setting, the lutein content of the 200 mg·L^{-1} ALA-treated fruit was significantly lower than that of the controls.

Relative Expression of Key Genes Involved in the Lycopene Synthetic and Metabolic Pathways

The relative expression levels of the five key genes involved in the lycopene synthetic and metabolic pathways are shown in **Figure 5**. Compared with control fruits, the expression level of *GGPPS* increased in the 200 mg·L^{-1} ALA treatment and reached its highest level 32 days after fruit setting (**Figure 5A**). On the 32nd and 36th day after fruit setting, the expression level of *GGPPS* in 200 mg·L^{-1} ALA-treated fruit was 0.81- and 0.64-fold higher than that of the control. As shown in **Figure 5B**, the expression levels of *PSY1* in ALA-treated fruit increased gradually 28–36 days after fruit setting, reaching a maximum 36 days after fruit setting. The expression level of *PSY1* decreased slightly on the 40th day compared with the 36th day after fruit setting. Moreover, 200 mg·L^{-1} ALA significantly upregulated *PSY1* expression compared with that of 100 mg·L^{-1} ALA and the control group 32–40 days after fruit setting. Compared with the control, both 100 and 200 mg·L^{-1} ALA treatments significantly upregulated *PDS* and *LCY-B* in tomato fruits. By 32–40 days after fruit setting, the expression levels of *PDS* and *LCY-B* in fruits treated with 200 mg·L^{-1} ALA were significantly higher than those in the 100 mg·L^{-1} ALA treatment and control groups (**Figures 5C,D**).

Effects of ALA on Endogenous Metabolic Derivatives of the ALA Metabolic Pathway

As shown in **Figure 6A**, 24–32 days after fruit setting, the endogenous ALA content in ALA-treated fruits was no significant difference compared with the control. However, on the 36th day after fruit setting, endogenous ALA content in tomato fruit treated with ALA decreased significantly. Subsequently, endogenous ALA content increased with increasing treatment concentration. Under exogenous ALA treatments, the Proto IX, Mg-Proto IX, and Pchlide contents of the fruits initially increased and then later decreased (**Figures 6B–D**). On the 32nd day after fruit setting, they reached their highest levels in all treatments. In addition, their values in fruits under 200 mg L^{-1} ALA treatment

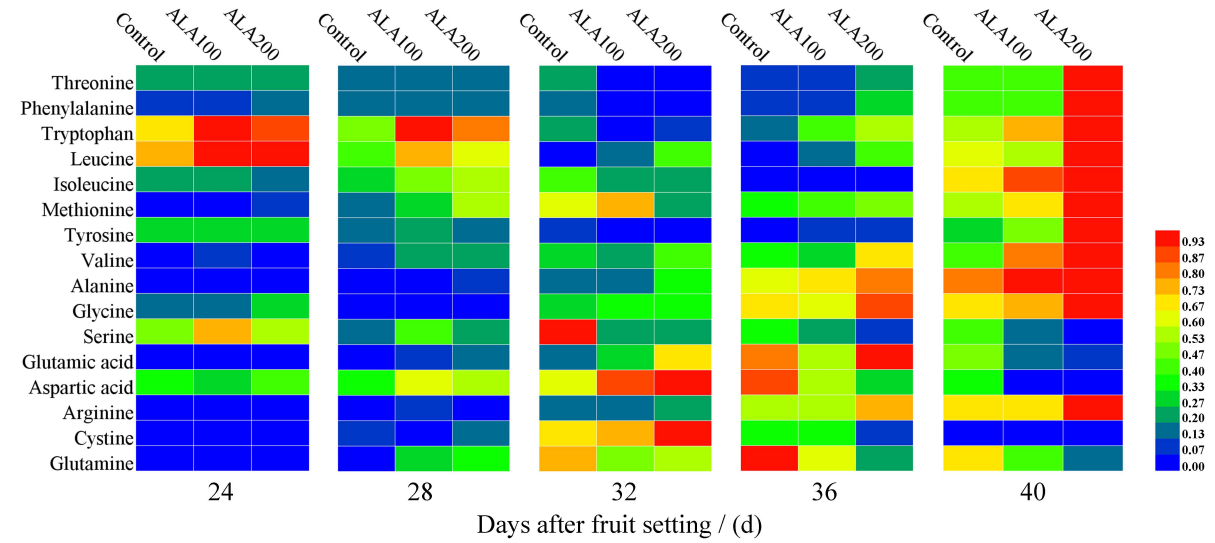


FIGURE 3 | Heat map of the effects of ALA on amino acid components in tomato fruit. Min-Max normalization method was used to standardize the data (Mohamad and Usman, 2013). The color block represents the relative value of amino acid components in the corresponding position.

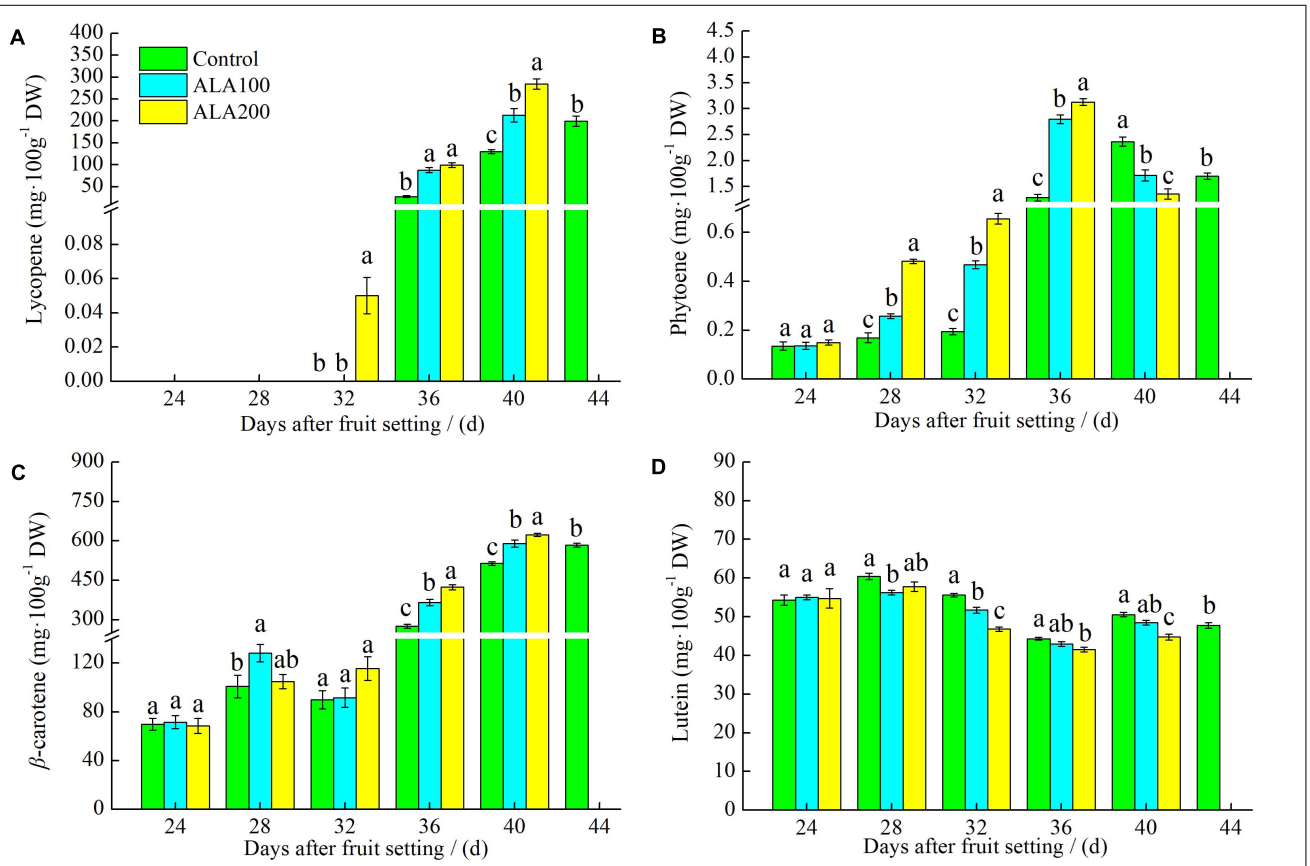


FIGURE 4 | The effects of ALA on the intermediates in lycopene synthesis and metabolic pathway. **(A)** Lycopene content; **(B)** the phytoene content; **(C)** the β-carotene content; and **(D)** the lutein content of tomato fruits at 24th–44th day after fruit setting under different treatments. The 44th day after fruit setting data of the control group and the 40th day after fruit setting data of other treatments were analyzed by analyzed by analysis of variance (ANOVA) to separate its significance. Vertical bars represent mean ± SE from three independent replicates and the different letters denote significant differences ($p < 0.05$).

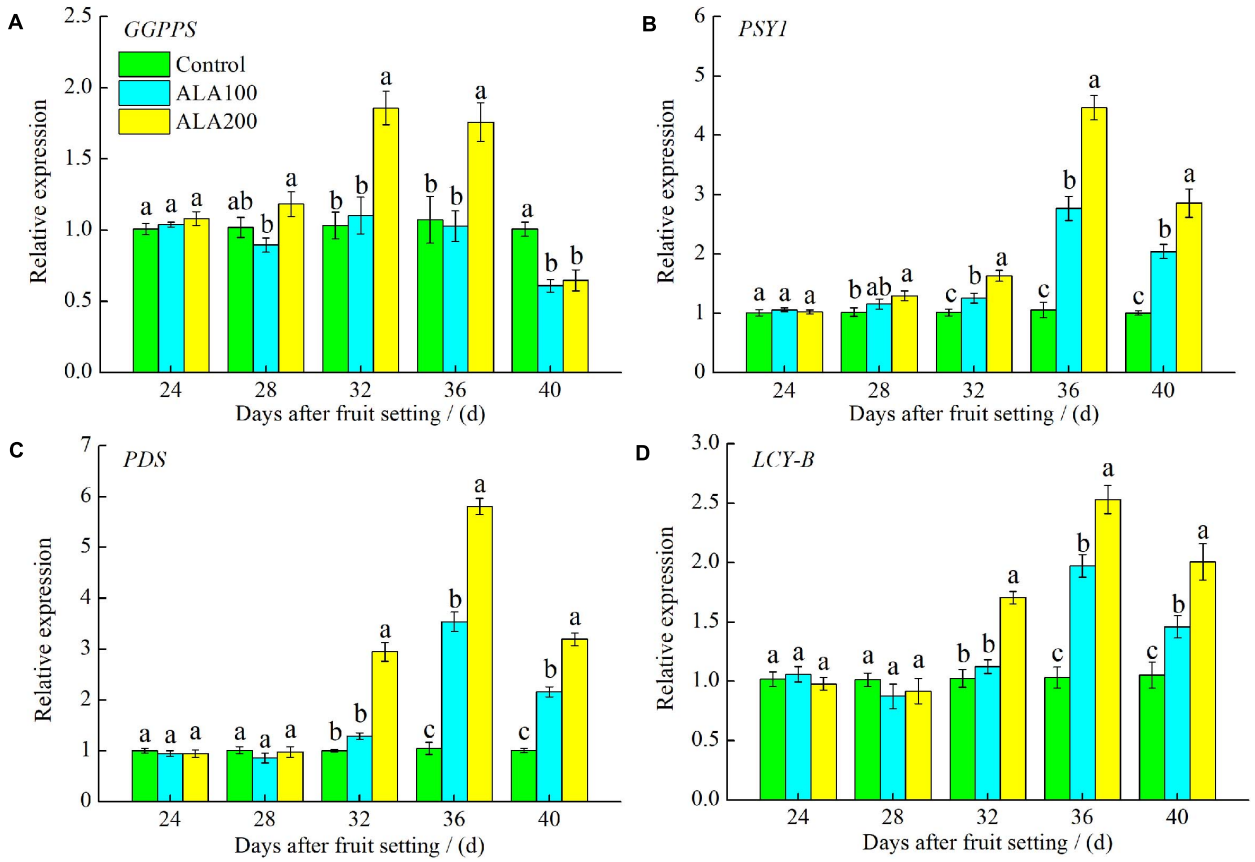


FIGURE 5 | Relative expression levels of key genes involved in lycopene synthesis and metabolism pathway. **(A)** Relative expression of *GGPPS*, encoding geranylgeranyl diphosphate synthase; **(B)** relative expression of *PSY1*, encoding phytoene synthase; **(C)** relative expression of *PDS*, encoding phytoene desaturase; and **(D)** relative expression of *LCY-B*, encoding lycopene β-cyclase. Vertical bars represent mean ± SE from three independent replicates and the different letters denote significant differences ($p < 0.05$). The control group was used as reference at each sampling time point.

were significantly lower than those of the control group on the 40th day after fruit setting. As shown in **Figures 6E,F**, on the 28th day after fruit setting, the chlorophyll a content in fruits was slightly increased by exogenous ALA, but there was no significant difference compared with the control. However, the chlorophyll *b* content was significantly higher than that of the control. Application of exogenous ALA inhibited the total content of chlorophyll 32–40 days after fruit setting due to the reduction of both chlorophyll *a* and *b* contents. In addition, for 200 mg·L^{-1} ALA treatment, chlorophyll *a* and *b* contents were significantly decreased compared with the control.

Relative Expression Levels of Key Genes Involved in the ALA Metabolic Pathway

The relative expression levels of genes involved in the ALA metabolic pathway during tomato fruit ripening were determined and are shown in **Figure 7**. By 28–32 days after fruit setting, the expression level of *CHLH* was significantly increased by exogenous ALA. In addition, the expression level of *CHLH* showed a decline by 36–40 days after fruit setting (**Figure 7A**). The expression level of *POR* was significantly increased by ALA treatment by the 28th day after fruit setting but was subsequently inhibited (**Figure 7B**).

DISCUSSION

As a plant growth regulator, ALA has the great potential for use in agricultural production (Akram and Ashraf, 2013), especially in the field of improving fruit color. For example, the application of exogenous ALA to apple fruits significantly increased the anthocyanin content in the fruit skin, thereby improving fruit color (Xie et al., 2013; Feng et al., 2016). Moreover, ALA significantly improved the fruit coloring of "Feizixiao" lychee at harvest (Feng et al., 2015). Thus, in the production of red fruits, exogenous ALA seems to be widely used to improve fruit color (Zheng et al., 2018). However, little information is available on regulatory mechanisms behind ALA-induced tomato fruit coloration. In the present study, ALA (100 and 200 mg L^{-1}) improved the color of tomato fruits and accelerated the ripening process (including color break, pink, and red stages), and the harvesting process occurred 4 days earlier than the control. Harvesting early reduces capital and energy

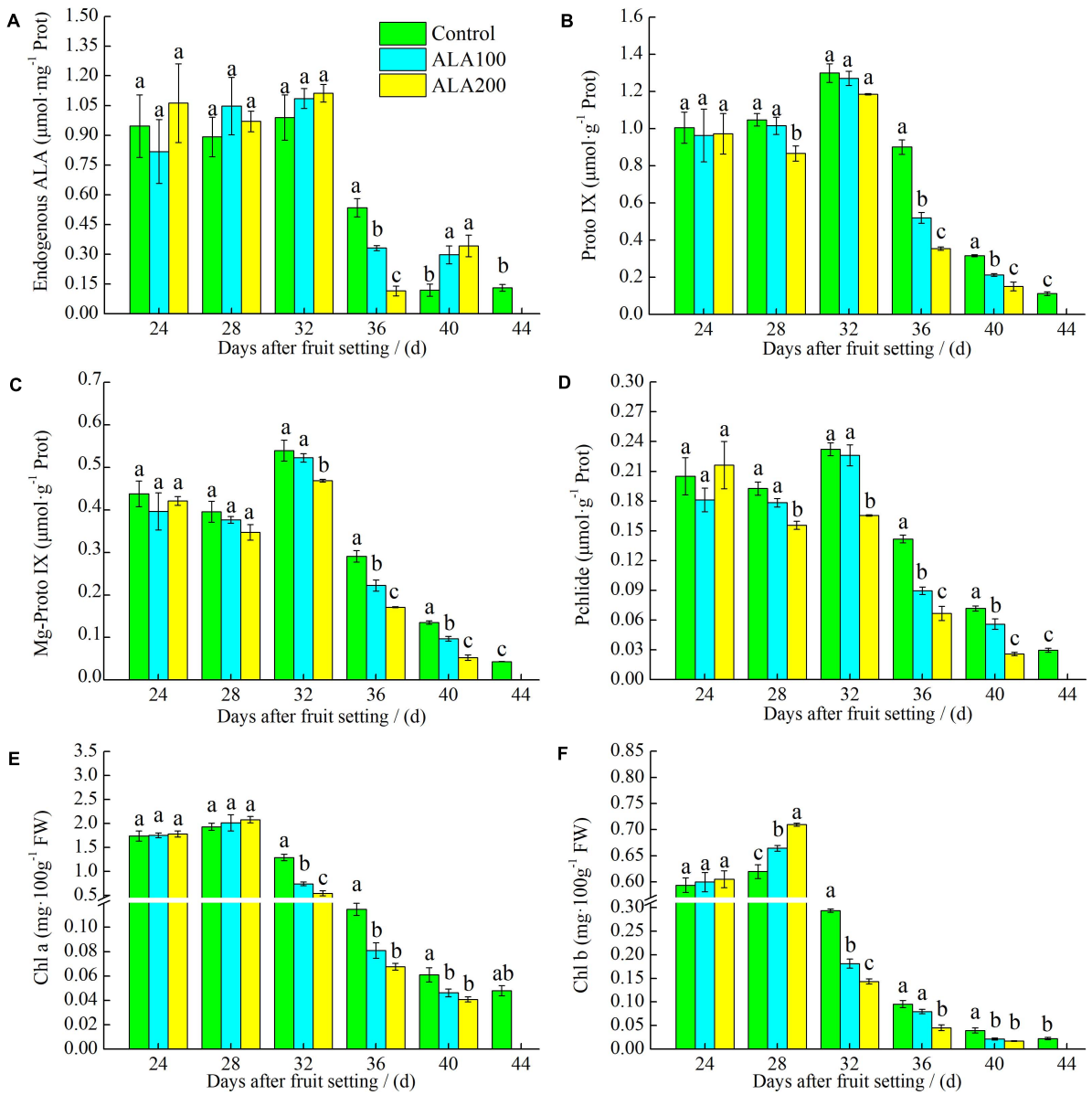


FIGURE 6 | The effects of ALA on endogenous derivatives of ALA metabolic pathway. **(A)** Endogenous ALA content; **(B)** Proto? content; **(C)** Mg-Proto? content; **(D)** Pchlide content; **(E)** Chl *a* content; and **(F)** Chl *b* content of tomato fruits at 24th–44th day after fruit setting. The 44th day after fruit setting data of the control group and the 40th day after fruit setting data of other treatments were analyzed by ANOVA to separate its significance. Vertical bars represent mean ± SE from three independent replicates and the different letters denote significant differences ($p < 0.05$).

inputs (Xie et al., 2017) and allows for early marketing to obtain economic benefits (Wang et al., 2012).

The color of tomato fruit is mainly related to its pigments, including chlorophyll, carotenoids, and anthocyanins, and their relative proportions (Borghesi et al., 2016). And coloration is mainly attributable to lycopene accumulation in red tomato fruits (Ip et al., 2013). In the present study, ALA application promoted the accumulation of carotenoids in tomato fruits. In particular, on the 40th day after fruit setting, the lycopene content of tomato fruits treated with 200 mg·L^{-1} ALA was significantly higher than that of the controls, indicating that exogenous ALA promoted the synthesis and accumulation of lycopene, which promoted the coloring of tomato fruit. However, the molecular mechanism of ALA on lycopene accumulation in tomato fruits have not been elucidated. In fruits of higher plants, lycopene biosynthesis and metabolism are intricate processes involving a series of physiological and biochemical reactions and various genes (such as *GGPPS*, *PSY*, *PDS*, and *LCY-B*) (Li et al., 2020). PSY is a key rate-limiting enzyme of lycopene biosynthesis in ripening tomato fruits (Rodríguez-Villalón et al., 2010; Stuart et al., 2011). The absence of *PSY1* in tomato fruits results in a yellow-flesh phenotype (Kang et al., 2014). Loss of *PSY1* gene

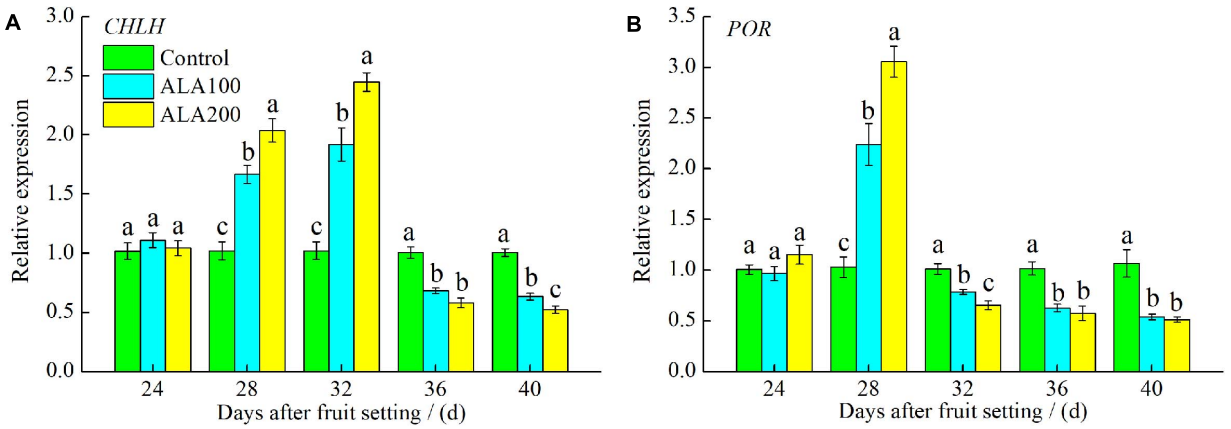


FIGURE 7 | Relative expression of genes involved in ALA metabolic pathway. **(A)** Relative expression of *CHLH*, encoding Mg-chelatase; **(B)** relative expression of *POR*, encoding protochlorophyllide oxidoreductase. Vertical bars represent mean ± SE from three independent replicates and the different letters denote significant differences ($p < 0.05$). The control group was used as reference at each sampling time point.

function by gene silencing and CRISPR/Cas9 techniques resulted in yellow tomato fruits, confirming the function of the *PSY1* gene (D'Ambrosio et al., 2018). In the present study, the overall expression of genes related to lycopene synthesis was upregulated by exogenous ALA in tomato fruits. Relative expression levels of *GGPPS*, *PSY1*, and *PDS* 32–36 days after fruit setting were increased by the application of 200 mg L^{-1} ALA, thus promoting lycopene accumulation. Furthermore, when the tomato fruit is fully ripe, all-*trans*-lycopene is converted to β- and α-carotene, catalyzed by lycopene β-cyclase (LCY-B) and lycopene ε-cyclase (LCY-E), respectively (Cunningham et al., 1994; Ronen et al., 1999). β- and α-carotene are precursors of zeaxanthin and lutein, respectively (Fraser et al., 2002). Overexpression of *NtLCYB* results in tomato fruit with high β-carotene content (Ralley et al., 2016), indicate *LCY-B* plays an important role in lycopene metabolism. In the present study, ALA significantly upregulated the expression of *LCY-B*, thereby increasing the content of β-carotene. The expression patterns of the genes involved in carotenoids metabolism after ALA treatment were consistent with carotenoids accumulation, these results further indicate that exogenous ALA can improve the external color of tomato fruit. ALA secreted by *Rhodopseudomonas* sp. inoculant in the cultivation substrate could increase tomato fruit lycopene content (Lee et al., 2008). Therefore, the positive role of ALA in lycopene accumulation in fruits is probably caused by ALA-induced gene expression during lycopene synthesis.

With the maturity of tomato fruit, the color of fruit changed significantly, mainly in the carotenoids content increase and the degradation of chlorophyll (Borghesi et al., 2016). As a precursor of chlorophyll synthesis, the ALA metabolic pathway and chlorophyll degradation are closely related to fruit ripening (Senge et al., 2014). For example, during tomato fruit ripening, it was found that *glutamate-1-semialdehyde aminotransferase* (*GAST*) was downregulated at the transcription level (Kyriacou et al., 1996). Meanwhile, 5-aminolevulinic acid dehydratase (ALAD), a key enzyme in ALA metabolism, was significantly downregulated at the translation and enzymatic activity levels, and the content of chlorophyll in the fruit decreased (Polking et al., 1999). These results indicate that chlorophyll synthesis is inhibited during tomato ripening. In the present study showed that ALA application increased chlorophyll synthesis (including Proto IX, Mg-Proto IX, and Pchlide) in the early stage of fruit development, which subsequently decreased rapidly 36 days after fruit setting. In *Brassica napus*, the relative expression of Glutamyl–tRNA synthetase (*GLUTS*), a gene in the ALA biosynthetic pathway, was upregulated by exogenous ALA, and Proto IX, Mg-Proto IX, and Pchlide levels were increased (Xiong et al., 2018). Moreover, spraying ALA on cucumber leaves significantly increased their chlorophyll content (Wu et al., 2018). Similar results were found in the present study; the contents of chlorophyll *a* and *b* increased during early fruit development after ALA application, and subsequently, chlorophyll synthesis was significantly inhibited during the late stage of fruit development. In addition, during the early stage of fruit maturity (24–32 days after fruit setting), the endogenous ALA maintained a relative stable level in tomato fruit. When fruits grew into breaker stage (36th day after fruit setting), endogenous ALA significantly declined by exogenous ALA application. Then, it was accumulated when the fruits were in pink stage (40th day after fruit setting). In the early growth stage, the fruit is a photosynthetic tissue (Hiratsuka et al., 2015). We believe that exogenous ALA promotes chlorophyll synthesis. However, application of ALA advanced the breaker stage of fruit and promoted the synthesis of carotenoid pigments. Then, chlorophyll synthesis was inhibited in the late stage of fruit development, which resulted in the inhibition of ALA metabolism in the fruit. These results suggested that the metabolism of ALA and biosynthesis of carotenoid in tomato fruit might have some interaction regulative mechanism, which should be deeply explored in further studies. In higher plants, MCH and POR are the main catalytic enzymes involved in chlorophyll biosynthesis (Nickelsen et al., 2011; Akram and Ashraf, 2013; Sobotka, 2014). MCH consists of three subunits, CHLH, CHLI, and CHLD, in higher plants; among these,

CHLH is primarily responsible for the catalytic action of MCH (Richter and Grimm, 2013). Introduction of the HEMA-RNA-interference (RNAi) gene into tobacco (*Nicotiana tabacum* L.) resulted in a decline in MCH activity and caused a decrease in chlorophyll content (Hedtke et al., 2007). In the present study, 28–32 days after fruit setting, *CHLH* expression was significantly increased by exogenous ALA. However, the gene expression of *CHLH* was downregulated 36–40 days after fruit setting. These results are consistent with the change in the Mg-Proto IX content after ALA treatment. Moreover, ALA treatment significantly promoted *POR* gene expression on the 28th day after fruit setting. Subsequently, *POR* expression was downregulated immediately before the tomato fruit reached the color break stage (32 days after fruit setting). The downregulation of *POR* resulted in the accumulation of Pchlide, which led to a decline in ALA metabolism since there is feedback regulation between ALA and Pchlide synthesis (Richter et al., 2010). These results further indicated that exogenous ALA treatment significantly promoted chlorophyll synthesis at the early stage of fruit development and that feedback inhibition eventually led to the suppression of chlorophyll biosynthesis during the late period of fruit growth. In addition, some studies have shown that inhibition of lycopene cyclase results in the accumulation of a large amount of chlorophyll synthesis precursors in plant tissues, indicating an interaction between the lycopene synthetic pathway and the ALA metabolic pathway (La Rocca et al., 2007). In the present study, the accumulation and synthesis of lycopene in tomato fruits treated with exogenous ALA were higher than those in the control fruits. Possible reasons for this phenomenon are as follows. First, during the fruit coloration period, chlorophyll began to break down, and lycopene synthesis was dominant. It is possible that feedback regulation of the ALA downstream metabolic pathway might relate to lycopene synthesis (Richter et al., 2010). Second, we speculate that ALA promotes lycopene synthesis by activating endogenous ethylene synthesis (Rupasinghe, 1995; Klee and Giovannoni, 2011). However, the specific mechanism has not been elucidated and therefore requires further investigation.

The results showed that application of exogenous ALA could not only improve the external quality of fruit, but also increase the internal quality (Xie et al., 2013). For example, the content and proportion of sugars and acids are important factors in fruit internal flavor quality (Hecke et al., 2006; Kafkas et al., 2007). Exogenous ALA could promote the accumulation of photosynthetic products, such as sugar and starch, thus promoting crop quality (Hotta et al., 1997). In grapefruit, the soluble solid content increased by 2.7%, and the organic acid content decreased significantly with the application of 100 mg·L^{-1} ALA (Watanabe et al., 2006). In the present study, we applied 200 mg·L^{-1} ALA on the 24th day after fruit setting (the mature green stage); this increased the soluble sugar content of the tomato fruits, decreased the titratable acid content between days 36 and 40 after fruit setting, and increased the sugar-acid ratio, resulting in sweeter fruit. It has been suggested that exogenous ALA increases the fructan (polyfructosylsucrose) content, suggesting that ALA is related to the transfer and storage of carbohydrates, as well as to the formation of polysaccharides in higher plants (Bingshan et al., 1998). Moreover, the sugar and acid contents in fruit treated with 200 mg·L^{-1} ALA at its mature stage (40th day after fruit setting) were consistent with the control fruit levels at maturity (44 days after fruit setting). Because proteins are composed of different amino acids, their content can be determined by the amounts, proportions, and availability of their amino acids (Gressler et al., 2010). The results of the present study showed that exogenous ALA significantly increased the contents of soluble protein and total free amino acids in the tomato fruits, and they changed in the same way. Recently, similar results were observed when rhizospheric irrigation with 160 mg·L^{-1} ALA significantly increased the soluble protein content in apple fruit (Zheng et al., 2017). The free amino acid content of *Brassica napus* was further increased by foliar application of ALA (Naeem et al., 2010). Vitamin C plays an important role in protecting human health by effectively halting tumor development, and vitamin C plays an important role in the growth and development of plants (Drisko et al., 2018). Ye et al. (2017) found that when 200 or 400 mg·L^{-1} ALA solution was sprayed to the fruit surface before the peach fruit reached maturity, and the vitamin C content in fruit flesh was significantly higher than that in control. Exogenous application of ALA to lychee peel, the vitamin C content of the fruits increased by 9–13% at harvest (Feng et al., 2015). In the present study, at 36th–40th day after fruit setting, application of 100 and 200 mg·L^{-1} ALA solution to the tomato fruit surface significantly increased the vitamin C content compared with the control. This result is likely related to the participation of vitamin C in plant respiration, ALA may weaken the respiration of plants by promoting the photosynthesis of tomato fruit, leading to increase in vitamin C content in fruit (Ye et al., 2017).

Amino acid is an important parameter reflecting the flavor and nutritional value of tomato fruit (Goff and Klee, 2006; Sorrequieta et al., 2010). It cannot only be used to regulate protein synthesis, maintain nitrogen balance, and other related physiological functions, but also closely related to human taste perception (Salvioli et al., 2012). Some amino acids, such as aspartic acid and glutamic acid, may contribute to sourness, while alanine, glycine and serine more contribute to sweetness (Kader, 2008). In the present study, the contents of threonine, phenylalanine, tryptophan, leucine, isoleucine, methionine, tyrosine, valine, alanine, glycine, and arginine of fruit treated with 200 mg·L^{-1} ALA was significantly higher than that of the control, 40 days after fruit setting. Glutamic acid, as the highest content of amino acid in tomato fruit, has more contribution to fruit flavor quality (Cheng et al., 2019). In the present study, after exogenous 200 mg·L^{-1} ALA treatments, the content of glutamic acid was significantly higher than that of the control on the 36th day after fruit setting. This is because glutamic acid is the source of ALA synthesis (Czarnecki and Grimm, 2012), while the synthesis of endogenous ALA in fruit treated with 200 mg·L^{-1} ALA was inhibited on the 36th day after fruit setting. Eventually leading to the accumulation of glutamic acid. These results further indicate that exogenous ALA can improve the flavor quality of tomato fruit. In summary, exogenous ALA application to mature green stage tomato fruits could promote coloration and ripening and improve internal qualities.

CONCLUSION

Exogenous ALA, the optimal effect on 200 mg L^{-1}, had positive effects on tomato fruit coloration and improved carotenoid biosynthesis by upregulating the expression of genes related to lycopene synthesis and metabolism (including *GGPPS*, *PSY1*, *PDS*, and *LCY-B*). Moreover, the chlorophyll synthesis pathway was inhibited mainly by downregulating the related genes (*CHLH* and *POR*) simultaneously. In addition, the application of exogenous ALA increased the contents of soluble sugar, soluble protein, vitamin C, and total free amino acids as well as 11 kinds of amino acid components in tomato fruits and reduced the content of titratable acid, thus improving fruit quality. Our study showed that tomato fruits treated with exogenous ALA reached maturity 4 days earlier than the controls. In summary, the application of an appropriate concentration of ALA (200 mg·L^{-1}) during ripening enhances fruit nutritional qualities, coloration and promotes fruit maturation in tomato.

DATA AVAILABILITY STATEMENT

The original contributions presented in the study are included in the article/**Supplementary Material**, further inquiries can be directed to the corresponding authors.

AUTHOR CONTRIBUTIONS

YW and JY conceived and designed the research. JW, JZ, and JLi conducted the experiments. JW, JZ, and YW analyzed the data and prepared the figures and illustrations. JW wrote the manuscript. MD, BA, ZT, JLy, XX, LH, and JX read the manuscript and made valuable inputs. All authors read and approved the submission of the manuscript.

FUNDING

This work was financially supported by the Special Fund for Talent of Gansu Agricultural University (GAU-KYQD-2018-34), the National Key Research and Development Program of China (2018YFD0201205), the Agriculture Research System of China (CARS-23-C-07), and the Special Project of Central Government Guiding Local Science and Technology Development (ZCYD-2020-5).

SUPPLEMENTARY MATERIAL

The Supplementary Material for this article can be found online at: https://www.frontiersin.org/articles/10.3389/fpls.2021.683868/full#supplementary-material

REFERENCES

Ahmad, P., Hakeem, K. R., Kumar, A., Ashraf, M., and Akram, N. A. (2012). Salt-induced changes in photosynthetic activity and oxidative defense system of three cultivars of mustard (*Brassica juncea* L). *Afr. J. Biotechnol.* 11, 2694–2703. doi: 10.1007/s11356-017-8603-7

Akram, N. A., and Ashraf, M. (2013). Regulation in plant stress tolerance by a potential plant growth regulator, 5-aminolevulinic acid. *J. Plant Growth Regul.* 32, 663–679. doi: 10.1007/s00344-013-9325-9

Ali, B., Tao, Q. J., Zhou, Y. F., Mwamba, T. M., Rafiq, M. T., Xu, L., et al. (2013b). 5-Aminolevolinic acid mitigates the cadmium-induced changes in Brassica napus as revealed by the biochemical and ultra-structural evaluation of roots. *Ecotox. Environ. Safe.* 92, 271–280. doi: 10.1016/j.ecoenv.2013.02.006

Ali, B., Wang, B., Ghani, M. A., Hayat, M. T., Yang, C., Xu, L., et al. (2013a). 5-Aminolevulinic acid ameliorates the growth, photosynthetic gas exchange capacity and ultrastructural changes under cadmium stress in *Brassica napus* L. *J. Plant Growth Regul.* 32, 604–614. doi: 10.1007/s00344-013-9328-6

Ali, B., Yang, S., Farooq, M. A., Liu, D., Daud, M. K., and Zhou, W. J. (2015). Up-regulation of cadmium-induced proteomic and metabolic changes by 5-aminolevulinic acid in leaves of *Brassica napus* L. *PLoS One.* 10:e0123328. doi: 10.1371/journal.pone.0123328

Bingshan, L., Yasushi, H., Qu, Y. L., Zhao, J. S., and Tanaka, T. (1998). Effects of 5-aminolevulinic acid on the growth and ripening of wheat. *J. Pestic. Sci.* 23, 300–303. doi: 10.1584/jpestics.23.300

Borghesi, E., Ferrante, A., Gordillo, B., Rodríguez-Pulido, F. J., Cocetta, G., Trivellini, A., et al. (2016). Comparative physiology during ripening in tomato rich-anthocyanins fruits. *Plant Growth Regul.* 80, 207–214. doi: 10.1007/s10725-016-0158-y

Buyuklu, M., Kandemir, F. M., Ozkaraca, M., Set, T., Bakirci, E. M., Topal, E., et al. (2015). Benefical effects of lycopene against contrast medium-induced oxidative stress, inflammation, autophagy, and apoptosis in rat kidney. *Hum. Exp. Toxicol.* 34, 487–496. doi: 10.1177/0960327114542964

Chen, M. (2014). Chlorophyll modifications and their spectral extension in oxygenic photosynthesis. *Annu. Rev. Biochem.* 83, 317–340. doi: 10.1146/annurev-biochem-072711-162943

Cheng, Y., Wan, H. J., Yao, Z. P., Ye, Q. J., Wang, R. Q., Yang, Y. J., et al. (2019). Comparative analysis of the amino acid constitution and flavor quality in different cherry tomato varieties. *J. Nuclear Agric. Sci.* 33, 2177–2185. doi: 10.11869/j.issn.100-8551.2019.11.2177

Cunningham, F. X., Sun, Z., Chamovitz, D., Hirschberg, J., and Gantt, E. (1994). Molecular structure and enzymatic function of lycopene cyclase from the cyanobacterium synechococcus sp strain PCC7942. *Plant Cell.* 6, 1107–1121. doi: 10.1105/tpc.6.8.1107

Czarnecki, O., and Grimm, B. (2012). Post-translational control of tetrapyrrole biosynthesis in plants, algae, and cyanobacteria. *J. Exp. Bot.* 63, 1675–1687. doi: 10.1093/jxb/err437

D'Ambrosio, C., Stigliani, A. L., and Giorio, G. (2018). CRISPR/Cas9 editing of carotenoid genes in tomato. *Transgenic Res.* 27, 367–378. doi: 10.1007/s11248-018-0079-9

Dorais, M., Ehret, D. L., and Papadopoulos, A. P. (2008). Tomato (*Solanum lycopersicum*) health components: from the seed to the consumer. *Phytochem. Rev.* 7, 231–250. doi: 10.1007/s11101-007-9085-x

Drisko, J. A., Serrano, O. K., Spruce, L. R., Chen, Q., and Levine, M. (2018). Treatment of pancreatic cancer with intravenous vitamin C: a case report. *Anti Cancer Drug.* 29, 373–379. doi: 10.1097/CAD.0000000000000603

Fantini, E., Falcone, G., Frusciante, S., Giliberto, L., and Giuliano, G. (2013). Dissection of tomato lycopene biosynthesis through virus-induced gene silencing. *Plant Physiol.* 163, 986–998. doi: 10.1104/pp.113.224733

Feng, S., Li, M. F., Wu, F., Li, W. L., and Li, S. P. (2015). 5-Aminolevulinic acid affects fruit coloration, growth, and nutrition quality of Litchi chinensis Sonn. cv. *Feizixiao Hainan Trop. China. Sci. Hortic.* 193, 188–194. doi: 10.1016/j.scienta.2015.07.010

Feng, X., An, Y., Zheng, J., Sun, M., and Wang, L. (2016). Proteomics and SSH Analyses of ALA-promoted fruit coloration and evidence for the involvement of a MADS-box gene. MdMADS1. *Front. Plant Sci.* 7:1615. doi: 10.3389/fpls.2016.01615

Fraser, P. D., Romer, S., Shipton, C. A., Mills, P. B., Kiano, J. W., Misawa, N., et al. (2002). Evaluation of transgenic tomato plants expressing an additional phytoene synthase in a fruit-specific manner. *Proc. Natl. Acad. Sci. U.S.A.* 99, 1092–1097. doi: 10.1073/pnas.241374598

Fu, J., Sun, Y., Chu, X., Xu, Y., and Hu, T. (2014). Exogenous 5-aminolevulenic acid promotes seed germination in elymus nutans against oxidative damage induced by cold stress. *PLoS One.* 9:e107152. doi: 10.1371/journal.pone.0107152

Gill, R. A., Ali, B., Islam, F., Farooq, M. A., Gill, M. B., Mwamba, T. M., et al. (2015). Physiological and molecular analyses of black and yellow seeded *Brassica napus* regulated by 5-aminolivulinic acid under chromium stress. *Plant Physiol. Bioch.* 94, 130–143. doi: 10.1016/j.plaphy.2015.06.001

Goff, S. A., and Klee, H. J. (2006). Plant volatile compounds: sensory cues for health and nutritional value. *Science.* 311, 815–819. doi: 10.1126/science.1112614

Grandy, A. S., Erich, M. S., and Porter, G. A. (2000). Suitability of the anthrone-sulfuric acid reagent for determining water soluble carbohydrates in soil water extracts. *Soil Biol. Biochem.* 32, 725–727. doi: 10.1016/S0038-0717(99)00203-5

Gressler, V., Yokoya, N. S., Fujii, M. T., Colepicolo, P., Filho, J. M., Torres, R. P., et al. (2010). Lipid, fatty acid, protein, amino acid and ash contents in four Brazilian red algae species. *Food Chem.* 120, 585–590. doi: 10.1016/j.foodchem.2009.10.028

Hadi, M. A. M. E., Zhang, F. J., Wu, F. F., Zhou, C. H., and Tao, J. (2013). Advances in fruit aroma volatile research. *Molecules.* 18, 8200–8229. doi: 10.3390/molecules18078200

Hecke, K., Herbinger, K., Veberic, R., Trobec, M., Toplak, H., Stampar, F., et al. (2006). Sugar, acid and phenol contents in apple cultivars from organic and integrated fruit cultivation. *Eur. J. Clin. Nutr.* 60, 1136–1140. doi: 10.1038/sj.ejcn.1602430

Hedtke, B., Alawady, A., Chen, S., Bornke, F., and Grimm, B. (2007). HEMA RNAi silencing reveals a control mechanism of ALA biosynthesis on Mg chelatase and Fe chelatase. *Plant Mol. Biol.* 64, 733–742. doi: 10.1007/s11103-007-9194-3

Hiratsuka, S., Suzuki, M., Nishimura, H., and Nada, K. (2015). Fruit photosynthesis in Satsuma mandarin. *Plant Sci.* 241, 65–69. doi: 10.1016/j.plantsci.2015.09.026

Hirschberg, J. (2001). Carotenoid biosynthesis in flowering plants. *Curr. Opin. Plant Biol.* 4, 210–218. doi: 10.1016/S1369-5266(00)00163-1

Hotta, Y., Tanaka, T., Takaoka, H., Takeuchi, Y., and Konnai, M. (1997). Promotive effects of 5-aminolevulinic acid on the yield of several crops. *Plant Growth Regul.* 22, 109–114. doi: 10.1023/A:1005883930727

Ip, B. C., Hu, K. Q., Liu, C., Smith, D. E., Obin, M. S., Ausman, L. M., et al. (2013). Lycopene metabolite, apo-10'-lycopenoic acid, inhibits diethylnitrosamine-initiated, high fat diet-promoted hepatic inflammation and tumorigenesis in mice. *Cancer Prev. Res.* 6, 1304–1316. doi: 10.1158/1940-6207.CAPR-13-0178

Isaacson, T., Ronen, G., Zamir, D., and Hirschberg, J. (2002). Cloning of tangerine from tomato reveals a carotenoid isomerase essential for the production of β-carotene and xanthophylls in plants. *Plant Cell.* 14, 333–342. doi: 10.1105/tpc.010303

Ito, Y., Nishizawa-Yokoi, A., Endo, M., Mikami, M., Shima, Y., Nakamura, N., et al. (2017). Re-evaluation of the rin mutation and the role of RIN in the induction of tomato ripening. *Nat. Plants.* 3, 866–874. doi: 10.1038/s41477-017-0041-5

Jarquín-Enríquez, L., Mercado-Silva, E. M., Maldonado, J. L., and Lopez-Baltazar, J. (2013). Lycopene content and color index of tomatoes are affected by the greenhouse cover. *Sci. Hortic.* 155, 43–48. doi: 10.1016/j.scienta.2013.03.004

Kader, A. A. (2008). Flavor quality of fruits and vegetables. *J. Sci. Food Agric.* 88, 1863–1868. doi: 10.1002/jsfa.3293

Kafkas, E., Kosar, M., Paydas, S., Kafkas, S., and Baser, K. H. C. (2007). Quality characteristics of strawberry genotypes at different maturation stages. *Food Chem.* 100, 1229–1236. doi: 10.1016/j.foodchem.2005.12.005

Kang, B., Gu, Q., Tian, P., Xiao, L., Cao, H., and Yang, W. (2014). A chimeric transcript containing Psy1 and a potential mRNA is associated with yellow flesh color in tomato accession PI 114490. *Planta* 240, 1011–1021. doi: 10.1007/s00425-014-2052-z

Kang, B., Zhao, W. E., Hou, Y., and Tian, P. (2010). Expression of carotenogenic genes during the development and ripening of watermelon fruit. *Sci. Hortic.* 124, 368–375. doi: 10.1016/j.scienta.2010.01.027

Klee, H. J., and Giovannoni, J. J. (2011). Genetics and control of tomato fruit ripening and quality attributes. *Annu. Rev. Genet.* 45, 41–59. doi: 10.1146/annurev-genet-110410-132507

Korkmaz, A., and Korkmaz, Y. (2009). Promotion by 5-aminolevulenic acid of pepper seed germination and seedling emergence under low-temperature stress. *Sci. Hortic.* 119, 98–102. doi: 10.1016/j.scienta.2008.07.016

Kyriacou, M. C., Polking, G. F., Hannapel, D. J., and Gladon, R. J. (1996). Activity of 5-Aminolevulinic acid dehydratase declines during tomato fruit development and ripening. *J. Am. Soc. Hortic. Sci.* 121, 91–95. doi: 10.21273/JASHS.121.1.91

La Rocca, N., Rascio, N., Oster, U., and Rudiger, W. (2007). Inhibition of lycopene cyclase results in accumulation of chlorophyll precursors. *Planta* 225, 1019–1029. doi: 10.2307/23389588

Lee, K. H., Koh, R. H., and Song, H. G. (2008). Enhancement of growth and yield of tomato by Rhodopseudomonas sp. under greenhouse conditions. *J. Microbiol.* 46, 641–646. doi: 10.1007/s12275-008-0159-2

Li, D. M., Zhang, J., Sun, W. J., Li, Q., Dai, A. H., and Bai, J. G. (2011). 5-Aminolevulinic acid pretreatment mitigates drought stress of cucumber leaves through altering antioxidant enzyme activity. *Sci. Hortic.* 130, 820–828. doi: 10.1016/j.scienta.2011.09.010

Li, L., Liu, Z., Jiang, H., and Mao, X. (2020). Biotechnological production of lycopene by microorganisms. *Appl. Microbiol Biot.* 104, 10307–10324. doi: 10.1007/s00253-020-10967-4

Lichtenthaler, H. K., and Wellburn, A. R. (1983). Determination of total carotenoids and chlorophylls A and B of leaf in different solvents. *Biochem. Soc. T.* 11, 591–592. doi: 10.1042/bst0110591

Liu, D., Wu, L., Naeem, M. S., and Liu, H. (2013). 5-Aminolevulinic acid enhances photosynthetic gas exchange, chlorophyll fluorescence and antioxidant system in oilseed rape under drought stress. *Acta Physiol. Plant.* 35, 2747–2759. doi: 10.1007/s11738-013-1307-9

Liu, J., Wang, J., Yao, X., Zhang, Y., Li, J., and Wang, X. (2015). Characterization and fine mapping of thermo-sensitive chlorophyll deficit mutant1 in rice (*Oryza sativa* L.). *Breeding Sci.* 65, 161–169. doi: 10.1270/jsbbs.65.161

Livak, K. J., and Schmittgen, T. D. L. (2001). Analysis of relative gene expression data using real-time quantitative PCR and the 2-ΔΔCT method. *Methods* 25, 402–408. doi: 10.1006/meth.2001.1262

Mohamad, I. B., and Usman, D. (2013). Standardization and its effects on K-means clustering algorithm. *Res. J. App. Sci. Eng. Technol.* 6, 3299–3303. doi: 10.19026/rjaset.6.3638

Mohamed, H. E., and Abu-Goukh, A. B. A. (2003). Effect of ethrel in aqueous solution and ethylene released from ethrel on mango fruit ripening. *J. Hortic. Sci. Biotech.* 78, 568–573. doi: 10.1080/14620316.2003.11511665

Mou, W., Li, D., Bu, J., Jiang, Y., Khan, Z. U., Luo, Z., et al. (2016). Comprehensive analysis of ABA effects on ethylene biosynthesis and signaling during tomato fruit ripening. *PLoS One.* 11:e0154072. doi: 10.1371/journal.pone.0154072

Naeem, M. S., Rasheed, M., Liu, D., Jin, Z. L., Ming, D. F., Yoneyama, K., et al. (2010). 5-Aminolevulinic acid ameliorates salinity-induced metabolic, water-related and biochemical changes in Brassica napus L. *Acta Physiol. Plant.* 33, 517–528. doi: 10.1007/s11738-010-0575-x

Naeem, M. S., Warusawitharana, H., Liu, H., Liu, D., Ahmad, R., Waraich, E. A., et al. (2012). 5-Aminolevulinic acid alleviates the salinity-induced changes in Brassica napus as revealed by the ultrastructural study of chloroplast. *Plant Physiol. Bioch.* 57, 84–92. doi: 10.1016/j.plaphy.2012.05.018

Nguyen, H., Kim, H. S., and Jung, S. (2015). Altered tetrapyrrole metabolism and transcriptome during growth-promoting actions in rice plants treated with 5-aminolevulinic acid. *Plant Growth Regul.* 78, 133–144. doi: 10.1007/s10725-015-0080-8

Nickelsen, J., Rengstl, B., Stengel, A., Schottkowski, M., Soll, J., and Ankele, E. (2011). Biogenesis of the cyanobacterial thylakoid membrane system-an update. *FEMS Microbiol. Lett.* 315, 1–5. doi: 10.1111/j.1574-6968.2010.02096.x

Nimbalkar, M. S., Pai, S. R., Pawar, N. V., Oulkar, D., and Dixit, G. B. (2012). Free amino acid profiling in grain amaranth using LC–MS/MS. *Food Chem.* 134, 2565–2569. doi: 10.1016/j.foodchem.2012.04.057

Nour, V., Trandafir, I., and Ionica, M. E. (2010). Compositional characteristics of fruits of several apple (*Malus domestica* Borkh.) cultivars. *Not. Bot. Horti. Agrobo.* 38, 228–233. doi: 10.1111/J.1364-3703.2010.00617.X

Okada, K., Saito, T., Nakagawa, T., Kawamukai, M., and Kamiya, Y. (2000). Five geranylgeranyl diphosphate synthases expressed in different organs are localized into three subcellular compartments in arabidopsis. *Plant Physiol.* 122, 1045–1056. doi: 10.1104/pp.122.4.1045

Palumbo, G., Carfagna, S., Stoleru, V., Torino, V., Romano, P. M., Letizia, F., et al. (2020). Environmental sustainability fruit quality and production in mycorrhizal tomato plants without P fertilizing. *Agron. Res.* 18, 2535–2549. doi: 10.15159/AR.20.204

Perveen, R., Suleria, H. A. R., Anjum, F. M., Butt, M. S., Pasha, I., and Ahmad, S. (2015). Tomato (*Solanum lycopersicum*) carotenoids and lycopenes chemistry;

metabolism, absorption, nutrition, and allied health claims - a comprehensive review. *Crit. Rev. Food Sci.* 55, 919–929. doi: 10.1080/10408398.2012.657809

Polking, G. F., Hannapel, D. J., and Gladon, R. J. (1999). Regulation of glutamate-l-semialdehyde aminotransferase expression during tomato (*Lycopersicon esculentum* Mill.) fruit development. *J. Plant Physiol.* 155, 41–47. doi: 10.1016/S0176-1617(99)80138-2

Porra, R. J., Thompson, W. A., and Kriedemann, P. E. (1989). Determination of accurate extinction coefficients and simultaneous equations for assaying chlorophylls a and b extracted with four different solvents: verification of the concentration of chlorophyll standards by atomic absorption spectroscopy. *BBA-Bioenergetics.* 975, 384–394. doi: 10.1016/S0005-2728(89)80347-0

Ralley, L., Schuch, W., Fraser, P. D., and Bramley, P. M. (2016). Genetic modification of tomato with the tobacco lycopene beta-cyclase gene produces high beta-carotene and lycopene fruit. *Z. Naturforsch. C.* 71, 295–301. doi: 10.1515/znc-2016-0102

Richter, A. S., and Grimm, B. (2013). Thiol-based redox control of enzymes involved in the tetrapyrrole biosynthesis pathway in plants. *Front. Plant Sci.* 4:371. doi: 10.3389/fpls.2013.00371

Richter, A., Peter, E., Pors, Y., Lorenzen, S., Grimm, B., and Czarnecki, O. (2010). Rapid dark repression of 5-aminolevulinic acid synthesis in green barley leaves. *Plant Cell Physiol.* 51, 670–681. doi: 10.1093/pcp/pcq047

Rodríguez-Villalón, A., Gas, E., and Rodríguez-Concepción, M. (2010). Phytoene synthase activity controls the biosynthesis of carotenoids and the supply of their metabolic precursors in dark-grown arabidopsis seedlings. *Plant J.* 60, 424–435. doi: 10.1111/j.1365-313X.2009.03966.x

Ronen, G., Cohen, M., Zamir, D., and Hirschberg, J. (1999). Regulation of carotenoid biosynthesis during tomato fruit development expression of the gene for lycopene epsilon-cyclase is down-regulated during ripening and is elevated in the mutant Delta. *Plant J.* 17, 341–351. doi: 10.1046/j.1365-313X.1999.00381.x

Rupasinghe, H. P. V. (1995). *Glutamic Acid and 5-Aminolevulinic Acid May Function as Precursors of System II Ethylene in Ripening Tomato Fruits. Ph. D, Thesis*. Iowa: Iowa State University, doi: 10.31274/rtd-180813-8186

Sagar, M., Chervin, C., Mila, I., Hao, Y., Roustan, J. P., Benichou, M., et al. (2013). SlARF4, an auxin response factor involved in the control of sugar metabolism during tomato fruit development. *Plant Physiol.* 161, 1362–1374. doi: 10.1104/pp.113.213843

Saltveit, M. E. (1999). Effect of ethylene on quality of fresh fruits and vegetables. *Postharvest Biol. Tec.* 15, 279–292. doi: 10.1016/S0925-5214(98)00091-X

Salvioli, A., Zouari, I., Chalot, M., and Bonfante, P. (2012). The arbuscular mycorrhizal status has an impact on the transcriptome profile and amino acid composition of tomato fruit. *BMC Plant Bio.* 12:44. doi: 10.1186/1471-2229-12-44

Sedmak, J. J., and Grossberg, S. E. (1977). A rapid, sensitive, and versatile assay for protein using coomassie brilliant blue G250. *Anal. Biochem.* 79, 544–552. doi: 10.1016/0003-2697(77)90428-6

Senge, M., Ryan, A., Letchford, K., Macgowan, S., and Mielke, T. (2014). Chlorophylls, symmetry, chirality, and photosynthesis. *Symmetry* 6, 781–843. doi: 10.3390/sym6030781

Sobotka, R. (2014). Making proteins green; biosynthesis of chlorophyll-binding proteins in cyanobacteria. *Photosynth. Res.* 119, 223–232. doi: 10.1007/s11120-013-9797-2

Sorrequieta, A., Ferraro, G., Boggio, S. B., and Valle, E. M. (2010). Free amino acid production during tomato ripening: a focus on L-glutamate. *Amino Acids.* 38, 1523–1532. doi: 10.1007/s00726-009-0373-1

Stuart, M., Tzfadia, O., Vallabhaneni, R., Gehring, C., and Wurtzel, E. T. (2011). A transcriptional analysis of carotenoid, chlorophyll and plastidial isoprenoid biosynthesis genes during development and osmotic stress responses in Arabidopsis thaliana. *BMC Syst. Biol.* 5:77. doi: 10.1186/1752-0509-5-77

Wang, M., Zheng, Y., Khuong, T., and Lovatt, C. J. (2012). Effect of harvest date on the nutritional quality and antioxidant capacity in 'Hass' avocado during storage. *Food Chem.* 135, 694–698. doi: 10.1016/j.foodchem.2012.05.022

Wang, T., Rao, J. P., Song, Y. L., Zhang, H. Y., and Zou, Z. R. (2008). Effects of 5-aminolevulinic acid on the quality and post harvest physiology of tomato fruit. *J. North. Univer. (Nat. Sci. Ed.)* 36, 127–131. doi: 10.13207/j.cnki.jnwafu.2008.10.018

Wang, Y., Wang, Y., Ji, K., Dai, S., Hu, Y., Sun, L., et al. (2013). The role of abscisic acid in regulating cucumber fruit development and ripening and its transcriptional regulation. *Plant Physiol. Bioch.* 64, 70–79. doi: 10.1016/j.plaphy.2012.12.015

Watanabe, K., Nishihara, E., Watanabe, S., Tanaka, T., Takahashi, K., and Takeuchi, Y. (2006). Enhancement of growth and fruit maturity in 2-year-old grapevines cv. Delaware by 5-Aminolevulinic acid. *Plant Growth Regul.* 49, 35–42. doi: 10.1007/s10725-006-0024-4

Wu, Y., Jin, X., Liao, W., Hu, L., Dawuda, M. M., Zhao, X., et al. (2018). 5-Aminolevulinic acid (ALA) alleviated salinity stress in cucumber seedlings by enhancing chlorophyll synthesis pathway. *Front. Plant Sci.* 9:635. doi: 10.3389/fpls.2018.00635

Xie, B. X., Wei, J. J., Zhang, Y. T., Song, S. W., Su, W., Sun, G. W., et al. (2019). Supplemental blue and red light promote lycopene synthesis in tomato fruits. *J. Integr. Agr.* 18, 590–598. doi: 10.1016/S2095-3119(18)62062-3

Xie, J., Yu, J., Chen, B., Feng, Z., Li, J., Zhao, C., et al. (2017). Facility cultivation systems "设施农业": a Chinese model for the planet. *Adv. Agron.* 145, 1–42. doi: 10.1016/bs.agron.2017.05.005

Xie, L., Wang, Z. H., Cheng, X. H., Gao, J. J., Zhang, Z. P., and Wang, L. J. (2013). 5-Aminolevulinic acid promotes anthocyanin accumulation in Fuji apples. *Plant Growth Regul.* 69, 295–303. doi: 10.1007/s10725-012-9772-5

Xiong, J. L., Wang, H. C., Tan, X. Y., Zhang, C. L., and Naeem, M. (2018). 5-aminolevulinic acid improves salt tolerance mediated by regulation of tetrapyrrole and proline metabolism in *Brassica napus* L. seedlings under NaCl stress. *Plant Physiol. Bioch.* 124, 88–99. doi: 10.1016/j.plaphy.2018.01.001

Xu, F., Wang, W., and Yu, D. (2012). Effect of 5-aminolevulinic acid on yield and quality of lettuce in sunlit greenhouse. *Afr. J. Biotechnol.* 11, 11591–11594. doi: 10.5897/AJB12.792

Xu, L., Zhang, W., Ali, B., Islam, F., Zhu, J., and Zhou, W. (2015). Synergism of herbicide toxicity by 5-aminolevulinic acid is related to physiological and ultra-structural disorders in crickweed (*Malachium aquaticum* L.). *Pestic. Biochem. Phys.* 125, 53–61. doi: 10.1016/j.pestbp.2015.06.002

Ye, J., Yang, X., Chen, Q., Xu, F., and Wang, G. (2017). Promotive effects of 5-aminolevulinic acid on fruit quality and coloration of *Prunus persica* (L.) Batsch. *Sci. Hortic.* 217, 266–275. doi: 10.1016/j.scienta.2017.02.009

Ye, M., Wu, Q., Zhang, M., and Huang, J. (2016). Lycopene inhibits the cell proliferation and invasion of human head and neck squamous cell carcinoma. *Mol. Med. Rep.* 14, 2953–2958. doi: 10.3892/mmr.2016.5597

Yokotani, N., Tamura, S., Nakano, R., Inaba, A., McGlasson, W. B., and Kubo, Y. (2004). Comparison of ethylene- and wound-induced responses in fruit of wild-type, rin and nor tomatoes. *Postharvest Biol. Tec.* 32, 247–252. doi: 10.1016/j.postharvbio.2004.01.001

Yu, Y., Weng, Q., and Zhou, B. (2016). Effects of exogenous ABA on contents of lycopene and endogenous hormone in tomato pericarp. *British Biotechnol. J.* 16, 1–5. doi: 10.9734/BBJ/2016/28767

Zheng, J., An, Y. Y., Feng, X. X., and Wang, L. J. (2017). Rhizospheric application with 5-aminolevulinic acid improves coloration and quality in 'Fuji' apples. *Sci. Hortic.* 224, 74–83. doi: 10.1016/j.scienta.2017.06.004

Zheng, J., An, Y., and Wang, L. (2018). 24-Epibrassinolide enhances 5-ALA-induced anthocyanin and flavonol accumulation in calli of 'Fuji' apple flesh. *Plant Cell Tiss. Org.* 134, 319–330. doi: 10.1007/s11240-018-1418-5

Zhu, T., Tan, W. R., Deng, X. G., Zheng, T., Zhang, D. W., and Lin, H. H. (2015). Effects of brassinosteroids on quality attributes and ethylene synthesis in postharvest tomato fruit. *Postharvest Biol. Tec.* 100, 196–204. doi: 10.1016/j.postharvbio.2014.09.016

Zhu, Z., Zhang, Y., Liu, J., Chen, Y., and Zhang, X. (2018). Exploring the effects of selenium treatment on the nutritional quality of tomato fruit. *Food Chem.* 252, 9–15. doi: 10.1016/j.foodchem.2018.01.064

Conflict of Interest: The authors declare that the research was conducted in the absence of any commercial or financial relationships that could be construed as a potential conflict of interest.

Copyright © 2021 Wang, Zhang, Li, Dawuda, Ali, Wu, Yu, Tang, Lyu, Xiao, Hu and Xie. This is an open-access article distributed under the terms of the Creative Commons Attribution License (CC BY). The use, distribution or reproduction in other forums is permitted, provided the original author(s) and the copyright owner(s) are credited and that the original publication in this journal is cited, in accordance with accepted academic practice. No use, distribution or reproduction is permitted which does not comply with these terms.

frontiers in Plant Science

ORIGINAL RESEARCH
published: 15 June 2021
doi: 10.3389/fpls.2021.702303

Genome-Wide Investigation of N6-Methyladenosine Regulatory Genes and Their Roles in Tea (*Camellia sinensis*) Leaves During Withering Process

Chen Zhu[1,2,3,4], Shuting Zhang[1,2], Chengzhe Zhou[1,2,3,4], Siyi Xie[1,3,4], Guangwu Chen[1,3,4], Caiyun Tian[1,3,4], Kai Xu[1,3,4], Yuling Lin[1,2], Zhongxiong Lai[1,2] and Yuqiong Guo[1,3,4]**

[1]College of Horticulture, Fujian Agriculture and Forestry University, Fuzhou, China, [2]Institute of Horticultural Biotechnology, Fujian Agriculture and Forestry University, Fuzhou, China, [3]Key Laboratory of Tea Science in Universities of Fujian Province, Fujian Agriculture and Forestry University, Fuzhou, China, [4]Tea Industry Research Institute, Fujian Agriculture and Forestry University, Fuzhou, China

OPEN ACCESS

Edited by:
Xinchao Wang,
Tea Research Institute,
Chinese Academy of Agricultural Sciences (CAAS), China

Reviewed by:
Lanting Zeng,
South China Botanical Garden,
Chinese Academy of Sciences (CAS), China
Hunseung Kang,
Chonnam National University,
South Korea

***Correspondence:**
Zhongxiong Lai
laizx01@163.com
Yuqiong Guo
guoyq828@163.com

Specialty section:
This article was submitted to Crop and Product Physiology, a section of the journal Frontiers in Plant Science

Received: 29 April 2021
Accepted: 24 May 2021
Published: 15 June 2021

Citation:
Zhu C, Zhang S, Zhou C, Xie S, Chen G, Tian C, Xu K, Lin Y, Lai Z and Guo Y (2021) Genome-Wide Investigation of N6-Methyladenosine Regulatory Genes and Their Roles in Tea (Camellia sinensis) Leaves During Withering Process. Front. Plant Sci. 12:702303. doi: 10.3389/fpls.2021.702303

N6-methyladenosine (m6A), one of the internal modifications of RNA molecules, can directly influence RNA abundance and function without altering the nucleotide sequence, and plays a pivotal role in response to diverse environmental stresses. The precise m6A regulatory mechanism comprises three types of components, namely, m6A writers, erasers, and readers. To date, the research focusing on m6A regulatory genes in plant kingdom is still in its infancy. Here, a total of 34 m6A regulatory genes were identified from the chromosome-scale genome of tea plants. The expansion of m6A regulatory genes was driven mainly by whole-genome duplication (WGD) and segmental duplication, and the duplicated gene pairs evolved through purifying selection. Gene structure analysis revealed that the sequence variation contributed to the functional diversification of m6A regulatory genes. Expression pattern analysis showed that most m6A regulatory genes were differentially expressed under environmental stresses and tea-withering stage. These observations indicated that m6A regulatory genes play essential roles in response to environmental stresses and tea-withering stage. We also found that RNA methylation and DNA methylation formed a negative feedback by interacting with each other's methylation regulatory genes. This study provided a foundation for understanding the m6A-mediated regulatory mechanism in tea plants under environmental stresses and tea-withering stage.

Keywords: RNA methylation, *Camellia sinensis*, abiotic stress, withering process, flavonoid

INTRODUCTION

Methylation, one of the representative epigenetic modifications, can directly influence gene expression and function without altering the gene sequence. At the molecular level, DNA methylation is a pervasive modification that plays a broad role in myriad biological processes. Recently, extensive studies have shown that methylation occurs not only on DNAs but also

on RNAs (Fu et al., 2014; Yang et al., 2018). RNA methylation is one of the internal modifications of RNA molecules. Among diverse methylation types found on RNAs, N6-methyladenosine (m6A) is the best-characterized and most predominant form of eukaryotic RNA methylation, accounting for up to 80% of RNA methylation in animals and plants. Similar to DNA methylation, recent studies have shown that m6A modification within multiple types of RNAs is a dynamic and reversible process. The m6A abundance depends on two pivotal proteins, namely, methyltransferases (MTs; m6A writers) and demethylases (m6A erasers). Writers and erasers are involved in adding or removing methyl groups to the conserved sequence. In addition to these two pivotal proteins, the third proteins (m6A readers) recognize specifically m6A marks and ultimately perform the specific biological functions of m6A-modified RNAs. In general, writers, erasers, and readers form a sophisticated regulatory system that guides the formation, removal, and decoding of m6A modifications.

Although many efforts have been made to investigate the m6A modification in animals, the research focusing on m6A regulatory genes in the plant kingdom is still in its infancy. Recently, major components of m6A writer complexes have been systemically identified and investigated in *Arabidopsis* (Yue et al., 2019). The addition of m6A modification is not controlled by a single RNA MT, but by a protein complex formed by a series of m6A writer components (Śledź et al., 2016). As the first m6A writer component discovered in plants, the MT family can be sorted into three subfamilies, namely, methyltransferase A (MTA), methyltransferase B (MTB), and methyltransferase C (MTC). MTA contained a catalytic core domain (MT-A70) that exerted RNA modification activity. Subsequently, the other MT member, MTB, was identified and considered to be the second most-active enzyme in regulating m6A level. In addition, previous research has shown that MTB not only has a supporting role in interacting with MTA to form a stable MTA–MTB heterodimer but also plays a crucial role in binding m6A writer complexes to RNA substrates (Wang et al., 2016a; Knuckles et al., 2018). As a newly discovered subfamily of MT family, there are few studies on MTC and its specific role in m6A modification (Liang et al., 2020). More research is needed to determine the role of MTC in m6A writing. It has not been proposed whether MTC is also involved in the formation and maintenance of MTA–MTB heterodimer. Except for the aforementioned MT family, the composition of m6A writer complex also required a series of other important components, including FKBP interacting protein 37 (FIP37), virilizer (VIR), and E3 ubiquitin ligase HAKAI. Among them, FIP37 was considered as an ortholog of Wilms' tumor 1-associating protein (WTAP). Inhibition of FIP37 expression was found to significantly reduce the overall m6A level (Shen et al., 2016). It has shown that FIP37 also plays an indispensable role in sculpting m6A modification. The third core component of the m6A writer complex, VIR, is known for guiding the MTA–MTB heterodimer to the target region of specific RNAs. Similar to the function of FIP37, downregulation of HAKAI expression can cause a significant decrease in relative m6A levels (Růžička et al., 2017). Additionally, it has been found that HAKAI can interact with other m6A writer complex members and was required for RNA methylation.

The level of RNA methylation in plants is not only regulated by m6A writers, but also by m6A erasers. Previous studies have confirmed that m6A marks are removed by α-ketoglutarate-dependent dioxygenase homolog (ALKBH) that can wipe methyl groups off m6A-modified RNAs and restore the m6A to unmethylated adenosine (Scarrow et al., 2020). In contrast to RNA methylation that is catalyzed by an m6A write complex, m6A demethylation process required only a single m6A demethylase family. ALKBH, which contained a conserved clavaminate synthase-like domain, has catalytic activity and can effectively reverse m6A marks. The high abundance of ALKBH in *Arabidopsis thaliana* and *Solanum lycopersicum* was correlated with the decrease in the relative m6A level (Martínez-Pérez et al., 2017; Zhou et al., 2019a). However, the functional roles of m6A eraser in species outside of the *Arabidopsis* and tomato need to be further discovered. Besides, decoding of m6A marks was tightly bound up with the implementation of m6A biological function, which required m6A reader to recognize m6A-modified sites and perform varying functions during mRNA processing. Two classes of m6A readers have been reported, namely, evolutionarily conserved C-terminal region (ECT) and cleavage and polyadenylation specificity factor 30 (CPSF30; Addepalli and Hunt, 2007; Arribas-Hernández et al., 2018). ECT containing the conserved YTH domain can specifically recognize m6A marks through a canonical aromatic cage. Moreover, the absence of ECT results in the loss of m6A binding affinity, which is similar to the phenomenon caused by the knockdown of *MTA* expression (Scutenaire et al., 2018). As another m6A reader, CPSF30, contained a highly conserved C3H1-type zinc finger domain at N-terminal region, which was mainly responsible for scavenging deleterious mRNA transcripts through m6A-assisted polyadenylation processing (Pontier et al., 2019).

To date, existing reports clearly demonstrate that RNA methylation plays a prominent role in response to diverse environmental stresses, including drought (Scutenaire et al., 2018; Miao et al., 2020), cold (Hu et al., 2019), and UV radiation stresses (Dominissini et al., 2012). Under external stress, the increase of m6A marks in the 5' untranslated region (UTR) promoted the translation of drought-resistant mRNA (Meyer et al., 2015). Meanwhile, m6A RNA methylation can also alleviate the damage of abiotic stress *via* modulating mRNA abundance, splicing, stability, and decay (Zhou et al., 2015, 2018; Duan et al., 2017; Kramer et al., 2020). Additionally, recent studies have shown that the dynamic redistribution of m6A levels under stress leads to m6A marks mainly enriched in genes related to primary and secondary metabolisms (Liu et al., 2020). At present, the major knowledge on the biological function and regulatory mechanism of m6A has been limited to a handful of model plant taxa. There is still a significant gap surrounding m6A-mediated regulatory mechanism in crop plants, especially horticultural plants.

Tea plant (*Camellia sinensis*), which originated in southwest China, is one of the most economically important crop plants around the world. During the lifespan of tea plants, tea yield and

quality are tightly linked to the environmental condition. With the more frequent occurrence of extreme climate, sustainable development of the global tea industry is also continuously threatened by a multitude of external stresses, particularly extreme cold and drought. Increasing studies have focused on molecular mechanisms of tea plants underlying the stress response (Wang et al., 2016b; Guo et al., 2017; Shen et al., 2019a; Zhang et al., 2020a). An array of stress-induced genes and core transcription factors have been identified in tea plants, and they play vital roles in coping with multiple stresses (Zhu et al., 2018a; Shen et al., 2019b; Zhou et al., 2019b; Li et al., 2020a; Wang et al., 2020). Additionally, oolong tea, one of the Chinese premium tea processes, is well-known for its mellow taste and elegant floral-fruity fragrance. The unique flavor of oolong tea is closely linked to its manufacturing process. Reportedly, withering is the first indispensable step to improve the quality of oolong tea during postharvest manufacturing process (Hu et al., 2018; Wang et al., 2019). Similar to preharvest tea leaves, postharvest leaves were also exposed to various environmental stresses during tea-withering stage. Moreover, it is reported that plants respond to environmental stress through DNA methylation and histone methylation modifications. More recently, DNA methylation and histone methylation-related regulatory genes have been investigated and found to play pivotal functions in stress response (Zhu et al., 2020; Chen et al., 2021). However, the roles of RNA methylation and related regulatory genes in tea plants against various stresses during preharvest and postharvest processing are still far from clear to date. The chromosome-scale genome of tea plants provides an opportunity to accurately investigate m6A regulatory genes and systemically dissect the potential functions of RNA methylation in tea plants during preharvest and postharvest processing. Here, we initially identified and classified the m6A regulatory genes from tea plants and analyzed their evolutionary relationships, chromosomal distribution, and gene structure at the whole genome scale. Then, we examined the expression profiles of m6A regulatory genes under abiotic stresses and withering process. Finally, the relationship between m6A regulatory genes and m6A level as well as the roles of RNA methylation during preharvest and postharvest processes was explored through functional assessment. Our findings lay a foundation for exploring the diverse functions of m6A regulatory genes in tea plants under environmental stresses and highlight the underlying effects of m6A modifications on the precise regulation of tea quality during the withering stage of postharvest processing.

MATERIALS AND METHODS

Identification and Characterization of m6A Regulatory Genes in Tea Plants

To identify all members of the m6A regulatory genes, the known sequences of m6A regulatory genes in *A. thaliana* and *S. lycopersicum* were obtained from The Arabidopsis Information Resource (TAIR; Berardini et al., 2015) and Sol Genomics Network (SGN) database (Bombarely et al., 2010), respectively. These sequences were queried against the chromosome-level genome of tea plant (Xia et al., 2020) using BLAST algorithm with the parameter E-value < $1.0E^{-5}$. Then, the hidden Markov model (HMM) profiles of the MT-A70 family (PF05063), WTAP family (PF17098) and virilizer domain (PF15912), 2OG-Fe(II) oxygenase superfamily (PF13532), and YTH domain were used to evaluate the deduced protein sequences of m6A regulatory genes in *C. sinensis*. The obtained sequences were further confirmed using Simple Modular Architecture Research Tool (SMART; Letunic and Bork, 2017) and Conserved Domain Database (CDD; Lu et al., 2019). The physicochemical parameters of the relevant proteins were examined using the ExPASy tool (Artimo et al., 2012). The Plant-mPLoc program (Chou and Shen, 2010) was used to analyze the potential subcellular localization of these proteins. The percent identity matrix of m6A regulatory genes was calculated using the Clustal Omega program (Li et al., 2015). The conserved domains in m6A regulatory proteins were detected using the PfamScan tool (Madeira et al., 2019).

The Phylogenetic Classifications, Chromosomal Distributions, and Gene Structures of m6A Regulatory Genes in Tea Plants

The phylogenetic trees were generated using the neighbor-joining (NJ) algorithm with 1,000 bootstrap replicates in MEGA X software (Kumar et al., 2018) and then were visualized using the Evolview v3 server (Subramanian et al., 2019). The detailed protein sequences from the dicotyledonous species (*C. sinensis*, *A. thaliana*, *S. lycopersicum*, *Vitis vinifera*, and *Gossypium hirsutum*), monocotyledonous species (*Zea mays*, *Triticum aestivum*, and *Oryza sativa*), pteridophyte species (*Selaginella moellendorffii*), and moss species (*Marchantia polymorpha* and *Physcomitrella patens*) were listed in **Supplementary Table S1**.

On the basis of the genome annotation files at the Tea Plant Information Archive (TPIA) database (Xia et al., 2019), the chromosomal distributions and gene structures of m6A regulatory genes were visualized using the TBtools software (Chen et al., 2020a). The MEME suite (Bailey et al., 2009) was employed to investigate the conserved motifs in m6A regulatory proteins.

The Protein–Protein Interactions, Evolutionary Selections, Gene Duplication Events, and Collinearity Analysis of m6A Regulatory Genes in Tea Plants

The protein–protein interaction networks of m6A regulatory proteins were constructed using the STRING v11.0 database (Szklarczyk et al., 2018). The gene duplication events were investigated using MCScanX software (Wang et al., 2012) with the default parameters. The TBtools software was used for the collinearity analysis of m6A regulatory genes. To reckon the evolutionary selections of m6A regulatory genes, the TBtools software was used to calculate the nonsynonymous substitution rate (Ka), synonymous substitution rate (Ks), and Ka/Ks ratio of each duplicated gene pair. The divergence time

(T) of duplicated gene pairs was calculated according to the formula $T = Ks/(2 \times 6.5 \times 10^{-9}) \times 10^{-6}$ million years ago (Mya; Wei et al., 2018).

Analysis of *cis*-Acting Elements in the Promoter Regions of m6A Regulatory Genes in Tea Plants

The promoter sequences of the m6A regulatory genes, which were 2,000 bp upstream from the translation start site, were collected from the TPIA database. The obtained sequences were then submitted to the PlantCARE database for *cis*-acting element analysis (Lescot et al., 2002).

Expression Profiles of m6A Regulatory Genes in Tea Plants Based on Transcriptome Data

Public transcriptome data, including eight representative tissues (apical buds, young leaves, mature leaves, old leaves, stems, roots, flowers, and fruits) and different withering processes (FL, fresh leaves; IW, indoor-withered leaves; SW, solar-withered leaves), were collected from the Sequence Read Archive (SRA) database (accession numbers PRJNA274203 and PRJNA562623). After quality trimming, all clean reads were mapped to the chromosome-level genome of tea plant using the HISAT software (Kim et al., 2015), and then the RSEM (Li and Dewey, 2011) was used to calculate the fragments per kilobase per million mapped reads (FPKM) value. The expression profiles of m6A regulatory genes were visualized using the TBtools software based on the normalized FPKM values.

Plant Materials and Treatments

The tea plants (*C. sinensis* cv. Tieguanyin) were grown at Fujian Agriculture and Forestry University, Fuzhou, Fujian Province, China (E 119°14′, N 26°05′). Referring to the previous method (Zhu et al., 2020), the tea plants were subjected to abiotic stress treatments. To simulate drought treatment, tea leaves were sprayed with 15% (w/v) PEG-4000 solution. For cold treatment, the tea plants were transferred to the artificial climatic chamber, and temperature was set to 4°C. Then, all the tender leaves from treated tea plants were sampled at 0, 12, 24, 36, and 48 h, respectively. Three independent biological replicates were conducted for each sample.

For the withering process of oolong tea, the tender shoot containing one bud and first three leaves were picked uniformly from tea plants. The picked leaves were evenly divided into three parts. The first part was collected immediately as the FL. The second part was exposed to sunlight for 45 min. The third part was subjected to indoor-withering for 45 min. The detailed parameters in the solar-withering and indoor-withering were described in the previous study (Zhu et al., 2020). The FL, IW leaves, and SW leaves were sampled for further analyses. Each sample was performed in three independent biological replicates. All collected samples were immersed in liquid nitrogen immediately and then maintained at −80°C until further investigation.

Total RNA Isolation and Relative Expression Analysis of m6A Regulatory Genes in Tea Plants

Total RNA was isolated separately from the above-mentioned samples using the Trizol reagent (TransGen Biotech, Beijing, China). The isolated RNA integrity was verified by gel electrophoresis and Agilent Bioanalyzer 2100 system (Thermo Fisher Scientific, MA, United States). Then RNA was used to synthesize the first-strand cDNA using the TransScript First-Strand cDNA Synthesis SuperMix Kit (TransGen Biotech, Beijing, China). The quantitative real-time polymerase chain reaction (qRT-PCR) of m6A regulatory genes was conducted on the LightCycler 480 platform (Roche Applied Sciences, Basel, Switzerland) according to our previous method (Zhu et al., 2020). *Glyceraldehyde-3-phosphate dehydrogenase* (*GAPDH*) and *β-actin* were used to normalize the gene expression. The relative gene expression was calculated using $2^{-\Delta\Delta CT}$ method (Livak and Schmittgen, 2001). All specific primers are listed in **Supplementary Table S2**. Three biological replicates were performed for each qRT-PCR analysis.

Quantitative Analyses of Global N6-Methyladenosine RNA Methylation and 5-Methylcytosine DNA Methylation

Global m6A RNA methylation level in tea leaves was determined using the EpiQuik m6A RNA Methylation Quantification Kit (Epigentek, Farmingdale, NY, United States), according to the manufacturer's instructions. The m6A level was detected colorimetrically by reading the absorbance in the Infinite M200 PRO enzyme-labeled instrument (Tecan, Switzerland).

To evaluate the global 5mC DNA methylation level in tea leaves, genomic DNA from FL, IW, and SW was extracted separately using EasyPure Plant Genomic DNA kit (TransGen Biotech, Beijing, China). The extracted DNA was checked in gel electrophoresis and quantified by Agilent Bioanalyzer 2100 system. According to the manufacturer's protocols as previously described (Zhou et al., 2019a), the integrated DNA was used to detect the 5mC level by MethylFlash Global DNA Methylation ELISA Easy Kit (Epigentek, Farmingdale, NY, United States). Each experiment was repeated three times independently.

Functional Assessment of m6A Regulatory Genes in Tea Leaves by siRNA-Mediated Gene Silencing

To uncover the potential functions of m6A regulatory genes in tea leaves, gene suppression was performed as previously described (Zhao et al., 2020) with minor modifications. The freshly apical buds with first leaves were picked uniformly from eight-year-old tea plants (*C. sinensis* cv. Tieguanyin) at the development stage of one bud with three leaves. Tea shoots (the apical buds with first leaves) were then incubated in 1.5-mL microcentrifuge tubes containing 1 ml of 20 μM siRNA solution at room temperature. Shoots incubated with the same concentrations of siRNA-negative control (siRNA-NC) were used as the internal control. After 12- and 24-h incubations, the collected shoots were used for methylation level and

qRT-PCR analyses. The flavonoid content of these shoots was also determined as described elsewhere (Zhu et al., 2019). The specific siRNAs targeting m6A regulatory genes were synthesized from GenePharma (Shanghai, China). Detailed information on siRNA and siRNAs-NC is provided in **Supplementary Table S2**.

Statistical Analyses

All data were presented as the mean ± SD. Group differences were conducted by one-way analysis of variance followed by Tukey's *post-hoc* test, and all statistical analyses were conducted on SPSS 25 software. The rMATS software was employed to detect the alternative splicing (AS) events (Shen et al., 2014). The correlation analysis of m6A regulatory genes, 5mC regulatory genes, m6A level, and 5mC level was performed based on Pearson's correlation coefficient. The expression levels of 5mC regulatory genes were obtained from our previous study (Zhu et al., 2020).

RESULTS

Identification and Characterization of m6A Regulatory Genes in Tea Plants

After thoroughly screened the whole genome of tea plant, a total of nine m6A writer, 16 m6A eraser, and nine m6A reader genes were ultimately ascertained. All m6A regulatory genes were named according to their homologs of *A. thaliana*. Their protein lengths and predicted molecular weights (MWs) varied widely (**Supplementary Table S3**). The lengths of putative m6A regulatory proteins ranged from 242 (CsALKBH2) to 1,387 (CsVIR1 and CsVIR2) amino acids, and the MW of m6A regulatory proteins was between 27.52 (CsALKBH2) and 152.50 (CsVIR1). Likewise, the m6A regulatory proteins had considerably different theoretical isoelectric point. CsALKBH3 had the highest theoretical isoelectric point (9.30), while CsALKBH5A had the lowest theoretical isoelectric point (4.77). Additionally, the subcellular localization of these proteins showed that a total of 30 m6A regulatory proteins (88.24%) were localized in the nucleus, with the remaining four proteins (CsALKBH5C, CsALKBH9, CsALKBH11, and CsECT5) targeted to the cytoplasmic region.

The Phylogenetic Classifications and Structural Features of m6A Regulatory Genes in Tea Plants

To gain an insight into the evolutionary history of the m6A regulatory genes in the plant kingdom, the m6A writer, m6A eraser, and m6A reader proteins from five dicotyledons, three monocotyledons, one pteridophyte, and two mosses were used to construct phylogenetic trees. The m6A writer can be naturally grouped into four categories, namely, MT, FIP37, VIR, and HAKAI. As per phylogenetic analysis, the MT gene family can split into three distinct clades named as MTA, MTB, and MTC (**Figure 1A**). Two CsMTAs, two CsMTBs, and one CsMTC were, respectively, distributed in their corresponding evolutionary clades. The MTA, MTB, and MTC were present in all dicotyledons, monocotyledons, and mosses. However, both MTB and MTC subfamilies were absent in the pteridophyte, and only MTA subfamily was identified from this plant. Similarly, only FIP37 was detected in the pteridophyte (**Figures 1B–D**). However, there was an absence of VIR and HAKAI proteins from this species. On the other hand, the phylogenetic tree of ALKBH family was stringently clustered into three groups (**Figure 2A**). In each group, most ALKBH proteins from moss and pteridophyte lie in a distinct branch, while ALKBH proteins belonging to spermatophyte were grouped into other branches. In the phylogenetic tree of m6A readers, a total of 154 ECT and 15 CPSF30 proteins fell into two distinct clades (YTHDF and YTHDC; **Figure 2B**), which were similar to the previous report (Scutenaire et al., 2018). Intriguingly, most m6A reader proteins from moss were closely clustered with their homologs in pteridophyte than in spermatophyte.

Besides, the number of m6A regulatory genes varied greatly among the 11 plant species (**Figure 2C**). The number of m6A regulatory genes in hexaploid wheat (*T. aestivum*) and tetraploid cotton (*G. hirsutum*) was observed almost double of several plant species, including *C. sinensis* (34), *O. sativa* (32), and *A. thaliana* (32), indicating that the m6A regulatory genes in polyploid plants have exhibited large-scale expansion. Notably, a total of 34 m6A regulatory genes were screened in tea plants, which had the fourth-highest number of m6A regulatory genes among the seven plant species.

To analyze the sequential characteristics of m6A regulatory components from tea plants, the conserved domains and motif sequences were identified from these proteins. The typical MT-A70 domain was found in each member of CsMT family (**Figure 3A**). Among other m6A writer components, we found that CsFIP37 protein was conserved with one WTAP domain. On the other hand, both two CsVIR proteins contained one conserved VIR-N domain, and the CsHAKAI had a ZnF-C2H2 domain. Unlike the m6A writer components that contain diverse conserved domains, all members of ALKBH family had one 2OG-Fell-Oxy-2 domain (**Figure 3B**) and shared a high level of similarity with each other. It is worth noting that both CsALKBH4A and CsALKBH4B harbored one additional PRONE domain. Similarly, one highly conserved YTH domain was identified in all ECT proteins belonging to m6A readers (**Figure 3C**). Another key component of the m6A readers, CPSF30, possessed one extra ZnF-C3H1 domain.

Among different m6A writer components, the motif number varied from 1 to 10 (**Supplementary Figure S1**). CsFIP37 and CsHAKAI harbored only one motif. In contrast, homologous CsMTA1 and CsMTA2 contained all 10 motifs. With the exception of the CsALKBH10, the other members of ALKBH family had one motif 1. Further, motif 10 was found to be specific to CsECT8 and CsCPSF30 of YTHDC subfamily, while motifs 1 and 2 only existed in the YTHDF subfamily. Thereafter, the analysis of the exon–intron organizations showed that there was a large variation in the exon number of m6A regulatory genes. Both *CsVIR1* and *CsVIR2* contain up to 23 exons. Contrastingly, *CsHAKAI* was found to be intronless. In general, most m6A regulatory proteins in the adjacent branches exhibited similar motif distribution and the exon–intron compositions.

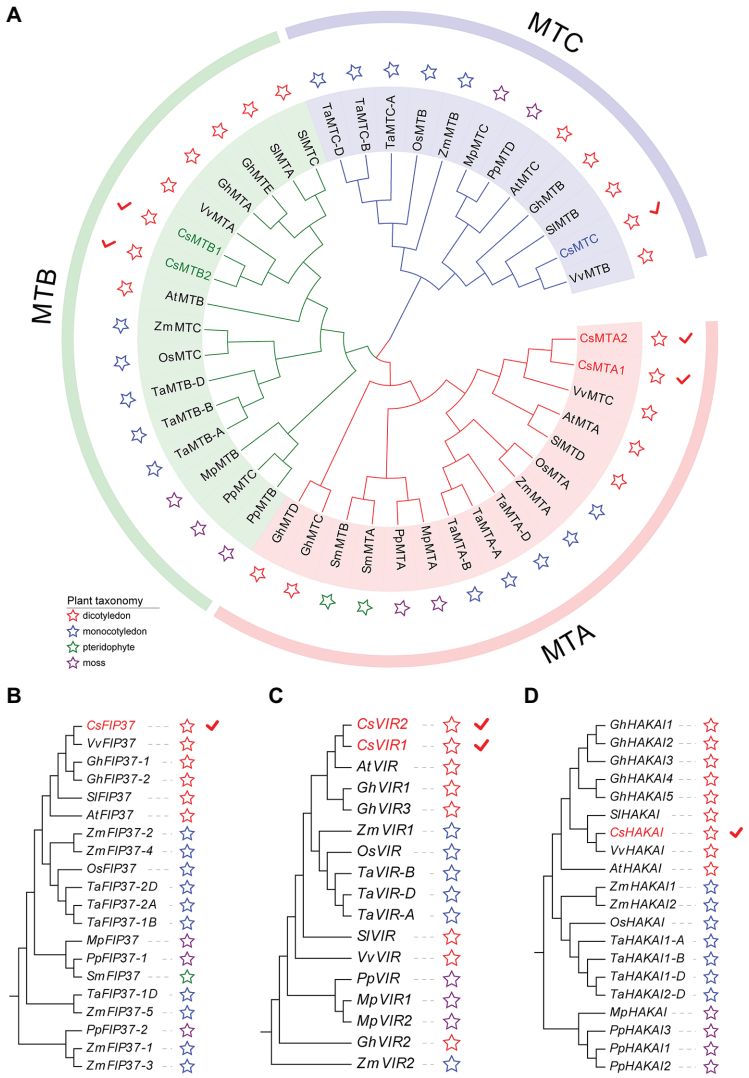


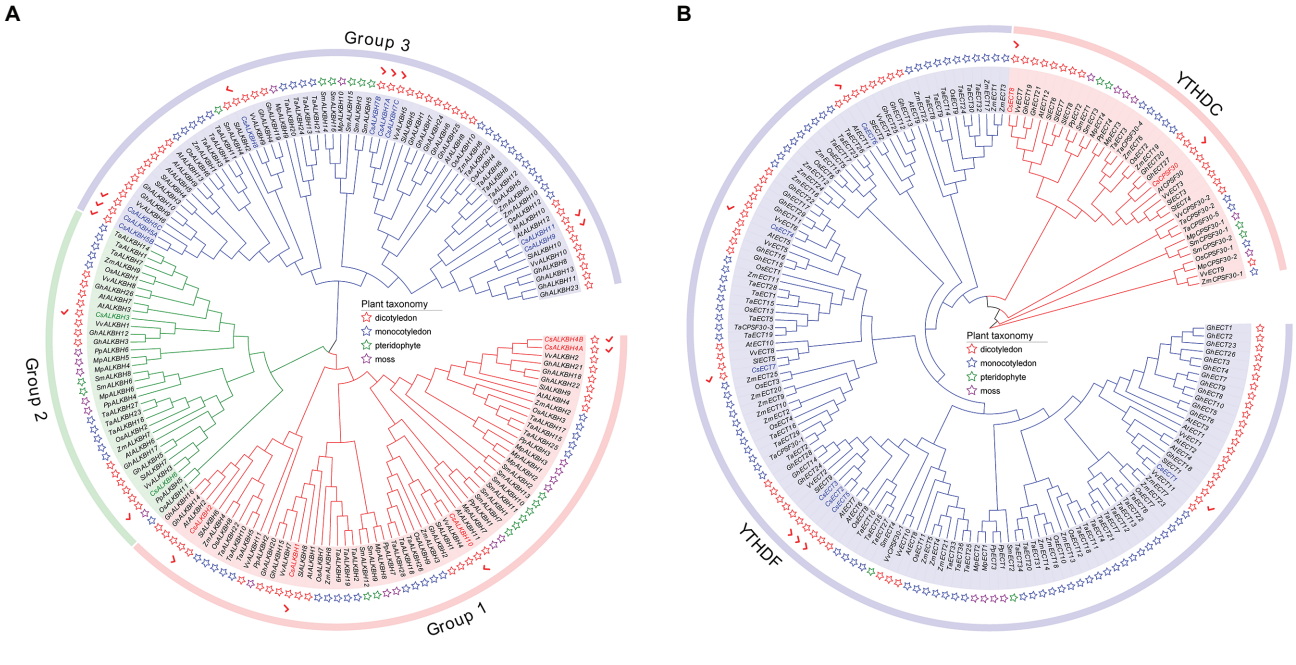
FIGURE 1 | Phylogenetic analysis of m6A writer genes from five dicotyledons, three monocotyledons, one pteridophyte, and two mosses. **(A)** Phylogenetic tree of *MT* genes. **(B)** Phylogenetic tree of *FIP37* genes. **(C)** Phylogenetic tree of *VIR* genes. **(D)** Phylogenetic tree of *HAKAI* genes.

The Chromosomal Distributions, Gene Duplication Events, and Evolutionary Selection of m6A Regulatory Genes in Tea Plants

In total, 30 m6A regulatory genes were randomly distributed on 13 chromosomes, and the remaining four genes were located on the unanchored contigs (**Figure 4**). Both chromosomes 2 and 14 harbored the highest number of m6A regulatory genes (4), whereas chromosomes 4, 5, 7, and 8 contained only one gene. Besides, a total of five duplicated gene pairs involved in nine m6A regulatory genes were observed in the tea genome, namely, two m6A writer genes, four m6A eraser genes, and three m6A reader genes. Additionally, these nine m6A regulatory genes may experience the segmental duplication or whole-genome duplication (WGD) events.

To further explore the evolution patterns of the m6A regulatory genes in different plant species, the comparative collinearity analyses of tea plants associated with four representative species were performed (**Figure 5**). A total of 24 m6A regulatory genes in tea plants exhibited the collinearity relationships with those in *V. vinifera*, followed by *S. lycopersicum* (17), *A. thaliana* (14), and *O. sativa* (3). Curiously, the number of collinearity gene decreased sharply between dicotyledons and monocotyledons. The number of homologous m6A regulatory genes between tea plants and other dicotyledons is far more than that between tea plants and monocotyledons. This result indicated that the expansion events of m6A regulatory genes may occur after the monocot–dicot divergence. In addition, four ALKBH members (CsALKBH5B1, CsALKBH5C, CsALKBH9, and CsALKBH1) and two ECT members (CsECT1 and CsECT5) were shown to have more than one pair of collinearity gene.

To explore the evolutionary trajectory acting on these m6A regulatory genes, we calculated the Ka, Ks, and, Ka/Ks ratio



C

	m6A writer						m6A eraser			m6A reader	
	MTA	MTB	MTC	FIP37	VIR	HAKAI	Group 1	Group 2	Group 3	YTHDF	YTHDC
Zea mays	1	1	1	5	2	2	4	2	4	22	3
Triticum aestivum	3	3	3	4	3	4	12	6	11	37	4
Oryza sativa	1	1	1	1	1	1	4	3	5	12	2
Vitis vinifera	1	1	1	1	1	1	4	3	4	9	4
Arabidopsis thaliana	1	1	1	1	1	1	4	3	5	11	2
Gossypium hirsutum	1	1	1	2	3	5	8	5	13	25	4
Solanum lycopersicum	1	1	1	1	1	1	4	1	5	4	5
Camellia sinensis	2	2	1	1	2	1	5	2	9	7	2
Selaginella moellendorffii	1	1	0	1	0	0	8	2	6	2	4
Physcomitrella patens	1	1	1	2	1	3	4	3	0	2	2
Marchantia polymorpha	1	1	1	1	2	1	5	3	2	2	4

Monocot
Dicot
Pteridophyte
Moss

FIGURE 2 | Evolutionary analysis of m6A regulatory genes from five dicotyledons, three monocotyledons, one pteridophyte, and two mosses. **(A)** Phylogenetic tree of m6A eraser genes. **(B)** Phylogenetic tree of m6A reader genes. **(C)** Number of m6A regulatory genes in different plant species.

for each duplicated pair of m6A regulatory genes in tea plants (**Table 1**). The Ka/Ks ratio of five duplicated pairs of m6A regulatory genes ranged from 0.2130 to 0.3838, with an average of 0.2837, indicating that these m6A regulatory genes evolved through strong purifying selection, which limited the divergences of gene functions after segmental duplication or WGD events. Based on the previously defined criteria (Xia et al., 2020), the divergence time of duplicated gene pairs can be estimated using Ks value. In the present study, the Ks values of these five duplicated gene pairs were distributed between 0.0160 and 0.5217. Among them, the duplicated gene pair (*CsECT2-CsECT3*) possessed the lowest Ks value (0.0160), implying that it probably generated from the recent segmental duplication or WGD event. The Ka values of the other four duplicated gene pairs were in the range of 0.35–0.53, demonstrating that they might be associated with the ancient duplication events.

The Protein–Protein Interaction Network of the m6A Regulatory Proteins in Tea Plants

A total of 14 m6A regulatory proteins were aligned to the corresponding homologs of *A. thaliana*, namely, nine m6A writer components, three m6A eraser components, and two m6A reader components (**Figure 6**). There were strong interactions of all m6A writer components, indicating that they may be participated in m6A modifications by forming protein complexes. Meanwhile, two m6A reader components (ECT8 and CPSF30) interacted with FIP37 and HAKAI in m6A writer components. This result suggested that ECT8 and CPSF30 may immediately bind m6A sites and play ultimate regulatory roles for modified RNA. In addition, we found that ALKBH2 simultaneously interacted with the other two ALKBH members (ALKBH3 and ALKBH6), which might be associated with their special roles in the removal of m6A modification and reduction of the overall m6A level.

Detection of *cis*-Acting Elements in the Promoter Regions of m6A Regulatory Genes in Tea Plants

To better understand the transcriptional regulation and potential biological functions of m6A regulatory genes from tea plants, the *cis*-acting elements in the 2,000-bp promoter regions of 34 m6A regulatory genes were analyzed using the PlantCare

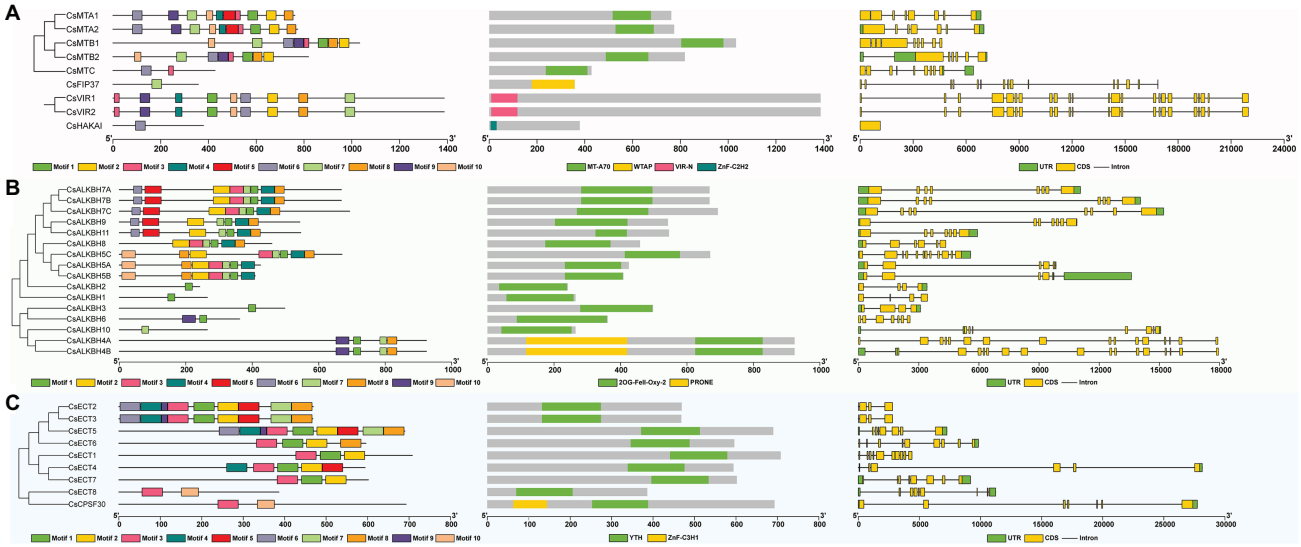


FIGURE 3 | Phylogenetic relationships, conserved motifs, functional domains, and exon–intron organizations of m6A regulatory genes in tea plants. **(A)** Structure analysis of m6A writer genes. **(B)** Structure analysis of m6A eraser genes. **(C)** Structure analysis of m6A reader genes.

database (**Figure 7**). In m6A regulatory components, stress-responsive, light-responsive, and phytohormone-responsive elements are more common than plant growth and development-related elements. In stress-responsive category, several types of stress-responsive elements were identified in the promoter regions of m6A regulatory genes. With the exception of *CsFIP37* and *CsALKBH6*, other 32 m6A regulatory genes contained the STRE element. Contrastingly, GC-motif element was observed in only three m6A regulatory genes (*CsMTC*, *CsALKBH7B*, and *CsECT4*). Differences in stress-responsive element types may be associated with the different functions of these genes under environmental stresses. Moreover, light-responsive elements were evenly present in the promoter regions of all m6A regulatory genes, indicating that the expression levels of m6A regulatory genes might be regulated by light signaling.

Tissue-Specific Expression of m6A Regulatory Genes in Tea Plants

The expression profiles of m6A regulatory genes in eight representative tea plant tissues were retrieved from published transcriptome datasets (**Figure 8**). Among nine m6A writer genes, we discovered that a few m6A regulatory genes showed high expression in all studied tissues (FPKM > 10). On the contrary, the major m6A regulatory genes were seldom expressed (FPKM < 1) or expressed at moderate levels (FPKM > 1 and FPKM < 10) in eight representative tissues. It is noteworthy that *CsMTB2*, *CsHAKAI*, *CsECT1*, and *CsECT6* were continuously expressed at high levels in all tissues, implying that these m6A regulatory genes inevitably play important roles in numerous tissues. Besides, most m6A writer genes exhibited lower expression levels in young leaves than in mature leaves and old leaves. In contrast, a multitude of m6A eraser genes were more highly expressed in young leaves than in mature leaves and old leaves.

Expression Patterns of m6A Regulatory Genes in Tea Plants Under Environmental Stresses

To unveil the possible functions of m6A regulatory genes in response to environmental stresses, the expression patterns of m6A regulatory genes under drought and cold stresses were detected (**Figure 9**). All m6A writer genes were slightly downregulated under drought treatment. Among them, the expression levels of *CsMTB1* and *CsMTC* decreased sharply from 0 to 12 h, and then gradually decreased to the lowest level after 48-h treatment. In addition, *CsMTA1*, *CsMTA2*, *CsMTB2*, and *CsVIR2* showed no significant expression changes from 0 to 24 h but were significantly downregulated during the late stage (36–48 h) of drought stress. Remarkably, the remaining m6A genes showed no significant changes in transcript levels, suggesting that these genes might not perform the important roles under drought stress. Unlike the transcript patterns of m6A writer genes, almost all m6A eraser genes were markedly elevated with prolonged drought stress. Nine m6A eraser genes were rapidly upregulated under drought stress, but the expression levels of the other seven m6A eraser genes increased slightly at the early stage (0–24 h) of drought stress and increased significantly at 36 h after drought treatment. Similarly, the transcript levels of most m6A reader genes increased continuously and peaked at 48 h after drought treatment.

The expression patterns of all m6A regulatory genes under cold stress were similar to those under drought stress. In m6A writer genes, only *CsMTA1* and *CsMTA2* were markedly

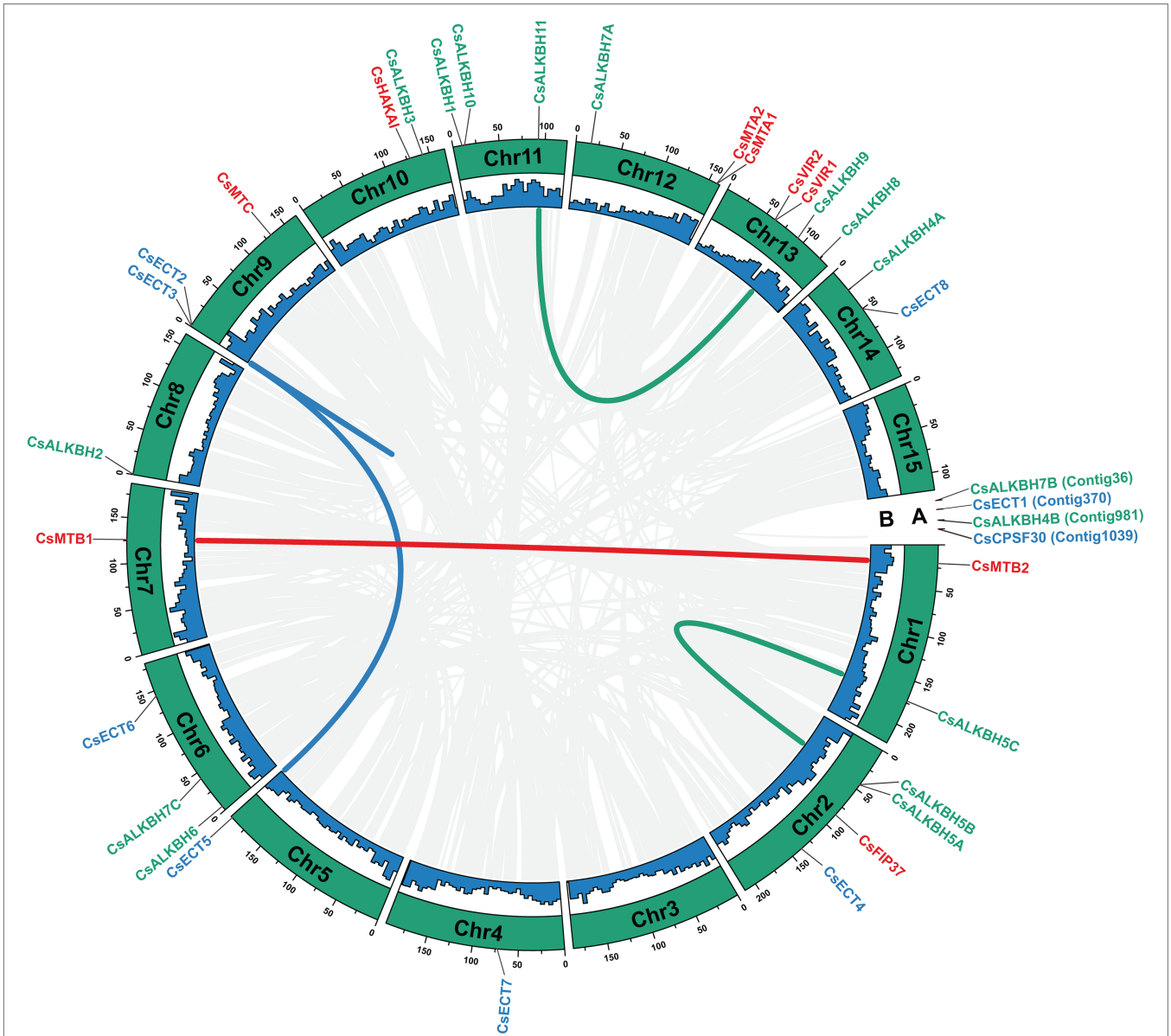


FIGURE 4 | Chromosomal distribution and collinearity analysis of m6A regulatory genes in tea plants. **(A)** Chromosomal number. **(B)** GC content. The gray lines represent all collinear blocks in the genome of tea plant. The other colored lines represent all collinear relationships of m6A regulatory genes.

downregulated at 48 h after cold treatment, and the transcript levels of the seven m6A writer genes were not significantly altered during the whole periods of cold stress. With the exception of *CsALKBH7* and *CsALKBH9*, other m6A eraser genes were upregulated and persisted at high expression levels during the late period of cold stress. Similarly, we noted that the transcript abundance of most m6A reader genes was dramatically induced under cold stress. Four genes (*CsECT5*, *CsECT7*, *CsECT8*, and *CsCPSF30*) were upregulated immediately at 24 h, whereas the expression levels of remaining m6A reader genes were not significantly altered at the early period of cold treatments and then notably increased with prolonged cold stress.

Effects of Withering Process on the Expression of m6A Regulatory Genes and Correlation Analyses of m6A Regulatory Genes, 5mC Regulatory Genes, m6A Levels, and 5mC Levels

In this study, the transcript levels of 34 m6A regulatory genes were analyzed in the FL, IW, and SW based on the previous transcriptome datasets (**Figure 10A**). The expression of most m6A writer genes was not affected by indoor-withering and solar-withering, while the transcript abundance of *CsMTC* was strongly reduced at IW and SW. Regarding the expression of m6A eraser genes, half of m6A eraser genes were insensitive after withering treatments, while the other eight m6A eraser

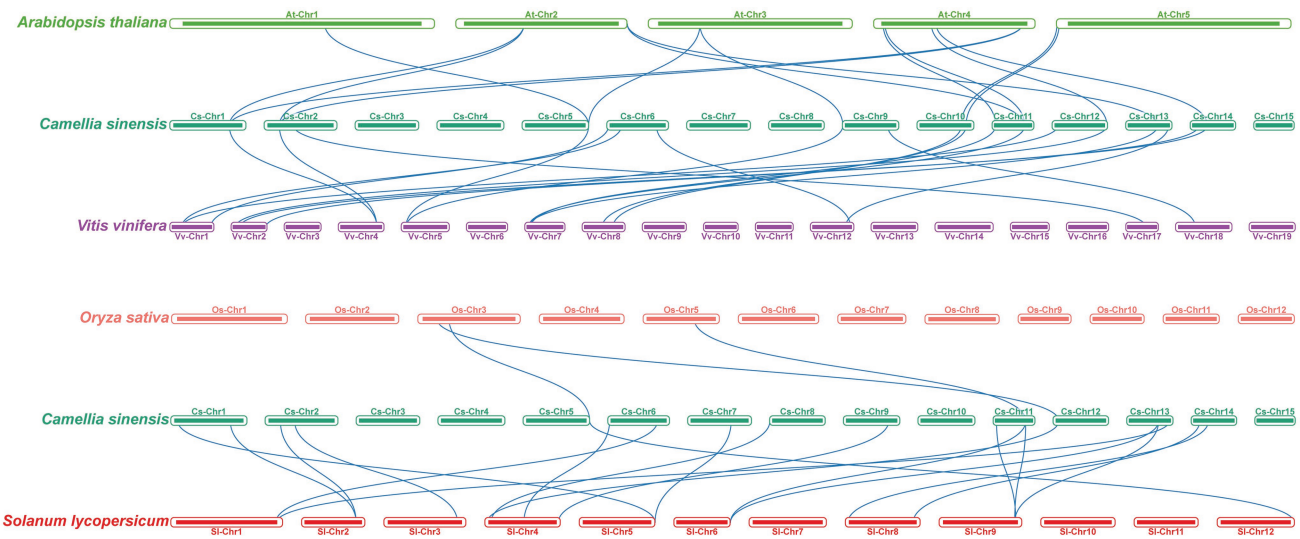


FIGURE 5 | Collinearity analysis of m6A regulatory genes between tea plants and four representative plant species. The blue lines represent all collinear relationships of m6A regulatory genes between tea plants and other plants.

TABLE 1 | The evolutionary analysis of duplicated m6A regulatory genes in tea plants.

Gene 1	Gene 2	Ka	Ks	Ka/Ks ratio	Divergence time (Mya)	Duplication type
CsMTB1	CsMTB2	0.1280	0.3573	0.3581	27.4853	WGD
CsALKBH5B	CsALKBH5C	0.1521	0.3962	0.3838	30.4747	WGD
CsALKBH9	CsALKBH11	0.1111	0.5217	0.2130	40.1309	WGD
CsECT2	CsECT3	0.0037	0.0160	0.2308	1.2288	Segmental duplication
CsECT3	CsECT5	0.0895	0.3846	0.2327	29.5868	WGD

WGD: whole-genome duplication.

genes were significantly upregulated at IW or SW. Among these eight genes, *CsALKBH1* and *CsALKBH3* were not significantly altered by indoor-withering, while the expression levels of these genes were dramatically elevated at SW. In contrast, the transcript levels of the other six *CsALKBH* genes were noticeably enhanced in IW and SW than in FL. In m6A reader genes, the expression levels of *CsECT5*, *CsECT7*, and *CsECT8* were signally higher in IW than in FL. Furthermore, the transcript abundance of all m6A reader genes was substantially upregulated and maintained at a highest level after solar-withering. These results showed that the expression levels of major m6A regulatory genes were more affected by solar-withering than by indoor-withering. Notably, we observed that a large number of alternative spliced isoforms were detected after withering treatment (**Table 2**), suggesting withering process may promote the occurrence of AS events. To further validate the expression patterns of all m6A regulatory genes retrieved from the transcriptome datasets, we conducted qRT-PCR analyses to determine the expression levels of these genes (**Figure 10B**). The overall transcript levels of the detected m6A regulatory genes were consistent with those obtained from the transcriptome datasets.

To comprehensively ascertain whether there may exist the interplay between RNA and DNA methylation, we examined the m6A and 5mC levels during tea-withering process. The overall m6A levels were 0.287, 0.236, and 0.173% in the FL, IW, and SW, respectively (**Figure 11A**). The results showed that the overall m6A level was declined after tea-withering process. We then assessed the 5mC levels in the same samples. Similarly, the 5mC level was significantly higher in FL (3.480%) and IW (2.975%) than in SW (2.363%). These results showed that the dynamic changes of m6A levels were similar to those of 5mC levels during withering process. Thereafter, we investigated the functional relationship between methylation levels and corresponding regulatory genes during tea-withering process. For these analyses, correlation networks among the expression profiles of the identified m6A regulatory genes and 5mC regulatory genes, as well as the m6A levels and 5mC levels, were conducted (**Figure 11B**). The m6A modifications were strongly positively correlated with the transcript abundance of RNA MT genes, but significantly negatively correlated with the transcript abundance of RNA demethylase genes. In 5mC modifications, we also detected a strong positive interaction between 5mC levels and the transcript abundance of the corresponding DNA MT genes. Contrastingly, the DNA methylation status was negatively correlated with the expression levels of DNA demethylase genes. Additionally, we found that several RNA MT genes were positively correlated with DNA MT genes.

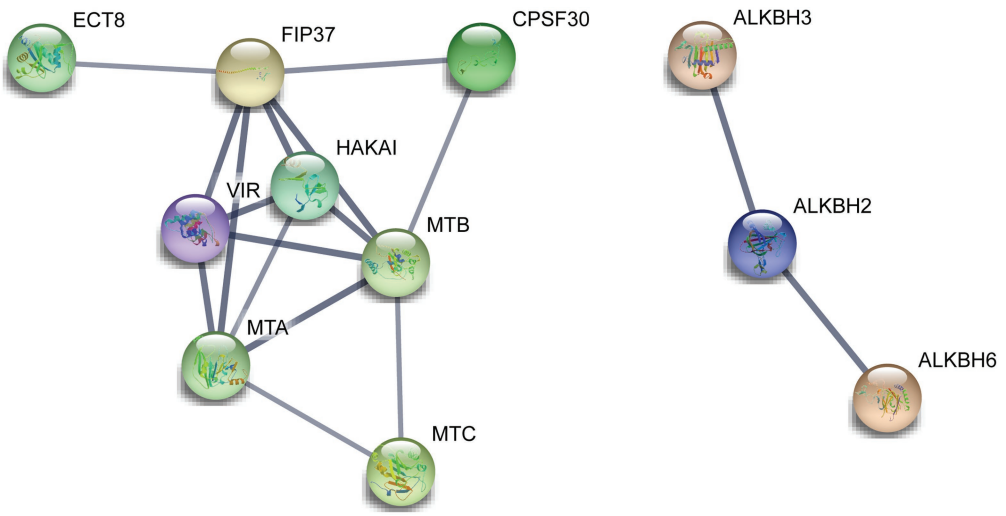


FIGURE 6 | Functional protein–protein interaction network of the m6A regulatory proteins in tea plants. The protein–protein interaction network of m6A regulatory proteins was constructed using the STRING v11.0 database. The orthologous protein was found using Tea Plant Information Archive (TPIA) database, and further, the homologous proteins were also considered as STRING proteins based on the high bit score.

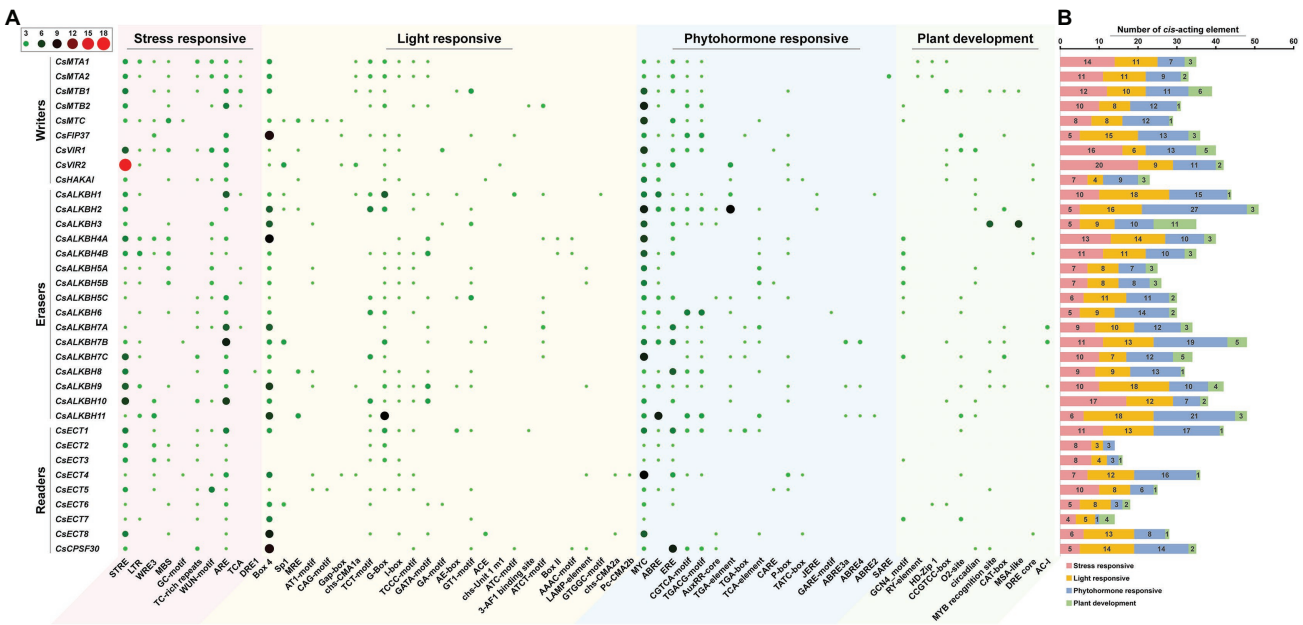


FIGURE 7 | Analysis of *cis*-acting elements in the promoter regions of m6A regulatory genes in tea plants. **(A)** The distribution of *cis*-acting elements in the promoter regions of m6A regulatory genes. **(B)** The histogram of *cis*-acting elements in each category.

Likewise, positive correlations were detected between some RNA demethylase genes and DNA demethylase genes.

Functional Assessment of m6A Regulatory Genes in Tea Plants

To further unravel the potential roles of m6A regulatory genes in tea plants, the representative m6A writer gene (*CsMTC*), m6A eraser gene (*CsALKBH9*), and m6A reader gene (*CsECT8*) were selected for functional assessment *via* an siRNA-mediated silencing method. After *CsMTC*-silenced treatment, the expression level of *CsMTC* at 12 and 24 h was considerably declined compared with that at 0 h (**Figure 12A**). As expected, both *CsALKBH9* and *CsECT8* were also significantly downregulated at 12 and 24 h after corresponding siRNA treatments. In contrast, the transcript levels of these three m6A regulatory genes in tea leaves treated with siRNA-NC were not obviously altered. Then, the m6A level, 5mC level, and flavonoid content in gene-silenced tea leaves were also determined (**Figures 12B,C**).

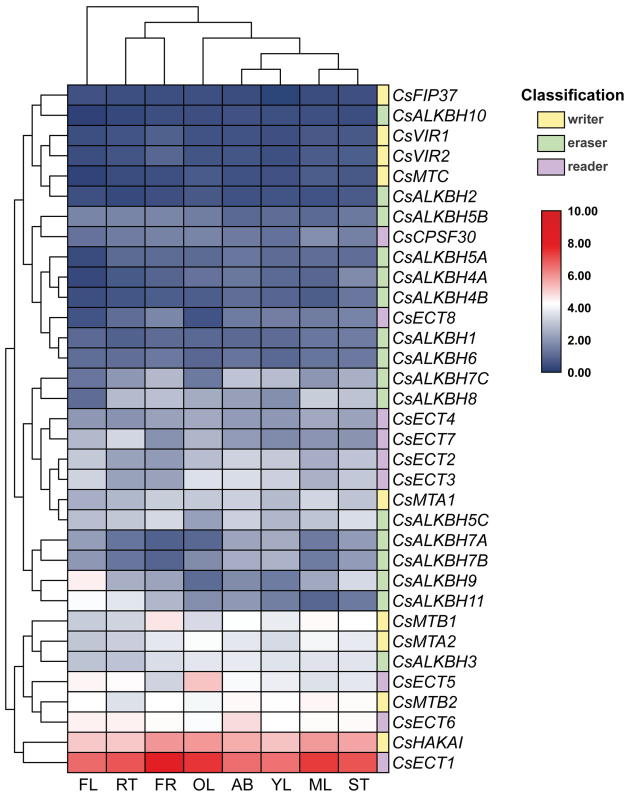


FIGURE 8 | Expression profiles of m6A regulatory genes in eight tea plant tissues. The expression values of m6A regulatory genes were normalized by log_2-transformed (FPKM+1). FL: flowers; RT: roots; FR: fruits; OL: old leaves; AB: apical buds; YL: young leaves; ML: mature leaves; ST: stems. Public transcriptome data were collected from the NCBI Sequence Read Archive (SRA) database under accession number PRJNA274203.

The m6A and 5mC levels were markedly declined after siRNA-*CsMTC* treatment, while the m6A and 5mC levels in tea level treated with siRNA-*CsALKBH9* were both sharply increased. However, the downregulation of *CsECT8* did not affect m6A level and 5mC levels. In addition, the flavonoid content was also significantly changed after siRNA-*CsECT8* treatment, whereas no obvious alterations of flavonoid contents in *CsMTC*- and *CsALKBH9*-silenced tea leaves were detected.

DISCUSSION

Evolutionary Relationships and Structural Features of m6A Regulatory Genes in Tea Plants

In the current study, a total of 34 m6A regulatory genes were ultimately identified from the chromosome-scale genome of tea plants. Compared with other plant species, the number of m6A regulatory genes in tea plants appears greater than that in *A. thaliana* (32), *O. sativa* (32), *V. vinifera* (30), *S. lycopersicum* (26), *S. moellendorffii* (25), *M. polymorpha* (23), and *P. patens* (20). Since the genome size of tea plants (2.94 Gb) is almost several-fold larger than that of these plant species, the increasing number of m6A regulatory genes may be linked with a series of gene duplication and expansion events during the long-term evolutionary process of tea plants (Xia et al., 2020). Similarly, hexaploid wheat possessed the largest number of m6A regulatory genes, which may be attributed to the large and complex genome size (17 Gb) that has undergone polyploidization. Because the genome size of upland cotton and maize was larger than that of tea plant, more m6A regulatory genes were identified in upland cotton and maize than in tea plants, indicating that m6A modification in these two plant species may require more m6A regulatory genes to form a precise regulatory mechanism.

In phylogenetic trees of these plant taxa, the majority of m6A regulatory genes from pteridophyte and moss tend to form independent branches (**Figures 1, 2**), while those genes from monocotyledon and dicotyledon were generally clustered together. It suggested that these genes may have experienced expansion events after the divergence of moss and spermatophyte. Remarkably, *VIR* and *HAKAI* genes were not identified from pteridophyte. We speculated that the loss of *VIR* and *HAKAI* in pteridophyte might be due to other writer genes taking over the biological functions of these two writer genes or another alternative mechanism for RNA methylation. Gene duplication portrayed a major driving force for producing a large number of coding gene families (Defoort et al., 2019). In fact, a total of 24 m6A regulatory genes in tea plants had homologous copies in several representative dicotyledons and monocotyledons. More homologous m6A regulatory gene pairs were detected in two dicots than in monocot–dicot. This indicated that the biological functions of m6A regulatory genes may enrich and diversify after monocot–dicot divergence, and more neofunctionalization in m6A regulatory genes required to participate in this precise mechanism to cope with more complex and changeable environments during the long-term evolutionary course. Furthermore, there are five duplicated gene pairs involved in m6A regulatory genes of tea plants (**Figure 4**). All these duplicated gene were demonstrated to be formed after segmental duplication or WGD events. Combined with previously reported WGD events in tea genomes (Wei et al., 2018), four duplicated gene pairs were found to have experienced the WGD events, while only *CsECT2-CsECT3* gene pair underwent segmental duplication. Notably, no tandem duplicated gene pairs were detected from m6A regulatory genes. Thus, the expansion of m6A regulatory genes in tea plants was driven mainly by WGD and segmental duplication, rather than tandem duplication. In addition, duplicated event was a well-known precursor to the functional diversity of gene family, and it can confer genes with new roles in plant growth and resistance against the environmental stresses *via* neofunctionalization and subfunctionalization. The predominant traces of gene functional differentiation were tightly associated with the variation of gene sequence, structure, and expression profile (Tian et al., 2020). The Ka/Ks ratios of all duplicated m6A regulatory gene pairs were far less than 1.0 (**Table 1**), confirming that these m6A regulatory genes obtained from WGD or segmental duplication have experienced strong purifying selection to maintain the new acquisition of vital traits. It reflected that these duplicated genes may be conserved in the composition of their domains

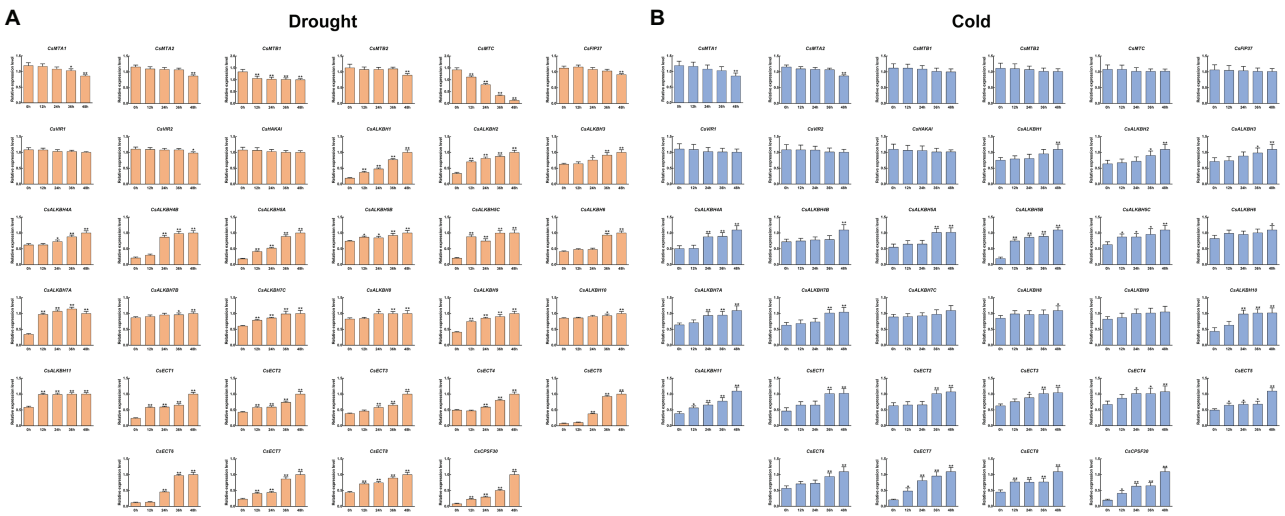


FIGURE 9 | Expression patterns of m6A regulatory genes under abiotic stresses determined by qRT-PCR. **(A)** Drought stress; **(B)** Cold stress. Data are presented as mean ± SD. Single asterisk indicates significant difference ($p < 0.05$); double asterisks indicate highly significant difference ($p < 0.01$). The stress treatment was performed on the healthy two-year-old tea plants (*C. sinensis* cv. Tieguanyin) at the development stage of one bud with three leaves. To simulate drought treatment, tea leaves were sprayed with 15% (w/v) PEG-4000 solution. For cold treatment, the tea plants were transferred to the artificial climatic chamber and the temperature was set to 4°C. Then, all the tender leaves from treated tea plants were sampled at 0, 12, 24, 36, and 48 h, respectively. Three independent biological replicates were conducted for each sample.

and motifs. Also, the functional differentiation of these genes after WGD or segmental duplication might be not conducive to the modification of RNA methylation in tea plants. In actuality, both two members of each duplicated pair were found to possess the same domains and conserved motifs (**Figure 3**). However, there were especially obvious differences in exon–intron structures of five duplicated gene pairs. These results clearly demonstrated that instead of a variation in conserved domain and motif, the gain or loss of exons and introns in gene sequence may contribute to the functional diversification of m6A regulatory genes. Gene expression profiling usually provided a useful indicator for dissecting its biological roles (Sun et al., 2020). In the duplicated gene pair of *CsMTB1* and *CsMTB2*, the *CsMTB1* was highly expressed in stem and root, whereas its low expression was found in flower and young leaf. The difference was that *CsMTB2* displayed a higher expression in young leaves and flower buds. Meanwhile, the lower expression of *CsMTB2* was observed in the root. In essence, the newly duplicated m6A regulatory genes and their ancestral genes tend to have divergent spatiotemporal expression profiles, which were consistent with previous results of gene families from *A. thaliana* (Zhang et al., 2020b). This indicated that the newly duplicated *CsMTB2* obtained unique functions that complemented the original functions of ancestral gene *CsMTB1* through subfunctionalization. Subsequently, we observed the expression patterns of these duplicated genes under abiotic stresses and also supported the hypothesis that the newly duplicated m6A regulatory genes have complementary features to the biological functions of their ancestral genes.

In general, gene duplication events, especially WGD accompanied by chromosomal rearrangements, are the major force acting upon the expansion of m6A regulatory genes and lay the foundation for triggering the functional innovation of these genes. Subsequently, the combined variations in gene sequence and expression abundance of m6A regulatory genes may further enrich the functional diversification of these duplicated gene members in tea plants. These factors coordinately facilitated the more explicit roles of m6A regulatory genes in different plant tissues and environmental adaptations and may contribute to the formation of a precise m6A regulatory mechanism in tea plants.

The m6A Regulatory Genes Act as Essential Roles in Resistance Against the Environmental Stresses and Tea-Withering Stage

Accumulating evidence from prior reports uncovered that m6A modification displays high sensitivity and plays an essential role in response to various abiotic stresses (Hu et al., 2019; Zheng et al., 2020). In the present study, a large number of *cis*-acting elements related to stress responsiveness were presented in the promoter regions of major m6A regulatory genes, indicating that m6A regulatory genes may be involved in stress response. Two m6A writer genes, *CsMTB1* and *CsMTC*, exhibited sustained descending expression trends under drought stress, whereas the transcript levels of most m6A writer genes were marginally decreased (**Figure 9**). Likewise, only *CsMTA1* and *CsMTA2* were significantly downregulated during the late stage of cold stress. The expression levels of other m6A writer genes were not significantly modulated. On the contrary, the majority of m6A eraser genes were upregulated under drought and cold stresses, which were consistent with the expression patterns of these genes detected in *Arabidopsis* and rice under environmental stresses (Ma et al., 2006; Merret et al., 2015;

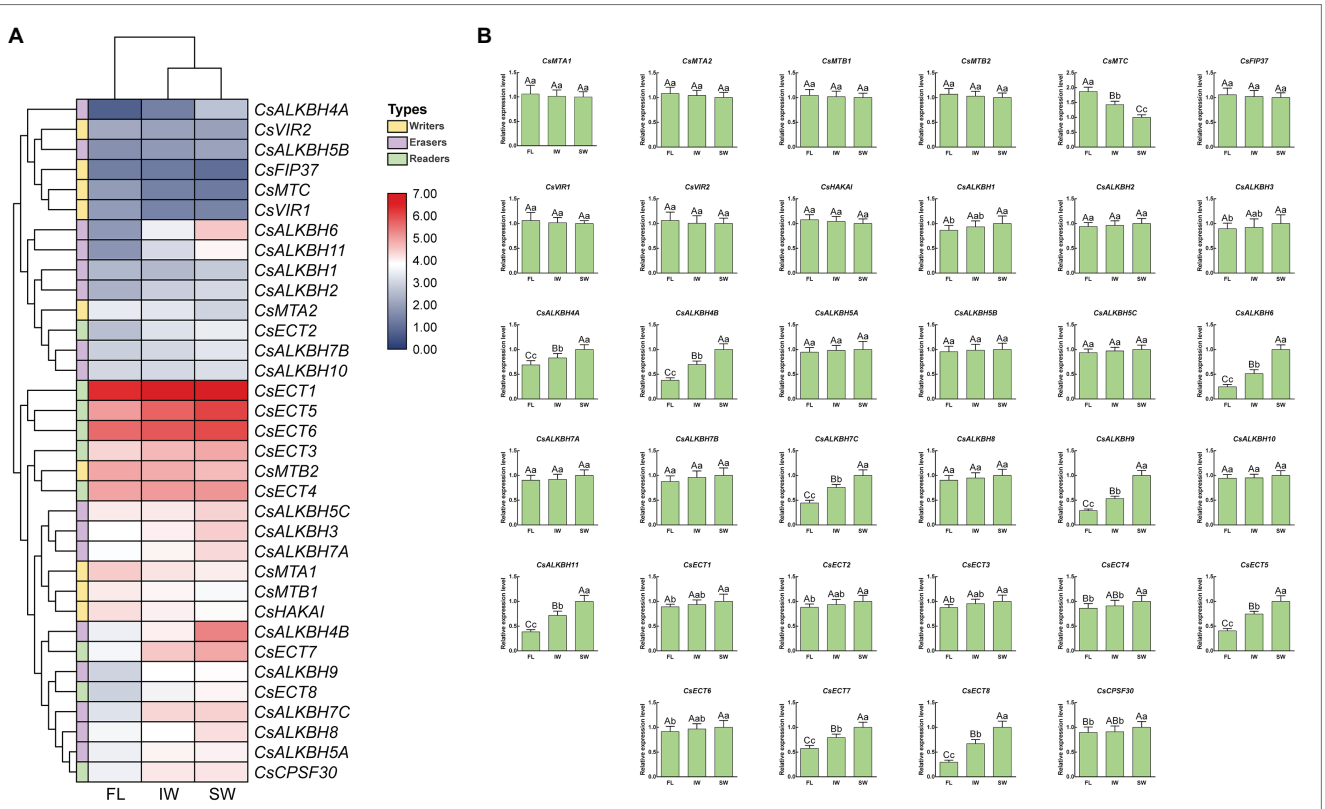


FIGURE 10 | Expression patterns of m6A regulatory genes during tea-withering. **(A)** The heat map of m6A regulatory genes during tea-withering based on the transcriptome data. The expression values of m6A regulatory genes were normalized by $\log_2$-transformed (FPKM + 1). **(B)** Expression patterns of m6A regulatory genes during tea-withering determined by qRT-PCR. Data are presented as mean ± SD. Lowercase letter indicates significant difference ($p < 0.05$); uppercase letter indicates highly significant difference ($p < 0.01$). FL: fresh leaves; IW: indoor-withered leaves; SW: solar-withered leaves. Public transcriptome data were collected from the NCBI Sequence Read Archive (SRA) database under accession number PRJNA562623. The freshly apical buds with first leaves were picked uniformly from eight-year-old tea plants (*C. sinensis* cv. Tieguanyin) at the development stage of one bud with three leaves. The picked leaves were evenly divided into three parts. The first part was collected immediately as the FL. The second part was exposed to sunlight for 45 min. The third part was subjected to indoor-withering for 45 min. The FL, IW, and SW were sampled, respectively. Each sample was performed in three independent biological replicates.

TABLE 2 | Statistics of alternative splicing events at fresh leaves (FL), indoor-withered leaves (IW), and solar-withered leaves (SW).

Sample	Alternative 5′ splice site	Alternative 3′ splice site	Mutually exclusive exon	Retained intron	Skipped exon	Total
FL	818	1,469	347	1,411	6,047	10,092
IW	797	1,404	403	1,343	6,387	10,334
SW	856	1,501	449	1,481	7,159	11,446

Anderson et al., 2018). Combined with no significant alteration in most m6A writer genes, the upregulation of m6A eraser genes was considered to be responsible for the dynamic changes of RNA methylation level in tea plants under environmental stress. Global m6A hypomethylation was detected in maize under drought stress, which has been highlighted as a crucial contributor in the regulation of drought resistance (Miao et al., 2020). Therefore, we speculated that the dynamic changes of RNA methylation level in tea plants played indispensable roles in response to environmental stresses.

Reportedly, the m6A reader can recognize methylated transcripts and further regulate their fates through mRNA processing (Wang et al., 2015; Roundtree et al., 2017). In our research, different from m6A writer and erasers genes, a greater number of m6A reader genes exhibited significant expression variations in response to abiotic stresses. In particular, *CsECT8* and *CsCPSF30* belonging to the YTHDC subfamily were induced rapidly and persisted at high expression levels under drought and cold stresses. Previous studies proposed that YTHDC subfamily is mainly responsible for interacting with splicing factors to mediate AS events in the nucleus (Xu et al., 2014; Xiao et al., 2016). Moreover, AS is known to be one of the main contributors to posttranscriptional gene regulation *via* producing multiple mRNA transcripts and enhancing their coding

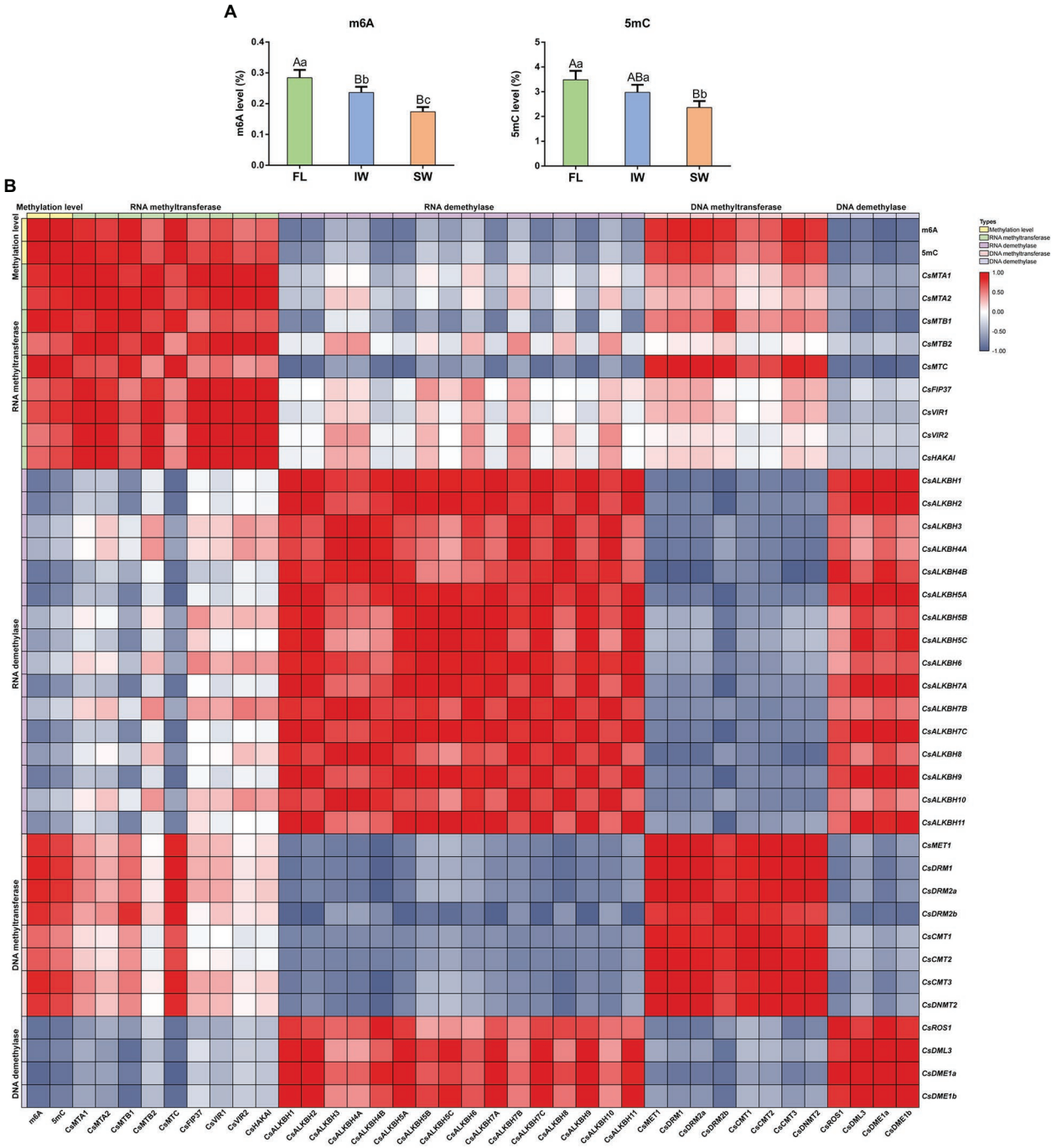


FIGURE 11 | Dynamics of RNA methylation (m6A) and DNA methylation (5mC) in fresh leaves (FL), indoor-withered leaves (IW), and solar-withered leaves (SW) and correlation analyses of m6A regulatory genes, 5mC regulatory genes, m6A levels, and 5mC levels. **(A)** The levels of m6A and 5mC. **(B)** Correlation analyses of m6A level, 5mC level, and corresponding regulatory gene expression. Data are presented as mean ± SD. Lowercase letter indicates significant difference ($p < 0.05$); uppercase letter indicates highly significant difference ($p < 0.01$). To comprehensively ascertain whether there may exist the interplay between RNA and DNA methylation during tea-withering, the correlation between methylation level and corresponding regulatory gene expression was evaluated by Pearson's correlation coefficient. Pearson's correlation coefficient was determined by SPSS 25 software. A correlation coefficient greater than 0 indicates a positive correlation, while a correlation coefficient less than 0 indicates a negative correlation.

potential from the same gene (Filichkin et al., 2015). In the plant kingdom, plants also trigger AS events to generate a large amount of stress-resistant mRNAs to cope with various environmental stresses (Cui and Xiong, 2015; Chen et al., 2020b). Notably, it has been recently observed that the increase in the number of AS events and differentially expressed AS transcripts

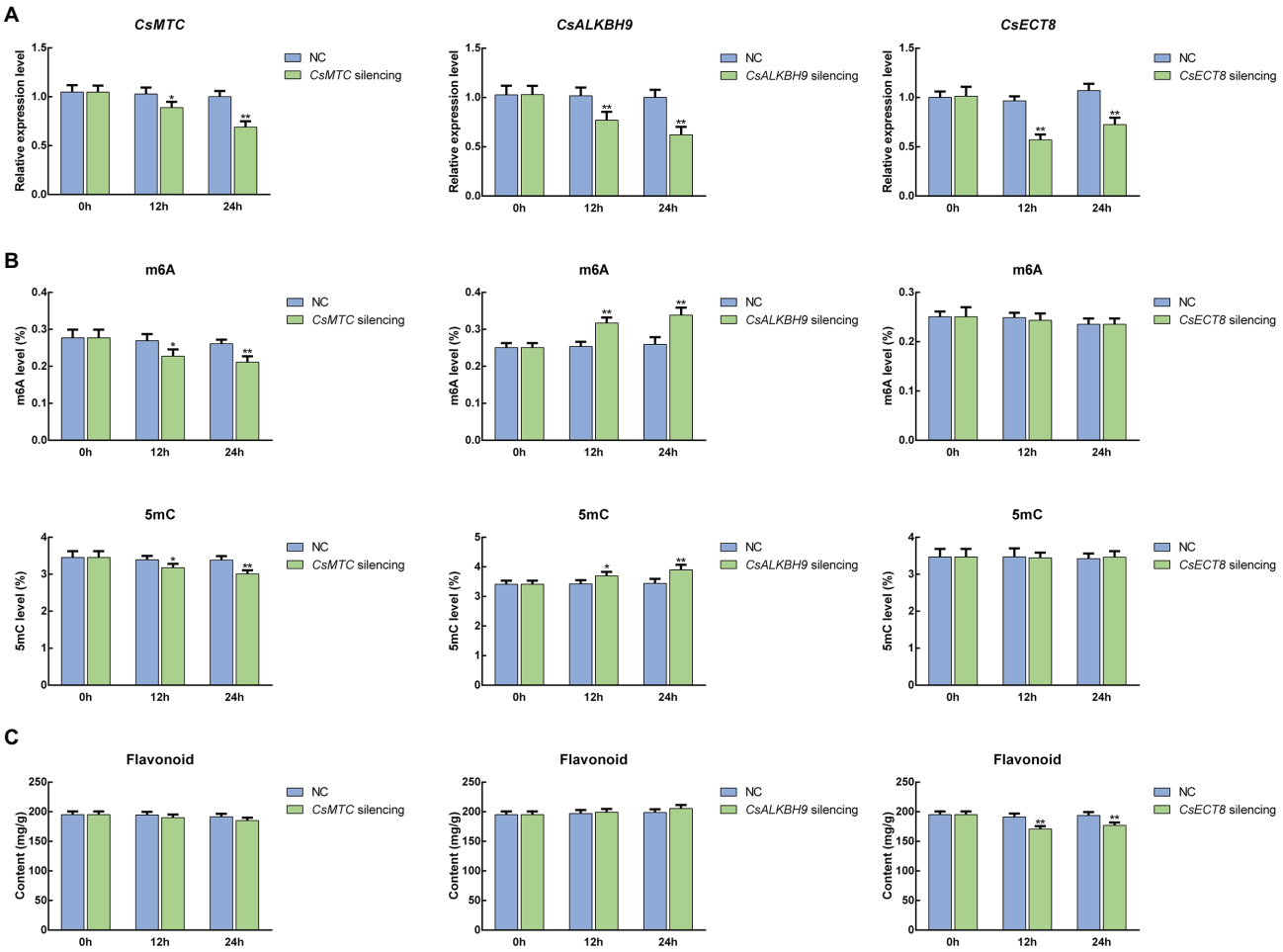


FIGURE 12 | Functional assessment of m6A regulatory genes in tea leaves by siRNA-mediated transient gene silencing. **(A)** Expression patterns of m6A regulatory genes in siRNA-treated tea leaves. **(B)** The levels of RNA methylation (m6A) and DNA methylation (5mC) in siRNA-treated tea leaves. **(C)** Flavonoid content in siRNA-treated tea leaves. Data are presented as mean ± SD. Single asterisk indicates significant difference ($p < 0.05$); double asterisks indicate highly significant difference ($p < 0.01$). The freshly apical buds with first leaves were picked uniformly from eight-year-old tea plants (*C. sinensis* cv. Tieguanyin) at the development stage of one bud with three leaves. Tea shoots (the apical buds with first leaves) were then incubated in 1.5-ml microcentrifuge tubes containing 1 ml of 20 μM siRNA solution at room temperature. Shoots incubated with the same concentrations of siRNA-negative control (siRNA-NC) were used as the internal control. After 12- and 24-h incubations, the collected shoots were used for RNA isolation and flavonoid extraction.

contributes to the adaptation of tea plants to environmental stresses (Ding et al., 2020; Li et al., 2020b). Accordingly, we inferred that upregulation of *CsECT8* and *CsCPSF30* may be the upstream factors that activate the AS regulatory mechanism and further enhance the resistance of tea plants under abiotic stresses through regulating the transcript abundance of AS-induced isoforms.

Similar to the effects of abiotic stress on tea plants, FL were exposed to various abiotic stresses during the withering stage. Therefore, the underlying mechanism of m6A regulatory genes during the withering process also needs in-depth dissection. In this study, almost all of m6A eraser genes were insensitive after withering treatments, whereas the expression level of *MTC* was dramatically plummeted at IW and SW (**Figure 10**). In contrast, the transcript levels of six m6A eraser genes and three m6A reader genes were substantially elevated in IW and SW than in FL. Consistent with the environmental stress, withering also significantly altered the transcript levels of m6A regulatory genes. In IW vs. SW comparison, the up-regulation of m6A gene expression in SW may be due to the fact that solar-withering accelerated the dehydration of tea leaves, which is more severe than the stress experienced by leaves withered indoors. Reportedly, epigenetic mechanisms are widely implicated in abiotic stress response, including high temperature and UV radiation (Chang et al., 2020). Concomitantly, the significant alteration in global m6A level was detected after high-temperature and UV radiation treatments (Xiang et al., 2017; Scutenaire et al., 2018; Li et al., 2020c; Liu et al., 2020). Therefore, we speculated that m6A regulatory genes with a different expression between these two withering treatments may play the roles in response to the high-temperature and UV radiation. Additionally, it was noteworthy that *CsECT8* and *CsCPSF30* were also highly

expressed in SW than in FL and IW, suggesting that the withering process may also produce a large number of AS events. As expected, we also observed that the number of AS events in SW was tremendously higher than that of FL and IW, clearly indicating that transcript abundance of these two genes was positively correlated with AS number. It has also been reported that AS is not only considered to be a vital role in response to various environmental stresses but also involved in the biosynthesis of secondary metabolites (Yuan et al., 2009; Xu et al., 2017; Liu et al., 2018). Flavonoids are characteristic metabolites associated with the bitterness and astringency of tea flavor, and their accumulation in tea plants has also been found to be regulated by AS events (Zhu et al., 2018b). Moreover, a previous study found that the flavonoid content in SW was significantly lower than that in FL and IW (Zhu et al., 2019). Accordingly, we speculated that m6A regulatory genes may be implicated in flavonoid metabolism through AS regulatory mechanism, thereby affecting the formation of tea flavor during the withering process. To validate this hypothesis, we performed the gene silencing on representative m6A regulatory genes (*CsMTC*, *CsALKBH9*, and *CsECT8*), and examined the flavonoid content in the related gene-silenced tea leaves, respectively. We observed that only the downregulation of *CsECT8* significantly suppressed the flavonoid accumulation after *CsECT8*-silenced treatment (**Figure 12**). These results hinted that, combined with the inhibition of flavonoid biosynthesis triggered by the withering process, high expression levels of m6A reader genes were considered to be mainly responsible for the suppression of flavonoid biosynthesis *via* modulating AS regulatory mechanism. Simultaneously, downregulation of m6A writer genes and upregulation of m6A eraser genes also synergistically reduced the flavonoid content. In addition, previous reports have shown that decreased flavonoid content may help form a weakly bitterness and mellow taste in tea infusions (Scharbert et al., 2004; Zeng et al., 2020). Consequently, m6A regulatory genes may also play crucial roles in improving the tea palatability during the withering process, which also confirms that solar-withering is superior to indoor-withering regarding the development of a premium flavor in oolong tea.

The Complex Interplay Between RNA Methylation and DNA Methylation Contributes to the Flavor of Oolong Tea

In the central dogma, RNA is a bridge connecting DNA and protein to flow genetic information. Previous reports have shown that DNA methylation modifications occur on genomic DNA, and the modified DNA may be subject to RNA methylation for another round of reversible chemical modifications after being transcribed into RNA (Fu et al., 2014). Furthermore, our results showed that overall levels of 5mC and m6A contained a similar dynamic trend, and both of them have declined significantly after withering (**Figure 11**). It is noteworthy that the expression levels of several RNA MT genes were positively correlated with those of DNA MT genes. Likewise, the transcript levels of some RNA demethylase genes and DNA demethylase genes were highly correlated during tea-withering. Therefore, we speculated that there may exist a complex correlation between RNA methylation and DNA methylation during tea-withering process. Remarkably, the suppression of *CsMTC* significantly reduced m6A and 5mC levels, whereas both m6A and 5mC levels were markedly increased after *CsALKBH9*-silenced treatment. These results suggested that significant changes in the expression levels of m6A writer and eraser genes were not only involved in regulating the m6A level but also involved in modulating 5mC level.

As previously reported, the promoter regions of major *SlALKBHs* in tomato harbored distinct differentially DNA methylated regions, and hypermethylation of *SlALKBHs* substantially repressed their transcript levels (Zhou et al., 2019a). Meanwhile, accumulating evidence revealed that DNA methylation is highly interconnected with histone modifications at the posttranscriptional level (Sonmez et al., 2011; Jabre et al., 2019; Tian et al., 2019). More specifically, H3 methylation and DNA methylation in rice have a synergistic effect on suppressing gene expression (Zhou et al., 2016). Reportedly, RNA methylation is considered to be associated with chromatin remodeling *via* the combination of *ALKBH10* with multiple H3 modification markers (Jeong et al., 2009; Scarrow et al., 2020). These findings indicated that DNA methylation can be linked with RNA methylation through complex interactions. In addition, it is evident from a previous study that RNA demethylase genes can mediate the m6A modification status of DNA demethylase genes, thereby modulating its mRNA abundance, while DNA demethylase genes can influence the DNA methylation levels in the promoter regions of RNA demethylation genes (Zhou et al., 2019a). Data from this study also showed that transcript abundance of RNA demethylase was positively correlated with that of DNA demethylase genes during the withering process, whereas the expression levels of these demethylase genes were negatively correlated with the 5mC level and m6A level, respectively. Therefore, high expression levels of DNA demethylase genes in SW can stimulate the transcription of RNA demethylase genes by removing the DNA methylation marks, thereby indirectly inhibiting the flavonoid biosynthesis and improving the palatability of oolong tea. This helps to explain why solar-withering is beneficial to the production of high-quality oolong tea. Accordingly, we inferred that RNA methylation and DNA methylation formed a negative feedback by interacting with each other's methylation regulatory genes, and the intertwined connection between DNA methylation and RNA methylation contributed to oolong tea flavor. In summary, a possible model is proposed to explain the biological functions of m6A regulatory genes in resistance against the environmental stresses and tea-withering stage (**Figure 13**).

CONCLUSION

On the basis of the chromosome-scale genome of tea plants, we conducted a comprehensive genome-wide survey of m6A regulatory genes in tea plants for the first time. A total of 34 m6A regulatory genes were ultimately identified and grouped

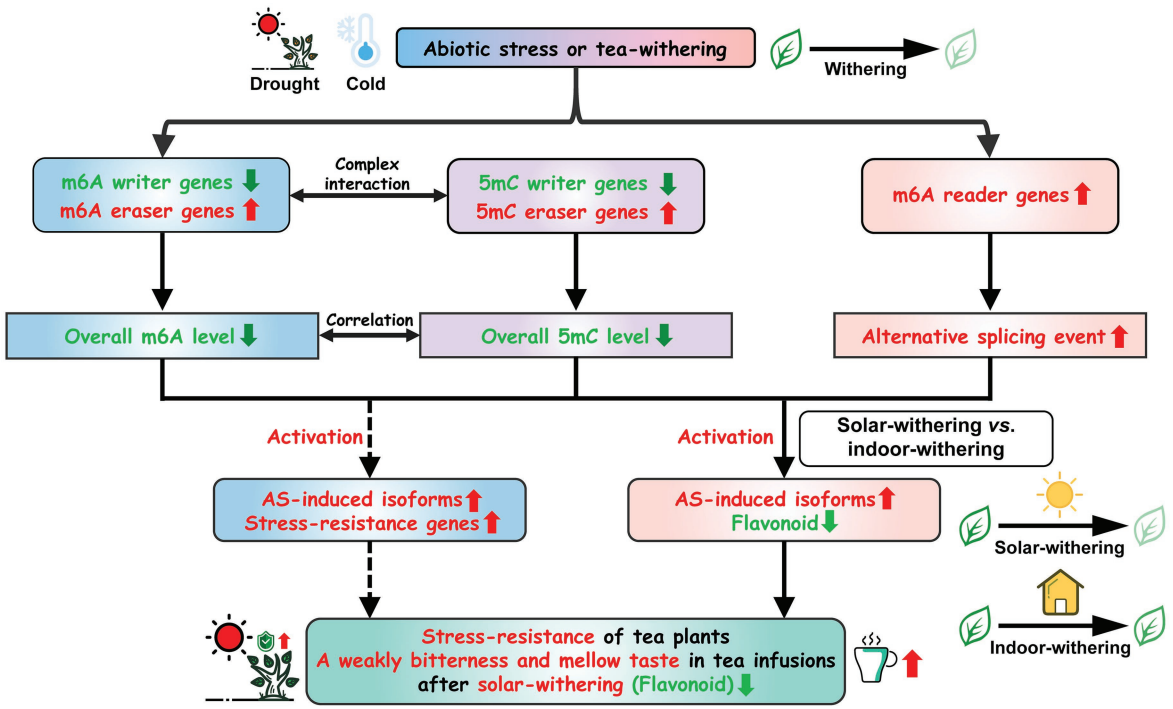


FIGURE 13 | Schematic model for the roles of m6A regulatory genes in tea plants under abiotic stresses and tea-withering. Arrows represent the direct interaction; dotted arrows represent the indirect interaction.

into three categories, namely, m6A writers, erasers, and readers. Then, we systematically analyzed chromosomal distribution, and gene duplication, and evolutionary selection of these m6A regulatory genes. In total, 30 m6A regulatory genes were randomly distributed on 13 chromosomes, and the remaining four genes were located on the unanchored contigs. We also found that segmental duplication and WGD events are the main contributors to the expansion of m6A regulatory genes. Additionally, gene structure analysis revealed instead of variation in conserved domain and motif, the gain or loss of exons and introns in gene sequence may contribute to the functional diversification of m6A regulatory genes. Subsequently, we detected the expression patterns of the identified m6A regulatory genes under environmental stresses and the tea-withering process. The results suggested that the m6A regulatory genes act as essential roles in resistance against the environmental stresses and tea-withering stage. Remarkably, we found that RNA methylation and DNA methylation formed a negative feedback by interacting with each other's methylation regulatory genes, and high expression levels of DNA demethylase genes can stimulate the transcription of RNA demethylase genes by removing the DNA methylation marks, thereby indirectly inhibiting the flavonoid biosynthesis and improving the palatability of oolong tea. This study provided a solid framework for exploring the diverse functions of m6A regulatory genes in tea plants under environmental stresses and opened up new perspectives for understanding m6A-mediated regulatory mechanism on the improvement of tea palatability during the withering stage of postharvest processing.

DATA AVAILABILITY STATEMENT

The original contributions presented in the study are included in the article/**Supplementary Material**, further inquiries can be directed to the corresponding authors.

AUTHOR CONTRIBUTIONS

YG, ZL, and CZhu conceived and designed the study. YG, CZhu, and SZ performed the experiments and wrote the manuscript. YG, CZhu, SZ, CZhou, SX, GC, CT, and KX analyzed the experimental data. CZhu, SZ, CZhou, and YL performed the plant treatments and revised the manuscript. All authors have read and approved the manuscript.

FUNDING

This work was supported by the Earmarked Fund for China Agriculture Research System (CARS-19), the Scientific Research Foundation of Graduate School of Fujian Agriculture and Forestry University (324-1122yb070), the Scientific Research Foundation of Horticulture College of Fujian Agriculture and Forestry University (2019B01), the Rural Revitalization Tea Industry Technical Service Project of Fujian Agriculture and Forestry University (11899170145), the "Double First-Class" scientific and technological innovation capacity and enhancement cultivation plan of Fujian

Agriculture and Forestry University (KSYLP004), 6.18 Tea Industry Technology Branch of Collaborative Innovation Institute (K1520001A), Fujian Agriculture and Forestry University Construction Project for Technological Innovation and Service System of Tea Industry Chain (K1520005A01), and the Construction of Plateau Discipline of Fujian Province (102/71201801101).

SUPPLEMENTARY MATERIAL

The Supplementary Material for this article can be found online at: https://www.frontiersin.org/articles/10.3389/fpls.2021.702303/full#supplementary-material

Supplementary Figure S1 | Sequence logos of conserved motifs in m6A regulatory genes **(A)** m6A writer genes; **(B)** m6A eraser genes; **(C)** m6A reader genes.

REFERENCES

Addepalli, B., and Hunt, A. G. (2007). A novel endonuclease activity associated with the *Arabidopsis* ortholog of the 30-kDa subunit of cleavage and polyadenylation specificity factor. *Nucleic Acids Res.* 35, 4453–4463. doi: 10.1093/nar/gkm457

Anderson, S. J., Kramer, M. C., Gosai, S. J., Yu, X., Vandivier, L. E., Nelson, A. D., et al. (2018). N^6-methyladenosine inhibits local ribonucleolytic cleavage to stabilize mRNAs in *Arabidopsis*. *Cell Rep.* 25, 1146–1157. doi: 10.1016/j.celrep.2018.10.020

Arribas-Hernández, L., Bressendorff, S., Hansen, M. H., Poulsen, C., Erdmann, S., and Brodersen, P. (2018). An m^6A-YTH module controls developmental timing and morphogenesis in *Arabidopsis*. *Plant Cell* 30, 952–967. doi: 10.1105/tpc.17.00833

Artimo, P., Jonnalagedda, M., Arnold, K., Baratin, D., Csardi, G., de Castro, E., et al. (2012). ExPASy: SIB bioinformatics resource portal. *Nucleic Acids Res.* 40, W597–W603. doi: 10.1093/nar/gks400

Bailey, T. L., Boden, M., Buske, F. A., Frith, M., Grant, C. E., Clementi, L., et al. (2009). MEME suite: tools for motif discovery and searching. *Nucleic Acids Res.* 37, W202–W208. doi: 10.1093/nar/gkp335

Berardini, T. Z., Reiser, L., Li, D. H., Mezheritsky, Y., Muller, R., Strait, E., et al. (2015). The arabidopsis information resource: making and mining the "gold standard" annotated reference plant genome. *Genesis* 53, 474–485. doi: 10.1002/dvg.22877

Bombarely, A., Menda, N., Tecle, I. Y., Buels, R. M., Strickler, S., Fischer-York, T., et al. (2010). The sol genomics network (solgenomics.net): growing tomatoes using Perl. *Nucleic Acids Res.* 39, D1149–D1155. doi: 10.1093/nar/gkq866

Chang, Y. N., Zhu, C., Jiang, J., Zhang, H. M., Zhu, J. K., and Duan, C. G. (2020). Epigenetic regulation in plant abiotic stress responses. *J. Integr. Plant Biol.* 62, 563–580. doi: 10.1111/jipb.12901

Chen, C. J., Chen, H., Zhang, Y., Thomas, H. R., Frank, M. H., He, Y. H., et al. (2020a). TBtools: an integrative toolkit developed for interactive analyses of big biological data. *Mol. Plant* 13, 1194–1202. doi: 10.1016/j.molp.2020.06.009

Chen, Q. H., Hu, S. L., Guo, F., Zhao, H., Wang, M. L., Ni, D. J., et al. (2021). Characterization of the *SET DOMAIN GROUP* gene family members in *Camellia sinensis* and functional analysis of the *SDG43* gene in abiotic stresses. *Environ. Exp. Bot.* 182:104306. doi: 10.1016/j.envexpbot.2020.104306

Chen, M. X., Zhang, K. L., Zhang, M., Das, D., Fang, Y. M., Dai, L., et al. (2020b). Alternative splicing and its regulatory role in woody plants. *Tree Physiol.* 40, 1475–1486. doi: 10.1093/treephys/tpaa076

Chou, K. C., and Shen, H. B. (2010). Plant-mPLoc: a top-down strategy to augment the power for predicting plant protein subcellular localization. *PLoS One* 5:e11335. doi: 10.1371/journal.pone.0011335

Cui, P., and Xiong, L. M. (2015). Environmental stress and pre-mRNA splicing. *Mol. Plant* 8, 1302–1303. doi: 10.1016/j.molp.2015.07.006

Defoort, J., Van de Peer, Y., and Carretero-Paulet, L. (2019). The evolution of gene duplicates in angiosperms and the impact of protein-protein interactions and the mechanism of duplication. *Genome Biol. Evol.* 11, 2292–2305. doi: 10.1093/gbe/evz156

Ding, Y. Q., Wang, Y., Qiu, C., Qian, W. J., Xie, H., and Ding, Z. T. (2020). Alternative splicing in tea plants was extensively triggered by drought, heat and their combined stresses. *PeerJ* 8:e8258. doi: 10.7717/peerj.8258

Dominissini, D., Moshitch-Moshkovitz, S., Schwartz, S., Salmon-Divon, M., Ungar, L., Osenberg, S., et al. (2012). Topology of the human and mouse m^6A RNA methylomes revealed by m^6A-seq. *Nature* 485, 201–206. doi: 10.1038/nature11112

Duan, H. C., Wei, L. H., Zhang, C., Wang, Y., Chen, L., Lu, Z., et al. (2017). ALKBH10B is an RNA N^6-methyladenosine demethylase affecting *Arabidopsis* floral transition. *Plant Cell* 29, 2995–3011. doi: 10.1105/tpc.16.00912

Filichkin, S., Priest, H. D., Megraw, M., and Mockler, T. C. (2015). Alternative splicing in plants: directing traffic at the crossroads of adaptation and environmental stress. *Curr. Opin. Plant Biol.* 24, 125–135. doi: 10.1016/j.pbi.2015.02.008

Fu, Y., Dominissini, D., Rechavi, G., and He, C. (2014). Gene expression regulation mediated through reversible m^6A RNA methylation. *Nat. Rev. Genet.* 15, 293–306. doi: 10.1038/nrg3724

Guo, Y. Q., Zhao, S. S., Zhu, C., Chang, X. J., Yue, C., Wang, Z., et al. (2017). Identification of drought-responsive miRNAs and physiological characterization of tea plant (*Camellia sinensis* L.) under drought stress. *BMC Plant Biol.* 17:211. doi: 10.1186/s12870-017-1172-6

Hu, C. J., Li, D., Ma, Y. X., Zhang, W., Lin, C., Zheng, X. Q., et al. (2018). Formation mechanism of the oolong tea characteristic aroma during bruising and withering treatment. *Food Chem.* 269, 202–211. doi: 10.1016/j.foodchem.2018.07.016

Hu, J. Z., Manduzio, S., and Kang, H. S. (2019). Epitranscriptomic RNA methylation in plant development and abiotic stress responses. *Front. Plant Sci.* 10:500. doi: 10.3389/fpls.2019.00500

Jabre, I., Reddy, A. S., Kalyna, M., Chaudhary, S., Khokhar, W., Byrne, L. J., et al. (2019). Does co-transcriptional regulation of alternative splicing mediate plant stress responses? *Nucleic Acids Res.* 47, 2716–2726. doi: 10.1093/nar/gkz121

Jeong, J. H., Song, H. R., Ko, J. H., Jeong, Y. M., Kwon, Y. E., Seol, J. H., et al. (2009). Repression of *FLOWERING LOCUS T* chromatin by functionally redundant histone H3 lysine 4 demethylases in *Arabidopsis*. *PLoS One* 4:e8033. doi: 10.1371/journal.pone.0008033

Kim, D., Langmead, B., and Salzberg, S. L. (2015). HISAT: a fast spliced aligner with low memory requirements. *Nat. Methods* 12, 357–360. doi: 10.1038/nmeth.3317

Knuckles, P., Lence, T., Haussmann, I. U., Jacob, D., Kreim, N., Carl, S. H., et al. (2018). Zc3h13/Flacc is required for adenosine methylation by bridging the mRNA-binding factor Rbm15/Spenito to the m^6A machinery component Wtap/Fl(2)d. *Genes Dev.* 32, 415–429. doi: 10.1101/gad.309146.117

Kramer, M. C., Janssen, K. A., Palos, K., Nelson, A. D. L., Vandivier, L. E., Garcia, B. A., et al. (2020). N^6-methyladenosine and RNA secondary structure affect transcript stability and protein abundance during systemic salt stress in *Arabidopsis*. *Plant Direct* 4:e239. doi: 10.1002/pld3.239

Kumar, S., Stecher, G., Li, M., Knyaz, C., and Tamura, K. (2018). MEGA X: molecular evolutionary genetics analysis across computing platforms. *Mol. Biol. Evol.* 35, 1547–1549. doi: 10.1093/molbev/msy096

Lescot, M., Déhais, P., Thijs, G., Marchal, K., Moreau, Y., Van de Peer, Y., et al. (2002). PlantCARE, a database of plant *cis*-acting regulatory elements and a portal to tools for *in silico* analysis of promoter sequences. *Nucleic Acids Res.* 30, 325–327. doi: 10.1093/nar/30.1.325

Letunic, I., and Bork, P. (2017). 20 years of the SMART protein domain annotation resource. *Nucleic Acids Res.* 46, D493–D496. doi: 10.1093/nar/gkx922

Li, W. Z., Cowley, A., Uludag, M., Gur, T., McWilliam, H., Squizzato, S., et al. (2015). The EMBL-EBI bioinformatics web and programmatic tools framework. *Nucleic Acids Res.* 43, W580–W584. doi: 10.1093/nar/gkv279

Li, B., and Dewey, C. N. (2011). RSEM: accurate transcript quantification from RNA-Seq data with or without a reference genome. *BMC Bioinform.* 12:323. doi: 10.1186/1471-2105-12-323

Li, M. S., Lu, J., Tao, M. M., Li, M. R., Yang, H., Xia, E. H., et al. (2020a). Genome-wide identification of seven polyamine oxidase genes in *Camellia sinensis* (L.) and their expression patterns under various abiotic stresses. *Front. Plant Sci.* 11:544933. doi: 10.3389/fpls.2020.544933

Li, Y. Y., Mi, X. Z., Zhao, S. Q., Zhu, J. Y., Guo, R., Xia, X. B., et al. (2020b). Comprehensive profiling of alternative splicing landscape during cold acclimation in tea plant. *BMC Genomics* 21:65. doi: 10.1186/s12864-020-6491-6

Li, D., Zhu, X. H., Li, Y. X., and Zeng, X. Y. (2020c). Novel insights into the roles of RNA N^6-methyladenosine modification in regulating gene expression during environmental exposures. *Chemosphere* 261:127757. doi: 10.1016/j.chemosphere.2020.127757

Liang, Z., Riaz, A., Chachar, S., Ding, Y. K., Du, H., and Gu, X. F. (2020). Epigenetic modifications of mRNA and DNA in plants. *Mol. Plant* 13, 14–30. doi: 10.1016/j.molp.2019.12.007

Liu, G. F., Liu, J. J., He, Z. R., Wang, F. M., Yang, H., Yan, Y. F., et al. (2018). Implementation of *CsLIS/NES* in linalool biosynthesis involves transcript splicing regulation in *Camellia sinensis*. *Plant Cell Environ.* 41, 176–186. doi: 10.1111/pce.13080

Liu, G. F., Wang, J., and Hou, X. L. (2020). Transcriptome-wide N^6-methyladenosine (m^6A) methylome profiling of heat stress in Pak-choi (*Brassica rapa ssp. chinensis*). *Plan. Theory* 9:1080. doi: 10.3390/plants9091080

Livak, K. J., and Schmittgen, T. D. (2001). Analysis of relative gene expression data using real-time quantitative PCR and the $2^{-\Delta\Delta CT}$ method. *Methods* 25, 402–408. doi: 10.1006/meth.2001.1262

Lu, S. N., Wang, J. Y., Chitsaz, F., Derbyshire, M. K., Geer, R. C., Gonzales, N. R., et al. (2019). CDD/SPARCLE: the conserved domain database in 2020. *Nucleic Acids Res.* 48, D265–D268. doi: 10.1093/nar/gkz991

Ma, J. F., Tamai, K., Yamaji, N., Mitani, N., Konishi, S., Katsuhara, M., et al. (2006). A silicon transporter in rice. *Nature* 440, 688–691. doi: 10.1038/nature04590

Madeira, F., Park, Y. M., Lee, J., Buso, N., Gur, T., Madhusoodanan, N., et al. (2019). The EMBL-EBI search and sequence analysis tools APIs in 2019. *Nucleic Acids Res.* 47, W636–W641. doi: 10.1093/nar/gkz268

Martínez-Pérez, M., Aparicio, F., López-Gresa, M. P., Bellés, J. M., Sánchez-Navarro, J. A., and Pallás, V. (2017). *Arabidopsis* m^6A demethylase activity modulates viral infection of a plant virus and the m^6A abundance in its genomic RNAs. *Proc. Natl. Acad. Sci. U. S. A.* 114, 10755–10760. doi: 10.1073/pnas.1703139114

Merret, R., Nagarajan, V. K., Carpentier, M. C., Park, S., Favory, J. J., Descombin, J., et al. (2015). Heat-induced ribosome pausing triggers mRNA co-translational decay in *Arabidopsis thaliana*. *Nucleic Acids Res.* 43, 4121–4132. doi: 10.1093/nar/gkv234

Meyer, K. D., Patil, D. P., Zhou, J., Zinoviev, A., Skabkin, M. A., Elemento, O., et al. (2015). 5' UTR m6A promotes cap-independent translation. *Cell* 163, 999–1010. doi: 10.1016/j.cell.2015.10.012

Miao, Z. Y., Zhang, T., Qi, Y. H., Song, J., Han, Z. X., and Ma, C. (2020). Evolution of the RNA N^6-methyladenosine methylome mediated by genomic duplication. *Plant Physiol.* 182:345. doi: 10.1104/pp.19.00323

Pontier, D., Picart, C., El Baidouri, M., Roudier, F., Xu, T., Lahmy, S., et al. (2019). The m6A pathway protects the transcriptome integrity by restricting RNA chimera formation in plants. *Life Sci. Alliance* 2:e201900393. doi: 10.26508/lsa.201900393

Roundtree, I. A., Evans, M. E., Pan, T., and He, C. (2017). Dynamic RNA modifications in gene expression regulation. *Cell* 169, 1187–1200. doi: 10.1016/j.cell.2017.05.045

Růžička, K., Zhang, M., Campilho, A., Bodi, Z., Kashif, M., Saleh, M., et al. (2017). Identification of factors required for m6A mRNA methylation in *Arabidopsis* reveals a role for the conserved E3 ubiquitin ligase HAKAI. *New Phytol.* 215, 157–172. doi: 10.1111/nph.14586

Scarrow, M., Chen, N., and Sun, G. L. (2020). Insights into the N6-methyladenosine mechanism and its functionality: progress and questions. *Crit. Rev. Biotechnol.* 40, 639–652. doi: 10.1080/07388551.2020.1751059

Scharbert, S., Holzmann, N., and Hofmann, T. (2004). Identification of the astringent taste compounds in black tea infusions by combining instrumental analysis and human bioresponse. *J. Agric. Food Chem.* 52, 3498–3508. doi: 10.1021/jf049802u

Scutenaire, J., Deragon, J. M., Jean, V., Benhamed, M., Raynaud, C., Favory, J. J., et al. (2018). The YTH domain protein ECT2 is an m^6A reader required for normal trichome branching in *Arabidopsis*. *Plant Cell* 30, 986–1005. doi: 10.1105/tpc.17.00854

Shen, W., Li, H., Teng, R. M., Wang, Y. X., Wang, W. L., and Zhuang, J. (2019b). Genomic and transcriptomic analyses of HD-zip family transcription factors and their responses to abiotic stress in tea plant (*Camellia sinensis*). *Genomics* 111, 1142–1151. doi: 10.1016/j.ygeno.2018.07.009

Shen, L. S., Liang, Z., Gu, X. F., Chen, Y., Teo, Z. W., Hou, X. L., et al. (2016). N6-methyladenosine RNA modification regulates shoot stem cell fate in *Arabidopsis*. *Dev. Cell* 38, 186–200. doi: 10.1016/j.devcel.2016.06.008

Shen, S. H., Park, J. W., Lu, Z. X., Lin, L., Henry, M. D., Wu, Y. N., et al. (2014). RMATS: robust and flexible detection of differential alternative splicing from replicate RNA-Seq data. *Proc. Natl. Acad. Sci. U. S. A.* 111, E5593–E5601. doi: 10.1073/pnas.1419161111

Shen, J. Z., Zhang, D. Y., Zhou, L., Zhang, X. Z., Liao, J. R., Duan, Y., et al. (2019a). Transcriptomic and metabolomic profiling of *Camellia sinensis* L. cv. 'Suchazao' exposed to temperature stresses reveals modification in protein synthesis and photosynthetic and anthocyanin biosynthetic pathways. *Tree Physiol.* 39, 1583–1599. doi: 10.1093/treephys/tpz059

Śledź, P., Jinek, M., and Nilsen, T. W. (2016). Structural insights into the molecular mechanism of the m6A writer complex. *eLife* 5:e18434. doi: 10.7554/eLife.18434

Sonmez, C., Bäurle, I., Magusin, A., Dreos, R., Laubinger, S., Weigel, D., et al. (2011). RNA 3' processing functions of *Arabidopsis* FCA and FPA limit intergenic transcription. *Proc. Natl. Acad. Sci. U. S. A.* 108, 8508–8513. doi: 10.1073/pnas.1105334108

Subramanian, B., Gao, S. H., Lercher, M. J., Hu, S. N., and Chen, W. H. (2019). Evolview v3: a webserver for visualization, annotation, and management of phylogenetic trees. *Nucleic Acids Res.* 47, W270–W275. doi: 10.1093/nar/gkz357

Sun, W. J., Ma, Z. T., and Liu, M. Y. (2020). Cytochrome P450 family: genome-wide identification provides insights into the rutin synthesis pathway in Tartary buckwheat and the improvement of agricultural product quality. *Int. J. Biol. Macromol.* 164, 4032–4045. doi: 10.1016/j.ijbiomac.2020.09.008

Szklarczyk, D., Gable, A. L., Lyon, D., Junge, A., Wyder, S., Huerta-Cepas, J., et al. (2018). STRING v11: protein-protein association networks with increased coverage, supporting functional discovery in genome-wide experimental datasets. *Nucleic Acids Res.* 47, D607–D613. doi: 10.1093/nar/gky1131

Tian, R. Z., Yang, Y., and Chen, M. H. (2020). Genome-wide survey of the amino acid transporter gene family in wheat (*Triticum aestivum* L.): identification, expression analysis and response to abiotic stress. *Int. J. Biol. Macromol.* 162, 1372–1387. doi: 10.1016/j.ijbiomac.2020.07.302

Tian, Y. K., Zheng, H., Zhang, F., Wang, S. L., Ji, X. R., Xu, C., et al. (2019). PRC2 recruitment and H3K27me3 deposition at *FLC* require FCA binding of *COOLAIR*. *Sci. Adv.* 5:u7246. doi: 10.1126/sciadv.aau7246

Wang, P., Doxtader, K. A., and Nam, Y. (2016a). Structural basis for cooperative function of Mettl3 and Mettl14 methyltransferases. *Mol. Cell* 63, 306–317. doi: 10.1016/j.molcel.2016.05.041

Wang, Y. C., Lu, Q. H., Xiong, F., Hao, X. Y., Wang, L., Zheng, M. X., et al. (2020). Genome-wide identification, characterization, and expression analysis of nucleotide-binding leucine-rich repeats gene family under environmental stresses in tea (*Camellia sinensis*). *Genomics* 112, 1351–1362. doi: 10.1016/j.ygeno.2019.08.004

Wang, Y. P., Tang, H. B., DeBarry, J. D., Tan, X., Li, J. P., Wang, X. Y., et al. (2012). MCScanX: a toolkit for detection and evolutionary analysis of gene synteny and collinearity. *Nucleic Acids Res.* 40:e49. doi: 10.1093/nar/gkr1293

Wang, W. D., Xin, H. H., Wang, M. L., Ma, Q. P., Wang, L., Kaleri, N. A., et al. (2016b). Transcriptomic analysis reveals the molecular mechanisms of drought-stress-induced decreases in *Camellia sinensis* leaf quality. *Front. Plant Sci.* 7:385. doi: 10.3389/fpls.2016.00385

Wang, X., Zhao, B. S., Roundtree, I. A., Lu, Z. K., Han, D. L., Ma, H. H., et al. (2015). N^6-methyladenosine modulates messenger RNA translation efficiency. *Cell* 161, 1388–1399. doi: 10.1016/j.cell.2015.05.014

Wang, Y., Zheng, P. C., Liu, P. P., Song, X. W., Guo, F., Li, Y. Y., et al. (2019). Novel insight into the role of withering process in characteristic flavor formation of teas using transcriptome analysis and metabolite profiling. *Food Chem.* 272, 313–322. doi: 10.1016/j.foodchem.2018.08.013

Wei, C. L., Yang, H., Wang, S. B., Zhao, J., Liu, C., Gao, L. P., et al. (2018). Draft genome sequence of *Camellia sinensis var. sinensis* provides insights into the evolution of the tea genome and tea quality. *Proc. Natl. Acad. Sci. U. S. A.* 115, E4151–E4158. doi: 10.1073/pnas.1719622115

Xia, E. H., Li, F. D., Tong, W., Li, P. H., Wu, Q., Zhao, H. J., et al. (2019). Tea plant information archive: a comprehensive genomics and bioinformatics platform for tea plant. *Plant Biotechnol. J.* 17, 1938–1953. doi: 10.1111/pbi.13111

Xia, E. H., Tong, W., Hou, Y., An, Y. L., Chen, L. B., Wu, Q., et al. (2020). The reference genome of tea plant and resequencing of 81 diverse accessions

provide insights into its genome evolution and adaptation. *Mol. Plant* 13, 1013–1026. doi: 10.1016/j.molp.2020.04.010

Xiang, Y., Laurent, B., Hsu, C. H., Nachtergaele, S., Lu, Z. K., Sheng, W. Q., et al. (2017). RNA m^{6}A methylation regulates the ultraviolet-induced DNA damage response. *Nature* 543, 573–576. doi: 10.1038/nature21671

Xiao, W., Adhikari, S., Dahal, U., Chen, Y. S., Hao, Y. J., Sun, B. F., et al. (2016). Nuclear m^{6}A reader YTHDC1 regulates mRNA splicing. *Mol. Cell* 61, 507–519. doi: 10.1016/j.molcel.2016.01.012

Xu, C., Wang, X., Liu, K., Roundtree, I. A., Tempel, W., Li, Y. J., et al. (2014). Structural basis for selective binding of m^{6}A RNA by the YTHDC1 YTH domain. *Nat. Chem. Biol.* 10, 927–929. doi: 10.1038/nchembio.1654

Xu, Q. S., Zhu, J. Y., Zhao, S. Q., Hou, Y., Li, F. D., Tai, Y. L., et al. (2017). Transcriptome profiling using single-molecule direct RNA sequencing approach for in-depth understanding of genes in secondary metabolism pathways of *Camellia sinensis*. *Front. Plant Sci.* 8:1205. doi: 10.3389/fpls.2017.01205

Yang, Y., Hsu, P. J., Chen, Y. S., and Yang, Y. G. (2018). Dynamic transcriptomic m6A decoration: writers, erasers, readers and functions in RNA metabolism. *Cell Res.* 28, 616–624. doi: 10.1038/s41422-018-0040-8

Yuan, Y., Chung, J. D., Fu, X. Y., Johnson, V. E., Ranjan, P., Booth, S. L., et al. (2009). Alternative splicing and gene duplication differentially shaped the regulation of isochorismate synthase in *Populus* and *Arabidopsis*. *Proc. Natl. Acad. Sci. U. S. A.* 106, 22020–22025. doi: 10.1073/pnas.0906869106

Yue, H., Nie, X. J., Yan, Z. G., and Song, W. N. (2019). N6-methyladenosine regulatory machinery in plants: composition, function and evolution. *Plant Biotechnol. J.* 17, 1194–1208. doi: 10.1111/pbi.13149

Zeng, L. T., Zhou, X. C., Su, X. G., and Yang, Z. Y. (2020). Chinese oolong tea: An aromatic beverage produced under multiple stresses. *Trends Food Sci. Technol.* 106, 242–253. doi: 10.1016/j.tifs.2020.10.001

Zhang, X. X., Li, X. X., Zhao, R., Zhou, Y., and Jiao, Y. N. (2020b). Evolutionary strategies drive a balance of the interacting gene products for the *CBL* and *CIPK* gene families. *New Phytol.* 226, 1506–1516. doi: 10.1111/nph.16445

Zhang, C. Y., Wang, M. H., Chen, J. J., Gao, X. Z., Shao, C. Y., Lv, Z. D., et al. (2020a). Survival strategies based on the hydraulic vulnerability segmentation hypothesis, for the tea plant [*Camellia sinensis*(L.) O. Kuntze] in long-term drought stress condition. *Plant Physiol. Biochem.* 156, 484–493. doi: 10.1016/j.plaphy.2020.09.034

Zhao, M. Y., Zhang, N., Gao, T., Jin, J. Y., Jing, T. T., Wang, J. M., et al. (2020). Sesquiterpene glucosylation mediated by glucosyltransferase UGT91Q2 is involved in the modulation of cold stress tolerance in tea plants. *New Phytol.* 226, 362–372. doi: 10.1111/nph.16364

Zheng, H. X., Li, S. M., Zhang, X. S., and Sui, N. (2020). Functional implications of active N^6-methyladenosine in plants. *Front. Cell Dev. Biol.* 8:291. doi: 10.3389/fcell.2020.00291

Zhou, S. L., Liu, X. Y., Zhou, C., Zhou, Q. W., Zhao, Y., Li, G. L., et al. (2016). Cooperation between the H3K27me3 chromatin mark and non-CG methylation in epigenetic regulation. *Plant Physiol.* 172, 1131–1141. doi: 10.1104/pp.16.01238

Zhou, L. L., Tian, S. P., and Qin, G. Z. (2019a). RNA methylomes reveal the m^{6}A-mediated regulation of DNA demethylase gene *SlDML2* in tomato fruit ripening. *Genome Biol.* 20:156. doi: 10.1186/s13059-019-1771-7

Zhou, J., Wan, J., Gao, X. W., Zhang, X. Q., Jaffrey, S. R., and Qian, S. B. (2015). Dynamic m6A mRNA methylation directs translational control of heat shock response. *Nature* 526, 591–594. doi: 10.1038/nature15377

Zhou, J., Wan, J., Shu, X. E., Mao, Y. H., Liu, X. M., Yuan, X., et al. (2018). N6-methyladenosine guides mRNA alternative translation during integrated stress response. *Mol. Cell* 69, 636–647. doi: 10.1016/j.molcel.2018.01.019

Zhou, C. Z., Zhu, C., Fu, H. F., Li, X. Z., Chen, L., Lin, Y. L., et al. (2019b). Genome-wide investigation of *superoxide dismutase* (*SOD*) gene family and their regulatory miRNAs reveal the involvement in abiotic stress and hormone response in tea plant (*Camellia sinensis*). *PLoS One* 14:e223609. doi: 10.1371/journal.pone.0223609

Zhu, J. Y., Wang, X. W., Guo, L. X., Xu, Q. S., Zhao, S. Q., Li, F. D., et al. (2018a). Characterization and alternative splicing profiles of the lipoxygenase gene family in tea plant (*Camellia sinensis*). *Plant Cell Physiol.* 59, 1765–1781. doi: 10.1093/pcp/pcy091

Zhu, J. Y., Wang, X. W., Xu, Q. S., Zhao, S. Q., Tai, Y. L., and Wei, C. L. (2018b). Global dissection of alternative splicing uncovers transcriptional diversity in tissues and associates with the flavonoid pathway in tea plant (*Camellia sinensis*). *BMC Plant Biol.* 18:266. doi: 10.1186/s12870-018-1497-9

Zhu, C., Zhang, S. T., Fu, H. F., Zhou, C. Z., Chen, L., Li, X. Z., et al. (2019). Transcriptome and phytochemical analyses provide new insights into long non-coding RNAs modulating characteristic secondary metabolites of oolong tea (*Camellia sinensis*) in solar-withering. *Front. Plant Sci.* 10:1638. doi: 10.3389/fpls.2019.01638

Zhu, C., Zhang, S. T., Zhou, C. Z., Chen, L., Fu, H. F., Li, X. Z., et al. (2020). Genome-wide investigation and transcriptional analysis of cytosine-5 DNA methyltransferase and DNA demethylase gene families in tea plant (*Camellia sinensis*) under abiotic stress and withering processing. *PeerJ* 8:e8432. doi: 10.7717/peerj.8432

Conflict of Interest: The authors declare that the research was conducted in the absence of any commercial or financial relationships that could be construed as a potential conflict of interest.

Copyright © 2021 Zhu, Zhang, Zhou, Xie, Chen, Tian, Xu, Lin, Lai and Guo. This is an open-access article distributed under the terms of the Creative Commons Attribution License (CC BY). The use, distribution or reproduction in other forums is permitted, provided the original author(s) and the copyright owner(s) are credited and that the original publication in this journal is cited, in accordance with accepted academic practice. No use, distribution or reproduction is permitted which does not comply with these terms.

frontiers in Plant Science

ORIGINAL RESEARCH
published: 30 June 2021
doi: 10.3389/fpls.2021.698796

Effects of Soil Type on Trace Element Absorption and Fruit Quality of Pepper

*Zhoubin Liu[1,2,3], Yu Huang[1,2,3], Fangjun Tan[4], Wenchao Chen[4] and Lijun Ou[1,2,3]**

[1]College of Horticulture, Hunan Agricultural University, Changsha, China, [2]ERC for Germplasm Innovation and New Variety Breeding of Horticultural Crops, Changsha, China, [3]Key Laboratory of Vegetable Biology of Hunan Province, Changsha, China, [4]Vegetable Institution of Hunan Academy of Agricultural Science, Changsha, China

The inbred "SJ11-3" pepper was cultured in yellow brown soil, paddy soil, fluvo-aquic soil, and pastoral soil, and the factors affecting the absorption of trace elements and fruit quality were analyzed. The results showed that the physicochemical properties of the soils were significantly different, which led to differences in the nutritional quality of pepper fruits. The pH value had a significant effect on the absorption of trace elements in pepper. The increase of pH promoted the absorption of magnesium and molybdenum but inhibited the absorption of zinc, copper, manganese, and iron. The stepwise multivariable regression analysis showed that the amount of molybdenum in soil was the main factor affecting the total amino acid content of pepper. Total nitrogen, zinc, and copper were the main factors that contributed to the soluble sugar content of pepper, and the available potassium was the major determinant of the vitamin C content of pepper. This study provides new insight on the pepper fruit quality grown on different types of soil with varying levels of trace elements.

Keywords: pepper, soil, trace element, fruit quality, nutritional quality

OPEN ACCESS

Edited by:
Pei Xu,
China Jiliang University, China

Reviewed by:
Zhi Wei Wang,
Hainan University, China
Minghua Deng,
Yunnan Agricultural University, China

***Correspondence:**
Lijun Ou
ou9572@hunau.edu.cn

Specialty section:
This article was submitted to Crop and Product Physiology, a section of the journal Frontiers in Plant Science

Received: *22 April 2021*
Accepted: *31 May 2021*
Published: *30 June 2021*

Citation:
Liu Z, Huang Y, Tan F, Chen W and Ou L (2021) Effects of Soil Type on Trace Element Absorption and Fruit Quality of Pepper. Front. Plant Sci. 12:698796. doi: 10.3389/fpls.2021.698796

INTRODUCTION

Pepper is one of the main vegetable crops in China with an annual planting area of 1.33 million hm^2. The total economic output is more than 70 billion CNY per year, illustrating its economic significance in many provinces and cities in China (Ma, 2011). With the improvement of living standards, the nutritional value of peppers has received more and more attention. While fruit quality is a complex trait composed of many factors, the absorption, accumulation, and metabolic transformation of soluble solid nutrients, sugars, acids, vitamins, and some special substances during fruit development are important factors determining the flavor and nutritional quality as well as its commercial value. It is well known that the nutritional value of pepper is mainly determined by genetic factors and as well as the environment. As an important agro-ecological factor, the changes in the soil (pH, fertilizer efficiency, enzyme activity, and soil microbe) have an important impact on the quality of pepper.

Recently, research on the nutritional value of crops under different soil conditions (roots) has received increasing attention (Jansen et al., 2012; He et al., 2019). Bao et al. (2006) investigated the soil nutrient status of Newhall navel orange orchard in Hubei Province and its effect on fruit quality. They found a significant linear correlation between soluble solid

content and available P and available K content. Base application of selenium fertilizer can increase some essential amino acid content and total amino acid content in the forage and grain of buckwheat (Li et al., 2012). Zhang et al. (2015) demonstrated that nitrogen, phosphorus, and potassium combined with organic fertilizer could increase the content of vitamin C, soluble solids, soluble protein, and soluble sugar in tomato and augment yield. Moreover, Liu et al. (2012) reported that the soluble solid of kiwi fruit was negatively correlated with soil available magnesium and boron, soluble sugar was negatively correlated with soil available magnesium and manganese, and titratable acid was negatively correlated with soil organic matter. In addition, Kong et al. (2013) indicated that organic matter did not contribute to the synthesis of soluble solids and total amino acids. These findings suggest that the impact of soil on crop quality is highly complicated, and the higher efficacy of the fertilizer does not necessarily lead to improved quality.

At present, the traditional cultivation of peppers is mainly based on the theory of "more water and more fertilizer." Its practice probably can deteriorate the soil structure, reduce the function, waste resource, and cause water pollution and other issues that affect the nutritional quality and safety of pepper. Therefore, in this study, the relationship between different soil conditions and the quality of pepper was investigated by examining the physical and chemical properties, nutrient content, soil microbial and enzyme activities, the nutrient quality, and mineral nutrient absorption of different soil types. These results provide guidance for the improvement of pepper planting soil, proper fertilization, and the enhancement of the quality of pepper.

MATERIALS AND METHODS

Materials and Treatments

This experiment is based on the inbred line "SJ11-3" provided by the Hunan Provincial Vegetable Research Institute. It has long, spirally shaped fruit, good taste, and high vitamin C content, which is widely used in the breeding of screw pepper. It was planted from April to September 2016 in the yellow brown soil (Xiangyin County, 112°52' E, 28°14' N), paddy soil (Ningxiang County, 112°33' E, 28°16' N), pastoral soil (Changsha County, 113°4' E, 28°14' N), and fluvo-aquic soil (Changde City, 111°41' E, 29°1' N), and each soil was divided into three plots. The four soil types are distributed in the central and northern parts of Hunan Province with little difference in geographical location: longitude and latitude. Therefore, the temperature change, light intensity, and precipitation during the planting period were generally consistent, and there was no significant climate difference.[1] The tested pepper seeds were seeded in the plug tray after germination, and the seedlings with strong and consistent growth were obtained in the five-leaf period. For transplantation, 30 peppers were planted in each plot, and the row spacing × plant spacing was 40 cm × 40 cm. All the plants were planted in open field, and fertilization and water management were consistent during planting. After planting, the pepper green ripe fruits were obtained at 35 days after flowering, and 20 peppers were taken from each plot. Meanwhile, nine plants with picked peppers were selected and 200 g soil was taken from the roots of 0–15 cm deep of each plant. The obtained peppers and soil were frozen at −80°C by liquid nitrogen and used for the following experiments.

[1]http://hn.cma.gov.cn/

Determination of Physical and Chemical Properties

The pH value of soil was determined by potentiometric electrode method. The bulk density was quantified by the ring knife method. The contents of zinc, copper, manganese, and molybdenum in soil and pepper fruit were measured by inductively coupled plasma mass spectrometry method. The total nitrogen content in soil was determined by semi-micro Kay method. The content of nitrogen was examined by the alkali diffusion method. The content of total phosphorus was measured by $HClO_4$-H_2SO_4 digestion molybdenum ruthenium colorimetric method. The content of available phosphorus was calculated by sodium bicarbonate extraction-molybdenum ruthenium colorimetry. The total potassium content was determined by H_2SO_4-H_2O_2 digestion-flame photometric method. The available potassium content was quantified by ammonium acetate extraction-flame photometry.

The urease activity of soil was determined by sodium phenolate-sodium hypochlorite colorimetric method. The phosphatase activity was measured by the phenyl phosphonate colorimetric method. The invertase activity was quantified by 3,5-dinitrosalicylic acid colorimetric method. The catalase activity was examined by potassium permanganate titration. The enzyme activities are expressed as the amount of substance produced by the unit weight of air-dried soil during the culture period.

The soluble sugar of pepper fruit was determined by the anthrone colorimetric method. The total amino acid, vitamin E, and vitamin C were quantified by kit (Nanjing Institute of Bioengineering).

Analysis of Soil Microbial Diversity

Extraction of Total Soil Microbial DNA

The total soil microbial DNA was extracted with Soil DNA Extraction Kit (Stamford, CT, United States). The integrity of DNA was verified with 1% agarose gel electrophoresis. The concentration and purity of the extracted DNA were measured with Mini-Drop (Thermo Fisher Scientific, Waltham, MA, United States).

PCR Amplification and Sequencing

The extracted total DNA was used as the template for PCR amplification. Primers targeting V3 + V4 regions of bacterial 16S rDNA gene (F:5'-ACTCCTAC GGGAGGCAGCA-3'; R: 5'-GGACTACHVGGGTWTCTAAT-3') and primers targeting fungal ITS1 region (F: 5'-CTTGGTCATTTAGAGGAAGTAA-3'; R: 5'-GCTGCGT TCTTCATCGATGC-3') were designed by Biomarker Science and Technology Service (Beijing, China),

and V3 + V4 regions and ITS1 region were amplified with PCR, respectively. The PCR reaction system was as follows: pre-denaturation at 95°C for 5 min, followed by 25 cycles of denaturation at 95°C for 30 s, annealing at 50°C for 30 s, extension at 72°C for 40 s, and the final extension at 72°C for 7 min. The amplified DNA products were purified, quantified, and uniformed to form the sequencing library. The PCR-amplified DNA products were sequenced using Illumina MiSeq 2500 by Biomarker Science and Technology Service (Beijing, China).

DNA Sequencing Analysis

(1) Merge of PE Reads: The merger of the original sequences obtained was conducted with FLASH v1.2.7 software. According to the minimum overlap length of 10 bp, the maximal mismatched ratio that was allowed in the overlapping region was 0.2. Merge of reads of each sample was conducted, and the merger sequences were obtained, i.e., the original Tags data (Raw Tags). (2) Filtration of Tags: the Raw Tags obtained by merger were filtrated with Trimmomatic v0.33. The parameter was set as the 50 bp window. If the mean quantity value was lower than 20, the back-end nucleotide bases starting from the window were removed. After filtration and quantity control, the length of DNA fragments was shorter than 75% of the Tags. The high-quality Tags (Clean Tags) were obtained. (3) Removal of Chimera: the chimera sequences were identified and removed with UCHIME v4.2 software. Finally, the effective tags were obtained. UCLUST in QIIME (version 1.8.0) was used to conduct cluster analysis of Tags at the level of 97% similarity. OTU and RDP classification for all the sequences was conducted to obtain OTUs based on the bacterial and fungal taxonomic databases, and the numbers of OTU were calculated for statistical tests.

Data Analysis

In this study, the results were expressed as "mean ± standard error," and data analysis was performed using Excel 2010 and SPSS 17.0. The significance of multiple comparisons was determined by Duncan's test.

RESULTS

Differences in Physical and Chemical Properties of Different Soils

According to the soil pH and bulk weight grading standards, we found a significant difference in pH among the four types of soil: yellow brown soil, paddy soil, fluvo-aquic soil, and pastoral soil ($p < 0.05$), and the range was 4.20–6.42, all of which were acidic soils (**Table 1**). The paddy soil was strongly acidic, with the lowest pH. On the contrary, the pastoral soil was slightly acidic, and the pH value was significantly higher than that of the other three types ($p < 0.05$). Also, the overall bulk density of the four soils is relatively high, considered as compact or semi-compact. The fluvo-aquic soil has the highest compactness, with no significant difference with the paddy soil, but is 11.53% higher than the yellow brown soil with the lowest bulk density.

TABLE 1 | Soil acidity and bulk density grading.

Soils	pH	pH grading	Bulk density/g/cm^3	Compactness
Yellow brown soil	4.95b	Acidic	1.30c	Partial tight
Paddy soil	4.20c	Strong acidic	1.44a	Tight
Fluvo-aquic soil	4.82b	Acidic	1.45a	Tight
Pastoral soil	6.42a	Slightly acidic	1.35b	Partial tight

Each value is the mean ± standard deviation (SD, n = 6). The effects are significant at $p < 0.05$ with a one-way ANOVA. Different lowercase letters represent significant differences.

Comparison of Nutrient Contents in Different Soils

The fertility of rhizosphere is significantly dependent on the soil type (**Table 2**). The content of total nitrogen and alkali nitrogen was the highest in paddy soil, which was 99.37 and 66.49% higher than that in the lowest pastoral soil. The total phosphorus and available phosphorus were the highest in fluvo-aquic soil, followed by pastoral soil, and the lowest in yellow brown soil, which were only 41.26 and 7.08% of the fluvo-aquic soil, respectively. The highest content of total potassium was detected in the yellow brown soil, which was significantly higher than that in the other soils. There was no significant difference in the content of total potassium among paddy soil, fluvo-aquic soil, and pastoral soil. The available potassium content was the highest in paddy soil, followed by fluvo-aquic soil and pastoral soil. The content of available potassium was the lowest in yellow brown soil, which is only 19.82% of that in the paddy soil.

Comparison Enzyme Activities in Different Soils

There were significant differences in enzyme activities among the four soils (**Figure 1**). The soil urease activity was the highest in pastoral soil, which was significantly higher than the other soils ($p < 0.05$). The urease activity was the lowest in paddy soil, which was only 26.01% of that in pastoral soil. No significant difference in urease activity was observed between yellow brown soil and fluvo-aquic soil ($p < 0.05$). Fluvo-aquic soil exhibited the highest activity of sucrase among the four types of soil, which was 36.19% higher than that of pastoral soil, which showed the lowest activity of sucrase. Soil phosphatase displayed the highest activity in fluvo-aquic soil and yellow brown soil, followed by paddy soil, and no significant difference was detected among the three ($p < 0.05$), with the lowest phosphatase activity in the pastoral soil. However, catalase activity was the highest in the pastoral soil, followed by yellow brown soil, and the lowest in the paddy soil, which was only 17.23% of the activity in the pastoral soil.

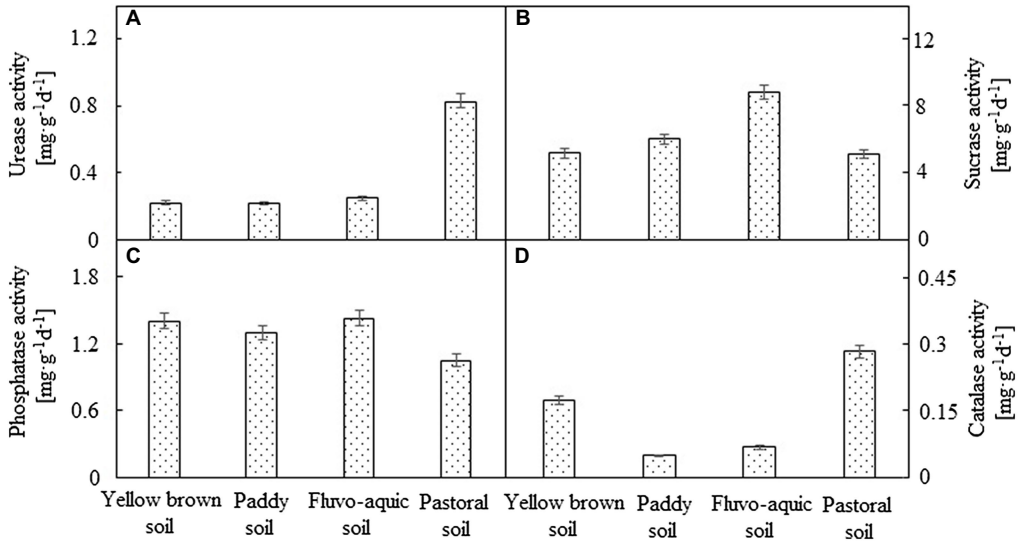


FIGURE 1 | The enzyme activities of different soils. **(A–D)** represented urease, sucrase, phosphatase and catalase activity, respectively.

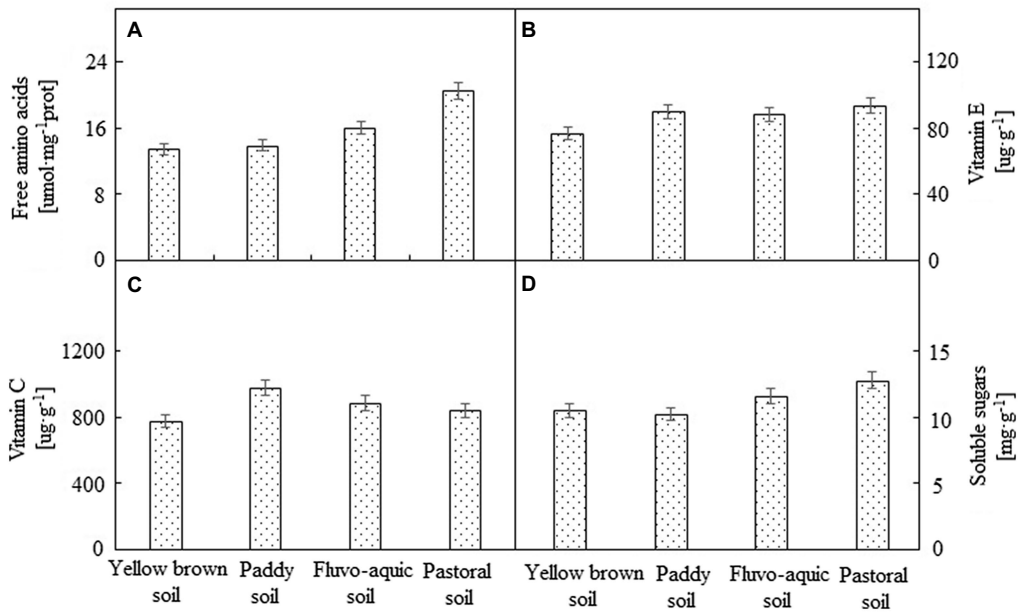


FIGURE 2 | The nutrient composition of pepper grown in different soils. **(A–D)** represented Free amino acid, vitamin E,vitamin C and soluble sugars, respectively.

TABLE 2 | Analysis of nutrient contents in different soils.

	Total nitrogen g/kg	Total phosphorus mg/kg	Total potassium mg/kg	Alkaline hydrolyzed nitrogen mg/kg	Available phosphorus mg/kg	Available potassium mg/kg
Yellow brown soil	2.60 ± 0.22b	302.61 ± 7.99d	8.50 ± 0.17a	90.77 ± 4.45bc	11.36 ± 0.56c	13.23 ± 1.52d
Paddy soil	3.17 ± 0.30a	453.84 ± 19.81c	7.35 ± 0.23b	128.53 ± 8.94a	60.49 ± 5.27b	66.74 ± 4.81a
Fluvo-aquic soil	1.97 ± 0.19bc	733.34 ± 18.03a	7.95 ± 0.25b	107.38 ± 3.22b	160.44 ± 6.33a	45.31 ± 2.47b
Pastoral soil	1.59 ± 0.16c	587.50 ± 34.43b	7.58 ± 0.16b	77.20 ± 5.32c	65.37 ± 6.25b	23.76 ± 1.35c

Each value is the mean ± standard deviation (SD, n = 6). The effects are significant at $p < 0.05$ with a one-way ANOVA. Different lowercase letters represent significant differences.

TABLE 3 | Effects of different soil trace elements on the absorption of trace elements in pepper.

		Yellow brown soil	Paddy soil	Fluvo-aquic soil	Pastoral soil
Zinc	Pepper (mg/kg)	3.07 ± 0.19b	5.14 ± 0.12a	3.25 ± 0.11b	5.18 ± 0.21a
	Soil (mg/kg)	108.13 ± 3.22d	123.26 ± 2.51b	115.41 ± 1.09c	151.98 ± 4.89a
Copper	Pepper (mg/kg)	1.12 ± 0.08b	1.47 ± 0.15a	0.75 ± 0.11c	0.76 ± 0.04c
	Soil (mg/kg)	16.85 ± 0.86c	25.39 ± 1.02b	15.77 ± 0.63c	43.60 ± 1.26a
Magnesium	Pepper (g/kg)	0.11 ± 0.01a	0.07 ± 0.01b	0.12 ± 0.02a	0.10 ± 0.01a
	Soil (g/kg)	5.07 ± 0.26a	3.24 ± 0.19c	5.27 ± 0.34a	3.75 ± 0.22b
Manganese	Pepper (mg/kg)	1.64 ± 0.09d	4.47 ± 0.17a	2.39 ± 0.23bc	2.02 ± 0.19c
	Soil (mg/kg)	347.10 ± 12.88b	143.41 ± 7.57c	483.20 ± 18.03a	507.37 ± 25.42a
Molybdenum	Pepper (μg/kg)	4.71 ± 0.11d	7.92 ± 0.23c	9.15 ± 0.17b	27.03 ± 0.98a
	Soil (mg/kg)	1.60 ± 0.07c	2.52 ± 0.09b	1.74 ± 0.06c	3.02 ± 0.13a
Ferrum	Pepper (mg/kg)	15.41 ± 0.14c	27.44 ± 0.33a	15.93 ± 0.17c	20.25 ± 0.27b
	Soil (g/kg)	3.37 ± 0.19b	3.25 ± 0.09b	3.21 ± 0.11b	4.12 ± 0.22a

Each value is the mean ± standard deviation (SD, n = 6). The effects are significant at p < 0.05 with a one-way ANOVA. Different lowercase letters represent significant differences.

Comparison of Nutrient Composition of Pepper Grown in Different Soils

The nutrient composition of pepper varied due to the type of soil (**Figure 2**). The total amino acid content of pepper grown in the pastoral soil was significantly higher than that of the other three soils, which was 28.28% higher than that of the second highest fluvo-aquic soil. No significant difference in amino acid content ($p < 0.05$) was observed among the peppers grown in fluvo-aquic soil, paddy soil, and yellow brown soil. The content of soluble sugar was the highest in the pepper grown in the pastoral soil, followed by the pepper planted in the fluvo-aquic soil. There was no significant difference between the two ($p < 0.05$). The content of soluble sugar was the lowest in the pepper grown in the paddy soil, which was 19.92% lower than that in the pastoral soil. The highest vitamin E content was determined in the pepper grown in the pastoral soil, and there was no significant difference among the other three soils ($p < 0.05$). The content of vitamin C was the highest in the paddy soil, followed by the fluvo-aquic soil and pastoral soil. The pepper planted in the yellow brown soil showed the lowest vitamin C content, which was only 79.68% of the paddy soil.

Effects of Trace Element Contents in Different Soils on the Absorption of Trace Elements in Pepper

The contents of trace elements zinc, copper, magnesium, manganese, molybdenum, and iron were significantly different among different soil types and pepper fruits (**Table 3**). The content of zinc in the four types of soils was significantly different ($p < 0.05$), among which the content of pastoral soil was the highest, and the content of yellow brown soil was the lowest, which was 28.85% lower than that of pastoral soil. The content of zinc in pepper was the highest in the pastoral and paddy soils, which is significantly higher than that in pepper planted in the fluvo-aquic and yellow brown soil ($p < 0.05$). The content of copper was the highest content in the pastoral soil and the lowest in the yellow brown and fluvo-aquic soils, and there was no significant difference between the two ($p < 0.05$). The copper content in the pepper was the highest in the paddy soil, followed by the yellow brown soil, while the amount of copper in pepper grown in the pastoral soil and fluvo-aquic soil was the lowest. The content of magnesium in fluvo-aquic soil and yellow brown soil was the highest and was the lowest in paddy soil, which was only 61.48% of that of pastoral soil. The magnesium in pepper was the highest in fluvo-aquic soil, but it is not significantly different from that in yellow brown soil and pastoral soil ($p < 0.05$). The content of manganese in the soil was the highest in the pastoral soil and fluvo-aquic soil, and the lowest in the paddy soil, which was significantly lower than that in all the other soils ($p < 0.05$). In the pepper, the content of manganese in the paddy soil was the highest, which was 172.56% higher than that in the lowest yellow brown soil. The content of molybdenum was the highest in pastoral soil, which was significantly higher than all the other soils ($p < 0.05$), and the lowest in fluvo-aquic soil and yellow brown soil,; there was no significant difference between them ($p < 0.05$). The content of molybdenum was the highest in peppers planted in the pastoral soil, while the peppers planted in the yellow brown soil were the lowest, which was only 17.40% of that in the pastoral soil. The content of iron in the pastoral soil was the highest, which was significantly higher than that in the other soils. The content of iron in pepper was the highest in the paddy soil, which was significantly higher than that in the other soils ($p < 0.05$).

Analysis of Microbial Diversity in Different Soils

The microbial diversity was high in different soils, and the number of bacterial species of different soil types was significantly higher than the fungal species (**Figures 3A,B**). The bacteria in the pepper planting soil were mainly *Alphaproteobacteria, Acidobacteria, Gammaproteobacteria, Betaproteobacteria, Gemmatimonadetes,* and *Actinobacteria,* which accounted for more than 60% in number. Among them, α-proteobacteria, acid bacillus, and β-proteobacteria were mostly identical in number, while γ-proteobacteria was the most diverse in paddy soil and the least diverse in yellow brown soils. *Gemmatimonadetes* were the most enriched

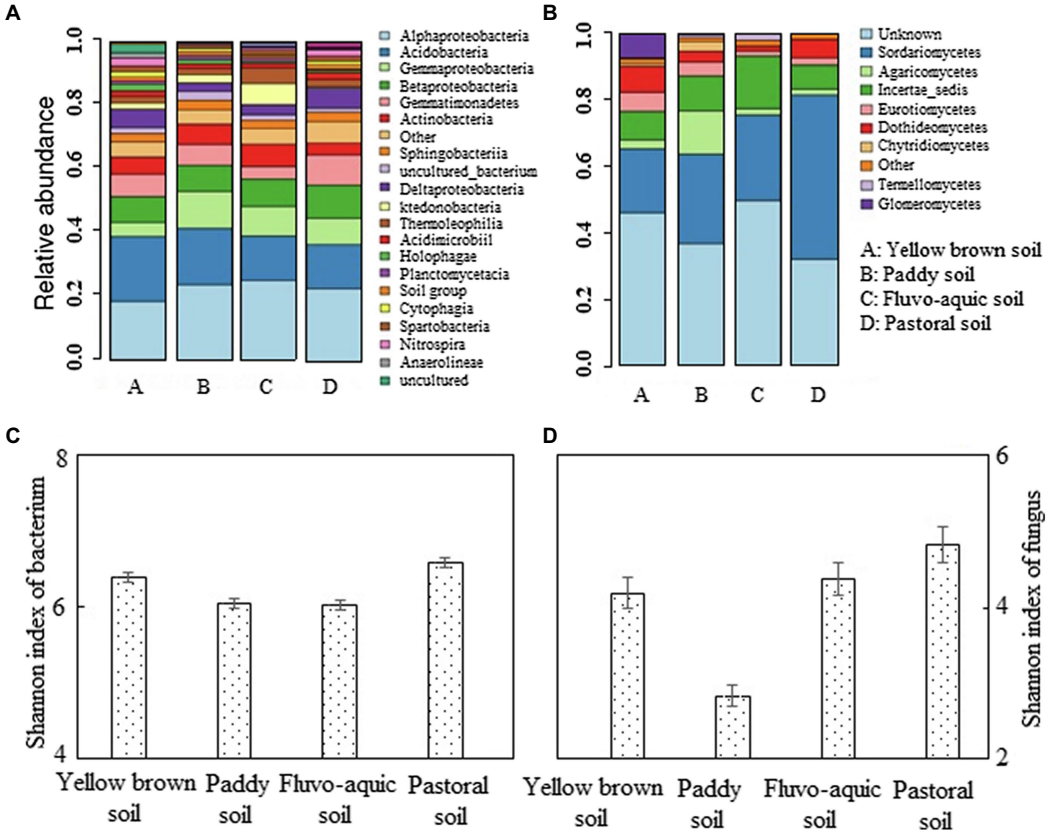


FIGURE 3 | Analysis of bacterial and fungal levels in different soils. **(A,B)** represented the abundance of bacterium and fungus, respectively. **(C,D)** represented the shannon index of bacterium and fungus, respectively.

in pastoral soil, while is the lowest in number in fluvo-aquic soil. *Actinomycetes* were the most abundant in paddy soil and fluvo-aquic soil, and the rarest in pastoral soil. The Shannon index of bacterial community in Pastoral soil and yellow brown soil was 6.58 and 6.39, which were significantly higher than those in paddy soil and fluvo-aquic soil ($p < 0.05$; **Figure 3C**). The differences in fungi species in pepper-planted soils were more evident. The fungi in the four soils were mainly unknown fungi, *Sordariomycetes, Agaricomycetes, and Incertae sedis*, with unknown fungi and *Sordariomycetes* accounting for 60–80% of the total fungal species in the four soils. Among them, the species of *Sordariomycetes* were the most abundant in the pastoral soil, and the lowest in the yellow brown soil. The species of the *Agaricomycetes* were the most abundant in the paddy soil, which was significantly higher than the other three soils. The *incertae sedis* was the most dominant in the fluvo-aquic soil, followed by the paddy soil. The Shannon index of the fungal community in the four regions was also significantly different ($p < 0.05$; **Figure 3D**). The Shannon index of fungal community in pastoral soil was the highest, which was 4.83. The Shannon index of paddy soil fungus community was the lowest, which was 41.40% lower than that of pastoral soil.

Multiple Regression Analysis of Nutrients and Soil Factors in Pepper

Since the nutrient level of the soil will change plant growth, development, and metabolism, and the soil composition is a complex system, it is imperative to transform the measured factors to eliminate the nonlinearity in the linear regression analysis. Therefore, soil factors, including pH (X1), bulk density (X2), bacterial Shannon index (X3), fungal Shannon index (X4), total nitrogen (X5), total phosphorus (X6), total potassium (X7), alkaline hydrolyzed nitrogen (X8), available phosphorus (X9), available potassium (X10), urease (X11), invertase (X12), phosphatase (X13), catalase (X14), zinc (X15), copper (X16), magnesium (X17), manganese (X18), molybdenum (X19), and iron (X20), were treated as independent variables, and the total amino acid content (Y1), soluble sugar (Y2), vitamin E (Y3), and vitamin C (Y4) of pepper were considered as the dependent variables. We eliminated the least influential factor in the objective function by stepwise multiple regression. The stepwise multiple regression function between the nutrient composition of the pepper and the main soil factors was determined as follows: $Y1 = 12.145 + 0.974 \times X19$, $R2 = 0.949$; $Y2 = 13.784 - 0.981 \times X5 + 0.301 \times X15 + 0.013 \times X16$, $R2 = 0.908$; and $Y4 = 786.235 + 0.876 \times X10 + 0.154 \times X15 - 0.058 \times X7$, $R2 = 0.984$, while the valid function for Y3 was not obtained.

These results showed that the main factor affecting the total amino acid content of pepper was the content of molybdenum in soil, the main factors determining the content of soluble sugar were the contents of total nitrogen, zinc, and copper in soil, and the main factor controlling the content of vitamin C is the contents of available potassium, zinc, and total potassium in soil.

DISCUSSION

Zinc, copper, magnesium, manganese, molybdenum, and iron are heavy metal elements and trace elements that play an important role in the growth and development of living organisms. pH is one of the most important factors affecting the absorption and distribution of heavy metals (Anderson and Rubin, 1982). Studies have shown that elevated pH prompts the increase of rhizosphere copper (Lexmond and Vorm, 1981; Chaignon et al., 2002), while leads to a decrease in copper in plants (Li, 2005). Li et al. (2003) found that the application of acidic rhizosphere fertilizer reduced the soil pH within 2 cm of the fertilization area, which increased the effective iron content in the area and promoted the absorption of iron by plants. In this experiment, the content of copper and iron in the pastoral soil was the highest, but the content of copper and iron in the pepper was at a low level, whose level in the paddy soil was the highest. This was because the pH value of the pastoral soil is significantly higher than the other soils, causing the copper and iron to be enriched in the soil. However, this enrichment may be mainly in the form of copper or ferrous salts, rather than the ions which are easily absorbed by plants. This is consistent with previous studies on the adsorption of copper and iron in soil (Wallace et al., 1980; Xu et al., 2005). Previous studies have found that the availability of zinc and manganese in the rhizosphere and the absorption of zinc and manganese by plants are negatively correlated with soil pH (Eriksson, 1989; He and Singh, 1994; Zhang et al., 2012). Fu et al. (2013) examined the soil in Bijie tobacco region and demonstrated that the effective Mn and effective Zn in soil were the highest when pH <5. In the current experiments, the amount of zinc and manganese in other soils was significantly lower than that in the paddy soil. Also, no significant difference was observed between the zinc content in the peppers grown in the paddy soil and pastoral soil, while the manganese content was significantly higher in the paddy soil. This result could be resulted from the higher pH of the pastoral soil, which enhanced the adsorption of soil to Zn^{2+} and Mn^{2+}, and reduced the concentration of these ions in the soil. Moreover, it decreased the available zinc and manganese which are conducive to the absorption of plants and vice versa in the paddy soil with a low pH. In general, the absorption of molybdenum and magnesium by plants is positively correlated with the content of the elements in the soil, but the molybdate is barely soluble in acidic soils (Shen, 2010). However, the exchangeable magnesium is enhanced with the increasing soil acidity (Diao et al., 2013). In this experiment, the relatively high pH of the pastoral soil promoted the activity of available molybdenum and exchangeable magnesium in the soil and prompted the absorption of molybdenum and magnesium by the pepper, which resulted in the molybdenum element of the plant being significantly higher than the other three soils. The content of magnesium was not significantly different from the yellow brown soil and fluvo-aquic soil with high magnesium level in the soil. Although the paddy soil had higher total molybdenum content, the low soil pH decreased the effective molybdenum content, resulting in lower molybdenum content in the fruit, which was consistent with the results of Ye et al. (2011). Therefore, the current study suggests that elevated soil pH can promote the absorption of magnesium and molybdenum by pepper, and reduced the absorption of zinc, copper, manganese, and iron. It also indicates that pH can affect the absorption of trace elements in pepper by regulating their availability in the soil.

Amino acids, soluble sugars, vitamin E, and vitamin C are important determinants of pepper quality, whose contents determine not only the nutritional but also the commercial value of peppers. Studies have demonstrated that the total amino acid in plants is positively correlated with the N, P, and K absorbed (Shi et al., 2019; Wen et al., 2020; Zhao et al., 2020). In this experiment, the content of nutrients in paddy soil and fluvo-aquic soil was higher, but the total amino acid of the planted pepper was not significantly different from that of yellow brown soil with lower soil nutrient, but significantly lower than that of other soils with lower nutrient level. This indicates that in addition to the nutrient-related accumulation of total amino acids, other factors are regulating their accumulation in plants. Yang and Jiang (2016) reported that the high soil sucrase and phosphatase activities inhibited the accumulation of total ginsenosides, total water-soluble proteins, and total amino acids. Nie et al. (2008) investigated pakchoi and found that the application of molybdenum significantly increased the content of some essential amino acids and non-essential amino acids. In this study, the stepwise multivariable regression analysis indicated that the content of molybdenum in soil is the most important factor that determines the total amino acid content of pepper, which is consistent with the results of previous studies in soybean (Liu and Yang, 2003). It suggests that the effects of other factors, such as invertase and phosphatase on the total amino acids of pepper, are far less than those of molybdenum. Changes in stress, soil pH, and trace element content can affect the amount of soluble sugar in plants. Tang et al. (2007) found that zinc fertilizer had a significant effect on the soluble sugar content of pakchoi, whose content first increased and then decreased with the increase of zinc fertilizer application. Also, they demonstrated that zinc significantly boosted the vitamin C content in pakchoi. Zhang et al. (2015) uncovered that the soluble sugar content in tomato was significantly positively correlated with soil urease and catalase. Also, Zhang et al. (2016) reported that the proper application of copper micro-fertilizer significantly increased the soluble sugar, soluble protein, and starch of the bulb of saffron. This result is consistent with our current study that the highest content of zinc and copper is in the pastoral soil and the highest soluble sugar content in the planted pepper. The results of the stepwise regression analysis illustrated that soil nitrogen, zinc, and copper were the main factors affecting the soluble sugar of pepper, while urease and catalase were not, which were rather mainly involved in the transformation of nutrients in the soil, but not directly involved in on the plants.

Soil total nitrogen is the most important factor affecting soluble sugar content. Studies have shown that proper nitrogen application can facilitate the accumulation of soluble sugar, while excessive nitrogen application will lead to a decrease in soluble sugar (Karimi and Koulivand, 2019). The changes in soil nitrogen content can consequently regulate the conversion and transfer of soluble sugar in plants (Sung et al., 2015). In production, attention should be paid to improve the availability of nitrogen and efficacy of its usage, and not blindly increase the nitrogen content in the soil. Potassium is known as the "quality-controlling element," which promotes fruit enlargement, increases yield, and improves nutritional quality (Pettigrew, 2010). Previous reports have demonstrated that the application of potassium increases vitamin C in fruits (Chen et al., 2011; Ning et al., 2011; Lu et al., 2015). In this study, the content of available potassium in paddy soil was the highest, leading to the highest content of vitamin C in peppers. The stepwise regression showed that available potassium was the most important factor affecting the content of vitamin C in pepper. On the other hand, the total potassium in soil negatively affected the content of vitamin C. This may indicate that it is not the potassium content in the soil that determines the vitamin C content of the pepper, but the content of available potassium in the soil. Therefore, when applying potassium fertilizer, efforts should be made to increase the content of available potassium rather than enhancing the total amount of potassium. In addition to available potassium and total potassium, zinc is also a major factor affecting vitamin C. Studies have indicated that zinc can increase the vitamin C content of fruits in red dates (Kang and Li, 2012) and eggplant (Wang et al., 2011). We did not obtain the formula for vitamin E by stepwise regression, which indicates that vitamin E content is not affected by several major factors, but the overall effects of all soil factors. Zhang et al. (2009) reported that a high level of calcium and phosphorus have an effect on the accumulation of vitamin E in wheat germ callus, and the effect from the phosphorus is much stronger. In the current study, the available phosphorus content of the four types of soils was significantly different from each other. However, the content of vitamin E in the fruit was similar among the four soils. This may be because the amount of effective phosphorus in the soil affects the absorption in the plant with a critical saturation of 30 mg/kg, beyond which the increase of the application of phosphate fertilizer cannot generate further effects (Fan et al., 2005).

Soil microbes are the driving force for the transformation and circulation of soil organic matter and nutrient and play an important role in many aspects of the formation and development of soil fertility. The soil microbial diversity is also closely related to soil function and maintains the dynamic balance of the soil system (Nathalia and Daniel, 2011; Haytham and Sharkawi, 2012). The Shannon-Werner diversity index of bacteria and fungi in the pastoral soil in this study was higher than the other soils, indicating that the microbial population of the pastoral soil is richer and more active. Soil microbes function as an important part of the cyclical transformation of soil C, N, P, and other nutrients, and it also plays a critical role in promoting the energy exchange between plants and soil, which explains the higher nutrient content of pepper grown in the pastoral soil. In addition, the analysis of bacterial diversity in the four soil types demonstrated that the rhizosphere of pepper was enriched with a large number of deformed bacteria. Presently, the enrichment of deformed bacteria has been observed in the rhizosphere of *Arabidopsis thaliana* (Fierer et al., 2007) and maize (Peiffer et al., 2013), indicating that the deformed bacteria can adapt to the rhizosphere microenvironment of various plants. However, results from the current study do not support the hypothesis that soil microbes can directly affect the nutritional quality of pepper. Na et al. (2016) found that the content of total phosphorus and available phosphorus was significantly correlated with the ratio of *Acidobacteria, Sordariomycetes, Basidiomycetes, and Zygomycetes.* This result suggests that changes in soil microbes may indirectly affect crops by changing the nutrient composition and activity of the soil. In summary, many factors, including soil nutrient, pH, enzyme activity, and soil microbe, contribute to the quality of pepper. In the future, to maximize the efficacy of improving the nutrient quality of pepper, more attention should also be paid to the effects of microorganism when adjusting the particular nutrient composition of the soil.

CONCLUSION

In this study, the nutritional quality of pepper fruits grown in soil with different physical and chemical properties was different, indicating that there was a certain relationship between pepper quality and soil properties. The results of stepwise multivariable regression analysis showed that the amount of molybdenum in soil is the main factor affecting the total amino acid content of pepper. Total nitrogen, zinc, and copper are the main factors that contribute to the amount of soluble sugar of pepper. Also, available potassium is the major determinant of the vitamin C content of pepper. This study provides a new insight for analyzing the relationship between soil trace elements and the pepper fruit quality.

DATA AVAILABILITY STATEMENT

The datasets presented in this study can be found in online repositories. The names of the repository/repositories and accession number(s) can be found at: https://www.ncbi.nlm.nih.gov/ (PRJNA577242 and PRJNA577978).

AUTHOR CONTRIBUTIONS

ZL: formal analysis and writing—original draft. LO: funding acquisition, project administration, supervision, and writing—review and editing. ZL and YH: investigation. ZL and FT: methodology. WC: resource. All authors have read and approved the final manuscript.

FUNDING

This work was supported by the China Agriculture Research System (CARS-24-A-05).

REFERENCES

Anderson, M. A., and Rubin, A. J. (1982). Adsorption of inorganics at solid-liquid interfaces. *Soil Sci.* 133, 257–258. doi: 10.1097/00010694-198204000-00010

Bao, J. F., Xia, R. X., Peng, S. A., and Li, G. H. (2006). Main soil nutrient status of Newhall orchards of Hubei province and its effect on fruit quality of Newhall orange. *Soil* 38, 75–80. doi: 10.13758/j.cnki.tr.2006.01.013

Chaignon, V., Bedin, F., and Hinsinger, P. (2002). Copper bioavailability and rhizosphere pH changes as affected by nitrogen supply for tomato and oilseed rape cropped on an acidic and a calcareous soil. *Plant Soil* 243, 219–228. doi: 10.1023/A:1019942924985

Chen, K., Liu, S. Q., Zhang, Z. K., Zhang, T., and Meng, F. L. (2011). Effects of potassium in nutrient solution on physiological and quality of garlic. *Acta Hortic. Sin.* 38, 556–562. doi: 10.16420/j.issn.0513-353x.2011.03.021

Diao, L. H., Peng, L. Z., Chun, C. P., Ling, L. L., Li, X., Xue, J., et al. (2013). Survey of soil available magnesium content at navel orange orchards in southern Jiangxi province. *J. Fruit Sci.* 30, 241–247. doi: 10.13925/j.cnki.gsxb.2013.02.013

Eriksson, J. E. (1989). The influence of pH, soil type and time on adsorbtion and uptake by plants of Cd added to the soil. *Water Air Soil Pollut.* 48, 317–335. doi: 10.1007/BF00283334

Fan, H., Hao, M., and Li, Z. (2005). Effect of wheat quality and amino acid quantity of different fertilizings in dryland of Loess Plateau. *J. Northwest Sci. Tech. Univ. Agri. For.* 33, 54–57. doi: 10.3321/j.issn:1671-9387.2005.12.011

Fierer, N., Bradford, M. A., and Jackson, R. B. (2007). Toward an ecological classification of soil bacteria. *Ecology* 88, 1354–1364. doi: 10.1890/05-1839

Fu, Y. P., Wang, X. C., Chen, X., Li, Y. F., Dai, C. M., Yu, Q. W., et al. (2013). Distribution of soil pH and its relationships with soil nutrients in Bijie tobacco-growing area. *Soil* 45, 46–51. doi: 10.13758/j.cnki.tr.2013.01.015

Haytham, M., and Sharkawi, E. (2012). Effect of nitrogen sources on microbial biomass nitrogen under different soil types. *ISRN Soil Sci.* 2012:310727. doi: 10.5402/2012/310727

He, F., Thiele, B., Watt, M., Kraska, T., and Kuhn, A. J. (2019). Effects of root cooling on plant growth and fruit quality of cocktail tomato during two consecutive seasons. *J. Food Qual.* 2019:3598172. doi: 10.1155/2019/3598172

He, Q. B., and Singh, B. R. (1994). Crop uptake of cadmium from phosphorus fertilizers: I. yield and cadmium content. *Water Air Soil Pollut.* 74, 251–265. doi: 10.1007/BF00479793

Jansen, G., Jürgens, H. U., Schliephake, E., and Ordon, F. (2012). Effect of the soil pH on the alkaloid content of *Lupinus angustifolius*. *Int. J. Agron.* 2012, 1–5. doi: 10.1155/2012/269878

Kang, P., and Li, J. G. (2012). Effects of zinc treatment on fruit quality in the growth process of jujube. *China For. Sci. Technol.* 26, 111–115. doi: 10.3969/j.issn.1000-8101.2012.05.029

Karimi, R., and Koulivand, M. (2019). Soluble sugars, phenolic acids and antioxidant capacity of grape berries as affected by iron and nitrogen. *Acta Physiol. Plant.* 41:117. doi: 10.1007/s11738-019-2910-1

Kong, X. J., Dou, L. J., Qian, D. N., and Zhou, Q. (2013). Correlation analysis between soil nutrient factors of red-peach production area in Jinhua-Yiwu and fruit internal quality. *Hortic. Seed.* 23, 20–22. doi: 10.3969/j.issn.2095-0896.2013.06.007

Lexmond, T. M., and Vorm, P. D. J. (1981). The effect of pH on copper toxicity to hydroponically grown maize. *Neth. J. Agric. Sci.* 29, 217–238. doi: 10.18174/njas.v29i3.17008

Li, H. S. (2005). A study on absorption and accumulation of aluminum, copper and mineral nutrients of tea seedlings under different pH levels. *J. Guangdong Educ. Inst.* 25, 78–81.

Li, M., Jie, X. L., Li, J. P., Guo, X., Hu, H. F., Huang, A. Q., et al. (2012). Effects of basal Se fertilizers on nutrition value and amino acid contents of naked oats. *Acta Agrestia Sin.* 20, 1086–1092. doi: 10.11733/j.issn.1007-0435.2012.06.017

Li, Y. T., Bai, D. S., Zhang, F. S., Jiang, R. F., and Mao, D. R. (2003). Effect of acidic rhizosphere fertilizer on the soil pH and Fe availability of calcareous soil. *J. Plant Nutr. Fert.* 9, 312–316. doi: 10.11674/zwyf.2003.0312

Liu, K. P., Huang, C. H., Leng, J. H., Chen, K., Yan, Y. P., Tu, G. Q., et al. (2012). Multivariate analysis between boil nutrients and fruit qualities in kiwifruit orchard. *J. Fruit Sci.* 29, 1047–1051. doi: 10.13925/j.cnki.gsxb.2012.06.021

Liu, P., and Yang, Y. A. (2003). Effect of molybdenum and boron on pollution on quality of soybean. *Chin. J. Appl. Environ. Biol.* 9, 594–597. doi: 10.3321/j.issn:1006-687X.2003.06.007

Lu, Y. L., Yang, X. L., Li, R., Li, S. L., and Tong, Y. A. (2015). Effects of different potassium fertilizer application periods on the yield and quality of Fuji apple. *Chin. J. Appl. Ecol.* 26, 1179–1185. doi: 10.13287/j.1001-9332.2015.0030

Ma, Y. Q. (2011). Analysis of the situation of China's pepper industry. *J. China Capsicum.* 11, 1–5. doi: 10.3969/j.issn.1672-4542.2011.01.001

Na, X. F., Zheng, G. Q., Peng, L., Lei, C. Y., Yang, H. Y., Ma, Y., et al. (2016). Microbial biodiversity in rhizosphere of *Lyceum bararum* L. relative to cultivation history. *Acta Pedol. Sin.* 53, 241–252. doi: 10.11766/trxb201503030643

Nathalia, F. Z., and Daniel, U. V. (2011). Biological and physicochemical parameters related to the nitrogen cycle in the rhizospheric soil of native potato (*Solanum phureja*) crops of Colombia. *Appl. Environ. Soil Sci.* 2011:847940. doi: 10.1155/2011/847940

Nie, Z. J., Hu, C. X., and Sun, X. C. (2008). Effects of molybdenum on leaf color, nutritional quality and nitrate contents of Chinese cabbage. *China Veg.* 28, 7–10.

Ning, X. J., Yu, H. J., Jiang, W. J., Liu, X. R., and Yang, X. Y. (2011). Effects of different potassium levels applied at blooming stage on the growth, yield and quality of tomato in greenhouse. *Soil Fert. Sci. China.* 48, 35–38. doi: 10.3969/j.issn.1673-6257.2011.06.006

Peiffer, J. A., Spor, A., Koren, O., Jin, Z., Tringe, S. G., Dangl, J. L., et al. (2013). Diversity and heritability of the maize rhizospheremicrobiome under field conditions. *Proc. Natl. Acad. Sci. U. S. A.* 110, 6548–6553. doi: 10.1073/pnas.1302837110

Pettigrew, W. T. (2010). Potassium influences on yield and quality production for maize, wheat, soybean and cotton. *Physiol. Plant.* 133, 670–681. doi: 10.1111/j.1399-3054.2008.01073.x

Shen, H. G. (2010). Influence of soil microelement on plant. *For. Sci. Technol. Inf.* 42, 12–14. doi: 10.3969/j.issn.1009-3303.2010.04.006

Shi, Z., Wei, F., Wan, R., Li, Y., Wang, Y., An, W., et al. (2019). Impact of nitrogen fertilizer levels on metabolite profiling of the *Lycium barbarum* L. fruit. *Molecules* 24:3879. doi: 10.3390/molecules24213879

Sung, J., Lee, S., Lee, Y., Ha, S., Song, B., Kim, T., et al. (2015). Metabolomic profiling from leaves and roots of tomato (*Solanum lycopersicum* L.) plants grown under nitrogen, phosphorus or potassium-deficient condition. *Plant Sci.* 241, 55–64. doi: 10.1016/j.plantsci.2015.09.027

Tang, X. L., Gu, M. H., Pan, L. H., Ling, G. Z., and Qian, D. X. (2007). Effect of combined application of N, P, K and Zn on the yield and quality of pakchoi. *Soil Fert. Sci. China.* 44, 47–51. doi: 10.3969/j.issn.1673-6257.2007.03.012

Wallace, A., Mueller, R. T., and Alexander, G. V. (1980). Effect of soil pH on iron uptake and its specific activity by two cultivars of soyabeans differing in ability to accumulate iron and by oleander. *J. Plant Nutr.* 2, 205–211. doi: 10.1080/01904168009362766

Wang, X. J., Wang, H. M., Wang, F., and Wang, Z. Y. (2011). Effects of zinc on the fruits' quality of two eggplant varieties. *Acta Ecol. Sin.* 31, 6125–6133.

Wen, G., Cambouris, A. N., Ziadi, N., Bertrand, A., and Khelifi, M. (2020). Nitrogen rate and source effects on foliar sugar, glycoalkaloid, and amino acid composition of potato Russet Burbank. *Can. J. Plant Sci.* 101, 61–72. doi: 10.1139/CJPS-2020-0096

Xu, M. G., Zeng, X. B., and Li, J. M. (2005). Effect of pH on adsorption and desorption of Cu^{2+} in latersol and yellow brown earth. *Chin. J. Soil Sci.* 36, 349–351. doi: 10.1016/j.msea.2006.04.103

Yang, Y. W., and Jiang, Y. T. (2016). Study on relationship between effective components and soil enzyme activity in different growth patterns of *Panax ginseng*. *China J. Chin. Materia Medica.* 41, 2987–2992. doi: 10.4268/cjcmm20161607

Ye, X., Guo, Y. L., Wang, G., and Ge, H. L. (2011). Investigation and analysis of soil molybdenum in the Tieguanyin tea plantations of Fujian Province. *Plant Nutr. Fert. Sci.* 17, 1372–1378. doi: 10.11674/zwyf.2011.1047

Zhang, C., Liu, G. B., Xie, S., and Zhang, C. S. (2012). Characteristics of soil microelements contents in the rhizospheres of different vegetation in hilly-gully region of Loess Plateau. *Chin. J. Appl. Ecol.* 23, 645–650. doi: 10.13287/j.1001-9332.2012.0087

Zhang, E. P., Tan, F. L., Wang, Y., Zhang, S. H., Duan, Y., and Zhou, F. (2015). Effects of NPK fertilizers and organic manure on nutritional quality, yield of tomato and soil enzyme activities. *Acta Hortic. Sin.* 42, 2059–2067. doi: 10.16420/j.issn.0513-353x.2015-0341

Zhang, H., Xu, Z., Sun, S., Li, W., Yu, J., and Zhao, S. (2009). Effect of calcium and phosphorus on accumulation of vitamin E in wheat embryo callus. *Sci. Tech. of. Food. Indust.* 11, 164–172. doi: 10.1360/972009-754

Zhang, H. F., Zhang, H. C., Wei, Q. C., and Li, C. Z. (2016). Effects of four microelement fertilizer on growth, quality and yield in *Crocus sativus* L. *J. Nanjing For. Univ.* 40, 169–173. doi: 10.3969/j.issn.1000-2006.2016.01.027

Zhao, Y., Zhang, C., Wang, C., Huang, Y., and Liu, Z. (2020). Increasing phosphate inhibits cadmium uptake in plants and promotes synthesis of amino acids in grains of rice. *Environ. Pollut.* 257:113496. doi: 10.1016/j.envpol.2019.113496

Conflict of Interest: The authors declare that the research was conducted in the absence of any commercial or financial relationships that could be construed as a potential conflict of interest.

Copyright © 2021 Liu, Huang, Tan, Chen and Ou. This is an open-access article distributed under the terms of the Creative Commons Attribution License (CC BY). The use, distribution or reproduction in other forums is permitted, provided the original author(s) and the copyright owner(s) are credited and that the original publication in this journal is cited, in accordance with accepted academic practice. No use, distribution or reproduction is permitted which does not comply with these terms.

frontiers in Plant Science

REVIEW
published: 23 September 2021
doi: 10.3389/fpls.2021.729448

The Formation of Fruit Quality in *Cucumis sativus* L.

Juping Zhang[1†], Shengjun Feng[1†], Jing Yuan[2†], Chen Wang[2], Tao Lu[3], Huasen Wang[1] and Chao Yu[1*]*

[1] Collaborative Innovation Center for Efficient and Green Production of Agriculture in Mountainous Areas, College of Horticulture Science, Zhejiang A&F University, Hangzhou, China, [2] State Key Laboratory of Subtropical Silviculture, Laboratory of Plant Molecular and Developmental Biology, College of Forestry and Biotechnology, Zhejiang A&F University, Hangzhou, China, [3] Institute of Vegetables and Flowers, Chinese Academy of Agricultural Sciences, Beijing, China

Cucumber is one of the most widely grown vegetables in China and an indispensable fresh fruit in the diet. With the development of society, the demand of people for cucumber quality is higher and higher. Therefore, cultivating high-quality cucumber varieties is one of the main goals of cucumber breeding. With the rapid development of biotechnology such as molecular marker, cucumber quality control network is becoming clear. In this review, we describe the formation mechanism of cucumber fruit quality from three aspects: (1) the commercial quality of cucumber fruit, (2) nutritional quality formation, and (3) flavor quality of cucumber fruit. In addition, the determinants of cucumber fruit quality were summarized from two aspects of genetic regulation and cultivation methods in order to provide ideas for cucumber researchers and cultivators to improve fruit quality.

Keywords: cucumber, fruit quality, QTLs, spine, bitterness, grafting

OPEN ACCESS

Edited by:
Pei Xu,
China Jiliang University, China

Reviewed by:
Zheng Li,
Northwest A&F University, China
Zhihui Chen,
University of Dundee, United Kingdom
Tao Yao,
Oak Ridge National Laboratory (DOE), United States

****Correspondence:***
Huasen Wang
wanghs@zafu.edu.cn
Chao Yu
yuch@zafu.edu.cn

[†] These authors have contributed equally to this work

Specialty section:
This article was submitted to Crop and Product Physiology, a section of the journal Frontiers in Plant Science

Received: *23 June 2021*
Accepted: *18 August 2021*
Published: *23 September 2021*

Citation:
Zhang J, Feng S, Yuan J, Wang C, Lu T, Wang H and Yu C (2021) The Formation of Fruit Quality in Cucumis sativus L. Front. Plant Sci. 12:729448. doi: 10.3389/fpls.2021.729448

INTRODUCTION

Cucumber (*Cucumis sativus* L.) is an annual herbaceous climbing fruit vegetable that belongs to the Cucurbitaceae family and originates from the tropical rainforest in the southern foot of the Himalayas. According to its geographical locations, it can be categorized into four groups such as the Indian group, the Eurasian group, the East Asian group, and the Xishuangbanna group (Qi et al., 2013). In China, cucumber can be subdivided into two geographic groups, such as the northern China group with dark green, dense spines and warts on fruits, and the southern China group with light green, sparse spines and warts on fruits (Jiang et al., 2015). Cucumber is an economically important crop in the world. Its fruits are fragrant and delicious with nutrient enrichment that can be consumed in fresh or processed into pickles. In addition, its fruits are also used in beauty products. However, with the constantly change in the cultivation environment and techniques, and the ever-rising living standards of people, the cucumber fruit quality is becoming much more concerned by the consumers.

With the continuous work on the formation of cucumber fruit quality by various research groups in recent years, some of the influencing factors and regulation mechanism of the formation of cucumber fruit quality can be understood now in a more in-depth and thorough manner. This review attempted to summarize the recent advances in the studies on the formation of cucumber fruit quality through physiological and molecular biological approaches in order to provide insights for further research studies on the formation of fruit quality of cucumber and other melons.

Fruit quality in cucumber can be defined by three aspects, namely, commercial quality, nutrient quality, and flavor quality (Lv et al., 1992). The commercial quality in cucumber contains the fruit size and shape, fruit spine characteristics (color, size, and density), fruit skin characteristics (color, ridges, and speckles), and flesh characteristics (color) (Wang et al., 2007; Lu et al., 2015; Zhang et al., 2016; Zhang C. et al., 2019). Fruit size and shape are the two most obvious appearances of quality traits in cucumber, which had become one of the criterions for breeders to select high fruit quality cultivars. The external fruit qualities, such as the fruit skin and spine color, the presence or absence of the wax on the cucumber surface, and the number, shape, size, distribution, and density of fruit spines (trichomes on cucumber fruit are called spines), are also important fruit quality traits for cucumber production (Choi et al., 2013; Li et al., 2013; Chen et al., 2014; Liu X. et al., 2016). In the late 1980s, the bloomless cucumber fruits are popular in Japan due to their distinct shiny appearance (Ohara et al., 2006). Besides, the character of spines could also have a big influence on consumer preference. For example, people in Europe prefer cucumber without spines, whereas people in Asia like cucumber with spines (Chen et al., 2014). Furthermore, epicuticular wax, which acts as the outermost barrier between the plants and their environment, is also one of the significant commercial quality traits in cucumber that can play significant roles in protecting the tissues against various biotic and abiotic stress (Samuels et al., 2008). Moreover, fruit flesh color that varies from white to green or yellow to orange is also an important fruit quality trait that influences the preference of consumers (Cuevas et al., 2010).

On the other hand, nutrition elements, such as soluble solids, vitamins, and minerals, constitute the nutrient quality in cucumber. In addition, flavor quality in cucumber, for one reason, contains all of the volatile compounds from cucumber, and for another reason, it is related to the non-volatile flavor substances (Kemp et al., 1974; Malundo et al., 1995). Ever since the 1960s, there have had research studies on the flavor of cucumber (Forss et al., 1962). Nowadays, there are more and more research studies on fruit flavor, which would help us to improve the fruit quality of cucumber.

GENETIC REGULATION OF FRUIT QUALITY IN CUCUMBER

Genetic Regulation of Commercial Quality in Cucumber

Cucumber commercial quality is determined mainly by its fruit-related traits. The genes related to the commercial quality traits of cucumber fruits are shown in **Figure 1** and **Table 1**. The ability of cucumber to produce large fruits is believed to have been evolved through long time domestication of wild cucumber, and *Cucumis sativus* L. var. hardwickii is regarded as the ancestor of cultivated cucumber. Its fruit is small and round and about 3–5 cm long. In addition, it has large amounts of spines on its epidermis. It is so bitter that it is difficult to eat (Sebastian et al., 2010; Yang et al., 2012). Nowadays, the fruit length of widely cultivated cucumber is about 10–30 cm, and the fruit shape has also become oblong, which has shown great variation compared with its ancestors. Besides, based on the whole genome sequencing and the construction of the high-resolution genetic map, we have gained a clearer understanding of the genetic mechanism of formation of fruit quality during their domestication processes (Huang et al., 2009; Qi et al., 2013).

The Size and Shape of Cucumber Fruits

Fruit size and shape, especially fruit length, are important fruit traits during cucumber domestication and diversifying selection. Wenzel et al. (1995) first identified the overall information of gene regulation on the cucumber fruit length, diameter, and other genetic traits. Yuan et al. (2008) constructed a 257-point genetic linkage map and found 78 quantitative trait locus (QTLs) related to fruit weight, fruit length, fruit diameter, and other four fruit-related traits, which can be used to conduct marker-assisted selection in cucumber breeding. Bo et al., also detected several QTLs of cucumber fruit-related traits, including five fruit length-related QTLs (*fl1.1, fl3.1, fl4.1, fl6.1,* and *fl7.1*), three fruit diameter-related QTLs (*fd1.1, fd4.1,* and *fd6.1*), and three fruit weight-related QTLs (*fw2.1, fw4.1,* and *fw6.1*). At the same time, they also found that the chromosomal rearrangements of cucumber ancestors between wild and cultivated cucumbers were mainly concentrated on chromosomes 4, 5, and 7 (Bo et al., 2015). Besides, Cheng et al. (2010) and Wang et al. (2014) also found 5 fruit length (Fl)-related QTLs that were distributed in chromosome 1, 4, and 6 and 4 stalk length (Fsl)-related QTLs that were located on chromosome 3, 4, and 6, respectively.

The enzyme 1-aminocyclopropane-1-carboxylic acid synthase (ACS) in the process of plant hormone ethylene synthesis plays an important role in cucumber sex determination. The genes involved in this process include *CsACS1G* (Kamachi et al., 1997), *CsACS2* (Knopf and Trebitsh, 2006; Li et al., 2009), and *CsACS11* (Boualem et al., 2015). Among them, the *CsACS2* mutation makes cucumber produce a bisexual flower phenotype. *CsACS2* gene was eliminated in addition to the above functions, and it is also related to the length of the cucumber fruit. Boualem et al. (2009) proved that an allele of *CsACS2* co-segregated with the M (andromonoecious) locus, resulting in a round fruit phenotype after the gene mutation. Subsequently, Tan et al. (2015) further studied through fine mapping and found that another allele mutation of *CsACS2* caused the cucumber to appear a long fruit phenotype. Later, Pan et al. (2017) found that round fruit shape in WI7239 cucumber was controlled by two interacting quantitative trait loci, such as *FS1.2* and *FS2.1*, and demonstrated that *FS2.1* may encode a homolog of tomato fruit shape gene *SUN*. They also identified a *FS5.2* QTL in Xishuangbanna cucumber that has great significance on round fruit determination (Pan et al., 2017). Besides, Zhao et al. (2019) further demonstrated that among the QTLs that have putative functions in regulating cucumber fruit length, a gain-of-function allele $CsFUL1^{A}$ can prevent the accumulation of auxin by inhibiting the expression of its transporters *PIN-FORMED1* (*PIN1*) and *PIN7*. This further analyzes the molecular mechanism of auxin regulating cucumber fruit development.

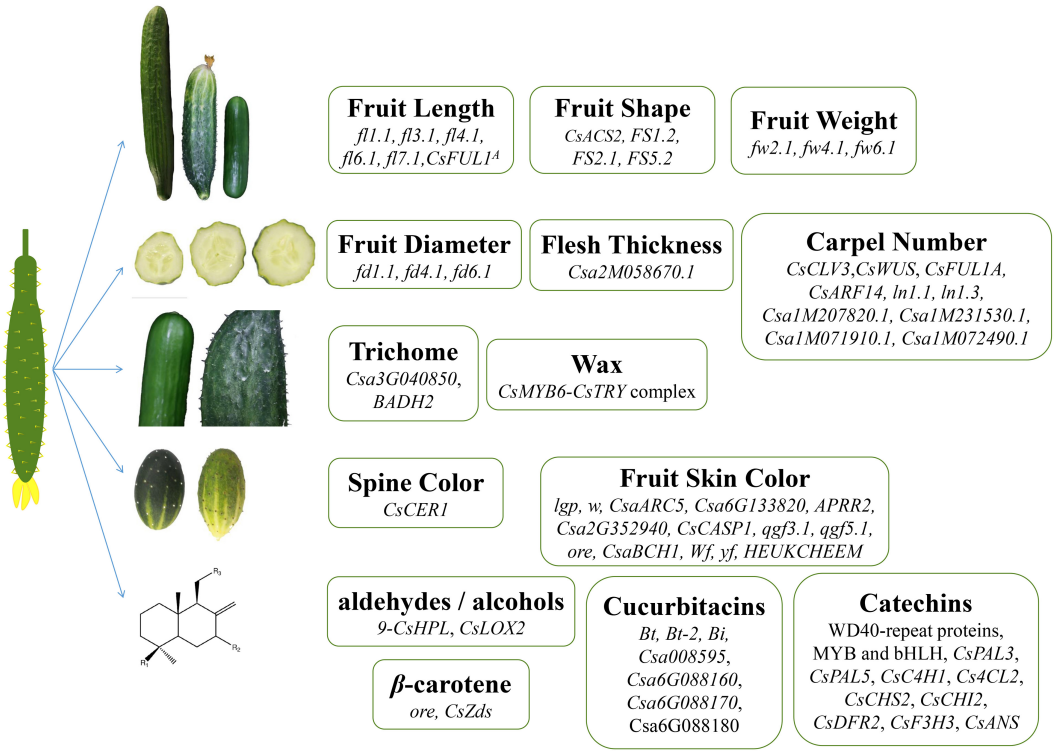


FIGURE 1 | Genes related to cucumber fruit quality. Genes regulating fruit length, fruit shape, weight, diameter, thickness, carpel number, trichome, wax, spine color, and synthesis of secondary metabolite in cucumber.

The Carpel Number and Flesh Thickness of Cucumber Fruits

In addition, factors that affect important fruit characteristics such as cucumber fruit shape, size, and internal quality also include the carpel number and the thickness of fruit flesh. The expression of *CsCLV3* in cucumber was negatively correlated with the number of carpels. *CsCLV3* and *CsWUS* act as negative regulators and positive regulators of changes in carpel number, respectively, and *CsWUS* can be directly combined with the promoter of *CsCLV3* to activate its expression. *CsFUL1*^{A} overexpression plants showed increased petals and carpels. Through the interaction of *CsARF14* and *CsWUS*, auxin can also participate in the change of cucumber carpel number (Che et al., 2020). The QTL mapping of Xishuangbanna cucumber revealed that *ln1.1* and *ln1.3* located on chromosome 1 are the main QTLs controlling multi-ventricular traits. At the same time, two genes, namely, *Csa1M207820.1* and *Csa1M231530.1,* involved in plant hormone signal transduction and two genes, namely, *Csa1M071910.1* and *Csa1M072490.1,* related to WD40 repeat protein are predicted as candidate genes (Zhang et al., 2015). By combining the separation and segmentation analysis with the sequencing of amplified fragments of specific lengths, the genes that regulate the pulp thickness of cucumber fruit were finely mapped, and the quantitative trait locus that controls the pulp thickness was located in the interval of about 0.19 Mb on chromosome 2. This 0.19-Mb region predicts and recognizes 20 genes, among which there is a 4 bp deletion mutation in the promoter region of the candidate gene *Csa2M058670.1* (a protein-lysine methyltransferase, PKMT), which may lead to the loss of its activity in the thin fruit line. This suggests that *Csa2M058670.1* may be a candidate gene for controlling cucumber pulp thickness (Xu et al., 2015). *Csa2M058670.1* belongs to the same subfamily as At2g18850, and the latter is related to the cell division and growth process of *Arabidopsis* (Horvath et al., 2003). At present, there are too many factors affecting the thickness of pulp and the number of ventricles in cucumber, and these two traits are easily affected by the environment, so a consistent conclusion has not yet been reached.

The Color of the Flesh and Skin of Cucumber Fruit

The colors of the fruit flesh and skin are also significant commercial quality traits in cucumber that have obvious influences on the choice of the consumers. Fruit color was determined by the regulation of pigment in the plants, and chlorophylls were declared to be the main factor to determine the fruit skin color (Egea et al., 2010). In cucumber, five genes controlled fruit skin color, such as dark green (*DG*), green (*dg*), yellow green (*yg*), light green (*lgp*), and white (*w*) peeling genes (Pierce and Wehner, 1990; Dong et al., 2012). Now, the fruit light green peel gene *lgp* and the white peel gene *w* have been identified (Wehner et al., 2001; Dong et al., 2012). The mutation of *CsaARC5* (*ACCUMULATION AND REPLICATION OF CHLOROPLASTS 5*), the ortholog

TABLE 1 | Genes related to the commercial quality of cucumber fruits.

Category	Traits	QTLs or Gene name	References
Commercial quality	Fruit length	*fl1.1, fl3.1, fl4.1, fl6.1,* and *fl7.1*	Bo et al., 2015
		CsFUL1^{A}	Zhao et al., 2019
	Fruit diameter	*fd1.1, fd4.1,* and *fd6.1*	Bo et al., 2015
	Fruit weight	*fw2.1, fw4.1,* and *fw6.1*	Bo et al., 2015
	Fruit shape	*CsACS2*	Tan et al., 2015
		FS1.2, *FS2.1,* and *FS5.2*	Pan et al., 2017
	Carpel number	*CsCLV3, CsWUS, CsFUL1*^{A}, and *CsARF14*	Che et al., 2020
		ln1.1, ln1.3, Csa1M207820.1, Csa1M231530.1, Csa1M071910.1, and *Csa1M072490.1*	Zhang et al., 2015
	Flesh thickness	*Csa2M058670.1*	Xu et al., 2015
	Fruit skin color	*lgp*	Wehner et al., 2001
		w	Dong et al., 2012
		CsaARC5	Zhou et al., 2015
		Csa6G133820	Lun et al., 2016
		APRR2	Liu H. et al., 2016
		Csa2G352940 and *CsCASP1*	Hao et al., 2018
		qgf3.1 and *qgf5.1*	Bo et al., 2019
		ore	Bo et al., 2012
		CsaBCH1	Qi et al., 2013
		wf and *yf*	Kooistra, 1971; Whalen, 2005; Lu et al., 2015
		HEUKCHEEM	Zhang C. et al., 2019
	Spine color	*CsCER1*	Wang et al., 2015
	Wax	*CsMYB6-CsTRY* complex	Yang et al., 2018
	Trichome	*Csa3G040850*	Wei et al., 2016
		BADH2	Yundaeng et al., 2015

gene of *Arabidopsis ARC5*, led to a light green fruit peel phenotype in cucumber (Zhou et al., 2015). Another Ycf54-like protein-encoding gene *Csa6G133820* can also determine the formation of light green fruits (Lun et al., 2016). Besides, a single-nucleotide insertion on *APRR2* disturbed the chlorophyll accumulation and chloroplast development so that leading to a white fruit color in cucumber (Liu H. et al., 2016). Identification of cucumber yellow green peel-related genes and research studies on their regulation mechanism have also progressed greatly in recent years. Research studies on a cucumber yellow green peel mutant (*ygp*) identified a *Csa2G352940* gene, encoding a MYB36 transcription factor, functioned to regulate a yellow green peel determination in cucumber. This study also revealed that *CsMYB36* may interact with the peel color development-related genes, such as Casparian strip (*CsCASP1*) and pigment synthesis protein (*CsMYC2*), to regulate yellow green peel determination in cucumber (Hao et al., 2018).

Besides fruit skin color, chlorophylls can also influence the formation of flesh color. Bo et al. (2019) revealed that two QTLs, *qgf3.1* and *qgf5.1*, can function together in regulating the formation of green fruit flesh in cucumber. When cucumber fruits developed to the mature stage, their flesh color changed from green to yellow or green to orange. High β-carotene content was demonstrated to be the main reason for cucumber to form fruits with orange flesh color, and further genetic analysis demonstrated that the quantity of β-carotene was controlled by the orange endocarp (*ore*) gene (Bo et al., 2012) and *CsaBCH1* (Qi et al., 2013). Cucumber fruits with white flesh and yellow flesh were proven to be controlled by two genes, *wf* and a single recessive gene named *yf*, respectively (Kooistra, 1971; Whalen, 2005; Lu et al., 2015). The study on the color of cucumber flesh and skin will help to promote the breeding process of cucumber with a different color.

External Quality of Cucumber Fruits

Several genes and transcription factors are involved in the regulation of the external quality of cucumber fruits. Zhang C. et al. (2019) found that spine color was regulated by the *HEUKCHEEM* gene, mutations in *HEUKCHEEM* leading to a white spine in cucumber. Wang et al. (2015) revealed that *CsCER1* significantly influenced the biosynthesis of alkane so that further influenced the wax synthesis of cucumber, and *CsCER1* overexpression lines showed more wax crystallization phenotypes, whereas its RNA interference (RNAi) lines exhibited fewer wax crystallizations. Liu et al. (2018) analyzed 91 *NAC* gene homologs in cucumber and identified 13 *NAC* genes that can control fruit spine development. Yang et al. (2018) found that *CsMYB6* and *CsTRY* can negatively regulate the trichome initiation in cucumber and revealed that *CsMYB6* functions the upstream of *CsTRY* and that they can also form *CsMYB6-CsTRY* complex to function together in this progress. These results provide a reference for the cultivation of non-spiny and prickly cucumbers.

Genetic Regulation of Flavor Quality in Cucumber

Research studies on flavor quality have become popular in recent years. Foods with good or special tastes will increase the pleasure in people and influence the digestion in people and absorption of nutrients (Beaulieu and Lea, 2006). The genes contributed to the flavor quality traits of cucumber fruits are shown again in **Figure 1** and **Table 2**. It is confirmed that the degradation of linoleic acid and linolenic acid occurred rapidly after the disruption of cucumber tissues and gave rise to the flavor of fresh cucumber (Ligor and Buszewski, 2008).

The Scent of Cucumber Fruits

Aldehydes and alcohols are thought to mainly contribute to the fresh cucumber scent (Kemp et al., 1974; Hatanaka et al., 1975; Palma-Harris et al., 2001; Ligor and Buszewski, 2008; Hao et al., 2013). Forss et al. (1962) first isolated 2,6-nonadienal from cucumber. Subsequently, Schieberle et al. (1990) found that (*E,Z*)-2,6-nonadienal mainly caused the flavor of cucumbers with fresh cucumber odor and identified (*E*)-2-nonenal as the second important odor compound in cucumber. Since six-carbon (C6) and nine-carbon (C9) aldehydes play an important role in flavor during fruit development, changes in volatile substances in developing cucumber fruits were investigated in two *Cucumis sativus* L. lines (No. 26 and No. 14). C6 aldehyde content was higher during the early stages, whereas the C9 aldehyde content was higher during the latter stages in both lines (Chen et al., 2015). Lipoxygenase (LOX) and hydroperoxide lyase (HPL) are the two key pre-regulatory factors in the synthesis of cucumber aldehydes. Thereinto, the expression patterns of *9-CsHPL* are similar to the trend of C9, and the expression of *CsLOX2* is also significantly correlated with changes in C9 aldehyde aroma content (Liu, 2018; Wei, 2018). Subsequently, Wei et al. (2016) analyzed 85 volatile chemicals in 23 different tissues of cucumber and further found that TPS15 (encoded by *Csa3G040850*) mediated the biosynthesis of volatile terpenoid in the fruit tissues, which will promote future research studies on the physiological function of volatiles and improve the cucumber flavor breeding. Except for fresh cucumber odor, Yundaeng et al. (2015) also found a special pandan (*Pandanus amaryllifolius*), like fragrance in PK2011T202 (PKT) cucumber cultivar in Thailand. They further found that 2-acetyl-1-pyrroline (2AP) generated this fragrance, and a *betaine aldehyde dehydrogenase 2* (*BADH2*) mutant caused the biosynthesis of 2AP so that produced the pandan-like fragrance in PKT (Yundaeng et al., 2015). Two cucumber accessions, PKT and 301,176 (301), an inbred line from Clover Seed Company, Hong Kong, possessing no fragrance, were used to determine the mode of inheritance of these recessive fragrance traits and each controlled by a specific gene (Pramnoi et al., 2013).

The Bitterness of Cucumber Fruits

The bitterness of cucumber fruits is also of great popularity in the research study of flavor quality traits. Research studies have demonstrated that the Cucurbitacins (Ct) caused the bitterness in cucumber fruits (Rice et al., 1981; Balkema-Boomstra et al., 2003). Since the production of bitterness will lead to fatal losses in the sale of cucumbers, cultivating varieties of cucumbers without bitterness is of great significance for improving the efficiency of cucumber sales. Genetic mechanism of cucumber bitterness showed great complexity. Wehner et al. (2001) found that two dominant genes, Bt (bitter fruit) and Bt-2 (bitter fruit-2), controlled the bitterness of cucumber. In addition, bi (bitter-free cotyledons) gene and the fruit bitterness need both Bi and Bt genes (Andeweg and Bruyn, 1959; Gu et al., 2004; Shang et al., 2014). Further research studies by Zhang et al. (2013) proved that the candidate gene of bi-1 is considered to be the terpene synthase gene named *Csa008595*. Besides, Shang et al. (2014) further demonstrated that Bt can regulate the biosynthesis of cucurbitacin C (CuC) in the cucumber fruits and identified 11 cucumber bitterness biosynthesis, regulation, and domestication-related genes. In addition, the biosynthetic pathway and main regulators of cucurbitacin in cucumber have also been identified. By applying a comparative genomic study, Zhou et al., reported that the independent mutations of the homologous transcription factor genes in the three cucurbits may lead to a significant reduction in fruit bitterness, which may be the reason for the convergence and domestication of bitter wild cucurbits. A syntenic gene cluster that regulates both the tissue-specific biosynthesis of cucurbitacin and the loss of bitter phenotypes associated with the fusion and domestication of wild cucurbits has also been reported in this study. They also found that *Csa6G088160*, *Csa6G088170,* and *Csa6G088180* in cucumber can participate in the biosynthesis of cucurbitacin C (Zhou et al., 2016).

In addition to cucurbitacin, catechins are also one of the key factors that cause cucumber to produce astringency. Xu et al. (2019a) found that tryptophan–aspartate acid (WD40)-repeat protein, avian myeloblastosis viral oncogene homolog (MYB), and basic helix–loop–helix (bHLH) also play an important role in the biosynthesis of catechins. They further found that some genes related to phenylalanine ammonia lyase (PAL)-*CsPAL3* and *CsPAL5*, to cinnamate 4-hydroxylase (C4H)-*CsC4H1*, to 4-coumarate-CoA ligase (4CL)-*Cs4CL2*, to chalcone synthase (CHS)-*CsCHS2*, to chalcone isomerase (CHI)-*CsCHI2*, to flavanone 3-hydroxylase (F3H)-*CsF3H3*, to dihydroflavonol 4-reductase (DFR)-*CsDFR2,* and to anthocyanidin synthase (ANS)-*CsANS* are important regulators of catechin biosynthesis in cucumber fruits (Xu et al., 2019b). But there is currently no clear evidence on how catechins are regulated.

Genetic Regulation of Nutrient Quality in Cucumber

Qiao et al. (2005) reported that crude protein, Vitamin C (VC), soluble reductive sugar, soluble solids, and moisture were five important nutrient components in cucumber. Meanwhile, soluble solids can directly affect nutritional quality, with the greatest impact, while VC, soluble reducing sugars, and crude protein indirectly affect nutritional quality through soluble solids (Qiao et al., 2005). The genes related to the nutrient quality traits of cucumber fruits are shown in **Figure 1** and **Table 2**. The heritability of the soluble sugar content of cucumber is higher, and the selection of early generation has a better effect on it

TABLE 2 | Genes related to the nutrient quality and flavor quality of cucumber fruits.

Category	Traits	QTLs or Gene name	References
Flavor quality	Aldehydes/alcohols	*9-CsHPL*	Liu, 2018
		CsLOX2	Wei, 2018
	Cucurbitacins	*Bt*, *Bt-2,* and *Bi*	Andeweg and Bruyn, 1959; Wehner et al., 2001; Gu et al., 2004; Shang et al., 2014
		Csa008595	Zhang et al., 2013
		Csa6G088160, *Csa6G088170*, and *Csa6G088180*	Zhou et al., 2016
	Catechins	WD40-repeat proteins, MYB, and bHLH	Xu et al., 2019a
		CsPAL3, *CsPAL5*, *CsC4H1*, *Cs4CL2*, *CsCHS2*, *CsCHI2*, *CsDFR2*, *CsF3H3*, and *CsANS*	Xu et al., 2019b
Nutrient quality	β-carotene	*ore*	Bo et al., 2012
		CsZds	Wang et al., 2012

(Xu et al., 2001). Zhang et al. (2020) found that the relationship between soluble sugar and water is positively correlated, while ascorbic acid is negatively correlated with water and soluble sugar. Besides, the contents of β-carotene, a provitamin A, were also important nutrient qualities in cucumber, its contents in cucumber were regulated by an *ore* gene, and seven simple sequence repeat (SSR) markers were identified linking to the locus controlling β-carotene quantity (Bo et al., 2012). On this basis, Wang et al. (2012) used RACE technology to successfully clone the complementary DNA (cDNA) sequence of the ζ-carotene dehydrogenase (ZDS) gene (*CsZds*) and speculated that the gene may be related to the accumulation of β-carotene in cucumber fruits. However, there existed fewer genetic research studies on nutrient qualities in cucumber even until now, and further studies are needed to identify factors related to nutrient qualities formation in cucumber.

PHYSIOLOGICAL REGULATION OF FRUIT QUALITY IN CUCUMBER

Physiological Regulation of Commercial Quality in Cucumber

Cucumber plants usually have poorly developed root systems, rending them vulnerable to infection by various pests and diseases; thus, the cucumber growers have to apply various techniques to improve the commercial quality of cucumber fruits (**Figure 2**). Grafting was wildly used to improve the stress resistance in cucumber, which could also generate positive influences on improvement in their fruit commercial quality (King et al., 2008; Colla et al., 2013). Grafting can also influence the transcript expression levels in cucumber. For example, Zhang J. et al. (2019) found that compared to those self-rooted cucumber, the grafted cucumber showed a higher expression level of the Apetala2/ethylene-responsive factor (AP2/ERF)-type transcription factor *CsWIN1*, and *CsWIN1* further promoted the expression of several key wax biosynthesis and transporter genes so that reflected a glossier appearance. Besides, the usage of plant growth regulators is also an effective measure to alter the fruit qualities in cucumber. Qian et al. (2018) found that N-(2-chloro-4-pyridyl)-N′-phenylurea (CPPU) treatment produced a positive effect on cucumber appearance for the increased flesh firmness. However, gibberellin A4 + A7 (GA4 + 7) treatment reduced its commercial quality (Qian et al., 2018). Hypoxia treatment can inhibit the fresh weight of cucumber fruit. Under hypoxia stress, increasing the amount of exogenous calcium can increase the fresh weight of the fruit (He et al., 2018).

Physiological Regulation of Flavor Quality in Cucumber

Grafting not only affects the commercial quality of cucumbers but also affects the total amount of aroma substances and characteristic esters in the fruit (Pérez et al., 2002). Dong et al. (2013) found that the increased content of volatile substances such as acetaldehyde in the fruits of cucumbers grafted to pumpkins led to a decrease in the flavor and taste of the fruits. Zhao et al., found that compared with those self-grafted cucumbers, the total content of alcohols, aldehydes, olefins, and acids increased of those cucumber plants that were grafted onto "Weisheng NO.1" (*Cucurbita moschata* hybrids) rootstock, so the flavor quality was significantly improved, while the cucumber plants grafted onto *Cucurbita ficifolia* rootstock showed the opposite trend. Grafting of different rootstocks will also significantly affect the expression of genes related to glycolysis, fructose metabolism, and α-linolenic acid metabolism in the scion, thereby changing the flavor quality of grafted cucumbers (Zhao et al., 2018). Different grafting methods will also affect the flavor of cucumber fruits (Lee, 1994). Peng et al. (2010) comprehensively evaluated the sweetness, bitterness, astringency, moisture, and other aspects of cucumber fruit and found that the taste quality of cucumber after double-cut root grafting was the best, while the taste quality of cucumber after double-root grafting was poor. Wang et al. (2019) found that compared with conventional grafting and self-rooting seedlings, the method of interstock grafting can significantly increase the types and contents of volatile substances in cucumber fruits. Besides, bagging was also an effective measure to improve the fruit quality. Shan et al. (2020) demonstrated that cucumber fruits were found to have enhanced fruit flavor

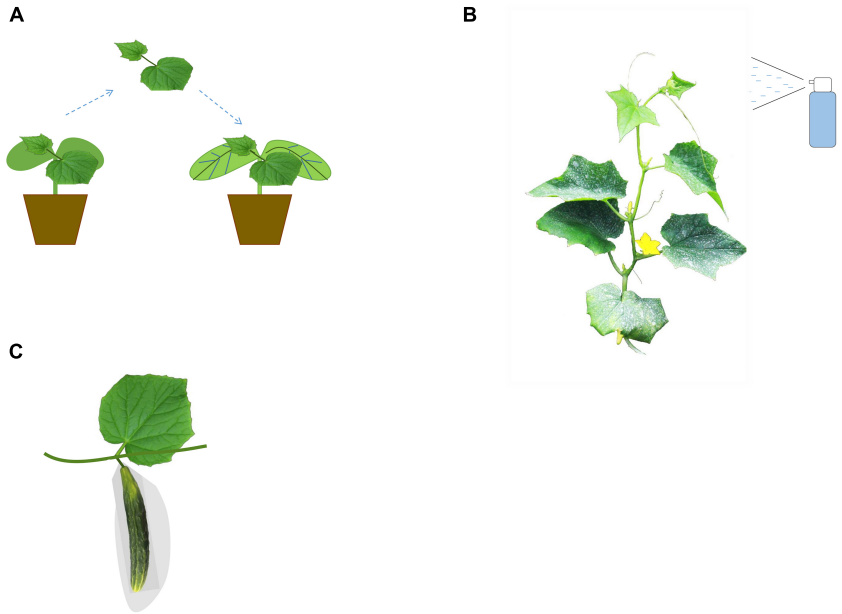


FIGURE 2 | Illustration of the cultivation techniques in cucumber fruit quality breeding. Grafting technique **(A)**, application of exogenous fertilizers and growth regulators **(B)**, and bagging technology **(C)** are widely used in cucumber fruit quality breeding.

quality after bagging, for the elevated relative proportion of C6 aldehyde, (*E,Z*)-2,6-nonadienal/(*E*)-2-nonenal ratio, and linoleic/α-linolenic acid ratio.

Physiological Regulation of Nutrient Quality in Cucumber

Grafting also has an influence on nutrient qualities in cucumber fruits. For example, in the study of Zhao et al. (2018) when cucumber was grafted onto "Weisheng NO.1," the soluble solid content in the fruit was significantly higher than that of the self-grafted group. Besides, the contents of the sugar, organic acids, amino acids, and alcohols were greatly increased when grafting "xintaimici" cucumber on the "GNo.45" pumpkin (*Cucurbita moschata*) (Miao et al., 2019). Dong et al. (2018) also found that elevated carbon dioxide (CO_2) concentration and high nitrogen (N) application can also increase the content of nutrients such as fructose and glucose in cucumber by promoting the carbon translocation from source leaves to fruits. Qian et al. (2018) also found that gibberellin GA4 + 7 treatment improved the nutrient quality in cucumber fruits but decreased its commercial quality. On the contrary, CPPU treatment had a negative effect on the nutritional quality of cucumber (Qian et al., 2018). Moreover, He et al. (2018) found that exogenous calcium treatment on cucumbers under hypoxic stress results in an increased soluble sugar content in cucumber fruits so that enhances its nutrient quality. Ali et al. (2019) found that cucumber growth can be improved by adding arbuscular mycorrhizal strain (AM: *Glomus versiforme* L.) inoculant with organic substrates (GS), and GS + AMF (arbuscular mycorrhizal fungi) treatments increase the total soluble solids of cucumber fruits and soluble sugar content, thereby improving the nutrient qualities of cucumber fruits. With the rapid development of facility cultivation technology, cucumber has now become one of the main crops cultivated in protected areas. Di-n-butyl phthalate (DBP) is widely used as a plasticizer in plastic films because it can increase the toughness and elasticity of products. However, one of its main components, dibromophenol, can cause agricultural pollution that leads to food safety problems, and it has been widely concerned (Heudorf et al., 2007). DBP stress has also a detrimental effect on the contents of organic acids, vitamin C, soluble protein, and soluble sugar in cucumber fruits and resulted in the residue of dibromophenol under protected cultivation conditions. Although the residual dibromophenol in cucumber fruits is below the risk threshold, the potential health risks cannot be ignored (Wang et al., 2016). Therefore, in the process of studying cucumbers, attention should also be paid to the safety of the protected cultivation of cucumbers.

PERSPECTIVE

Compared to the traditional model plants such as *Arabidopsis* and rice, cucumber has some advantages as a new model plant for studies on gene function during fruit development. However, the fruit development of cucumber is a complex biological process, which is affected both by internal genes and external environmental factors. We still need firstly a comprehensive understanding of cucumber quality traits and problems of cultivation skills such as the production of grafted rootstocks, genetic deterioration in breeding, and soil renovation under protected cultivation. Then, we should analyze the compositions of good-quality fruits, such as the types and content of flavor substances, the nutrients, and pigments in cucumber fruits by using high-throughput, high-resolution, and high-sensitivity

modern instrumental analysis methods. Combining with the taste evaluation system of consumers, the breeding goal of cucumber flavor quality can be established and then the genetic mechanism of formation of cucumber fruit quality can be explored. Molecular breeding techniques and methods are used to create new varieties with the best commercial quality (the top flower with thorns and straight strips), nutritional quality (rich in nutrients), and flavor quality (clear fragrance and no bitterness) to meet consumer demand eventually.

In recent years, biotechnologies such as fine mapping, cloning, and transgenesis of genes for important cucumber fruit traits have developed rapidly, and molecular markers combined with traditional breeding methods have been widely used. We will accelerate the completion of the improvement of fruit quality and achieve the breeding goal of high quality, high yield, and stable yield in cucumber fruit production.

AUTHOR CONTRIBUTIONS

CY, JZ, JY, and HW conceived the review, conducted the literature review, and wrote the manuscript. CW and TL collected the literature. SF provided critical comments on the manuscript. All authors read and approved the manuscript.

FUNDING

This study was supported by the National Key Research and Development Program of China (2018YFD1000800 and 2019YFD1000300), Natural Science Foundation of Zhejiang Province (LY21C150002), and National Natural Science Foundation of China (Grant Nos. 31872105, 31972221, 32002048, and 31801862).

REFERENCES

Ali, A., Ghani, M. I., Ding, H., Fan, Y., Cheng, Z., and Iqbal, M. (2019). Co-amended synergistic Interactions between arbuscular mycorrhizal fungi and the organic substrate-induced cucumber yield and fruit quality associated with the regulation of the AM-Fungal community structure under anthropogenic cultivated soil. *Int. J. Mol. Sci.* 20:1539. doi: 10.3390/ijms20071539

Andeweg, J. M., and Bruyn, J. (1959). Breeding of non-bitter cucumbers. *Euphytica* 8, 13–20. doi: 10.1007/BF00022084

Balkema-Boomstra, A. G., Zijlstra, S., Verstappen, F. W. A., Inggamer, H., Mercke, P. E., Jongsma, M. A., et al. (2003). Role of cucurbitacin C in resistance to spider mite (*Tetranychus urticae*) in Cucumber (*Cucumis sativus* L.). *J. Chem. Ecol.* 29, 225–235. doi: 10.1023/A:1021945101308

Beaulieu, J. C., and Lea, J. M. (2006). Quality changes in cantaloupe during growth, maturation, and in stored fresh-cut cubes prepared from fruit harvested at various maturities. *J. Am. Soc. Hortic. Sci.* 132, 127–139. doi: 10.1007/s10658-007-9180-2

Bo, K., Ma, Z., Chen, J., and Weng, Y. (2015). Molecular mapping reveals structural rearrangements and quantitative trait loci underlying traits with local adaptation in semi-wild Xishuangbanna cucumber (*Cucumis sativus* L. *var. xishuangbannanesis* Qi et Yuan). *Theor. Appl. Genet.* 128, 25–39. doi: 10.1007/s00122-014-2410-z

Bo, K., Song, H., Shen, J., Qian, C., Staub, J. E., Simon, P. W., et al. (2012). Inheritance and mapping of the ore gene controlling the quantity of β-carotene in cucumber (*Cucumis sativus* L.) endocarp. *Mol. Breed.* 30, 335–344. doi: 10.1007/s11032-011-9624-4

Bo, K., Wei, S., Wang, W., Miao, H., Dong, S., Zhang, S., et al. (2019). QTL mapping and genome-wide association study reveal two novel loci associated with green flesh color in cucumber. *BMC Plant Biol.* 19:243. doi: 10.1186/s12870-019-1835-6

Boualem, A., Troadec, C., Camps, C., Lemhemdi, A., Morin, H., Sari, M.-A., et al. (2015). A cucurbit androecy gene reveals how unisexual flowers develop and dioecy emerges. *Science* 350, 688–691. doi: 10.1126/science.aac8370

Boualem, A., Troadec, C., Kovalski, I., Sari, M.-A., Perl-Treves, R., and Bendahmane, A. (2009). A conserved ethylene biosynthesis enzyme leads to andromonoecy in two cucumis species. *PLoS One* 4:e6144. doi: 10.1371/journal.pone.0006144

Che, G., Gu, R., Zhao, J., Liu, X., Song, X., Zi, H., et al. (2020). Gene regulatory network controlling carpel number variation in cucumber. *Development* 147:dev184788. doi: 10.1242/dev.184788

Chen, C., Liu, M., Jiang, L., Liu, X., Zhao, J., Yan, S., et al. (2014). Transcriptome profiling reveals roles of meristem regulators and polarity genes during fruit trichome development in cucumber (*Cucumis sativus* L.). *J. Exp. Botany* 65, 4943–4958. doi: 10.1093/jxb/eru258

Chen, S., Zhang, R., Hao, L., Chen, W., and Cheng, S. (2015). Profiling of volatile compounds and associated gene expression and enzyme activity during fruit development in two cucumber cultivars. *PLoS One* 10:e0119444. doi: 10.1371/journal.pone.0119444

Cheng, Z., Gu, X., Zhang, S., Miao, H., Zhang, R., Liu, M., et al. (2010). QTL analysis for fruit length of cucumber. *China Vegetables* 12, 20–25.

Choi, E., Kim, B., Hwang, U., Han, W., and Dong, H. (2013). Characterization of blooming on cucumber fruits. *Korean J. Hortic. Sci. Technol.* 31, 159–164. doi: 10.7235/hort.2013.12160

Colla, G., Rouphael, Y., Jawad, R., Kumar, P., Rea, E., and Cardarelli, M. (2013). The effectiveness of grafting to improve NaCl and CaCl2 tolerance in cucumber. *Sci. Hortic.* 164, 380–391. doi: 10.1016/j.scienta.2013.09.023

Cuevas, H. E., Song, H., Staub, J. E., and Simon, P. W. (2010). Inheritance of beta-carotene-associated flesh color in cucumber (*Cucumis sativus* L.) fruit. *Euphytica* 171, 301–311. doi: 10.1007/s10681-009-0017-2

Dong, J., Xu, Q., Gruda, N., Chu, W., Li, X., and Duan, Z. (2018). Elevated and super-elevated CO2 differ in their interactive effects with nitrogen availability on fruit yield and quality of cucumber. *J. Sci. Food Agric.* 98, 4509–4516. doi: 10.1002/jsfa.8976

Dong, S., Cao, L., Zhang, S., Wang, G., Miao, H., Xie, B., et al. (2013). Effect of grafting on fruit appearance quality and flavor substances in cucumber. *China Vegetables* 22, 44–51.

Dong, S., Miao, H., Zhang, S., Liu, M., Wang, Y., and Gu, X. (2012). Genetic analysis and gene mapping of white fruit skin in cucumber (*Cucumis sativus* L.). *Acta Botanica Boreali-Occidentalia Sin.* 32, 2177–2181. doi: 10.1007/s11783-011-0280-z

Egea, I., Barsan, C., Bian, W., Purgatto, E., Latché, A., Chervin, C., et al. (2010). Chromoplast differentiation: current status and perspectives. *Plant Cell Physiol.* 51, 1601–1611. doi: 10.1093/pcp/pcq136

Forss, D., Dunstone, E., Ramshaw, E., and Stark, W. (1962). The flavor of cucumbers. *J. Food Sci.* 27, 90–93. doi: 10.1111/j.1365-2621.1962.tb00064.x

Gu, X., Zhang, S., Guo, Y., and Xu, C. (2004). Inheritance of bitterness in cucumber. *Acta Hortic. Sin.* 31, 613–616.

Hao, L., Chen, S., Wang, C., Chen, Q., Wan, X., Shen, X., et al. (2013). Aroma components and their contents in cucumbers from different genotypes. *J. Northwest A F Univ.* 41, 139–146. doi: 10.13207/j.cnki.jnwafu.2013.06.027

Hao, N., Du, Y., Li, H., Wang, C., Wang, C., Gong, S., et al. (2018). *CsMYB36* is involved in the formation of yellow green peel in cucumber (*Cucumis sativus* L.). *Theor. Appl. Genet.* 131, 1659–1669. doi: 10.1007/s00122-018-3105-7

Hatanaka, A., Kajiwara, T., and Harada, T. (1975). Biosynthetic pathway of cucumber alcohol: tr*ans*-2,*cis*-6-nonadienol via *cis*-3,*cis*-6-nonadienal. *Phytochemistry* 14, 2589–2592. doi: 10.1016/0031-9422(75)85230-7

He, L., Li, Y., Li, B., Du, N., and Guo, S. (2018). The effect of exogenous calcium on cucumber fruit quality, photosynthesis, chlorophyll fluorescence, and fast chlorophyll fluorescence during the fruiting period under hypoxic stress. *BMC Plant Biol.* 18:180. doi: 10.1186/s12870-018-1393-3

Heudorf, U., Mersch-Sundermann, V., and Angerer, J. (2007). Phthalates: toxicology and exposure. *Int. J. Hygiene Environ. Health* 210, 623–634. doi: 10.1016/j.ijheh.2007.07.011

Horvath, D. P., Schaffer, R., West, M., and Wisman, E. (2003). *Arabidopsis* microarrays identify conserved and differentially expressed genes involved in shoot growth and development from distantly related plant species. *Plant J.* 34, 125–134. doi: 10.1046/j.1365-313X.2003.01706.x

Huang, S., Li, R., Zhang, Z., Li, L., Gu, X., Fan, W., et al. (2009). The genome of the cucumber, *Cucumis sativus* L. *Nat. Genet.* 41, 1275–1281. doi: 10.1038/ng.475

Jiang, L., Yan, S., Yang, W., Li, Y., Xia, M., Chen, Z., et al. (2015). Transcriptomic analysis reveals the roles of microtubule-related genes and transcription factors in fruit length regulation in cucumber (*Cucumis sativus* L.). *Sci. Rep.* 5, 207–228. doi: 10.1038/srep08031

Kamachi, S., Sekimoto, H., Kondo, N., and Sakai, S. (1997). Cloning of a cDNA for a 1-aminocyclopropane-1-carboxylate synthase that is expressed during development of female flowers at the apices of *Cucumis sativus* L. *Plant Cell Physiol.* 38, 1197–1206. doi: 10.1093/oxfordjournals.pcp.a029106

Kemp, T., Knavel, D., and Stoltz, L. (1974). Identification of some volatile compounds from cucumber. *J. Agric. Food Chem.* 22, 717–718. doi: 10.1021/jf60194a006

King, S., Davis, A., Liu, W., and Levi, A. (2008). Grafting for Disease Resistance. *HortScience* 43, 1673–1676. doi: 10.21273/HORTSCI.43.6.1673

Knopf, R. R., and Trebitsh, T. (2006). The Female-Specific *Cs-ACS1G* Gene of Cucumber. A Case of Gene Duplication and Recombination between the Non-Sex-Specific 1-Aminocyclopropane-1-Carboxylate Synthase Gene and a Branched-Chain Amino Acid Transaminase Gene. *Plant Cell Physiol.* 47, 1217–1228. doi: 10.1093/pcp/pcj09

Kooistra, E. (1971). Inheritance of fruit flesh and skin colours in powdery mildew resistant cucumbers (*Cucumis Sativus* L.). *Euphytica* 20, 521–523. doi: 10.1007/BF00034206

Lee, J. (1994). Cultivation of Grafted Vegetables I. Current Status, Grafting Methods, and Benefits. *Hortscience* 29, 235–239. doi: 10.21273/HORTSCI.29.4.235

Li, Y., Wen, C., and Weng, Y. (2013). Fine mapping of the pleiotropic locus *B* for black spine and orange mature fruit color in cucumber identifies a 50kb region containing a R2R3-MYB transcription factor. *Theor. Appl. Genet.* 126, 2187–2196. doi: 10.1007/s00122-013-2128-3

Li, Z., Huang, S., Liu, S., Pan, J., Zhang, Z., Tao, Q., et al. (2009). Molecular isolation of the *M* gene suggests that a conserved-residue conversion induces the formation of bisexual flowers in cucumber plants. *Genetics* 182, 1381–1385. doi: 10.1534/genetics.109.104737

Ligor, T., and Buszewski, B. (2008). Single-drop microextraction and gas chromatography–mass spectrometry for the determination of volatile aldehydes in fresh cucumbers. *Anal. Bioanal. Chem.* 391, 2283–2289. doi: 10.1007/s00216-008-2098-5

Liu, H., Jiao, J., Liang, X., Liu, J., Meng, H., Chen, S., et al. (2016). Map-based cloning, identification and characterization of the *w* gene controlling white immature fruit color in cucumber (*Cucumis sativus L.*). *Theor. Appl. Genet.* 129, 1247–1256. doi: 10.1007/s00122-016-2700-8

Liu, X., Ezra, B., Cai, Y., and Ren, H. (2016). Trichome-related mutants provide a new perspective on multicellular trichome initiation and development in cucumber (*Cucumis sativus* L). *Front. Plant Sci.* 7:1187. doi: 10.3389/fpls.2016.01187

Liu, M. (2018). *Preliminary Functional Analysis of Cucumber Lipoxygenase CsLOX2 Involved in the Synthesis of C9 Aldehydes*. Xianyang: Northwest A&F University.

Liu, X., Wang, T., Ezra, B., Kezia, B., Dong, M., Zhang, Y., et al. (2018). Comprehensive analysis of NAC transcription factors and their expression during fruit spine development in cucumber (*Cucumis sativus* L.). *Hortic. Res.* 5:31. doi: 10.1038/s41438-018-0036-z

Lu, H., Miao, H., Tian, G., Wehner, T., Gu, X., and Zhang, S. (2015). Molecular mapping and candidate gene analysis for yellow fruit flesh in cucumber. *Mol. Breed.* 35, 1–8. doi: 10.1007/s11032-015-0263-z

Lun, Y., Wang, X., Zhang, C., Yang, L., Gao, D., Chen, H., et al. (2016). A *CsYcf54* variant conferring light green coloration in cucumber. *Euphytica* 208, 509–517. doi: 10.1007/s10681-015-1592-z

Lv, J., Li, M., Qian, W., and Qi, W. (1992). Vegetable quality, criterion and sensory identification. *J. Changjiang Vegetables* 6, 3–5.

Malundo, T., Shewfelt, R., and Scott, J. (1995). Flavor quality of fresh tomato (*Lycopersicon esculentum* Mill.) as affected by sugar and acid levels. *Postharvest Biol. Technol.* 6, 103–110. doi: 10.1016/0925-5214(94)00052-T

Miao, L., Di, Q., Sun, T., Li, Y., and Yu, X. (2019). Integrated metabolome and transcriptome analysis provide insights into the effects of grafting on fruit flavor of cucumber with different rootstocks. *Int. J. Mol. Sci.* 20, 289–302. doi: 10.3390/ijms20143592

Ohara, T., Sugiyama, M., and Sakata, Y. (2006). The history of melon and cucumber grafting in Japan. *Acta Hortic.* 767, 217–228. doi: 10.17660/ActaHortic.2008.767.22

Palma-Harris, C., Mcfeeters, R., and Fleming, H. (2001). Solid-phase microextraction (SPME) technique for measurement of generation of fresh cucumber flavor compounds. *J. Agric. Food Chem.* 49, 4203–4207. doi: 10.1021/jf010182w

Pan, Y., Qu, S., Bo, K., Gao, M., Haider, K. R., and Weng, Y. (2017). QTL mapping of domestication and diversifying selection related traits in round-fruited semi-wild Xishuangbanna cucumber (*Cucumis sativus* L. var. *xishuangbannanesis*). *Theor. Appl. Genet.* 130, 1531–1548. doi: 10.1007/s00122-017-2908-2

Peng, X., Chen, Z., Shi, F., Wu, X., Wang, Y., and Gao, L. (2010). Effects of different grafting methods on growth and fruit quality of cucumber in solar greenhouse. *Northern Hortic.* 15, 122–124.

Pérez, A. G., Olías, R., Luaces, P., and Sanz, C. (2002). Biosynthesis of strawberry aroma compounds through amino acid metabolism. *J. Agric. Food Chem.* 50, 4037–4042. doi: 10.1021/jf011465r

Pierce, L., and Wehner, T. (1990). Review of genes and linkage groups in cucumber. *Hortic. Sci.* 25, 605–615. doi: 10.1016/0304-4238(90)90105-N

Pramnoi, P., Somta, P., Chankaew, S., Juwattansomran, R., and Srinives, P. (2013). A single recessive gene controls fragrance in cucumber (*Cucumis sativus* L.). *J. Genet.* 92, 147–149. doi: 10.1007/s12041-013-0228-0

Qi, J., Liu, X., Shen, D., Miao, H., Xie, B., Li, X., et al. (2013). A genomic variation map provides insights into the genetic basis of cucumber domestication and diversity. *Nat. Genet.* 45, 1510–1515. doi: 10.1038/ng.2801

Qian, C., Ren, N., Wang, J., Xu, Q., Chen, X., and Qi, X. (2018). Effects of exogenous application of CPPU, NAA and GA_{4+7} on parthenocarpy and fruit quality in cucumber (*Cucumis sativus* L.). *Food Chem.* 243, 410–413. doi: 10.1016/j.foodchem.2017.09.150

Qiao, H., Zhu, F., Li, C., and Zhang, H. (2005). Inherited analysis on nutrient quality character of cucumber. *J. Northeast Agric. Univ.* 36, 290–293. doi: 10.19720/j.cnki.issn.1005-9369.2005.03.008

Rice, C., Rymal, K., Chambliss, O., and Johnson, F. (1981). Chromatographic and mass spectral analysis of cucurbitacins of three *Cucumis sativus* cultivars. *J. Agric. Food Chem.* 29, 194–196. doi: 10.1021/jf00103a051

Samuels, L., Kunst, L., and Jetter, R. (2008). Sealing plant surfaces: cuticular wax formation by epidermal cells. *Ann. Rev. Plant Biol.* 59, 683–707. doi: 10.1146/ANNUREV.ARPLANT.59.103006.093219

Schieberle, P., Ofner, S., and Grosch, W. (1990). Evaluation of potent odorants in cucumbers (*Cucumis sativus*) and muskmelons (*Cucumis melo*) by aroma extract dilution analysis. *J. Food Sci.* 55, 193–195. doi: 10.1111/j.1365-2621.1990.tb06050.x

Sebastian, P., Schaefer, H., Telford, I., and Renner, S. (2010). Cucumber (*Cucumis sativus*) and melon (*C. melo*) have numerous wild relatives in Asia and Australia, and the sister species of melon is from Australia. *Proc. Natl. Acad. Sci. U. S. A.* 107, 14269–14273. doi: 10.1073/pnas.1005338107

Shan, N., Gan, Z., Nie, J., Liu, H., Wang, Z., and Sui, X. (2020). Comprehensive characterization of fruit volatiles and nutritional quality of three cucumber (*Cucumis sativus* L.) genotypes from different geographic groups after bagging treatment. *Foods* 9:294. doi: 10.3390/foods9030294

Shang, Y., Ma, Y., Zhou, Y., Zhang, H., Duan, L., Chen, H., et al. (2014). Biosynthesis, regulation, and domestication of bitterness in cucumber. *Science* 346, 1084–1088. doi: 10.1126/science.1259215

Tan, J., Tao, Q., Niu, H., Zhang, Z., Li, D., Gong, Z., et al. (2015). A novel allele of *monoecious* (*m*) locus is responsible for elongated fruit shape and perfect flowers in cucumber (*Cucumis sativus* L.). *Theor. Appl. Genet.* 128, 2483–2493. doi: 10.1007/s00122-015-2603-0

Wang, G., Qin, Z., Zhou, X., and Zhao, Z. (2007). Genetic analysis and SSR markers of tuberculate trait in *Cucumis sativus*. *Chin. Bull. Botany* 24, 168–172.

Wang, J., Li, X., Wang, H., Qiu, Y., Song, J., Zhang, X., et al. (2012). Molecular cloning and expression analysis of ζ-carotene desaturase gene from *Cucumis sativus* L. *Mol. Plant Breed.* 10, 520–527. doi: 10.3969/mpb.010.000520

Wang, L., Dong, Y., Sun, X., and Liu, S. (2019). Effects of different grafting methods and different interstock graftings on fruit quality and volatile compounds in cucumber. *Plant Physiol. J.* 55, 867–874. doi: 10.13592/j.cnki.ppj.2018.0469

Wang, L., Sun, X., Chang, Q., Tao, Y., Wang, L., Dong, J., et al. (2016). Effect of di-n-butyl phthalate (DBP) on the fruit quality of cucumber and the health risk. *Environ. Sci. Pollut. Res.* 23, 24298–24304. doi: 10.1007/s11356-016-7658-1

Wang, M., Liu, S., Zhang, S., Miao, H., Wang, Y., Tian, G., et al. (2014). Quantitative trait loci associated with fruit length and stalk length in cucumber using RIL population. *Acta Botanica Boreali-Occidentalia Sin.* 34, 1764–1770.

Wang, W., Zhang, Y., Xu, C., Ren, J., Liu, X., Black, K., et al. (2015). Cucumber *ECERIFERUM1* (*CsCER1*), which influences the cuticle properties and drought tolerance of cucumber, plays a key role in VLC alkanes biosynthesis. *Plant Mol. Biol.* 87, 219–233. doi: 10.1007/s11103-014-0271-0

Wehner, T., Shetty, N., and Walters, S. (2001). Segregation and linkage of several genes in cucumber. *J. Am. Soc. Hortic. Sci.* 126, 442–450.

Wei, G., Tian, P., Zhang, F., Qin, H., Miao, H., Chen, Q., et al. (2016). Integrative analyses of nontargeted volatile profiling and transcriptome data provide molecular insight into VOC diversity in cucumber plants (*Cucumis sativus*). *Plant Physiol.* 172, 603–618. doi: 10.1104/pp.16.01051

Wei, W. (2018). *Preliminary Study on the Role of Hydroperoxide lyase CsHPLs in the Function of Aldehydes Aroma Synthesis in Cucumber*. Xianyang: Northwest A&F University.

Wenzel, G., Kennard, W., and Havey, M. (1995). Quantitative trait analysis of fruit quality in cucumber: QTL detection, confirmation, and comparison with mating-design variation. *Theor. Appl. Genet.* 91, 53–61. doi: 10.1007/bf00220858

Whalen, M. (2005). Host defence in a developmental context. *Mol. Plant Pathol.* 6, 347–360. doi: 10.1111/j.1364-3703.2005.00286.x

Xu, Q., Chen, X., Yu, J., Li, L., and Cao, B. (2001). Preliminary study on heritability and genetic correlation of quality characters in pickling cucumber (*Cucumis sativus* L.). *Jiangsu Agric. Res.* 22, 18–20.

Xu, X., Lu, L., Zhu, B., Xu, Q., Qi, X., and Chen, X. (2015). QTL mapping of cucumber fruit flesh thickness by SLAF-seq. *Sci. Rep.* 5, 895–906. doi: 10.1038/srep15829

Xu, X., Pan, J., He, M., Tian, H., Qi, X., Xu, Q., et al. (2019a). Transcriptome profiling reveals key genes related to astringency during cucumber fruit development. *3 Biotech* 9, 390–398. doi: 10.1007/s13205-019-1922-2

Xu, X., Tian, H., He, M., Gebretsadik, K., Qi, X., Xu, Q., et al. (2019b). Changes in catechin contents and expression of catechin biosynthesis-associated genes during early cucumber fruit development. *Acta Physiol. Plant.* 41, 130–138. doi: 10.1007/s11738-019-2925-7

Yang, L., Koo, D.-H., Li, Y., Zhang, X., Luan, F., Havey, M. J., et al. (2012). Chromosome rearrangements during domestication of cucumber as revealed by high-density genetic mapping and draft genome assembly. *Plant J.* 71, 895–906. doi: 10.1111/j.1365-313x.2012.05017.x

Yang, S., Cai, Y., Liu, X., Dong, M., Zhang, Y., Chen, S., et al. (2018). A *CsMYB6-CsTRY* module regulates fruit trichome initiation in cucumber. *J. Exp. Bot.* 69, 1887–1902. doi: 10.1093/jxb/ery047

Yuan, X., Pan, J., Cai, R., Guan, Y., Liu, L., Zhang, W., et al. (2008). Genetic mapping and QTL analysis of fruit and flower related traits in cucumber (*Cucumis sativus* L.) using recombinant inbred lines. *Euphytica* 164, 473–491. doi: 10.1007/s10681-008-9722-5

Yundaeng, C., Somta, P., Tangphatsornruang, S., Chankaew, S., and Srinives, P. (2015). A single base substitution in BADH/AMADH is responsible for fragrance in cucumber (*Cucumis sativus* L.), and development of SNAP markers for the fragrance. *Theor. Appl. Genet.* 128, 1881–1892. doi: 10.1007/s00122-015-2554-5

Zhang, C., Win, K. T., Kim, Y.-C., and Lee, S. (2019). Two types of mutations in the *HEUKCHEEM* gene functioning in cucumber spine color development can be used as signatures for cucumber domestication. *Planta* 250, 1491–1504. doi: 10.1007/s00425-019-03244-w

Zhang, J., Yang, J., Luo, J., Zheng, X., Wen, C., and Xu, Y. (2019). Transcription factor *CsWIN1* regulates pericarp wax biosynthesis in cucumber grafted on pumpkin. *Front. Plant Sci.* 10:1564. doi: 10.3389/fpls.2019.01564

Zhang, K., Song, H., Kai-Liang, B., Ji, L., Zheng, M., Lou, Q., et al. (2015). QTL Mapping of Multi-Locule-Number Trait in Xishuangbanna Cucumber. *Sci. Agric. Sin.* 48, 3211–3220.

Zhang, S., Liu, S., Miao, H., Wang, M., Liu, P., Wehner, T. C., et al. (2016). Molecular mapping and candidate gene analysis for numerous spines on the fruit of cucumber. *J. Heredity* 107, 471–477. doi: 10.1093/jhered/esw028

Zhang, S., Miao, H., Sun, R., Wang, X., Huang, S., Wehner, T., et al. (2013). Localization of a new gene for bitterness in cucumber. *J. Heredity* 104, 134–139. doi: 10.1093/jhered/ess075

Zhang, X., Zhang, B., Liu, L., and Liu, Z. (2020). Correlation analysis between main fruit characters and quality characters of South China type cucumber. *Hubei Agric. Sci.* 59, 389–391. doi: 10.14088/j.cnki.issn0439-8114.2020.S1.106

Zhao, J., Jiang, L., Che, G., Pan, Y., Li, Y., Hou, Y., et al. (2019). A functional allele of *CsFUL1* regulates fruit length through repressing *CsSUP* and inhibiting auxin transport in cucumber. *Plant Cell* 31, 1289–1307. doi: 10.1105/tpc.18.00905

Zhao, L., Liu, A., Song, T., Jin, Y., Xu, X., Gao, Y., et al. (2018). Transcriptome analysis reveals the effects of grafting on sugar and α-linolenic acid metabolisms in fruits of cucumber with two different rootstocks. *Plant Physiol. Biochem.* 130, 289–302. doi: 10.1016/j.plaphy.2018.07.008

Zhou, Q., Wang, S., Hu, B., Chen, H., Zhang, Z., and Huang, S. (2015). An ACCUMULATION AND REPLICATION OF CHLOROPLASTS 5 gene mutation confers light green peel in cucumber. *J. Integr. Plant Biol.* 57, 936–942. doi: 10.1111/jipb.12355

Zhou, Y., Ma, Y., Zeng, J., Duan, L., Xue, X., Wang, H., et al. (2016). Convergence and divergence of bitterness biosynthesis and regulation in Cucurbitaceae. *Nat. Plants* 2, 1251–1263. doi: 10.1038/nplants.2016.183

Conflict of Interest: The authors declare that the research was conducted in the absence of any commercial or financial relationships that could be construed as a potential conflict of interest.

Publisher's Note: All claims expressed in this article are solely those of the authors and do not necessarily represent those of their affiliated organizations, or those of the publisher, the editors and the reviewers. Any product that may be evaluated in this article, or claim that may be made by its manufacturer, is not guaranteed or endorsed by the publisher.

Copyright © 2021 Zhang, Feng, Yuan, Wang, Lu, Wang and Yu. This is an open-access article distributed under the terms of the Creative Commons Attribution License (CC BY). The use, distribution or reproduction in other forums is permitted, provided the original author(s) and the copyright owner(s) are credited and that the original publication in this journal is cited, in accordance with accepted academic practice. No use, distribution or reproduction is permitted which does not comply with these terms.

frontiers in Plant Science

ORIGINAL RESEARCH
published: 12 October 2021
doi: 10.3389/fpls.2021.737815

Anthocyanin Genes Involved in the Flower Coloration Mechanisms of *Cymbidium kanran*

Zhuang Zhou[1], Zhen Ying[1], Zhigang Wu[1], Yanping Yang[1], Shuangbin Fu[1], Wan Xu[1], Lijuan Yao[1], Aiping Zeng[1], Jian Huang[1], Siren Lan[2], Xiaole Wang[1†] and Zhongjian Liu[1*]*

[1] Zhejiang Institute of Subtropical Crops, Zhejiang Academy of Agricultural Sciences, Wenzhou, China, [2] Key Laboratory of National Forestry and Grassland Administration for Orchid Conservation and Utilization at College of Landscape Architecture, Fujian Agriculture and Forestry University, Fuzhou, China

The Orchidaceae, otherwise known as orchids, is one of the largest plant families and is renowned for its spectacular flowers and ecological adaptations. Various polymorphisms of orchid flower colour can attract pollinators and be recognised as valuable horticultural ornamentals. As one of the longest historic cultured orchids, *Cymbidium kanran* has been domesticated for more than 2,500 years and is an ideal species to study coloration mechanisms because of plentiful variations in floral coloration and abundant traditional varieties. In this study, we used two distinct colour-type flowers of *C. kanran* as experimental materials to elucidate the mechanism of flower coloration. High-performance liquid chromatography (HPLC) analysis revealed that anthocyanins in purple-red-type flowers include three types of anthocyanidin aglycones, peonidin, malvidin, and cyanidin, whereas anthocyanins are lacking in white-type flowers. Through comparative transcriptome sequencing, 102 candidate genes were identified as putative homologues of colour-related genes. Based on comprehensive correlation analysis between colour-related compounds and gene expression profiles, four candidates from 102 captured genes showed a positive correlation with anthocyanidin biosynthesis. Furthermore, transient expression of *CkCHS-1*, *CkDFR*, and *CkANS* by particle bombardment confirmed that recovery of their expression completed the anthocyanin pathway and produced anthocyanin compounds in white-type flowers. Collectively, this study provided a comprehensive transcriptomic dataset for *Cymbidium*, which significantly facilitate our understanding of the molecular mechanisms of regulating floral pigment accumulation in orchids.

Keywords: orchids, *Cymbidium kanran*, anthocyanins, *CkCHS-1, CkDFR, CkANS*, flower coloration

OPEN ACCESS

Edited by:
Pei Xu,
China Jiliang University, China

Reviewed by:
Xiang Lin,
Huazhong Agricultural University, China
Haibin Wang,
Nanjing Agricultural University, China

****Correspondence:***
Xiaole Wang
35337650@qq.com
Zhongjian Liu
zjliu@fafu.edu.cn

†Present address:
Xiaole Wang,
Ningbo Academy of Agricultural Sciences, Ningbo, China

Specialty section:
This article was submitted to Crop and Product Physiology, a section of the journal Frontiers in Plant Science

Received: *07 July 2021*
Accepted: *07 September 2021*
Published: *12 October 2021*

Citation:
Zhou Z, Ying Z, Wu Z, Yang Y, Fu S, Xu W, Yao L, Zeng A, Huang J, Lan S, Wang X and Liu Z (2021) Anthocyanin Genes Involved in the Flower Coloration Mechanisms of Cymbidium kanran. Front. Plant Sci. 12:737815. doi: 10.3389/fpls.2021.737815

INTRODUCTION

Orchids are important ornamental plants characterised by their fantastic floral morphology and high levels of corolla-colour polymorphism and variability, which have played an important role in pollination and have excited biologists since Darwin (Gigord et al., 2001; Aguiar et al., 2020; Basist et al., 2021). As an important member of orchids, *Cymbidium* species are probably the earliest orchid, having been cultivated since before the time of Confucius (551–479 BC) for traditional use in worship and ornamentation (Chen and Tang, 1982; Du Puy et al., 2007). Currently, members of

Cymbidium are still very prevalent and dominate the world floriculture markets (Singh et al., 2019). Although the mechanism of genes encoding enzymes for flower coloration in orchids has been studied in some species (Mudalige-Jayawickrama et al., 2005; Han et al., 2006; Hieber et al., 2006; Chen et al., 2011; Hsiao et al., 2011; Liu et al., 2012; Yu et al., 2018), as one of the longest historic floricultural plants, *Cymbidium kanran* attracts wide attention. However, its coloration mechanism remains unclear.

Anthocyanins, as a series of secondary metabolites, are water-soluble pigments that contribute colours from orange, pink, red, magenta, purple, blue, cyan to "black" (Hatier and Gould, 2007; Tanaka et al., 2008; Petroni and Tonelli, 2011; Moreau et al., 2012; Li et al., 2014). These pigments are an ideal model for genetics, molecular biology, and cell biology (Passeri et al., 2016). To date, hundreds of anthocyanins have been extensively studied and characterised, which were originally based on six common types of anthocyanidins (chromophores of anthocyanins), namely, petunidin, pelargonidin, delphinidin, cyanidin, malvidin, and peonidin. Accordingly, the synthetic route of anthocyanins and important related genes are well-studied and characterised in some model and non-model plants. Anthocyanins are derived from flavonoid biosynthetic pathways, and their biosynthesis has been divided into three stages (Grotewold, 2006). The first stage is phenylalanine and phenylpropanoid metabolism, which is shared among other secondary metabolisms. The second stage, flavonoid metabolism, is the crux of anthocyanin biosynthesis. Chalcone synthase (CHS) is the first key enzyme to produce chalcones, the precursor for all classes of flavonoids. Subsequently, an enzymatic reaction of chalcones to naringenins is catalysed by chalcone isomerase (CHI), which is followed by a conversion to dihydrokaempferol (DHK) by flavanone 3-hydroxylase (F3H). The last step involves two participants, flavonoid 3'-hydroxylase (F3'H) and flavonoid 3', 5'hydroxylase (F3' 5'H), corresponding to the respective products dihydroquercetin (DHQ) and dihydromyricetin (DHM). The final stage is anthocyanin metabolism, including two rate-limiting steps catalysed by dihydroflavonol reductase (DFR) and anthocyanidin synthase (ANS). Three kinds of products, delphinidin, pelargonidin, and cyanidin, undergo several modifications, such as glycosylation or methylation, by UDP-glucoside: flavonoid 3-O-glucosyltransferase (3GT) and anthocyanin methyltransferase (AMT).

Transgenic technology, expression, and suppression of the level of the anthocyanin synthetic gene have been verified as feasible to study the accumulation mechanism of anthocyanin in many plants. With the expression of *UFGT*, the skin colours of the *Vitis* and *Litchi* were turned red or violet from green (Ramazzotti et al., 2008; Zhao et al., 2012). Overexpression of *SmANS* from *Salvia miltiorrhiza* enhanced anthocyanin accumulation in the petals of *S. miltiorrhiza* f. *alba* and resulted in purple-red colour from white colour (Li et al., 2019). Using RNA interference (RNAi) technology to suppress *CHS*, *ANS*, and *F3'5'H*, the petals of gentian plants exhibited pure white to pale-blue and magenta flowers accordingly (Nakatsuka et al., 2008). Consequently, using transgenic approaches to introduce exogenous anthocyanin genes into the targeted plant can obtain the desired coloration traits to produce new flower colour (Meyer et al., 1987; Katsumoto et al., 2007).

Cymbidium kanran is an ideal species to study coloration mechanisms because of numerous variations in floral coloration and abundant traditional varieties. In this study, we used purple-red flowers (with many purple-red pigments) and white flowers (greenish-white without purple-red pigments) as research materials (**Figure 1**). Through a combination of transcriptome sequencing, chemical, and molecular analysis, the mechanism of anthocyanin deficiency in white was preliminarily revealed. This dataset provided a novel resource to study and to understand the molecular mechanisms of coloration in *C. kanran*.

MATERIALS AND METHODS

Plant Material and Freehand Sectioning

White-type flowers and purple-red-type flowers of *C. kanran* were used as research materials in this study and cultivated in the greenhouse of Zhejiang Institute of Subtropical Crops in Wenzhou City, China (120°37′53″E, 28°0′8″N). For the first one, it has white flowers (**Figure 1A**), for the second, it has purple-red flowers with purple-red sepals/petals and white lip with purple-red spots (**Figure 1B**). The buds were about 2, 3 cm, 1–2 days before anthesis, and opened flowers were used for Real-Time PCR analysis. At the same time, about 3 cm length buds were selected for transcriptome sequencing and fully opened flowers were selected for freehand sectioning and pigment analysis. When harvested, all the materials were immediately frozen in liquid nitrogen (LN) and stored at −80°C except the freehand sectioning samples. Petals or lips of fully opened flowers were perpendicularly cut quickly to their longitudinal axis by hand sectioning with a new sharp double-edged razor blade. The sections were immersed in water and observed under an optical microscope.

RNA Extraction, Library Construction, and RNA-seq

The total RNA of each sample was isolated using TRIzol Reagent (Invitrogen Life Technologies, Carlsbad, CA, USA). Then, the integrity and concentration were checked on a 1% agarose gel and a NanoDrop ND-1000 spectrophotometer (NanoDrop Technologies, Wilmington, DE, USA). The enriched mRNA was broken into short fragments, which were used to synthesise first- and second-strand cDNA. After that, the construction of the cDNA library was performed following the instructions of the manufacturer of the NEBNext Ultra RNA Library Prep Kit for Illumina (NEB, E7530, New England Biolabs, Ipswich, MA, USA) and NEBNext Multiplex Oligos for Illumina (NEB, E7500). Finally, the libraries of *C. kanran* buds were sequenced using an Illumina HiSeq^{TM} 2500 by Biomarker Biotechnology Corporation (Beijing, China).

RNA-seq Data Assembly, Annotation, and Differential Expression Analysis

Raw data obtained by RNA-seq were primarily processed through in-house Perl scripts. In this step, clean reads were acquired



FIGURE 1 | The phenotype of purple-red and white *Cymbidium kanran*. **(A)** The plant of purple-red *C. kanran*. **(B)** The plant of white *C. kanran*. **(C–G)** Flower, sepal, petal, lip, and gynostemium of white *C. kanran*. **(H–L)** Flower, sepal, petal, lip, and gynostemium of purple-red *C. kanran*. Scale bar = 1 cm.

by removing reads containing adapters, reads containing poly-N and low-quality reads from raw data. In addition, the Q20, Q30, GC content, and sequence duplication levels of the clean data were calculated to evaluate the sequencing quality. All the subsequent analyses were based on clean data with high quality. Transcriptome assembly was accomplished based on the fq file using Trinity software (https://github.com/trinityrnaseq/trinityrnaseq/wiki) (Grabherr et al., 2011) with min_kmer_cov set to two by default and all other parameters set to default.

Gene function was annotated by BLASTX (Altschul et al., 1997) program (http://www.ncbi.nlm.nih.gov/) based on the following databases: Nr (NCBI non redundant protein sequences); Nt (NCBI non-redundant nucleotide sequences); Pfam (Protein family); KOG/COG (Clusters of Orthologous Groups of proteins); Swiss-Prot (a manually annotated and reviewed protein sequence database); KO (KEGG Orthologue database); and GO (Gene Ontology).

Gene expression levels were estimated using RSEM software (http://deweylab.github.io/RSEM/) (Li and Dewey, 2011) for each sample. Differential expression analysis of the two samples was performed using DESeq (http://www.bioconductor.org/packages/3.8/bioc/html/DESeq.html). The resulting *P*-values were adjusted with the Benjamini-Hochberg method to control the false discovery rate. Genes with an adjusted $P < 0.05$ found by DESeq were identified as differentially expressed.

Gene Validation and Expression Analysis

Total RNA was isolated from *C. kanran* buds and flowers using the ZR Plant RNA MiniPrep Kit (Zymo Research, Irvine, CA, USA), and 1 μg RNA was used to synthesise oligo(dT)-primed first-strand cDNA by the QuantiTect Reverse Transcription

Kit (QIAGEN, Hilden, Germany) following the protocol of the manufacturer. The qRT-PCRs were performed in a 7300 Real-Time PCR System (Applied Biosystems, Foster Arthritis 5 City, CA, USA) using an SYBR premix Ex TaqTM Kit (TaKaRa, Kyoto, Japan). The reference gene we chose was actin (c114989.graph_c0). We calculated the relative expression level by the $2^{-\Delta\Delta}$CT method (Livak and Schmittgen, 2001).

Measurement of Flower Flavonoids

We used the relative quantitative method to analyze flavonoids from white and purple-red *C. kanran* opened flowers. Approximately 0.1 g (fresh weight) was extracted in 1 ml 70% methanol at 4°C for 1 day. After centrifugation for 5 min at 12,000 rpm, the supernatant was collected. Before analysis by high-performance liquid chromatography (HPLC), the extract was filtered to remove impurities. Samples were analysed using LC-ESI-QTRAP-MS/MS with an Agilent 1200 Series HPLC system (Agilent Technologies, Waldbronn, Germany) coupled to an Applied Biosystems 4000 QTRAP (Darmstadt, Germany), and quantification of flavonoids was carried out in MRM mode. The analytical conditions were as described previously (Chen et al., 2013). Data acquisition, peak integration, and calculations were performed using Analyst 1.5 software (AB Sciex, MA, USA). We quantified the anthocyanin and flavonol contents of white, purple-red, and intermediate phenotype *C. kanran* flowers for Pearson's correlation coefficient in a different way. Approximately, 0.2 g (fresh weight) was extracted in 1 ml methanol: acetic acid: water (80:2:18, by vol.) at 4°C for 1 day. After centrifugation for 5 min at 12,000 rpm, the supernatant was collected, and the pellet was re-extracted for the second time. The combined supernatant was hydrolyzed in boiling water for 1 h and then quantitated to 2 ml. Before analysis by HPLC, the extract was filtered to remove impurities. HPLC was performed as previously described (Wang et al., 2014). Myricetin, kaempferol, quercetin, peonidin, malvidin, delphinidin, pelargonidin, and cyanidin (Sigma-Aldrich, China) were used for qualitative and quantitative analysis. Mean values and SDs were obtained from three replicates.

Construction for Transient Expression by Particle Bombardment

According to the gene transcript level and flavonoid content, *CkCHS-1*, *CkDFR*, and *CkANS* were screened as key genes encoding enzymes in the flavonoid metabolic pathway of *C. kanran*. Therefore, the three genes were divided into three groups, single genes, double genes, and triple genes, to be validated for transient expression by particle bombardment. The genes driven individually by the 35S promoter were cloned into the pCAMBIA1305.1 vector at the NcoI restriction site. The recombinant plasmid DNA was extracted and purified using an EndoFree Plasmid Giga Kit (QIAGEN, Hilden, Germany). Before bombardment, healthy white-type *C. kanran* flowers were collected, and the following procedure was conducted as described in the study by Ma et al. (2008).

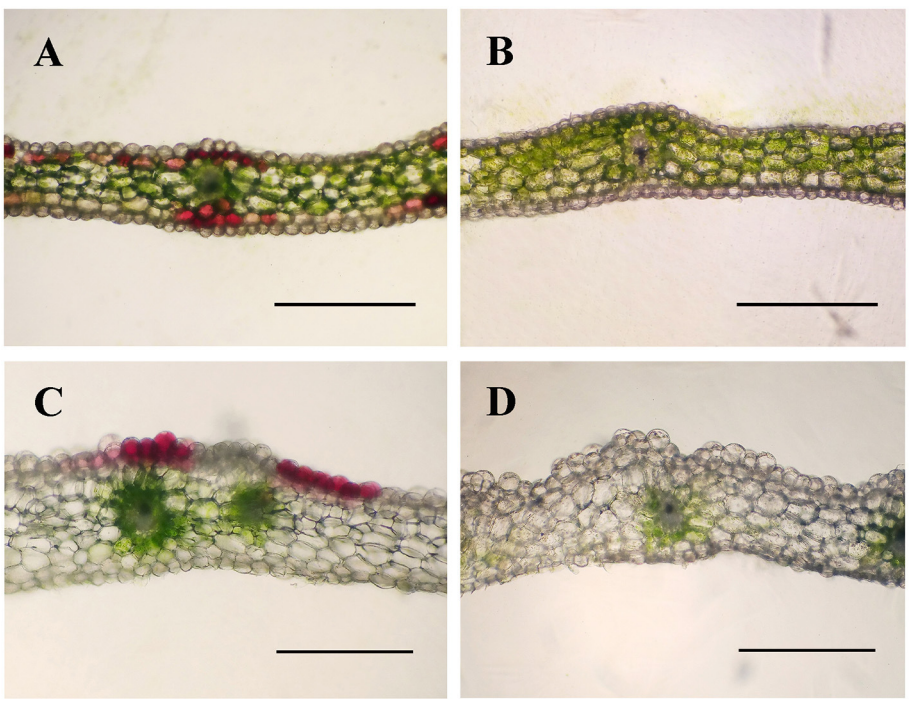


FIGURE 2 | Cross-sections of purple-red and white *C. kanran* showing the different colour patterns in petals and lips. Anatomic structure of purple-red *C. kanran* petals **(A)** and lips **(C)**, white *C. kanran* petals **(B)**, and lips **(D)**. Scale bar = 500 μm.

RESULTS

Phenotypic Characterisation

In the process of domestication and cultivation of *C. kanran*, it is important to note the colour variety of the flowers. The most well-known cultivar, white-type *C. kanran*, has greenish-white petals and a white lip, both with greenish stripes (**Figures 1A,C–G**). Compared with white-type flowers, purple-red flowers exhibited purple-red petals with stripes of the same colour and a white lip with red spots and greenish stripes (**Figures 1B,H–L**). Because of the striking contrast in flower colour, white and purple-red *C. kanran* are the optimal candidates to reveal the flower coloration mechanism. To study the distribution of anthocyanin production in perianth cells, we analysed petal and lip cross-sections from white and purple-red *C. kanran* (**Figure 2**). In the petals, anthocyanins accumulated in the region from subepidermal cells to the xylem (**Figure 2A**), while in the lip, anthocyanins accumulated only in the epidermal cells of the adaxial surface (**Figure 2C**). However, white flowers showed no purple-red pigments (anthocyanins) in cells except chlorophyll (**Figures 2B,D**).

Flavonoid Content

Anthocyanins, as the largest group of water-soluble pigments, are responsible for most of the purple, blue, and red colours in the plants. In this study, we quantified the flavonoids of purple-red and white *C. kanran* flowers by a relative quantitative method. In purple-red flowers, only cyanidin, peonidin, and malvidin were present, and the cyanidin content was far greater than that of peonidin and malvidin. Delphinidin and pelargonidin-type anthocyanins were not detected, which probably was due to their extremely low content. Interestingly, the contents of myricetin (MY), kaempferol (KA), and quercetin (QU) in the white petals were lower than those in the purple-red *C. kanran* petals. However, it is worth noting that QU was detected in the white lip at a concentration two times higher than that in the purple-red lip, while the concentrations of MY and KA were similar in both study objects (**Figure 3**).

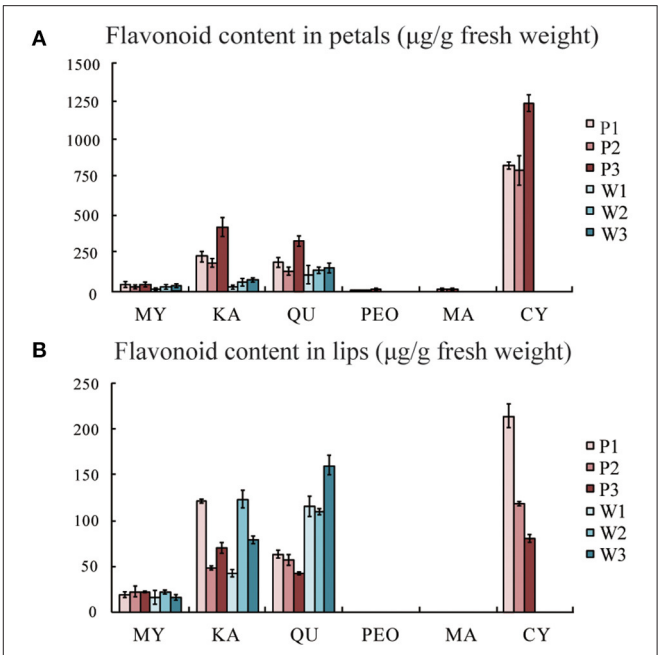


FIGURE 3 | Flavonoid composition analysis by HPLC from flowers of purple-red and white *C. kanran*. **(A)** Flavonoid content in petals. **(B)** Flavonoid content in lips. MY, myricetin; KA, kaempferol; QU, quercetin; PEO, peonidin; MA, malvidin; CY, cyanidin; P1, purple-red *C. kanran* 1; W1, white *C. kanran* 1.

RNA-seq, Assembly, and Differential Expression Analysis

To illustrate the mechanism underlying the variation in flower coloration and to identify potential genes involved in this process, the petals and lips of purple-red and white *C. kanran* were used to generate four libraries for high-throughput sequencing. After quality cheques, 61.90 Gb clean data were obtained, and the Q30 percentages (percentage of sequences with sequencing error rates <0.1%) of every sample were higher than 87.72%. These data showed that the sequencing quality and throughput were reliable enough to carry out further research. Short reads were then assembled into 181,335 transcripts and 74,713 unigenes by Trinity with mean lengths of 1,230 bp and 887 bp, respectively. After searching the reference sequences using BLASTX against KEGG, COG, KOG, GO, nr, and Swiss-Prot, we obtained a total of 26,930 unigenes providing a significant BLAST result.

Differentially expressed unigenes were grouped into 50 functional categories following KEGG annotation (**Figure 4**). The most prevalent functional category was photosynthesis, followed by phenylpropanoid metabolism, which was located upstream of flavonoid metabolism. Members involved in phenylalanine and flavonoid metabolism were also major parts of differentially expressed unigenes. These results indicated that the alternation of flavonoid metabolism was the underlying factor leading to a striking contrast in flower colour between purple-red and white *C. kanran*. Furthermore, the crucial genes taking part in three secondary metabolic pathways (phenylpropanoid, flavonoid, and anthocyanin metabolism referring to KEGG pathways) are listed in **Table 1**, consisting of 102 unigenes.

To compare levels of pigment biosynthesis-related gene expression, relative expression levels of "petals vs. lips of purple-red *C. kanran,*" "petals vs. lips of white *C. kanran,*" "petals of white *C. kanran* vs. petals of purple-red *C. kanran,*" and "lips of white *C. kanran* vs. lips of purple-red *C. kanran*" were conducted. Among the differences in the gene expression profile of white *C. kanran* vs. purple-red *C. kanran*, each one of cinnamate 4-hydroxylase (C4H), CHS, DFR, and ANS were downregulated, whereas each one of F 3'H, flavonol synthase (FLS), and CCoAOMT were upregulated. In the same flower, two C4H and each one of CHS, DFR, and ANS were upregulated but only one CHS was downregulated (petals vs. lips of purple-red *C. kanran*), however, there was only one CHS downregulated (petals vs. lips of white *C. kanran*) (**Table 2**).

Validating RNA-seq Data by qRT-PCR

To validate the RNA-seq expression profiles, seven differentially expressed unigenes encoding C4H, CHS, DFR, ANS, and FLS

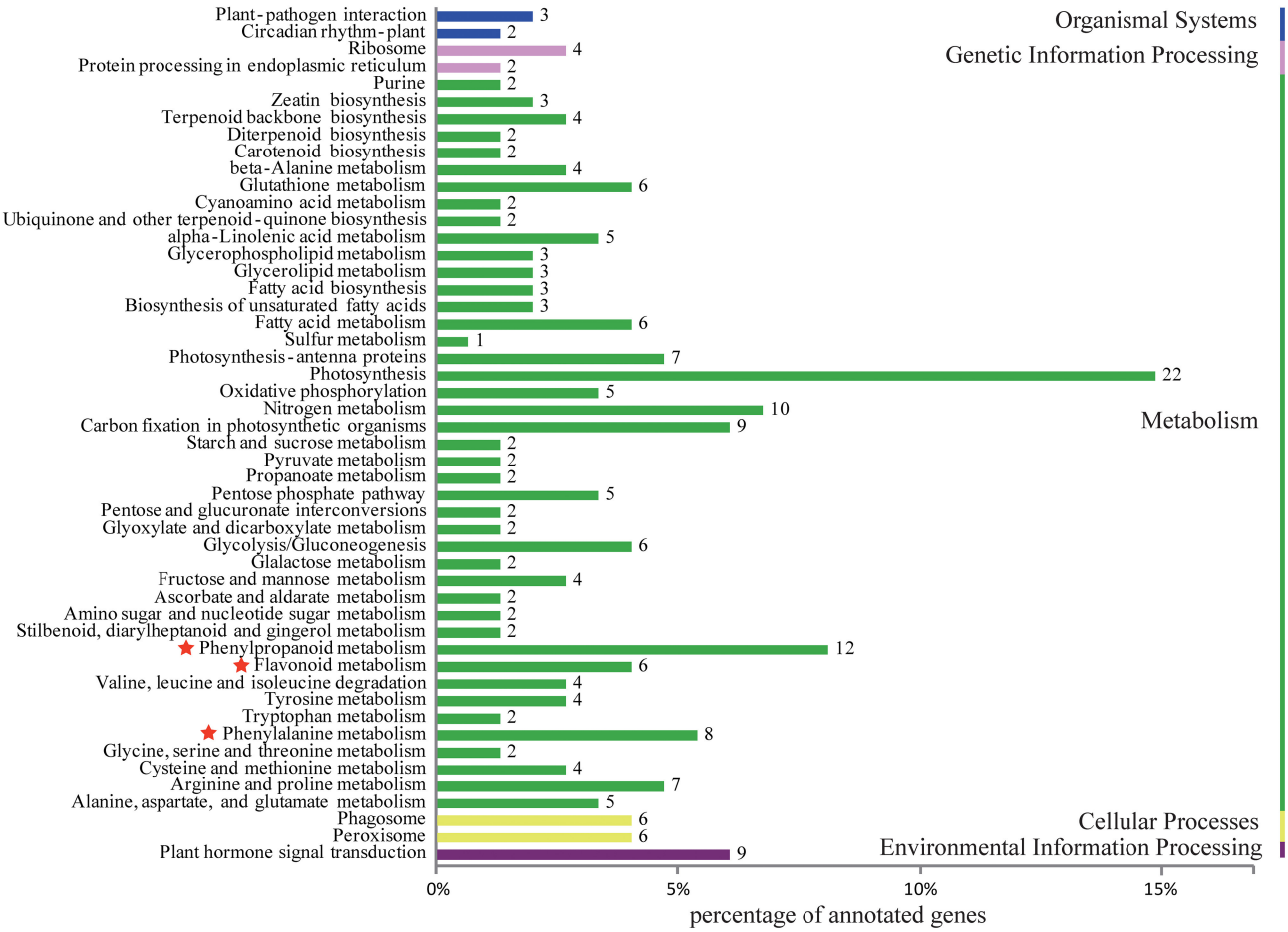


FIGURE 4 | Histogram of KEGG classification for different colours of *C. kanran*. Functional classification of differentially expressed unigenes, considering both purple-red and white *C. kanran*. Classification followed the KEGG annotations. The red star shows the category we focused on.

TABLE 1 | Candidate genes related to flower pigmentation of *Cymbidium kanran*.

Function	Name	Target description	KO id (EC No.)	No. All[a]
Phenylpropanoid biosynthesis	C4H	Trans-cinnamate 4-monooxygenase	K00487 (1.14.13.11)	4
	C3H	Coumaroylquinate 3′-monooxygenase	K09754 (1.14.13.36)	1
	CCoAOMT	Caffeoyl-CoAO-methyltransferase	K00588 (2.1.1.104)	7
	HCT	Shikimate hydroxycinnamoyl transferase	K13065 (2.3.1.133)	4
Flavonoid biosynthesis	CHS	Chalcone synthase	K00660 (2.3.1.74)	14
	CHI	Chalcone isomerase	K01859 (5.5.1.6)	2
	F3H	Flavanone 3-hydroxylase	K00475(1.14.11.9)	10
	F3′H	Flavonoid 3′-hydroxylase	K05280 (1.14.13.21)	9
	F3′5′H	Flavonoid 3′5′-hydroxylase	K13083 (1.14.13.88)	1
	DFR	Dihydroflavonol-4-reductase	K13082 (1.1.1.219)	3
	ANS	Anthocyanidin synthase	K05277 (1.14.11.19)	6
	ANR	Anthocyanidin reductase	K08695 (1.3.1.77)	1
	FNS	Flavone synthase	K13077 (1.14.11.22)	1
	FLS	Flavonol synthase	K05278 (1.14.11.23)	12
	C12RT1	Flavanone 7-O-glucoside 2′′-O-beta-L-rhamnosyltransferase	K12934 (2.3.1.172)	1

(Continued)

TABLE 1 | Continued

Function	Name	Target description	KO id (EC No.)	No. All[a]
	FOMT	Flavonol 3-O-methyltransferase	K05279 (2.1.1.76)	9
Anthocyanin modification	GT1	Anthocyanidin 5′,3′-O-glucosyltransferase	K12938 (2.4.1.-)	7
	3′GT	Anthocyanin 3′-O-beta-glucosyltransferase	K12939 (2.4.1.238)	1
	5 MaT1	Anthocyanin 5-O-glucoside-6‴-O-malonyltransferase	K12934 (2.3.1.172)	1
	UFGT	Anthocyanidin 3-O-glucosyltransferase	K12930 (2.4.1.115)	5
	CrOMT2	Myricetin O-methyltransferase	K13272 (2.1.1.149)	1
	LuOMT	Luteolin O-methyltransferase	\[d] (2.1.1.75)	2

[a]*No. All, the total number of unigenes investigated.*
[d]*Omission of numbers for the KO id.*

TABLE 2 | Shifts in the expression levels of candidate genes related to flower pigmentation.

Name	Target description	KO id (EC No.)	No. All[a]	No. Up[b]	No. Down[c]
Petals vs. lips of purple *C. kanran*					
C4H	Trans-cinnamate 4-monooxygenase	K00487 (1.14.13.11)	2	2	0
CHS	Chalcone synthase	K00660 (2.3.1.74)	2	1	1
DFR	Dihydroflavonol 4-reductase	K13082 (1.1.1.219)	1	1	0
ANS	Anthocyanidin synthase	K05277 (1.14.11.19)	1	1	0
Petals of white vs. petals of purple *C. kanran*					
C4H	Trans-cinnamate 4-monooxygenase	K00487 (1.14.13.11)	2	0	1
CHS	Chalcone synthase	K00660 (2.3.1.74)	1	0	1
DFR	Dihydroflavonol 4-reductase	K13082 (1.1.1.219)	1	0	1
FLS	Flavonol synthase	K05278 (1.14.11.23)	12	1	0
ANS	Anthocyanidin synthase	K05277 (1.14.11.19)	1	0	1
CCoAOMT	Caffeoyl-CoAO-methyltransferase	K00588 (2.1.1.104)	1	1	0
Petals vs. lips of white *C. kanran*					
CHS	Chalcone synthase	K00660 (2.3.1.74)	1	0	1
Lips of white vs. lips of purple *C. kanran*					
F3'H	Flavonoid 3′-monooxygenase	K05280 (1.14.13.21)	1	1	0
FLS	Flavonol synthase	K05278 (1.14.11.23)	12	1	0

[a]*No. All, the total number of unigenes investigated.*
[b]*No. Up, the number of unigenes with higher expression level in the former than the latter.*
[c]*No. Down, the number of unigenes with lower expression level in the former than the latter.*

were quantified by qRT-PCR (**Figures 5A–U**). The general expression profile obtained by qRT-PCR was perfectly consistent with that obtained by RNA-seq (**Figure 5V**), supporting the accuracy of the RNA-seq data.

CkC4H-3, *CkCHS-1*, *CkDFR*, and *CkANS* were highly expressed in purple-red floral tissues and expressed at low levels in white floral tissues (**Figures 5A–I, M–R**). Conversely, *CkFLS* was expressed at a higher level both in petals and the lip of white *C. kanran* than purple-red *C. kanran* (**Figures 5S,T**). Most of the anthocyanin-related genes exhibited higher expression levels in petals than in the lip, but the opposite results appeared in the *CkCHS-2* expression pattern (**Figures 5J–L**). More interestingly, *CkCHS-2* was abundantly expressed in white flowers but expressed at low levels in purple-red flowers (**Figures 5J,K**). Conversely, *CkCHS-1* was highly expressed in purple-red flowers but had low expression levels in white flowers (**Figures 5G,H**), suggesting that white and purple-red flowers may have different *CHSs* to participate in the flavonoid/anthocyanin biosynthesis pathway. Additionally, *CkDFR* expression in three shades of purple-red flowers displayed a reverse trend to *CkFLS* (**Figures 5W,X**), which is in agreement with the competition to the same substrate between DFR and FLS.

Pearson's Correlation Coefficient Between Gene Transcript Level and Flavonoid Content

To uncover the relationship between gene expression and flavonoid content, the transcript abundance of flavonoid pathway genes and the accumulation of related products were detected in three shades of flowers (white, purple-red, and intermediate phenotype *C. kanran*). As presented in **Figure 6**,

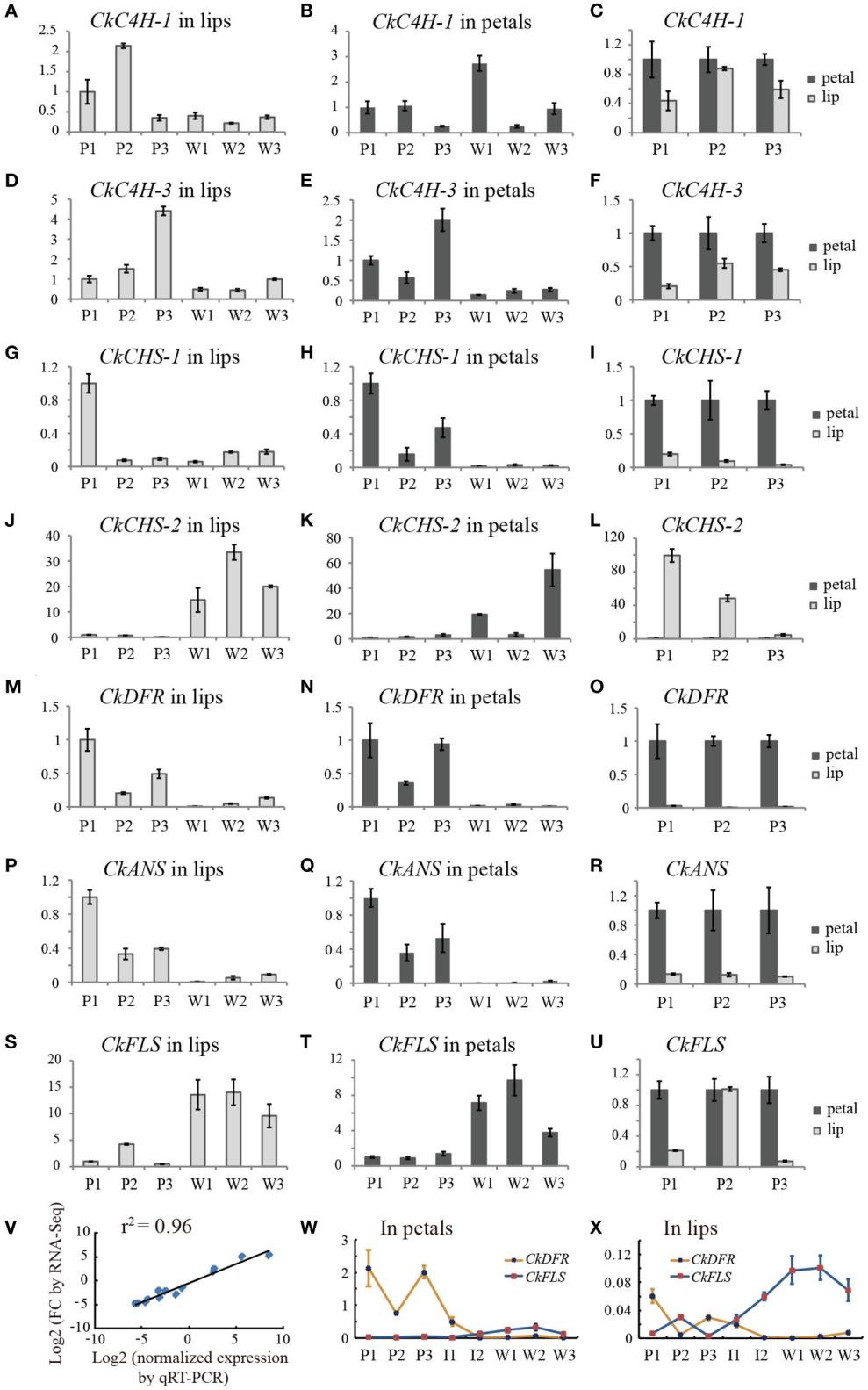


FIGURE 5 | Transcript accumulation measurements of colour-related genes involved in the anthocyanidin metabolic process. **(A–U)** The qRT-PCR analysis of differentially expressed genes from RNA-Seq analysis. **(V)** Correlation of gene expression results obtained by qRT-PCR analysis and RNA-Seq for colour-related genes of the purple-red and white flower buds (length of approximately 3.0 cm). **(W,X)** line charts of the relative expression levels of *DFR* and *FLS* in petals and lips, respectively. The Y-axis of all charts except V represents the relative expression level. P1, purple-red *C. kanran* 1; W1, white *C. kanran* 1; I1, intermediate phenotype *C. kanran* 1.

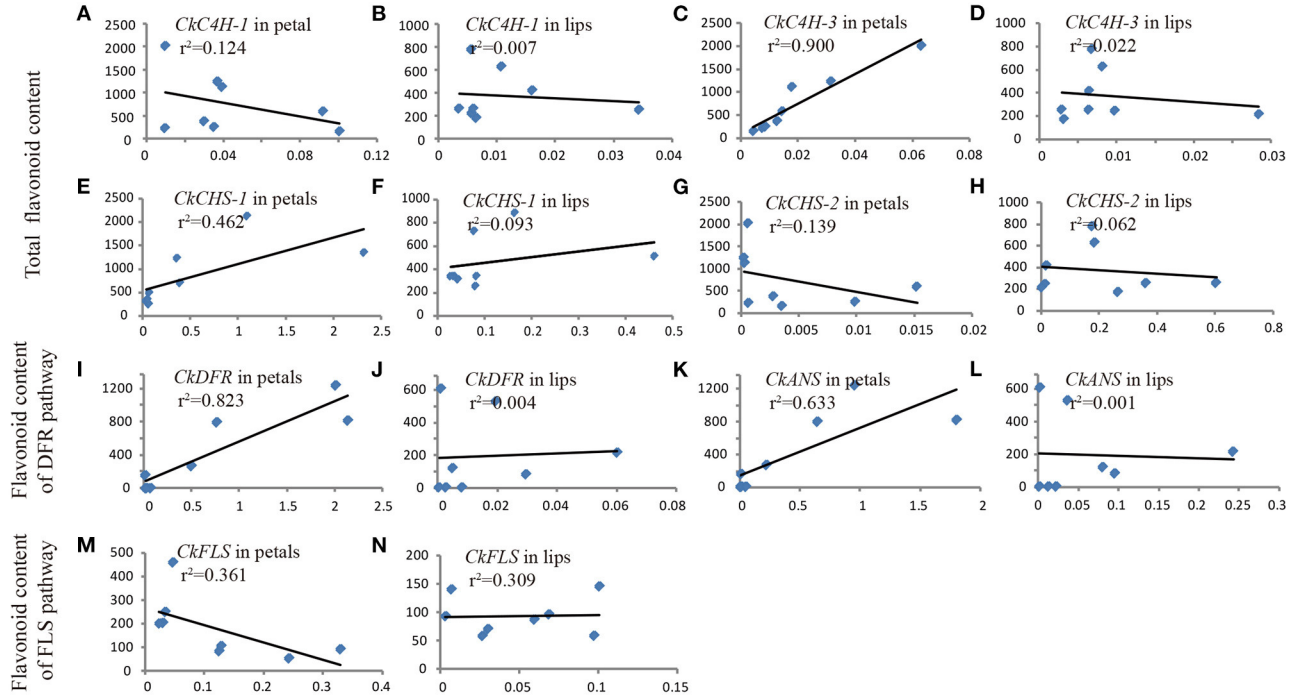


FIGURE 6 | Pearson's correlation coefficient between gene transcript level (X-axis) and flavonoid content (Y-axis) in petals **(A,C,E,G,I,K,M)** and the lip **(B,D,F,H,J,L,N)** of *C. kanran*. Total flavonoids included MY, KA, QU, PEO, MA, and CY. The anthocyanidins of the DFR pathway included PEO, MA, and CY. The flavonol of the FLS pathway included MY, KA, and QU.

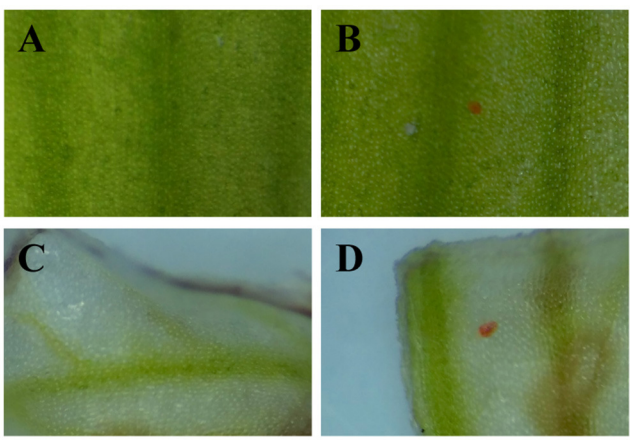


FIGURE 7 | Development of red spots in white petals and lips due to transient expression of *CkCHS-1*, *CkDFR*, and *CkANS* under the control of the 35S promoter. **(A)** A petal conducted by particle bombardment with empty vector plasmid. **(B)** A petal conducted by particle bombardment with the mixture of overexpression vector plasmids of the three genes. **(C)** A lip conducted by particle bombardment with empty vector plasmid. **(D)** A lip conducted by particle bombardment with the mixture of overexpression vector plasmids of the three genes.

the concentration of flavonoids varied with the expression level of different genes. Normally, two variables show a strong correlation if the correlation coefficient (r) exceeds 0.6 in the Pearson correlation analysis. The contents of total flavonoids were significantly positively correlated with the expression levels of *CkC4H-3* and *CkCHS-1* in petals ($r^2 = 0.9055$, $r^2 = 0.4642$) (**Figures 6C,E**). However, there was poor or no correlation between the total flavonoid content and *CkC4H-1* and *CkCHS-2* transcripts (**Figures 6AB,G,H**), which agreed with the qRT-PCR results showing ruleless expression levels in purple-red and white *C. kanran* (**Figures 6A–C,J–L**). *CkDFR* and *CkANS* were involved in the biosynthesis of CY, MA, and PEO and were positively correlated with the anthocyanidin content of the DFR pathway in petals (**Figures 6I,L**).

Production of Purple-Red Pigmentation in White *C. kanran* by Transient Expression of *CHS-1*, *DFR*, and *ANS* Genes

According to Pearson's correlation analysis in **Figure 6**, we conjectured that the recovery of the *CkCHS-1*, *CkDFR*, and *CkANS* genes in the white type could complete the anthocyanin pathway to display a red pigment similar to that of purple-red *C. kanran*. Hence, these three genes were divided into three groups, which are single genes, double genes, and triple genes, to be validated for transient expression by particle bombardment. Then, the three groups of genes were bombarded into white petals and lips. After incubation on 1/2 MS medium for 5 days, only the group of triple genes accumulated red spots in both petal and lip tissue (**Figure 7**). This result supported that anthocyanin absence in white-type *C. kanran* probably resulted from the expression deficiency of *CkCHS-1*, *CkDFR*, and *CkANS*. We further evaluated the temporal transcription of these three

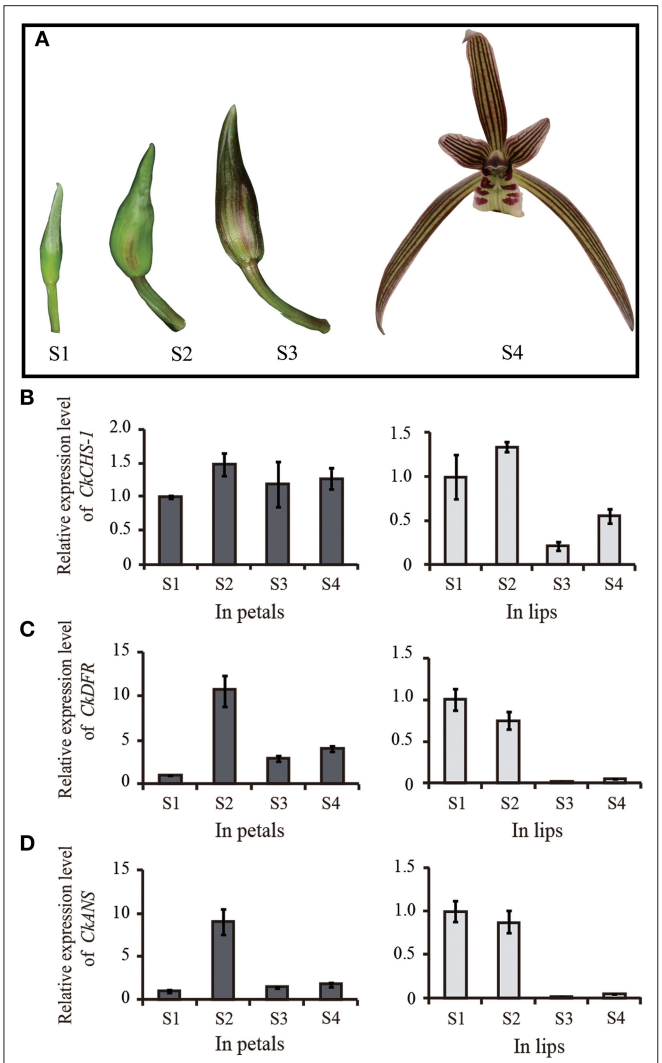


FIGURE 8 | *CkCHS-1*, *CkDFR*, and *CkANS* expression levels were measured by qRT-PCR in four stages. **(A)** Four development stages of purple-red flower. **(B–D)** The relative expression level of *CkCHS-1*, *CkDFR*, and *CkANS* in four development stages of petals and lips of purple-red flower, respectively. Four developmental stages: stage 1 (S1, bud length of approximately 2 cm), stage 2 (S2, bud length of approximately 3 cm), stage 3 (S3, 1–2 days before anthesis), and stage 4 (S4, the flower opened).

genes in four developmental stages: stage 1 (S1, bud length of approximately 2 cm), stage 2 (S2, bud length of approximately 3 cm), stage 3 (S3, 1–2 days before anthesis), and stage 4 (S4, the flower opened) (**Figure 8**). In petals, the transcriptional profile showed that *CkCHS-1*, *CkDFR*, and *CkANS* were all actively expressed gradually from S1 to S4 and reached maximal expression in S2. Both *CkDFR* and *CkANS* presented a sharp peak at S2, but *CkCHS-1* maintained similar transcriptional activity during all stages in petals. These three gene expression patterns in the lip displayed a similar trend of higher expression in early stages S1 and S2, while *CkDFR* and *CkANS* showed the same trend in both organs.

DISCUSSION

The main pigments targeted for orchid flowers are anthocyanins that contribute to a variety of colours, such as red, purple, pink, and blue, while studies have shown that the main types of anthocyanidin aglycones in orchids are cyanidin, peonidin, and delphinidin (Liu et al., 2012; Vignolini et al., 2012; Wang et al., 2014; Liang et al., 2020; Zhang et al., 2020). In *Oncidium* Gower Ramsey, the red portion of lips contained a mixture of cyanidin-3-O-glucoside, delphinidin-3-O-glucoside, and peonidin-3-O-glucoside compounds (Liu et al., 2012). Flowers of *Phalaenopsis* with red-purple, purple, purple-violet, and violet to violet-blue colour were due to highly accumulated cyanidin-based anthocyanins, but no true-blue colour and no delphinidin was detected (Liang et al., 2020). In some cultivars of *Cymbidium hybrids*, only cyanidin-, malvidin-, and peonidin-type anthocyanins were identified (Woltering and Somhorst, 1990; Johnson et al., 1999). In *C. kanran*, the flavonoid composition exhibited a sharp shift between purple-red and white flowers. Three types (cyanidin, peonidin, and malvidin) of anthocyanidins were also detected in purple-red flowers but were absent in white flowers. While the transcript level of the colour-related gene showed that *CkC4H-3*, *CkCHS-1*, *CkDFR*, and *CkANS* were highly expressed corresponding to purple-red floral tissues compared with white type floral tissues, but *CkFLS* had a higher level of expression in the white one, and a similar result was also achieved in *Pleione limprichtii* (Zhang et al., 2020). Dihydroflavonol reductase is a key enzyme in the biosynthesis of anthocyanins and can catalyze the reduction of three colourless dihydroflavonols, DHQ, DHK, and DHM, to leucoanthocyanidins. Because of the similar structure of the three substrates, it is easy to understand that DFRs from many species can utilise all three substrates (Heller et al., 1985; Meyer et al., 1987; Stich et al., 1992; Helariutta et al., 1993; Tanaka et al., 1995; Livak and Schmittgen, 2001; Ma et al., 2008; Chen et al., 2013). dihydroflavonol reductases from some species specifically convert one or two types of dihydroflavonols. In *Petunia* and *Cymbidium*, pelargonidin-based brick red/orange flowers do not exist in nature because DFRs cloned from these two species cannot reduce DHK efficiently (Gerats et al., 1982; Forkmann and Ruhnau, 1987; Johnson et al., 1999), suggesting that DFRs have a striking substrate specificity (Springob et al., 2003). In *Fragaria* species, two DFRs were isolated, and one enzyme variant strongly preferred DHK as a substrate, whereas the other had a higher specificity for DHQ than for DHM (Miosic et al., 2014). Similar results were also reported in *Ginkgo biloba* and *Freesia hybrida* (Cheng et al., 2013; Li et al., 2017). In *C. kanran*, relative quantification showed that cyanidin, peonidin, and malvidin were detected, and the cyanidin content was far greater than that of peonidin and malvidin, indicating that the DFR isolated from *C. kanran* could catalyze DHQ conversion to leucocyanidin. However, more *in vitro* enzyme assays are needed to verify the substrate specificity of DFR with DHM and DHK.

Orchid flowers are striking for their specific patterns of colours in the perianths, and the regulation and formation of pigmentation is determined by specific cells of the different floral organs (Yu and Goh, 2001). In the case of *C. kanran*, the

distributions of anthocyanin production depended on the tissue specificity. The pigmentation in the petals showed anthocyanins concentrated in the outer layer of subepidermal cells to the xylem (**Figure 2A**), but in the lip, the red anthocyanins only accumulated in epidermal cells (**Figure 2C**). Orchid flowers have three petals, and one of the petals is morphologically different in structure and is known as the lip or labellum. However, the differences between the petals and lip were represented not only in shape but also in tissue and genes. The epidermal cells in the lip displayed different forms, in which the adaxial side cells were large and bubble-like, but the abaxial side cells were similar to the petal epidermal cells, which were small and flat. However, anthocyanins accumulated in the region from subepidermal cells to the xylem in the petal (**Figure 2A**), while in the lip, anthocyanins accumulated only in the epidermal cells of the adaxial surface (**Figure 2C**). Accordingly, pigments in the adaxial side of lips displayed bright-coloured pigmentation compared with those in petals (**Figures 1J,K, 2A,C**). Similar results were also reported in the leaves of *Tipularia discolour* orchid, the same anthocyanins in different anatomical locations led to a broad range of colours (Hughes et al., 2020). In addition, differentially expressed genes in transcriptome analysis of *C. kanran* supported that the molecular changes also existed between the lip and petals. In petals, *CkCHS-1* was highly expressed, but *CkCHS-2* was inversely expressed in the lip. In the *Petunia hybrid*, 12 genes encode CHS from a gene family, which were detected specifically in the margin of the corolla throughout all stages of flower development. Among them, *CHS-A* and *CHS-J* were expressed predominantly. These results indicated that *CHS* expression is regulated by different mechanisms in marginal picotee petals (Saito et al., 2006). According to a previous study, MADS-box genes might collectively regulate the genes involved in colour differentiation in petals and sepals during *Cattleya* orchid flower development, which may result in the spatiotemporal expression of anthocyanin biosynthesis pathway structural genes to determine colour differentiation (Li et al., 2020).

Knowledge of the molecular genetic basis of the flavonoid biosynthetic pathway allows us to improve the colour quality of plants. The simplest strategy to modify flower colour is to change the amounts of endogenous anthocyanins by regulating the essential enzymes required for flavonoid biosynthesis. For example, transgenic gentian plants with a suppressed ANS showed pale-blue-coloured flowers, while those with a suppressed CHS exhibited a more serious phenotype, i.e., pale-blue to pure white flowers (Nakatsuka et al., 2008). The manipulation of DFR and FLS, which are competing steps for flux towards anthocyanins and flavonols, led to an increase or decrease in anthocyanin content in the flower (Davies and Schwinn, 2010). In addition, the approach of regulating endogenous modification genes has also been utilised

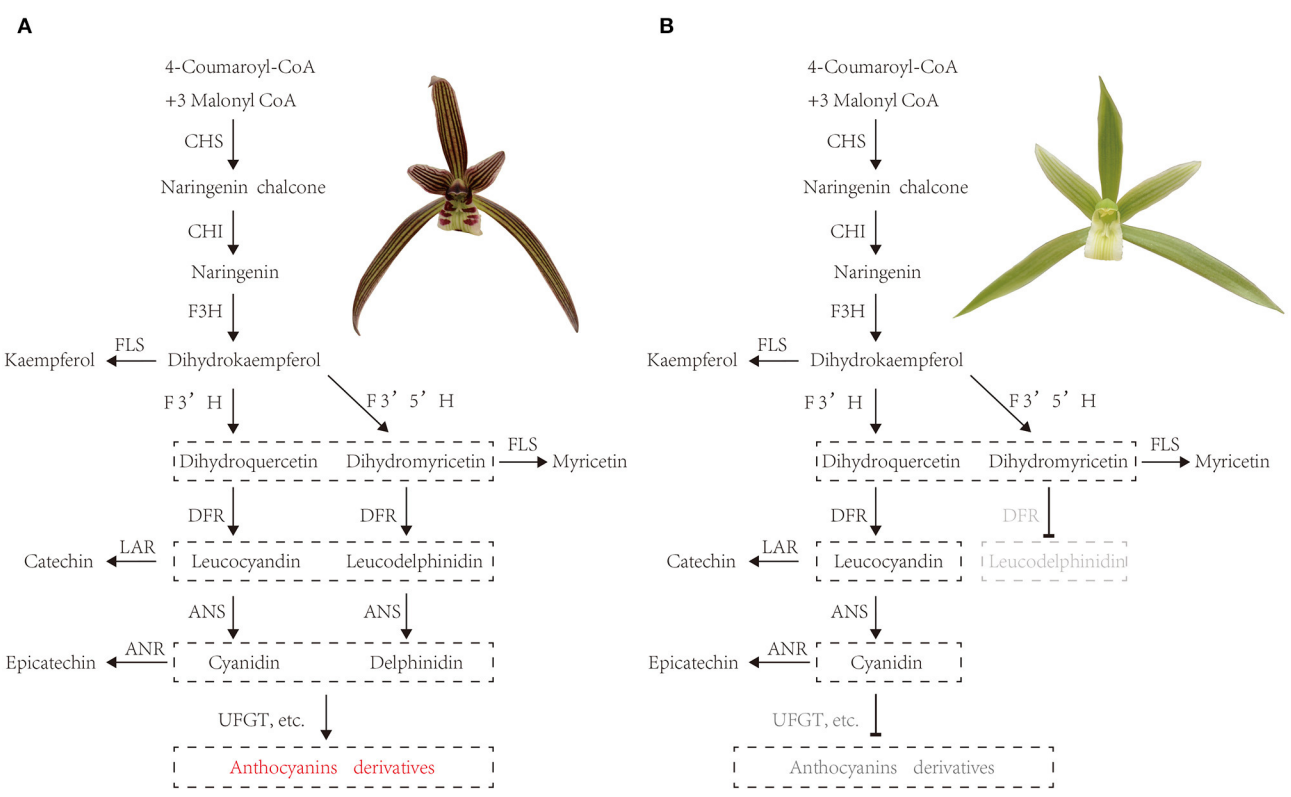


FIGURE 9 | Tentative pathways for **(A)** purple-red and white **(B)** *C. kanran*. CHS, chalcone synthase; CHI, chalcone isomerase; F3H, flavanone 3-hydroxylase; F3'H, flavonoid 3'-hydroxylase; F3'5'H, flavonoid 3'5'-hydroxylase; DFR, dihydroflavonol 4-reductase; ANR, anthocyanidin reductase; ANS, anthocyanidin synthase; FLS, flavonol synthase; LAR, leucoanthocyanidin reductase; UFGT, anthocyanidin 3-O-glucosyltransferase.

in genetic engineering. For example, F3'5'H suppression by RNAi induced a flower colour change from purple to red in cyclamen (Boase et al., 2010). Similar transformations were also displayed in both F3'5'H and A5/3'AT (anthocyanin 5,3'-aromaticacyltransferase)-suppressed transgenic gentian plants (Nishihara and Nakatsuka, 2010). In *C. kanran*, the validation of the transient expression of key genes involved in colour formation showed that only triple genes, *CkCHS-1*, *CkDFR*, and *CkANS* could accumulate red spots in both the petal and lip tissue, indicating that the regulatory mechanism of coloration is complicated. To date, studies on some genetically defined genotypes or mutants revealing blocks of anthocyanin pathway gene expression have already been verified in many plants. In *Forsythia*, it was shown to be blocked in anthers at both the DFR and ANS levels but at the ANS level, only in petals (Rosati et al., 1999). However, the absence of anthocyanins in the skins of white berry varieties is due to a block only of UFGT expression in *Vitis* (Boss et al., 1996). Additionally, a point mutation of the CHS gene could result in the formation of the white flower of *Matthiola incana* (Hemleben et al., 2004). Another study in *Oncidium* also revealed that the failure of anthocyanin accumulation may be due to the inactivation of *OgCHS* caused by epigenetic methylation of the 5'-upstream promoter regions (Liu et al., 2012). However, the silencing of three different CHS genes of the purple-colour flower of *Dianthus chinensis via* VIGS could obtain white or pale purple flower (Liu et al., 2021), suggesting that several CHS genes may be involved in the formation of coloration. In *C. kanran*, it is noteworthy that *CkCHS-2* was abundantly expressed in white flowers but expressed at low levels in purple-red flowers (**Figures 5J,K**), and *CkCHS-1* was highly expressed in purple-red flowers but had lower expression levels in white flowers (**Figures 5G,H**), indicating the complicated regulation of CHSs in *C. kanran*. Therefore, further studies need to be performed on the regulatory mechanism of anthocyanin pathway-related genes in *C. kanran*.

Thus, we tentatively speculated about the pathways for purple-red and white *C. kanran* (**Figure 9**). In purple-red *C. kanran*, flavonoids are initially derived from phenylalanine and phenylpropanoid metabolism. Subsequently, *CkCHS* is generated to produce chalcones, and *CkCHI* catalyzes chalcones into naringenin. Furthermore, naringenin can be converted through *CkF3H*, *CkF3'H*, and *CkF3'5'H* to produce dihydroxyflavonols including DHK, DHQ, and DHM. Following the above reaction, *CkDFR* and *CkANS* further catalyze the divergent conversion of dihydroflavonols to produce colourless cyanidin and delphinidin. In the end, *CkUFGT* and other GTs catalyze the glucosylation of anthocyanidins (peonidin, malvidin, and cyanidin). As for white *C. kanran*, the main divergence of flavonoid metabolism is anthocyanin metabolism, the GTs cannot be regulated and fulfilled to catalyze the glucosylation of anthocyanidins. White-type flowers of *Cymbidium* are uncommon in nature, and traditional division propagation requires a long period, which leads to a low reproductive rate and high price. In this study, the molecular mechanism of anthocyanidin deficiency in white-type flowers establishes a foundation for genetic engineering to generate white-type *C. kanran*. The simplest strategy is to suppress the expression levels of *CkCHS-1*, *CkDFR*, and *CkANS*.

Concurrently, the regulatory mechanism of genes involved in the anthocyanin metabolic pathway has also been carried out in orchids. In *Oncidium*, *OgMYB1* directly activated the expression of *OgCHI* and *OgDFR* to regulate anthocyanin accumulation in the lip (Chiou and Yeh, 2008). In *Phalaenopsis*, three MYB transcription factors determine full-red pigmentation, red spots, and venation patterns (Hsu et al., 2015). A recent study in *C. hybrids* also indicated that *CyMYB1* regulates temporal- and temperature-dependent anthocyanin accumulation in petals (Nakatsuka et al., 2019). In *C. kanran*, we also isolated several differentially expressed *MYB* genes by Biochemical and Biophysical Research Communications transcriptome analysis and attempted to reveal the molecular mechanism of *MYB* genes regulating pigmentation patterning, which may provide genetic resources for *C. kanran* molecular breeding in the future.

CONCLUSIONS

The white and purple-red phenotype *C. kanran* flowers had provided a unique experimental system to examine the mechanism for flower anthocyanin pigmentation. Compared with white flowers, purple-red flowers are comprised of three types of anthocyanidin compounds, namely, peonidin, malvidin, and cyanidin, which were shown by HPLC analysis. A total of 102 candidate genes involved in the flower coloration of *C. kanran* were identified using transcriptome analysis. Gene expression profiles showed that four of these genes were positively correlated with anthocyanidin biosynthesis by qRT-PCR. Transient expression of *CkCHS-1*, *CkDFR*, and *CkANS* by particle bombardment results in the accumulation of anthocyanins in white flowers. These results indicated that *CkCHS-1*, *CkDFR*, and *CkANS* are the key genes involved in floral pigment accumulation in *C. kanran*. This study also provided a platform for *C. kanran* functional genomic research.

DATA AVAILABILITY STATEMENT

The datasets presented in this study can be found in online repositories. The name of the repository and accession number can be found below: National Centre for Biotechnology Information (NCBI) BioProject, https://www.ncbi.nlm.nih.gov/bioproject/, PRJNA744371.

AUTHOR CONTRIBUTIONS

ZZ, XW, and ZL designed the experiments. ZZ, XW, YY, and ZY performed all experiments. ZZ, XW, and ZW analysed the data. ZZ and XW wrote the manuscript. ZL revised the manuscript. All the authors have read and agreed to the published version of the manuscript.

FUNDING

This research was funded by the Natural Science Foundation of Zhejiang Province (grant nos.

LY20C160005 and LY19C150003), National Key R & D Program of China (grant nos. 2018YFD1000401 and 2019YFD1000400), and Wenzhou Agricultural New Variety Breeding Cooperative Group Project (grant no. 2019ZX004-3).

ACKNOWLEDGMENTS

We would like to thank Biogle Gene Tech. Co., Ltd., and Dr. Jinda Wang (Fujian Agriculture and Forestry University) for the help with particle bombardment experimentation.

REFERENCES

Aguiar, J., Giurfa, M., and Sazima, M. (2020). A cognitive analysis of deceptive pollination: associative mechanisms underlying pollinators' choices in non-rewarding colour polymorphic scenarios. *Sci. Rep.* 10:9476. doi: 10.1038/s41598-020-66356-4

Altschul, S. F., Madden, T. L., Schäffer, A. A., Zhang, J., Zhang, Z., Miller, W., et al. (1997). Gapped BLAST and PSI BLAST: a new generation of protein database search programs, *Nucleic. Acids. Res.* 25, 3389–3402. doi: 10.1093/nar/25.17.3389

Basist, G., Dyer, A. G., Garcia, J. E., Raleigh, R. E., and Lawrie, A. C. (2021). Why variation in flower color may help reproductive success in the endangered Australian orchid *Caladenia fulva*. *Front. Plant Sci.* 12, 874. doi: 10.3389/fpls.2021.599874

Boase, M. R., Lewis, D. H., Davies, K. M., Marshall, G. B., Patel, D., Schwinn, K. E., et al. (2010). Isolation and antisense suppression of flavonoid 3', 5'-hydroxylase modifies flower pigments and color in cyclamen. *BMC Plant Biol.* 10:107. doi: 10.1186/1471-2229-10-107

Boss, P. K., Davies, C. H., and Robinson, S. P. (1996). Expression of anthocyanin biosynthesis pathway genes in red and white grapes. *Plant Mol. Biol.* 32, 565–569. doi: 10.1007/BF00019111

Chen, S. C., and Tang, T. A. (1982). "A general review of the orchid flora of China," in *Orchid Biology: Review and Perspectives, Vol. II*, ed J. Arditti (New York, NY: Cornell University Press), 39–87.

Chen, W., Gong, L., Guo, Z., Wang, W., Zhang, H., Liu, X., et al. (2013). A novel integrated method for large-scale detection, identification, and quantification of widely targeted metabolites: application in the study of rice metabolomics. *Mol. Plant*. 6:1769. doi: 10.1093/mp/sst080

Chen, W. H., Hsu, C. Y., Cheng, H. Y., Chang, H., Chen, H. H., and Ger, M. J. (2011). Downregulation of putative UDP-glucose: flavonoid 3-O-glucosyltransferase gene alters flower coloring in *Phalaenopsis*. *Plant Cell Rep.* 30, 1007–1017. doi: 10.1007/s00299-011-1006-1

Cheng, H., Li, L., Cheng, S., Cao, F., Xu, F., Yuan, H., et al. (2013). Molecular cloning and characterization of three genes encoding dihydroflavonol-4-reductase from *Ginkgo biloba* in anthocyanin biosynthetic pathway. *PLoS ONE* 8:e72017. doi: 10.1371/journal.pone.0072017

Chiou, C. Y., and Yeh, K. W. (2008). Differential expression of *MYB* gene (*OgMYB1*) determines color patterning in floral tissue of *Oncidium* Gower Ramsey. *Plant Mol. Biol.* 66, 379–388. doi: 10.1007/s11103-007-9275-3

Davies, K. M., and Schwinn, K. E. (2010). "Molecular biology and biotechnology of flower pigments," in *Plant Developmental Biology-Biotechnological Perspectives*, ed E. Pua and M. Davey, (Berlin, Heidelberg: Springer), 161–187.

Du Puy, D., Cribb, P., and Tibbs, M. (2007). The genus Cymbidium. Kew: Royal Botanic Gardens Kew.

Forkmann, G., and Ruhnau, B. (1987). Distinct substrate specificity of dihydroflavonol-4-reductase from flowers of *Petunia hybrid*. *Z. Naturforsch. C.* 42, 1146–1148. doi: 10.1515/znc-1987-9-1026

Gerats, A. G., Vlaming, P. D., Doodeman, M., Al, B., and Schram, A. W. (1982). Genetic control of the conversion of dihydroflavonols into flavonols and anthocyanins in flowers of *Petunia hybrid*. *Planta* 155, 364–368. doi: 10.1007/BF00429466

Gigord, L. D. B., Macnair, M. R., and Smithson, A. (2001). Negative frequency-dependent selection maintains a dramatic flower color polymorphism in the rewardless orchid *Dactylorhiza sambucina* (L.) Soò. *Proc. Natl. Acad. Sci. U.S.A.* 98, 6253–6255. doi: 10.1073/pnas.111162598

Grabherr, M. G., Haas, B. J., Yassour, M., Levin, J. Z., Thompson, D. A., Amit, I., et al. (2011). Full-length transcriptome assembly from RNA-Seq data without a reference genome. *Nat. Biotechnol.* 29:644. doi: 10.1038/nbt.1883

Grotewold, E. (2006). The genetics and biochemistry of floral pigments. *Annu. Rev. Plant Biol.* 57, 761–780. doi: 10.1146/annurev.arplant.57.032905.105248

Han, Y. Y., Ming, F., Wang, W., Wang, J. W., Ye, M. M., and Shen, D. L. (2006). Molecular evolution and functional specialization of chalcone synthase superfamily from *Phalaenopsis* orchid. *Genetica* 128, 429–438. doi: 10.1007/s10709-006-7668-x

Hatier, J. H. B., and Gould, K. S. (2007). Black coloration in leaves of *Ophiopogon planiscapus* 'Nigrescens'. Leaf optics, chromaticity, and internal light gradients. *Funct. Plant Biol.* 34, 130–138. doi: 10.1071/FP06220

Helariutta, Y., Elomaa, P., Kotilainen, M., Seppanen, P., and Teeri, T. H. (1993). Cloning of cDNA coding for dihydroflavonol-4-reductase (DFR) and characterization of *dfr* expression in the corollas of *Gerbera hybrida* var. regina (Compositae). *Plant Mol. Biol.* 22, 183–193. doi: 10.1007/BF00014927

Heller, W., Forkmann, G., Britsch, L., and Grisebach, H. (1985). Enzymatic reduction of (+)-dihydroflavonols to flavan-3,4-cis-diols with flower extracts from *Matthiola incana* and its role in anthocyanin biosynthesis. *Planta* 165, 284–287. doi: 10.1007/BF00395052

Hemleben, V., Dressel, A., Epping, B., Lukačin, R., Martens, S., and Austin, M. (2004). Characterization and structural features of a chalcone synthase mutation in a white-flowering line of *Matthiola incana* R. Br. (Brassicaceae). *Plant Mol. Biol.* 55, 455–465. doi: 10.1007/s11103-004-1125-y

Hieber, A. D., Mudalige-Jayawickrama, R. G., and Kuehnle, A. R. (2006). Color genes in the orchid *Oncidium* Gower Ramsey: identification, expression, and potential genetic instability in an interspecific cross. *Planta* 223, 521–531. doi: 10.1007/s00425-005-0113-z

Hsiao, Y. Y., Pan, Z. J., Hsu, C. C., Yang, Y. P., Hsu, Y. C., Chuang, Y. C., et al. (2011). Research on orchid biology and biotechnology. *Plant Cell Physiol.* 52, 1467–1486. doi: 10.1093/pcp/pcr100

Hsu, C. C., Chen, Y. Y., Tsai, W. C., Chen, W. H., and Chen, H. H. (2015). Three R2R3-MYB transcription factors regulate distinct floral pigmentation patterning in *Phalaenopsis* spp. *Plant Physiol.* 168, 175–191. doi: 10.1104/pp.114.254599

Hughes, N. M., Connors, M. K., Grace, M. H., Lila, M. A., and Wommack, A. J. (2020). The same anthocyanins served four different ways: insights into anthocyanin structure-function relationships from the wintergreen orchid, *Tipularia discolor*. *Plant Sci.* 303:110793. doi: 10.1016/j.plantsci.2020.110793

Johnson, E. T., Yi, H., Shin, B., Oh, B. J., Cheong, H., and Choi, A. G. (1999). *Cymbidium hybrida* dihydroflavonol 4-reductase does not efficiently reduce dihydrokaempferol to produce orange pelargonidin-type anthocyanins. *Plant J.* 19, 81–85. doi: 10.1046/j.1365-313X.1999.00502.x

Katsumoto, Y., Fukuchi-Mizutani, M., Fukui, Y., Brugliera, F., Holton, T. A., Karan, M., et al. (2007). Engineering of the rose flavonoid biosynthetic pathway successfully generated blue-hued flowers accumulating delphinidin. *Plant Cell Physiol.* 48, 1589–1600. doi: 10.1093/pcp/pcm131

Li, B., and Dewey, C. N. (2011). RSEM: accurate transcript quantification from RNA-Seq data with or without a reference genome. *BMC Bioinformatics* 12:323. doi: 10.1186/1471-2105-12-323

Li, B. J., Zheng, B. Q., Wang, J. Y., Tsai, W. C., Lu, H. C., Zou, L. H., et al. (2020). New insight into the molecular mechanism of colour differentiation among floral segments in orchids. *Commun. Biol.* 3:89. doi: 10.1038/s42003-020-0821-8

Li, H., Liu, J., Pei, T., Bai, Z., Han, R., and Liang, Z. (2019). Overexpression of *SmANS* enhances anthocyanin accumulation and alters phenolic acids content in *Salvia miltiorrhiza* and *Salvia miltiorrhiza* Bge f. alba plantlets. *Int. J. Mol. Sci.* 20, 2225. doi: 10.3390/ijms20092225

Li, Q., Wang, J., Sun, H. Y., and Shang, X. (2014). Flower color patterning in pansy (*Viola* × *wittrockiana* Gams.) is caused by the differential expression of three genes from the anthocyanin pathway in acyanic and cyanic flower areas. *Plant Physiol. Biochem.* 84, 134–141. doi: 10.1016/j.plaphy.2014.09.012

Li, Y., Liu, X., Cai, X., Shan, X., Gao, R., Yang, S., et al. (2017). Dihydroflavonol 4-reductase genes from *Freesia hybrida* play important and partially overlapping roles in the biosynthesis of flavonoids. *Front. Plant Sci.* 8:428. doi: 10.3389/fpls.2017.00428

Liang, C. Y., Rengasamy, K. P., Huang, L. M., Hsu, C. C., Jeng, M. F., Chen, W. H., et al. (2020). Assessment of violet-blue color formation in *Phalaenopsis* orchids. *BMC Plant Biol.* 20:212. doi: 10.1186/s12870-020-02402-7

Liu, J., Hao, X. L., and He, X. Q. (2021). Characterization of three chalcone synthase-like genes in *Dianthus chinensis*. *Plant Cell, Tissue Organ Cult*. 146, 483–492. doi: 10.1007/s11240-021-02081-8

Liu, X. J., Chuang, Y. N., Chiou, C. Y., Chin, D. C., Shen, F. Q., and Yeh, K. W. (2012). Methylation effect on chalcone synthase gene expression determines anthocyanin pigmentation in floral tissues of two *Oncidium* orchid cultivars. *Planta* 236, 401–409. doi: 10.1007/s00425-012-1616-z

Livak, K. J., and Schmittgen, T. D. (2001). Analysis of relative gene expression data using real-time quantitative PCR and the 2 (-Delta Delta C (T)) method. *Methods* 25, 402–408. doi: 10.1006/meth.2001.1262

Ma, H., Pooler, M., and Griesbach, R. (2008). Ratio of Myc and Myb transcription factors regulates anthocyanin production in orchid flowers. *J. Am. Soc. Hortic. Sci.* 133, 133–138. doi: 10.21273/JASHS.133.1.133

Meyer, P., Heidmann, I., Forkmann, G., and Saedler, H. (1987). A new petunia flower colour generated by transformation of a mutant with a maize gene. *Nature* 330, 677–678. doi: 10.1038/330677a0

Miosic, S., Thill, J., Milosevic, M., Gosch, C., Pober, S., Molitor, C., et al. (2014). Dihydroflavonol 4-reductase genes encode enzymes with contrasting substrate specificity and show divergent gene expression profiles in *Fragaria* species. *PLoS ONE* 9:e112707. doi: 10.1371/journal.pone.0112707

Moreau, C., Hill, L., Ellis, T. N., and Hofer, J. M. (2012). The *b* gene of pea encodes a defective flavonoid $3'5'$-hydroxylase, and confers pink flower color. *Plant Physiol.* 159, 759–768. doi: 10.1104/pp.112.197517

Mudalige-Jayawickrama, R. G., Champagne, M. M., Hieber, A. D., and Kuehnle, A. R. (2005). Cloning and characterization of two anthocyanin biosynthetic genes from *Dendrobium* orchid. *J. Am. Soc. Hortic. Sci.* 130, 611–618. doi: 10.21273/JASHS.130.4.611

Nakatsuka, T., Kei-Ichiro, M., Abe, Y., Kubota, A., Kakizaki, Y., Yamamura, S., et al. (2008). Flower color modification of gentian plants by RNAi-mediated gene silencing. *Plant Biotechnol.* 25, 61–68. doi: 10.5511/plantbiotechnology.25.61

Nakatsuka, T., Suzuki, T., Harada, K., Kobayashi, Y., Dohra, H., and Ohno, H. (2019). Floral organ- and temperature-dependent regulation of anthocyanin biosynthesis in *Cymbidium hybrid* flowers. *Plant Sci.* 287, 110173. doi: 10.1016/j.plantsci.2019.110173

Nishihara, M., and Nakatsuka, T. (2010). "Genetic engineering of novel flower colors in floricultural plants: recent advances via transgenic approaches," in *Protocols for In Vitro Propagation of Ornamental Plant*, ed S. Jain and S. Ochatt (Totowa, NJ: Humana Press), 325–347.

Passeri, V., Koes, R., and Quattrocchio, F. M. (2016). New challenges for the design of high value plant products: stabilization of anthocyanins in plant vacuoles. *Front. Plant Sci*. 7:153. doi: 10.3389/fpls.2016.00153

Petroni, K., and Tonelli, C. (2011). Recent advances on the regulation of anthocyanin synthesis in reproductive organs. *Plant Sci.* 181, 219–229. doi: 10.1016/j.plantsci.2011.05.009

Ramazzotti, S., Filippetti, I., and Intrieri, C. (2008). Expression of genes associated with anthocyanin synthesis in red-purplish, pink, pinkish-green and green grape berries from mutated 'Sangiovese' biotypes: a case study. *Vitis* 47, 147–151. doi: 10.5073/vitis.2008.47.147-151

Rosati, C., Cadic, A., Duron, M., Ingouff, M., and Simoneau, P. (1999). Molecular characterization of the anthocyanidin synthase gene in *Forsythia intermedia* reveals organ-specific expression during flower development. *Plant Sci.* 149, 73–79. doi: 10.1016/S0168-9452(99)00146-6

Saito, R., Fukuta, N., Ohmiya, A., Itoh, Y., Ozeki, Y., Kuchitsu, K., et al. (2006). Regulation of anthocyanin biosynthesis involved in the formation of marginal picotee petals in *Petunia*. *Plant Sci.* 170, 828–834. doi: 10.1016/j.plantsci.2005.12.003

Singh, D. R., Pamarthi, R. K., Kumar, R., Rai, D., Meitei, A. L., and Kiran Babu, P. (2019). Traditional artifacts from dried leaves of *Cymbidium* species (Orchidaceae) in Indian state of Sikkim. *Indian J. Tradit. Knowl.* 18, 390–394. http://nopr.niscair.res.in/handle/123456789/47067

Springob, K., Nakajima, J., Yamazaki, M., and Saito, K. (2003). Recent advances in the biosynthesis and accumulation of anthocyanins. *Nat. Prod. Rep*. 20, 288–303. doi: 10.1039/b109542k

Stich, K., Eidenberger, T., Wurst, F., and Forkmann, G. (1992). Enzymatic conversion of dihydroflavonols to flavan-3,4-diols using flower extracts of *Dianthus caryophyllus* L. (carnation). *Planta*. 187, 103–108. doi: 10.1007/BF00201630

Tanaka, Y., Fukui, Y., Fukuchi-Mizutani, M., Holton, T. A., Higgins, E., and Kusumi, T. (1995). Molecular cloning and characterization of *Rosa hybrida* dihydroflavonol 4-reductase gene. *Plant Cell Physiol*. 36, 1023–1031. doi: 10.1093/oxfordjournals.pcp.a078844

Tanaka, Y., Sasaki, N., and Ohmiya, A. (2008). Biosynthesis of plant pigments: anthocyanins, betalains, and carotenoids. *Plant J*. 54, 733–749. doi: 10.1111/j.1365-313X.2008.03447.x

Vignolini, S., Davey, M. P., Bateman, R. M., Rudall, P. J., Moyroud, E., Tratt, J., et al. (2012). The mirror crack'd: both pigment and structure contribute to the glossy blue appearance of the mirror orchid, Ophrys speculum. *New Phytol*. 196, 1038–1047. doi: 10.1111/j.1469-8137.2012.04356.x

Wang, L., Albert, N. W., Zhang, H., Arathoon, S., Boase, M. R., Ngo, H., et al. (2014). Temporal and spatial regulation of anthocyanin biosynthesis provide diverse flower color intensities and patterning in *Cymbidium* orchid. *Planta* 240, 983–1002. doi: 10.1007/s00425-014-2152-9

Woltering, E. J., and Somhorst, D. (1990). Regulation of anthocyanin synthesis in *Cymbidium* flowers: effects of emasculation and ethylene. *J. Plant Physiol.* 136, 295–299. doi: 10.1016/S0176-1617(11)80052-0

Yu, H., and Goh, C. J. (2001). Molecular genetics of reproductive biology in orchids. *Plant Physiol.* 127, 1390–1393. doi: 10.1104/pp.127.4.1390

Yu, Z., Liao, Y., Teixeira da Silva, J., Yang, Z., and Duan, J. (2018). Differential accumulation of anthocyanins in *Dendrobium officinale* stems with red and green peels. *Int. J. Mol. Sci.* 19:2857. doi: 10.3390/ijms19102857

Zhang, Y. Y., Zhou, T. H., Dai, Z. W., Dai, X. Y., Li, W., Cao, M. X., et al. (2020). Comparative transcriptomics provides insight into floral color polymorphism in a *Pleione limprichtii* orchid population. *Int. J. Mol. Sci*. 21:247. doi: 10.3390/ijms21010247

Zhao, Z. C., Hu, G. B., Hu, F. C., Wang, H. C., Yang, Z. Y., and Lai, B. (2012). The UDP glucose: flavonoid-3-O-glucosyltransferase (UFGT) gene regulates anthocyanin biosynthesis in litchi (*Litchi chinesis* Sonn.) during fruit coloration. *Mol. Biol. Rep*. 39, 6409–6415. doi: 10.1007/s11033-011-1303

Conflict of Interest: The authors declare that the research was conducted in the absence of any commercial or financial relationships that could be construed as a potential conflict of interest.

Publisher's Note: All claims expressed in this article are solely those of the authors and do not necessarily represent those of their affiliated organizations, or those of the publisher, the editors and the reviewers. Any product that may be evaluated in this article, or claim that may be made by its manufacturer, is not guaranteed or endorsed by the publisher.

Copyright © 2021 Zhou, Ying, Wu, Yang, Fu, Xu, Yao, Zeng, Huang, Lan, Wang and Liu. This is an open-access article distributed under the terms of the Creative Commons Attribution License (CC BY). The use, distribution or reproduction in other forums is permitted, provided the original author(s) and the copyright owner(s) are credited and that the original publication in this journal is cited, in accordance with accepted academic practice. No use, distribution or reproduction is permitted which does not comply with these terms.

frontiers in Plant Science

ORIGINAL RESEARCH
published: 25 October 2021
doi: 10.3389/fpls.2021.753261

Benzothiazole Treatment Regulates the Reactive Oxygen Species Metabolism and Phenylpropanoid Pathway of *Rosa roxburghii* Fruit to Delay Senescence During Low Temperature Storage

Boyu Dong[1]*, Hongmin Tang[1], Dequan Zhu[1], Qiuping Yao[1], Hongqiang Han[1], Kequn He[1] and Xiaochun Ding[2]*

[1]College of Ethnic-Minority Medicine, Guizhou Minzu University, Guiyang, China, [2]State Key Laboratory of Plant Resources Conservation and Sustainable Utilization, South China Botanical Garden, Chinese Academy of Sciences, Guangzhou, China

OPEN ACCESS

Edited by:
Xinchao Wang,
Tea Research Institute,
Chinese Academy of Agricultural Sciences (CAAS), China

Reviewed by:
Kamrun Nahar,
Sher-e-Bangla Agricultural University, Bangladesh
Morteza Soleimani Aghdam,
Imam Khomeini International University, Iran

***Correspondence:**
Boyu Dong
kuroro1986@163.com
Xiaochun Ding
dingxc111@scbg.ac.cn

Specialty section:
This article was submitted to Crop and Product Physiology, a section of the journal Frontiers in Plant Science

Received: *04 August 2021*
Accepted: *28 September 2021*
Published: *25 October 2021*

Citation:
Dong B, Tang H, Zhu D, Yao Q, Han H, He K and Ding X (2021) Benzothiazole Treatment Regulates the Reactive Oxygen Species Metabolism and Phenylpropanoid Pathway of Rosa roxburghii Fruit to Delay Senescence During Low Temperature Storage. Front. Plant Sci. 12:753261. doi: 10.3389/fpls.2021.753261

Rosa roxburghii fruit were used as research objects to study the effects of different concentrations of benzothiazole (BTH) treatment on quality parameters, reactive oxygen species (ROS) metabolism, and the phenylpropanoid pathway during storage at 4°C for 14 days. Results showed that BTH effectively delayed senescence with lower decay incidence, weight loss, and lipid peroxidation level and maintained the quality with higher contents of total soluble solid (TSS) content, titratable acidity (TA) in *R. roxburghii* fruit. Moreover, BTH increased hydrogen peroxide (H_2O_2) content, superoxide anion ($O_2^{\bullet-}$) production rate, and the activities and expression of superoxide dismutase (SOD), catalase (CAT), ascorbate peroxidase (APX), glutathione (GSH) reductase (GR), monodehydroascorbate reductase (MDHAR), dehydroascorbate reductase (DHAR), and peroxidase (POD), and the contents of GSH and ascorbic acid (AsA), but reduced the oxidized GSH (GSSG) content. In addition, the activities and gene expression of phenylalanine ammonia lyase (PAL), cinnamate 4-hydroxylase (C4H), and 4-coumarate-CoA ligase (4CL) and the concentrations of flavonoids, total phenols, and lignin were significantly elevated by BTH. These findings imply that BTH can delay senescence and maintain the quality of *R. roxburghii* fruit by modulating ROS metabolism and the phenylpropanoid pathway under low-temperature conditions.

Keywords: *Rosa roxburghii*, benzothiazole, fruit quality, reactive oxygen species metabolism, phenylpropanoid pathway

INTRODUCTION

Rosa roxburghii (*R. roxburghii*), a perennial deciduous shrub from the Rosaceae family, is widely distributed in southwest China. The vitamin C and superoxide dismutase (SOD) contents of *R. roxburghii* fruit are particularly rich and exhibit considerable promotion prospects in the market (Liu et al., 2016; Yang et al., 2020). However, *R. roxburghii* is

prone to rot due to water loss, softening, pathogen infection, and cell wall degradation during storage at room temperature. Rotting seriously affects the appearance and quality of *R. roxburghii* fruit, reducing their commercial value. *R. roxburghii* fruit can only be stored for approximately 8 days at room temperature. At present, studies on the postharvest storage of *R. roxburghii* fruit, including those regarding 1-methylcyclopropene and bagging treatments, are relatively rare (Fan et al., 2019; Zhang et al., 2020). To date, reports on the effects of inducer treatment on the phenylpropanoid pathway in *R. roxburghii* fruit and reactive oxygen species (ROS) metabolism remain few.

The structural analogue of salicylic acid, benzothiazole (BTH) has confirmed to induce the production and improvement of disease resistance in various plants (Lavergne et al., 2017). BTH can effectively increase the postharvest quality and delay the senescence of pear (Li et al., 2020a), muskmelon (Liu et al., 2014; Ge et al., 2015), grape (Ruiz-García et al., 2013), and strawberry (Cao et al., 2011) fruit. Previous studies have demonstrated that BTH treatment can induce disease resistance and maintain fruit quality; these activities are closely related to ROS metabolism (Ge et al., 2015) and the phenylpropanoid pathway (Liu et al., 2014).

Reactive oxygen species have been confirmed to act directly on pathogens and function as a defensive gene signals in plant defense responses (Oliveira et al., 2016). However, excessive ROS will damage cells and destroy the integrity of the cell membrane, leading to the accelerated senescence of fruit (Ray et al., 2012; Nath et al., 2017). Plants may eliminate excess ROS through the ascorbic acid (AsA)-glutathione (GSH) cycle, which is critical for balancing ROS metabolism and increasing the antioxidant capacity of fruit and vegetables (de Freitas-Silva et al., 2017; Zhu et al., 2019). Rasool et al. (2013) suggested that the AsA–GSH cycle comprises antioxidant enzymes and compounds, including SOD, catalase (CAT), ascorbate peroxidase (APX), GSH reductase (GR), monodehydroascorbate reductase (MDHAR), dehydroascorbate reductase (DHAR), AsA, and GSH. Research has demonstrated that increasing the activity and gene expression of enzymes involved in ROS metabolism increases the antioxidant capacity of blueberry (Ge et al., 2019b) and pear (Li et al., 2020a) fruit after harvest.

The phenylpropanoid pathway is a unique secondary metabolism in plants, and it is important in the development of plant disease resistance. Many major antibacterial substances, such as lignin, flavonoids, and phenolic compounds are directly or indirectly generated by the phenylpropanoid pathway (Ge et al., 2012). The buildup of phenylpropanoid pathway products can boost the antioxidant potential of muskmelons and blueberries (Liu et al., 2014; Ge et al., 2015, 2019b). The effects of BTH treatment on the antioxidant capacity and phenylpropanoid pathway of *R. roxburghii* remain unclear.

The current study aimed to investigate the effects of BTH treatment on the following: (1) the quality including: weight loss rate, decay incidence, malondialdehyde (MDA), cell membrane permeability, titratable acidity (TA), soluble solids (TSS), and AsA content of *R. roxburghii* fruit during low-temperature storage, (2) the ROS metabolism of *R. roxburghii* fruit during low-temperature storage, and (3) the phenylpropanoid pathway of *R. roxburghii* fruit. That is, this research intended to evaluate the potential of BTH in enhancing the postharvest quality and delaying the senescence of *R. roxburghii* fruit under low-temperature conditions.

MATERIALS AND METHODS

Fruit and Chemicals

R. roxburghii fruit harvested at 85 days after full blossom (about 70% maturity) without mechanical damage were obtained from an orchard planted with the AsA–GSH cycle comprises *R. roxburghii* in Anshun, Guizhou Province, China. Sigma-Aldrich provided support for BTH.

Treatment

Undamaged fruit were selected and washed three times with distilled water. All the selected fruit were immersed in 25, 50, 100, and 200 mg L^{-1} of BTH dissolving with 0.1 ml L^{-1} Tween-80 for 10 min, with distilled water as the control. All the processed fruit were air-dried at ambient temperature (22°C) before being stored at 4°C for 14 days. Each treatment consisted of three replicates, and each replicate comprised 80 fruits.

Sample Collection

On days 0, 2, 4, 6, 8, 10, 12, and 14 after BTH treatment, tissues were detached from 3 to 6 mm below the skin and around the equator of a fruit. Consequently, the collected samples were frozen in liquid nitrogen and immediately stored at −80°C.

Determination of Weight Loss and AsA Content

The weighing method used for evaluation and measurement was based on the following formula: weight loss rate/% = [(quality before storage−quality after storage)/quality before storage] × 100. The AsA content was assayed by applying the method of Ge et al. (2015) and was expressed as g kg^{-1} fresh weight (FW). The optimal concentration of BTH was determined on the basis of the weight loss rate and AsA content.

Determination of Decay Incidence

Decay index is divided into six levels. Level 0: no decay and mold; Level 1: small brown spots, no obvious decay area; Level 2: decay area <1/4 of the fruit surface area; Level 3: 1/4 < decay area < 1/3 of the fruit surface area; Level 4: 1/3 < decay area < 1/2 of the fruit surface area; and Level 5: decay area > 1/2 of the fruit surface area. The decay incidence (%) was calculated according to the following equation: $\sum$ (number of fruits × decay index)/(total number of fruits × the highest level of decay index) × 100.

Determination of TSS, TA, Integrity of the Cell Membrane, and MDA Content

Pulp tissues (2.0 g) from 10 fruits were homogenized. The supernatant was dropped onto a TF-65 handheld refractometer. Total soluble solid (TSS) content was expressed in %. Then, acid–base titration was performed with 0.1 mol L^{-1} of sodium hydroxide standard solution. The method of Sayyari et al. (2009) was adopted as a reference for cell membrane integrity. A sample was cut into 10 slices with a thickness of 2 mm. After soaking in double distilled water at 25°C for 3 h, conductivity was measured using a conductivity meter and denoted as CI. Conductivity was measured again after 30 min of boiling. After cooling to room temperature (22°C), the final conductivity was denoted as *CF*. Cell membrane integrity was estimated using the following formula: cell membrane integrity (%) = $[1-(CI/CF)]\times 100$. The study of Gao et al. (2018) was used as a reference for determining MDA content. Absorbance was measured at 450, 532, and 600 nm. MDA content was expressed in mmol kg^{-1} FW.

Measurement of the Hydrogen Peroxide (H_2O_2) Content, Superoxide Anion ($O_2^{\bullet-}$) Production Rate, GSH, and Oxidized GSH (GSSG) Content

The method of Ge et al. (2015) was used as a reference for determining the production rate of $O_2^{\bullet-}$. The rate of $O_2^{\bullet-}$ production was measured using an mmol g^{-1} min^{-1} FW scale. H_2O_2 content was determined in accordance with the method of Ren et al. (2012). Subsequently, 3 g of frozen tissue was homogenized in 3 ml of cold acetone at 4°C and then centrifuged at $9{,}000\times g$ for 20 min at 4°C. Thereafter, 1 ml of supernatant with 200 µl of 20% titanium tetrachloride dissolved in concentrated hydrochloric acid (HCl, v/v) was used in the reaction. The titanium–hydroperoxide complex precipitate was filtered three times in cold acetone before being dissolved in 3 ml of 1 M sulfuric acid and centrifuged for 10 min at 4°C at $9{,}000\times g$. H_2O_2 content was measured using an absorbance of 410 nm and expressed in µmol g^{-1} FW. GSH content was assayed by applying the method of Ge et al. (2015) and expressed as µmol g^{-1} FW. GSSG contents were determined using GSSG Detection Assay Kit (Beyotine, Shanghai, China) and were expressed as µmol g^{-1} FW.

Extraction of Crude Enzyme and Enzymatic Activity Assays

All the extractions were performed at 4°C. Liquid nitrogen was used to grind frozen tissues (1.0 g) into powder, which was subsequently extracted with the following solutions:

SOD and CAT: 3.0 ml of phosphate buffer (pH 7.4, 0.05 M) with 5.0 mM of dithiothreitol (DTT) and 10 g L^{-1} of polyvinyl polypyrrolidone (PVPP). SOD activity was determined using the method described by Ren et al. (2012). The reaction mixture was composed of 0.4 ml of crude enzyme, 1.5 ml of 50 mM sodium phosphate buffer (pH 7.8), 0.3 ml of 130 mM methionine, 0.3 ml of 100 µM ethylenediaminetetraacetic acid (EDTA), 0.3 ml of 750 µM nitro blue tetrazolium (NBT), and 0.3 ml of 20 µM riboflavin. Absorbance at 560 nm was used to track the development of blue formazan. Activity was denoted by U·g^{-1} protein, where U = 50% inhibition of NBT. CAT activity was determined using the method described by Ren et al. (2012). First, 3 ml of 0.01 mol L^{-1} H_2O_2 and 0.3 ml of crude enzyme extract were used in the reaction. The absorbance of the supernatant was then measured at 240 nm.

APX and DHAR: 3.0 ml of phosphate buffer (pH 7.5, 0.1 M) with 1.0 mM of EDTA. APX activity was determined as described by Ren et al. (2012). Briefly, 2 ml of 100 mM sodium phosphate buffer (pH 7.5), 0.5 ml of 30% (v/v) H_2O_2, and 0.2 ml of enzyme extract were used in the assay mixture. APX activity was measured in units of U mg^{-1} protein, i.e., 1 U = 0.01 Δ340 min^{-1}. DHAR activities were measured using the method of Ren et al. (2012) and expressed as U mg^{-1} protein, where 1 U = 0.01A290 min^{-1}.

GSH reductase: 0.1 M of phosphate buffer (pH 7.5, 1 mM of EDTA). The GR-dependent oxidation of NADPH was used to determine GR activity at 340 nm by using the method of Ren et al. (2012). An enzyme reaction mixture that contained 0.2 ml of crude enzyme, 3 ml of 100 mM sodium phosphate buffer (pH 7.5), 30 µl of 3 mM NADPH, and 0.1 ml of 10 mM oxidized GR was used. Activity was measured in units of U mg^{-1} protein.

MDHAR: 0.04 M of phosphate buffer (pH 7.5, 20 g L^{-1} of PVPP, and 5 mM of β-mercaptoethanol). MDHAR activities were measured using the method of Ren et al. (2012). Activities were measured in units of U mg^{-1} protein, where 1 U = 0.01A340 min^{-1}.

Peroxidase (POD): 0.05 M of phosphate buffer (pH 7.5, 1 ml of L^{-1} Triton X-100, and 20 g L^{-1} of PVPP). POD activity was assayed in accordance with the method of Liu et al. (2014). The oxidation of guaiacol into tetraguaiacol was observed spectrophotometrically at 470 nm for 2 min. Activity was expressed as U mg^{-1} protein, where 1 U = 0.01 Δ470 min^{-1}.

Phenylalanine ammonia lyase (PAL): 5 ml of sodium borate buffer (0.05 M, pH 8.8, 5 mM of mercaptoethanol, 2 mM of EDTA, and 20 g L^{-1} of PVPP). PAL activity was determined using the method of Liu et al. (2014). First, 1 ml of crude enzyme was incubated with 3 ml of l-phenylalanine for 60 min at 37°C. PAL activity was evaluated by measuring absorbance at 290 nm. Activity was indicated in units of U·mg^{-1} protein. Here, U = 0.01 ΔOD290 min^{-1}.

Cinnamate 4-hydroxylase (C4H): 5 ml of 50 mM Tris–HCl buffer (pH 8.9) with 4 mM of $MgCl_2$, 15 mM of mercaptoethanol, 10 M of leupeptin, 5 mM of l-ASA, 1 mM of phenylmethylsulfonyl fluoride, 1 g/L (w/v) of PVPP, and 10% (v/v) glycerin. C4H activity was determined in accordance with the method of Liu et al. (2014). It was measured in 0.01 ΔOD340/mg protein.

4-Coumarate-CoA ligase (4CL): 5 ml of 0.2 M Tris–HCl buffer (pH 7.5) with 25% glycerin and 0.1 M of DTT. The activity of 4CL was assessed using the technique of

Liu et al. (2014). Here, 0.5 ml of crude enzyme was added to a reaction mixture that contained 0.45 ml of 75 mM $MgCl_2$, 0.15 ml of 1 M coenzyme A (CoA), 0.15 ml of 0.8 mM adenosine triphosphate, and 0.15 ml of 2 mM p-cumaric acid. Activity was measured in $U{\cdot}mg^{-1}$ protein by using $U = 0.01\ \Delta OD333\ min^{-1}$.

Analysis of the Metabolite Content in the Phenylpropanoid Pathway

Total phenolic, flavonoid, and lignin contents were extracted and measured using the method described by Liu et al. (2014). Total phenolic and lignin concentrations were measured at OD280 and OD325, respectively and determined as $mg{\cdot}Kg^{-1}$ FW.

RNA Extraction and First-Strand Complementary DNA Synthesis

RNA was extracted from tissues (1.0 g) by using an RNeasy Plant Mini Kit (Takara, Japan) following meticulous procedures. First-strand complementary DNA (cDNA) was synthesized from 1 μg of total RNA by utilizing a Reverse-iT™ 1st Strand Synthesis Kit (Takara, Japan) and strictly following the manufacturer's instructions.

Real-Time Quantitative RT-PCR

A real-time quantitative PCR experiment was conducted by adding 10 μl of SYBR™ Green qPCR Master Mix, 1 μl of template cDNA, and 1 μl of 10 μM forward and reverse primers to each well with a 20 μl reaction volume. An ABI PRISM™ 7,000 Sequence Detection System was used for measurements (Applied Biosystems). Cycling conditions were 95°C for 10 min, followed by 40 cycles of 15 s at 95°C and 40 s at 60°C. The $2^{-\Delta\Delta t}$ formula was used to calculate the target gene expression and the *actin* gene was used as reference. Three duplicates of real-time PCR were conducted for each sample. Primers were indicated in **Supplementary Table 1**.

Data Analysis

By using SPSS 19.0, all data on enzyme activities and substance contents were evaluated using one-way ANOVA of least significant difference ($p < 0.05$).

RESULTS

Effects of Different BTH Concentrations on Weight Loss, Decay Incidence, and AsA Content

The weight loss of the BTH-treated fruit at 25, 50, 100, and 200 mg/L was compared with that of the control fruit, as presented in **Table 1**. As shown in the table, 100 mg/L of BTH significantly slowed down weight loss during the storage period. As shown in **Figure 1A**, from the sixth day of storage, the fruits of the different concentrations of BTH treatment and the control appeared to decay. On days 12 and 14, the fruit decay rate of the 100 mg/L BTH treatment was significantly lower than that of the control (**Figure 1A**). **Table 2** provides the AsA content of the BTH-treated and control fruit during the storage period. In this table, 100 mg/L of BTH exerted the best effect on increasing AsA content compared with the 25, 50, and 200 mg/L of BTH treatments of *R. roxburghii* fruit. Therefore, the concentration of 100 mg/L of BTH was selected for the subsequent experiments.

Effects of BTH Treatment on TSS, TA, MDA Content, and Cell Membrane Integrity

Throughout the storage period, TA continued to decrease in the control and BTH-treated fruit. However, BTH treatment slowed the decline of TA, and the BTH-treated fruit exhibited considerably higher TA levels than the control fruit on days 6–8 and 14 (**Figure 1B**). Similar to TA, TSS content continued to decrease in the control and BTH-treated fruit. However, TSS content in the BTH-treated fruit was always higher than that in the control fruit. It was considerably higher on days 2–6 and 14 (**Figure 1C**). The MDA content of the BTH-treated and control fruit increased throughout the storage period. However, BTH remarkably inhibited MDA increase on days 6–14 (**Figure 1D**). The BTH-treated fruit performed substantially better than the control fruit, with cell membrane integrity being considerably higher than that of the control group on days 6–14 (**Figure 1E**).

Changes in $O_2^{\bullet-}$ Production Rate, H_2O_2 Content, and SOD, CAT, and POD Activities After BTH Treatment

After BTH treatment, $O_2^{\bullet-}$ production rate increased rapidly on days 0–4 and reached the highest value on day 4, which

TABLE 1 | Effects of BTH treatment at different concentrations on the weight loss in *R. roxburghii* fruit.

Treatment	2 Days	4 Days	6 Days	8 Days	10 Days	12 Days	14 Days
Control	3.58 ± 0.07^{a}	5.29 ± 0.10^{a}	10.91 ± 0.69^{a}	11.80 ± 0.63^{a}	14.45 ± 0.34^{a}	16.40 ± 0.73^{a}	$17.43 \pm 0.34^{a,b}$
BTH (mg/L)							
25	3.30 ± 0.35^{a}	$5.13 \pm 0.46^{a,b}$	10.57 ± 0.24^{a}	$11.22 \pm 0.51^{a,b}$	14.83 ± 0.69^{a}	$15.52 \pm 0.78^{a,b}$	17.86 ± 0.44^{a}
50	3.12 ± 0.17^{a}	$4.86 \pm 0.33^{a,b}$	9.23 ± 0.17^{b}	$10.18 \pm 0.47^{b,c}$	$13.57 \pm 0.92^{a,b}$	15.77 ± 0.79^{a}	$16.44 \pm 0.38^{b,c}$
100	3.01 ± 0.03^{a}	4.43 ± 0.43^{b}	7.80 ± 0.81^{c}	9.70 ± 0.46^{c}	12.34 ± 1.82^{b}	14.41 ± 0.33^{b}	16.23 ± 0.83^{c}
200	3.57 ± 0.64^{a}	$5.06 \pm 0.42^{a,b}$	8.74 ± 0.21^{b}	$10.53 \pm 0.81^{b,c}$	14.76 ± 0.33^{a}	15.85 ± 0.66^{a}	17.97 ± 0.70^{a}

Different letters indicate significant differences between the BTH-treated and control fruit ($p < 0.05$).

was 48.2% higher than that of the control. During storage, the $O_2^{\bullet-}$ production rate of the BTH-treated fruit was higher than that of the control fruit. Moreover, it was considerably higher on days 2–4 (**Figure 2A**). H_2O_2 content increased on days 0–10 in the BTH-treated fruit and reached its peak on day 10, which was 54.3% higher than that of the control fruit, and then decreased. The H_2O_2 concentration of the BTH-treated fruit was greater than that of the control fruit throughout the preservation period. It was considerably higher on days 2–4 and 8–12 (**Figure 2B**). The SOD activity of the BTH-treated fruit was greater than that of the control fruit during storage, and it peaked on day 4, being 27.8% greater than that of the control fruit (**Figure 2C**). Substantial differences existed between the control and BTH-treated fruit on days 2–6 and 12. CAT activity increased during the storage period in two groups. On days 4–8 and 12, the CAT activity of the BTH-treated fruit was considerably higher (**Figure 2D**). On days 0–4, the POD activity of the BTH-treated fruit increased and peaked on day 4, which was 52.6% higher than that of the control fruit, before declining (**Figure 2E**). On days 4, 10, and 14, the POD activity of the BTH-treated fruit was considerably higher than that of the control group. In addition, the POD activity of the control fruit was always reduced during storage.

Effects of BTH Treatment on APX, GR, MDHAR, and DHAR Activities and GSH, GSSG Content

The APX activity of the fruit increased rapidly after BTH treatment on days 0–4. It peaked on day 4, when it was 48.9% greater than that of the control fruit, and then declined. During storage, the BTH-treated fruit exhibited a more activated APX than the control fruit, and significant differences were observed between the control and BTH-treated fruit on days 2, 4, 10, and 12 (**Figure 3A**). BTH treatment boosted GR activity, which increased rapidly after 8 days and peaked on day 10, when it was 39.6% greater than that of the control fruit (**Figure 3B**). MDHAR activity in the BTH-treated fruit increased on days 0–8, peaked on day 8 (45.1% greater than that of the control group), and then declined on days 8–14. On these days, the MDHAR activity of the BTH-treated fruit was substantially higher than that of the control fruit (**Figure 3C**). DHAR activity increased from days 0 to 8 and peaked on day 8 in the BTH-treated fruit, 34.4% higher than that of the control fruit (**Figure 3D**). As shown in **Figure 3E**, the GSH content peaked on day 6, after BTH treatment, when it was 20.8% higher than that of the control fruit. The BTH-treated fruit had considerably higher GSH than the control fruit on days 4–6 and 10 (**Figure 3E**). However, BTH-treated fruit showed lower GSSG levels than the control fruit throughout the storage period (**Figure 3F**).

Effects of BTH Treatment on PAL, C4H, and 4CL Activities and Total Phenolic, Flavonoid, and Lignin Contents

PAL activity was consistently higher in the BTH-treated fruit than in the control fruit throughout the storage period. On day 4, the PAL activity of the BTH-treated fruit peaked at 83.2% higher than that of the control fruit. A significant difference was observed between the two groups of fruit on days 4–10 (**Figure 4A**). C4H activity increased on days 0–4. The first peak, which appeared on day 4, was 51.8% higher than that of the control fruit and then declined. The second peak appeared on day 10 (85.0% higher than that in the control group). The BTH-treated fruit exhibited considerably higher

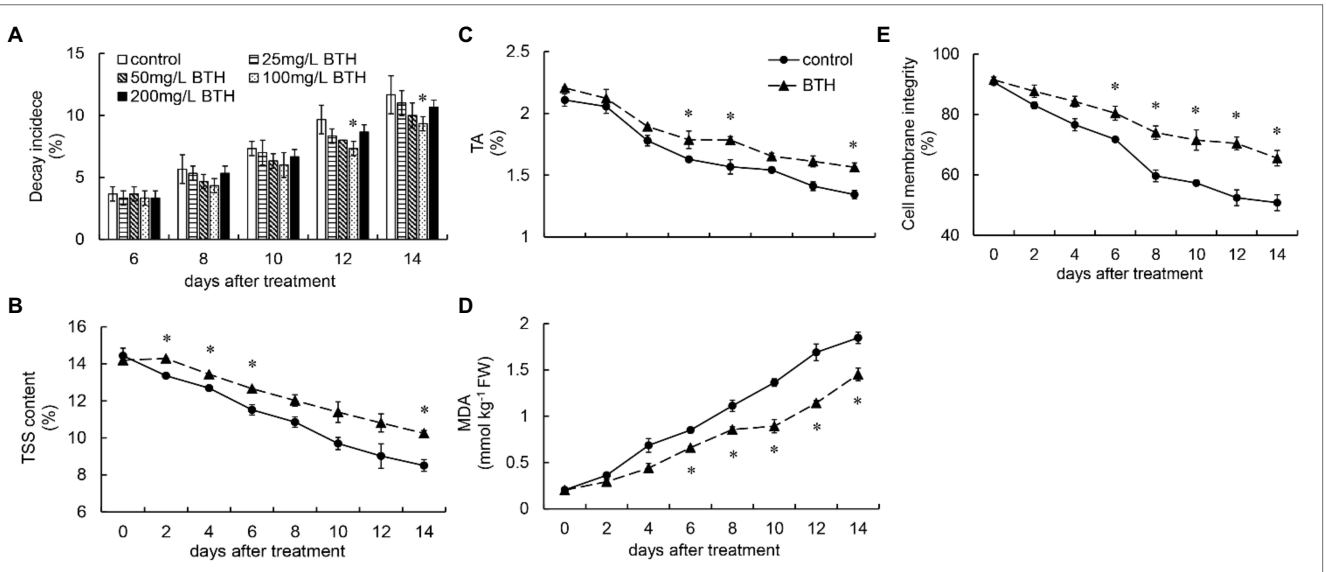


FIGURE 1 | Effect of benzothiazole (BTH) treatment on the decay incidence **(A)**, titratable acidity (TA; **B**), total soluble solid (TSS; **C**), malondialdehyde (MDA) content **(D)**, and cell membrane integrity **(E)** of *R. roxburghii* fruit. The significant differences at a level of 0.05 by Fisher's least significant difference (LSD) between the control and BTH-treated fruit are indicated by asterisks (*). Vertical bars represent the standard errors of the means (±SE).

TABLE 2 | Effects of BTH treatment at different concentrations on ascorbic acid (AsA) content in *R. roxburghii* fruit.

Treatment	0 Day	2 Days	4 Days	6 Days	8 Days	10 Days	12 Days	14 Days
Control	7.39 ± 0.35^{a}	7.53 ± 0.13^{a}	7.49 ± 0.10^{a}	7.48 ± 0.15^{a}	7.99 ± 0.37^{a}	7.58 ± 0.25^{a}	7.79 ± 0.46^{a,b}	6.41 ± 0.22^{a}
BTH (mg/L)								
25	7.52 ± 0.27^{a}	7.65 ± 0.81^{a}	7.83 ± 0.55^{a,b}	8.23 ± 0.54^{a}	8.83 ± 0.25^{a,b}	8.14 ± 0.60^{a}	7.34 ± 0.74^{a}	7.54 ± 0.57^{b,c}
50	7.45 ± 0.19^{a}	7.63 ± 0.52^{a}	7.52 ± 0.59^{a}	8.11 ± 0.20^{a}	9.43 ± 0.45^{b}	8.43 ± 0.39^{a}	8.65 ± 0.23^{b,c}	6.76 ± 0.57^{a,b}
100	7.43 ± 0.36^{a}	8.21 ± 0.43^{a}	8.82 ± 0.27^{b}	9.22 ± 0.52^{b}	11.71 ± 1.02^{c}	11.02 ± 0.84^{b}	9.48 ± 0.32^{c}	8.25 ± 0.67^{c}
200	7.24 ± 0.37^{a}	7.78 ± 0.30^{a}	8.23 ± 1.00^{a,b}	9.65 ± 0.69^{b}	9.75 ± 0.61^{b}	10.12 ± 0.91^{b}	8.73 ± 0.61^{b,c}	7.32 ± 0.77^{a,b,c}

Different letters indicate significant differences between the BTH-treated and control fruit ($p < 0.05$).

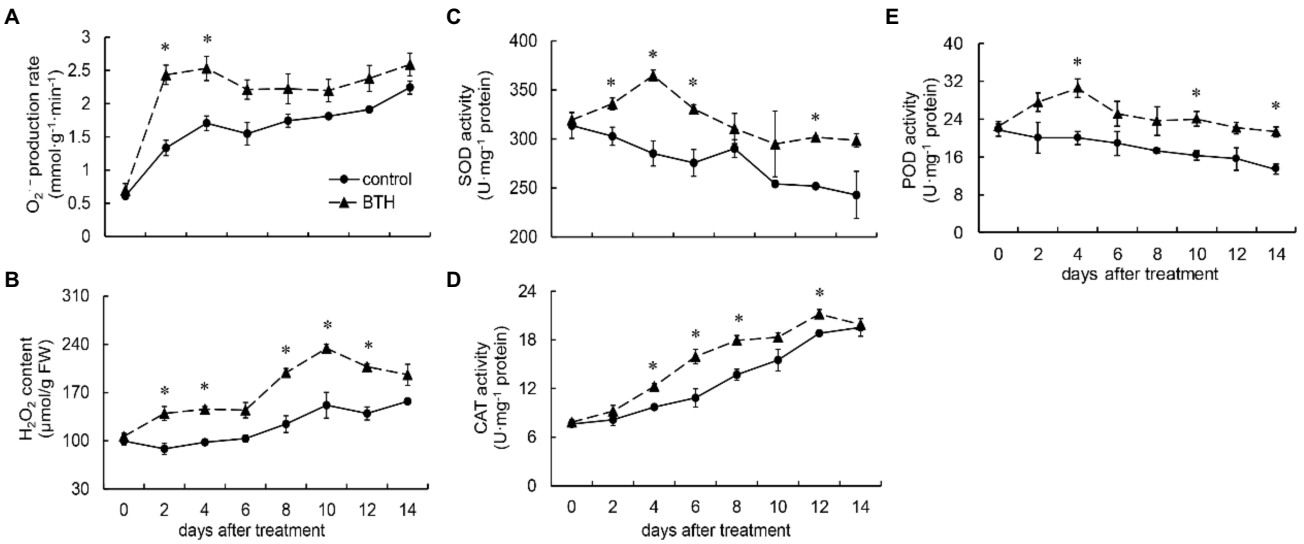


FIGURE 2 | Changes in superoxide anion ($O_2^{\bullet-}$) production rate **(A)**, hydrogen peroxide (H_2O_2) content **(B)**, and the activities of superoxide dismutase (SOD; **C**), catalase (CAT; **D**), and peroxidase (POD; **E**) in *R. roxburghii* fruit after BTH treatment during low temperature storage. The significant differences at a level of 0.05 by LSD between the control and BTH-treated fruit are indicated by asterisks (*). Vertical bars represent the standard errors of the means (±SE).

C4H activity than the control fruit on days 4–6 and 10–14 (**Figure 4B**). After BTH treatment, two peaks of 4CL activity appeared in *R. roxburghii* fruit on days 4 and 10. They were 21.9 and 33.3% greater than that of the control fruit, as shown in **Figure 4C**. BTH increased total phenolic content, which peaked on day 8 and was 24.0% greater than that of the control fruit. On days 4, 8, 12, and 14, the total phenolic content of the BTH-treated fruit was considerably greater than that of the control fruit (**Figure 4D**). The total phenolic content of the BTH-treated fruit was always higher than that of the control fruit during preservation. BTH increased flavonoid content, reaching a peak on day 6, which was 30.3% higher than that of the control fruit. The BTH-treated fruit contained considerably higher amounts of flavonoids on days 4–10, while the flavonoid content of the control fruit remained at a low level throughout the storage period (**Figure 4E**). The lignin contents of the BTH-treated and control fruit remained basically consistent during the first 6 days, while the lignin content of the BTH-treated fruit increased from day 8 and reached a peak on day 10 (22.6% higher than that of the control fruit). On days 8–14, BTH considerably increased lignin content (**Figure 4F**).

Effects of BTH Treatment on the Expression of *RrSOD*, *RrCAT*, *RrPOD*, *RrAPX*, *RrGR*, *RrMDHAR*, *RrDHAR*, *RrPAL*, *RrC4H*, and *Rr4CL*

Benzothiazole treatment increased *RrSOD* expression. The BTH-treated fruit reached their maximum value on day 2, which was 1.6 times that of the control fruit. *RrSOD* expression was greater than that in the control fruit on days 2–6 and 10–14 (**Figure 5A**). After BTH treatment, *RrCAT* expression increased rapidly during the first 6 days and reached its peak on day 6, which was two times as much as that of the control fruit. BTH largely increased *RrCAT* expression on days 2–6 (**Figure 5B**). Compared with the control fruit, BTH considerably enhanced *RrPOD* expression on days 2–6 and 10–12 (**Figure 5C**). BTH treatment considerably increased *RrAPX* expression during storage. On day 6, BTH-treated fruit exhibited the greatest relative gene expression, which was 1.6 times greater than the control fruit (**Figure 5D**). BTH treatment considerably increased *RrGR* expression on days 4–14. On day 10, the *RrGR* expression of the BTH-treated fruit reached its maximum value, which was 2.2 times that of the control fruit (**Figure 5E**). The *RrDHAR*

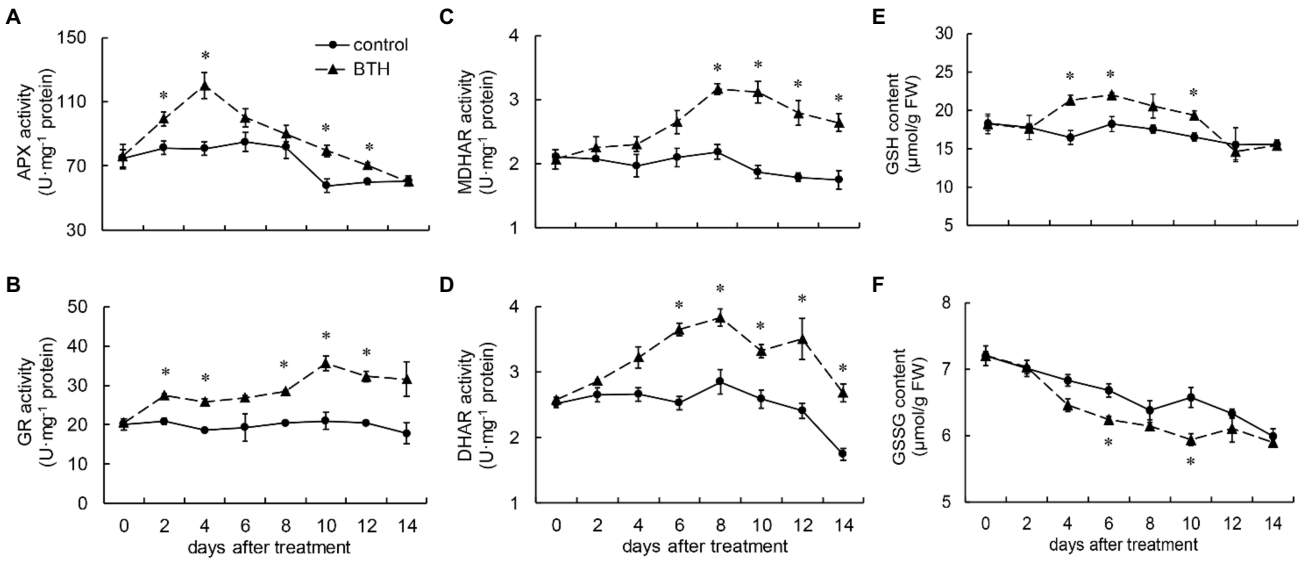


FIGURE 3 | Changes in the activities of ascorbate peroxidase (APX; **A**), Glutathione reductase (GR; **B**), monodehydroascorbate reductase (MDHAR; **C**), and dehydroascorbate reductase (DHAR; **D**) and the content of glutathione (GSH; **E**) and GSSG **(F)** in *R. roxburghii* fruit after BTH treatment during low temperature storage. The significant differences at a level of 0.05 by LSD between the control and BTH-treated fruit are indicated by asterisks (*). Vertical bars represent the standard errors of the means (±SE).

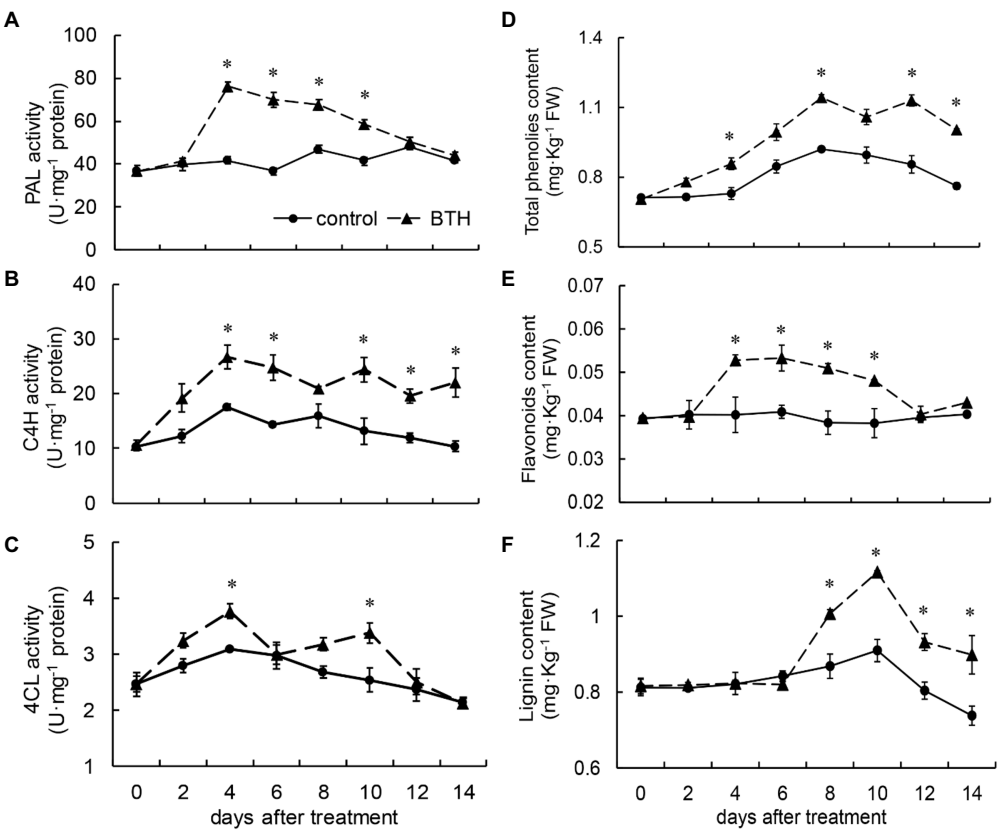


FIGURE 4 | Changes in the activities of phenylalanine ammonia lyase (PAL; **A**), cinnamate 4-hydroxylase (C4H; **B**), 4-coumarate-CoA ligase (4CL; **C**), and the content of total phenolic **(D)**, flavonoids **(E)**, and lignin **(F)** in *R. roxburghii* fruit after BTH treatment during low temperature storage. The significant differences at a level of 0.05 by LSD between the control and BTH-treated fruit are indicated by asterisks (*). Vertical bars represent the standard errors of the means (±SE).

expression of the treated fruit increased on days 0–6 and then decreased on days 6–12. The gene expression of the BTH-treated fruit was substantially higher than that of the control fruit. During preservation, the expression of *RrDHAR* in the control fruit did not change considerably (**Figure 5F**). Postharvest BTH treatment largely increased *RrMDHAR* expression on days 6 and 12, which were 3.1 and 1.4 times greater than that of the control fruit, respectively (**Figure 5G**). After BTH treatment, *RrPAL* expression in the BTH-treated fruit was considerably greater than that in the control group on days 6–8 and 10–12 (**Figure 5H**). Postharvest BTH treatment considerably increased *Rr4CL* expression on days 2, 6, and 8, reaching its peak on day 6, which was 1.5 times higher than that of the control (**Figure 5I**). BTH treatment notably increased *RrC4H* expression on days 2, 6, 8, and 12, i.e., 2.2, 1.6, 1.7, and 2.1 times greater than that of the control fruit, respectively (**Figure 5J**).

DISCUSSION

Moisture is an important guarantee for maintaining fruit freshness. Weight loss, which is mostly caused by respiration and transpiration, influences fruit quality. The current study found that BTH treatment can effectively reduce the weight loss rate of *R. roxburghii* fruit during storage. Du et al. (2021) determined that postharvest BTH treatment can reduce weight loss in oranges. Similar results have also been reported for apple fruit (Li et al., 2020b). BTH has been reported to induce systemic acquired resistance (SAR) in various plants (Lavergne et al., 2017), so we examined the effect of BTH treatment on decay rate in *R. roxburghii* fruit. Consistent with those reported in apples (Cao et al., 2011), strawberry (Romanazzi et al., 2013), muskmelon (Ren et al., 2012), and litchi (Xu et al., 2021), BTH inhibited *R. roxburghii* fruit decay. TA is primarily produced through the tricarboxylic acid cycle, and it can preserve the sugar-to-acid ratio in fruit, which is a key indicator for evaluating fruit quality (Ge et al., 2019a). The current research found that TA in the BTH-treated and control fruit declined during storage, with the BTH-treated fruit exhibiting lower TA than the control fruit. TSS is an important indicator for determining fruit maturity, and it directly affects fruit shelf quality. Similar to the findings for TA, the current research suggested that BTH treatment can significantly minimize the loss of TSS during storage. Previous studies have indicated that BTH treatment can effectively reduce TA content and increase TSS content in orange (Du et al., 2021), apple (Li et al., 2020b), and muskmelon (Li et al., 2015) fruit.

Cell membrane permeability and MDA can reflect the senescence level of fruit. MDA is a significant index of membrane lipid oxidative damage and peroxidation (Li et al., 2020b). The current study found that BTH treatment can effectively reduce the MDA content of *R. roxburghii* fruit during storage. Cell integrity is an important indicator of fruit quality. The present work determined that the cell membrane integrity of the BTH-treated and control fruit was decreased with prolonged storage. However, the cell membrane integrity of the BTH-treated fruit was significantly greater than that of the control fruit. Li et al. (2020a) demonstrated that treating pear fruit with BTH can essentially reduce MDA level during storage. The preceding results indicate that BTH treatment can effectively delay the senescence and maintain the quality of *R. roxburghii* fruit.

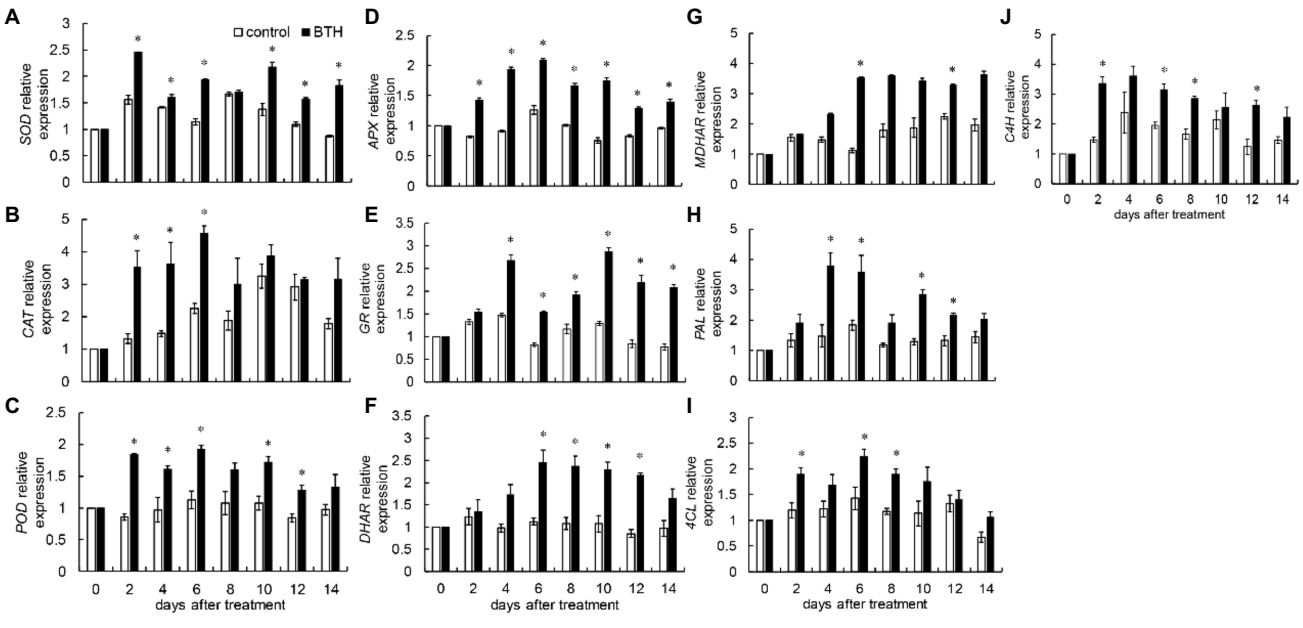


FIGURE 5 | Effects of BTH treatment on the expression of *RrSOD* **(A)**, *RrCAT* **(B)**, *RrPOD* **(C)**, *RrAPX* **(D)**, *RrGR* **(E)**, *RrDHAR* **(F)**, *RrMDHAR* **(G)**, *RrPAL* **(H)**, *Rr4CL* **(I)**, and *RrC4H* **(J)** in *R. roxburghii* fruit during low temperature storage. The significant differences at a level of 0.05 by LSD between the control and BTH-treated fruit are indicated by asterisks (*). Vertical bars represent the standard errors of the means (±SE).

Plant cells can accumulate large amounts of ROS as a result of biological and abiotic stressors, as asserted by Li et al. (2019). Low levels of ROS act as signal molecules from the following three aspects: (1) Activating ROS sensors to induce signal cascades and affect gene expression; (2) The components of signaling pathways could be directly oxidized by ROS; and (3) ROS modulates gene expression by regulating the activity of transcription factors (Apel and Hirt, 2004); thereby causing the production of defense genes and assisting in the cross-linking and lignification of cell walls, helping cells resist fungal infections (Jiang et al., 2017; Waszczak et al., 2018). However, excessive ROS can cause damage to cells (Jiang et al., 2017). The current study found that BTH treatment can rapidly increase the $O_2^{\bullet-}$ production rate of *R. roxburghii* fruit on days 0–4. In addition, H_2O_2 content was significantly greater than that of the control fruit during the majority of the storage period after BTH treatment. Wei et al. (2019) reported that postharvest BTH treatment increased H_2O_2 content in apple fruit. Ge et al. (2015) found that $O_2^{\bullet-}$ and H_2O_2 increased after the BTH dipping treatment of muskmelon fruit. Furthermore, a similar outcome was recorded in citrus fruit after the treatment of *Pichia membranaefaciens* (Luo et al., 2013).

The antioxidant defense system is composed of enzymes and non-enzymatic antioxidants that play an important role in scavenging ROS. Enzymatic reactive oxygen scavenging systems include SOD, POD, CAT, APX etc. (Apel and Hirt, 2004). SOD directly acts on $O_2^{\bullet-}$ to degrade it into H_2O_2. Subsequently, H_2O_2 is catalyzed and decomposed into H_2O and O_2 by CAT and APX, reducing excess H_2O_2 in plants and eliminating the damage caused by excess H_2O_2 to cells (Li et al., 2020b). POD is involved in various cell processes, such as the removal of H_2O_2, phenol oxidation, and lignification (Radhakrishnan et al., 2011; Wei et al., 2019). Our work determined that BTH treatment can increase the activity and expression of POD. Similar results have been found in studies on tomato (Małolepsza, 2006) and muskmelon (Ren et al., 2012) fruit. In the present study, BTH treatment increased the activities and gene expression of SOD, CAT, and APX. Ge et al. (2019b) found that postharvest BTH dipping treatment increased SOD, CAT, and APX activities, extending the storage life of blueberries. Similar results have been reported in pears (Li et al., 2020a), muskmelons (Ge et al., 2015), and peaches (Gao et al., 2016).

Non-enzymatic substances containing AsA and GSH have been reported to be involved in antioxidant scavenging in plants. AsA preserve the membrane structure and GSH directly decompose H_2O_2 into water. These two compounds contribute significantly to eliminate ROS in cells and protect the integrity of cell membranes (Wei et al., 2019). In our study, BTH treatment boosted the AsA and GSH contents of *R. roxburghii* fruit. Previous research has linked AsA and GSH contents to senescence in apples (Wei et al., 2019), pears (Li et al., 2020a), blueberries (Ge et al., 2019b), and strawberries (Romanazzi et al., 2013). This suggested that the delay of *R. roxburghii* fruit senescence by BTH treatment may be related to the increase of AsA and GSH content. The AsA-GSH cycle enzymes APX, MDHAR, DHAR, and GR play an important role in maintaining the dynamic balance between GSH and GSH disulfide in plants (Tao et al., 2019). Ren et al. (2012), Ge et al. (2019b), and Wei et al. (2019) reported that BTH treatment increased the activity and gene expression of GR, MDHAR, and DHAR to maintain the dynamic balance of AsA and GSH of the AsA–GSH cycle in apple and muskmelon fruit. Our result also found BTH increased the activities and gene expression of MDHAR, DHAR, and GR during the storage period. The AsA-GSH cycle enzymes APX, MDHAR, DHAR, and GR are directly related to the AsA and GSH degradation and recycling and that is why, the content of AsA and GSH are related to the activity of the AsA-GSH cycle enzymes (Nahar et al., 2015). One of the mechanisms of SAR is the induction of ROS production when plants are subjected to biotic or abiotic stress (Li et al., 2020c). BTH has been reported to activate the SA-mediated SAR response in plants, and further activate the activity and gene expression related to the metabolism of ROS (Terry et al., 2004). In our study, BTH induces a moderate increase in ROS content without damaging the organism, which might serve as a signal molecule to continuously induces the production of antioxidant scavenging enzymes to maintain cellular redox homeostasis, thereby improving the defense capabilities and delaying senescence in *R. roxburghii* fruit.

The phenylpropanoid pathway is a secondary metabolic pathway in plants. Many major antibacterial substances in plants, such as lignin, flavonoids, and phenolic compounds, are directly or indirectly produced by the phenylpropanoid pathway (Vogt, 2010). PAL is a rate-limiting enzyme in the phenylpropanoid pathway. C4H is the second key enzyme in the phenylpropanoid pathway, and its substrate is trans-cinnamic acid. 4CL can catalyze various hydroxycinnamic acids to generate the corresponding thioesters, entering the synthesis pathways of phenols, flavonoids, and anthocyanins (Liu et al., 2014). The present research demonstrated that BTH treatment can increase PAL and 4CL activities and gene expression in *R. roxburghii* fruit. Liu et al. (2014) found that postharvest BTH treatment increased the activities of PAL, C4H, and 4CL in muskmelon fruit. A similar result was obtained in the BTH treatment of blueberries (Ge et al., 2019b). Phenolic can enhance the buildup of lignin in the cell wall by acting as precursors for the synthesis of lignin and other anti-disease compounds and exhibiting a certain antibacterial effect. In addition, phenolic compounds can be oxidized into more toxic quinones under the action of polyphenol oxidase, effectively inhibiting the spread of pathogens (Liu et al., 2014). Flavonoids have antibacterial properties and can prevent spore germination, germ tubes elongation, and mycelial growth (Deng et al., 2008). In accordance with the results of the current study, the concentrations of total phenol, flavonoid, and lignin in *R. roxburghii* fruit can be increased by BTH treatment. The BTH treatment on apple (Ge et al., 2019a) and muskmelon (Liu et al., 2014) fruit exhibits similar effects.

The above results indicate that BTH treatment may delay fruit senescence by increasing the expression of key genes in the secondary metabolic pathway of phenylalanine synthesis, increasing PAL, C4H, and 4CL enzyme activity, and further

promoting the content of secondary metabolites such as lignin, total phenols, and total flavonoids.

CONCLUSION

Benzothiazole treatment significantly increased the activities and expression of SOD, CAT, APX, GR, POD, MDHAR, and DHAR and the contents of GSH and AsA in *R. roxburghii* fruit. It also increased $O_2^{\bullet-}$ production rate and H_2O_2 content, but reduced MDA content. BTH treatment effectively maintained the dynamic balance of ROS metabolism and delayed the senescence of *R. roxburghii* fruit. In addition, BTH also increased the activities and expression of PAL, C4H, and 4CL and the contents of total phenols, flavonoids, and lignin, enhancing the disease resistance of *R. roxburghii* fruit (**Figure 6**). Nevertheless, the investigation of the mechanism of BTH to delay *R. roxburghii* fruit senescence is still needed to be further studied at the molecular level. Future studies will consider using high-throughput sequencing technologies such as metabolome sequencing and RNA-seq to identify key gene regulatory networks and metabolic regulatory networks, revealing the molecular mechanisms by which BTH treatment delays senescence in *R. roxburghii* fruit.

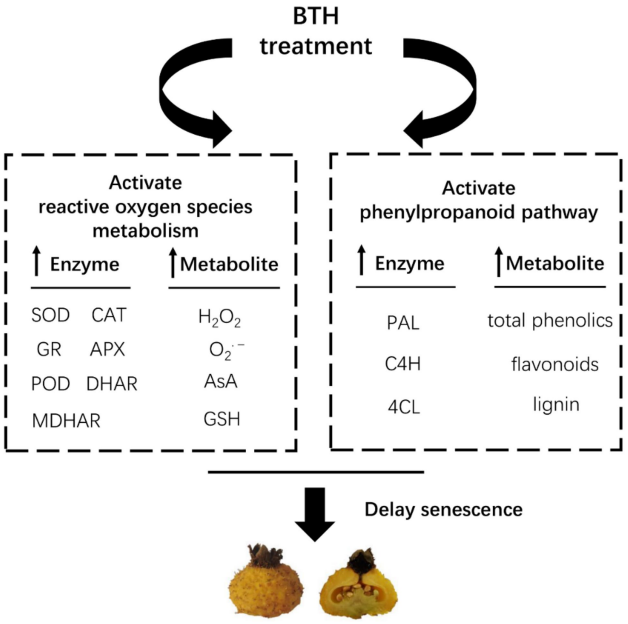


FIGURE 6 | A speculation to explain the role of BTH in regulating fruit senescence in *R. roxburghii*. Arrow up indicates promotion.

DATA AVAILABILITY STATEMENT

The original contributions presented in the study are included in the article/**Supplementary Material**; further inquiries can be directed to the corresponding authors.

AUTHOR CONTRIBUTIONS

BD: conceptualization, funding acquisition, resources, and writing – original draft. XD: investigation, data curation, formal analysis, methodology, funding acquisition, and writing – review and editing. HT: software, investigation, and methodology. DZ: resources and validation. QY: software and methodology. HH: methodology and validation. KH: supervision and resources. All authors contributed to the article and approved the submitted version.

FUNDING

This study was supported by the Science and Technology Program of Guizhou Province, China (2021172); National Natural Science Foundation of China (32002103), and Guangdong Basic and Applied Basic Research Foundation (2020A1515110092); and Major Research Project of Innovation Group of Guizhou Provincial Department of Education (2018017).

SUPPLEMENTARY MATERIAL

The Supplementary Material for this article can be found online at: https://www.frontiersin.org/articles/10.3389/fpls.2021.753261/full#supplementary-material

REFERENCES

Apel, K., and Hirt, H. (2004). Reactive oxygen species: metabolism, oxidative stress, and signal transduction. *Annu. Rev. Plant Biol.* 55, 373–399. doi: 10.1146/annurev.arplant.55.031903.141701

Cao, S. F., Hu, Z. C., Zheng, Y. H., Yang, Z. F., and Lu, B. H. (2011). Effect of BTH on antioxidant enzymes, radical-scavenging activity and decay in strawberry fruit. *Food Chem.* 125, 145–149. doi: 10.1016/j.foodchem.2010.08.051

de Freitas-Silva, L., Rodríguez-Ruiz, M., Houmani, H., da Silva, L. C., Palma, J. M., and Corpas, F. J. (2017). Glyphosate-induced oxidative stress in *Arabidopsis thaliana* affecting peroxisomal metabolism and triggers activity in the oxidative phase of the pentose phosphate pathway (OxPPP) involved in NADPH generation. *J. Plant Physiol.* 218, 196–205. doi: 10.1016/j.jplph.2017.08.007

Deng, Y. Y., Ming, J., and Zeng, K. F. (2008). Effects of chitosan coating on disease resistance and storage quality of navel orange fruit. *J. Food Sci.* 29, 656–661. doi: 10.3321/j.issn:1002-6630.2008.11.155

Du, H., Sun, Y., Yang, R., Zhang, W., Wan, C., Chen, J., et al. (2021). Benzothiazole (BTH) induced resistance of navel orange fruit and maintained fruit quality during storage. *J. Food Qual.* 2021:6631507. doi: 10.1155/2021/6631507

Fan, K. X., Xie, G. F., Liu, S., Wang, L., Zhao, Z., and Liu, Y. (2019). Effect of 1-MCP combined with PE bag on the quality of golden pear storage. *Food Sci. Technol.* 44, 71–76. doi: 10.13684/j.cnki.spkj.2019.02.012

Gao, H., Lu, Z., Yang, Y., Wang, D., Yang, T., Cao, M., et al. (2018). Melatonin treatment reduces chilling injury in peach fruit through its regulation of membrane fatty acid contents and phenolic metabolism. *Food Chem.* 245, 659–666. doi: 10.1016/j.foodchem.2017.10.008

Gao, H., Zhang, Z. K., Chai, H. K., Cheng, N., Yang, Y., Wang, D. N., et al. (2016). Melatonin treatment delays postharvest senescence and regulates reactive oxygen species metabolism in peach fruit. *Postharvest Biol. Technol.* 118, 103–110. doi: 10.1016/j.postharvbio.2016.03.006

Ge, Y. H., Bi, Y., Li, Y. C., and Wang, Y. (2012). Resistance of harvested fruits and vegetables to diseases induced by ASM and its mechanism. *Agric. Sci. China* 45, 3357–3362.

Ge, Y., Chen, Y., Li, C., Wei, M., Li, X., Li, S., et al. (2019a). Effect of trisodium phosphate dipping treatment on the quality and energy metabolism of apples. *Food Chem.* 274, 324–329. doi: 10.1016/j.foodchem.2018.08.142

Ge, Y. H., Deng, H. W., Bi, Y., Li, C. Y., Liu, Y. Y., and Dong, B. Y. (2015). Postharvest ASM dipping and DPI pre-treatment regulated reactive oxygen species metabolism in muskmelon (*Cucumis melo* L.) fruit. *Postharvest Biol. Technol.* 99, 160–167. doi: 10.1016/j.postharvbio.2014.09.001

Ge, Y., Tang, Q., Li, C., Duan, B., Li, X., Wei, M., et al. (2019b). Acibenzolar-S-methyl treatment enhances antioxidant ability and phenylpropanoid pathway of blueberries during low temperature storage. *LWT* 110, 48–53. doi: 10.1016/j.lwt.2019.04.069

Jiang, G., Xiao, L., Yan, H., Zhang, D., Wu, F., Liu, X., et al. (2017). Redox regulation of methionine in calmodulin affects the activity levels of senescence-related transcription factors in litchi. *Biochim. Biophys. Acta* 1861, 1140–1151. doi: 10.1016/j.bbagen.2017.02.004

Lavergne, F., Richard, C., Saudreau, M., Venisse, J. S., Fumanal, B., and Goupil, P. (2017). Effect of acibenzolar-S-methyl phototransformation on its elicitation activity in tobacco cells. *Plant Physiol. Biochem.* 118, 370–376. doi: 10.1016/j.plaphy.2017.07.008

Li, X., Bi, Y., Wang, J., Dong, B., Li, H., Gong, D., et al. (2015). BTH treatment caused physiological, biochemical and proteomic changes of muskmelon (*Cucumis melo* L.) fruit during ripening. *J. Proteome* 120, 179–193. doi: 10.1016/j.jprot.2015.03.006

Li, X., Li, C., Cheng, Y., Hou, J., Zhang, J., and Ge, Y. (2020a). Postharvest application of acibenzolar-s-methyl delays the senescence of pear fruit by regulating reactive oxygen species and fatty acid metabolism. *J. Agric. Food Chem.* 68, 4991–4999. doi: 10.1021/acs.jafc.0c01031

Li, T., Shi, D., Wu, Q., Zhang, Z., Qu, H., and Jiang, Y. (2019). Sodium Para-aminosalicylate delays pericarp browning of litchi fruit by inhibiting ROS-mediated senescence during postharvest storage. *Food Chem.* 278, 552–559. doi: 10.1016/j.foodchem.2018.11.099

Li, C., Wei, M., Ge, Y., Zhao, J., Chen, Y., Hou, J., et al. (2020b). The role of glucose-6-phosphate dehydrogenase in reactive oxygen species metabolism in apple exocarp induced by acibenzolar-S-methyl. *Food Chem.* 308:125663. doi: 10.1016/j.foodchem.2019.125663

Li, C., Zhang, J., Ge, Y., Li, X., Wei, M., Hou, J., et al. (2020c). Postharvest acibenzolar-S-methyl treatment maintains storage quality and retards softening of apple fruit. *J. Food Biochem.* 44:e13141. doi: 10.1111/jfbc.13141

Liu, Y., Ge, Y., Bi, Y., Li, C., Deng, H., Hu, L., et al. (2014). Effect of postharvest acibenzolar-S-methyl dipping on phenylpropanoid pathway metabolism in muskmelon (*Cucumis melo* L.) fruits. *Sci. Hortic.* 168, 113–119. doi: 10.1016/j.scienta.2014.01.030

Liu, M. H., Zhang, Q., Zhang, Y. H., Lu, X. Y., Fu, W. M., and He, J. Y. (2016). Chemical analysis of dietary constituents in *R. roxburghii* and Rosa sterilis fruits. *Molecules* 21:1204. doi: 10.3390/molecules21091204

Luo, Y., Zhou, Y., and Zeng, K. (2013). Effect of *Pichia membranaefaciens* on ROS metabolism and postharvest disease control in citrus fruit. *Crop Prot.* 53, 96–102. doi: 10.1016/j.cropro.2013.06.015

Małolepsza, U. (2006). Induction of disease resistance by acibenzolar-S-methyl and o-hydroxyethylorutin against *Botrytis cinerea* in tomato plants. *Crop Prot.* 25, 956–962. doi: 10.1016/j.cropro.2005.12.009

Nahar, K., Hasanuzzaman, M., Alam, M. M., and Fujita, M. (2015). Exogenous spermidine alleviates low temperature injury in mung bean (*Vigna radiata* L.) seedlings by modulating ascorbate-glutathione and glyoxalase pathway. *Int. J. Mol. Sci.* 16, 30117–30132. doi: 10.3390/ijms161226220

Nath, M., Bhatt, D., Prasad, R., and Tuteja, N. (2017). "Reactive oxygen species (ROS) metabolism and signaling in plant-mycorrhizal association under biotic and abiotic stress conditions," in *Mycorrhiza- Eco-Physiology, Secondary Metabolites, Nanomaterials*. eds. A. Varma, R. Prasad and N. Tuteja (Cham: Springer), 223–232.

Oliveira, M. D. M., Varanda, C. M. R., and Félix, M. R. F. (2016). Induced resistance during the interaction pathogen plant and the use of resistance inducers. *Phytochem. Lett.* 15, 152–158. doi: 10.1016/j.phytol.2015.12.011

Radhakrishnan, N., Alphonse, A. J., and Balasubramanian, R. (2011). Effect of Acibenzolar-S-methyl (ASM) pre-treatment in inducing resistance against *Pythium aphanidermatum* infection in *Curcuma longa*. *Crop Prot.* 30, 24–32. doi: 10.1016/j.cropro.2010.08.020

Rasool, S., Ahmad, A., Siddiqi, T. O., and Ahmad, P. (2013). Changes in growth, lipid peroxidation and some key antioxidant enzymes in chickpea genotypes under salt stress. *Acta Physiol. Plant.* 35, 1039–1050. doi: 10.1007/s11738-012-1142-4

Ray, P. D., Huang, B. W., and Tsuji, Y. (2012). Reactive oxygen species (ROS) homeostasis and redox regulation in cellular signaling. *Cell. Signal.* 24, 981–990. doi: 10.1016/j.cellsig.2012.01.008

Ren, Y. L., Wang, Y. F., Bi, Y., Ge, Y. H., Wang, Y., Fan, C. F., et al. (2012). Postharvest BTH treatment induced disease resistance and enhanced reactive oxygen species metabolism in muskmelon (*Cucumis melo* L.) fruit. *Eur. Food Res. Technol.* 234, 963–971. doi: 10.1007/s00217-012-1715-x

Romanazzi, G., Feliziani, E., Santini, M., and Landi, L. (2013). Effectiveness of postharvest treatment with chitosan and other resistance inducers in the control of storage decay of strawberry. *Postharvest Biol. Technol.* 75, 24–27. doi: 10.1016/j.postharvbio.2012.07.007

Ruiz-García, Y., Gil-Munoz, R., López-Roca, J. M., Martinez-Cutillas, A., Romero-Cascales, I., and Gomez-Plaza, E. (2013). Increasing the phenolic compound content of grapes by preharvest application of abcisic acid and a combination of methyl jasmonate and benzothiadiazole. *J. Agric. Food Chem.* 61, 3978–3983. doi: 10.1021/jf400631m

Sayyari, M., Babalar, M., Kalantari, S., Serrano, M., and Valero, D. (2009). Effect of salicylic acid treatment on reducing chilling injury in stored pomegranates. *Postharvest Biol. Technol.* 53, 152–154. doi: 10.1016/j.postharvbio.2009.03.005

Tao, D., Wang, J., Zhang, L., Jiang, Y., and Lv, M. (2019). 1-Methylcyclopropene alleviates peel browning of 'Nanguo'pears by regulating energy, antioxidant and lipid metabolisms after long term refrigeration. *Sci. Hortic.* 247, 254–263. doi: 10.1016/j.scienta.2018.12.025

Terry, L. A., and Joyce, D. C. (2004). Elicitors of induced disease resistance in postharvest horticultural crops: a brief review. *Postharvest Biol. Technol.* 32, 1–13. doi: 10.1016/j.postharvbio.2003.09.016

Vogt, T. (2010). Phenylpropanoid biosynthesis. *Mol. Plant* 3, 2–20. doi: 10.1093/mp/ssp106

Waszczak, C., Carmody, M., and Kangasjärvi, J. (2018). Reactive oxygen species in plant signaling. *Annu. Rev. Plant Biol.* 69, 209–236. doi: 10.1146/annurev-arplant-042817-040322

Wei, M., Ge, Y., Li, C., Han, X., Qin, S., Chen, Y., et al. (2019). G6PDH regulated NADPH production and reactive oxygen species metabolism to enhance disease resistance against blue mold in apple fruit by acibenzolar-S-methyl. *Postharvest Biol. Technol.* 148, 228–235. doi: 10.1016/j.postharvbio.2018.05.017

Xu, D. D., Xi, P. G., Lin, Z. M., Huang, J. H., Lu, S. H., Jiang, Z. D., et al. (2021). Efficacy and potential mechanisms of benzothiadiazole inhibition on postharvest litchi downy blight. *Postharvest Biol. Technol.* 181:111660. doi: 10.1016/j.postharvbio.2021.111660

Yang, Q. Q., Zhang, D., Farha, A. K., Yang, X., Li, H. B., Kong, K. W., et al. (2020). Phytochemicals, essential oils, and bioactivities of an underutilized wild fruit Cili (*R. roxburghii*). *Ind. Crop. Prod.* 143:111928. doi: 10.1016/j.indcrop.2019.111928

Zhang, Z. M., Hou, F. M., Li, J., Zhang, S., Li, X., and Wu, Q. (2020). Effect of 1-MCP and UV-C compound treatment on the preservation effect of pear fruit. *Food Sci. Technol.* 45, 31–38. doi: 10.13684/j.cnki.spkj.2020.06.006

Zhu, J. X., Wu, H., and Sun, Q. J. (2019). Preparation of crosslinked active bilayer film based on chitosan and alginate for regulating ascorbate-glutathione cycle of postharvest cherry tomato (*Lycopersicon esculentum*). *Int. J. Biol. Macromol.* 130, 584–594. doi: 10.1016/j.ijbiomac.2019.03.006

Conflict of Interest: The authors declare that the research was conducted in the absence of any commercial or financial relationships that could be construed as a potential conflict of interest.

Publisher's Note: All claims expressed in this article are solely those of the authors and do not necessarily represent those of their affiliated organizations, or those of the publisher, the editors and the reviewers. Any product that may be evaluated in this article, or claim that may be made by its manufacturer, is not guaranteed or endorsed by the publisher.

Copyright © 2021 Dong, Tang, Zhu, Yao, Han, He and Ding. This is an open-access article distributed under the terms of the Creative Commons Attribution License (CC BY). The use, distribution or reproduction in other forums is permitted, provided the original author(s) and the copyright owner(s) are credited and that the original publication in this journal is cited, in accordance with accepted academic practice. No use, distribution or reproduction is permitted which does not comply with these terms.

frontiers in Plant Science

ORIGINAL RESEARCH
published: 15 November 2021
doi: 10.3389/fpls.2021.769989

Genetic Mapping and Identification of the Candidate Genes for Mottled Rind in *Cucumis melo* L.

*Jia Shen, Xinyang Xu, Yuejian Zhang, Xiaowei Niu and Weisong Shou**

Institute of Vegetables, Zhejiang Academy of Agricultural Sciences, Hangzhou, China

The rind appearance of melon is one of the most vital commercial quality traits which determines the preferences and behavior of consumers toward the consumption of melon. In this study, we constructed an F_2 population derived from SC (mottled rind) and MG (non-mottled rind) lines for mapping the mottled rind gene(s) in melon. Genetic analysis showed that there were two dominant genes (*CmMt1* and *CmMt2*) with evidence of epistasis controlling the mottled rind. Meanwhile, the phenotypic segregation ratio implied that the immature rind color had an epistatic effect on the mottled rind, which was regulated by *CmAPRR2*. A Kompetitive Allele-Specific PCR (KASP) DNA marker ($CmAPRR2^{SNP(G/T)}$) was developed and shown to co-segregate with rind color, confirming that *CmAPRR2* was *CmMt1*. Using bulked segregant analysis sequencing and KASP assays, *CmMt2* was fine-mapped to an interval of 40.6 kb with six predicted genes. Functional annotation, expression analysis, and sequence variation analyses confirmed that *AtCPSFL1* homolog, *MELO3C026282*, was the most likely candidate gene for *CmMt2*. Moreover, pigment content measurement and transmission electron microscopy analysis demonstrated that *CmMt2* might participate in the development of chloroplast, which, in turn, decreases the accumulation of chlorophyll. These results provide insight into the molecular mechanism underlying rind appearance and reveal valuable information for marker-assisted selection breeding in melon.

Keywords: melon, mottled rind, spots, chlorophyll, mapping

OPEN ACCESS

Edited by:
Pei Xu,
China Jiliang University, China

Reviewed by:
Shi Liu,
Northeast Agricultural University, China
Angel Rene Del Valle Echevarria,
Hawaii Agriculture Research Center, United States
Meiling Gao,
Qiqihar University, China

***Correspondence:**
Weisong Shou
shouws@zaas.ac.cn

Specialty section:
This article was submitted to Crop and Product Physiology, a section of the journal Frontiers in Plant Science

Received: *03 September 2021*
Accepted: *18 October 2021*
Published: *15 November 2021*

Citation:
Shen J, Xu X, Zhang Y, Niu X and Shou W (2021) Genetic Mapping and Identification of the Candidate Genes for Mottled Rind in Cucumis melo L. Front. Plant Sci. 12:769989. doi: 10.3389/fpls.2021.769989

INTRODUCTION

Melon (*Cucumis melo* L. $2n = 24$) is an economically important vegetable crop grown throughout the world. Based on ovary pubescence, melon has been classified into two subspecies, *C. melo* ssp. *agrestis* and *C. melo* ssp. *melo* (Jeffrey, 1980). Recent studies revealed that there are two independent sets of domestication sweeps, resulting in diverse characteristics of these two subspecies during melon cultivation, especially the fruit characters (Zhao et al., 2019; Liu S. et al., 2020). External fruit (rind) appearance is an important commercial quality trait affecting the consumption of melon of consumers, which has abundant genetic diversity (Pitrat, 2016). In recent years, numerous genetic studies have focused on the rind appearance of melon, including rind color and rind pattern (Feder et al., 2015; Pereira et al., 2018; Oren et al., 2019; Zhao et al., 2019).

For convenience, the rind color could be divided into immature fruit and mature fruit color according to the development stage (Pitrat, 2016). Previous studies have shown that besides chlorophyll, the pigment regulation of immature rind color is inhibited early in fruit development, reflecting chlorophyll concentrations (Tadmor et al., 2010), and that rind color transforms during development leading to rich variation in mature fruit pigment profiles that include different

combinations of carotenoids, flavonoids, and chlorophylls (Tadmor et al., 2010; Feder et al., 2015). Therefore, compared with mature fruits, the rind color of immature melon fruits is relatively straightforward, dividing into light green and dark green (Pitrat, 2016). And the causative regulatory gene (*CmAPRR2*) of chlorophyll accumulation in the immature fruit rind of melon was identified (Oren et al., 2019). Xu et al. (2021) cloned the same gene with the genetic population constructed between subspecies, indicating the conservation of the *CmAPRR2*.

As for rind pattern, the presence of spots on the rind is an important rind pattern trait commonly found in commercial melon (Pitrat, 2016). Although the study of the genetic pattern of spots on the rind by multiple research groups is relatively early (Danin-Poleg et al., 2002; Zhao et al., 2019), they have given unconvincing and even conflicting results. A single gene, *Mt* (Mottled rind pattern), was reported to control the mottled rind, dominant to uniform color *mt* (Ganesan, 1988), while Perin et al. (2002) showed that the presence of dark spot on the rind has a monogenic recessive inheritance (*mt-2*). And *mt-2* was mapped to the linkage group II (Pitrat, 2008). Since the reference genome of melon was released in 2012 (Garcia-Mas et al., 2012), we were unable to define the physical position on the reference genome. And then, Pereira et al. (2018) detected that the mottled rind was controlled by a dominant gene *Mt*, which was identified on chromosome 2 within 850 kb by a genotyping-by-sequencing strategy. Recently, Lv et al. (2018) narrowed the *Mt* positioning interval to 280.872 kb of chromosome 2, although the interval was not completely coincident. Interestingly, it was also mapped on chromosome 4 within 172.8 kb (Liu et al., 2019). Thus, the mottled rind of melon may be relatively complex, and more effort should be required for the fine mapping and cloning of the *Mt* gene(s).

Research on melon rind appearance is very important both in theoretical studies and in applied practice for elucidating the mechanism of mottled rind and for the breeding of melon. In this study, two inbred accessions, namely, *C. melo* ssp. *agrestis* (SC, mottled rind) and *C. melo* ssp. *melo* (MG, non-mottled rind), were used to identify the pigment components of the dark spots formation on the melon rind. The inheritance of mottled rind was analyzed, and two dominant genes (*CmMt1* and *CmMt2*) with evidence of epistasis were responsible for the mottled rind. *CmAPRR2* was the candidate epistatic gene for *CmMt1*, and a candidate gene encoding *AtCPSFL1* homolog, *MELO3C026282,* was predicted by map-based cloning for *CmMt2*. The present results may highlight the understanding of the genetic basis for mottled rind formation and promote the breeding of melon with ideal rind appearance by marker-assisted selection.

MATERIALS AND METHODS

Plant Materials and Phenotypic Data Collection

An inbred line of *C. melo* spp. *agrestis* (Songwhan Charmi, SC) and an inbred line of *C. melo* ssp. *melo* (Mi Gua, MG) were employed to generate F_1, BC_1, and F_2 populations in this study. The female parent was mottled and dark green rind, while the male parent was uniform and light green rind. The SC and MG lines as well as their F_1, F_2, and BC_1 populations were used for genetic analyses. The $F_{2:3}$ families were developed and used in this study for the fine mapping. All the plants were hand pollinated with two staminate flowers and clamped with grafting clips to prevent re-pollination by entomophily or pollen dispersal. All the lines were grown in the plastics greenhouse at Zhejiang Academy of Agricultural Sciences under the natural sunlight in spring 2019 in Yangdu (120°46′ E, 30°45′ N).

Each plant, including the parental lines as well as F_1, BC_1, and F_2 individuals, was given an identification tag revealing its serial number, pollination date, and cross-combination type. The phenotype of the fruit rind was detected through visual observation and a digital portable colorimeter (Minolta CS-321) at 10–15 days after pollination (dap). And each fruit was photographed for reassessment. The young leaves of each plant were cut from the plant apex and flash-frozen in liquid nitrogen and maintained at −80°C for further use.

Pigment Content Measurement and Transmission Electron Microscopy

According to the initial stage of phenotypic differences between parents, rind samples from the immature fruits of melon at 15 days after pollination were collected to measure the chlorophyll and carotenoid contents. The pigment content was measured on three biological replicates for each sample analysis, each sample comprising three individual fruits.

The same samples were prepared for transmission electron microscopy (TEM). The samples were vacuumed in 2.5% glutaraldehyde, fixed at 4°C for 4 h, and then dehydrated in a graded ethanol series, and critical point drying was performed using liquid CO_2 in a Bal-Tec CPD 030 critical point drier. Later, the samples were coated with 15 nm gold on aluminum stubs in a Sputter Coater Bal-Tec SCD 005. A Hitachi S-3500N scanning electron microscope was subsequently used for sample observations. The chloroplast number and size in the rind cells (n = 10 for each sample) was measured by ultrathin section with CaseViewer 2.1 (3DHISTECH, Budapest, Hungary).

Bulked Segregant Analysis Sequencing

Bulked segregant analysis sequencing (BSA-seq) was used to map the *CmMt* gene. The genomic DNA was extracted from young leaves of F_2 individuals using the CTAB (Murray and Thompson, 1980). A mottled pool containing equal amounts of DNA from 20 mottled rind individuals and a uniform pool containing 20 individuals with uniform rind were prepared for whole-genome resequencing with an Illumina HiSeq 2500 (500 bp) in Novogene (Beijing, China). The clean data obtained from the DNA pools were aligned with the "DHL92" melon reference genome (v4.0) (Castanera et al., 2019). Variant calling including single-nucleotide polymorphism (SNP) and insertion and deletion polymorphisms (Indels), SNP and Indel filtering, index calculation, and mapping region identification were performed as described by Klein et al. (2018).

Fine Mapping With Kompetitive Allele-Specific PCR Markers

According to the BSA-seq analysis, 25 SNPs in the candidate region were selected for developing Kompetitive Allele-Specific PCR (KASP) marker. The KASP primers were validated with the two-parent lines and a small number of F_2 individuals first. Then, a total of 553 F_2 individuals with two parents were genotyped by the KASP markers, and the primers are shown in **Supplementary Table 1**. The linkage map was constructed using QTL IciMapping 4.2 (CAAS, Beijing, China) (Meng et al., 2015). The KASP assays were performed as described previously (Yang et al., 2020). Briefly, KASP reaction mixture contained 2.0 μl of template DNA, 0.07 μl of primer mixture (10 μM), 0.43 μl of RNase-free water, and 5 μl of KASP master mixture (2×; LGC, Middlesex, United Kingdom). The PCR cycling started with an initial denaturation at 95°C for 15 min, followed by 10 cycles for 20 s at 95°C, 60 s at initially 65°C, decreasing by 1°C per cycle, finally by 30 cycles for 10 s at 95°C and 60 s at 57°C. The components required for the KASP reaction were added to a 1,536-well plate. Two fluorescence, namely, FAM and HEX, were selected for the PCR reaction in the CFX Connect™ Real-Time System and the terminal fluorescence signal was read after the reaction.

Real-Time Quantitative PCR Analysis

The rind of the parents had been collected for real-time quantitative PCR (RT-qPCR) from the immature fruits of melon at 15 days after pollination, when there were phenotypic differences between parents. For each parent, the rind samples from three individual plants were used as one biological replicate, with a total of three biological replicates. The RT-qPCR was performed with the StepOne PCR System (Thermo Fisher Scientific, Waltham, MA, United States), and amplification was conducted using Maxima SYBR Green qPCR Master Mix (Thermo Fisher Scientific, Waltham, MA, United States) with 40 cycles of denaturation at 94°C for 30 s, annealing at 60°C for 30 s, and extension at 72°C for 30 s. The amplification specificity was tested by a dissociation curve (65–90°C) to compare the results from different reactions and samples. The primers are shown in **Supplementary Table 2**. The expression levels of genes were normalized to the value for *Actin* (*MELO3C008032*). At least three independent biological and technical replicates were tested per sample. The primer efficiencies were estimated with a dilution series, and the relative gene expression levels were determined by $2^{-\Delta\Delta Ct}$ formula (Livak and Schmittgen, 2001).

Statistical Analysis

The mean values and SD of pigment contents and the expression levels of the related genes were calculated based on three independent biological replicates. Significant differences ($p < 0.05$) were statistically determined by Student's *t*-test and Duncan's method performed on SPSS version 20.0 software (IBM, Chicago, IL, United States).

RESULTS

Phenotypic Characterization of the Melon Rind

The phenotypic analyses showed significant differences in rind pattern between the two parental lines. Compared with the light green and non-mottled (uniform) rind of MG (P_2, **Figure 1A**), SC (P_1, **Figure 1B**) showed mottled with spots on the dark green rind at the immature fruit stage (visible approximately 10–15 dap). The spots were distributed longitudinally and stable even after fruit ripening.

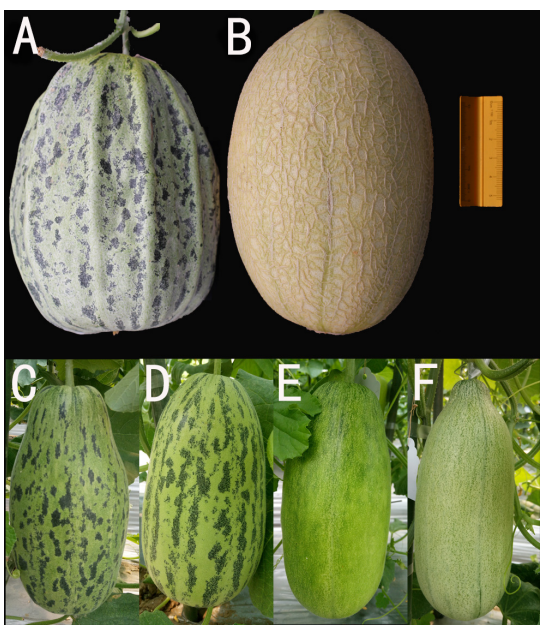


FIGURE 1 | Mature melon fruits of the parents and immature melon fruits of F_1 and F_2 individuals. **(A)** SC, the maternal parent with mottled rind (35 dap). **(B)** MG, the paternal parent with non-mottled rind (40 dap). **(C)** F_1 hybrid from SC × MG. **(D–F)** F_2 individuals with the typical phenotype (15 dap).

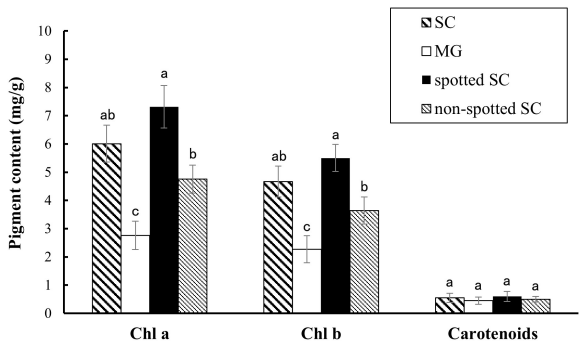


FIGURE 2 | Pigment contents analysis. Contents of chlorophyll and carotenoids in the 15-dap peels of two parental lines, SC and MG. All data are shown as mean ± SD of three replicates. Different letters indicate significant difference (Duncan's multiple range test, $p < 0.05$). Spotted SC, spotted part of SC peel; non-spotted SC, non-spotted part of SC peel; Chl *a*, chlorophyll *a*; Chl *b*, chlorophyll *b*.

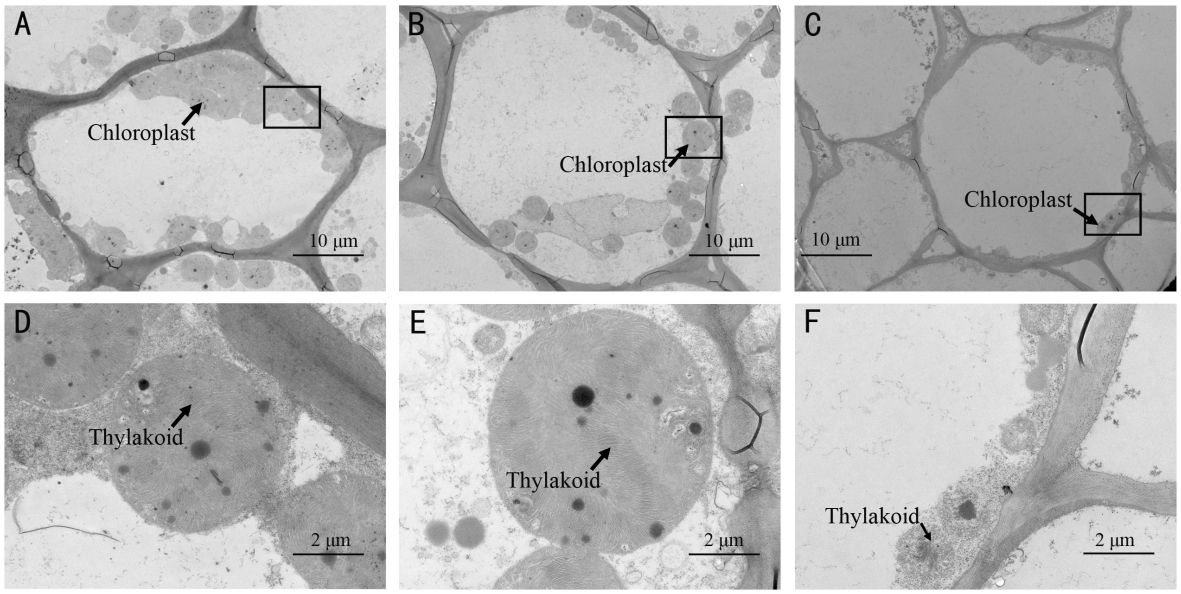


FIGURE 3 | Transmission electron microscopy (TEM) observation of chloroplasts in the spotted peels of SC **(A,D)** and non-spotted peels of SC **(B,E)**, and MG **(C,F)**. **(D–F)** Magnified views of the boxed regions in **(A–C)**, respectively.

Pigment content measurement showed that the rind of SC had a higher chlorophyll content, including Chl *a* and Chl *b*, than that of MG. The level of carotenoids was similar between the two parental lines (**Figure 2**). In addition, the spotted part of SC had a higher chlorophyll content than the non-spotted part, while no difference was found in carotenoid contents between the spotted and non-spotted part of SC.

Furthermore, TEM observations showed that there were more chloroplasts in the rind cells of the spotted part of SC than that in MG or non-spotted part of SC (**Figures 3A–C** and **Supplementary Table 3**). There was no evident difference in the chloroplast numbers of the rind cells between the non-spotted part of SC and MG, while the chloroplast was much bigger in SC than that in MG (**Figures 3D–F** and **Supplementary Table 3**). Meanwhile, a much more tightly stacking lamella structure of chloroplast was obviously observed in the rind cells of SC than MG. Consequently, the mottled rind of melon was due to the abnormal development of chloroplast number and the chlorophyll accumulation during the fruit development. And the developmental state of thylakoid structure in chloroplasts might be the reason for the difference of immature rind color between the two parental lines.

TABLE 1 | Inheritance of the mottled rind in melon.

Crosses	Generation	Mottled	Non-mottled	Expected ratio (M:N)	Chi-square	p^a
SC	P_1	10	0			
MG	P_2	0	10			
SC × MG	F_1	20	0			
MG × SC	F'_1	19	0			
(SC × MG) × MG	BC_1P_2	39	132	1:3	0.439	0.508
(SC × MG)⊗	F_2	318	235	9:7	0.354	0.552

M, mottled; N, non-mottled.
Phenotypic observations for the fruit rind were at 10–15 days after pollination (dap).
[a]Segregation ratios are statistically consistent with the expected ratios (χ^2 test, $p < 0.05$).

Genetic Analysis of Mottled Rind in Melon

To investigate the genetic inheritance of mottled rind in melon, reciprocal crosses between SC and MG were performed. The resulting F_1 or F'_1 plants exhibited the dark green and mottled rind (**Figure 1C**), similar to the parent, SC. In the F_2 population, the segregation ratio was 9:7 (mottled/non-mottled ratio of 318:235, $\chi^2 = 0.354$) (**Table 1**). Among the BC_1P_2 population (171 individuals), 39 showed the mottled rind, and 132 showed the non-mottled rind, corresponding to a segregation ratio of 1:3 by the Chi-square test. These results indicated that two dominant and epistatic genes, namely, *CmMt1* and *CmMt2*, were involved in the genetics of the mottled rind pattern in SC-MG melon. It could be concluded that mottled rind pattern of melon fruit was controlled by two dominant complementary genes, comparing with non-mottled rind. Consequently, SC should contain two dominant alleles, while MG should contain two recessive alleles. Coincidentally, we identified a 9:3:4 segregation ratio for dark green mottled, dark green non-mottled, and light green non-mottled traits by analyzing the above F_2 segregating population (**Figures 1D–F** and **Table 2**), indicating that the dominant allele of rind color gene is necessary for the development of the spots on the rind. Statistical evidence of deviation from the 1:1 expected segregation ratio was measured with a χ^2 goodness-of-fit test in another BC_1 segregating population derived from a cross between

TABLE 2 | Segregation ratio of rind patterns and immature rind color in the F_2 populations.

Crosses	Generation	Dark green		Light green		Expected ratio	Chi-square	*p*[a]
		Mottled	Non-mottled	Mottled	Non-mottled			
(SC × MG)⊗	F_2	318	102	0	133	9:3:4	0.381	0.944

[a]*Segregation ratios are statistically consistent with the expected ratios (χ^2 test, $p < 0.05$).*

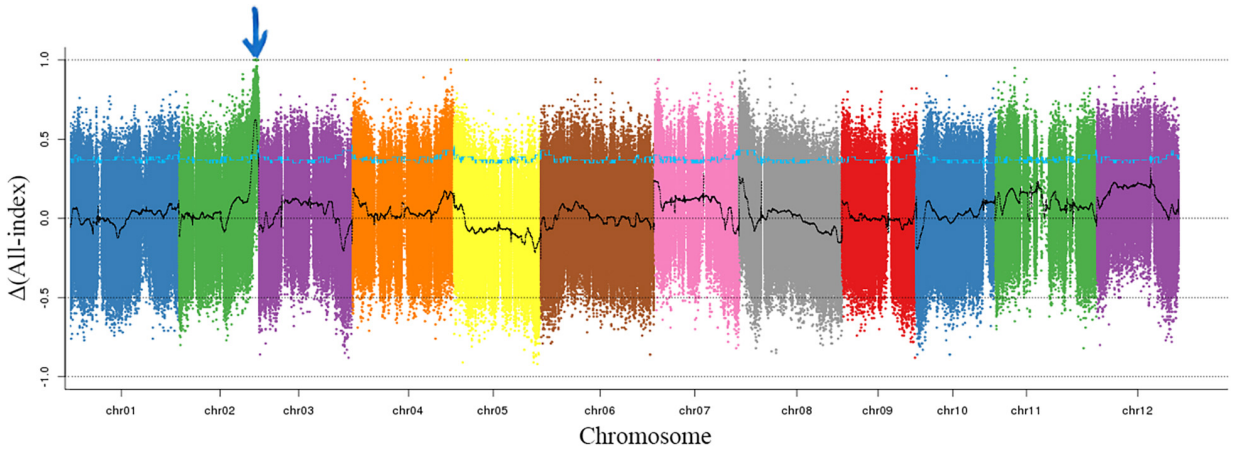


FIGURE 4 | Δ(All-index) graphs from BSA-seq. The Δ(all-index) was calculated at a 1-Mb intervals with a 50-kb sliding window. One candidate region was identified on chromosome 2 indicating with the blue arrow.

a dark green mottled rind line HPG and a dark green non-mottled rind line MR-5 (**Supplementary Figure 1**). And the segregation ratio fits a 1:1 ratio as determined by a Chi-square test ($\chi^2 = 0.281$, $p = 0.596$) (**Supplementary Table 4**), which further proved the abovementioned conclusions.

Previous studies have confirmed that *CmAPRR2* was the key gene controlling rind color in immature fruit rind, and the causative variants at the *CmAPRR2* alleles were found in the parental lines based on next-generation sequencing of genomic DNA (Oren et al., 2019; Xu et al., 2021). Therefore, genotyping was performed in the F_2 segregating population with the developed KASP DNA marker ($CmAPRR2^{SNP(G/T)}$). The results further validated that all the mottled individuals had one or two copies of *CmAPRR2* from the female parent (SC) (**Supplementary Table 5**) and that the genotyping results were consistent with the phenotype. In summary, those results indicated that the *CmAPRR2* regulating young fruit rind color in melon was the candidate epistatic gene (*CmMt1*) to the mottled rind. However, it is also possible that *CmAPRR2* was only closely linked to the target epistatic gene (*CmMt1*) and the results need to be further confirmed.

Whole-Genome Resequencing-Bulked Segregant Analysis and Linkage Mapping of the *CmMt2* Locus

To exclude the influence of epistatic gene, only the individuals with dark green rind were used to map the *CmMt2*. For BSA-seq, 20 mottled (M-pool) and 20 non-mottled (N-pool) F_2 plants and two parental lines, such as SC and MG, were selected. In total, 13.6, 11.1, 16.9, and 14.6 GB of clean data were generated for M-pool, N-pool, SC, and MG, representing approximately 28-, 23-, 37-, and 30-fold genome coverage, respectively, based on the estimated genome size of 417 Mb. The clean reads of each sample were mapped to the reference genome of the DHL92 (version 4.0). After filtering, a total of 3,002,120 SNPs and 671,480 Indels, which were distributed merely on 12 chromosomes, were identified between the M-pool and the N-pool. To identify the causal region, the Δ(SNP-index) and Δ(Indel-index) of each position were calculated for sliding window analysis, and the results showed that the Δ(All-index) values were approximately 0.5 for most parts of the genome. A single 2.0-Mb genomic region on chromosome 2 was identified as the candidate region for mottled rind trait at a 95% significant level (**Figure 4**).

To precisely narrow down the candidate region, the resequencing data of SC and MG were analyzed to identify polymorphisms for the 2.0-Mb region between the two parental lines and develop KASP markers. Ten validated KASP markers were genotyped in 135 individuals with dark green rind, which was randomly selected from the F_2 population. The initial linkage map was constructed using QTL IciMapping version 4.2, and the order of the markers in the map is consistent with that in the physical map. The results showed that the *CmMt2* locus was localized within the 0.5 cM regions, co-segregating with CmSNP19 (**Figure 5A**). All the dark green rind individuals of the F_2 population were adopted to fine-map the *CmMt2* locus using flanking markers and eight newly developed markers. Consequently, the results delimited the *CmMt2* to a 40.6-kb region on chromosome 2 between the markers CmSNP18

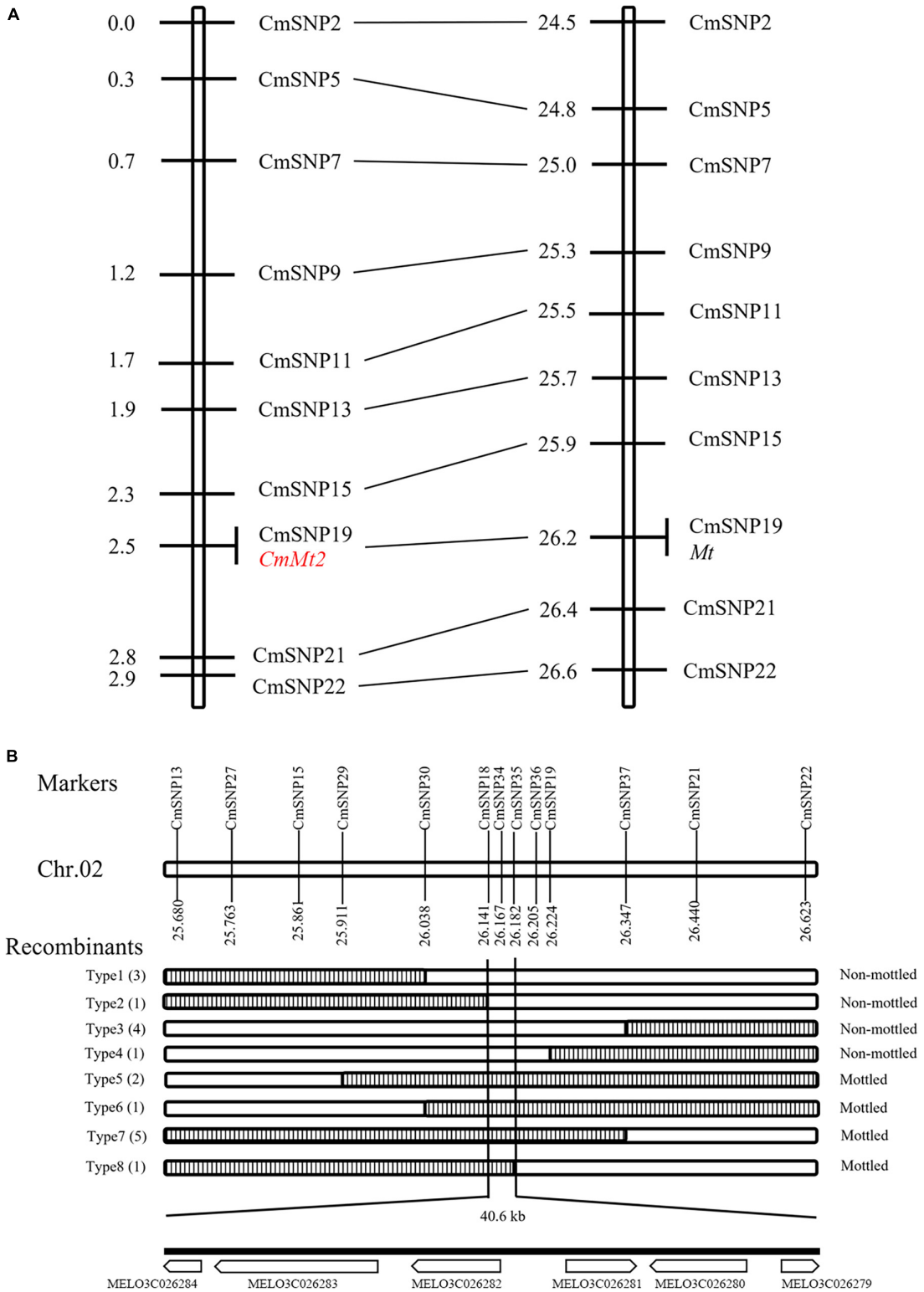


FIGURE 5 | Initial and fine mapping of the *CmMt2* gene in melon. **(A)** Initial mapping of *CmMt2*. Genetic map of *CmMt2* is on the left, with cM as the unit. The corresponding physical map (right, unit: Mb) is also shown. **(B)** Fine mapping of *CmMt2*. The *CmMt2* gene was delimited to an interval between CmSNP18 and CmSNP35, with an estimated length of 40.6 kb, and six genes were annotated in this region based on the reference genome sequence. The genetic structure of each recombinant type is depicted as white for homozygous non-mottled rind and striped for heterozygous mottled alleles. The number of each recombinant type is indicated in bracket.

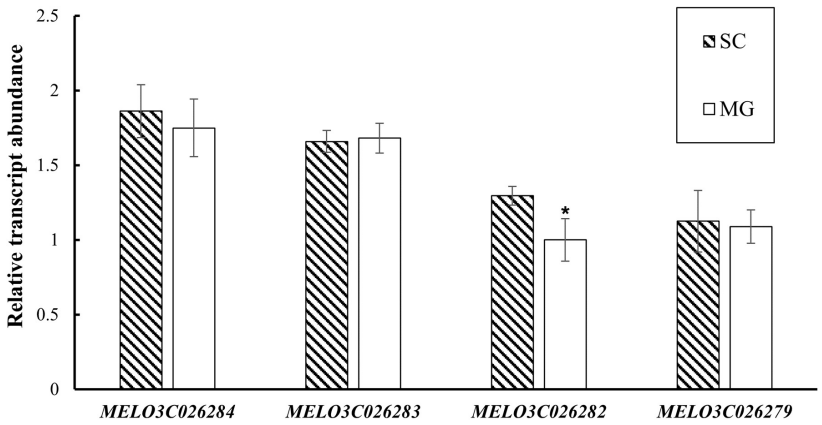


FIGURE 6 | Expression evaluation of *MELO3C026284*, *MELO3C026283*, *MELO3C026282*, and *MELO3C026279* by qRT-PCR. The values are shown as mean ± SD of three biological and three technical replicates. *Significant differences (*t*-test, $p < 0.05$).

and CmSNP35, each with one recombinant (type 2 and type 8) (**Figure 5B**).

Candidate Gene Analysis

Based on the fine-mapping results of *CmMt2*, the DNA sequences in the abovementioned 40.6 kb interval were analyzed according to the "DHL92" melon genome (version 4.0). As a result, six predicted genes were identified in the mapping region (**Supplementary Table 6**). To pinpoint the candidate gene of *CmMt2*, the resequencing data of SC, MG, and the two BSA pools were analyzed by alignment. In total, 231 SNPs and 52 Indel were detected in the region corresponding to the reference genome. Among them, 266 mutation sites were in the intergenic region or intron region, and 17 were located in protein-coding gene regions, which were the sites of our concerns. For the 16 SNPs and 1 Indel, 5 SNPs caused a synonymous variant, while the other 12 variations caused a non-synonymous mutation between the two parents, indicating that these SNPs or Indel might be the causative sites for the mottled rind. These 12 variation sites were distributed in four genes, including *MELO3C026284*, *MELO3C026283*, *MELO3C026282*, and *MELO3C026279*. qRT-PCR was performed on 15 dap rinds of SC and MG plants to determine the candidate gene. The results revealed that the *MELO3C026282* was highly expressed in the mottled rind parent (SC) than in the non-mottled rind parent (MG), while the other three genes (i.e., *MELO3C026284*, *MELO3C026283*, and *MELO3C026279*) exhibited a similar transcript level between the two parents (**Figure 6**). Besides, *MELO3C026282* was predicted to encode a Sec14p-like phosphatidylinositol transfer family protein, homolog to *AtCPSFL1*, which is essential for chloroplast development (Pan et al., 2013). Taken together, our results indicated that *MELO3C026282* gene was the most likely candidate gene for *CmMt2*.

In the "DHL92" genome, *MELO3C026282* was 4,345 bp in length with 8 exons and encoded a protein of 261 amino acids. To characterize the sequence of the candidate gene in the parental lines, the coding sequences of *MELO3C026282* were amplified. The CDS of *MELO3C026282* in the parental lines was 786 bp in length. Sequence alignment between the parental lines revealed that there were five SNPs in the exon, including three base substitutions resulting in synonymous mutations and two base substitutions resulting in non-synonymous mutations. Conserved domain analysis in EMBL-EBI showed that the MELO3C026282 contained an N-terminal CRAL_TRIO domain and a C-terminal CRAL_TRIO domain with the chloroplast targeting sequences at the beginning. The two non-synonymous mutations leading amino acid substitution were in the N-terminal CRAL_TRIO domain, which may cause a loss of the conserved domain and ultimately lose the function of the CmMt2 protein.

DISCUSSION

Rind pattern is an important appearance quality of fruits, which is contributing to their commercial value (Liu G. et al., 2020). Therefore, the identification of genes or closely linked markers would be of great value for breeding, especially for fruits of horticultural crops (Sanseverino et al., 2015; Zhao et al., 2019). Previous studies showed that the spots on the melon fruit are a dominant trait controlled by a single gene (Liu et al., 2016; Lv et al., 2018; Pereira et al., 2018), whereas the mapping results are quite different and localized on chromosomes 2 and 4, respectively. We found that the mottled rind (spots on the rind) was controlled by two dominant genes (i.e., *CmMt1* and *CmMt2*) with epistatic effects and that two candidate genes were located close to previous reports. Due to the different parental materials, the conclusions are inconsistent. Here, we extended the genetic model of mottled rind and showed evidence of epistasis, which may explain the genetically diverse progenies in rind pattern crossing from the parents without spots on the rind (Li et al., 2019). Considering that the population was constructed with an inter-subspecific hybrid, our results reveal more genetic variation information about mottled rind in melon.

Coincidentally, the segregation ratio of rind traits showed that the rind color of immature fruit was an epistatic to the mottled

rind, which is regulated by *CmAPRR2* (Oren et al., 2019; Xu et al., 2021). In addition, the genotyping results of *CmAPRR2* confirmed the results of phenotypic segregation. Previous reports indicated that the orthologous genes of *CmAPRR2* in cucumber (*Cucumis sativus* L.) (Liu et al., 2016), watermelon [*Citrullus lanatus* (Thunb.) Matsum. & Nakai] (Oren et al., 2019), pepper (*Capsicum annuum* L.), and tomato (*Solanum lycopersicum*) (Pan et al., 2013) have been proven to have similar functions controlling the chlorophyll accumulation on fruit rind. Compared with non-mottled rind, the number of chloroplasts and the chlorophyll content in the mottled rind were much higher. Thus, we suspected that *CmAPRR2* was the candidate gene for *CmMt1*. Based on the phenotype of the F_2 individuals with a dark green rind, the *CmMt2* controlling mottled melon rind was mapped to an interval of 40.6 kb on chromosome 2 using BSA and KASP analysis. Further, according to the qRT-PCR results, the expression level of *MELO3C026282* in MG with non-mottled rind was significantly lower than that in SC with mottled rind. Therefore, *MELO3C026282* was the most likely candidate gene for *CmMt2*, which codes a Sec14p-like phosphatidylinositol transfer family protein playing a significant role in chloroplast development (Hertle et al., 2020). Studies in tomato and cucumber have confirmed that *APRR2* has the activity of transcription factors, closer with *GLK2-like* and *MYB* transcription factors family (Jiao et al., 2017). In monkeyflowers (*Mimulus*), an *R2R3-MYB* activator and an *R3-MYB* repressor produce spotted pigment patterning in flowers (Ding et al., 2020). Whether there is a similar system in melon needs to be further studied. And there were two SNPs in *MELO3C026282* coding sequences between the parental lines. The mechanism by which SNP affects the differential expression of *MELO3C026282* in the rind requires further investigation.

In addition, the mottled fruit is a common phenomenon in horticultural crops (Zhai et al., 2019), including pear (*Pyrus bretschneideri*), tomato, and apple (*Malus pumila*); however, the mechanism responsible for this uneven distribution of pigments remains largely unknown (Ding et al., 2020). In tomato, *TAGL1* was cloned, which regulated diversified chloroplast development and pigment accumulation (Hertle et al., 2020). Our study validated the mottled rind of melon was mainly caused by the difference in chloroplast development and chlorophyll accumulation. In summary, we assumed that *CmMt1* regulated the accumulation of chlorophyll and *CmMt2* might be involved in the development of chloroplast number, which cooperated to control the formation of mottled rind in melon.

CONCLUSION

We reported that mottled rind in melon is controlled by two dominant genes with epistatic effects. The epistatic gene *CmMt1* was co-segregated with *CmAPRR2* controlling the pigment accumulation in immature melon fruit, which suggested that *CmAPRR2* was the candidate gene for *CmMt1*. Furthermore, the *CmMt2* locus was mapped between 24.53 and 26.57 Mb on chromosome 2 and fine-mapped in an interval of 40.6 kb with KASP analysis. The candidate gene *MELO3C026282* for *CmMt2* within the interval that is involved in the mottled rind formation was predicted through functional annotation, expression analysis, and sequence variation analyses. Our study provides insight into the molecular mechanism underlying rind appearance and reveals valuable information for marker-assisted selection breeding in melon.

DATA AVAILABILITY STATEMENT

The datasets presented in this study can be found in online repositories. The names of the repository/repositories and accession number(s) can be found below: https://www.ncbi.nlm.nih.gov/genbank/, PRJNA759737.

AUTHOR CONTRIBUTIONS

JS conceived and designed the study. XX performed the analyses. XN and YZ prepared the melon samples. JS, XX, and WS wrote the manuscript. All authors checked and approved the final version.

FUNDING

This study was funded by the Major Science and Technology Project of Plant Breeding in Zhejiang Province (Grant Number 2021C02065) and the Natural Science Foundation of Zhejiang Province (Grant Number LY20C150005).

ACKNOWLEDGMENTS

The authors thank Sujuan Li for technical help with the KASP experiment and Jiajing Chen for technical help with phenotypic data collection.

SUPPLEMENTARY MATERIAL

The Supplementary Material for this article can be found online at: https://www.frontiersin.org/articles/10.3389/fpls.2021.769989/full#supplementary-material

REFERENCES

Castanera, R., Ruggieri, V., Pujol, M., Garcia-Mas, J., and Casacuberta, J. M. (2019). An improved melon reference genome with single-molecule sequencing uncovers a recent burst of transposable elements with potential impact on genes. *Front. Plant Sci.* 10:1815. doi: 10.3389/fpls.2019.01815

Danin-Poleg, Y., Tadmor, Y., Tzuri, G., Reis, N., Hirschberg, J., and Katzir, N. (2002). Construction of a genetic map of melon with molecular markers and

horticultural traits, and localization of genes associated with ZYMV resistance. *Euphytica* 125, 373–384. doi: 10.1023/a:1016021926815

Ding, B., Patterson, E. L., Holalu, S. V., Li, J., Johnson, G. A., Stanley, L. E., et al. (2020). Two MYB proteins in a self-organizing activator-inhibitor system produce spotted pigmentation patterns. *Curr. Biol.* 30, 802–814. doi: 10.1016/j.cub.2019.12.067

Feder, A., Burger, J., Gao, S., Lewinsohn, E., Katzir, N., Schaffer, A. A., et al. (2015). A Kelch domain-containing F-Box coding gene negatively regulates flavonoid accumulation in muskmelon. *Plant Physiol.* 169, 1714–1726. doi: 10.1104/pp.15.01008

Ganesan, J. (1988). *Genetic Studies on Certain Characters of Economic Importance in Muskmelon (Cucumis melo L.)*. Chidambaram: Annamalai University.

Garcia-Mas, J., Benjak, A., Sanseverino, W., Bourgeois, M., Mir, G., Gonzalez, V. M., et al. (2012). The genome of melon (*Cucumis melo* L.). *Proc. Natl. Acad. Sci. U.S.A.* 109, 11872–11877. doi: 10.1073/pnas.1205415109

Hertle, A. P., Garcia-Cerdan, J. G., Armbruster, U., Shih, R., Lee, J. J., Wong, W., et al. (2020). A Sec14 domain protein is required for photoautotrophic growth and chloroplast vesicle formation in *Arabidopsis thaliana*. *Proc. Natl. Acad. Sci. U.S.A.* 117, 9101–9111. doi: 10.1073/pnas.1916946117

Jeffrey, C. (1980). A review of the *Cucurbitaceae*. *Bot. J. Linn. Soc.* 81, 233–247. doi: 10.1111/j.1095-8339.1980.tb01676.x

Jiao, J., Liu, H., Liu, J., Cui, M., Xu, J., Meng, H., et al. (2017). Identification and functional characterization of APRR2 controlling green immature fruit color in cucumber (*Cucumis sativus* L.). *Plant Growth Regul.* 83, 233–243. doi: 10.1007/s10725-017-0304-1

Klein, H., Xiao, Y., Conklin, P. A., Govindarajulu, R., Kelly, J. A., Scanlon, M. J., et al. (2018). Bulked-segregant analysis coupled to whole genome sequencing (BSA-Seq) for rapid gene cloning in maize. *G3 (Bethesda)* 8, 3583–3592. doi: 10.1534/g3.118.200499

Li, S., Ni, X., Xia, Q., Li, Y., Dong, X., Hou, J., et al. (2019). Rapid characterization of the genetic loci controlling commodity traits of Chinese Hami Melon (*Cucumis melo* var. Saccharinensis Naud.) through multiplexed shotgun genotyping. *Agronomy* 9:430. doi: 10.3390/agronomy9080430

Liu, G., Li, C., Yu, H., Tao, P., Yuan, L., Ye, J., et al. (2020). GREEN STRIPE, encoding methylated TOMATO AGAMOUS-LIKE 1, regulates chloroplast development and Chl synthesis in fruit. *New Phytol.* 228, 302–317. doi: 10.1111/nph.16705

Liu, H., Jiao, J., Liang, X., Liu, J., Meng, H., Chen, S., et al. (2016). Map-based cloning, identification and characterization of the w gene controlling white immature fruit color in cucumber (*Cucumis sativus* L.). *Theor. Appl. Genet.* 129, 1247–1256. doi: 10.1007/s00122-016-2700-8

Liu, L., Sun, T., Liu, X., Guo, Y., Huang, X., Gao, P., et al. (2019). Genetic analysis and mapping of a striped rind gene (st3) in melon (*Cucumis melo* L.). *Euphytica* 215:20. doi: 10.1007/s10681-019-2353-1

Liu, S., Gao, P., Zhu, Q., Zhu, Z., Liu, H., Wang, X., et al. (2020). Resequencing of 297 melon accessions reveals the genomic history of improvement and loci related to fruit traits in melon. *Plant Biotechnol. J.* 18, 2545–2558. doi: 10.1111/pbi.13434

Livak, K. J., and Schmittgen, T. D. (2001). Analysis of relative gene expression data using real-time quantitative PCR and the $2^{-\Delta\Delta Ct}$ method. *Methods* 25, 402–408. doi: 10.1006/meth.2001.1262

Lv, J., Fu, Q., Lai, Y., Zhou, M., and Wang, H. (2018). Inheritance and gene mapping of spotted to non-spotted trait gene CmSp-1 in melon (*Cucumis melo* L. var. chinensis Pangalo). *Mol. Breed.* 38:105. doi: 10.1007/s11032-018-0860-8

Meng, L., Li, H., Zhang, L., and Wang, J. (2015). QTL IciMapping: integrated software for genetic linkage map construction and quantitative trait locus mapping in biparental populations. *Crop J.* 3, 269–283. doi: 10.1016/j.cj.2015.01.001

Murray, M. G., and Thompson, W. F. (1980). Rapid isolation of high molecular weight plant DNA. *Nucleic Acids Res.* 8, 4321–4325. doi: 10.1093/nar/8.19.4321

Oren, E., Tzuri, G., Vexler, L., Dafna, A., Meir, A., Faigenboim, A., et al. (2019). The multi-allelic APRR2 gene is associated with fruit pigment accumulation in melon and watermelon. *J. Exp. Bot.* 70, 3781–3794. doi: 10.1093/jxb/erz182

Pan, Y., Bradley, G., Pyke, K., Ball, G., Lu, C., Fray, R., et al. (2013). Network inference analysis identifies an APRR2-like gene linked to pigment accumulation in tomato and pepper fruits. *Plant Physiol.* 161, 1476–1485. doi: 10.1104/pp.112.212654

Pereira, L., Ruggieri, V., Pérez, S., Alexiou, K. G., Fernández, M., Jahrmann, T., et al. (2018). QTL mapping of melon fruit quality traits using a high-density GBS-based genetic map. *BMC Plant Biol.* 18:324. doi: 10.1186/s12870-018-1537-5

Perin, C., Hagen, S., De Conto, V., Katzir, N., Danin-Poleg, Y., Portnoy, V., et al. (2002). A reference map of *Cucumis melo* based on two recombinant inbred line populations. *Theor. Appl. Genet.* 104, 1017–1034. doi: 10.1007/s00122-002-0864-x

Pitrat, M. (2008). "Melon," in *Vegetables*, eds J. Prohens and F. Nuez (New York, NY: Springer), 283–315. doi: 10.1007/978-0-387-30443-4_9

Pitrat, M. (2016). "Melon genetic resources: phenotypic diversity and horticultural taxonomy: genetics and genomics of *Cucurbitaceae*," in *Plant Genetics and Genomics: Crops and Models*, eds R. Grumet, N. Katzir, and J. Garcia-Mas (Cham: Springer), 25–60.

Sanseverino, W., Henaff, E., Vives, C., Pinosio, S., Burgos-Paz, W., Morgante, M., et al. (2015). Transposon insertions, structural variations, and SNPs contribute to the evolution of the melon genome. *Mol. Biol. Evol.* 32, 2760–2774. doi: 10.1093/molbev/msv152

Tadmor, Y., Burger, J., Yaakov, I., Feder, A., Libhaber, S. E., Portnoy, V., et al. (2010). Genetics of flavonoid, carotenoid, and chlorophyll pigments in melon fruit rinds. *J. Agric. Food Chem.* 58, 10722–10728. doi: 10.1021/jf1021797

Xu, X., Shen, J., Zhang, Y., Li, G., Niu, X., and Shou, W. (2021). Fine mapping of an immature rind color gene GR in melon. *Sci. Agric. Sin.* 54, 3308–3319. doi: 10.3864/j.issn.0578-1752.2021.15.014

Yang, S., Yu, W., Wei, X., Wang, Z., Zhao, Y., Zhao, X., et al. (2020). An extended KASP-SNP resource for molecular breeding in Chinese cabbage (*Brassica rapa* L. ssp. pekinensis). *PLoS One* 15:e0240042. doi: 10.1371/journal.pone.0240042

Zhai, R., Wang, Z., Yang, C., Lin-Wang, K., Espley, R., Liu, J., et al. (2019). PbGA2ox8 induces vascular-related anthocyanin accumulation and contributes to red stripe formation on pear fruit. *Hortic. Res.* 6:137. doi: 10.1038/s41438-019-0220-9

Zhao, G., Lian, Q., Zhang, Z., Fu, Q., He, Y., Ma, S., et al. (2019). A comprehensive genome variation map of melon identifies multiple domestication events and loci influencing agronomic traits. *Nat. Genet.* 51, 1607–1615. doi: 10.1038/s41588-019-0522-8

Conflict of Interest: The authors declare that the research was conducted in the absence of any commercial or financial relationships that could be construed as a potential conflict of interest.

Publisher's Note: All claims expressed in this article are solely those of the authors and do not necessarily represent those of their affiliated organizations, or those of the publisher, the editors and the reviewers. Any product that may be evaluated in this article, or claim that may be made by its manufacturer, is not guaranteed or endorsed by the publisher.

Copyright © 2021 Shen, Xu, Zhang, Niu and Shou. This is an open-access article distributed under the terms of the Creative Commons Attribution License (CC BY). The use, distribution or reproduction in other forums is permitted, provided the original author(s) and the copyright owner(s) are credited and that the original publication in this journal is cited, in accordance with accepted academic practice. No use, distribution or reproduction is permitted which does not comply with these terms.

frontiers in Plant Science

ORIGINAL RESEARCH
published: 25 November 2021
doi: 10.3389/fpls.2021.751853

Genome-Wide Identification and Expression Analysis of Terpene Synthase Genes in *Cymbidium faberi*

Qian-Qian Wang[1], Meng-Jia Zhu[2], Xia Yu[1], Yuan-Yang Bi[1], Zhuang Zhou[1,3], Ming-Kun Chen[1], Jiating Chen[1], Diyang Zhang[1], Ye Ai[1], Zhong-Jian Liu[1,3,4] and Siren Lan[1,2]**

[1]Key Laboratory of National Forestry and Grassland Administration for Orchid Conservation and Utilization at College of Landscape Architecture, Fujian Agriculture and Forestry University, Fuzhou, China, [2]College of Forestry, Fujian Agriculture and Forestry University, Fuzhou, China, [3]Zhejiang Institute of Subtropical Crops, Zhejiang Academy of Agricultural Sciences, Wenzhou, China, [4]Institute of Vegetable and Flowers, Shandong Academy of Agricultural Sciences, Jinan, China

OPEN ACCESS

Edited by:
Xinchao Wang,
Tea Research Institute,
Chinese Academy of Agricultural Sciences (CAAS), China

Reviewed by:
Xinlu Chen,
The University of Tennessee, Knoxville, United States
Mingle Wang,
Huazhong Agricultural University, China

***Correspondence:**
Zhong-Jian Liu
zjliu@fafu.edu.cn
Siren Lan
lkzx@fafu.edu.cn

Specialty section:
This article was submitted to Crop and Product Physiology, a section of the journal Frontiers in Plant Science

Received: *02 August 2021*
Accepted: *01 November 2021*
Published: *25 November 2021*

Citation:
Wang Q-Q, Zhu M-J, Yu X, Bi Y-Y, Zhou Z, Chen M-K, Chen J, Zhang D, Ai Y, Liu Z-J and Lan S (2021) Genome-Wide Identification and Expression Analysis of Terpene Synthase Genes in Cymbidium faberi. Front. Plant Sci. 12:751853. doi: 10.3389/fpls.2021.751853

Terpene synthases (TPSs) are essential for forming terpenes, which play numerous functional roles in attracting pollinators, defending plants, and moderating the interaction between plants. TPSs have been reported in some orchids, but genome-wide identification of terpenes in *Cymbidium faberi* is still lacking. In this study, 32 putative TPS genes were classified in *C. faberi* and divided into three subfamilies (TPS-a, TPS-b, and TPS-e/f). Motif and gene structure analysis revealed that most *CfTPS* genes had the conserved aspartate-rich DDxxD motif. TPS genes in the TPS-a and TPS-b subfamilies had variations in the RRX_8W motif. Most *cis*-elements of *CfTPS* genes were found in the phytohormone responsiveness category, and MYC contained most of the numbers associated with MeJA responsiveness. The *Ka*/*Ks* ratios of 12/13 *CfTPS* gene pairs were less than one, indicated that most *CfTPS* genes have undergone negative selection. The tissue-specific expression patterns showed that 28 genes were expressed in at least one tissue in *C. faberi*, and TPS genes were most highly expressed in flowers, followed by leaves and pseudobulbs. In addition, four *CfTPS* genes were selected for the real-time reverse transcription quantitative PCR (RT-qPCR) experiment. The results revealed that *CfTPS12*, *CfTPS18*, *CfTPS23*, and *CfTPS28* were mainly expressed in the full flowering stage. *CfTPS18* could convert GPP to β-myrcene, geraniol, and α-pinene *in vitro*. These findings of *CfTPS* genes of *C. faberi* may provide valuable information for further studies on TPSs in orchids.

Keywords: terpenes, terpene synthase, orchids, floral scent, expression analysis, *Cymbidium*

INTRODUCTION

Terpenes, which contain isoprene (C5), monoterpenes (C10), sesquiterpenes (C15), and diterpenes (C20), constitute the most prominent family of volatile components in plants (Nagegowda, 2010; Tholl, 2015). They play significant roles in attracting pollinators, defending plants against herbivores and pathogens, and moderating the interaction between plants (Wagner and Elmadfa, 2003; Dudareva et al., 2006). Terpenoids are dominant compounds in orchid floral scents (Ramya et al., 2018). For example, sesquiterpenes are the major floral scent compounds in *Cymbidium goeringii* (Ramya et al., 2019). The monoterpenes linalool, ocimene, and linalool

oxide are the major scent components of *Vanda* Mini Palmer flowers (Mohd-Hairul et al., 2010). The floral scent in orchids is closely related to flower development stages and is vital for pollination ecology (Ramya et al., 2018).

Isopentenyl diphosphate (IPP) and dimethylallyl diphosphate (DMAPP) are precursors of terpene formation, and they are generated by cytosolic mevalonate acid (MVA) and the plastid methylerythritol phosphate (MEP) pathways (Dudareva et al., 2006). A plastid prenyltransferase synthesizes geranyl diphosphate (GPP), and the second type of plastid prenyltransferase produces geranylgeranyl diphosphate (GGPP) from the condensation of IPP and DMAPP. The condensation of DMAPP and IPP forms farnesyl diphosphate (FPP) in the cytosol (**Figure 1**). Plants have terpene synthases (TPSs) that catalyze monoterpene formation, sesquiterpene formation, and diterpene formation from GPP, FPP, and GGPP, respectively (Pichersky et al., 2006; Vranová et al., 2013).

Most full-length TPSs contain two conserved domains defined in PFAM: PF01397 (N-terminal) containing a conserved RRX_8W motif and PF03936 (C-terminal) containing a DDxxD motif and NSE/DTE motif (El-Gebali et al., 2019; Jiang et al., 2019). In addition, TPSs can be divided into seven major categories: TPS-a, TPS-b, TPS-c, TPS-d, TPS-e/f, TPS-g, and TPS-h (Chen et al., 2011). TPS-a, TPS-b, and TPS-g categories are angiosperm-specific. The TPS-a category can encode sesquiterpene synthases of these three categories and can be further classified into monocot-specific TPS-a-1 and dicot-specific TPS-a-2 groups. In recent reports, all characterized TPSs in TPS-b with RRX_8W motifs are monoterpene synthases. The TPS-g category can encode monoterpene synthases without the RRX_8W motif. In addition, TPS-d is a gymnosperm-specific category that encodes monoterpenes, sesquiterpenes, and diterpenes. TPS-e/f can encode kaurene or copalyl diphosphate synthases that function in gibberellic acid synthesis in vascular plants. TPS-c may represent the ancestral category, and TPS-h only appears in *Selaginella moellendorffii* in recent reports (Chen et al., 2011; Li et al., 2012).

Genome-wide TPS families have been identified in *Arabidopsis thaliana*, *Vitis vinifera*, *Malus domestica*, *Camellia sinensis*, *Glycine max*, *Daucus carota*, and *Dendrobium. officinale* (Aubourg et al., 2002; Martin et al., 2010; Nieuwenhuizen et al., 2013; Liu et al., 2014; Keilwagen et al., 2017; Yu et al., 2020; Zhou et al., 2020). Terpenoids are predominant components in orchid flower volatiles, but genome-wide TPS identification is limited in orchids (Ramya et al., 2018; Yu et al., 2020). Orchidaceae comprises five subfamilies, and in recent reports, a few TPS genes have been identified in *Apostasia shenzhenica* in Apostasioideae subfamily; *Vanilla planifolia* in Vanilloideae subfamily; and *Phalaenopsis equestris* and *Dendrobium catenatum* in Epidendroideae subfamily (Huang et al., 2021). However, genome-wide TPS genes identification in Orchidoideae was limited.

Cymbidium faberi is a plant of Orchidaceae with a long history of cultivation due to its characteristic flower fragrance and beautiful flower shape (Ramya et al., 2018). There are over 100 compounds in the *C. faberi* floral scent, and some terpenes have been identified in the blooming *C. faberi* flowers by headspace vapors (Omata et al., 1990). This study first analyzed the classification, phylogenetics, and expression patterns of TPS genes in *C. faberi*. Our results will provide valuable information for further studies on *C. faberi* and other orchids.

MATERIALS AND METHODS

Plant Materials

The wild *C. faberi* collected in this study were cultivated in the greenhouse at Forest Orchid Garden in Fujian Agriculture and Forestry University (Fuzhou, Fujian Province, China) under natural light and temperatures. The temperature was about 20–25°C. Flowers, leaves, and pseudobulbs of *C. faberi* were sampled at the flowering stage. The buds about 1 cm before anthesis, semi-open flowers about 3 cm, and fully open flowers were also used in this study. All samples of *C. faberi* were frozen in liquid nitrogen for storage at −80°C until use.

Identification of *CfTPS* Genes in the *C. faberi* Protein Database

Two domains – PF01397 representing the TPS N-terminal domain and PF03936 representing the TPS C-terminal domain from PFAM[1] – were used as queries to search the *C. faberi* protein database (El-Gebali et al., 2019). The *C. faberi* genome data will be published separately. An HMM search (built-in Tbtools) was used in this study with an e-value cut at 10^{-3}. To avoid missing potential TPS genes, TPS sequences from *A. thaliana* in the TAIR database[2] were also used to screen the *C. faberi* protein database using BLASTP (built-in Tbtools; Chen et al., 2018). The candidate TPS genes were checked manually by Pfam to verify putative full-length TPS genes, and TPS genes lacking either PF03936 or PF01397 were excluded. The grand average of hydrophobicity (GRAVY), molecular weight (Mw), isoelectric points (pI), aliphatic index (AI), and instability index (II) of the TPS proteins were predicted by the ExPASy database (Artimo et al., 2012).[3] Subcellular localization was predicted by Plant-mPloc (Chou and Shen, 2010),[4] AtSubP (Kaundal et al., 2010),[5] and Ploc-mPlant (Cheng et al., 2017).[6] Terzyme[7] and BLATP[8] were used to predict gene function (Priya et al., 2018).

Abbreviations: AI, Aliphatic index; bp, Base pair; DMAPP, Dimethylallyl diphosphate; FPP, Farnesyl diphosphate; FPKM, Fragments per kilobase of transcript per million fragments mapped; GGPP, Geranylgeranyl diphosphate; GPP, Geranyl diphosphate; GRAVY, Grand average of hydrophobicity; II, Instability index; IPP, Isopentenyl diphosphate; MeJA, Methyl jasmonate; MEP, Methylerythritol phosphate; Mw, Molecular weight; MVA, Mevalonate acid; NCBI, National Center for Biotechnology Information; NJ, Neighbor-joining; pI, Isoelectric point; RT-qPCR, Real-time reverse transcription quantitative PCR; TPS, Terpene synthase.

[1]http://pfam.xfam.org/
[2]https://www.arabidopsis.org/
[3]https://www.expasy.org/
[4]http://www.csbio.sjtu.edu.cn/bioinf/plant-multi/
[5]http://bioinfo3.noble.org/AtSubP/
[6]https://www.swmath.org/software/25191
[7]http://www.nipgr.ac.in/terzyme.html
[8]http://blast.ncbi.nlm.nih.gov

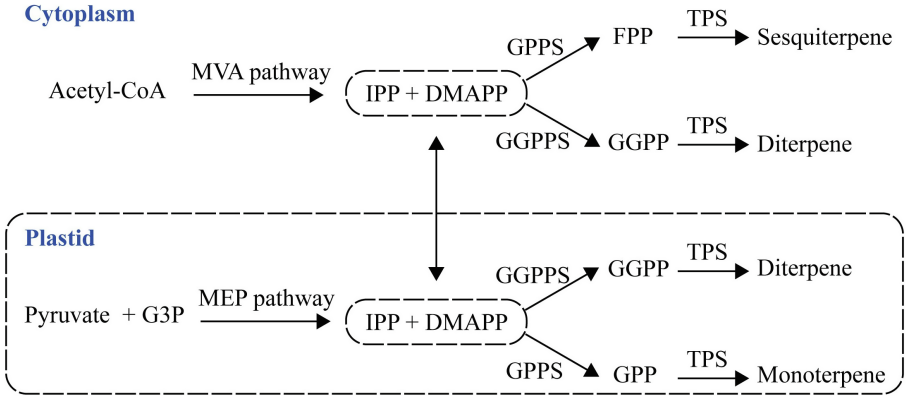


FIGURE 1 | The pathway of plant terpenes biosynthesis. Terpenes are synthesized from two precursors generated by the cytosolic mevalonate acid (MVA) and plastid methylerythritol phosphate (MEP) pathways. G3P, glyceraldehyde 3-phosphate; IPP, isopentenyl diphosphate; DMAPP, dimethylallyl diphosphate; GPP, geranyl diphosphate; GPPS, GPP synthase; FPP, farnesyl diphosphate; FPPS, FPP synthase; GGPP, geranylgeranyl diphosphate; GGPPS, GGPP synthase; and TPS, terpene synthase.

Motifs and Gene Structure Analysis

Conserved motifs in the *C. faberi* TPS sequences were employed and analyzed by MEME software[9] with default parameters (Bailey et al., 2009). We identified 20 motifs in this study. The exon-intron structure of the sequences was determined using GSDS software (Hu et al., 2015).[10]

Phylogenetic Analysis of TPS Genes

The transcriptomes of TPS sequences from *P. equestris* and *A. shenzhenica* were downloaded from their genome databases. TPS sequences from *S. moellendorffii* were downloaded from NCBI.[11] TPS sequences from *Picea abies* were downloaded from UniProt,[12] and TPS protein sequences from *A. thaliana* and *Oryza sativa* were downloaded from Phytozome.[13] All these sequences were aligned with MAFFT (Rozewicki et al., 2019). The maximum likelihood (ML) method was used for the phylogenetic tree, which was constructed with RAxML on the CIPRES Science Gateway web server (RAxML-HPC2 on XSEDE; Miller et al., 2011). Bootstrap values were 1,000 replicates with the JTT model. The most appropriate protein evolution model for the alignment was predicted by ProTest (Darriba et al., 2011). The generated tree was redrawn and annotated by EVOLVIEW (He et al., 2016).[14] The sequences of the *CfTPS* proteins used in this study are listed in **Supplementary Table S7**.

Promoter Element Analysis of TPS Genes

Tbtools software extracted the promoter sequences and 2,000 bp regions upstream of 32 *CfTPS* genes (Chen et al., 2018). Afterward, the online software PlantCARE[15] was used to identify the *cis*-active regulatory elements in the promoter regions of the *CfTPS* genes (Lescot et al., 2002).

Calculation of *Ka* and *Ks* Ratios

Gene pairs with similar genetic relationships were selected based on the phylogenetic tree. DNAMAN software was used to select the gene pairs with a consistency greater than 60%. Tbtools software was then used to calculate *Ka* (non-synonymous rate), *Ks* (synonymous substitution), and *Ka*/*Ks* (evolutionary constraint) values. Divergence time (T) was calculated by using the formula $T = Ks/(2 \times 9.1 \times 10^{-9}) \times 10^{-6}$ million years ago (Mya; Zhang et al., 2018). In general, $Ka/Ks < 1.0$ represents purifying or negative selection, $Ka/Ks = 1.0$ represents neutral selection, and $Ka/Ks > 1.0$ represents positive selection (Zhang et al., 2006).

Transcriptome Data and GO Classification Analysis

An RNA sequencing transcriptome database of leaves, pseudobulbs, petals, sepals, labellums, and gynostemium was established to study the expression patterns of *CfTPS* genes. Fragments per kilobase of transcript per million mapped reads (FPKM) values of *CfTPS* genes were used to evaluate translation abundance. DESeq was used to conduct gene differential expression analysis, and gene ontology (GO) classification analysis was performed based on the differentially expressed gene analysis. The heatmaps of *CfTPS* expression patterns were drawn by Tbtools software, and the color in the heatmap was expressed as the log2-transformed expression levels of each *CfTPS* gene (Chen et al., 2018).

Extraction of RNA and RT-qPCR Analysis

RNA was isolated from flowers of *C. faberi* at the flowering stage using the Biospin Plant Total RNA Extraction Kit (Bioer Technology, Hangzhou, China). First-strand DNA was synthesized with TransScript® All-in-One First-Strand cDNA Synthesis SuperMix for quantitative PCR (qPCR; TransGen Biotech, Beijing, China). TransScript® All-in-One First-Strand cDNA

[9]http://meme-suite.org/
[10]http://gsds.gao-lab.org/
[11]https://www.ncbi.nlm.nih.gov/genbank/
[12]https://www.UniProt.org/
[13]https://phytozome.jgi.doe.gov/
[14]https://evolgenius.info/
[15]http://bioinformatics.psb.ugent.be/webtools/plantcare/html/

Synthesis SuperMix for qPCR was also used to remove genomic DNA. The real-time reverse transcription quantitative PCR (RT-qPCR) primers of *CfTPS* were designed by Primer Premier 5 software and can be found in **Supplementary Table S12**. Primer specificity was confirmed using Primer-BLAST on the NCBI website.[16] PerfectStart™ Green qPCR SuperMix (TransGen Biotech, Beijing, China) was used for RT-qPCR analysis. The *C. faberi* reference gene GAPDH (GenBank Accession: JX560732; Tian et al., 2020) was used as the internal control and quantified by the $2^{-\triangle\triangle CT}$ method (Livak and Schmittgen, 2001). There were three biological replicates in the RT-qPCR analysis.

CfTPS18 Enzyme Assays

The ORF of *CfPS18* was synthesized and ligated into pET28a vector. Then, the recombinant plasmid was transformed into *Escherichia coli* BL21 (DE3) pLysS cells (Transgen, China). Primers are given in **Supplementary Table S12**. The positive clones were incubated with shaking at 200 rpm, 37°C until $OD_{600} = 0.6$, and then at 37°C for 3 h with shaking and 0.1 mM IPTG. Recombinant *CfTPS18* enzyme was induced at 16°C for 16 h with 0.1 mM IPTG. The precipitate was resuspended in extraction buffer [50 mM NaH_2PO_4, 500 mM NaCl, 10% (v/v) glycerol, and pH 7.0] and disrupted with a sonicator at 200 W for 60 s. The protein was purified with Ni-NTA agarose (Clontech). Purified *CfTPS18* protein was examined by SDS-PAGE using Tris-HCl buffer (pH 7.5). The recombinant protein was performed in assay buffer [25 mM HEPES, 10 mM $MgCl_2$, 100 mM KCl, 5 mM DTT, 10% (v/v) glycerol, and 30 μM GPP], and 30 μg of *CfTPS18* protein at pH 7.2 and 30°C for 1 h[24].

GC-MS Analysis

The volatiles were exposed to SPME fiber with 50/30 μm DVB/CAR/PDMS (divinylbenzene/carboxen/polydimethylsiloxane; Supelco Co., Bellefonte, PA, United States). The extract was analyzed using a gas chromatograph (Agilent 6,890 N) and mass spectrometer (Agilent 5975B, Santa Clara, CA, United States) outfitted with a silica capillary column (DB-5MS; 60 m × 0.25 mm × 0.25 μm). The temperature program was as follows: 55°C for 2 min, 3°C min^{-1} up to 80°C, 5°C min^{-1} up to 180°C, 10°C min^{-1} up to 230°C, and finally, 20°C min^{-1} to 250°C. The ion source temperature was 230°C, and the electron energy was 70 eV. The GC-MS interface zone temperature was 250°C, and the scan range was 50–500 m/z. Reactions only added with GPP were used as the blank control. There were three biological replicates for the experiment. The retention time was compared with the NIST Mass Spectral Library.

RESULTS

TPS Gene Identification and Protein Features in *C. faberi*

To retrieve the TPS genes in *C. faberi*, two domains, PF01397 and PF03936 in the PFAM, were used to search the *C. faberi* protein database (El-Gebali et al., 2019). BLASTP (built-in Tbtools) was also used to screen the *C. faberi* protein database (Chen et al., 2018). After removing artefacts, 32 TPS genes were obtained. The deduced proteins of these genes were in the range of 115 for *CfTPS1* and *CfTPS2* to 902 amino acids for *CfTPS12* and had predicted molecular weights (Mw) in the range of 10.24 for *CfTPS12* to 103.89 KDA for *CfTPS31*. The theoretical isoelectric point (pI) values were in the range of 4.86 for *CfTPS1* and *CfTPS2* to 9.28 for *CfTPS26*, and the deduced grand average of hydrophilic (GRAVY) values were in the range of −0.358 for *CfTPS26* to 0.073 for *CfTPS6*, suggesting that most *CfTPS* proteins were hydrophilic except for *CfTPS1*, *CfTPS2*, and *CfTPS6*. Additionally, the aliphatic index (AI) of *CfTPS*-deduced proteins was in the range of 87.09 for *CfTPS21* to 107.22 for *CfTPS6*, and the instability index (II) was in the range of 28.62 for *CfTPS1* and *CfTPS2* to 52.36 for *CfTPS5*. To retrieve information on the subcellular localization of *CfTPS* proteins, three predictors were used in this study: AtSubp, Plant-mPLoc, and pLoc-mPLant (Chou and Shen, 2010; Kaundal et al., 2010; Cheng et al., 2017). The results showed that 16 *CfTPS* proteins were marked in the chloroplast, and 16 *CfTPS* proteins were marked in chloroplast or cytoplasm, indicating that these three predictors produce different results and need to be further analyzed. We also annotated 32 *CfTPS* genes using BLASTP[17] and Terzyme software (**Supplementary Table S4**; Priya et al., 2018). The results showed that 11 *CfTPSs* were annotated sesquiterpene synthases, 15 *CfTPSs* were annotated monoterpene synthases, and six *CfTPSs* were annotated diterpene synthases. The secondary structure predicted by the SOPMA program revealed that the average of α-helices, random coils, extended strands, and β-turns comprised 70.86, 21.37, 4.35, and 3.63% of the structure, respectively (Geourjon and Deléage, 1995). The results showed that α-helices were predominant in all *CfTPS* proteins (**Table 1**).

Motif and Gene Structure Analysis

To understand the intron-exon structure of *CfTPS* genes, we analyzed TPS gene structure with GSDS software (Hu et al., 2015). The exons in *CfTPS* genes ranged in numbers from 2 to 15, and the results showed that most of the genes in the same category contained a similar intron-exon structure.

To further analyze the motifs of the *CfTPS* genes, we identified 20 motifs using MEME software (Bailey et al., 2009). The numbers of *C. faberi* TPS motifs ranged in length from 4 to 16. *CfTPS3* and *CfTPS23* contained the most motifs, with 16, while *CfTPS1*, *CfTPS2* had only four motifs. Motif 3 can be found in all *CfTPS* proteins except *CfTPS9* and *CfTPS16*. Motif 4 was also the most common *CfTPS* protein (28/32). Twenty-five *CfTPS* genes contained the RRX_8W motif (motif 1), and 30 *CfTPS* genes contained the DDxxD motif (motif 2; **Figure 2C**). Accordingly, different clusters have different forms of motifs. The same cluster's *CfTPS* proteins generally contained similar motifs. These results of intron-exon structure

[16]https://blast.ncbi.nlm.nih.gov/Blast.cgi

[17]http://blast.ncbi.nlm.nih.gov

TABLE 1 | A list of TPS genes in *C. faberi*, their characteristics, and functional annotation.

Gene ID[1]	Name	AA[2] (aa)	pI[3]	Mw[4] (kDa)	AI[5]	II[6]	GRAVY[7]	Localization[8]	Function[9]
HL002300	*CfTPS1*	115	4.86	13.43	100.18	28.62	0.004	Chloroplast[a,b]/Cytoplasm[c]	C15
HL002301	*CfTPS2*	115	4.86	13.43	100.18	28. 62	0.004	Chloroplast[a,b]/Cytoplasm[c]	C15
HL003318	*CfTPS3*	609	6.00	70.70	97.68	47. 96	−0.274	Chloroplast[a,b,c]	C10
HL003423	*CfTPS4*	806	6.03	90.68	93.49	44. 18	−0.114	Chloroplast[a,b,c]	C20
HL008810	*CfTPS5*	374	6.02	43.53	96.27	52. 36	−0.294	Chloroplast[a,b]/Cytoplasm[c]	C10
HL012959	*CfTPS6*	321	5.45	37.26	107.22	40. 93	0.073	Chloroplast[a,b,c]	C20
HL015149	*CfTPS7*	435	5.30	49.81	98.66	48.37	−0.109	Chloroplast[a,b]/Cytoplasm[c]	C10
HL015150	*CfTPS8*	448	5.43	51.45	101.25	45.47	−0.112	Chloroplast[a,b]/Cytoplasm[c]	C10
HL017747	*CfTPS9*	429	6.08	48.50	98.13	46.48	−0.074	Chloroplast[a,b,c]	C20
HL018937	*CfTPS10*	250	5.00	28.44	91.77	46.95	−0.163	Chloroplast[a,b,c]	C10
HL020199	*CfTPS11*	405	5.17	46.73	92.00	42.44	−0.291	Chloroplast[a,b,c]	C20
HL021067	*CfTPS12*	902	6.18	10.24	95.35	38.05	−0.160	Chloroplast[a,b]/Nucleus[a]/Cytoplasm[c]	C10
HL023892	*CfTPS13*	455	5.18	52.81	101.21	42.22	−0.072	Chloroplast[a,b]/Cytoplasm[c]	C20
HL024326	*CfTPS14*	501	5.91	58.85	101.00	48.05	−0.139	Chloroplast[a,b]/Cytoplasm[c]	C20
HL024478	*CfTPS15*	528	6. 35	62.29	98.60	35.68	−0.230	Chloroplast[a,b]/Cytoplasm[c]	C10
HL025052	*CfTPS16*	421	5.07	49.19	89.67	45.71	−0.270	Chloroplast[a,b,c]	C20
HL025282	*CfTPS17*	617	6.46	69.77	93.26	52.75	−0.124	Chloroplast[a]/Mitochondrion[b]/Cytoplasm[c]	C10
HL025366	*CfTPS18*	463	5.57	54.22	106.80	49.56	−0.174	Chloroplast[a,b,c]	C10
HL025643	*CfTPS19*	490	5.30	57.56	98.18	39. 76	−0.095	Chloroplast[a,b,c]	C20
HL025987	*CfTPS20*	445	5.27	51.22	97.09	50.28	−0.055	Chloroplast[a,b]/Cytoplasm[c]	C10
HL026777	*CfTPS21*	653	8.57	75.5	87.09	42.52	−0.257	Chloroplast[a,b,c]	C20
HL026987	*CfTPS22*	178	5.09	21.16	104.18	37.38	−0.237	Chloroplast[a,b]/Cytoplasm[c]	C10
HL027027	*CfTPS23*	569	5.30	66.31	95.63	37. 83	−0.277	Chloroplast[a,b]/Cytoplasm[c]	C10
HL027466	*CfTPS24*	508	5.17	59.33	98.70	41.50	−0.090	Chloroplast[a,b]/Cytoplasm[c]	C20
HL027610	*CfTPS25*	398	6.12	46.21	99.97	52.70	−0.221	Chloroplast[a,b]/Cytoplasm[c]	C10
HL027633	*CfTPS26*	562	9.28	65.60	87.47	42.35	−0.358	Chloroplast[a,b,c]	C20
HL028595	*CfTPS27*	281	5.83	33.37	99.21	47.13	−0.312	Chloroplast[a,b]/Cytoplasm[c]	C10
HL029155	*CfTPS28*	311	5.53	36.76	105.65	42.67	−0.126	Chloroplast[a,b]/Cytoplasm[c]	C10
HL029581	*CfTPS29*	550	5.38	64.34	101.58	50.85	−0.189	Chloroplast[a,b,c]	C20
HL029624	*CfTPS30*	454	5.60	53.09	100.68	49.99	−0.174	Chloroplast[a,b]/Cytoplasm[c]	C20
HL029782	*CfTPS31*	895	6.68	103.89	88.87	40.62	−0.249	Chloroplast[a,c]/Unknown[b]	C20
HL030142	*CfTPS32*	321	5.38	37.77	97.84	38. 32	−0.085	Chloroplast[a]/Unknown[b]/Cytoplasm[c]	C20

[1]*Gene ID is annotated in C. faberi genome.*

[2]*AA, exhibits amino acid.*

[3]*pI, exhibits theoretical isoelectric point.*

[4]*Mw, exhibits molecular weight.*

[5]*AI, exhibits aliphatic index.*

[6]*II, exhibits instability index.*

[7]*GRAVY, exhibits the grand average of hydrophobicity.*

[8]*Subcellular localization depended on Plant-mPloc, AtSubP, and Ploc-mPlant, respectively (Chou and Shen, 2010; Kaundal et al., 2010; Cheng et al., 2017).*

[9]*Gene function predicted by Terzyme website.*

C10, C15, and C20 represent monoterpene, sesquiterpene, and diterpene, respectively. Row data is listed in ***Supplementary Tables S1–S5****.*

[a, b, c]*exhibit Plant-mPloc, AtSubP, and Ploc-mPlant website results, respectively.*

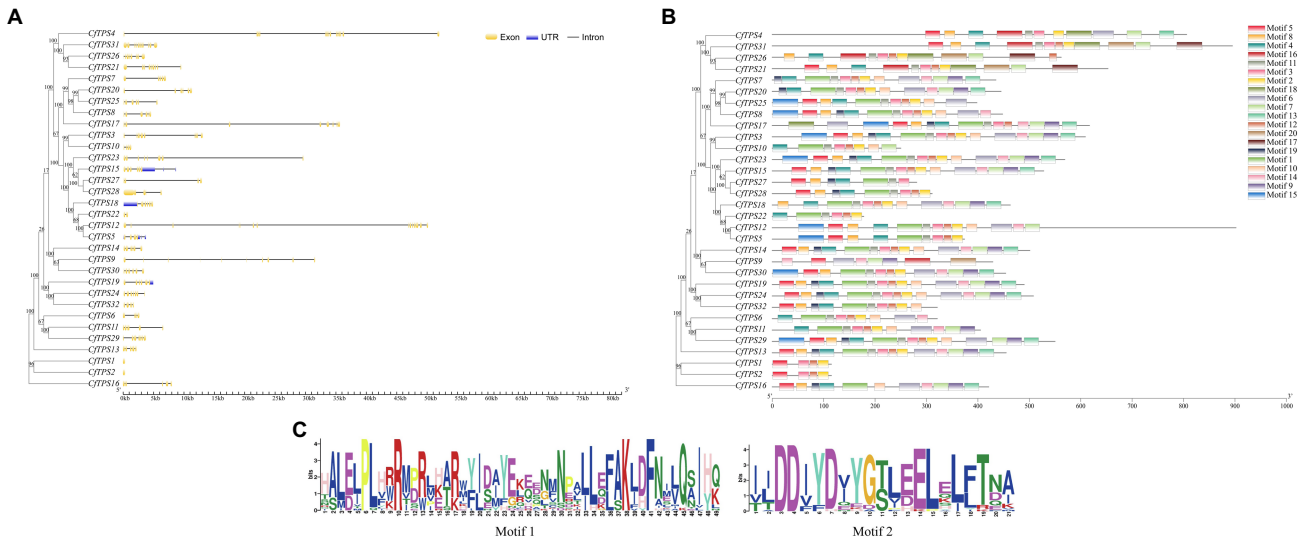


FIGURE 2 | Phylogenetic tree and intron-exon structure of *CfTPS* genes. **(A)** Phylogenetic tree and intron-exon structure of *CfTPS* genes. The maximum likelihood (ML) method was used for the phylogenetic tree, which was constructed with RAxML on the CIPRES Science Gateway web server (RAxML-HPC2 on XSEDE; Miller et al., 2011). Bootstrap values were 1,000 replicates with the JTT model. The intron-exon structure was drawn by the GSDS website (Hu et al., 2015). Yellow boxes, blue boxes, and black lines exhibit exons, introns, and upstream or downstream-untranslated regions. **(B)** Phylogenetic tree and conserved motifs of *CfTPS* genes. Conserved motifs were determined by MEME software with default parameters (Kaundal et al., 2010). **(C)** Sequence logo of motif 1 (RRX_8W) and motif 2 (DDxxD). Motif 1 shows the N-terminal motif RRX_8W, and motif 2 shows the C-terminal motif DDxxD motif. Conserved motifs are available in **Supplementary Table S6**.

and motif analysis verified the closeness of the phylogenetic tree in *C. faberi* (**Figure 2**).

Phylogenetic Analysis of *CfTPS* Genes

A phylogenetic tree was constructed to analyze the evolutionary patterns of the *CfTPS* genes. Thirty-two *CfTPS* genes were used, and TPS protein sequences from six species (*A. shenzhenica*, *P. equetris*, *O. sativa*, *A. thaliana*, *P. abies*, and *S. moellendorfii*) were used. The maximum likelihood (ML) method was used for the phylogenetic tree, which was constructed with RAxML on the CIPRES Science Gateway web server (RAxML-HPC2 on XSEDE; Miller et al., 2011). Bootstrap values were 1,000 replicates with the JTT model. The phylogenetic tree indicated that TPS proteins belonged to seven categories. This classification result was consistent with a recent study: TPS-a, TPS-b, TPS-c, TPS-d, TPS-e/f, TPS-g, and TPS-h (Chen et al., 2011). Thirty-two *CfTPS* proteins belonged to three categories according to the phylogenetic tree (**Figure 3**): TPS-a, TPS-b, and TPS-e/f. Of these three categories, the TPS-a and TPS-b clades contained the most members and were the most expanded categories, with 13 and 15 genes, respectively, and were consistent with other plant species, such as *A. thaliana*, *C. sinensis*, *V. planifolia*, *D. catenatum*, *P. equestris*, and *D. officinale* (Aubourg et al., 2002; Yu et al., 2020; Zhou et al., 2020; Huang et al., 2021). The remaining four TPS genes belonged to the TPS-e/f subfamily.

We aligned the multiple sequences using MAFFT to analyze the TPS RRX_8W motif in the N-terminus, DDxxD, and NSE/DTE motifs in the C-terminus (Rozewicki et al., 2019). The alignment showed that almost all the *CfTPS* proteins in the TPS-a and TPS-b subfamilies had the highly conserved aspartate-rich motif DDxxD, except *CfTPS9* and *CfTPS16* in the TPS-a subfamily and *CfTPS17*, *CfTPS27*, and *CfTPS28* in the TPS-b subfamily (Jiang et al., 2019). TPS genes in TPS-a and TPS-b had variations in the RRX_8W and RxR motif. However, in the TPS-a and TPS-b categories, the RRX_8W motif was not found in nine *CfTPS* genes. The RRX_8W motif was absent in the TPS-e/f subfamily, and the NSE/DTE motif was found in 16 *CfTPS* genes (**Figure 4**). Among them, DDxxD and NSE/DTE are important in the metal-dependent ionization of the prenyl diphosphate substrate, and the RRX_8W motif is essential in the cyclization of monoterpene synthase (Bohlmann et al., 1998; Chen et al., 2011; Jiang et al., 2019). In addition, the members in the TPS-a subfamily detected in both dicot and monocot plants encode only sesquiterpenes (Jiang et al., 2019). The secondary "R" in this family is not conserved (Martin et al., 2010). TPS-b encodes monoterpenes containing the conserved RRX_8W motif (Chen et al., 2011; Jiang et al., 2019).

Promoter Analysis of *CfTPS* Genes

To retrieve the potential function of *CfTPS* genes, we obtained a 2,000-bp region upstream of the 32 *CfTPS* genes and analyzed them using the online software Plantcare (Lescot et al., 2002). In total, we found 784 *cis*-acting regulatory elements in the promoter areas of *CfTPS* genes. We classified them into three categories according to the function of these elements: plant growth and development, stress responsiveness, and phytohormone responsiveness. The plant growth and dependent category (166/784) contained nine *cis*-acting regulatory elements and consists of AAGAA motifs, As-1 elements, A1-rich elements, etc. Most of them had As-1 elements (66/166), which are related to shoot expression. The stress responsiveness category (216/874) contained ARE, DRE, LTR, ST-RE, ABRE, etc.

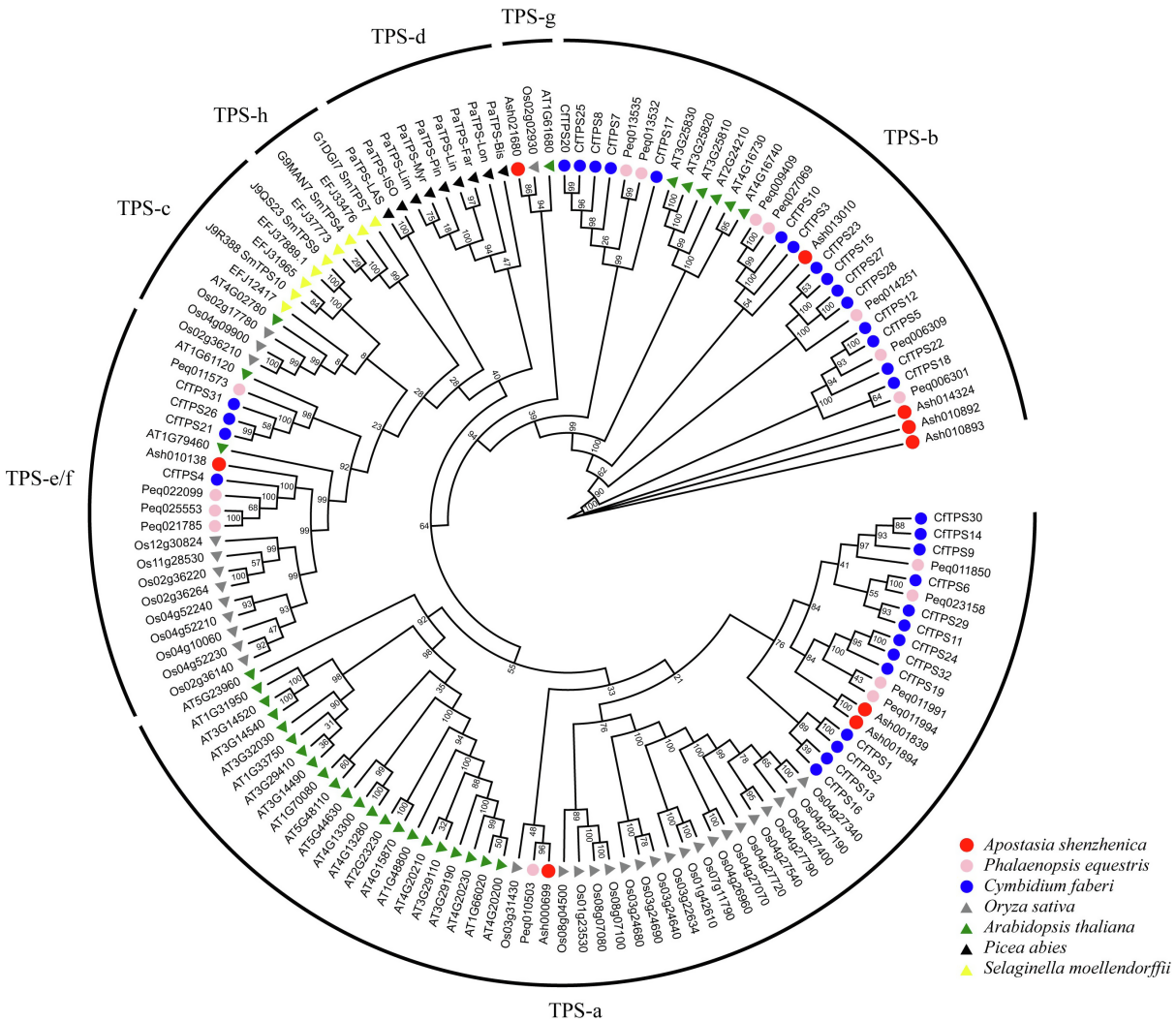


FIGURE 3 | Phylogenetic tree of *CfTPS* genes based on the TPS protein sequences of seven plant species. The ML method was used for the phylogenetic tree, which was constructed with RAxML on the CIPRES Science Gateway web server (RAxML-HPC2 on XSEDE; Miller et al., 2011). The bootstrap values were 1,000 replicates with the JTT model. The generated tree was redrawn and annotated by the EVOLVIEW website (He et al., 2016). The TPS family was classified into seven categories: TPS-a, TPS-b, TPS-c, TPS-d, TPS-e/f, TPS-g, and TPS-h (Chen et al., 2011). TPS protein sequences in *Cymbidium faberi* are available in **Supplementary Table S7**.

STRE (48/216) is an essential element in the promoter that is related to stress. Interestingly, most of the *cis*-elements (401/784) were in the phytohormone responsiveness category, which contained CGTCA motifs, EREs, MYC motifs, TGAGG motifs, etc. Among them, most *cis*-elements were MYC (137/401), which is associated with MeJA responsiveness (Dombrecht et al., 2007). The results indicated that the *CfTPS* gene expression patterns might be regulated by MeJA treatment (**Figure 5**).

Ka/*Ks* Analysis in *C. faberi*

The *Ka*/*Ks* ratio can show positive selection (*Ka*/*Ks* > 1), negative or purifying selection (*Ka*/*Ks* < 1), and neutral selection (*Ka*/*Ks* = 1) during the evolution (Zhang et al., 2006). In this study, 13 gene pairs with similar genetic relationships were selected for *Ka*/*Ks* calculation. The results showed that the *Ka*/*Ks* ratios of 12/13 *CfTPS* genes were less than one, indicated that most *CfTPS* genes underwent negative selection (**Table 2**). The divergence time of 13 *CfTPS* gene pairs was in the range of 0.75 for *CfTPS1* and *CfTPS2* to 60.46 for *CfTPS3* and *CfTPS10*.

Expression Patterns in Different *C. faberi* Organs and GO Classification of TPS Genes

An RNA sequencing transcriptome database of leaves, pseudobulbs, petals, sepals, labellums, and gynostemium was established to study the expression patterns of *CfTPS* genes. Eighteen genes were expressed in both leaves and flowers, and 20 genes were expressed in the labellums. Twenty-five genes were found in sepals and 24 in gynostemium. Four genes were not found to be expressed in any of the tissues.

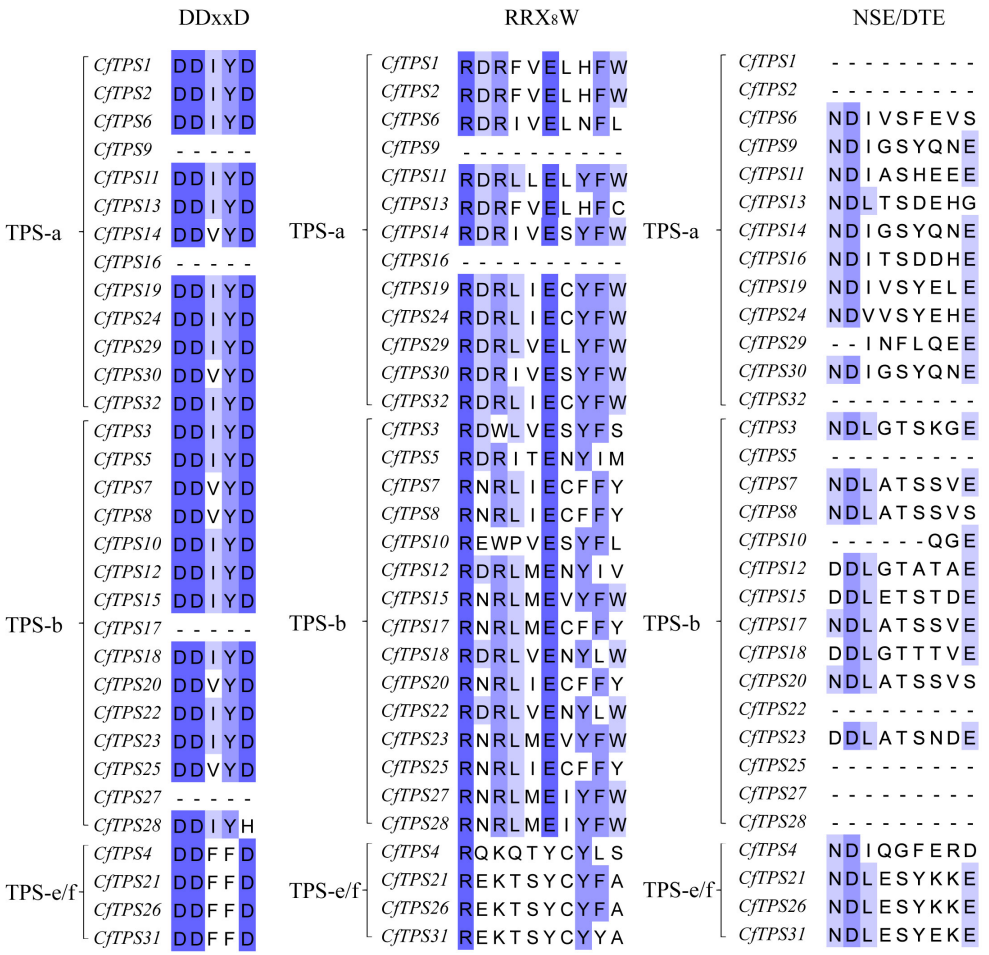


FIGURE 4 | RRX_8W, DDxD, and NSE/DTE motifs in the *CfTPS* protein amino acid sequences. Multiple sequence alignments were constructed by MAFFT, and Jalview software was used to visualize the sequences (Troshin et al., 2011; Rozewicki et al., 2019).

CfTPS12, *CfTPS15*, and *CfTPS23* exhibited a high level of expression in leaves and pseudobulbs. Notably, *CfTPS3*, *CfTPS12*, *CfTPS15*, *CfTPS17*, *CfTPS18*, *CfTPS28*, and *CfTPS31* displayed high transcript abundance in floral organs, suggesting that these TPS genes might be related to flower scent in *C. faberi* (**Figure 6**).

Gene ontology classification analysis was performed based on the differentially expressed gene analysis. According to the classification results, molecular function contained most genes, and genes were mostly enriched in lyase activity, magnesium binding, and terpene synthase activity (**Figure 7**).

Expression Patterns of *CfTPS* in Flowers at Three Floral Developmental Stages

Real-time reverse transcription quantitative PCR was performed to investigate the expression patterns of *CfTPS* genes in flowers at three floral developmental stages. Four putative functional genes, *CfTPS12*, *CfTPS18*, *CfTPS23*, and *CfTPS28*, which are highly expressed in floral organs, were used. They were expressed differently among the three floral stages. Interestingly, these genes were mainly expressed in the full flowering stage (**Figure 8**). Notably, *CfTPS18* had the highest transcript levels during the floral developmental stages, consistent with the expression patterns displayed in **Figure 5**. Gene annotation indicated that *CfTPS12*, *CfTPS18*, *CfTPS23*, and *CfTPS28* likely encoded monoterpene synthases and clustered in TPS-b subfamily (**Table 1**).

Functional Characterization of *CfTPS18* in *E. coli*

To investigate the enzyme activity, the full-length ORF sequence of *CfTPS18* was cloned to vector pET28a and ectopically expressed in *E. coli*. Recombinant *CfTPS18* enzyme was induced with 0.1 mM isopropyl-β-d-galactopyranoside and purified with Ni-NTA agarose (Clontech). SDS-PAGE analysis of *CfTPS18* recombinant protein can be found in **Supplementary Figure S1**. After using GPP as substrate in the reactions, the products were analyzed by GC-MS. The result indicated that *CfTPS18* could convert GPP into β-myrcene, geraniol, and α-pinene which were validated by the NIST Mass Spectral Library (**Figure 9**). The blank control with only GPP added to the reactions could not produce

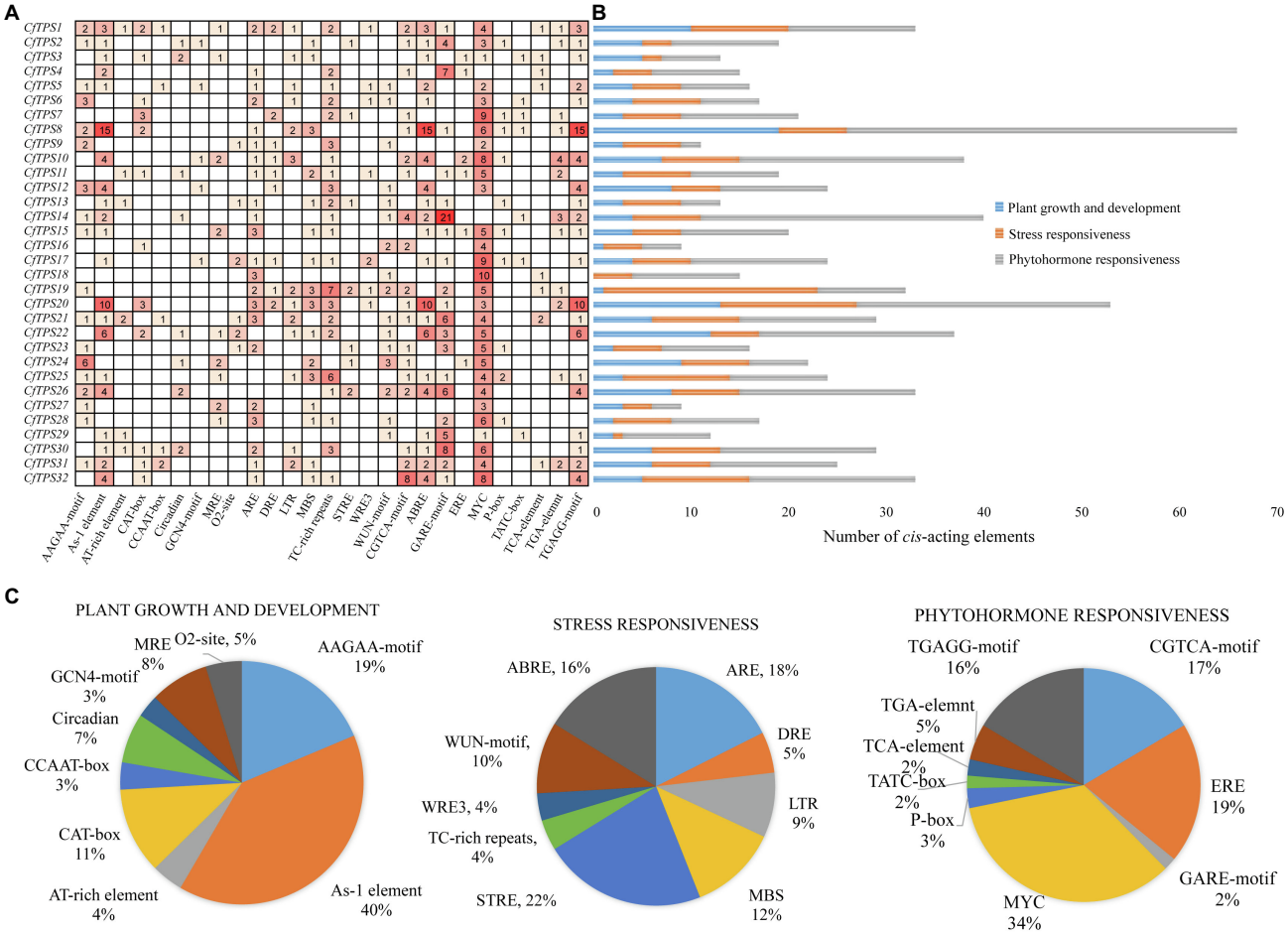


FIGURE 5 | Promoter analysis of *CfTPS* genes. **(A)** The numbers in the box exhibit the number of *cis*-acting elements in *CfTPS*. **(B)** Blue, orange, and gray colors exhibit *cis*-acting elements in plant growth and development, stress responsiveness, and phytohormone responsiveness. **(C)** The proportion of different *cis*-acting elements in plant growth and development, stress responsiveness, and phytohormone responsiveness.

monoterpenes. Thus, *CfTPS18* was considered a monoterpene synthase.

DISCUSSION

Orchids are among the largest angiosperm families in angiosperms and demonstrate a diversity of epiphytic and terrestrial growth forms (Hsiao et al., 2011). *Cymbidium faberi* is one of the longest cultivated orchids planted in China and has high ornamental value due to its characteristic flower scent and beautiful flower shape (Omata et al., 1990; Hsiao et al., 2011; Sun et al., 2016). Terpenoids play an essential role in floral scent and can attract pollinating insects and defend against environmental stresses (Wagner and Elmadfa, 2003; Dudareva et al., 2006; Sun et al., 2016). Plants have enzymes called TPSs, which encode the synthesis of monoterpene (C10), sesquiterpene (C15), or diterpenes (C20) from DMAPP, GPP, and GGPP, respectively (Pichersky et al., 2006). Terpenoids are dominant in the flower scent of orchids. In this study, we systematically retrieved and classified TPS genes in *C. faberi*.

We identified 32 *CfTPS* genes in the *C. faberi* genome according to the TPS N-terminal and C-terminal domains (**Table 1**). We classified them into three categories: TPS-a, TPS-b, and TPS-e/f. TPS-b was the most expanded category, which was consistent with patterns in *D. officinale*, *V. planifolia*, and *D. catenatum*, and *C. faberi* have more genes in TPS-b than *P. equestris* (Yu et al., 2020; Huang et al., 2021). However, it was not consistent with *A. thaliana*, *O. sativa*, and *S. bicolor*, which have a dominant subfamily TPS-a (Aubourg et al., 2002; Chen et al., 2011). These results suggest that orchids have more TPS genes in TPS-b than other angiosperm dicot species and are related to emit floral scent to attract pollinators (Huang et al., 2021). According to the phylogenetic tree, most of the TPS-b genes are present in dicots. TPS-a genes can be further split into monocot-specific TPS-a-1 and dicot-specific TPS-a-2 clades. The TPS gene family is a medium-sized family, and the numbers of TPS genes range from approximately 20–100 (Chen et al., 2011). For instance,

TABLE 2 | *Ka/Ks* analysis of TPS genes in *C. faberi*.

Gene pairs	*Ka*[1]	*Ks*[2]	*Ka/Ks*[3] Ratio	Date (Mya)
CfTPS5-CfTPS12	0.036349	0.060903	0.596841353	3.346319222
CfTPS18-CfTPS22	0.183699	0.58801	0.31240786	32.30822426
CfTPS27-CfTPS28	0.061668	0.086265	0.71486064	4.739845716
CfTPS15-CfTPS23	0.040242	0.038395	1.048087536	2.109640277
CfTPS3-CfTPS10	0.329855	1.100284	0.299790513	60.45518349
CfTPS20-CfTPS7	0.035647	0.054369	0.655636934	2.987330286
CfTPS25-CfTPS8	0.052051	0.057777	0.900881064	3.174578759
CfTPS1-CfTPS2	0	0.01373	0	0.754415417
CfTPS13-CfTPS16	0.207258	0.585853	0.353772093	32.1897194
CfTPS11-CfTPS29	0.108769	0.203168	0.535365599	11.16305388
CfTPS14-CfTPS30	0.035698	0.0446	0.800403031	2.450539375
CfTPS24-CfTPS32	0.028484	0.045777	0.622244514	2.515215271
CfTPS21-CfTPS26	0.04343	0.044138	0.983976748	2.425138016

[1]*Ka, non-synonymous rate.*
[2]*Ks, synonymous substitution.*
[3]*Ka/Ks, evolutionary constraint.*
Divergence time (T) was calculated by using the formula $T = Ks/(2 \times 9.1 \times 10^{-9}) \times 10^{-6}$ *million years ago (Mya, Zhang et al., 2018). The details of Ka/Ks calculation are listed in* ***Supplementary Table S8****.*

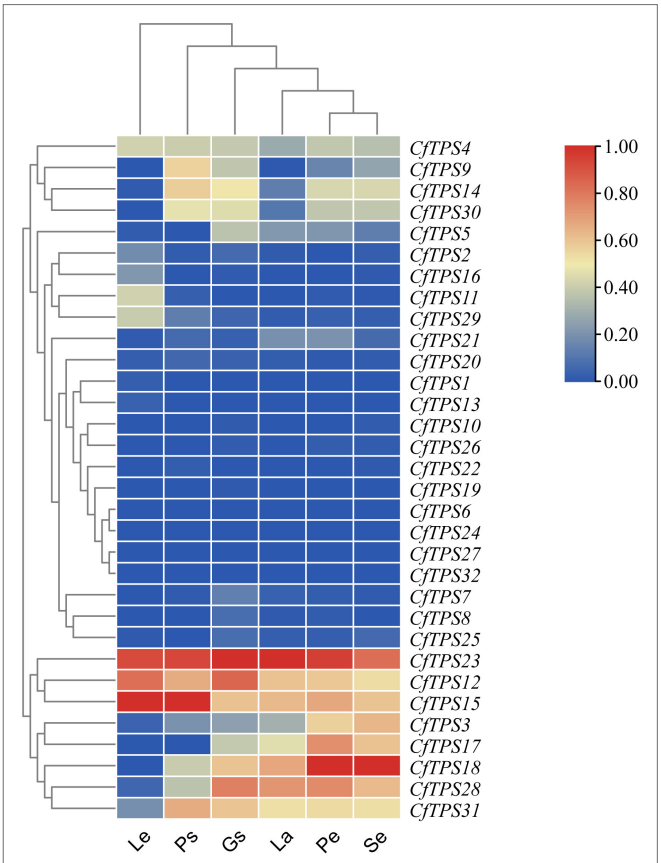


FIGURE 6 | Expression patterns of *CfTPS* genes in different organs. The heatmap was produced in Tbtools (Chen et al., 2018). The tissues were leaves (L), pseudobulbs (Ps), petals (Pe), sepals (Se), labellum (La), and gynostemium (Gs) in wild *C. faberi*. The fragments per kilobase of transcript per million fragments (FPKM) values are listed in **Supplementary Table S9**.

14 *SmTPS*, 23 *GmTPS*, 32 *AtTPS*, 34 *DoTPS*, 23 *CsTPS*, and 69 *VvTPS* were found in *S. moellendorfii*, *G. max*, *A. thaliana*, *D. officinale*, *C. sinensis*, and *V. vinifera*, respectively (Li et al., 2012; Yu et al., 2020; Zhou et al., 2020). In addition, TPS occupied 0.26 genes/M in *A. thaliana* (125 M), 0.14 genes/M in *V. vinifera* (487 M), 0.13 genes/M in *S. moellendorfii* (106 M), 0.02 genes/M in *D. officinale* (1.35 G), 0.02 genes/M in *G. max* (1.011 G), and 0.01 genes/M in *C. faberi* (3.77 G; Jaillon et al., 2007; Schmutz et al., 2010; Poczai et al., 2014; Zhang et al., 2016). These results indicate that the TPS family has undergone expansion throughout the evolutionary history of land plants, and different species may show a difference in the expansion mechanism (Chen et al., 2011; Jiang et al., 2019).

We also annotated 32 *CfTPS* genes, and the results showed that all TPSs in the TPS-a clade encode sesquiterpenes, and all TPSs in the TPS-b clade encode monoterpenes (**Table 1**). All the *CfTPS* in the TPS-e/f clade were annotated as diterpene synthases. This is consistent with a recent study in which most TPS genes in the TPS-a subfamily were determined to be sesquiterpene synthases. TPS-e/f encoded monoterpene, sesquiterpene, and diterpene in a recent study (Chen et al., 2011). Sesquiterpenes, diterpenes, and monoterpenes are important to emit floral scents to attract pollinators and defend against environmental stress (Huang et al., 2021).

Each full-length TPS had two conserved domains, including the N-terminal domain containing the RRX_8W motif and the C-terminal domain containing two highly conserved aspartate-rich motifs: DDxxD and NSE/DTE (Starks et al., 1997; Jiang et al., 2019). DDxxD and NSE/DTE are significant in the metal-dependent ionization of the prenyl diphosphate substrate, and the RRX_8W motif is essential in the cyclization of monoterpene synthase (Bohlmann et al., 1998; Chen et al., 2011; Jiang et al., 2019). The secondary "R" in the TPS-a subfamily is not conserved (Martin et al., 2010). TPS-b contains the conserved RRX_8W motif, which is related to monoterpene formation. TPS-c does not include the DDxxD motif (Chen et al., 2011; Jiang et al., 2019). Motif RxR was also conserved in TPS-a and TPS-b subfamilies. In this study, multiple sequence alignments showed that 28/32 *CfTPS* had highly conserved DDxxD motifs, 16/32 *CfTPS* had RRX_8W motifs, 16/32 *CfTPS* had NSE/DTE motifs, and 9/32 *CfTPS* had RxR motifs. The RRX_8W motif was not found in 11 *CfTPSs* in the TPS-a and TPS-b clades, and it was absent in the TPS-e/f subfamily. The results indicated that motif loss might have appeared during family evolution in *C. faberi* and that different subfamilies have different motif features.

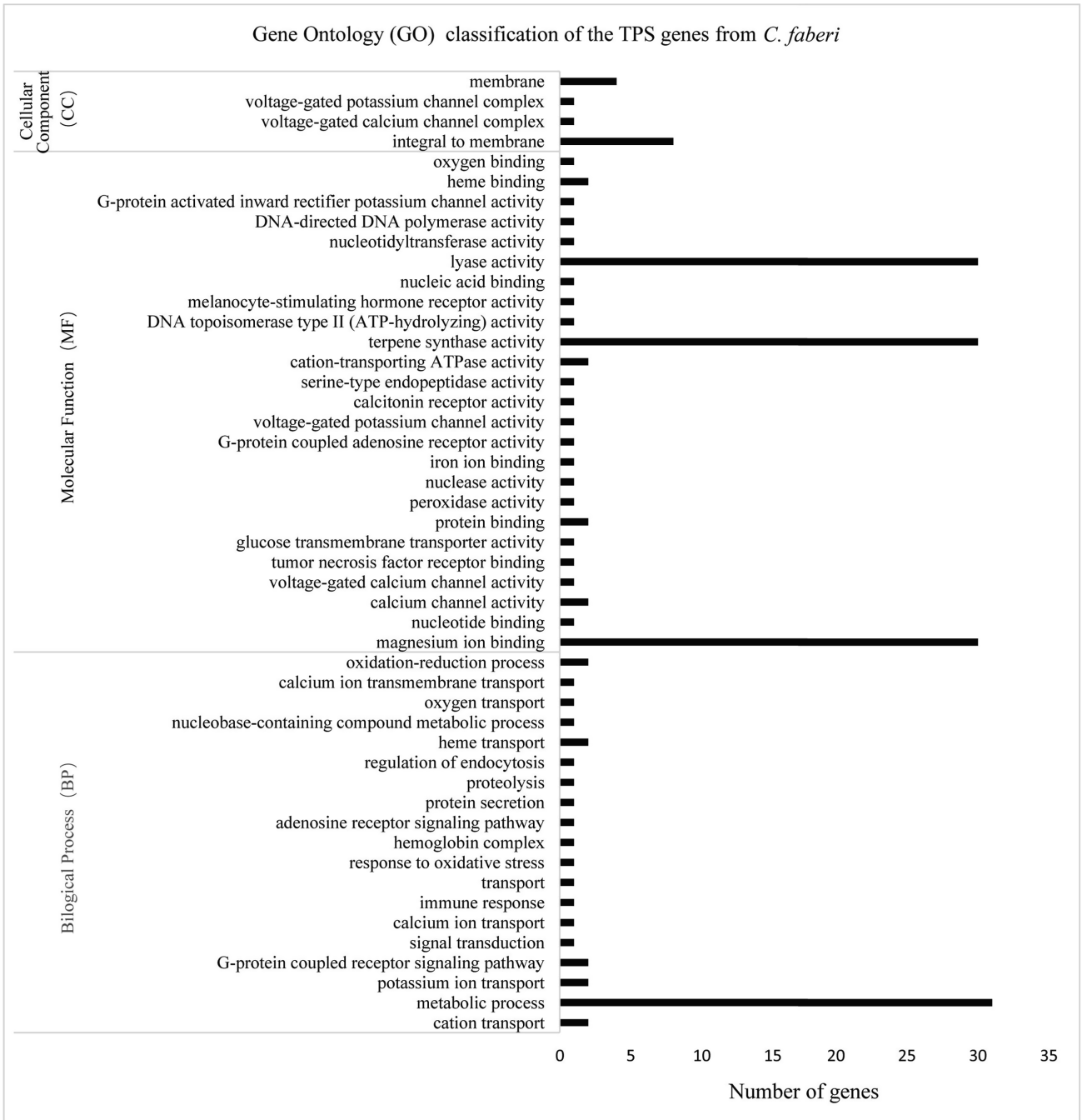


FIGURE 7 | Gene ontology (GO) classification of *CfTPS* genes. GO annotation details are listed in **Supplementary Table S10**.

Different elements were observed in promoter areas of *CfTPS* genes. Most of the *cis*-elements were in the phytohormone responsiveness group, and the number of MYCs associated with MeJA responsiveness contained most of this group. The results indicated that the expression patterns of *CfTPS* may be regulated by MeJA treatment and may respond to multiple environmental stresses (Chaiprasongsuk et al., 2018). In recent studies, MeJA was shown to regulate TPS gene expression in *D. officinale* and *C. sinensis* (Yu et al., 2020; Zhao et al., 2020; Zhou et al., 2020). However, this needs to be further investigated in *C. faberi*. The *Ka*/*Ks* ratio analysis indicated that the TPS gene family in *C. faberi* mainly underwent negative selection, making it more stable during the evolution. GO annotation analysis of *CfTPS* genes indicated that molecular function contained most genes, and genes were mostly enriched in lyase activity, magnesium binding, and terpene synthase activity. Expression pattern analysis indicated that *CfTPS*

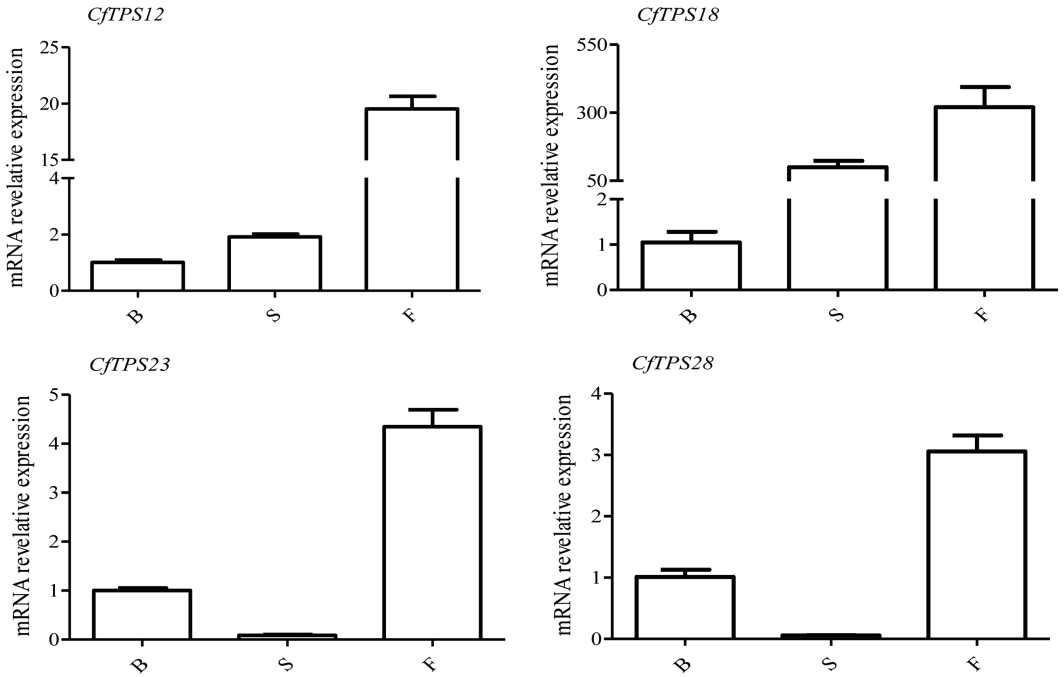


FIGURE 8 | Real-time reverse transcription quantitative PCR (RT-qPCR) validation of transcriptomic data of the *CfTPS* genes at three flowering stages. B, budding flowers; S, semi-open flowers; and F, fully open flowers. The error bars indicate three RT-qPCR biological replicates. The values were standardized by the *C. faberi* reference gene GAPDH (GenBank Accession: JX560732; Tian et al., 2020). The expression values of *CfTPS* genes are listed in **Supplementary Table S11**, and the RT-qPCR primers of *CfTPS* are listed in **Supplementary Table S12**.

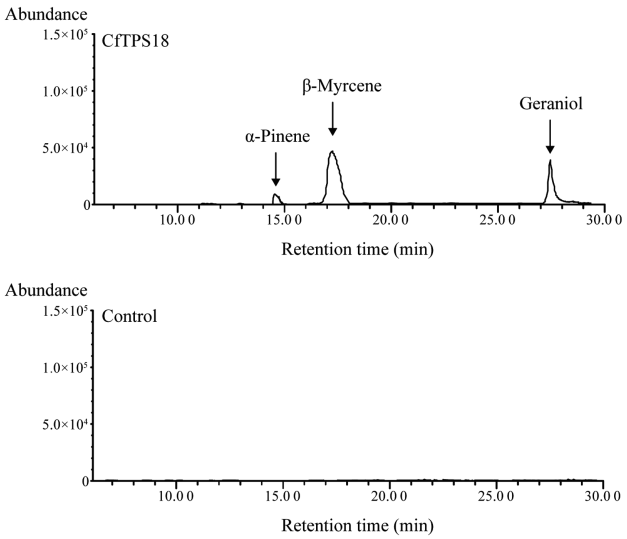


FIGURE 9 | Enzymatic assays after incubating recombinant *CfTPS18*. Reactions only performed with GPP were used as the blank control. The retention time was compared with the NIST Mass Spectral Library.

genes were mainly expressed in the floral organs of *C. faberi*, indicating that they were related to floral scent. We selected four *CfTPS* genes with the highest transcript levels in floral organs for qRT-PCR analysis at three flowering stages. The results showed that they all belonged to the TPS-b clade and were mainly expressed in the full flowering stage. According to our annotation, four genes were all annotated as monoterpene synthases, which may play essential roles in floral scent and attracting pollinators in *C. faberi*. Enzymatic assays suggested that *CfTPS18* could convert GPP to β-myrcene, geraniol, and α-pinene. In recent reports, *DoTPS10* in *D. officinale* can convert GPP to linalool *in vitro* (Yu et al., 2020). *DoGES1* in *D. officinale* can catalyze geraniol *in vitro* and *in vivo* (Zhao et al., 2020). Linalool and geraniol belong to monoterpenes which play essential roles in floral scents. TPS that catalyze terpenes can also be found in *V. vinifera*, *M. domestica*, and *Litsea cubeba* (Martin et al., 2010; Nieuwenhuizen et al., 2013; Chen et al., 2020). To better understand terpenes production and function in *C. faberi*, more studies of expression profiles should be developed.

CONCLUSION

In this study, 32 *CfTPS* genes were identified from the genomes of *C. faberi*. We analyzed their conserved motifs, exon-intron structure, phylogeny, *Ka*/*Ks* ratios, and *cis*-acting regulatory elements. We also analyzed the expression patterns of *CfTPS* genes in leaves, pseudobulbs, petals, sepals, labellums, and gynostemium in wild *C. faberi*. Four putatively functional genes highly expressed in floral organs were used to analyze the expression patterns at three flowering stages. Enzymatic assays

indicated that *CfTPS18* could convert GPP to β-myrcene, geraniol, and α-pinene. The results will provide valuable information for further studies on floral scents in *C. faberi* and other orchids.

DATA AVAILABILITY STATEMENT

The original contributions presented in the study are included in the article/**Supplementary Material**, further inquiries can be directed to the corresponding authors.

AUTHOR CONTRIBUTIONS

SL, Z-JL, and DZ contributed to conceptualization and validation. Q-QW, M-JZ, and ZZ prepared the original draft. Q-QW, Y-YB, and XY analyzed the data. M-KC, YA, and JC contributed to the visualization. All authors contributed to the article and approved the submitted version.

FUNDING

This research was funded by The National Key Research and Development Program of China (2019YFD1001000), The National Natural Science Foundation of China (no. 31870199), The Key Laboratory of National Forestry and Grassland Administration for Orchid Conservation and Utilization Construction Funds (Grant 115/118990050, 115/KJG18016A), Natural Science Foundation of Zhejiang Province (Grant nos. LY20C160005, LY19C150003), Key Research and Development Program of Zhejiang Province (Grant no. 2021C02043), and Wenzhou Agricultural New Variety Breeding Cooperative Group Project (Grant no. 2019ZX004-3).

SUPPLEMENTARY MATERIAL

The Supplementary Material for this article can be found online at: https://www.frontiersin.org/articles/10.3389/fpls.2021.751853/full#supplementary-material

REFERENCES

Artimo, P., Jonnalagedda, M., Arnold, K., Baratin, D., Csardi, G., De Castro, E., et al. (2012). ExPASy: SIB bioinformatics resource portal. *Nucleic Acids Res.* 40, 597–603. doi: 10.1093/nar/gks400

Aubourg, S., Lecharny, A., and Bohlmann, J. (2002). Genomic analysis of the terpenoid synthase (*AtTPS*) gene family of *Arabidopsis thaliana*. *Mol. Gen. Genomics* 267, 730–745. doi: 10.1007/s00438-002-0709-y

Bailey, T. L., Boden, M., Buske, F. A., Frith, M., Grant, C. E., Clementi, L., et al. (2009). MEME suite: tools for motif discovery and searching. *Nucleic Acids Res.* 37, 1–7. doi: 10.1093/nar/gkp335

Bohlmann, J., Meyer-Gauen, G., and Croteau, R. (1998). Plant terpenoid synthases: molecular biology and phylogenetic analysis. *Proc. Natl. Acad. Sci. U. S. A.* 95, 4126–4133. doi: 10.1073/pnas.95.8.4126

Chaiprasongsuk, M., Zhang, C., Qian, P., Chen, X., Li, G., Trigiano, R. N., et al. (2018). Biochemical characterization in Norway spruce (*Picea abies*) of SABATH methyltransferases that methylate phytohormones. *Phytochemistry* 149, 146–154. doi: 10.1016/j.phytochem.2018.02.010

Chen, C., Chen, H., He, Y., and Xia, R. (2018). TBtools, a toolkit for biologists integrating various biological data handling tools with a user-friendly interface. bioRxiv [Preprint]. doi: 10.1101/289660

Chen, Y. C., Li, Z., Zhao, Y. X., Gao, M., Wang, J. Y., Liu, K. W., et al. (2020). The Litsea genome and the evolution of the laurel family. *Nat. Commun.* 11, 1–14. doi: 10.1038/s41467-020-15493-5

Chen, F., Tholl, D., Bohlmann, J., and Pichersky, E. (2011). The family of terpene synthases in plants: a mid-size family of genes for specialized metabolism that is highly diversified throughout the kingdom. *Plant J.* 66, 212–229. doi: 10.1111/j.1365-313X.2011.04520.x

Cheng, X., Xiao, X., and Chou, K. C. (2017). PLoc-mPlant: predict subcellular localization of multi-location plant proteins by incorporating the optimal GO information into general PseAAC. *Mol. BioSyst.* 13, 1722–1727. doi: 10.1039/C7MB00267J

Chou, K. C., and Shen, H. B. (2010). Plant-mPLoc: a top-down strategy to augment the power for predicting plant protein subcellular localization. *PLoS One* 5:e11335. doi: 10.1371/journal.pone.0011335

Darriba, D., Taboada, G. L., Doallo, R., and Posada, D. (2011). ProtTest 3: fast selection of best-fit models of protein evolution. *Bioinformatics* 27, 1164–1165. doi: 10.1093/bioinformatics/btr088

Dombrecht, B., Gang, P. X., Sprague, S. J., Kirkegaard, J. A., Ross, J. J., Reid, J. B., et al. (2007). MYC2 differentially modulates diverse jasmonate-dependent functions in *Arabidopsis*. *Plant Cell* 19, 2225–2245. doi: 10.1105/tpc.106.048017

Dudareva, N., Negre, F., Nagegowda, D. A., and Orlova, I. (2006). Plant volatiles: recent advances and future perspectives. *Crit. Rev. Plant Sci.* 25, 417–440. doi: 10.1080/07352680600899973

El-Gebali, S., Mistry, J., Bateman, A., Eddy, S. R., Luciani, A., Potter, S. C., et al. (2019). The Pfam protein families database in 2019. *Nucleic Acids Res.* 47, D427–D432. doi: 10.1093/nar/gky995

Geourjon, C., and Deléage, G. (1995). Sopma: significant improvements in protein secondary structure prediction by consensus prediction from multiple alignments. *Comput. Appl. Biosci.* 11, 681–684. doi: 10.1093/bioinformatics/11.6.681

He, Z., Zhang, H., Gao, S., Lercher, M. J., Chen, W. H., and Hu, S. (2016). Evolview v2: an online visualization and management tool for customized and annotated phylogenetic trees. *Nucleic Acids Res.* 44, W236–W241. doi: 10.1093/nar/gkw370

Hsiao, Y. Y., Pan, Z. J., Hsu, C. C., Yang, Y. P., Hsu, Y. C., Chuang, Y. C., et al. (2011). Research on orchid biology and biotechnology. *Plant Cell Physiol.* 52, 1467–1486. doi: 10.1093/pcp/pcr100

Hu, B., Jin, J., Guo, A. Y., Zhang, H., Luo, J., and Gao, G. (2015). GSDS 2.0: an upgraded gene feature visualization server. *Bioinformatics* 31, 1296–1297. doi: 10.1093/bioinformatics/btu817

Huang, L. M., Huang, H., Chuang, Y. C., Chen, W. H., Wang, C. N., and Chen, H. H. (2021). Evolution of terpene synthases in Orchidaceae. *Int. J. Mol. Sci.* 22:6947. doi: 10.3390/ijms22136947

Jaillon, O., Aury, J. M., Noel, B., Policriti, A., Clepet, C., Casagrande, A., et al. (2007). The grapevine genome sequence suggests ancestral hexaploidization in major angiosperm phyla. *Nature* 449, 463–467. doi: 10.1038/nature06148

Jiang, S. Y., Jin, J., Sarojam, R., and Ramachandran, S. (2019). A comprehensive survey on the terpene synthase gene family provides new insight into its evolutionary patterns. *Genome Biol. Evol.* 11, 2078–2098. doi: 10.1093/gbe/evz142

Kaundal, R., Saini, R., and Zhao, P. X. (2010). Combining machine learning and homology-based approaches to accurately predict subcellular localization in *Arabidopsis*. *Plant Physiol.* 154, 36–54. doi: 10.1104/pp.110.156851

Keilwagen, J., Lehnert, H., Berner, T., Budahn, H., Nothnagel, T., Ulrich, D., et al. (2017). The terpene synthase gene family of carrot (*Daucus carota* L.): identification of QTLs and candidate genes associated with terpenoid volatile compounds. *Front. Plant Sci.* 8:1930. doi: 10.3389/fpls.2017.01930

Lescot, M., Déhais, P., Thijs, G., Marchal, K., Moreau, Y., Van De Peer, Y., et al. (2002). PlantCARE, a database of plant *cis*-acting regulatory elements and a portal to tools for in silico analysis of promoter sequences. *Nucleic Acids Res.* 30, 325–327. doi: 10.1093/nar/30.1.325

Li, G., Köllner, T. G., Yin, Y., Jiang, Y., Xu, Y., Gershenzon, J., et al. (2012). Correction for Li et al., nonseed plant *Selaginella moellendorfii* has both

seed plant and microbial types of terpene synthases. *Proc. Natl. Acad. Sci. U. S. A.* 109, 20774–20774. doi: 10.1073/pnas.1204300109

Liu, J., Huang, F., Wang, X., Zhang, M., Zheng, R., Wang, J., et al. (2014). Genome-wide analysis of terpene synthases in soybean: functional characterization of GmTPS3. *Gene* 544, 83–92. doi: 10.1016/j.gene.2014.04.046

Livak, K. J., and Schmittgen, T. D. (2001). Analysis of relative gene expression data using real-time quantitative PCR and the 2-ΔΔCT method. *Methods* 25, 402–408. doi: 10.1006/meth.2001.1262

Martin, D. M., Aubourg, S., Schouwey, M. B., Daviet, L., Schalk, M., Toub, O., et al. (2010). Functional annotation, genome organization and phylogeny of the grapevine (*Vitis vinifera*) terpene synthase gene family based on genome assembly, FLcDNA cloning, and enzyme assays. *BMC Plant Biol.* 10:226. doi: 10.1186/1471-2229-10-226

Miller, M. A., Pfeiffer, W., and Schwartz, T. (2011). "The CIPRES science gateway: A community resource for phylogenetic analyses." in *Proceedings of the TeraGrid 2011 Conference: Extreme Digital Discovery, TG'11*.

Mohd-Hairul, A. R., Namasivayam, P., Lian, G. E. C., and Abdullah, J. O. (2010). Terpenoid, benzenoid, and phenylpropanoid compounds in the floral scent of *Vanda* Mimi palmer. *J. Plant Biol.* 53, 358–366. doi: 10.1007/s12374-010-9123-x

Nagegowda, D. A. (2010). Plant volatile terpenoid metabolism: biosynthetic genes, transcriptional regulation and subcellular compartmentation. *FEBS Lett.* 584, 2965–2973. doi: 10.1016/j.febslet.2010.05.045

Nieuwenhuizen, N. J., Green, S. A., Chen, X., Bailleul, E. J. D., Matich, A. J., Wang, M. Y., et al. (2013). Functional genomics reveals that a compact terpene synthase gene family can account for terpene volatile production in apple. *Plant Physiol.* 161, 787–804. doi: 10.1104/pp.112.208249

Omata, A., Nakamura, S., Yomogida, K., Moriai, K., Ichikawa, Y., and Watanabe, I. (1990). Volatile components of to-Yo-ran flowers (*Cymbidium faberi* and *Cymbidium virescens*). *Agric. Biol. Chem.* 54, 1029–1033. doi: 10.1080/00021369.1990.10870040

Pichersky, E., Noel, J. P., and Dudareva, N. (2006). Biosynthesis of plant volatiles: nature's diversity and ingenuity. *Science* 311, 808–811. doi: 10.1126/science.1118510

Poczai, P., Cernák, I., Varga, I., and Hyvönen, J. (2014). Analysis of the genome sequence of the flowering plant *Arabidopsis thaliana*. *Genet. Resour. Crop. Evol.* 61, 796–815. doi: 10.1134/S1022795411020074

Priya, P., Yadav, A., Chand, J., and Yadav, G. (2018). Terzyme: a tool for identification and analysis of the plant terpenome. *Plant Methods* 14, 1–18. doi: 10.1186/s13007-017-0269-0

Ramya, M., An, H. R., Baek, Y. S., Reddy, K. E., and Park, P. H. (2018). Orchid floral volatiles: biosynthesis genes and transcriptional regulations. *Sci. Hortic.* 235, 62–69. doi: 10.1016/j.scienta.2017.12.049

Ramya, M., Park, P. H., Chuang, Y. C., Kwon, O. K., An, H. R., Park, P. M., et al. (2019). RNA sequencing analysis of *cymbidium goeringii* identifies floral scent biosynthesis related genes. *BMC Plant Biol.* 19:337. doi: 10.1186/s12870-019-1940-6

Rozewicki, J., Li, S., Amada, K. M., Standley, D. M., and Katoh, K. (2019). MAFFT-DASH: integrated protein sequence and structural alignment. *Nucleic Acids Res.* 47, W5–W10. doi: 10.1093/nar/gkz342

Schmutz, J., Cannon, S. B., Schlueter, J., Ma, J., Mitros, T., Nelson, W., et al. (2010). Genome sequence of the palaeopolyploid soybean. *Nature* 463, 178–183. doi: 10.1038/nature08670

Starks, C. M., Back, K., Chappell, J., and Noel, J. P. (1997). Structural basis for cyclic terpene biosynthesis by tobacco 5-epi- aristolochene synthase. *Science* 277, 1815–1820. doi: 10.1126/science.277.5333.1815

Sun, Y., Wang, G., Li, Y., Jiang, L., Yang, Y., and Guan, S. (2016). De novo transcriptome sequencing and comparative analysis to discover genes related to floral development in *Cymbidium faberi* Rolfe. *Springerplus* 5:1458. doi: 10.1186/s40064-016-3089-1

Tholl, D. (2015). Biosynthesis and biological functions of terpenoids in plants. *Adv. Biochem. Eng. Biotechnol.* 148, 63–106. doi: 10.1007/10_2014_295

Tian, C., Liu, S., Jiang, L., Tian, S., and Wang, G. (2020). The expression characteristics of methyl jasmonate biosynthesis–related genes in *Cymbidium faberi* and influence of heterologous expression of *CfJMT* in *Petunia hybrida*. *Plant Physiol. Biochem.* 151, 400–410. doi: 10.1016/j.plaphy.2020.03.051

Troshin, P. V., Procter, J. B., and Barton, G. J. (2011). Java bioinformatics analysis web services for multiple sequence alignment-JABAWS:MSA. *Bioinformatics* 27, 2001–2002. doi: 10.1093/bioinformatics/btr304

Vranová, E., Coman, D., and Gruissem, W. (2013). Network analysis of the MVA and MEP pathways for isoprenoid synthesis. *Annu. Rev. Plant Biol.* 64, 665–700. doi: 10.1146/annurev-arplant-050312-120116

Wagner, K. H., and Elmadfa, I. (2003). Biological relevance of terpenoids: overview focusing on mono-, di- and tetraterpenes. *Ann. Nutr. Metab.* 47, 95–106. doi: 10.1159/000070030

Yu, Z., Zhao, C., Zhang, G., Teixeira da Silva, J. A., and Duan, J. (2020). Genome-wide identification and expression profile of TPS gene family in *Dendrobium officinale* and the role of *DoTPS10* in linalool biosynthesis. *Int. J. Mol. Sci.* 21, 1–22. doi: 10.3390/ijms21155419

Zhang, J., Li, Y., Liu, B., Wang, L., Zhang, L., Hu, J., et al. (2018). Characterization of the Populus Rab family genes and the function of PtRabE1b in salt tolerance. *BMC Plant Biol.* 18:124. doi: 10.1186/s12870-018-1342-1

Zhang, Z., Li, J., Zhao, X. Q., Wang, J., Wong, G. K. S., and Yu, J. (2006). KaKs_calculator: calculating Ka and Ks through model selection and model averaging. *Genomics Proteomics Bioinformatics* 4, 259–263. doi: 10.1016/S1672-0229(07)60007-2

Zhang, G. Q., Xu, Q., Bian, C., Tsai, W. C., Yeh, C. M., Liu, K. W., et al. (2016). The *Dendrobium catenatum* Lindl. genome sequence provides insights into polysaccharide synthase, floral development and adaptive evolution. *Sci. Rep.* 6, 1–10. doi: 10.1038/srep19029

Zhao, C., Yu, Z., Teixeira da Silva, J. A., He, C., Wang, H., Si, C., et al. (2020). Functional characterization of a *Dendrobium officinale* geraniol synthase *DoGES1* involved in floral scent formation. *Int. J. Mol. Sci.* 21:7005. doi: 10.3390/ijms21197005

Zhou, H. C., Shamala, L. F., Yi, X. K., Yan, Z., and Wei, S. (2020). Analysis of terpene synthase family genes in *Camellia sinensis* with an emphasis on abiotic stress conditions. *Sci. Rep.* 10:933. doi: 10.1038/s41598-020-57805-1

Conflict of Interest: The authors declare that the research was conducted in the absence of any commercial or financial relationships that could be construed as a potential conflict of interest.

Publisher's Note: All claims expressed in this article are solely those of the authors and do not necessarily represent those of their affiliated organizations, or those of the publisher, the editors and the reviewers. Any product that may be evaluated in this article, or claim that may be made by its manufacturer, is not guaranteed or endorsed by the publisher.

Copyright © 2021 Wang, Zhu, Yu, Bi, Zhou, Chen, Chen, Zhang, Ai, Liu and Lan. This is an open-access article distributed under the terms of the Creative Commons Attribution License (CC BY). The use, distribution or reproduction in other forums is permitted, provided the original author(s) and the copyright owner(s) are credited and that the original publication in this journal is cited, in accordance with accepted academic practice. No use, distribution or reproduction is permitted which does not comply with these terms.

frontiers in Plant Science

REVIEW
published: 14 January 2022
doi: 10.3389/fpls.2021.802802

S1-bZIP Transcription Factors Play Important Roles in the Regulation of Fruit Quality and Stress Response

Hong Wang[1,2†], Yunting Zhang[2,3†], Ayla Norris[4] and Cai-Zhong Jiang[2,4]*

[1] Jiangsu Key Laboratory for Horticultural Crop Genetic Improvement, Institute of Pomology, Jiangsu Academy of Agricultural Sciences, Nanjing, China, [2] Department of Plant Sciences, University of California at Davis, Davis, CA, United States, [3] College of Horticulture, Sichuan Agricultural University, Chengdu, China, [4] Crops Pathology and Genetics Research Unit, United States Department of Agriculture, Agricultural Research Service, Davis, CA, United States

Sugar metabolism not only determines fruit sweetness and quality but also acts as signaling molecules to substantially connect with other primary metabolic processes and, therefore, modulates plant growth and development, fruit ripening, and stress response. The basic region/leucine zipper motif (bZIP) transcription factor family is ubiquitous in eukaryotes and plays a diverse array of biological functions in plants. Among the bZIP family members, the smallest bZIP subgroup, S1-bZIP, is a unique one, due to the conserved upstream open reading frames (uORFs) in the 5′ leader region of their mRNA. The translated small peptides from these uORFs are suggested to mediate Sucrose-Induced Repression of Translation (SIRT), an important mechanism to maintain sucrose homeostasis in plants. Here, we review recent research on the evolution, sequence features, and biological functions of this bZIP subgroup. S1-bZIPs play important roles in fruit quality, abiotic and biotic stress responses, plant growth and development, and other metabolite biosynthesis by acting as signaling hubs through dimerization with the subgroup C-bZIPs and other cofactors like SnRK1 to coordinate the expression of downstream genes. Direction for further research and genetic engineering of S1-bZIPs in plants is suggested for the improvement of quality and safety traits of fruit.

Keywords: uORF, amino acid metabolism, sugar metabolism, biotic and abiotic stress, plant growth and development

OPEN ACCESS

Edited by:
Pei Xu,
China Jiliang University, China

Reviewed by:
Chong Cai,
China Jiliang University, China
Rakesh Srivastava,
National Botanical Research Institute (CSIR), India

***Correspondence:**
Cai-Zhong Jiang
cjiang@ucdavis.edu;
caizhong.jiang@usda.gov

† These authors have contributed equally to this work

Specialty section:
This article was submitted to Crop and Product Physiology, a section of the journal Frontiers in Plant Science

Received: *27 October 2021*
Accepted: *20 December 2021*
Published: *14 January 2022*

Citation:
Wang H, Zhang Y, Norris A and Jiang C-Z (2022) S1-bZIP Transcription Factors Play Important Roles in the Regulation of Fruit Quality and Stress Response. Front. Plant Sci. 12:802802. doi: 10.3389/fpls.2021.802802

INTRODUCTION

Plants have developed diverse mechanisms to regulate their biological and metabolic processes via transcription factor (TF) regulatory networks (Riechmann et al., 2000). Among the TF families, the basic leucine zipper (bZIP) family is present in all eukaryotes and is one of the largest and most diverse TF groups in higher plants. There are about four times more bZIP genes in the *Arabidopsis* genome than in the genomes of other model organisms such as *Saccharomyces cerevisiae*, *Caenorhabditis elegans*, and *Drosophila melanogaster* (Riechmann et al., 2000). Large numbers of bZIP TF family members have been found in many plant species including rice (Nijhawan et al., 2008), maize (Wei et al., 2012), tomato (Li D. et al., 2015), common wheat (Li X. et al., 2015), sorghum (Wang et al., 2011), soybean (Liao et al., 2008), banana (Hu et al., 2016a), cassava (Hu et al., 2016b), grape (Liu J. et al., 2014), peach (Wang et al., 2015), strawberry (Wang et al., 2015; Zhang et al., 2022), apple (Wang et al., 2015; Li et al., 2016), rapeseed (Zhou et al., 2017), radish (Fan et al., 2019), cucumber (Baloglu et al., 2014), tea plant (Xue et al., 2018), sweet potato

(Yang Y. et al., 2019), watermelon/melon (Unel et al., 2019), Chinese jujube (Zhang et al., 2020a), pepper (Gai et al., 2020), Chinese pear (Manzoor et al., 2021), poplar (Zhao et al., 2021), quinoa (Li et al., 2020) and plum (Li et al., 2021).

The bZIP family is phylogenetically categorized into different groups, with different species having various members of homologs. For example, the *Arabidopsis* AtbZIP family members were systematically classified into 10 groups (A–I and S) based on conserved motifs (Jakoby et al., 2002). Subsequently, a more complete classification was expanded into 13 groups, designated as A-J, M, and S (Corrêa et al., 2008). The tomato SlbZIPs were classified as nine clades (Li D. et al., 2015). The cucumber CsbZIPs and sorghum SbbZIPs were separately categorized into six and seven groups (Wang et al., 2011; Baloglu et al., 2014). The bZIP family in both rice and maize has 11 groups which are the same as castor bean (Nijhawan et al., 2008; Wei et al., 2012; Jin et al., 2014). The plum PmbZIP proteins were divided into 12 groups (Li et al., 2021). Chinese pear PbbZIPs were categorized into 13 groups (Manzoor et al., 2021). Several interspecies clustering studies indicate that the S group found in *Arabidopsis* has especially high homology across different species (Li D. et al., 2015; Li et al., 2020; Manzoor et al., 2021), although some clades might be specific to *Arabidopsis* compared to peach, strawberry, and apple (Wang et al., 2015).

These classifications, phylogeny, and homology analyses define the possible biological roles of bZIPs in green plant evolution (Corrêa et al., 2008). Basic leucine zipper TFs orchestrate a diverse array of functions in multiple biological processes including flower development (Chuang et al., 1999; Walsh and Freeling, 1999; Strathmann et al., 2001; Abe et al., 2005; Wigge et al., 2005; Muszynski et al., 2006; Romera-Branchat et al., 2020) and pollen development (Gibalová et al., 2009; Iven et al., 2010), seed maturation (Izawa et al., 1994; Toh et al., 2012; Zinsmeister et al., 2016; Jain et al., 2018), senescence (Smykowski et al., 2015), light signaling (Chen et al., 2013; Abbas et al., 2014; Xu, 2020), anthocyanin and chlorophyll biosynthesis (An et al., 2017; Wang et al., 2020), nutrient signaling (Dröge-Laser and Weiste, 2018; Pedrotti et al., 2018; Yang Z. et al., 2019), hormone signaling such as salicylic acid, ABA, ethylene, auxin, and cytokinin (Singh et al., 2002; Li et al., 2011; Weiste and Dröge-Laser, 2014; Zong et al., 2016; Xu et al., 2018; Lv et al., 2019; Srivastava et al., 2019), sugar signaling (Kang et al., 2010; Ma et al., 2011; Thalor et al., 2012; Sagor et al., 2016), and abiotic/biotic stress signaling (Tsugama et al., 2012, 2016; Alves et al., 2013; Zong et al., 2016; Sun et al., 2017; Li et al., 2019; Yang J. et al., 2019; Carianopol et al., 2020) in plants.

Group S is the largest bZIP subgroup in several species such as *Arabidopsis* (Jakoby et al., 2002) and safflower (Li et al., 2020) and comprises three to four even smaller subgroups. In this review, we focus on the well-studied S1-bZIP subgroup, whose members contain unique conserved upstream open reading frames (uORFs) in the 5′ region of their transcripts and play important regulatory roles in many metabolic processes relating to fruit quality and stress responses. Our review aims to provide perspectives for further surveying the biological function, exploring regulatory mechanisms, and genome engineering the S1-bZIPs to obtain desirable traits for quality improvement in horticultural plants.

CLASSIFICATION AND STRUCTURE OF S1-bZIPs

Of the AtbZIPs, the 17 members of the S group are further separated into three subgroups based on homology: S1, S2, and S3 (Ehlert et al., 2006). The S1 subgroup (S1-bZIP) in *Arabidopsis* contains five members: AtbZIP1, −2, −11, −44, and −53. Recent studies indicate that other species, including many horticultural plants, also have multiple members of the S1-bZIP subgroup (**Figure 1A** and **Supplementary Table 1**). Like other bZIP members, those in the S1 subgroup are characterized by a conserved bZIP domain, composed of two functionally distinct motifs (a basic region and a leucine zipper) located on a contiguous α-helix. The basic region of −18 amino acids contains, sequentially, a nuclear localization signal and an invariant N-x7-R/K-x9 motif for DNA binding. This motif preferentially binds to the A-box, C-box, and G-box of target promoters which contain DNA sequences with an ACGT core (Jakoby et al., 2002; Dröge-Laser et al., 2018; Li et al., 2021). The leucine zipper comprises a heptad repeat of leucines or other numerous hydrophobic amino acids (L-x_6-L-x_6-L) (**Figure 1B**). Compared to other groups, members of the S group include the extraordinarily high number of eight hydrophobic amino acid repeats (Ehlert et al., 2006; Dröge-Laser et al., 2018) (**Figure 1B**). The two subunits form a zipper structure that binds DNA to form dimers through interactions with the hydrophobic sides of the helices (Jakoby et al., 2002). Of three S subgroups, only members of the S1 subgroup show specific heterodimerization with C group bZIP proteins (C-bZIPs), whereas weak homodimerization within members of the S1 subgroup is detected (Ehlert et al., 2006; Peviani et al., 2016). Phylogenetic analysis between S1 and C group bZIPs from angiosperms, gymnosperms, mosses, and algae suggests that the S1 and C groups evolved from a proto-S/C bZIP in algae species that homodimerized, which has since diverged into heterodimerizing pairs prior to the evolution of seeds plants (Peviani et al., 2016).

UNIQUE UPSTREAM OPEN READING FRAME STRUCTURE AND TRANSLATIONAL REGULATION MECHANISM OF S1-bZIPs

Besides their common structural features, S1-bZIPs are unique in that they have an unusually long 5′-leader sequence in the upstream region of the main open reading frame (mORF) of the mRNA. This leader sequence contains several upstream open reading frames (uORFs) that encode small peptides (Dröge-Laser et al., 2018). Among those, the second uORF is conserved and encodes a Sucrose Control peptide (SC-peptide) of 28 residues, which regulates the translation of the mORF and reduces protein expression through a mechanism known as Sucrose-Induced Repression of Translation (SIRT), which contributes to sucrose

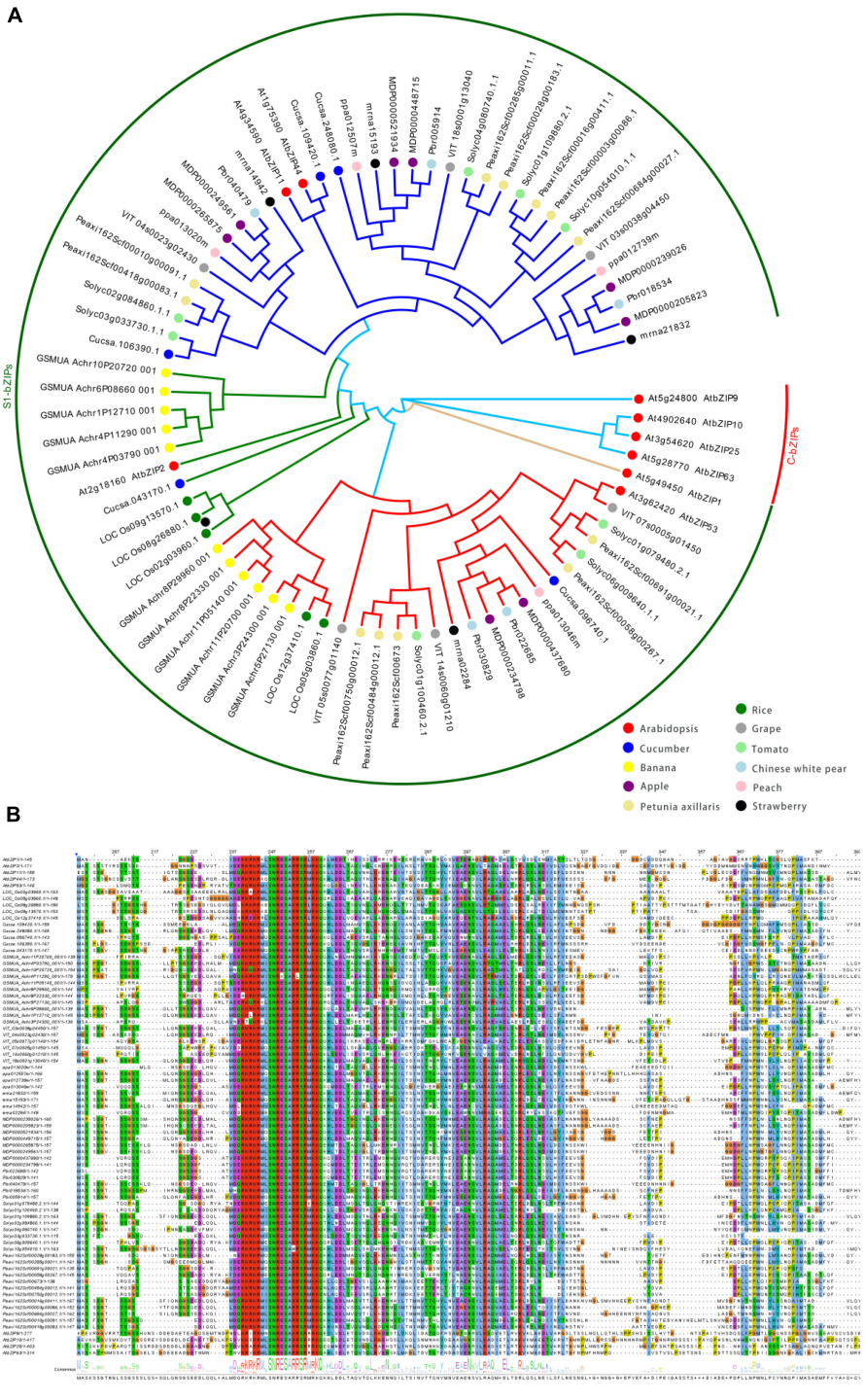


FIGURE 1 | Phylogenetic analysis of S1-bZIPs in some species. **(A)** The phylogenetic tree was constructed by the neighbor-joining method (NJ) using MEGAx software. The phylogenetic trees were drawn with EvoView at the following URL: https://www.evolgenius.info/evolview/. Colored dots represent members from various species. The proteins were classified into six different clades. Each clade was assigned a different color according to their inclusion of each *Arabidopsis* S1-bZIP member. **(B)** The predicted amino acid sequences encoded by the *Arabidopsis* S1 and C group bZIP mORFs are aligned with the S1 homologs from other species using the multiple sequence alignment tools of ClustalW (Chenna et al., 2003) and the alignment results were displayed using Jalview (Waterhouse et al., 2009). The addition of the *Arabidopsis* C-bZIP serves as an outgroup.

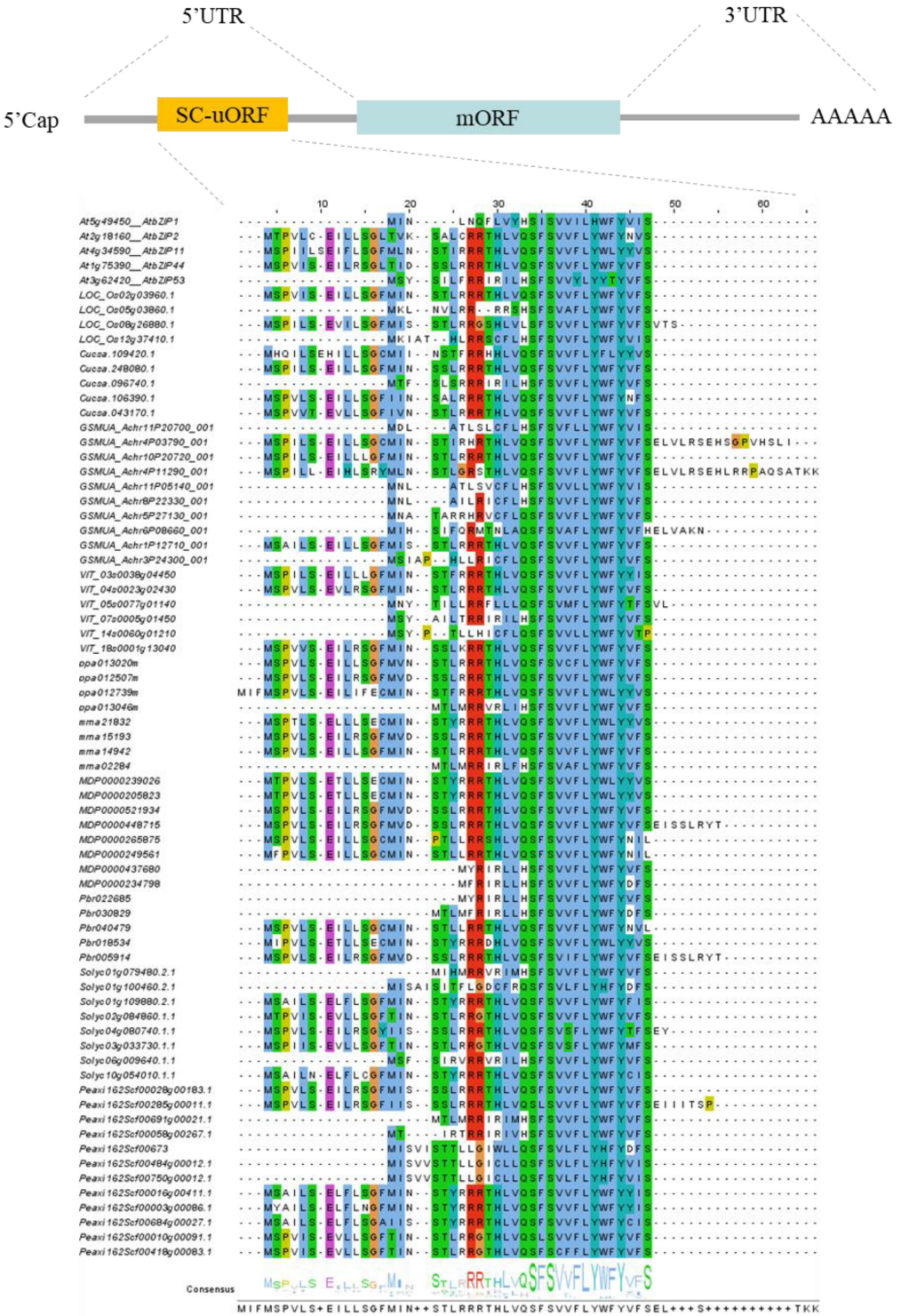


FIGURE 2 | Full-length gene structure of the S1-bZIPs, and alignment of the highly conserved S1-bZIP uORFs encoding the sucrose control peptide (SC-peptide) from some species. Conserved amino acids are depicted in color.

homeostasis in the cells (Wiese et al., 2004; Rahmani et al., 2009). Here, we summarize uORFs of the S1-bZIP subgroup from different horticultural plants, including banana (Hu et al., 2016a), grape (Liu J. et al., 2014), apple (Wang et al., 2015), peach (Wang et al., 2015), cucumber (Baloglu et al., 2014), strawberry (Baloglu et al., 2014; Zhang et al., 2022), petunia

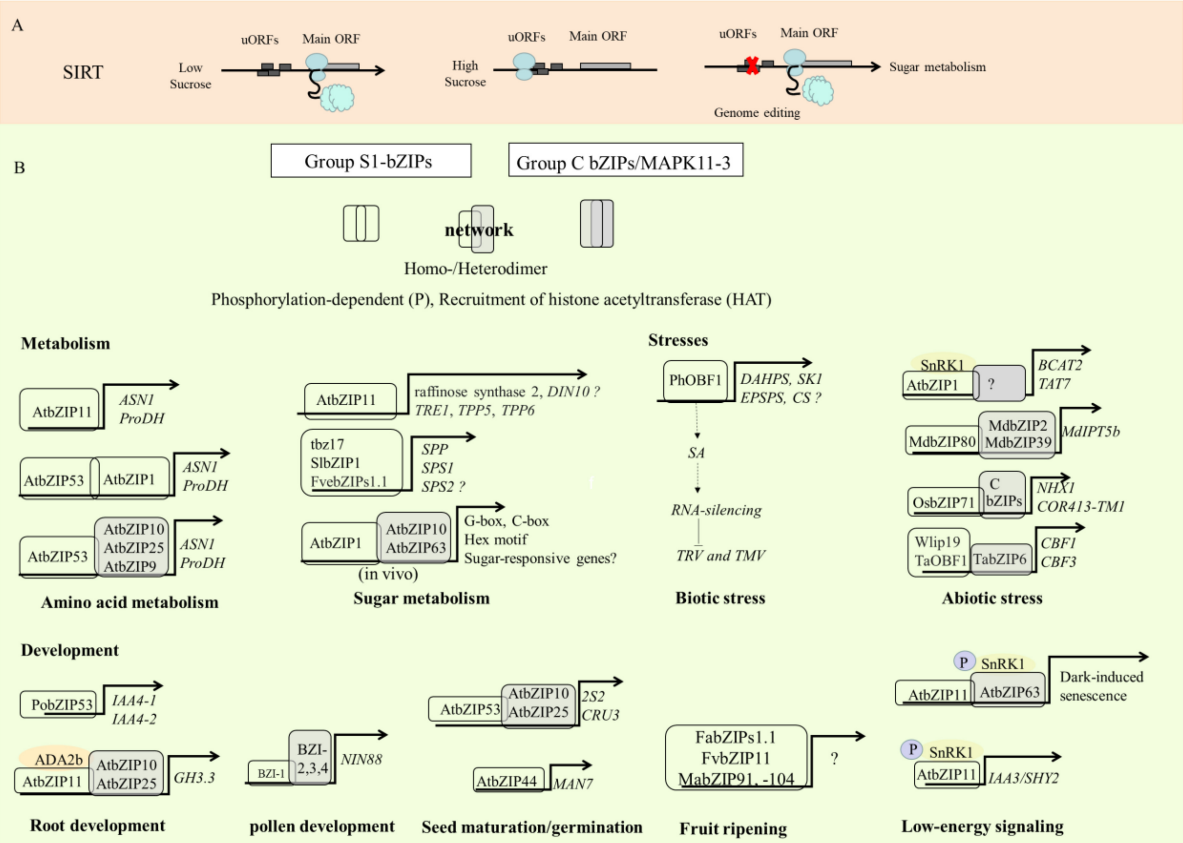


FIGURE 3 | Multiple levels of regulation and biological function of S1-bZIPs. **(A)** Translation regulation of S1-bZIPs by SIRT. SIRT: Sucrose-induced repression of translation. **(B)** Biological function and target genes regulated by S1-bZIP. The regulated target genes by S1-bZIP (white) or heterodimers of S1-bZIPs and C-bZIPs (gray). Gene names: *ASN1*, *ASPARAGINE SYNTHETASE 1*; *ProDH*, *Proline Dehydrogenase*; *TRE1*, *Trehalase 1*; *TPP5/-6*, *trehalose-phosphate phosphatase 5/-6*; *SPP*, *sucrose-phosphatase*; *SPS1/-2*, *sucrose-phosphate synthase 1/-2*; *HXK1*, *hexokinase 1*; *DAHPS*, *3-Deoxy-D-arabino-heptulosonate 7-phosphate synthase*; *SK1*, *shikimate kinase 1*; *EPSPS*, *5-enolpyruvylshikimate 3-phosphate synthase*; *CS*, *chorismate synthase*; *BCAT2, BRANCHED-CHAIN AMINO ACID TRANSAMINASE2; TAT7*, *TYROSINE AMINOTRANSFERA- SE7; IPT5b*, *Isopentenyltransferase 5b*; *NHX1*, *Na+/H+exchanger 1*; *COR413-TM1*, cold acclimation protein; *CBF1/-3*, *C-repeat/DRE binding factor 1/-3*; ADA2b: transcriptional adapter ADA2b; *IAA4-1/4-2/-3*, *INDOL-3-ACETIC ACID INDUCIBLE 4-1/4-2/-3*; *SHY2*, *SHORT HYPOCOTYL 2*; *GH3.3*, *Indole-3-acetic acid-amido synthetase*; *NIN88*, *Defective invertase*; *2S2*, *SEED STORAGE ALBUMIN*; *CRU3*, *CRUCIFERIN* 3; *MAN7*, *endo-beta-mannase 7*; P, phosphorylation.

(Sun et al., 2017), and white pear (Wu et al., 2013) (**Figure 2** and **Supplementary Table 1**).

The regulation of gene expression involves different layers, including transcriptional and translational controls (van der Horst et al., 2020). Compared with transcriptional regulation, translational control allows more immediate responses to adjust protein expression and reprogram metabolism upon cellular signals or environmental stimuli (Jorgensen and Dorantes-Acosta, 2012; Chen et al., 2020). The translation process of mRNA includes four major steps: initiation, elongation, termination, and ribosome re-initiation (van der Horst et al., 2020). Translation initiation is the major step that determines the rate of protein biosynthesis and is regulated by multiple mechanisms (Sonenberg and Hinnebusch, 2009; Jackson et al., 2010; Hinnebusch et al., 2016; Zhang et al., 2019; van der Horst et al., 2020). uORFs have been suggested to play a critical role in regulating the translation of the mORF (Morris and Geballe, 2000; Kochetov, 2008; Ruiz-Orera and Albà, 2019). uORFs of S1-bZIPs are involved in the translational regulation in a SIRT manner (Jorgensen and Dorantes-Acosta, 2012; von Arnim et al., 2014). The SC-peptide encoded by the uORF in the 5′leader region of *AtbZIP11* is capable of repressing translation of the subsequent mORF in the presence of sucrose (Rahmani et al., 2009). High sucrose levels enhance ribosome stalling on the uORF, which results in poor translation of the mORF (Rook et al., 1998; Hummel et al., 2009; Peviani et al., 2016; Merchante et al., 2017; van der Horst et al., 2020) (**Figure 3A**). The members of the *Arabidopsis* S1-bZIP subfamily show similar responses to sucrose. Translation of *AtbZIP1*, *AtbZIP2*, *AtbZIP11*, *AtbZIP44* and *AtbZIP53* is downregulated by sucrose (Rook et al., 1998; Price et al., 2004; Kang et al., 2010). Transgenic seedlings with 35S:bZIP11 5′ leader::LUC show significantly reduced luciferase activities when treated with sucrose while those incubated in media lacking sucrose show two- to three-fold higher luciferase activities (Rahmani et al., 2009). SIRT-mediating S1-bZIP orthologs exist in all seed plants (Peviani et al., 2016).

Previous research showed that amino acids such as serine, leucine, and tyrosine in the conserved peptide of uORF are essential for SIRT (Rahmani et al., 2009). However, it has been shown that expressing the gymnosperm 5′uORF sequence, which only contains the conserved leucine and tyrosine in *Arabidopsis* cells efficiently mediates the translational repression of the LUC reporter gene in response to sucrose (Peviani et al., 2016). This study suggests that the SIRT mechanism most likely depends on structural conformation, but not on recognition of specific sequence motifs (Peviani et al., 2016). Recently, interesting research conducted using gene-editing technology in strawberry demonstrated that uORFs are involved in regulating protein translation efficiency and sucrose content (Xing et al., 2020) (**Figure 3A**). In the study, to manipulate the SC-uORF of *FvebZIPs1.1*, the start codons of the uORF and the codons encoding a conserved pair of amino acid arginine within the SC-peptide were edited using the CRISPR/Cas9 system. Mutations in the start codons and the conserved C-terminal region of the SC-peptide significantly reduced translation of the SC-uORF. This consequently enhanced the translation efficiency of the downstream mORF. Seven novel alleles with C-to-T substitutions and small deletions within the uORF were identified. To test if phenotypic effects were additive in heterozygous and biallelic plants, 4000 T1 seedlings were generated by crossing the biallelic and homozygous T0 mutants to each other and to wild type. 35 novel genotypes were obtained in T1 and inherited in T2 generation. In comparison with wild-type fruits, the mutants had significantly higher levels of fructose, glucose, and total sugar contents, demonstrating that engineering the conserved SC-uORF of *FvebZIPs1.1* can increase the sugar content in strawberry (Xing et al., 2020). In addition, the citric acid content was slightly lower in the homozygous mutants than that in wild type. A continuum of gradual increase of sugar contents was generated in T1 by combining heterozygous, homozygous, and biallelic mutants, and inherited in T2 generation by propagating stolons of these T1 mutants, therefore confirming the transmissibility of novel genotypes and phenotypes from T1 to T2 by asexual propagation (Xing et al., 2020). Given that sugars can modulate multiple growth and development processes, the agricultural traits including leaf shapes, leaf areas, plant height, growth rates, pollination, fruit size and fruit weight were further evaluated in *FvebZIPs1.1* uORF mutants. Remarkably, editing SC-uORF does not severely impair plant growth. The agricultural traits in *FvebZIPs1.1* uORF mutants were similar to wild-type (Xing et al., 2020), whereas impaired phenotypes and retarded growth are observed in transgenic lines with the overexpression of *AtbZIP11*, *tbz17*, and *FvbZIP11* mORF (Ma et al., 2011; Thalor et al., 2012; Zhang et al., 2022). Taken together, this suggests a broad application of editing uORFs of S1-bZIPs for quality improvement in horticultural plants.

S1-bZIPs AFFECT AMINO ACID METABOLISM

Amino acids are not only involved in plant response to stress but also influence fruit flavor (Keutgen and Pawelzik, 2008). For example, asparagine is present in almost all fruits and determines fruit flavor and quality in a concentration-dependent manner (Aisala et al., 2020). Glutamate is responsible for "umami" or savory taste (Lindemann, 2001). Glycine, alanine, serine, threonine, proline, glutamine, and lysine are highly correlated with sweetness (Sagor et al., 2016), while phenylalanine and tyrosine are bitter (Belitz et al., 2001). The molecular taste receptor, found in humans and rodents, responds to asparagine and aspartic acid (Nelson et al., 2002). Asparagine is considered to serve as a nitrogen storage molecule and synthesized at night under low-carbon conditions (Lam et al., 1994; Hanson et al., 2008). Asparagine and glutamate are synthesized from aspartate and glutamine through ASPARAGINE SYNTHETASE1 (ASN) (Lam et al., 1994; Hanson et al., 2008). A high sugar content represses the expression of *ASN* and reduces asparagine content (Lam et al., 1994). Likewise, proline levels change in response to energy levels. PROLINE DEHYDROGENASE (ProDH) converts proline to glutamate (Hayashi et al., 2000). Recent studies demonstrate that S1-bZIPs directly regulate the expression of *ProDH* and *ASN1 via* binding to the C-boxes, ACT motifs (ACTCAT), and G-boxes in their promoters, thereby influencing amino acid metabolism (Weltmeier et al., 2006; Hanson et al., 2008; Dietrich et al., 2011). Overexpression of *tbz17* mORF in tobacco significantly induces the expression of *ASN*, whereas silencing of *tbz17* represses the expression of *ProDH* and *ASN* (Thalor et al., 2012). One of the target genes of AtbZIP53 is *ProDH2* (Satoh et al., 2004). Overexpression of *SlbZIP1* and *AtbZIP11* mORFs in the transgenic tomato and *Arabidopsis* significantly up-regulates the expression of *ASN1* and *ProDH2* and affects amino acid contents (Hanson et al., 2008; Dietrich et al., 2011; Thalor et al., 2012; Sagor et al., 2016). For example, overexpression of *SlbZIP1* increases the content of alanine, aspartic acid, glutamate, serine, threonine, tyrosine, and total amino acid content. Energy deprivation induces the expression of *ASN1* and *ProDH*, which contributes to the recycling of amino acids to mitigate deficits of carbon, nitrogen, and energy (Dietrich et al., 2011). Many amino acid catabolism related genes induced by *AtbZIP11* are largely repressed by treatments with sugar (Hanson et al., 2008). Moreover, under high-sucrose conditions, the translation of AtbZIP11 is inhibited *via* a uORF (Hanson et al., 2008; Yamashita et al., 2017). These findings indicate that *ASN1* and *ProDH* are ultimately regulated in a sugar-dependent manner, with AtbZIP11 acting as the link between sugar signaling and amino acid/nitrogen metabolism (Hanson et al., 2008). Additionally, AtbZIP1 and AtbZIP53 are also involved in modulating amino acid metabolism during stress responses (Baena-González et al., 2007; Hartmann et al., 2015). In *Arabidopsis*, it has been demonstrated that AtbZIP53 preferentially forms heterodimers with group C-bZIP members like AtbZIP9, AtbZIP10, and AtbZIP25 for controlling the gene expression of *ASN1* and *ProDH* (Weltmeier et al., 2006; Garg et al., 2019) (**Figure 3B**). However, the interacting partners between the S1- and C-bZIPs are not identified in many other crops and need to be investigated in the future.

S1-bZIPs AFFECT SUGAR METABOLISM

Overexpression of S1-bZIP mORFs induces sugar-related gene expression and increases sugar content (**Figure 3B**). Previous studies have shown that overexpression of *tbz17* and *SlbZIP1* mORF up-regulates the expression level of genes encoding sucrose phosphate synthase (*SPS*) and sucrose phosphate phosphatase (*SPP*), whereas silencing *tbz17* down-regulates the expression of these genes (Thalor et al., 2012). Knockout and overexpression of *AtbZIP1* affects sugar-responsive gene expression (Kang et al., 2010). Furthermore, it has been demonstrated that constitutive expression of the *S1-bZIP1*s such as *tbz17 and AtbZIP11* mORF significantly increases the sucrose concentration in transgenic lines (Ma et al., 2011; Thalor et al., 2012). Interestingly, the contents of glucose and fructose were significantly increased and the citric acid content was significantly decreased in transgenic plants with overexpression *AtbZIP11* (Ma et al., 2011). The induction of the *AtbZIP11* mORF also results in the up-regulation of genes associated with the metabolism of trehalose, myo-inositol and raffinose. Transgenic *Arabidopsis* lines overexpressing *AtbZIP11* showed decreased contents of the trehalose-6-phosphate (T6P), limiting the plant's ability to use available sugars, thereby slowing plant growth. This growth inhibition in *Arabidopsis* cannot be reversed by the exogenous application of metabolizable sugars such as glucose and sucrose (Ma et al., 2011). The use of the fruit-specific E8 promoter to drive overexpression of *SlbZIP1* increases the sugar contents in tomato while avoiding growth impairment (Sagor et al., 2016). Remarkably, sucrose contents were approximately sixfold higher in transgenic lines with approximately 1.5-fold higher fructose, glucose, and total sugar contents than in wild type. Similar effects such as significantly increased glucose and fructose contents and significantly reduced citric acid content were observed in mutants with enhanced *FvebZIP1.1* mORF protein expression due to the uORFs mutation (Xing et al., 2020). In a recent study, heterologous overexpression of strawberry *FvbZIP11* affects fruit quality and flavor in tomato (Zhang et al., 2022). In comparison with wild type, the total soluble solid was significantly increased at the breaker, pink and red ripe stages in three transgenic tomato lines. The soluble sugar (SS) content was significantly accumulated at 30–50 days after anthesis in transgenic line 6. In addition, the titratable acid content (TTA) was significantly reduced at 30 days after anthesis, while SS/TTA ratio was significantly increased from 20 to 50 days after anthesis in the transgenic tomato line (Zhang et al., 2022). Taken together, these studies demonstrate that the S1-bZIPs play important roles in the regulation of sugar metabolism for quality improvement in plants.

REGULATORY ROLES OF S1-bZIPs IN RESPONSE TO BIOTIC AND ABIOTIC STRESSES

S1-bZIPs play an essential role in plant adaptation to unfavorable conditions (Alves et al., 2013; Sornaraj et al., 2016; Noman et al., 2017) (**Figure 3B**). It has been documented that S1-bZIPs play important roles in plant innate immunity, especially against attack by various pathogens (Lee et al., 2002; Alves et al., 2013), and in response to abiotic stresses, such as cold (Shimizu et al., 2005; Kobayashi et al., 2008), drought (Ditzer and Bartels, 2006; Shekhawat and Ganapathi, 2014), and salinity (Hartmann et al., 2015). It has been demonstrated that the C-/S1-bZIP-SnRK1 complex participates in the reprogramming of primary metabolism related to carbohydrate and amino acid and induces salt stress tolerance through ABA-independent signaling in *Arabidopsis* roots (Hartmann et al., 2015). Similarly, C-/S1-bZIP-SnRK1 signaling is involved in defenses against biotic stresses, which are also energy-consuming processes that require metabolic readjustment in plants (Hulsmans et al., 2016). Research in our laboratory has suggested that petunia PhOBF1, a homolog of AtbZIP11, is involved in plant defenses against a wide range of viral pathogens (Sun et al., 2017). In the study, silencing *PhOBF1* resulted in the reduction of RNA silencing-related gene expression, including RNA-dependent RNA polymerases, Dicer-like RNase III enzymes, and Argonaut. *PhOBF1*-RNAi plants displayed a compromised resistance to tobacco rattle virus (TRV) and tobacco mosaic virus (TMV). On the other hand, overexpression of *PhOBF1* in petunia enhances resistance to these virus infections. Interestingly, *PhOBF1*-silenced petunia lines produced much lower levels of the compounds associated with the shikimate and phenylpropanoid pathways such as free salicylic acid (SA), salicylic acid glucoside, and phenylalanine, but much higher levels of those were detected in *PhOBF1* overexpressing plants (Sun et al., 2017). Intriguingly, *PhbZIP44*, a paralog of *PhOBF1* appears to be unable to participate in this antiviral process, suggesting functional diversity and specificity among the S1-bZIPs (Sun et al., 2017).

In *Arabidopsis,* S1-bZIPs AtbZIP11/ATB2, AtbZIP44, AtbZIP2/GBF5, and AtbZIP53 can bind to a 6-bp *cis*-acting element (ACTCAT) located in the promoter of *ProDH* (Satoh et al., 2004), which is responsive to hypoosmolarity and proline. AtbZIP53 directly and strongly promotes hypoosmolarity-induced transcription of *ProDH*, which is enhanced by the synergistic interplay between AtbZIP53 and the group C member AtbZIP10 (Satoh et al., 2004; Weltmeier et al., 2006). Analysis of transcriptome data has revealed the complexity of the response to abiotic stresses by S1-AtbZIPs. For instance, the transcript level of *AtbZIP53* was found to be strongly up-regulated by salt stress in roots and by osmotic stress in green tissues. Cold, osmotic, and salt elicitors were found to remarkably increase the expression of *AtbZIP1* in roots and *AtbZIP11* in green tissues but inhibit the expression of *AtbZIP2* in green tissues. *AtbZIP44* shows a solid and specific response to cold stress in the root and to salinity in green tissues (Kilian et al., 2007; Weltmeier et al., 2009). The expression of *AtbZIP1* in roots was significantly induced by salt treatment. *Arabidopsis bzip1 bzip53* double mutant reprograms carbohydrate and amino acid metabolism to help roots adapt to salt stress. Furthermore, AtbZIP1 binds the promoter of *BCAT2* and *TAT7* and plays a role as a signalling module of SnRK1-bZIP1 under salt stress. This pathway is independent of ABA-SnRK2-AREB signaling pathways, whereas *bZIP53* transcription partially depends on the SnRK2/AREB pathway (Hartmann et al., 2015). In tomato, *SlbZIP1* increases

salt tolerance by increasing the gene expression related to ABA biosynthesis and signal transduction (Zhu et al., 2018). In response to water deficiency, two cucumber S1-bZIP member (*CsbZIP6* and *CsbZIP30*) transcripts accumulated in the root but decreased in leaves (Baloglu et al., 2014). Likewise, in sweet potato, the expression of *IbbZIP1* is highly induced by treatments with NaCl and ABA. Abiotic stress-related genes are significantly up-regulated in the transgenic *Arabidopsis* overexpressing *IbbZIP1*, suggesting the role of *IbbZIP1* in salt and drought tolerance (Kang et al., 2019). In apple, an S1-bZIP, *MdbZIP80*, has been shown to negatively regulate cytokinin-mediated drought and salt tolerance (Feng et al., 2021). This study shows that MdbZIP80 specifically heterodimerizes with C-bZIPs MdbZIP2 and MdbZIP39. The formed C-/S1-bZIP complex then binds to the ACTCAT motif in the promoter of *MdIPT5b*, a gene encoding the rate-limiting enzyme isopentenyltransferase in the cytokinin biosynthesis pathway, thereby suppressing its expression. This leads to drought and salt stress response through the cytokinin pathway by delaying drought-induced premature leaf senescence by reducing oxidative damage and maintaining plant growth (Feng et al., 2021). Another study demonstrates that low temperature stress induces *mlipl5* expression, and the protein subsequently binds to the promoter region of *Adh1* (Kusano et al., 1995). Interestingly, mechanical damage in tea leaves leads to the activation of S1-bZIPs such as *CsbZIP2*, *−11*, *−14*, *−16*, *−20*, *−21*, *−28* and *−30* (Xue et al., 2018). Overall, it appears that the expression levels of these *S1-bZIPs* respond to stress signals in a tissue-specific manner. The members of S1-bZIP share partially redundant functions but play a role in unique regulatory mechanisms. Generally, the S1- and C-AtbZIPs heterodimerize to mediate stress signal transduction cascades. For example, S1-bZIP AtbZIP53 forms heterodimers with group C-bZIP members such as AtbZIP10 or AtbZIP25 and increases DNA binding activity, resulting in strong activation of the target genes. These heterodimers can also form tertiary complexes with the non-bZIP protein ABI3 (ABSCISIC ACID INSENSITIVE 3) to play a synergistic role in target gene expression (Alonso et al., 2009; Weltmeier et al., 2009); however, it needs to be demonstrated whether other members of S1-bZIP such as AtbZIP1 heterodimers are formed under stress conditions (Hartmann et al., 2015).

The S1-bZIP gene *low-temperature-induced protein 19* (*lip19*) is significantly induced by low temperature in monocots (Shimizu et al., 2005; Kobayashi et al., 2008; Cai et al., 2018). The LIP19 protein appears to be unable to form homodimers and bind to DNA in rice (Kobayashi et al., 2008). However, the counterpart of LIP19 proteins in maize and wheat can form homodimers and bind to *cis*-elements in DNA sequences (Kobayashi et al., 2008; Cai et al., 2018). The WLIP19 can heterodimerize with wheat TaOBF1, another low temperature-responsive S1-bZIP member. The stable heterodimerization between LIP19-type and OBF1-type proteins seems to induce the expression of target genes in response to different abiotic stresses, especially cold stress (Shimizu et al., 2005; Kobayashi et al., 2008; Cai et al., 2018). However, there is no definitive evidence showing that the formation of heterodimers or homodimers between WLIP19 and TaOBF1 directly affects the expression of the downstream stress-responsive genes including *COR* (cold-responsive) and *LEA* (late embryogenesis-abundant) genes (Lee et al., 2002). Recent research indicates that a group C-bZIP TabZIP6 dimerizes with WLIP19, TaOBF1, or itself and then binds to the promoters of genes encoding CBFs (C-repeat binding factors), resulting in inhibition of their expression. These dimers can also inhibit the expression of some *COR* genes (Liu C. et al., 2014). Rice S1-bZIP plays a vital role in ABA-mediated drought and salt stress response. One of the S1-bZIPs, OsbZIP71, appears to be able to form homodimers and heterodimers with group C-bZIP members OsbZIP15, OsbZIP20, OsbZIP33, and OsbZIP88. It has been speculated that these heterodimers help OsbZIP71 bind to the promoters of its target genes, *OsNHX1,* and *COR413-TM1* because OsbZIP71 on its own has weak DNA-binding activity to the G-box element and no transcriptional activation activity (Liu C. et al., 2014). Thus, the interplay between C-group and S1-subgroup is proposed to affect plant response to stress.

BIOLOGICAL ROLES OF S1-bZIPs AS REGULATORS OF PLANT GROWTH AND DEVELOPMENT

Plant growth and development are tightly interlinked with the control of metabolism, especially energy homeostasis. Transient energy deprivation causes plants to adjust their metabolism to adapt to daily light/dark cycles and unpredictable environmental changes. It has been proposed that the Snf1-related kinase 1 (SnRK1) and Target of Rapamycin (TOR) kinase function to reprogram plant metabolism in response to the energy status (Baena-González et al., 2007; Hulsmans et al., 2016). Evidence suggests that SnRK1 mediates the phosphorylation of S1-bZIPs to control plant growth and development under starvation and nutrient-replete conditions (Lastdrager et al., 2014) (**Figure 3B**). As the transcriptional regulators downstream of SnRK1, AtbZIP11 can directly control a subset of SnRK1-dependent genes *via* binding to G-box elements in their promoter regions (Pedrotti et al., 2018). Furthermore, heterodimerization between group C- and S1-bZIPs is enhanced by the phosphorylation of group C-bZIPs by SnRK1. Phosphorylation of AtbZIP63 provides the structural basis for forming the AtbZIP63-AtbZIP1-SnRK1/AtbZIP63-AtbZIP11-SnRK1 complex and ultimately leads to the adjustment of metabolism to ensure plant survival under low energy conditions (Pedrotti et al., 2018). Notably, the formation of the complex is dependent on the SnRK1-specific phosphorylation sites, which are pivotal for the function of AtbZIP1 and AtbZIP53 (Hartmann et al., 2015). Additionally, the identification of many SnRK1-independent genes regulated by AtbZIP11 indicates a function of AtbZIP11 beyond SnRK1 signaling (Dröge-Laser et al., 2018). It seems that heterodimers within the C-/S1-bZIP network function as a hub to integrate SnRK1-dependent and -independent signals to adjust growth/development and stress responses (Mair et al., 2015). Recent studies showed that S1-bZIPs regulate the root apical meristem size through controlling polar auxin flux (Weiste et al., 2017). Under low-energy conditions, *AtbZIP2*, *AtbZIP11*, and *AtbZIP44* directly

activate the transcription of *INDOLE-3-ACETIC ACID PROTEIN 3/SHORT HYPOCOTYL 2* (*IAA3*/*SHY2*), a negative regulator of auxin signaling, which leads to the down-regulation of *PIN-FORMED (PIN)* genes, limiting polar auxin transport to the root tip and blocking auxin-driven primary root growth (Weiste et al., 2017).

S1-bZIPs play essential roles in plant growth and development, especially seed maturation, root growth, and flower development (**Figure 3B**). For example, the transcript abundance of *AtbZIP53* is markedly induced during the late stages of seed development (Weltmeier et al., 2009). AtbZIP53 enhances the gene expression associated with seed maturation by specific heterodimerization with group C-bZIPs (Alonso et al., 2009). AtbZIP11 and AtbZIP44 play a role in embryogenesis. *AtbZIP44* shows high transcript levels at the early stage of seed development and is involved in micropylar endosperm loosening and seed coat rupture via its interaction with the promoter of *AtMAN7* (Weltmeier et al., 2009). The *atbzip44* knock-out mutant shows slower germination and reduced expression of *AtMAN7* (Iglesias-Fernández et al., 2013). In *Populus*, the binding of poplar bZIP53 to the promoter of *IAA4-1* and *IAA4-2* inhibits adventitious root development (Zhang et al., 2020b). In horticultural plants, three S1-bZIP members (*VvbZIP07*, *14,* and *47*) are highly expressed in grape seed (Liu J. et al., 2014), but their regulatory mechanisms have yet to be elucidated. Other studies have shown that S1-bZIPs are related to floral development. For example, *CsbZIP-06* is highly expressed in female cucumber flowers and ovaries (Baloglu et al., 2014). Transgenic lines overexpressing mORF of *BZI-4* show reduced flower size and impaired pollen development (Iven et al., 2010). Overexpressing *AtbZIP1*, *AtbZIP53*, *tbz17*, *MusabZIP53,* and *FvbZIP11* shortened internode length, and stunted vegetative growth (Alonso et al., 2009; Dietrich et al., 2011; Thalor et al., 2012; Shekhawat and Ganapathi, 2014). *FabZIPs1.1* and *FvbZIP11* have been shown to be involved in fruit ripening in strawberry (Chen et al., 2020; Zhang et al., 2022). Banana *MabZIP91* and *MabZIP104,* which belong to S1-bZIP subgroup, showed high transcript abundance during fruit development and ripening (Chen et al., 2020). These studies illustrate the various roles of S1-bZIPs as a regulator of plant growth and development (**Figure 3B**).

CONCLUDING REMARKS AND FUTURE PERSPECTIVES

The S1-bZIP subgroup, with their functional diversity in all plants, reflects their importance as regulators. The literature covered in this review suggests that the small but unique and crucial S1-bZIP transcription factors play essential roles in the balance of carbon and amino acid metabolism, plant growth and development, and stress responses (**Figure 3**). S1-bZIPs also play important roles in regulating fruit quality and stress response. Through heterodimerization with group C-bZIPs, S1-bZIPs orchestrate an array of downstream transcriptional and metabolic control. However the C group bZIP dimerization partners of many S1-bZIPs have yet to be identified. The S1-bZIPs regulate sugar signaling and amino acid metabolism under energy-deprived conditions, which involves the Sucrose Induced Repression of Translation mechanism of the uORFs and through interaction with the SnRK1 pathway. However, further research is needed to explore whether and how SnRK1 and TOR kinase interact with C- and S1-bZIPs complex. The SC-uORF negatively regulates the translation of S1-bZIP mORFs and, in turn, downstream targets of the S1-bZIPs, which further affect fruit quality and other metabolite biosynthesis. Evidence suggests that overexpression of S1-bZIP mORFs significantly increased the fruit sugar content and sweetness, showing the potential for improvement of fruit quality (Thalor et al., 2012; Sagor et al., 2016; Chen et al., 2020; Zhang et al., 2022). In addition, functional diversity and specificity among the S1-bZIPs need to be further defined. Using substitution of conserved amino acid residues in the DNA-binding domain could be a useful approach to clarify specific interconnections among S1-bZIPs and their dimerization partners in horticultural plants (Garg et al., 2019). Using CRISPR technology to create indel mutations in uORF start codons or enhancing the expression of S1-bZIPs using fruit-specific promoters could provide broad applications to control the levels of sucrose and other nutrients for the improvement of the quality of fruits, vegetables, and flowers, and to improve stress response without the detrimental effects on plant growth and development in horticultural plants (Corrêa et al., 2008; Shipman et al., 2021).

AUTHOR CONTRIBUTIONS

HW, YZ, AN, and C-ZJ collected data and wrote and revised the manuscript. All authors contributed to the article and approved the submitted version.

FUNDING

This work was partially supported by the General Program of the National Natural Science Foundation of China (Grant No. 31872078), United States Department of Agriculture (USDA) CRIS project 2032-21000-025-00D, and Jiangsu Agricultural Science and Technology Independent Innovation Fund [CX(20)2020]. The funders had no role in study design, data collection, and analysis.

ACKNOWLEDGMENTS

We thank Yujing Shi (Bioatgcn Biotechnologies Co. Ltd., Nanjing, China) for providing bioinformatics analysis.

SUPPLEMENTARY MATERIAL

The Supplementary Material for this article can be found online at: https://www.frontiersin.org/articles/10.3389/fpls.2021.802802/full#supplementary-material

REFERENCES

Abbas, N., Maurya, J. P., Senapati, D., Gangappa, S. N., and Chattopadhyay, S. (2014). *Arabidopsis* CAM7 and HY5 physically interact and directly bind to the HY5 promoter to regulate its expression and thereby promote photomorphogenesis. *Plant Cell* 26, 1036–1052. doi: 10.1105/tpc.113.122515

Abe, M., Kobayashi, Y., Yamamoto, S., Daimon, Y., Yamaguchi, A., Ikeda, Y., et al. (2005). FD, a bZIP protein mediating signals from the floral pathway integrator FT at the shoot apex. *Science* 309, 1052–1056. doi: 10.1126/science.1115983

Aisala, H., Manninen, H., Laaksonen, T., Linderborg, K. M., Myoda, T., Hopia, A., et al. (2020). Linking volatile and non-volatile compounds to sensory profiles and consumer liking of wild edible Nordic mushrooms. *Food Chem.* 304:125403. doi: 10.1016/j.foodchem.2019.125403

Alonso, R., Oñate-Sánchez, L., Weltmeier, F., Ehlert, A., Diaz, I., Dietrich, K., et al. (2009). A pivotal role of the basic leucine zipper transcription factor bZIP53 in the regulation of *Arabidopsis* seed maturation gene expression based on heterodimerization and protein complex formation. *Plant Cell* 21, 1747–1761. doi: 10.1105/tpc.108.062968

Alves, M. S., Dadalto, S. P., Gonçalves, A. B., De Souza, G. B., Barros, V. A., and Fietto, L. G. (2013). Plant bZIP transcription factors responsive to pathogens: a review. *Int. J. Mol. Sci.* 14, 7815–7828. doi: 10.3390/ijms14047815

An, J., Qu, F., Yao, J., Wang, X., You, C., Wang, X., et al. (2017). The bZIP transcription factor MdHY5 regulates anthocyanin accumulation and nitrate assimilation in apple. *Hort. Res.* 4:17023. doi: 10.1038/hortres.2017.23

Baena-González, E., Rolland, F., Thevelein, J. M., and Sheen, J. (2007). A central integrator of transcription networks in plant stress and energy signaling. *Nature* 448, 938–942. doi: 10.1038/nature06069

Baloglu, M. C., Eldem, V., Hajyzadeh, M., and Unver, T. (2014). Genome-wide analysis of the bZIP transcription factors in cucumber. *PLoS One* 9:e96014. doi: 10.1371/journal.pone.0096014

Belitz, H. D., Grosch, W., and Schieberle, P. (2001). *Lehrbuch der Lebensmittelchemie: 1.2 Aminosäuren*, 5th Edn. Berlin: Springer Verlag, 9–33.

Cai, W., Yang, Y., Wang, W., Guo, G., Liu, W., and Bi, C. (2018). Overexpression of a wheat (*Triticum aestivum* L.) bZIP transcription factor gene, *TabZIP6*, decreased the freezing tolerance of transgenic *Arabidopsis* seedlings by down-regulating the expression of *CBFs*. *Plant Physiol. Biochem.* 124, 100–111. doi: 10.1016/j.plaphy.2018.01.008

Carianopol, C. S., Chan, A. L., Dong, S., Provart, N. J., Lumba, S., and Gazzarrini, S. (2020). An abscisic acid-responsive protein interaction network for sucrose non-fermenting related kinase1 in abiotic stress response. *Commun. Biol.* 3:145. doi: 10.1038/s42003-020-0866-8

Chen, D., Xu, G., Tang, W., Jing, Y., Ji, Q., Fei, Z., et al. (2013). Antagonistic basic helix-loop-helix/bZIP transcription factors form transcriptional modules that integrate light and reactive oxygen species signaling in *Arabidopsis*. *Plant Cell* 25, 1657–1673. doi: 10.1105/tpc.112.104869

Chen, Q., Tang, Y., Wang, Y., Sun, B., Chen, T., Lei, D., et al. (2020). Enhance sucrose accumulation in strawberry fruits by eliminating the translational repression of *FabZIPs1.1*. *Sci. Hortic.* 259:108850. doi: 10.1016/j.scienta.2019.108850

Chenna, R., Sugawara, H., Koike, T., Lopez, R., Gibson, T. J., Higgins, D. G., et al. (2003). Multiple sequence alignment with the Clustal series of programs. *Nueleic Acid Res.* 31, 3479–3500. doi: 10.1093/nar/gkg500

Chuang, C. F., Running, M. P., Williams, R. W., and Meyerowitz, E. M. (1999). The *PERIANTHIA* gene encodes a bZIP protein involved in the determination of floral organ number in *Arabidopsis thaliana*. *Genes Dev.* 13, 334–344. doi: 10.1101/gad.13.3.334

Corrêa, L. G. G., Riaño-Pachón, D. M., Schrago, C. G., Dos Santos, R. V., Mueller-Roeber, B., and Vincentz, M. (2008). The role of bZIP transcription factors in green plant evolution: adaptive features emerging from four founder genes. *PLoS One* 3:e2944. doi: 10.1371/journal.pone.0002944

Dietrich, K., Weltmeier, F., Ehlert, A., Weiste, C., Stahl, M., Harter, K., et al. (2011). Heterodimers of the *Arabidopsis* transcription factors bZIP1 and bZIP53 reprogram amino acid metabolism during low energy stress. *Plant Cell* 23, 381–395. doi: 10.1105/tpc.110.075390

Ditzer, A., and Bartels, D. (2006). Identification of a dehydration and ABA-responsive promoter regulon and isolation of corresponding DNA binding proteins for the group 4 *LEA* gene *CpC2* from *C. plantagineum*. *Plant Mol. Biol.* 61, 643–663. doi: 10.1007/s11103-006-0038-3

Dröge-Laser, W., and Weiste, C. (2018). The C/S1 bZIP Network: a regulatory hub orchestrating plant energy homeostasis. *Trends Plant Sci.* 23, 422–433. doi: 10.1016/j.tplants.2018.02.003

Dröge-Laser, W., Snoek, B. L., Snel, B., and Weiste, C. (2018). The Arabidopsis bZIP transcription factor family-an update. *Curr. Opin. Plant Biol.* 45, 36–49. doi: 10.1016/j.pbi.2018.05.001

Ehlert, A., Weltmeier, F., Wang, X., Mayer, C. S., Smeekens, S., Vicente-Carbajosa, J., et al. (2006). Two-hybrid protein-protein interaction analysis in *Arabidopsis* protoplasts: establishment of a heterodimerization map of group C and group S bZIP transcription factors. *Plant J.* 46, 890–900. doi: 10.1111/j.1365-313X.2006.02731.x

Fan, L., Xu, L., Wang, Y., Tang, M., and Liu, L. (2019). Genome- and transcriptome-wide characterization of bZIP gene family identifies potential members involved in abiotic stress response and anthocyanin Aiosynthesis in Radish (*Raphanus sativus* L.). *Int. J. Mol. Sci.* 20:E6334. doi: 10.3390/ijms20246334

Feng, Y., Wang, Y., Zhang, G., Gan, Z., Gao, M., Lv, J., et al. (2021). Group-C/S1 bZIP heterodimers regulate *MdIPT5b* to negatively modulate drought tolerance in apple species. *Plant J.* 107, 399–417. doi: 10.1111/tpj.15296

Gai, W., Ma, X., Qiao, Y., Shi, B., Ul Haq, S., Li, Q., et al. (2020). Characterization of the bZIP transcription factor family in pepper (*Capsicum annuum* L.): *CabZIP25* positively modulates the salt tolerance. *Front. Plant Sci.* 11:139. doi: 10.3389/fpls.2020.00139

Garg, A., Kirchler, T., Fillinger, S., Wanke, F., Stadelhofer, B., Stahl, M., et al. (2019). Targeted manipulation of bZIP53 DNA-binding properties influences Arabidopsis metabolism and growth. *J. Exp. Bot.* 70, 5659–5671. doi: 10.1093/jxb/erz309

Gibalová, A., Renák, D., Matczuk, K., Dupľáková, N., Cháb, D., Twell, D., et al. (2009). *AtbZIP34* is required for *Arabidopsis* pollen wall patterning and the control of several metabolic pathways in developing pollen. *Plant Mol. Biol.* 70, 581–601. doi: 10.1007/s11103-009-9493-y

Hanson, J., Hanssen, M., Wiese, A., Hendriks, M. M. W. B., and Smeekens, S. (2008). The sucrose regulated transcription factor bZIP11 affects amino acid metabolism by regulating the expression of *ASPARAGINE SYNTHETASE1* and *PROLINE DEHYDROGENASE2*. *Plant J.* 53, 935–949. doi: 10.1111/j.1365-313X.2007.03385.x

Hartmann, L., Pedrotti, L., Weiste, C., Fekete, A., Schierstaedt, J., Göttler, J., et al. (2015). Crosstalk between two bZIP signaling pathways orchestrates salt-induced metabolic reprogramming in *Arabidopsis* roots. *Plant Cell* 27, 2244–2260. doi: 10.1105/tpc.15.00163

Hayashi, F., Ichino, T., Osanai, M., and Wada, K. (2000). Oscillation and regulation of proline content by *P5CS* and *ProDH* gene expressions in the light/dark cycles in *Arabidopsis thaliana L. Plant Cell Physiol.* 41, 1096–1101. doi: 10.1093/pcp/pcd036

Hinnebusch, A. G., Ivanov, I. P., and Sonenberg, N. (2016). Translational control by 5'-untranslated regions of eukaryotic mRNAs. *Science* 352, 1413–1416. doi: 10.1126/science.aad9868

Hu, W., Wang, L., Tie, W., Yan, Y., Ding, Z., Liu, J., et al. (2016a). Genome-wide analyses of the bZIP family reveal their involvement in the development, ripening and abiotic stress response in banana. *Sci. Rep.* 6:30203. doi: 10.1038/srep30203

Hu, W., Yang, H., Yan, Y., Wei, Y., Tie, W., Ding, Z., et al. (2016b). Genome-wide characterization and analysis of bZIP transcription factor gene family related to abiotic stress in cassava. *Sci. Rep.* 6:22783. doi: 10.1038/srep22783

Hulsmans, S., Rodriguez, M., De Coninck, B., and Rolland, F. (2016). The SnRK1 energy sensor in plant biotic interactions. *Trends Plant Sci.* 21, 648–661. doi: 10.1016/j.tplants.2016.04.008

Hummel, M., Rahmani, F., Smeekens, S., and Hanson, J. (2009). Sucrose-mediated translational control. *Ann. Bot.* 104, 1–7. doi: 10.1093/aob/mcp086

Iglesias-Fernández, R., Barrero-Sicilia, C., Carrillo-Barral, N., Oñate-Sánchez, L., and Carbonero, P. (2013). *Arabidopsis thaliana* bZIP44: a transcription factor affecting seed germination and expression of the mannanase-encoding gene *AtMAN7*. *Plant J.* 74, 767–780. doi: 10.1111/tpj.12162

Iven, T., Strathmann, A., Böttner, S., Zwafink, T., Heinekamp, T., Guivarc'h, A., et al. (2010). Homo- and heterodimers of tobacco bZIP proteins counteract as positive or negative regulators of transcription during pollen development. *Plant J.* 63, 155–166. doi: 10.1111/j.1365-313X.2010.04230.x

Izawa, T., Foster, R., Nakajima, M., Shimamoto, K., and Chua, N. H. (1994). The rice bZIP transcriptional activator RITA-1 is highly expressed during seed development. *Plant Cell* 6, 1277–1287. doi: 10.1105/tpc.6.9.1277

Jackson, R. J., Hellen, C. U. T., and Pestova, T. V. (2010). The mechanism of eukaryotic translation initiation and principles of its regulation. *Nat. Rev. Mol. Cell Biol.* 11, 113–127. doi: 10.1038/nrm2838

Jain, P., Shah, K., and Rishi, V. (2018). Potential in vitro and ex vivo targeting of bZIP53 involved in stress response and seed maturation in *Arabidopsis thaliana* by five designed peptide inhibitors. *Biochim. Biophys. Acta Proteins Proteom.* 1866, 1249–1259. doi: 10.1016/j.bbapap.2018.09.007

Jakoby, M., Weisshaar, B., Dröge-Laser, W., Vicente-Carbajosa, J., Tiedemann, J., Kroj, T., et al. (2002). bZIP transcription factors in *Arabidopsis*. *Trends Plant Sci.* 7, 106–111. doi: 10.1016/s1360-1385(01)02223-3

Jin, Z., Xu, W., and Liu, A. (2014). Genomic surveys and expression analysis of bZIP gene family in castor bean *(Ricinus communis* L.). *Planta* 239, 299–312. doi: 10.1007/s00425-013-1979-9

Jorgensen, R. A., and Dorantes-Acosta, A. E. (2012). Conserved peptide upstream open reading frames are associated with regulatory genes in angiosperms. *Front. Plant Sci.* 3:191. doi: 10.3389/fpls.2012.00191

Kang, C., Zhai, H., He, S., Zhao, N., and Liu, Q. (2019). A novel sweet potato bZIP transcription factor gene, *IbbZIP1,* is involved in salt and drought tolerance in transgenic *Arabidopsis*. *Plant Cell Rep.* 38, 1373–1382. doi: 10.1007/s00299-019-02441-x

Kang, S. G., Price, J., Lin, P., Hong, J. C., and Jang, J. (2010). The *Arabidopsis* bZIP1 transcription factor is involved in sugar signaling, protein networking, and DNA binding. *Mol. Plant* 3, 361–373. doi: 10.1093/mp/ssp115

Keutgen, A. J., and Pawelzik, E. (2008). Contribution of amino acids to strawberry fruit quality and their relevance as stress indicators under NaCl salinity. *Food Chem.* 111, 642–647. doi: 10.1016/j.foodchem.2008.04.032

Kilian, J., Whitehead, D., Horak, J., Wanke, D., Weinl, S., Batistic, O., et al. (2007). The AtGenExpress global stress expression data set: protocols, evaluation and model data analysis of UV-B light, drought and cold stress responses. *Plant J.* 50, 347–363. doi: 10.1111/j.1365-313X.2007.03052.x

Kobayashi, F., Maeta, E., Terashima, A., Kawaura, K., Ogihara, Y., and Takumi, S. (2008). Development of abiotic stress tolerance via bZIP-type transcription factor LIP19 in common wheat. *J. Exp. Bot.* 59, 891–905. doi: 10.1093/jxb/ern014

Kochetov, A. V. (2008). Alternative translation start sites and hidden coding potential of eukaryotic mRNAs. *Bioessays* 30, 683–691. doi: 10.1002/bies.20771

Kusano, T., Berberich, T., Harada, M., Suzuki, N., and Sugawara, K. (1995). A maize DNA-binding factor with a bZIP motif is induced by low temperature. *Mol. Gen. Genet.* 248, 507–517. doi: 10.1007/BF02423445

Lam, H. M., Peng, S. S., and Coruzzi, G. M. (1994). Metabolic regulation of the gene encoding glutamine-dependent asparagine synthetase in *Arabidopsis thaliana*. *Plant Physiol.* 106, 1347–1357. doi: 10.1104/pp.106.4.1347

Lastdrager, J., Hanson, J., and Smeekens, S. (2014). Sugar signals and the control of plant growth and development. *J. Exp. Bot.* 65, 799–807. doi: 10.1093/jxb/ert474

Lee, S. J., Lee, M. Y., Yi, S. Y., Oh, S. K., Choi, S. H., Her, N. H., et al. (2002). PPI1: a novel pathogen-induced basic region-leucine zipper (bZIP) transcription factor from pepper. *Mol. Plant Microbe Interact.* 15, 540–548. doi: 10.1094/MPMI.2002.15.6.540

Li, D., Fu, F., Zhang, H., and Song, F. (2015). Genome-wide systematic characterization of the bZIP transcriptional factor family in tomato (*Solanum lycopersicum* L.). *BMC Genomics* 16:771. doi: 10.1186/s12864-015-1990-6

Li, F., Liu, J., Guo, X., Yin, L., Zhang, H., and Wen, R. (2020). Genome-wide survey, characterization, and expression analysis of bZIP transcription factors in *Chenopodium quinoa*. *BMC Plant Biol.* 20:405. doi: 10.1186/s12870-020-02620-z

Li, P., Zheng, T., Li, L., Wang, J., Cheng, T., and Zhang, Q. (2021). Genome-wide investigation of the bZIP transcription factor gene family in *Prunus mume:* classification, evolution, expression profile and low-temperature stress responses. *Hort. Plant J.* 15:281. doi: 10.1016/j.hpj.2021.01.009

Li, Q., Jia, R., Dou, W., Qi, J., Qin, X., Fu, Y., et al. (2019). CsBZIP40, a BZIP transcription factor in sweet orange, plays a positive regulatory role in citrus bacterial canker response and tolerance. *PLoS One* 14:e0223498. doi: 10.1371/journal.pone.0223498

Li, X., Gao, S., Tang, Y., Li, L., Zhang, F., Feng, B., et al. (2015). Genome-wide identification and evolutionary analyses of bZIP transcription factors in wheat and its relatives and expression profiles of anther development related *TabZIP* genes. *BMC Genomics* 16:976. doi: 10.1186/s12864-015-2196-7

Li, Y., Meng, D., Li, M., and Cheng, L. (2016). Genome-wide identification and expression analysis of the bZIP gene family in apple (*Malus domestica*). *Tree Genet. Genomes* 12:82. doi: 10.1007/s11295-016-1043-6

Li, Z., Zhang, L., Yu, Y., Quan, R., Zhang, Z., Zhang, H., et al. (2011). The ethylene response factor AtERF11 that is transcriptionally modulated by the bZIP transcription factor HY5 is a crucial repressor for ethylene biosynthesis in *Arabidopsis*. *Plant J.* 68, 88–99. doi: 10.1111/j.1365-313X.2011.04670.x

Liao, Y., Zou, H., Wei, W., Hao, Y., Tian, A., Huang, J., et al. (2008). Soybean *GmbZIP44*, *GmbZIP62* and *GmbZIP78* genes function as negative regulator of ABA signaling and confer salt and freezing tolerance in transgenic *Arabidopsis*. *Planta* 228, 225–240. doi: 10.1007/s00425-008-0731-3

Lindemann, B. (2001). Receptors and transduction in taste. *Nature* 412, 219–225. doi: 10.1038/35093032

Liu, C., Mao, B., Ou, S., Wang, W., Liu, L., Wu, Y., et al. (2014). OsbZIP71, a bZIP transcription factor, confers salinity and drought tolerance in rice. *Plant Mol. Biol.* 84, 19–36. doi: 10.1007/s11103-013-0115-3

Liu, J., Chen, N., Chen, F., Cai, B., Dal Santo, S., Tornielli, G. B., et al. (2014). Genome-wide analysis and expression profile of the bZIP transcription factor gene family in grapevine (*Vitis vinifera*). *BMC Genomics* 15:281. doi: 10.1186/1471-2164-15-281

Lv, Z., Guo, Z., Zhang, L., Zhang, F., Jiang, W., Shen, Q., et al. (2019). Interaction of bZIP transcription factor TGA6 with salicylic acid signaling modulates artemisinin biosynthesis in *Artemisia annua*. *J. Exp. Bot.* 70, 3969–3979. doi: 10.1093/jxb/erz166

Ma, J., Hanssen, M., Lundgren, K., Hernández, L., Delatte, T., Ehlert, A., et al. (2011). The sucrose-regulated *Arabidopsis* transcription factor bZIP11 reprograms metabolism and regulates trehalose metabolism. *New Phytol.* 191, 733–745. doi: 10.1111/j.1469-8137.2011.03735.x

Mair, A., Pedrotti, L., Wurzinger, B., Anrather, D., Simeunovic, A., Weiste, C., et al. (2015). SnRK1-triggered switch of bZIP63 dimerization mediates the low-energy response in plants. *eLife* 4:e05828. doi: 10.7554/eLife.05828

Manzoor, M. A., Manzoor, M. M., Li, G., Abdullah, M., Han, W., Wenlong, H., et al. (2021). Genome-wide identification and characterization of bZIP transcription factors and their expression profile under abiotic stresses in Chinese pear (*Pyrus bretschneideri*). *BMC Plant Biol.* 21:413. doi: 10.1186/s12870-021-03191-3

Merchante, C., Stepanova, A. N., and Alonso, J. M. (2017). Translation regulation in plants: an interesting past, an exciting present and a promising future. *Plant J.* 90, 628–653. doi: 10.1111/tpj.13520

Morris, D. R., and Geballe, A. P. (2000). Upstream open reading frames as regulators of mRNA translation. *Mol. Cell Biol.* 20, 8635–8642. doi: 10.1128/MCB.20.23.8635-8642.2000

Muszynski, M. G., Dam, T., Li, B., Shirbroun, D. M., Hou, Z., Bruggemann, E., et al. (2006). *Delayed flowering1* encodes a basic leucine zipper protein that mediates floral inductive signals at the shoot apex in maize. *Plant Physiol.* 14, 1523–1536. doi: 10.1104/pp.106.088815

Nelson, G., Chandrashekar, J., Hoon, M. A., Feng, L., Zhao, G., Ryba, N. J. P., et al. (2002). An amino-acid taste receptor. *Nature* 416, 199–202. doi: 10.1038/nature726

Nijhawan, A., Jain, M., Tyagi, A. K., and Khurana, J. P. (2008). Genomic survey and gene expression analysis of the basic leucine zipper transcription factor family in rice. *Plant Physiol.* 146, 333–350. doi: 10.1104/pp.107.112821

Noman, A., Liu, Z., Aqeel, M., Zainab, M., Khan, M. I., Hussain, A., et al. (2017). Basic leucine zipper domain transcription factors: the vanguards in plant immunity. *Biotechnol. Lett.* 39, 1779–1791. doi: 10.1007/s10529-017-2431-1

Pedrotti, L., Weiste, C., Nägele, T., Wolf, E., Lorenzin, F., Dietrich, K., et al. (2018). Snf1-RELATED KINASE1-controlled C/S1-bZIP signaling activates alternative mitochondrial metabolic pathways to ensure plant survival in extended darkness. *Plant Cell* 30, 495–509. doi: 10.1105/tpc.17.00414

Peviani, A., Lastdrager, J., Hanson, J., and Snel, B. (2016). The phylogeny of C/S1 bZIP transcription factors reveals a shared algal ancestry and the pre-angiosperm translational regulation of S1 transcripts. *Sci. Rep.* 6:30444. doi: 10.1038/srep30444

Price, J., Laxmi, A., St Martin, S. K., and Jang, J. (2004). Global transcription profiling reveals multiple sugar signal transduction mechanisms in *Arabidopsis*. *Plant Cell* 16, 2128–2150. doi: 10.1105/tpc.104.022616

Rahmani, F., Hummel, M., Schuurmans, J., Wiese-Klinkenberg, A., Smeekens, S., and Hanson, J. (2009). Sucrose control of translation mediated by an upstream open reading frame-encoded peptide. *Plant Physiol.* 150, 1356–1367. doi: 10.1104/pp.109.136036

Riechmann, J. L., Heard, J., Martin, G., Reuber, L., Jiang, C., Keddie, J., et al. (2000). *Arabidopsis* transcription factors: genome-wide comparative analysis among eukaryotes. *Science* 290, 2105–2110. doi: 10.1126/science.290.5499.2105

Romera-Branchat, M., Severing, E., Pocard, C., Ohr, H., Vincent, C., Née, G., et al. (2020). Functional divergence of the *Arabidopsis* florigen-interacting bZIP transcription factors FD and FDP. *Cell Rep.* 31:107717. doi: 10.1016/j.celrep.2020.107717

Rook, F., Gerrits, N., Kortstee, A., Van Kampen, M., Borrias, M., Weisbeek, P., et al. (1998). Sucrose-specific signalling represses translation of the *Arabidopsis ATB2* bZIP transcription factor gene. *Plant J.* 15, 253–263. doi: 10.1046/j.1365-313x.1998.00205.x

Ruiz-Orera, J., and Albà, M. M. (2019). Translation of small open reading frames: roles in regulation and evolutionary innovation. *Trends Genet.* 35, 186–198. doi: 10.1016/j.tig.2018.12.003

Sagor, G. H. M., Berberich, T., Tanaka, S., Nishiyama, M., Kanayama, Y., Kojima, S., et al. (2016). A novel strategy to produce sweeter tomato fruits with high sugar contents by fruit-specific expression of a single bZIP transcription factor gene. *Plant Biotechnol. J.* 14, 1116–1126. doi: 10.1111/pbi.12480

Satoh, R., Fujita, Y., Nakashima, K., Shinozaki, K., and Yamaguchi-Shinozaki, K. (2004). A novel subgroup of bZIP proteins functions as transcriptional activators in hypoosmolarity-responsive expression of the *ProDH* gene in *Arabidopsis*. *Plant Cell Physiol.* 45, 309–317. doi: 10.1093/pcp/pch036

Shekhawat, U. K. S., and Ganapathi, T. R. (2014). Transgenic banana plants overexpressing *MusabZIP53* display severe growth retardation with enhanced sucrose and polyphenol oxidase activity. *Plant Cell Tiss. Organ. Cult.* 116, 387–402. doi: 10.1007/s11240-013-0414-z

Shimizu, H., Sato, K., Berberich, T., Miyazaki, A., Ozaki, R., Imai, R., et al. (2005). LIP19, a basic region leucine zipper protein, is a Fos-like molecular switch in the cold signaling of rice plants. *Plant Cell Physiol.* 46, 1623–1634. doi: 10.1093/pcp/pci178

Shipman, E. N., Yu, J., Zhou, J., Albornoz, K., and Beckles, D. M. (2021). Can gene editing reduce postharvest waste and loss of fruit, vegetables, and ornamentals? *Hortic. Res.* 8:1. doi: 10.1038/s41438-020-00428-4

Singh, K., Foley, R. C., and Oñate-Sánchez, L. (2002). Transcription factors in plant defense and stress responses. *Plant Cell Physiol.* 46, 1623–1634.

Smykowski, A., Fischer, S. M., and Zentgraf, U. (2015). Phosphorylation affects DNA-binding of the senescence-regulating bZIP transcription factor GBF1. *Plants (Basel)* 4, 691–709. doi: 10.3390/plants4030691

Sonenberg, N., and Hinnebusch, A. G. (2009). Regulation of translation initiation in eukaryotes: mechanisms and biological targets. *Cell* 136, 731–745. doi: 10.1016/j.cell.2009.01.042

Sornaraj, P., Luang, S., Lopato, S., and Hrmova, M. (2016). Basic leucine zipper (bZIP) transcription factors involved in abiotic stresses: a molecular model of a wheat bZIP factor and implications of its structure in function. *Biochim. Biophys. Acta* 1860, 46–56. doi: 10.1016/j.bbagen.2015.10.014

Srivastava, A. K., Dutta, S., and Chattopadhyay, S. (2019). MYC2 regulates *ARR16*, a component of cytokinin signaling pathways, in Arabidopsis seedling development. *Plant Direct.* 3:e00177. doi: 10.1002/pld3.177

Strathmann, A., Kuhlmann, M., Heinekamp, T., and Dröge-Laser, W. (2001). BZI-1 specifically heterodimerises with the tobacco bZIP transcription factors BZI-2, BZI-3/TBZF and BZI-4, and is functionally involved in flower development. *Plant J.* 28, 397–408. doi: 10.1046/j.1365-313x.2001.01164.x

Sun, D., Li, S., Niu, L., Reid, M. S., Zhang, Y., and Jiang, C. (2017). *PhOBF1*, a petunia ocs element binding factor, plays an important role in antiviral RNA silencing. *J. Exp. Bot.* 68, 915–930. doi: 10.1093/jxb/erw490

Thalor, S. K., Berberich, T., Lee, S. S., Yang, S. H., Zhu, X., Imai, R., et al. (2012). Deregulation of sucrose-controlled translation of a bZIP-type transcription factor results in sucrose accumulation in leaves. *PLoS One* 7:e33111. doi: 10.1371/journal.pone.0033111

Toh, S., Mccourt, P., and Tsuchiya, Y. (2012). HY5 is involved in strigolactone-dependent seed germination in *Arabidopsis*. *Plant Signal. Behav.* 7, 556–558. doi: 10.4161/psb.19839

Tsugama, D., Liu, S., and Takano, T. (2012). A bZIP protein, VIP1, is a regulator of osmosensory signaling in *Arabidopsis*. *Plant Physiol.* 159, 144–155. doi: 10.1104/pp.112.197020

Tsugama, D., Liu, S., and Takano, T. (2016). The bZIP protein VIP1 is involved in touch responses in *Arabidopsis* roots. *Plant Physiol.* 171, 1355–1365. doi: 10.1104/pp.16.00256

Unel, N. M., Cetin, F., Karaca, Y., Celik Altunoglu, Y., and Baloglu, M. C. (2019). Comparative identification, characterization, and expression analysis of bZIP gene family members in watermelon and melon genomes. *Plant Growth Regul.* 87, 227–243. doi: 10.1007/s10725-018-0465-6

van der Horst, S., Filipovska, T., Hanson, J., and Smeekens, S. (2020). Metabolite control of translation by conserved peptide uORFs: the ribosome as a metabolite multisensor. *Plant Physiol.* 182, 110–122. doi: 10.1104/pp.19.00940

von Arnim, A. G., Jia, Q., and Vaughn, J. N. (2014). Regulation of plant translation by upstream open reading frames. *Plant Sci.* 214, 1–12. doi: 10.1016/j.plantsci.2013.09.006

Walsh, J., and Freeling, M. (1999). The *liguleless2* gene of maize functions during the transition from the vegetative to the reproductive shoot apex. *Plant J.* 19, 489–495. doi: 10.1046/j.1365-313x.1999.00541.x

Wang, J., Zhou, J., Zhang, B., Vanitha, J., Ramachandran, S., and Jiang, S. (2011). Genome-wide expansion and expression divergence of the basic leucine zipper transcription factors in higher plants with an emphasis on sorghum. *J. Integr. Plant Biol.* 53, 212–231. doi: 10.1111/j.1744-7909.2010.01017.x

Wang, X., Zhong, Y., Cheng, Z., and Xiong, J. (2015). Divergence of the bZIP gene family in strawberry, peach, and apple suggests multiple modes of gene evolution after duplication. *Int. J. Genomics* 2015:536943. doi: 10.1155/2015/536943

Wang, Y., Zhang, X., Zhao, Y., Yang, J., He, Y., Li, G., et al. (2020). Transcription factor PyHY5 binds to the promoters of *PyWD40* and *PyMYB10* and regulates its expression in red pear 'Yunhongli No. 1'. *Plant Physiol. Biochem.* 154, 665–674. doi: 10.1016/j.plaphy.2020.07.008

Waterhouse, A. M., Procter, J. B., Martin, D. M. A., Clamp, M., and Barton, G. J. (2009). Jalview Version 2—a multiple sequence alignment editor and analysis workbench. *Bioinformatics* 25, 1189–1191. doi: 10.1093/bioinformatics/btp033

Wei, K., Chen, J., Wang, Y., Chen, Y., Chen, S., Lin, Y., et al. (2012). Genome-wide analysis of bZIP-encoding genes in maize. *DNA Res.* 19, 463–476. doi: 10.1093/dnares/dss026

Weiste, C., and Dröge-Laser, W. (2014). The *Arabidopsis* transcription factor bZIP11 activates auxin-mediated transcription by recruiting the histone acetylation machinery. *Nat. Commun.* 5:3883. doi: 10.1038/ncomms4883

Weiste, C., Pedrotti, L., Selvanayagam, J., Muralidhara, P., Fröschel, C., Novák, O., et al. (2017). The *Arabidopsis* bZIP11 transcription factor links low-energy signalling to auxin-mediated control of primary root growth. *PLoS Genet.* 13:e1006607. doi: 10.1371/journal.pgen.1006607

Weltmeier, F., Ehlert, A., Mayer, C. S., Dietrich, K., Wang, X., Schütze, K., et al. (2006). Combinatorial control of *Arabidopsis* proline dehydrogenase transcription by specific heterodimerisation of bZIP transcription factors. *EMBO J.* 25, 3133–3143. doi: 10.1038/sj.emboj.7601206

Weltmeier, F., Rahmani, F., Ehlert, A., Dietrich, K., Schütze, K., Wang, X., et al. (2009). Expression patterns within the *Arabidopsis* C/S1 bZIP transcription factor network: availability of heterodimerization partners controls gene expression during stress response and development. *Plant Mol. Biol.* 69, 107–119. doi: 10.1007/s11103-008-9410-9

Wiese, A., Elzinga, N., Wobbes, B., and Smeekens, S. (2004). A conserved upstream open reading frame mediates sucrose-induced repression of translation. *Plant Cell* 16, 1717–1729. doi: 10.1105/tpc.019349

Wigge, P. A., Kim, M. C., Jaeger, K. E., Busch, W., Schmid, M., Lohmann, J. U., et al. (2005). Integration of spatial and temporal information during floral induction in *Arabidopsis*. *Science* 309, 1056–1059. doi: 10.1126/science.1114358

Wu, J., Wang, Z., Shi, Z., Zhang, S., Ming, R., Zhu, S., et al. (2013). The genome of the pear (*Pyrus bretschneideri* Rehd.). *Genome Res.* 23, 396–408. doi: 10.1101/gr.144311.112

Xing, S., Chen, K., Zhu, H., Zhang, R., Zhang, H., Li, B., et al. (2020). Fine-tuning sugar content in strawberry. *Genome Biol.* 21:230. doi: 10.1186/s13059-020-02146-5

Xu, C., Cao, H., Zhang, Q., Wang, H., Xin, W., Xu, E., et al. (2018). Control of auxin-induced callus formation by bZIP59-LBD complex in *Arabidopsis* regeneration. *Nat. Plants* 4, 108–115. doi: 10.1038/s41477-017-0095-4

Xu, D. (2020). COP1 and BBXs-HY5-mediated light signal transduction in plants. *New Phytol.* 228, 1748–1753. doi: 10.1111/nph.16296

Xue, Y., Zhang, Z., Wang, L., Yu, Y., Xiao, J., Hou, J., et al. (2018). Genome-wide systematic characterization and its regulatory expression reprogramming process of the bZIP transcription factors during trauma response in *Camellia sinensis*. *Can. J. For. Res.* 48, 1279–1291. doi: 10.1139/cjfr-2018-0135

Yamashita, Y., Takamatsu, S., Glasbrenner, M., Becker, T., Naito, S., and Beckmann, R. (2017). Sucrose sensing through nascent peptide-meditated ribosome stalling at the stop codon of *Arabidopsis bZIP11* uORF2. *FEBS Lett.* 591, 1266–1277. doi: 10.1002/1873-3468.12634

Yang, J., Wang, M., Li, W., He, X., Teng, W., Ma, W., et al. (2019). Reducing expression of a nitrate-responsive bZIP transcription factor increases grain yield and N use in wheat. *Plant Biotechnol. J.* 17, 1823–1833. doi: 10.1111/pbi.13103

Yang, Y., Li, J., Li, H., Yang, Y., Guang, Y., and Zhou, Y. (2019). The bZIP gene family in watermelon: genome-wide identification and expression analysis under cold stress and root-knot nematode infection. *PeerJ* 7:e7878. doi: 10.7717/peerj.7878

Yang, Z., Sun, J., Chen, Y., Zhu, P., Zhang, L., Wu, S., et al. (2019). Genome-wide identification, structural and gene expression analysis of the bZIP transcription factor family in sweet potato wild relative *Ipomoea trifida*. *BMC Genet.* 20:41. doi: 10.1186/s12863-019-0743-y

Zhang, H., Wang, Y., and Lu, J. (2019). Function and evolution of upstream ORFs in eukaryotes. *Trends Biochem. Sci.* 44, 782–794. doi: 10.1016/j.tibs.2019.03.002

Zhang, Y., Gao, W., Li, H., Wang, Y., Li, D., Xue, C., et al. (2020a). Genome-wide analysis of the bZIP gene family in Chinese jujube (*Ziziphus jujuba Mill.*). *BMC Genomics* 21:483. doi: 10.1186/s12864-020-06890-7

Zhang, Y., Li, S., Chen, Y., Liu, Y., Lin, Y., Li, M., et al. (2022). Heterologous overexpression of strawberry bZIP11 induces sugar accumulation and inhibits plant growth of tomato. *Sci. Hortic.* 292:110634. doi: 10.1016/j.scienta.2021.110634

Zhang, Y., Yang, X., Cao, P., Xiao, Z., Zhan, C., Liu, M., et al. (2020b). The *bZIP53-IAA4* module inhibits adventitious root development in *Populus*. *J. Exp. Bot.* 71, 3485–3498. doi: 10.1093/jxb/eraa096

Zhao, K., Chen, S., Yao, W., Cheng, Z., Zhou, B., and Jiang, T. (2021). Genome-wide analysis and expression profile of the bZIP gene family in poplar. *BMC Plant Biol.* 21:122. doi: 10.1186/s12870-021-02879-w

Zhou, Y., Xu, D., Jia, L., Huang, X., Ma, G., Wang, S., et al. (2017). Genome-wide identification and structural analysis of bZIP transcription factor genes in *Brassica napus*. *Genes* 8:E288. doi: 10.3390/genes8100288

Zhu, M., Meng, X., Cai, J., Li, G., Dong, T., and Li, Z. (2018). Basic leucine zipper transcription factor SlbZIP1 mediates salt and drought stress tolerance in tomato. *BMC Plant Biol.* 18:83. doi: 10.1186/s12870-018-1299-0

Zinsmeister, J., Lalanne, D., Terrasson, E., Chatelain, E., Vandecasteele, C., Vu, B. L., et al. (2016). ABI5 is a regulator of seed maturation and longevity in legumes. *Plant Cell* 28, 2735–2754. doi: 10.1105/tpc.16.00470

Zong, W., Tang, N., Yang, J., Peng, L., Ma, S., Xu, Y., et al. (2016). Feedback regulation of ABA signaling and biosynthesis by a bZIP transcription factor targets drought-resistance-related genes. *Plant Physiol.* 171, 2810–2825. doi: 10.1104/pp.16.00469

Conflict of Interest: The authors declare that the research was conducted in the absence of any commercial or financial relationships that could be construed as a potential conflict of interest.

Publisher's Note: All claims expressed in this article are solely those of the authors and do not necessarily represent those of their affiliated organizations, or those of the publisher, the editors and the reviewers. Any product that may be evaluated in this article, or claim that may be made by its manufacturer, is not guaranteed or endorsed by the publisher.

Copyright © 2022 Wang, Zhang, Norris and Jiang. This is an open-access article distributed under the terms of the Creative Commons Attribution License (CC BY). The use, distribution or reproduction in other forums is permitted, provided the original author(s) and the copyright owner(s) are credited and that the original publication in this journal is cited, in accordance with accepted academic practice. No use, distribution or reproduction is permitted which does not comply with these terms.

frontiers in Plant Science

ORIGINAL RESEARCH
published: 21 January 2022
doi: 10.3389/fpls.2021.792832

Evolutionary Origin of the Carotenoid Cleavage Oxygenase Family in Plants and Expression of Pepper Genes in Response to Abiotic Stresses

Yixiu Yao[1,2†], Li Jia[3†], Yuan Cheng[2], Meiying Ruan[2], Qingjing Ye[2], Rongqing Wang[2], Zhuping Yao[2], Guozhi Zhou[2], Jia Liu[4], Jiahong Yu[2,4], Peng Zhang[4], Yuhe Yin[4], Weiping Diao[5] and Hongjian Wan[1,2,6]**

[1] State Key Laboratory for Managing Biotic and Chemical Threats to the Quality and Safety of Agro-Products, Zhejiang Academy of Agricultural Sciences, Hangzhou, China, [2] Institute of Vegetables, Zhejiang Academy of Agricultural Sciences, Hangzhou, China, [3] Institute of Horticulture, Anhui Academy of Agricultural Sciences, Hefei, China, [4] Wulanchabu Academy of Agricultural and Forestry Sciences, Wulanchabu, China, [5] Jiangsu Key Laboratory for Horticultural Crop Genetic Improvement, Institute of Vegetable Crops, Jiangsu Academy of Agricultural Sciences, Nanjing, China, [6] Australia-China Research Centre for Crop Improvement, Zhejiang Academy of Agricultural Sciences, Hangzhou, China

OPEN ACCESS

Edited by:
Pei Xu,
China Jiliang University, China

Reviewed by:
Hao Li,
Northwest A&F University, China
Ziji Liu,
Tropical Crops Genetic Resources Institute, Chinese Academy of Tropical Agricultural Sciences, China

***Correspondence:**
Weiping Diao
diaowp@jaas.ac.cn
Hongjian Wan
wanhongjian@sina.com

† These authors have contributed equally to this work

Specialty section:
This article was submitted to Crop and Product Physiology, a section of the journal Frontiers in Plant Science

Received: *11 October 2021*
Accepted: *08 December 2021*
Published: *21 January 2022*

Citation:
Yao Y, Jia L, Cheng Y, Ruan M, Ye Q, Wang R, Yao Z, Zhou G, Liu J, Yu J, Zhang P, Yin Y, Diao W and Wan H (2022) Evolutionary Origin of the Carotenoid Cleavage Oxygenase Family in Plants and Expression of Pepper Genes in Response to Abiotic Stresses. Front. Plant Sci. 12:792832. doi: 10.3389/fpls.2021.792832

Plant carotenoid cleavage oxygenase (CCO) is an enzyme that catalyzes the synthesis of carotenoids and participates in many important physiological functions. The plant CCOs exist in two forms, namely carotenoid cleavage dioxygenase (CCD) and nine-*cis* epoxide carotenoid dioxygenase (NCED). Although studies have shown that this gene family has been identified in many species, such as *Arabidopsis*, grape, and tomato, the evolutionary origin of the CCO family and the expression pattern of pepper genes in response to H_2O_2 and other abiotic stresses are still unclear. In this study, we used the bioinformatics method to identify and analyze the members of the *CCO* gene family from pepper and other 13 plants from lower to higher plant species based on the whole genome sequence. A total of 158 *CCO* genes were identified in different plant species and further divided into two groups (e.g., groups I and II). The former was subdivided into CCD7 and CCD8 and have independent evolutionary origins, respectively, while the latter was subdivided into CCD1, CCD4, CCD-like, and NCED, which may have come from a common ancestor. In addition, the results of RNA-seq showed that the expression patterns of pepper *CaCCO* genes were different in the tissues tested, and only few genes were expressed at high levels such as *CaCCD1a*, *CaCCD4a*, *CaNCED3*, and *CaCCD1b*. For hydrogen peroxide (H_2O_2) and other abiotic stresses, such as plant hormones, heat, cold, drought, and NaCl treatments, induction of about half of the *CaCCO* genes was observed. Moreover, the expression patterns of CaCCOs were further investigated under heat, cold, drought, and NaCl treatments using quantitative real-time PCR (qRT-PCR), and most members were responsive to these stresses, especially some CaCCOs with significant expression changes were identified, such as *CaCCD4c, CaCCD-like1, CaCCD8*, and *CaCCD1b*, suggesting the important roles of CaCCOs in abiotic stress responses. All these results will provide a valuable analytical basis for understanding the evolution and functions of the CCO family in plants.

Keywords: pepper, phylogenetic analysis, gene expression, abiotic stress, NCED

INTRODUCTION

As is known to all, due to the global climate change, plant resources and genetic diversity as well as the world food security has had a certain impact, so environmental stress has become the focus of attention of people (Raza et al., 2020). Plants are often subjected to various environmental stresses during their life, such as drought, high salt, high temperature, or invasion of pathogenic bacteria. These abiotic stresses or biotic stresses will have a certain impact on the growth and development of plants (Roychoudhury et al., 2013). Carotenoids are important lipid-soluble compounds, contain a large family over 700 types of structures (Britton et al., 2004), and perform a series of important biotic and abiotic stress functions. Apocarotenoids, or carotenoid cleavage products, were produced by carotenoid cleavage oxygenases (CCOs) of specific cleavage of carotenoids. Plant CCOs are a class of dioxygenases that catalyze the cleavage of carotenoids and their conjugate double bonds in plants. The CCOs can be further divided into nine-*cis*-epoxide carotenoid dioxygenase (NCED) and carotenoid cleavage dioxygenase (CCDs), based on their substrate informing an epoxy structure (Tan et al., 2003; Auldridge et al., 2006).

The first *NCED* gene *vp14* was identified in maize (Schwartz et al., 1997; Tan et al., 1997). Since then, the function of *NCED* gene has been widely studied. The *NCED* genes in these species exist in plants in the form of gene family (Yang and Guo, 2007), and their expression sites and functions are also different (Lefebvre et al., 2010). It is reported that the *NCED* genes play a certain role in the growth and development of plants. For example, in *Arabidopsis*, the *NCED1* gene can respond to water stress (Blankenship and Sisler, 1993). Similarly, according to the phenotypic analysis of *NCED5*, *NCED6*, and *NCED9* mutants at specific time and tissue, the results show that the three genes work together to induce seed dormancy (Frey et al., 2012). Seo et al. (2009) showed that spatiotemporal expression of the *NCED* gene is particularly important for the regulation of abscisic acid (ABA) level, which affects the seed dormancy and germination (Nambara et al., 2010). Furthermore, the inhibition of far-red light on *Arabidopsis* seed germination was reported in part due to the photoreversible regulation of *NCED6* to maintain the ABA levels (Seo et al., 2006), and Toh et al. (2008) suggested that three different *NCED* genes, namely, *NCED2*, *NCED5*, and *NCED9*, inhibited germination by increasing the ABA levels at high temperatures. Finally, two (*PaNCED1* and *PaNCED3*) of three avocado *NCED* genes cloned were highly expressed at ripening (Chernys and Zeevaart, 2000).

In addition, studies have shown that the *NCED* gene not only involves in the growth and development of plants but also plays an important role in their stress tolerance (Gómez et al., 2002). It has been reported that the *NCED* gene can upregulate ABA biosynthesis (Chernys and Zeevaart, 2000; Rodrigo, 2006). Overexpression of the *NCED* gene can enhance the resistance of plants to abiotic stresses (Xian et al., 2014). For example, overexpression of the *AtNCED3* gene can increase the content of ABA and increase the water loss tolerance of *Arabidopsis thaliana*. Previous reports have shown that overexpression of the *LeNCED1* gene can improve the drought tolerance of tomato (Thompson et al., 2000). The heterologous overexpression of *MhNCED3* in *Malus crabapple* alleviated oxidative damage and enhanced the tolerance of *A. thaliana* to chlorine stress (Zhang et al., 2014, 2015). The real-time PCR (RT-PCR) analysis of *OsNCED3*, *OsNCED4*, and *OsNCED5* on the root of rice seedlings showed that the three *NCED* genes were induced by salt and ABA treatments (Welsch et al., 2008). More recently, Hwang et al. (2018) studied the sugar sensitivity and drought tolerance of the allograft expression of rice *OsNCED4* in *A. thaliana* and found that the allograft expression of *OsNCED4* increased ABA levels, changed plant size and leaf shape, and delayed seed germination, leading to oversensitivity to sugar after germination and enhanced tolerance to drought. There are few reports on the involvement of the *NCED* gene in disease resistance regulation, but some studies have found that *AtNCED5* was overexpressed in *A. thalli* mutants, the endogenous ABA level was increased by about 2 times, and the susceptibility of this mutant was significantly improved. After inoculation with *Pseudomonas syringa*, *AtNCED2*, *AtNCED3*, and *AtNCED5* were significantly induced, and ABA was also accumulated in large quantities (Fan et al., 2009).

Hydrogen peroxide (H_2O_2) and NO are important signals involved in plant growth and abiotic stress tolerance (Neill et al., 2002; Uchida et al., 2002). The exogenous ABA treatment can induce the production of H_2O_2 and NO, resulting in stomatal closure, and improve the expression and activity of antioxidant enzymes (Jiang and Zhang, 2003; Desikan et al., 2004; Zhou et al., 2005; Zhang et al., 2007). Especially, research reported that rice *OsNECD3* regulates plant growth and enhances abiotic stress tolerance. Huang et al. (2018) showed that under H_2O_2 stress, *OsNCED3* was expressed in different tissues, and the *OsNCED3* gene avoided oxidative damage by increasing ABA biosynthesis when the plant was subjected to oxidative stress. Other studies have pointed out that the expression of the *NCED* gene increased the ABA and the H_2O_2 contents in roots in the non-saline side increased. Exogenous H_2O_2 can reduce ABA content by downregulating the *NCED* gene, indicating that there is a feedback mechanism between ABA and H_2O_2 (Kong et al., 2016).

Compared with the *NCED* gene family, only few studies were reported on the *CCD* gene family. Researchers reported that each member of this gene family had formed a functional carotenoid, such as β-ionone and geranylacetone, which were vital for the flavor of vegetable and fruit plants (Simkin et al., 2004a,b; Sun et al., 2008; Ilg et al., 2009). The *CCD1* enzymes have cleavage activities on 5,6 (5', 6') double bonds position, while *CCD4* were also found to have a 9,10 (9', 10') cleavage activity (Huang et al., 2009; Campbell et al., 2010; Brandi et al., 2011). In addition, the researchers reported that the cooperation of *CCD7* and *CCD8* can regulate plant architectures and reproductive development (Snowden et al., 2005; Liu et al., 2013).

Presently, nine members of the *CCO* gene family have been identified in *Arabidopsis*: four of which were designed as CCDs (*CCD1*, *CCD4*, *CCD7*, and *CCD8*) and the remaining genes were proven to be NCEDs (*NCED2*, *NCED3*, *NCED5*, *NCED6*, and *NCED9*) (Schwartz et al., 1997). In recent years, with the completion of plant genome sequencing, this gene family

has been identified in different plant species, such as tomato (Burbidge et al., 1999), avocado (Chernys and Zeevaart, 2000), and bean (Qin and Zeevaart, 2002). Although identification and the roles of many CCOs in plants have been completed, members of the *CCO* gene family in pepper "zunla-1" have not been reported. Recently, the whole genome of "zunla-1" in pepper was sequenced (Qin et al., 2014). In this study, we systematically surveyed the *CCO* gene family from 14 plant species, ranging from lower to higher plant species, and analyzed their evolutionary origins. In addition, the expression profiles of the members of the pepper *CCO* gene family in response to H_2O_2 and other biotic stresses were also further investigated. These results will provide the value information of understanding of evolutionary modes and theoretical basis for exploring the functional roles of *CCO* in pepper.

MATERIALS AND METHODS

Data Retrieval of Carotenoid Cleavage Oxygenase Gene Families in Different Plant Species

To identify the *CaCCO* gene family members, the predicted pepper gene sequences were downloaded from the Pepper Genome Database[1,2]. The genome information of *Arabidopsis* was derived from the database[3]. In addition, twelve plant species were also selected for analyses, including *Volvox carteri*, *Chlamydomonas reinhardtii*, *Marchantia polymorpha, Physcomitrella patens*, *Selaginella moellendorffii*, *Oryza sativa*, *Zea mays*, *Solanum lycopersicum*, *Brachypodium distachyon*, *Setaria italic*, *Aquilegia coerulea*, and *Solanum tuberosum*. Genome sequences of these plant species were downloaded from JGI[4].

Identification and Chromosome Localization of the Carotenoid Cleavage Oxygenase Gene Family in Pepper

The *CCO* gene sequences were downloaded from *A. thaliana* genome database and used as a seed sequence to retrieve the pepper genome database to obtain the candidate genes. To confirm the members of the pepper *CCO* family, BlastP methods were performed using the conserved domain of *Arabidopsis* CCO protein as a query sequence in the local database. The pepper *CCO* genes with e-value less than 1e − 5 were used for further analysis. Then, the Hidden Markov Model (HMM) profile of the PF03055 (RPE65) conserved domain was downloaded from the Pfam protein family database[5] with e-value < 1e − 5. Finally, all of the putative CaCCO sequences with incomplete domains were excluded by the HMM analysis. Genome sequences of other 12 plant species were used to construct the local database using Bioedit 7.0 software[6].

The physicochemical properties of *CaCCO* genes were analyzed using the online ExPASy-ProtParam tool[7], which included several amino acids, molecular weight (MW), and theoretical isoelectric point (p*I*) of deduced CaCCO proteins. According to the information in the pepper gene database, chromosome localization of the *CCO* genes was further performed using MapDrawV2.1 software.

Phylogenetic Analysis of Carotenoid Cleavage Oxygenase Gene Family in Pepper and Other Plant Species

To explore the phylogenetic relationships of the pepper *CCO* genes, multiple sequence comparison was conducted using CCO amino acid sequences of pepper and other plant species using ClustalW program, and MEGA5.0 software[8] was used to construct neighbor-joining (NJ) tree (Ilg et al., 2009).

Spatiotemporal Expression Analysis of CaCCO Genes in Various Tissues of Pepper

To study the spatiotemporal expression patterns of the pepper *CCO* genes, data of reported RNA-seq were selected for analyses (see text footnote 2). Previously, a pepper variety (Line 6421) with good heat resistance, drought resistance, and disease resistance was selected as the preparation materials of various samples for RNA sequencing. The seeds were surface disinfected with 5% sodium hypochlorite solution for 15 min. After rinsing with water, the seeds were sown in 200-well vermiculite-filled seedling trays and placed in an environment of 25/18^{o}C day/night temperature, 16/8 h light/dark cycle, 60–70% relative humidity, and 6,000 lux light intensity. The RNA-seq sequencing data of various tissue development stages of pepper, including seeds and placenta (ST1–ST2), seed (S3–S11), placenta (T3–T11), flower (F1–F9), petal (P10), ovary (O10), stamen (STA10), leaf (L1–L9), fruits (FST0–FST1), and peel (G1–G11), were used to make heat maps, and the heat map of tissue-specific expression patterns of the *CCO* genes was drawn using the MeV software[9]. All samples were collected in quadruplicate from each of the sampling points, and five seedlings were randomly picked and mixed as one biological replicate.

Expression Analysis of CaCCO Genes Under Abiotic Stresses

Similarly, to determine the response of the *CaCCO* gene to abiotic stresses (heat, cold, drought, and NaCl treatments), 40-day-old seedlings were treated and RNA samples were extracted from leaves and roots. Salt stress was carried out by adding NaCl with a final concentration of 200 mM to the nutrient solution, and

[1]http://passport.pepper.snu.ac.kr/?t=PGENOME
[2]http://pepperhub.hzau.edu.cn/
[3]https://www.arabidopsis.org/
[4]https://phytozome-next.jgi.doe.gov/
[5]http://pfam.sanger.ac.uk/
[6]https://bioedit.software.informer.com/
[7]http://web.expasy.org/protparam/
[8]https://www.megasoftware.net/
[9]https://sourceforge.net/projects/mev-tm4/

osmotic stress was carried out by adding mannitol with a final concentration of 400 mM. For high/low-temperature treatment, the seedlings at the fourth true leaf stage will be transferred to the 42°C (high temperature) or 10°C (low temperature) of the growth chamber, photoperiod, and relative humidity consistent with the untreated plants. The control was treated with nutrient solution only. The leaves and roots were selected for RNA-seq analysis at 0, 1, 6, and 24 h after treatment.

Expression Analysis of CaCCO Genes in Response to Hormone Stresses

To study the expression of these genes under different hormone treatments, 30 μM ABA, 2 mM salicylic acid (SA), and 10 μM methyl jasmonic acid (MeJA) were used to treat the seedling for 40 days. These three different hormones (ABA, MeJA, and SA) were selected and added to the nutrient solution. The leaves and roots were selected for RNA-seq analysis (see text footnote 2) at 0, 1, 6, and 24 h after treatment. An isometric histogram was drawn using OriginPro7.5[10].

Expression Analysis of CaCCO Genes in Response to H_2O_2 Stress

The oxidative stress was also applied by adding H_2O_2 into the nutrient solution to a final concentration of 30 mM. Then, the leaves and roots were selected for RNA-seq analysis (see text footnote 2) at 0, 1, 6, and 24 h after treatment. The heat map of expression patterns of *CCO* genes in response to H_2O_2 treatment was drawn using the MeV software.

RNA Isolation and Quantitative Real-Time PCR Analysis

Total RNA was extracted from the pepper leaves using E.Z.N.A.® Plant RNA Kit (OMEGA, United States). The first strand cDNA was synthesized using FastKing RT Kit (with gDNase) (TIANGEN, China) according to the instructions of the manufacturer. Gene-specific primers were designed using the Genscript online tool[11], and the detailed information is listed in **Supplementary Table 2**. The pepper *GAPDH* gene was utilized as an internal control for normalizing the expression levels. The use of primers was diluted according to the synthetic instructions. The reaction system followed the instructions of SYBR Green Master Mix reagent of Vazyme using CFX96 Real Time System (Bio-Rad, United States) with AceQ® qPCR SYBR® Green Master Mix with 20 μl reaction mixture of volume. The reaction volume consists of 10 μl SYBR® Green Master Mix, 0.4 μl of each primer (10 μM), 1 μl of the cDNA template, and 7.8 μl of RNase free H_2O. Thermal cycling parameters for the amplification were as follows: 95°C, 10 min, followed by 40 cycles at 95°C, 15 s, and 55°C, 1 min. Three technical repeats were performed for each gene, and the data were analyzed according to the $2^{-\Delta\Delta Ct}$ method.

[10]https://www.originlab.com/

[11]https://www.genscript.com

RESULTS

Identification of the CaCCO Gene Family in Pepper and Other Plant Species

To identify the members of the *CCO* gene family at the genome-wide levels, the whole genome sequence of pepper was searched using HMM and BLAST. The results showed that a total of 158 candidate *CCO* genes were identified in various plant species, each with a distinct number of variants. In addition, fourteen CCO DNA binding domains containing proteins were encoded in the pepper genome. The detailed information of these proteins is shown in **Table 1**, including gene name, genome location, coding sequence length, amino acid sequence length, MW, and isoelectric point. The predicted size of the CaCCO proteins was from 321 to 744 AA (for *CaCCD4b* and *CaCCD7*, respectively; **Table 1**). The MW of these genes ranged from 36.33 (*CaCCD4b*) to 83.79 kDa (*CaCCD7*), while their estimated p*I* values ranged from 5.16 (*CaCCD4b*) to 8.25 (CaNCED1). Most CaCCO proteins were acidic (p*I*-values 7) according to the p*I* values.

Evolutionary Origin of Carotenoid Cleavage Oxygenase Gene Family in Plant Species

To investigate the evolutionary origin, a total of 158 CCOs (CCDs and NCEDs) from 14 plant species were identified (**Supplementary Table 1**). A phylogenetic tree was constructed based on the amino acid sequences of these genes using the NJ method in MEGA 5.0 software (Tamura et al., 2011). As shown in **Figure 1**, all of the CCOs in different plants ranging from green algae to higher plant species were divided into two groups (groups I and II), and the former was further separated into two subgroups (*CCD7* and *CCD8*). Both of these two subgroups contained the members from the lower to higher plant species, suggesting that they have independent evolutionary origins, respectively. Inversely, the latter was subdivided into *CCD1*, *CCD4*, *CCD-like*, and *NCED*. The *CCD1* subgroup was composed of members from green algae to higher plant species, both *NCED* and *CCD-like* subgroups contained *CCO* genes from moss to higher plant species, and *CCD4* was composed of *CCO* genes from angiosperm. This showed that group II may have come from a common ancestor, and *NCED*, *CCD-like*, and *CCD4* were produced from multiple duplication events in land plant species.

Chromosome Distribution of the CaCCO Gene Family Members

In this study, the chromosome distribution of the pepper *CaCCO* gene was analyzed based on the genome sequence of the pepper. Except for *CaNCED3*, the remaining thirteen genes in the fourteen CaCCO members were irregularly distributed on five of the twelve pepper chromosomes, according to the findings (**Figure 2**). Among them, most of the genes are located on the first chromosome (Chr1), and there are seven genes, namely, *CaCCD1a*, *CaNCED2*, *CaCCD4a*, *CaCCD1b*, *CaCCD4c*, *CaCCD7*, and *CaCCD4b*. The third and fifth chromosomes

TABLE 1 | Information for the *CaCCO* gene family in pepper.

	Gene name	Gene ID	Protein length (AA)	Molecular weight (kD)	Isoelectric point
CaCCD	CaCCD1a	Capana01g002623	581	65.81	6.49
	CaCCD1b	Capana01g002624	565	63.14	5.86
	CaCCD4a	Capana01g000948	603	66.05	6.34
	CaCCD4	Capana01g000946/Capana01g000947	321	36.33	5.16
	CaCCD4c	Capana01g004038	568	63.13	7.85
	CaCCD7	Capana01g003456	744	83.79	6.67
	CaCCD8	Capana08g000570	501	56.15	6.04
	CaCCD-like1	Capana08g000589	567	64.06	6.18
	CaCCD-like2	Capana11g000021	565	64.72	5.56
	CaCCD-like3	Capana11g000005	442	49.35	5.49
CaNCED	CaNCED1	Capana05g002276	579	64.67	8.25
	CaNCED2	Capana01g003704	596	66.49	6.64
	CaNCED3	Capana00g003114	506	56.47	5.6
	CaNCED4	Capana03g002722/Capana03g002723	353	40.04	6.16

had only one member (*CaNCED4* and *CaNCED1*, respectively). Furthermore, two genes are found to be present on each of the two chromosomes (Chr8 and 11). None of the *CaCCO* genes was mapped on Chr2, 4, 6, 7, 9, 10, and 12. Subsequently, we further analyzed the tandem and segmental duplications of the *CaCCO* genes in pepper. We found that both of the tandem duplication and segmental duplication events were not found in the *CaCCO* gene family.

Expression Analysis of CaCCO Genes in Different Tissues

It is well known that RNA-seq data have a wide range of applications and can be used to conveniently analyze the differential expression of genes in higher plant species (del Río et al., 2006). In this study, the expression patterns of fourteen *CaCCO* genes were analyzed using RNA-seq data from seeds, leaves, flowers, and fruits. The results revealed that most of the *CaCCO* genes in these organs were completely unexpressed in all of the examined tissues (**Figure 3**). In different developmental stages of leaves from L1 to L9, expression levels of 10 of 14 *CaCCO* genes were not detected, including *CaNCED1*, *CaNCED2*, *CaCCD4c*, *CaCCD7*, *CaCCD-like1*, *CaCCD8*, *CaCCD-like2*, *CaCCD-like3*, *CaNCED4*, and *CaCCD4b*. Three genes (*CaCCD1a*, *CaCCD4a*, and *CaCCD1b*) were expressed constitutively in all of the stages that were analyzed. The expression of *CaNCED3* is weak and gradually decreases along with the development.

The expression patterns of all *CaCCO* genes in the flower organs were explored, including twelve different tested stages (F1–F9), petals (P10), ovary (O10), and stamens (STA10). As shown in **Figure 3**, among 14 *CaCCO* genes, three members (*CaCCD1a*, *CaNCED3*, and *CaCCD1b*) were expressed in all twelve tested stages. The expression levels of *CaNCED2* and *CaNCED3* increased gradually in different developmental stages, but those of *CaCCD4a* and *CaCCD1b* decreased gradually in different stages, and *CaCCD4a* was not expressed in stamens. *CaCCD1a* has the highest expression in all periods, while *CaCCD4b* only has the expression in F8, F9, and STA10, and the expression in STA10 is the highest.

In pepper fruit, three tissues (placenta, seeds, and pericarp) were selected for analyzing the expression patterns of the *CaCCO* genes. The developmental stages in each of the tissues (placenta: T3–T11, seed: S3–S11, pericarp: G1–G11, fruits at days 3 and 7: FST0, FST1, and seeds and placenta at days 10 and 15: ST1, ST2) were included. As shown in **Figure 3**, half members of the *CaCCO* gene family have relatively high expression levels, and the mean of the log-signal values of each gene is within the range of 10 to 20. On the contrary, nine genes show relatively low expression levels with the mean of the log-signal values of each gene ranging from 0 to 1.

In the placenta and seed, the results showed that most of the *CaCCO* genes were expressed in different developmental stages. Some genes such as *CaCCD1a*, *CaNCED2*, *CaCCD4a*, *CaNCED3*, and *CaCCD1b* were highly expressed in the seeds and placenta of capsicum, indicating that these genes may play an important role in the development of capsicum plants. The gene *CaCCD1a* was highly expressed in T3–T11, and *CaNCED1* was in S5–S11. The *CaNCED3* and *CaCCD1b* were highly expressed in ST1–T11. The transcript levels of *CaCCD1b* were highly expressed in S3. In pericarp, there were four members with high expression, namely, *CaCCD1a*, *CaCCD4a*, *CaNCED3*, and *CaCCD1b*. Among them, *CaCCD1a* and *CaCCD1b* have the highest expression in each stage of fruit development; *CaCCD4a* has a higher expression in the early stage of fruit development and a lower expression in the later stage, but not in the G11 stage. *CaCCD4c*, *CaCCD7*, *CaCCD-like1*, *CaCCD8*, *CaCCD-like2*, *CaCCD-like3*, *CaCCD4b*, and *CaNCED1* gene has a similar expression in different period of time, such as FST0–G11. The *CaCCO* gene has a lower expression. These results indicate that half of *CaCCO* genes are involved in plant growth and development.

Expression of CaCCOs in Response to Hormone Treatments

Previous studies have shown that hormones, including cytokinins (CKs), gibberellins (GAs), salicylic acid (SA), jasmonic acid



FIGURE 1 | Evolutionary origin of carotenoid cleavage oxygenase (CCO) proteins in plant species. The unrooted tree was constructed using the neighbor-joining (NJ) method in MEGA5.0 software. The parameters were 1,000 bootstraps. The CCO proteins were classified into two groups: I and II. The former was subdivided into CCD7 and CCD8, while the latter was subdivided into CCD1, CCD-like, CCD4, and NCED.

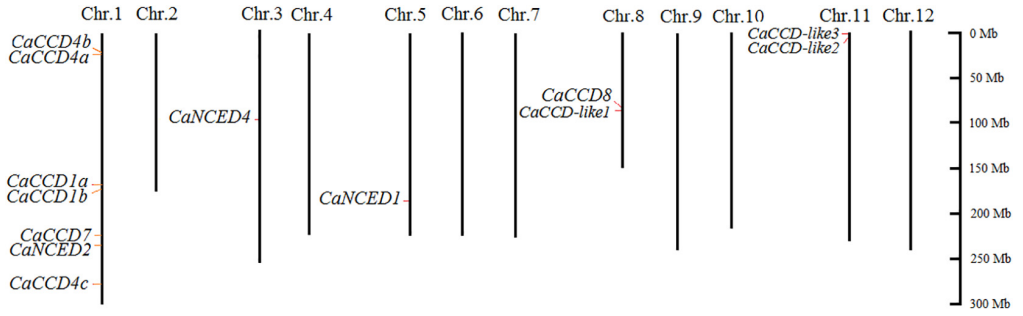


FIGURE 2 | Chromosomal mapping of the *CCO* genes in *Capsicum annuum*. The chromosome number is shown at the top of each bar chart, while the size of the chromosome is shown in its relative length. The scale on the right is in MB, and the short line represents the approximate positions of the *CaCCO* genes on the respective chromosome.

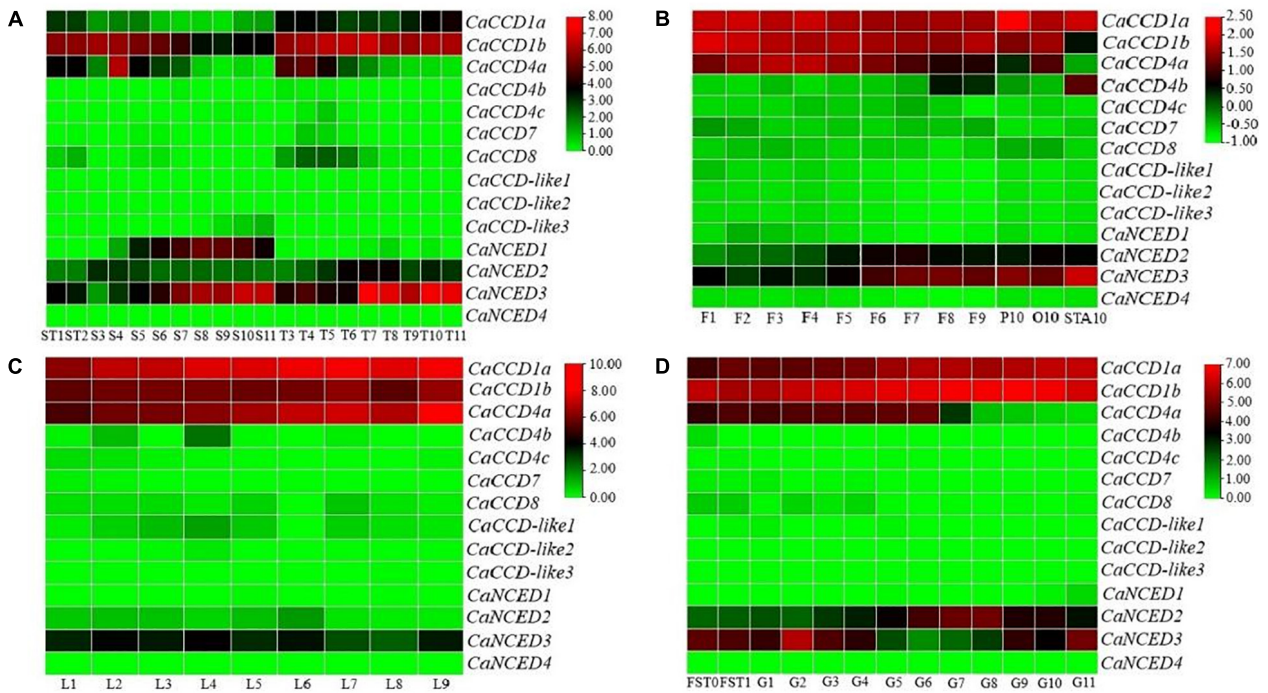


FIGURE 3 | Expression patterns of CaCCOs in different tissues of pepper. Key: red, strong expression; black, weak expression; green, no expression. The expression data were hierarchically clustered based on MeV software. **(A)** Seeds and placenta, **(B)** flowers, **(C)** leaf, and **(D)** fruit and peel.

(MeJA), ethylene (ET), ABA, and brassinosteroids (BRs), play a key role in regulating plant growth and development, adapting to environmental stress and complex signal networks (Vallabhaneni et al., 2010). To further analyze the expression patterns of *CaCCO* genes under stress-related stimulation, the expression profiles of leaves and roots of *CaCCO* genes under ABA, MeJA, and SA-hormone treatments were analyzed.

As illustrated in **Figure 4**, we found that fourteen *CaCCO* genes have different expression patterns in roots and leaves under three different hormone treatments. Among them, five *CaCCO* genes had high expression levels, while the remaining nine genes had low or even no expression levels. The five genes were induced significantly by ABA, MeJA, and SA treatments. Among the five genes, the root expressions of *CaCCD1a* and *CaCCD4a* significantly decreased after treatment with ABA, MeJA, and SA for 1, 6, and 24 h, while the expression levels in leaves showed a trend of first increasing and then decreasing. Among them, the expression levels of *CaCCD4a* under treatment with different hormones were the highest at 6 h for ABA, MeJA, and SA, while the expressions of *CaCCD1a* and *CaNCED3* were in reverse manner. Expression levels were decreased at 6 h for ABA, MeJA, and SA.

Expression of CaCCOs in Response to Cold, Heat, Drought, and NaCl Treatments

Abiotic stresses (heat, cold, drought, and salt) affected the plant growth and development and were the major factors limiting crop production (Simkin et al., 2004a; Ohmiya et al., 2006; Sun et al., 2008; Adami et al., 2013; Liu et al., 2013; Bai et al., 2017). To illustrate the roles of *CaCCO* gene family members in abiotic stresses, the RNA-seq data of pepper under four treatments (heat, cold, drought, and NaCl) have been selected. Interestingly, similar expression patterns of most of the *CaCCO* genes were observed in pepper, whereas some differences in expression patterns can be carefully shown. The results showed that at least four genes were significantly induced under different stresses, and these genes have similar expression patterns, such as *CaCCD1a*, *CaCCD4a*, *CaNCED3*, *CaCCD1b*, and *CaCCD8*. The remaining *CaCCO* genes are not regulated under low temperature, high temperature, drought, and salt stresses.

For cold stress (**Figure 5**), *CaCCD1a* and *CaCCD4a* share a similar expression pattern, and the upregulated expression was followed by a downregulated expression in FL1–FL24. However, in roots, the expression of these two genes was downregulated after cold treatment. The expressions of *CaNCED3* and *CaCCD1b* were upregulated in leaves under low-temperature treatment, especially the expression level of *CaNCED3* was increased about 200 times after 24 h of low-temperature treatment. Under heat treatment conditions, the *CaCCD1a* and *CaCCD4a* slightly upregulated the stage of CL0 and HL1, then the *CaCCD1a* and *CaCCD4a* gene was downregulated in all the stages analyzed. However, in roots, the expression of these two genes was significantly decreased after high-temperature treatment.

Under drought stress (**Figure 5**), the expression of *CaCCD4a* in leaves was upregulated first and then downregulated, and the highest expression level was reached after 4 h of

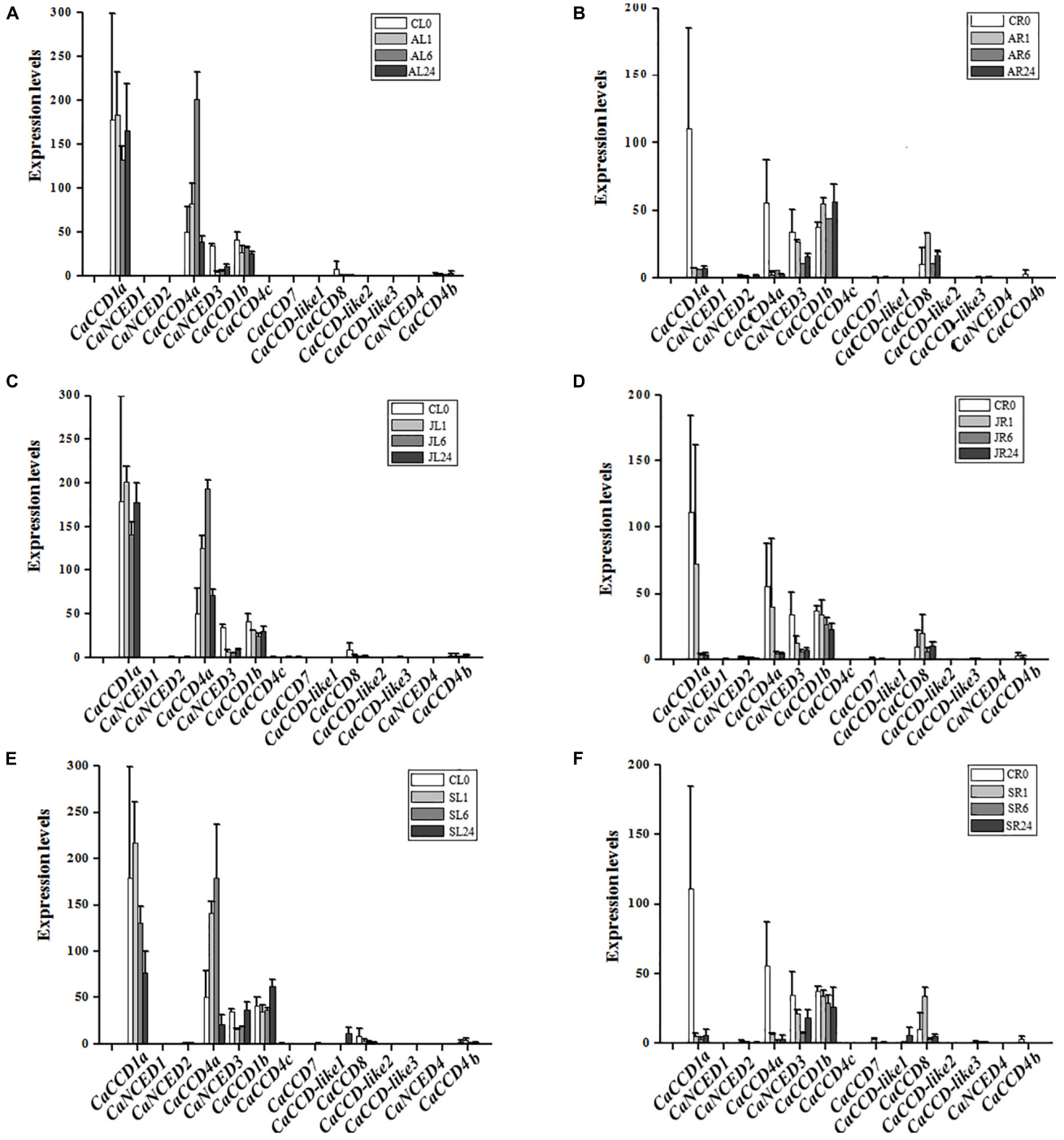


FIGURE 4 | Expression of *CaCCO* genes under different hormone treatments. **(A)** Leaves under abscisic acid (ABA) treatment, **(B)** roots under ABA treatment, **(C)** leaves under jasmonic acid (MeJA) treatment, **(D)** roots under MeJA treatment, **(E)** leaves under salicylic acid (SA) treatment, and **(F)** roots under SA treatment.

drought treatment. However, the expression of this gene was significantly downregulated in roots. The expression of *CaNCED3* was the highest in leaves and roots at 1 h after drought treatment and then decreased. Of the fourteen genes, about half responded to salt stress, suggesting that these genes were involved in coping with environmental changes. In leaves, a total of 6 genes were upregulated, among which the most significant ones were *CaCCD1a* and *CaCCD4a*, followed by *CaNCED3* and *CaNCCD1b*, and the expressions of *CaCCD8* and *CaCCD4b* were the lowest. The expression pattern of the *CaCCO* gene family in roots under salt stress was the same as that in roots under

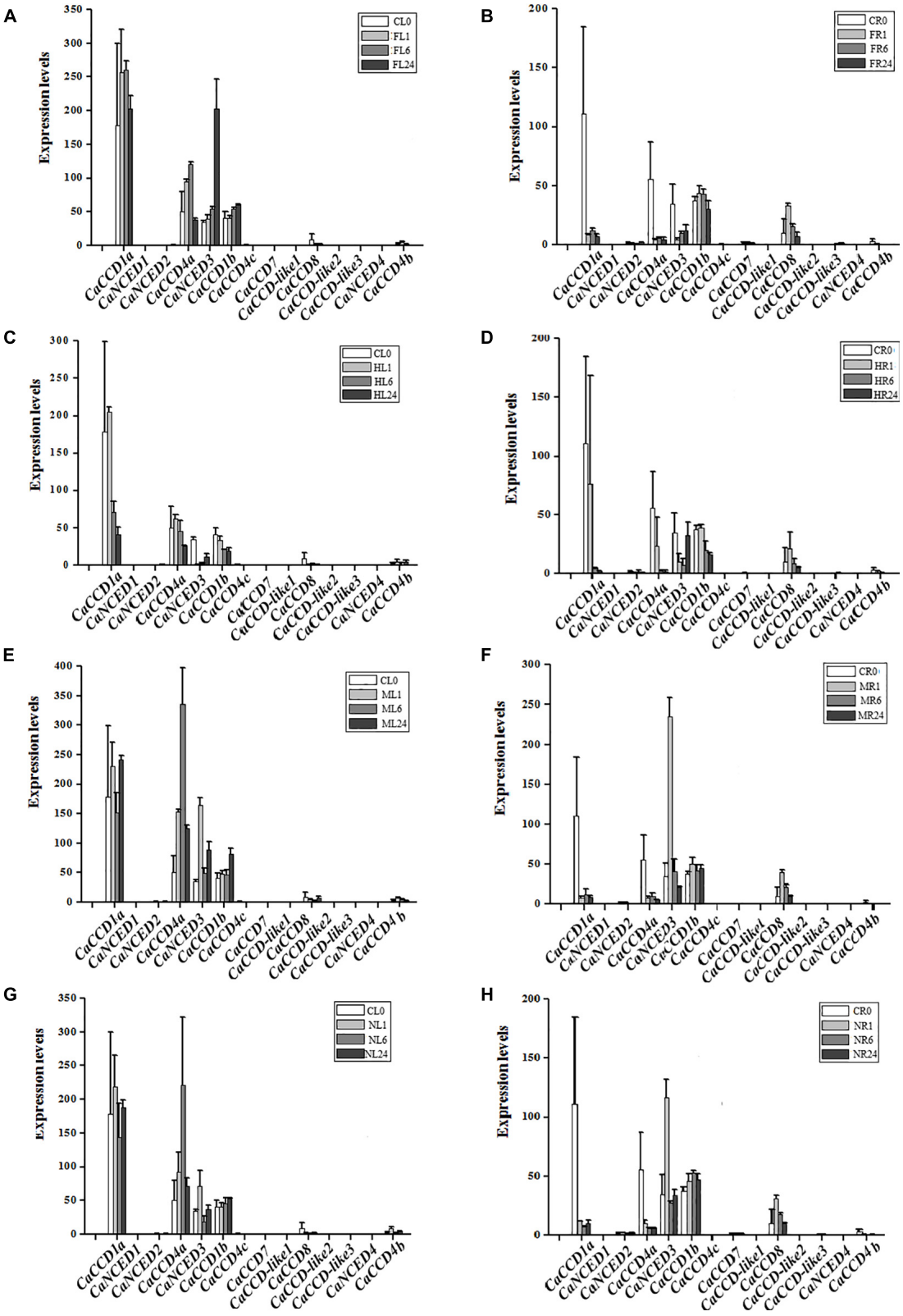


FIGURE 5 | Expression patterns of *CaCCO* genes under low/high temperature, drought, and salt stresses. **(A)** Leaves under cold stress, **(B)** roots under cold stress, **(C)** leaves under heat stress, **(D)** roots under heat stress, **(E)** leaves under drought stress, **(F)** roots under drought stress, **(G)** leaves under NaCl stress, and **(H)** roots under NaCl stress.

drought treatment, the expressions of *CaCCD1a* and *CaCCD4a* were significantly downregulated, and the expressions of *CaNCED3*, *CaCCD1b*, and *CaCCD8* were upregulated first and then downregulated.

Expression of CaCCOs in Response to H_2O_2 Treatments

Under the H_2O_2 treatment condition (**Figure 6**), expressions of 6 *CaCCO* genes were induced in pepper leaf, including *CaCCD1a*, *CaCCD4a*, *CaNCED3*, *CaCCD1b*, *CaCCD8*, and *CaCCD4b*. Among them, the expression levels of *CaCCD1a* and *CaCCD4a* were first increased and then decreased. The expression level of *CaCCD1a* was the highest at 1 h of H_2O_2 treatment, while *CaCCD4a* reached the maximum at 6 h of H_2O_2 treatment. In addition, the trend of *CaNCED3* and *CaCCD1b* treated with H_2O_2 was opposite to the former. The expression levels reached a peak at 24 h after treatment. In root, expressions of 8 *CaCCO* genes were induced, namely *CaCCD1a*, *CaNCED2*, *CaCCD4a*, *CaNCED3*, *CaCCD1b*, *CaCCD7*, *CaCCD8*, and *CaCCD4b*. Among them, the expression levels of *CaCCD1a*, *CaCCD4a*, and *CaNCED3* decreased gradually, while *CaCCD1b* and *CaCCD8* increased first and then decreased. The expression levels of *CaCCD1b* reached the highest at 1 h and *CaCCD8* reached the peak at 6 h.

Quantitative RT-PCR Analysis of Members of *CaCCO* Gene Family in Response to Abiotic Stresses

The expression levels of the CaCCOs were investigated under heat, cold, drought, and NaCl treatments using qRT-PCR to understand their possible roles in responses to abiotic stresses (**Table 2**). Under heat stress, the expression levels of half of the genes were significantly downregulated with large-fold changes at the 0.5, 1, 4.5, and 6 h, respectively, while *CaCCD4a*, *CaCCD4c*, and *CaCCD-like1* were first upregulated and then downregulated at three of the four time points (**Figure 7**). Notably, some *CaCCDs* exhibited significant differences across the four time points. *CaCCD4a* and *CaCCD4c* reached the maximum value at 0.5 h. Three members (*CaCCD1a*, *CaCCD1b*, and *CaCCD-like1*) significantly elevated at 1 h. *CaNCED3* expression was significantly downregulated at 0.5 h, but significantly upregulated at 6 h after heat treatment. Under cold stress, we found that expression levels of *CaCCD4c*, *CaCCD7*, *CaCCD8*, *CaCCD-like3*, *CaNCED1*, and *CaNCED2* were significantly downregulated at all of the four time points (**Figure 8**). In addition, the expression levels of four genes, namely, *CaCCD1a*, *CaCCD1b*, *CaCCD4a*, and *CaNCED3*, showed a trend of upregulation and then downregulation, respectively. Notably, *CaCCD1a*, *CaCCD1b*, *CaCCD4a*, and *CaCCD-like2* all peaked at 3 h after cold treatment.

To explore the expression patterns of CCO gene family in pepper in response to drought and NaCl stresses, based on the RNA-seq data, we showed the upregulated in leaves, selected to verify using qRT-PCR analysis at 1, 6, 12, and 24 h expression patterns after treatments. For drought stress, nine genes were downregulated (**Figure 9**), including *CaCCD1a*, *CaCCD1b*, *CaCCD4a*, *CaCCD4c*, *CaCCD7*, *CaCCD8*, *CaCCD-like2*, *CaCCD-like3*, and *CaNCED2*. In addition, only *CaNCED1* and *CaNCED3* showed upregulation before downregulation among the twelve genes. However, the difference between the two groups was that the expression level of the former reached its peak at 1 h under drought treatment, increased by 5.7 times compared with the control, while the latter reached its peak at 6 h and increased by 7.7 times compared with the control. In addition, under 400 mM NaCl treatment (**Figure 10**), our results found that the expression levels of most genes were downregulated, including *CaCCD1a*, *CaCCD1b*, *CaCCD4a*, *CaCCD4c*, *CaCCD7*, *CaCCD8*, *CaCCD-like1*, *CaCCD-like3*, *CaNCED1*, and *CaNCED2*. However, only *CaCCD-like2* and *CaNCED3* were upregulated and then downregulated. Notably, the expression of *CaCCD-like2* was the highest after 12 h of stress treatment, while the expression of *CaNCED3* was the highest after 1 h of stress treatment. These results showed that the *CaCCD* gene family has a certain function in plant response to abiotic

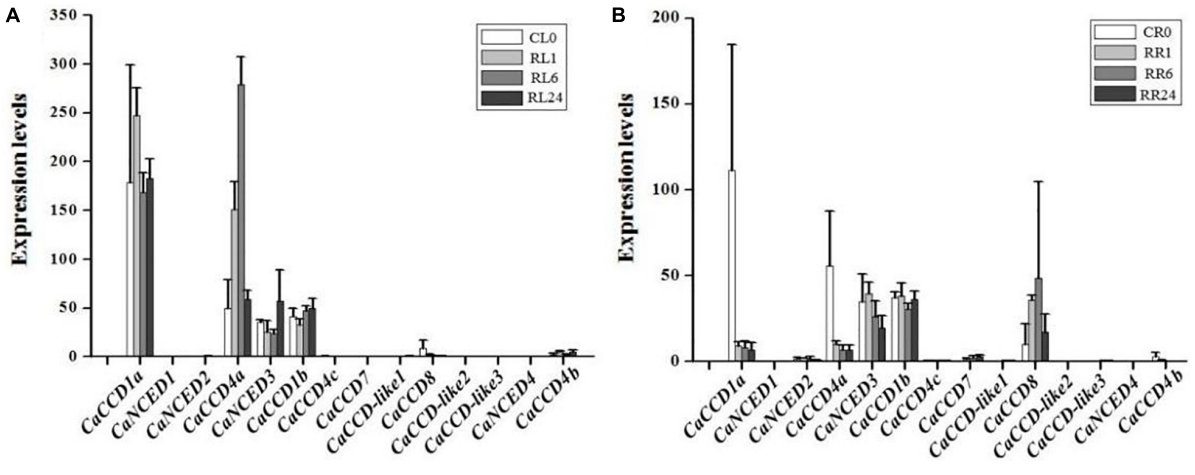


FIGURE 6 | Expression of *CaCCO* genes under hydrogen peroxide (H_2O_2) treatment. **(A)** Leaves under H_2O_2 stress and **(B)** roots under H_2O_2 stress.

TABLE 2 | Sequences of the primers used in quantitative real-time PCR (qRT-PCR) analysis in this study.

Gene name	Forward primers	Reverse primers
GAPDH	ATGATGATGTGAAAGCAGCG	TTTCAACTGGTGGCTGCTAC
CaCCD1a	GCGTCATGCAAGATCCAGTT	AAAGCGAGCCTTCTTTGTGG
CaCCD1b	TCGTCCGAAGGAAATGGTGA	CCAAGCGTTGGCATTATGGA
CaCCD4a	TCTTCCACGTGGTCCTTACC	AGGCAGAGAGACCGTTGAAA
CaCCD4c	TGGACCTAATTCGCCCAAGA	AGGGTTCCCAATAGCTGCAT
CaCCD7	GGATATGTTGCTCCCTCGGA	TGCTGTCATTGACCCAGGAA
CaCCD8	GTGTAAAGCCAGTGGCAACA	CGGAGATTGTCAAGGCGAAG
CaCCD-like1	GTGTTGAGGTTTGGCGTGAT	GCTTTCTTTGGGTGGCTTGT
CaCCD-like2	AAGATGAGGTGGTGGTGAGG	GAAGTTTGGCTAGCCCTCCA
CaCCD-like3	TGCGAGAATTGGAATAATGCCT	CTACTGCGATAGCCGGTCTT
CaNCED1	CTGCTTCTGCATGCATCTGT	CCGTTTGGTTGACTCACCTG
CaNCED2	GAAGAGCCAGAGACGGATGA	TCGTTTCCTCGACTCTCCAG
CaNCED3	TGGCATGGTTCATGCTGTTC	CCGAAGAGTCCACGAGCATA

stress, but its molecular mechanism may be different among different genes.

DISCUSSION

Plant *CCO* gene family, a class of specific enzymes, can catalyze conjugated double-bond system of carotenoids and their apocarotenoids to form smaller compounds (Ilg et al., 2009; Walter et al., 2010). These CCO proteins catalyze the cleavage of carotenoids and help to adjust the plant responses to stress (Espasandin et al., 2014). Therefore, it is very important to understand the evolutionary relationship and function of *CCO* genes in plant species. In this study, our results showed that plant *CCO* genes could be divided into two subfamilies (groups I and II). Group I was subdivided into *CCD7* and *CCD*, and group II was composed of *CCD1*, *CCD4*, *CCD-like*, and *NCED*. We found that orthology groups (*CCD7* and *CCD8*) appeared to be conserved only as single- or low-copy genes in all plants, whereas group II genes underwent several duplication events, resulting in multiple gene copies. These duplication events were due to whole-genome duplications in plants. Our results indicate that group II genes had strikingly different patterns of gene duplication from genes from *CCD7* and *CCD8*. The *CCD1* genes expanded during the histories of land plants (**Figure 1**). Unlike *CCO* genes from group II, other types of plant *CCO* genes (*CCD7* and *CCD8*) are single- or low-copy genes. The stably maintained low-copy numbers for these *CCO* genes suggest the functional conservation during the process of evolution in plants. These results also suggested that differential evolution of members of the *CCO* gene family with conservative and divergent patterns were observed.

The gene expression profiles often have some connection with gene function. To date, although the expression patterns of *CCO* genes have been determined in other plants, there are few detailed studies on the expression of *CCO* genes in pepper. To determine whether there were differences in the expression of *CaCCO* genes, the transcriptional levels of each member in pepper were analyzed spatially and temporally. In four different organs, about half of the *CaCCO* genes were not fully expressed at all stages of detection. In leaf, the *CaCCD1a*, *CaCCD4a*, *CaNCED3*, and *CaCCD1b* were expressed in all of the detected stages. Compared with the other three genes, the expression of *CaNCED3* was lower at all stages. We concluded that they are likely to act as a housekeeping gene of pepper cells under normal growth conditions. In flower, high expression levels of four genes (*CaCCD1a*, *CaCCD4a*, *CaNCED3*, and *CaCCD1b*) were observed in all the stages analyzed (F1–F9), indicating that these genes were involved in the growth and development of the flower. The *CaNCED2* and *CaNCED3* are transcribed at the late stage (F5–F9), while *CaCCD1a*, *CaCCD4a*, and *CaCCD1b* are transcribed in the whole development stage (F1–F9). These results suggest that these genes may play different functional roles at different stages of development.

We further analyzed the expression profiles of these *CaCCO* genes in the placenta, seed, and pericarp. In the placenta, all genes were expressed at different stages. Among them, the expressions of *CaCCD1a*, *CaNCED2*, *CaNCED3*, and *CaCCD1b* were the highest (T3–T11), and the expression of *CaNCED1* was the lowest in the whole placenta development period. The expression levels of *CaCCD4a* and *CaCCD8* were highest in the early placental stage (T1–T6) and decreased in the late placental stage (T7–T11). In seeds, *CaCCD4a* was expressed preferentially in the early stage (S1–S7), while *CaNCED1* was transcribed in the late stage (S5–S11). The expression level of *CaCCD1b* was the highest in each period, and the expression level of *CaNCED3* was the highest in all periods except S3–S4. The results indicated that these genes are related to seed development and maturation in pepper plants. The expression levels of two genes (*CaCCD1a* and *CaCCD1b*) in the pericarp were the highest (FST0–G11) during the whole development period. *CaCCD4a* and *CaNCED3* were expressed in the early stage (G1–G4), and *CaCCD4c* and *CaCCD1b* were expressed in the late stage (G5–G11). We concluded that these genes play important roles in the formation and maturity of pepper pericarp. In conclusion, these *CaCCO* genes may have specific functions in different organs and stages.

Under abiotic stress, the effects of heat and cold stress on plant growth induced the expression of multiple *CaCCO* genes in leaves. Under heat stress, *CaCCD1a*, *CaCCD4a*, and *CaCCD1b* genes were downregulated at different stages. Under cold stress, four *CaCCO* genes (*CaCCD1a*, *CaCCD4a*, *CaNCED3*, and *CaCCD1b*) were obviously induced, while *CaCCD8* and *CaCCD4b* were slightly induced. Drought stress and salt stress also induced this trend.

The NCED, a key rate-limiting enzyme in ABA biosynthesis, plays an important role in regulating plant growth and development and stress responses. Some studies have reported that ABA synthesis in plants can respond to oxidative stress, and oxidative reaction has the function of reactive oxygen species (ROS) clearance. ROS are biological molecules that are necessary for seed dormancy and germination. Among them, H_2O_2 can maintain cell homeostasis and participate in the regulation of photosynthesis, seed germination, and stomatal characteristics, and other physiological activities. O^{2-} and other ROS such as hydroxyl radical (OH), perhydroxy radical (HO^2), alkoxy radicals (RO), H_2O_2, and singlet oxygen ($^1O_2$) are produced

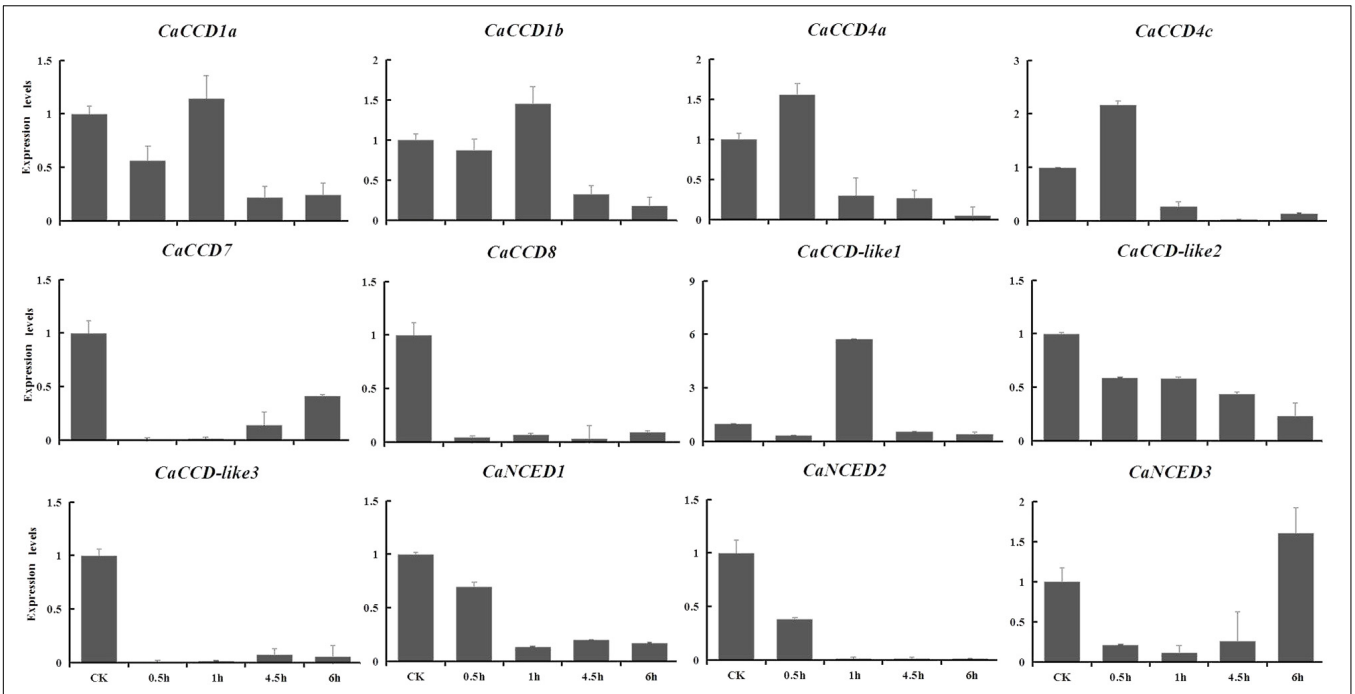


FIGURE 7 | Expression patterns of *CaCCO* genes in response to heat stress at different time points.

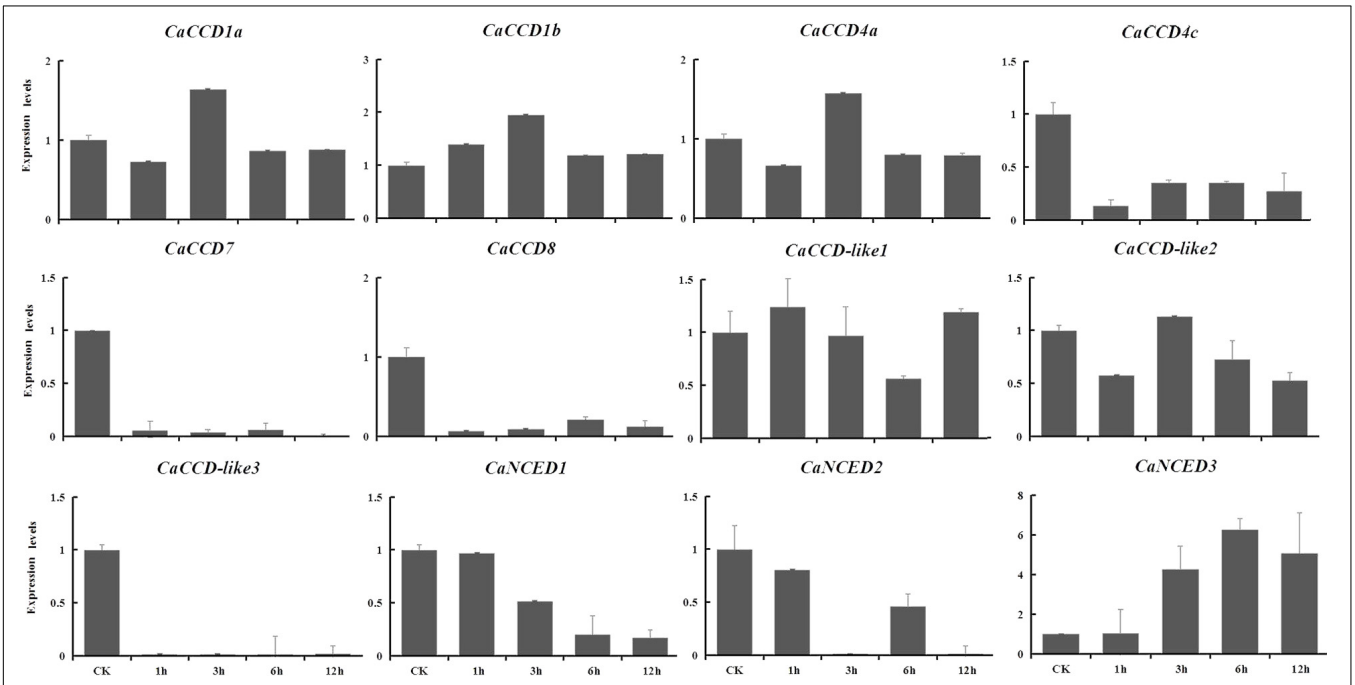


FIGURE 8 | Expression patterns of *CaCCO* genes in response to cold stress at different time points.

continuously as byproducts of various metabolic pathways that are localized in different cellular compartments including mitochondria, chloroplast, and peroxisomes (del Río et al., 2006; Navrot et al., 2007). Under stable conditions, ROS can be removed and maintained in equilibrium utilizing antioxidants or antioxidant enzymes (Gill and Tuteja, 2010). In the study, the results indicate that about half of the *CCO* genes can be induced by H_2O_2 stress in both roots and leaves, and their expression levels in leaves are upregulated first and downregulated later, which may be related to ABA synthesis and stress regulation.

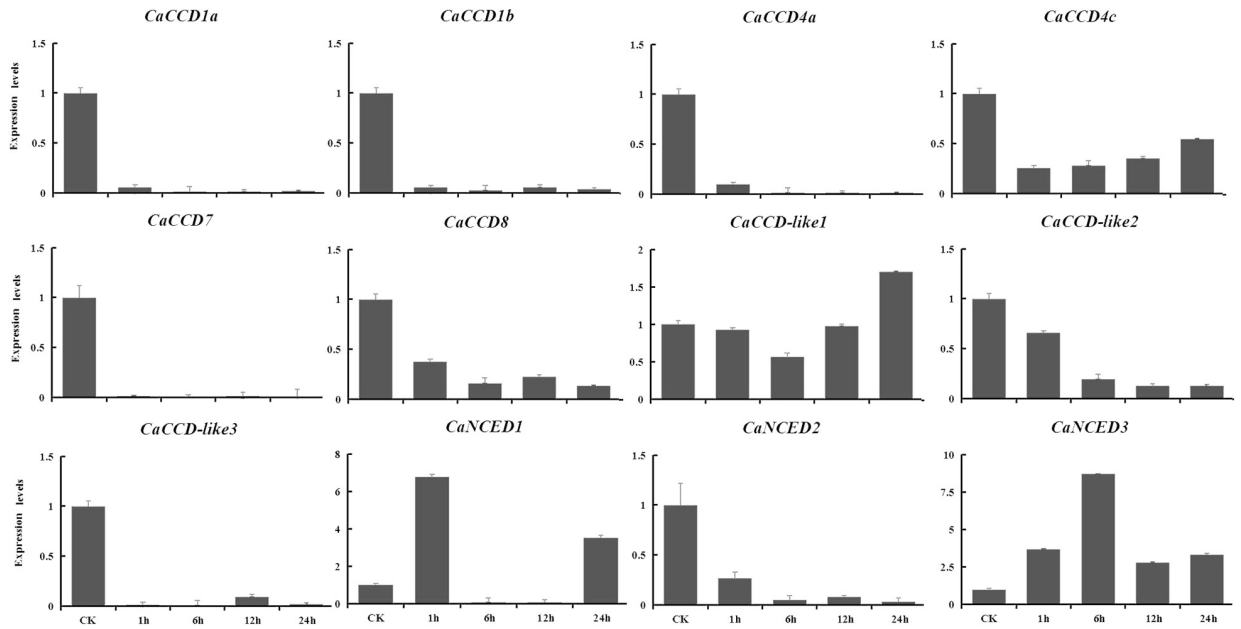


FIGURE 9 | Expression patterns of *CaCCO* genes in response to drought stress at different time points.

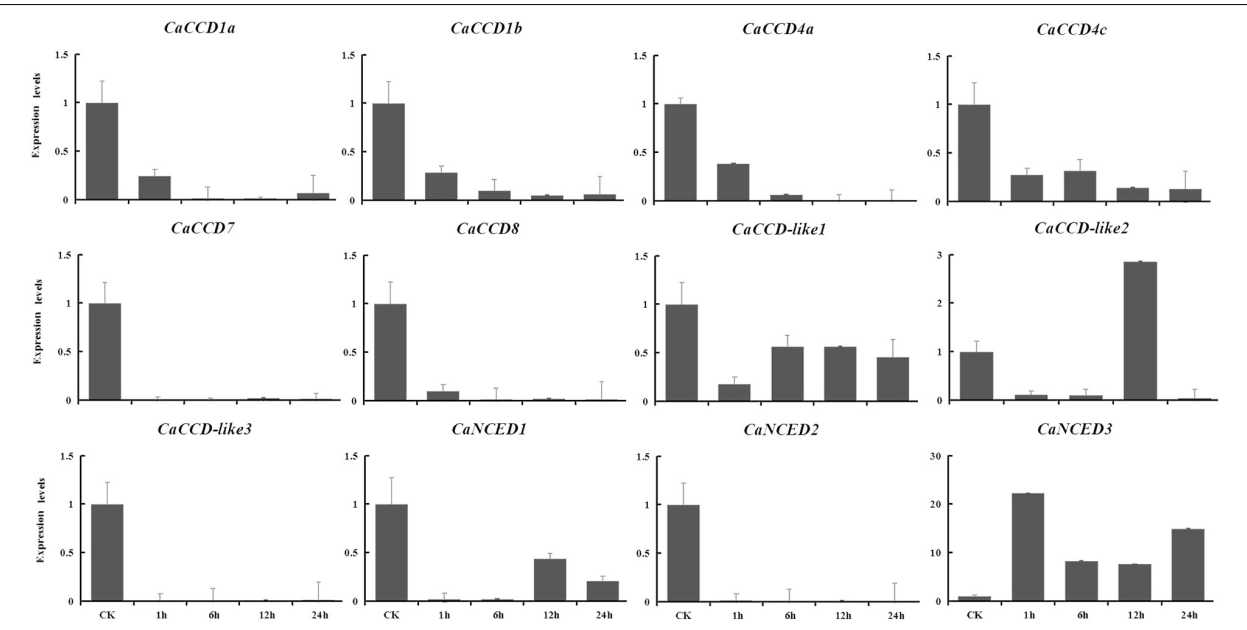


FIGURE 10 | Expression patterns of *CaCCO* genes in response to salt stress at different time points.

The specific mechanism of *CCO* genes needs to be confirmed by further experiments.

CONCLUSION

The RNA-seq analysis of the *CaCCO* gene family provides a solid foundation for us to fully understand the functions of the *CCO* gene in pepper growth and development and abiotic stress. However, the functions of these genes in each genome are still unclear and need to be verified by further experiments.

DATA AVAILABILITY STATEMENT

The original contributions presented in the study are included in the article/**Supplementary Material**, further inquiries can be directed to the corresponding authors.

AUTHOR CONTRIBUTIONS

YXY, LJ, and HW conceived and designed the research. YC, MR, QY, RW, ZY, and GZ performed the experiments. JL, JY, PZ, and YHY analyzed the data and wrote the manuscript. YXY, WD, and HW revised the manuscript. All authors have read and agreed to the published version of the manuscript.

FUNDING

This research was partially supported by the National Key Research and Development Program of China (2018YFD1000800 and 2017YFE0114500), China Agriculture Research System of MOF and MARA (CARS-23-G-44), National Natural Science Foundation of China (31772294, 31960601, and 32060446), and Natural Science Foundation of Inner Mongolia Autonomous Region of China (2021MS03106 and 2021MS03071).

SUPPLEMENTARY MATERIAL

The Supplementary Material for this article can be found online at: https://www.frontiersin.org/articles/10.3389/fpls.2021.792832/full#supplementary-material

REFERENCES

Adami, M., Franceschi, P., Brandi, F., Liverani, A., Giovannini, D., Rosati, C., et al. (2013). Identifying a carotenoid cleavage dioxygenase (CCD4) gene controlling yellow/white fruit flesh color of peach. *Plant Mol. Biol. Rep.* 31, 1166–1175. doi: 10.1007/s11105-013-0628-6

Auldridge, M. E., Block, A., Vogel, J. T., Dabney-Smith, C., and Klee, H. J. (2006). Characterization of three members of the *Arabidopsis* carotenoid cleavage dioxygenase family demonstrates the divergent roles of this multifunctional enzyme family. *Plant J.* 45, 982–993. doi: 10.1111/j.1365-313X.2006.02666.x

Bai, G., Yang, D. H., Yao, H., and Xie, H. (2017). Identification and analysis of NtNCED gene in tobacco. *Mol. Plant Breed.* 10, 73–78. doi: 10.13271/j.mpb.015.003907

Blankenship, S. M., and Sisler, E. C. (1993). Response of apples to diazocyclopentadiene inhibition of ethylene binding. *Postharvest Biol. Technol.* 3, 95–101. doi: 10.1016/0925-5214(93)90001-J

Brandi, F., Bar, E., Mourgues, F., Horváth, G., Turcsi, E., Giuliano, G., et al. (2011). Study of' 'Redhave' peach and its white-fleshed mutant suggests a key role of CCD4 carotenoid dioxygenase in carotenoid and norisoprenoid volatile metabolism. *BMC Plant Biol.* 11:24. doi: 10.1186/1471-2229-11-24

Britton, G., Liaaen-Jensen, S., and Pfander, H. P. (2004). *Handbook of Carotenoids*. Basel: Birkhäuser

Burbidge, A., Grieve, T. M., Jackson, A., Thompson, A., McCarty, D. R., and Taylor, I. B. (1999). Characterization of the ABA-deficient tomato mutant notabilis and its relationship with maize Vp14. *Plant J.* 17, 427–431. doi: 10.1046/j.1365-313x.1999.00386.x

Campbell, R., Ducreux, L. J., Morris, W. L., Morris, J. A., Suttle, J. C., Ramsay, G., et al. (2010). The metabolic and developmental roles of carotenoid cleavage dioxygenase 4 from potato. *Plant Physiol.* 154, 656–664. doi: 10.1104/pp.110.158733

Chernys, J. T., and Zeevaart, J. A. (2000). Characterization of the 9-cis-epoxycarotenoid dioxygenase gene family and the regulation of abscisic acid biosynthesis in avocado. *Plant Physiol.* 124, 343–353. doi: 10.1104/pp.124.1.343

del Río, L. A., Sandalio, L. M., Corpas, F. J., Palma, J. M., and Barroso, J. B. (2006). Reactive oxygen species and reactive nitrogen species in peroxisomes. production, scavenging, and role in cell signaling. *Plant Physiol.* 141, 330–335. doi: 10.1104/pp.106.078204

Desikan, R., Cheung, M. K., Bright, J., Henson, D., Hancock, J. T., and Neill, S. J. (2004). ABA, hydrogen peroxide and nitric oxide signalling in stomatal guard cells. *J. Exp. Bot.* 55, 205–212. doi: 10.1093/jxb/erh033

Espasandin, F. D., Maiale, S. J., Calzadilla, P., Ruiz, O. A., and Sansberro, P. A. (2014). Transcriptional regulation of 9-cis-epoxycarotenoid dioxygenase (NCED) gene by putrescine accumulation positively modulates ABA synthesis and drought tolerance in *Lotus tenuis* plants. *Plant Physiol. Biochem.* 76, 29–35. doi: 10.1016/j.plaphy.2013.12.018

Fan, J., Hill, L., Crooks, C., Doerner, P., and Lamb, C. (2009). Abscisic acid has a key role in modulating diverse plant-pathogen interactions. *Plant Physiol.* 150, 1750–1761. doi: 10.1104/pp.109.137943

Frey, A., Effroy, D., Lefebvre, V., Seo, M., Perreau, F., Berger, A., et al. (2012). Epoxycarotenoid cleavage by NCED5 fine-tunes ABA accumulation and affects seed dormancy and drought tolerance with other NCED family members. *Plant J.* 70, 501–512. doi: 10.1111/j.1365-313X.2011.04887.x

Gill, S., and Tuteja, N. (2010). Reactive oxygen species and antioxidant machinery in abiotic stress tolerance in crop plants. *Plant Physiol. Biochem.* 48, 909–930. doi: 10.1016/j.plaphy.2010.08.016

Gómez, C. A., Arbona, V., Jacas, J., Primo-Millo, E., and Talon, M. (2002). Abscisic acid reduces leaf abscission and increases salt tolerance in citrus plants. *J. Plant Growth Regul.* 21, 234–240. doi: 10.1007/s00344-002-0013-4

Huang, F. C., Molnár, P., and Schwab, W. (2009). Cloning and functional characterization of carotenoid cleavage dioxygenase 4 genes. *J. Exp. Bot.* 60, 3011–3022. doi: 10.1093/jxb/erp137

Huang, Y., Guo, Y., Liu, Y., Zhang, F., Wang, Z., Wang, H., et al. (2018). 9-cis-epoxycarotenoid dioxygenase 3 regulates plant growth and enhances multi-abiotic stress tolerance in rice. *Front. Plant Sci.* 9:162. doi: 10.3389/fpls.2018.00162

Hwang, S. G., Lee, C. Y., and Tseng, C. S. (2018). Heterologous expression of rice 9–cis–epoxycarotenoid dioxygenase 4 (OsNCED4) in *Arabidopsis* confers sugar oversensitivity and drought tolerance. *Bot. Stud.* 59:2. doi: 10.1186/s40529-018-0219-9

Ilg, A., Beyer, P., and Babili, S. (2009). Characterization of the rice carotenoid cleavage dioxygenase 1 reveals a novel route for geranial biosynthesis. *FEBS J.* 276, 736–747. doi: 10.1111/j.1742-4658.2008.06820.x

Jiang, M., and Zhang, J. (2003). Cross-talk between calcium and reactive oxygen species originated from NADPH oxidase in abscisic acid-induced antioxidant defense in leaves of maize seedlings. *Plant Cell Environ.* 26, 929–939. doi: 10.1046/j.1365-3040.2003.01025.x

Kong, X., Luo, Z., Dong, H., Eneji, A. E., and Li, W. (2016). H2O2 and ABA signaling are responsible for the increased Na+ efflux and water uptake in *Gossypium hirsutum* L. roots in the non-saline side under non-uniform root zone salinity. *J. Exp. Bot.* 8:2247. doi: 10.1093/jxb/erw026

Lefebvre, V., North, H., Frey, A., Sotta, B., Seo, M., Okamoto, M., et al. (2010). Functional analysis of *Arabidopsis* NCED6 and NCED9 genes indicates that ABA synthesized in the endosperm is involved in the induction of seed dormancy. *Plant J.* 45, 309–319. doi: 10.1111/j.1365-313X.2005.02622.x

Liu, J., Novero, M., Charnikhova, T., Ferrandino, A., Schubert, A., Ruyter Spira, C., et al. (2013). Carotenoid cleavage dioxygenase 7 modulates plant growth, reproduction, senescence, and determinate nodulation in the model legume *Lotus japonicus*. *J. Exp. Bot.* 64, 1967–1981. doi: 10.1093/jxb/ert056

Nambara, E., Okamoto, M., Tatematsu, K., Yano, R., Seo, M., and Kamiya, Y. (2010). Abscisic acid and the control of seed dormancy and germination. *Seed Sci. Res.* 20, 55–67. doi: 10.1017/S0960258510000012

Navrot, N., Rouhier, N., Gelhaye, E., and Jaquot, J. P. (2007). Reactive oxygen species generation and antioxidant systems in plant mitochondria. *Physiol. Plant.* 129, 185–195. doi: 10.1111/j.1399-3054.2006.00777.x

Neill, S. J., Desikan, R., Clarke, A., Hurst, R. D., and Hancock, J. T. (2002). Hydrogen peroxide and nitric oxide as signaling molecules in plants. *J. Exp. Bot.* 53, 1237–1247. doi: 10.1093/jexbot/53.372.1237

Ohmiya, A., Kishimoto, S., Aida, R., Yoshioka, S., and Sumitomo, K. (2006). Carotenoid cleavage dioxygenase (CmCCD4a) contributes to white color

formation in chrysanthemum petals. *Plant Physiol.* 142, 1193–1201. doi: 10.1104/pp.106.087130

Qin, C., Yu, C. S., Shen, Y. O., Fang, X. D., Chen, L., Min, J. M., et al. (2014). Whole-genome sequencing of cultivated and wild peppers provides insights into Capsicum domestication and specialization. *Proc. Natl. Acad. Sci. U.S.A.* 14, 5135–5140. doi: 10.1073/pnas.1400975111

Qin, X., and Zeevaart, J. A. D. (2002). Overexpression of a 9-cis-epoxycarotenoid dioxygenase gene in *Nicotiana plumbaginifolia* increases abscisic acid and phaseic acid levels and enhances drought tolerance. *Plant Physiol.* 128, 544–551. doi: 10.1104/pp.010663

Raza, A., Ashraf, F., Zou, X. L., Zhang, X. K., and Tosif, H. (2020). "Plant adaptation and tolerance to environmental stresses: mechanisms and perspectives," in *Plant Ecophysiology and Adaptation Under Climate Change: Mechanisms and Perspectives I*, ed. M. Hasanuzzaman (Berlin: Springer), 117–145.

Rodrigo, M. J. (2006). Cloning and characterization of two 9-cis-epoxycarotenoid dioxygenase genes, differentially regulated during fruit maturation and under stress conditions, from orange (*Citrus sinensis* L. Osbeck). *J. Exp. Bot.* 57, 633–643. doi: 10.1093/jxb/erj048

Roychoudhury, A., Paul, S., and Basu, S. (2013). Cross-talk between abscisic acid-dependent and abscisic acid-independent pathways during abiotic stress. *Plant Cell Rep.* 32, 985–1006. doi: 10.1007/s00299-013-1414-5

Schwartz, S. H., Tan, B. C., Gage, D. A., Zeevaart, J. A., and Mccarty, D. R. (1997). Specific oxidative cleavage of carotenoids by VP14 of maize. *Science* 276, 1872–1874. doi: 10.1126/science.276.5320.1872

Seo, M., Hanada, A., Kuwahara, A., Endo, A., Okamoto, M., Yamauchi, Y., et al. (2006). Regulation of hormone metabolism in *Arabidopsis* seeds: phytochrome regulation of abscisic acid metabolism and abscisic acid regulation of gibberellin metabolism. *Plant J.* 48, 354–366. doi: 10.1111/j.1365-313X.2006.02881.x

Seo, M., Nambara, E., Choi, G., and Yamaguchi, S. (2009). Interaction of light and hormone signals in germinating seeds. *Plant Mol. Biol.* 69, 463–472. doi: 10.1007/s11103-008-9429-y

Simkin, A. J., Schwartz, S. H., Auldridge, M., Taylor, M. G., and Klee, H. J. (2004a). The tomato carotenoid cleavage dioxygenase 1 genes contribute to the formation of the flavor volatiles β-ionone, pseudoionone, and geranylacetone. *Plant J.* 40, 882–892. doi: 10.1111/j.1365-313X.2004.02263.x

Simkin, A. J., Underwood, B. A., Auldridge, M., Loucas, H. M., Shibuya, K., Schmelz, E., et al. (2004b). Circadian regulation of the PhCCD1 carotenoid cleavage dioxygenase controls emission of β-ionone, a fragrance volatile of petunia flowers. *Plant Physiol.* 136, 3504–3514. doi: 10.1104/pp.104.049718

Snowden, K. C., Simkin, A. J., Janssen, B. J., Templeton, K. R., Loucas, H. M., Simons, J. L., et al. (2005). The decreased apical dominance 1/petunia hybrida carotenoid cleavage dioxygenase 8 gene affects branch production and plays a role in leaf senescence, root growth, and flower development. *Plant Cell* 17, 746–759. doi: 10.1105/tpc.104.027714

Sun, Z., Hans, J., Walter, M. H., Matusova, R., Beekwilder, J., Verstappen, F. W., et al. (2008). Cloning and characterisation of a maize carotenoid cleavage dioxygenase (ZmCCD1) and its involvement in the biosynthesis of apocarotenoids with various roles in mutualistic and parasitic interactions. *Planta* 228, 789–801. doi: 10.1007/s00425-008-0781-6

Tamura, K., Peterson, D., Peterson, N., Stecher, G., Nei, M., and Kumar, S. (2011). MEGA5: molecular evolutionary genetics analysis using maximum likelihood, evolutionary distance, and maximum parsimony methods. *Mol. Biol. Evol.* 28, 2731–2739. doi: 10.1093/molbev/msr121

Tan, B. C., Joseph, L. M., Deng, W. T., Liu, L., Li, Q., Cline, K., et al. (2003). Molecular characterization of the *Arabidopsis* 9-cis-epoxycarotenoid dioxygenase gene family. *Plant J.* 35, 44–56. doi: 10.1046/j.1365-313x.2003.01786.x

Tan, B. C., Schwartz, S. H., Zeevaart, J. A., and McCarty, D. R. (1997). Genetic control of abscisic acid biosynthesis in maize. *Proc. Natl. Acad. Sci. U.S.A.* 94, 12235–12240. doi: 10.1073/pnas.94.22.12235

Thompson, A. J., Jackson, A. C., Symonds, R. C., Mulholland, B. J., Dadswell, A. R., Blake, P. S., et al. (2000). Ectopic expression of a tomato 9-cis-epoxycarotenoid dioxygenase gene causes over-production of abscisic acid. *Plant J.* 23, 363–374. doi: 10.1046/j.1365-313x.2000.00789.x

Toh, S., Imamura, A., Watanabe, A., Nakabayashi, K., Okamoto, M., Jikumaru, Y., et al. (2008). High temperature-induced abscisic acid biosynthesis and its role in the inhibition of gibberellin action in *Arabidopsis* seeds. *Plant Physiol.* 146, 1368–1385. doi: 10.1104/pp.107.113738

Uchida, A., Jagendorf, A. T., Hibino, T., Takabe, T., and Takabe, T. (2002). Effect of hydrogen peroxide and nitric oxide on both salt and heat stress tolerance in rice. *Plant Sci.* 163, 515–523. doi: 10.1016/S0168-9452(02)00159-0

Vallabhaneni, R., Bradbury, L. M., and Wurtzel, E. T. (2010). The carotenoid dioxygenase gene family in maize, sorghum, and rice. *Arch. Biochem. Biophys.* 504, 104–111. doi: 10.1016/j.abb.2010.07.019

Walter, M. H., Floss, D. S., and Strack, D. (2010). Apocarotenoids: hormones, mycorrhizal metabolites and aroma volatiles. *Planta* 232, 1–17. doi: 10.1007/s00425-010-1156-3

Welsch, R., Wüst, F., Bär, C., Al-Babili, S., and Beyer, P. (2008). A third phytoene synthase is devoted to abiotic stress-induced abscisic acid formation in rice and defines functional diversification of phytoene synthase genes. *Plant Physiol.* 147, 367–380. doi: 10.1104/pp.108.117028

Xian, L. H., Sun, P. P., Hu, S. S., Wu, J., and Liu, J. H. (2014). Molecular cloning and characterization of CrNCED1, a gene encoding 9-cis-epoxycarotenoid dioxygenase in *Citrus reshni*, with functions in tolerance to multiple abiotic stresses. *Planta* 239, 61–77. doi: 10.1007/s00425-013-1963-4

Yang, J., and Guo, Z. (2007). Cloning of a 9-cis-epoxycarotenoid dioxygenase gene (SgNCED1) from Stylosanthes guianensis and its expression in response to abiotic stresses. *Plant Cell Rep.* 26, 1383–1390. doi: 10.1007/s00299-007-0325-8

Zhang, A., Jiang, M., Zhang, J., Ding, H., Xu, S., Hu, X., et al. (2007). Nitric oxide induced by hydrogen peroxide mediates abscisic acid-induced activation of the mitogen-activated protein kinase cascade involved in antioxidant defense in maize leaves. *New Phytol.* 175, 36–50. doi: 10.1111/j.1469-8137.2007.02071.x

Zhang, W. W., Yang, H. Q., You, S. Z., Fan, S. L., and Ran, K. (2015). MhNCED3, a gene encoding 9-cis-epoxycarotenoid dioxygenase in *Malus hupehensis* Rehd., enhances plant tolerance to Cl- stress by reducing Cl-accumulation. *Plant Physiol. Biochem.* 89, 85–91. doi: 10.1016/j.plaphy.2015.02.012

Zhang, W. W., Yang, H. Q., You, S. Z., Xu, Y. T., Ran, K., and Fan, S. (2014). Cloning, characterization and functional analysis of the role MhNCED3, a gene encoding 9-cis-epoxycarotenoid dioxygenase in *Malus hupehensis* Rehd. plays in plant tolerance to osmotic and Cd2+ stresses. *Plant Soil* 381, 143–160. doi: 10.1007/s11104-014-2120-y

Zhou, B., Guo, Z., Xing, J., and Huang, B. (2005). Nitric oxide is involved in abscisic acid-induced antioxidant activities in *Stylosanthes guianensis*. *J. Exp. Bot.* 56, 3223–3228. doi: 10.1093/jxb/eri319

Conflict of Interest: The authors declare that the research was conducted in the absence of any commercial or financial relationships that could be construed as a potential conflict of interest.

Publisher's Note: All claims expressed in this article are solely those of the authors and do not necessarily represent those of their affiliated organizations, or those of the publisher, the editors and the reviewers. Any product that may be evaluated in this article, or claim that may be made by its manufacturer, is not guaranteed or endorsed by the publisher.

Copyright © 2022 Yao, Jia, Cheng, Ruan, Ye, Wang, Yao, Zhou, Liu, Yu, Zhang, Yin, Diao and Wan. This is an open-access article distributed under the terms of the Creative Commons Attribution License (CC BY). The use, distribution or reproduction in other forums is permitted, provided the original author(s) and the copyright owner(s) are credited and that the original publication in this journal is cited, in accordance with accepted academic practice. No use, distribution or reproduction is permitted which does not comply with these terms.

frontiers in Plant Science

ORIGINAL RESEARCH
published: 27 January 2022
doi: 10.3389/fpls.2021.807514

Genome-Wide Identification of the *PMEI* Gene Family in Tea Plant and Functional Analysis of *CsPMEI2* and *CsPMEI4* Through Ectopic Overexpression

Bo Li[1,2†], Huan Wang[1,2†], Shan He[1,2], Zhaotang Ding[1,2], Yu Wang[1,2], Nana Li[3,4], Xinyuan Hao[3,4], Lu Wang[3,4], Yajun Yang[3,4] and Wenjun Qian[1,2]*

[1] College of Horticulture, Qingdao Agricultural University, Qingdao, China, [2] Engineering Laboratory of Genetic Improvement of Horticultural Crops of Shandong Province, Qingdao, China, [3] National Center for Tea Plant Improvement, Tea Research Institute, Chinese Academy of Agricultural Sciences, Hangzhou, China, [4] Key Laboratory of Tea Biology and Resources Utilization, Ministry of Agriculture, Hangzhou, China

OPEN ACCESS

Edited by:
Pei Xu,
China Jiliang University, China

Reviewed by:
Weidong Wang,
Northwest A&F University, China
Chuan Yue,
Fujian Agriculture and Forestry University, China

***Correspondence:**
Wenjun Qian
qau-wenjunqian@qau.edu.cn

[†]These authors have contributed equally to this work

Specialty section:
This article was submitted to Crop and Product Physiology, a section of the journal Frontiers in Plant Science

Received: *02 November 2021*
Accepted: *14 December 2021*
Published: *27 January 2022*

Citation:
Li B, Wang H, He S, Ding Z, Wang Y, Li N, Hao X, Wang L, Yang Y and Qian W (2022) Genome-Wide Identification of the PMEI Gene Family in Tea Plant and Functional Analysis of CsPMEI2 and CsPMEI4 Through Ectopic Overexpression. Front. Plant Sci. 12:807514. doi: 10.3389/fpls.2021.807514

Pectin methylesterase inhibitor (PMEI) inhibits pectin methylesterase (PME) activity at post-translation level, which plays core roles in vegetative and reproductive processes and various stress responses of plants. However, the roles of PMEIs in tea plant are still undiscovered. Herein, a total of 51 *CsPMEIs* genes were identified from tea plant genome. *CsPMEI1-4* transcripts were varied in different tea plant tissues and regulated by various treatments, including biotic and abiotic stresses, sugar treatments, cold acclimation and bud dormancy. Overexpression of *CsPMEI4* slightly decreased cold tolerance of transgenic *Arabidopsis* associated with lower electrolyte leakage, soluble sugars contents and transcripts of many cold-induced genes as compared to wild type plants. Under long-day and short-day conditions, *CsPMEI2/4* promoted early flowering phenotypes in transgenic *Arabidopsis* along with higher expression levels of many flowering-related genes. Moreover, overexpression of *CsPMEI2/4* decreased PME activity, but increased sugars contents (sucrose, glucose, and fructose) in transgenic *Arabidopsis* as compared with wild type plants under short-day condition. These results indicate that *CsPMEIs* are widely involved in tea plant vegetative and reproductive processes, and also in various stress responses. Moreover, *CsPMEI4* negatively regulated cold response, meanwhile, *CsPMEI2/4* promoted early flowering of transgenic *Arabidopsis* via the autonomous pathway. Collectively, these results open new perspectives on the roles of PMEIs in tea plant.

Keywords: ***Camellia sinensis*, *Arabidopsis*, pectin methylesterase inhibitor, expression patterns, biotic and abiotic stresses, overexpression, cold, flowering**

INTRODUCTION

Pectin is one of three major polysaccharides in plant primary cell walls, which plays vital roles in different plant tissues and developmental stages, and also in responses to biotic and abiotic stresses. Galacturonic acid (GalA) is the main component of pectin, which can be subdivided into five classes, including apiogalacturonan (AP), homogalacturonan (HG), rhamnogalacturonan I

(RG-I), rhamnogalacturonan II (RG-II), and xylogalacturonan (XGA) (Wormit and Usadel, 2018). Among them, HG is the backbone of pectin that constitutes about 65% of total pectin, and its properties could be affected by acetylating at C2–C3 atom and methylesterifing at C6 atom of GalA, respectively (Wolf et al., 2009). Within cell walls, the highly methylesterified HG could be de-methylesterified (DM) by pectin methylesterases (PMEs, E.C. 3.1.1.11) to produce negatively charged carboxyl groups and release methanol and protons (Cantarel et al., 2009). Meanwhile, PMEs activities are regulated by a type of endogenous inhibitors called pectin methylesterases inhibitors (PMEIs) (Juge, 2006).

It is now clear that PMEIs are encoded by a large multigene family both in monocotyledons and dicotyledons, and a conserved PMEI domain (PF04043) was contained in PMEI protein. In plant, the first PMEI protein (AcPMEI) was identified and purified from kiwi fruit, which has been verified to effectively repress PME activity through formation of a 1:1 non-covalent complex (Balestrieri, 1990; Di Matteo et al., 2005). Crystallographic structural analysis showed that AcPMEI is almost all helical mainly consisting of four long helices (α1–4) arranged in an anti-parallel way to form a classical up-and-down four-helical bundle (Di Matteo et al., 2005). The amino acid sequence of PMEI contains an N-terminal signal peptide and four highly conserved cysteine (Cys, C) residues. The four C residues are mainly involved in the formation of two disulfide bridges (S–S), which is critical for the stabilization of four-helical bundle structure (Wormit and Usadel, 2018). However, these structural properties are also found in a type of invertase inhibitor (INH) that shared a structural superimposition with PMEI though their sequence identity is only 20–30%. The main differences between PMEI and INH lie in the N-terminal region and the loops connecting the bundle helix. In particular, an amino acid inserted into helix α2 of INH that partially distorts the helix (Di Matteo et al., 2005). With the development of biological technology, lots of *PMEI* genes have been identified, and their functions have been explored in different plant species recently. At present, 78 *AtPMEIs* in *Arabidopsis* (Müller et al., 2013), 83 *LuPMEIs* in flax (Pinzon-Latorre and Deyholos, 2014), 49 *OsPMEIs* in rice (Nguyen et al., 2016), 95 *BoPMEIs* in *Brassica oleracea* (Liu et al., 2018a), 100 *BcPMEIs* in *Brassica campestris* (Liu et al., 2018b), 55 *SbPMEIs* in *Sorghum bicolor* (Ren et al., 2019), and 42 *PbrPMEIs* in *Pyrus bretschneideri* (Zhu et al., 2021) etc. have been identified and characterized in succession.

Until now, many research findings have revealed that PMEIs play key roles in plant vegetative and reproductive processes. With the help of mutation and overexpression techniques, the functions of many *PMEIs* have been extensively explored. In *Arabidopsis*, there have been more than 12 *AtPMEIs* verified to mediate plant growth and development. Among them, AtPMEI1 (At1g48020) and AtPMEI2 (At3g17220) inhibited plant-derived PME activity rather than microbial PME activity, which shared 38% sequence identity with AcPMEI from kiwi fruit (Raiola et al., 2004). Similarly, a functional PMEI of *Vitis vinifera*, VvPMEI1, also typically inhibited the plant PME activity but not microbial PME activity (Lionetti et al., 2015). In addition, the recombinant OsPMEI28 protein showed high inhibitory activity against PME protein, overexpression of *OsPMEI28* caused dwarf phenotypes and reduced culm diameter in transgenic rice lines (Nguyen et al., 2017). Similarly, overexpression of *AtPMEI3* resulted in hyper-methyl-esterification of HG and effected the formation of flower primordia (Lionetti et al., 2007). The expression of *AtPMEI6* showed a spatio-temporal pattern in seed coat epidermal cells, and overexpression of *AtPMEI6* inhibited the endogenous PME activity and decreased the total methylesterification of mucilage fractions and demucilaged seeds in transgenic plants (Saez-Aguayo et al., 2013). GUS staining results showed that the promoter of a flower-specific gene, *SlPMEI*, expressed specifically in mature pollen of tomato and reproductive organs of transgenic *Arabidopsis* (Raiola et al., 2004).

In addition to mediate plant growth and development, PMEIs have also been reported to participate in defending pathogen infection and responding to environment stresses. In *Arabidopsis*, the expressions of three PMEIs genes, *AtPMEI10*/*11*/*12*, were induced by *Botrytis cinerea* infection mainly through jasmonic acid and ethylene signaling. Moreover, the reverse genetic approach results found that the PME activity was increased but the DM of pectin was decreased in *pmei10*/*11*/*12* mutants, respectively, which finally increased lesion formation during *B. cinerea* infection. These results indicated that AtPMEI10/11/12 served as mediators to maintain cell wall integrity in plant immunity (Lionetti et al., 2017).

Tea plant (*Camellia sinensis*) is a type of evergreen economic plant, which is appropriate to growth at normal temperature, high humidity and acid soil (pH 5.5) environments. However, with the frequency of extreme climate in recent years, tea plants usually cannot overwinter safely or grow normally when suffered from drought, chilling, freezing, or cold spell damages. Therefore, more and more studies have been focused on the molecular mechanisms of tea plant stress responses. At present, many functional genes involved in vegetative (Xia et al., 2021), reproductive (Jing et al., 2020), nutrient uptake (Arkorful et al., 2020), secondary metabolism (Yu et al., 2021; Zhao et al., 2021), and stress response (Qian et al., 2018; Wang et al., 2018; Yao et al., 2020) have been extensively explored. However, the functions of PMEIs in tea plant still remain unknown. Herein, we performed a genome-wide identification and characterization analysis of *CsPMEIs*, analyzed the tissue-specific profiles and spatio-temporal patterns of four *CsPMEIs* (*CsPMEI1-4*), and finally explored the functions of *CsPMEI2*/*4* in transgenic *Arabidopsis*, respectively. Our study opened the door for the functional study of pectin in tea plant, and these results also provided a firm foundation for deeply exploring the functions of PMEs and PMEIs in tea plant.

MATERIALS AND METHODS

Plant Materials and Multiple Treatments

For tissue-specific analysis, the apical buds, the first leaves, the second leaves, the third leaves, young fruits, mature fruits, young stems, flowers, and roots were sampled from 4-year-old clonal potted seedlings of the 'LongJing43' cultivar during flowering season (October). Each tissue contains three independent

biological replicates, and all tissues were frozen in liquid nitrogen and then stored at −80°C until used.

For various abiotic stress treatments, 1-year-old clonal hydroponic seedlings of the 'LongJing43' cultivar with the similar growth potential were used for 4°C, PEG-6000 [10% (w/v)], 150 mmol·L^{-1} NaCl and 100 μmol·L^{-1} ABA treatments. The detailed treatment methods were carried out as described by Qian et al. (2016). The nutrient solution formulation was shown in **Supplementary Table 1**. Five-year-old clonal seedlings of the 'LongJing43' cultivar at one bud and five leaf stages were used for *Colletotrichum fructicola* (*C. fructicola*) infection. The detailed infection method was performed as described by Wang et al. (2016). 15-year-old of four-tea cultivars, including two cold-resistant cultivars ('ZheNong113' and 'LongJing43') and two cold-susceptible cultivars ('ZheNong12' and 'DaMianBai') as demonstrated by Wang et al. (2019), were used for cold acclimation (CA) analysis in 2018–2019. The sampling methods were performed according to the methods stated by Qian et al. (2018). 15-year-old clonal tea plants of the 'LongJing43' cultivar that planted in field were used for bud dormancy analysis. The sampling methods were implemented as described by Hao et al. (2018). The above mentioned treatments were, respectively, performed three independent biological replicates, and all samples were quickly frozen in liquid nitrogen and then stored at −80°C until used.

2-year-old clonal potted cuttings of the 'LongJing43' cultivar at two different growth stages, including one bud and one leaf (OBOL) stage and one bud and three leaves (OBTL) stage, were used for cold treatment. Before proceeding, the cuttings were moved into the greenhouse for normal culture. The growth conditions were as follows: lighting time, 14 h/10 h (light/dark); temperature, 23°C; and humidity, 75%. When the cuttings reached the standards, the temperature of greenhouse was plummeted to 4°C without changing lighting time and humidity. The cuttings with OBOL were continued for 3 days at 4°C, and the samples (OBOL) were collected at 0, 1, 3, 6, 12, 24, 48, and 72 h, respectively. Similarly, the cuttings with OBTL were continued for 8 days at 4°C, and the samples (OBTL) were collected at 0, 1, 2, 3, 4, 5, 6, 7, and 8 days, respectively. Subsequently, the cuttings were returned to 25°C for 2 days, and the samples (OBTL) were collected at 1 and 2 days. All samples were immediately frozen in liquid nitrogen and then stored at −80°C until used. Each sampling time point was performed five biological replicates, and each biological replicate contains 10 pots of tea plants and each pot contained three cuttings.

One-year-old clonal hydroponic cuttings of the 'LongJing43' cultivar were used for sugar treatment. 3% sucrose (Suc), 3% glucose (Glu), 3% fructose (Fru), and 3% mannose (Man) treatments were, respectively, performed as described by Qian et al. (2018). Each sampling time point was performed three independent biological replicates, and each biological replicate contains four pots of tea plants and each pot contains eight cuttings. The nutrient solution formulation was shown in **Supplementary Table 1**.

The wild-type (WT) *Arabidopsis thaliana* (*Columbia*-0 ecotype) was used to construct overexpression (OE) lines of the opening reading frame of *CsPMEI2* and *CsPMEI4*. The seeds of the homozygous OE lines and WT were surface sterilized and vernalized for 2 days, and then sown on 1/2 MS medium (1.5% Suc, 0.8% Agar, pH 5.7) for 2 weeks. Thereafter, the seedlings were transplanted on the seedling block in the growth chamber under short-day (SD) (8 h light at 22°C/16 h dark at 20°C) or long-day (LD) (16 h light at 22°C/8 h dark at 20°C) conditions. The light intensity was 100 μmol/m^2s both under SD and LD conditions. The OE lines of blank vector were omitted in this study as a same phenotype detected in WT as demonstrated by Qian et al. (2018). Under LD condition, 4-week-old seedlings of both WT and *CsPMEI2*/*4*-OE lines were sampled for analyzing the expressions of flowering-related genes. Under SD condition, 10-week-old seedlings of both WT and *CsPMEI2*/*4*-OE lines were sampled for measuring PME activities, sugars (sucrose, glucose, and fructose) contents, and flowering-related genes expressions.

Genome-Wide Identification of *CsPMEIs*

The hidden Markov models (HMM) file of PMEI domain (PF04043) downloaded from Pfam database[1] was used to obtain CsPMEIs similar sequences from the tea plant protein database of 'ShuChaZao' cultivar (Wei et al., 2018) by using HMMER 3.0 software with the default parameters. Subsequently, all of these sequences were performed alignment analysis to delete the sequence that contains only one or two conserved Cys residues. The redundant sequences were submitted to the SMART server[2] and the Conserved Domain Database of NCBI[3] for verifying whether they had conserved the PMEI domain. Finally, the sequences that contain only one conserved PMEI domain were retained for further analyses.

Bioinformatics Analysis of *CsPEMIs* in Tea Plant

The bioinformatics of *CsPEMIs*, including ORF lengths, amino acid numbers, molecular weights, signal peptides, transmembrane regions, and subcellular locations were performed as described by Wang et al. (2021). For phylogenetic analysis, 262 PMEI domain contained proteins (**Supplementary Table 2**), including 78 AtPEMIs from *Arabidopsis*, 55 SbPEMIs from *Sorghum bicolor*, 55 PbrPEMIs from pear, 2 AcPEMIs from kiwi fruit, 51 CsPEMIs from tea plant and 21 INHs, were used to generate phylogenetic tree by MEGA 7.0 software. The parameters were set as follows: maximum likelihood method, 1,000 bootstrap replications, Jones–Taylor–Thornton (JTT) model, and partial deletion. Thereafter, the generated tree was uploaded to the ITOL website[4] for further beautification. The exon–intron structures of *CsPMEIs* were predicted by using GSDS 2.0 website[5]. The *cis*-acting elements of 2,000-bp promoter sequences of *CsPMEIs* were predicted by using PlantCARE website[6]. Multiple amino acids sequences alignment analysis was

[1]http://pfam.xfam.org/

[2]http://smart.embl-heidelberg.de/

[3]https://www.ncbi.nlm.nih.gov/cdd/advanced

[4]https://itol.embl.de/

[5]http://gsds.cbi.pku.edu.cn/

[6]http://bioinformatics.psb.ugent.be/webtools/plantcare/html/

carried out by using Clustlx2.0 software, and then output the result with the help of GENEDOC software.

Cloning the Full-Length of *CsPMEIs*

Before the tea plant genome sequenced, 20 expressed sequence tags (EST) that annotated as PMEI domain containing proteins were identified from the transcriptome data of the tea plant under CA condition (Wang et al., 2013). After assembled by Seqman software, a total of 4 contigs were obtained and served as templates to design RT-PCR primers for TA cloning. The TA cloning method was performed as described by Qian et al. (2016). The amplified and purified PCR products were inserted into the *pEASY-Blunt Zero* vector (TransGen Biotech, Beijing, China), then transferred into *Trans5α* chemically competent cell (TransGen Biotech, Beijing, China) and sequenced finally. All RT-PCR primers were listed in **Supplementary Table 3**.

Vector Construction, Plant Transformation, and Cold Treatment of Transgenic Plants

The vector construction and plant transformation methods were carried out as stated by Qian et al. (2018) with some modification. The Gateway technology was used to construct overexpression vectors (Landy, 1989). Simply, the ORF of *CsPMEI2* and *CsPMEI4* without stop codons were firstly cloned into the entry vector (*pENTR/D-TOPO*) (Invitrogen, CA, United States) following the instruction of manufacturer, respectively. After verified by sequencing, the ORF of *CsPMEI2* and *CsPMEI4* were transferred into the destination vector (*pH7FWG2*) by using LR Clonase II enzyme mix kit (Invitrogen, Carlsbad, CA, United States) (Ishimaru et al., 2005), respectively. The plasmids of recombined vectors of *CsPMEI2* and *CsPMEI4* were separately mobilized into *Agrobacterium tumefaciens* strain *GV3101*, and finally transformed into *Arabidopsis* via *Agrobacterium*-mediated floral infiltration (Clough and Bent, 2010). The positive *CsPMEI2*-OE lines and *CsPMEI4*-OE lines were obtained by *hygromycin* B screening, and the transcript abundances of *CsPMEI2* and *CsPMEI4* in each OE-line were quantified by qRT-PCR. Finally, three OE-lines with different transcript abundances of *CsPMEI2* and *CsPMEI4* were, respectively, used to proceed further experiments. The primers used for vector construction were listed in **Supplementary Table 3**.

Cold and ABA Treatments of Transgenic Plants

For cold treatment, the seeds of WT plants and three *CsPMEI4*-OE lines (OE4-2, OE4-7, and OE4-11) were sterilized and vernalized firstly, and then they were sown onto 1/2 MS medium for germinating in the growth chamber with photoperiod (10 h light at 22°C/14 h dark at 20°C) and 100 μmol/m^2s. Two weeks later, the seedlings with four rosette leaves were transplanted on the seedling blocks and grown in the growth chamber for another 2 weeks. For cold treatment, both WT plants and *CsPMEI4*-OE plants were treated at 4°C for 7 days without changing the light time and intensity. The rosette leaves were collected to measure total soluble sugar (TSS) and the expressions of cold-responsive genes. To detect electrolyte leakage, 4-week-old seedlings of both WT plants and *CsPMEI4*-OE plants were exposed to −6°C for 8 h without changing the light time and intensity. The control seedlings were grown normally in the growth chamber. Each treatment contained three independent biological replicates, and each replicate contained six seedlings of each OE lines and WT plants, respectively.

ABA treatment was performed as described by Jing et al. (2020). Two-week-old seedlings of *CsPMEI2/4*-OE lines and WT plants were sprayed with a 20 μM ABA solution twice a week until flowering under LD condition. Meanwhile, the controls were sprayed with distilled water. The phenotypes, flowering time, and leaf number were recorded. Each treatment contained three independent biological replicates, and each replicate contained fifteen seedlings of each OE lines and WT plants, respectively.

Flowering Time, Leaf Number, and Plant Height Measurements

The methods used for evaluating the flowering time and other phenotypes were conducted as described by Jing et al. (2020). The WT and OE-lines were cultured in seedling blocks under LD and SD conditions, respectively. The time from seed sterilization to floral bud formation was recorded as flowering time, and the total number of rosette leaves were counted at the same time. The plant heights of WT and OE-lines were measured once the plants stop flowering. The sizes of the leaves, flowers and seeds of WT and OE-lines were also surveyed as described by Wang et al. (2012). Three independent biological replicates were performed, and each replicate contained fifteen seedlings of each OE lines and WT plants, respectively.

Electrolyte Leakage and Sugar Contents Measurements

The electrolyte leakage (EL) was assayed as described by Qian et al. (2018). For detecting soluble sugars contents, 0.1 g fresh sample was extracted with 1.0 mL extraction buffer in a pre-cooled mortar on ice box, and then transferred into 1.5 mL microcentrifuge tube to water bath at 80°C for 10 min. After centrifuged at 25°C, 4,000 × *g* for 10 min, the supernatants were decolorized. Thereafter, 1.0 mL extraction buffer was added and centrifuged at 25°C, 4,000 × *g* for 10 min again. The supernatant was used for total soluble sugar (TSS), Suc, Glc, and Fru measurements according to the instructions of the corresponding sugar measurement kits (Suzhou Comin Biotechnology, Suzhou, China), respectively.

Pectin Methylesterase Activity Measurements

Pectin methylesterase activity was assayed by using NaOH indirect titration method as the manufacture's introduction (Suzhou Comin Biotechnology, Suzhou, China). 1 g sample was thoroughly ground in an ice bath with 2 mL pre-cooled extraction buffer. After centrifuged at 4°C, 12,000 × *g* for 10 min, the supernatant was used.

Quantitative Real-Time RT-PCR Analysis

Total RNA isolation, first-strand cDNA synthesis and qRT-PCR analysis of all samples were conducted as demonstrated by Qian et al. (2018). The qRT-PCR reaction system was mixed as follows: 5.0 μL SYBR Premix Ex *Taq*, 1 μL cDNA, 0.8 μL forward/reverse primers, and 3.2 μL distilled water. The qRT-PCR program was run as follows: 95°C, 15 s for predegeneration; then 94°C, 5 s and 58°C, 30 s for amplification with 40 cycles; finally, a melting curve was added. Two housekeeping genes, *CsPTB* of tea plant (Hao et al., 2014) and *AtEF* of *Arabidopsis* (Yuan et al., 2008), were, respectively, used to quantify the relative expression levels of the target genes based on $2^{-\Delta Ct}$ or $2^{-\Delta\Delta Ct}$ method (Livak and Schmittgen, 2001). Each cDNA was performed three parallel technical repeats, and the calculated results were visualized as the mean values ± standard error (±SE). The qRT-PCR primers were shown in **Supplementary Table 4**.

Statistical Analysis

Statistical differences between WT and *CsPMEI2/4*-OE lines under different conditions were analyzed by one-way Analysis of Variance (ANOVA) followed by Tukey's HSD test and/or Duncan's test.

RESULTS

Identification, Cloning, Bioinformatics Analysis of *CsPMEIs* in Tea Plant

Based on PMEI domain (PF04043), 51 *CsPMEIs* and 2 *CsVIF/CIFs* were identified from tea plant genome. The ORF lengths of *CsPMEIs* were varied from 420 to 924 bp, the encoded amino acids were ranged from 139 to 307 aa, the molecular weights (MW) were changed from 15.48 to 34.12 kD, and the theoretical isoelectric points (pIs) were ranged from 3.93 to 9.76 pIs. More than 35 CsPMEIs were predicted to be stable proteins that are located in cytoplasm. 46 CsPMEIs were predicted to contain N-terminal signal peptides and 10 CsPMEIs were predicted to contain transmembrane helices (TMHs) (**Table 1**). Meanwhile, four *CsPMEIs* genes, named as *CsPMEI1-4* (accession number: KU884479, KU884480, KU884481, and KU884482), were cloned based on the ESTs sequences as found in the previous transcriptome data. Alignment analysis results found that CsPMEI1-4 shared more than 99% identities with XP_028079167, XP_028079378, XP_028097250, and XP_028127647, respectively. Amino acid alignment analysis result showed that all of the identified CsPMEIs and CsVIF/CIFs contained four conserved and representative Cys residues except for CsPMEI5 (**Supplementary Figure 1**).

Phylogenetic analysis result showed that 262 PMEI domain contained proteins were clustered into five clades. However, CsPMEIs and CsVIF/CIFs were only grouped into four clades, among them, 35 of CsPMEIs were clustered into Clade I. In addition, we found that CsVIF/CIFs showed closet relationship with lots of known VIF/CIFs, but most of CsPMEIs showed closet relationship with PbrPMEIs (**Figure 1**). Moreover, the DNA structure of each *CsPMEI* contains only one exon except for *CsPMEI34* and *CsPMEI42* (**Supplementary Figure 2A**). *cis*-acting elements prediction results showed that *CsPMEIs* could be regulated by MYB and MYC transcription factors, auxins (GA, MeJ, SA, and ABA etc.) and multiple stresses (drought, cold, and anaerobic etc.) (**Supplementary Figure 2B**). To verify this conclusion, the expressions of four genes, *CsPMEI1-4*, were detected under different conditions. Meanwhile, the functions of *CsPMEI2* and *CsPMEI4* were further explored by means of overexpression technology in *Arabidopsis*.

Expression Profiles of *CsPMEIs* in Various Tissues, and in Responding to Various Abiotic Stresses in Tea Plant Leaves and Roots

The tissue-specific of *CsPMEI1-4* were analyzed in nine different tea plant tissues. As shown in **Figure 2A**, *CsPMEI1-4* showed diverse transcription abundances in various tissues. Among them, *CsPMEI1/2* were highly expressed in tender leaves and root, *CsPMEI3* was highly expressed in mature fruit. However, *CsPMEI4* presented the highest expressions in each detected tissue than the other three *CsPMEIs*, especially in young fruit, young stem and bud, suggesting that *CsPMEIs*, especially *CsPMEI4*, widely involved in the vegetative and reproductive processes of tea plant.

Within 5 days of different abiotic stresses treatments, the expressions of *CsPMEIs* showed diverse changes both in tea plant mature leaves and roots at different processing time points (**Figure 2B**). In mature leaves, *CsPMEI1* transcripts were declined by cold treatment, but induced by drought and NaCl treatments; *CsPMEI2/3* transcripts were highly induced by different abiotic stresses within 9 h of treatments, then *CsPMEI2* was reduced by different abiotic stresses until the 5 days of time point; besides, *CsPMEI4* transcripts were significantly decreased within 5 days of different abiotic stresses. In roots, *CsPMEI1* transcripts were highly upregulated by drought and NaCl treatments, but downregulated by cold treatment; *CsPMEI2* transcripts were highly induced by drought, NaCl and ABA stresses within 5 days of different abiotic stresses, except for a few time points; *CsPMEI3* transcripts were increased within 3 h of cold stress and 1 day of drought and NaCl stresses, respectively, but decreased within 5 days of ABA treatment; the mRNA level of *CsPMEI4* was reduced by various abiotic stresses after 3 h of treatments, even though it was induced by drought and NaCl within 3 h of treatments. The above results indicated that *CsPMEI1-4* play important roles in dealing with various abiotic stresses in tea plant.

Differential Expressions of *CsPMEIs* Under Biotic, Cold and Sugars Treatments

Here, we detected the expression patterns of *CsPMEI1-4* under *C. fructicola* infection condition. As **Figure 3A** shown, *CsPMEI1-4* transcripts were reduced by *C. fructicola*, especially *CsPMEI1/2* were remarkably downregulated by *C. fructicola* infection.

Besides, a time-course expressions of *CsPMEI1-4* were separately performed in OBOL and OBTL tissues under 4°C

condition. As **Figures 3B,C** shown, the expression patterns of *CsPMEI1-4* were varied in OBOL and OBTL. At OBOL stage, *CsPMEI1/3* were continuously up-regulated with 6 h and 2 days of cold treatment (CT), respectively; *CsPMEI2* was also induced by CT within 2 days; *CsPMEI4* showed a highest expression at 3 h, and then gradually decreased until 3 days. At OBTL stage, *CsPMEI1/4* were gradually downregulated within 8 days of CT, and then recovered to normal expression levels following the

TABLE 1 | Basic information of *CsPMEIs*.

Gene name	Accession number	ORF (bp)	AA	MW (kDa)	pI	Instability index	Loc	SignalP	TMHs
CsPMEI1	KU884479	594	197	21.70	4.31	Stable	Nucleus	Yes	No
CsPMEI2	KU884480	591	196	21.52	3.93	Stable	Cytoplasm	Yes	No
CsPMEI3	KU884481	630	209	22.55	9.16	Stable	Nucleus	Yes	1
CsPMEI4	KU884482	639	212	22.86	7.67	Stable	Cytoplasm	Yes	No
CsPMEI5	XP_028119293.1	816	271	28.74	4.5	Unstable	Nucleus	Yes	No
CsPMEI6	XP_028063476.1	504	167	18.27	5.79	Stable	Cytoplasm	Yes	No
CsPMEI7	XP_028078455.1	561	186	20.39	4.37	Stable	Nucleus	Yes	No
CsPMEI8	XP_028080229.1	552	183	19.8	9.1	Stable	Cytoplasm	Yes	No
CsPMEI9	XP_028096826.1	798	265	29.6	5.34	Stable	Cytoplasm	No	1
CsPMEI10	XP_028103971.1	585	194	20.53	6.27	Stable	Nucleus	Yes	No
CsPMEI11	XP_028105374.1	636	211	23	9.32	Unstable	Nucleus	Yes	No
CsPMEI12	XP_028106458.1	615	204	22.25	9.73	Stable	Nucleus	Yes	No
CsPMEI13	XP_028108659.1	639	212	23.28	8.51	Unstable	Nucleus	Yes	No
CsPMEI14	XP_028108660.1	630	209	22.68	9.24	Stable	Cytoplasm	Yes	1
CsPMEI15	XP_028108661.1	639	212	23.14	8.71	Unstable	Nucleus	Yes	No
CsPMEI16	XP_028112715.1	564	187	21.02	9.12	Stable	Nucleus	Yes	1
CsPMEI17	XP_028117331.1	651	216	23.89	4.58	Unstable	Cytoplasm	Yes	No
CsPMEI18	XP_028118374.1	546	181	20.92	4.65	Stable	Nucleus	Yes	No
CsPMEI19	XP_028118383.1	546	181	20.7	4.64	Stable	Cytoplasm	Yes	No
CsPMEI20	XP_028118385.1	546	181	20.96	4.64	Stable	Cytoplasm	Yes	No
CsPMEI21	XP_028118830.1	582	193	21.11	6.42	Stable	Nucleus	Yes	No
CsPMEI22	XP_028118831.1	630	209	22.65	9.36	Stable	Cytoplasm	Yes	No
CsPMEI23	XP_028118832.1	642	213	23.24	8.88	Stable	Cytoplasm	Yes	No
CsPMEI24	XP_028118833.1	618	205	22.21	8.29	Stable	Cytoplasm	Yes	No
CsPMEI25	XP_028118856.1	588	195	20.96	9.25	Stable	Cytoplasm	Yes	No
CsPMEI26	XP_028122572.1	504	167	18.18	5.28	Stable	Cytoplasm	Yes	No
CsPMEI27	XP_028123747.1	630	209	22.68	9.76	Stable	Cytoplasm	Yes	No
CsPMEI28	XP_028123748.1	621	206	21.9	6.09	Stable	Cytoplasm	Yes	No
CsPMEI29	XP_028123765.1	555	184	19.46	5.8	Stable	Chloroplast	No	No
CsPMEI30	XP_028051078.1	630	209	22.7	8.92	Stable	Chloroplast	Yes	No
CsPMEI31	XP_028051784.1	582	193	20.86	9.41	Stable	Cytoplasm	Yes	No
CsPMEI32	XP_028055798.1	504	167	18.17	5.63	Stable	Cytoplasm	Yes	No
CsPMEI33	XP_028056276.1	609	202	22.01	9.47	Unstable	Cytoplasm	Yes	No
CsPMEI34	XP_028061043.1	585	194	21.09	5.59	Stable	Cytoplasm	Yes	No
CsPMEI35	XP_028061148.1	627	208	22.14	8.85	Stable	Cytoplasm	Yes	1
CsPMEI36	XP_028063328.1	420	139	15.48	5.04	Stable	Cytoplasm	No	No
CsPMEI37	XP_028063329.1	558	185	20.33	4.54	Stable	Cytoplasm	Yes	1
CsPMEI38	XP_028063330.1	552	183	20.36	5.27	Stable	Cytoplasm	Yes	1
CsPMEI39	XP_028063858.1	573	190	21.3	6.23	Unstable	Cytoplasm	Yes	1
CsPMEI40	XP_028069427.1	606	201	21.49	4.52	Stable	Cytoplasm	Yes	No
CsPMEI41	XP_028069450.1	621	206	21.96	6.09	Stable	Cytoplasm	Yes	No
CsPMEI42	XP_028073478.1	567	188	20.52	9.14	Stable	Cytoplasm	No	No
CsPMEI43	XP_028073497.1	540	179	19.67	7.66	Stable	Cytoplasm	Yes	No
CsPMEI44	XP_028074709.1	516	171	18.5	6.29	Stable	Cytoplasm	Yes	No
CsPMEI45	XP_028079349.1	504	167	18.27	5.13	Stable	Cytoplasm	Yes	No
CsPMEI46	XP_028079849.1	564	187	21.58	8.82	Unstable	Cytoplasm	Yes	1
CsPMEI47	XP_028081340.1	762	253	27.12	5.11	Stable	Cytoplasm	No	1

(Continued)

TABLE 1 | (Continued)

Gene name	Accession number	ORF (bp)	AA	MW (kDa)	pI	Instability index	Loc	SignalP	TMHs
CsPMEI48	XP_028082183.1	606	201	21.98	9.33	Stable	Cytoplasm	Yes	No
CsPMEI49	XP_028082302.1	621	206	21.93	6.09	Stable	Cytoplasm	Yes	No
CsPMEI50	XP_028082397.1	540	179	19.6	8.32	Stable	Cytoplasm	Yes	No
CsPMEI51	XP_028090516.1	924	307	34.12	8.92	Unstable	Cytoplasm	Yes	No
CsVIF/CIF1	XP_028053538.1	525	174	18.71	9.23	Stable	Cytoplasm	Yes	No
CsVIF/CIF2	XP_028100701.1	522	173	18.48	9.57	Stable	Cytoplasm	Yes	No

ORF, opening reading fame; AA, the numbers of amino acid residues; MW, molecule weight; pI, theoretical isoelectric point; Loc, subcellular location; SignalP, signal peptide; TMHs, transmembrane helices.

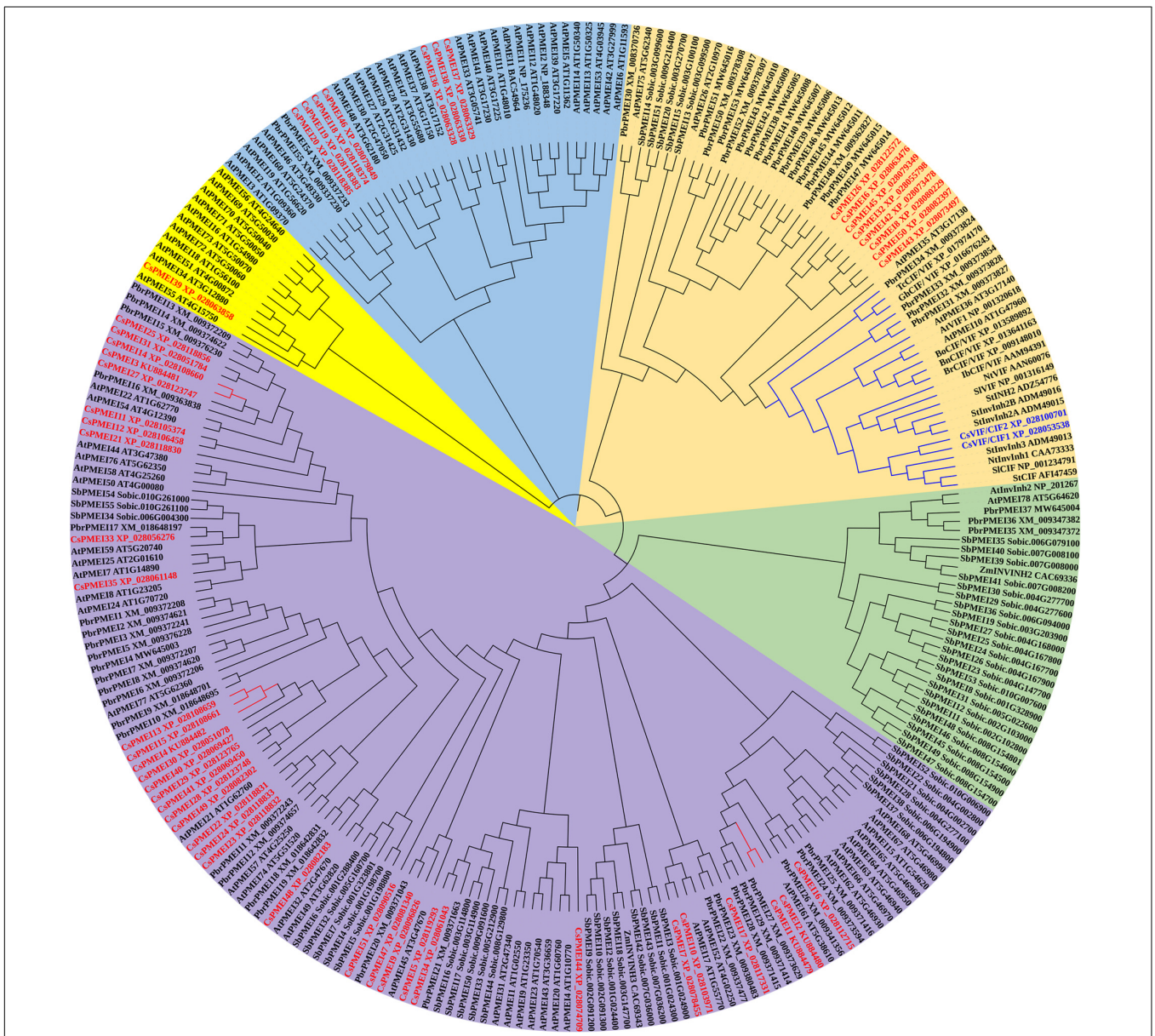


FIGURE 1 | Phylogenetic analysis of *CsPMEIs* and known PMEIs in *Arabidopsis*, *Sorghum bicolor,* pear, and kiwi fruit. A total of 262 PMEI domain contained proteins that were used to construct phylogenetic tree by using MEGA 7.0 software. *CsPMEIs* are highlighted with red color, and different PMEIs subfamilies were covered with different colors.

temperature increased; in contrast, *CsPMEI2/3* were, respectively, upregulated within 8 and 4 days of CT, and also recovered to normal expression levels under normal temperature condition. These results indicated that *CsPMEI1-4* had different levels and timings of expressions in different tissues of tea plant under CT condition.

Furthermore, we found exogenous sugars, including Suc, Glc, Fru, and Man independently induced the expression of *CsPMEI2* under normal temperature (NT) condition, while *CsPMEI2* was reduced within 2 days of CT treatment, except for Man that enhanced the expression of *CsPMEI2* under CT treatment. In contrast, the expression of *CsPMEI4* were decreased under NT condition, but remarkably induced by exogenous sugars within 4 days of CT. Specifically, *CsPMEI4* transcripts were increased more than twofold within 1 days of CT (**Figure 3D**). These results demonstrated that the cold response of *CsPMEI2/4* in tea plant could be mediated by sugar signaling pathway.

Differential Expressions of *CsPMEIs* During Cold Acclimation and Bud Dormancy Periods

Four-tea cultivars with different cold-resistance were used for exploring the expression patterns of *CsPMEI1-4* during CA periods. As **Figure 4A** shown, *CsPMEIs* showed similar expressions patterns among these four-tea cultivars during CA periods. Briefly, *CsPMEIs* transcripts were decreased during CA periods (from 15 November to 16 December), except for *CsPMEI3*. Subsequently, the expressions of *CsPMEI1/2* were increased from 16 December to 27 March. However, *CsPMEI3/4* transcripts were firstly increased from 16 December to 10 February, and then decreased with increasing temperature.

We also detected the expressions of *CsPMEI1-4* in axillary buds during bud dormancy period. As **Figure 4B** shown, *CsPMEI1/2/4* transcripts were decreased throughout the bud dormancy period, but increased with the dormancy released and at bud sprouting stages. However, the expression of *CsPMEI3* was not changed during para- and endo-dormancy periods (from 30 September to 16 December), but increased during eco-dormancy (after 28 December) and bud sprouting stages (after 27 March). In a word, *CsPMEI1-4* involved in the bud dormancy and release of axillary buds in tea plant, but the comprehensive molecular mechanisms need to be further explored.

Overexpression Analysis of *CsPMEI2* and *CsPMEI4* in Transgenic *Arabidopsis*

CsPMEI4 Decreased the Cold Resistance of Transgenic *Arabidopsis*

As described in **Figures 2**, **3**, *CsPMEI4* was significantly repressed by CT in tea plant. Here, we further explored the cold resistance of *CsPMEI4*-OE lines under CT conditions. Three independent *CsPMEI4*-OE lines (OE4-2, OE4-7, and OE4-11) with different transcription abundances were separately selected to perform the following experiments (**Figure 5A**). Unfortunately, the phenotypes had not shown obvious difference between *CsPMEI4*-OE lines and WT plants under CT condition (data not shown). However, *CsPMEI4*-OE lines showed higher EL, but lower TSS contents than the WT plants even though no significant difference detected between them (**Figure 6A**). Besides, the expression levels of many cold-induced genes (*AtCBF1-3*, *AtCOR47A*, *AtRD29A*, *AtGR1*, *AtZAT12*, *AtHSFC1,* and *AtCZF1*) in *CsPMEI4*-OE lines were lower than that in WT plants under CT condition. In addition, the transcript abundances of four cold-repressors (*AtAZF* and *AtMYB7/44/73*), two antioxidant-related genes (*AtCAT1* and *AtAPX1*), and one ROS-producing enzyme NADPH oxidase gene (*AtRbohD*) were decreased both in *CsPMEI4*-OE lines and WT plants under CT condition (**Figure 6B**). These results suggested that overexpression of *CsPMEI4* slightly reduced the cold-resistance of transgenic *Arabidopsis*.

CsPMEI2 and *CsPMEI4* Promote Early Flowering in Transgenic *Arabidopsis* Both Under Long-Day and Short-Day Conditions

Apart from influencing cold tolerance of transgenic *Arabidopsis*, an obvious difference was observed on the flowering time between *CsPMEI2/4*-OE lines and WT plants.

Three independent *CsPMEI2*-OE lines (OE2-2, OE2-4, and OE2-7) and *CsPMEI4*-OE lines (OE4-2, OE4-7, and OE4-11) with different transcription abundances were separately selected to perform the following experiments (**Figures 5A**, **7A**). Under LD condition, both *CsPMEI2*-OE lines and *CsPMEI4*-OE lines present early flowering than the WT plants (**Figures 5B**, **7B**). Concretely, the WT plants require *c.* 36 days from seeds sterilization to floral bud formation, while *CsPMEI2*-OE lines and *CsPMEI4*-OE lines require *c.* 30 and 31 days, respectively (**Figures 5C**, **7C**). It is now clear that early-flowering plants usually possess less leaves during flowering periods (Xiong et al., 2019). The similar phenotypes were also detected in *CsPMEI2/4*-OE lines, where we found that both *CsPMEI2*-OE lines and *CsPMEI4*-OE lines formed *c.* 9 rosette leaves, while the WT plants formed *c.* 12 rosette leaves as the first flower opened (**Figures 5C**, **7C**). In addition, both *CsPMEI2*-OE lines and *CsPMEI4*-OE lines showed earlier senescence phenotypes than the WT plants (**Figures 5B**, **7B**). As compared to WT plants, the plant heights of *CsPMEI2*-OE lines were taller, while *CsPMEI4*-OE lines were shorter (**Figures 5C**, **7C**). Besides, the flower sizes of *CsPMEI2*-OE lines are longer and slender, and the pistils are smaller than the WT plants, while the flower structures (numbers of sepals, petals, and stamens) and the sizes of seeds have not shown significant distances among them (**Figure 7B**). However, the flower sizes, the flower structures (numbers of sepals, petals, stamens, and pistils) and the sizes of seeds of *CsPMEI4*-OE lines are similar to the WT plants (**Figure 5B**).

Similarly, *CsPMEI2/4*-OE lines also promote early flowering in transgenic *Arabidopsis* under SD condition as compared to WT plants. Concretely, *CsPMEI2*-OE lines and *CsPMEI4*-OE lines, respectively, need *c.* 38 days and *c.* 58 days from seeds sterilization to the floral bud formation, while WT plants need more than 3 months to bloom. Correspondingly, *CsPMEI2*-OE lines and *CsPMEI4*-OE lines formed *c. 15* and *c. 20* rosette leaves, while

the WT plants formed *c.* 38 rosette leaves as the first flower bloomed (**Figures 8A**, **9A**). These results indicate that *CsPMEI2* and *CsPMEI4* mediating flowering control may be independent of photoperiod pathway.

CsPMEI2 and *CsPMEI4* Affect PME Activities and Sugar Contents in Transgenic *Arabidopsis* Under Short-Day Condition

Under SD condition, the seedlings were sampled to validate the effects of *CsPMEI2* and *CsPMEI4* on PME activities of transgenic *Arabidopsis*. As **Figures 8B**, **9B** show, the PME activities seem to be not significantly inhibited by the exogenous overexpression of *CsPMEI2* or *CsPMEI4*, except for the highest expressions OE-lines (OE2-7 and OE4-11). In addition, the sugars contents, including Suc, Glu, and Fru were increased both in *CsPMEI2*-OE and *CsPMEI4*-OE lines. Particularly, Suc and Fru contents in OE lines were significantly higher than that in WT plants, and the ratios of (Glu + Fru)/Suc were also higher both in *CsPMEI2*-OE and *CsPMEI4*-OE lines than the WT plants, except for OE4-2 (**Figures 8C**, **9C**). These results indicate that *CsPMEI2* and *CsPMEI4* mediated flowering was associated with the changes of sugars contents.

CsPMEI2 and *CsPMEI4* Affect Multiple Flowering-Relate Genes Transcripts in Transgenic *Arabidopsis*

To explore the molecular mechanisms of early flowering phenotype of *CsPMEI2*-OE lines and *CsPMEI4*-OE lines, we further conducted the expression levels of many flowering responsive genes.

Under LD condition, the expressions of two floral integrators, *FLOWERING LOCUS T* (*FT*) and *SUPPRESSOR OF OVEREXPRESSION OF CONSTANS 1* (*SOC1*), were remarkably increased, while a key flowering repressor gene, *FLOWERING LOCUS C* (*FLC*), was significantly inhibited both in *CsPMEI2*-OE lines and *CsPMEI4*-OE lines as compared to WT plants. In addition, three floral meristem identity genes, *APETALA1* (*AP1*), *FLOWERING CONTROL LOCAL A* (*FCA*), and *FLOWERING LOCUS T* (*FY*) were also upregulated both in *CsPMEI2*-OE lines and *CsPMEI4*-OE lines (**Figures 5D**, **7D**). Similarly, under SD condition, the expressions of *FT*, *SOC1*, *FCA*, and *FY* were upregulated both in *CsPMEI2*-OE lines and *CsPMEI4*-OE lines, especially for *FT* gene, which is induced at least *c.* 20-fold and *c.* 400-fold in *CsPMEI2*-OE lines and *CsPMEI4*-OE lines, respectively. Meanwhile, the mRNA levels of *FLC* and an ABA stimulated positive factors, *ABSCISIC ACID-INSENSITIVE 5* (*ABI5*) were decreased both in *CsPMEI2*-OE lines and *CsPMEI4*-OE lines (**Figures 8D**, **9D**). These results suggested that *CsPMEI2* and *CsPMEI4* promoting early flowering may partially depend on ABA-dependent pathway. This inference was supported by ABA treatments, where we found the flowering times of *CsPMEI2*-OE and *CsPMEI4*-OE lines were delayed by the application of exogenous ABA, even though the development of all plants retarded by ABA treatment (**Supplementary Figure 3**).

.

DISCUSSION

CsPMEIs Exist in Large Multigene Family Exhibiting Diverse Expression Patterns in Tea Plant

At post-translation level, the activity of PME is antagonized by PMEI. As a type of small molecular protein, PMEI is encoded by large multigene family in various plant species, such as *Arabidopsis* (Müller et al., 2013), *B. campestris* (Liu et al., 2018b), rice (Nguyen et al., 2016), pear (Zhu et al., 2021), etc. It is now clear that both PMEI and INH share moderate sequence homology, in particular the presence of four conserved Cys residues that form two disulfide bridges (S–S) (Camardella et al., 2000; Hothorn et al., 2004). However, PMEI and INH are selectively targeted toward PMEs and plant acid INVs (CWIN and VIN), respectively. For INH, a conserved amino acid motif 'PKF' (Proline, Lysine, and Phenylalanine) has been demonstrated as core motif that directly targets the active site of the CWIN/VIN (Hothorn et al., 2010). Herein, 53 genes with intact and conserved PMEI domains were identified from 'ShuChaZao' tea plant cultivar genome. Bioinformatics analysis results showed that most of *CsPMEIs* contain one exon on DNA level encoding a type of 21 KD proteins with an N-signal peptide. Phylogenetic analysis result showed that CsPMEIs were clustered into four clades, which are similar to the phylogenetic results of PbrPMEIs (Zhu et al., 2021) and BcPMEIs (Liu et al., 2018b). In addition, we found 2 CsVIF/CIFs showed closet relationships with many known INHs, and only these two CsVIF/CIFs contain the conserved 'PKF' motif that directly targets the INV active site (**Supplementary Figure 1**). These two genes have been cloned and sequenced recently, and their functions will be further explored in future. Besides, phylogenetic analysis result showed that PMEIs and INHs were clearly clustered into different subgroups, most of known INHs, including CsVIF/CIFs, were clustered into subgroup I, while CsPMEI2/4 were clustered into subgroup III (**Supplementary Figure 4A**). This result was further verified by the amino acid alignment result, where we found all members of subgroup I contain the conserved 'PKF' motif, but PMEIs do not contain this motif (**Supplementary Figure 4B**). Collectively, we considered that 51 *CsPMEIs* and 2 *CsVIF/CIFs* genes were identified from 'ShuChaZao' tea plant cultivar genome, and CsPMEI2/4 belonged to PMEI family members.

In recent years, lots of experiments have validated that PMEIs function in various biological processes, including seed germination (Müller et al., 2013), pollen growth (Zhu et al., 2021), fertility (Andres-Robin et al., 2020), organ formation and separation, fruit ripening (Srivastava et al., 2012), biotic and abiotic stress response (An et al., 2008; Volpi et al., 2011; Lionetti et al., 2017). Recently, many *PMEIs* genes involved in abiotic stresses also have been identified and explored in plants, while their molecular regulation mechanisms are rarely studied. Microarray data analysis results showed that many *AtPMEIs* were differentially expressed in response to different abiotic stresses (Liu et al., 2018b). Similarly, the meta-transcriptional

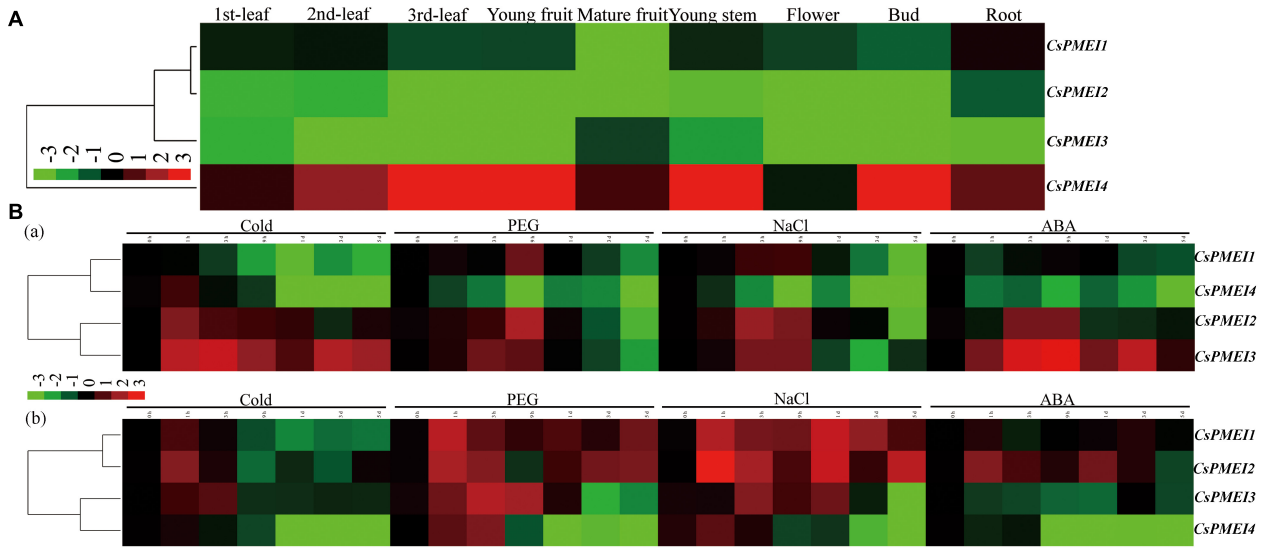


FIGURE 2 | Expression profiles of *CsPMEIs* in tea plant. **(A)** Tissue-specifc expression patterns of *CsPMEIs* in different tea plant tissues. The relative expression levels were calculated by using $2^{-\Delta\ Ct}$ method. The colorbar was displayed on the lower-left of the heat map, red and green colors represent higher and lower expression levels, respectively. **(B)** Temporal-spatial expression patterns of *CsPMEIs* both in tea plant mature leaves and roots under various abiotic stresses. **(a)** The expression patterns of *CsPMEIs* in mature leaves; **(b)** The expression patterns of *CsPMEIs* in roots. Samples at 0 h were used as control, and the final results were calculated with $2^{-\Delta\ \Delta\ Ct}$ method. The colorbar was presented on the left side of the heat map, red and green colors represent higher and lower expression levels, respectively. Data are shown as the means ± SE (n = 3).

analysis results found that lots of *OsPMEIs* were transcriptionally up- or down-regulated by abiotic and biotic stresses (Nguyen et al., 2016). Exogenous overexpression of *CaPMEI* enhanced drought tolerance and alleviated the sensitive to mannitol-induced osmotic stress in transgenic *Arabidopsis* seedlings as compared to WT plants (An et al., 2008). Herein, *CsPMEI1-4* exist transcriptional diversity and functional division. In various tea plant tissues, *CsPMEI4* transcripts were remarkably accumulated in each detected tissue, suggesting that it may play an important role in response to various biological processes in tea plant. Besides, *CsPMEI1-4* were up- or down-regulated by various abiotic stresses in a certain period of treatment time, suggesting that CsPMEIs possess functional specialization, and a balance mechanism of pectin regulation exists in tea plant in response to abiotic stresses. This assumption was also supported by the results of **Table 1**, which indicated that the PME activity of tea plant was co-regulated by CsPMEI superfamily genes at the post-translational level, rather than by several CsPMEI genes.

Previous studies found that pectin contents, PME activity and the low-methylated pectin contents increased in the leaves of winter oil-seed rape during CA period, while a contrary tendency exhibited as the de-acclimation proceeded (Solecka et al., 2008). Similarly, Baldwin et al. (2014) found that the levels of arabinose, galactose, galacturonic acid and xylose residues changed in *Pisum sativum* under CA condition. Moreover, the degree of DM increased after 10–20 days of CA and 2 days of frost treatment as compared to non-CA plants. Meanwhile, the PME activity increased after 10–20 days of CA, but decreased after 2 days of frost treatment in frost-tolerant genotype 'Champagne' as compared to non-CA 'Champagne,' which indicated that methylesterification of pectins contributes to improving frost-tolerance of pea during CA period (Baldwin et al., 2014). In this study, we found that the expressions of *CsPMEI1-2* declined in tea plant leaves during CA period, while increased with the process of de-acclimation. Meanwhile, *CsPMEI1-4* transcripts decreased throughout the bud dormancy period, but increased with the breaking dormancy and the bud sprouting. These results inferred that the PME activity, pectin contents and the methyl-esterification degree of pectins may be dynamically changed by temperature both in tea plant leaves and axillary buds. However, this assumption still needs to be further verified due to PME activity was inhibited by a large superfamily members of CsPMEIs as showed in **Table 1**. Therefore, the expression analysis of all CsPMEIs, the assay of PME activity and pectins contents should be further performed in order to extensively explore the specific regulation mechanism of CsPMEIs involved in freezing tolerance of tea plant.

In addition to responding to abiotic stress, *PMEIs* transcripts are also affected by hormones. As Srivastava et al. (2012) demonstrated that the expression of a ripening related gene, *MaPMEI*, relies on ethylene-dependent pathway indirectly during banana ripening. Similarly, the transcription levels of a wheat *PMEI* gene, *TaPMEI*, were regulated by SA, ABA, and MeJA in leaves, stem and root (Hong et al., 2010). Meanwhile, the expression levels of *CaPMEI1* were not only induced by abiotic stresses, but also by ABA, SA, ethylene and MeJA at various time intervals, suggesting that *CaPMEI1* may be mediated the early active defense responses to bacterial pathogen infection and exogenous hormones treatment (An et al., 2008). Herein, we

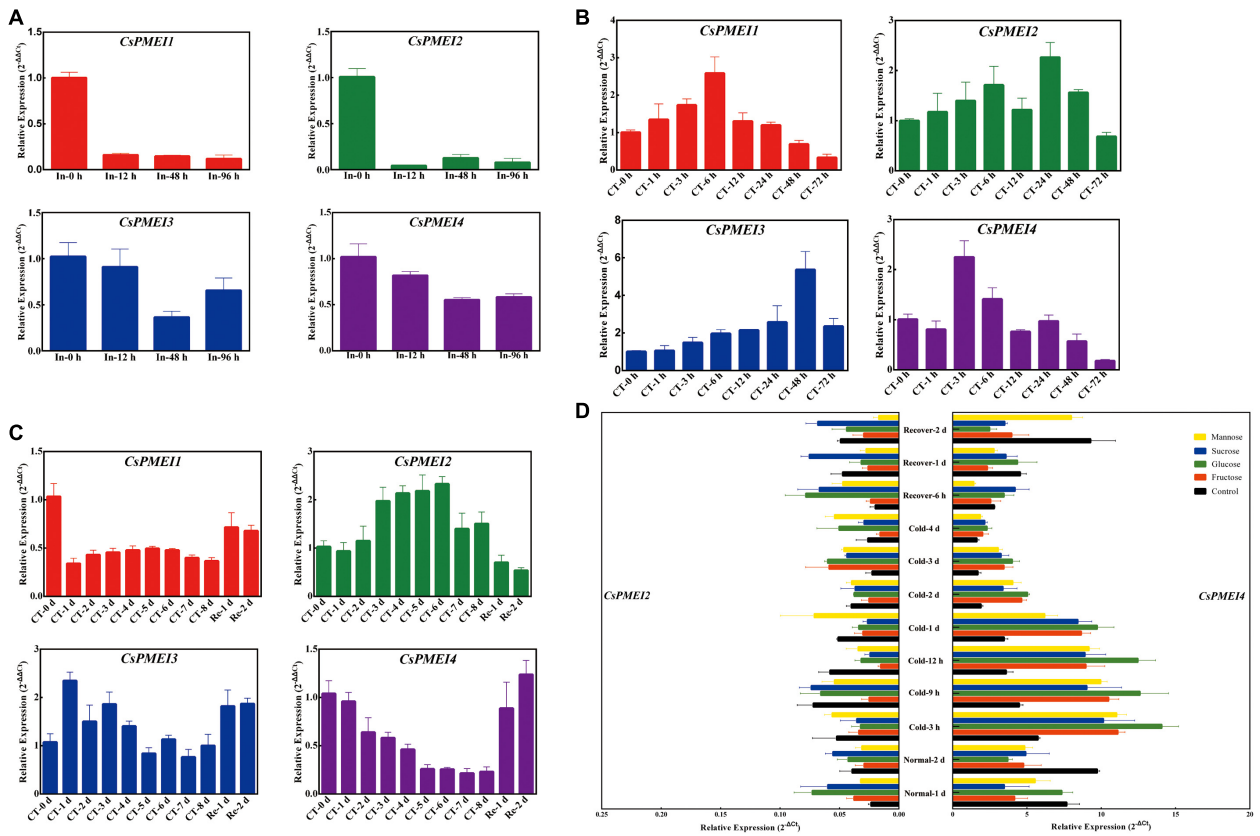


FIGURE 3 | Temporal-spatial expression patterns of *CsPMEIs* in response to biotic, cold and various sguar treatments. **(A)** Expression profiles of *CsPMEIs* under *C. fructicola* infection condition. Samples at 0 h were used as control, and the final results were calculated with $2^{-\Delta\Delta Ct}$ method. 'In' represents infection treatment. Data are shown as the means ± SE (n = 3). **(B)** Expression profiles of *CsPMEIs* at one bud and one leaf stage of tea plant under cold condition. Samples at 0 h were used as control, and the final results were calculated with $2^{-\Delta\Delta Ct}$ method. 'CT' represents cold treatment. Data are shown as the means ± SE (n = 3). **(C)** Expression profiles of *CsPMEIs* at one bud and three leaves stage of tea plant under cold condition. Samples at 0 h were used as control, and the final results were calculated with $2^{-\Delta\Delta Ct}$ method. 'CT' represents cold treatment. Data are shown as the means ± SE (n = 3).**(D)** Expression analysis of *CsPMEIs* in tea plant leaves under different sugar and temperature conditions. All results were calculated by using the $2^{-\Delta Ct}$ method. Data are shown as the means ± SE (n = 3).

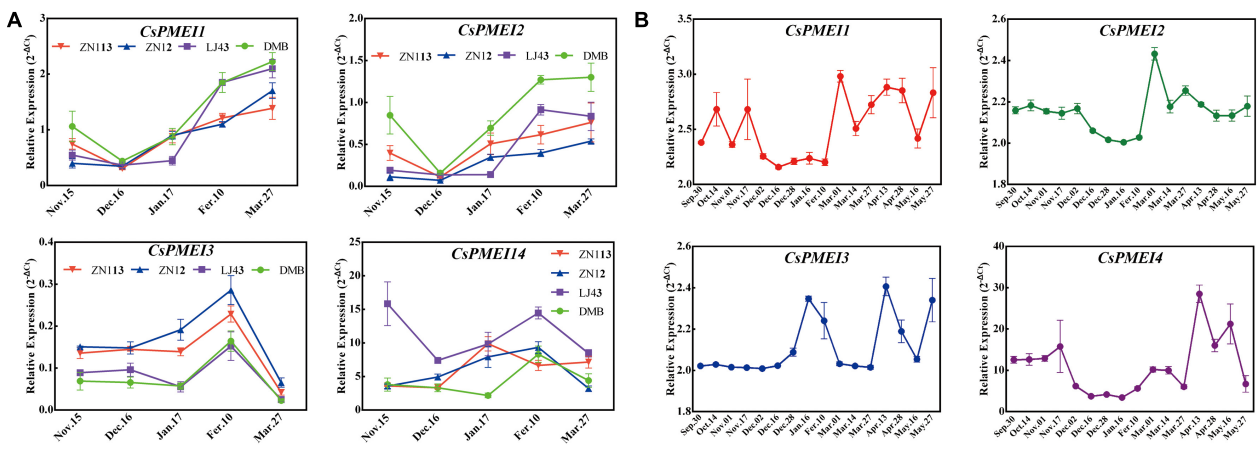


FIGURE 4 | Expression analysis of *CsPMEIs* during CA and bud dormancy periods. **(A)** Expression analysis of *CsPMEIs* in the mature leaves of four-tea cultivars during CA periods. 'DMB,' 'LJ43,' 'ZN12,' and 'ZN113' mean 'DaMianBai,' 'LongJing43,' 'ZheNong12,' and 'ZheNong113' tea plant cultivar, respectively. The relative expression levels were calculated by using $2^{-\Delta Ct}$ method. Data are shown as the means ± SE (n = 3). **(B)** Expression analysis of *CsPMEIs* in axillary buds of 'LJ43' cultivar during bud dormancy period. The relative expression levels were calculated by using $2^{-\Delta Ct}$ method. Data are shown as the means ± SE (n = 3).

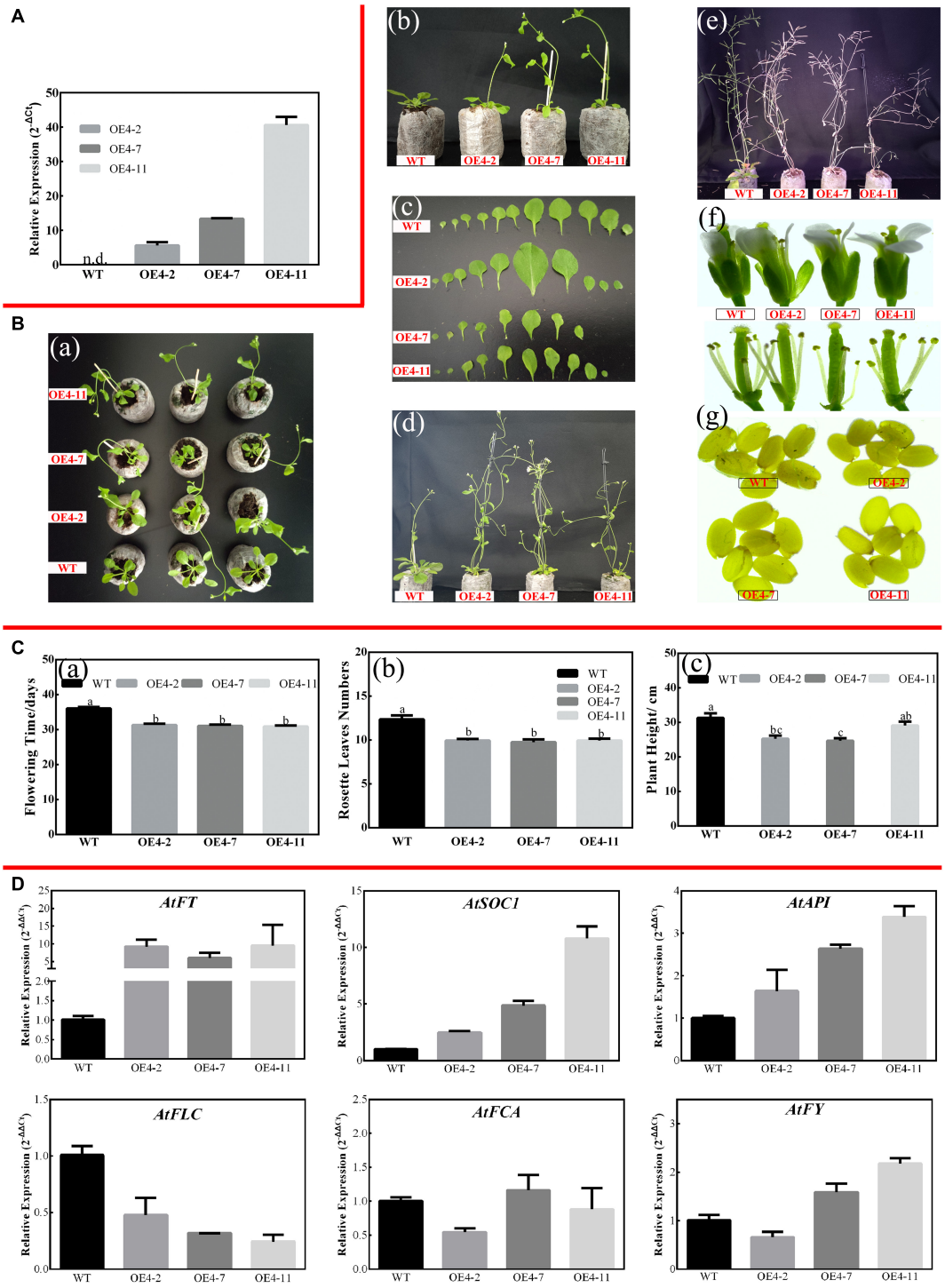


FIGURE 5 | Overexpression of *CsPMEI4* promotes early flowering in transgenic *Arabidopsis* under LD condition. **(A)** The expression of *CsPMEI4* in three *CsPMEI4*-OE lines and WT plants. The relative expression levels were calculated by using $2^{-\Delta Ct}$ method. Data are shown as the means ± SE (n = 3). **(B)** Early flowering phenotypes of *CsPMEI4*-OE lines grown under LD condition. **(a)** Early-flowering phenotype; **(b)** phenotypes of *CsPMEI4*-OE lines and WT plants after 30 d of growth under LD condition; **(c)** leaf size; **(d)** phenotype of *CsPMEI4*-OE lines and WT plants after 40 days of growth under LD condition; **(e)** phenotype of *CsPMEI4*-OE lines and WT plants at senescence stage; **(f)** flowers sizes of WT and *CsPMEI4*-OE lines; **(g)** seed size of WT and *CsPMEI4*-OE lines. **(C)** Flowering time, rosette leaves numbers, and plant height of WT and *CsPMEI4*-OE lines at the just bolting stage. **(a)** Flowering time; **(b)** rosette leaves numbers; **(c)** plant height. **(D)** Expression analysis of flowering-related genes. The final results were calculated with $2^{-\Delta\Delta Ct}$ method. Data are shown as the means ± SE (n = 3).

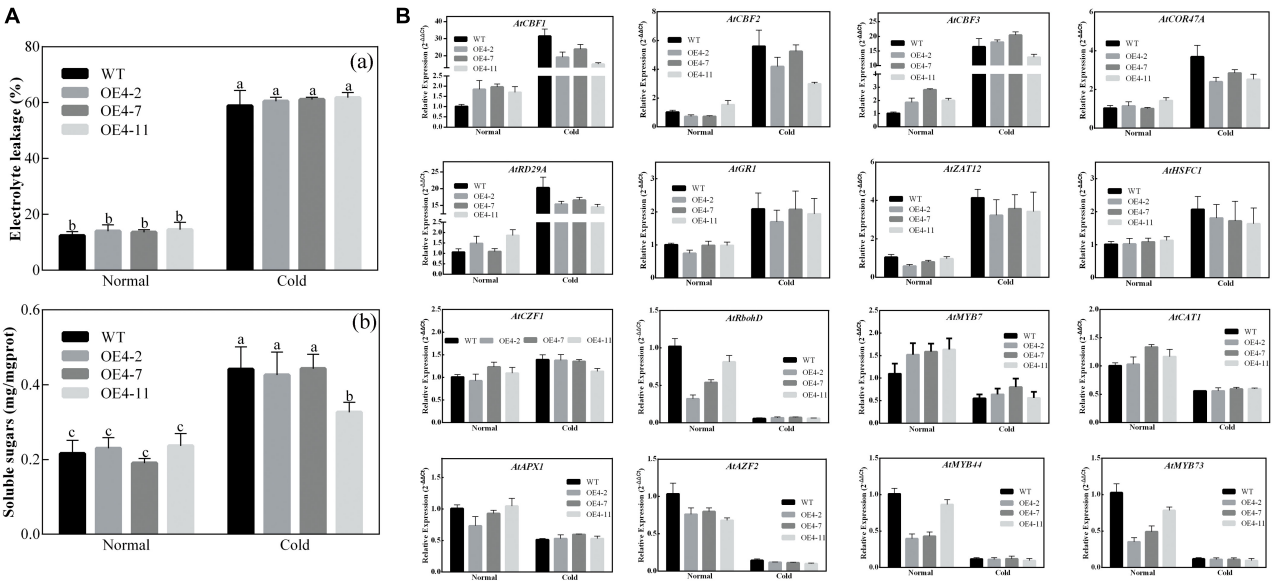


FIGURE 6 | Analysis of EL, TSS contents and cold-related genes transcripts in *CsPMEI4*-OE lines and WT plants. **(A)** EL and TSS contents of *CsPMEI4*-OE lines and WT plants under different temperature conditions. **(a)** Electrolyte leakage, EL; **(b)** total soluble sugar content. Data are shown as the means ± SE (n = 3). **(B)** Expression analysis of cold-related genes in *CsPMEI4*-OE lines and WT plants under cold condition. The final results were calculated with $2^{-\Delta\Delta Ct}$ method. Data are shown as the means ± SE (n = 3).

found the transcription abundance of *CsPMEI2/3* were strongly induced after 9 h of ABA treatment, while *CsPMEI1/4* were significantly declined during ABA treatment period, suggesting that *CsPMEI2/3* may be involved in hormone-related signaling pathways associated with defense-responsive.

At present, lots of evidences have verified that PMEIs are involved in plant defense against pathogen infection. CaPMEI1 exhibited basal disease resistance against a variety of plant pathogenic fungi, overexpression of *CaPMEI1* enhanced the anti-fungal ability in transgenic *Arabidopsis*, which indicated that the increased PMEI activity may cause the decrease accessibility of fungal pectin degrading-enzymes and thus enhance disease resistance of transgenic *Arabidopsis* (An et al., 2008). Similar results were also found in *AtPMEI-1* or *AtPMEI-2* overexpressed *Arabidopsis* lines after infected by *B. cinerea* (Lionetti et al., 2007). However, it has been reported that increasing PME activity also improved the ability of pathogen immunity. During pattern-triggered immunity and after inoculation with necrotrophic fungus and bacterial hemibiotroph in *Arabidopsis*, the PME activity increased, but the degree of pectin methylesterification decreased. Further research found that pathogen-induced PME activity was dependent on JA signaling pathway. Mutating the selected *pme* gene resulted in high sensitivity to pathogen, but the total PME activity was not influenced in *pme* mutants, suggesting that PME enhancing the immunity responsive was not determined by total PME activity, but by some specific effect of PMEs, such as methyl-esterification degree of pectins (Bethke et al., 2014). For tea plant, lots of differentially expressed metabolites (e.g., gluconic acid, fatty acid, amino acid, organic acid, etc.) have been identified after being inoculated with *C. camelliae*. Meanwhile, the contents of JA and IAA were significantly increased, accompanied by the transcription accumulation of a pathogenesis-related protein 4 (*PR4*) in JA signaling pathway, which indicated that tea plant-*Colletotrichum* interaction may be mainly mediated by JA signaling pathway (Lu et al., 2020). Herein, all four *CsPMEIs* transcripts were significantly inhibited by *C. fructicola* infection in tea plant, suggesting that the low transcription abundance of *CsPMEIs* may result in the decrease of PMEI activity, and thus increasing PME activity may change the methyl-esterification degree of pectins depending on JA signaling pathway.

Exogenous Overexpression of *CsPMEIs* Affects Cold-Resistance and Flowering Time in Transgenic *Arabidopsis*

It has been reported that the PME activity, pectins content and the methyl-esterification degree of pectins were dynamically changed under cold conditions (Solecka et al., 2008; Baldwin et al., 2014). In present study, there are no obvious phenotypic differences observed between *CsPMEI4*-OE lines and WT plants under cold condition. However, the higher EL, but the lower TSS contents and the lower expressions of many cold-induced genes were found in *CsPMEI4*-OE lines as compared with WT plants, suggesting that *CsPMEI4* may play negative roles in responding to cold stress in transgenic *Arabidopsis*. A similar result was also obtained by Chen et al. (2018), where they found overexpression of *CbPMEI* from *Chorispora bungeana* or *PMEI13* (AT5G62360) from *Arabidopsis* decreased PME activity and the content of low-DM pectins in transgenic *Arabidopsis*. Furthermore, both *CbPMEI*-OE and *PMEI13*-OE lines are sensitive to freezing stress, while tolerant to salt stress. Expression

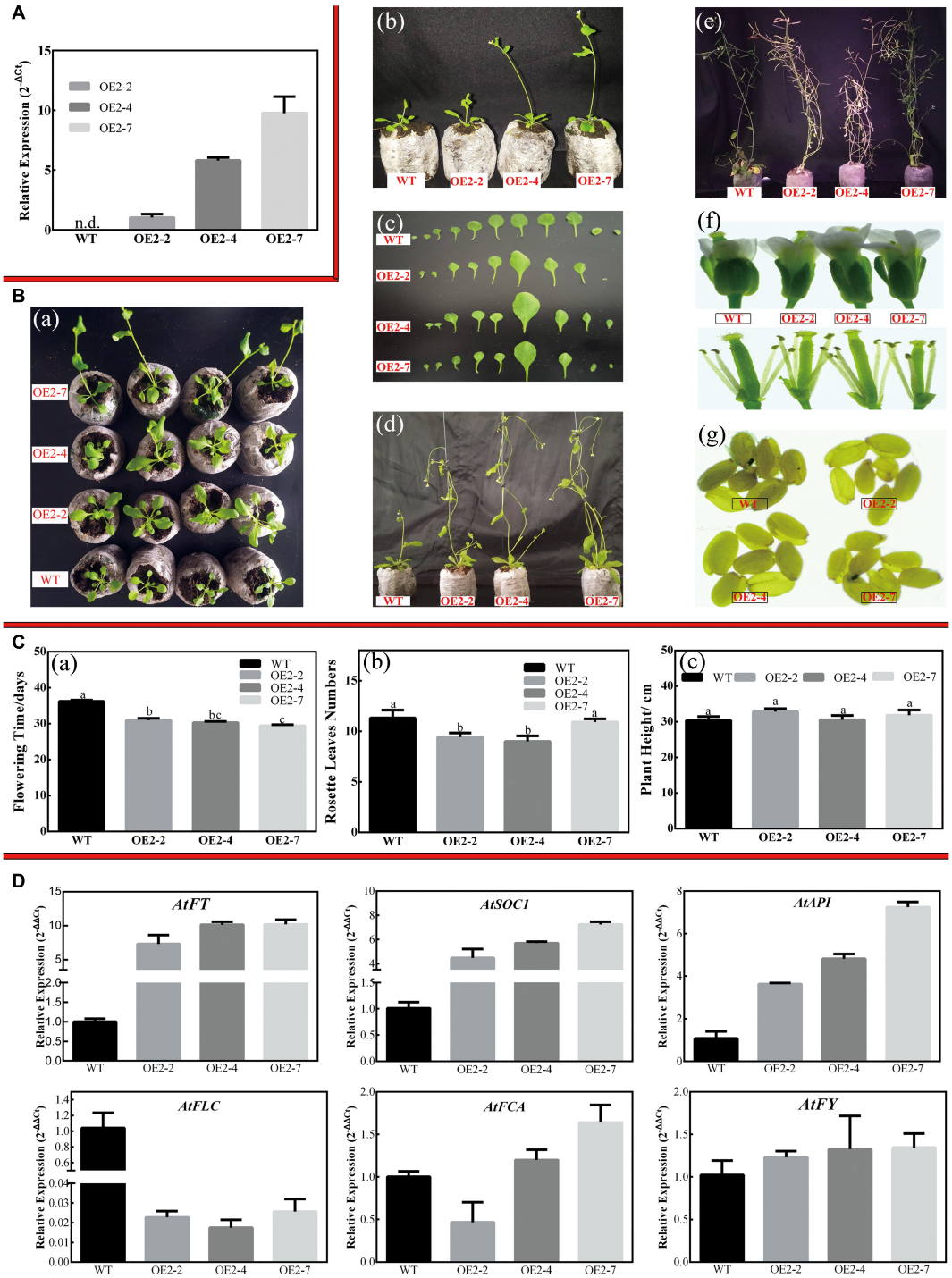


FIGURE 7 | Overexpression of *CsPMEI2* promotes early flowering in transgenic *Arabidopsis* under LD condition. **(A)** The expression of *CsPMEI2* in three *CsPMEI2*-OE lines and WT plants. The relative expression levels were calculated by using $2^{-\Delta\ Ct}$ method. Data are shown as the means ± SE (n = 3). **(B)** Early flowering phenotypes of *CsPMEI2*-OE lines grown under LD condition. **(a)** Early-flowering phenotype; **(b)** phenotypes of *CsPMEI2*-OE lines and WT plants after 29 days of growth under LD condition; **(c)** leaf size; **(d)** phenotypes of *CsPMEI2*-OE lines and WT plants after 38 days of growth under LD condition; **(e)** phenotypes of *CsPMEI2*-OE lines and WT plants at senescence stage; **(f)** flowers of WT and *CsPMEI2*-OE lines; **(g)** seed size of WT and *CsPMEI2*-OE lines. **(C)** Flowering time, rosette leaves, and plant height of WT and *CsPMEI2*-OE lines at the just bolting stage. **(a)** Flowering time; **(b)** rosette leaves numbers; **(c)** plant height. **(D)** Expression analysis of flowering-related genes. The final results were calculated with $2^{-\Delta\ \Delta\ Ct}$ method. Data are shown as the means ± SE (n = 3).

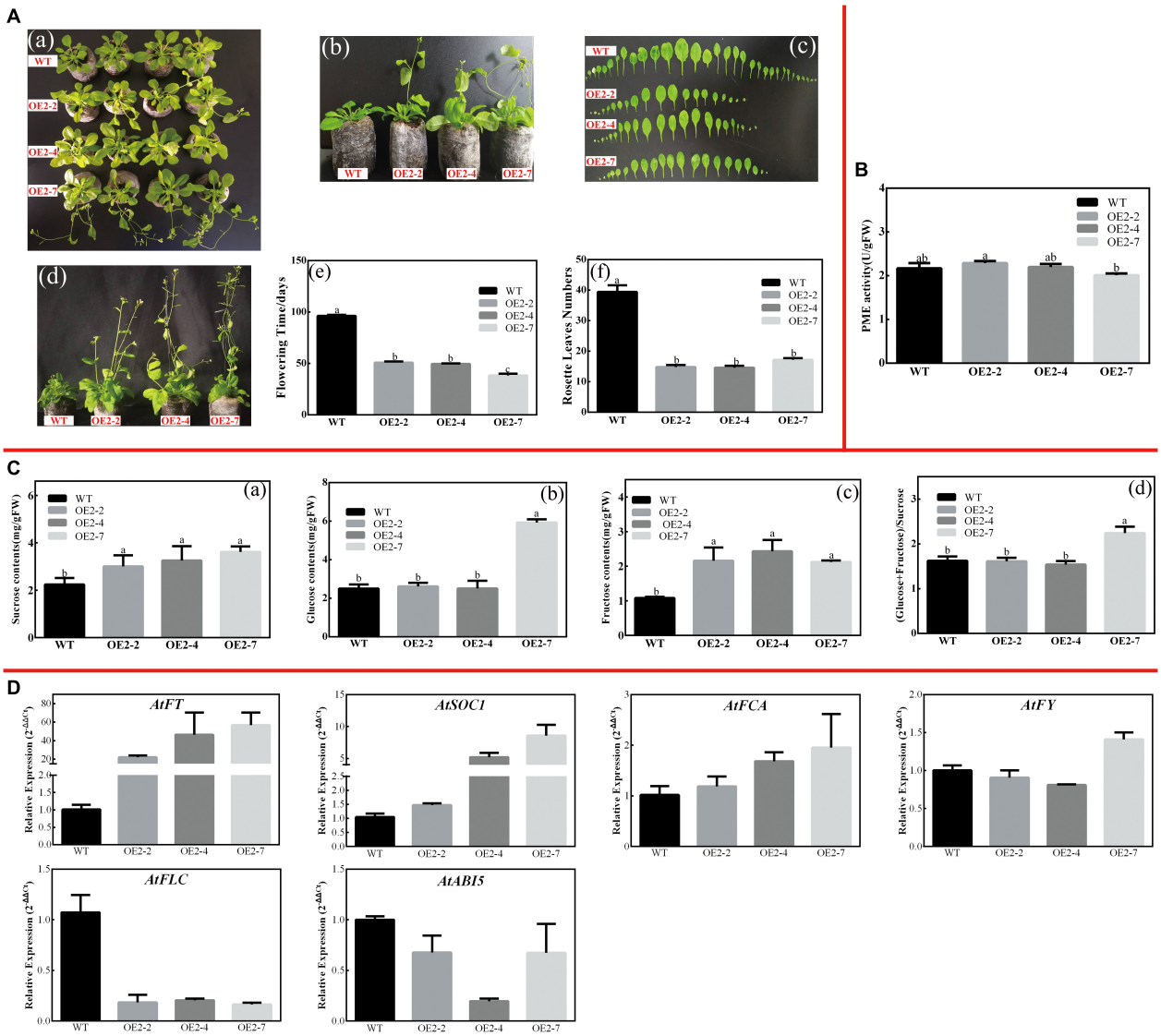


FIGURE 8 | Overexpression of *CsPMEI2* promotes early flowering in transgenic *Arabidopsis* under SD condition. **(A)** Early flowering phenotypes of *CsPMEI2*-OE lines grown under SD condition. **(a)** Early-flowering phenotype; **(b)** phenotypes of *CsPMEI2*-OE lines and WT plants after 38 d of growth under SD condition; **(c)** leaf size; **(d)** phenotypes of *CsPMEI2*-OE lines and WT plants after 96 days of growth under SD condition; **(e)** flowering time; **(f)** rosette leaves numbers. **(B)** PME activities of WT and *CsPMEI2*-OE lines under SD condition. **(C)** Sugar contents of WT and *CsPMEI2*-OE lines under SD condition. **(a)** Suc contents; **(b)** Glu contents; **(c)** Fru contents; **(d)** the ratio of hexose/Suc. **(D)** Expression analysis of flowering-related genes. The final results were calculated with $2^{-\Delta\Delta Ct}$ method. Data are shown as the means ± SE (n = 3).

analysis results showed that *CbPMEI* and *PMEI13* mediated freezing tolerance may be independent on *CBF* pathway due to *CBFs* and *CORs* transcripts were not consistently declined in transgenic lines (Chen et al., 2018). However, the molecular and genetic mechanisms of PMEIs involved in abiotic stress tolerance still remain poorly understood, how the increased PMEI activity affects abiotic resistance needs to be further explored.

It is now clear that PMEIs are involved in pollen tube growth through inhibiting PME activity and hence affect cell wall stability (Rockel et al., 2008). A *PMEI* gene, *BoPMEI*, has been demonstrated as a pollen-specific gene, which is critical to pollen tube growth. Antisense expression of *BoPMEIl* in *Arabidopsis* suppressed the transcriptions of an orthologous gene, *Atlgl0770*, which resulted in partial male sterility and decreased seed set (Zhang et al., 2010). In *B. campestris*, many *BcPMEIs* transcripts were highly expressed in inflorescences, in particular 10 *BcPMEIs* transcripts were specifically expressed during flower development periods (Liu et al., 2018b). Moreover, mature transcripts of two *PMEI* genes, *Tdpmei2.1* and *Tdpmei2.2*, were predominantly detected in floral organs of durum wheat, which indicated that *Tdpmei2.1* and *Tdpmei2.2* play key roles in flower development, in particular in anther and pollen

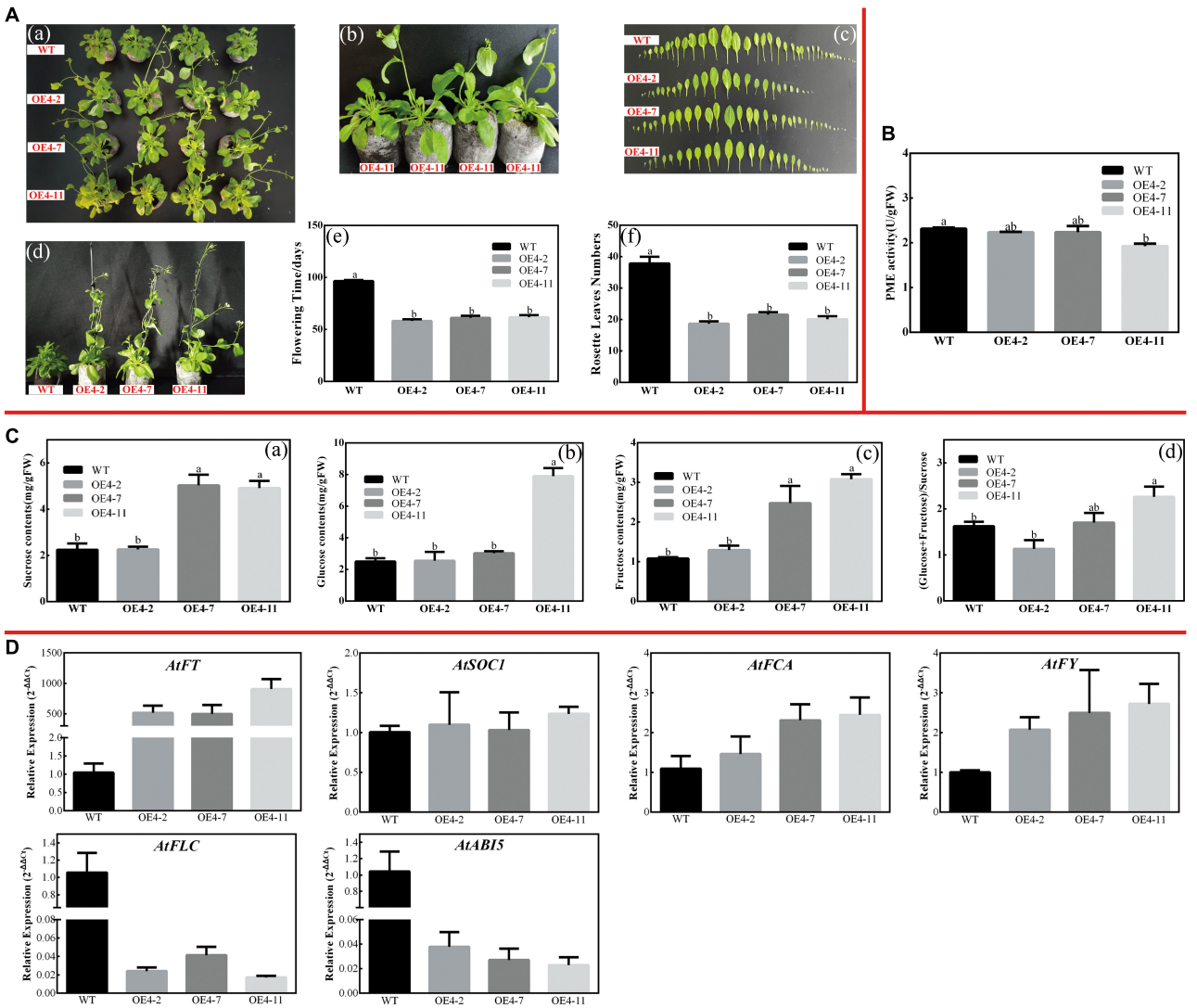


FIGURE 9 | Overexpression of *CsPMEI4* promotes early flowering in transgenic *Arabidopsis* under SD condition. **(A)** Early flowering phenotypes of *CsPMEI4*-OE lines grown under SD condition. **(a)** Early-flowering phenotype; **(b)** phenotypes of *CsPMEI4*-OE lines and WT plants after 58 d of growth under SD condition; **(c)** leaf size; **(d)** phenotypes of *CsPMEI4*-OE lines and WT plants after 96 days of growth under SD condition; **(e)** flowering time; **(f)** rosette leaves numbers. **(B)** PME activities of WT and *CsPMEI4*-OE lines under SD condition. **(C)** Sugar contents of WT and *CsPMEI4*-OE lines under SD condition. **(a)** Suc contents; **(b)** Glu contents; **(c)** Fru contents; **(d)** the ratio of hexose/Suc. **(D)** Expression analysis of flowering-related genes. The final results were calculated with $2^{-\Delta\Delta Ct}$ method. Data are shown as the means ± SE (n = 3).

development (Rocchi et al., 2012). Since many studies have demonstrated that PMEIs are involved in the reproductive process of plant, the roles in promoting flowering have not been reported. In the present study, both *CsPMEI2*-OE and *CsPMEI4*-OE lines exhibited early flowering phenotypes as compared to WT plants both under LD and SD conditions. Meanwhile, we found the PME activities were slightly decreased under SD condition. It is well known that the inhibition of PME activity leads to an increase in methylesterification of cell wall HGs, but the changes to cell walls were spatially regulated (Müller et al., 2013). Here, we failed to detect the methylesterification contents as the technology restriction. Instead, we found the degradation productions contents of pectins, including Suc, Glu and Fru were significantly increased both in *CsPMEI2*-OE and *CsPMEI4*-OE lines, suggesting that overexpression of *CsPMEI2/4* induced the changes of carbohydrate metabolism, and hence affected reproductive process. However, the specific regulation mechanisms need to be further explored. Actually, a similar result was also found by Müller et al. (2013), where they demonstrated that overexpression of *AtPMEI5* in *Arabidopsis* resulted in lower PME activity and higher contents of neutral sugars (i.e., Glu, fucose, and rhamnose) in cell wall, but the levels of uronic acids were not significantly changed as compared with WT plants.

In terms of flowering, at least four major pathways, including autonomous, gibberellin, photoperiod, and vernalization pathways, have been identified to participate in floral promotion (Wang et al., 2012; Jing et al., 2020). During flowering period, two flowering pathway integrators (*FT* and *SOC1*), which are commonly regulated by these four pathways, will activate two floral meristem identity genes (*AP1* and *LFY*) to promote the formation of floral meristems (Wang et al., 2012). However, such integrators are negatively regulated by a central upstream regulator, *FLC*, which encodes a MADS box transcription factor and mediates the autonomous or vernalization pathways (Michaels and Amasino, 2001). The transcription accumulation of genes involved in the autonomous pathway (e.g., *FCA* and *FY*) would suppress the expression of *FLC* through chromatin or RNA modification (Wang et al., 2012). As expected, the transcriptions of *FT*, *SOC1*, and *AP1* and some genes involved in the autonomous pathway, including *FCA* and *FY*, were accumulated, while the expression of *FLC* was declined both in *CsPMEI2*-OE and *CsPMEI4*-OE lines as compared to WT plants under LD and SD condition. A similar phenotype was also found in *CsUGT85A53*-OE transgenic *Arabidopsis*. The expressions of *FT*, *SOC1*, *AP1*, *LFY*, *FY*, and *FCA* were increased, while the mRNA level of *FLC* was repressed in *CsUGT85A53*-OE lines. Further research found that overexpression of *CsUGT85A53* increased the DNA methylation levels of *FLC*, but decreased the free ABA contents via ABA glucosylation in transgenic *Arabidopsis*. However, the early flowering phenotype was restored by the application of exogenous ABA (Jing et al., 2020). In this study, we found the expression of an activator of *FLC* gene, *ABI5*, was also declined both in *CsPMEI2*-OE and *CsPMEI4*-OE lines. However, exogenous ABA treatment did not completely inhibit early flowering phenomenon of *CsPMEI2*-OE and *CsPMEI4*-OE lines, suggesting that the early flowering phenomenon in transgenic *Arabidopsis* may be partially dependent on ABA signaling pathway, and the changes of carbohydrate metabolism may also contribute to this phenomenon. Still, the detailed molecular mechanism of the roles of *CsPMEI2/4* in flowering needs to be deeply explored.

DATA AVAILABILITY STATEMENT

The datasets presented in this study can be found in online repositories. The names of the repository/repositories and accession number(s) can be found in the article/ **Supplementary Material**.

AUTHOR CONTRIBUTIONS

WQ conceived and designed the experiments. WQ and HW wrote the original draft. HW and BL performed the experiments. YW, NL, LW, and XH sampled the materials. SH, BL, and WQ analyzed the results and performed figures. ZD and YY reviewed and edited the manuscript. All authors read and approved the final manuscript.

FUNDING

This work was supported by the National Natural Science Foundation of China (31800588), the Sub Project of Shandong Agricultural Elite Variety Project (2321401), and the School Fund Project of Qingdao Agricultural University (1118025).

SUPPLEMENTARY MATERIAL

The Supplementary Material for this article can be found online at: https://www.frontiersin.org/articles/10.3389/fpls.2021.807514/full#supplementary-material

Supplementary Figure 1 | Conserved domains analysis of CsPMEIs and CsVIF/CIFs. Four conserved and representative Cys (C) residues were contained in the red boxes, respectively.

Supplementary Figure 2 | The exon–intron structures, and *cis*-acting elements of *CsPMEIs*. **(A)** Exon–intron structure of *CsPMEIs*. The coding sequence and the corresponding genomic sequence of each *CsPMEI* were compared by using GSDS2.0. Blue boxes represent untranslated upstream/downstream regions, green double sided wedges represent exons, and black lines indicate introns. **(B)** The *cis*-acting regulatory elements of *CsPMEIs*. 2,000-bp upstream non-coding region sequences of each *CsPMEI* gene, except for *CsPMEI3/20*, were used to predict *cis*-acting elements, and different colored blocks represent different elements.

Supplementary Figure 3 | Phenotypes, flowering time and rosette leaves numbers of *CsPMEI2/4*-OE lines under ABA treatment condition. **(A)** Phenotypes, flowering time and rosette leaves numbers of *CsPMEI2*-OE lines under ABA treatment condition. **(a)** Phenotypes of *CsPMEI2*-OE lines and WT plants after 31 days of growth under ABA treatment condition; **(b)** phenotypes of *CsPMEI2*-OE lines and WT plants after 41 days of growth under ABA treatment condition; **(c)** phenotypes of *CsPMEI2*-OE lines and WT plants after 51 days of growth under ABA treatment condition; **(d)** flowering time; **(e)** rosette leaves numbers. **(B)** Phenotypes, flowering time and rosette leaves numbers of *CsPMEI4*-OE lines under ABA treatment condition. **(a)** Phenotypes of *CsPMEI4*-OE lines and WT plants after 35 days of growth under ABA treatment condition; **(b)** phenotypes of *CsPMEI4*-OE lines and WT plants after 41 days of growth under ABA treatment condition; **(c)** phenotypes of *CsPMEI4*-OE lines and WT plants after 51 days of growth under ABA treatment condition; **(d)** flowering time; **(e)** rosette leaves numbers.

Supplementary Figure 4 | Phylogenetic and conserved domains analysis of INHs and PMEIs. **(A)** A total of 30 INHs and PMEIs were used to construct phylogenetic tree by using MEGA 7.0 software. CsVIF/CIFs highlighted with red squares and CsPMEIs are highlighted with red triangle, and different subgroups were covered with different colors. **(B)** Conserved domains analysis of INHs and PMEIs. The conserved 'PKF' motif was contained in the blue box, and the four conserved and representative Cys (C) residues were contained in the red boxes, respectively.

Supplementary Table 1 | Nutrient solution formulation.

Supplementary Table 2 | All sequences used to construct phylogenetic tree.

Supplementary Table 3 | Primer sequences used in ORF of *CsPMEI2/4* cloning and vector construction.

Supplementary Table 4 | Primers information used in qRT-PCR detection.

REFERENCES

An, S., Sohn, K., Choi, H., Hwang, I., Lee, S., and Hwang, B. (2008). Pepper pectin methylesterase inhibitor protein CaPMEI1 is required for antifungal activity, basal disease resistance and abiotic stress tolerance. *Planta* 228, 61–78. doi: 10.1007/s00425-008-0719-z

Andres-Robin, A., Reymond, M. C., Brunoud, G., Martin-Magniette, M. L., Moneger, F., and Scutt, C. P. (2020). Immediate targets of ETTIN suggest a key role for pectin methylesterase inhibitors in the control of *Arabidopsis gynecium* development. *Plant Signal Behav.* 15:1771937. doi: 10.1080/15592324.2020.1771937

Arkorful, E., Hu, S., Zou, Z., Yu, Y., Chen, X., and Li, X. (2020). Metabolomic analyses provide new insights into signaling mechanisms for nutrient uptake by lateral roots of pruned tea plant (*Camellia sinensis*). *J. Agric. Food Chem.* 68, 7890–7903. doi: 10.1021/acs.jafc.0c02053

Baldwin, L., Domon, J. M., Klimek, J. F., Fournet, F., Sellier, H., Gillet, F., et al. (2014). Structural alteration of cell wall pectins accompanies pea development in response to cold. *Phytochemistry* 104, 37–47. doi: 10.1016/j.phytochem.2014.04.011

Balestrieri, C. (1990). A glycoprotein inhibitor of pectin methylesterase in kiwi fruit. *Eur. J. Biochem.* 193, 183–187. doi: 10.1111/j.1432-1033.1990.tb19321.x

Bethke, G., Grundman, R., Sreekanta, S., Truman, W., Katagiri, F., and Glazebrook, J. (2014). Arabidopsis pectin methylesterases contribute to immunity against *Pseudomonas* syringae. *Plant physiol.* 164, 1093–1107. doi: 10.1104/pp.113.227637

Camardella, L., Carratore, V., Ciardiello, M., Servillo, L., Balestrieri, C., and Giovane, A. (2000). Kiwi protein inhibitor of pectin methylesterase amino-acid sequence and structural importance of two disulfide bridges. *Eur. J. Biochem.* 267, 4561–4565. doi: 10.1046/j.1432-1327.2000.01510.x

Cantarel, B. L., Coutinho, P. M., Rancurel, C., Bernard, T., Lombard, V., and Henrissat, B. (2009). The carbohydrate-active enzymes database (CAZy): an expert resource for Glycogenomics. *Nucleic Acids Res.* 37, D233–D238. doi: 10.1093/nar/gkn663

Chen, J., Chen, X., Zhang, Q., Zhang, Y., Ou, X., An, L., et al. (2018). A cold-induced pectin methyl-esterase inhibitor gene contributes negatively to freezing tolerance but positively to salt tolerance in *Arabidopsis*. *J. Plant Physiol.* 222, 67–78. doi: 10.1016/j.jplph.2018.01.003

Clough, S. J., and Bent, A. F. (2010). Floral dip: a simplified method for agrobacterium-mediated transformation of *Arabidopsis thaliana*. *Plant J.* 16, 735–743. doi: 10.1046/j.1365-313x.1998.00343.x

Di Matteo, A., Giovane, A., Raiola, A., Camardella, L., Bonivento, D., De Lorenzo, G., et al. (2005). Structural basis for the interaction between pectin methylesterase and a specific inhibitor protein. *Plant Cell* 17, 849–858. doi: 10.1105/tpc.104.028886

Hao, X. Y., Horvath, D., Chao, W., Yang, Y. J., Wang, X. C., and Xiao, B. (2014). Identification and evaluation of reliable reference genes for quantitative real-time PCR analysis in tea plant (*Camellia sinensis* (L.) O. Kuntze). *Int. J. Mol. Sci.* 15, 22155–22172. doi: 10.3390/ijms151222155

Hao, X. Y., Tang, H., Wang, B., Wang, L., Cao, H. L., Wang, Y. C., et al. (2018). Gene characterization and expression analysis reveal the importance of auxin signaling in bud dormancy regulation in tea plant. *J. Plant Growth Regul.* 38, 225–240. doi: 10.1007/s00344-018-9834-7

Hong, M., Kim, D., Lee, T., Jeon, W., and Seo, Y. (2010). Functional characterization of pectin methylesterase inhibitor (PMEI) in wheat. *Genes Genet. Syst.* 85, 97–106. doi: 10.1266/ggs.85.97

Hothorn, M., Van den Ende, W., Lammens, W., Rybin, V., and Scheffzek, K. (2010). Structural insights into the pH-controlled targeting of plant cell-wall invertase by a specific inhibitor protein. *Proc. Natl. Acad. Sci. U.S.A.* 107, 17427–17432. doi: 10.1073/pnas.1004481107

Hothorn, M., Wolf, S., Aloy, P., Greiner, S., and Scheffzek, K. (2004). Structural insights into the target specificity of plant invertase and pectin methylesterase inhibitory proteins. *Plant Cell* 16, 3437–3447. doi: 10.2307/3872361

Ishimaru, T., Hirose, T., Matsuda, T., Akitoshi, G., Kazunari, T., Haruto, S., et al. (2005). Expression patterns of genes encoding carbohydrate-metabolizing enzymes and their relationship to grain filling in rice (*Oryza sativa* L.): comparison of caryopses located at different positions in a panicle. *Plant Cell Physiol.* 46, 620–628. doi: 10.1093/pcp/pci066

Jing, T., Zhang, N., Gao, T., Wu, Y., Zhao, M., Jin, J., et al. (2020). UGT85A53 promotes flowering via mediating abscisic acid glucosylation and FLC transcription in *Camellia sinensis*. *J. Exp. Bot.* 71, 7018–7029. doi: 10.1093/jxb/eraa373

Juge, N. (2006). Plant protein inhibitors of cell wall degrading enzymes. *Trends Plant Sci.* 11, 359–367. doi: 10.1016/j.tplants.2006.05.006

Landy, A. (1989). Dynamic, structural, and regulatory aspects of lambda site-specific recombination. *Annu. Rev. Biochem.* 58, 913–949. doi: 10.1146/annurev.bi.58.070189.004405

Lionetti, V., Fabri, E., De Caroli, M., Hansen, A. R., Willats, W. G., Piro, G., et al. (2017). Three pectin methylesterase inhibitors protect cell wall integrity for *Arabidopsis* immunity to botrytis. *Plant Physiol.* 173, 1844–1863. doi: 10.1104/pp.16.01185

Lionetti, V., Raiola, A., Camardella, L., Giovane, A., Obel, N., Pauly, M., et al. (2007). Overexpression of pectin methylesterase inhibitors in *Arabidopsis* restricts fungal infection by Botrytis cinerea. *Plant Physiol.* 143, 1871–1880. doi: 10.1104/pp.106.090803

Lionetti, V., Raiola, A., Mattei, B., and Bellincampi, D. (2015). The grapevine VvPMEI1 gene encodes a novel functional pectin methylesterase inhibitor associated to grape berry development. *PLoS One* 10:e0133810. doi: 10.1371/journal.pone.0133810

Liu, T., Yu, H., Xiong, X., Yu, Y., Yue, X., Liu, J., et al. (2018a). Genome-wide identification and characterization of pectin methylesterase inhibitor genes in Brassica oleracea. *Int. J. Mol. Sci.* 19:338. doi: 10.3390/ijms19113338

Liu, T., Yu, H., Xiong, X., Yue, X., Yu, Y., Huang, L., et al. (2018b). Genome-wide identification, molecular evolution, and expression profiling analysis of pectin methylesterase inhibitor genes in Brassica campestris ssp. chinensis. *Int. J. Mol. Sci.* 19:338. doi: 10.3390/ijms19051338

Livak, K. J., and Schmittgen, T. D. (2001). Analysis of relative gene expression data using real-time quantitative PCR and the 2(-Delta Delta C(T)) method. *Methods* 25, 402–408. doi: 10.1006/meth.2001

Lu, Q., Wang, Y., Xiong, F., Hao, X., Zhang, X., Li, N., et al. (2020). Integrated transcriptomic and metabolomic analyses reveal the effects of callose deposition and multihormone signal transduction pathways on the tea plant-*Colletotrichum camelliae* interaction. *Sci. Rep.* 10:12858. doi: 10.1038/s41598-020-69729-x

Michaels, S., and Amasino, R. M. (2001). Loss of Flowering locus c activity eliminates the late-flowering phenotype of FRIGIDA and autonomous pathway mutations but not responsiveness to vernalization. *Plant Cell* 13, 935–941. doi: 10.2307/3871350

Müller, K., Levesque-Tremblay, G., Fernandes, A., Wormit, A., Bartels, S., Usadel, B., et al. (2013). Overexpression of a pectin methylesterase inhibitor in *Arabidopsis thaliana* leads to altered growth morphology of the stem and defective organ separation. *Plant Signal. Behav.* 8:e26464. doi: 10.4161/psb.26464

Nguyen, H. P., Jeong, H. Y., Jeon, S. H., Kim, D., and Lee, C. (2017). Rice pectin methylesterase inhibitor28 (OsPMEI28) encodes a functional PMEI and its overexpression results in a dwarf phenotype through increased pectin methylesterification levels. *J. Plant Physiol.* 208, 17–25. doi: 10.1016/j.jplph.2016.11.006

Nguyen, H. P., Jeong, H. Y., Kim, H., Kim, Y. C., and Lee, C. (2016). Molecular and biochemical characterization of rice pectin methylesterase inhibitors (OsPMEIs). *Plant Physiol. Biochem.* 101, 105–112. doi: 10.1016/j.plaphy.2016.01.021

Pinzon-Latorre, D., and Deyholos, M. K. (2014). Pectinmethylesterases (PME) and pectinmethylesterase inhibitors (PMEI) enriched during phloem fiber development in flax (*Linum usitatissimum*). *PLoS One* 9:e105386. doi: 10.1371/journal.pone.0105386

Qian, W. J., Xiao, B., Wang, L., Hao, X. Y., Yue, C., Cao, H. L., et al. (2018). CsINV5, a tea vacuolar invertase gene enhances cold tolerance in transgenic *Arabidopsis*. *BMC Plant Biol.* 18:228. doi: 10.1186/s12870-018-1456-5

Qian, W. J., Yue, C., Wang, Y. C., Cao, H. L., Li, N. N., Wang, L., et al. (2016). Identification of the invertase gene family (INVs) in tea plant and their expression analysis under abiotic stress. *Plant Cell Rep.* 35, 2269–2283. doi: 10.1007/s00299-016-2033-8

Raiola, A., Camardella, L., Giovane, A., Mattei, B., De Lorenzo, G., Cervone, F., et al. (2004). Two *Arabidopsis thaliana* genes encode functional pectin

methylesterase inhibitors 1. *FEBS Lett.* 557, 199–203. doi: 10.1016/s0014-5793(03)01491-1

Ren, A., Ahmed, R. I., Chen, H., Han, L., Sun, J., Ding, A., et al. (2019). Genome-wide identification, characterization and expression patterns of the pectin methylesterase inhibitor genes in *Sorghum bicolor*. *Genes (Basel)* 10:755. doi: 10.3390/genes10100755

Rocchi, V., Janni, M., Bellincampi, D., Giardina, T., and D'Ovidio, R. (2012). Intron retention regulates the expression of pectin methyl esterase inhibitor (Pmei) genes during wheat growth and development. *Plant Biol.* 14, 365–373. doi: 10.1111/j.1438-8677.2011.00508.x

Rockel, N., Wolf, S., Kost, B., Rausch, T., and Greiner, S. (2008). Elaborate spatial patterning of cell-wall PME and PMEI at the pollen tube tip involves PMEI endocytosis, and reflects the distribution of esterified and de-esterified pectins. *Plant J.* 53, 133–143. doi: 10.1111/j.1365-313X.2007.03325.x

Saez-Aguayo, S., Ralet, M. C., Berger, A., Botran, L., Ropartz, D., Marion-Poll, A., et al. (2013). PECTIN METHYLESTERASE INHIBITOR6 promotes Arabidopsis mucilage release by limiting methylesterification of homogalacturonan in seed coat epidermal cells. *Plant Cell* 25, 308–323. doi: 10.1105/tpc.112.106575

Solecka, D., Zebrowski, J., and Kacperska, A. (2008). Are pectins involved in cold acclimation and de-acclimation of winter oil-seed rape plants? *Ann. Bot.* 101, 521–530. doi: 10.1093/aob/mcm329

Srivastava, S., Gupta, S. M., Sane, A. P., and Nath, P. (2012). Isolation and characterization of ripening related pectin methylesterase inhibitor gene from banana fruit. *Physiol. Mol. Biol. Plants* 18, 191–195. doi: 10.1007/s12298-012-0102-1

Volpi, C., Janni, M., Lionetti, V., Bellincampi, D., Favaron, F., and D'Ovidio, R. (2011). The ectopic expression of a pectin methyl esterase inhibitor increases pectin methyl esterification and limits fungal diseases in wheat. *Mol. Plant Microbe In.* 24, 1012–1019. doi: 10.1094/mpmi-01-11-0021

Wang, B., Jin, S. H., Hu, H. Q., Sun, Y. G., Wang, Y. W., Han, P., et al. (2012). UGT87A2, an Arabidopsis glycosyltransferase, regulates flowering time via FLOWERING LOCUS C. *New Phytol.* 194, 666–675. doi: 10.1111/j.1469-8137.2012.04107.x

Wang, H., Ding, Z., Gou, M., Hu, J., Wang, Y., Wang, L., et al. (2021). Genome-wide identification, characterization, and expression analysis of tea plant autophagy-related genes (CsARGs) demonstrates that they play diverse roles during development and under abiotic stress. *BMC Genomics* 22:121. doi: 10.1186/s12864-021-07419-2

Wang, L., Yao, L., Hao, X., Li, N., Qian, W., Yue, C., et al. (2018). Tea plant SWEET transporters: expression profiling, sugar transport, and the involvement of CsSWEET16 in modifying cold tolerance in *Arabidopsis*. *Plant Mol. Biol.* 96, 577–592. doi: 10.1007/s11103-018-0716-y

Wang, L. Y., Hao, X. Y., Li, N. N., Wang, Y. C., Ding, C. Q., Lei, L., et al. (2019). Transcriptional and physiological analyses reveal the association of ROS metabolism with cold tolerance in tea plant. *Environ. Exp. Bot.* 160:14. doi: 10.1016/j.envexpbot.2018.11.011

Wang, X. C., Zhao, Q. Y., Ma, C. L., Zhang, Z. H., Cao, H. L., Kong, Y. M., et al. (2013). Global transcriptome profiles of *Camellia sinensis* during cold acclimation. *BMC Genomics* 14:415. doi: 10.1186/1471-2164-14-415

Wang, Y. C., Qian, W. J., Li, N. N., Hao, X. Y., Wang, L., Xiao, B., et al. (2016). Metabolic changes of caffeine in tea plant (*Camellia sinensis* (L.) O. kuntze) as defense response to *Colletotrichum fructicola*. *J. Agric. Food. Chem.* 64, 6685–6693. doi: 10.1021/acs.jafc.6b02044

Wei, C., Yang, H., Wang, S., Zhao, J., Liu, C., Gao, L., et al. (2018). Draft genome sequence of *Camellia sinensis* var. sinensis provides insights into the evolution of the tea genome and tea quality. *Proc. Natl. Acad. Sci. U.S.A.* 115, E4151–E4158. doi: 10.1073/pnas.1719622115

Wolf, S., Mouille, G., and Pelloux, J. (2009). Homogalacturonan methyl-esterification and plant development. *Mol. Plant* 2, 851–860. doi: 10.1093/mp/ssp066

Wormit, A., and Usadel, B. (2018). The multifaceted role of pectin methylesterase inhibitors (PMEIs). *Int. J. Mol. Sci.* 19:878. doi: 10.3390/ijms19102878

Xia, X., Mi, X., Jin, L., Guo, R., Zhu, J., Xie, H., et al. (2021). CsLAZY1 mediates shoot gravitropism and branch angle in tea plants (*Camellia sinensis*). *BMC Plant Biol.* 21:243. doi: 10.1186/s12870-021-03044-z

Xiong, F., Ren, J. J., Yu, Q., Wang, Y. Y., Lu, C. C., Kong, L. J., et al. (2019). AtU2AF65b functions in abscisic acid mediated flowering via regulating the precursor messenger RNA splicing of ABI5 and FLC in *Arabidopsis*. *New Phytol.* 223, 277–292. doi: 10.1111/nph.15756

Yao, L. N., Ding, C. Q., Hao, X. Y., Zeng, J. M., Yang, Y. J., Wang, X. C., et al. (2020). CsSWEET1a and CsSWEET17 mediate growth and freezing tolerance by promoting sugar transport across the plasma membrane. *Plant Cell Physiol.* 61, 1669–1682. doi: 10.1093/pcp/pcaa091

Yu, S., Li, P., Zhao, X., Tan, M., Ahmad, M. Z., Xu, Y., et al. (2021). CsTCPs regulate shoot tip development and catechin biosynthesis in tea plant (*Camellia sinensis*). *Hortic Res.* 8:104. doi: 10.1038/s41438-021-00538-7

Yuan, Y., Wu, H., Wang, N., Jie, L., Zhao, W., Du, J., et al. (2008). FIT interacts with AtbHLH38 and AtbHLH39 in regulating iron uptake gene expression for iron homeostasis in *Arabidopsis*. *Cell Res.* 18, 385–397. doi: 10.1038/cr.2008.26

Zhang, G. Y., Feng, J., Wu, J., and Wang, X. (2010). BoPMEI1, a pollen-specific pectin methylesterase inhibitor, has an essential role in pollen Tube growth. *Planta* 231, 1323–1334. doi: 10.1007/s00425-010-1136-7

Zhao, X., Zeng, X., Lin, N., Yu, S., Fernie, A. R., and Zhao, J. (2021). CsbZIP1-CsMYB12 mediates the production of bitter-tasting flavonols in tea plants *(Camellia sinensis*) through a coordinated activator-repressor network. *Hortic Res.* 8:110. doi: 10.1038/s41438-021-00545-8

Zhu, X., Tang, C., Li, Q., Qiao, X., Li, X., Cai, Y., et al. (2021). Characterization of the pectin methylesterase inhibitor gene family in rosaceae and role of PbrPMEI23/39/41 in methylesterified pectin distribution in pear pollen tube. *Planta* 253:118. doi: 10.1007/s00425-021-03638-9

Conflict of Interest: The authors declare that the research was conducted in the absence of any commercial or financial relationships that could be construed as a potential conflict of interest.

Publisher's Note: All claims expressed in this article are solely those of the authors and do not necessarily represent those of their affiliated organizations, or those of the publisher, the editors and the reviewers. Any product that may be evaluated in this article, or claim that may be made by its manufacturer, is not guaranteed or endorsed by the publisher.

Copyright © 2022 Li, Wang, He, Ding, Wang, Li, Hao, Wang, Yang and Qian. This is an open-access article distributed under the terms of the Creative Commons Attribution License (CC BY). The use, distribution or reproduction in other forums is permitted, provided the original author(s) and the copyright owner(s) are credited and that the original publication in this journal is cited, in accordance with accepted academic practice. No use, distribution or reproduction is permitted which does not comply with these terms.

frontiers in Plant Science

ORIGINAL RESEARCH
published: 28 January 2022
doi: 10.3389/fpls.2021.817861

Melatonin Treatment Delays Senescence and Maintains the Postharvest Quality of Baby Mustard (*Brassica juncea* var. *gemmifera*)

Hongmei Di[1†], Zhiqing Li[1†], Yating Wang[1], Yi Zhang[1], Jinlin Bian[1], Jingyi Xu[1], Yangxia Zheng[1], Ronggao Gong[1], Huanxiu Li[2], Fen Zhang[1] and Bo Sun[1]**

[1] College of Horticulture, Sichuan Agricultural University, Chengdu, China, [2] Institute of Pomology and Olericulture, Sichuan Agricultural University, Chengdu, China

OPEN ACCESS

Edited by:
Pei Xu,
China Jiliang University, China

Reviewed by:
Guang-Long Wang,
Huaiyin Institute of Technology, China
Athanasios Koukounaras,
Aristotle University of Thessaloniki, Greece

***Correspondence:**
Fen Zhang
zhangf@sicau.edu.cn
Bo Sun
bsun@sicau.edu.cn

[†] These authors have contributed equally to this work

Specialty section:
This article was submitted to Crop and Product Physiology, a section of the journal Frontiers in Plant Science

Received: 18 November 2021
Accepted: 27 December 2021
Published: 28 January 2022

Citation:
Di H, Li Z, Wang Y, Zhang Y, Bian J, Xu J, Zheng Y, Gong R, Li H, Zhang F and Sun B (2022) Melatonin Treatment Delays Senescence and Maintains the Postharvest Quality of Baby Mustard (Brassica juncea var. gemmifera). Front. Plant Sci. 12:817861. doi: 10.3389/fpls.2021.817861

The effect of melatonin treatment on the visual quality and content of health-promoting compounds in baby mustard (*Brassica juncea* var. *gemmifera*) at 20°C was investigated in this study. Application of 100 μmol L^{-1} melatonin was the most effective in prolonging the shelf life of baby mustard among all of the concentrations tested (1, 50, 100, and 200 μmol L^{-1}). The 100 μmol L^{-1} melatonin treatment also delayed the increase in weight loss and the decrease in sensory parameter scores; retarded the decline of chlorophyll content; slowed the decline in antioxidant capacity by maintaining the content of carotenoids and ascorbic acid, as well as increasing the levels of total phenolics; and increased the content of individual and total glucosinolates in the lateral buds of baby mustard. These findings indicate that melatonin treatment is effective for maintaining the sensory and nutritional qualities of postharvest baby mustard.

Keywords: melatonin, baby mustard (*Brassica juncea* var. *gemmifera*), sensory, antioxidant, glucosinolate

INTRODUCTION

Baby mustard (*Brassica juncea* var. *gemmifera*) is becoming increasingly popular among consumers for its sensory and nutritional properties. The lateral buds are tender with a sweet and fragrant flavor. Baby mustard contains numerous health-promoting compounds including ascorbic acid, carotenoids, phenolics, and glucosinolates (Sun et al., 2019). However, the lateral buds of baby mustard are susceptible to dehydration, browning, and the loss of health-promoting compounds during postharvest storage at room temperature (Sun et al., 2018, 2021). Several methods have been used to preserve the quality of postharvest baby mustard, such as long-term freezing treatment (Zhang et al., 2021), low temperature storage (Sun et al., 2020), and light exposure (Sun et al., 2021). Given the inconvenience and high costs of these methods, there is a need to develop improved techniques to extend the shelf life and preserve the postharvest quality of baby mustard during storage at room temperature.

Melatonin (*N*-acetyl-5-methoxytryptamine) is a derivative of tryptophan that occurs in all living organisms, including bacteria, fungi, plants, and mammals (Tang et al., 2020; Wu X. et al., 2021). This indoleamine is a pleiotropic molecule with a wide range of cellular and physiological functions in plants (Arnao and Hernández-Ruiz, 2019; Deng et al., 2021). In addition to its key role in plant growth and development, melatonin has been shown to be effective in promoting the postharvest

quality of fruits and vegetables, including delaying senescence, controlling disease, and alleviating chilling injury (Zhang et al., 2020). A delay in browning and other forms of quality deterioration caused by melatonin have been observed in numerous horticultural plants, such as peaches (Cao et al., 2016; Gao et al., 2016), pears (Zhai et al., 2018; Zheng et al., 2019), cassavas (Ma et al., 2016), bamboo shoots (Li et al., 2019), broccoli florets (Miao et al., 2020; Wei et al., 2020; Wu C. H. et al., 2021), and Chinese flowering cabbages (Tan et al., 2019, 2021). For example, melatonin treatment has been reported to delay the senescence of Chinese flowering cabbages by suppressing chlorophyll degradation and ABF-mediated abscisic acid biosynthesis (Tan et al., 2019). Melatonin treatment has also been shown to maintain the chlorophyll content in broccoli florets (Miao et al., 2020; Wu C. H. et al., 2021). Melatonin is widely known to be a direct scavenger of reactive oxygen species (ROS). Melatonin treatment can also reduce the accumulation of ROS indirectly by enhancing the activity of the ROS-scavenging system including major antioxidant enzymes (SOD, CAT, APX, etc.) and other natural antioxidants (carotenoids, ascorbic acid, phenolics, etc.) (Gao et al., 2016). It can also increase the levels of beneficial substances, such as amino acids, sugars, and soluble solids and thus enhance the nutritional quality of apples (Onik et al., 2021) and plums (Bal, 2019) postharvest. Furthermore, it can maintain the content of glucosinolates and positively affect the glucoraphanin-sulforaphane system in broccoli florets (Miao et al., 2020; Wei et al., 2020). These findings indicate that melatonin can be used for the postharvest preservation of fruits and vegetables because of its multiple effects.

Although melatonin treatment has been shown to be useful for the postharvest preservation of various fruits and vegetables, there is little information on the effect of melatonin on postharvest baby mustard. The aim of the current study was to explore the effects of melatonin on the sensory quality, chlorophyll, carotenoids, ascorbic acid, total phenolics, antioxidant capacity, and glucosinolates in baby mustard during storage.

MATERIALS AND METHODS

Plant Materials and Melatonin Treatments

Baby mustard (*B. juncea* var. *gemmifera*), harvested early in the morning, was obtained from a local farm in Chengdu City, China, and transported to the laboratory within 2 h under ambient temperature. In experiment I, 120 lateral buds were randomly divided into five batches in quadruplicate (six lateral buds per replicate) and were immersed in 0 (control), 1, 50, 100, and 200 μmol L^{-1} melatonin solutions for 5 min. The lateral buds were then removed from the solutions and air-dried. All the procedures were performed at room temperature. Afterward, each replicate was placed in a transparent polypropylene container and stored at 20°C with a relative humidity of 75% for 6 days. Samples were treated and stored in the dark (<0.01 μmol m^{-2} s^{-1}) to prevent melatonin decomposition. Treatment with 100 μmol L^{-1} melatonin significantly extended the shelf life of baby mustard compared with other treatment groups and the control.

In experiment II, a total of 168 lateral buds were assigned to two groups (0 and 100 μmol L^{-1} melatonin). Similarly, there are four replicates in both groups, and each replicate contains six lateral buds. Samples were taken before melatonin treatment (time 0) and at 2-day intervals during storage for measurements. Among the six lateral buds in each replicate, three lateral buds were tested for analyses of sensory quality and weight loss; the remaining three are lyophilized and stored at −20°C for further analyses of phytochemicals and antioxidant capacity.

Shelf Life and Sensory Quality Evaluation

Shelf life and sensory quality of the baby mustard lateral buds were assessed daily and on sampling day, respectively. The lateral buds were considered to have reached the end of their shelf life when they became soft, shrank, and exhibited browning (Sun et al., 2021). Sensory attributes were quantified on a scale from 5 (best) to 1 (worst). Color was rated using 5 = bright green without defects, 3 = lighter green with a few browning spots, and 1 = yellowish lateral buds with severe browning. Form was rated using 5 = the leaves on the upper of lateral buds are fresh and straight, 3 = shrinkage appears to the leaves of lateral buds, and 1 = the leaves shrink significantly. Odor was rated using 5 = no off-odors, 3 = slight but obvious off-odor, and 1 = strong off-odor. Texture was rated using 5 = very tight and firm, 3 = slightly soften but acceptable, and 1 = very soften. Acceptance was rated using 5 = excellent and having a freshly harvested appearance, 3 = average, and 1 = unmarketable.

Weight Loss

Weight loss (%) was calculated by the formula $(W_x - W_0)/W_0 \times 100$, where W_0 is the weight at 0 day, and W_x is the weight at a certain day after storage (Sun et al., 2021).

Chlorophyll and Carotenoid Content

The powder of lateral bud was ground and extracted with acetone, and the supernatant was filtered and analyzed by high-performance liquid chromatography (HPLC). Samples (10 μL) were separated using isopropanol and 80% acetonitrile–water at a flow rate of 0.5 mL min^{-1} (Sun et al., 2021).

Ascorbic Acid Content

The sample powder was extracted with 1.0% oxalic acid, and then centrifuged. Each sample was filtered through a 0.45 μm cellulose acetate filter, and analyzed by HPLC. The amount of ascorbic acid was calculated from absorbance values at 243 nm (Sun et al., 2018).

Total Phenolics Content

Total phenolics were extracted with 50% ethanol, and the supernatant was mixed with Folin-Ciocalteu reagent, after 3 min, saturated sodium carbonate was added. The absorbance was measured at 760 nm with the spectrophotometer (Sun et al., 2018).

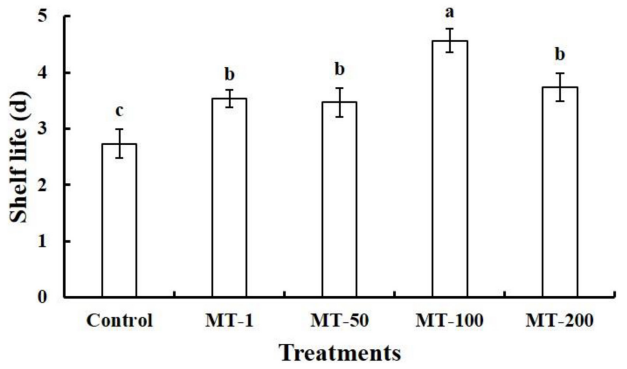


FIGURE 1 | Shelf life of different concentrations of melatonin-treated lateral buds of baby mustard during storage at 20°C. Different letters in the figure indicate statistically significant differences among treatments ($P < 0.05$). MT-1, 1 μmol L^{-1} melatonin treatment; MT-50, 50 μmol L^{-1} melatonin treatment; MT-100, 100 μmol L^{-1} melatonin treatment; and MT-200, 200 μmol L^{-1} melatonin treatment.

Ferric Reducing Antioxidant Power

The extracted samples were added to the ferric reducing antioxidant power (FRAP) working solution incubated at 37°C. The absorbance was then recorded at 593 nm using a spectrophotometer after the mixture had been incubated in at 37°C for 10 min, and then the value was calculated (Sun et al., 2018).

2,2-Azinobis (3-Ethyl-Benzothiazoline-6-Sulfonic Acid) (ABTS) Assay

An aliquot of 300 μL of each extracted sample was added to 3 mL of $ABTS^{+}$ solution. The absorbance was measured spectrophotometrically at 734 nm after exactly 2 h, and then the value was calculated. The percentage inhibition was calculated according to the formula:% inhibition = $[(A_{control} - A_{sample})/A_{control}] \times 100\%$ (Sun et al., 2018).

Glucosinolate Composition and Content

Freeze-dried samples (100 mg) were boiled in 5 mL water for 10 min to destroy the activity of myrosinases and prevent glucosinolates from hydrolysis. The supernatant was collected and applied to a DEAE-Sephadex A-25 column. The glucosinolates were converted into their desulpho analogues by treated with aryl sulphatase, and the desulphoglucosinolates were eluted, and then analyzed by HPLC. Glucosinolates were quantified by using *ortho*-Nitrophenyl β-D-galactopyranoside as the internal standard and considering the response factor of each glucosinolate (Sun et al., 2018).

Data Analysis

Data were analyzed using one-way ANOVAs. A time-related trajectory analysis based on a principal component analysis map was used to visualize temporal changes in postharvest quality between different treatments (Sun et al., 2021).

RESULTS

Shelf Life

In experiment I, all of the melatonin treatments significantly extended the shelf life of the lateral buds of baby mustard (**Figure 1**). The shelf life was the longest for the 100 μmol L^{-1} melatonin treatment (4.6 days), which was 1.7-fold greater than that of the control (2.7 days). No significant differences in the shelf life were observed between the other three melatonin treatments (average of 3.4 days). Thus, 100 μmol L^{-1} melatonin was used in subsequent experiments.

Sensory Quality

The treatment of 100 μmol L^{-1} melatonin notably suppressed the deterioration of the external aspect of the lateral buds. The control group showed obvious browning and yellowing at 4 and 6 days, respectively. In the melatonin-treated group, slight browning was observed at 6 days (**Figure 2A**).

At 4 days, the sensory parameter scores, with the exception of odor, were less than 3 in the control, which means that they were unsaleable (**Figures 2B–F**). The treatment with 100 μmol L^{-1} melatonin had significantly higher color, form, texture, and acceptance scores compared with the control at 6 days (**Figures 2B,C,E,F**). The color and acceptance scores of the melatonin-treated group at 6 days were still higher than those of the control at 4 days of storage (**Figures 2B,F**). No differences in the odor scores were observed between the control and melatonin treatment during the entire storage period and were 3.4 and 3.6 at 6 days, respectively (**Figure 2D**).

Weight Loss

Weight loss increased regardless of whether the lateral buds were treated with melatonin during storage (**Figure 2G**). The weight loss observed during the storage period was significantly lower in the melatonin treatment than in the control. The weight loss in the control reached a maximum value of 19% at 6 days, whereas the level of weight loss was only 12% in the melatonin treatment, indicating that the weight loss of baby mustard was substantially reduced by melatonin during postharvest storage.

Chlorophyll and Carotenoids

The total chlorophylls content in the control and melatonin-treated samples decreased during storage (**Figure 3A**). However, the content in the melatonin-treated group was always significantly higher than that of the control, which was consistent with the change in the acceptance score (**Figure 2F**). At 6 days, the total chlorophylls content in the treated samples was 1.3-fold higher compared with the control, with reductions of 31 and 47%, respectively, compared with day 0.

The total carotenoids content in the control significantly decreased over the first 2 days of storage and then remained stable. The total carotenoids content in the treated group was significantly lower at 6 days than at 0 day. However, at 6 days of storage, the total carotenoids content in samples treated with

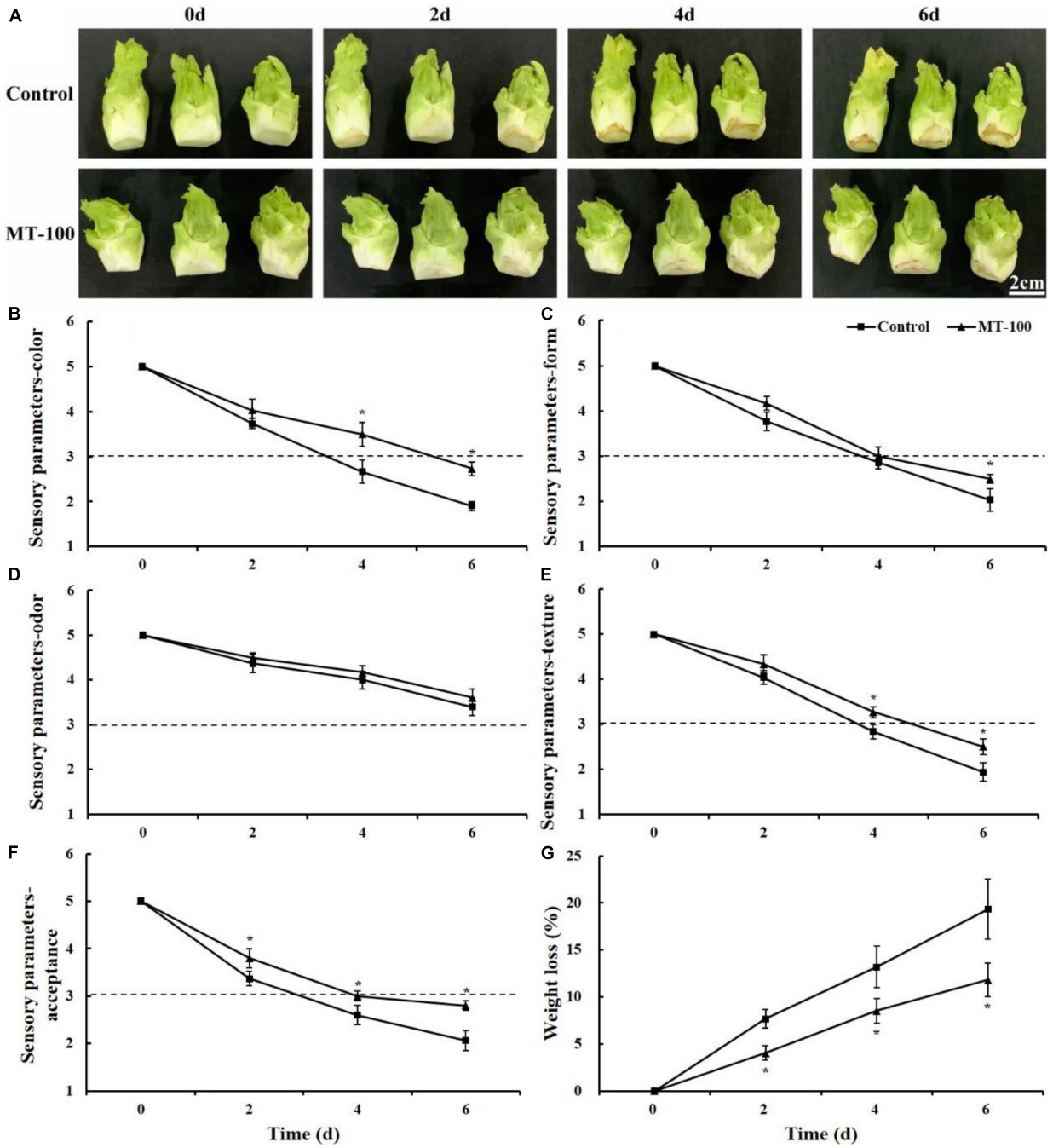


FIGURE 2 | Sensory quality and weight loss of 100 μmol L^{-1} melatonin-treated lateral buds of baby mustard during storage at 20°C. **(A)** Lateral buds of baby mustard at each sampling time. **(B–F)** Sensory parameters including color, form, odor, texture, and acceptance of lateral buds. **(G)** weight loss. MT-100, 100 μmol L^{-1} melatonin treatment. Each value is presented as the mean ± standard error of four biological replicates. Asterisks (*) indicate the significant differences ($P < 0.05$) between control and melatonin-treated lateral buds during storage.

100 μmol L^{-1} melatonin was 1.2-fold higher compared with the control (**Figure 3B**).

Ascorbic Acid and Total Phenolics

The content of ascorbic acid decreased in both the control and melatonin treatment during storage. Nevertheless, melatonin treatment significantly inhibited the decrease in the content of ascorbic acid during the entire storage period; the ascorbic acid content was 17, 21, and 14% higher than the control at 2, 4, and 6 days, respectively (**Figure 4A**).

The total phenolics content increased early during storage and decreased thereafter. The maximum values of the total

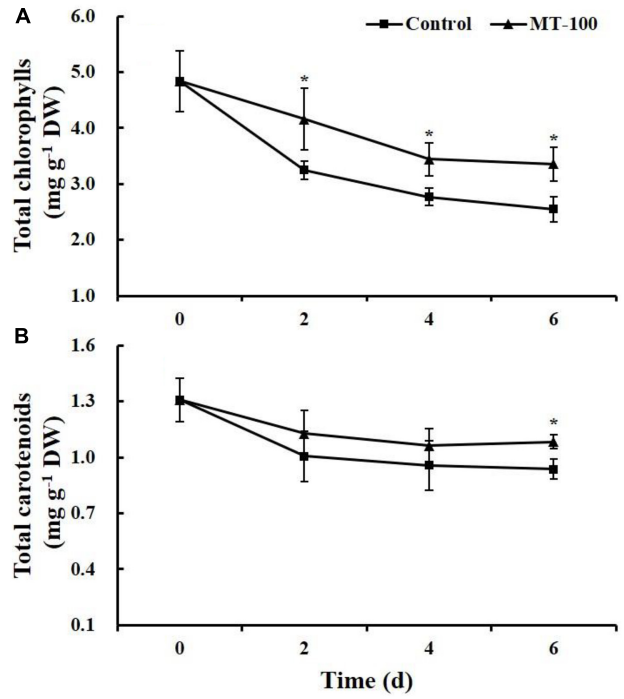


FIGURE 3 | Total chlorophyll **(A)** and carotenoid **(B)** content of 100 μmol L^{-1} melatonin treated lateral buds of baby mustard during storage at 20°C. MT-100, 100 μmol L^{-1} melatonin treatment. Each value is presented as the mean ± standard error of four biological replicates. Asterisks (*) indicate the significant differences ($P < 0.05$) between control and melatonin-treated lateral buds during storage.

phenolics content in both groups were observed at 4 days. During storage, the total phenolics levels in treated baby mustard were significantly higher compared with the control. The total phenolics content was 11% higher in melatonin-treated samples than in the control at 6 days (**Figure 4B**).

Antioxidant Capacity

Ferric reducing antioxidant power and 2,2-azinobis (3-ethylbenzothiazoline-6-sulfonic acid) (ABTS) levels decreased in control baby mustard during storage but were basically maintained in the melatonin treatment. The decrease in FRAP was significantly lower in melatonin-treated baby mustard than in the control at 2 days of storage. The FRAP levels were 10 and 9% higher in the melatonin treatment than in the control at 4 and 6 days, respectively (**Figure 4C**). The ABTS level was significantly higher (by 13%) in the melatonin-treated baby mustard than in the control at the end of storage (**Figure 4D**).

Glucosinolates

Nine glucosinolates, including four aliphatic glucosinolates, four indolic glucosinolates, and one aromatic glucosinolate, were detected in the lateral buds of baby mustard (**Figure 5**). Among aliphatic glucosinolates, the content of sinigrin and gluconapin in control lateral buds decreased significantly during storage by 61 and 67% at 6 days, respectively. In contrast, the content of sinigrin and gluconapin in the melatonin-treated samples decreased significantly with a loss of no more than 45% at 6 days (**Figures 5A,D**). The content of progoitrin and glucoiberin increased slightly in the first 2 days of storage and then decreased substantially in both the control and melatonin treatment. Nevertheless, the content of progoitrin and glucoiberin was 37 and 17% higher, respectively, in melatonin-treated samples than in the control at 6 days (**Figures 5G,J**). Because of the large proportion of sinigrin, the changes in the total aliphatic and total glucosinolate content were similar to the change in sinigrin: their content was 1.4-fold higher in melatonin-treated baby mustard than in the control at 6 days (**Figures 5F,L**).

For indolic glucosinolates, the glucobrassicin and neoglucobrassicin content in the control decreased by 58 and 53% at 4 days, respectively. The content of glucobrassicin and neoglucobrassicin was 1.9- and 1.5-fold, respectively, in the melatonin treatment compared with the control at 4 days (**Figures 5B,E**). The 4-methoxyglucobrassicin and 4-hydroxyglucobrassicin content in the treated samples were significantly higher compared with the control throughout storage, and no difference was observed in the total indolic glucosinolate content in the first 2 days because of the two other predominant glucosinolates (**Figures 5H,K,I**).

Gluconasturtiin was the only type of aromatic glucosinolate detected in baby mustard. The gluconasturtiin content was 1.3- and 1.2-fold higher in the melatonin treatment than in the control at 4 and 6 days, respectively (**Figure 5C**).

Time-Related Trajectory Analysis

The different storage times and treatments of baby mustard were separated, and greater distances from day 0 corresponded to a greater degree of deterioration of postharvest baby mustard. Both control and melatonin-treated groups showed large changes in their distances in the last 2 days. The control showed the longest distance change in the first 2 days. The melatonin-treated group had shorter distance changes than the control group throughout storage. The distance from the origin under the melatonin treatment at 4 days was even shorter than that in the control at 2 days and approximately half of that in the control at 6 days (**Figure 6**). These results indicate that the postharvest deterioration of baby mustard was clearly delayed by the 100 μmol L^{-1} melatonin treatment.

DISCUSSION

The ability of melatonin to extend the shelf life and improve the quality of postharvest fruits and vegetables has been previously studied, and the optimal concentration for postharvest preservation differs among plant species (Zhang et al., 2020; Wu X. et al., 2021). For example, 1,000 μmol L^{-1} melatonin treatment was optimal for delaying the lignification of bamboo shoots, as this treatment significantly decreased the degree of firmness, as well as the lignin and cellulose content (Li et al., 2019). Low doses of melatonin (1 μmol L^{-1}) were optimal for preserving antioxidants in broccoli florets, such as ascorbic acid, carotenoids, and total phenolics, as well as glucosinolates

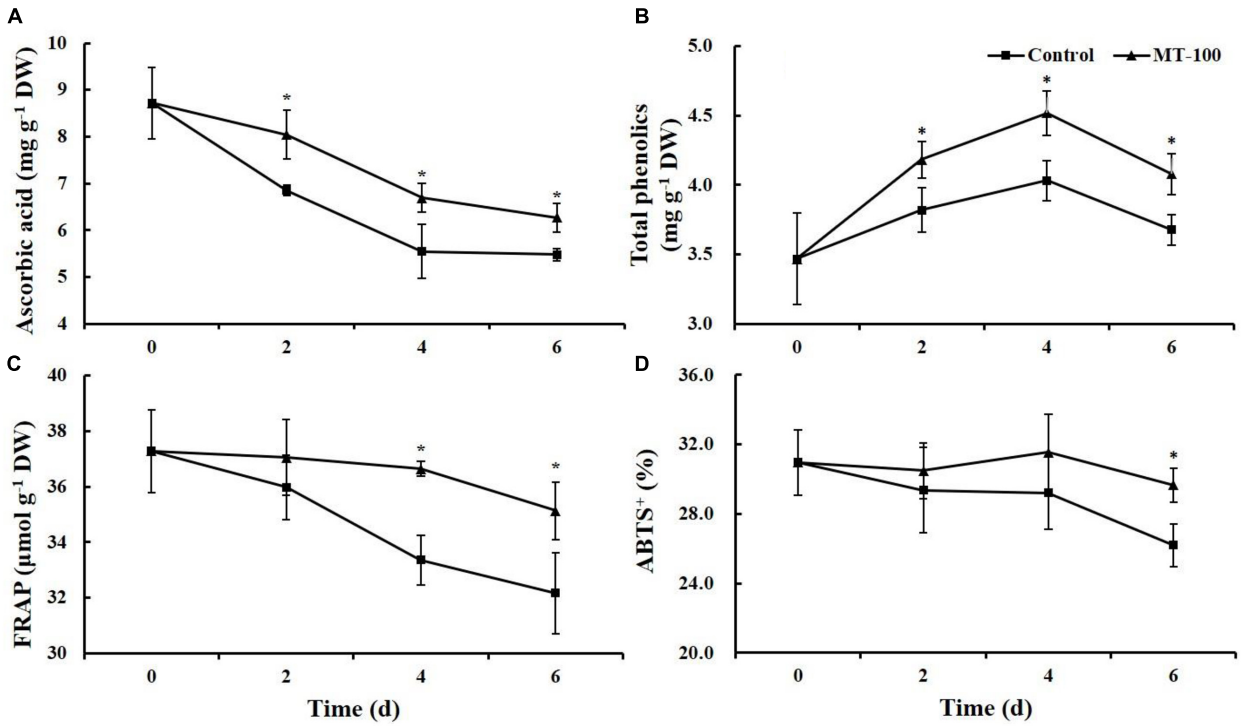


FIGURE 4 | Main antioxidants content and antioxidant capacity levels of 100 μmol L^{-1} melatonin treated lateral buds of baby mustard during storage at 20°C. **(A)** Ascorbic acid; **(B)** total phenolics; **(C)** FRAP; **(D)** $ABTS^{+}$. MT-100, 100 μmol L^{-1} melatonin treatment. Each value is presented as the mean ± standard error of four biological replicates. Asterisks (*) indicate the significant differences ($P < 0.05$) between control and melatonin-treated lateral buds during storage.

(Miao et al., 2020). In our study, treatment with 100 μmol L^{-1} melatonin was more effective for extending the shelf life of baby mustard (**Figure 1**), which is consistent with Chinese flowering cabbage and several types of fruits, such as peach (Cao et al., 2016; Gao et al., 2016), pear (Zhai et al., 2018; Zheng et al., 2019), sweet cherry (Wang F. et al., 2019; Miranda et al., 2020), and pomegranate (Jannatizadeh, 2019). In addition to plant species, the optimal concentrations of melatonin can vary with the stages of fruit development, different treatment conditions (e.g., application method and duration), and storage conditions (Ma et al., 2016; Onik et al., 2021).

Melatonin treatment improves the sensory quality of vegetables. In this study, melatonin-treated baby mustard had higher sensory parameter scores than control baby mustard (**Figure 2B-F**). The color and acceptance scores of baby mustard were correlated with the chlorophyll content and yellowing. Melatonin treatment markedly inhibited the chlorophyll degradation of baby mustard (**Figure 3A**). The protective effect of melatonin on chlorophyll has been observed in previous studies of barley leaves (Arnao and Hernández-Ruiz, 2009) and detached apple leaves (Wang et al., 2012). Tan et al. (2019) found that melatonin treatment suppressed the expression of chlorophyll catabolic and senescence marker genes in Chinese flowering cabbage. Similar results have been obtained with broccoli florets (Miao et al., 2020; Wu C. H. et al., 2021). Melatonin treatment can keep the chloroplasts intact as well as inhibit the expression of genes and the activity of enzymes involved in chlorophyll degradation (Wu C. H. et al., 2021). The results of our study indicated that melatonin can prevent chlorophyll from degrading. Fruits and vegetables are highly susceptible to water loss because of their metabolic activity, respiration, and transpiration after harvest (Bal, 2019). The 100 μmol L^{-1} melatonin treatment significantly decreased the weight loss of baby mustard throughout the storage period compared with the control. This may be ascribed to the increased skin strength under melatonin treatment (Liu et al., 2018; Miranda et al., 2020). Melatonin treatment has also been shown to significantly reduce the weight loss of peach (Gao et al., 2016) and strawberry (Liu et al., 2018) fruits during storage.

Antioxidants, such as carotenoids, ascorbic acid, and phenolics, are important phytochemicals in baby mustard that protect cells against oxidative stress (Xiao et al., 2012; Sun et al., 2018; Moloto et al., 2020). The content of carotenoids and ascorbic acid decreased during postharvest storage period, and melatonin treatment reduced the magnitude of the decrease (**Figures 3B**, **4A**). The content of total phenolics increased continuously during the first 4 days of storage and decreased thereafter (**Figure 4B**), which could be caused by postharvest stress; these findings are consistent with the results of Miao et al. (2020) showing that phenolic compounds increased in broccoli florets at 5 days of storage at 20°C. Melatonin exposure delayed the decrease in FRAP and $ABTS^{+}$ levels in postharvest baby mustard. Similar results have also been obtained in other studies of strawberry (Liu et al., 2018), plum (Bal, 2019), and

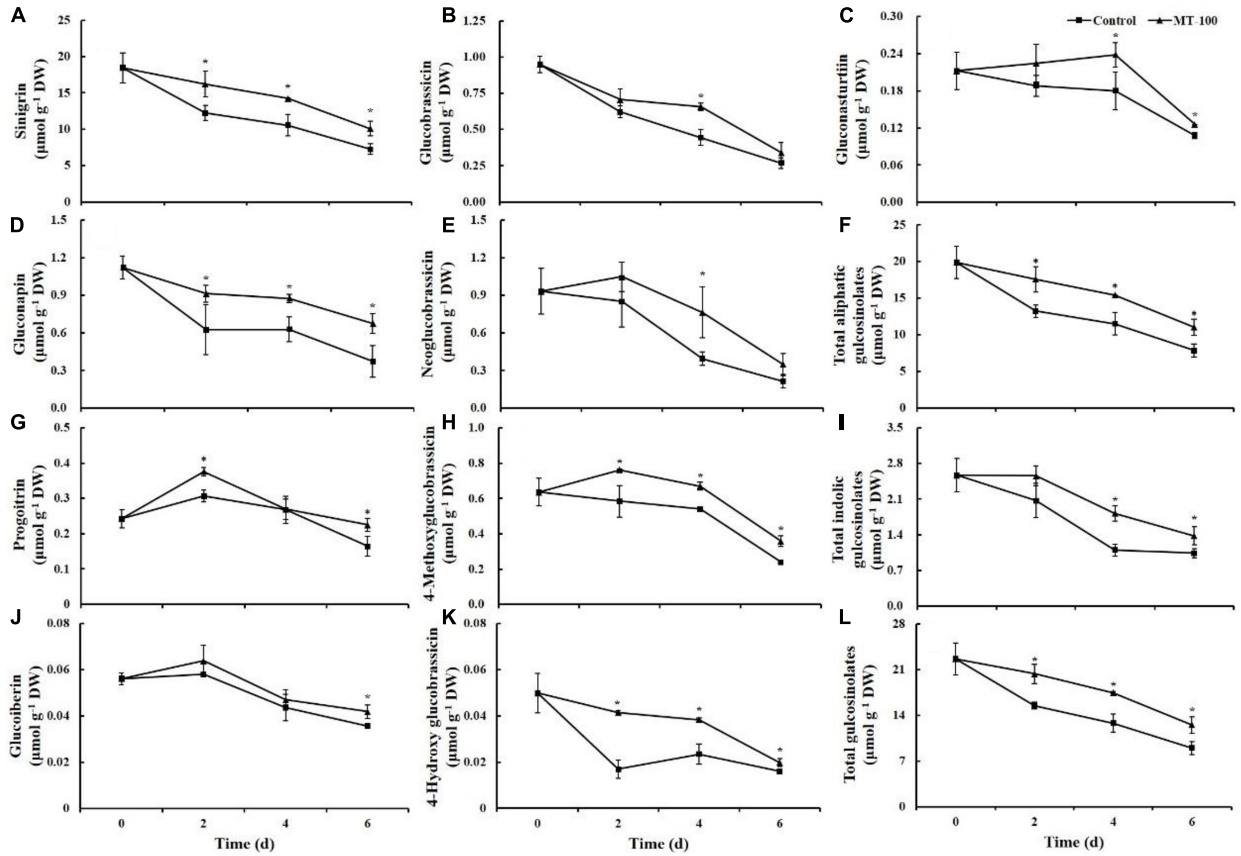


FIGURE 5 | Glucosinolate content of 100 μmol L^{-1} melatonin treated lateral buds of baby mustard during storage at 20°C. **(A)** Sinigrin; **(B)** glucobrassicin; **(C)** gluconasturtiin; **(D)** gluconapin; **(E)** neoglucobrassicin; **(F)** total aliphatic gulcosinolates; **(G)** progoitrin; **(H)** 4-methoxyglucobrassicin; **(I)** total indolic gulcosinolates; **(J)** glucoiberin; **(K)** 4-hydroxy glucobrassicin; **(L)** total gulcosinolates. MT-100, 100 μmol L^{-1} melatonin treatment. Each value is presented as the mean ± standard error of four biological replicates. Asterisks (*) indicate the significant differences ($P < 0.05$) between control and melatonin-treated lateral buds during storage.

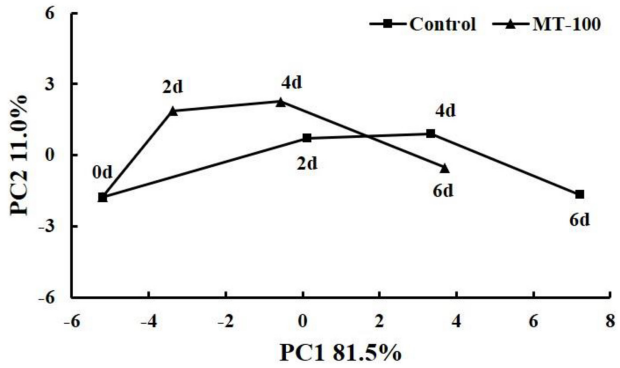


FIGURE 6 | Time-related trajectory plot showing the time-related responses of sensory and nutritional qualities in the lateral buds of baby mustard plants under 100 μmol L^{-1} melatonin treatment during storage.

pomegranate (Aghdam et al., 2020). Melatonin plays a role not only as an antioxidant by scavenging ROS directly but also augment the activity of antioxidant enzymes and the content of other antioxidants mentioned above and thus increases the postharvest life of fruits and vegetables (Ahammed et al., 2020). Conferring delaying the senescence in sweet cherries (Wang F. et al., 2019) and chilling tolerance in pomegranate (Jannatizadeh, 2019) were partly ascribed to the higher SOD, CAT, and APX activity under the melatonin treatment, which attenuated H_2O_2 accumulation. Moreover, melatonin treatment indued the expression of the key gene *PAL*, which encodes an enzyme in the phenylpropanoid pathway, contributing to the accumulation of total phenolics in postharvest fresh-cut pear (Zheng et al., 2019). These findings differ slightly from those obtained for bamboo shoots (Li et al., 2019). Melatonin treatment increased the antioxidant potential of bamboo shoots during postharvest storage; however, it significantly inhibited PAL activity compared with control shoots. PAL might also play a role in catalyzing the polymerization of monolignols in the lignification of bamboo shoots, and the effect of melatonin on PAL activity varies among species and organs (Boudet, 2000; Mastropasqua et al., 2016).

Glucosinolates are important health-promoting compounds unique to *Brassica* vegetables (Jia et al., 2009; Li et al., 2018; Wang J. S. et al., 2019; Wu et al., 2019; Zeng et al., 2021). Thus, maintaining the content of glucosinolates in postharvest

baby mustard is essential for maintaining its nutritional quality. Our results indicated that individual and total glucosinolates content in postharvest baby mustard decreased during storage at room temperature, which was accompanied by a high rate of senescence (**Figure 5**). However, the decrease was alleviated by melatonin treatment; the total glucosinolate content was 1.4-fold higher in melatonin-treated baby mustard than in control baby mustard at the end of storage (**Figure 5L**). As baby mustard aged, cellular integrity was destroyed, and vacuoles burst, which made glucosinolates and myrosinase come into contact, resulting in the degradation of glucosinolates (Sun et al., 2012). However, the contact between glucosinolates and myrosinase was delayed under melatonin treatment because cell structures were preserved, which helped maintain the glucosinolate content (Arnao and Hernández-Ruiz, 2018). Melatonin treatment has also been shown to be effective in preserving glucosinolates in postharvest broccoli (Miao et al., 2020; Wei et al., 2020).

Safety is a critical point for the consumer. Melatonin is approved as a dietary supplexment by the United States Food and Drug Administration (FDA), and can be purchased over-the-counter in both the United States and Canada (Foster, 2021). Ministry of Public Health of China has also approved melatonin as health products (Liu and Sun, 2017). There's not enough information yet about possible side effects but evidence suggests that melatonin supplements promote sleep and are safe for short-term use (National Center for Complementary and Integrative Health, 2021). The concentration of melatonin used as a postharvest treatment on horticultural crops ranges from 1 to 1,000 μmol L^{-1}, and generally adopts the application method of immersing or spraying. In our experiment, the optimal concentration of the melatonin solution for immersing is 100 μmol L^{-1}, and the residual melatonin in lateral bud is very limited compared with the usual dose of melatonin (1–3 mg per day) as a dietary supplement (Lutterschmidt et al., 2003). Morevoer, as for people, melatonin is not easy to accumulate in the body: the half-life is short; and there is a liver metabolic pathway, 70% of the metabolites are excreted in the urine (Lutterschmidt et al., 2003; Bagci et al., 2011). Even if consumers still have concerns, the light-decomposing properties of melatonin can reassure them: exposure to light after melatonin treatment can reduce the residue (Ma et al., 2021). Therefore, melatonin treatment is safe to use for postharvest preservation of fruit and vegetables.

In sum, application of 100 μmol L^{-1} melatonin was the most effective for prolonging the shelf life and maintaining the quality of postharvest baby mustard. Treatment with 100 μmol L^{-1} melatonin delayed sensory quality deterioration by inhibiting the degradation of chlorophyll and decreasing the degree of yellowness; sustained the antioxidant potential of postharvest baby mustard by maintaining higher levels of antioxidants and antioxidant capacity; and slowed decreases in the content of individual and total glucosinolates. Treatment with 100 μmol L^{-1} melatonin is effective for preserving the postharvest quality of baby mustard.

DATA AVAILABILITY STATEMENT

The original contributions presented in the study are included in the article/supplementary material, further inquiries can be directed to the corresponding authors.

AUTHOR CONTRIBUTIONS

HD and YW: investigation and writing—original draft preparation. ZL: data curation and writing—original draft preparation. YiZ, JB, JX, YaZ, and RG: data curation. HL: investigation and funding acquisition. FZ: conceptualization, funding acquisition, and writing—reviewing and editing. BS: funding acquisition, writing—reviewing and editing, and conceptualization. All authors: review and editing.

FUNDING

This work was supported by National Natural Science Foundation of China (32072586 and 31500247), Project of New Varieties Breeding of Sichuan Vegetable Innovation Team (sccxtd-2020-05), and Undergraduate Research Interest Cultivation Project of Sichuan Agricultural University (2021298).

REFERENCES

Aghdam, M. S., Luo, Z. S., Li, L., Jannatizadeh, A., Fard, J. R., and Pirzad, F. (2020). Melatonin treatment maintains nutraceutical properties of pomegranate fruits during cold storage. *Food Chem.* 303:125385. doi: 10.1016/j.foodchem.2019.125385

Ahammed, G. J., Wu, M. J., Wang, Y. Q., Yan, Y. R., Mao, Q., Ren, J. J., et al. (2020). Melatonin alleviates iron stress by improving iron homeostasis, antioxidant defense and secondary metabolism in cucumber. *Sci. Hortic.* 265:109205. doi: 10.1016/j.scienta.2020.109205

Arnao, M. B., and Hernández-Ruiz, J. (2009). Protective effect of melatonin against chlorophyll degradation during the senescence of barley leaves. *J. Pineal Res.* 46, 58–63. doi: 10.1111/j.1600-079X.2008.00625.x

Arnao, M. B., and Hernández-Ruiz, J. (2018). Melatonin and its relationship to plant hormones. *Ann. Bot.* 121, 195–207. doi: 10.1093/aob/mcx114

Arnao, M. B., and Hernández-Ruiz, J. (2019). Melatonin: a new plant hormone and/or a plant master regulator? *Trends Plant Sci.* 24, 38–48. doi: 10.1016/j.tplants.2018.10.010

Bagci, S., Yildizdas, D., Horoz, Ö. Ö., Reinsberg, J., Bartmann, P., and Mueller, A. (2011). Use of nocturnal melatonin concentration and urinary 6-sulfatoxymelatonin excretion to evaluate melatonin status in children with severe sepsis. *J. Pediatr. Endocrinol. Metab.* 24, 1025–1030. doi: 10.1515/JPEM.2011.402

Bal, E. (2019). Physicochemical changes in 'Santa Rosa' plum fruit treated with melatonin during cold storage. *J. Food Meas. Charact.* 13, 1713–1720. doi: 10.1007/s11694-019-00088-6

Boudet, A. (2000). Lignins and lignification: selected issues. *Plant Physiol. Biochem.* 38, 81–96. doi: 10.1016/S0981-9428(00)00166-2

Cao, S. F., Song, C. B., Shao, J. R., Bian, K., Chen, W., and Yang, Z. F. (2016). Exogenous melatonin treatment increases chilling tolerance and induces

defense response in harvested peach fruit during cold storage. *J. Agric. Food Chem.* 64, 5215–5222. doi: 10.1021/acs.jafc.6b01118

Deng, B. L., Xia, C. B., Tian, S., and Shi, H. J. (2021). Melatonin reduces pesticide residue, delays senescence, and improves antioxidant nutrient accumulation in postharvest jujube fruit. *Postharvest Biol. Technol.* 173:111419. doi: 10.1016/j.postharvbio.2020.111419

Foster, R. G. (2021). Melatonin. *Curr. Biol.* 31, R1456–R1458. doi: 10.1016/j.cub.2021.10.029

Gao, H., Zhang, Z. K., Chai, H. K., Cheng, N., Yang, Y., Wang, D. N., et al. (2016). Melatonin treatment delays postharvest senescence and regulates reactive oxygen species metabolism in peach fruit. *Postharvest Biol. Technol.* 118, 103–110. doi: 10.1016/j.postharvbio.2016.03.006

Jannatizadeh, A. (2019). Exogenous melatonin applying confers chilling tolerance in pomegranate fruit during cold storage. *Sci. Hortic.* 246, 544–549. doi: 10.1016/j.scienta.2018.11.027

Jia, C. G., Xu, C. J., Wei, J., Yuan, J., Yuan, G. F., Wang, B. L., et al. (2009). Effect of modified atmosphere packaging on visual quality and glucosinolates of broccoli florets. *Food Chem.* 114, 28–37. doi: 10.1016/j.foodchem.2008.09.009

Li, B. H., Tang, M., Nelson, A., Caligagan, H., Zhou, X., Clark-Wiest, C., et al. (2018). Network-guided discovery of extensive epistasis between transcription factors involved in aliphatic glucosinolate biosynthesis. *Plant Cell* 30, 178–195. doi: 10.1105/tpc.17.00805

Li, C. T., Suo, J. W., Xuan, L. L., Ding, M. Z., Zhang, H., Song, L. L., et al. (2019). Bamboo shoot-lignification delay by melatonin during low temperature storage. *Postharvest Biol. Technol.* 156:110933. doi: 10.1016/j.postharvbio.2019.110933

Liu, C. H., Zheng, H. H., Sheng, K. L., Liu, W., and Zheng, L. (2018). Effects of melatonin treatment on the postharvest quality of strawberry fruit. *Postharvest Biol. Technol.* 139, 47–55. doi: 10.1016/j.postharvbio.2018.01.016

Liu, Z. Y., and Sun, Z. (2017). The research progress of melatonin metabolic patterns. *Chin. Bull. Life Sci.* 29, 209–214. doi: 10.13376/j.cbls/2017028

Lutterschmidt, D. I., Lutterschmidt, W. I., and Hutchison, V. H. (2003). Melatonin and thermoregulation in ectothermic vertebrates: a review. *Can. J. Zool.* 81, 1–13. doi: 10.1139/z02-189

Ma, Q. L., Lin, X., Wei, Q. J., Yang, X. Z., Zhang, Y. N., and Chen, J. Y. (2021). Melatonin treatment delays postharvest senescence and maintains the organoleptic quality of 'Newhall' navel orange (*Citrus sinensis* (L.) Osbeck) by inhibiting respiration and enhancing antioxidant capacity. *Sci. Hortic.* 286:110236. doi: 10.1016/j.scienta.2021.110236

Ma, Q. X., Zhang, T., Zhang, P., and Wang, Z. Y. (2016). Melatonin attenuates postharvest physiological deterioration of cassava storage roots. *J. Pineal Res.* 60, 424–434. doi: 10.1111/jpi.12325

Mastropasqua, L., Tanzarella, P., and Paciolla, C. (2016). Effects of postharvest light spectra on quality and health-related parameters in green *Asparagus officinalis* L. *Postharvest Biol. Technol.* 112, 143–151. doi: 10.1016/j.postharvbio.2015.10.010

Miao, H. Y., Zeng, W., Zhao, M., Wang, J. S., and Wang, Q. M. (2020). Effect of melatonin treatment on visual quality and health-promoting properties of broccoli florets under room temperature. *Food Chem.* 319:126498. doi: 10.1016/j.foodchem.2020.126498

Miranda, S., Vilches, P., Suazo, M., Pavez, L., García, K., Méndez, M. A., et al. (2020). Melatonin triggers metabolic and gene expression changes leading to improved quality traits of two sweet cherry cultivars during cold storage. *Food Chem.* 319:126360. doi: 10.1016/j.foodchem.2020.126360

Moloto, M. R., Phan, A. D. T., Shai, J. L., Sultanbawa, Y., and Sivakumar, D. (2020). Comparison of phenolic compounds, carotenoids, amino acid composition, in vitro antioxidant and anti-diabetic activities in the leaves of seven cowpea (*Vigna unguiculata*) cultivars. *Foods* 9:1285. doi: 10.3390/foods9091285

National Center for Complementary and Integrative Health (2021). *Melatonin: What You Need To Know*. Available online at: https://www.nccih.nih.gov/health/melatonin-what-you-need-to-know (accessed January, 2021).

Onik, J. C., Wai, S. C., Li, A., Lin, Q., Sun, Q. Q., Wang, Z. D., et al. (2021). Melatonin treatment reduces ethylene production and maintains fruit quality in apple during postharvest storage. *Food Chem.* 337:127753. doi: 10.1016/j.foodchem.2020.127753

Sun, B., Di, H. M., Zhang, J. Q., Xia, P. X., Huang, W. L., Jian, Y., et al. (2021). Effect of light on sensory quality, health-promoting phytochemicals and antioxidant capacity in post-harvest baby mustard. *Food Chem.* 339:128057. doi: 10.1016/j.foodchem.2020.128057

Sun, B., Lin, P. X., Xia, P. X., Di, H. M., Zhang, J. Q., Zhang, C. L., et al. (2020). Low-temperature storage after harvest retards the deterioration in the sensory quality, health-promoting compounds, and antioxidant capacity of baby mustard. *RSC Adv.* 10, 36495–36503. doi: 10.1039/d0ra07177c

Sun, B., Tian, Y. X., Chen, Q., Zhang, Y., Luo, Y., Wang, Y., et al. (2019). Variations in the glucosinolates of the individual edible parts of three stem mustards (*Brassica juncea*). *R. Soc. Open Sci.* 6:182054. doi: 10.1098/rsos.182054

Sun, B., Tian, Y. X., Jiang, M., Yuan, Q., Chen, Q., Zhang, Y., et al. (2018). Variation in the main health-promoting compounds and antioxidant activity of whole and individual edible parts of baby mustard (*Brassica juncea* var. *gemmifera*). *RSC Adv.* 8, 33845–33854. doi: 10.1039/c8ra05504a

Sun, B., Yan, H. Z., Liu, N., Wei, J., and Wang, Q. M. (2012). Effect of 1-MCP treatment on postharvest quality characters, antioxidants and glucosinolates of Chinese kale. *Food Chem.* 131, 519–526. doi: 10.1016/j.foodchem.2011.09.016

Tan, X. L., Fan, Z. Q., Kuang, J. F., Lu, W. J., Reiter, R. J., Lakshmanan, P., et al. (2019). Melatonin delays leaf senescence of Chinese flowering cabbage by suppressing ABFs-mediated abscisic acid biosynthesis and chlorophyll degradation. *J. Pineal Res.* 67:e12570. doi: 10.1111/jpi.12570

Tan, X. L., Fan, Z. Q., Zeng, Z. X., Shan, W., Kuang, J. F., Lu, W. J., et al. (2021). Exogenous melatonin maintains leaf quality of postharvest Chinese flowering cabbage by modulating respiratory metabolism and energy status. *Postharvest Biol. Technol.* 177:111524. doi: 10.1016/j.postharvbio.2021.111524

Tang, Q., Li, C. Y., Ge, Y. H., Li, X., Cheng, Y., Hou, J. B., et al. (2020). Exogenous application of melatonin maintains storage quality of jujubes by enhancing anti-oxidative ability and suppressing the activity of cell wall degrading enzymes. *LWT Food Sci. Technol.* 127:109431. doi: 10.1016/j.lwt.2020.109431

Wang, F., Zhang, X. P., Yang, Q. Z., and Zhao, Q. F. (2019). Exogenous melatonin delays postharvest fruit senescence and maintains the quality of sweet cherries. *Food Chem.* 301:125311. doi: 10.1016/j.foodchem.2019.125311

Wang, J. S., Yu, H. F., Zhao, Z. Q., Sheng, X. G., Shen, Y. S., and Gu, H. G. (2019). Natural variation of glucosinolates and their breakdown products in broccoli (*Brassica oleracea* var. *italica*) seeds. *J. Agric. Food Chem.* 67, 12528–12537. doi: 10.1021/acs.jafc.9b06533

Wang, P., Yin, L. H., Liang, D., Li, C., Ma, F. W., and Yue, Z. Y. (2012). Delayed senescence of apple leaves by exogenous melatonin treatment: toward regulating the ascorbate–glutathione cycle. *J. Pineal Res.* 53, 11–20. doi: 10.1111/j.1600-079x.2011.00966.x

Wei, L. Y., Liu, C. H., Zheng, H. H., and Zheng, L. (2020). Melatonin treatment affects the glucoraphanin-sulforaphane system in postharvest fresh-cut broccoli (*Brassica oleracea* L.). *Food Chem.* 307:125562. doi: 10.1016/j.foodchem.2019.125562

Wu, C. H., Cao, S. F., Xie, K. Q., Chi, Z. Y., Wang, J., Wang, H. F., et al. (2021). Melatonin delays yellowing of broccoli during storage by regulating chlorophyll catabolism and maintaining chloroplast ultrastructure. *Postharvest Biol. Technol.* 172:111378. doi: 10.1016/j.postharvbio.2020.111378

Wu, Q. Y., Wang, J. W., Mao, S. X., Xu, H. R., Wu, Q., Liang, M. T., et al. (2019). Comparative transcriptome analyses of genes involved in sulforaphane metabolism at different treatment in Chinese kale using full-length transcriptome sequencing. *BMC Genomics* 20:377. doi: 10.1186/s12864-019-5758-2

Wu, X., Ren, J., Huang, X. Q., Zheng, X. Z., Tian, Y. C., Shi, L., et al. (2021). Melatonin: Biosynthesis, content, and function in horticultural plants and potential application. *Sci. Hortic.* 288:110392. doi: 10.1016/j.scienta.2021.110392

Xiao, Z. L., Leater, G. E., Luo, Y. G., and Wang, Q. (2012). Assessment of vitamin and carotenoid concentrations of emerging food products: edible microgreens. *J. Agric. Food Chem.* 60, 7644–7651. doi: 10.1021/jf300459b

Zeng, W., Tao, H., Li, Y. B., Wang, J. S., Xia, C. C., Li, S. W., et al. (2021). The flavor of Chinese kale sprouts is affected by genotypic variation of glucosinolates and their breakdown products. *Food Chem.* 359:129824. doi: 10.1016/j.foodchem.2021.129824

Zhai, R., Liu, J. L., Liu, F. X., Zhao, Y. X., Liu, L. L., Fang, C., et al. (2018). Melatonin limited ethylene production, softening and reduced physiology disorder in pear (*Pyrus communis* L.) fruit during senescence. *Postharvest Biol. Technol.* 139, 38–46. doi: 10.1016/j.postharvbio.2018.01.017

Zhang, F., Zhang, J. Q., Di, H. M., Xia, P. X., Zhang, C. L., Wang, Z. H., et al. (2021). Effect of long-term frozen storage on health-promoting compounds and

antioxidant capacity in baby mustard. *Front. Nutr.* 8:665482. doi: 10.3389/fnut.2021.665482

Zhang, W. L., Cao, J. K., Fan, X. G., and Jiang, W. B. (2020). Applications of nitric oxide and melatonin in improving postharvest fruit quality and the separate and crosstalk biochemical mechanisms. *Trends Food Sci. Technol.* 99, 531–541. doi: 10.1016/j.tifs.2020.03.024

Zheng, H. H., Liu, W., Liu, S., Liu, C. H., and Zheng, L. (2019). Effects of melatonin treatment on the enzymatic browning and nutritional quality of fresh-cut pear fruit. *Food Chem.* 299:125116. doi: 10.1016/j.foodchem.2019.125116

Conflict of Interest: The authors declare that the research was conducted in the absence of any commercial or financial relationships that could be construed as a potential conflict of interest.

Publisher's Note: All claims expressed in this article are solely those of the authors and do not necessarily represent those of their affiliated organizations, or those of the publisher, the editors and the reviewers. Any product that may be evaluated in this article, or claim that may be made by its manufacturer, is not guaranteed or endorsed by the publisher.

Copyright © 2022 Di, Li, Wang, Zhang, Bian, Xu, Zheng, Gong, Li, Zhang and Sun. This is an open-access article distributed under the terms of the Creative Commons Attribution License (CC BY). The use, distribution or reproduction in other forums is permitted, provided the original author(s) and the copyright owner(s) are credited and that the original publication in this journal is cited, in accordance with accepted academic practice. No use, distribution or reproduction is permitted which does not comply with these terms.

frontiers in Plant Science

SYSTEMATIC REVIEW
published: 02 February 2022
doi: 10.3389/fpls.2021.807736

Practice in Nursery Weed Control—Review and Meta-Analysis

*Ping Yu and Stephen Christopher Marble**

Department of Environmental Horticulture, Mid-Florida Research and Education Center, University of Florida Institute of Food and Agricultural Sciences, Apopka, FL, United States

Weeds, as one of the biggest challenges in the nursery industry, have been controlled by various methods, such as chemical and non-chemical practices. Although these practices have been widely established and tested to control weeds, there is no systematic or meta-analysis review to provide quantitative weed control efficacy information of these practices. To provide a systematic understanding of weed control practices in nursery production, a visualization research trend, a systematic review, and a meta-analysis were conducted. A total of 267 relevant studies were included for the research trend and 83 were included in the meta-analysis. The results in this study showed that interests in nursery weed control have switched dramatically in the past 2–3 decades (1995–2021) from chemical dominant weed control to chemical coexistent with non-chemical techniques. Developing new management tactics and implementing diverse combinations of integrated weed management present the future trend for weed control. The systematic review results showed that chemical methods had the highest weed control efficacy, while non-chemical had the lowest on average, nonetheless, all three weed control practices (chemical, non-chemical, and combined) reduced the weed biomass and density significantly compared with when no strategy was employed. Weed control challenges could be the catalyst for the development of new non-chemical and integrated weed control techniques.

Keywords: container, weed efficacy, herbicide, non-chemical, integrated control, citespace

OPEN ACCESS

Edited by:
Pei Xu,
China Jiliang University, China

Reviewed by:
Barbara De Lucia,
University of Bari Aldo Moro, Italy
Weimin Dai,
Nanjing Agricultural University, China

***Correspondence:**
Stephen Christopher Marble
marblesc@ufl.edu

Specialty section:
This article was submitted to Crop and Product Physiology, a section of the journal Frontiers in Plant Science

Received: *02 November 2021*
Accepted: *30 December 2021*
Published: *02 February 2022*

Citation:
Yu P and Marble SC (2022) Practice in Nursery Weed Control—Review and Meta-Analysis. Front. Plant Sci. 12:807736. doi: 10.3389/fpls.2021.807736

INTRODUCTION

Weeds present one of the important challenges in the nursery industry as weeds significantly affect nursery crop values by reducing their growth and salability (Amoroso et al., 2009). For instance, redroot pigweed (*Amaranthus retroflexus* L.) and large crabgrass [*Digitaria sanguinalis* (L.) Scop.] reduced Japanese holly (*Ilex crenata* Thunb. 'Convexa') growth by 47 and 60%, respectively, making it less or not salable (Fretz, 1972). Similarly, eclipta (*Eclipta prostrata* L.) caused a 43% reduction in Fashion azalea (*Rhododendron* × *'Fashion'*) growth, largely reducing its marketability (Berchielli-Robertson et al., 1990).

To control weeds, various methods have been tested, such as chemical, non-chemical, and the integrated chemical and non-chemical practices (Marble, 2015; Stewart et al., 2017). Chemical weed control primarily uses herbicides to control weeds (Altland et al., 2004) whereas non-chemical weed control utilizes different cultural practices, such as mulching, irrigation, and fertilization to reduce

the weed growth (Case et al., 2005; Amoroso et al., 2009; Marble et al., 2019; Saha et al., 2019b). To reduce herbicide usage while maintaining the promising weed control results, combined chemical and non-chemical weed control have been widely developed (Altland et al., 2004; Stewart et al., 2018).

Weed control efficacy varies largely with control methods and weed species. In a field study, Diuron application at a rate of 4 kg ha^{-1} controlled 94% of weeds, which were dominated with johnsongrass (*Sorghum halepense* (L.) Pers.), green foxtail [*Setaria viridis* (L.) P. Beauv.], annual bluegrass (*Poa annua* L.), goosefoot grass (*Chenopodium album* L.), bindweed (*Convolvulus arvensis* L.), broadleaf woodsorrel (*Oxalis latifolia* Kunth.), field sow-thistle (*Sonchus arvensis* L.), bird-eye speedwell (*Veronica persica* Poir.), frost aster (*Aster pilosus* (Willd.) G.L. Nesom), black nightshade (*Solanum nigrum* L.), and scarlet pimpernel (*Anagallis arvensis* L.), however, unpunched black polyethylene resulted in 100% control of these weeds (Dalal et al., 2008). Similarly, in a container study, applying granular Broadstar 0.25 G (flumioxazin) 0.4 kg ai ha^{-1} alone controlled 92% of bittercress (*Cardamine* spp.), while combining herbicide and pine bark mini-nuggets (7.62 cm) led to 100% control efficacy (Richardson et al., 2008).

Table 1 summarizes the commonly tested weed species reported in literature from 1995 to 2021 with total 114 records. Approximately half of the studies did not specify weed species. Among the specified studies, spurge (*Euphorbia* spp.) and sedge *(Cyperus* spp.) presented to be the most tested weed species with 17 reports, followed by bittercress (*Cardamine* spp.) with 12, crabgrass (*Digitaria* spp.) with 11, and woodsorrel (*Oxalis* spp.) with 10. Bittercress (*Cardamine* spp.), spurge (*Euphorbia* spp.), and woodsorrel (*Oxalis* spp.) were mainly tested in container studies, while other weed species were reported from both field and container studies or field studies only.

Although herbicides have been largely used for nursery weed control, many challenges have emerged due to their overuse. Many tested weeds species (**Table 1**), such as goosegrass (*Eleusine indica* (L.) Gaertn.), annual bluegrass (*P. annua* L.), large crabgrass (*D. sanguinalis* L.), smooth crabgrass (*Digitaria ischaemum* Schreb.), and prostrate spurge (*Euphorbia humistrata* L.) have developed resistance to herbicides (Jalaludin et al., 2010; Powles and Yu, 2010; Derr et al., 2020; Boyd and Steed, 2021). In addition, it takes a long time (generally 5–10 years) to develop and register new herbicides, depending on herbicide characteristics along with other manufacturer and registration variables. The lack of discovery in new mode of reactions in recent years presented another challenge for new herbicide developments (Duke, 2012). Moreover, the overuse of herbicides, has created safety, environmental, and economic concerns due to running off, leaching, and drifting (Collins et al., 2001; Riley, 2003; Chalker-Scott, 2007).

Several weed-control reviews have been published in the past decade with focusing on one or two aspects. In Altland et al. (2003), a review focusing on different herbicides with respect to their chemical class, mode of action, and rates for field nursery was published. In Case et al. (2005) published a review on container nursery weed control practices, discussing commonly used herbicides for container nurseries, other control practices (mulching, irrigation, and combining tactics). In Marble (2015) reviewed herbicide and mulch interactions, suggesting that high mulch depths (>7 cm) resulted in a high level of weed control regardless of herbicide use. In Stewart et al. (2017), another review on container nursery and landscape weed control was published, focusing on irrigation, nutrient, and substrate management effects on the weed growth and herbicide performance. However, the evolution of a knowledge domain was rarely reported, not to mention the efficacy comparison of weed control methods, effects on weed density or biomass.

Exploring and visualizing the evolution of a knowledge domain in the past years can be achieved by detecting remarkable articles in citation and co-citation networks from each time interval, and major changes between adjacent time series in a panoramic view (Chen, 2004). Chen (2004) proposed using the software CiteSpace to visualize salient nodes in merged networks from a specific knowledge area, and described three types of nodes: (a) landmark node with a large radius, representing the most highly cited documents; (b) hub node with a large degree, indicating widely cited papers with significantly intellectual contributions; and (c) pivot nodes with two networks exclusively connected by few lines, presenting common knowledge shared by different knowledge focus areas.

Systematic reviews and meta-analyses have been widely used for quantitative research reviews as they rely on the quantitative information and allow for the testing of hypotheses that cannot be satisfactorily answered by a single study (Shrestha et al., 2016; Osipitan et al., 2018). Systematic reviews reduce bias by appraising and synthesizing the surveyed studies based on a set of criteria to answer a specific question (Phan et al., 2015). Meta-analysis is a statistical technique summarizing the data extracted through a systematic review into a single quantitative estimate of effect sizes (Haddaway et al., 2015).

As such, this research aimed at analyzing how the evolution of knowledge domains in nursery weed control changed over time and visualizing the trends and linkages of the main scientific research areas. A systematic analysis was also conducted to evaluate the different weed control methods efficacy. Additionally, a meta-analysis was carried out to evaluate the relative impact of different weed control methods on weed biomass and density.

MATERIALS AND METHODS

Literature Search and Data Collection

The primary literature search was performed by using the Web of Science database using the term "nursery weed control" on August 31, 2021. No language restriction was applied, and years of publication were from 1995 to 2021, resulting in 267 records in total. Additional relevant peer-reviewed publications were searched using "Google scholar™" with the keyword "weed control." Duplicate references were removed (**Figure 1**). Studies with reports on weed efficacy, weed density, and/or weed biomass were selected for the meta-analysis to estimate the common truth for the different control methods effects,

TABLE 1 | Weed species reported in literature (total 114 records) from 1995 to 2021.

Weed types	Common name	Scientific name	Number of reports	Type of study
	Forbs	*Abutilon theophrasti* Medik.	2	Field
	Common ragweed	*Ambrosia artemisiifolia* L.	2	Field
Wort and moss (5)	Mug wort	*Artemisia vulgaris* L.	1	Field
	Silver thread moss	*Bryum argenteum* Hedw.	1	Container
	Liverwort	*Marchantia polymorpha* L.	3	Container
Bittercress (12)	Wavy bittercress	*Cardamine flexuosa* With.	2	Container
	Bittercress	*Cardamine* spp.	6	Container
	Hairy bittercress	*Cardamine hirsuta* L.	4	Container
Spurge (17)	Garden spurge	*Euphorbia hirta* L.	1	Container
	Prostrate spurge	*Euphorbia humistrata* L.	8	Container
	Spotted spurge	*Euphorbia maculata* L.	8	Container
	Goosefoot	*Chenopodium* spp.	3	Field
	Horseweed	*Conyza canadensis* L.	3	Field
Sedge (17)	Sedge	*Cyperus* spp.	8	Field (7) Container
	Yellow nutsedge	*Cyperus esculentus* L.	7	Field (6) Container
	Purple nutsedge	*Cyperus rotundus* L.	2	Field
Crabgrass (11)	Southern crabgrass	*Digitaria ciliaris* Retz.	1	Container
	Smooth crabgrass	*Digitaria ischaemum* Schreb.	1	Field
	Large crabgrass	*Digitaria sanguinalis* L.	9	Container (8), Field
Barnyard grass (6)	Barnyard grass	*Echinochloa* spp.	2	Field, Container
	Awnless barnyard grass	*Echinochloa colonum* L.	2	Field
	Eclipta	*Eclipta prostrata* Roxb.	9	Container
	Goosegrass	*Eleusine indica* (L.) Gaertn.	2	Field, Container
Morning glory (3)	Ivy-leaf morning-glory	*Ipomoea hederacea* L.	1	Field
	Pitted morning-glory	*Ipomoea lacunosa* L.	1	Container
	Morning-glory	*Ipomoea* spp.	1	Field
Mallow (5)	Little mallow	*Malva parviflora* L.	3	Field
	Common mallow	*Malva sylvestris* L.	2	Field
	California burclover	*Medicago polymorpha* L.	2	Field
Woodsorrel (10)	Creeping woodsorrel	*Oxalis corniculata* L.	5	Container
	Broadleaf woodsorrel	*Oxalis latifolia* Kunth.	1	Field
	Yellow woodsorrel	*Oxalis stricta* L.	4	Container
	Annual bluegrass	*Poa annua* L.	7	Container (5), Field
	Common purslane	*Portulaca oleracea* L.	3	Field (2), Container
	Common groundsel	*Senecio vulgaris* L.	4	Container
Foxtail (5)	Giant foxtail	*Setaria faberi* Herrm.	2	Field
	Green foxtail	*Setaria viridis* L.	3	Field (2), Container
	Common chickweed	*Stellaria media* L.	8	Field, Container
	Dandelion	*Taraxacum officinale* (L.) Weber ex F.H.Wigg.	2	Field, Container
	Broadleaf weed		9	Field

categorized in chemical, non-chemical, and integrated chemical and non-chemical practices. The meta-analysis included 83 publications in total with studies from 11 countries (**Figure 2**). Some of the reports were selected for all categories because they reported all the parameters (weed efficacy, weed density, and weed biomass). Biological weed control was not included or discussed in this study.

Criteria for Paper and Data Selection

In CiteSpace, two criteria were used for the paper selection: g-index and top 50 usages since 2013. References with citations numbers more than 2 were displayed. For systematic and meta-analysis reviews, the best weed control methods with the highest weed efficacy, and/or the lowest weed biomass and density were selected in each study. Both field studies and container studies were included, with weed density units for field and container studies being weed number per square meter and weed number per container, respectively. Units for biomass were unified to gram (g), both fresh weight and dry weight were included. All three parameters (weed efficacy, weed biomass, and weed density) were compared with non-weed control treatments.

Data Extraction and Analysis

Software GetData Graph Digitizer (version 2.26) was used to extract data from figures. When SEs were not presented or could not be calculated, we assumed a SE of 10% of the mean

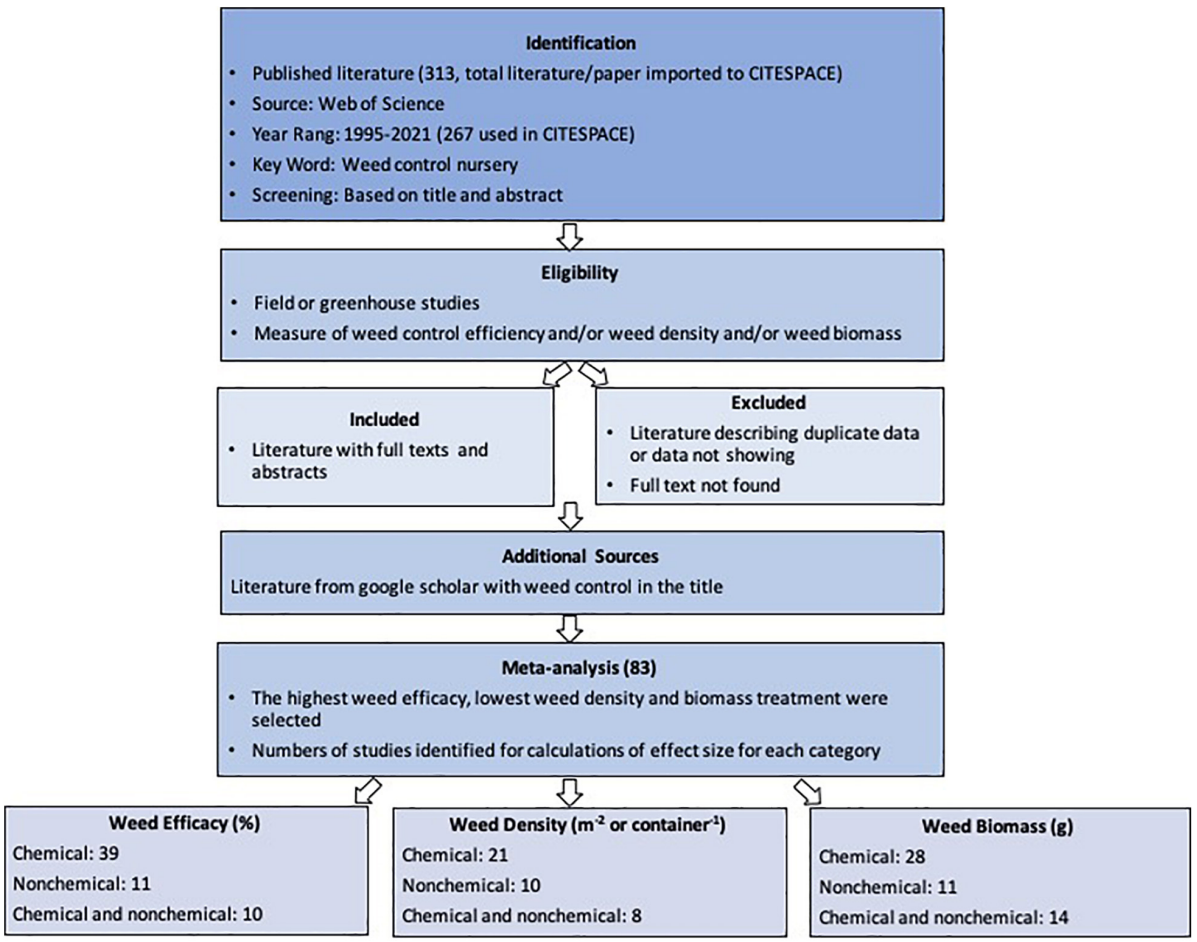


FIGURE 1 | Flow diagram showing the study selection procedure.

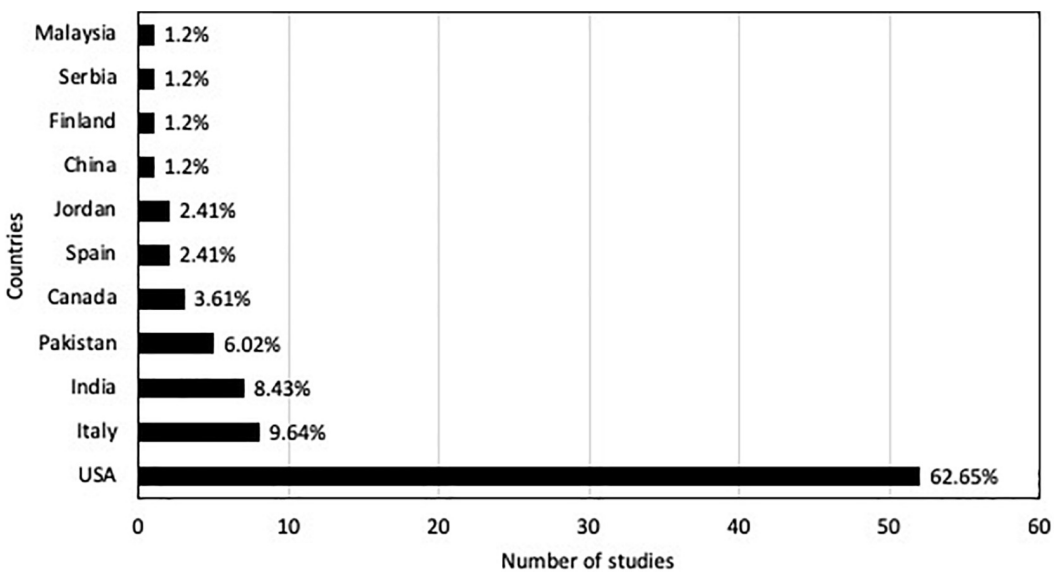


FIGURE 2 | Countries of the studies reported in the articles used for the meta-analysis.

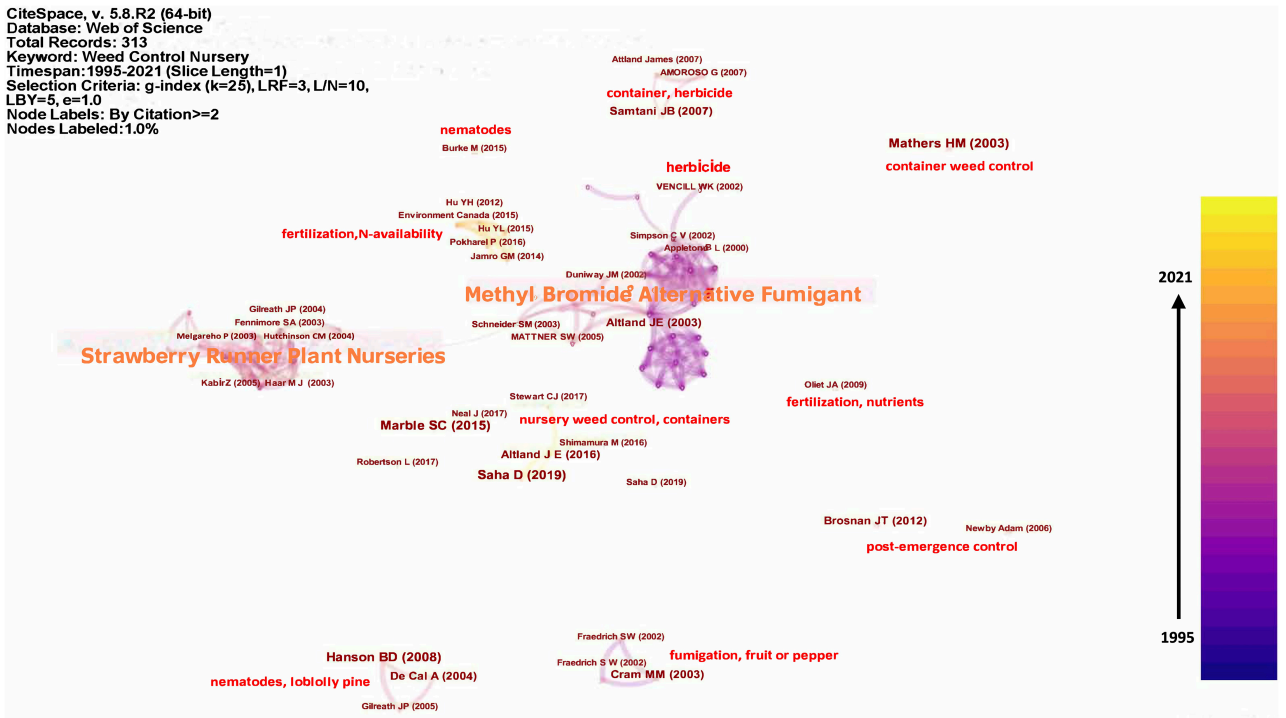


FIGURE 3 | CiteSapce generated knowledge networks from 1995 to 2021. The red texts are keywords derived from the clusters or the literature next to them.

(Rose et al., 2014). All the citations (full report) were analyzed with the software CiteSpace (current version 5.8. R2). A meta-analysis was conducted by using the *meta* package in R Studio (Version 1.3.1093). Fixed and random-effects models were both used in the meta-analysis to provide more unbiased information: fixed effects assume all studies with the size of their effect come from a single population (with a single source of variance), studies with greater precision (large study number and small SE) have a higher weight to affect overall effects; random effects add another variance in addition to the fixed effects to count for the variability of the true effect size, in this case, small studies play more important roles in overall effects (Harrer et al., 2021). A meta-analysis was conducted for weed density and biomass, respectively. Since the weed efficacy for the control was 0, we analyzed the weed control efficacy with boxplots using the R Studio.

RESULTS

Research Trends

The network was divided into different clusters based on the influential articles and their citations (**Figures 3**, **4**), with the more intense crosslink (where nodes gather together) labeled by the most frequently used title terms from the literature (Chen, 2006). In **Figure 3**, "methyl bromide alternative fumigant" was the hub node connecting the common knowledge or the close research areas, meaning the focus on weed control in nurseries was the methyl bromide alternative fumigants while the pivot nodes connecting other topics (e.g., herbicide) and strawberry runner plant nurseries. Other pivot nodes at different time slices were distributed at different places and were not connected to the hub nodes as indicated by the scattered/non-connected pivot nodes.

Based on the pub nodes and pivot nodes, two clusters were divided and labeled by index terms from their citers. In the first decade (1995–2005), chemical, primarily methyl bromide alternative fumigants, along with the strawberry runner plant nurseries, were the main focuses in the nursery weed control (Duniway, 2002; Cal et al., 2004; De Cal et al., 2005; Hanson et al., 2010). At this time, weeds and pathogens (mainly nematodes) were primarily controlled using methyl bromide alternatives (Schneider et al., 2003; Gilreath et al., 2004; De Cal et al., 2005; Hanson et al., 2010). Besides the two major clusters, other literature focused on herbicides, container weed control, and/or nematodes but not necessarily closely related to the hub nodes (Vencill, 2002; Mathers, 2003; Gilreath et al., 2005).

In the following years (2006–2021), the research focus switched more toward nursery/container weed control and weed practices. New weed control methods, such as chemicals, primarily herbicides, as well as non-chemical, primarily mulching, and fertilization have gained more attention in recent years. In **Figure 3**, the separated pivot nodes at different time slices show that the studies on nursery/container weed control, fertilizers, and herbicides are not well connected. The literature was widely distributed based on various topics, such as weed control methods (herbicide, fertilization, and mulch) as well as crops (pine trees, peaches, and ornamentals), indicated

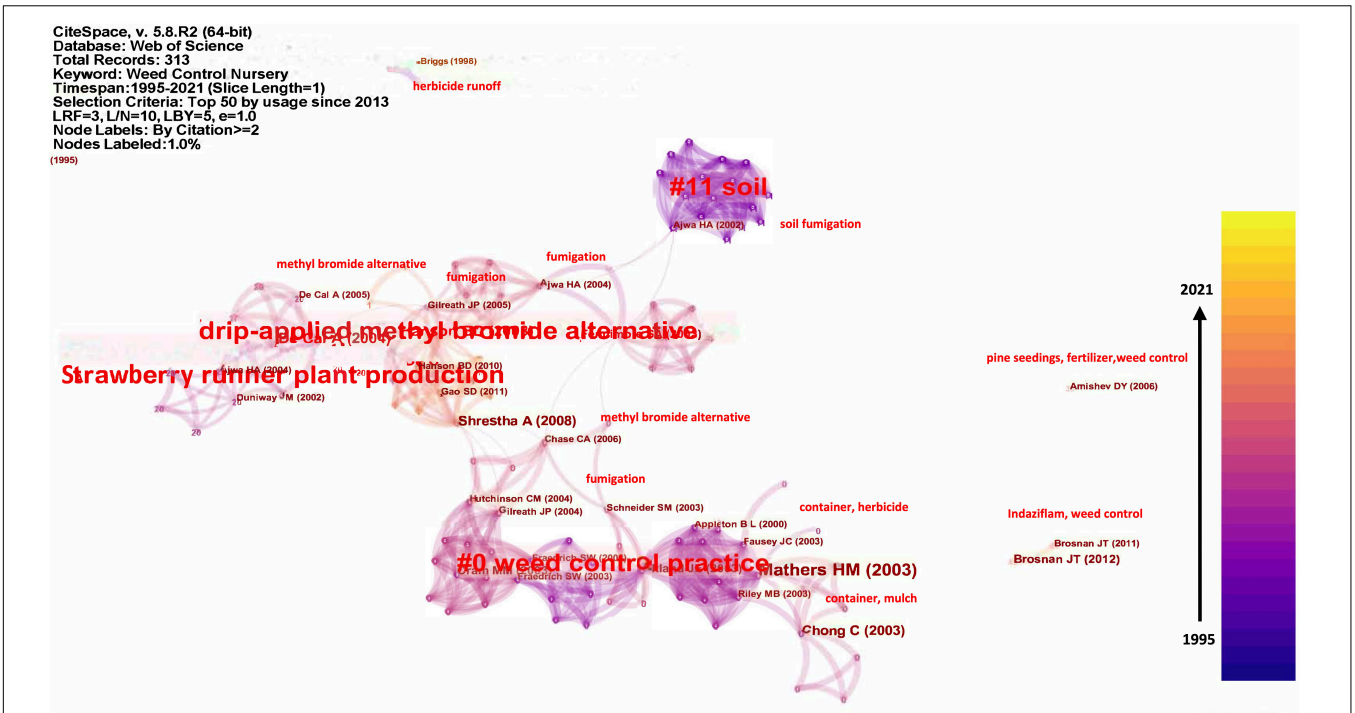


FIGURE 4 | CiteSapce generated knowledge networks on the top 50 pieces of literature used since 2013. The small red texts are keywords derived from the clusters or the literature next to them.

by the scattered pivot nodes (Hanson and Schneider, 2008; Brosnan et al., 2012; Altland et al., 2016; Stewart et al., 2018; Massa et al., 2019; Saha et al., 2019a).

Since research interests have been largely switched from the first decade (1995–2005) to the following years (2006–2021), we derived a literature usage on "nursery weed control" since 2013 (**Figure 4**). In **Figure 4**, "weed control practice" became the hub node, meaning that the research interests have switched to different weed control practices, such as herbicide, mulching, fertilization, combinations of herbicide, and other practices since 2013. The pivot nodes connecting different time slices showed that the integration of studies on weed control practices, methyl bromide alternatives, strawberry runner plant productions, and soil fumigations were well connected (Chen, 2006).

Based on the pub nodes and pivot nodes, four clusters were divided and labeled by index terms from their citers, such as weed control practices, strawberry runner plant production, drip-applied methyl bromide alternative, and soil fumigation. The weed control practice literature group was mainly cited by container studies investigating mulching, fertilization, herbicides, or chemical and non-chemical combinations. However, the other three groups were cited by field studies in the first decade and both field and container studies in the following years.

Different Weed Control Methods on Weed Control Efficacy

The highest weed control efficacy was 100% and all three weed control methods can reach 100% efficacy depending on weed species and practices (**Figure 5**). The lowest weed control efficacy for chemical, non-chemical, and the combined were 74, 74.3, and 81.8%, respectively. On average, chemical methods had the highest weed control efficacy mean (94.39%), and non-chemical had the lowest mean (90.45%) among the three, although no significant difference was detected ($p = 0.429$).

Chemical Effects on Weed Biomass and Density

For both fixed and random models, the application of chemical weed control method decreased weed biomass and density (**Figures 6**, **7**). Diamonds in the meta-analysis showed the overall effects (or standard mean differences, SMD) and its 95% *CI* of comparing chemical application with no chemical application. There was an overall mean difference between with or without chemical application effects on weed biomass (SMD = −9.39; 95% *CI* = −11.28, −7.5; $p < 0.01$, random model) and weed density (SMD = −8.9; 95% *CI* = −10.95, −6.85; $p < 0.01$, random model). Overall, there was moderate heterogeneity (I^2 = 68 and 55%, respectively) among studies on chemical effects on the weed biomass and density (Mikolajewicz and Komarova, 2019).

Non-chemical Effects on Weed Biomass and Density

Similarly, non-chemical weed control methods decreased the weed biomass and density (**Figures 8**, **9**). There was an overall mean difference between with or without non-chemical

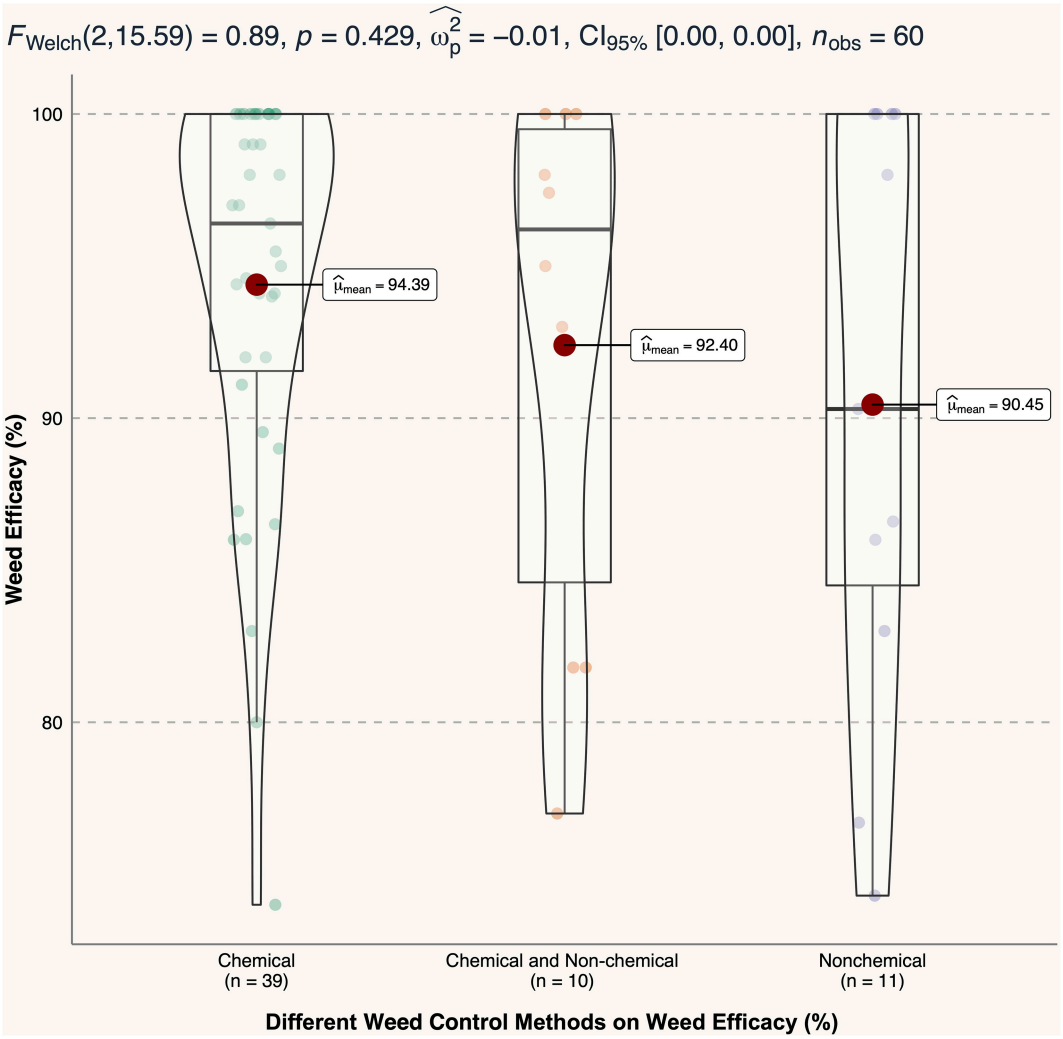


FIGURE 5 | Different weed control methods (chemical, chemical and non-chemical combined, and non-chemical) effects on weed control efficacy.

method effects on the weed biomass (SMD = −4.84; 95% *CI* = −7.97, −1.91; $p < 0.01$, random model) and weed density (SMD = −10.33; 95% *CI* = −13.19, −7.47; $p = 0.04$, random model). Overall, there was moderate heterogeneity ($I^2 = 71$ and 50%) among studies on non-chemical effects on the weed biomass and density, respectively.

Chemical and Non-chemical Effects on Weed Biomass and Density

For both fixed and random models, integrated chemical and non-chemical weed control methods decreased the weed biomass and density (**Figures 10**, **11**). There was an overall mean difference between with or without integrated chemical and non-chemical method effects on weed biomass (SMD = − 8.57; 95% *CI* = −11.49, −5.65; $p < 0.01$, random model) and weed density (SMD = −9.54; 95% *CI* = −12.34, −6.74; $p < 0.01$, random model). The heterogeneity among studies on integrated chemical and non-chemical effects on the weed biomass was high ($I^2 = 88\%$) and moderate on weed density ($I^2 = 64\%$, respectively).

DISCUSSION

Meta-Analysis Heterogeneity

Heterogeneity was defined as the proportion of total variance between studies, indicating the inconsistency between studies (Mikolajewicz and Komarova, 2019). The value of I^2 ranges from 0 to 100% and does not depend on the number of comparisons in the meta-analysis. The values of I^2 at 25, 50, and 75% reflect low, moderate, and high heterogeneity, respectively (Higgins and Thompson, 2002). The decision to use a fixed-effects or random-effects model based on these statistics is subjective; however, we would consider using a random-effects model on I^2 values greater than 50% (Osipitan et al., 2018). There

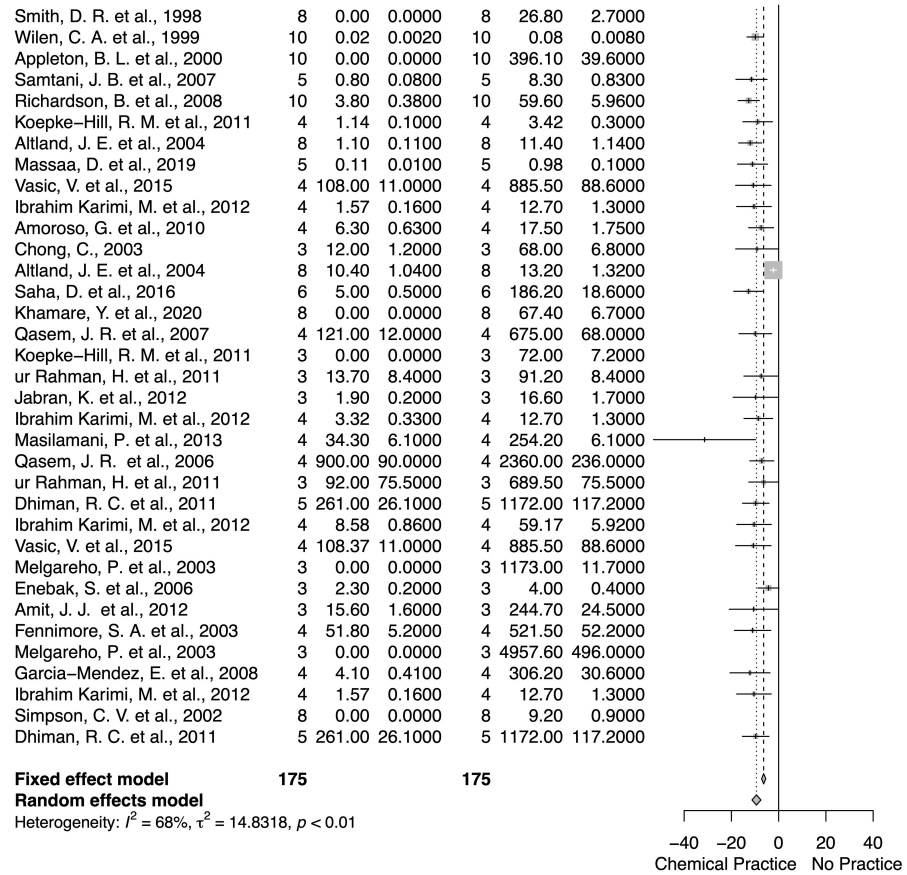


FIGURE 6 | Meta-analysis for the chemical weed control method on weed biomass.

was high heterogeneity among studies for most measurements of weed biomass and density, with the highest I^2 being 88%, found in chemical and non-chemical combined effects on weed biomass studies (**Figure 10**). However, among the studies for the effects of non-chemical weed control method on weed density, 50% of the primary studies were at variance. The moderate heterogeneity was acceptable and might be because some research studies (e.g., container studies) were conducted with more replications and less variance than others (e.g., field studies).

The main sources of heterogeneity in this study could because of the differences in weed species and control practices: weed species, such as spotted spurge (*Euphorbia maculata* L.), oxalis (*Oxalis corniculate* L.), northern willowherb (*Epilobium ciliatum* Raf.), and common groundsel (*Senecio vulgaris* L.); practices, such as use rice hull mulch, steaming, fertilizer placements, and different chemicals (isoxaben, trifluralin, indaziflam, prodiamine, methyl bromide, and chloropicrin). To address differences among the primary studies, a random-effects model was included and used for the meta-analysis. The random model recognized the variance among studies and summarized the effect sizes as weighted means based on these differences (Osipitan et al., 2018; Mikolajewicz and Komarova, 2019).

Research Trend in Nursery Weed Control

The research interests in nursery weed control have switched dramatically in the past 2–3 decades (1995–2021) from chemical dominant weed control to chemical coexist with other techniques. In the first decade, chemical weed control obtained the major research focus, specifically methyl bromide alternatives, due to the phase-out of methyl bromide (Keddy et al., 1996; Duniway, 2002; Cal et al., 2004; Enebak et al., 2006; Fennimore et al., 2008; Garcia-Mendez et al., 2008). Among the 267 pieces of literature, 27 focused on methyl bromide alternatives. In the meantime, non-chemical weed control techniques, specifically disks, occupied a small portion (2 out of 267) of the research interests (Chong, 2003; Knox et al., 2012). As a result of methyl bromide phase-out, herbicide become a research hot spot in the nursery weed control (78 out of 267). Since 2013, due to the increasing environmental concerns, research switched to weed control practices (**Figure 3**, 128 out of 267), specifically on non-chemical as well as chemical and non-chemical integrated. Among them, mulch started to draw

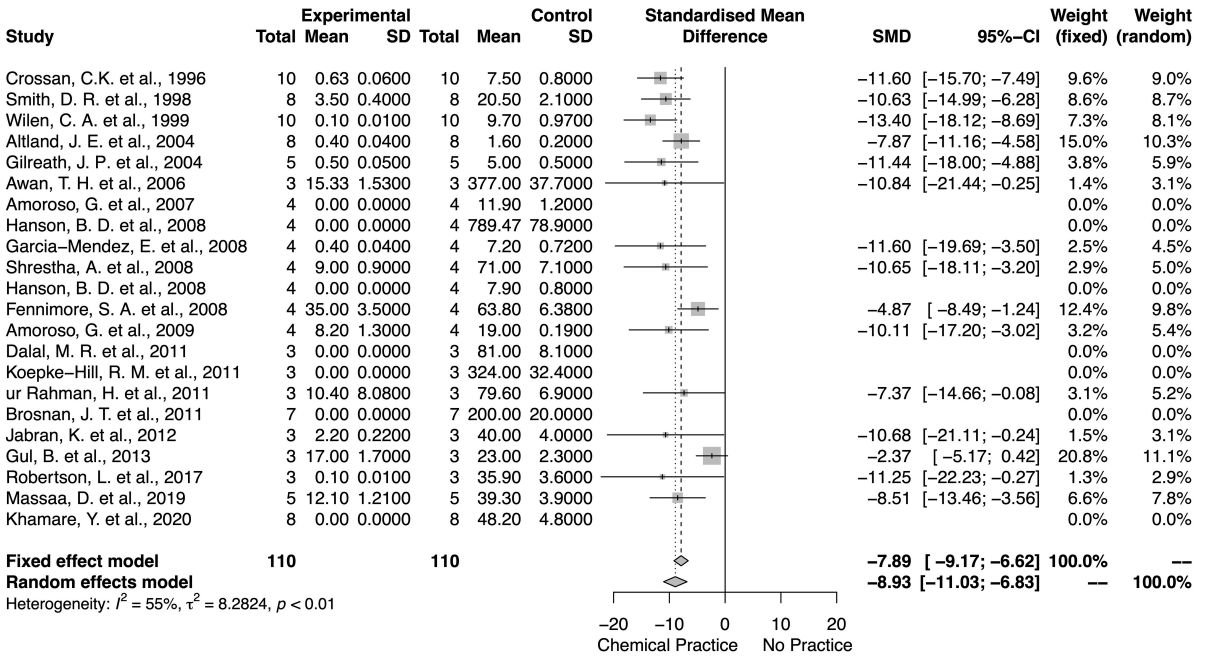


FIGURE 7 | Meta-analysis for the chemical weed control method on weed density.

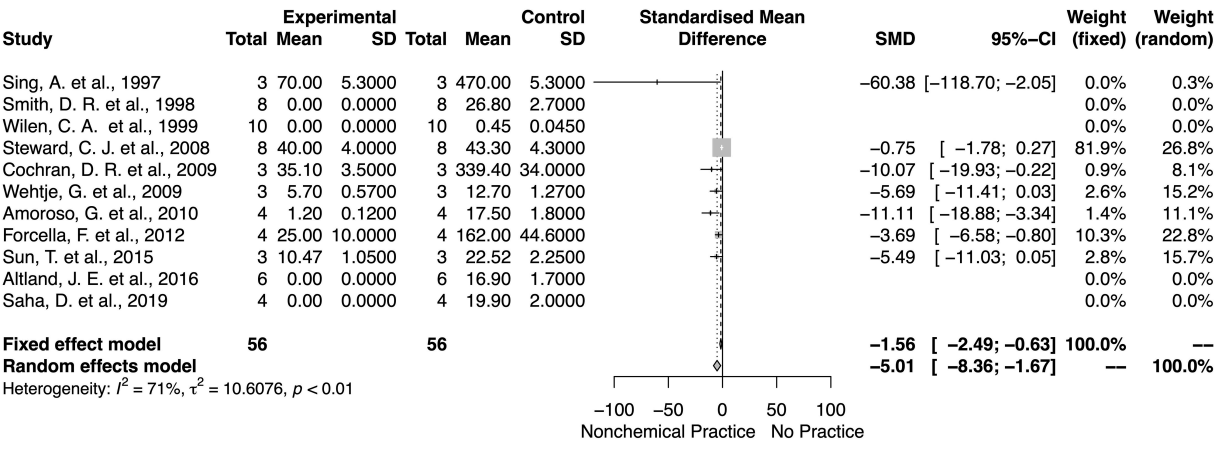


FIGURE 8 | Meta-analysis for the non-chemical weed control method on weed biomass.

attention of researchers and became the widest tested method (29 out of 267).

Not only research interests have changed dramatically, but also chemical products used in weed control. At methyl bromide phase-out times, the common tested chemicals included chloropicrin, metam sodium, 1,3-dichloropropene, iodomethane, dazomet, anhydrous ammonia, and their combinations with different formulations (Reynolds et al., 2002; Schneider et al., 2003; Gilreath et al., 2004, 2005; Fennimore et al., 2008; Shrestha et al., 2008; Schneider and Hanson, 2009; Hanson et al., 2010). Some of those chemicals, such as iodomethane reached a 100% weed control efficacy (Fennimore et al., 2008). Later, herbicides, such as oryzalin, glyphosate, flumioxazin, oxyfluorfen, pendimethalin, isoxaben, trifluralin, and their combinations become more widely tested, other herbicides that have both preemergence and postemergence effects, such as quinoclamine was also tested in different studies (Porter, 1996; Willoughby et al., 2003; Altland et al., 2004, 2007, 2008, 2011; Awan et al., 2006; Judge and Neal, 2006; Qasem, 2006, 2007; Richardson and Zandstra, 2009; Wehtje et al., 2010a,b, 2012; Rahman et al., 2011; Abit and Hanson, 2013; Ramalingam et al., 2013; Vasic et al., 2015; Marble et al., 2016b). Most of the herbicides, such as oxadiazon, flumioxazin, and prodiamine, presented satisfactory weed control performances (Judge and Neal, 2006; Amoroso et al., 2009; Wehtje et al., 2010a).

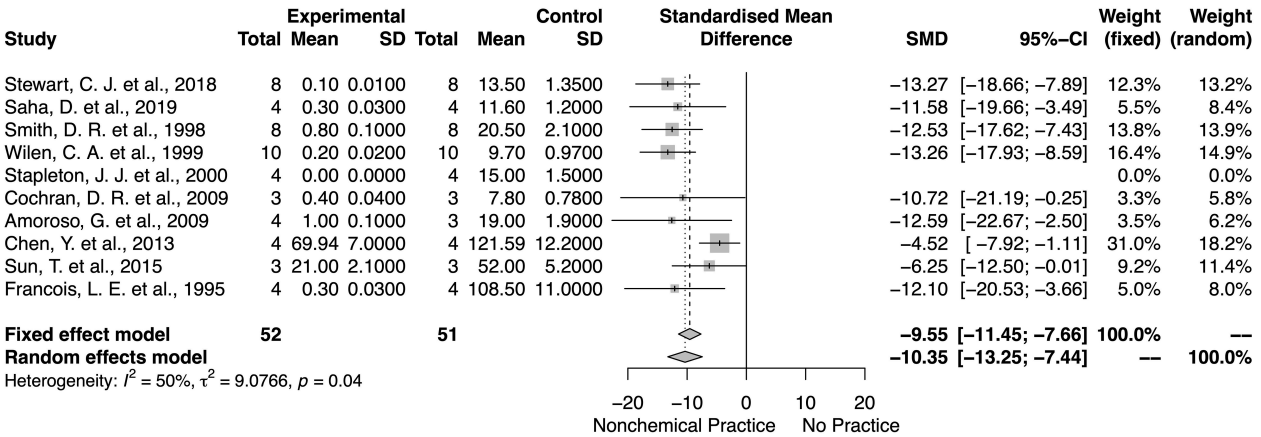


FIGURE 9 | Meta-analysis for the non-chemical weed control method on weed density.

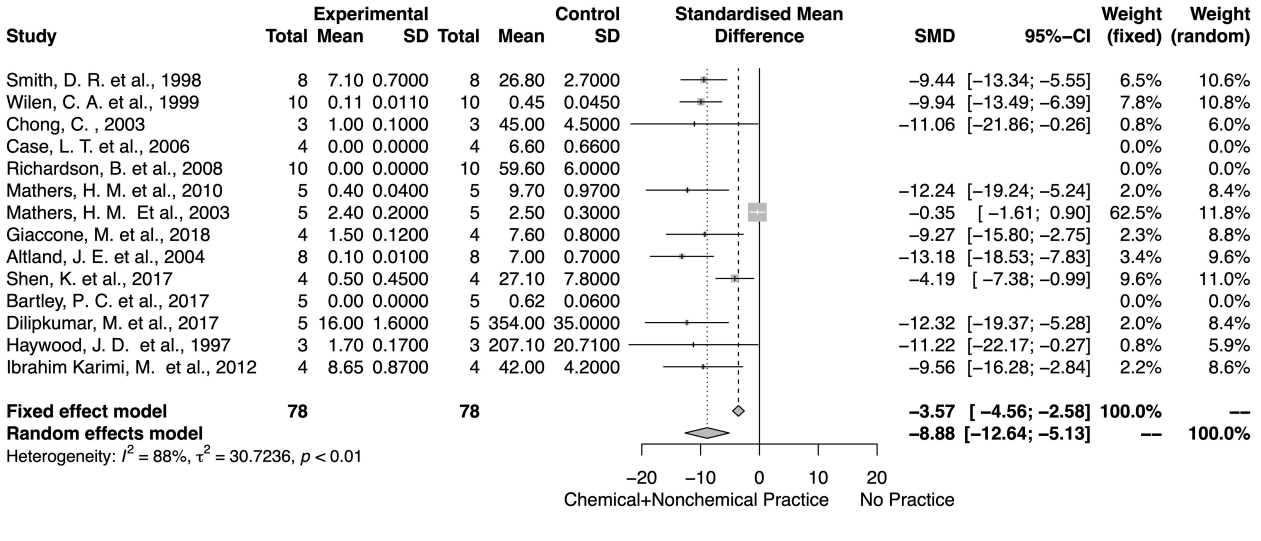


FIGURE 10 | Meta-analysis for the chemical and non-chemical combined weed control method on weed biomass.

Similarly, non-chemical weed control experienced significant change. In the early years of the evaluation period, different disks, such as Geo-disk, non-woven polypropylene fabric, plastic lids, and polyethylene sleeves were tested (Case et al., 2005; Lanthier et al., 2006; Knox et al., 2012; Sun et al., 2015). However, due to the poor weed control performance, most weed disks introduced during the past 15 years were no longer being used or sold (Chong, 2003). Later, mulches stood out among other non-chemical practices and became a research hot spot due to their easy availability and low prices (Chalker-Scott, 2007). The widely tested mulches, such as pine bark, rice hull, Douglas fir bark, coconut coir, newspaper pellets, and waste paper (Pellett and Heleba, 1995; Penny and Neal, 2003; Amoroso et al., 2009; Mathers and Case, 2010; Chen et al., 2013; Marble, 2015; Bartley et al., 2017; Burrows, 2017; Masilamany et al., 2017; Marble et al., 2019; Massa et al., 2019). Adding mulches (2.54–7.62 cm) can reach satisfactory weed control results depending on mulch types and weed species (Richardson et al., 2008; Cochran et al., 2009; Altland et al., 2016; Massa et al., 2019; Särkkä and Tahvonen, 2020). In addition, innovative non-chemical weed control methods, such as fertilizer placement, irrigation, flaming, steaming, oil palm, real-time robotics have been proposed and tested (Rainbolt et al., 2013; Frasconi et al., 2014; Masilamany et al., 2017; Pokharel et al., 2017; Stewart et al., 2017, 2018; Saha et al., 2019b; Raja et al., 2020).

Similarly, the chemical and non-chemical integrated weed control practices evolved from herbicide combined with mechanical to herbicide combined with mulch. In the first decades, chemical and disks were the two main ways for weed control, only a few studies tested chemical and non-chemical (mechanical or hand weeding) combined (Zheljazkov et al., 1996). In recent years, researchers integrated mulches and herbicides for weed control, aiming to reduce herbicide usage (or increase weed control performance) while maintaining the sufficient weed control (Somireddy, 2011; Masilamany et al., 2017; Shen and Zheng, 2017; Giaccone et al., 2018;

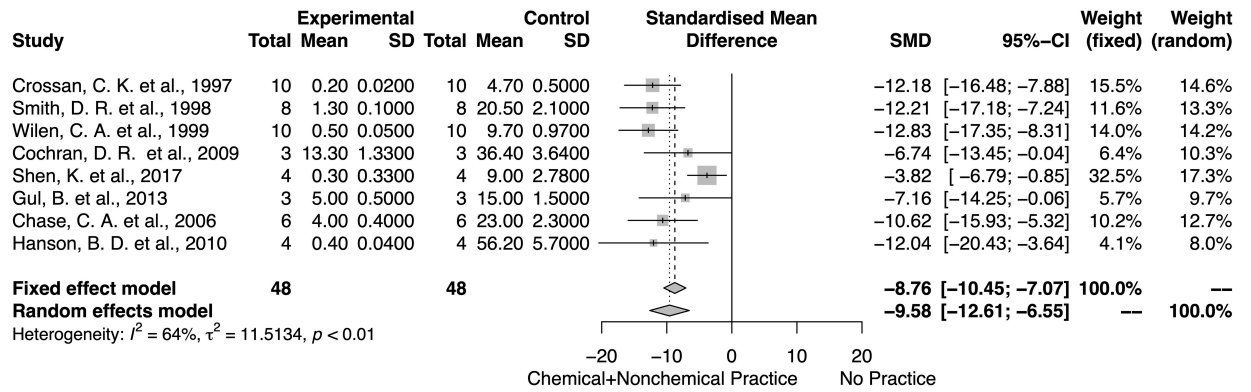


FIGURE 11 | Meta-analysis for the chemical and non-chemical combined weed control method on weed density.

Anthony and Witcher, 2020). Case and Mathers (2006) showed that applying SureGuard (flumioxazin) at half manufacturer label rate (0.19 kg ai ha^{-1}) to hardwood or rice hull significantly reduced spurge (*Euphorbia maculata* L.), annual bluegrass (*P. annua* L.), and common chickweed (*Stellaria media* L.) biomass. In addition, Richardson et al. (2008) showed that applying pine bark mini-nugget mulch (3.8 cm) with Broadstar (flumioxazin) herbicide increased weed control efficacy comparing with the non-treated control, herbicide alone, or mulch alone, achieved a 100% weed control efficacy for both bittercress (*Cardamine* spp.) and oxalis (*Oxalis stricta* L.). Other combinations of herbicides and other non-chemical practices have also been tested (Wehtje et al., 2009).

With the rising environmental concerns and potential restrictions, herbicide alternatives are becoming more important (Chong, 2003). Weed science is extending from a discipline emphasizing herbicides toward a multidiscipline integrating several weed control methods (Hamill et al., 2004). Developing new management tactics, and implementing diverse combinations of integrated weed management present the future trend for weed control (Harker and O'Donovan, 2013; Stewart et al., 2017).

Weed Control Efficacy in Nursery Weed Control

For the same weed species, different methods led to the varied weed control. For a mix of annual bluegrass (*P. annua* L.), common groundsel (*Senecio vulgaris* L.), and shepherd's purse (*Capsella bursa-pastoris* L.), applying Diuron 80DF (diuron) alone at 1.12 kg ai ha^{-1} resulted in 86% control; however, treating weeds with diuron at 1.12 kg ai ha^{-1} and rice hull (0.51 cm) reached to 98% control; leaf pellet application controlled 50% weeds (Samtani et al., 2007). Similarly, in a container study, applying Rout (oxytluorfen + oryzalin) at 3.3 kg ai ha^{-1} for spotted spurge (*Euphorbia maculata* L.) resulted in 3.5 weed density (number per container); treating weeds with fabric disk plus Spin Out (PGR) led to 1.3; yet using recycled paper pellets reduced weed density to 0.8 (Smith et al., 1998).

The target weed species had a significant impact on weed control efficacy. Granular flumioxazin at 0.41 kg ai ha^{-1} controlled 84% doveweed (*Murdannia nudiflora* L.) but only 22% crabgrass (*D. sanguinalis* (L.) Scop.). Pendimethalin + dimethanamid-P (2.24 + 1.68 kg ai ha^{-1}) resulted in 100% weed control on doveweed (*Murdannia nudiflora* L.) and large crabgrass (*D. sanguinalis* (L.) Scop.), but only 19% on eclipta (*Eclipta prostrata* L.) (Saha et al., 2016). In a container study, applying pine bark mini nuggets at 2.54 cm controlled 87% spotted spurge (*Euphorbia maculata* L.) and 89% eclipta (*Eclipta alba* L.) (Cochran et al., 2009). In a field study, hand weeding followed by 0.0024 kg ai ha^{-1} imazethapyr-treated oil palm frond mulch (3.4 t ha^{-1}) controlled 94.5% Ganges primrose [*Asystasia gangetica* (L.) T. Anderson], 94.0% of junglerice [*Echinochloa colona* (L.) Link], 96.4% of mixed switchgrass species (*Panicum* spp.), 99.0% mile-a-minute (*Mikania micrantha* Kunth), and 96.8% of gale-of-the-wind (*Phyllanthus amarus* L.) 3 months after treatment in the coconut plantations (Masilamany et al., 2017).

It is commonly known that weed control is determined by both methods and species. How do we select the right practice for weed control? In general, chemical methods had better weed control efficacy compared with other control methods (**Figure 5**). However, weed density and biomass results varied as practices changed. Applying chemical products reduced weed density the most (by 94.6%), followed by non-chemical (85.7%), and integrated (80.8%). However, integrated methods reduced weed biomass the most (by 95.0%), followed by non-chemical (86.4%), and chemical (82.6%).

Unlike agronomic crops, most nursery crops are sold and marketed based on the aesthetic value, and consumers demand weed-free pots (Simpson et al., 2002). Thus, we removed all the field studies and got the average weed control results for each method. The non-chemical method reduced weed density the most (by 97.1%), followed by chemical (by 87.1%), and integrated (by 80.6%). In terms of weed biomass, these three methods presented similar effectiveness for weed control, although the chemical had the most control effects (by 95.3%), followed by integrated (by 93.2%) and non-chemical (by 90.3%).

As such, in container studies, non-chemical methods can reach the best weed control performance as comparing with chemical or integrated methods. The average number of weed per container was 0.4 for non-chemical method and was 2.8 for chemical. Although only one non-chemical study showed 100% control for weed density (Stapleton et al., 2002), other non-chemical studies had nearly 0 weed density (0.2–0.4) (Wilen et al., 1999; Cochran et al., 2009; Saha et al., 2019a). For chemicals, however, although some studies had close to 0 weed density (e.g., 0.1 per container) (Robertson and Derr, 2017), many other studies had larger weed density (e.g., 3.5–12.1) (Smith et al., 1998; Massa et al., 2019). For both weed density and biomass, the integrated method presented a medium effect on weed control, similar to the weed efficacy results (**Figure 5**). The reason might be because some studies showed relatively high control performance for weed density (0.2–0.3) and biomass (0 g) (Crossan et al., 1997; Bartley et al., 2017; Shen and Zheng, 2017).

Challenges and Opportunities in Nursery Weed Control

Since 2005 following the phase-out of methyl bromide, herbicides have become the dominant chemical weed control method in nurseries because they are highly effective on most weeds. Herbicides account for 60% of the pesticides used worldwide, and most large-scale crop production systems rely extensively on synthetic herbicides to manage weeds (Dayan, 2019). About 2.2 Mt of herbicide was used worldwide in 2019 with the United States contributing 0.26 Mt of herbicide usage, ranking the second largest herbicide usage country following China (FAOSTAT, 2021).

However, the wide use of herbicides has brought many challenges, with the first being herbicide-resistant weeds. Weeds can adapt to new herbicides and exhibit herbicide resistance in a short time (Burrows, 2017). Since 1985, reports of herbicide-resistant weeds increased from less than 100 cases in 1985 to nearly 500 cases globally in 2019. Over 23 weed species from 20 countries have been confirmed glyphosate resistance, and triazine resistant weed species have been largely confirmed in recent years (Powles and Yu, 2010; Derr et al., 2020).

The wide use of herbicides has caused environmental concerns and economic losses due to its leaching, runoff, and spray-drift (Briggs et al., 2002; Riley, 2003; Case and Mathers, 2006). For instance, up to 86% of a granular applied herbicide can be lost by misapplication and non-target loss, depending on the pot spacing and species (Gilliam et al., 1992). In addition, to maintain an acceptable weed control, nurseries often conduct frequent reapplications, leading to more runoff and leaching, causing environmental concerns (Horowitz and Elmore, 1991; Crossan et al., 1996, 1997; Bana et al., 2020). Moreover, herbicides drift from nearby farm fields could lead to crop damaged greater than 50%, causing huge economic losses depending on the farm size and plant species (Derr et al., 2020).

The costly and time-consuming herbicides development and regulation present another big challenge, especially in the ornamental industry (Altland et al., 2004; Duke, 2012). In the last 20 years, only a few new modes of action (e.g., indaziflam cellulose biosynthesis inhibitors) have been registered for use in nurseries (Duke, 2012; Brabham et al., 2014). Additionally, for the last 10 years, only very few new herbicides have become available to the landscape sector, with fewer postemergence herbicides (Case and Mathers, 2006; Marble, 2015).

However, on the bright side, herbicide weed control challenges could be the catalyst for the development of new non-chemical and integrated weed control techniques, creating new opportunities (Walsh et al., 2013). For instance, new mulch materials with satisfactory weed control performance could be explored and developed (Marble, 2015). Exploring new substrates and testing how different substrates can affect the weed growth can be another research direction. More research on how properties of mulches, such as particle size and feedstock influence the nursery weed control need to be conducted. Studies on how different mulch–herbicide combinations affect the weed growth need to be examined, especially with postemergence herbicides (Marble, 2015; Marble et al., 2016a). Furthermore, how different mulch materials affect herbicide leaching and runoff after application need to be determined (Marble, 2015). Moreover, understanding the mechanisms of how mulch controls weed will help the horticulture industry (Saha et al., 2018).

CONCLUSION

In this review, we provided a visualization and systematic understanding of research trend on nursery weed control. The results showed that interests in nursery weed control have switched dramatically in the last 2–3 decades (1995–2021) from chemical dominant weed control to chemical coexist with non-chemical techniques. The meta-analysis results indicated that all three weed control practices (chemical, non-chemical, and combined) reduced weed biomass and density significantly. With the rising environmental concerns and potential restrictions, developing new management tactics, implementing diverse combinations of integrated weed management present the future trend for weed control.

DATA AVAILABILITY STATEMENT

The original contributions presented in the study are included in the article/supplementary material, further inquiries can be directed to the corresponding author.

AUTHOR CONTRIBUTIONS

PY conducted the literature searching, collected and analyzed the data, and wrote the manuscript with the assistance of SCM. Both authors contributed to the article and approved the submitted version.

ACKNOWLEDGMENTS

The authors would like to thank KQ for his valuable comments on an earlier version of this manuscript.

REFERENCES

Abit, M. J. M., and Hanson, B. D. (2013). Evaluation of preemergence and post-directed herbicides on rootstock safety in field-grown almond nursery stock. *HortTechnology* 23, 462–467. doi: 10.21273/HORTTECH.23.4.462

Altland, J. E., Boldt, J. K., and Krause, C. C. (2016). Rice hull mulch affects germination of bittercress and creeping woodsorrel in container plant culture. *Am. J. Plant Sci.* 7, 2359–2375. doi: 10.4236/ajps.2016.716207

Altland, J. E., Fain, G. B., and Arx, K. V. (2004). Fertilizer placement and herbicide rate affect weed control and crop growth in containers. *J. Environ. Horticult.* 22, 93–99. doi: 10.24266/0738-2898-22.2.93

Altland, J. E., Gilliam, C. H., and Wehtje, G. (2003). Weed control in field nurseries. *HortTechnology* 13, 9–14. doi: 10.21273/HORTTECH.13.1.0009

Altland, J. E., Wehtje, G., Gilliam, C. H., and Miller, M. E. (2007). Liverwort (*Marchantia polymorpha*) control with quinoclamine. *Weed Technol.* 21, 483–488. doi: 10.1614/WT-06-116.1

Altland, J. E., Wehtje, G., Mckee, M. L., and Gilliam, C. H. (2008). Liverwort (*Marchantia polymorpha*) response to Quinoclamine in a pine bark substrate. *Weed Sci.* 56, 762–766. doi: 10.1614/WS-07-167.1

Altland, J. E., Wehtje, G., Sibley, J., Miller, M. E., Gilliam, C. H., and Krause, C. (2011). Differential response of liverwort (*Marchantia polymorpha*) tissue to post-applied quinoclamine. *Weed Technol.* 25, 580–585. doi: 10.1614/WT-D-10-00135.1

Amoroso, G., Fini, A., Piatti, R., and Frangi, P. (2009). Mulching as alternative to chemical weed control in nursery containerized crops. *Adv. Hortic. Sci.* 23:276. doi: 10.1400/121245

Anthony, L., and Witcher, I. P. (2020). Pre-emergence herbicides and mulches for weed control in cutting propagation. *Agronomy* 10:1249. doi: 10.3390/agronomy10091249

Awan, T., Safdar, M., Manzoor, Z., and Ashraf, M. (2006). Screening of herbicides as post-emergence application for effective weed control without affecting growth and yield of direct seeded rice plant. *J. Anim. Plant Sci.* 16, 60–64.

Bana, R. S., Singh, D., Nain, M. S., Kumar, H., Kumar, V., and Sepat, S. (2020). Weed control and rice yield stability studies across diverse tillage and crop establishment systems under on-farm environments. *Soil Tillage Res.* 204:104729. doi: 10.1016/j.still.2020.104729

Bartley, P. C., Wehtje, G. R., Murphy, A.-M., Foshee, W. G., and Gilliam, C. H. (2017). Mulch type and depth influences control of three major weed species in nursery container production. *HortTechnology* 27, 465–471. doi: 10.21273/HORTTECH03511-16

Berchielli-Robertson, D. L., Gilliam, C. H., and Fare, D. C. (1990). Competitive effects of weeds on the growth of container-grown plants. *HortScience* 25, 77–79. doi: 10.21273/HORTSCI.25.1.77

Boyd, N. S., and Steed, S. (2021). Potted tropical ornamental tolerance to multiple Pre herbicides. *Weed Technol.* 35, 623–627. doi: 10.1017/wet.2020.133

Brabham, C., Lei, L., Gu, Y., Stork, J., Barrett, M., and Debolt, S. (2014). Indaziflam herbicidal action: a potent cellulose biosynthesis inhibitor. *Plant Physiol.* 166, 1177–1185. doi: 10.1104/pp.114.241950

Briggs, J. A., Whitwell, T., Fernandez, R. T., and Riley, M. B. (2002). Formulation effects on isoxaben and trifluralin in runoff water from container plant nurseries. *Weed Sci.* 50, 536–541.

Brosnan, J. T., Breeden, G. K., McCullough, P. E., and Henry, G. M. (2012). Pre and Post control of annual bluegrass (*Poa annua*) with indaziflam. *Weed Technol.* 26, 48–53. doi: 10.1614/WT-D-11-00088.1

Burrows, M. (2017). *Evaluation of Pine Bark Mulch-Herbicide Combinations for Weed Control in Nursery Containers.* Master thesis. Auburn: Auburn University.

Cal, A. D., Martinez-Treceno, A., Lopez-Aranda, J., and Melgarejo, P. (2004). Chemical alternatives to methyl bromide in Spanish strawberry nurseries. *Plant Dis.* 88, 210–214. doi: 10.1094/PDIS.2004.88.2.210

Case, L., and Mathers, H. (2006). Herbicide-treated mulches for weed control in nursery container crops. *J. Environ. Hortic.* 24, 84–90. doi: 10.24266/0738-2898-24.2.84

Case, L., Mathers, H., and Senesac, A. (2005). A review of weed control practices in container nurseries. *HortTechnology* 15, 535–545. doi: 10.21273/HORTTECH.15.3.0535

Chalker-Scott, L. (2007). Impact of mulches on landscape plants and the environment—a review. *J. Environ. Hortic.* 25, 239–249. doi: 10.24266/0738-2898-25.4.239

Chen, C. (2004). Searching for intellectual turning points: progressive knowledge domain visualization. *Proc. Natl. Acad. Sci. U.S.A.* 101(Suppl. 1), 5303–5310.

Chen, C. (2006). CiteSpace II: detecting and visualizing emerging trends and transient patterns in scientific literature. *J. Am. Soc. Inform. Sci. Technol.* 57, 359–377. doi: 10.1002/asi.20317

Chen, Y., Strahan, R. E., and Bracy, R. P. (2013). Effects of mulching and preemergence herbicide placement on yellow nutsedge control and ornamental plant quality in landscape beds. *HortTechnology* 23, 651–658. doi: 10.21273/HORTTECH.23.5.651

Chong, C. (2003). Experiences with weed discs and other nonchemical alternatives for container weed control. *HortTechnology* 13, 23–27. doi: 10.21273/HORTTECH.13.1.0023

Cochran, D. R., Gilliam, C. H., Eakes, D. J., Wehtje, G. R., Knight, P. R., and Olive, J. (2009). Mulch depth affects weed germination. *J. Environ. Hortic.* 27, 85–90. doi: 10.24266/0738-2898-27.2.85

Collins, K. B., McNiel, R. E., and Weston, L. A. (2001). Evaluation of sulfentrazone for weed control and phytotoxicity in field-grown landscape plants. *J. Environ. Hortic.* 19, 189–194. doi: 10.24266/0738-2898-19.4.189

Crossan, C., Gilliam, C., Eakes, D., Keever, G., Wehtje, G., and Dozie, W. Jr. (1996). Weed control with herbicide-coated or-blended fertilizer in 'August Beauty'gardenia. *J. Environ. Hortic.* 14, 5–8. doi: 10.24266/0738-2898-14.1.5

Crossan, C., Gilliam, C., Keever, G., Eakes, D., Wehtje, G., and Dozie, W. Jr. (1997). Weed control in container-grown crops with herbicide-coated fertilizers. *J. Environ. Hortic.* 15, 138–141. doi: 10.24266/0738-2898-15.3.138

Dalal, M. R., Pandit, A. H., Wani, W. M., Mir, M. A., Bhat, K. M., and Malik, A. R. (2008). "Effects of different weed control measures on weed population and growth parameters of apple nursery plants," in *Proceedings of the IX International Symposium on Integrating Canopy, Rootstock and Environmental Physiology in Orchard Systems 903*, Geneva, NY, 1017–1022.

Dayan, F. E. (2019). Current status and future prospects in herbicide discovery. *Plants* 8:341. doi: 10.3390/plants8090341

De Cal, A., Martinez-Treceno, A., Salto, T., López-Aranda, J., and Melgarejo, P. (2005). Effect of chemical fumigation on soil fungal communities in Spanish strawberry nurseries. *Appl. Soil Ecol.* 28, 47–56. doi: 10.1016/j.apsoil.2004.06.005

Derr, J. F., Neal, J. C., and Bhowmik, P. C. (2020). Herbicide resistance in the nursery crop production and landscape maintenance industries. *Weed Technol.* 34, 437–446. doi: 10.1017/wet.2020.40

Duke, S. O. (2012). Why have no new herbicide modes of action appeared in recent years? *Pest Manage. Sci.* 68, 505–512. doi: 10.1002/ps.2333

Duniway, J. M. (2002). Status of chemical alternatives to methyl bromide for pre-plant fumigation of soil. *Phytopathology* 92, 1337–1343. doi: 10.1094/PHYTO.2002.92.12.1337

Enebak, S. S., Starkey, T., and McCraw, D. (2006). "Tree seedling quality and weed control with Basamid, MBR and methyl iodide," in *Proceedings of the Annual International Research Conference on Methyl Bromide Alternatives*, Orlando, FL.

FAOSTAT (2021). *Pestcides Use*. Rome: Food and Agriculture Organization of the United Nations.

Fennimore, S. A., Haar, M. J., Goodhue, R. E., and Winterbottom, C. Q. (2008). Weed control in strawberry runner plant nurseries with methyl bromide alternative fumigants. *HortScience* 43, 1495–1500. doi: 10.21273/HORTSCI.43.5.1495

Frasconi, C., Fontanelli, M., Raffaelli, M., Martelloni, L., and Peruzzi, A. (2014). "Experiences on physical weed control in nursery container production," in *Proceedings of the 10 th EWRS Workshop on Physical and Cultural Weed Control*, Alnarp.

Fretz, T. A. (1972). Weed competition in container grown Japanese holly. *HortScience* 7, 485–486.

Garcia-Mendez, E., García-Sinovas, D., Becerril, M., De Cal, A., Melgarejo, P., Martinez-Treceno, A., et al. (2008). Chemical alternatives to methyl bromide for weed control and runner plant production in strawberry nurseries. *HortScience* 43, 177–182. doi: 10.21273/HORTSCI.43.1.177

Giaccone, M., Cirillo, C., Scognamiglio, P., Teobaldelli, M., Mataffo, A., Stinca, A., et al. (2018). Biodegradable mulching spray for weed control in the cultivation

of containerized ornamental shrubs. *Chem. Biol. Technol. Agric.* 5, 1–8. doi: 10.1186/s40538-018-0134-z

Gilliam, C., Fare, D., and Beasley, A. (1992). Nontarget herbicide losses from application of granular Ronstar to container nurseries. *J. Environ. Hortic.* 10, 175–176. doi: 10.24266/0738-2898-10.3.175

Gilreath, J. P., Motis, T. N., and Santos, B. M. (2005). *Cyperus* spp. Control with reduced methyl bromide plus chloropicrin doses under virtually impermeable films in pepper. *Crop Prot.* 24, 285–287. doi: 10.1016/j.cropro.2004.08.008

Gilreath, J. P., Noling, J. W., and Santos, B. M. (2004). Methyl bromide alternatives for bell pepper (*Capsicum annuum*) and cucumber (*Cucumis sativus*) rotations. *Crop Prot.* 23, 347–351. doi: 10.1016/j.cropro.2003.09.006

Haddaway, N., Woodcock, P., Macura, B., and Collins, A. (2015). Making literature reviews more reliable through application of lessons from systematic reviews. *Conserv. Biol.* 29, 1596–1605. doi: 10.1111/cobi.12541

Hamill, A. S., Holt, J. S., and Mallory-Smith, C. A. (2004). Contributions of weed science to weed control and management. *Weed Technol.* 18, 1563–1565.

Hanson, B. D., and Schneider, S. A. (2008). Evaluation of weed control and crop safety with herbicides in open field tree nurseries. *Weed Technol.* 22, 493–498. doi: 10.1614/WT-08-021.1

Hanson, B. D., Gerik, J. S., and Schneider, S. M. (2010). Effects of reduced-rate methyl bromide applications under conventional and virtually impermeable plastic film in perennial crop field nurseries. *Pest Manage. Sci.* 66, 892–899. doi: 10.1002/ps.1959

Harker, K. N., and O'Donovan, J. T. (2013). Recent weed control, weed management, and integrated weed management. *Weed Technol.* 27, 1–11. doi: 10.1614/WT-D-12-00109.1

Harrer, M., Cuijpers, P., Furukawa, T. A., and Ebert, D. D. (2021). *Doing Meta-Analysis with R: A Hands-On Guide (1st ed.)*. Boca Raton: Chapman and Hall/CRC.

Higgins, J. P., and Thompson, S. G. (2002). Quantifying heterogeneity in a meta-analysis. *Stat. Med.* 21, 1539–1558. doi: 10.1002/sim.1186

Horowitz, M., and Elmore, C. L. (1991). Leaching of oxyfluorfen in container media. *Weed Technol.* 5, 175–180.

Jalaludin, A., Ngim, J., Bakar, B. H., and Alias, Z. (2010). Preliminary findings of potentially resistant goosegrass (*Eleusine indica*) to glufosinate-ammonium in Malaysia. *Weed Biol. Manage.* 10, 256–260. doi: 10.1111/j.1445-6664.2010.00392.x

Judge, C. A., and Neal, J. C. (2006). Preemergence and early postemergence control of selected container nursery weeds with Broadstar, OH_2, and Snapshot TG. *J. Environ. Hortic.* 24, 105–108. doi: 10.24266/0738-2898-24.2.105

Keddy, C. O., Klaus, I., Jensen, N., and Harris, S. M. (1996). "Results of alternative applications on weed control in a strawberry nursery," in *Proceedings of the 1996 Annual Research Conference on Methyl Bromide Alternatives and Emissions Reduction*, Orlando, FL.

Knox, G. W., Chappell, M., and Stamps, R. H. (2012). *Alternatives to Synthetic Herbicides for Weed Management in Container Nurseries*. Available online at: http://edis.ifas.ufl.edu (accessed September 28, 2021).

Lanthier, M., Peters, S., Harel, S., and McInnis, M. (2006). "Non-chemical weed control with mulches and disks for nursery container production," in *60th Canadian Weed Science Society*, Victoria, BC.

Marble, S. C. (2015). Herbicide and mulch interactions: a review of the literature and implications for the landscape maintenance industry. *Weed Technol.* 29, 341–349. doi: 10.1614/WT-D-14-00165.1

Marble, S. C., Chandler, A., and Archer, M. (2016b). Impact of application rate, timing, and indaziflam formulation on early postemergence control of *Oxalis stricta*. *Weed Technol.* 30, 701–707. doi: 10.1614/WT-D-16-00002.1

Marble, S. C., Chandler, A., and Saha, D. (2016a). Postemergence control of *Pilea microphylla* (Artillery Weed). *Proc. Florida State Hortic. Soc.* 129, 243–245.

Marble, S. C., Steed, S. T., Saha, D., and Khamare, Y. (2019). On-Farm evaluations of wood-derived, waste paper, and plastic mulch materials for weed control in Florida container nurseries. *HortTechnology* 29, 866–873. doi: 10.21273/HORTTECH04437-19

Masilamany, D., Mat, M. C., and Seng, C. T. (2017). The potential use of oil palm frond mulch treated with imazethapyr for weed control in Malaysian coconut plantation. *Sains Malaysiana* 46, 1171–1181. doi: 10.17576/jsm-2017-4608-02

Massa, D., Benvenuti, S., Cacini, S., Lazzereschi, S., and Burchi, G. (2019). Effect of hydro-compacting organic mulch on weed control and crop performance in the cultivation of three container-grown ornamental shrubs: old solutions meet new insights. *Sci. Horticult.* 252, 260–267. doi: 10.1016/j.scienta.2019.03.053

Mathers, H. M. (2003). Novel methods of weed control in containers. *HortTechnology* 13, 28–34. doi: 10.21273/HORTTECH.13.1.0028

Mathers, H. M., and Case, L. T. (2010). Microencapsulated herbicide-treated bark mulches for nursery container weed control. *Weed Technol.* 24, 529–537. doi: 10.1614/WT-09-048.1

Mikolajewicz, N., and Komarova, S. V. (2019). Meta-analytic methodology for basic research: a practical guide. *Front. Physiol.* 10:203. doi: 10.3389/fphys.2019.00203

Osipitan, O. A., Dille, J. A., Assefa, Y., and Knezevic, S. Z. (2018). Cover crop for early season weed suppression in crops: systematic review and meta-analysis. *Agron. J.* 110, 2211–2221. doi: 10.2134/agronj2017.12.0752

Pellett, N. E., and Heleba, D. A. (1995). Chopped newspaper for weed control in nursery crops. *J. Environ. Hortic.* 13, 77–81. doi: 10.24266/0738-2898-13.2.77

Penny, G. M., and Neal, J. C. (2003). Light, temperature, seed burial, and mulch effects on mulberry weed (*Fatoua villosa*) seed germination. *Weed Technol.* 17, 213–218.

Phan, K., Tian, D. H., Cao, C., Black, D., and Yan, T. D. (2015). Systematic review and meta-analysis: techniques and a guide for the academic surgeon. *Ann. Cardiothor. Surg.* 4:112. doi: 10.3978/j.issn.2225-319X.2015.02.04

Pokharel, P., Kwak, J.-H., and Chang, S. X. (2017). Growth and nitrogen uptake of jack pine seedlings in response to exponential fertilization and weed control in reclaimed soil. *Biol. Fertility Soils* 53, 701–713. doi: 10.1007/s00374-017-1213-1

Porter, W. C. (1996). Isoxaben and isoxaben combinations for weed control in container-grown herbaceous flowering perennials. *J. Environ. Hortic.* 14, 27–30. doi: 10.24266/0738-2898-14.1.27

Powles, S. B., and Yu, Q. (2010). Evolution in action: plants resistant to herbicides. *Annu. Rev. Plant Biol.* 61, 317–347. doi: 10.1146/annurev-arplant-042809-112119

Qasem, J. (2006). Chemical weed control in seedbed sown onion (*Allium cepa* L.). *Crop Prot.* 25, 618–622. doi: 10.1016/j.cropro.2005.09.008

Qasem, J. (2007). Weed control in cauliflower (*Brassica oleracea* var. Botrytis L.) with herbicides. *Crop Prot.* 26, 1013–1020. doi: 10.1016/j.cropro.2006.09.010

Rahman, H. U., Ullah, K., Sadiq, M., Zubiar, M., Javaria, S., and Khan, M. A. (2011). Relative efficacy of different weed control methods in onion (*Allium cepa* L.) crop. *Pak. J. Weed Sci. Research* 17, 343–350.

Rainbolt, C. M., Samtani, J. B., Fennimore, S. A., Gilbert, C. A., Subbarao, K. V., Gerik, J. S., et al. (2013). Steam as a preplant soil disinfestant tool in California cut-flower production. *HortTechnology* 23, 207–214. doi: 10.21273/HORTTECH.23.2.207

Raja, R., Nguyen, T. T., Slaughter, D. C., and Fennimore, S. A. (2020). Real-time weed-crop classification and localisation technique for robotic weed control in lettuce. *Biosyst. Eng.* 192, 257–274. doi: 10.1111/avsc.12495

Ramalingam, S. P., Chinnagounder, C., Perumal, M., and Palanisamy, M. A. (2013). Evaluation of new formulation of oxyfluorfen (23.5% EC) for weed control efficacy and bulb yield in onion. *Am. J. Plant Sci.* 4, 890–895. doi: 10.4236/ajps.2013.44109

Reynolds, J. P., Greene, T. A., and Britt, J. R. (2002). "Effects of lifting method, seedling size, and herbaceous weed control on first-year growth of loblolly pine seedlings," in *Proceedings of the the Eleventh Biennial Southern Silvicultural Research Conference*, (Asheville, NC: United States Department of Agriculture, Forest Service, Southern Research Station), 51–54.

Richardson, B., Gilliam, C. H., Fain, G., and Wehtje, G. (2008). Nursery container weed control with pinebark mininuggets. *J. Environ. Hortic.* 26, 144–148. doi: 10.24266/0738-2898-26.3.144

Richardson, R. J., and Zandstra, B. H. (2009). Weed control in Christmas trees with flumioxazin and other residual herbicides applied alone or in tank mixtures. *HortTechnology* 19, 181–186. doi: 10.21273/HORTSCI.19.1.181

Riley, M. B. (2003). Herbicide losses in runoff of containerized plant production nurseries. *HortTechnology* 13, 16–22. doi: 10.21273/HORTTECH.13.1.0016

Robertson, L., and Derr, J. F. (2017). Dimethenamid persistence and leaching potential in a soilless mix. *J. Environ. Hortic.* 35, 99–102. doi: 10.24266/0738-2898-35.3.99

Rose, M. T., Patti, A. F., Little, K. R., Brown, A. L., Jackson, W. R., and Cavagnaro, T. R. (2014). A meta-analysis and review of plant-growth response to humic substances: practical implications for agriculture. *Adv. Agron.* 124, 37–89. doi: 10.1016/B978-0-12-800138-7.00002-4

Saha, D., Marble, S. C., and Pearson, B. J. (2018). Allelopathic effects of common landscape and nursery mulch materials on weed control. *Front. Plant Sci.* 9:733. doi: 10.3389/fpls.2018.00733

Saha, D., Marble, S. C., Boyd, N. S., and Steed, S. (2016). "Impacts of preemergence herbicide formulation on cost and weed control efficacy for container nursery crop producers© ," in *Proceedings of the 2016 Annual Meeting of the International Plant Propagators'. Society 1174*, Virginia, 319–324. doi: 10.17660/ActaHortic.2017.1174.64

Saha, D., Marble, S. C., Torres, N., and Chandler, A. (2019b). Fertilizer placement affects growth and reproduction of three common weed species in pine bark–based soilless nursery substrates. *Weed Sci.* 67, 682–688. doi: 10.1017/wsc.2019.49

Saha, D., Marble, S. C., Pearson, B. J., Pérez, H. E., MacDonald, G. E., and Odero, D. C. (2019a). Mulch type and depth, herbicide formulation, and postapplication irrigation volume influence on control of common landscape weed species. *HortTechnology* 29, 65–77. doi: 10.21273/HORTTECH04208-18

Samtani, J. B., Kling, G. J., Mathers, H. M., and Case, L. (2007). Rice hulls, leaf-waste pellets, and pine bark as herbicide carriers for container-grown woody ornamentals. *HortTechnology* 17, 289–295. doi: 10.21273/HORTTECH.17.3.289

Särkkä, L., and Tahvonen, R. (2020). Control of liverwort (*Marchantia polymorpha* L.) growth in nursery plants with mulches of Sphagnum moss and blackcurrant stem pieces. *Agric. Food Sci.* 29, 250–256. doi: 10.23986/afsci.90687

Schneider, S. M., and Hanson, B. D. (2009). Effects of fumigant alternatives to methyl bromide on pest control in open field nursery production of perennial fruit and nut plants. *HortTechnology* 19, 526–532. doi: 10.21273/HORTSCI.19.3.526

Schneider, S. M., Rosskopf, E. N., Leesch, J. G., Chellemi, D. O., Bull, C. T., and Mazzola, M. (2003). United States Department of Agriculture—Agricultural Research Service research on alternatives to methyl bromide: pre-plant and post-harvest. *Pest Manage. Sci.* 59, 814–826. doi: 10.1002/ps.728

Shen, K., and Zheng, Y. (2017). Efficacy of bio-based liquid mulch on weed suppression and water conservation in container nursery production. *J. Environ. Hortic.* 35, 161–167. doi: 10.24266/0738-2898-35.4.161

Shrestha, A., Browne, G. T., Lampinen, B. D., Schneider, S. M., Simon, L., and Trout, T. J. (2008). Perennial crop nurseries treated with methyl bromide and alternative fumigants: effects on weed seed viability, weed densities, and time required for hand weeding. *Weed Technol.* 22, 267–274. doi: 10.1614/WT-07-122.1

Shrestha, U., Augé, R. M., and Butler, D. M. (2016). A meta-analysis of the impact of anaerobic soil disinfestation on pest suppression and yield of horticultural crops. *Front. Plant Sci.* 7:1254. doi: 10.3389/fpls.2016.01254

Simpson, C. V., Gilliam, C. H., Altland, J., Wehtje, G., and Sibley, J. (2002). Postemergence oxalis control in container. *Southern Nursery Assoc. Res. Conf.* 47, 376–379.

Smith, D., Gilliam, C., Edwards, J., Olive, J., Eakes, D., and Williams, J. (1998). Recycled waste paper as a non-chemical alternative for weed control in container production. *J. Environ. Hortic.* 16, 69–75. doi: 10.24266/0738-2898-16.2.69

Somireddy, U. R. (2011). *Effect of Herbicide-Organic Mulch Combinations on Weed Control and Herbicide Persistence.* Doctoral. Columbus, OH: The Ohio State University.

Stapleton, J. J., Prather, T. S., Mallek, S. B., Ruiz, T. S., and Elmore, C. L. (2002). High temperature solarization for weed control in container soil and potting mixes. *HortTechnology* 12, 697–700. doi: 10.21273/HORTTECH.12.4.697

Stewart, C. J., Marble, S. C., Jackson, B. E., Pearson, B. J., and Wilson, P. C. (2018). Effects of three fertilization methods on weed growth and herbicide performance in soilless nursery substrates. *J. Environ. Hortic.* 36, 133–139. doi: 10.24266/0738-2898-36.4.133

Stewart, C. J., Marble, S. C., Pearson, B. J., and Wilson, P. C. (2017). Impact of container nursery production practices on weed growth and herbicide performance. *HortScience* 52, 1593–1600. doi: 10.21273/HORTSCI12241-17

Sun, T., Zhang, Z., Ning, T., Mi, Q., Zhang, X., Zhang, S., et al. (2015). Colored polyethylene film mulches on weed control, soil conditions and peanut yield. *Plant Soil Environ.* 61, 79–85. doi: 10.17221/882/2014-PSE

Vasic, V., Orlovic, S., Pap, P., Kovacevic, B., Drekic, M., Pajnik, L. P., et al. (2015). Application of pre-emergence herbicides in poplar nursery production. *J. Forest. Res.* 26, 143–151. doi: 10.1007/s11676-015-0040-1

Vencill, W. K. (2002). *Herbicide Handbook*. Lawrence, KS: Weed Science Society of America.

Walsh, M., Newman, P., and Powles, S. (2013). Targeting weed seeds in-crop: a new weed control paradigm for global agriculture. *Weed Technol.* 27, 431–436. doi: 10.1614/WT-D-12-00181.1

Wehtje, G., Altland, J. E., Gilliam, C. H., Marble, S. C., Van Hoogmoed, A. J., and Fain, G. B. (2009). Weed growth and efficacy of pre-applied herbicides in alternative rooting substrates used in container-grown nursery crops. *Weed Technol.* 23, 455–459. doi: 10.1614/WT-09-011.1

Wehtje, G., Gilliam, C. H., and Marble, S. C. (2010a). Interaction of prodiamine and flumioxazin for nursery weed control. *Weed Technol.* 24, 504–509. doi: 10.1614/WT-D-10-00020.1

Wehtje, G., Gilliam, C. H., and Marble, S. C. (2010b). Postemergence weed control with glyphosate plus flumioxazin combinations. *Weed Technol.* 24, 356–360. doi: 10.1614/WT-D-09-00038.1

Wehtje, G., Gilliam, C. H., and Marble, S. C. (2012). Duration of flumioxazin-based weed control in container-grown nursery crops. *Weed Technol.* 26, 679–683. doi: 10.1614/WT-D-11-00180.1

Wilen, C. A., Schuch, U. K., and Elmore, C. L. (1999). Mulches and subirrigation control weeds in container production. *J. Environ. Hortic.* 17, 174–180.

Willoughby, I., Clay, D., and Dixon, F. (2003). The effect of pre-emergent herbicides on germination and early growth of broadleaved species used for direct seeding. *Forestry* 76, 83–94. doi: 10.1093/forestry/76.1.83

Zheljazkov, V., Yankov, B., and Topalov, V. (1996). Effect of mechanical and chemical weed control on the growth, development and productivity of *Mentha piperita* and *M. arvensis* var. piperascens grown for planting material. *J. Essential Oil Res.* 8, 171–176. doi: 10.1080/10412905.1996.9700585

Conflict of Interest: The authors declare that the research was conducted in the absence of any commercial or financial relationships that could be construed as a potential conflict of interest.

Publisher's Note: All claims expressed in this article are solely those of the authors and do not necessarily represent those of their affiliated organizations, or those of the publisher, the editors and the reviewers. Any product that may be evaluated in this article, or claim that may be made by its manufacturer, is not guaranteed or endorsed by the publisher.

Copyright © 2022 Yu and Marble. This is an open-access article distributed under the terms of the Creative Commons Attribution License (CC BY). The use, distribution or reproduction in other forums is permitted, provided the original author(s) and the copyright owner(s) are credited and that the original publication in this journal is cited, in accordance with accepted academic practice. No use, distribution or reproduction is permitted which does not comply with these terms.

frontiers in Plant Science

ORIGINAL RESEARCH
published: 17 February 2022
doi: 10.3389/fpls.2022.828209

Genome-Wide Identification and Expression Profiling of CONSTANS-Like Genes in Pepper (*Capsicum annuum*): Gaining an Insight to Their Phylogenetic Evolution and Stress-Specific Roles

Zhinan Huang[1†], Xueying Bai[1†], Weike Duan[1], Boqing Chen[1], Guodong Chen[1], Binghua Xu[2], Rui Cheng[2] and Jizhong Wang[1]*

[1] College of Life Science and Food Engineering, Huaiyin Institute of Technology, Huai'an, China, [2] Huai'an Key Laboratory for Facility Vegetables, Huaiyin Institute of Agricultural Sciences of Xuhuai Region in Jiangsu, Huai'an, China

CONSTANS-like (*COL*) genes play important regulatory roles in multiple growth and development processes of plants but have rarely been studied in *Capsicum annuum*. This study explored the evolutionary relationship and expression patterns of *COL* genes from *C. annuum*. A total of 10 *COL* genes were identified in the genome of the cultivated pepper *Zunla-1* and were named *CaCOL01–10*. These genes were unequally distributed among five chromosomes and could be divided into three groups based on differences in gene structure characteristics. During evolutionary history, duplications and retentions were divergent among different groups of *COL* genes. Tandem duplication caused amplification of group I genes. Genetic distance among *COL* genes was the largest in group III, suggesting that group III genes undergo more relaxed selection pressure compared with the other groups. Expression patterns of *CaCOLs* in tissues were significantly different, with *CaCOL08* exhibiting the highest expression in stem and leaf. Some *COL* orthologous genes showed markedly different expression patterns in pepper compared with tomato, such as COL_1 orthologs, which may be involved in fruit development in pepper. In addition, *CaCOLs* participated in the regulation of abiotic stresses to varying degrees. Five *CaCOL* genes were induced by cold, and *CaCOL02* and *CaCOL03* were specifically upregulated by cold and downregulated by heat. This study provides a theoretical basis for the in-depth understanding of the functions of *COL* genes in pepper and their molecular mechanisms involved in growth and development and responses to abiotic stresses.

Keywords: COL, phylogenetic relationship, expression pattern, abiotic stress, *Capsicum annuum*

OPEN ACCESS

Edited by:
Pei Xu,
China Jiliang University, China

Reviewed by:
Arun K. Pandey,
China Jiliang University, China
Yuan Cheng,
Zhejiang Academy of Agricultural Sciences, China

****Correspondence:***
Weike Duan
weikeduan@126.com

† These authors have contributed equally to this work

Specialty section:
This article was submitted to Crop and Product Physiology, a section of the journal Frontiers in Plant Science

Received: *03 December 2021*
Accepted: *14 January 2022*
Published: *17 February 2022*

Citation:
Huang Z, Bai X, Duan W, Chen B, Chen G, Xu B, Cheng R and Wang J (2022) Genome-Wide Identification and Expression Profiling of CONSTANS-Like Genes in Pepper (Capsicum annuum): Gaining an Insight to Their Phylogenetic Evolution and Stress-Specific Roles. Front. Plant Sci. 13:828209. doi: 10.3389/fpls.2022.828209

INTRODUCTION

CONSTANS (*CO*), a crucial gene in the photoperiod flowering induction pathway of plants, is located in the circadian clock output pathway and promotes the flowering of plants by activating expression of the downstream floral gene *FLOWERING LOCUS T* (*FT*) (Putterill et al., 1995). *CO* was subsequently found to belong to a class of genes called the *CONSTANS-like* (*COL*) gene family (Griffiths et al., 2003). The *COL* gene family is widely distributed and the members vary greatly among different plant species. For example, 17 *COL* genes were identified in *Arabidopsis thaliana* (Griffiths et al., 2003), 9 in barley (Griffiths et al., 2003), 16 in rice (Griffiths et al., 2003), 26 in soybean (Wu et al., 2014), 42 in cotton (Cai et al., 2017), 19 in maize (Song et al., 2018), 20 in radish (Hu et al., 2018), 13 in tomato (Yang et al., 2020), and 22 in sunflower (Niu et al., 2022). *COL* genes are characterized based on two conservative domains. The first is the CONSTANS, CONSTANS-LIKE, TOC1 (CCT) domain at the C-terminus, which comprises 43 amino acids and conservatively plays a role in promoter elements binding, transcription regulation, and nuclear localization. The N-terminus of *COL* genes generally contains one to two B-box type zinc finger structures that can interact with ubiquitin ligase, receptor proteins, and transcriptional regulators (Robson et al., 2001; Valverde et al., 2004). According to the number and conservation of B-boxes, the *A. thaliana COL* gene family can be divided into three groups (Griffiths et al., 2003). Furthermore, in most other studied plants, the *COL* gene family clusters into three groups with strong bootstrap values. Both group I and group III genes stably contain two B-box domains in terrestrial plants before *Amborella trichopoda*. After the angiosperm whole-genome duplication (WGD) events, the first B-box domain in group I and the second B-box domain in group III were lost in some plant species (Song et al., 2015). Differentiation of the B-box domain has a crucial role in the phyletic evolution of *COL* genes (Song et al., 2015; Niu et al., 2022).

As transcription factors, *CO* was the first cloned in *A. thaliana*, regulating the flowering time in the photoperiod pathway (Putterill et al., 1995; Li and Xu, 2017). The function of *CO* may be conserved across the angiosperms. For example, *CrCO* (of *Chlamydomonas reinhardtii*) was overexpressed in *A. thaliana* to make flowering in advance (Tenorio et al., 2003), and *PtCO* was found to promote the early flowering of plants (Bohlenius et al., 2006). However, during evolutionary history, *COL* genes often exist in plants as multiple copies, displaying apparent functional differentiation in different plants. Moreover, not all the genes of this family are photoperiod related; several reports have demonstrated that *COL* genes are associated with plant development and even abiotic stress responses. *CrCO* may also participate in cell division and regulation of starch synthesis (Tenorio et al., 2003). In *Populus*, *PtCO* was involved in plant growth and bud differentiation (Bohlenius et al., 2006). *AtCOL3* promoted the development of lateral roots and shoot branches (Datta et al., 2006). *VvCOL1* was involved in regulating the maintenance and induction of bud dormancy in grape (Almada et al., 2009). *MaCOL1*, a transcriptional activator in banana, was reported to be associated with fruit ripening and abiotic stress tolerance (Chen et al., 2012). *AtCOL4* was proven to positively regulate tolerance to abiotic stresses (acid, salt, and osmotic stress) in the plant (Min et al., 2015). In rice, *Ghd2* participated in regulating leaf senescence and drought tolerance (Liu J. et al., 2016). *OsCOL9* was reported to regulate disease resistance dependent on ethylene and salicylic acid (SA) signaling pathways (Liu H. et al., 2016). *BnCOL2* in *Brassica napus* responded to drought stress (Liu et al., 2020), while *HaCOL3*, *HaCOL6*, and *HaCOL19* were induced by cadmium (Cd), heat, and drought stresses in sunflower (Niu et al., 2022). In adapting to adverse environments, *COL* genes have developed essential new functions in response to abiotic stresses.

CONSTANS-like genes have been studied in many plants, but there are no systematic reports of *COLs* in *Capsicum annuum*, a vital vegetable crop. Publication of the whole-genome sequence and high-quality physical map of *C. annuum* has laid the foundation for phylogenetic evolution and functional research of *COL* genes (Kim et al., 2014; Qin et al., 2014). Systematically analyzing conserved domains, evolutionary relationships, and the functional expression of *CaCOL* genes would provide theoretical support for further investigation of the molecular mechanism of *CaCOL* genes and vegetable-breeding research.

RESULTS

Members of the *CaCOL* Gene Family

Based on genome-wide identification and validation, all 10 *COL* gene family members were identified in the *C. annuum* cv. *Zunla-1* genome and were named *CaCOL01-CaCOL10* in order of chromosomal location (**Table 1**). Simultaneously, nine *COLs* were identified in *C. annuum* cv. *CM334* (**Supplementary Table 1**). The lengths of the 10 *COL* genes in the "*Zunla-1*" genome varied, with a maximum of 1410 bp (*CaCOL09*) and a minimum of 1,032 bp (*CaCOL01*). The molecular weights of CaCOLs were predicted to be between 37.93∼51.67 kD, and the isoelectric points were concentrated in 4.85∼7.07 (**Table 1**). Comparative analysis indicated that *CaCOL* genes and *AtCOL* genes had high sequence similarity (*E*-value < 5E-44).

Phylogenetic and Structure Characterization of CaCOLs

To understand the phylogenetic evolution of CaCOLs, the COL sequences of *A. thaliana*, tomato, and *C. annuum* cv. *Zunla-1* and *CM334* were selected for analysis. The COLs were divided into three groups (I, II, and III). In "*Zunla-1*," group I contained six COLs (*CaCOL01*, *CaCOL02*, *CaCOL03*, *CaCOL04*, *CaCOL07*, and *CaCOL08*), which was similar to the number of COLs in group I of *A. thaliana* and tomato. Group II of "*Zunla-1*" contained only one gene (*CaCOL05*), while group III contained three COLs (*CaCOL06*, *CaCOL09*, and *CaCOL10*) (**Figure 1A**). In the "*CM334*" genome, there were five COLs in group I, with one missing compared to "*Zunla-1*," groups II and III contained the same number of COLs as "*Zunla-1*." There were eight pairs of homologous COLs in the two varieties of *C. annuum* (**Figure 1A**).

TABLE 1 | The information of COL gene family in pepper *Zunla-1*.

Gene name	Gene accession No.	Size/aa	Length/bp	Chromosome location	MW/kD	pI	*Arabidopsis* homologous	*E*-value
CaCOL01	Capana01g004030	343	1,032	Chr01:278243944..278245872	37.93	5.44	AtCOL4	5.00E-94
CaCOL02	Capana02g003199	404	1,215	Chr02:157107846..157110095	44.56	5.42	AtCOL2	2.00E-97
CaCOL03	Capana02g003200	398	1,197	Chr02:157118313..157120062	43.89	5.23	AtCOL2	5.00E-44
CaCOL04	Capana02g003201	407	1,224	Chr02:157124787..157126407	45.39	5.27	AtCOL2	7.00E-84
CaCOL05	Capana03g000377	382	1,149	Chr03:5273465..5275489	43.46	5.52	AtCOL6	3.00E-90
CaCOL06	Capana03g003558	387	1,164	Chr03:228734754..228738294	43.34	5.45	AtCOL13	7.00E-83
CaCOL07	Capana07g000030	384	1,155	Chr07:1563552..1565426	42.54	6.99	AtCOL5	1.00E-89
CaCOL08	Capana12g000414	356	1,071	Chr12:8179392..8181909	39.43	5.24	AtCOL4	2.00E-97
CaCOL09	Capana00g001486	469	1,410	Chr00:399610115..399614902	51.67	7.07	AtCOL14	1.00E-97
CaCOL10	Capana00g004489	426	1,281	Chr00:649683777..649686080	46.86	4.85	AtCOL12	7.00E-103

MW, molecular weight; pI, isoelectric point.

There was apparent differentiation in gene structure characteristics among the three subgroups of COLs, but a relatively similar gene structure was present within the groups (**Figure 1B**). The number of exons in groups I and II was approximately two to three but reached approximately five in group III. In addition, the intron lengths of COLs in groups I and II were similar. *CaCOL09* and *SlyCOL10*, contained longer introns than the other genes, exceeding 4 kb. Such phenomenon of intron-exon structural alienation may be due to differentiation of gene function during evolution.

Through analysis of the conserved domains of *A. thaliana* and *C. annuum* cv. *Zunla-1* COL proteins (**Figure 2**), 10 conserved motifs were identified and annotated. Each COL protein contained Motif 1 and 2, indicating that the CCT domain and the B-box domain were the essential functional domains. However, in the three subgroups, there was significant differentiation of B-box domains. Groups I and III both contained two B-boxes, but only one B-box domain was conserved, with the first B-box in group I and the second B-box in group III exhibiting markedly different structures. There was only one B-box domain in group II (**Figure 2**). Among the three subgroups, group I had the most complex structure and contained seven types of motifs, group II had the simplest motif type, with only three types, and group III contained four types of motifs. COL homologous proteins of *A. thaliana* and *C. annuum* had similar conserved domains, indicating that they may have similar functions (**Figure 2**).

Cis-Elements Analysis in the Promoters of *CaCOL* Genes

The *cis*-elements in the upstream 2-kb regions of the *CaCOL* gene sequences were analyzed to predict the functions of *CaCOLs*. The promoter regions of *CaCOL* genes contained different types and numbers of *cis*-elements (**Figure 3**). All 10 genes contained light response *cis*-elements, the stress response *cis*-element (MYB), and the cold resistance *cis*-element recognition site (MYC). In addition, two of the *CaCOL* genes contained the drought response *cis*-element (MBS), and nine of the genes contained the abscisic acid response *cis*-element (ABRE). The *CaCOL* genes also included a variety of hormone response *cis*-elements. These findings indicated that *CaCOLs* might participate in plant growth, development, and resistance to adversity stresses.

Chromosomal Location and Homologous Genes of *CaCOL* Genes

Chromosome location analysis showed that eight of the ten *CaCOL* genes were anchored on five chromosomes of *C. annuum*—Chr01, Chr02, Chr03, Chr07, and Chr12 (**Figure 4A**). Three tandem duplicated genes were found on Chr02 (**Figure 4A**).

COL homologous analysis identified six orthologous gene pairs between *A. thaliana* and *C. annuum*, eight pairs between *A. thaliana* and tomato, and 13 pairs between *C. annuum* and tomato. In addition, only three paralogous gene pairs were found in *C. annuum* and tomato, while seven were identified in *A. thaliana* (**Figure 4B** and **Supplementary Table 2**).

Evolution Pattern Analysis of CONSTANS-Like Genes

CONSTANS-like gene family members of 12 plant species (*Arabidopsis thaliana*, *Brassica rapa*, *Carica papaya*, *Populus trichocarpa*, *Fragaria vesca*, *Vitis vinifera*, *Solanum tuberosum*, *Solanum lycopersicum*, *C. annuum* cv. *Zunla-1, Zea mays*, *Oryza sativa*, and *Amborella trichopoda*) were selected to reconstruct a phylogenetic tree (**Supplementary Table 3**) and further explore the evolutionary history of COLs. In the chosen angiosperms, *A. trichopoda* is one of the species known to exist for the longest time among existing angiosperms without experiencing ancient hexaploid (γ) events, while *C. papaya*, *P. trichocarpa*, and *V. vinifera* did not undergo α and β duplications, and Solanaceae crops have experienced unique whole-genome triplication (WGT) events. All *COL* genes were divided into three subgroups: groups I, II, and III (**Figure 5A**). Genetic distance was analyzed to further determine the relationship among the three subgroups (**Figure 5B**). The box plot revealed that genetic distances of the *COL* genes were the smallest in group I and the largest in group III, indicating that the degree of sequence divergence of group I was the lowest. The genetic distance of group II versus group III was higher than those of group I versus group II and group I versus group III, indicating that groups II and III may be differentiated from group I during the evolutionary process. The genetic distance was bigger among the three groups than within the three

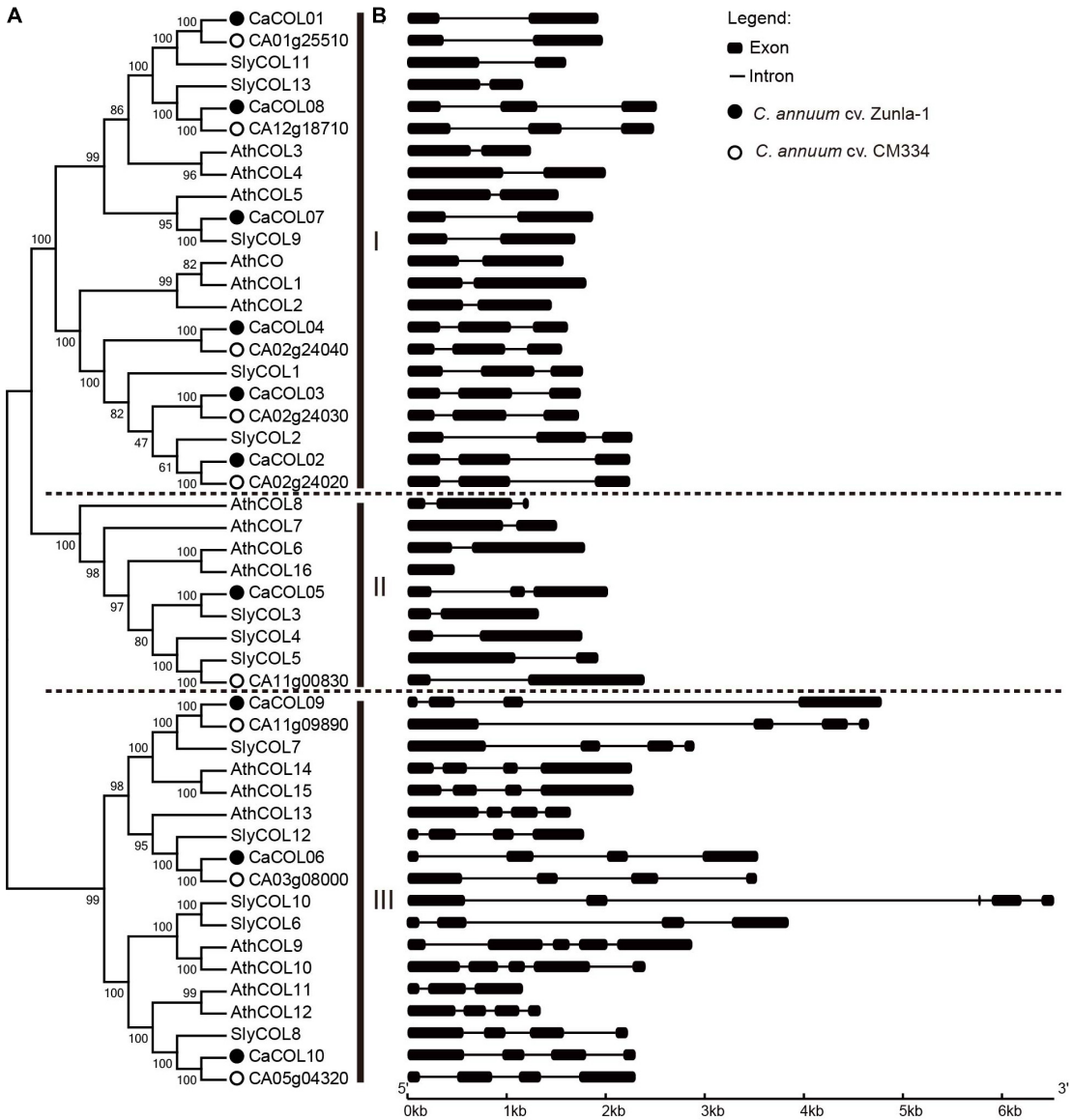


FIGURE 1 | Phylogenetic analysis **(A)** and gene structures **(B)** of COL homologs in *Capsicum annuum*, *Solanum lycopersicum*, and *Arabidopsis thaliana*. The phylogenetic relationship of COLs categorized them into three groups (I, II, and III). COLs of *C. annuum Zunla-1* and CM334 are indicated by black balls and hollow circles, respectively. Exons and introns are represented by black boxes and black lines, respectively.

groups, confirming that the COL gene family was divided into three groups.

Copy number variation of the COL family in the 12 selected plant species was subsequently determined (**Figure 6**). The COLs in *A. trichopoda* had already been divided into three subgroups (**Figure 6**). In *A. thaliana* and *B. rapa*, the cruciferous plants, groups I and III had the most apparent gene amplification (**Figure 6**). The number of *COL* genes in *Z. mays* and *O. sativa* was the same, but group III genes of *O. sativa* had been significantly amplified and differentiated, indicating that these genes may play a regulatory role in the growth of *O. sativa* (**Figure 6**). In the three Solanaceae crops, the copy number of *COL* genes was significantly different; *S. tuberosum* contained the most, while *C. annuum* had the least. Moreover, in *C. annuum*, only one group II gene was retained (**Figure 6**).

Expression Divergence of the *CaCOL* Genes in Different Tissues

To investigate the divergence of *COL* homologs, the expression patterns of *CaCOL* genes were analyzed based on the transcriptome data of different tissues and fruit development stages of *C. annuum* cv. *Zunla-1*. The expression patterns of *CaCOL* genes showed tissue specificity and a high degree of similarity between genes from the same clade of the phylogenetic tree (**Figure 7A**). In group I, the genes were clustered into

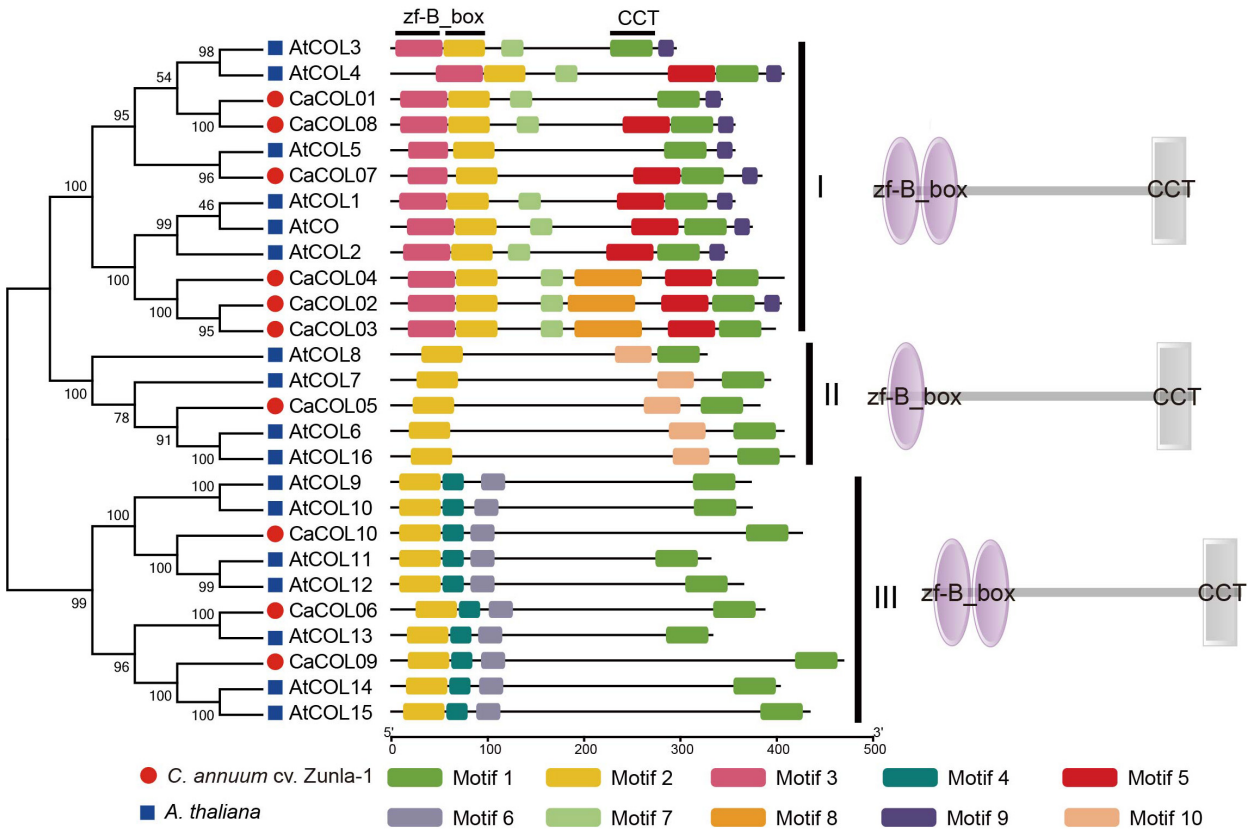


FIGURE 2 | Analysis of conserved domains of COL proteins in *Capsicum annuum* and *Arabidopsis thaliana.* CaCOLs and AtCOLs are indicated by red balls and blue boxes, respectively. B-box and CCT domains were annotated by the SMART database.

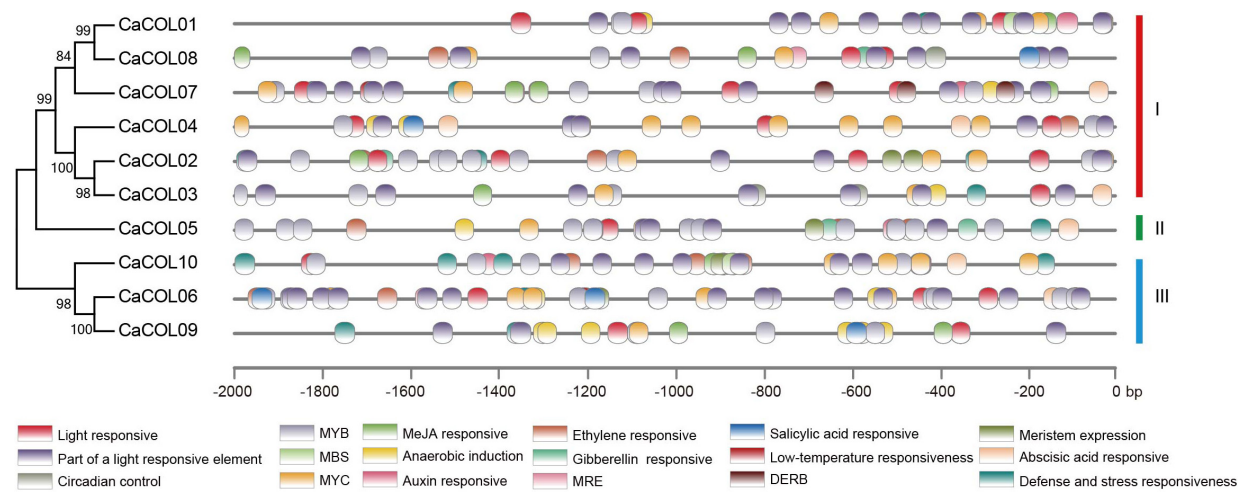


FIGURE 3 | Predicted *cis*-elements in the promoter regions of *CaCOL* genes. Promoter sequences (-2000 bp) of *CaCOL* genes were analyzed. The elements are identified as different colored boxes.

two clades. The first clade included *CaCOL01*, *CaCOL07*, and *CaCOL08*, All three of these genes exhibited high expression in the primary tissues, with *CaCOL08* showing the highest expression of all *CaCOL* genes in the stem and leaf, while *CaCOL07* was expressed at a low level once the fruit had turned color. The second clade of group I comprised *CaCOL02*, *CaCOL03*, and *CaCOL04*, and these genes were either not expressed or were expressed at low levels in most of the

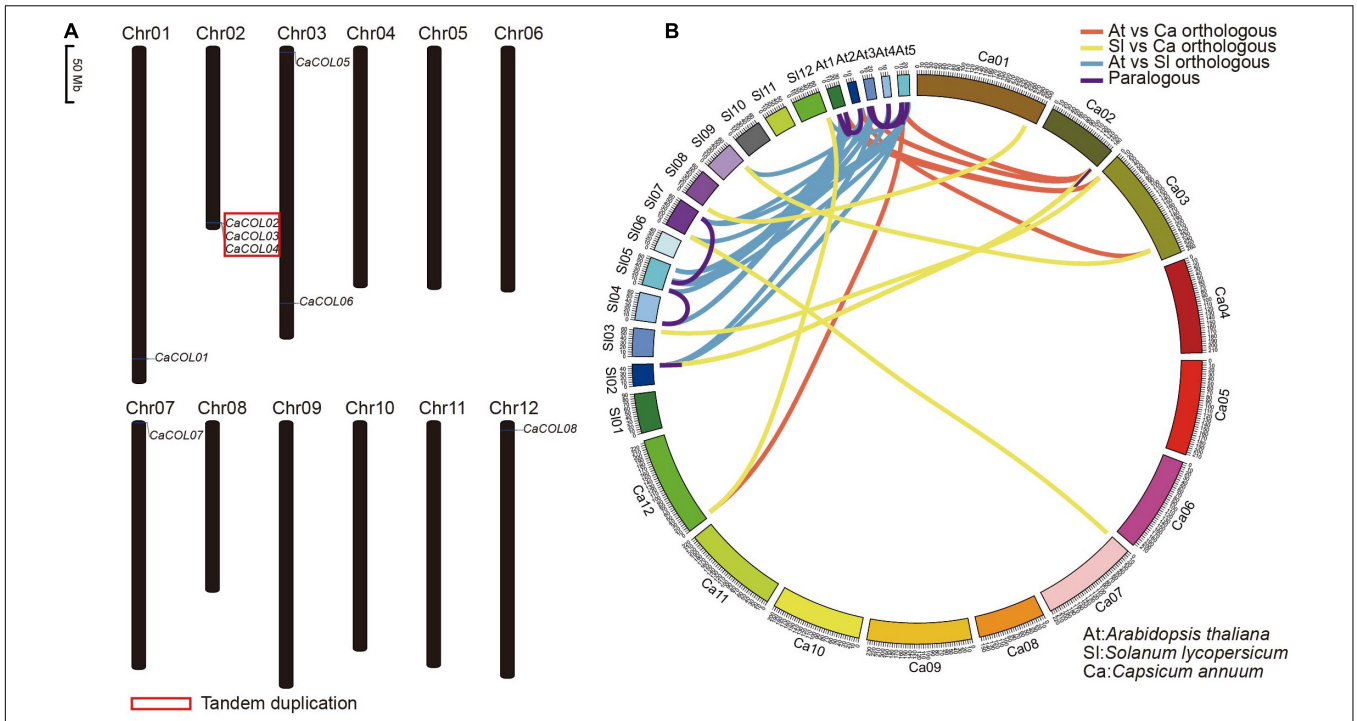


FIGURE 4 | Chromosomal localization of *CaCOL* genes **(A)** and the relationship of *COL* homologous genes among *Capsicum annuum*, *Solanum lycopersicum*, and *Arabidopsis thaliana* **(B)**. The red box indicates tandem duplicated genes. Lines showing orthologous gene pairs between *A. thaliana* and *C. annuum* are red; those between *S. lycopersicum* and *C. annuum* are yellow; and those between *A. thaliana* and *S. lycopersicum* are blue. Lines showing paralogous gene pairs are pink.

investigated tissues, except for *CaCOL02*, which was only expressed at moderate levels in the stem. The sole gene of group II—*CaCOL05*—was expressed at high levels in the stem and leaf but exhibited low or no expression in other tissues. In group III, *CaCOL06*, *CaCOL09*, and *CaCOL10* showed two distinct expression patterns. *CaCOL10* was barely expressed in all tissues except in the stem, while *COL06* and *CaCOL09* were expressed at high or moderate levels in all tissues tested. These findings indicate that *CaCOL* genes play a crucial role in plant growth and undergo functional differentiation (**Figure 7A**).

To further understand the correlation between *CaCOL* genes and their homologous genes, correlation between the expression trends of *CaCOL* genes was explored by calculating Pearson Correlation Coefficient (PCC) values and then constructing a co-regulatory network by screening significantly co-expressed gene pairs (**Figure 7B**). *CaCOL06* and *CaCOL09* were at the central node of the co-expression network, and *CaCOL06* had a strong co-expression relationship with four genes simultaneously, indicating that this gene may be at the central node position in the *C. annuum* growth and development regulatory network (**Figure 7B**).

Subsequently, transcriptome data of different tissues and developmental stages of *C. annuum* cv. *CM334* and tomato were analyzed (**Supplementary Figures 1, 2**), and the expression patterns of seven groups of *COL* orthologous genes were compared (**Supplementary Figure 3**). The expression patterns of *COL* orthologous genes were both similar and opposite in pepper and tomato. Four of the seven groups of *COL* orthologous genes showed almost identical expression patterns, namely COL_2, COL_5, COL_6, and COL_7. Orthologous genes in the COL_2 group were highly expressed in leaf tissues of both tomato and pepper, and at low levels during fruit development, especially at breaker stage. In the COL_5 group, the orthologous genes were expressed highly in bud tissues. Both COL_6 and COL_7 orthologous genes were expressed in all tissues tested, but expression levels were higher in pepper compared with tomato (**Supplementary Figure 3**). The other three groups of orthologous genes (COL_1, COL_3, and COL_4) showed different expression patterns in the two plant species. COL_1 genes were highly expressed in pepper fruit but not in tomato fruit at the breaker stage, while COL_3 genes were the opposite, with very low expression or almost no expression in pepper fruit and higher expression in tomato fruit. COL_4 genes were barely expressed in all tissues of pepper but were expressed in tomato throughout fruit development (**Supplementary Figure 3**). The expression patterns of most genes were consistent in both pepper varieties, with only the COL_2 genes being expressed in the "*Zunla-1*" stem at higher levels than in "*CM334*" (**Supplementary Figure 3**).

Diurnal Rhythm Expression Patterns of *CaCOL* Genes

CONSTANS-like genes are reported to exhibit prominent circadian rhythm characteristics. Therefore, the expression patterns of 10 *CaCOLs* during 24 h were studied under long-day

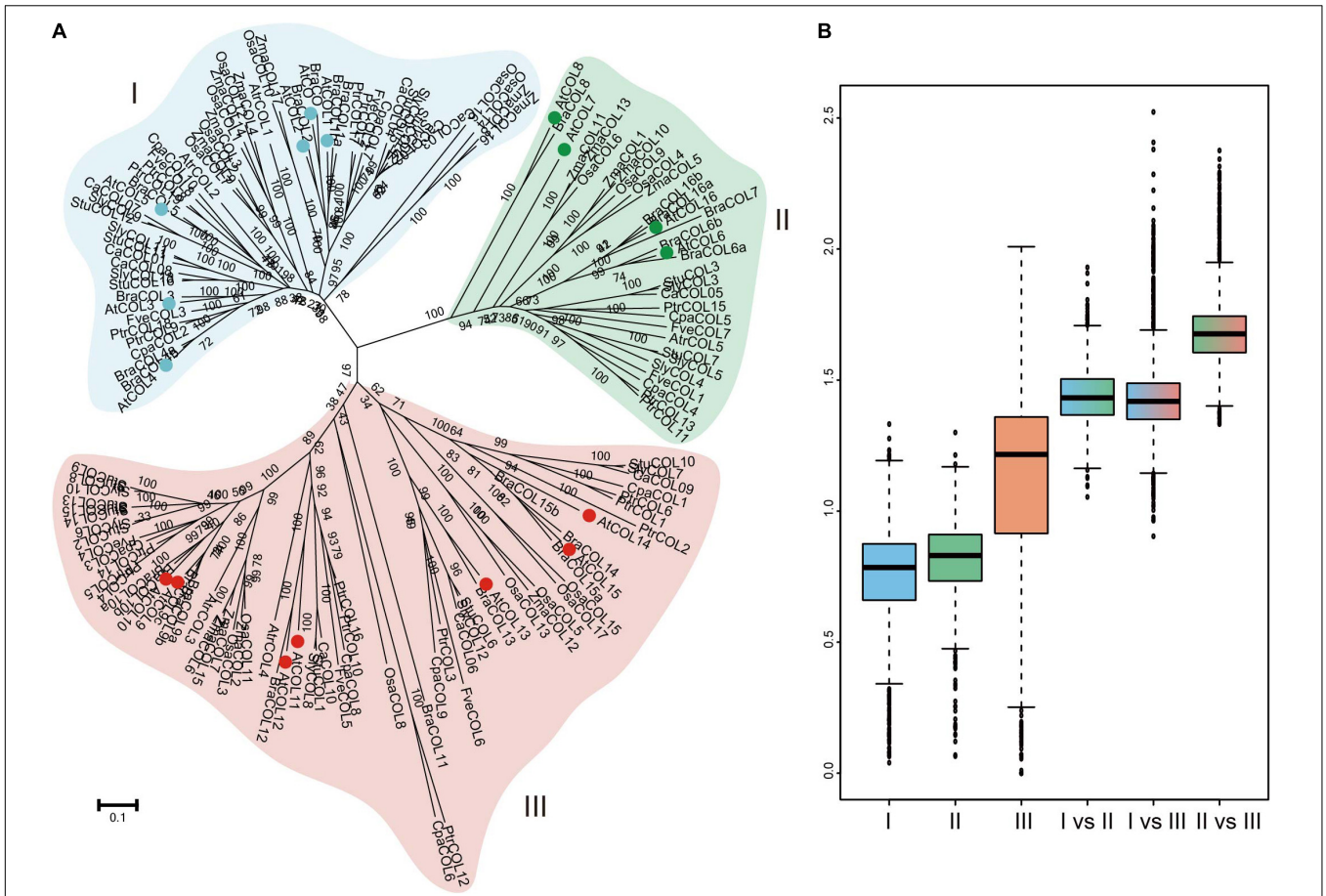


FIGURE 5 | Phylogenetic relationship of *COL* gene family members in 12 selected plant species **(A)** and nucleotide distance of group I, II, and III *COL* genes **(B)**. Group I, II and III of AtCOLs are indicated by blue, green and red balls, respectively.

(LD) conditions. All genes, except *CaCOL04* and *CaCOL10*, could be induced by light conditions (**Figure 8**). During the 24 h cycle, the expression of *CaCOL01*, *CaCOL02*, *CaCOL03*, *CaCOL05*, and *CaCOL08* peaked and then decreased at 4 or 8 h after dawn and did not change significantly in the dark (**Figure 8**). *CaCOL07* reached a peak at 12 h, while *CaCOL06* peaked at 16 h, and *CaCOL09* maintained a high expression level from 4 to 16 h (**Figure 8**).

Expression Patterns of CaCOLs Under Abiotic Stresses

The expression patterns of the 10 *CaCOL* genes under four abiotic stresses (cold, heat, salt, and osmotic) were analyzed by qRT-PCR (**Figure 9**). Under cold treatment, five *CaCOL* genes were induced, among which the expression of *CaCOL02*, *CaCOL03*, *CaCOL07*, and *CaCOL8* peaked at 12 h after treatment and then decreased, while *CaCOL06* expression peaked at 24 h. Eight *CaCOL* genes participated in the resistance to high-temperature adversity to varying degrees—five genes (*CaCOL01*, *CaCOL06*, *CaCOL07*, *CaCOL08*, and *CaCOL09*) were upregulated, and three genes (*CaCOL02*, *CaCOL03*, and *CaCOL05*) were downregulated. Most genes did not respond strongly to NaCl treatment, with some genes presenting a downward trend in expression, including *CaCOL02*, *CaCOL05*, and *CaCOL07*. Under osmotic stress, the expression levels of *CaCOL02*, *CaCOL03*, *CaCOL07*, and *CaCOL08* were upregulated after 2 h of treatment, while the other genes showed little or no change in expression (**Figure 9**).

DISCUSSION

To meet physiological needs and adapt to the external environment during the process of growth and development, plants usually control gene expression in vivo from multiple dimensions and levels, among which transcription level regulation is a crucial step (Jiao et al., 2007; Fornara et al., 2010). CO, located in the output pathway of the circadian clock, specifically activates the *FT* gene promoter to upregulate expression of the genes *FT* and *SUPPRESSOR OF OVEREXPRESSION OF CONSTANS 1* (*SOC1*), thus CO is an essential gene that regulates the photoperiod pathway and plays a central regulatory role (Yoo et al., 2005; Jiao et al., 2007; Tiwari et al., 2010). Members of the *COL* gene family have been identified in detail in the model plant *A. thaliana* and many

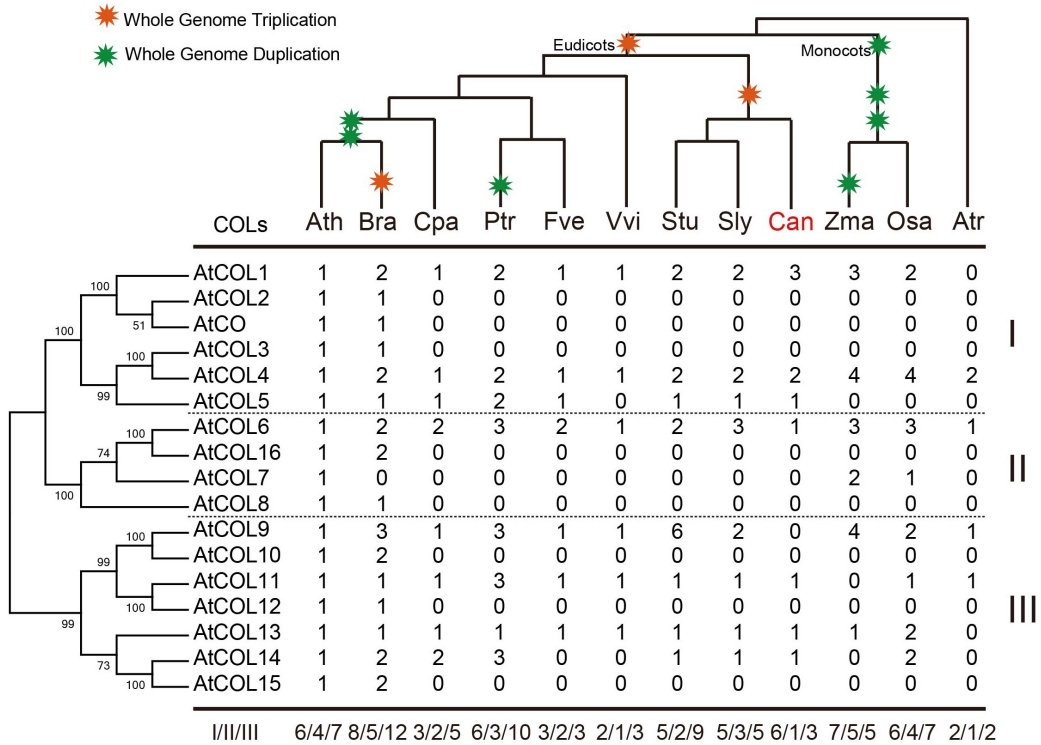


FIGURE 6 | Copy number variation of the COL family in 12 selected plant species. The phylogenetic tree of AtCOLs is shown on the left, and the species tree is shown at the top. Whole-genome duplication and triplication events are indicated on the tree branches according to the Plant Genome Duplication Database. Numbers are copy numbers of each gene in *Arabidopsis thaliana* (Ath), *Brassica rapa* (Bra), *Carica papaya* (Cpa), *Populus trichocarpa* (Ptr), *Fragaria vesca* (Fve), *Vitis vinifera* (Vvi), *Solanum tuberosum* (Stu), *Solanum lycopersicum* (Sly), *Capsicum annuum* (Can), *Zea mays* (Zma), *Oryza sativa* (Osa), and *Amborella trichopoda* (Atr). Statistics of copy number variation of the *COL* genes are based on the phylogenetic relationships.

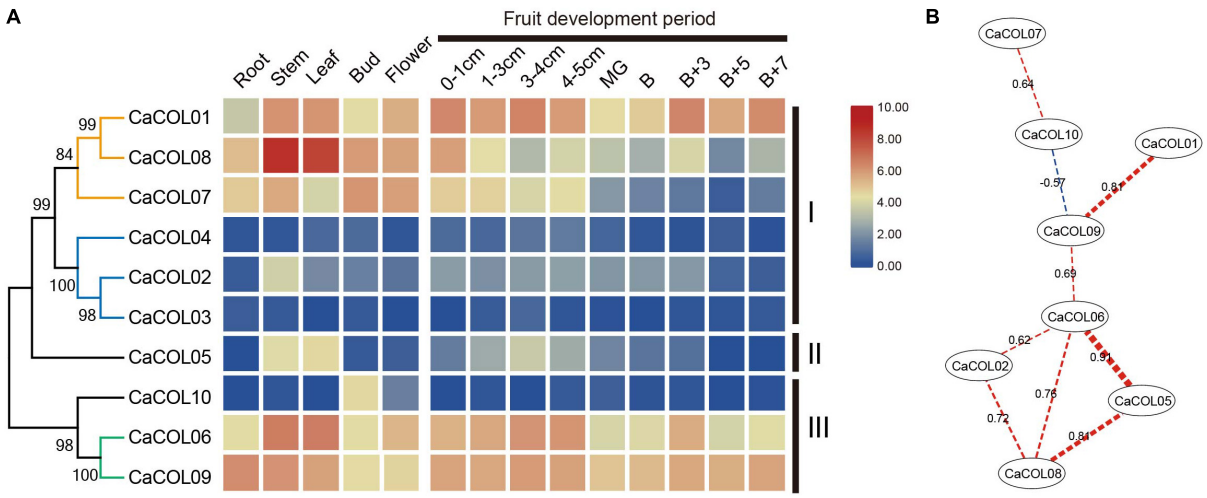


FIGURE 7 | Expression patterns **(A)** and co-expression networks **(B)** of *CaCOL* genes in different tissues and at different stages of the fruit development process. Co-expression networks of *CaCOL* genes were established based on the PCCs of these gene pairs using transcriptome data, which involved eight nodes and nine regulatory edges.

other species (Griffiths et al., 2003; Song et al., 2015). *C. annuum* is an important vegetable crop, but there are limited studies on *COL* genes in this species. In the current study, 10 and 9 *COL* genes were identified in the genomes of two varieties—"*Zunla-1*" and "*CM334*"—of *C. annuum*, respectively, and these genes could be divided into three subgroups. *COL* genes of "*Zunla-1*"

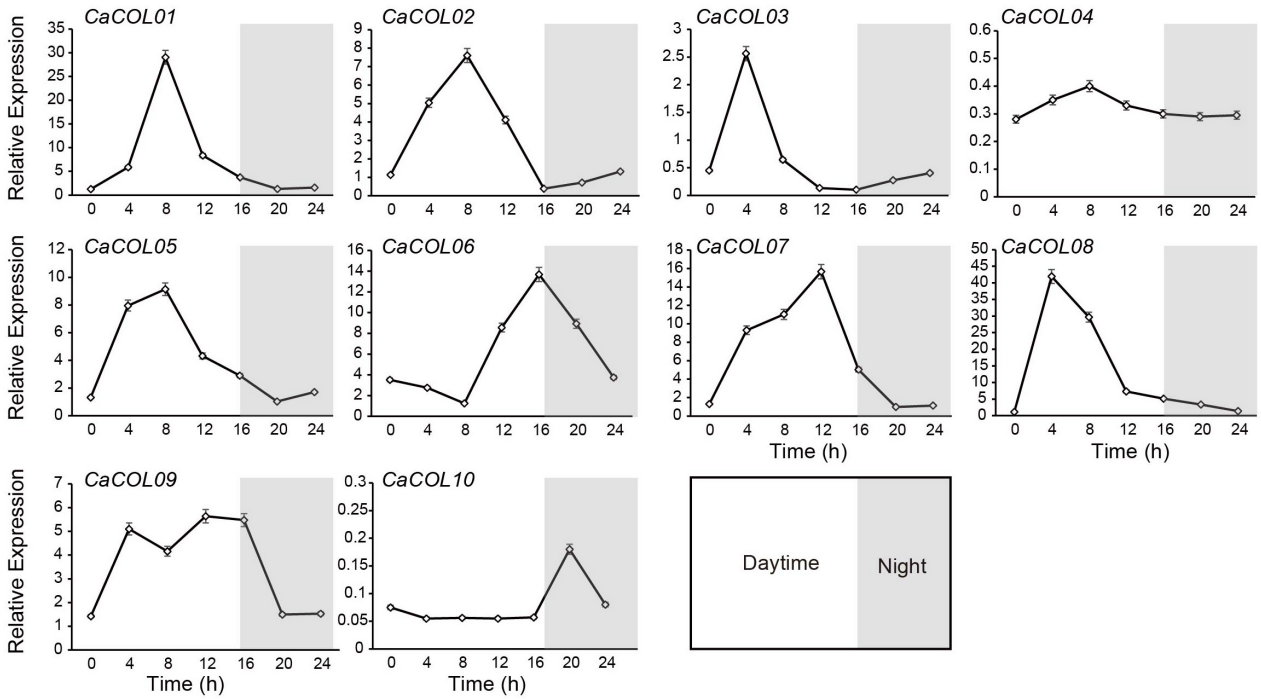


FIGURE 8 | Effect of light on the expression patterns of *COLs* in pepper leaves. Line charts indicate transcript levels of *COL* genes. For each sample, transcript levels were normalized with those of actin (control). Data are the mean values ± standard deviation (SD) of three individual experiments ($n = 3$).

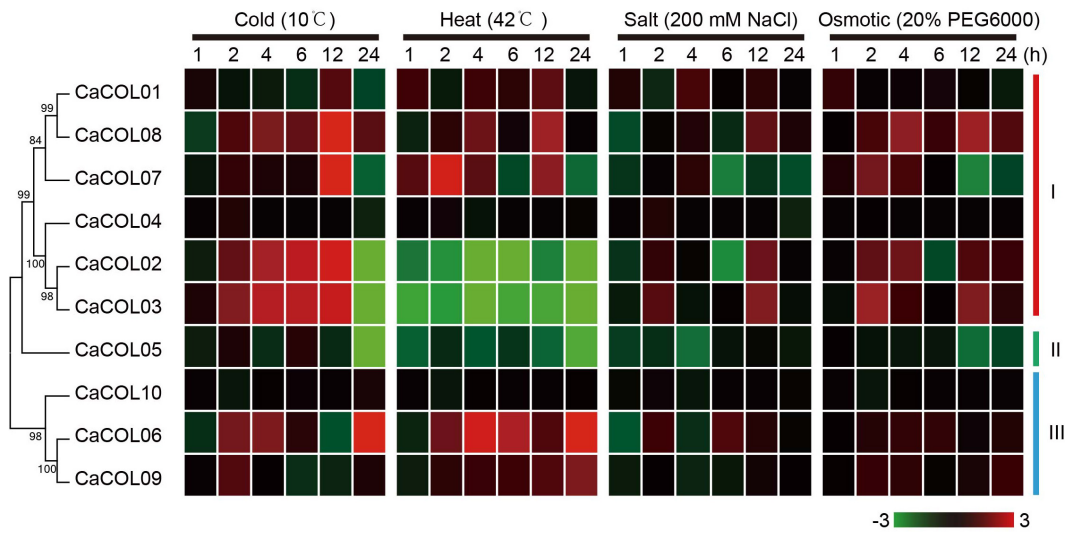


FIGURE 9 | Expression of *CaCOL* genes under cold, heat, salt, and osmotic stress. The bar at the bottom of each heat map represents the relative expression values.

were distributed on five chromosomes, while those of "*CM334*" were distributed on six chromosomes. This may be due to chromosomal splicing or gene differentiation between varieties of *C. annuum*.

CONSTANS-like family members possess three conserved domains, two B-box domains and a CCT domain (Griffiths et al., 2003). B-box domains were markedly differentiated among the *CaCOL* genes, while the CCT domain was relatively more conserved. Phylogenetic analysis indicated that the B-box domain plays a crucial role in the phyletic evolution of *COL* gene family, which is consistent with previous studies (Griffiths et al., 2003; Song et al., 2015). The evolution of plant regulatory genes is relatively fast and the evolutionary rate is significantly different among different regions of COL family

genes (Lagercrantz and Axelsson, 2000). Although both group I and group III COLs contain B-box domains, the domains of the two groups differ significantly. B-box domains of groups I and III were missing in some dicots (Song et al., 2015), but such loss was not observed in *C. annuum*. Compared with *A. thaliana*, the gene structures of *CaCOL* genes were relatively conserved in groups I and II, while those of group III showed apparent differentiation. Investigation of genetic diversity was critical in linking selection pressure to specific genes (Fu et al., 2010; Fiil et al., 2011; Wei et al., 2011). The lower the nucleotide diversity, the greater the selection pressure (Whitt et al., 2002). In the current study, COLs of 12 representative plants (*A. thaliana*, *B. rapa*, *C. Papaya*, *P. trichocarpa*, *F. vesca*, *V. vinifera*, *S. tuberosum*, *S. lycopersicum*, *C. annuum* cv. *Zunla-1*, *Z. mays*, *O. sativa*, and *A. trichopoda*) were analyzed to further explore the evolutionary history of the COLs. Genetic distance between *COL* genes was the biggest in group III and the smallest in group I, suggesting that *COL* genes in group III undergo more relaxed selection pressure during evolution compared with genes of the other two groups. The more extensive selection pressure and structural differences in group III may account for the functional differentiation of group III *COL* genes. Among the three groups of COLs, genetic distance was the smallest between groups I and III, and the largest between groups II and III, suggesting that groups II and III may be differentiated from group I (**Figure 5B**).

During their long evolutionary history, angiosperms have undergone different WGD events that induced gene duplication and differentiation (Taylor and Raes, 2004; Lee et al., 2012; Rensing, 2014). Due to the different regions and external environments of different plants, homologous genes are partially lost and partially retained during evolution. Retained genes undergo functional differentiation, leading to gradually different regulatory mechanisms (Wang et al., 2015). Analysis of the replication and retention of *COL* genes in the 12 selected plants demonstrated that *COL* genes had also undergone duplication, loss, retention, and differentiation during the evolutionary history of the plants, especially during the genome duplication event. Starting from the relict plant *A. trichopoda*, angiosperm genomes have undergone different WGD or WGT events (Clark and Donoghue, 2018), with the *COL* genes of groups I, II, and III presenting unequal amplification among the 12 angiosperm species. Compared with other angiosperms, group I *COL* genes of *C. annuum* had the highest proportion of retained genes, which was mainly caused by tandem replication. However, the tandem duplication genes (*CaCOL02*, *CaCOL03*, and *CaCOL04*) in group I were not significantly expressed in different tissues but did respond to abiotic stresses, thus they may exist as backup genes in response to other environmental factors, as indicated in a previous study (Qian et al., 2010; Duan et al., 2016). Among the other species, group III had the most retained genes, especially in *B. rapa*, which had up to 25 genes. Segmental duplications may be one of the reasons for this phenomenon (Song et al., 2015). Therefore, amplification of group III is presumed to be the main reason for the increase in the number of genes in the COL family. COLs play an essential regulatory role in the photoperiod pathway, but in the 12 selected species, which included typical long- and short-daylight plants, no obvious retention rule was found for *COL* genes. This indicated that photoperiod regulation had not affected the number of retained *COL* genes. Specific gene structures or functional differentiation of individual genes may account for their functions.

Obvious functional differentiation was also found in *COL* orthologous genes of the two varieties of *C. annuum*. Among these orthologous genes, four pairs had an identity up to 100%, while the remaining four pairs exhibited an average identity of 97.79%. The eight pairs of orthologous genes displayed similar expression trends in leaves, but in root tissue, only one gene was highly expressed in "*CM334*" and three genes were highly expressed in "*Zunla-1*." Most of the *COL* orthologous genes in *C. annuum* and tomato had similar expression patterns in different tissues and developmental stages, but with considerable differences in some expression levels. These findings and analyses demonstrated that *COL* genes display great conservation but have also experienced loss and differentiation. This may be because different selection pressures in different environments result in different degrees of retention of *COL* genes, and during the retention process, some genes have undergone new functionalization or sub-functionalization.

COLs are instrumental in photoperiod regulation. Previous studies showed that transcription levels of COLs in tomato and *Arabidopsis* were regulated by circadian rhythms (Suarez-Lopez et al., 2001; Steinbach, 2019; Yang et al., 2020). In the current study, the expression patterns of *CaCOL* genes also exhibited a clear circadian rhythm under light induction. Under LD conditions, the expression trends of most homologous genes in pepper and tomato were similar, but they differed significantly from those in *Arabidopsis* (Suarez-Lopez et al., 2001; Yang et al., 2020). Expression patterns analysis showed that expression of *CaCOL01*, *CaCOL02*, *CaCOL03*, and *CaCOL08* peaked at 4 or 8 h after dawn, and their homologs in tomato had similar expression trends (Yang et al., 2020). However, *CaCOL01* and *CaCOL08*, as homologous genes of *AtCOL4*, were expressed at different levels in LD conditions. Additionally, the *CaCOL* genes showed different circadian rhythms (**Figure 8**), suggesting functional divergence of these genes in multiple aspects of plant development in response to the photoperiod. This may be because different species have different photoperiod requirements and that structurally similar genes have diverged functionally within or between species. In addition, COLs are also involved in the regulation of the development of different tissues, such as *GmCOL9* in soybeans and *MaCOL1* in bananas (Huang et al., 2011; Chen et al., 2012). In *C. annuum*, *CaCOL01*, *CaCOL06*, *CaCOL08*, and *CaCOL09* were highly expressed in stem and leaf. In addition, *CaCOL01*, *CaCOL08*, and *CaCOL07* were homologous to CO have higher expression in flower buds and flower tissues, and *CaCOL01*, *CaCOL06*, and *CaCOL09* were highly expressed during fruit development. These findings indicated that *CaCOL* genes play an important regulatory role in *C. annuum* growth and development.

Analysis of the promoter regions of the *CaCOL* genes revealed that the regions contained not only light response elements but also a variety of adversity stress response elements, suggesting *CaCOL* genes may be associated with resistance to abiotic stress. *COL* homologous genes, such as *MaCOL1* (Chen et al., 2012),

AtCOL4 (Min et al., 2015), OsCOL9 (Liu H. et al., 2016), *Ghd2* (Liu J. et al., 2016), and *BnCOL2* (Liu et al., 2020), were reported to be involved in adversity expression in other plant species. In pepper, five *CaCOL* genes (*CaCOL02*, *CaCOL03*, *CaCOL06*, *CaCOL07*, and *CaCOL08*) were expressed under the four adversity treatments (cold, heat, salt, and osmotic stress), with all five genes significantly expressed in the temperature treatments. *CaCOL02* and *CaCOL03* were upregulated in low temperatures and downregulated in high temperatures. A previous study showed that the CO-HOS1 module was crucial for fine-tuning of photoperiodic flowering under short-term temperature fluctuations (Jung et al., 2012). This may be one of the reasons why *COL* genes respond to temperature regulation. The *CaCOL* genes may help plants better adapt to the survival environment by changing the flowering time in response to adversity. Results from the current study provide a specific direction for studying stress-tolerance mechanisms in plants.

CONCLUSION

This study investigated the evolutionary characteristics and expression function of *C. annuum COL* genes and included structural characteristics, replication types, evolutionary patterns, and expression analysis. Findings from this study lay the foundation for the in-depth understanding of the function of the *COL* gene family members in *C. annuum* and will facilitate research on the molecular response mechanism of these genes during growth and development.

MATERIALS AND METHODS

Identification of CONSTANS-Like Gene Family in Pepper

Pepper (*C. annuum* cv. *Zunla-1* and *CM334*) genome data were downloaded from Solanaceae Genomics Network[1] (Kim et al., 2014; Qin et al., 2014). To identify all COL family genes in the pepper genome, a batch Basic Local Alignment Search Tool (BLAST) search was performed against the pepper genome data using the full-length amino acid sequences of COs and COLs of *Arabidopsis* (Griffiths et al., 2003) as queries with an *E*-value cut-off of 1×10^{-10}. All retrieved protein sequences were submitted to Pfam[2] databases to annotate the protein domains. Only proteins containing the N-terminal B-box domain (PF00643.19) and C-terminal CCT domain (PF06203.9) were considered to be COL homologs in pepper. Candidate genes were verified in Simple Modular Architecture Research Tool (SMART) and National Center for Biotechnology Information (NCBI) databases to derive the final sequences.

Physical and chemical properties of the CaCOL proteins, including molecular weight (MV) and isoelectric point (pI), were determined and analyzed using EMBOSS programs[3].

[1]https://solgenomics.net/organism/Capsicum_annuum/genome

[2]http://pfam.xfam.org/

[3]https://www.ebi.ac.uk/Tools/emboss/

Phylogenetic Tree, Gene Structure, and Conserved Domain Analysis of CONSTANS-Like Gene Family Members

Multiple sequence alignment analyses were performed using the CLUSTALW program (Thompson et al., 2002). Phylogenetic trees were then reconstructed by the Neighbor-Joining (NJ) method with a bootstrap value of 1000, using MEGA 6.0 software. The genetic distance of *COL* genes was also calculated using MEGA 6.0 software (Tamura et al., 2013).

Gene structure was plotted using the online tool Gene Structure Display Server (GSDS)[4]. Based on the *Arabidopsis thaliana* General Feature Format (GFF) file and *C. annuum* genome annotation information, the local Perl program was used to extract the location information of exons and introns and convert them into a GSDS readable bed. Online software MEME 4.9.0 was used to predict and analyze structural domains of COL protein sequences of *A. thaliana* and *C. annuum*; the motif search value was set to 10, the structural domain width was set to a minimum of 10 and a maximum of 100, and the other parameters used default settings. MEME structures were plotted using Tbtool software (Chen et al., 2020). The COL domain model was analyzed through the SMART database[5].

Chromosome Location and Orthologous and Paralogous Genes of the CaCOL Gene Family

Chromosome position information of *CaCOL* genes was obtained through the GFF file of annotation information of *the C. annuum* genome. The local Perl program was used to extract location information and construct the *C. annuum* chromosome map. The duplication type of *CaCOL* genes was analyzed by duplicate_gene_classifier, the downstream program of MCScanX (Wang et al., 2012).

OrthoMCL[6] software was used to identify orthologous and paralogous *COL* genes of *C. annuum*, *S. lycopersicum*, and *A. thaliana* (Li et al., 2003). Orthologous and paralogous relationship diagrams of *COL* genes in the three genomes were plotted using Circos software[7] (Krzywinski et al., 2009).

Prediction of *Cis*-Elements in Promoters of CaCOL Genes

Based on the genome sequence of *C. annuum* cv. *Zunla-1* (Qin et al., 2014), the upstream 2-kb sequences of *CaCOL* genes were extracted using the local Perl program and submitted to the PlantCARE website[8] for prediction of *cis*-acting elements. Finally, a *cis*-element distribution map was plotted by Tbtool software (Chen et al., 2020).

[4]http://gsds.cbi.pku.edu.cn

[5]http://smart.embl-heidelberg.de

[6]http://orthomcl.org/orthomcl/

[7]http://circos.ca/

[8]http://bioinformatics.psb.ugent.be/webtools/plantcare/html/

Analysis of Expression of CaCOL Genes in Different Tissues

Transcriptome data from different tissues and fruit development stages of *C. annuum* cv. *Zunla-1*, *C. annuum* cv. *CM334*, and tomato were explored in this study (Tomato Genome Consortium, 2012; Kim et al., 2014; Qin et al., 2014). An expression heatmap was plotted using R software (R Core Team, 2013). Pearson correlation coefficient (PCC) values of the expression relationships among *CaCOL* genes in different tissues were calculated by the local Perl program, and the co-expression network was constructed with the Cytoscape 3.7 program (Shannon et al., 2003).

Planting and Treating of Pepper

The pepper cultivar "Xianhong No. 1" was used for expression pattern analysis. Seeds were disinfected (2% sodium hypochlorite) and sown in the growth room of Huaiyin Institute of Technology, Jiangsu Province, China at 25/18°C day/night temperature, and with a 16/8-h light/dark cycle, relative humidity of 60–70%, and light intensity of 6000 Lux. Various treatments were applied to 45-day old seedlings and samples for RNA extraction were collected from leaves. Consistently robust 45-day-old plants were selected for 24 h sampling, collecting leaf tissues from the same leaf position at an interval of 4 h and performing three biological replicates. For abiotic stress treatments, the seedlings were placed over a plastic box filled with Japanese garden test nutrient solution, pH 6.0. Salt stress was applied by adding NaCl to a final concentration of 200 mmol/L in the nutrient solution; osmotic stress was imitated by adding polyethylene glycol 6000 (PEG6000) to a final concentration of 20%; cold or heat stress treatments were applied by transferring the seedlings into a growth chamber at 10 or 42°C, respectively. The illumination, photoperiod, and relative humidity of the treated plants were kept the same as the plants without abiotic stress treatments. A parallel control (normal growth) was set for each treatment. The second true leaves were sampled at 0, 1, 2, 4, 6, 12, and 24 h after treatment, and three biological replicates were performed at each time point. All samples were wrapped in tin foil, quickly placed in liquid nitrogen, and then stored in a refrigerator at –80°C.

RNA Extraction and qRT-PCR Expression Analysis

A Simple Total RNA Kit (TIANGEN) was used to extract high-quality RNA from pepper leaves, and cDNA was derived by reverse transcription using a PrimeScript RT reagent kit (TaKaRa kit). Actin (GenBank accession number GQ339766.1) was used as an internal reference gene. qRT-PCR was performed (three technical repeats) according to the instructions of the SYBR premix Ex Taq kit (TaKaRa). The $2^{-\Delta\Delta CT}$ method was used to calculate the relative expression of *CaCOL* genes (Heid et al., 1996). Primers used for the expression analysis are listed in **Supplementary Table 4**.

DATA AVAILABILITY STATEMENT

The original contributions presented in the study are included in the article/**Supplementary Material**, further inquiries can be directed to the corresponding author/s.

AUTHOR CONTRIBUTIONS

WD and ZH conceived the study and collected the public dataset of the researched species. XB and ZH contributed to data analysis, bioinformatics analysis, and manuscript preparation. GC, BX, and RC participated in the qRT-PCR experiment. All authors read and approved the final version of the manuscript.

FUNDING

This work was supported by the National Natural Science Foundation of China (31902021, 31701931, and 31801829).

ACKNOWLEDGMENTS

Our deepest gratitude goes to the reviewers for their careful work and thoughtful suggestions that have helped to improve the manuscript substantially.

SUPPLEMENTARY MATERIAL

The Supplementary Material for this article can be found online at: https://www.frontiersin.org/articles/10.3389/fpls.2022.828209/full#supplementary-material

REFERENCES

Almada, R., Cabrera, N., Casaretto, J. A., Ruiz-Lara, S., and Gonzalez Villanueva, E. (2009). VvCO and VvCOL1, two CONSTANS homologous genes, are regulated during flower induction and dormancy in grapevine buds. *Plant Cell Rep.* 28, 1193–1203. doi: 10.1007/s00299-009-0720-4

Bohlenius, H., Huang, T., Charbonnel-Campaa, L., Brunner, A. M., Jansson, S., Strauss, S. H., et al. (2006). CO/FT regulatory module controls timing of flowering and seasonal growth cessation in trees. *Science* 312, 1040–1043. doi: 10.1126/science.1126038

Cai, D., Liu, H., Sang, N., and Huang, X. (2017). Identification and characterization of CONSTANS-like (COL) gene family in upland cotton (*Gossypium hirsutum* L.). *PLoS One* 12:e0179038. doi: 10.1371/journal.pone.0179038

Chen, C., Chen, H., Zhang, Y., Thomas, H. R., Frank, M. H., He, Y., et al. (2020). TBtools: an integrative toolkit developed for interactive analyses of big biological data. *Mol. Plant* 13, 1194–1202. doi: 10.1016/j.molp.2020.06.009

Chen, J., Chen, J. Y., Wang, J. N., Kuang, J. F., Shan, W., and Lu, W. J. (2012). Molecular characterization and expression profiles of MaCOL1, a CONSTANS-like gene in banana fruit. *Gene* 496, 110–117. doi: 10.1016/j.gene.2012.01.008

Clark, J. W., and Donoghue, P. C. J. (2018). Whole-genome duplication and plant macroevolution. *Trends Plant Sci.* 23, 933–945. doi: 10.1016/j.tplants.2018.07.006

Datta, S., Hettiarachchi, G. H., Deng, X. W., and Holm, M. (2006). Arabidopsis CONSTANS-LIKE3 is a positive regulator of red light signaling and root growth. *Plant Cell* 18, 70–84. doi: 10.1105/tpc.105.038182

Duan, W., Ren, J., Li, Y., Liu, T., Song, X., Chen, Z., et al. (2016). Conservation and expression patterns divergence of ascorbic acid d-mannose/l-galactose pathway genes in brassica rapa. *Front. Plant Sci.* 7:778. doi: 10.3389/fpls.2016.00778

Fiil, A., Lenk, I., Petersen, K., Jensen, C. S., Nielsen, K. K., Schejbel, B., et al. (2011). Nucleotide diversity and linkage disequilibrium of nine genes with putative effects on flowering time in perennial ryegrass (*Lolium perenne* L.). *Plant Science* 180, 228–237. doi: 10.1016/j.plantsci.2010.08.015

Fornara, F., De Montaigu, A., and Coupland, G. (2010). SnapShot: control of flowering in arabidopsis. *Cell* 141, e551–e552. doi: 10.1016/j.cell.2010.04.024

Fu, Z., Yan, J., Zheng, Y., Warburton, M. L., Crouch, J. H., and Li, J.-S. (2010). Nucleotide diversity and molecular evolution of the PSY1 gene in zea mays compared to some other grass species. *Theor. Appl. Genet.* 120, 709–720. doi: 10.1007/s00122-009-1188-x

Griffiths, S., Dunford, R. P., Coupland, G., and Laurie, D. A. (2003). The evolution of CONSTANS-like gene families in barley, rice, and arabidopsis. *Plant Physiol.* 131, 1855–1867. doi: 10.1104/pp.102.016188

Heid, C. A., Stevens, J., Livak, K. J., and Williams, P. M. (1996). Real time quantitative PCR. *Genome Res.* 6, 986–994.

Hu, T., Wei, Q., Wang, W., Hu, H., Mao, W., Zhu, Q., et al. (2018). Genome-wide identification and characterization of CONSTANS-like gene family in radish (*Raphanus sativus*). *PLoS One* 13:e0204137. doi: 10.1371/journal.pone.0204137

Huang, G., Ma, J., Han, Y., Chen, X., and Fu, Y.-F. (2011). Cloning and expression analysis of the soybean CO-like gene GmCOL9. *Plant Mol. Biol. Rep.* 29, 352–359. doi: 10.1007/s11105-010-0240-y

Jiao, Y., Lau, O. S., and Deng, X. W. (2007). Light-regulated transcriptional networks in higher plants. *Nat. Rev. Genet* 8, 217–230. doi: 10.1038/nrg2049

Jung, J.-H., Seo, P. J., and Park, C.-M. (2012). The E3 ubiquitin ligase HOS1 regulates arabidopsis flowering by mediating CONSTANS degradation under cold stress. *J. Biol. Chem.* 287, 43277–43287. doi: 10.1074/jbc.M112.394338

Kim, S., Park, M., Yeom, S. I., Kim, Y. M., Lee, J. M., Lee, H. A., et al. (2014). Genome sequence of the hot pepper provides insights into the evolution of pungency in capsicum species. *Nat. Genet.* 46, 270–278. doi: 10.1038/ng.2877

Krzywinski, M., Schein, J., Birol, I., Connors, J., Gascoyne, R., Horsman, D., et al. (2009). Circos: an information aesthetic for comparative genomics. *Genome Res.* 19, 1639–1645. doi: 10.1101/gr.092759.109

Lagercrantz, U., and Axelsson, T. (2000). Rapid evolution of the family of CONSTANS LIKE genes in plants. *Mol. Biol. Evol.* 17, 1499–1507. doi: 10.1093/oxfordjournals.molbev.a026249

Lee, T.-H., Tang, H., Wang, X., and Paterson, A. H. (2012). PGDD: a database of gene and genome duplication in plants. *Nucleic Acids Res.* 41, D1152–D1158. doi: 10.1093/nar/gks1104

Li, L., Stoeckert, C. J. Jr., and Roos, D. S. (2003). OrthoMCL: identification of ortholog groups for eukaryotic genomes. *Genome Res.* 13, 2178–2189. doi: 10.1101/gr.1224503

Li, Y., and Xu, M. (2017). CCT family genes in cereal crops: a current overview. *Crop J.* 5, 449–458. doi: 10.1016/j.cj.2017.07.001

Liu, H., Dong, S., Sun, D., Liu, W., Gu, F., Liu, Y., et al. (2016). CONSTANS-Like 9 (OsCOL9) interacts with receptor for activated C-kinase 1 (OsRACK1) to regulate blast resistance through salicylic acid and ethylene signaling pathways. *PLoS One* 11:e0166249. doi: 10.1371/journal.pone.0166249

Liu, J., Shen, J., Xu, Y., Li, X., Xiao, J., and Xiong, L. (2016). Ghd2, a CONSTANS-like gene, confers drought sensitivity through regulation of senescence in rice. *J. Exp. Bot.* 67, 5785–5798. doi: 10.1093/jxb/erw344

Liu, L., Ding, Q., Liu, J., Yang, C., Chen, H., Zhang, S., et al. (2020). Brassica napus COL transcription factor BnCOL2 negatively affects the tolerance of transgenic arabidopsis to drought stress. *Environ. Exp. Bot.* 178:104171. doi: 10.1016/j.envexpbot.2020.104171

Min, J. H., Chung, J. S., Lee, K. H., and Kim, C. S. (2015). The CONSTANS-like 4 transcription factor, AtCOL4, positively regulates abiotic stress tolerance through an abscisic acid-dependent manner in arabidopsis. *J. Int. Plant Biol.* 57, 313–324. doi: 10.1111/jipb.12246

Niu, T., Wang, X., Abbas, M., Shen, J., Liu, R., Wang, Z., et al. (2022). Expansion of CONSTANS-like genes in sunflower confers putative neofunctionalization in the adaptation to abiotic stresses. *Industr. Crops Prod.* 176:114400. doi: 10.1016/j.indcrop.2021.114400

Putterill, J., Robson, F., Lee, K., Simon, R., and Coupland, G. (1995). The CONSTANS gene of arabidopsis promotes flowering and encodes a protein showing similarities to zinc finger transcription factors. *Cell* 80, 847–857. doi: 10.1016/0092-8674(95)90288-0

Qian, W., Liao, B. Y., Chang, A. Y., and Zhang, J. (2010). Maintenance of duplicate genes and their functional redundancy by reduced expression. *Trends Genet.* 26, 425–430. doi: 10.1016/j.tig.2010.07.002

Qin, C., Yu, C., Shen, Y., Fang, X., Chen, L., Min, J., et al. (2014). Whole-genome sequencing of cultivated and wild peppers provides insights into capsicum domestication and specialization. *Proc. Natl. Acad. Sci. U.S.A.* 111, 5135–5140. doi: 10.1073/pnas.1400975111

Rensing, S. A. (2014). Gene duplication as a driver of plant morphogenetic evolution. *Curr. Opin. Plant Biol.* 17, 43–48. doi: 10.1016/j.pbi.2013.11.002

Robson, F., Costa, M. M., Hepworth, S. R., Vizir, I., Pineiro, M., Reeves, P. H., et al. (2001). Functional importance of conserved domains in the flowering-time gene CONSTANS demonstrated by analysis of mutant alleles and transgenic plants. *Plant J.* 28, 619–631. doi: 10.1046/j.1365-313x.2001.01163.x

Shannon, P., Markiel, A., Ozier, O., Baliga, N. S., Wang, J. T., Ramage, D., et al. (2003). Cytoscape: a software environment for integrated models of biomolecular interaction networks. *Genome Res.* 13, 2498–2504. doi: 10.1101/gr.1239303

Song, N., Xu, Z., Wang, J., Qin, Q., Jiang, H., Si, W., et al. (2018). Genome-wide analysis of maize CONSTANS-LIKE gene family and expression profiling under light/dark and abscisic acid treatment. *Gene* 673, 1–11. doi: 10.1016/j.gene.2018.06.032

Song, X., Duan, W., Huang, Z., Liu, G., Wu, P., Liu, T., et al. (2015). Comprehensive analysis of the flowering genes in Chinese cabbage and examination of evolutionary pattern of CO-like genes in plant kingdom. *Sci. Rep.* 5:14631. doi: 10.1038/srep14631

Steinbach, Y. (2019). The *Arabidopsis thalianaconstans*-LIKE 4 (COL4)–a modulator of flowering time. *Front. Plant Sci.* 10:651.

Suarez-Lopez, P., Wheatley, K., Robson, F., Onouchi, H., Valverde, F., and Coupland, G. (2001). CONSTANS mediates between the circadian clock and the control of flowering in Arabidopsis. *Nature* 410, 1116–1120. doi: 10.1038/35074138

Tamura, K., Stecher, G., Peterson, D., Filipski, A., and Kumar, S. (2013). MEGA6: molecular evolutionary genetics analysis version 6.0. *Mol. Biol. Evol.* 30, 2725–2729. doi: 10.1093/molbev/mst197

Taylor, J. S., and Raes, J. (2004). Duplication and divergence: the evolution of new genes and old ideas. *Ann. Rev. Genet.* 38, 615–643. doi: 10.1146/annurev.genet.38.072902.092831

R Core Team (2013). *R: A Language and Environment for Statistical Computing*. Vienna: R Foundation for Statistical Computing.

Tenorio, G., Orea, A., Romero, J. M., and Merida, A. (2003). Oscillation of mRNA level and activity of granule-bound starch synthase I in arabidopsis leaves during the day/night cycle. *Plant Mol. Biol.* 51, 949–958. doi: 10.1023/a:1023053420632

Thompson, J. D., Gibson, T. J., and Higgins, D. G. (2002). Multiple sequence alignment using clustalw and clustalx. *Curr. Protoc. Bioinform.* Chapter 2:Unit2.3. doi: 10.1002/0471250953.bi0203s00

Tiwari, S. B., Shen, Y., Chang, H. C., Hou, Y., Harris, A., Ma, S. F., et al. (2010). The flowering time regulator CONSTANS is recruited to the FLOWERING LOCUS T promoter via a unique cis-element. *New Phytol.* 187, 57–66. doi: 10.1111/j.1469-8137.2010.03251.x

Tomato Genome Consortium (2012). The tomato genome sequence provides insights into fleshy fruit evolution. *Nature* 485:635. doi: 10.1038/nature11119

Valverde, F., Mouradov, A., Soppe, W., Ravenscroft, D., Samach, A., and Coupland, G. (2004). Photoreceptor regulation of CONSTANS protein in photoperiodic flowering. *Science* 303, 1003–1006. doi: 10.1126/science.1091761

Wang, Y., Tang, H., Debarry, J. D., Tan, X., Li, J., Wang, X., et al. (2012). MCScanX: a toolkit for detection and evolutionary analysis of gene synteny and collinearity. *Nucleic Acids Res.* 40:e49. doi: 10.1093/nar/gkr1293

Wang, Z., Zhou, Z., Liu, Y., Liu, T., Li, Q., Ji, Y., et al. (2015). Functional evolution of phosphatidylethanolamine binding proteins in soybean and arabidopsis. *Plant Cell* 27, 323–336. doi: 10.1105/tpc.114.135103

Wei, S., Peng, Z., Zhou, Y., Yang, Z., Wu, K., and Ouyang, Z. (2011). Nucleotide diversity and molecular evolution of the WAG-2 gene in common wheat (*Triticum aestivum* L) and its relatives. *Genet. Mol. Biol.* 34, 606–615. doi: 10.1590/S1415-47572011000400013

Whitt, S. R., Wilson, L. M., Tenaillon, M. I., Gaut, B. S., and Buckler, E. S. (2002). Genetic diversity and selection in the maize starch pathway. *Proc. Natl. Acad. Sci. U.S.A.* 99, 12959–12962. doi: 10.1073/pnas.202476999

Wu, F., Price, B. W., Haider, W., Seufferheld, G., Nelson, R., and Hanzawa, Y. (2014). Functional and evolutionary characterization of the CONSTANS gene family in short-day photoperiodic flowering in soybean. *PLoS One* 9:e85754. doi: 10.1371/journal.pone.0085754

Yang, T., He, Y., Niu, S., Yan, S., and Zhang, Y. (2020). Identification and characterization of the CONSTANS (CO)/CONSTANS-like (COL) genes related to photoperiodic signaling and flowering in tomato. *Plant Sci.* 301:110653. doi: 10.1016/j.plantsci.2020.110653

Yoo, S. K., Chung, K. S., Kim, J., Lee, J. H., Hong, S. M., Yoo, S. J., et al. (2005). CONSTANS activates SUPPRESSOR OF OVEREXPRESSION OF CONSTANS 1 through FLOWERING LOCUS T to promote flowering in arabidopsis. *Plant Physiol.* 139, 770–778. doi: 10.1104/pp.105.066928

Conflict of Interest: The authors declare that the research was conducted in the absence of any commercial or financial relationships that could be construed as a potential conflict of interest.

Publisher's Note: All claims expressed in this article are solely those of the authors and do not necessarily represent those of their affiliated organizations, or those of the publisher, the editors and the reviewers. Any product that may be evaluated in this article, or claim that may be made by its manufacturer, is not guaranteed or endorsed by the publisher.

Copyright © 2022 Huang, Bai, Duan, Chen, Chen, Xu, Cheng and Wang. This is an open-access article distributed under the terms of the Creative Commons Attribution License (CC BY). The use, distribution or reproduction in other forums is permitted, provided the original author(s) and the copyright owner(s) are credited and that the original publication in this journal is cited, in accordance with accepted academic practice. No use, distribution or reproduction is permitted which does not comply with these terms.

frontiers in Plant Science

REVIEW
published: 23 February 2022
doi: 10.3389/fpls.2022.843004

Overview of Witloof Chicory (*Cichorium intybus* L.) Discolorations and Their Underlying Physiological and Biochemical Causes

*Isabel De Jaegere[1], Yannah Cornelis[2], Tim De Clercq[2], Alain Goossens[3,4] and Bram Van de Poel[1]**

[1]*Laboratory of Molecular Plant Hormone Physiology, Division of Crop Biotechnics, Department of Biosystems, University of Leuven, Leuven, Belgium,* [2]*Praktijkpunt Landbouw Vlaams-Brabant, Herent, Belgium,* [3]*Department of Plant Biotechnology and Bioinformatics, Ghent University, Ghent, Belgium,* [4]*VIB Center for Plant Systems Biology, Ghent, Belgium*

Many fruits and vegetables suffer from unwanted discolorations that reduce product quality, leading to substantial losses along the supply chain. Witloof chicory (*Cichorium intybus* L. var. *foliosum*), a specialty crop characterized by its unique bitter taste and crunchiness, is particularly sensitive to various types of red and brown discolorations. The etiolated vegetable suffers from three predominant color disorders, i.e., core browning, internal leaf reddening, and leaf edge browning. Additionally, several less frequently observed color disorders such as hollow pith, external red, and *point noir* can also negatively affect crop quality. In this article, we bring together fragmented literature and present a comprehensive overview of the different discoloration types in chicory, and discuss their potential underlying physiological causes, including laticifer rupture, calcium deficiency, and a disturbed water distribution. We also describe the role of environmental cues that influence discoloration incidence, including cultivation and postharvest storage conditions such as forcing and storage temperature, root ripeness and the duration of the forcing process. Finally, we zoom in on the underlying biochemical pathways that govern color disorders in witloof chicory, with a strong emphasis on polyphenol oxidase.

Keywords: chicory, witloof, quality, discolorations, polyphenol oxidase

OPEN ACCESS

Edited by:
Xinchao Wang,
Tea Research Institute (CAAS), China

Reviewed by:
Hossein Sadeghi,
Shiraz University, Iran
Rajko Vidrih,
University of Ljubljana, Slovenia

****Correspondence:***
Bram Van de Poel
bram.vandepoel@kuleuven.be

Specialty section:
This article was submitted to Crop and Product Physiology, a section of the journal Frontiers in Plant Science

Received: *24 December 2021*
Accepted: *31 January 2022*
Published: *23 February 2022*

Citation:
De Jaegere I, Cornelis Y, De Clercq T, Goossens A and Van de Poel B (2022) Overview of Witloof Chicory (Cichorium intybus L.) Discolorations and Their Underlying Physiological and Biochemical Causes. Front. Plant Sci. 13:843004. doi: 10.3389/fpls.2022.843004

INTRODUCTION

Witloof chicory (*Cichorium intybus* L. var. *foliosum*, syn. Belgian endive, chicon) is a leafy vegetable with firm white-yellow leaves and a characteristic bitter taste. In Europe, chicory has a long history of cultivation for its taproot and leaves, but the particular method that produces the etiolated buds known as witloof chicory, was only introduced in the 19th century in the region of Brussels in Belgium (van Kruistum and Zwanepol, 1997; Lucchin et al., 2008). Today, production of witloof chicory is mainly localized in Western Europe, with the Netherlands, Belgium, France, Italy, and Germany as main producers. However, the global market is rapidly expanding, as chicons are exported to distant markets such as the United States, Canada, Japan, Qatar, and Israel, adding to a world trade value of 102 million United States dollar in 2019 (OEC, 2021). New markets, such as the United States, are ramping up their local witloof

chicory production (Corey et al., 1990), highlighting the growing international interest in this specialty bitter vegetable.

Chicory is a member of the *Asteraceae* family, more specifically the *Cichorieae* tribe, which is typified by the presence of milky latex and homogamous ligulate capitula and includes well-known relatives such as lettuce and dandelion (Kilian et al., 2009). Within the species, *C. intybus* shows a broad genetic diversity, harboring a wide range of different ecotypes and numerous cultivated varieties (Lucchin et al., 2008; Ghanaatiyan and Sadeghi, 2016, 2017). In accordance with their different uses, chicory cultivars can be divided into three subtypes, i.e., root chicory, leaf chicory, and witloof chicory, which show a clear genetic diversion (Raulier et al., 2016). Due to its biennial life cycle, witloof chicory is produced in two stages. During the first, vegetative stage, the crop is sown during late spring in open fields to produce a rosette of green leaves with a fleshy taproot, which is harvested in the late fall and stored at low temperature to initiate generative growth. The duration of the root storage period thereby depends on the cultivar and its subsequent forcing window, during which chicon yield and quality are optimal. During the second stage, the vernalized taproot is stimulated to produce an etiolated apical bud in a dark, humid environment; a process known as forcing. Traditionally, growers covered the taproots with soil to induce chicon growth, but today, most witloof chicory is grown hydroponically in a multilayer system in dark growth chambers (van Kruistum and Zwanepol, 1997). The combination of hydroponic forcing systems, together with the introduction of hybrid cultivars and a well-balanced long-term root storage program, enables chicon production all year round (de Proft et al., 2003).

Witloof chicory is typically subjected to rigorous quality standards regarding shape, firmness, and visual appearance. Chicons should be symmetrical with tightly-packed turgid leaves tapering to a pointed tip. The leaves are cream-colored with smooth, yellow edges and free of any pigmentation by chlorophyll. The occurrence of physiological disorders such as brown or red discolorations on either the leaves or pith can largely reduce the economic value and may diminish shelf life, nutritional value, and consumer appreciation (Yoruk and Marshall, 2003). Although discolorations already occurred in traditionally grown soil chicory, a lot of color defects arose upon the introduction of high-yielding cultivars bred specifically for hydroponic systems (Den Outer, 1989; Reerink, 1994). Color defects are still pertinent nowadays, considering that 10–50% of chicons can suffer discolorations after postharvest storage (personal communication Praktijkpunt Landbouw Vlaams-Brabant). Past studies have described the issue of discolorations in witloof chicory but profound fundamental knowledge about the exact causes of these physiological disorders is largely lacking. In this review, we bring together the current knowledge to categorize and illustrate the different types of discolorations in witloof chicory, and we provide insight into the physiological and biochemical factors that govern these disorders.

OVERVIEW OF DISCOLORATION TYPES

Unwanted discolorations in chicons of witloof chicory can be grouped into three major types i.e., leaf reddening, leaf edge browning, and pith disorders. In addition, a number of less frequent discoloration types may occur as a result of specific environmental or postharvest storage conditions, including *point noir* and chilling injury. Here, we illustrate and describe the different color disorders and briefly present the underlying physiological causes. More details on the factors influencing color disorders and the biochemical processes causing discolorations, will be presented in the next section.

Leaf Reddening

A common quality disorder in chicory involves the development of red discolorations on some of the leaves. A distinction is made between internal red and external red, based on the localization of the symptoms and their occurrence throughout the forcing season.

Internal Red

Red discolorations that occur adaxially on the basal part of the leaves are referred to as internal red. This color disorder occurs predominantly during late forcing (spring) and develops mostly postharvest. It is initiated by the appearance of crisp red spots on the lower half of the midrib of medial leaves. In a later stage, the red color may spread further into the leaf lamina, resulting in a red haze throughout the basal part of the leaf (Reerink, 1994; **Figures 1A,B**). Veen (1999) and Coppenolle et al. (2001) pointed out that internal red is associated with gaps that are formed between the adaxial epidermis and the subepidermal parenchyma cell layers. After harvest, the continued growth of the flower stalk or pith may attribute to the progression of this red lesion by extracting water and perhaps also nutrients from the leaves, as well as exerting mechanical stress on the tightly packed medial leaves.

External Red

Whereas internal red occurs predominantly during late forcing, external reddening manifests mainly during early forcing (autumn). External red occurs on the outer leaves of the chicon, showing elongated red spots on the abaxial side that run parallel to the vascular bundles (Reerink, 1994; van Kruistum and Zwanepol, 1997; **Figure 1C**). The spots are diffuse and occur mostly on the basal part of the leaf, but can extend toward the tip. External red presumably develops when forcing temperatures are relatively high at the start of the forcing season, which leads to rapid elongation of the leaves during the last days of forcing. The high rate of water uptake associated with a fast cellular elongation can cause laticifer cells to rupture. This results in leakage of latex into surrounding tissue and the subsequent development of discolorations. Asymmetric turgor pressure differences between laticifers and the surrounding parenchyma cells, as well as weakened cell wall structures due to calcium deficiency, have been proposed to play a role in the development of external red (Reerink, 1994).

Pith Disorders

Several discoloration types can develop in the pith, which is the central core of the chicon that develops into a flowering

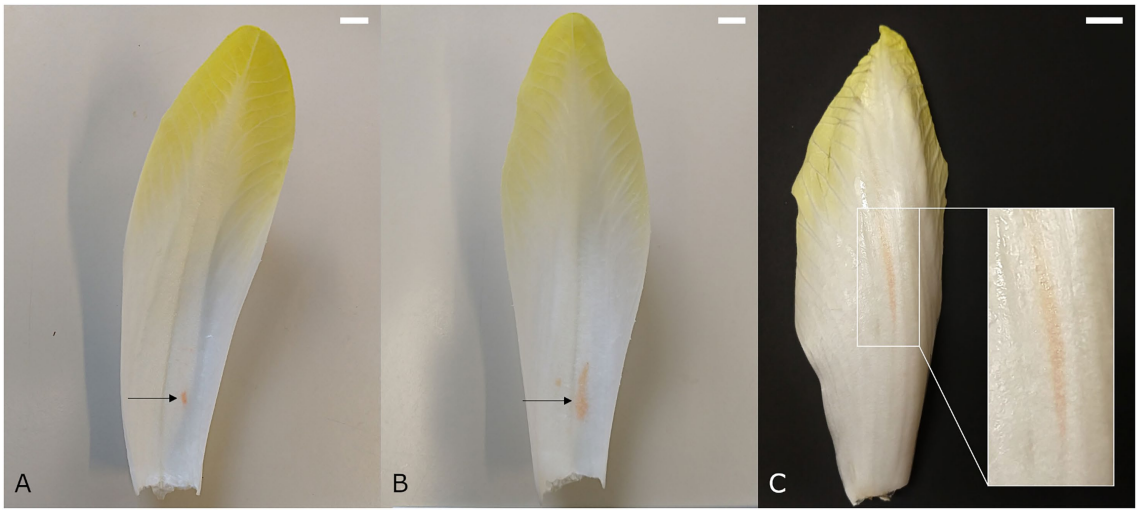


FIGURE 1 | Medial chicon leaf showing internal red discoloration with **(A)** initial and **(B)** more advanced symptoms. **(C)** Chicory leaf with external red discoloration symptoms. Scale bars represent 1 cm.

stem when allowed to grow in the light. The most studied pith disorder is core browning, but other physiological defects such as apple pith, pink axis, and hollow pith also occur on a regular basis.

Core Browning

Core browning (syn. brown pith, internal browning) appears as brown or dark red discolorations in the core parenchyma. The first symptoms arise during forcing and can gradually aggravate as the pith continues to grow during postharvest storage. A brown pith can occur in two distinct forms. The first type involves spot-like core browning, in which the core tissue turns translucent and subsequently yellow-brown to dark brown due to an increasing loss of cellular integrity (de Barsy and Bronchart, 1991; **Figure 2A**). The second type involves the discoloration of several layers of pith tissue and is referred to as layered core browning (**Figure 2B**). According to Den Outer (1989), layered core browning is associated with a disturbed cellular organization in the central core due to irregular cell division. Later, cells undergo plasmolysis, followed by the discoloration of the cell content, and finally cellular collapse. Around the discolored core tissue, series of radial cells are produced that separate the affected region from the healthy surrounding pith tissue. It is thought that core browning is associated with an inadequate supply of calcium during chicon development. A lack of calcium can lead to disintegration of the middle lamellae and the detachment of cell walls, which causes a gradual loss of structural integrity and eventually cellular collapse (Den Outer, 1989; de Barsy and Bronchart, 1991).

Apple Pith

The name of this disorder refers to its resemblance to the cross-section of an apple seed. Apple pith designates an area of opaque white tissue that is sharply delineated by a dark red-brown border, usually situated around the center of the core near the base (**Figure 2C**). In severe cases, the affected central tissue may collapse, leaving only the colored outer edge and thus a hollow pith (van Kruistum and Zwanepol, 1997). Symptomatic similarities between apple pith and the sharply delineated discolorations observed in layered core browning, make it plausible that apple pith is a more severe manifestation of core browning.

Pink Axis

Sometimes, a pink discoloration can be seen along the longitudinal axis of the pith (**Figure 2D**). It usually develops during postharvest storage, especially when the pith is very elongated. Symptoms vary in intensity from a nearly indistinguishable haze to a bright pink stripe.

Textural Pith Disorders

Several other physiological pith disorders, including porous, hollow—and glassy pith, are not necessarily color disorders but rather textural defects of the core parenchyma tissue. A porous pith (**Figure 2D**) shows core tissue that is sponge-like and has an opaque white appearance, as opposed to the glossy white appearance of healthy pith tissue. Typically, a porous pith develops postharvest and is often seen in combination with a pink axis (**Figure 2D**). Hollow pith designates a cavity that usually occurs along the central axis and can take on a number of different forms, depending on the physiological process that caused the cavity (**Figure 2E**). This disorder occurs quite frequently and can reduce product quality, especially when visible from the base. A glassy pith (**Figure 2F**), is characterized by a yellow and vitreous appearance of the core, similar to the initial stage of spotted core browning, and is often overlooked.

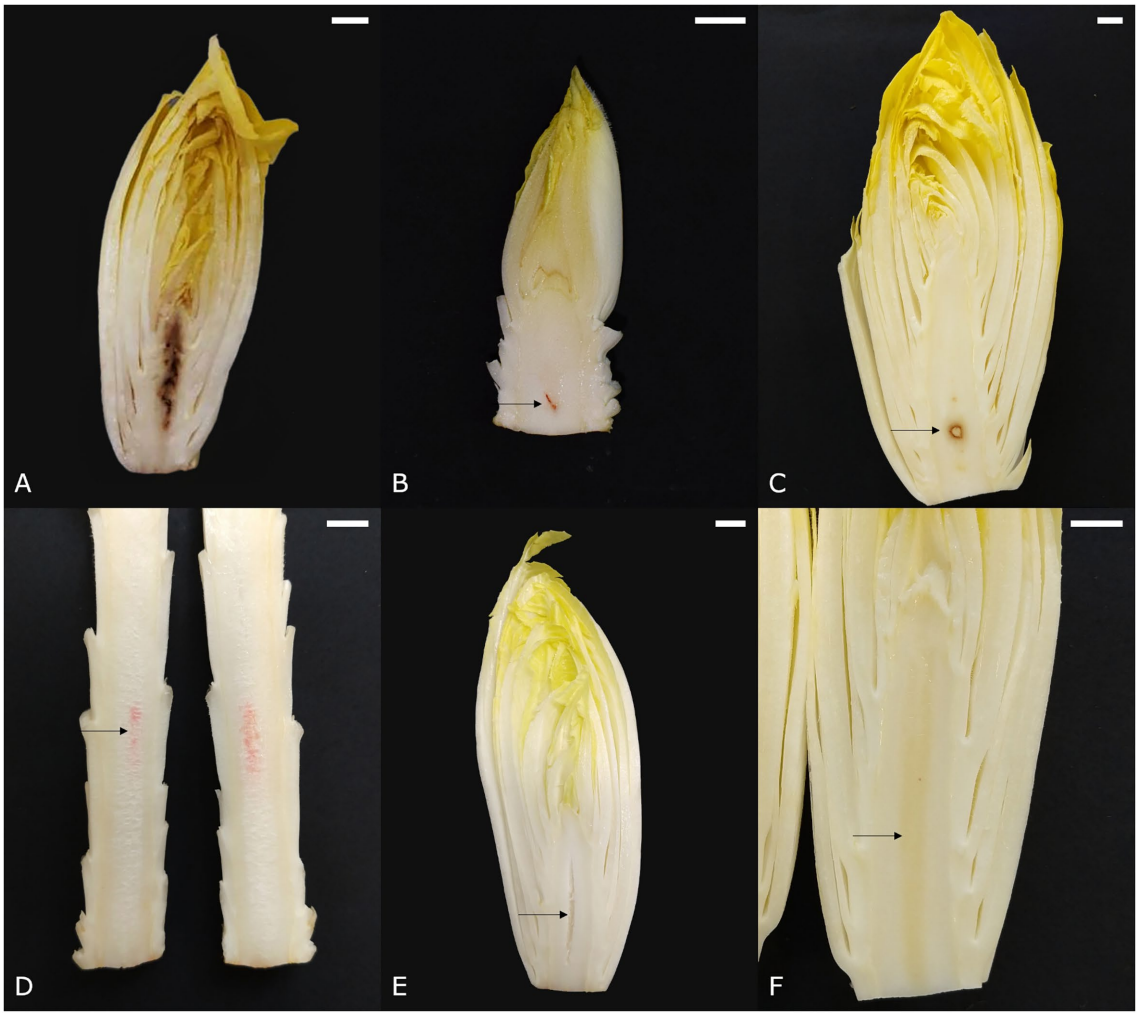


FIGURE 2 | Symptoms of pith discolorations in witloof chicory. **(A)** Spotted core browning, **(B)** layered core browning, **(C)** apple pith, **(D)** porous pith with pink discoloration, **(E)** hollow pith, and **(F)** glassy pith. Scale bars represent 1 cm.



FIGURE 3 | Symptoms of **(A)** mild and **(B)** severe leaf edge browning of the external leaves. Scale bars represent 1 cm.

Leaf Edge Browning

Chicons with brown edges on the external leaves are encountered rather frequently and symptoms can range from a few brown spots near the edge in the middle of the leaf (**Figure 3A**) to completely brown and necrotic leaf edges (**Figure 3B**). This color disorder is usually seen on cultivars with thin outer leaves and develops predominantly postharvest (Reerink, 1994). Leaf edge browning in chicory resembles a number of browning disorders in other crops, such as tipburn in lettuce, which are typically related to cellular disintegration as a result of calcium deficiency in young leaves that have little transpiration (Reerink, 1994; Barta and Tibbitts, 2000). However, the link between leaf edge browning and calcium has not been studied in chicory and in contrast to other crops, it occurs mainly in the oldest leaves of the chicon, which are most exposed to the environment. Alternatively, leaf edge browning could also

be linked to leaf dehydration, causing mesophyll cells in the thin leaf margin to collapse, thus leading to browning of the disintegrated tissue (van Kruistum, 1992).

Less Frequently Encountered Discolorations

Point Noir

Point noir, French for "black spot," refers to the development of a black region of necrotic tissue on the leaves (**Figure 4A**). Subsequent growth of healthy tissue around the affected spot results in an atypically bent leaf. The *point noir* disorder can also occur in the pith, causing chicon growth to be seriously hampered and resulting in the development of a cavity in the core around the black spot (**Figure 4B**). *Point noir* typically occurs during early and winter forcing (October–January), becoming more pronounced after prolonged storage of the roots. Its incidence is more outspoken when chicory plants suffered dry conditions during the preceding field cultivation phase. A significant reduction of *point noir* symptoms can be achieved when roots were treated with $CaCl_2$ before forcing (van den Broek, 1994).

Chilling Injury

Inadequate cooling after chicon harvest can lead to the development of superficial red-brown depressed spots on the abaxial side of leaves (**Figure 4C**). This disorder is also referred to as low temperature injury and manifests itself predominantly when the harvested chicons are stored at an intermediate temperature (±18°C) for 1–2 days before actual long term storage at 1°C. The symptoms become more apparent when chicons are again exposed to higher temperatures (±15°C). Sensitivity to this disorder is highly variable among cultivars (van Kruistum et al., 1995).

Blue or Black Discolored Leaves

Occasionally, patches of dark discolored tissue can be seen on the leaves of the chicon (**Figure 5A**). These blue or black discolorations typically occur in the vascular tissue (**Figure 5B**) and are thought to be caused by excessive uptake of iron due to low soil pH or low calcium content in ferrous, oxygen-deprived soils during root cultivation or soil-covered forcing. The dark pigment likely results from a complexation reaction between iron and polyphenols. This type of discoloration occurs more frequently in traditional soil forced chicory, because the composition of the nutrient solution can be managed more precisely in a hydroponic forcing system (van Kruistum and Zwanepol, 1997).

EXTERNAL FACTORS INFLUENCING COLOR DISORDERS

The occurrence of chicory discolorations varies considerably throughout the forcing season and between successive years, indicating that root age and environmental conditions during field cultivation and root storage can have a major impact on subsequent chicon quality (Godts et al., 2012). Past research has improved our understanding of the conditions that influence the development of color disorders and has led to the formulation of a range of guidelines for cultivation and postharvest storage practices that can effectively reduce the prevalence of certain disorders. Apart from cultivation conditions and postharvest storage procedures, the genetic differences between cultivars may also account for a lot of the variability in discoloration sensitivity.

Cultivation Practice and Postharvest Storage

Past research on chicory discolorations has focused primarily on the influence of different cultivation techniques and forcing

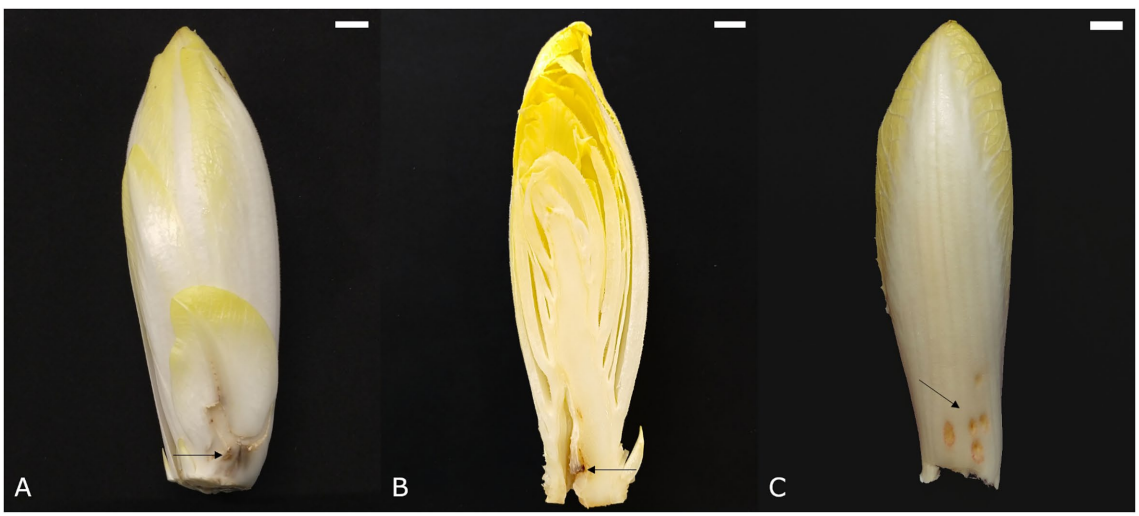


FIGURE 4 | Symptoms of point noir on **(A)** an outer leaf and **(B)** the pith. **(C)** Symptoms of chilling injury. Scale bars represent 1 cm.

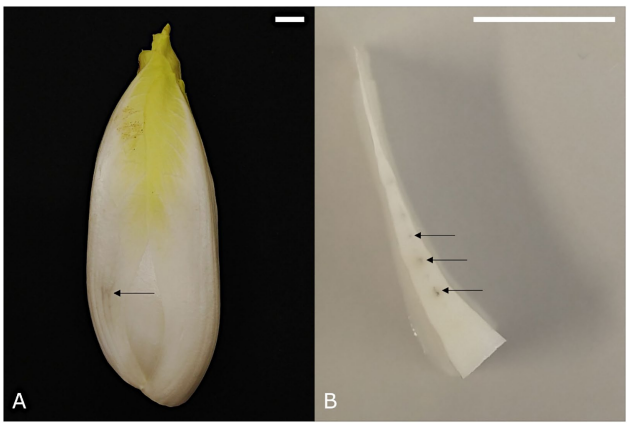


FIGURE 5 | (A) Symptoms of black discoloration of a chicon and **(B)** the localization of black pigment in the vascular tissue on a cross section. Scale bars represent 1 cm.

conditions on the development of color disorders. This has led to the identification of a number of influencing factors and the formulation of cultivation guidelines to minimize discolorations. In general, controlling color disorders requires a balance between yield and product quality, since conditions that promote high yield can jeopardize chicon quality. This is especially true for internal red and leaf edge browning, which are both considerably reduced by harvesting the chicons in time and by using a sufficiently low forcing temperature to prevent rapid chicon growth (Reerink, 1994; Godts et al., 2012). Likewise, the treatment of root heads with $CaCl_2$ before forcing has been shown to reduce core browning and hollow pith, but comes at the cost of a slightly reduced yield (van den Broek, 1994; Versluis, 1994). Although climatological conditions and soil properties can seriously influence the sensitivity to color disorders such as tipburn and pinking in lettuce (Olson et al., 1967; Hunter et al., 2017), these factors have not been reported to play an important role in the development of the most prevalent discolorations in chicory. With regard to postharvest storage, it is imperative that chicons are cooled down swiftly after harvest and stored at low temperature to minimize the development of color disorders (Godts et al., 2012). Additionally, storage under modified atmosphere conditions may further reduce the incidence of certain discoloration types, as was shown for internal red and leaf edge browning (Reerink, 1994; Vanstreels et al., 2002).

Table 1 summarizes a number of cultivation, forcing, and postharvest factors that influence sensitivity to internal red, leaf edge browning, and core browning. Some factors are specific for certain discoloration types while others, such as root ripeness, are more general. The influence of forcing and storage practices is more important than the chemical composition of the roots, especially with respect to the development of internal red (Seynnaeve et al., 2000). As a consequence, roots with an identical origin (cultivar/field/harvest date/storage conditions), may develop chicons with varying levels of discoloration when grown in different forcing facilities (van Kruistum, 1992; Coppenolle et al., 2001). Similarly, roots of variable origins

TABLE 1 | Overview of influencing factors during root cultivation, forcing and postharvest storage of witloof chicory on the sensitivity toward the development of internal red, core browning, and leaf edge browning.

	Influencing factor	Discoloration type		
		Internal red	Core browning	Leaf edge browning
Root characteristics	Composition	High N content: ↓ (van Kruistum and Zwanepol, 1997)	High N content: ↑ (van Kruistum, 1992)	
	Diameter	Large: ↑ (van Kruistum, 1992)	Large: ↑ (van Kruistum, 1992; Van Stallen et al., 2005)	Small: ↑ (van Kruistum, 1992)
	Ripeness*	Unripe/overripe: ↑ (van Kruistum and Zwanepol, 1997)	Unripe/overripe: ↑ (van Kruistum and Zwanepol, 1997)	Unripe/overripe: ↑ (van Kruistum and Zwanepol, 1997)
	Dry matter content	High DM: ↓ (Reerink, 1994)		
Forcing conditions	Root treatment	Shortening root: ↓ (Coppenolle et al., 2001)	$CaCl_2$ treatment: ↓ (Versluis, 1994)	
		Boron treatment: ↓ (Hunter et al., 2017)		
	Temperature**	High: ↑ (Coppenolle et al., 2001)		High: ↑ (Reerink, 1994)
	Duration**	Long: ↑ (Reerink, 1994)		Long: ↑ (van Kruistum, 1992; van Kruistum and Zwanepol, 1997)
	Nutrient solution	More K^+ toward end of forcing: ↓ (Reerink, 1994)	More K^+: ↓ (Reerink, 1993)	More K^+ toward end of forcing: ↓ (Reerink, 1994)
Postharvest storage	Storage temperature	High: ↑ (Reerink, 1994)		High: ↑ (Reerink, 1994)
	Storage duration	Long: ↑ (Reerink, 1994)		Long: ↑ (Reerink, 1994)
	Atmosphere	10% O_2 + 10% CO_2 at 5°C: ↓ (Vanstreels et al., 2002)		10% O_2 + 10% CO_2 at 5°C: ↓ (Vanstreels et al., 2002)

↑ = *increased sensitivity*, ↓ = *decreased sensitivity.*

**Root ripeness indicates the moment when forcing will result in optimal chicon yield and quality.*

***Level of factors should be interpreted relative to standard practice, which may differ with respect to cultivar and time of year.*

will produce chicons with a different sensitivity to discolorations when forced in the same facility (van Kruistum, 1992; Coppenolle et al., 2001).

GENETIC DETERMINANT OF COLOR DISORDERS

Contrary to the role of cultivation and postharvest factors, the genetic determinant of chicory discolorations has not received much attention to date. It is assumed that the narrow genetic diversity among witloof chicory hybrids may explain the persistence of discoloration problems over many years (de Proft et al., 2003). It has previously been established that discoloration sensitivity varies between cultivars. For example, leaf edge browning tends to occur more often in cultivars with thin and translucent outer leaves. Likewise, chilling injury, internal reddening, and pith browning were shown to be highly cultivar dependent (van Kruistum, 1992; van den Broek, 1994; van Kruistum et al., 1995; Coppenolle et al., 2001; Godts et al., 2012). Although this genetic factor has often been reported, little is known that can explain discoloration differences between cultivars. A QTL analysis showed genetic linkage for pith browning and hollow pith, but not up to the level of single gene resolution (Van Stallen et al., 2005). Future studies that will deploy new genetic tools and use novel genomic resources, could improve our understanding of the genetic regulation of color disorders in chicory (Barcaccia et al., 2016; Bernard et al., 2019; Bogdanović et al., 2019; Aldahak et al., 2021).

PHYSIOLOGICAL CAUSES OF COLOR DISORDERS

Over the years, a number of physiological causes have been linked with the development of color disorders in chicory, ranging from laticifer rupture to calcium deficiency. Here, we will discuss the most prevalent hypotheses concerning common discoloration types.

Laticifer Rupture

Laticifer cells are present in approximately 10% of all flowering plants and compose a tubular network filled with milky latex, which contains a broad range of specialized metabolites and defense proteins (Castelblanque et al., 2016). Although its specific function is not entirely clear, latex is thought to play a role in plant defense by creating a physical and chemical barrier against pests. Coagulated latex facilitates wound closure and pest entrapment, while secretory compounds within the latex may have an antibiotic effect (Castelblanque et al., 2020). In chicory, articulated laticifers compose an anastomosing network that is tightly associated with the phloem in the vascular bundles (Vertrees and Mahlberg, 1978). Chicory laticifers contain no phenolic compounds, but exhibit both polyphenol oxidase and peroxidase activity (Mohamed-Yasseen and Splittstoesser, 1990). The absence of phenols may explain the lack of browning in exuded latex after wounding, much in contrast to the immediate browning reaction that occurs in the polyphenol-rich latex of related dandelion species (*Taraxacum* spp.; Wahler et al., 2009). However, the release of latex may elicit a discoloration reaction with the phenolic compounds located in the surrounding mesophyll cells or apoplast. In lettuce, fluctuating water availability in combination with local calcium deficiency leads to overpressure in laticifer vessels, resulting in deformations of the weakened cell walls and leakage of latex into neighboring tissue, which causes the browning phenomenon tipburn (Olson et al., 1967; Tibbitts et al., 1985; Barta and Tibbitts, 2000). Similarly, in growing chicory leaves, rapid water uptake during cell elongation, is thought to cause excessive asymmetrical pressure between laticifers and the surrounding tissue. This can cause laticifer cells to rupture and bleed latex into the intercellular space, causing the elongated red spots that are typical for external red discoloration of the leaves. The rupture of laticifer cells has also been mentioned in the context of internal red and leaf edge browning. However, cells affected by internal reddening are usually situated under the upper epidermis, relatively far away from the laticifer-encased vasculature in the center or toward the abaxial side of the leaf. Moreover, it was found that the latex-exuding functionality of laticifer cells was not compromised in leaves affected by internal red discolorations (Veen, 1999). As for leaf edge browning, the association with laticifer rupture is uncertain, because this disorder occurs typically in the oldest outer leaves, in which the laticifer system has long been developed. Additionally, laticifer cells in chicory are predominantly localized on the abaxial side of the leaf, while brown edge symptoms can occur at both sides (Reerink, 1994).

Calcium Deficiency

Calcium ions play a critical role in the maintenance of cellular integrity by promoting cell wall rigidity and stability of the cell membranes and the middle lamellae (de Barsy and Bronchart, 1991; White and Broadley, 2003). Long-distance calcium transport to the shoot occurs *via* the xylem and is thereby dependent on transpiration. Subsequently, Ca^{2+} ions are further mobilized predominantly *via* the apoplast and enter the cell passively through Ca^{2+} channels (White and Broadley, 2003). In a range of different crops, an inadequate supply of Ca^{2+} is associated with physiological color disorders in developing tissues that have a low transpiration rate, such as young leaves, enclosed tissues, and storage organs (Den Outer, 1989; White and Broadley, 2003; Adams and Brown, 2007). For example, internal necrosis in potato, which is caused by a calcium deficiency, shows a striking similarity to pith disorders in chicory (Thornton et al., 2020). Furthermore, many leafy vegetables can develop calcium-related discolorations that resemble the symptoms of leaf edge browning in chicons, such as tipburn in lettuce (Reerink, 1994). Chicory roots, which are naturally low in calcium (±2.3 mg g^{-1} DW), are forced under conditions of low root pressure and limited transpiration (Den Outer, 1989; Reerink, 1993). During the first half of the forcing period, translocation of calcium from the nutrient solution to the apical bud is very low and as a result, the growing chicon relies entirely on the limited redistribution of calcium from the

taproot (Limami and Lamaze, 1991; Reerink, 1993). Toward the end of the forcing period, when secondary roots have developed and more water can be taken up for rapid cell elongation, calcium translocation from the nutrient solution to the chicon increases, reaching approximately 3.5–5 mg g^{-1} DW in the harvested chicon. This is considerably lower than calcium levels in leaves of other crops, which usually range from 7 to 65 mg g^{-1} DW (Reerink, 1994). Local calcium deficiencies have been proposed to be involved in multiple color disorders in chicory, but are particularly associated with the development of a brown pith (Den Outer, 1989; de Barsy and Bronchart, 1991). A pre-treatment of chicory roots with $CaCl_2$ before forcing alleviates the symptoms of brown pith, hollow pith, and point noir, but not of internal red (van den Broek, 1994; Versluis, 1994). Moreover, symptoms of pith browning are initiated during the early forcing stage characterized by low calcium uptake and mobilization, in contrast to the symptoms of internal red and leaf edge, which mainly develop during postharvest storage (Fouldrin and Limami, 1993). Calcium distribution within a chicon is comparable to other crops, with higher Ca^{2+} concentrations in older leaves and lowest Ca^{2+} levels in younger leaves (Veen, 1999). The occurrence of reddening in the medial leaves and leaf edge browning in the old leaves does not correlate with their relatively high calcium content, which makes these disorders less likely to be caused by a calcium deficiency. A dedicated analysis of the calcium content in the leaf edge, upper rib, and lower rib (where reddening usually occurs), revealed a slightly lower calcium content in the lower rib, but no relation with reddening could be deduced (Veen, 1999). However, the incidence of a temporary calcium deficiency in these tissues cannot be ruled out.

Water Distribution

Both a surplus and a loss of water can play an important role in the development of color disorders in chicory. Excessive uptake of water for cell elongation during the final stage of forcing may lead to pressure imbalances between the continuous laticifer system and the surrounding mesophyll tissue (Reerink, 1994). Consequent laticifer rupture can then facilitate the oxidation of phenolic substrates by polyphenol oxidase, resulting in the elongated red spots that typify external red discolorations. In contrast, both internal red and leaf edge browning are more likely to result from loss of water in the affected tissue, independent of laticifers. Coppenolle et al. (2001) showed that leaves displaying the most intense reddening symptoms also have the highest water potential. After harvest, this makes them more prone to internal water redistribution toward the pith, which has a more negative water potential and keeps growing after harvest (Coppenolle et al., 2001). This process was validated by imposing an external potential pressure on harvested chicory heads by storing them with their base in either distilled water or in a sorbitol solution with a more negative water potential than the pith. This resulted, respectively, in a decrease and increase of the reddening symptoms, indicating that a strong negative water potential of the pith causes strong gradients in water content that can give rise to internal red. Similarly, postharvest storage of chicons detached from or attached to their taproot, resulted in more and less red discoloration of the leaves (Veen, 1999), confirming that water loss from the leaves leads to internal reddening. Finally, loss of water from the outer leaves due to desiccation is likely to be the driving force behind the development of leaf edge browning after harvest (van Kruistum, 1992). Differences in the transpiration rate between cultivars could help to explain the observed variation in sensitivity to leaf edge browning.

Tissue Tension

The closed conformation of a chicory head imposes some mechanical stress on the inner surface of the medial leaves. According to Veen (1999), tissue tension is maximal just below the upper epidermis and may attribute to the development of internal red discolorations by promoting the development of tears in the tissue just below the adaxial epidermis. Additionally, Gillis et al. (2001) showed that the application of a mechanical load on individual leaves induced red discoloration symptoms corresponding to the pattern of stress distribution within the leaves. Presumably, tissue tension can lead to loss of cellular integrity, resulting in unwanted discolorations in the affected tissue.

BIOCHEMISTRY OF DISCOLORATION IN CHICORY AND RELATED SPECIES

Many browning reactions in fruits and vegetables are attributed to the enzymatic activity of polyphenol oxidases (PPOs; Martinez and Whitaker, 1995; Tomás-Barberán and Espín, 2001; Yoruk and Marshall, 2003). PPOs and their phenolic substrates, which are localized in the plastids and the vacuole, respectively, can be decompartmentalized when cellular integrity is lost, e.g., due to senescence, dehydration, or mechanical trauma. This enables subsequent enzymatic oxidation and discoloration of the affected tissue (Yoruk and Marshall, 2003). Although this mechanism has long been thought to cause discolorations in witloof chicory, little research has been done to validate this hypothesis. The discoloration process in lettuce, however, has received far more attention in recent years and could serve as a paradigm for chicon discolorations (Hunter et al., 2017; Saltveit, 2018). It is worth noting that not all browning reactions of fresh produce are associated with PPO activity. For example in lettuce, researchers showed that the formation of yellow-brown lettucenin sesquiterpenes contributed significantly to the browning of cut tissues (Mai and Glomb, 2014). Nevertheless, phenolic oxidation by PPO remains a major source of discolorations in fruit and vegetable products and is therefore an interesting target for research on color disorders in chicory.

PPO in Plants

Polyphenol oxidase proteins are type-III copper enzymes that are nearly ubiquitous in higher plants. They are typically localized in the plastids and can be either soluble or membrane-bound (Martinez and Whitaker, 1995; Kampatsikas et al., 2019). Much

of the research on PPOs in plants has focused on their negative impact on fresh produce quality e.g., browning reactions in apple, potato, and lettuce (Yoruk and Marshall, 2003). However, PPOs play an important role in plant defense by contributing to wound healing and immune responses against pathogens and pests (Kampatsikas et al., 2019). Additionally, some PPO isoforms have a specific function in the biosynthesis of specialized metabolites. The distribution of the *PPO* gene family is highly variable among plant taxa. Different isoforms show diverse substrate specificities and their expression is subject to both temporal and spatial regulation in response to environmental conditions (Tran et al., 2012; Dirks-Hofmeister et al., 2014). This flexibility allows PPO enzymes to fulfill a range of physiological functions in different tissues during different developmental stages.

PPO Reaction Mechanism and Phenolic Substrates in Chicory

Phenolic compounds are synthesized by the phenylpropanoid pathway, of which phenylalanine lyase (PAL) is the first and rate-determining enzyme (Hunter et al., 2017). Generally, the amount of *PAL* transcript and PAL activity is low, but expression can be induced by wounding or exposure to hormonal levels of ethylene (Tomás-Barberán and Espín, 2001; Kang and Saltveit, 2003). In chicory, phenolic compounds are highly abundant in parenchyma cells and to a lesser extent in the vicinity of the vascular tissue (Reerink, 1994). Interestingly, chicory laticifers contain no phenolic compounds as evidenced by the lack of browning in exuded latex (Mohamed-Yasseen and Splittstoesser, 1990). PPO catalyzes the first step in the oxidation of phenolic compounds to complex brown polymers or melanins, which are typically associated with color disorders in fresh produce. Depending on the type of PPO, the enzyme can catalyze the oxidation of monophenols and/or *o*-diphenols to *o*-quinones in the presence of molecular oxygen (Kampatsikas et al., 2019). These highly reactive and colored *o*-quinones can then lead to the formation of melanin *via* non-enzymatic reactions with different cellular components, such as proteins, amino acids, and other quinones (Martinez and Whitaker, 1995; Yoruk and Marshall, 2003).

Substrate specificity of PPOs toward different phenolic compounds varies considerably between species (Yoruk and Marshall, 2003). For lettuce PPO, the highest substrate specificity was observed for caffeic acid and chlorogenic acid, resulting in the formation of a pink and green quinone, respectively (Saltveit, 2018). In etiolated endive, the relative contribution of caffeic acid derivatives to the total phenolic content was shown to be increased in comparison to that of regular endive, which also developed less enzymatic discolorations than its dark-grown counterpart (Reerink, 1994). Caffeic acid and its derivatives also make up a major part of the total phenolic content in chicory, thus identifying them as potential precursors in the development of color disorders in chicons (Hanotel et al., 1995). The red color of several discoloration types of chicory may be the result of an interaction between PPO reaction products and free amino acids such as proline and tryptophan. Accordingly, the amount of free amino acids in chicory heads was found to be strongly correlated to the incidence of internal red during postharvest storage (Godts et al., 2012). Alternatively, the red pigment could result from the interaction between caffeic acid quinone and cellulose in the cell walls, which results in a stable pink complex as described in lettuce (Saltveit, 2018).

Strategies to Reduce Enzymatic Discoloration

Several approaches targeting the PPO enzyme family have proven to be successful in reducing browning reactions in fruits and vegetables. Since the rate of browning depends on both PAL and PPO activity, as well as substrate availability, O_2 concentration, pH, and temperature, each of these factors can be managed in order to reduce the occurrence of color disorders (Martinez and Whitaker, 1995). As such, several postharvest approaches have proven to be successful in diminishing oxidative discoloration in fresh produce. This includes physical methods such as heat treatments, modified atmosphere packaging, storage at low temperature and irradiation, and chemical treatments such as the application of reducing agents, copper-chelating agents, natural anti-browning compounds, and acidification (Moon et al., 2020). In chicory, successful postharvest interventions have mainly aimed to tackle color disorders *via* the use of a sufficiently low storage temperature and modified atmosphere packaging (see also **Table 1**). For example, the combination of 10% CO_2 and 10% O_2 at 5°C led to a maximal reduction of internal red discoloration and additionally reduced symptoms of leaf edge browning, rot and continuation of pith growth (Vanstreels et al., 2002). One study also indicated the feasibility of reducing red discoloration of the chicon base using a heat-shock treatment of 2 min at 42°C after harvest (Jung and Kang, 2014). This reduction is thought to be achieved by the suppression of wounding-induced PAL synthesis due to a preferential synthesis of heat-shock proteins, thereby reducing accumulation of phenolic compounds and subsequent base discoloration (Kang and Saltveit, 2003). In practice, the only strategy that is consistently used to decrease discoloration incidence in chicons, is postharvest storage at low temperature, which is also essential for good shelf-life. Storage under modified atmosphere, however, is not standard practice and requires additional investments in specialized equipment.

Other than postharvest interventions, breeding strategies addressing the phenylpropanoid or PPO biosynthesis pathway could also be an effective solution (Hunter et al., 2017). There have been several successful attempts to silence *PPO* expression and thereby reduce discolorations in fresh produce, resulting in commercial applications such as Arctic® apple and Innate® Potato (Richael, 2021; Stowe and Dhingra, 2021). However, it is possible that the suppression of *PPOs* results in an increased susceptibility toward disease, due to their role in plant defense (Kampatsikas et al., 2019). Additionally, the PPO enzyme is not necessarily responsible for the full array of discolorations

in a particular crop. Both in lettuce and chicory, a direct link between PPO activity, phenolic content, and the degree of discolorations could not always be observed (Jung and Kang, 2014; Saltveit, 2018). This may limit the applicability of *PPO* silencing in species were these enzymes play an important role in plant defense or when other specialized metabolites are at play. Alternatively, breeding efforts could target PAL or an enzyme downstream of PAL in the biosynthesis pathway of PPO substrates (Hunter et al., 2017). An improved understanding of the discoloration biochemistry and the nature of the different discoloration compounds in witloof chicory would be invaluable to identify novel targets for future breeding efforts to prevent color disorders.

AUTHOR CONTRIBUTIONS

ID performed literature research and took pictures. ID and BP wrote the manuscript. YC, TD, and AG provided feedback and corrected the manuscript. All authors approved the final manuscript.

FUNDING

This work was financially supported by Flanders Innovation & Entrepreneurship (VLAIO) through the LA-traject grant "ChiQon" (HBC.2018.2218).

REFERENCES

Adams, J., and Brown, H. (2007). Discoloration in raw and processed fruits and vegetables. *Crit. Rev. Food Sci. Nutr.* 47, 319–333. doi: 10.1080/10408390600762647

Aldahak, L., Salem, K. F. M., Al-Salim, S. H. F., and Al-Khayri, J. M. (2021). "Volume 10: Leaves, flowerheads, green pods, mushrooms and truffles," in *Advances in Plant Breeding Strategies: Vegetable Crops. 1st Edn.* eds. J. M. Al-Khayri, S. M. Jain and D. V. Johnson (Cham: Springer), 3–57.

Barcaccia, G., Ghedina, A., and Lucchin, M. (2016). Current advances in genomics and breeding of leaf chicory (*Cichorium intybus* L.). *Agriculture* 6:50. doi: 10.3390/agriculture6040050

Barta, D. J., and Tibbitts, T. W. (2000). Calcium localization and tipburn development in lettuce leaves during early enlargement. *J. Am. Soc. Hortic. Sci.* 125, 294–298. doi: 10.21273/JASHS.125.3.294

Bernard, G., Gagneul, D., Alves Dos Santos, H., Etienne, A., Hilbert, J.-L., and Rambaud, C. (2019). Efficient genome editing using CRISPR/Cas9 technology in chicory. *Int. J. Mol. Sci.* 20:1155. doi: 10.3390/ijms20051155

Bogdanović, M., Cankar, K., Todorović, S., Dragicević, M., Simonović, A., van Houwelingen, A., et al. (2019). Tissue specific expression and genomic organization of bitter sesquiterpene lactone biosynthesis in *Cichorium intybus* L. (Asteraceae). *Ind. Crop. Prod.* 129, 253–260. doi: 10.1016/j.indcrop.2018.12.011

Castelblanque, L., Balaguer, B., Marti, C., Rodriguez, J., Orozco, M., and Vera, P. (2016). Novel insights into the organization of laticifer cells: a cell comprising a unified whole system. *Plant Physiol.* 172, 1032–1044. doi: 10.1104/pp.16.00954

Castelblanque, L., García-Andrade, J., Martínez-Arias, C., Rodríguez, J. J., Escaray, F. J., Aguilar-Fenollosa, E., et al. (2020). Opposing roles of plant laticifer cells in the resistance to insect herbivores and fungal pathogens. *Plant Commun.* 2:100112. doi: 10.1016/j.xplc.2020.100112

Coppenolle, H., Beuselinck, A., and Gillis, N. (2001). *Integraal Kwaliteitsbeheer Bij Productie, Behandeling en Verwerking van Witloof* KU Leuven, Leuven.

Corey, K. A., Marchant, D. J., and Whitney, L. F. (1990). "Witloof chicory: a new vegetable crop in the United States," in *Advances in New Crops*, eds. J. Janick and J. E. Simon (Portland, OR: Timber Press), 414–418.

de Barsy, T., and Bronchart, R. (1991). Ultrastructural study of the brown core of Witloof chicory chicon. *Sci. Hortic.* 45, 191–197. doi: 10.1016/0304-4238(91)90063-5

de Proft, M., van Stallen, N., and Noten, V. (2003). "Breeding and cultivar idenitification of *Cichorium intybus* L. var. foliosum Hegi," in *Eucarpia Leafy Vegetables*, eds. Th. J. L. van Hintum, A. Lebeda, D. Pink and J. W. Schut (Netherland, Wageningen: Center for Genetic Resources (CGN)), 83–90.

Den Outer, R. W. (1989). Internal browning of witloof chicory (*Cichorium intybus* L.). *J. Hortic. Sci.* 64, 697–704. doi: 10.1080/14620316.1989.11516011

Dirks-Hofmeister, M. E., Singh, R., Leufken, C. M., Inlow, J. K., and Moerschbacher, B. M. (2014). Structural diversity in the dandelion (*Taraxacum officinale*) polyphenol oxidase family results in different responses to model substrates. *PLoS One* 9:e99759. doi: 10.1371/journal.pone.0099759

Fouldrin, K., and Limami, A. (1993). Calcium (45 Ca) mobility in chicory root (*Cichorium intybus* L.) as affected by the anionic composition of the nutrient solution during forcing. *J. Am. Soc. Hortic. Sci.* 118, 587–592. doi: 10.21273/JASHS.118.5.587

Ghanaatiyan, K., and Sadeghi, H. (2016). Divergences in hormonal and enzymatic antioxidant responses of two chicory ecotypes to salt stress. *Planta Daninha* 34, 199–208. doi: 10.1590/S0100-83582016340200001

Ghanaatiyan, K., and Sadeghi, H. (2017). Differential responses of chicory ecotypes exposed to drought stress in relation to enzymatic and non-enzymatic antioxidants as well as ABA concentration. *J. Hortic. Sci. Biotechnol.* 92, 404–410. doi: 10.1080/14620316.2017.1286235

Gillis, N., Verlinden, B. E., Van Hecke, P., De Baerdemaeker, J., and Nicolaï, B. M. (2001). Finite element analysis of mechanical damage in chicory (*Cichorium intybus* L). *Acta Hortic.* 553, 527–530. doi: 10.17660/actahortic.2001.553.123

Godts, C., Ceusters, J., Eylen, T., François, I., and De Proft, M. (2012). Characterisation of reddening in etiolated chicory leaves (*Cichorium intybus* L. var. *foliosum*). *Acta Hortic.* 936, 463–470. doi: 10.17660/ActaHortic.2012.936.62

Hanotel, L., Fleuriet, A., and Boisseau, P. (1995). Biochemical changes involved in browning of gamma-irradiated cut witloof chicory. *Postharvest Biol. Technol.* 5, 199–210. doi: 10.1016/0925-5214(94)00028-Q

Hunter, P. J., Atkinson, L. D., Vickers, L., Lignou, S., Oruna-Concha, M. J., Pink, D., et al. (2017). Oxidative discolouration in whole-head and cut lettuce: biochemical and environmental influences on a complex phenotype and potential breeding strategies to improve shelf-life. *Euphytica* 213:180. doi: 10.1007/s10681-017-1964-7

Jung, H. J., and Kang, H. M. (2014). Effect of hot-water dipping on inhibiting red discoloration of basal part in chicon. *Korean J. Hortic. Sci. Technol.* 32, 353–358. doi: 10.7235/hort.2014.13159

Kampatsikas, I., Bijelic, A., and Rompel, A. (2019). Biochemical and structural characterization of tomato polyphenol oxidases provide novel insights into their substrate specificity. *Sci. Rep.* 9:4022. doi: 10.1038/s41598-019-39687-0

Kang, H.-M., and Saltveit, M. (2003). Wound-induced PAL activity is suppressed by heat-shock treatments that induce the synthesis of heat-shock proteins. *Physiol. Plant.* 119, 450–455. doi: 10.1034/j.1399-3054.2003.00190.x

Kilian, N., Gemeinholzer, B., and Lack, H. (2009). "Cichorieae," in *Systematics, Evolution, and Biogeography of Compositae*, eds. V. A. Funk, A. Susanna, T. F. Stuessy and R. J. Bayer (Vienna: International Association for Plant Taxonomy (iapt)). 343–383.

Limami, A., and Lamaze, T. (1991). Calcium (45Ca) accumulation and transport in chicory (*Cichorium intybus* L.) root during bud development (forcing). *Plant Soil* 138, 115–121. doi: 10.1007/BF00011813

Lucchin, M., Varotto, S., Barcaccia, G., and Parrini, P. (2008). "Chicory and endive," in *Vegetables I: Asteraceae, Brassicaceae, Chenopodicaceae, and Cucurbitaceae. Vol. 1*, eds. P. Jaime and N. Fernando (New York: Springer), 3–48.

Mai, F., and Glomb, M. A. (2014). Lettucenin sesquiterpenes contribute significantly to the browning of lettuce. *J. Agric. Food Chem.* 62, 4747–4753. doi: 10.1021/jf500413h

Martinez, M. V., and Whitaker, J. R. (1995). The biochemistry and control of enzymatic browning. *Trends Food Sci. Technol.* 6, 195–200. doi: 10.1016/S0924-2244(00)89054-8

Mohamed-Yasseen, Y., and Splittstoesser, W. E. (1990). Phenolic compounds, oxidative enzymes and their relationship with discoloration in endive (*Cichorium intybus* L.). *Proc. Inter. Soc. Trop. Hort.* 79–82.

Moon, K. M., Bin Kwon, E., Lee, B., and Kim, C. Y. (2020). Recent trends in controlling the enzymatic browning of fruit and vegetable products. *Molecules* 25:2754. doi: 10.3390/molecules25122754

OEC (2021). "Witloof chicory, fresh or chilled," Observatory of Economic Complexity. Available at: https://oec.world/en/profile/hs92/witloof-chicory-fresh-or-chilled (Accessed April 07, 2021).

Olson, K. C., Tibbitts, T., and Struckmeyer, B. E. (1967). Morphology and significance of laticifer rupture in lettuce tipburn. *J. Am. Soc. Hortic. Sci.* 91, 377–385.

Raulier, P., Maudoux, O., Notté, C., Draye, X., and Bertin, P. (2016). Exploration of genetic diversity within *Cichorium endivia* and *Cichorium intybus* with focus on the gene pool of industrial chicory. *Genet. Resour. Crop. Evol.* 63, 243–259. doi: 10.1007/s10722-015-0244-4

Reerink, J. A.. (1993). "*Onderzoek Naar Factoren en Processen Die de Produktie en Kwaliteit van Witlof Beïnvloeden*." Cabo-dlo, Wageningen.

Reerink, J. A.. (1994). "*Bestaande Kennis Over Fysiologische Kwaliteitsafwijkingen Bij Witlof*." Ab-dlo, Wageningen.

Richael, C. M. (2021). "Development of the genetically modified innate® potato," in *Plant Breeding Reviews*, ed. I. Goldman (Hoboken, NJ: John Wiley & Sons, Inc.), 57–78.

Saltveit, M. (2018). Pinking of lettuce. *Postharvest Biol. Technol.* 145, 41–52. doi: 10.1016/j.postharvbio.2018.06.001

Seynnaeve, M. C., Sarrazyn, R., Vanderschelden, C., and Calus, A. (2000). Study on red discoloration of chicory heads. *Acta Hortic.* 511, 89–98. doi: 10.17660/ActaHortic.2000.511.10

Stowe, E., and Dhingra, A. (2021). "Development of the Arctic® apple," in *Plant Breeding Reviews*, ed. I. Goldman (Hoboken, NJ: John Wiley & Sons, Inc.), 273–296.

Thornton, M., Olsen, N., and Liang, X. (2020). "Physiological disorders," in *Potato Production Systems*. eds. J. C. Stark, M. Thornton and P. Nolte (Cham: Springer International Publishing), 447–478.

Tibbitts, T., Bensink, J., Kuiper, F., and Hobe, J. (1985). Association of latex pressure with tipburn injury of lettuce. *J. Am. Soc. Hortic. Sci.* 110, 362–365.

Tomás-Barberán, F. A., and Espín, J. C. (2001). Phenolic compounds and related enzymes as determinants of quality in fruits and vegetables. *J. Sci. Food Agric.* 81, 853–876. doi: 10.1002/jsfa.885

Tran, L. T., Taylor, J. S., and Constabel, C. P. (2012). The polyphenol oxidase gene family in land plants: lineage-specific duplication and expansion. *BMC Genomics* 13:395. doi: 10.1186/1471-2164-13-395

van den Broek, R. D. F. (1994). "De Fysiologische Afwijking 'Point Noir' in Witlof." ROC Zwaagdijk, Zwaagdijk.

van Kruistum, G. (1992). "*Fysiologische Afwijkingen van de Witlofkrop, Hoe te Vermijden?*" PAGV, Lelystad.

van Kruistum, G., Biesheuvel, A. R., van de Broek, R. C. F., Geelen, P. M. T. M., and Jeurissen, J. G. M. (1995). "*Beheersing van Lage-Temperatuurbederf Bij Witlof*." PAGV, Lelystad.

van Kruistum, G., and Zwanepol, S.. (1997). "*Productie van Witlof en Roodlof*." PAGV, Lelystad.

Van Stallen, N., Vandenbussche, B., Londers, E., Noten, V., and De Proft, M. (2005). QTL analysis of important pith characteristics in a cross between two inbred lines of chicory (*Cichorium intybus* var. *foliosum*): a preliminary study. *Plant Breed.* 124, 54–58. doi: 10.1111/j.1439-0523.2005.00955.x

Vanstreels, E., Lammertyn, J., Verlinden, B., Gillis, N., Schenk, A., and Nicolai, B. M. (2002). Red discoloration of chicory under controlled atmosphere conditions. *Postharvest Biol. Technol.* 26, 313–322. doi: 10.1016/S0925-5214(02)00060-1

Veen, B. W.. (1999). "*Roodverkleuring in Witlof: Invloed van Mineralenhuishouding en Kropontwikkeling*." Ab-dlo, Wageningen.

Versluis, H. P.. (1994). "*Behandeling Witlofwortels Met Calciumchloride*." PAGV, Westmaas. PAGV, Lelystad.

Vertrees, G. L., and Mahlberg, P. G. (1978). Structure and ontogeny of laticifers in *Cichorium intybus* (Compositae). *Am. J. Bot.* 65, 764–771. doi: 10.1002/j.1537-2197.1978.tb06135.x

Wahler, D., Gronover, C. S., Richter, C., Foucu, F., Twyman, R. M., Moerschbacher, B. M., et al. (2009). Polyphenoloxidase silencing affects latex coagulation in *Taraxacum* species. *Plant Physiol.* 151, 334–346. doi: 10.1104/pp.109.138743

White, P. J., and Broadley, M. R. (2003). Calcium in plants. *Ann. Bot.* 92, 487–511. doi: 10.1093/aob/mcg164

Yoruk, R., and Marshall, M. R. (2003). Physicochemical properties and function of plant polyphenol oxidase: a review. *J. Food Biochem.* 27, 361–422. doi: 10.1111/j.1745-4514.2003.tb00289.x

Conflict of Interest: The authors declare that the research was conducted in the absence of any commercial or financial relationships that could be construed as a potential conflict of interest.

Publisher's Note: All claims expressed in this article are solely those of the authors and do not necessarily represent those of their affiliated organizations, or those of the publisher, the editors and the reviewers. Any product that may be evaluated in this article, or claim that may be made by its manufacturer, is not guaranteed or endorsed by the publisher.

Copyright © 2022 De Jaegere, Cornelis, De Clercq, Goossens and Van de Poel. This is an open-access article distributed under the terms of the Creative Commons Attribution License (CC BY). The use, distribution or reproduction in other forums is permitted, provided the original author(s) and the copyright owner(s) are credited and that the original publication in this journal is cited, in accordance with accepted academic practice. No use, distribution or reproduction is permitted which does not comply with these terms.

frontiers in Plant Science

ORIGINAL RESEARCH
published: 24 February 2022
doi: 10.3389/fpls.2022.848349

Integrative Transcriptome and Proteome Analysis Reveals the Absorption and Metabolism of Selenium in Tea Plants [*Camellia sinensis* (L.) O. Kuntze]

Hengze Ren[1†], Xiaoman Li[1,2†], Lina Guo[1], Lu Wang[1], Xinyuan Hao[1] and Jianming Zeng[1*]*

[1] National Center for Tea Improvement, Key Laboratory of Tea Biology and Resources Utilization, Ministry of Agriculture and Rural Affairs, Tea Research Institute, Chinese Academy of Agricultural Sciences, Hangzhou, China, [2] College of Horticulture, Fujian Agriculture and Forestry University, Fuzhou, China

Certain tea plants (*Camellia sinensis*) have the ability to accumulate selenium. In plants, the predominant forms of bioavailable Se are selenite (SeO_3^{2-}) and selenate (SeO_4^{2-}). We applied transcriptomics and proteomics to hydroponically grown plants treated with selenite or selenate for 48 h in the attempt to elucidate the selenium absorption and assimilation mechanisms in tea. A total of 1,844 differentially expressed genes (DEGs) and 691 differentially expressed proteins (DEPs) were obtained by comparing the Na_2SeO_3 and Na_2SeO_4 treatments against the control. A GO analysis showed that the genes related to amino acid and protein metabolism and redox reaction were strongly upregulated in the plants under the Na_2SeO_3 treatment. A KEGG pathway analysis revealed that numerous genes involved in amino acid and glutathione metabolism were upregulated, genes and proteins associated with glutathione metabolism and ubiquinone and terpenoid-quinone biosynthesis were highly expressed. Genes participating in DNA and RNA metabolism were identified and proteins related to glutathione metabolism were detected in tea plants supplemented with Na_2SeO_4. ABC, nitrate and sugar transporter genes were differentially expressed in response to selenite and selenate. Phosphate transporter (*PHT3;1a*, *PHT1;3b*, and *PHT1;8*) and aquaporin (*NIP2;1*) genes were upregulated in the presence of selenite. Sulfate transporter (*SULTR1;1* and *SULTR2;1*) expression increased in response to selenate exposure. The results of the present study have clarified Se absorption and metabolism in tea plants, and play an important theoretical reference significance for the breeding and cultivation of selenium-enriched tea varieties.

Keywords: ***Camellia sinensis*, transcriptome, proteome, selenite, selenate**

OPEN ACCESS

Edited by:
Pei Xu,
China Jiliang University, China

Reviewed by:
Wanping Fang,
Nanjing Agricultural University, China
Antonio Masi,
University of Padua, Italy

***Correspondence:**
Xinyuan Hao
haoxy@tricaas.com
Jianming Zeng
zengjm@tricaas.com

† These authors have contributed equally to this work

Specialty section:
This article was submitted to Crop and Product Physiology, a section of the journal Frontiers in Plant Science

Received: *04 January 2022*
Accepted: *02 February 2022*
Published: *24 February 2022*

Citation:
Ren H, Li X, Guo L, Wang L, Hao X and Zeng J (2022) Integrative Transcriptome and Proteome Analysis Reveals the Absorption and Metabolism of Selenium in Tea Plants [Camellia sinensis (L.) O. Kuntze]. Front. Plant Sci. 13:848349. doi: 10.3389/fpls.2022.848349

INTRODUCTION

Selenium (Se) is a trace non-metal element that is sometimes regarded as a metalloid. It is an essential mineral nutrient for humans, animals, and certain microorganisms. At the appropriate concentrations, it is beneficial for plant growth (Guignardi and Schiavon, 2017). Selenium may be toxic or beneficial depending on the dosage. High Se concentrations are phytotoxic as they cause

oxidative stress. Moreover, they form selenoamino acids that interfere with protein folding and function (Guignardi and Schiavon, 2017). At optimal doses, Se protects plants against oxidative stress, reduces the toxicity of harmful elements, regulates growth, photosynthesis, respiration, and improves yield and quality (Hu et al., 2003; Feng et al., 2013; Yu et al., 2019; Chauhan et al., 2020; Niu et al., 2020). In humans, optimal Se doses improve antioxidant capacity, prevent cancer, and reduce heavy metal toxicity (Pieczyñska and Grajeta, 2015). However, global Se distribution is highly heterogeneous. Over 15% of the world's population suffers from Se deficiency characterized by Kashin–Beck and Keshan diseases (Tan et al., 2016). Tea [*Camellia sinensis* (L.) O. Kuntze] is an economically important perennial woody plant grown in many Asian, African, and Latin American countries. It is used to prepare a non-alcoholic beverage consumed by over three billion people in 160 countries (Xia et al., 2017; Wang et al., 2020). Certain tea cultivars can accumulate selenium. Within the plant, 80% of the Se occurs as moieties of organic compounds that can be absorbed through the human digestive tract (Gao et al., 2014). In regions where the soil Se content is low, the amount of Se in tea is actually greater than the available Se in maize, rice, beans, or potatoes (Xiang et al., 2012). Thus, tea may be an ideal alternative Se supplement for humans. However, little is known about the mechanisms by which tea plants absorb, translocate, or metabolize Se.

In nature, the existence valence of Se mainly includes −2 in selenide, 0 in elemental selenium, +2 in thioselenate, +4 in selenites, +6 in selenates. The predominant inorganic forms of Se available to plants are selenate in oxic soils ($pE + pH > 15$) and selenite in anaerobic soils ($7.5 < pE + pH < 15$) (Sors et al., 2005; White, 2016). Plants absorb selenate and selenite via sulfate and phosphate transporters, respectively. Tea and other plants have four different types of sulfate transporters (Gigolashvili and Kopriva, 2014; Zhang et al., 2021). In *Arabidopsis thaliana*, *SULTR1;1* and *SULTR1;2* are high-affinity sulfate transporters that absorb selenate. *SULTR2;1* and *SULTR2;2* are low-affinity sulfate transporters that mediate selenate translocation from the roots to the leaves (Takahashi et al., 2000; El Kassis et al., 2007; Takahashi, 2019). *CsSULTR1;2/2;1/3;3/3;5* were upregulated in response to Se^{4+} and Se^{6+} exposure in *Camellia sinensis* (Zhang et al., 2021). Plant phosphate transporters are classified into subfamilies PHT1–5 (Liu et al., 2016; Wang et al., 2017). Selenite uptake is mediated by phosphate transporters (Zhang et al., 2014; Song et al., 2017). Only PHT1, PHT3, PHT4, and PHO were identified in *C. sinensis* (Cao et al., 2021). A transcriptome analysis of tea plants treated with selenite showed that their phosphate transporters may participate in selenite absorption and translocation (Cao et al., 2021). Nevertheless, the phosphate transporters involved in the uptake and translocation of Se species with different valences remain to be further elucidated.

After selenate is absorbed by the roots, it can be reduced to selenite via ATP sulfurylase and APS reductase. The selenite is then reduced to Se^{2-} (selenide) either enzymatically by sulfite reductase or non-enzymatically via glutathione. Cysteine and methionine synthases may then catalyze the formation of the selenoamino acids selenocysteine and selenomethionine, respectively (Guignardi and Schiavon, 2017). Few studies to date have been conducted on the metabolism of Se with different valences in tea plants.

Transcriptomics, metabolomics, and proteomics have been used to study Se disposition in living organisms (Zhang C. et al., 2019; Chauhan et al., 2020; Rao et al., 2021). Accordingly, multiple omics technologies should also be applied to explore Se uptake and metabolism in tea plants. In the present study, we integrated transcriptomics and proteomics to clarify the mechanisms of selenite and selenate uptake and metabolism in tea plants. We believe that the results of this research will provide theoretical guidance for breeding and cultivating Se-accumulating tea varieties.

MATERIALS AND METHODS

Plant Materials and Treatments

One-year-old tea plant cuttings (*C. sinensis* cv. 'Zhongcha 108') were placed in black containers holding 1/4 nutrient solution (pH 5.0) consisting of ammonium salt (80.04 mg/L), KH_2PO_4 (8.53 mg/L), K_2SO_4 (52.27 mg/L), $MgSO_4$ (80.64 mg/L), $CaCl_2$ (58.82 mg/L), $Al_2(SO_4)_3$ (23.33 mg/L), EDTA-FeNa (1.77 mg/L), H_3BO_3 (0.43 mg/L), $MnSO_4{\cdot}H_2O$ (0.17 mg/L), $ZnSO_4{\cdot}7H_2O$ (0.19 mg/L), $CuSO_4{\cdot}5H_2O$ (0.03 mg/L), and $(NH_4)_2MoO_4$ (0.06 mg/L) (Ruan et al., 2007). The solution was renewed once weekly. The plants were grown in a greenhouse under a 12-h photoperiod and at 22°C and 70% RH. After the adventitious roots emerged, the cuttings were transferred to fresh 1/4 nutrient solution without Se or supplemented with 5 μM Na_2SeO_3 or 5 μM Na_2SeO_4. Each treatment consisted of four pots and each pot held 40 cuttings. After 48 h, roots and young shoots (two leaves and one bud) were sampled for total Se content determination. Other roots were promptly frozen in liquid nitrogen and stored at −80°C until the transcriptomic and proteomic analyses. Four biological replicates were conducted per analysis.

Se Content Determination

The roots were rinsed with MilliQ water containing 2 mM MES and 1 mM $CaSO_4$ and dried with absorbent paper. The roots and shoots were freeze-dried for 24 h in a lyophilizer (TF-FD-1; Zhejiang Nade Scientific Instrument Co. Ltd., Hangzhou, China). The samples were then pulverized for total Se content determination according to a previously described method (Zhang H. et al., 2019).

RNA Isolation, Library Construction, and Illumina Sequencing

Total RNA was isolated from the roots according to a previously described method (Chang et al., 1993). The integrity of the total RNA was assessed with the RNA Nano 6000 Assay Kit and the Bioanalyzer 2100 System (Agilent Technologies, Santa Clara, CA, United States). The library was prepared with a NEB Next Ultra RNA Library Prep Kit (New England Biolabs, Ipswich, MA, United States) according to a previously described method (Parkhomchuk et al., 2009) and sequenced on an Illumina Novaseq platform (Illumina, San Diego, CA, United States).

Transcriptomic Data Analysis

Clean reads were obtained by removing low-quality reads and those with adapter sequences from the raw data. They were then mapped to the reference genome with HISAT2 v. 2.0.5[1]. Novel genes were identified with StringTie v. 1.3.3b[2]. The expected numbers of fragments per kilobase of transcript sequence per million base pairs sequenced (FPKM) were calculated with FeatureCounts v. 1.5.0-p3[3]. Differentially expressed genes (DEGs) were filtered with padj < 0.05 and $|\log_2(\text{FoldChange})| > 0.5$ using DESeq2 v. 1.20.0[4] (Love et al., 2014). Gene ontology (GO) and Kyoto Encyclopedia of Genes and Genomes (KEGG) enrichment analyses were performed on all DEGs as previously described (Wang L. et al., 2019).

Gene Expression via RT-qPCR

One hundred milligrams tea roots was used for total RNA extraction in the RNAprep Pure Plant Plus Kit [Tiangen Biotech (Beijing) Co. Ltd., Beijing, China]. RNA samples (1 mg) were then treated with RNase-free DNase I (TaKaRa Bio Inc., Kusatsu, Japan) to remove residual genomic DNA. The cDNA was then synthesized with a PrimerScript RT Reagent Kit (TaKaRa Bio Inc., Kusatsu, Japan) according to the manufacturer's protocol. The cDNA products were diluted tenfold and used as a PCR template. The RT-qPCR was conducted as previously described (Hao et al., 2018). The *CsPTB* reference gene was the internal control (Hao et al., 2014).

Proteome Profiling

The protein was extracted and quantified as previously described (Wu et al., 2014), labeled with TMT labeling reagent, mixed in equal volumes, desalted, and lyophilized (Zhang et al., 2016). The powder was then dissolved in 2% (v/v) acetonitrile (pH 10.0) and centrifuged at 12,000 $\times$ *g* and 25°C for 10 min. The samples were then fractionated in a C18 column (Waters BEH C18; 4.6 mm $\times$ 250 mm; 5 μm; Waters Corp., Milford, MA, United States) on a Rigol L3000 HPLC system (Arc Scientific, Boston, MA, United States). The eluates were measured at 214 nm, collected every minute, and combined into ten fractions. The latter were dried under vacuum and reconstituted in 0.1% (v/v) formic acid. A 1-μg sample was analyzed by ultra-high performance liquid chromatography (EASY-nLC 1200 UHPLC, Thermo Fisher Scientific, Waltham, MA, United States) coup^{TM}led with tandem mass spectrometry (Q Exactive^{TM} HF-X, Thermo Fisher Scientific, Waltham, MA, United States). The proteome profiling results were presented in **Supplementary Tables 1**, **2**.

Proteomic Data Analysis

Each spectrum was separately searched with Proteome Discoverer v. 2.4 (PD 2.4; Thermo Fisher Scientific, Waltham, MA, United States). To improve output quality, the results were filtered with PD 2.4. Data with credibility >99% were identified as Peptide Spectrum Matches (PSMs). Each identified protein contained at least one unique peptide. The PSMs and protein were retained and analyzed using a false discovery rate (FDR) $\leq$ 1.0%. Protein quantitation was statistically analyzed with a *t*-test. Differentially expressed proteins (DEPs) were identified as those with $P < 0.05$. A GO functional analysis was conducted using an interproscan program against the non-redundant protein databases Pfam[5], PRINTS[6], ProDom[7], SMART[8], ProSite[9], and PANTHER[10] (Jones et al., 2014). KEGG (Kyoto Encyclopedia of Genes and Genomes) was used to analyze the protein pathway.

Transcriptome and Proteome Correlation Analyses

Alignment analyses of the gene sequences identified from the transcriptome and protein sequences were conducted at https://magic.novogene.com. The DEG and DEP data were integrated, GO enrichment and KEGG pathway analyses were performed, and the results were displayed in a heatmap.

Statistical Analysis

Transcriptomic sequencing, proteomic analysis, and RT-qPCR were conducted in four biological replicates. Statistical analyses were run in SPSS Statistics v. 19 (IBM Corp., Armonk, NY, United States) and consisted of ANOVA followed by the LSD test at $P < 0.05$. Column plots were drawn with GraphPad Prism 8 (GraphPad Software, La Jolla, CA, United States). Heatmaps were plotted with Tbtools[11] (Chen et al., 2020). Adobe Photoshop CS5[12] was used to assemble the figures.

RESULTS

Effects of Selenite and Selenate Exposure on Root and Leaf Se Content

Total Se was measured in the roots and leaves of tea plants subjected to Na_2SeO_3 or Na_2SeO_4 for 48 h. Samples without selenium supplementation served as the control. The total Se content in the roots significantly ($P < 0.05$) increased in response to Na_2SeO_3 treatment (**Figure 1**). The tea plants absorbed selenite more effectively than selenate. The total Se content in the leaves significantly ($P < 0.05$) increased in response to Na_2SeO_4 treatment. However, there was no significant difference between the Na_2SeO_3 treatment and the control in terms of foliar Se content (**Figure 1**). Hence, selenate was relatively more efficiently transported than selenite from the roots to the leaves.

[1]http://daehwankimlab.github.io/hisat2/

[2]https://ccb.jhu.edu/software/stringtie/

[3]http://subread.sourceforge.net/featureCounts.html

[4]https://bioconductor.org/packages/release/bioc/html/DESeq2.html

[5]https://pfam.xfam.org/search

[6]http://130.88.97.239/PRINTS/index.php

[7]http://prodom.prabi.fr/prodom/current/html/home.php

[8]smart.embl-heidelberg.de

[9]https://prosite.expasy.org

[10]pantherdb.org

[11]https://github.com/CJ-Chen/TBtools

[12]https://softmany.com/adobe-photoshop-cs5/

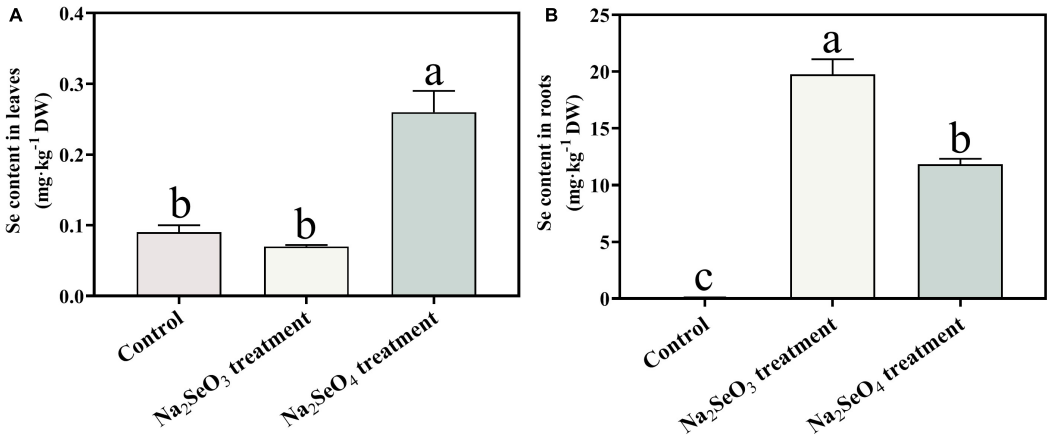


FIGURE 1 | Total Se content in leaves **(A)** and roots **(B)** of tea plants treated with selenite and selenate. Different lowercase letters in the figure indicate the significant difference at $P < 0.05$ level.

Differentially Expressed Genes and Proteins in Response to Selenite and Selenate

To elucidate the Se absorption and metabolism mechanisms in tea plants exposed to selenite and selenate, we compared relative gene and protein expression in untreated hydroponic ZC108 and in those subjected to 5 μM Na_2SeO_3 or 5 μM Na_2SeO_4 for 48 h. RNA-seq revealed 532.02 million clean reads (79.80 Gb) after data filtering and quality evaluation. The reads ranged in size from 5.98 to 7.16 Gb per sample (**Supplementary Table 3**). A heatmap analysis showed 2,272 DEGs based on comparisons of the three transcriptional datasets (padj < 0.05; $|\log_2(\text{FoldChange})| > 0.5$) (**Figure 2A**). Venn analyses revealed 806 and 939 unique genes for Na_2SeO_3 vs. control and Na_2SeO_4 vs. control, respectively. However, 99 genes were common to both groups (**Figure 2B**). In addition, 601 and 308 DEGs were upregulated while 730 and 304 DEGs were downregulated for Na_2SeO_3 vs. control and Na_2SeO_4 vs. control, respectively (**Figure 2B**).

The TMT generated 41,038 peptides and 6,632 proteins. Of the latter, 6,596 were quantified (**Supplementary Table 4**). Moreover, 192 and 201 DEPs were upregulated while 218 and 164 DEPs were downregulated for Na_2SeO_3 vs. control and Na_2SeO_4 vs. control, respectively ($P < 0.05$) (**Figures 2C,D**).

We conducted correlation analyses of the DEGs and DEPs to disclose mutual regulation between genes and proteins in response to selenite and selenate. For Na_2SeO_3 vs. control and Na_2SeO_4 vs. control, 23 and 11 DEPs and their corresponding DEGs were identified, respectively (**Figures 2E,F**).

Differentially Expressed Genes and Differentially Expressed Proteins Gene Ontology Enrichment and Kyoto Encyclopedia of Genes and Genomes Pathway Analyses

We subjected the unique 905 and 1,038 DEGs separately identified for Na_2SeO_3 vs. control and Na_2SeO_4 vs. control to GO enrichment and KEGG pathway analyses. For Na_2SeO_3 vs. control, DEGs related to protein metabolism and redox reaction were highly enriched. GO terms such as 'cellular protein catabolic process,' 'proteolysis involved in cellular protein catabolic process,' 'protein catabolic process,' and 'peptide biosynthetic process' under biological process, 'proteasome core complex,' 'peptidase complex,' and 'ribonucleoprotein complex' under cellular component, and 'oxidoreductase activity acting as donors,' 'oxidoreductase activity acting as donors and acceptor,' and 'oxidoreductase activity acting on paired donors' under molecular function were enriched (**Supplementary Figure 1**). For the KEGG pathway analysis, 'glutathione metabolism,' 'ribosome,' and 'proteasome' were highly enriched (**Figure 3**). For Na_2SeO_4 vs. control, four of the top ten GO terms under biological process were related to RNA and DNA metabolism. These included 'mRNA metabolic process,' 'RNA processing,' 'DNA repair,' and 'cellular response to DNA damage stimulus.' Under cellular component, the GO terms were related mainly to nuclear, plasma membrane, and organellar processes. Under molecular function, ADP binding was significantly enriched (**Supplementary Figure 1**). For the KEGG pathway analysis, 'RNA transport,' 'nitrogen metabolism,' and 'mismatch repair' were highly enriched (**Figure 3**). The DEPs were also subjected to KEGG pathway analysis. 'Metabolic pathways,' 'glutathione metabolism,' and 'fatty acid metabolism' were highly enriched for Na_2SeO_3 vs. control while 'metabolic pathways,' 'biosynthesis of secondary metabolites,' and 'RNA degradation' were highly enriched for Na_2SeO_4 vs. control (**Figure 3**). Among the top twenty KEGG pathways, 'glutathione metabolism' and 'tyrosine metabolism' were enriched in the transcriptomic and proteomic analyses of Na_2SeO_3 vs. control while 'RNA polymerase' was enriched in the transcriptomic and proteomic analyses of Na_2SeO_4 vs. control (**Figure 3**).

Differentially Expressed Genes Involved in Putative Se Transport and Assimilation

The transcriptome revealed 1,119 transporters. Of these, 85 were differentially expressed in response to selenite and selenate treatment (padj < 0.05; $|\log_2(\text{FoldChange})|$

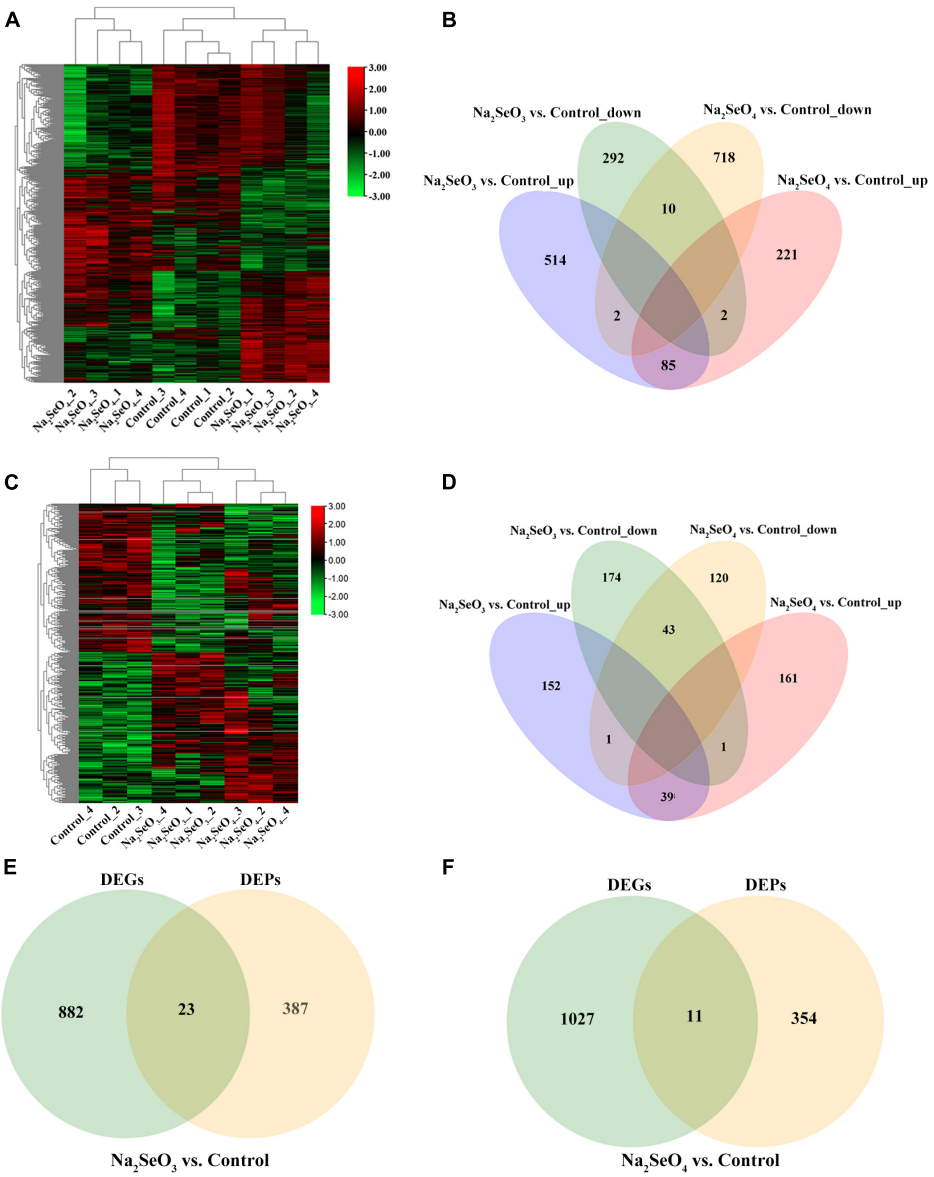


FIGURE 2 | Heatmap and Venn diagram analyses of differentially expressed genes (DEGs) and differentially expressed proteins (DEPs) in response to selenite and selenate treatments. **(A)** DEG heatmap. **(B)** Venn diagram showing overlap in numbers of upregulated and downregulated DEGs between Na_2SeO_3 vs. control and Na_2SeO_4 vs. control. **(C)** DEP heatmap. **(D)** Venn diagram showing overlap in numbers of upregulated and downregulated DEPs between Na_2SeO_3 vs. control and Na_2SeO_4 vs. control. **(E,F)** Venn diagram showing overlap in numbers of DEGs and DEPs for Na_2SeO_3 vs. control and for Na_2SeO_4 vs. control, respectively.

> 0.5). Seventy-three genes were categorized into calcium-transporting ATPase and the following transporters: ABC, sulfate, phosphate, triose-phosphate, magnesium, potassium, ZIP zinc, ferroportin, metal, cation, nitrate, auxin, lysine histidine, amino acid, peptide, sugar (and other), and others (**Figure 4**). For Na_2SeO_3 vs. control, 24 ABC transporter genes were identified. Three (evm.TU.Cha14g001230, evm.TU.ChaUn7937.2, and evm.TU.Cha13g008780) were upregulated 3. 60-, 5. 23-, and 3.63-fold, respectively, while 13 were downregulated. Of the nine nitrate transporter DEGs, four were upregulated and the expression levels of evm.TU.ChaUn9581.1 and evm.TU.Cha06g016450 had increased 4.79- and 2.01-fold, respectively. Of the eight sugar (and other) transporter DEGs, six were upregulated and the expression levels of evm.TU.Cha07g012310 and evm.TU.Cha01g007050 had increased by 2.41- and 2.51-fold, respectively. For Na_2SeO_4 vs. control, evm.TU.Cha04g018600 and evm.TU.Cha14g012510 of the ABC transporter were upregulated by 7.16- and 2.58-fold, respectively, and 18 genes were downregulated. Eight of the nitrate transporters genes were upregulated. Of these, evm.TU.ChaUn9581.1, evm.TU.ChaUn11309.1, and evm.TU.Cha02g011960 were upregulated by 7. 93-, 3. 04-, and

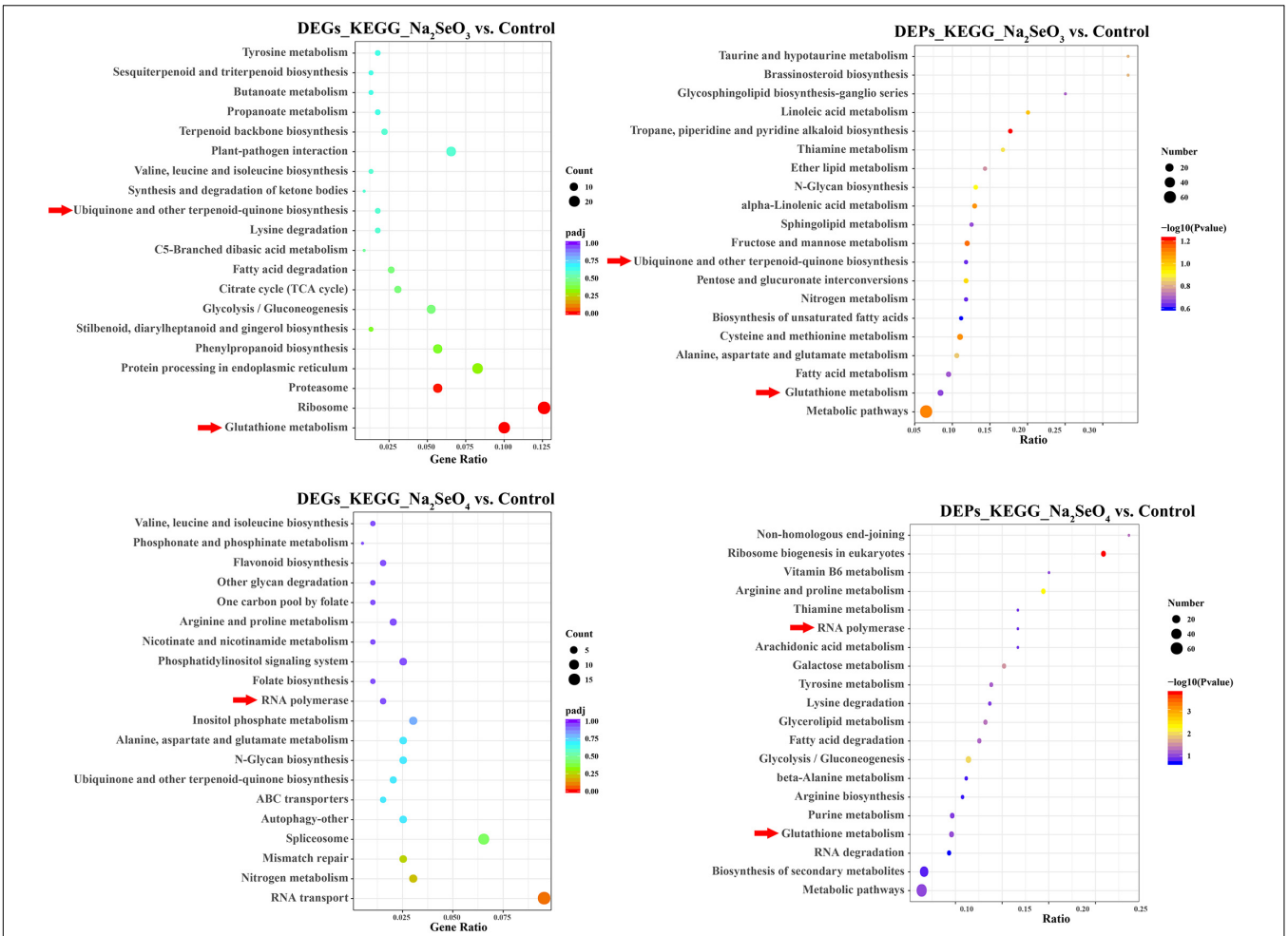


FIGURE 3 | Kyoto Encyclopedia of Genes and Genomes (KEGG) pathway analysis of DEGs and DEPs in response to selenite and selenate treatment, respectively.

2.00-fold, respectively. Six sugar (and other) transporter genes were upregulated and evm.TU.Cha02g009910 was upregulated by 4.64-fold (**Supplementary Table 5**). Hence, certain genes regulating the ABC, nitrate, and sugar transporters might also control selenite and selenate uptake and allocation.

Sulfate transporters mediate selenate uptake whereas phosphate transporters and aquaporin move selenite (White, 2016). However, only one sulfate and five phosphate transporter genes were identified for Na_2SeO_3 vs. control and Na_2SeO_4 vs. control, respectively, and no aquaporin gene was identified. We analyzed the expression patterns of all transporter-related genes to clarify their roles in response to selenite and selenate exposure in tea plants. For Na_2SeO_4 vs. control, the sulfate transporters evm.TU.Cha02g013540 (*SULTR1;1*) and evm.TU.Cha03g013130 (*SULTR2;1*) were upregulated 1.61- and 2.51-fold, respectively. For Na_2SeO_3 vs. control, the phosphate transporters evm.TU.Cha15g006520 (*PHT3;1a*), evm.TU.Cha09g013980 (*PHT3;1b*), and evm.TU.Cha09g000330 (*PHT1;8*) were upregulated 1. 53-, 1. 69-, and 1.51-fold, respectively. For Na_2SeO_3 vs. control, the aquaporins evm.TU.Cha01g023000 (*NIP2;1*) and evm.TU.Cha15g008600 (*NIP5;1*), were upregulated 5.95- and 1.53-fold, respectively (**Supplementary Figure 2**). For Na_2SeO_4 vs. control, only evm.TU.Cha09g014690 (ATP sulfurylase 1) was related to selenate reduction and its expression level was 1.59-fold higher in the selenate treatment than the control (**Figure 5**).

Differentially Expressed Genes Involved in Amino Acid Biosynthesis and Cysteine and Methionine Metabolism

The GO enrichment and KEGG pathway analyses showed that the terms and pathways related to amino acid metabolism were highly enriched. Therefore, we analyzed the expression pattern of the DEGs related to amino acid biosynthesis and cysteine and methionine metabolism (**Figure 5**). For Na_2SeO_3 vs. control, 14 of 24 DEGs associated with amino acid biosynthesis were upregulated while evm.TU.Cha14g006470, evm.TU.Cha11g006230, and evm.TU.ChaUn6796.5 had increased by 3. 22-, 2. 25-, and 2.18-fold, respectively. For Na_2SeO_4 vs. control, 12 DEGs associated with amino acid biosynthesis were upregulated, evm.TU.Cha14g006470

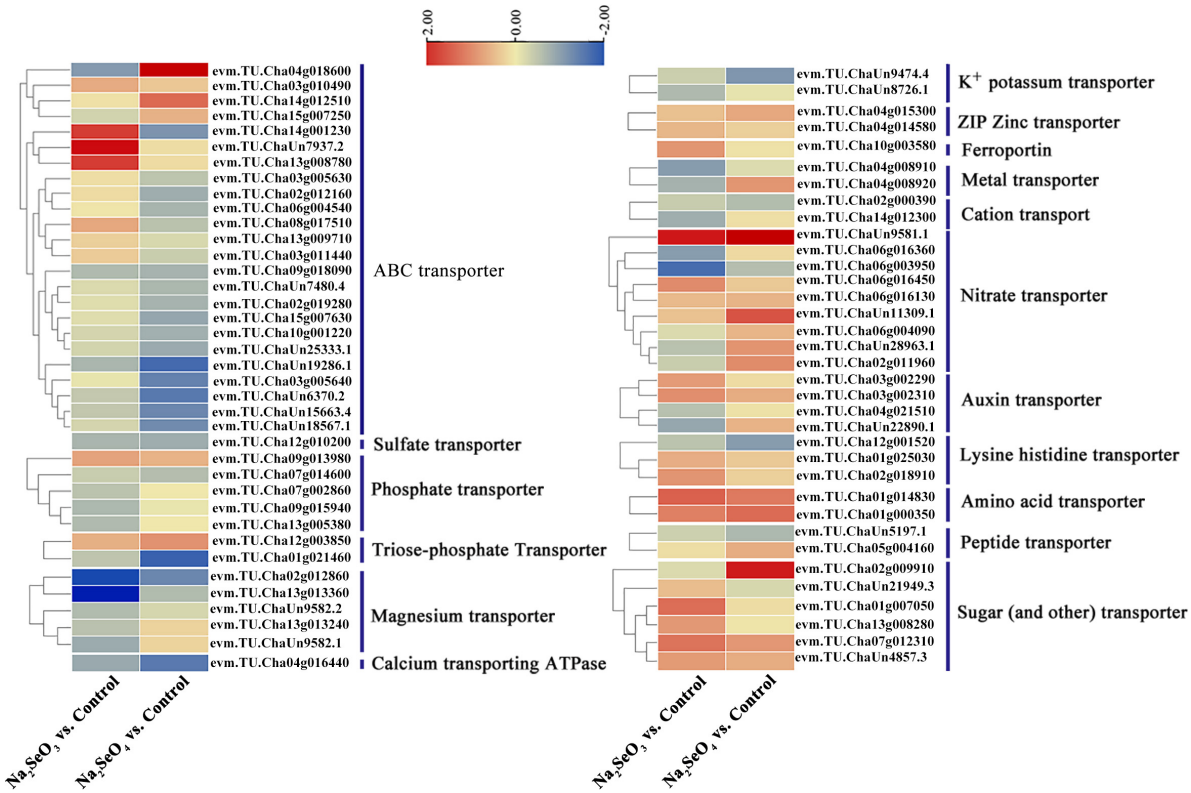


FIGURE 4 | Heatmap of putative Se transporters identified from DEGs. Different colors indicate different gene expression levels based on $\log_2$ FoldChange. The same below.

expression had increased 2.17-fold, and 12 other genes were downregulated. For cysteine and methionine metabolism, evm.TU.Cha08g010320, evm.TU.Cha12g001220, and evm.TU.ChaUn15902.4 were upregulated 11. 31-, 4. 25-, and 2.11-fold, respectively, in response to selenite treatment. By contrast, no gene was upregulated by more than twofold in response to selenate treatment (**Supplementary Table 6**). Thus, the genes related to amino acid metabolism were more strongly induced by selenite than selenate.

Differentially Expressed Genes and Differentially Expressed Proteins Involved in Glutathione Metabolism

A KEGG pathway analysis of the top 20 enrichments disclosed that the DEGs related to glutathione metabolism were enriched for both Na_2SeO_3 vs. control and Na_2SeO_4 vs. control. However, the DEPs related to glutathione metabolism were upregulated for Na_2SeO_4 vs. control (**Figure 3**). The combination of transcriptomic and proteomic data revealed 49 DEGs and their corresponding DEPs in the glutathione metabolism pathway (**Figure 6**). After selenite treatment, 29 DEGs of EC 2.5.1.8 (glutathione *S*-transferase, GST) and their DEPs were identified. Of these, 22 were upregulated. The genes evm.TU.Cha06g019020 and evm.TU.Cha08g013730 were upregulated at both the transcriptional and post-transcriptional levels. The genes evm.TU.Cha06g001700 and evm.TU.ChaUn4653.1 of EC PepA (leucyl aminopeptidase) as well as evm.TU.Cha11g005300 and novel.5164 of EC 1.11.1.11 (L-ascorbate peroxidase) were upregulated. Few genes responded to selenate fertilization (**Supplementary Table 7**). Hence, glutathione metabolism pathway was more strongly induced by selenite than selenate.

Integrated Transcriptomic and Proteomic Dataset Analysis

The GO enrichment and KEGG pathway analyses were conducted on integrated DEG and DEP data. For Na_2SeO_3 vs. control, the upregulated DEPs and DEGs were categorized under the GO terms 'oxidation-reduction process,' 'protein binding,' 'response to stress,' 'single-organism process,' 'metabolic process,' and 'ammonium transport,' and under the KEGG terms 'protein processing in endoplasmic reticulum,' 'glutathione metabolism,' and 'metabolic pathways.' For Na_2SeO_4 vs. control, the upregulated DEPs and DEGs were categorized under the GO terms 'response to stress' and 'metabolic process' and under the KEGG term 'metabolic pathways' (**Figure 7**).

Differentially Expressed Genes Validation by RT-qPCR

To verify RNA-Seq data accuracy and reliability, 28 genes related to the ABC, sulfate, and phosphate transporters, glutathione and

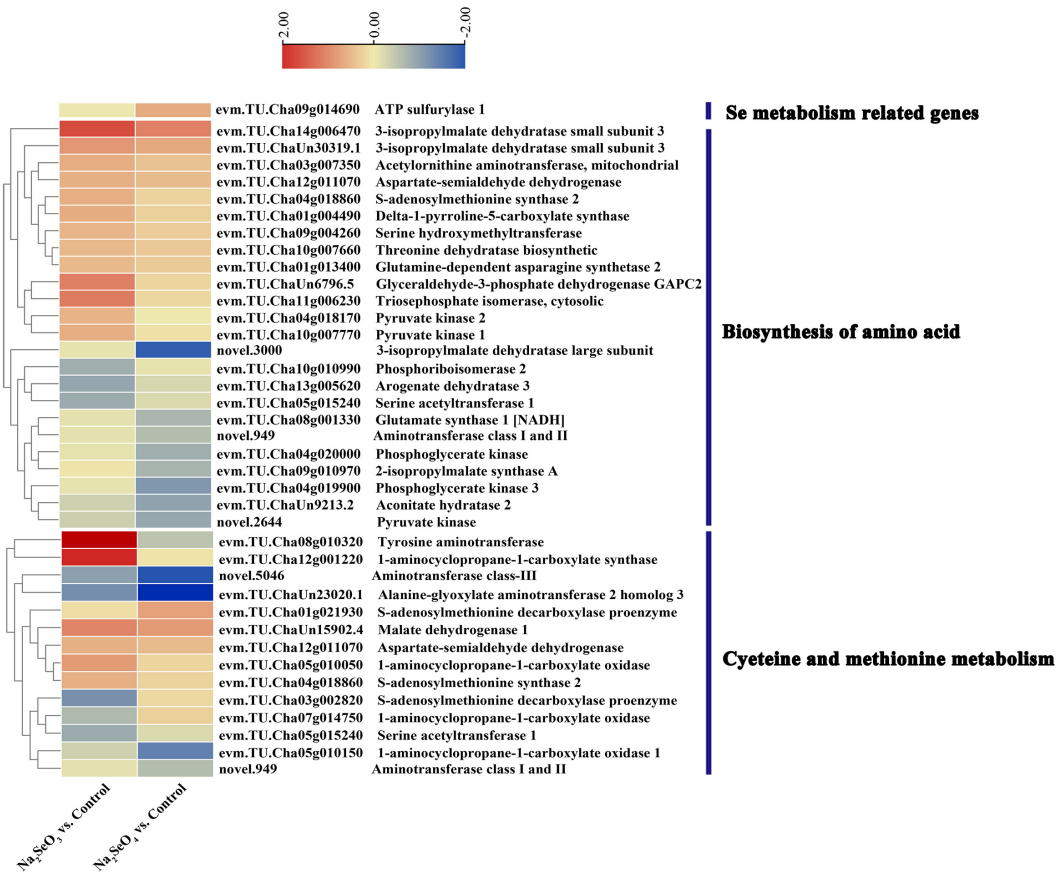


FIGURE 5 | Heatmap of DEGs related to selenium and amino acid metabolism in response to selenite and selenate exposure.

amino acid metabolism, and others were selected for RT-qPCR analysis. The expression patterns demonstrated by RNA-Seq and RT-qPCR were consistent for 24 genes under Na_2SeO_4 vs. control and for 26 genes under Na_2SeO_3 vs. control (**Figure 8**). Therefore, the RNA-seq data were reliable.

DISCUSSION

Multi-omics technologies have been implemented in studies related to selenium disposition in many other plants. However, single omics method was usually applied toward this particular research in tea plants (Cao et al., 2018; Jia et al., 2020). In this study, both transcriptome and proteome techniques were applied to explore the transcriptional and post-transcriptional changes in tea plants after treated with selenite and selenate, respectively, illustrating the primary mechanism of selenium disposition in tea plants. Independent and joint analyses were carried out using the transcriptomic and proteomic data, and DEGs, DEPs and enrichment pathways were comprehensive discovered. In joint omics analysis, only a minimal fraction of DEPs and corresponding DEGs were identified, and the gene expression and protein expression also correlated modestly. Such observations are not unprecedented. Poor correlation between protein expression and gene expression changes were also commonly found in other species. We also speculated that the relative low-concentration of selenium of 5 $\mu mol \cdot L^{-1}$ and a short-time of 48 h treatment, which might not be sufficient to induce a large number of DEGs and DEPs, may account for this phenomenon. On the whole, the quality control and expression verification of omics data confirmed that our data are reliable, which will provide beneficial support for the study of selenium enrichment mechanism in tea plants.

Se Uptake and Metabolism

After roots absorb selenite, they accumulate it and rapidly convert it to organoselenium compounds such as selenocysteine (SeCys), selenomethionine (SeMet), selenomethionine Se-oxide (SeOMet), and Se-methyl-selenocysteine (MeSeCys). By contrast, roots immediately translocate the selenate they absorb to the shoot (Li et al., 2008; White, 2016). Here, the highest total Se content was detected in the roots of plants supplemented with selenite and in the leaves of plants supplemented with selenate. Similar results were reported for maize and wheat (Li et al., 2008; Longchamp et al., 2015).

Integrated transcriptome and proteome analyses were conducted to clarify selenite and selenate uptake, translocation, and assimilation in tea plants. The ABC, nitrate, and sugar

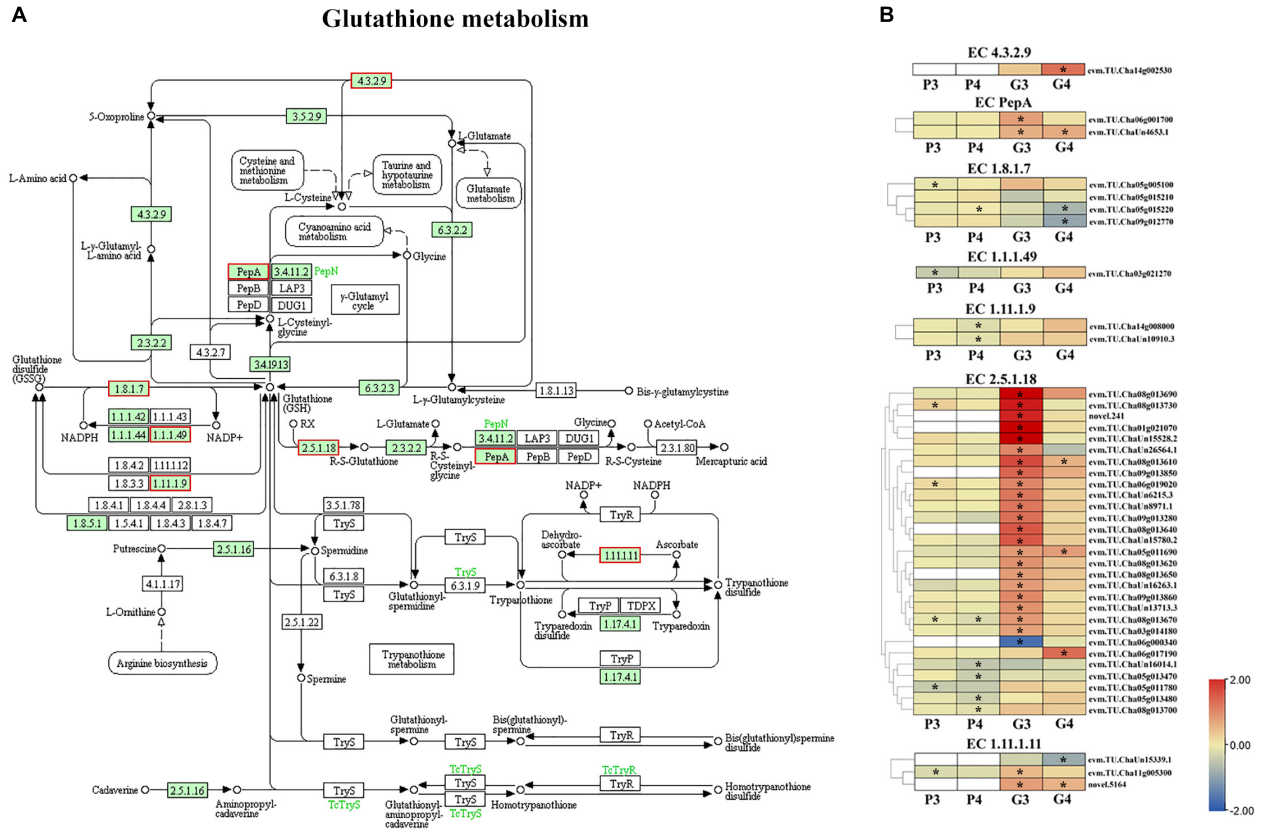


FIGURE 6 | Genes and proteins involved in glutathione metabolism pathway. **(A)** Red rectangles represent DEGs or DEPs. **(B)** DEG and DEP heatmaps. P3 and P4 represent DEPs for Na_2SeO_3 vs. control and for Na_2SeO_4 vs. control, respectively. G3 and G4 represent DEGs for Na_2SeO_3 vs. control and for Na_2SeO_4 vs. control, respectively. Different colors indicate different levels of protein or gene expression based on log_2 FoldChange. White rectangles indicate no DEGs or DEPs. Asterisks represent DEPs with $P < 0.05$ or DEGs with padj < 0.05.

transporters were all responsive to selenite and selenate. The ABC transporter catalyzes ATP and provides energy for the transmembrane transport of substrates such as simple ions, peptides, complex lipids, and small proteins. The ABC transporter also plays important roles in biotic and abiotic stress response (Theodoulou and Kerr, 2015). In perennial ryegrass, ABCA transporters regulate Se movement and accumulation. *ATH* genes in the ABCA subfamily were upregulated in response to selenite exposure (Byrne et al., 2010). ABCC family genes control the disposition of cytotoxic and xenobiotic compounds and play crucial roles in stress tolerance (Kim et al., 2013). *ABCG14* participates in phytohormone transport (Gräfe and Schmitt, 2021). Selenite treatment upregulated the extracellular ABC transporter genes *ABCA2* and *ABCC4* while selenate exposure increased *ABCC8* and *ABCG14* expression. Therefore, the foregoing genes may also control Se uptake and tolerance in tea plants. Nitrate transporters regulate plant nitrate uptake and allocation. *NRT1;11* moves nitrate to young leaves. *NRT2;4* and *NRT2;5* regulate root nitrate absorption from the soil (Wang et al., 2018). Here, we found that selenite exposure induced *NRT2;4* and *NRT2;5* whereas *NRT1;11* and *NRT2;4* were upregulated by selenate in tea plants. NRTs may mediate both selenite uptake and selenate allocation. Sugar transporters mediate long-distance sucrose movement in the phloem (Julius et al., 2017). In this study, eight and six sugar transporter genes were upregulated in response to selenite and selenate treatment, respectively. Thus, sugar transporters might be implicated in selenite and selenate transport.

Sulfate transporters participate in selenate uptake while selenite absorption is mediated mainly by phosphate transporters and aquaporin. When tea plants were subjected to low-Se treatment (30 $\mu mol \cdot L^{-1}$ Se) for 4 days, 23 genes were downregulated and only *CsPHT3;1* was upregulated. When the tea plants were exposed to high Se levels (500–10,000 $\mu mol \cdot L^{-1}$ Se), most of their *CsPHT* genes were upregulated (Cao et al., 2021). Only a few DEGs, one sulfate transporter gene, and five phosphate transporter genes were identified in the present study possibly because the tea plants were exposed to only 5 $\mu mol \cdot L^{-1}$ Se. Therefore, we conducted other expression analyses on sulfate and phosphate transporters and aquaporin based on raw transcriptomic data. For the sulfate transporter, the high-affinity genes *SULTR1;1* and *SULTR1;2* are involved in selenate absorption (Rouached et al., 2008). The low-affinity genes *SULTR2;1* and *SULTR2;2* mediate sulfate transport from

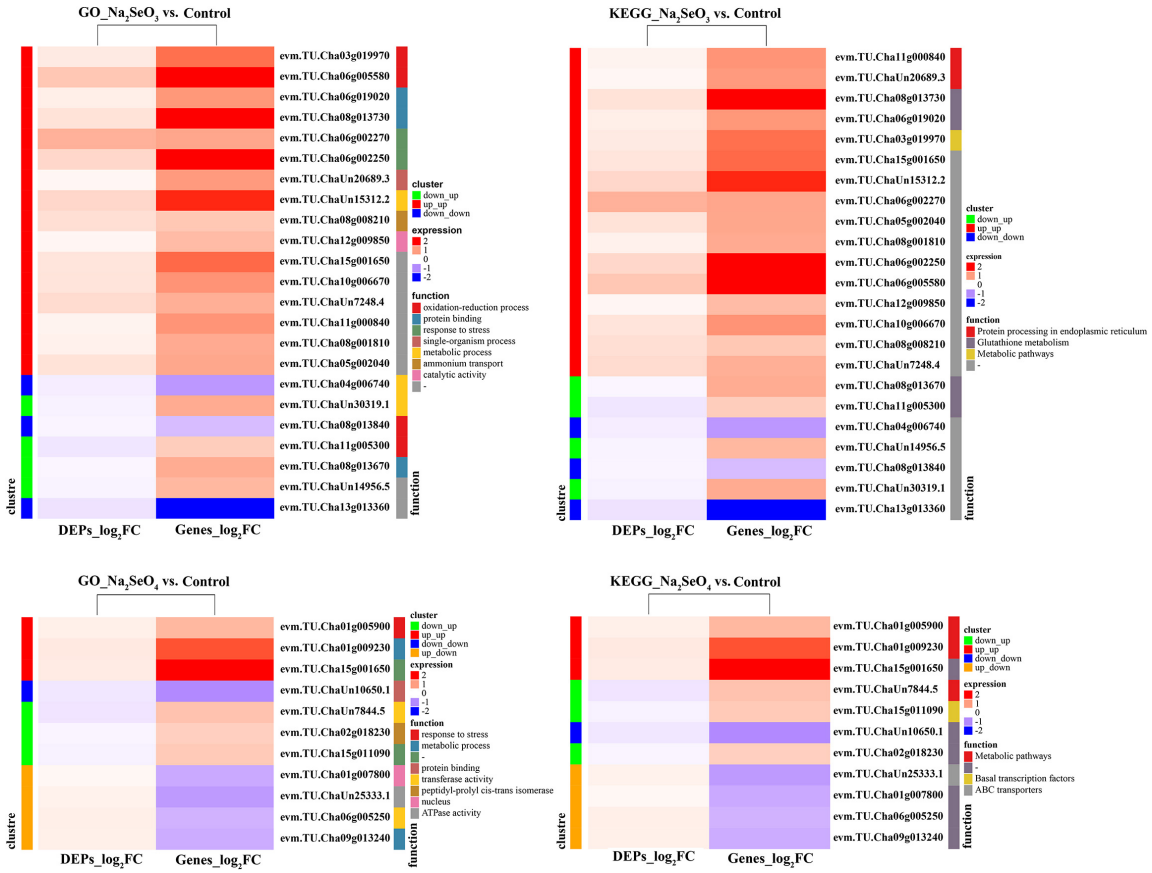


FIGURE 7 | Heatmap of GO enrichment and KEGG pathway analyses of DEPs and their corresponding DEGs.

the roots to the leaves (Takahashi et al., 2000). We found that *CsSULTR1;1* and *CsSULTR2;1* were upregulated in response to selenate treatment. In tea plants exposed to selenate, Se accumulation was relatively greater in the leaves.

Most members of the PHT1 subfamily are associated with selenite and Pi uptake and translocation in plants (Song et al., 2017; Wang et al., 2017; Cao et al., 2021). PHT3 proteins play vital roles in Pi exchange between the cytoplasm and the mitochondrial matrix and are essential for ATP biosynthesis (Wang et al., 2017). Aquaporins are permeable to selenite and *OsNIP2;1* is related to selenite uptake (Zhao et al., 2010). In this study, *CsPHT1;3b*, *CsPHT1;8,* and *CsPHT3;1a* were upregulated in response to selenite treatment. Compared with the control, *CsNIP2;1* expression increased 5.95-fold following selenite exposure. For these reasons, *CsPHT1*, *CsPHT3*, and *CsNIP2;1* might play important roles in selenite uptake in tea plants.

Absorbed selenate utilizes the sulfur assimilation pathway, is reduced to adenosine 5′-phosphoselenate (APSe) and SeO_3^{2-}, and eventually forms organoselenium compounds (Guignardi and Schiavon, 2017). ATP sulfurylase (*APS*) is the first rate-limiting enzyme in selenate assimilation into APSe (Pilon-Smits and LeDuc, 2009). We found that *CsAPS1* was upregulated in the roots of tea plants subjected to selenate. Consequently, *CsAPS1* may play a vital role in selenate reduction.

Selenite assimilation occurs either enzymatically or non-enzymatically via glutathione (GSH). After selenite is absorbed by the roots, it is converted into organoselenium compounds (Pilon-Smits and Quinn, 2010; Guignardi and Schiavon, 2017). Here, we found that most genes related to glutathione metabolism were highly upregulated in the roots of tea plants treated with selenite. Hence, genes related to glutathione metabolism may be involved in selenite assimilation in tea roots.

Responses of Amino Acid Metabolism-Related Genes to Selenite and Selenate

Selenite and selenate application for 4 weeks can significantly enhance the total amino acid content in tea plants (Hu et al., 2003). Here, selenite supplementation highly enriched GO terms related to amino acids, peptides, and proteins metabolism. Certain genes related to amino acid metabolism were differentially expressed in response to selenite and selenate treatment. Glyceraldehyde-3-phosphate dehydrogenase (GAPDH) induces protein expression and DNA repair (White and Garcin, 2017). Triose phosphate isomerase (TPI) plays an important role in the tricarboxylic acid (TCA) cycle and is indispensable in energy production (Lone et al., 2018).

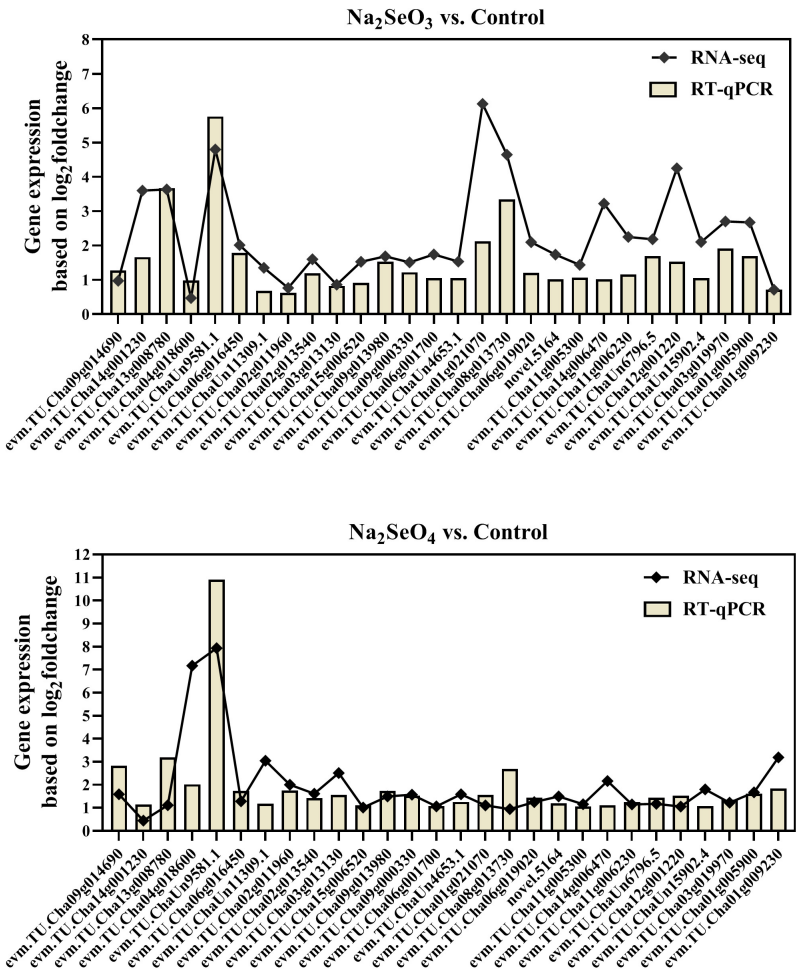


FIGURE 8 | Validation of gene expression by RT-qPCR.

ACC synthase (1-aminocyclopropane-1-carboxylate synthase) catalyzes the biosynthesis of ethylene which plays a crucial role in plant tolerance to biotic and abiotic stress (Houben and Van de Poel, 2019). Malate dehydrogenase (MDH) oxidize oxaloacetic acid to malate and also enhances plant stress tolerance (Wu et al., 2007). Tyrosine aminotransferase (TAT) catalyzes the biosynthesis of the free radical scavenger vitamin E (Sandorf and Holländer-Czytko, 2002). Here, the foregoing genes were upregulated by over twofold in response to selenite fertilization but by not more than twofold following selenate supplementation. In tea plants, selenite treatment promoted amino acid and protein biosynthesis and enhanced stress tolerance in tea plants to a greater extent than selenate fertilization.

Redox and Antistress-Related Gene and Protein Expression in Response to Selenite and Selenate

High Se concentrations are phytotoxic as they cause non-specific, disruptive selenoamino acid incorporation into proteins (Guignardi and Schiavon, 2017). Genes and proteins related to glutathione metabolism play important roles in assimilation and tolerance of Se in plants (Chauhan et al., 2020; Rao et al., 2021). After long-term selenite treatment on tea seedlings, glutathione metabolism was differentially regulated (Cao et al., 2018), remarkably, the expression of glutathione metabolism related genes and proteins were highly induced even with the short-term treatments of selenate and selenite in this study. Particularly, the antioxidant enzyme L-ascorbate peroxidase (APX) gene, related to glutathione metabolism and playing roles in protecting plants against oxidative stress (Uarrota et al., 2016), was significantly upregulated in the both treatments. Moreover, the importance of glutathione metabolism in tea plant response to selenate and selenite may not be the same. In response to selenite treatment here, 22/29 *GSTs* were upregulated in the roots and two of these genes were upregulated at both the transcriptional and post-transcriptional levels. By contrast, only three *GST* genes were upregulated in tea roots exposed to selenate. A GO enrichment analysis integrating transcriptome and proteome data showed that the two genes responding to selenite stress were upregulated at both the transcriptional and post-transcriptional

levels. Nevertheless, only a single gene responding to selenate treatment was upregulated at both the transcriptional and post-transcriptional levels. The positive roles of GST in enhancing stress tolerance are highlighted in plants (Brentner et al., 2008; Xu et al., 2016; Wang M. et al., 2019). These findings suggest that for tea plants, selenite is relatively more phytotoxic than selenate and GST-mediated metabolism may be essential for tea plant detoxification. Definitely, further functional studies on the redox and antistress-related genes in the absorption and metabolism of selenium in tea plants should be undertaken in future.

CONCLUSION

The present study combined transcriptome and proteome analyses to elucidate selenite and selenate uptake, allocation, and metabolism in tea plants. The Se content significantly increased in the roots of tea plants supplemented with selenite but significantly increased in the leaves of tea plants supplemented with selenate. The selenite treatment induced genes regulating the ABC, nitrate, and sugar transporters. The putative selenite uptake- and transport-regulating genes *PHT3;1a*, *PHT1;3b*, *PHT1;8*, and *NIP2;1* were also upregulated in tea plants subjected to selenite. Most genes and certain proteins associated with amino acid and glutathione metabolism and stress response were upregulated and may mediate Se assimilation and tolerance in tea plants. The selenate treatment induced genes regulating the ABC, nitrate, and sugar transporters as well as *SULTR1;1* and *SULTR2;1*. The latter two may participate in selenate absorption and translocation. Selenate exposure also induced ATP sulfurylase 1 which is the first rate-limiting step in selenate assimilation into APSe. The integrated analyses of Se content, genes, and proteins in this study may help clarify the mechanisms of selenite and selenate absorption and metabolism in tea plants.

DATA AVAILABILITY STATEMENT

The datasets presented in this study can be found in online repositories. The names of the repository/repositories and accession number(s) can be found below: National Center for Biotechnology Information (NCBI) BioProject database under accession number PRJNA795019. The mass spectrometry proteomics data deposited to the ProteomeXchange Consortium (http://proteomecentral.proteomexchange.org) have been permitted and assigned the dataset identifier PXD030944.

AUTHOR CONTRIBUTIONS

XH and JZ conceived and supervised the experiments. HR, XL, and LG performed the experiments. HR, XL, XH, and LW analyzed the results. HR wrote the manuscript. XH and JZ reviewed and edited the manuscript. All authors contributed to the article and approved the submitted version.

FUNDING

This work was supported by the Agricultural Science and Technology Innovation Program of the Chinese Academy of Agricultural Sciences (No. CAAS-XTCX20190025-7), the Special R&D Program Project of the Chinese Academy of Se-Enriched Industry (Nos. 2019QCY-1.2 and 2019QCY-1.3), and the Agricultural Sciences and Technology Innovation Program of the Chinese Academy of Agricultural Sciences (ASTIP).

SUPPLEMENTARY MATERIAL

The Supplementary Material for this article can be found online at: https://www.frontiersin.org/articles/10.3389/fpls.2022.848349/full#supplementary-material

Supplementary Figure 1 | Gene ontology (GO) enrichment analysis of differentially expressed genes (DEGs) in response to selenite and selenate treatment in tea plants.

Supplementary Figure 2 | Heatmap of transcriptomic data related to putative selenite and selenate transporters. Different colors indicate different gene expression levels based on log2 FoldChange.

REFERENCES

Brentner, L. B., Mukherji, S. T., Merchie, K. M., Yoon, J. M., Schnoor, J. L., and Van Aken, B. V. (2008). Expression of glutathione S-transferases in poplar trees (*Populus trichocarpa*) exposed to 2,4,6-trinitrotoluene (TNT). *Chemosphere* 73, 657–662. doi: 10.1016/j.chemosphere.2008.07.059

Byrne, S. L., Durandeau, K., Nagy, I., and Barth, S. (2010). Identification of ABC transporters from *Lolium perenne* L. that are regulated by toxic levels of selenium. *Planta* 231, 901–911. doi: 10.1007/s00425-009-1096-y

Cao, D., Liu, Y., Ma, L., Jin, X., Guo, G., Tan, R., et al. (2018). Transcriptome analysis of differentially expressed genes involved in selenium accumulation in tea plant (*Camellia sinensis*). *PLoS One* 13:e0197506. doi: 10.1371/journal.pone.0197506

Cao, D., Liu, Y., Ma, L., Liu, Z., Li, J., Wen, B., et al. (2021). Genome-wide identification and characterization of phosphate transporter gene family members in tea plants (*Camellia sinensis* L. O. Kuntze) under different selenite levels. *Plant Physiol Biochem.* 166, 668–676. doi: 10.1016/j.plaphy.2021.06.038

Chang, S., Puryear, J., and Cairney, J. (1993). A simple and efficient method for isolating RNA from pine trees. *Plant Mol. Biol.* 11, 113–116. doi: 10.1007/BF02670468

Chauhan, R., Awasthi, S., Indoliya, Y., Chauhan, A. S., Mishra, S., Agrawal, L., et al. (2020). Transcriptome and proteome analyses reveal selenium mediated amelioration of arsenic toxicity in rice (*Oryza sativa* L.). *J. Hazard. Mater.* 390:122122. doi: 10.1016/j.jhazmat.2020.122122

Chen, C., Chen, H., Zhang, Y., Thomas, H. R., Frank, M. H., He, Y., et al. (2020). TBtools: an integrative toolkit developed for interactive analyses of big biological data. *Mol. Plant.* 13, 1194–1202. doi: 10.1016/j.molp.2020.06.009

El Kassis, E., Cathala, N., Rouached, H., Fourcroy, P., Berthomieu, P., Terry, N., et al. (2007). Characterization of a selenate-resistant *Arabidopsis mutant*. Root growth as a potential target for selenate toxicity. *Plant Physiol.* 143, 1231–1241. doi: 10.1104/pp.106.091462

Feng, R., Wei, C., and Tu, S. (2013). The roles of selenium in protecting plants against abiotic stresses. *Environ. Exp. Bot.* 87, 58–68. doi: 10.1016/j.envexpbot.2012.09.002

Gao, Z., Cai, H., Peng, C., and Dong, Y. (2014). Distribution rule and combined forms of selenium in selenium-enriched tea. *Food Nutr. China.* 20, 31–33.

Gigolashvili, T., and Kopriva, S. (2014). Transporters in plant sulfur metabolism. *Front. Plant Sci.* 5:442. doi: 10.3389/fpls.2014.00442

Gräfe, K., and Schmitt, L. (2021). The ABC transporter G subfamily in *Arabidopsis thaliana*. *J. Exp. Bot.* 72, 92–106. doi: 10.1093/jxb/eraa260

Guignardi, Z., and Schiavon, M. (2017). Biochemistry of plant selenium uptake and metabolism. *Plant Ecophysiol.* 6, 21–34. doi: 10.1007/978-3-319-56249-0_2

Hao, X., Horvath, D. P., Chao, W. S., Yang, Y., Wang, X., and Xiao, B. (2014). Identification and evaluation of reliable reference genes for quantitative real-time PCR analysis in tea plant (*Camellia sinensis* (L.) O. Kuntze). *Int. J. Mol. Sci.* 15, 22155–22172. doi: 10.3390/ijms151222155

Hao, X., Tang, H., Wang, B., Yue, C., Wang, L., Zeng, J., et al. (2018). Integrative transcriptional and metabolic analyses provide insights into cold spell response mechanisms in young shoots of the tea plant. *Tree Physiol.* 38, 1655–1671. doi: 10.1093/treephys/tpy038

Houben, M., and Van de Poel, B. (2019). 1-aminocyclopropane-1-carboxylic acid oxidase (ACO): the enzyme that makes the plant hormone ethylene. *Front. Plant Sci.* 10:695. doi: 10.3389/fpls.2019.00695

Hu, Q., Xu, J., and Pang, G. (2003). Effect of selenium on the yield and quality of green tea leaves harvested in early spring. *J. Agric. Food Chem.* 51, 3379–3381. doi: 10.1021/jf0341417

Jia, W., Liu, Y., Shi, L., and Chu, X. (2020). Investigation of differentially expressed proteins induced by alteration of natural Se uptake with ultrahigh-performance liquid chromatography quadrupole Orbitrap uncovers the potential nutritional value in Se-enriched green tea. *J. Agric. Food Chem.* 68, 6316–6332. doi: 10.1021/acs.jafc.0c02130

Jones, P., Binns, D., Chang, H. Y., Fraser, M., Li, W., McAnulla, C., et al. (2014). InterProScan 5: genome-scale protein function classification. *Bioinformatics* 30, 1236–1240. doi: 10.1093/bioinformatics/btu031

Julius, B. T., Leach, K. A., Tran, T. M., Mertz, R. A., and Braun, D. M. (2017). Sugar transporters in plants: new insights and discoveries. *Plant Cell Physiol.* 58, 1442–1460. doi: 10.1093/pcp/pcx090

Kim, Y., Park, S. Y., Kim, D., Choi, J., Lee, Y. H., Lee, J. H., et al. (2013). Genome-scale analysis of ABC transporter genes and characterization of the ABCC type transporter genes in *Magnaporthe oryzae*. *Genomics* 101, 354–361. doi: 10.1016/j.ygeno.2013.04.003

Li, H. F., McGrath, S. P., and Zhao, F. J. (2008). Selenium uptake, translocation and speciation in wheat supplied with selenate or selenite. *New Phytol.* 178, 92–102. doi: 10.1111/j.1469-8137.2007.02343.x

Liu, T. Y., Huang, T. K., Yang, S. Y., Hong, Y. T., Huang, S. M., Wang, F. N., et al. (2016). Identification of plant vacuolar transporters mediating phosphate storage. *Nat. Commun.* 7:11095. doi: 10.1038/ncomms11095

Lone, S. N., Maqbool, R., Parray, F. Q., and Ul Hussain, M. (2018). Triose-phosphate isomerase is a novel target of miR-22 and miR-28, with implications in tumorigenesis. *J. Cell. Physiol.* 233, 8919–8929. doi: 10.1002/jcp.26821

Longchamp, M., Castrec-Rouelle, M., Biron, P., and Bariac, T. (2015). Variations in the accumulation, localization and rate of metabolization of selenium in mature Zea mays plants supplied with selenite or selenate. *Food Chem.* 182, 128–135. doi: 10.1016/j.foodchem.2015.02.137

Love, M. I., Huber, W., and Anders, S. (2014). Moderated estimation of fold change and dispersion for RNA-Seq data with DESeq2. *Genome Biol.* 15:550. doi: 10.1186/s13059-014-0550-8

Niu, H., Zhan, K., Xu, W., Peng, C., Hou, C., Li, Y., et al. (2020). Selenium treatment modulates fluoride distribution and mitigates fluoride stress in tea plant (*Camellia sinensis* (L.) O. Kuntze). *Environ. Pollut.* 267:115603. doi: 10.1016/j.envpol.2020.115603

Parkhomchuk, D., Borodina, T., Amstislavskiy, V., Banaru, M., Hallen, L., Krobitsch, S., et al. (2009). Transcriptome analysis by strand-specific sequencing of complementary DNA. *Nucleic Acids Res.* 37:e123. doi: 10.1093/nar/gkp596

Pieczyñska, J., and Grajeta, H. (2015). The role of selenium in human conception and pregnancy. *J. Trace Elem. Med. Biol.* 29, 31–38. doi: 10.1016/j.jtemb.2014.07.003

Pilon-Smits, E. A. H., and LeDuc, D. L. (2009). Phytoremediation of selenium using transgenic plants. *Curr. Opin. Biotechnol.* 20, 207–212. doi: 10.1016/j.copbio.2009.02.001

Pilon-Smits, E. A. H., and Quinn, C. F. (2010). Selenium metabolism in plants. *Plant Cell Monogr.* 7, 225–241. doi: 10.1016/j.bbagen.2018.05.006

Rao, S., Yu, T., Cong, X., Lai, X., Xiang, J., Cao, J., et al. (2021). Transcriptome, proteome, and metabolome reveal the mechanism of tolerance to selenate toxicity in *Cardamine violifolia*. *J. Hazard. Mater.* 406:124283. doi: 10.1016/j.jhazmat.2020.124283

Rouached, H., Wirtz, M., Alary, R., Hell, R., Arpat, A. B., Davidian, J. C., et al. (2008). Differential regulation of the expression of two high-affinity sulfate transporters, SULTR1.1 and SULTR1.2, in *Arabidopsis*. *Plant Physiol.* 147, 897–911. doi: 10.1104/pp.108.118612

Ruan, J., Gerendás, J., Härdter, R., and Sattelmacher, B. (2007). Effect of nitrogen form and root-zone pH on growth and nitrogen uptake of tea (*Camellia sinensis*) plants. *Ann. Bot.* 99, 301–310. doi: 10.1093/aob/mcl258

Sandorf, I., and Holländer-Czytko, H. (2002). Jasmonate is involved in the induction of tyrosine aminotransferase and tocopherol biosynthesis in *Arabidopsis thaliana*. *Planta* 216, 173–179. doi: 10.1007/s00425-002-0888-0

Song, Z., Shao, H., Huang, H., Shen, Y., Wang, L., Wu, F., et al. (2017). Overexpression of the phosphate transporter gene OsPT8 improves the Pi and selenium contents in *Nicotiana tabacum*. *Environ. Exp. Bot.* 137, 158–165. doi: 10.1016/j.envexpbot.2017.02.011

Sors, T. G., Ellis, D. R., and Salt, D. E. (2005). Selenium uptake, translocation, assimilation and metabolic fate in plants. *Photosynth. Res.* 86, 373–389. doi: 10.1007/s11120-005-5222-9

Takahashi, H. (2019). Sulfate transport systems in plants: functional diversity and molecular mechanisms underlying regulatory coordination. *J. Exp. Bot.* 70, 4075–4087. doi: 10.1093/jxb/erz132

Takahashi, H., Watanabe-Takahashi, A., Smith, F. W., Blake-Kalff, M., Hawkesford, M. J., and Saito, K. (2000). The roles of three functional sulphate transporters involved in uptake and translocation of sulphate in *Arabidopsis thaliana*. *Plant J.* 23, 171–182. doi: 10.1046/j.1365-313x.2000.00768.x

Tan, L. C., Nancharaiah, Y. V., van Hullebusch, E. D., and Lens, P. N. L. (2016). Selenium: environmental significance, pollution, and biological treatment technologies. *Biotechnol. Adv.* 34, 886–907. doi: 10.1016/j.biotechadv.2016.05.005

Theodoulou, F. L., and Kerr, I. D. (2015). ABC transporter research: going strong 40 years on. *Biochem. Soc. Trans.* 43, 1033–1040. doi: 10.1042/BST20150139

Uarrota, V. G., Moresco, R., Schmidt, E. C., Bouzon, Z. L., Nunes, E. C., Neubert, E. O., et al. (2016). The role of ascorbate peroxidase, guaiacol peroxidase, and polysaccharides in cassava (*Manihot esculenta* Crantz) roots under postharvest physiological deterioration. *Food Chem.* 197, 737–746. doi: 10.1016/j.foodchem.2015.11.025

Wang, D., Lv, S., Jiang, P., and Li, Y. (2017). Roles, regulation, and agricultural application of plant phosphate transporters. *Front. Plant Sci.* 8:817. doi: 10.3389/fpls.2017.00817

Wang, L., Yao, L., Hao, X., Li, N., Wang, Y., Ding, C., et al. (2019). Transcriptional and physiological analyses reveal the association of ROS metabolism with cold tolerance in tea plant. *Environ. Exp. Bot.* 160, 45–58. doi: 10.1016/j.envexpbot.2018.11.011

Wang, M., Wang, Y., Zhang, Y., Li, C., and Gong, S. (2019). Comparative transcriptome analysis of salt-sensitive and salt-tolerant maize reveals potential mechanisms to enhance salt resistance. *Genes Genom.* 41, 781–801. doi: 10.1007/s13258-019-00793-y

Wang, X., Feng, H., Chang, Y., Ma, C., Wang, L., Hao, X., et al. (2020). Population sequencing enhances understanding of tea plant evolution. *Nat. Commun.* 11:4447. doi: 10.1038/s41467-020-18228-8

Wang, Y. Y., Cheng, Y. H., Chen, K. E., and Tsay, Y. F. (2018). Nitrate transport, signaling, and use efficiency. *Annu. Rev. Plant Biol.* 69, 85–122. doi: 10.1146/annurev-arplant-042817-040056

White, M. R., and Garcin, E. D. (2017). D-glyceraldehyde-3-phosphate dehydrogenase structure and function. *Subcell. Biochem.* 83, 413–453. doi: 10.1007/978-3-319-46503-6_15

White, P. J. (2016). Selenium accumulation by plants. *Ann. Bot.* 117, 217–235. doi: 10.1093/aob/mcv180

Wu, J. L., Wu, Q. P., Huang, J. M., Chen, R., Cai, M., and Tan, J. B. (2007). Effects of L-malate on physical stamina and activities of enzymes related to the malate-aspartate shuttle in liver of mice. *Physiol. Res.* 56, 213–220. doi: 10.33549/physiolres.930937

Wu, X., Xiong, E., Wang, W., Scali, M., and Cresti, M. (2014). Universal sample preparation method integrating trichloroacetic acid/acetone precipitation with phenol extraction for crop proteomic analysis. *Nat. Protoc.* 9, 362–374. doi: 10.1038/nprot.2014.022

Xia, E. H., Zhang, H. B., Sheng, J., Li, K., Zhang, Q. J., Kim, C., et al. (2017). The tea tree genome provides insights into tea flavor and independent evolution of caffeine biosynthesis. *Mol. Plant.* 10, 866–877. doi: 10.1016/j.molp.2017.04.002

Xiang, C., Li, W., Ren, H., Wu, S., and Huang, F. (2012). Selenium content determination in edible parts of crops in Zhangjiajie city. *Nat. Prod. Res. Dev.* 24, 1084–1088.

Xu, J., Tian, Y. S., Xing, X. J., Peng, R. H., Zhu, B., Gao, J. J., et al. (2016). Over-expression of AtGSTU19 provides tolerance to salt, drought and methyl viologen stresses in *Arabidopsis*. *Physiol. Plant.* 156, 164–175. doi: 10.1111/ppl.12347

Yu, Y., Zhuang, Z., Luo, L. Y., Wang, Y. Q., and Li, H. F. (2019). Difference between selenite and selenate in selenium transformation and the regulation of cadmium accumulation in *Brassica chinensis*. *Environ. Sci. Pollut. Res. Int.* 26, 24532–24541. doi: 10.1007/s11356-019-05705-x

Zhang, C., Xu, B., Zhao, C. R., Sun, J., Lai, Q., and Yu, C. (2019). Comparative de novo transcriptomics and untargeted metabolomic analyses elucidate complicated mechanisms regulating celery (*Apium graveolens* L.) responses to selenium stimuli. *PLoS One* 14:e0226752. doi: 10.1371/journal.pone.0226752

Zhang, H., Hao, X., Zhang, J., Wang, L., Wang, Y., Li, N., et al. (2021). Genome-wide identification of SULTR genes in tea plant and analysis of their expression in response to sulfur and selenium. *Protoplasma* 259, 127–140. doi: 10.1007/s00709-021-01643-z

Zhang, H., Liu, T., Zhang, Z., Payne, S. H., Zhang, B., McDermott, J. E., et al. (2016). Integrated proteogenomic characterization of human high-grade serous ovarian Cancer. *Cell* 166, 755–765. doi: 10.1016/j.cell.2016.05.069

Zhang, H., Zhao, Z., Zhang, X., Zhang, W., Huang, L., Zhang, Z., et al. (2019). Effects of foliar application of selenate and selenite at different growth stages on selenium accumulation and speciation in potato (*Solanum tuberosum* L.). *Food Chem.* 286, 550–556. doi: 10.1016/j.foodchem.2019.01.185

Zhang, L., Hu, B., Li, W., Che, R., Deng, K., Li, H., et al. (2014). OsPT2, a phosphate transporter, is involved in the active uptake of selenite in rice. *New Phytol.* 201, 1183–1191. doi: 10.1111/nph.12596

Zhao, X. Q., Mitani, N., Yamaji, N., Shen, R. F., and Ma, J. F. (2010). Involvement of silicon influx transporter OsNIP2;1 in selenite uptake in rice. *Plant Physiol.* 153, 1871–1877. doi: 10.1104/pp.110.157867

Conflict of Interest: The authors declare that the research was conducted in the absence of any commercial or financial relationships that could be construed as a potential conflict of interest.

Publisher's Note: All claims expressed in this article are solely those of the authors and do not necessarily represent those of their affiliated organizations, or those of the publisher, the editors and the reviewers. Any product that may be evaluated in this article, or claim that may be made by its manufacturer, is not guaranteed or endorsed by the publisher.

Copyright © 2022 Ren, Li, Guo, Wang, Hao and Zeng. This is an open-access article distributed under the terms of the Creative Commons Attribution License (CC BY). The use, distribution or reproduction in other forums is permitted, provided the original author(s) and the copyright owner(s) are credited and that the original publication in this journal is cited, in accordance with accepted academic practice. No use, distribution or reproduction is permitted which does not comply with these terms.

frontiers in Plant Science

ORIGINAL RESEARCH
published: 03 March 2022
doi: 10.3389/fpls.2022.832669

Ethylene-Inducible AP2/ERF Transcription Factor Involved in the Capsaicinoid Biosynthesis in *Capsicum*

Jinfen Wen[1†], Junheng Lv[2†], Kai Zhao[2†], Xiang Zhang[2†], Zuosen Li[2†], Hong Zhang[2†], Jinlong Huo[2†], Hongjian Wan[3], Ziran Wang[2], Haishan Zhu[2] and Minghua Deng[2]*

[1]Faculty of Architecture and City Planning, Kunming University of Science and Technology, Kunming, China, [2]College of Horticulture and Landscape, Yunnan Agricultural University, Kunming, China, [3]Institute of Vegetables, Zhejiang Academy of Agricultural Sciences, Hangzhou, China

OPEN ACCESS

Edited by:
Xinchao Wang,
Tea Research Institute (CAAS), China

Reviewed by:
Changming Chen,
South China Agricultural University, China
Liu Qianqian,
Qingdao Agricultural University, China

***Correspondence:**
Minghua Deng
dengminghua2013@sina.com
orcid.org/0000-0001-8293-9035

[†]These authors have contributed equally to this work

Specialty section:
This article was submitted to Crop and Product Physiology, a section of the journal Frontiers in Plant Science

Received: 10 December 2021
Accepted: 14 February 2022
Published: 03 March 2022

Citation:
Wen J, Lv J, Zhao K, Zhang X, Li Z, Zhang H, Huo J, Wan H, Wang Z, Zhu H and Deng M (2022) Ethylene-Inducible AP2/ERF Transcription Factor Involved in the Capsaicinoid Biosynthesis in Capsicum. Front. Plant Sci. 13:832669. doi: 10.3389/fpls.2022.832669

Ethylene is very important in the process of plant development and regulates the biosynthesis of many secondary metabolites. In these regulatory mechanisms, transcription factors (TFs) that mediate ethylene signals play a very important role. Capsaicinoids (CAPs) are only synthesized and accumulated in *Capsicum* species, causing their fruit to have a special pungent taste, which can protect against attack from herbivores and pathogens. In this study, we identified the TF *CcERF2*, which is induced by ethylene, and demonstrated its regulatory effect on CAPs biosynthesis. Transcriptome sequencing analysis revealed that the expression patterns of *CcERF2* and multiple genes associated with CAPs biosynthesis were basically the same. The spatiotemporal expression results showed *CcERF2* was preferentially expressed in the placenta of the spicy fruit. Ethylene can induce the expression of *CcERF2* and CAPs biosynthesis genes (CBGs). *CcERF2* gene silencing and 1-methylcyclopropene (1-MCP) and pyrazinamide (PZA) treatments caused a decrease in expression of CBGs and a sharp decrease in content of CAPs. The results indicated that *CcERF2* was indeed involved in the regulation of structural genes of the CAPs biosynthetic pathway.

Keywords: *CcERF2*, pepper, capsaicinoids, ethylene, VIGS

INTRODUCTION

Peppers (*Capsicum* spp.) are important vegetables worldwide. Pepper fruits are diverse in color, rich in nutrients, have a special pungency and aroma, and so are widely used as food additives (Ou et al., 2018). The pungency of pepper fruit is derived from capsaicinoids (CAPs), which are only biosynthesized in *Capsicum* plants (Iwai et al., 1979; Liu et al., 2019). The CAPs have the effect of curbing attack by herbivores and microorganisms. At the same time, CAPs are also widely used in many fields such as food, medicine, cosmetics, and agricultural pest control; CAPs are also widely used in riot prevention, personal defense, and in the military and national defense (Lejeune et al., 2007; Tewksbury et al., 2008; Ludy et al., 2012).

The CAPs are synthesized and accumulated in fruit placental tissues (Iwai et al., 1979). So far, more than 22 CAPs have been identified in peppers. The most important components of CAPs are capsaicin (CaP) and dihydrocapsaicin (DhCaP), and these represent approximately 90% of the total content of CAPs. The accumulation of CAPs is affected by many factors, including endogenous (for example, variety and developmental stage of the fruit) and exogenous factors (for example, light, temperature, water conditions, and biological stress; Phimchan and Techawongstien, 2012; Garruña-Hernández et al., 2013). Genotype is the most important determinant of CAPs content (Bosland et al., 2012; Liu et al., 2017); among the five domesticated species of *Capsicum*, *Capsicum chinense*, and *Capsicum frutescens* accumulate significantly higher contents of CAPs (Deng et al., 2009; Bosland et al., 2012). It is reported that factors such as plant growth regulators, chemicals, temperature, light, and drought stress can change the content of CAPs (Gurung et al., 2011).

The CAPs are synthesized by the fusion of phenylpropane and branched-chain fatty acid pathways in the placenta (Aluru et al., 2003; Blum et al., 2003; Mazourek et al., 2009). The CAPs biosynthesis genes (CBGs) that have been determined to be involved in biosynthesis of CAPs include *PAL*, *Ca4H*, *4CL*, *BCAT*, *Kas*, *FatA*, *ACL*, *ACS*, *CoMT*, *pAMT*, and *CS* (Abraham-Juárez et al., 2008; Liu et al., 2013). The biosynthetic mechanism of CAPs has been widely elucidated using bioinformatics analysis and multi-omics (Qin et al., 2014). As CAPs have considerable application value and commercial use, and much effort has gone into enhancing their content. However, their biosynthesis greatly changes spatiotemporally, and expression of CBGs is precisely regulated at the transcriptional level. Manipulating the expression level of crucial CBGs seems to determine increasing the content of CAPs (Abraham-Juárez et al., 2008; Sun et al., 2019; Zhu et al., 2019). In highly spicy peppers, the transcription level of CBGs (such as *pAMT*, *Kas*, and *CS*) is always higher than that of less spicy varieties (Abraham-Juárez et al., 2008). It is very important that manipulating the expression levels of some transcription factors (TFs) usually change the transcription levels of all genes in the metabolic pathway, thereby affecting the final content of the compound.

For example, the TFs *CaMYB31*, *CaMYB108*, *CaMYB48*, *Erf*, and *Jerf* are associated with regulating the content of CAPs (Keyhaninejad et al., 2014; Phimchan et al., 2014; Arce-Rodríguez and Ochoa-Alejo, 2017; Sun et al., 2019; Zhu et al., 2019). It was found that the Solanaceae-specific TF *MYB31* affects the accumulation of CAPs by directly targeting CBGs, resulting in changing the expression level of CBGs (Zhu et al., 2019). The TF *CaMYB108* activates the CBG promoters, especially those of *COMT*, *pAMT*, and *KasI*, and promotes enhanced expression of CBGs, thereby promoting the biosynthesis of CAPs (Sun et al., 2019). By directly binding and regulating the expression of CBGs, TF *CaMYB48* participates in the biosynthesis of CAPs, but the transcriptional regulation of CAPs biosynthesis has not been fully clarified (Sun et al., 2020). Therefore, it is necessary to identify TFs associated with the biosynthesis of CAPs.

Ethylene plays a significant role in the plant life process (Hu et al., 2020). After synthesis of ethylene, it binds to the receptor ETR and transmits the signal to the nucleus through MAPKK and EIN2 (Gray, 2004). The EIN2 binds to EIN3/EIL1 and EIN3/EIL1 binds to the *ERF1* promoter. The ERF1 binds to the GCC-box-containing genes in the downstream promoter region specifically and their expression can promote secondary metabolism product synthesis (Fujimoto et al., 2000; Brown et al., 2003; Paul et al., 2020). For example, in tobacco, ERF189 and ERF163 can bind to the GCC-box in the promoter region of the tobacco nicotine synthesis-related gene *PMT2* specifically, and directly promote synthesis of tobacco alkaloids (Shoji et al., 2010). The B3 subfamily proteins ORCA3 and ORA59 of the ERF family are two typical TFs associated with the regulation of secondary metabolites. The ORCA3 can upregulate the expression level of indole alkaloid synthesis-related genes in terpenoids, and promote the terpenoid indole biosynthesis (van der Fits and Memelink, 2000, 2001). *Lithospermum erythrophyllum LeERF-1* affects the secondary metabolites of shikonin positively through a mechanism similar to that of ORCA3 in affecting secondary metabolites (Zhang et al., 2011). In *Catharanthus roseus*, *CrERF5* upregulates the biosynthesis and accumulation of bisindole alkaloids (Pan et al., 2019).

The TFs and key enzymes in ethylene synthesis and its signal transduction can promote the biosynthesis of secondary metabolites. In many cases (plants, cells, and hairy roots), the addition of ethylene, addition of 1-aminocyclopropane 1-carboxylic acid (ACC), and overexpression of related TFs can increase the biosynthesis of secondary metabolites (Pan et al., 2000; Gantet and Memelink, 2002; Zhao et al., 2004; Buer et al., 2006; De Boer et al., 2011). In previous studies, *PAL* genes possessed a homolog of the GCC-box in their promoters and *ERF* genes could combine with their cis-acting element (Ohme-Takagi and Shinshi, 1995; Keyhaninejad et al., 2014). Both *Erf* and *Jerf* in pepper have been proposed to be involved in accumulation of pungency (Keyhaninejad et al., 2014). Many of the ERF family are TFs that are candidates for regulating CAP biosynthesis (Song et al., 2020). However, how CAP biosynthesis is regulated at the transcription level is still unknown in peppers.

In this paper, the ethylene-induced AP2/ERF TF *CcERF2*, which was particularly expressed in the placenta was identified. We confirmed that *CcERF2* was associated with CAPs biosynthesis.

MATERIALS AND METHODS

Experimental Materials

The *C. chinense* inbred line SL08 has a high CAPs content and was derived from Shuan La, the hottest pepper genotype in China (Deng et al., 2009). The *Capsicum annuum* inbred line H19 has a low CAPs content, and was derived from Xiangtan Chi Ban Jiao. Pepper seeds germinated in the soil of cell plastic flats in complete darkness at 28°C. The seedlings were grown in a greenhouse of Yunnan Agricultural University on campus under normal conditions.

Extraction and Detection of CaP and DhCaP

The CaP and DhCaP were extracted and detected according to Deng et al. (2009). The total CAPs content was calculated as (CaP + DhCaP)/0.91 (Deng et al., 2009). Fruits in different development stages of SL08 and H19 were used as material for extraction and detection of CaP and DhCaP. All experiments were repeated three times.

RNA-Seq and Analysis

RNA-seq was performed according to Liu et al. (2012). Fruits of SL08 at 4, 14, 24, 34, 44, and 54 days after pollination (DAP) were used to isolate total RNA. All of RNA-seq data generated in this study are available from the NCBI Short Read Archive (SRA, BioProject ID: PRJNA789050), and the raw RNA-seq data are freely available at https://www.ncbi.nlm.nih.gov/bioproject/PRJNA789050.

Exogenous Substance Treatments

Fruit at 24 DAP was used to investigate the effect of different exogenous substances on expression level of *CcERF2* and CBGs after 0.5, 1.0, 1.5, 3.5, 5.5, 8.5, and 11.5 h. Treated with exogenous substances, the 24-DAP fruits of SL08 were soaked in sterile water with 0.01 g/L 6-benzylaminopurine (6-BA), 20 g/L PEG6000, 30% H_2O_2, 0.17 g/L gibberellic acid (GA_3), 0.14 g/L salicylic acid (SA), 17.53 g/L NaCl, 90 g/L glutamate (Glu), or 0.1 mmol/L ethephon (with sterile water as control) under normal conditions (16 h of light at 30 ± 2°C and 8 h of darkness at 20 ± 2°C). After treatment, all fruits were frozen in liquid nitrogen and immediately stored at −80°C for gene expression analysis. All experiments were repeated three times.

CcERF2 Cloning and Bioinformatics Analysis

The open reading frame of *CcERF2* was cloned according to Deng et al. (2012). The primers used in the experiment are shown in **Supplementary Table S1**. The BLAST-protein-nucleic acid (BLASTP) analysis was performed on *CcERF2* through a database[1]; PSORT Prediction was performed for subcellular location prediction; and MEME was used to analyze the amino acid sequence motif. The Portparam tool was used to predict the physical and chemical properties of the protein. SignalP-5.0, TMHMM, and Nepos were used for signal peptide, transmembrane structure, and phosphorylation site of the protein prediction, respectively; SOPMA was used to predict its secondary structure; and ClustalX was used for sequence alignment and phylogenetic analysis. The MEGA 6.0 software was used to construct a phylogenetic tree based on the amino acid sequence through the neighbor joining method, and the bootstrap method was used to evaluate the reliability of each node in the tree, repeated 1,000 times.

Subcellular Localization and Transcriptional Activation Analysis

Subcellular localization and transcriptional activation analysis were performed according to Zhu et al. (2019) and Sun et al. (2020). The full-length coding sequences of *CcERF2* was cloned into the pAN580 (green fluorescent protein, GFP) vector and fused to the N-terminus of GFP under the control of the CaMV 35S promoter. The constructs were separately introduced into tobacco protoplasts for transient expression, and the GFP fluorescence signals were detected using a Zeiss lsm710 confocal laser scanning microscope (Carl Zeiss Inc., Jena, Germany).

Gene Expression Analysis

The RNAiso Plus (Takara, Dalian, P. R. China) was used to extract total RNA from pepper fruit. The synthesis of cDNA first strand refers to the instructions of the High Fidelity PrimeScript® RT-PCR Kit (Takara). According to the sequence of related genes revealed by transcriptome sequencing data, specific primers were respectively designed, and the internal reference was the *β-ACTIN* gene. Quantitative real-time PCR (qRT-PCR) was performed according to the method provided by the SYBR®Premix Ex TaqTM II (Tli RNaseH Plus) kit (Takara). The primers used in this study are shown in **Supplementary Table S1**.

VIGS Analysis

A fragment of the *CcERF2* coding sequence (CDS) with low similarity to other genes was cloned into pTRV2 and generated the silencing vector pTRV2–*CcERF2*. The VIGS were carried as reported (Zhu et al., 2019). In short, the pTRV2–*CcERF2* and pTVR1 vectors were co-injected into the cotyledon stage seedlings of line SL08. The empty vectors pTRV2 and pTVR1 were co-infiltrated as a control, and pTRV2–PDS and pTVR1 were co-infiltrated as a technical control. The RNA isolated from 24-DAP fruits was used for expression analysis, and 34-DAP fruits were used for CaP and DhCaP measurement. The primer information used in this study is shown in **Supplementary Table S1**.

Effects of 1-Methylcyclopropene and Pyrazinamide on Expression of CBGs and Content of CAPs

The SL08 pepper fruit of 24 DAP was used to study the effects of 1-methylcyclopropene (1-MCP) and pyrazinamide (PZA) on expression of CBGs and content of CAPs. The 1-MCP treatment follows: 1 μl L^{-1} 1-MCP fumigated for 12 h and kept in darkness at a temperature of 20 ± 2°C and humidity of 85 ± 5%. The PZA treatment follows: 100 mM PZA was sprayed onto the surface of the fruit until there were droplets, and kept in darkness at a temperature of 20 ± 2°C and humidity of 85 ± 5%. The fruits after 5 days of treatment were stored in liquid nitrogen and used for subsequent analysis. All experiments were repeated three times.

Ethylene Release Rate Determination

Ethylene release rate was determined according to Xu et al. (2018).

Statistical Analyses

Each experiment contained three biological replicates and three technical replicates. The error bars indicate SEs. One-way

[1]www.ncbi.nlm.nih.gov

ANOVA was performed to identify significant differences. The relative gene expression was calculated using the $2^{-\Delta\Delta CT}$ method (Livak and Schmittgen, 2001). Control expression was without induction at the 0 h time point.

RESULTS AND ANALYSIS

Accumulation of CAPs

Accumulation of CaP and DhCaP was detected in both lines, but the content of CaP was much higher (about 3–4 times) than that of DhCaP. The CaP and DhCaP contents were much higher in the placenta of SL08 than in H19 (**Supplementary Figure S1**). Both CaP and DhCaP began to accumulate at 9 DAP in the placenta of SL08, reached a peak at 44 DAP, and then began to decline. Both CaP and DhCaP began to accumulate at 11 DAP in the placenta of H19, and began to decrease at 49 DAP. The CaP, DhCaP, and total CAPs contents in the placenta of SL08 were 44.4, 63.1, and 48.0 times those in H19, respectively.

Expression of *CcERF2* and CBGs Is Consistent With CAPs Biosynthesis

Expression patterns of CBGs during development stages of the placenta were analyzed using transcriptome sequencing data of the placenta and pericarp of line SL08 during the early stage of the laboratory study (**Figure 1**). Expressions of *CcPAL*, *CcCa4H*, *Cc4CL*, *CcCoMT*, *CcpAMT*, *CcCS*, *CcBCAT*, *CcKAS*, *CcACL*, *CcFAT*, and *CcACS* genes were positively associated with accumulation of CAPs in SL08. The expression of these genes (except *CcACL*) showed a low expression level in fruit at 4 DAP, increased, and then decreased. Gene *CcCS* (*Capana05g000531*) was not expressed in 4-DAP fruit, and reached a maximum in 24-DAP fruit. Expression of *CcCoMT* (*Capana03g001811*), *CATCcBCAT* (*Capana04g000751*), *CcKAS* (*Capana01g000111*), and *CcFATA* (*Capana06g000197*) reached their highest values in 14-DAP fruit. Expression of *CcCa4H* (*Capana06g000272*) and *CcpAMT* (*Capana10g001341*) genes reached their maximum in 34-DAP fruit. Expression of *CcPAL* (*Capana09g002199*) reached its highest value in 44-DAP fruit.

Based on the transcriptome sequencing data of lines SL08 and H19 at different developmental stages of placenta completed in the laboratory, combined with the changes in the CaP and DhCaP contents of the placenta of both lines (**Supplementary Figure S1**), the AP2/ERF TF *CcERF2* (*Capana01g000677*) was identified. Its expression pattern was similar to that of CBGs (**Figure 1**). Expression of *CcERF2* was almost undetectable in the early stage of placenta (4 DAP), then rose rapidly, reached a maximum at 34 DAP, and then decreased.

We measured the expression level of *CcERF2* in some tissues of line SL08 and found that it was mainly expressed in the placenta (**Figure 2A**). It also showed considerable level of expression in seeds and pericarp, meaning that it has a role in these tissues. We also investigated *CcERF2* expression in the placenta of both lines, and found significantly higher expression in SL08 than in H19 (**Figure 2B**). Expression of *CcERF2* in the placenta had the same pattern as the contents of CaP and DhCaP. Thus, our results indicated that *CcERF2* may play a vital role in CAPs biosynthesis.

CcERF2 Gene Cloning and Bioinformatics Analysis

Based on our transcriptome sequencing data of SL08 and the pepper genome data in the public database, specific primers were designed to clone the full-length CDS of *CcERF2* from SL08. Nucleotide sequence analysis showed that *CcERF2* length

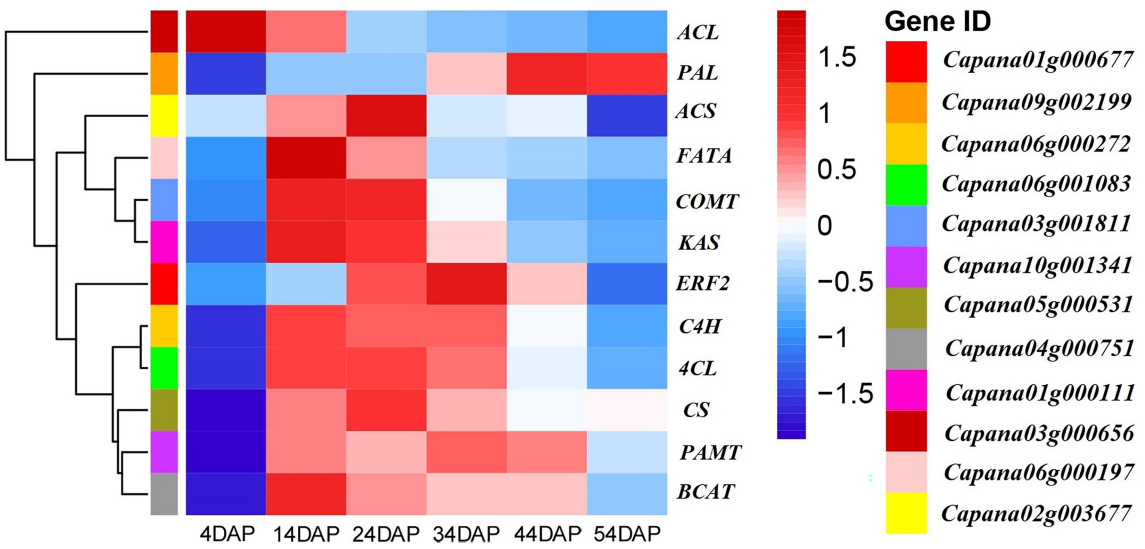


FIGURE 1 | Heat map indicating the capsaicinoids (CAPs) biosynthesis genes (CBGs) and *CcERF2* expression patterns in fruit of inbred line SL08. The heatmap was generated by transcriptome sequencing data with R software packages. The data were normalized in each row, and the numbers on the right side of the figure indicate the gene expression level corresponding to color.

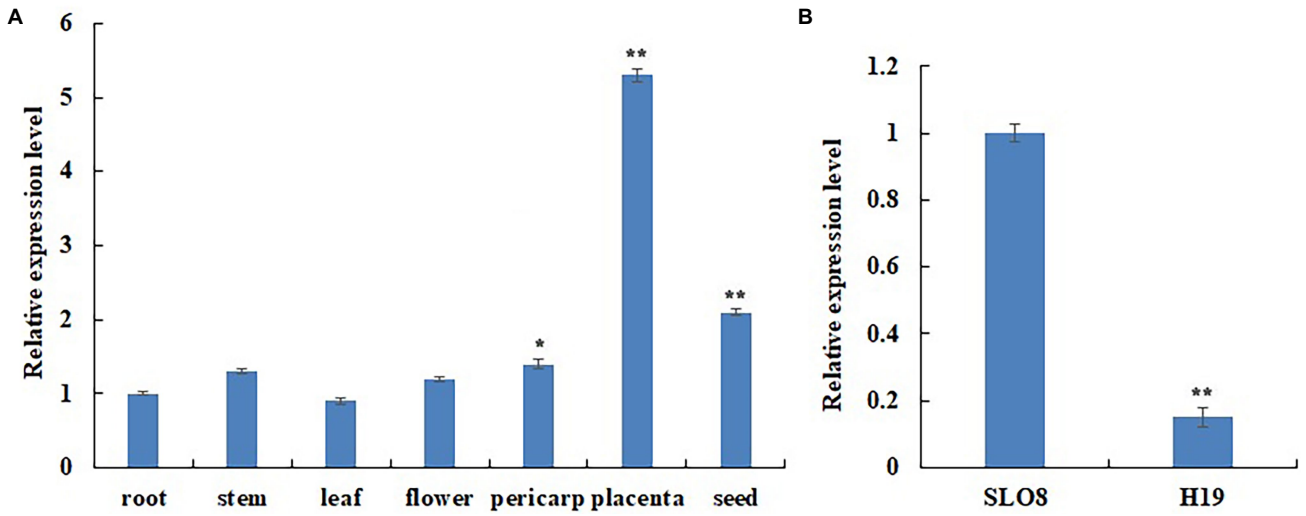


FIGURE 2 | Differential expression assays of *CcERF2*. **(A)** Differential expression assays of *CcERF2* in different tissues of pepper inbred line SL08; Roots, stems, leaves and flowers were collected from 30-day-old seedlings. Fruits at 24 days after pollination (DAP) was collected and was divided into pericarps, placentas and seeds. The relative expression of the root was set to 1, and that of all the other tissues was measured relative to that of the root. **(B)** Differential expression assays of *CcERF2* in pepper inbred line SL08 and H19 fruits. Fruits at 24 DAP was collected to investigate the *CcERF2* expression. The relative expression of the SL08 was set to 1, and that of H19 was measured relative to that of the SL08. The experiments were replicated three biological times and three technical times. Data are expressed as the mean ± SD ($n = 9$). Student's *t*-test was used to identify significant differences compared to the control (*$p < 0.05$, **$p < 0.01$).

was 795 bp. The molecular formula of CcERF2 is $C_{1328}H_{2050}N_{376}O_{409}S_9$, molecular weight is 30,115.70 D, and theoretical isoelectric point is 5.74. It is a fat-soluble, hydrophilic, and unstable protein. CcERF2 had no signal peptide and no transmembrane structure, and is located in the nucleus (88.8% probability).

The protein domain prediction results showed that *CcERF2* belonged to the AP2 superfamily, and the conservative amino acid sequence position was 74–131 (LYRGIRQRPWGKWAAEI RDPRKGVRVWLGTFNTAEEAARAYDKEARKIRGEKAKVN FP; **Figure 3A**). This domain specifically bound to the 11-bp GCC-box of the ethylene response element and was essential for the ethylene response. Based on BLAST, 48 amino acid sequences including CcERF2 were obtained, and 43 motifs were obtained after motif significance test and analysis. On the whole, the predicted motifs differed within the same family, but the conserved motifs in the same subgroup were almost the same; that is, the closer the related species, the more similar were the motifs. For peppers, they all contained 13 conserved motifs: 1–8, 11, 12, 17, 19, and 22. Of these, motifs 1, 3, and 5 covered the AP2 conserved structure domain (**Figure 3B**). The secondary structure of CcERF2 protein contained 73 alpha helices (27.56%), 22 extension chains (8.42%), and nine beta turns (3.41%). There were 160 random coils (60.61%). The evolutionary relationship of amino acid sequences showed that the selected ERF sequences were grouped together in different families. This meant that they were conserved in the evolutionary relationship. In genetic relationship, CcERF2 protein was the closest to Solanaceae. In the Solanaceae, it was closest to *Capsicum* and *Solanum*, and most distant to *Petunia* (**Figure 3C**). The phosphorylation sites of CcERF2 protein were predicted, and 19 amino acid residue types were screened: six types of T, three types of Y, and 10 types of S. The CcERF2 was localized to the cell nucleus (**Figure 4A**) and the CcERF2 protein had strong activation activity (**Figure 4B**).

CcERF2 Is a TF Induced by Ethylene

Exogenous substances were applied to the 24-DAP fruit of SL08 to test the regulation model. Expression of *CcERF2* in placental tissues was analyzed using qRT-PCR (**Figure 5**).

The fruits were treated with ethephon, which significantly induced *CcERF2* expression. Compared with the control, *CcERF2* expression increased by 64 times within 11.5 h of applying ethephon. At the same time, the effects of exogenous 6-BA, PEG, H_2O_2, GA_3, SA, NaCl, and Glu on *CcERF2* expression were also tested. Of these, 6-BA, H_2O_2, GA_3, SA, and NaCl significantly induced *CcERF2* expression. Compared with the control, these exogenous substances increased *CcERF2* expression; however, the modes of induced expression were not the same. In the test time range, under the 6-BA, H_2O_2, and NaCl treatments, the *CcERF2* expression showed a trend of initial increase and then decrease; however, under GA_3 and SA treatment, *CcERF2* expression showed an increasing trend. Treatment with Glu had no significant effect on *CcERF2* expression and PEG treatment was inhibitory.

Effect of Ethephon on Expression of CBGs

Ethephon treatment could significantly increase the expression level of CBGs, but the induction effect was inconsistent. Compared to controls, within 11.5 h of applying ethephon, gene expression levels of *CcPAL*, *CcCoMT*, and *CcFAT* were increased about 2.3–5.0 times; of *CcCa4H*, *CcpAmt*, *CcBCAT*,

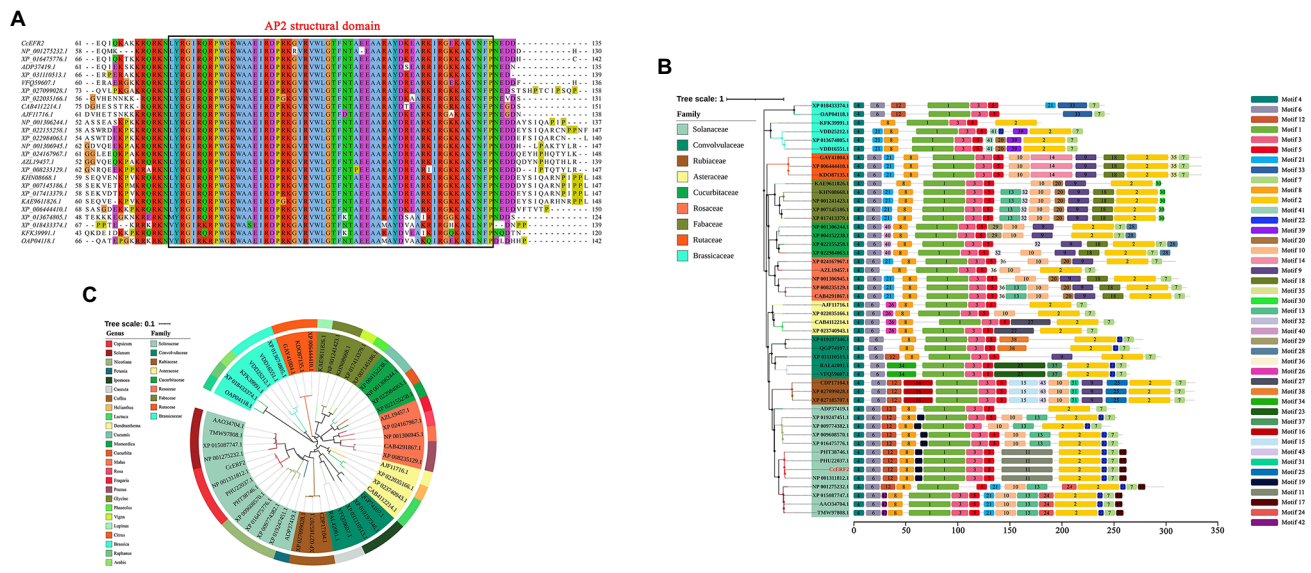


FIGURE 3 | Phylogenic tree of ERF transcription factors (TFs), analysis of promoter cis-acting elements and multiple amino acid sequence alignment of CcERF2 TFs. **(A)** Multiple amino acid sequence alignment of ERF2 TFs. **(B)** Promoter cis-acting elements comprising *CcERF2* in *Capsicum chinense* and 47 *ERF2* promoters in plant. **(C)** Phylogenetic tree comprising CcERF2 in *C. chinense* and 47 ERF2 TFs in plant.

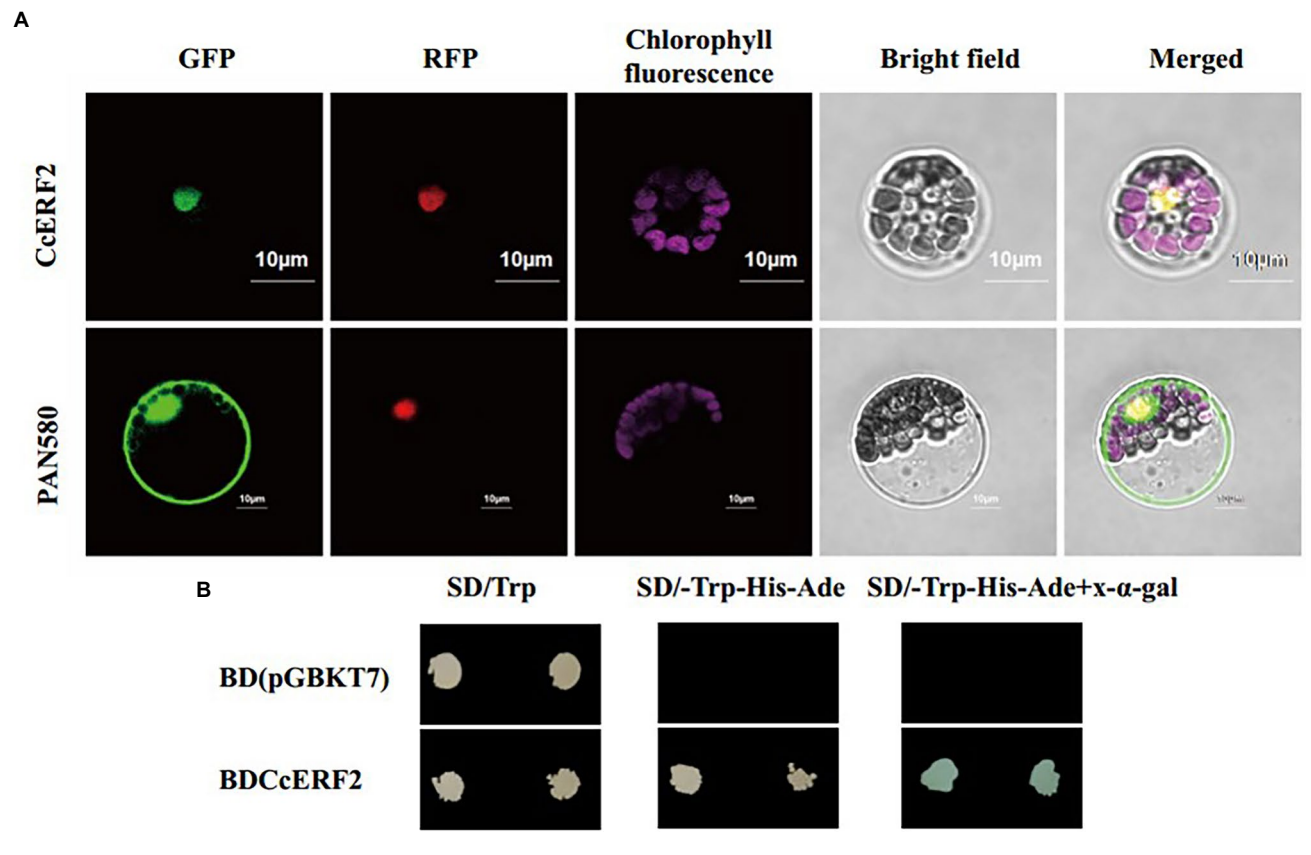


FIGURE 4 | Subcellular localization and transcriptional activation analysis. **(A)** Green fluorescent protein (GFP) signals indicated that CcERF2 was localized to nucleus. GFP fluorescence signals were detected using a Zeiss lsm710 confocal laser scanning microscope (Carl Zeiss, Inc., Jena, Germany). Scale bars: 10 μm. **(B)** Auxotroph plates of SD/–Leu–His–Ade (middle) and SD/–Leu–His–Ade–x-α-gal (right) showing transcriptional activation of protein. SD/Trp, medium lacking tryptophan; SD/-Trp-His-Ade, medium lacking tryptophan, histidine, and adenine.

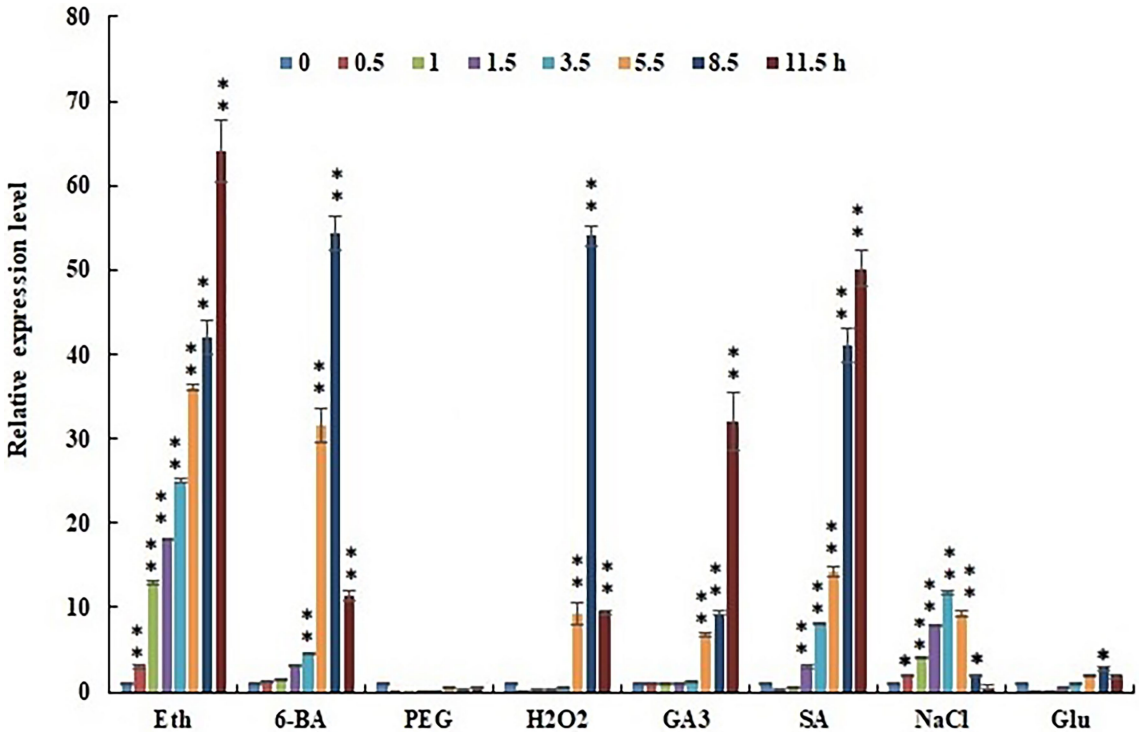


FIGURE 5 | Effect of elicitors (Eth, 6-BA, PEG, H_2O_2, GA_3, SA, NaCl, and Glu) on *CcERF2* expression. The 24 DAP pepper fruits were treated with elicitors (Eth, 6-BA, PEG, H_2O_2, GA_3, SA, NaCl, or Glu), and the fruit were sampled after elicitation for 0.5, 1.0, 1.5, 3.5, 5.5, 8.5, and 11.5 h. Without induction at the 0 h time point was used as control expression. The experiments were replicated three biological times and three technical times. Data are expressed as the mean ± SD ($n = 9$). Student's *t*-test was used to identify significant differences compared to the control ($^{*}p < 0.05$, $^{**}p < 0.01$).

CcACL, and *CcACS* were increased about 5.8–8.3 times; of *CcKAS* was increased about 11.1 times; and of *CcCS* was increased more than 100 times. Considering that ethephon significantly induced the expression of *CcERF2*, our results showed that *CcERF2* was a key factor in ethylene-mediated biosynthesis of CAPs (**Figure 6**).

Effects of 1-MCP on CBGs Expression and CAPs Contents

The effect of blocking ethylene signal transmission by 1-MCP on CBG expression and CAP contents was studied. The 1-MCP treatment remarkably reduced the expression of *PAL*, *C4H*, *COMT*, *pAMT*, and *CS* genes (**Figure 7A**). The 1-MCP treatment significantly reduced the content of CAPs (**Figure 7B**). The results indicated that ethylene signal transduction was involved in the regulation of CAP biosynthesis.

Effects of PZA on CBGs Expression and CAPs Contents

The results indicated that after pepper fruits were treated with ethylene biosynthesis inhibitor PZA for 12 h, the expression of *ACC oxidase-2* (*ACO2*) gene was extremely reduced (**Figure 7C**); expression of CBGs such as *PAL*, *C4H*, *COMT*, *pAMT*, and *CS* was inhibited (**Figure 7C**); CAPs contents were also obviously reduced (**Figure 7D**); and the endogenous ethylene release rate was conspicuously reduced (**Figure 7E**). This indicated that the content of endogenous ethylene significantly affected biosynthesis of CAPs.

The Effect of *CcERF2*-Silenced on CAPs Content and Metabolic Pathways

The VIGS vector pTRV2–*CcERF2* was constructed using a vector derived from tobacco rattle virus (TRV), and a *CcERF2*-silenced experiment was performed. The 24-DAP fruits of SL08 were used for the study. It was demonstrated that *Agrobacterium* infection with an empty pTRV2 vector resulted in distinctive changes in expression level of CBGs in pepper fruits (Abraham-Juárez et al., 2008). Compared with empty vector plants, the fruits infected with the pTRV2–*CcERF2* construct showed a distinctive reduction in *CcERF2* expression (22.4% of the empty vector; **Figure 8A**). Consistent with the expression level of *CcERF2*, CBGs in silent plants were also significantly downregulated. In the *CcERF2*-silent placenta, the expression of genes derived from fatty acid metabolism pathways (such as *CcKAS*, *CcACL*, *CcFAT*, and *CcACS*) only slightly changed. However, expression of genes derived from the phenylpropane pathway (such as *CcPAL*, *CcCa4H*, *Cc4CL*, *CcComt*, and *CcpAmt*) and *CcCS* underwent significant changes, and the genes whose expression was altered were consistent with the transcription level of *CcERF2* (**Figure 8A**).

The CAPs contents of the pepper fruits infected with the empty pTRV2 vector were similar to those of uninfected plants

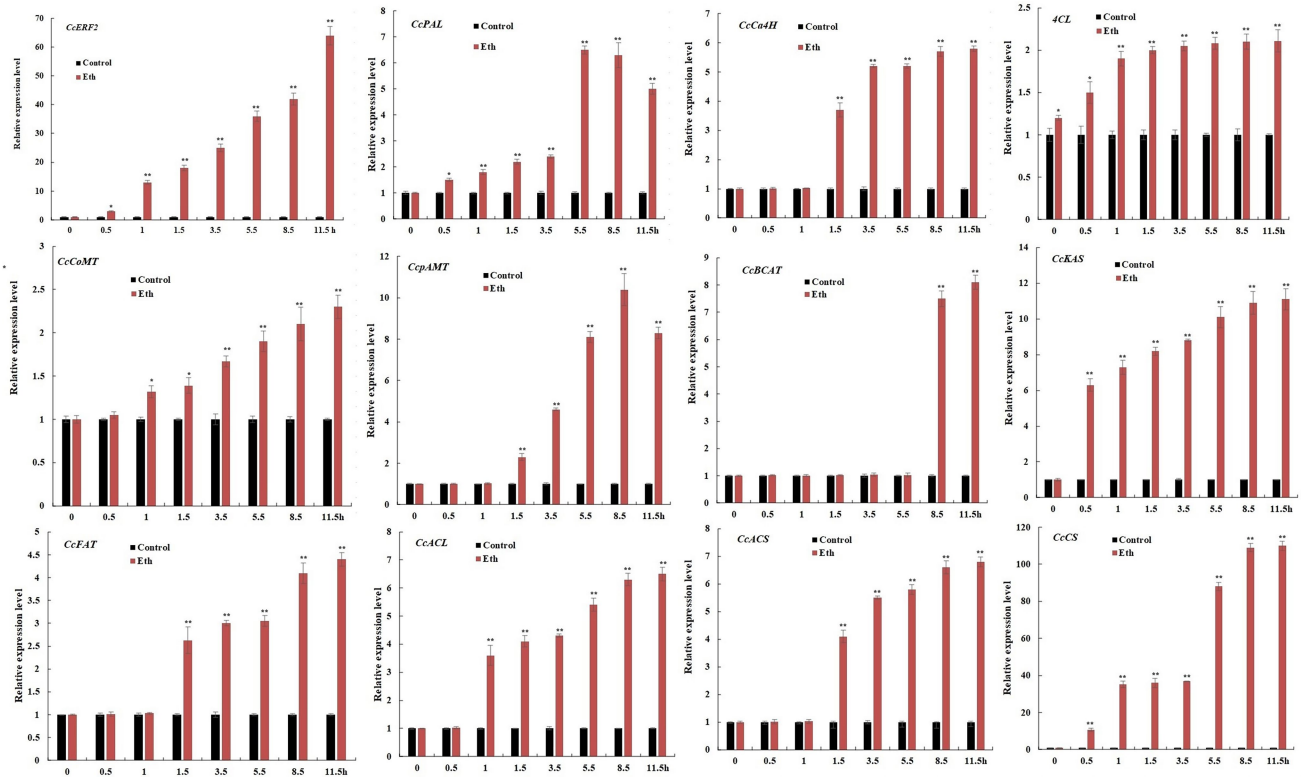


FIGURE 6 | Expression profiles of CBGs after treatment with Eth. The 24 DAP pepper fruits were treated with Eth, and the fruit were sampled after elicitation for 0.5, 1.0, 1.5, 3.5, 5.5, 8.5, and 11.5 h. Without induction at the 0 h time point was used as control expression. The experiments were replicated three biological times and three technical times. Data are expressed as the mean ± SD ($n = 9$). Student's *t*-test was used to identify significant differences compared to the control ($^*p < 0.05$, $^{**}p < 0.01$).

(Abraham-Juárez et al., 2008). The 34-DAP fruits were used to study the effect of *CcERF2* silencing on the CaP and DhCaP contents. Compared with fruits infected with empty pTRV2, the CaP and DhCaP contents in fruits infected with pTRV2–*CcERF2* were significantly reduced by 74.2 and 73.0%, respectively (**Figure 8B**). The above results strongly supported that *CcERF2* regulated certain CBGs to control CAPs biosynthesis.

DISCUSSION

Plant secondary metabolism comprises the life activity, formed in the long-term evolutionary process. The secondary metabolites are not only associated with the regulation of plant growth, but also allow plants to effectively deal with all kinds of stresses, such as fungi, pests, and herbivores (Dangl and Jones, 2001). The distribution of secondary metabolites is usually specific to species, organs, and tissues; CAPs are uniquely synthesized in the fruit placenta of *Capsicum* and have obvious specificity (Mazourek et al., 2009). A variety of stress conditions (such as high temperature, hydropenia, and herbivore invasion) can induce the production of secondary metabolites, and this process is affected by a lot of plant endogenous hormones (such as ethylene). Studies have found that low temperature promotes the accumulation of CAPs in pepper fruits (Keyhaninejad et al., 2014; Arce-Rodríguez and Ochoa-Alejo, 2017); drought induces biosynthesis of CAPs (Phimchan et al., 2014); and injury significantly increases the CAPs content of pepper fruits (Arce-Rodríguez and Ochoa-Alejo, 2017). Plants under stress (such as high temperature, hydropenia, and herbivore attack) usually show an increase in ethylene content, which can increase the formation of secondary metabolites. Ethylene plays a vital factor in response to all kinds of stresses (Fang et al., 2014; Hu et al., 2020). However, the effect of CAPs biosynthesis induced by ethylene needs further study.

We investigated the mechanism of ethylene on the expression of *CcERF2* and CBGs. After fruits of line SL08 were treated with ethephon, expressions of *CcERF2* and CBGs were significantly increased, equivalent to 2.1–110.3 times that of the control. However, the response pattern of each gene induced by ethephon slightly differed (**Figure 5**). Many studies have indicated that ethephon can upregulate the expression of multiple genes in the phenylpropane metabolic pathway, thereby promoting biosynthesis of flavonoids, anthocyanins, rutin, lignin, and procyanidins (El-Kereamy et al., 2003; Buer et al., 2006; Hossain et al., 2009; Pan et al., 2019; Hu et al., 2020; Paul et al., 2020; Zhao et al., 2020). Our experimental results are similar to those reports.

Most AP2/ERF family proteins have conserved AP2 domains, and it was reported that this type of TF can regulate the

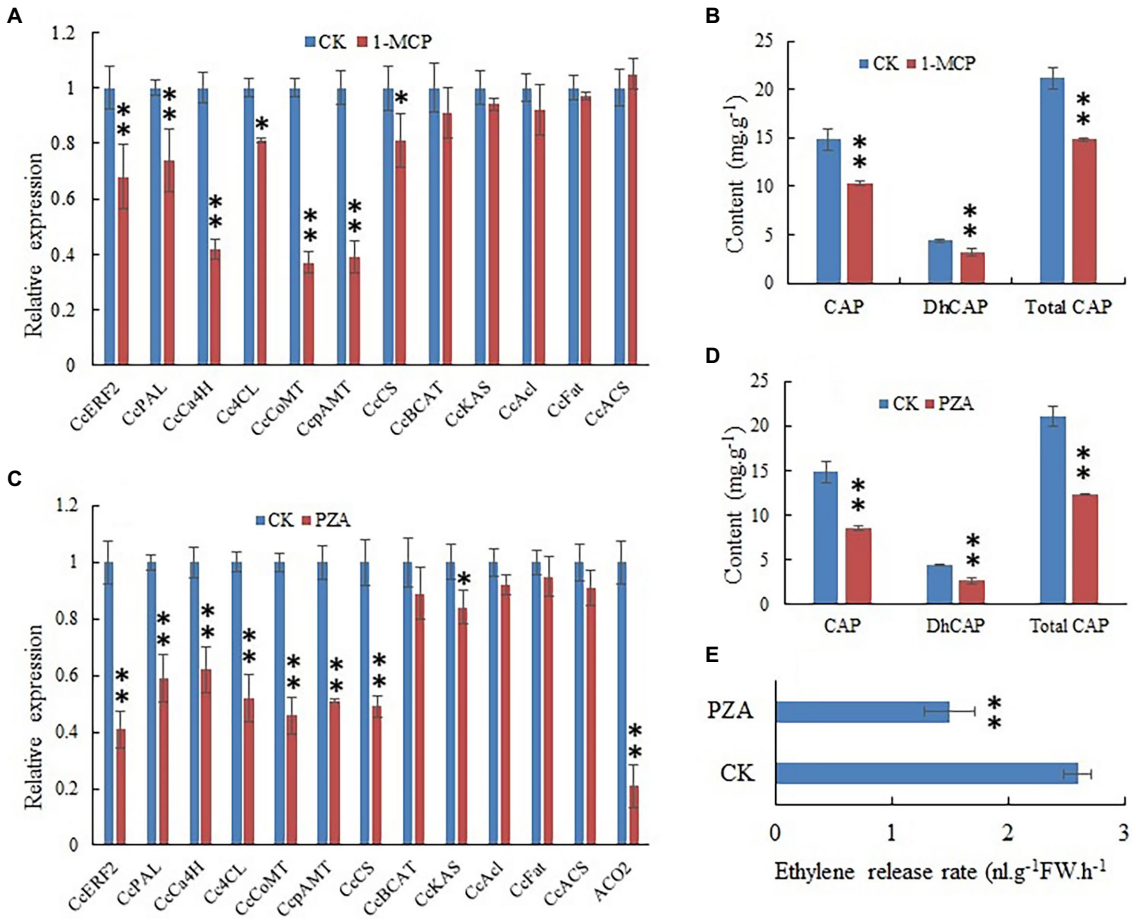


FIGURE 7 | Expression level of CBGs and *CcERF2*, relative contents of capsaicin (CaP), dihydrocapsaicin (DhCaP), and CAPs in 1-methylcyclopropene (1-MCP) and pyrazinamide (PZA) treatment fruit. **(A)** Expression level of CBGs and *CcERF2* in the 1-MCP treatment fruit. Fruits at 24 DAP was sampled to perform the expression level of CBGs and *CcERF2*. The relative expression level of the CBGs and *CcERF2* in the control were set to 1, and that of in 1-MCP treatment fruit were measured relative to that in the control. **(B)** Relative contents of CaP, DhCaP, and CAPs in the 1-MCP treatment fruit at 29 DAP. **(C)** Expression level of CBGs, *CcERF2*, and *ACC oxidase-2* (*ACO2*) in the PZA treatment fruit. Fruits at 24 DAP was sampled to perform the expression level of CBGs and *CcERF2*. The relative expression level of the CBGs and *CcERF2* in the control were set to 1, and that of in PZA treatment fruit were measured relative to that in the control. **(D)** Relative contents of CaP, DhCaP, and CAPs in the PZA treatment fruit at 29 DAP. **(E)** Ethylene release rate in the PZA treatment fruit at 29 DAP. The experiments were replicated three biological times and three technical times. Data are expressed as the mean ± SD ($n = 9$). Student's *t*-test was used to identify significant differences compared to the control ($^{*}p < 0.05$, $^{**}p < 0.01$).

synthesis of plant secondary metabolites (Paul et al., 2020). These AP2/ERF factors seem to play a similar role in regulation metabolic genes (Hu et al., 2020). In this paper, the AP2/ERF TF *CcERF2*, which can be used as a transcription activator to regulate CAPs biosynthesis was identified. There were 43 motifs obtained by analyzing the motif significance of the CcERF2 protein. On the whole, the predicted motifs differed within the same family, but the conserved motifs in the same subgroups were almost the same. That is, the closer the related species, the more similar were the motifs. The peppers all contained 13 conserved motifs (1–8, 11, 12, 17, 19, and 22), of which motifs 1, 3, and 5 covered the conserved AP2 structural domain. Our results showed that the function of CcERF2 was convergent and divergent among different plant species.

Various genes related to CAPs biosynthesis have been studied (Aluru et al., 2003). However, very few TFs associated with CAPs biosynthesis have been isolated and characterized, except for some MYB TFs (Arce-Rodríguez and Ochoa-Alejo, 2017; Sun et al., 2019, 2020; Zhu et al., 2019). We need to identify some TFs, especially AP2/ERF family TFs, which can be used as positive regulators to promote accumulation of CAPs. In the current study, based on transcription data, the AP2/ERF TF *CcERF2* was selected for further analysis, because *CcERF2* had a similar expression pattern to the CBGs in the transcriptome data. Silencing *CcERF2* downregulated the expression of CBGs, especially the expression level of genes associated with the phenylpropane pathway, and therefore reduced its CAPs content. The results showed that *CcERF2* was involved in regulating this metabolic process.

The 1-MCP is an ethylene receptor inhibitor (Sisler and Serek, 1997; Huber, 2008). It can effectively inhibit ethylene signal transduction (Du et al., 2021). A large number of studies

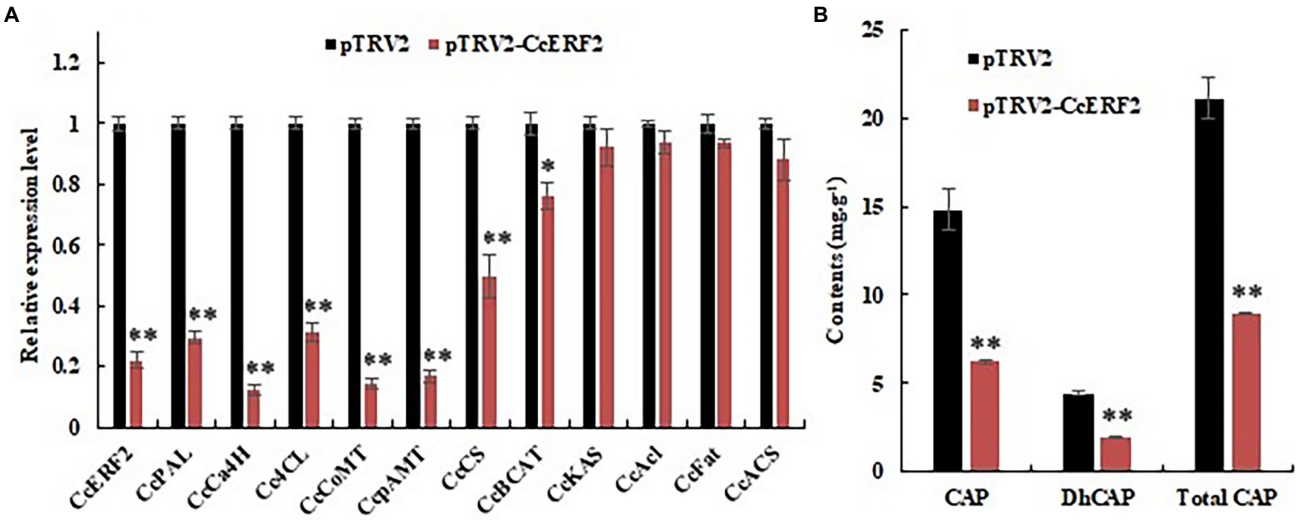


FIGURE 8 | Expression level of CBGs and *CcERF2*, relative contents of CaP, DhCaP, and CAPs in the control (empty vector) and *CcERF2*-silenced fruit. **(A)** Expression level of CBGs and *CcERF2* in the control (empty vector) and *CcERF2*-silenced fruit. Fruits at 24 DAP was sampled to perform the expression level of CBGs and *CcERF2*. The relative expression level of the CBGs and *CcERF2* in the control were set to 1, and that of in the *CcERF2*-silenced fruit were measured relative to that in the control. **(B)** Relative contents of CaP, DhCaP, and CAPs in the control (empty vector) and *CcERF2*-silenced fruit at 34 DAP. The experiments were replicated three biological times and three technical times. Data are expressed as the mean ± SD ($n = 9$). Student's *t*-test was used to identify significant differences compared to the control ($^{*}p < 0.05$, $^{**}p < 0.01$).

have shown that 1-MCP can affect the maturation, senescence, and secondary metabolism of non-climacteric fruits by blocking ethylene signal transduction (Gómez-Lobato et al., 2012; Li et al., 2016; Zhang et al., 2018). Our research results showed that 1-MCP significantly reduced the expression of some capsaicin biosynthesis genes, and obviously reduced the content of CAPs in fruits.

The PZA is a new type of ethylene biosynthesis inhibitor that acts by inhibiting expression of *ACO2* (Sun et al., 2017). Our research showed that PZA obviously reduced *ACO2* expression in pepper fruits and remarkably reduced ethylene production. At the same time, PZA treatment greatly reduced the expression of some genes related to capsaicin biosynthesis, thereby reducing the content of CAPs.

CONCLUSION

This study showed strong evidence that ethylene induced the expression of *CcERF2* and CBGs, and 1-MCP and PZA treatments caused a decrease in expression of CBGs and a sharp decrease in content of CAPs in fruit. It also demonstrated that *CcERF2* could promote CAP biosynthesis in *Capsicum*. It is necessary to further study whether *CcERF2* acts directly on the promoter of CBGs of the CAP pathway or through formation of a complex with other TFs.

DATA AVAILABILITY STATEMENT

The original contributions presented in the study are publicly available. This data can be found at: National Center for Biotechnology Information (NCBI) BioProject database under accession number PRJNA789050.

AUTHOR CONTRIBUTIONS

MD and KZ conceived and designed the study. JL, XZ, ZL, HZ, JH, and HW performed the research. ZW, HZ, XZ, and JW analyzed the data. MD, XZ, and JW prepared the paper. All authors contributed to the article and approved the submitted version.

FUNDING

This study was supported by the Natural Science Foundation of China (Grant Nos. 31560556 and 31160394) and the Major Science and Technology Projects in Yunnan Province (2018BB020).

SUPPLEMENTARY MATERIAL

The Supplementary Material for this article can be found online at: https://www.frontiersin.org/articles/10.3389/fpls.2022.832669/full#supplementary-material

Supplementary Figure S1 | Capsaicin (CaP), dihydrocapsaicin (DhCaP), and total capsaicinoids (CAPs) contents determination in inbred line SL08 and H19 fruits. Fifteen fruits were sampled for the measurement of the contents of CAP, DhCAP, and total CAPD at each developmental stage. The experiments were replicated three biological times and three technical times. Data are expressed as the mean ± SD ($n = 9$).

REFERENCES

Abraham-Juárez, M. R., Rocha-Granados, M. C., López, M. G., Rivera-Bustamante, R. F., and Ochoa-Alejo, N. (2008). Virus-induced silencing of *Comt*, *pAmt* and *Kas* genes results in a reduction of capsaicinoid accumulation in chili pepper fruits. *Planta* 227, 681–695. doi: 10.1007/s00425-007-0651-7

Aluru, M. R., Mazourek, M., Landry, L. G., Curry, J., Jahn, M., and O'Connell, M. A. (2003). Differential expression of fatty acid synthase genes, *Acl*, *Fat* and *Kas*, in *Capsicum* fruit. *J. Exp. Bot.* 54, 1655–1664. doi: 10.1093/jxb/erg176

Arce-Rodríguez, M. L., and Ochoa-Alejo, N. (2017). An R2R3-MYB transcription factor regulates capsaicinoid biosynthesis. *Plant Physiol.* 174, 1359–1370. doi: 10.1104/pp.17.00506

Blum, E., Mazourek, M., O'Connell, M. A., Curry, J., Thorup, T., Liu, K., et al. (2003). Molecular mapping of capsaicinoid biosynthesis genes and quantitative trait loci analysis for capsaicinoid content in *Capsicum*. *Theor. Appl. Genet.* 108, 79–86. doi: 10.1007/s00122-003-1405-y

Bosland, P. W., Coon, D., and Reeves, G. (2012). Trinidad moruga scorpion pepper is the world's hottest measured chile pepper at more than two million scoville heat units. *HortTechnology* 22, 534–538. doi: 10.21273/HORTTECH.22.4.534

Brown, R. L., Kazan, K., McGrath, K. C., Maclean, D. J., and Manners, J. M. (2003). A role for the GCC-box in jasmonate-mediated activation of the *PDF1.2* gene of *Arabidopsis*. *Plant Physiol.* 132, 1020–1032. doi: 10.1104/pp.102.017814

Buer, C. S., Sukumar, P., and Muday, G. K. (2006). Ethylene modulates flavonoid accumulation and gravitropic responses in roots of *Arabidopsis*. *Plant Physiol.* 140, 1384–1396. doi: 10.1104/pp.105.075671

Dangl, J. L., and Jones, J. D. G. (2001). Plant pathogens and integrated defence responses to infection. *Nature* 411, 826–833. doi: 10.1038/35081161

De Boer, K., Tilleman, S., Pauwels, L., Vanden Bossche, R., De Sutter, V., Vanderhaeghen, R., et al. (2011). APETALA2/ETHYLENE RESPONSE FACTOR and basic helix-loop-helix tobacco transcription factors cooperatively mediate jasmonate-elicited nicotine biosynthesis. *Plant J.* 66, 1053–1065. doi: 10.1111/j.1365-313X.2011.04566.x

Deng, M. H., Wen, J. F., Huo, J. L., Zhu, H. S., Wang, P., Dai, X. Z., et al. (2012). Molecular characterization and prokaryotic expression of *orf507* sterility-associated gene in chilli pepper (*Capsicum annum* L.) cytoplasmic male sterility. *Pak. J. Bot.* 44, 1497–1502.

Deng, M. H., Wen, J. F., Zhu, H. S., and Zou, X. X. (2009). The hottest pepepr variety in China. *Genet. Resour. Crop. Evol.* 56, 605–608. doi: 10.1007/s10722-009-9445-z

Du, Y., Jin, T., Zhao, H., Han, C., Sun, F., Chen, Q., et al. (2021). Synergistic inhibitory effect of 1-methylcyclopropene (1-MCP) and chlorine dioxide (ClO2) treatment on chlorophyll degradation of green pepper fruit during storage. *Postharvest Biol. Technol.* 171:111363. doi: 10.1016/j.postharvbio.2020.111363

El-Kereamy, A., Chervin, C., Roustan, J. P., Cheynier, V., Souquet, J. M., Moutounet, M., et al. (2003). Exogenous ethylene stimulates the long-term expression of genes related to anthocyanin biosynthesis in grape berries. *Physiol. Plant.* 119, 175–182. doi: 10.1034/j.1399-3054.2003.00165.x

Fang, R. J., Zhao, H., Liao, R. H., Tang, C. Y., Wu, F. Y., Zhu, Y., et al. (2014). Dual regulating effects of ethylene on the formation of plant secondary metabolites. *Chin. Bull. Bot.* 49, 626–639. doi: 10.3724/SP.J.1259.2014.00626

Fujimoto, S. Y., Ohta, M., Usui, A., Shinshi, H., and Ohme-Takagi, M. (2000). *Arabidopsis* ethylene-responsive element binding factors act as transcriptional activators or repressors of GCC box-mediated gene expression. *Plant Cell* 12, 393–404. doi: 10.1105/tpc.12.3.393

Gantet, P., and Memelink, J. (2002). Transcription factors: tools to engineer the production of pharmacologically active plant metabolites. *Trends Pharmacol. Sci.* 23, 563–569. doi: 10.1016/S0165-6147(02)02098-9

Garruña-Hernández, R., Monforte-González, M., Canto-Aguilar, A., Flota, F. V., and Orellana, R. (2013). Enrichment of carbon dioxide in the atmosphere increases the capsaicinoids content in Habanero peppers (*Capsicum chinense* Jacq.). *J. Agric. Food Chem.* 93, 1385–1388. doi: 10.1002/jsfa.5904

Gómez-Lobato, M. E., Hasperue, J. H., Civello, P. M., Chaves, A. R., and Martínez, G. A. (2012). Effect of 1-MCP on the expression of chlorophyll degrading genes during senescence of broccoli (*Brassica oleracea* L.). *Sci. Hortic.* 144, 208–211. doi: 10.1016/j.scienta.2012.07.017

Gray, W. M. (2004). Hormonal regulation of plant growth and development. *PLoS Biol.* 2:E311. doi: 10.1016/j.scienta.2012.07.017

Gurung, T., Techawongstien, S., Suriharn, B., and Techawongstien, S. (2011). Impact of environments on the accumulation of capsaicinoids in *Capsicum* spp. *HortScience* 46, 1–6. doi: 10.2514/1.16041

Hossain, M. A., Kim, S., Kim, K. H., Lee, S. J., and Lee, H. (2009). Flavonoid compounds are enriched in lemon balm (*Melissa officinalis*) leaves by a high level of sucrose and confer increased antioxidant activity. *HortScience* 44, 1907–1913. doi: 10.21273/HORTSCI.44.7.1907

Hu, Y.-T.，Xu, Z.-C.，Tian, Y.，Gao, R.-R.，Ji, A.-J.，Pu, X.-D., et al. (2020). Genome-wide identification and analysis of AP2/ERF transcription factors related to camptothecin biosynthesis in *Camptotheca acuminate*. *Chin. J. Nat. Med.* 18, 582–593. doi:10.1016/S1875-5364(20)30070-4

Huber, D. J. (2008). Suppression of ethylene responses through application of 1-methylcyclopropene: a powerful tool for elucidating ripening and senescence mechanisms in climacteric and nonclimacteric fruits and vegetables. *HortScience* 43, 106–111. doi: 10.21273/HORTSCI.43.1.106

Iwai, K., Suzuki, T., and Fujiwake, H. (1979). Formation and accumulation of pungent principle of hot pepper fruits, capsaicin and its analogues, in *Capsicum annuun* var. annuun cv. karayatsubusa at different growth stages after flowering. *Agric. Biol. Chem.* 43, 2493–2498. doi: 10.1080/00021369.1979.10863843

Keyhaninejad, N., Curry, J., Romero, J., and O'Connell, M. A. (2014). Fruit specific variability in capsaicinoid accumulation and transcription of structural and regulatory genes in *Capsicum* fruit. *Plant Sci.* 215–216, 59–68. doi: 10.1016/j.plantsci.2013.10.013

Lejeune, M. P. G. M., Kovacs, E. M. R., and Westerterp-Plantenga, M. S. (2007). Effect of capsaicin on substrate oxidation and weight maintenance after modest bodyweight loss in human subjects. *Brit. J. Nutr.* 90, 651–659. doi: 10.1079/BJN2003938

Li, L., Lichter, A., Chalupowicz, D., Gamrasni, D., Goldberg, T., Nerya, O., et al. (2016). Effects of the ethylene-action inhibitor 1-methylcyclopropene on postharvest quality of non-climacteric fruit crops. *Postharvest Biol. Technol.* 111, 322–329. doi: 10.1016/j.postharvbio.2015.09.031

Liu, S. Q., Chen, C. M., Chen, G. J., Cao, B. H., Chen, Q. H., and Lei, J. J. (2012). RNA-sequencing tag profiling of the placenta and pericarp of pungent pepper provides robust candidates, contributing to capsaicinoid biosynthesis. *Plant Cell Tissue Organ Cult.* 110, 111–121. doi: 10.1007/s11240-012-0135-8

Liu, F., Deng, Y., Zheng, J., Liu, M., Ou, L., Yang, B., et al. (2017). PepperHub, an informatics hub for the chili pepper research community. *Mol. Plant* 10, 1129–1132. doi: 10.1016/j.molp.2017.03.005

Liu, S., Li, W., Wu, Y., Chen, C., and Lei, J. (2013). De novo transcriptome assembly in chili pepper (*Capsicum frutescens*) to identify genes involved in the biosynthesis of capsaicinoids. *PLoS One* 8:e48156. doi: 10.1371/journal.pone.0048156

Liu, Y., Lv, J., Liu, Z., Wang, J., Yang, B., Chen, W., et al. (2019). Integrative analysis of metabolome and transcriptome reveals the mechanism of color formation in pepper fruit (*Capsicum annuum* L.). *Food Chem.* 306:125629. doi: 10.1016/j.foodchem.2019.125629

Livak, K. J., and Schmittgen, T. D. (2001). Analysis of relative gene expression data using real-time quantitative PCR and the 2(-Delta Delta C(T)) method. *Methods* 25, 402–408. doi: 10.1006/meth.2001.1262

Ludy, M. J., Moore, G. E., and Mattes, R. D. (2012). The effects of capsaicin and capsiate on energy balance: critical review and meta-analyses of studies in humans. *Chem. Senses* 37, 103–121. doi: 10.1093/chemse/bjr100

Mazourek, M., Pujar, A., Borovsky, Y., Paran, I., Mueller, L., and Jahn, M. M. (2009). A dynamic interface for capsaicinoid symstems biology. *Plant Physiol.* 150, 1806–1821. doi: 10.1104/pp.109.136549

Ohme-Takagi, M., and Shinshi, H. (1995). Ethylene-inducible DNA binding proteins that interact with an ethylene-responsive element. *Plant Cell* 7, 173–182. doi: 10.1105/tpc.7.2.173

Ou, L., Li, D., Lv, J., Chen, W., Zhang, Z., Li, X., et al. (2018). Pan-genome of cultivated pepper (*Capsicum*) and its use in gene presence-absence variation analyses. *New Phytol.* 220:360. doi: 10.1111/nph.15413

Pan, Q., Wang, C., Xiong, Z., Wang, H., Fu, X., Shen, Q., et al. (2019). *CrERF5*, an AP2/ERF transcription factor, positively regulates the biosynthesis of

bisindole alkaloids and their precursors in *Catharanthus roseus*. *Front. Plant Sci.* 10:931. doi: 10.3389/fpls.2019.00931

Pan, Z. W., Wang, H. Q., and Zhong, J. J. (2000). Scale-up study on suspension cultures of *Taxus chinensis* cells for production of taxane diterpene. *Enzym. Microb. Technol.* 27, 714–723. doi: 10.1016/S0141-0229(00)00276-3

Paul, P., Singh, S. K., Patra, B., Liu, X., Pattanaik, S., and Yuan, L. (2020). Mutually regulated AP2/ERF gene clusters modulate biosynthesis of specialized metabolites in plants. *Plant Physiol.* 182, 840–856. doi: 10.1104/pp.19.00772

Phimchan, P., Chanthai, S., Bosland, P. W., and Techawongstien, S. (2014). Enzymatic changes in phenylalanine ammonia-lyase, cinnamic-4-hydroxylase, capsaicin synthase, and peroxidase activities in *Capsicum* under drought stress. *J. Agric. Food Chem.* 62, 7057–7062. doi: 10.1021/jf4051717

Phimchan, P., and Techawongstien, S. (2012). Impact of drought stress on the accumulation of capsaicinoids in *Capsicum* cultivars with different initial capsaicinoid levels. *HortScience* 47, 1204–1209. doi: 10.21273/HORTSCI.47.9.1204

Qin, C., Yu, C., Shen, Y., Fang, X., Chen, L., Min, J., et al. (2014). Whole-genome sequencing of cultivated and wild peppers provides insights into Capsicum domestication and specialization. *Proc. Natl. Acad. Sci. U. S. A.* 111, 5135–5140. doi: 10.1073/pnas.1400975111

Shoji, T., Kajikawa, M., and Hashimoto, T. (2010). Clustered transcription factor genes regulate nicotine biosynthesis in tobacco. *Plant Cell* 22, 3390–3409. doi: 10.1105/tpc.110.078543

Sisler, E. C., and Serek, M. (1997). Inhibitors of ethylene responses in plants at the receptor level: recent developments. *Physiol. Plant.* 100, 577–582. doi: 10.1111/j.1399-3054.1997.tb03063.x

Song, J., Chen, C., Zhang, S., Wang, J., Huang, Z., Chen, M., et al. (2020). Systematic analysis of the Capsicum ERF transcription factor family: identification of regulatory factors involved in the regulation of species-specific metabolites. *BMC Genomics* 21:573. doi: 10.1186/s12864-020-06983-3

Sun, X., Li, Y., He, W., Ji, C., Xia, P., Wang, Y., et al. (2017). Pyrazinamide and derivatives block ethylene biosynthesis by inhibiting ACC oxidase. *Nat. Commun.* 8:15758. doi: 10.1038/ncomms15758

Sun, B., Zhou, X., Chen, C., Chen, C., Chen, K., Chen, M., et al. (2020). Coexpression network analysis reveals an MYB transcriptional activator involved in capsaicinoid biosynthesis in hot peppers. *Hortic. Res.* 7:162. doi: 10.1038/s41438-020-00381-2

Sun, B., Zhu, Z., Chen, C., Chen, G., Cao, B., Chen, C., et al. (2019). Jasmonate-inducible R2R3-MYB transcription factor regulates capsaicinoid biosynthesis and stamen development in *Capsicum*. *J. Agric. Food Chem.* 67, 10891–10903. doi: 10.1021/acs.jafc.9b04978

Tewksbury, J. J., Reagan, K. M., Machnicki, N. J., Carlo, T. A., Haak, D. C., Peñaloza, L. C., et al. (2008). Evolutionary ecology of pungency in wild chilies. *Proc. Natl. Acad. Sci. U. S. A.* 105, 11808–11811. doi: 10.1073/pnas.0802691105

van der Fits, L., and Memelink, J. (2000). *ORCA3*, a jasmonateresponsive transcriptional regulator of plant primary and secondary metabolism. *Science* 289, 295–297. doi: 10.1126/science.289.5477.295

van der Fits, L., and Memelink, J. (2001). The jasmonateinducible AP2/ERF-domain transcription factor *ORCA3* activates gene expression via interaction with a jasmonate-responsive promoter element. *Plant J.* 25, 43–53. doi: 10.1046/j.1365-313x.2001.00932.x

Xu, L., Yue, Q., Xiang, G., Bian, F., and Yao, Y. (2018). Melatonin promotes ripening of grape berry via increasing the levels of ABA, H_2O_2, and particularly ethylene. *Hortic. Res.* 5, 1–11. doi: 10.1038/s41438-018-0045-y

Zhang, X. M., Li, J. P., Fu, M. R., Jin, T., Yang, X. Y., Han, C., et al. (2018). Effects of the combination of 1-MCP and ClO_2 on shelf life quality of green pepper. *Sci. Technol. Food Ind.* 39, 275–280. doi: 10.13386/j.issn1002-0306.2018.13.050

Zhang, W., Zou, A., Miao, J., Yin, Y., Tian, R., Pang, Y., et al. (2011). *LeERF-1*, a novel AP2/ERF family gene within the B3 subcluster, is down-regulated by light signals in *Lithospermum erythrorhizon*. *Plant Biol.* 13, 343–348. doi: 10.1111/j.1438-8677.2010.00375.x

Zhao, C., Liu, X., Gong, Q., Cao, J., Shen, W., Yin, X., et al. (2020). Three AP2/ERF family members modulate flavonoid synthesis by regulating type IV chalcone isomerase in citrus. *Plant Biotechnol. J.* 19, 671–688. doi: 10.1111/pbi.13494

Zhao, J., Zheng, S. H., Fujita, K., and Sakai, K. (2004). Jasmonate and ethylene signaling and their interaction are integral parts of the elicitor signaling pathway leading to β-thujaplicin biosynthesis in *Cupressus lusitanica* cell cultures. *J. Exp. Bot.* 55, 1003–1012. doi: 10.1093/jxb/erh127

Zhu, Z., Sun, B., Cai, W., Zhou, X., Mao, Y., Chen, C., et al. (2019). Natural variations in the MYB transcription factor *MYB31* determine the evolution of extremely pungent peppers. *New Phytol.* 223, 922–938. doi: 10.1111/nph.15853

Conflict of Interest: The authors declare that the research was conducted in the absence of any commercial or financial relationships that could be construed as a potential conflict of interest.

Publisher's Note: All claims expressed in this article are solely those of the authors and do not necessarily represent those of their affiliated organizations, or those of the publisher, the editors and the reviewers. Any product that may be evaluated in this article, or claim that may be made by its manufacturer, is not guaranteed or endorsed by the publisher.

Copyright © 2022 Wen, Lv, Zhao, Zhang, Li, Zhang, Huo, Wan, Wang, Zhu and Deng. This is an open-access article distributed under the terms of the Creative Commons Attribution License (CC BY). The use, distribution or reproduction in other forums is permitted, provided the original author(s) and the copyright owner(s) are credited and that the original publication in this journal is cited, in accordance with accepted academic practice. No use, distribution or reproduction is permitted which does not comply with these terms.

frontiers in Plant Science

REVIEW
published: 08 March 2022
doi: 10.3389/fpls.2022.836515

Advances in Understanding and Harnessing the Molecular Regulatory Mechanisms of Vegetable Quality

Luyao Gao[1,2,3], Ning Hao[4,5], Tao Wu[1,2,3] and Jiajian Cao[1,2,3]**

[1] College of Horticulture, Hunan Agricultural University, Changsha, China, [2] Engineering Research Center for Horticultural Crop Germplasm Creation and New Variety Breeding, Ministry of Education, Changsha, China, [3] Key Laboratory for Vegetable Biology of Hunan Province, Changsha, China, [4] College of Horticulture and Landscape Architecture, Northeast Agricultural University, Harbin, China, [5] Graduate School of Agricultural and Life Sciences, The University of Tokyo, Tokyo, Japan

The quality of vegetables is facing new demands in terms of diversity and nutritional health. Given the improvements in living standards and the quality of consumed products, consumers are looking for vegetable products that maintain their nutrition, taste, and visual qualities. These requirements are directing scientists to focus on vegetable quality in breeding research. Thus, in recent years, research on vegetable quality has been widely carried out, and many applications have been developed via gene manipulation. In general, vegetable quality traits can be divided into three parts. First, commodity quality, which is most related to the commerciality of plants, refers to the appearance of the product. The second is flavor quality, which usually represents the texture and flavor of vegetables. Third, nutritional quality mainly refers to the contents of nutrients and health ingredients such as soluble solids (sugar), vitamin C, and minerals needed by humans. With biotechnological development, researchers can use gene manipulation technologies, such as molecular markers, transgenes and gene editing to improve the quality of vegetables. This review attempts to summarize recent studies on major vegetable crops species, with *Brassicaceae, Solanaceae*, and *Cucurbitaceae* as examples, to analyze the present situation of vegetable quality with the development of modern agriculture.

Keywords: gene manipulation, vegetables, quality, *Brassicaceae*, *Solanaceae*, *Cucurbitaceae*

OPEN ACCESS

Edited by:
Pei Xu,
China Jiliang University, China

Reviewed by:
Xueyong Yang,
Insititute of Vegetables and Flowers (CAAS), China
Li Tian,
Zhejiang Agriculture and Forestry University, China

****Correspondence:***
Tao Wu
wutao@hunau.edu.cn
Jiajian Cao
caojiajian@hunau.edu.cn

Specialty section:
This article was submitted to Crop and Product Physiology, a section of the journal Frontiers in Plant Science

Received: *15 December 2021*
Accepted: *28 January 2022*
Published: *08 March 2022*

Citation:
Gao L, Hao N, Wu T and Cao J (2022) Advances in Understanding and Harnessing the Molecular Regulatory Mechanisms of Vegetable Quality. Front. Plant Sci. 13:836515. doi: 10.3389/fpls.2022.836515

INTRODUCTION

With the improvement of living standards, an increasing number of people are paying close attention to the nutritional components and taste of vegetables. On the market, high-quality vegetables, such as broccoli, which contains high glucoraphanin levels, and cucumbers, which have glossy peels, are popular with consumers (Jin et al., 2014; Zhang et al., 2021). With the development of society and the improvement of people's living standards, consumers not only seek vegetables to eat but also have a wide range of choices of vegetables, with the accompanying expectations that they are attractive, nutritionally rich, delicious, fresh, safe and environmentally friendly. Given the requirements for the quality of vegetables, researchers have focused their efforts on systematic studies about the nutritional value of vegetables. In general, vegetable quality includes sensory characteristics and biochemical properties, which can be divided into three aspects, i.e., appearance, texture, and flavor, whereas biochemical properties can be used in the analysis and evaluation of the nutritional value and safety of vegetable crop species (Aung and Chang, 2014; Liu et al., 2017; Bort et al., 2019; Zhao et al., 2019).

The quality evaluation criteria of different vegetables and the regulatory mechanisms behind these traits are quite different (**Figure 1**). Therefore, summarizing the quality characteristics of different crop species is necessary to improve vegetable quality by gene manipulation. Currently, in addition to traditional radiation mutagenesis, chemical mutagenesis, and hybrid breeding methods, genetic manipulation is gradually being applied in the innovation of vegetable crop germplasm resources, but its specific application in quality improvement remains unclear. This paper summarizes the application of genetic manipulation to improve vegetable quality.

QUALITY CHARACTERISTICS OF *Brassicaceae*

Consumers often judge the quality of vegetable crops by their appearance. For example, consumers prefer densely colored cabbage leaves because they believe that the short light time and/or short growth cycle cause(s) the color of cabbage to be light, which leads to a relatively low nutritional quality (Amagai et al., 2021). Moreover, different consumers make various choices regarding vegetable quality due to their different needs or preferences. For instance, someone may prefer loose-type cabbage because they find its leaves to be crisp and sweet when chewing. Conversely, firm cabbage has a higher plant fiber content and is softer and more flexible. Therefore, germplasm resources of different qualities must be created to align with various consumer expectations.

Commodity Quality of *Brassicaceae*

Commodity quality refers to morphological characteristics that can be evaluated by appearance, including plant type, plant height, leaf size, leaf color, petiole characteristics, handle color, and handle shape (Cox et al., 2003; Cheng et al., 2009; Olfati et al., 2010; Kim et al., 2020). There are regional differences in the requirements for the quality of vegetables due to different eating and consumption habits. Many kinds of large-leaf Chinese cabbage can be found in northeast China, while small-leaf Chinese cabbage is most popular in southern China. For *Brassicaceae*, leaves are the most important organ because they are often edible or are involved in nutrient accumulation, and leaf size determines product yields. Current evidence shows that the *Brassicaceae* leaf area is connected with phytohormones. The transcription factor *AINTEGUMENTA* (*ANT*), which encodes the *APETALA2/ETHYLENE RESPONSE FACTOR* (*AP2/ERF*) family, responds to auxin and regulates downstream gene expression related to organogenesis and cell proliferation, indicating that *ANT* promotes leaf growth by regulating cell division (Klucher et al., 1996; Note-Wilson et al., 2010; Ding et al., 2018; Karamat et al., 2021). Three *ANT* and six *ANT-like* (*BrAIL*) genes were identified in Chinese cabbage; the expression of the *BrANT* gene and three *BrAIL* genes increased with auxin treatment, and the leaf size increased (Ding et al., 2018). *ETHYLENE RESPONSE FACTORS* (*ERFs*) encode AP2/ERF superfamily transcription factors, which are the central components of the ethylene signaling pathway (Muller and Munne-Bosch, 2015). Overexpression of *BrERF4* in *Arabidopsis thaliana* can reduce leaf size by inhibiting cell expansion. For *BrERF4* overexpression, two *EXPANSIN* (*EXP*) genes, *AtEXPA5* and *AtEXPA10,* are downregulated in *A. thaliana* (Park et al., 2012). Thus, ethylene can effectively regulate *Brassicaceae* leaf size. In addition to leaf size, leaf shape can affect consumer choice; for example, some consumers prefer split-leaf Chinese cabbage, but others prefer round leaves. *LOST MERISTEM2* (*BrLOM2*) may be the main factor regulating the phenotype of split leaves. A comparison of the round-leaf Chinese cabbage with split-leaf near isogenic lines shows that the expression of *BrLOM2* in split leaves increases synchronously with the number of leaf edge cracks (Shu-juan et al., 2016). Moreover, the plant surface is crucial in determining vegetable quality, including brightness and color. The wax content in *Brassicaceae* is the main factor controlling brightness, and it also affects stress defense. One principal component analysis of different waxy materials showed that the expression of the *LIPID TRANSFER PROTEINS* (*LTP2*) gene is higher in the least waxy lines and that of the *ECERIFERUM3* (*CER3*) gene is more highly expressed in the most waxy lines in *Brassica oleracea* var. *capitata*, indicating that *LTP2* and *CER3* may be related to the wax content (Laila et al., 2017). Scanning electron microscopy and gas chromatography–mass spectrometry (GC–MS) revealed that the wax content of the *CRISPR-BoCER1* plant "*CW1-3*" is significantly lower than that of the wild type, proving that *BoCER1* is crucial in the biosynthesis of cabbage epidermal wax (Cao et al., 2021). In addition to affecting glossiness, wax-related genes play an important role in defense against adverse stresses and are worthy of further exploration. In terms of color, for example, purple leaf *Brassicaceae* varieties are popular on the market. Given the different colors of vegetables, the contents of pigments also varies. Li et al. (2019) found that the relative expression of *BASIC HELIX-LOOP-HELIX49* (*bHLH49*) in stalks and young leaves of Zicaitai "Xianghongtai 01" is significantly higher than that in Caitai "Yinong50D," indicating that *bHLH49* affects the color formation of Zicaitai. These studies on the appearance of *Brassicaceae* will help enrich commodity quality and provide consumers with more choices.

Flavor Quality of *Brassicaceae*

Brassicaceae flavor quality includes sweetness, crispness, softness, juiciness and the lack of undesirable smells. In particular, the leaves and petioles tend to be soft, the odor should be fresh and fragrant, and the material should be tender and strong (Wright et al., 2006). Moreover, high oxygen atmospheric packaging (> 70 kPa, HOAP) can maintain vegetable quality. HOAP affects the production of hydrogen peroxide (H_2O_2), increases cabbage tissue firmness, and significantly reduces the contents of hemicellulose, cellulose, and lignin in the stem. Therefore, the decrease in the H_2O_2 signal in hemicellulose, cellulose, and lignin biosynthesis may be related to the differential accumulation of oxidative stress-related proteins that are induced by HOAP treatment (Wang et al., 2020). At present, studies about *Brassicaceae* flavor quality are limited, and the mechanism by which special flavors are formed has not yet been found.

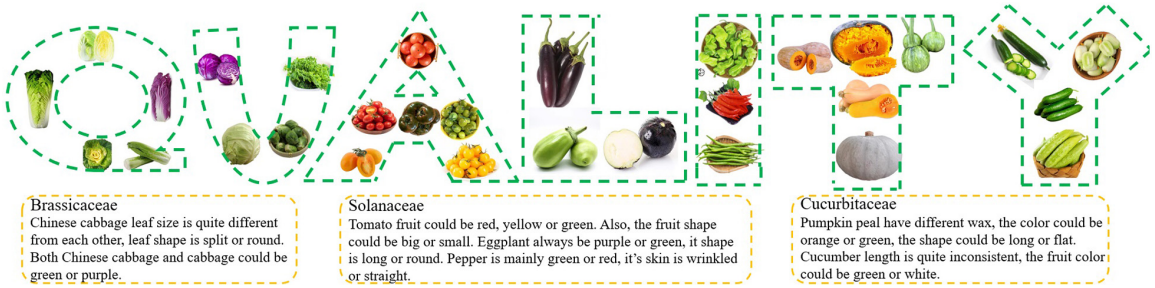


FIGURE 1 | Overview of the different vegetable commodity characteristics, with *Brassicaceae*, *Solanaceae*, and *Cucurbitaceae* as examples. Extensive research has been performed to optimize leaf size (e.g., split or round Chinese cabbages), leaf color (e.g., green or purple cabbages), fruit color (e.g., red, yellow or green tomatoes, purple or green eggplants, and orange or green pumpkins), fruit shape (e.g., big or small tomatoes, wrinkled or straight eggplants, and long or flat pumpkins), and fruit size (e.g., cucumbers of different lengths). Vegetables are usually optimized to meet consumer expectations for product quality, including appearance, taste, and texture.

Nutritional Quality of *Brassicaceae*

Nutritional quality refers to nutritional value, which is mainly determined by the contents of nutrients but is also affected by the contents of harmful components and pollutant residues. The nutritional quality of *Brassicaceae* requires high contents of flavonoids, L (+)-ascorbic acid (AsA), dry matter, soluble solids, and vitamins; a moderate content of crude fiber; a low content of nitrate; and absence of pollutant residues such as pesticides. The unique nutritional quality of *Brassicaceae* is attributed to flavonoids. Watercress is a special plant rich in flavonoids. Four important watercress varieties were compared with non-heading Chinese cabbage by ultrahigh-performance liquid chromatography-electrospray ionization-tandem mass spectrometry (UHPLC–ESI–MS/MS). A total of one hundred thirty-two flavonoid metabolites were detected: eight anthocyanins, two dihydroflavonoids, three dihydroflavonols, one flavonoid, twenty-two flavonoids, eleven flavonol carbon glycosides, eighty-two flavonols and three isoflavones. Marked differences in flavonoid metabolites were found in different samples, and all of them exhibited their own unique metabolites (Ma et al., 2021). The most important nutritional quality of *Brassicaceae* is the content of AsA, which can be regenerated from monodehydroascorbate and dehydroascorbate by *MONODEHYDROASCORBATE REDUCTASE* (*MDHAR*). Overexpression of *MDHAR1* from non-heading Chinese cabbage reduces the AsA level and growth in transgenic tobacco (Ren et al., 2015). Additionally, there is a very significant negative correlation between the nitrate content and AsA content in leaf lettuce (Koyama et al., 2012). These results provide a reference for enhancing the nutritional quality of *Brassicaceae* crop species.

QUALITY CHARACTERISTICS OF *Solanaceae*

Given that people eat only the fruits of solanaceous crop species, the key to improving the quality of solanaceous crops is to focus on fruit quality. Consumers have different evaluation standards for the fruit quality of *Solanaceae*. For example, tomatoes with uniform color, thin skin, and no cracks are more popular than their counterparts. When the taste is sweet and sour, the quality of tomatoes is considered high. Similarly, uniform color and strong luster are important qualities for peppers. Plump and juicy peppers taste better and are more popular with consumers than their counterparts. Less spicy peppers with moderate aromas sell well in northern China. However, peppers with high levels of spiciness and strong scents are highly popular among consumers in southern China, such as Sichuan and Hunan Provinces. In addition, factors such as cooking techniques and geographical restrictions lead to different consumer needs, so many varieties of solanaceous crops exist on the market.

Commodity Quality of *Solanaceae*

Tomatoes, peppers, and eggplants are common *Solanaceae* vegetables and are important parts of our table dishes. Given that the main edible part of solanaceous crops is the fruit, fruit shape and color are important commodity qualities. For example, the best-selling tomato requires uniform coloring, bright color, small cracks in the apical pedicel, and no longitudinal or ring cracks (Yildiz and Baysal, 2007; Liu et al., 2020; Xue et al., 2020). Currently, most consumers prefer bright red or pink fruit colors, and a few prefer an orange fruit color, which varies with the changes in eating habits in different regions (Veerappan et al., 2016; Yang et al., 2019). Similar to *Brassicaceae*, pigments, such as chlorophyll, lutein, carotene, and anthocyanin, affect the color of tomatoes. The expression of the structural flavonoid genes is closely followed by *MYB12*, suggesting that *MYB12* regulates the production of flavonoids in tomato fruit by activating the transcription of the genes encoding these pathway enzymes, and *MYB12* is also reported to be suppressed in pink line tomatoes (Adato et al., 2009; Ballester et al., 2010). *SlMYB12* mutation leads to premature termination of the amino acid sequence and structural changes, resulting in a colorless epidermis phenotype in tomato fruits (Veerappan et al., 2016). Compared with yellow tomatoes, *ISOPENTENYL DIPHOSPHATE ISOMERASE 1* (*IDI1*) is a cytoplasmic enzyme involved in the biosynthesis of isoprenoids,

including cholesterols, that inserts a single T base into exon 6 in apricot tomatoes, resulting in a decrease in carotenoid content and yellow pericarp (Nakamura et al., 2015; Shin et al., 2019; Chattopadhyay et al., 2021). Several genes and their mutant alleles related to carotenoid biosynthesis have been identified and characterized in tomato fruit. *PHYTOENE SYNTHASE* (*PSY1*), *CAROTENOID ISOMERASE* (*CrtISO*), *LYCOPENE BETA CYCLASE* (*CYC-B*), and *LYCOPENE* E-*CYCLASE* (*LCY-E*) mutations can affect the carotene content and change the color of the tomato epidermis, but the mechanisms of the formation of different colors remain unclear (Hwang et al., 2016; Yoo et al., 2017; Chen et al., 2019). For purple eggplant, pericarp color intensity is an important economic characteristic. Many factors are considered in assigning the final color intensity, one of which is the accumulation of anthocyanins and chlorophyll. Comparing two advanced purple eggplant lines, EP26 and EP28, with different pericarp color intensities, a higher anthocyanin content and lower chlorophyll content were observed in EP26, and deeper pericarp color intensity was observed at two developmental stages. In addition, comparative transcriptome analysis of EP26 and EP28 showed that 131 transcription factors, including those of the MYB, bHLH, WRKY and NO APICAL MERISTEM, *Arabidopsis* TRANSCRIPTION ACTIVATION FACTOR1/2, and CUP-SHAPED COTYLEDON (NAC) families, displayed dynamic changes, which may have been due to the changes in fruit pigment accumulation between EP26 and EP28 (Zhou et al., 2021). Although some genes related to *Solanaceae* fruit color have been clarified, the mechanism by which different colors are formed has yet to be elucidated. Further research on the molecular regulatory mechanism of color is necessary to create multicolor germplasm resources.

Tomato cracking generally occurs during fruit ripening and is affected by genetic or environmental factors such as fruit firmness, cuticle characteristics, abscisic acid (ABA), gibberellins (GAs), water, light and nutrients (Cox et al., 2003; Bargel and Neinhuis, 2005; Khadivi-Khub, 2015; Yang et al., 2016; Jiang et al., 2019). Cracking greatly reduces the edible value of tomatoes, and tomatoes with no cracks are highly popular on the market. One crack-resistance gene, *Cr3a*, was found by mapping. The water content of cracked tomato fruit during the green ripening period was significantly higher than that of the *Cr3a* crack-resistant tomato. However, no significant difference in the thickness of the cuticle or the number of epidermal cells was found between these two kinds of tomatoes, and the mechanism remains unclear (Yu et al., 2020). In addition to these genetic or environmental factors, tomato cracking is related to the pectin content. POLYGALACTURONASE (PG) can degrade the pectin backbone, and EXPANSIN (EXP) is a non-enzymatic cell wall active protein. PG and EXP cooperatively disassemble wall polysaccharide networks and contribute to the softening of fruit. By suppressing *SlPG* and *SlEXP1* expression in tomato fruit (*pg/exp*), the content of water-soluble pectin decreases in the pericarp, whereas the content of propectin increases. Although the cell wall and wax layer become thicker and the *pg/exp* fruit hardens, the rate of fruit cracking is reduced due to the firm protopectin (Jiang et al., 2019).

The texture of the fruit, especially the firmness, is the main quality of fresh tomatoes evaluated by consumers (Hongsoongnern and Chambers, 2008; Brashlyanova et al., 2014). Most consumers prefer hard tomatoes, which have better cooking characteristics. The factors affecting the firmness of tomatoes are epidermal toughness, pulp firmness and the internal structure of fruits (Chapman et al., 2012; Romero and Rose, 2019). *FIRM SKIN 1* (*FIS1*) encodes a GA2-oxidase, and changes in the level of GAs can induce parthenocarpic development and affect fruit maturity in tomatoes (Martinez-Bello et al., 2015; Li et al., 2019). Early termination of the *FIS1* gene increases the biological activity of GA, the biosynthesis of thorny and waxy layers, and the shelf life and firmness of fruits in tomato (Li et al., 2020). These changes improve the firmness of tomato fruits, thereby increasing transportability and yielding more economic benefits.

Flavor Quality of *Solanaceae*

For tomato, the main factors affecting flavor quality are the contents of sugar and acid and the ratio of sugar to acid (Beckles, 2012). High sugar and low acid contents make the tomato taste light, whereas a low ratio of sugar to acid makes the tomato taste sour. When both are low, the fruit is tasteless. For good flavor, the fruit must have a high sugar content and high sugar:acid ratio. In recent years, given the obvious diversification of consumer groups, tomato fruits with increased acidity have been favored by special groups such as beverage lovers under the premise of a high sugar content. The cell wall *CONVERTING ENZYME INHIBITOR 1* (*SlCIF1*) gene, which is involved in tomato glucose metabolism, activates the small *HEAT SHOCK PROTEIN 17.7* (*SlHSP17.7*) gene to control the flavor of tomato. In *SlHSP17.7*-RNA interference (RNAi) lines, the sweetness of tomato is significantly decreased by modulation of the contents of sucrose and fructose (Zhang et al., 2018).

Spicy taste is a unique flavor quality of pepper. Whole-genome sequencing and assembly of the hot pepper (Mexican landrace of *Capsicum annuum* cv. CM334) revealed fifty-four *CAPSAICINOID BIOSYNTHETIC GENES* (*CBGs*) related to the spicy taste of pepper; *CBGs* are specifically expressed in the placenta of pepper, but the mechanisms behind these genes are unclear (Kim et al., 2014). *MYB31* is a transcription factor specifically expressed in pepper placenta. Transcription level analysis revealed that *MYB31* is highly coexpressed with *CBG*. Further experiments revealed that *MYB31* directly regulates *ACYLTRANSFERASE* 3(*AT3*), which exhibits developmentally regulated placenta-specific expression and participates in capsaicin biosynthesis by binding to MYB *cis*-elements. Moreover, *MYB31* directly regulates *CBG* expression and participates in capsaicin biosynthesis (Zhu et al., 2019). Consumer preferences for pepper spiciness are affected by subjective factors, so breeders can select corresponding varieties depending on the preferences of local consumers.

Nutritional Quality of *Solanaceae*

The content of AsA is an important index of quality. *MYO-INOSITOL OXYGENASE* (*MIOX*) is a critical enzyme in the plant AsA biosynthesis pathway. *MIOX4* overexpression tomato lines show a significant increase in total ascorbate in

leaves and red fruits compared to the control (Munir et al., 2020). After the knockout of *ASCORBATE OXIDASE* (*AO*) and mitochondrial *ASCORBATE PEROXIDASE* (*mitAPX*), the decreased AO enzyme activity and significantly improved AsA content in tomato fruit were observed to be correlated with *AO* gene suppression, and the downregulated *mitAPX* expression and APX enzyme activity led to an increase in the content of AsA in tomato fruits compared with the wild type, indicating that *AO* and *APX* can improve the content of AsA (Zhang et al., 2011a,b).

QUALITY CHARACTERISTICS OF *Cucurbitaceae*

The common *Cucurbitaceae* vegetable crops include cucumbers (*Cucumis sativus* L.) and pumpkins (*Cucurbita moschata*), and their morphological characteristics are quite different from each other. Cucumbers with a slender and uniform body are preferred for cooking and fresh eating in China. To make pickled cucumbers, Russians prefer short fruits. Moreover, some people believe that cucumbers with small and dense thorns are better, and those with large and sparse thorns do not have the unique flavor of cucumbers. However, other people like cucumber fruit without thorns and growths. For yellow or green pumpkin, people believe that the darker the pumpkin is, the greater the sweetness. Consumers also find that yellow pumpkin is suitable for steaming or cooking porridge to make various cakes, while green pumpkin is suitable for fried food. In addition to cucumbers and pumpkins, *Cucurbitaceae* vegetables such as melons and watermelons exist in various shapes and colors. Therefore, *Cucurbitaceae* crops of different qualities should be cultivated to meet the demands of consumers.

Commodity Quality of *Cucurbitaceae*

The main edible part of *Cucurbitaceae* crop species such as cucumber is the fruit. Together with tomato and other *Solanaceae* crops, pericarp color, pulp color, and fruit luster are also important commodity qualities of *Cucurbitaceae* vegetables (Zhang et al., 2019; Gebretsadik et al., 2021; Mashiane et al., 2021). Fruit length and wax powder are the unique commodity qualities of *Cucurbitaceae* crops and have long been the focus of research (Hu et al., 2011; Dou et al., 2018; Ding et al., 2020). For cucumbers, it is difficult to select for fruit firmness during breeding. Peterson et al. found that cucumber firmness was quantitatively inherited with sufficient additive effects, so environmental effects and polygenic heritability were obvious. Fruit length is important to *Cucurbitaceae* crops, especially cucumber. Similar to *Brassicaceae*, some key genes controlling cucumber fruit length have been identified that are related to plant hormones, especially auxin. Knockout of the *FRUITFULL 1* (*CsFUL1*) gene results in further elongation of cucumber fruit, while the high expression of the *CsFUL1* gene significantly shortens cucumber fruit. In addition, *CsFUL1* inhibits the expression of the auxin transporters *PIN-FORMED1* (*PIN1*) and *PIN7,* resulting in a decrease in auxin accumulation in fruit, thereby affecting the fruit length of cucumber (Jiang et al., 2015; Zhao et al., 2019). To clarify the effect of plant hormones on the length of cucumber fruit, researchers can adjust the morphology of high-quality cucumbers in the actual production process. Wax powder is one of the factors affecting the glossiness of fruit. The *AtWAX2* homolog *CsWAX2* in cucumber was cloned and found to be highly expressed in synthetic waxy epidermis. The ectopic expression of *CsWAX2* in the *Arabidopsis wax2* mutant can partially complement the bright stem phenotype (Wang et al., 2015). Additionally, grafting cucumber onto pumpkin rootstock is an effective way to produce glossy cucumber fruits. *AtWIN1* is a regulator of wax biosynthesis that can activate the expression of wax biosynthesis genes such as *CER1*, *CER2*, and *KCS1*; when the expression is enhanced, the mutant *Arabidopsis* became glossier than the wild type (Broun et al., 2004). *CsWIN1* and several key wax biosynthesis genes, including *CsCER1*, *CsCER1-1*, *CsCER*, *4,3-KETOACYL-CoA SYNTHASE* (*CsKCS1*) and the wax transport gene *ATP-BINDING CASSETTE (CsABC)*, are significantly upregulated in cucumber grafted onto pumpkin, so these genes are positively correlated with wax synthesis. More wax esters (C20 fatty acid composition) and fewer alkanes (C29 and C31) were deposited in the grafted cucumber pericarp, probably due to the high wax ester content and the high integration of small trichomes in the pericarp (Zhang et al., 2019). However, there are few studies on the glossiness of *Cucurbitaceae*, and the mechanism needs to be further clarified.

Flavor Quality of *Cucurbitaceae*

Using cucumber as an example, its flavor quality generally refers to its unique smell and taste (Shimomura et al., 2016). The bitterness of *Cucurbitaceae* is caused by cucurbitacin. The transcription factors *BITTER LEAF* (*BL*) and *BITTER FRUIT* (*BT*) can be used to regulate bitterness formation in leaves and fruits, respectively, by applying the integrative bioinformatics and molecular biology approaches described above. Researchers have identified four additional *P450* genes (*Csa3G698490*, *Csa3G903540*, *Csa3G903550*, and *Csa1G044890*) that are coexpressed with the *BI* cluster (Shang et al., 2014). In addition to bitterness, unique aromatic substances and some non-volatile substances have been reported in cucumber. Researchers used GC–MS to analyze eighty-five volatile chemicals, including thirty-six volatile terpenes in twenty-three different tissues of cucumber, and found that TERPENE SYNTHASE11 (TPS11)/TPS14, TPS01, and TPS15 are responsible for volatile terpenoid production in the roots, flowers, and fruit tissues of cucumber plants and can improve cucumber flavor (Wei et al., 2016). Many kinds of cucumber flavor substances have been identified, of which (E,Z)-2,6-non-adienal (NDE) is an important commercial flavor. NDE has been found in various plant materials, but cucumbers are considered the best source of this flavor substance. NDE production is reduced by acidification, enhanced by linolenic acid, and unaffected by unsaturated fatty acids, NaCl or $CaCl_2$ (Buscher and Buscher, 2001). Cucurbitacin is a unique substance of cucumbers. The mechanism of cucumber bitterness must be clarified to combine the non-bitterness characteristics with other excellent characteristics to cultivate high-quality cucumbers.

Nutritional Quality of *Cucurbitaceae*

Nutritional quality mainly refers to the nutrition and health care ingredients needed by the human body. For cucumber, pumpkin and other *Cucurbitaceae* crops, AsA, soluble solids, soluble protein, soluble sugar and other traits are important for the measurement of nutritional quality (Ge et al., 2017; Gao et al., 2018; de Almeida et al., 2019; Buzigi et al., 2021). ASCORBATE OXIDASE is a copper-containing enzyme localized at the apoplast, where it catalyzes the oxidation of AsA to dehydroascorbic acid (DHA) via a monodehydroascorbic acid (MDHA) intermediate. Similar to solanaceous crops, AO can also affect the content of AsA in *Cucurbitaceae* crops. The reduction in AO activity increases the AsA content in melon (*Cucumis melo* L.) fruit, which is due to the oxidation of AsA and the expression of certain biosynthetic and recycling genes, such as *CmAPX1*, *CmMDHAR*, and *CmDHAR* (Chatzopoulou et al., 2020). Consequently, the ascorbate redox state is altered in the apoplast. Interestingly, transgenic melon, which suppresses AO expression, displays an increased ethylene production rate coinciding with elevated activity and gene expression levels of 1-aminocyclopropane-1-carboxylic acid (ACC) oxidase (ACO), which might contribute to early ripening; moreover, AO participates in the rapid fruit growth of *Cucurbitaceae in vivo* (Chatzopoulou et al., 2020). Sugars provide a strong, pleasant, sweet taste and deliver energy when ingested; appetite regulatory centers respond to the energy content of sugar, which has a major influence on human health (Anderson, 1995). Thus, studies on the soluble sugar content of vegetables are of great significance. Comparing two cultivated pumpkin lines with different sweetness, C. *maxima* inbred lines "98-2" and "312-2," the glucose content of "312-1" decreased rapidly in the early stage of fruit development, which may have been related to the high expression of sucrose *INVERTASE* (*INV*) and *HEXOKINASE (HK*) at this stage. In contrast, *FRUCTOSE KINASE* (*FK*), which is responsible for fructose metabolism, is differentially expressed at different stages of fruit development. These results suggest that *INV, HK*, and *FK* may serve important roles in promoting sucrose biosynthesis during pumpkin fruit development (Wang et al., 2020).

COMPLEXITY OF VEGETABLE QUALITY REGULATION

From the above, many studies on the genes related to the regulation of vegetable quality have been conducted, and genes that are highly conserved or belong to the same gene family in different varieties are likely to have close functional correlations (**Figure 2**). For example, MDHAR, the key enzyme in AsA synthesis, can catalyze the reduction of MDHA to AsA (Park et al., 2016). When *MDHAR* was silenced in different species, such as melon, acerola, and Chinese cabbage, the content of AsA decreased (Eltelib et al., 2011). Moreover, *SUN* is one of the main genes controlling tomato fruit shape and encodes a member of the *IQ67-DOMAIN* (*IQD*) family of calmodulin-binding proteins. When *SUN* expressed at high levels in the fruit, tomato showed an elongated shape (Xiao et al., 2008). More precisely, SUN controls tomato shape through redistribution of mass that is mediated by increased cell division in the longitudinal direction and decreased cell division in the transverse direction of the fruit (Wu et al., 2011, 2015). The cucumber *CsSUN* gene is also involved in the regulation of cucumber spherical fruit development, and the round-fruited WI7239 had a 161-bp deletion in the first exon of *CsSUN*. The expression of *CsSUN* in round-fruited WI7239 was significantly lower than that in long-fruited WI7238 (Pan et al., 2017). Although *SUN* has some effect on the fruit shape of tomato and cucumber, *SUN* affects the length of tomato and changes the width of cucumber fruits. It is necessary to understand the specific mechanism of *SUN* in different crops. Thus, although the genes regulating quality traits are conserved in different vegetables, their mechanisms of action remain to be further confirmed.

Constituting a common factor in vegetable quality regulation, phytohormones have diverse effects on vegetable quality. The same hormones can regulate the same phenotypes in different species, but the mechanisms are not consistent; for example, auxin can influence vegetable leaf or fruit size. *CsFUL1* inhibited the expression of the auxin transporters *PIN1* and *PIN7*, resulting in a decrease in auxin accumulation in fruit, thereby affecting the fruit length of cucumber (Zhao et al., 2019). *BrANT* responds to auxin and regulates downstream gene expression of organogenesis and cell proliferation, indicating that ANT promotes leaf growth by regulating cell division (Ding et al., 2018). These observations suggest that auxin controls many aspects of vegetable organ development in different ways (Pattison et al., 2014). Additionally, the same quality traits of vegetables may be affected by different phytohormones. Taking tomato firmness as an example, Moneymaker (MM) tomato has a higher compression resistance than *Solanum lycopersicum* var. *cerasiforme* LA1310 (CC). Compared with the fruits of the near-isogenic line with the CC *qFIRM SKIN 1* (q*FIS1*) allele (NIL-$FIS1^{CC}$) Li *et al.* found that bioactive GAs, including GA1, GA3, and GA7, were dramatically increased, whereas the metabolic products of GA2-oxidases, including GA8 and GA34, were decreased in the fruits of the near-isogenic line with the MM q*FIS1* allele (NIL-$FIS1^{MM}$) (Li et al., 2020). By spraying exogenous GA3 on NIL-$FIS1^{CC}$ mature green fruits, researchers found significantly increased compression resistance in treated fruits compared to untreated controls, indicating that GA levels contribute to higher fruit firmness (Li et al., 2020). Moreover, researchers treated wild type tomato fruit with exogenous ABA and found that fruit firmness decreased, and the suppression of *9-CIS-EPOXYCAROTENOID DIOXYGENASE* (*SlNCED1*), which encodes a key enzyme in ABA biosynthesis, significantly induced tomato fruit firmness (Sun et al., 2012). GA and ABA can both affect tomato firmness, but the specific mechanism of action and the connection between the two require further analysis. Furthermore, there is extensive cross-talk between different phytohormones that control growth and development, such as auxin and GA. AUXIN RESPONSE FACTORS (ARFs) are transcription factors that respond to auxin signals and activate or repress downstream gene expression, thus delivering the signal for the regulation of a set of genes (Roosjen et al., 2018). As critical transcriptional downstream

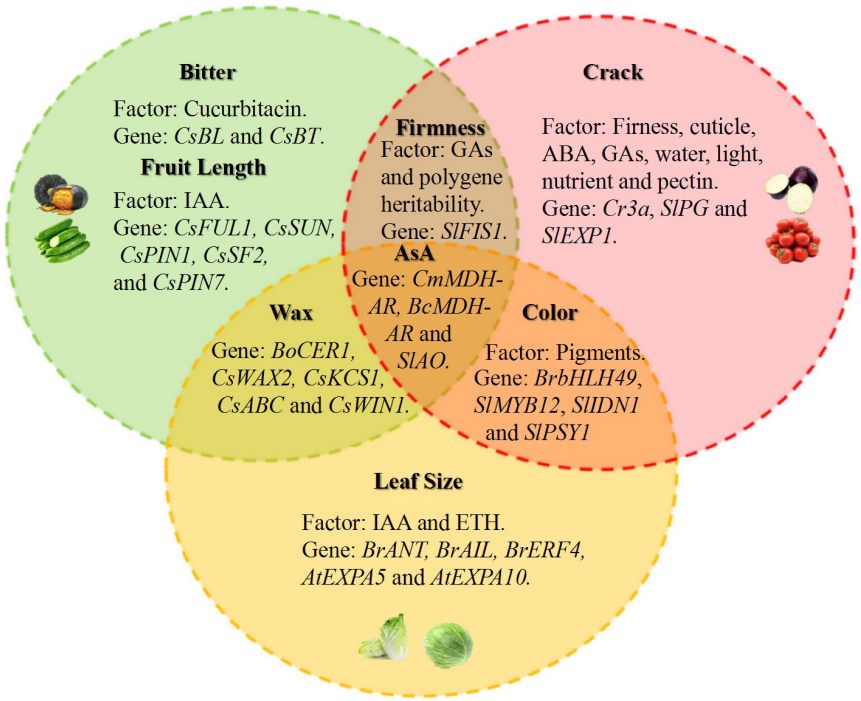


FIGURE 2 | Overview of the factors and genes related to vegetable quality, taking *Brassicaceae*, *Solanaceae* and *Cucurbitaceae* as examples. Phytohormones represent the main factor that can influence fruit length (*Cucurbitaceae*), leaf size (*Brassicaceae*), firmness (*Solanaceae*) and cracking (*Solanaceae*). Cucurbitacin is a unique substance of cucumbers that affects bitterness. Genes regulate different quality characteristics of vegetables, such as fruit length in cucumber (*CsFUL1*, *CsSUN*, *CsPIN1*, *CsPIN7* and *CsSF2*), cracks in tomato (*Cr3a*, *SlPG* and *SlEXP1*) and leaf size in Chinese cabbage (*BrANT*, *BrAIL* and *BrERF4*). Some homologous genes such as *MDHAR* also play similar roles in vegetable quality, which affects the content of AsA in non-heading Chinese cabbage and melon.

targets of *ARF2*, *CARBON-METABOLISM INVOLVED* (*GNC*) and *GNC-LIKE* (*GNL*) are involved in plant greening, flowering time, and senescence (Richter et al., 2013). It has been reported that the constitutive activation of GA signaling is sufficient to suppress *arf2* mutant phenotypes, causing increased chlorophyll accumulation and delayed senescence through repression of *GNC* and *GNL* (Richter et al., 2013). These and other aspects of different pathways suggest complex crosstalk in multiple phytohormone signals, reflecting their pleiotropic effects on vegetable growth and ripening. Finally, phytohormones act as common factors regulating vegetable quality, and deepening the mechanistic understanding of molecular events related to phytohormones will help to elucidate the regulatory networks that affect vegetable quality.

GENETIC MANIPULATION APPLIED IN VEGETABLE QUALITY

Many researchers have identified the key genes that affect vegetable qualities. For example, Wiesner et al. (2014) identified genes coding for polypeptide four of the cytochrome P450 (CYP) monooxygenase subfamily CYP81F and examined their metabolic roles in indole glucosinolate biosynthesis in *Brassica rapa* ssp. *chinensis* by microarray. Li et al. (2016) found that exogenous auxin alters the expression patterns of ethylene and auxin signaling-related genes that are induced or repressed in the normal ripening process by Illumina RNA sequencing. Kompetitive allele-specific PCR (KASP) is a proprietary technology of LGC genomics that can distinguish alleles at variant loci (Semagn et al., 2014; Steele et al., 2018). Paudel et al. (2019) used the four loci to facilitate marker-assisted selection (MAS) for watermelon seed coat color. The results of these studies can be applied to actual production processes to improve vegetable quality. With the development of molecular biology technology, the regulation of vegetable quality is not confined to traditional methods, such as grafting techniques and the application of exogenous fertilizers, but regulation at the molecular level is becoming increasingly common.

DNA molecular marker technologies are marker techniques based on nucleotide differences between individuals. This refers to genetic markers based on DNA. In other words, direct response to genetic material variation at the DNA level may accurately reveal interspecific and intraspecific differences (Vieira et al., 2007; Alim et al., 2011; Ferguson et al., 2012; Xu et al., 2019; El-Mansy et al., 2021).

DNA molecular markers are widely used in vegetable breeding research, including the construction of genetic maps to facilitate the selection of breeding parents, the stable and objective analysis of genetic relationships and plant origin and evolution, and the mapping of agronomic trait genes (**Table 1**). Restriction fragment

TABLE 1 | Different types of molecular markers.

Type	Molecular markers	References
Molecular hybridization	RFLP	Gebhardt et al., 1991; Sakamoto et al., 2000
PCR	SSR SNP	Shirasawa et al., 2010; Wang et al., 2012; Gharsallah et al., 2016; Ohyama et al., 2017; Paudel et al., 2019; Zhang et al., 2020a
PCR and Restriction Enzyme Digestion Technology	AFLP	Xu et al., 2014

TABLE 2 | Application of transgenic and genome editing technology in vegetables.

Type	Method	Gene	Quality	Challenges
Transgenic technology	RNAi	*SlABCG36 SlABCG42*	Tomato has a thinner stratum corneum	The safety of genetically modified vegetables is still unclear
	VIGS	*CaCCS CaPSY CaLCYB CaCRTZ*	Pepper fruits turn orange or yellow	
Genome editing technology	CRISPR	*SlFIS1*	Increase tomato firmness	Traits do not coexist with others
		CsSF2	Shoot cucumber fruit	The serious growth inhibition of homozygous plants

length polymorphism (RFLP) is the earliest DNA molecular marker technology. By mapping chromosome-specific tomato RFLP markers in potato and conversely mapping potato markers in tomato, the different potato and tomato RFLP maps were aligned, and the similarity of the potato and tomato genomes was confirmed (Gebhardt et al., 1991). RFLP has also been used for the identification of S-haplotypes of breeding lines in broccoli and cabbage (*B. oleracea* L.) and in purity tests of F_1 hybrid seeds (Sakamoto et al., 2000). Simple sequence repeat (SSR) markers have been widely used to obtain new germplasm in recent years. When 32 SSR pairs of primers derived from the *A. thaliana* chloroplast genome and another 21 SSR primers from the *B. napus* mitochondrial genome sequences were compared, six types of cabbage cytoplasmic male sterility (CMS) were found, namely, NigCMS, OguCMSR (1), OguCMSR (2), OguCMSR (3), OguCMSHY, and PolCMS (Wang et al., 2012). Additionally, Gharsallah et al. (2016) genotyped cultivars using nineteen polymorphic SSRs out of twenty-five tested to produce a total of seventy alleles with an average of 3.68 alleles per locus and polymorphism information content (PIC) values ranging from 0.22 to 0.82 in saline tolerant, mildly tolerant and saline sensitive tomatoes, so SSR marker-genotypes can be used to find potential salt tolerance sources in tomato. Furthermore, the single nucleotide polymorphism (SNP) markers screened in tomato cultivar lines can be used to estimate the transferability of these SNPs to other breeding materials (Shirasawa et al., 2010). A core set of twenty-four SNPs can distinguish 99% of the two hundred and sixty-one cucumber varieties (Zhang et al., 2020a). These methods can be used comprehensively. For example, amplified fragment length polymorphism (AFLP) and SSR techniques combined with bulk segregant analysis (BSA) can be used to map the *RESTORER GENE* (*BrRFP*) in heading Chinese cabbage using the F_2 segregating population developed by crossing the polima (pol)-like CMS line 06J45 and the restorer line 01S325 (Xu et al., 2014). Ohyama et al. (2017) identified thirteen important agronomic quantitative trait loci (QTLs) in tomato by SSR molecular markers. Xu et al. (2019) developed thirty-five informative InDel markers that were successfully used to analyze the genetic diversity of thirty-six cabbage germplasms, providing molecular marker data for genetic mapping and germplasm identification and promoting genetic improvement in cabbage breeding.

Transgenic Technology to Regulate the Quality of Vegetables

Transgenic technology involves the use of modern biotechnology to artificially separate, recombine, introduce, and integrate required target genes into the genome of organisms, thereby improving the original traits or providing new desirable traits (Kumar et al., 2020). Given that the essence of transgenic technology and traditional technology is genetic improvement through the acquisition of excellent genes, the close combination of transgenic technology and conventional breeding techniques can enable breeding of new varieties with multiresistance, high quality, high yield and high efficiency. This approach can greatly improve the efficiency of variety development, reduce the input of pesticides and fertilizers, and enable great potential in alleviating resource constraints, ensuring food safety, protecting the ecological environment and expanding agricultural functions (Ndimba et al., 2017).

Transgenic experiments play an important role in the verification of gene function (**Table 2**). The tomato genes *ATP-BINDING CASSETTE TRANSPORTER G 36* (*SlABCG36*) and *SlABCG42*, which encode proteins that are highly homologous to *AtABCG32*, can be downregulated using RNAi techniques, resulting in the deposition of the stratum corneum in the tomato fruit and the formation of a thinner stratum corneum; ABCG transporter protein affects the transport of keratin precursors (Elejalde-Palmett et al., 2021). Zhang et al. (2020b) used *A. thaliana* as a material and overexpressed *AtMYB49* to improve the ability of plants to resist oxidative stress. Arce-Rodriguez and Ochoa-Alejo designed a virus-induced gene silencing (VIGS) system for *Capsicum*, providing a new means for the study of gene function in this genus (Arce-Rodriguez and Ochoa-Alejo, 2020). The pepper color genes *CAPSANTHIN/CAPSORUBIN SYNTHASE* (*CCS*), PHYTOENE SYNTHASE (PSY), *LYCOPENE-BETA-CYCLASE* (*LCYB*), and *BETA-CAROTENE HYDROXYLASE* (*CRTZ*) were silenced separately through VIGS technology, and pepper fruits from red

fruit cultivars turned orange or yellow. Moreover, these four genes were silenced simultaneously; the fruits did not show the normal red color ation (Tian et al., 2014). Recently, researchers applied VIGS of pepper genes via a pTRV2-GFP-CaPDS vector, which can visualize TRV spread and monitor VIGS efficiency, thereby enriching the research methods for vegetable germplasm resources (Zhou et al., 2021).

Gene Editing Technology to Regulate the Quality of Vegetables

Gene editing, also known as genome editing or genome engineering, is a relatively accurate genetic engineering technology or process that can modify specific target genes in the genome of organisms (Schindele and Puchta, 2020). Clustered regularly interspaced short palindromic repeats/Cas (CRISPR/Cas) technology is the third generation of genome editing technology developed in recent years. It is a means to study gene function and improve crop yield. Gene editing shows great potential in gene research and genetic improvement because it can efficiently edit the targeted genome (Li et al., 2021).

At present, CRISPR technology has been applied to the targeted editing of genomes of various organisms (**Table 2**). Li et al. (2020) used CRISPR/Cas9 technology to edit *FIS1* to verify its effect on tomato firmness (Li et al., 2020). *SHORT-FRUIT 2* (*SF2*) encodes histone deacetylase proteins, which participate in diverse and tissue-specific developmental processes by forming various corepressor complexes with different regulatory subunits. Researchers knocked out the *SF2* gene by CRISPR/Cas9 and proved that *SF2* controls fruit cell proliferation by targeting the biosynthesis and metabolism of cytokinin and polyamines (Zhang et al., 2020c).

PERSPECTIVES

Currently, there are new demands for vegetable quality in terms of diversity and nutritional health. Improving vegetable quality is an important topic in contemporary vegetable research. Scientists have conducted in-depth research on the molecular development, regulatory mechanisms and biosynthesis of vegetable quality traits. Studies have mainly included the identification of candidate genes, and their loci, which are responsible for fruit quality traits of different varieties of vegetables, as well as the physiological and metabolic pathways that directly or indirectly affect fruit quality traits. In addition, the establishment of efficient genetic transformation methods and the use of gene-editing technology help verify the function of these determinants or regulators. These applications for improving quality attributes make sense when traditional breeding is difficult because of the reproductive isolation between species.

Studies have shown that molecular breeding combined with genome editing technology is growing rapidly, and that this approach can shorten the breeding cycle and greatly improve breeding efficiency, which has become a new direction in vegetable breeding (Ueta et al., 2017). Genome editing has been generally applied in horticulture, and gene edited crops mainly include *Solanum lycopersicum, Solanum pimpinellifolium, Solanum tuberosum, Brassica oleracea, Brassica napus, Brassica carinata, Lettuce sativa, Cucumis sativus, Camelina sativa, Daucus carota,* etc. (Xu et al., 2019). Through the application of genome editing technology, new germplasms have been created, such as lettuce with high AsA and strawberry with different sugar contents, and *de novo* domestication of tomato was realized (Li et al., 2018; Zhang et al., 2018; Xing et al., 2020). However, gene manipulation technologies still face challenges in improving vegetable quality. However, whether or not gene-edited vegetables should be regulated as transgenic vegetables has aroused international controversy (Hashimoto et al., 1999; Friedrichs et al., 2019). Thus, gene-edited vegetables are in urgent need of policy support to promote the industrialization of new technologies and products. On the other hand, the precise regulatory mechanisms of complex vegetable traits still need to be further explored. Important agronomic traits might be regulated by multiple gene loci, and one gene may be involved in multiple agronomic traits. For example, *SF2*, which encodes histone deacetylase protein, not only affects fruit quality but also participates in the normal growth of plants. The cucumber *sf2* knockout mutant exhibits severely hindered growth and cannot develop further. The application of CRISPR technology can only be used to analyze the functional mechanism by which *CsSF2* regulates cucumber fruit length and cannot be applied to the actual production process (Zhang et al., 2020c). Therefore, one of the biggest challenges facing future gene manipulation technologies is to identify precise trait regulatory networks and disrupt the unwanted linkages between different traits.

Furthermore, the development of genomics, molecular biology, imaging, remote sensing informatics, and big data technology will promote the development of breeding science (Mahlein et al., 2012; Boukar et al., 2019; Walter et al., 2019; Zhao et al., 2019). In particular, the application of big data technology in gene breeding plays a huge role in screening for functional variants, since it improves the efficiency and accuracy of variant detection. The target of genetic variation detection in plants has shifted from single SNP to structural variation and insertion or deletion allelic variation though big data technology (Wong et al., 2019). In summary, although challenges remain, the application of genetic manipulation in horticultural crop species improvement will further create and enhance vegetable quality through the inclusion of desirable traits.

AUTHOR CONTRIBUTIONS

LG and NH analyzed the gene manipulation effects on the quality of vegetables. TW and JC conceived the original idea for the review. All authors wrote the manuscript.

FUNDING

This study was supported by the National Key Research and Development Program of China (2018YFD1000800), the National Natural Science Foundation of China (31972429, 31972407, and 32011540003), and the Hunan Provincial Natural Science Foundation of China (2020JJ4363 and 2021JJ10032).

REFERENCES

Adato, A., Mandel, T., Mintz-Oron, S., Venger, I., Levy, D., Yativ, M., et al. (2009). Fruit-surface flavonoid accumulation in tomato is controlled by a SIMYB12-regulated transcriptional network. *PLoS Genet.* 5:e1000777. doi: 10.1371/journal.pgen.1000777

Alim, M. A., Sun, D. X., Zhang, Y., and Faruque, M. O. (2011). Genetic markers and their application in buffalo production. *J. Anim. Vet. Adv.* 10, 1789–1800. doi: 10.3923/javaa.2011.1789.1800

Amagai, Y., Lu, N., Hayashi, E., Takagaki, M., Kikuchi, M., Ibaraki, Y., et al. (2021). External green light as a new tool to change colors and nutritional components of inner leaves of head cabbages. *J. Food Meas.* 16, 269–280. doi: 10.1007/s11694-021-01150-y

Anderson, G. H. (1995). Sugars, sweetness, and food intake. *Am. J. Clin. Nutr.* 62(Suppl. 1), 195S–201S. doi: 10.1093/ajcn/62.1.195S

Arce-Rodriguez, M. L., and Ochoa-Alejo, N. (2020). Virus-induced gene silencing (VIGS) in chili pepper (*Capsicum* spp.). *Methods Mol. Biol.* 2172, 27–38. doi: 10.1007/978-1-0716-0751-0_3

Aung, M. M., and Chang, Y. S. (2014). Traceability in a food supply chain: safety and quality perspectives. *Food Control* 39, 172–184. doi: 10.1016/j.foodcont.2013.11.007

Ballester, A. R., Molthoff, J., de Vos, R., Hekkert, B. T. L., Orzaez, D., Fernandez-Moreno, J. P., et al. (2010). Biochemical and molecular analysis of pink tomatoes: deregulated expression of the gene encoding transcription factor S1MYB12 leads to pink tomato fruit color. *Plant Physiol.* 152, 71–84. doi: 10.1104/pp.109.147322

Bargel, H., and Neinhuis, C. (2005). Tomato (*Lycopersicon esculentum* Mill.) fruit growth and ripening as related to the biomechanical properties of fruit skin and isolated cuticle. *J. Exp. Bot.* 56, 1049–1060. doi: 10.1093/jxb/eri098

Beckles, D. M. (2012). Factors affecting the postharvest soluble solids and sugar content of tomato (*Solanum lycopersicum* L.) fruit. *Postharvest Biol. Technol.* 63, 129–140. doi: 10.1016/j.postharvbio.2011.05.016

Bort, A., Sanchez, B. G., Spinola, E., Mateos-Gomez, P. A., Rodriguez-Henche, N., and Diaz-Laviada, I. (2019). The red pepper's spicy ingredient capsaicin activates AMPK in HepG2 cells through CaMKK beta. *PLoS One* 14:e0211420. doi: 10.1371/journal.pone.0211420

Boukar, O., Belko, N., Chamarthi, S., Togola, A., Batieno, J., Owusu, E., et al. (2019). Cowpea (*Vigna unguiculata*): genetics, genomics and breeding. *Plant Breed.* 138, 415–424. doi: 10.1111/pbr.12589

Brashlyanova, B., Zsivanovits, G., and Ganeva, D. (2014). Texture quality of tomatoes as affected by different storage temperatures and growth habit. *Emir. J. Food Agric.* 26, 750–756. doi: 10.9755/ejfa.v26i9.17484

Broun, P., Poindexter, P., Osborne, E., Jiang, C.-Z., and Riechmann, J. L. (2004). WIN1, a transcriptional activator of epidermal wax accumulation in *Arabidopsis*. *Proc. Natl. Acad. Sci. U.S.A.* 101, 4706–4711. doi: 10.1073/pnas.0305574101

Buscher, R. H., and Buscher, R. W. (2001). Production and stability of (E, Z)-2,6-nonadienal, the major flavor volatile of cucumbers. *J. Food Sci.* 66, 357–361. doi: 10.1111/j.1365-2621.2001.tb11346.x

Buzigi, E., Pillay, K., and Siwela, M. (2021). Potential of pumpkin to combat vitamin A deficiency during complementary feeding in low and middle income countries: variety, provitamin A carotenoid content and retention, and dietary reference intakes. *Crit. Rev. Food Sci. Nutr.* 8, 1–10. doi: 10.1080/10408398.2021.1896472

Cao, W. X., Dong, X., Ji, J. L., Yang, L. M., Fang, Z. Y., Zhuang, M., et al. (2021). BoCER1 is essential for the synthesis of cuticular wax in cabbage (*Brassica oleracea* L. var. *capitata*). *Sci. Hortic.* 277:109801. doi: 10.1016/j.scienta.2020.109801

Chapman, N. H., Bonnet, J., Grivet, L., Lynn, J., Graham, N., Smith, R., et al. (2012). High-resolution mapping of a fruit firmness-related quantitative trait locus in tomato reveals epistatic interactions associated with a complex combinatorial locus. *Plant Physiol.* 159, 1644–1657. doi: 10.1104/pp.112.200634

Chattopadhyay, T., Hazra, P., Akhtar, S., Maurya, D., Mukherjee, A., and Roy, S. (2021). Skin colour, carotenogenesis and chlorophyll degradation mutant alleles: genetic orchestration behind the fruit colour variation in tomato. *Plant Cell Rep.* 40, 767–782. doi: 10.1007/s00299-020-02650-9

Chatzopoulou, F., Sanmartin, M., Mellidou, I., Pateraki, I., Koukounaras, A., Tanou, G., et al. (2020). Silencing of ascorbate oxidase results in reduced growth, altered ascorbic acid levels and ripening pattern in melon fruit. *Plant Physiol. Biochem.* 156, 291–303. doi: 10.1016/j.plaphy.2020.08.040

Chen, L. L., Li, W. Z., Li, Y. P., Feng, X. C., Du, K. Y., Wang, G., et al. (2019). Identified trans-splicing of YELLOW-FRUITED TOMATO 2 encoding the PHYTOENE SYNTHASE 1 protein alters fruit color by map-based cloning, functional complementation and RACE. *Plant Mol. Biol.* 100, 647–658. doi: 10.1007/s11103-019-00886-y

Cheng, Y., Wang, Q., Ban, Q. Y., Geng, J. F., Zhang, X. W., Yi, Y., et al. (2009). Unconditional and conditional quantitative trait loci mapping for plant height in nonheading Chinese cabbage. *Hortscience* 44, 268–273. doi: 10.21273/hortsci.44.2.268

Cox, M. C. H., Millenaar, F. F., Van Berkel, Y. E. M. J., Peeters, A. J. M., and Voesenek, L. A. C. J. (2003). Plant movement. Submergence-induced petiole elongation in *Rumex palustris* depends on hyponastic growth. *Plant Physiol.* 132, 282–291. doi: 10.1104/pp.102.014548

de Almeida, A. B., de Lima, T. M., de Oliveira, J. G., Santana, R. V., Lima, D. S., Moreira, E. A., et al. (2019). Relation between physicochemical characteristics and sensory profiles of cooked pumpkin varieties. *Emir. J. Food Agric.* 31, 697–707. doi: 10.9755/ejfa.2019.v31.i9.2007

Ding, Q., Cui, B., Li, J. J., Li, H. Y., Zhang, Y. H., Lv, X. H., et al. (2018). Ectopic expression of a *Brassica rapa* AINTEGUMENTA gene (BrANT-1) increases organ size and stomatal density in *Arabidopsis*. *Sci. Rep.* 8:10528. doi: 10.1038/s41598-018-28606-4

Ding, X. T., Yu, L. Y., Jiang, Y. P., Yang, S. J., He, L. Z., Zhou, Q., et al. (2020). Changes in leaf length, width, area, and photosynthesis of fruit cucumber in a greenhouse production system. *Hortscience* 55, 995–999. doi: 10.21273/hortsci14637-19

Dou, J. L., Zhao, S. J., Lu, X. Q., He, N., Zhang, L., Ali, A., et al. (2018). Genetic mapping reveals a candidate gene (ClFS1) for fruit shape in watermelon (*Citrullus lanatus* L.). *Theor. Appl. Genet.* 131, 947–958. doi: 10.1007/s00122-018-3050-5

El-Mansy, A. B., Abd El-Moneim, D., Alshamrani, S. M., Alsafhi, F. A., Abdein, M. A., and Ibrahim, A. A. (2021). Genetic diversity analysis of tomato (*Solanum lycopersicum* L.) with morphological, cytological, and molecular markers under heat stress. *Horticulturae* 7:65. doi: 10.3390/horticulturae7040065

Elejalde-Palmett, C., San Segundo, I. M., Garroum, I., Charrier, L., De Bellis, D., Mucciolo, A., et al. (2021). ABCG transporters export cutin precursors for the formation of the plant cuticle. *Curr. Biol.* 31, 2111–2123.e9. doi: 10.1016/j.cub.2021.02.056

Eltelib, H. A., Badejo, A. A., Fujikawa, Y., and Esaka, M. (2011). Gene expression of monodehydroascorbate reductase and dehydroascorbate reductase during fruit ripening and in response to environmental stresses in acerola (*Malpighia glabra*). *J. Plant Physiol.* 168, 619–627. doi: 10.1016/j.jplph.2010.09.003

Ferguson, M., Rabbi, I., Kim, D. J., Gedil, M., Lopez-Lavalle, L. A. B., and Okogbenin, E. (2012). Molecular markers and their application to cassava breeding: past, present and future. *Trop. Plant Biol.* 5, 95–109. doi: 10.1007/s12042-011-9087-0

Friedrichs, S., Takasu, Y., Kearns, P., Dagallier, B., Oshima, R., Schofield, J., et al. (2019). Meeting report of the OECD conference on "Genome editing: applications in agriculture-implications for health, environment and regulation". *Transgenic Res.* 28, 419–463. doi: 10.1007/s11248-019-00154-1

Gao, L., Zhao, S. J., Lu, X. Q., He, N., Zhu, H. J., Dou, J. L., et al. (2018). Comparative transcriptome analysis reveals key genes potentially related to soluble sugar and organic acid accumulation in watermelon. *PLoS One* 13:e0190096. doi: 10.1371/journal.pone.0190096

Ge, H. L., Liu, Z. H., and Zhang, F. L. (2017). Effect of *Rhodopseudomonas palustris* G5 on seedling growth and some physiological and biochemical characteristics of cucumber under cadmium stress. *Emir. J. Food Agric.* 29, 816–821. doi: 10.9755/ejfa.2017.v29.i11.1327

Gebhardt, C., Ritter, E., Barone, A., Debener, T., Walkemeier, B., Schachtschabel, U., et al. (1991). RFLP maps of potato and their alignment with the homoeologous tomato genome. *Theor. Appl. Genet.* 83, 49–57. doi: 10.1007/bf00229225

Gebretsadik, K., Qiu, X. Y., Dong, S. Y., Miao, H., and Bo, K. L. (2021). Molecular research progress and improvement approach of fruit quality traits in cucumber. *Theor. Appl. Genet.* 134, 3535–3552. doi: 10.1007/s00122-021-03895-y

Gharsallah, C., Ben Abdelkrim, A., Fakhfakh, H., Salhi-Hannachi, A., and Gorsane, F. (2016). SSR marker-assisted screening of commercial tomato genotypes under salt stress. *Breed. Sci.* 66, 823–830. doi: 10.1270/jsbbs.16112

Hashimoto, W., Momma, K., Katsube, T., Ohkawa, Y., Ishige, T., Kito, M., et al. (1999). Safety assessment of genetically engineered potatoes with designed soybean glycinin: compositional analyses of the potato tubers and digestibility of the newly expressed protein in transgenic potatoes. *J. Sci. Food Agric.* 79, 1607–1612. doi: 10.1002/(sici)1097-0010(199909)79:12<1607::aid-jsfa408<3.0.co;2-t

Hongsoongnern, P., and Chambers, E. (2008). A lexicon for texture and flavor characteristics of fresh and processed tomatoes. *J. Sens. Stud.* 23, 583–599. doi: 10.1111/j.1745-459X.2008.00174.x

Hu, D. L., Richards, P., and Alexeev, A. (2011). The growth of giant pumpkins: how extreme weight influences shape. *Int. J. Nonlin. Mech.* 46, 637–647. doi: 10.1016/j.ijnonlinmec.2010.12.013

Hwang, I., Kim, Y., Han, J., and Nou, I. S. (2016). Orange color is associated with CYC-B expression in tomato fleshy fruit. *Mol. Breed.* 36, 1–10. doi: 10.1007/s11032-016-0465-z

Jiang, F. L., Lopez, A., Jeon, S., de Freitas, S. T., Yu, Q. H., Wu, Z., et al. (2019). Disassembly of the fruit cell wall by the ripening-associated polygalacturonase and expansin influences tomato cracking. *Hortic. Res.* 6:17. doi: 10.1038/s41438-018-0105-3

Jiang, L., Yan, S. S., Yang, W. C., Li, Y. Q., Xia, M. X., Chen, Z. J., et al. (2015). Transcriptomic analysis reveals the roles of microtubule-related genes and transcription factors in fruit length regulation in cucumber (*Cucumis sativus* L.). *Sci. Rep.* 5:8031. doi: 10.1038/srep08031

Jin, X., Oliviero, T., van der Sman, R. G. M., Verkerk, R., Dekker, M., and van Boxtel, A. J. B. (2014). Impact of different drying trajectories on degradation of nutritional compounds in broccoli (*Brassica oleracea* var. *italica*). *LWT Food Sci. Technol.* 59, 189–195. doi: 10.1016/j.lwt.2014.05.031

Karamat, U., Sun, X. X., Li, N., and Zhao, J. J. (2021). Genetic regulators of leaf size in *Brassica* crops. *Hortic. Res.* 8:91. doi: 10.1038/s41438-021-00526-x

Khadivi-Khub, A. (2015). Physiological and genetic factors influencing fruit cracking. *Acta Physiol. Plant.* 37:1718. doi: 10.1007/s11738-014-1718-2

Kim, K. D., Suh, J. T., Lee, J. N., Yoo, D. L., Nam, J. H., Sohn, H. B., et al. (2020). Development of evaluation methods and determination of hardness variation with leaf order and tissue type of Kimchi cabbage during summer harvest. *Hortic. Environ. Biotechnol.* 61, 815–824. doi: 10.1007/s13580-020-00266-2

Kim, S., Park, M., Yeom, S. I., Kim, Y. M., Lee, J. M., Lee, H. A., et al. (2014). Genome sequence of the hot pepper provides insights into the evolution of pungency in *Capsicum* species. *Nat. Genet.* 46, 270–278. doi: 10.1038/ng.2877

Klucher, K. M., Chow, H., Reiser, L., and Fischer, R. L. (1996). The AINTEGUMENTA gene of *Arabidopsis* required for ovule and female gametophyte development is related to the floral homeotic gene APETALA2. *Plant Cell* 8, 137–153. doi: 10.1105/tpc.8.2.137

Koyama, R., Itoh, H., Kimura, S., Morioka, A., and Uno, Y. (2012). Augmentation of antioxidant constituents by drought stress to roots in leafy vegetables. *Horttechnology* 22, 121–125. doi: 10.21273/horttech.22.1.121

Kumar, K., Gambhir, G., Dass, A., Tripathi, A. K., Singh, A., Jha, A. K., et al. (2020). Genetically modified crops: current status and future prospects. *Planta* 251:91. doi: 10.1007/s00425-020-03372-8

Laila, R., Robin, A. H. K., Yang, K., Park, J. I., Suh, M. C., Kim, J., et al. (2017). Developmental and genotypic variation in leaf wax content and composition, and in expression of wax biosynthetic genes in *Brassica oleracea* var. *capitata*. *Front. Plant Sci.* 7:1972. doi: 10.3389/fpls.2016.01972

Li, G. H., Chen, H. C., Liu, J. L., Luo, W. L., Xie, D. S., Luo, S. B., et al. (2019). A high-density genetic map developed by specific-locus amplified fragment (SLAF) sequencing and identification of a locus controlling anthocyanin pigmentation in stalk of Zicaitai (*Brassica rapa* L. ssp. *chinensis* var. *purpurea*). *BMC Genomics* 20:343. doi: 10.1186/s12864-019-5693-2

Li, H., Wu, H., Qi, Q., Li, H. H., Li, Z. F., Chen, S., et al. (2019). Gibberellins play a role in regulating tomato fruit ripening. *Plant Cell Physiol.* 60, 1619–1629. doi: 10.1093/pcp/pcz069

Li, J. Y., Tao, X. Y., Li, L., Mao, L. C., Luo, Z. S., Khan, Z. U., et al. (2016). Comprehensive RNA-Seq analysis on the regulation of tomato ripening by exogenous auxin. *PLoS One* 11:e0156453. doi: 10.1371/journal.pone.0156453

Li, R., Sun, S., Wang, H., Wang, K., Yu, H., Zhou, Z., et al. (2020). FIS1 encodes a GA2-oxidase that regulates fruit firmness in tomato. *Nat. Commun.* 11:5844. doi: 10.1038/s41467-020-19705-w

Li, T. D., Yang, X. P., Yu, Y., Si, X. M., Zhai, X. W., Zhang, H. W., et al. (2018). Domestication of wild tomato is accelerated by genome editing. *Nat. Biotechnol.* 36, 1160–1163. doi: 10.1038/nbt.4273

Li, Y., Li, W. J., and Li, J. (2021). The CRISPR/Cas9 revolution continues: from base editing to prime editing in plant science. *J. Genet. Genomics* 48, 661–670. doi: 10.1016/j.jgg.2021.05.001

Liu, J. Y., Shi, M. J., Wang, J., Zhang, B., Li, Y. S., Wang, J., et al. (2020). Comparative transcriptomic analysis of the development of sepal morphology in tomato (*Solanum lycopersicum* L.). *Int. J. Mol. Sci.* 21:5914. doi: 10.3390/ijms21165914

Liu, Y. W., Pu, H. B., and Sun, D. W. (2017). Hyperspectral imaging technique for evaluating food quality and safety during various processes: a review of recent applications. *Trends Food Sci. Technol.* 69, 25–35. doi: 10.1016/j.tifs.2017.08.013

Ma, X. Q., Ding, Q., Hou, X. L., and You, X. (2021). Analysis of flavonoid metabolites in watercress (*Nasturtium officinale* R. Br.) and the non-heading Chinese cabbage (*Brassica rapa* ssp. *chinensis* cv. Aijiaohuang) using UHPLC-ESI-MS/MS. *Molecules* 26:5825. doi: 10.3390/molecules26195825

Mahlein, A. K., Oerke, E. C., Steiner, U., and Dehne, H. W. (2012). Recent advances in sensing plant diseases for precision crop protection. *Eur. J. Plant Pathol.* 133, 197–209. doi: 10.1007/s10658-011-9878-z

Martinez-Bello, L., Moritz, T., and Lopez-Diaz, I. (2015). Silencing C-19-GA 2-oxidases induces parthenocarpic development and inhibits lateral branching in tomato plants. *J. Exp. Bot.* 66, 5897–5910. doi: 10.1093/jxb/erv300

Mashiane, P., Mashitoa, F. M., Slabbert, R. M., and Sivakumar, D. (2021). Impact of household cooking techniques on colour, antioxidant and sensory properties of African pumpkin and pumpkin leaves. *Int. J. Gastron. Food Sci.* 23:100307. doi: 10.1016/j.ijgfs.2021.100307

Muller, M., and Munne-Bosch, S. (2015). Ethylene response factors: a key regulatory hub in hormone and stress signaling. *Plant Physiol.* 169, 32–41. doi: 10.1104/pp.15.00677

Munir, S., Mumtaz, M. A., Ahiakpa, J. K., Liu, G. Z., Chen, W. F., Zhou, G. L., et al. (2020). Genome-wide analysis of Myo-inositol oxygenase gene family in tomato reveals their involvement in ascorbic acid accumulation. *BMC Genomics* 21:284. doi: 10.1186/s12864-020-6708-8

Nakamura, K., Mori, F., Tanji, K., Miki, Y., Yamada, M., Kakita, A., et al. (2015). Isopentenyl diphosphate isomerase, a cholesterol synthesizing enzyme, is localized in Lewy bodies. *Neuropathology* 35, 432–440. doi: 10.1111/neup.12204

Ndimba, R. J., Kruger, J., Mehlo, L., Barnabas, A., Kossmann, J., and Ndimba, B. K. (2017). A comparative study of selected physical and biochemical traits of wild-type and transgenic sorghum to reveal differences relevant to grain quality. *Front. Plant Sci.* 8:952. doi: 10.3389/fpls.2017.00952

Note-Wilson, S., Azhakanandam, S., and Franks, R. G. (2010). Polar auxin transport together with AINTEGUMENTA and REVOLUTA coordinate early *Arabidopsis* gynoecium development. *Dev. Biol.* 346, 181–195. doi: 10.1016/j.ydbio.2010.07.016

Ohyama, A., Shirasawa, K., Matsunaga, H., Negoro, S., Miyatake, K., Yamaguchi, H., et al. (2017). Bayesian QTL mapping using genome-wide SSR markers and segregating population derived from a cross of two commercial F-1 hybrids of tomato. *Theor. Appl. Genet.* 130, 1601–1616. doi: 10.1007/s00122-017-2913-5

Olfati, J. A., Peyvast, G., Shabani, H., and Nosratie-Rad, Z. (2010). An estimation of individual leaf area in cabbage and broccoli using non-destructive methods. *J. Agric. Sci. Technol.* 12, 627–632. doi: 10.1111/j.1744-697X.2010.00192.x

Pan, Y. P., Liang, X. J., Gao, M. L., Liu, H. Q., Meng, H. W., Weng, Y. Q., et al. (2017). Round fruit shape in WI7239 cucumber is controlled by two interacting quantitative trait loci with one putatively encoding a tomato SUN homolog. *Theor. Appl. Genet.* 130, 573–586. doi: 10.1007/s00122-016-2836-6

Park, A. K., Kim, I. S., Do, H., Jeon, B. W., Lee, C. W., Roh, S. J., et al. (2016). Structure and catalytic mechanism of monodehydroascorbate reductase, MDHAR, from *Oryza sativa* L. *japonica*. *Sci. Rep.* 6:33903. doi: 10.1038/srep33903

Park, J. B., Sendon, P. M., Kwon, S. H., Seo, H. S., Park, S. K., Kim, J. H., et al. (2012). Overexpression of stress-related genes, BrERF4 and AtMYB44, in *Arabidopsis thaliana* alters cell expansion but not cell proliferation during leaf growth. *J. Plant Biol.* 55, 406–412. doi: 10.1007/s12374-012-0114-y

Pattison, R. J., Csukasi, F., and Catala, C. (2014). Mechanisms regulating auxin action during fruit development. *Physiol. Plant.* 151, 62–72. doi: 10.1111/ppl.12142

Paudel, L., Clevenger, J., and McGregor, C. (2019). Chromosomal locations and interactions of four loci associated with seed coat color in watermelon. *Front. Plant Sci.* 10:788. doi: 10.3389/fpls.2019.00788

Ren, J., Duan, W. K., Chen, Z. W., Zhang, S., Song, X. M., Liu, T. K., et al. (2015). Overexpression of the monodehydroascorbate reductase gene from non-heading Chinese cabbage reduces ascorbate level and growth in transgenic tobacco. *Plant Mol. Biol. Rep.* 33, 881–892. doi: 10.1007/s11105-014-0797-y

Richter, R., Behringer, C., Zourelidou, M., and Schwechheimer, C. (2013). Convergence of auxin and gibberellin signaling on the regulation of the GATA transcription factors GNC and GNL in *Arabidopsis thaliana*. *Proc. Natl. Acad. Sci. U.S.A.* 110, 13192–13197. doi: 10.1073/pnas.1304250110

Romero, P., and Rose, J. K. C. (2019). A relationship between tomato fruit softening, cuticle properties and water availability. *Food Chem.* 295, 300–310. doi: 10.1016/j.foodchem.2019.05.118

Roosjen, M., Paque, S., and Weijers, D. (2018). Auxin response factors: output control in auxin biology. *J. Exp. Bot.* 69, 179–188. doi: 10.1093/jxb/erx237

Sakamoto, K., Kusaba, M., and Nishio, T. (2000). Single-seed PCR-RFLP analysis for the identification of S haplotypes in commercial F1 hybrid cultivars of broccoli and cabbage. *Plant Cell Rep.* 19, 400–406. doi: 10.1007/s002990050747

Schindele, P., and Puchta, H. (2020). Engineering CRISPR/LbCas12a for highly efficient, temperature-tolerant plant gene editing. *Plant Biotechnol. J.* 18, 1118–1120. doi: 10.1111/pbi.13275

Semagn, K., Babu, R., Hearne, S., and Olsen, M. (2014). Single nucleotide polymorphism genotyping using Kompetitive Allele Specific PCR (KASP): overview of the technology and its application in crop improvement. *Mol. Breed.* 33, 1–14. doi: 10.1007/s11032-013-9917-x

Shang, Y., Ma, Y. S., Zhou, Y., Zhang, H. M., Duan, L. X., Chen, H. M., et al. (2014). Biosynthesis, regulation, and domestication of bitterness in cucumber. *Science* 346, 1084–1088. doi: 10.1126/science.1259215

Shimomura, K., Horie, H., Sugiyama, M., Kawazu, Y., and Yoshioka, Y. (2016). Quantitative evaluation of cucumber fruit texture and shape traits reveals extensive diversity and differentiation. *Sci. Hortic.* 199, 133–141. doi: 10.1016/j.scienta.2015.12.033

Shin, J. H., Yoo, H. J., Yeam, I., and Lee, J. M. (2019). Distinguishing two genetic factors that control yellow fruit color in tomato. *Hortic. Environ. Biotechnol.* 60, 59–67. doi: 10.1007/s13580-018-0093-0

Shirasawa, K., Isobe, S., Hirakawa, H., Asamizu, E., Fukuoka, H., Just, D., et al. (2010). SNP discovery and linkage map construction in cultivated tomato. *DNA Res.* 17, 381–391. doi: 10.1093/dnares/dsq024

Shu-juan, Z., Fang-fang, Y., Zhao-jun, Y., Ming-ke, Z., and Mai-xia, H. (2016). Cloning and expression analysis of *BrLOM2*, a gene involved in lobed leaf development in pak choi. *Acta Hortic. Sin.* 43, 2029–2038. doi: 10.16420/j.issn.0513-353x.2016-0252

Steele, K. A., Quinton-Tulloch, M. J., Amgai, R. B., Dhakal, R., Khatiwada, S. P., Vyas, D., et al. (2018). Accelerating public sector rice breeding with high-density KASP markers derived from whole genome sequencing of indica rice. *Mol. Breed.* 38:38. doi: 10.1007/s11032-018-0777-2

Sun, L., Sun, Y. F., Zhang, M., Wang, L., Ren, J., Cui, M. M., et al. (2012). Suppression of 9-cis-epoxycarotenoid dioxygenase, which encodes a key enzyme in abscisic acid biosynthesis, alters fruit texture in transgenic tomato. *Plant Physiol.* 158, 283–298. doi: 10.1104/pp.111.186866

Tian, S. L., Li, L., Chai, W. G., Shah, S. N. M., and Gong, Z. H. (2014). Effects of silencing key genes in the capsanthin biosynthetic pathway on fruit color of detached pepper fruits. *BMC Plant Biol.* 14:314. doi: 10.1186/s12870-014-0314-3

Ueta, R., Abe, C., Watanabe, T., Sugano, S. S., Ishihara, R., Ezura, H., et al. (2017). Rapid breeding of parthenocarpic tomato plants using CRISPR/Cas9. *Sci. Rep.* 7:507. doi: 10.1038/s41598-017-00501-4

Veerappan, K., Jung, H. J., Hwang, I., Kho, K. H., Chung, M. Y., and Nou, I. S. (2016). Sequence variation in SlMYB12 is associated with fruit peel color in pink tomato cultivars. *Hortic. Environ. Biotechnol.* 57, 274–279. doi: 10.1007/s13580-016-0041-9

Vieira, E. A., de Carvalho, F. I. F., Bertan, I., Kopp, M. M., Zimmer, P. D., Benin, G., et al. (2007). Association between genetic distances in wheat (*Triticum aestivum* L.) as estimated by AFLP and morphological markers. *Genet. Mol. Biol.* 30, 392–399. doi: 10.1590/s1415-47572007000300016

Walter, J., Edwards, J., Cai, J. H., McDonald, G., Miklavcic, S. J., and Kuchel, H. (2019). High-throughput field imaging and basic image analysis in a wheat breeding programme. *Front. Plant Sci.* 10:449. doi: 10.3389/fpls.2019.00449

Wang, C. J., Wang, Y. L., Wang, M. M., Han, H. Y., Luo, Y. S., Ding, W. Q., et al. (2020). Soluble sugars accumulation and related gene expression during fruit development in *Cucurbita maxima* Duchesne. *Sci. Hortic.* 272:109520. doi: 10.1016/j.scienta.2020.109520

Wang, L., Wen, M., Chen, F. P., Luo, Z., Yin, J., Chen, Y. L., et al. (2020). High oxygen atmospheric packaging (HOAP) reduces H_2O_2 production by regulating the accumulation of oxidative stress-related proteins in Chinese flowering cabbage. *Postharvest Biol. Technol.* 165:111183. doi: 10.1016/j.postharvbio.2020.111183

Wang, Q. B., Zhang, Y. Y., Fang, Z. Y., Liu, Y. M., Yang, L. M., and Zhuang, M. (2012). Chloroplast and mitochondrial SSR help to distinguish allo-cytoplasmic male sterile types in cabbage (*Brassica oleracea* L. var. *capitata*). *Mol. Breed.* 30, 709–716. doi: 10.1007/s11032-011-9656-9

Wang, W. J., Liu, X. W., Gai, X. S., Ren, J. J., Liu, X. F., Cai, Y. L., et al. (2015). *Cucumis sativus* L. WAX2 plays a pivotal role in wax biosynthesis, influencing pollen fertility and plant biotic and abiotic stress responses. *Plant Cell Physiol.* 56, 1339–1354. doi: 10.1093/pcp/pcv052

Wei, G., Tian, P., Zhang, F. X., Qin, H., Miao, H., Chen, Q. W., et al. (2016). Integrative analyses of nontargeted volatile profiling and transcriptome data provide molecular insight into VOC diversity in cucumber plants (*Cucumis sativus*). *Plant Physiol.* 172, 603–618. doi: 10.1104/pp.16.01051

Wiesner, M., Schreiner, M., and Zrenner, R. (2014). Functional identification of genes responsible for the biosynthesis of 1-methoxy-indol-3-ylmethyl-glucosinolate in *Brassica rapa* ssp *chinensis*. *BMC Plant Biol.* 14:124. doi: 10.1186/1471-2229-14-124

Wong, K. C., Zhang, J., Yan, S. K., Li, X. T., Lin, Q. Z., Kwong, S., et al. (2019). DNA sequencing technologies: sequencing data protocols and bioinformatics tools. *ACM Comput. Surv.* 52, 1–30. doi: 10.1145/3340286

Wright, J. M., Carunchia Whetstine, M. E., Miracle, R. E., and Drake, M. (2006). Characterization of a cabbage off-flavor in whey protein isolate. *J. Food Sci.* 71, C86–C90. doi: 10.1111/j.1365-2621.2006.tb08887.x

Wu, S., Clevenger, J. P., Sun, L., Visa, S., Kamiya, Y., Jikumaru, Y., et al. (2015). The control of tomato fruit elongation orchestrated by sun, ovate and fs8.1 in a wild relative of tomato. *Plant Sci.* 238, 95–104. doi: 10.1016/j.plantsci.2015.05.019

Wu, S., Xiao, H., Cabrera, A., Meulia, T., and van der Knaap, E. (2011). SUN regulates vegetative and reproductive organ shape by changing cell division patterns. *Plant Physiol.* 157, 1175–1186. doi: 10.1104/pp.111.181065

Xiao, H., Jiang, N., Schaffner, E., Stockinger, E. J., and van der Knaap, E. (2008). A retrotransposon-mediated gene duplication underlies morphological variation of tomato fruit. *Science* 319, 1527–1530. doi: 10.1126/science.1153040

Xing, S. N., Chen, K. L., Zhu, H. C., Zhang, R., Zhang, H. W., Li, B. B., et al. (2020). Fine-tuning sugar content in strawberry. *Genome Biol.* 21:230. doi: 10.1186/s13059-020-02146-5

Xu, J. M., Hua, K., and Lang, Z. B. (2019). Genome editing for horticultural crop improvement. *Hortic. Res.* 6:113. doi: 10.1038/s41438-019-0196-5

Xu, X. Y., Sun, X. L., Zhang, Y., Zhang, L. G., and Fang, Z. Y. (2014). Identification of AFLP and SSR markers linked with the male fertility restorer gene of CMS 06J45 in heading Chinese cabbage (*Brassica rapa* L. ssp *pekinensis*). *Plant Breed.* 133, 615–619. doi: 10.1111/pbr.12200

Xu, Y. Y., Zeng, A. S., Song, L. X., Li, J. Q., and Yan, J. Y. (2019). Comparative transcriptomics analysis uncovers alternative splicing events and molecular markers in cabbage (*Brassica oleracea* L.). *Planta* 249, 1599–1615. doi: 10.1007/s00425-019-03108-3

Xue, L. Z., Sun, M. T., Wu, Z., Yu, L., Yu, Q. H., Tang, Y. P., et al. (2020). LncRNA regulates tomato fruit cracking by coordinating gene expression via a hormone-redox-cell wall network. *BMC Plant Biol.* 20:162. doi: 10.1186/s12870-020-02373-9

Yang, T. X., Deng, L., Zhao, W., Zhang, R. X., Jiang, H. L., Ye, Z. B., et al. (2019). Rapid breeding of pink-fruited tomato hybrids using the CRISPR/Cas9 system. *J. Genet. Genomics* 46, 505–508. doi: 10.1016/j.jgg.2019.10.002

Yang, Z., Wu, Z., Zhang, C., Hu, E. M., Zhou, R., and Jiang, F. L. (2016). The composition of pericarp, cell aging, and changes in water absorption in two

tomato genotypes: mechanism, factors, and potential role in fruit cracking. *Acta Physiol. Plant.* 38:215. doi: 10.1007/s11738-016-2228-1

Yildiz, H., and Baysal, T. (2007). Color and lycopene content of tomato puree affected by electroplasmolysis. *Int. J. Food Prop.* 10, 489–495. doi: 10.1080/10942910600909063

Yoo, H. J., Park, W. J., Lee, G. M., Oh, C. S., Yeam, I., Won, D. C., et al. (2017). Inferring the genetic determinants of fruit colors in tomato by carotenoid profiling. *Molecules* 22:764. doi: 10.3390/molecules22050764

Yu, Z., Lina, A., Zejun, H., Yongchen, D., Yanmei, G., Junming, L., et al. (2020). Fine mapping of fruit cracking-resistant gene Cr3a in tomato. *Acta Hortic. Sin.* 47, 275–286. doi: 10.16420/j.issn.0513-353x.2019-0260

Zhang, C., Win, K. T., Kim, Y. C., and Lee, S. (2019). Two types of mutations in the HEUKCHEEM gene functioning in cucumber spine color development can be used as signatures for cucumber domestication. *Planta* 250, 1491–1504. doi: 10.1007/s00425-019-03244-w

Zhang, H. W., Si, X. M., Ji, X., Fan, R., Liu, J. X., Chen, K. L., et al. (2018). Genome editing of upstream open reading frames enables translational control in plants. *Nat. Biotechnol.* 36, 894–898. doi: 10.1038/nbt.4202

Zhang, J., Yang, J. J., Yang, Y., Luo, J., Zheng, X. Y., Wen, C. L., et al. (2019). Transcription factor CsWIN1 regulates pericarp wax biosynthesis in cucumber grafted on pumpkin. *Front. Plant Sci.* 10:1564. doi: 10.3389/fpls.2019.01564

Zhang, J., Yang, J. J., Zhang, L. K., Luo, J., Zhao, H., Zhang, J. A., et al. (2020a). A new SNP genotyping technology target SNP-seq and its application in genetic analysis of cucumber varieties. *Sci. Rep.* 10:5623. doi: 10.1038/s41598-020-62518-6

Zhang, P., Wang, R. L., Yang, X. P., Ju, Q., Li, W. Q., Lu, S. Y., et al. (2020b). The R2R3-MYB transcription factor AtMYB49 modulates salt tolerance in *Arabidopsis* by modulating the cuticle formation and antioxidant defence. *Plant Cell Environ.* 43, 1925–1943. doi: 10.1111/pce.13784

Zhang, Z., Wang, B. W., Wang, S. H., Lin, T., Yang, L., Zhao, Z. L., et al. (2020c). Genome-wide target mapping shows histone deacetylase complex1 regulates cell proliferation in cucumber fruit. *Plant Physiol.* 182, 167–184. doi: 10.1104/pp.19.00532

Zhang, J. P., Feng, S. J., Yuan, J., Wang, C., Lu, T., Wang, H. S., et al. (2021). The formation of fruit quality in *Cucumis sativus* L. *Front. Plant Sci.* 12:729448. doi: 10.3389/fpls.2021.729448

Zhang, N., Shi, J. W., Zhao, H. Y., and Jiang, J. (2018). Activation of small heat shock protein (SlHSP17.7) gene by cell wall invertase inhibitor (SlCIF1) gene involved in sugar metabolism in tomato. *Gene* 679, 90–99. doi: 10.1016/j.gene.2018.08.077

Zhang, Y. Y., Li, H. X., Shu, W. B., Zhang, C. J., and Ye, Z. B. (2011a). RNA interference of a mitochondrial APX gene improves vitamin C accumulation in tomato fruit. *Sci. Hortic.* 129, 220–226. doi: 10.1016/j.scienta.2011.03.025

Zhang, Y. Y., Li, H. X., Shu, W. B., Zhang, C. J., Zhang, W., and Ye, Z. B. (2011b). Suppressed expression of ascorbate oxidase gene promotes ascorbic acid accumulation in tomato fruit. *Plant Mol. Biol. Rep.* 29, 638–645. doi: 10.1007/s11105-010-0271-4

Zhao, C. J., Zhang, Y., Du, J. J., Guo, X. Y., Wen, W. L., Gu, S. H., et al. (2019). Crop phenomics: current status and perspectives. *Front. Plant Sci.* 10:714. doi: 10.3389/fpls.2019.00714

Zhao, J., Jiang, L., Che, G., Pan, Y., Li, Y., Hou, Y., et al. (2019). A functional allele of CsFUL1 regulates fruit length through repressing CsSUP and inhibiting auxin transport in cucumber. *Plant Cell* 31, 1289–1307. doi: 10.1105/tpc.18.00905

Zhou, X. H., Liu, S. Y., Liu, Y. P., Liu, J., Yang, Y., Wang, D., et al. (2021). Extensive transcriptome changes underlying the fruit skin colour intensity variation in purple eggplant. *Notulae Bot. Horti Agrobot. Cluj Napoca* 49:12434. doi: 10.15835/nbha49312434

Zhou, Y. J., Deng, Y. T., Liu, D., Wang, H. Z., Zhang, X., Liu, T. T., et al. (2021). Promoting virus-induced gene silencing of pepper genes by a heterologous viral silencing suppressor. *Plant Biotechnol. J.* 19, 2398–2400. doi: 10.1111/pbi.13724

Zhu, Z. S., Sun, B. M., Cai, W., Zhou, X., Mao, Y. H., Chen, C. J., et al. (2019). Natural variations in the MYB transcription factor MYB31 determine the evolution of extremely pungent peppers. *New Phytol.* 223, 922–938. doi: 10.1111/nph.15853

Conflict of Interest: The authors declare that the research was conducted in the absence of any commercial or financial relationships that could be construed as a potential conflict of interest.

Publisher's Note: All claims expressed in this article are solely those of the authors and do not necessarily represent those of their affiliated organizations, or those of the publisher, the editors and the reviewers. Any product that may be evaluated in this article, or claim that may be made by its manufacturer, is not guaranteed or endorsed by the publisher.

Copyright © 2022 Gao, Hao, Wu and Cao. This is an open-access article distributed under the terms of the Creative Commons Attribution License (CC BY). The use, distribution or reproduction in other forums is permitted, provided the original author(s) and the copyright owner(s) are credited and that the original publication in this journal is cited, in accordance with accepted academic practice. No use, distribution or reproduction is permitted which does not comply with these terms.

frontiers in Plant Science

ORIGINAL RESEARCH
published: 21 March 2022
doi: 10.3389/fpls.2022.832619

The Effect of Anti-browning Agent Activated Carbon and Polyvinyl Pyrrolidone on the Rooting of Embryo Seedlings of "FengDan" and Its Transcriptome Analysis

Xia Chen[1†], Chao Yu[2†], Jingtao Nie[2†], Hongmin Yang[3†], Wen Ji[1], Gangwei Xu[1], Huijun Zhu[1], Songheng Jin[1] and Xiangtao Zhu[1,4]*

[1] College of Jiyang, Zhejiang A&F University, Zhuji, China, [2] College of Horticulture Science, Zhejiang A&F University, Hangzhou, China, [3] Educational Technology Center of Zhejiang Province, Hangzhou, China, [4] Zhejiang Provincial Key Laboratory of Germplasm Innovation and Utilization for Garden Plants, Zhejiang A&F University, Hangzhou, China

Peony is an excellent ornamental, medicinal, and oily plant. Its traditional seed propagation methods have the disadvantages of low propagation coefficient, long seedling cycle, and low seedling emergence rate, which severely restrict the supply of seedlings for the peony industry. Efficient tissue culture technology is an important basis for accelerating its breeding and reproduction, and *in vitro* seed embryo culturing into seedlings can also effectively avoid the above problems. However, the browning phenomenon caused by man-made damage in the process of seed embryo stripping leads to problems such as low induction rate and difficulty in rooting, and the relationship between anti-browning agents and seed embryo root formation is still unclear. This study intends to improve the induction rate of peony seedlings by using different anti-browning agents and different combinations and to clarify the relationship between anti-browning agents and seedling rooting using transcriptome sequencing methods. The results show that both anti-browning agents, activated carbon (AC) and polyvinyl pyrrolidone (PVP), can increase the germination rate of seed embryos. Testing with 0.9 g/L of AC showed excellent performance of peony rooting rate and seedling growth, but only AC and the combination of AC and PVP can further promote rooting development. Through transcriptome analysis, we found that the AC vs. control check (CK), AC vs. PVP, and PVP vs. AC and PVP groups have significantly more differentially expressed genes than the AC vs. AC and PVP groups. Pathway enrichment analysis shows that "phenylpropanoid biosynthesis"/"cutin, suberin, and wax biosynthesis" is significantly enriched in these groups, while the AC vs. AC and PVP groups are mainly enriched in "cytochrome P450," indicating that AC may promote the further development of roots into seedlings by stimulating "phenylpropanoid biosynthesis" and biosynthesis of stratum cutin and suberin. This study can lay the foundation for understanding the potential molecular mechanism of the anti-browning agent promoting the rooting of seed embryo seedlings and also provide a theoretical basis for perfecting the construction of the peony tissue culture and rapid propagation system.

Keywords: ***Paeonia suffruticosa*** **Andr., embryo seedling, anti-browning agent, root, transcriptome**

OPEN ACCESS

Edited by:
Xinchao Wang,
Tea Research Institute (CAAS), China

Reviewed by:
Gang Li,
University of Adelaide, Australia
Liguo Feng,
Yangzhou University, China

****Correspondence:***
Xiangtao Zhu
zxt8202@163.com

† These authors have contributed equally to this work

Specialty section:
This article was submitted to Crop and Product Physiology, a section of the journal Frontiers in Plant Science

Received: *10 December 2021*
Accepted: *24 January 2022*
Published: *21 March 2022*

Citation:
Chen X, Yu C, Nie J, Yang H, Ji W, Xu G, Zhu H, Jin S and Zhu X (2022) The Effect of Anti-browning Agent Activated Carbon and Polyvinyl Pyrrolidone on the Rooting of Embryo Seedlings of "FengDan" and Its Transcriptome Analysis. Front. Plant Sci. 13:832619. doi: 10.3389/fpls.2022.832619

INTRODUCTION

Peony (*Paeonia suffruticosa* Andr.) has excellent garden ornamental value and medicinal value (Li et al., 2015). The current peony propagation method is mainly seed propagation, attached to grafting, ramets, cuttings, and other asexual propagation (Yang, 2009; Yang et al., 2015; Zhu et al., 2018), and its low reproduction coefficient, long seedling cycle, low seedling emergence, and uneven quality (Wang, 2016) have made the current supply of seedlings a bottleneck, restricting the development of the peony industry. As a new method of plant propagation, tissue culture technology has been widely popularized. The advantage is that it can multiply a large number of fine varieties in a short period of time, breaking the limitations of traditional breeding techniques and can use genetic transformation technology to cultivate new varieties of peony (Li et al., 2018). Therefore, solving the problems in the conventional breeding process of peony through tissue culture technology will be an inevitable trend for the development of peony to commercialization and industrialization, and it is also an effective measure to accelerate its reproduction and breeding (Xiu et al., 2017). This study on peony tissue culture technology mainly focuses on callus induction, suitable growth regulator ratio, explant selection, transplantation and domestication, etc. (Li et al., 2008; Cheng et al., 2019; Ma X. L. et al., 2019; Huang, 2020; Shi et al., 2021; Zhang et al., 2021). Although certain progress has been made, there are still problems in the process of peony tissue culture, such as serious pollution, prone to browning and vitrification in the subculture, difficulty in rooting, and low survival rate of transplanting (Jia and Liu, 2014), which result in the failure to establish an efficient and stable system and are unable to provide assistance to the actual production.

Studies have shown that using seed embryos as explants for *in vitro* culture can not only effectively avoid the above problems but also enable the embryos to germinate into seedlings quickly and advance the germination time, and it is of great significance to save hybrid embryo abortion, relieve seed dormancy, advance the breeding cycle, and increase the germination rate (Yu et al., 2013; He, 2019; Lian et al., 2020). The seed embryo culture technology has been successful in many crops and horticultural plants (Li et al., 2020; Ongagna et al., 2020; Bhatia et al., 2021), and research has also been done in the rapid propagation of peony. For example, Liu et al. (2011) used the peony variety "FengDan" as the material to explore the rapid growth technology of mature embryos through the combination of different hormones and basic media and has found that adding 1.5 mg/L of 6-BA and 1.0 mg/L of NAA to 1/2 Murashige and Skoog (MS) medium had the best effect. Nevertheless, this technology still has many unresolved problems such as low induction rate, poor growth, and development of test-tube plantlets, difficulty in rooting, and low survival rate after transplanting. Among them, the browning phenomenon caused by artificial damage during the process of stripping embryos leads to a low induction rate and difficulty in rooting, which are important factors that restrict and affect the rapid growth of seedlings of peony embryos. In tissue culture, browning is caused by the formation of quinones by phenolic acids under the catalysis of a variety of oxidases after plant materials are injured. Quinones produce colored substances through polymerization to cause tissues to become brown, and this brown substance will gradually spread into the culture medium, poisoning the entire tissue (Li et al., 2008). In plants, phenolic substances are closely related to the metabolism of auxin (IAA) (Fu, 2012), which seriously affects the origin and development of plant adventitious roots. Shang et al. (2020) studied the effects of phenolic substances of different types and concentrations on adventitious root formation of peony test-tube seedlings by adding phenolic substances in the rooting medium and have found that exogenous phenolic substances had a higher rooting rate and rooting index on test-tube seedlings than the control. In addition, endogenous phenols can react with IAA under the action of polyphenol oxidase, and the product has auxin activity and can also promote root formation. To a certain extent, this reveals the relationship between endogenous phenolic substance metabolism and root formation during the rooting process of peony test-tube plantlets. Paeonia is a plant species with a high content of phenolic substances, and its body contains a large amount of phenolic acids (Zhang and Fan, 2008); it can be seen that, in the rapid seedling formation technology of peony embryo culture, preventing the oxidative browning of phenolic acids in seed embryos caused by artificial damage is crucial to promoting the rooting of seed embryo seedlings. At present, the main method to prevent browning in tissue culture is to add anti-browning agents, of which activated carbon (AC), polyvinyl pyrrolidone (PVP), vitamin C, sodium thiosulfate, cysteine and ethylene synthesis inhibitor of aminoethoxyvinylglycine (AVG), silver nitrate, and silver thiosulfate (Li et al., 2008), are commonly used, among which, AC and PVP are the most widely used and have better effects. However, the research on the relationship between anti-browning agents and root formation of peony embryo seedlings is still blank.

Therefore, we studied the effects of two browning inhibitors, namely, AC and PVP, and their combination on the browning control during embryo culture of the peony variety "FengDan" and the effect on the rooting of seedling embryos, in order to improve the induction rate of peony embryo rapid seedling; at the same time, we conducted a transcriptome comparative analysis of the root and leaf mixed tissues of different treatments of peony embryo seedlings to understand the potential molecular mechanism of the anti-browning agent to promote the rooting of seedlings, laying a foundation for further research on the rooting mechanism of peony test-tube seedlings and providing a theoretical basis for the construction of the peony rapid propagation system.

MATERIALS AND METHODS

Plant Materials and Culture Conditions

The peony variety "FengDan" was used as the test material and was planted in the Peony Experimental Base of Jiyang College, Zhejiang Agriculture and Forestry University. Fresh seeds with good growth conditions were picked 120 days after flowering as the source of embryonic explants. The seeds were peeled out of the pods for sterilization, washed with detergent, and rinsed

TABLE 1 | Composition of media for different treatment combinations.

Group	Basal medium	PVP ($g \cdot L^{-1}$)	AC($g \cdot L^{-1}$)
CK		–	–
1P		1.5	–
2P		2.0	–
3P		2.5	–
4P		3.0	–
1A	MS 4.74 g/L	–	0.3
2A	Agar 8.5 g/L	–	0.6
3A	Suc 30.0 g/L	–	0.9
4A	IAA 1.4 mg/L	–	2.0
1P-A		1.5	0.9
2P-A		2.0	0.9
3P-A		2.5	0.9
4P-A		3.0	0.9

1–4P represents the groups added with different concentrations of PVP; 1–4A represents the groups added with different concentrations of AC; and 1–4P-A represents the groups added with different concentrations of AC and PVP combinations.

under running water for 10 min. They were transferred to the ultra-clean workbench, soaked in 2% of NaClO solution for 20 min, rinsed with sterile water for 3–5 times, sterilized with 75% of alcohol for 10–30 s, rinsed with sterile water for 3–5 times, then placed on a sterile filter paper to absorb the water, carefully peeled off the seed embryo with a scalpel and tweezers, and inoculated in the MS medium where the seed embryo germinates. The composition of different treatment media is shown in **Table 1**. The pH value was 5.8. After inoculation, the seeds were cultured in the dark for 30 days to observe the growth status of seed embryos, and the germination rates of *in vitro* embryos of "FengDan" seeds in different treatments were counted and then switched to light for 17 h day^{-1} with the light intensity of 30–50 $\mu mol\ m^{-2}\ s^{-1}$, using an LED (70% red light + 30% blue light) at a temperature of 24(±2)°C to observe the rooting situation. A total of 30 biological replicates were prepared for each group, with 4 seed embryos in each replicate. SPSS 20.0 software (IBM, Untied States) was used for statistical analysis.

To further analyze the effect mechanism of different types and combinations of anti-browning agents on seed embryo seedling rooting, among different treatment groups, the samples were collected from the group with better germination rates and obvious rooting differences. Each sample is composed of 10 mixed leaves and roots of separate seed embryos. Three biological replicates were paired for each sample, immediately frozen in liquid nitrogen, and stored at −80°C.

mRNA Isolation and cDNA Library Construction and Transcriptome Sequencing

Total RNA was isolated using a TRIzol total RNA extraction kit (ComWin, Beijing, China), following the instructions of the manufacturer, which yielded >2 μg of total RNA per sample. RNA quality was examined using 0.8% agarose gel electrophoresis and spectrophotometer. High-quality RNA with a 260/280 absorbance ratio of 1.8–2.2 was used for library construction and sequencing. Illumina HiSeq library construction was performed according to the instructions of the manufacturer' (Illumina, United States). Oligo-dT primers were used to transverse mRNA to obtain cDNA (APExBIO, Cat. No. K1159). cDNA was amplified for the synthesis of the second chain of cDNA. cDNA products were purified using magnetic beads. After library construction, library fragments were enriched by PCR amplification and selected according to a fragment size of 350–550 bp. The library was quality-assessed using an

TABLE 2 | Primers used in qRT-PCR.

Gene names	Forward primer (5′ to 3′)	Reverse Primer (5′ to 3′)
TRINITY_DN1028_c0_g1	GGAGAGTAGGAAGTGGTGGG	ACCTCCTGCACTTCTTCCTC
TRINITY_DN11050_c1_g1	GATGGGTCTAGTCCTGCTCC	GGGGACAAACTCATGAGCAC
TRINITY_DN1323_c0_g1	CACATTTGCCAGGCTCAACT	AGTTGGGGTGATGATGGGAG
TRINITY_DN6_c0_g3	CCTATGGCGACTACTGGAGG	AACTTCTTCTTCCCTCGCCA
TRINITY_DN42643_c0_g1	CGTGTCAGTCTTGTGTGTCG	AGGTAGAGAAAGGCACGGAC
TRINITY_DN960_c0_g1	TTGCAGTGGGATTAGGGGTC	CAGCTGACTTCAAGCACCTG
TRINITY_DN10171_c0_g1	TTGTGCTGCGGTGAAGAAAA	TATTGCAGCGCTTGGGAATG
TRINITY_DN10_c0_g1	TCTCCTTAATCTGGCCCACC	ACCGGCACTTACGATTCCTA
TRINITY_DN12346_c0_g1	ATGCAGTTGTTGACGTTGCT	GCTGACGTTACACAAGCCAA
TRINITY_DN1083_c0_g1	CTTGCAGACACCCACAACTC	AATTAGGGCTTCGGGGATCC
TRINITY_DN1166_c1_g1	GCAGCACTGTATCGAAGGTG	ATGGCTGTAACATGCAACCC
TRINITY_DN11019_c1_g1	AGGCTGAATCACCCATGGAA	TCCTGCACCTTGTCCGTTAT
TRINITY_DN1430_c0_g3	GGGATGGTCAACTGGGAGAA	CTCCTCTCCTTTCCCTGCAA
TRINITY_DN1131_c0_g1	ACCCCAAACCCAGATCGATT	GATTTTCCCAGTGACCGACG
TRINITY_DN16973_c0_g1	ATGGTCCTAGCTTGCATGGT	GGCATGGGGTTAGGCTTCTA
TRINITY_DN1271_c0_g1	AACCCATCCAACTGACCGAT	ATAAGGTCCAGAGGTTGCCG
TRINITY_DN11889_c1_g1	CGGATTGAGGTGGAGCGTAT	CTGGTTATGGTTACGGTGCG
TRINITY_DN15648_c0_g1	CGTTCGCATGTACAACCCAA	CGTGGATAGGAAGACGGTCA
TRINITY_DN10081_c0_g1	GTGTGTCGTCTATTTGCTCGGTCTC	TCTCTGGCCGATGGATGCCCACC

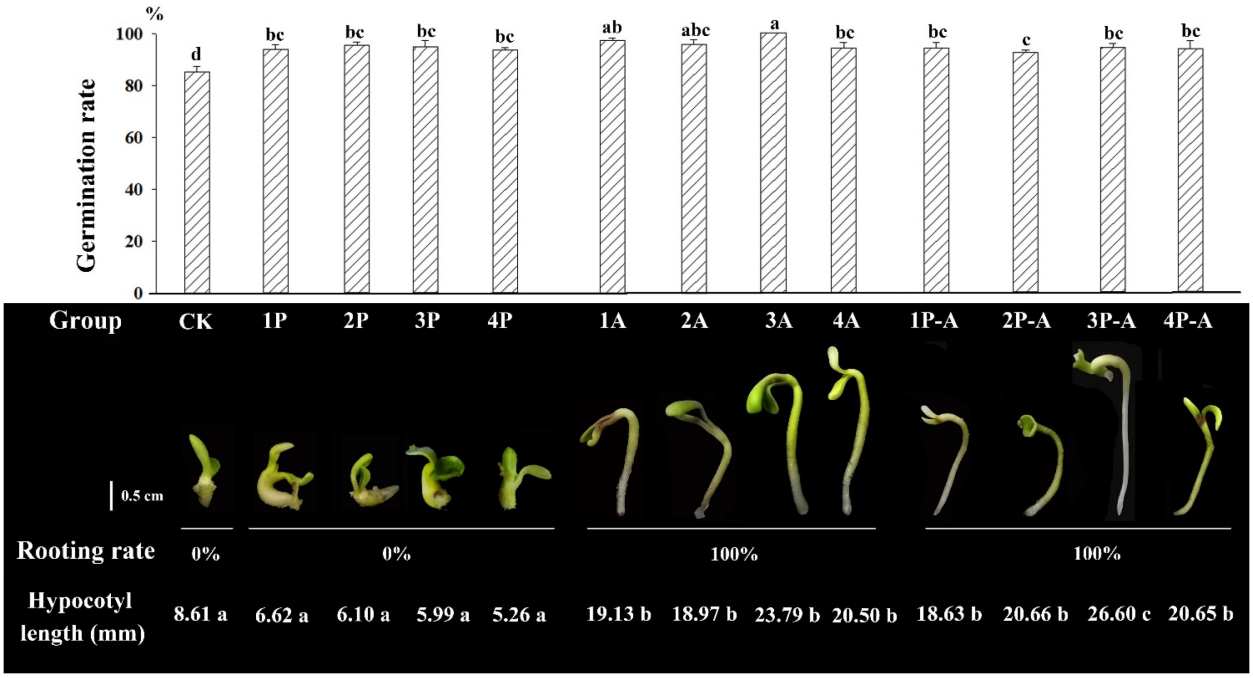


FIGURE 1 | Germination rate, rooting rate, hypocotyl length, and seedling morphology of seed embryos treated with different anti-browning agents. CK represents the control group; 1–4P represents the addition of PVP anti-browning agent groups with concentrations of 1.5, 2.0, 2.5, and 3.0 g•L^{-1}, respectively. 1–4A represents the addition of AC anti-browning agent with concentrations of 0.3, 0.6, 0.9, and 2.0 g•L^{-1}, respectively. 1–4P-A represents the groups added with 1.5, 2.0, 2.5, and 3.0 g•L^{-1} PVP and 0.9 g•L^{-1} AC anti-browning agent combinations, respectively. Rooting rate (%) = (Number of rooting seedlings/Number of germinated seedlings) × 100%. Different lowercase letters represent significant difference at 0.01 level (Duncan, $P = 0.01$).

Agilent 2100 Bioanalyzer (Agilent, United States). The library was sequenced using the Illumina NovaSeq 6000 sequencing platform (Paired end150) to generate raw reads (APExBIO Co. Ltd., China).

De novo Transcriptome Assemblies

The raw reads of 12 individual assemblies were filtered to remove low-quality reads and reads containing adapter sequence before performing the assembly using the TrimGalore (version 0.6.4) software.[1] *De novo* transcriptome assembly was accomplished using the Trinity software (version 2.4.0) (Haas et al., 2013), by which transcripts and unigenes (the longest transcript of a set of transcripts that appear to stem from the same transcription locus) were obtained.

Quantification for Assembled Transcripts

The assembled transcriptome was used as a reference database, and clean reads were mapped back to the reference transcriptome by using Bowtie (version 1.2.3) (Langmead, 2009), and all assembled unigenes counts were quantified using RSEM (version 1.3.3) (Dewey and Li, 2011). Then, the data were normalized for variation in sequencing depth using the transcripts per million (TPM) method (Patro et al., 2017).

[1]http://www.bioinformatics.babraham.ac.uk/projects/trim_galore/

Functional Annotation of Transcripts

Transcriptome functional annotation was performed using Trinotate pipeline (version 3.2.2) (Bryant et al., 2017). Gene functions of all the assembled unigenes were annotated based on the following databases with a cut-off *E*-value of 1.0×10^{-5}: Nr (NCBI nonredundant protein sequences), Pfam (protein

TABLE 3 | Base information statistics.

Sample	Read Num	Base Num	Q20 (%)	GC (%)
CK-1	49,145,224	6,748,074,777	97.27	45.61
CK-2	45,773,602	6,305,053,688	97.29	46.36
CK-3	41,531,112	5,722,152,220	97.14	45.87
PVP-1	51,767,768	7,058,031,299	97.39	46.8
PVP-2	54,583,640	7,382,919,737	97.09	46.71
PVP-3	45,214,764	6,193,826,414	97.32	46.83
AC-1	43,164,922	5,875,079,356	97.44	46.24
AC-2	42,173,928	5,845,653,992	97.48	46.44
AC-3	42,522,386	5,873,716,564	97.39	46.52
AC-and-PVP–1	43,128,464	6,044,250,064	96.75	46.23
AC-and-PVP–2	38,896,362	5,403,657,085	97.24	47.2
AC-and-PVP–3	24,363,904	3,415,330,847	90.75	47.08

Read Num represents the total number of reads; Base Num represents the total number of bases; Q20 represents the percentage of bases with a Phred value greater than 20 to the total bases; and GC represents the number of G/C bases as a percentage of the total number of bases.

family), and Swiss-Prot (a manually annotated and reviewed protein sequence database). Gene Ontology (GO) and Kyoto Encyclopedia of Genes and Genomes (KEGG) annotation results were retrieved from eggNOG-mapper[2] and GhostKOALA.[3]

Sequence Mapping and Differential Expression Analysis

DEGseq2 R package (version 1.28.1) (Love et al., 2014) was used for differential expression analysis using raw read counts. The *P*-value was adjusted using Benjamini–Hochberg methods as adjusted *P*-value. Adjusted *P*-value < 0.05 and $|\log2\ FC\ (\text{fold change})| > 1$ were defined as the threshold for differentially expressed genes (DEGs). Expression profiles of DEGs were examined by functional and pathway enrichment analysis using GO data and KEGG terms. For GO and KEGG enrichment analysis, we used the cluster Profiler R Package (version 3.16.1) (Yu et al., 2012).

[2]http://eggnog-mapper.embl.de/

[3]https://www.kegg.jp/ghostkoala/

TABLE 4 | Genome assembly quality evaluation.

Index	All	Average length	Median length	Total assembled bases	N50
Transcript	199,689	588.17	337	117,450,803	898
Unigene	130,956	515.16	293	67,462,977	724

N50 indicates that half of the assembled bases were incorporated into unigenes with a length of at least. All represents the total number of assembled transcripts and Unigene; average length represents the average gene size of the assembled transcript and Unigene; median length represents the median size of all assembled transcripts and Unigene; and total assembled bases represents the number of bases assembled in all transcripts and Unigene.

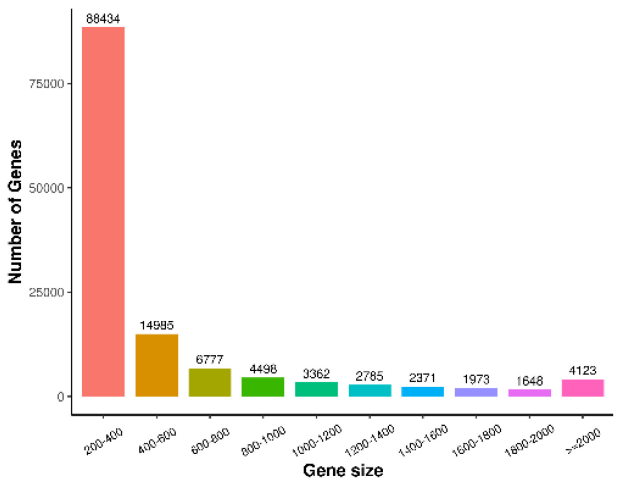


FIGURE 2 | Length distribution statistics of assembly results. *X*-axis represents the range of gene length, and *Y*-axis represents the number of gene lengths within this range.

Real-Time Quantitative PCR Verification Analysis

To verify the reliability of the transcriptome information, 19 DEGs were randomly selected for real-time quantitative PCR (qRT-PCR). The selected gene names and primer information are shown in **Table 2**. RNA extraction and reverse transcription were performed according to the methods described by Chen et al. (2021). The peony ubiquitin (Wang et al., 2012) gene was used as the housekeeping gene (ubiquitin-F: GACCTATACCAAGCCGAAG and ubiquitin-R: CGTTCCAGCACCACAATC), and the relative expression level of the genes was analyzed by qRT-PCR using the applied biosystem PowerUp SYBR Green kit. Three technical replicates for each sample were analyzed. The reaction system is as follows: 50°C for 2 min, 95°C for 2 min, 1 cycle; 95°C for 15 s, 60°C for 15 s, 72°C for 1 min, 40 cycles; 95°C for 15 s, 60°C for 1 min, 95°C for 15 s, 1 cycle.

RESULTS

Effects of Different Browning Agents on Germination and Rooting of Peony Embryo Seedlings

Figure 1 shows that the germination rate of seedlings after adding the anti-browning agent is significantly higher than that of the CK group. Among them, the germination rate of 3A group can reach 100%, but the seedlings of different treatment groups show different morphologies. The hypocotyls of the embryo seedlings of the CK group were not significantly elongated, the average elongation length was 8.61 mm, the cotyledons and hypocotyls were enlarged, the growth rate was relatively slow, and the rooting rate was 0%. For the group added with PVP anti-browning agent (1P, 2P, 3P, and 4P), the embryonic seedling morphology was similar to that of the control group, the growth of roots was inhibited, there was no significant difference in the average elongation length of hypocotyl between different PVP treatment concentration groups and the CK group, and they have no difference in their growth. For the group added with AC antibrowning agent (1A, 2A, 3A, and 4A), the hypocotyl elongation was obvious, the mean elongation length was significantly longer than the CK and PVP groups (as shown in **Figure 1**), the cotyledons were not enlarged and were flat and wide at all treatment concentrations, but the effect of promoting rooting was significant, and the rooting rate was 100%. Testing with 0.9 g/L AC showed an excellent performance of peony rooting rate and seedling growth overall. The hypocotyls of the group added with two anti-browning agents (1P-A, 2P-A, 3P-A, and 4PA) were elongated, similar to adding the AC group only, but the hypocotyls were thinner, the cotyledons were smaller, except for 3P-A, the hypocotyl length was not significantly different at other concentrations (**Figure 1**), and the rooting rate can also reach 100%, indicating that both PVP and AC can increase the seedling induction rate of seed embryo by reducing browning, but only AC has the effect of promoting embryonic seedling hypocotyl elongation and rooting.

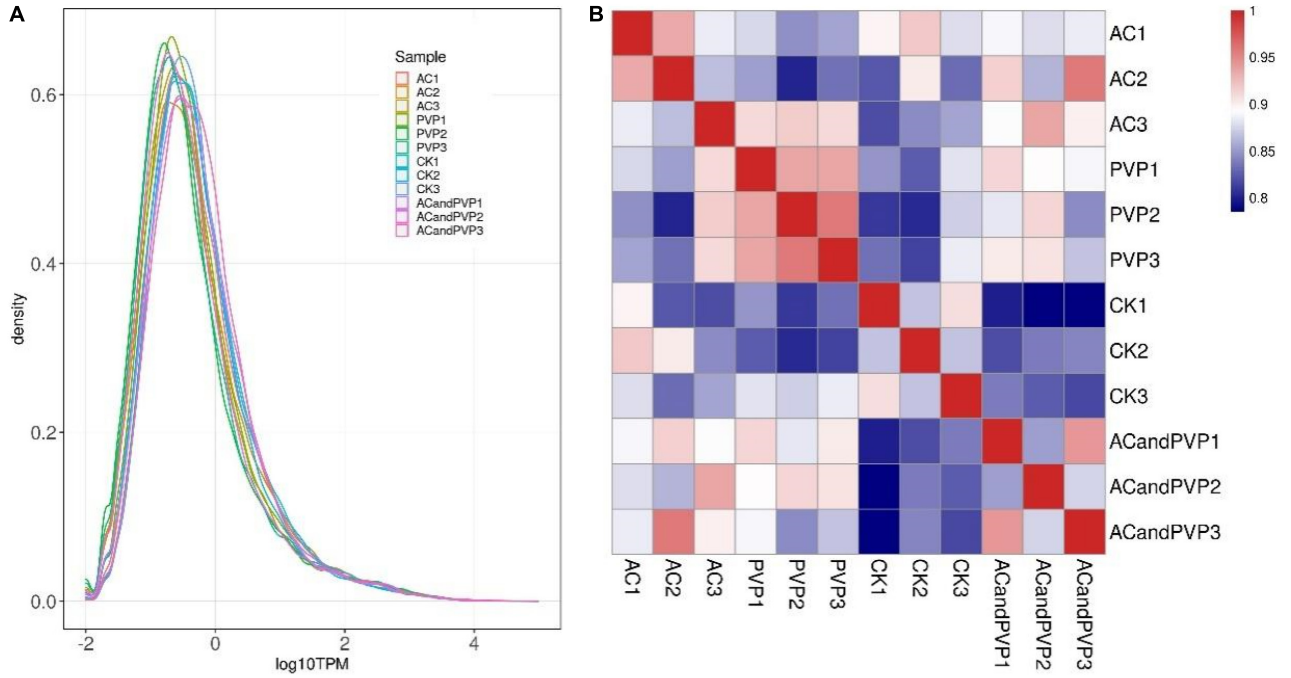


FIGURE 3 | Gene expression abundance distribution map and sample correlation heat map. **(A)** The curves in different colors in the figure represent different samples, with the *X*-axis representing log10 (TPM) of the corresponding gene and the *Y*-axis representing probability density. Generally speaking, the number of differentially expressed genes (DEGs) only accounts for a small part of the whole gene, and a few DEGs have little influence on the distribution of the expression level of samples. In most cases, samples should have a similar distribution of expression levels; **(B)** the closer the correlation coefficient is to 1, the higher the similarity of expression patterns between samples, and the degree of correlation is positively correlated with the depth of color.

RNA-Seq Analysis and Data Acquisition

Four groups (CK, 2P, 3A, and 3P-A) with better germination rates and obvious rooting differences in different treatment groups (marked directly as CK, PVP, AC, AC, and PVP) were selected for the comparative analysis of transcriptome sequencing. The Read Num and Base Num produced by 12 samples are shown in **Table 3**, and the Q20 percentages were over 90%, and the GC (number of G/C bases as a percentage of the total number of bases) percentages were over 45%.

We used Trinity to assemble and select the longest transcript of each gene as a unigene (unigene is the only one obtained after de-redundancy and deduplication of all genes in each sample) and evaluated the assembly quality of all transcripts and unigenes (**Table 4**). All the sequences were assembled, and a total of 130,956 unigenes were generated. The statistics of the number of genes of different gene sizes are shown in **Figure 2**; the average length and median length were 515.16 and 293, respectively; the N50 was 724 nt.

Five authoritative databases of Swiss-Prot, PFAM, GO, KEGG, and eggNOG have been used to annotate these unigenes. Unigenes 22,483, 28,968, 29,101, 17,281, and 17,885 could be annotated to the eggNOG, GO, KEGG, PFAM, Swiss-Prot, and Swiss-Prot databases, respectively.

We standardized the sequencing depth and gene length and obtained the TPM value of the gene for subsequent analysis. Low-quality genes that were not expressed in more than 80% of the samples were deleted. The TPM values of qualified genes are shown in **Supplementary Table 1**. Different samples have similar gene expression distribution diagrams (**Figure 3A**). At the same time, the TPM expression of all genes in any two samples was used to analyze the correlation between biological replicate samples. The results showed that the Pearson correlation coefficients between the three biological replicate samples in each group were all greater than 0.8. It reveals that the three biological repeats are highly correlated and reproducible, which can be used for gene expression analysis (**Figure 3B**).

Analysis of Differentially Expressed Genes Between Different Groups

We found that most of the genes were expressed in different groups, and the genes expressed in a group alone are relatively few compared with the total number of genes (**Figure 4B**), indicating that the addition of different anti-browning agents has little effect on the expression of the total number of genes in embryo seedlings. The number of DEGs between different groups is also relatively small compared with the total number of genes (**Supplementary Tables 2–5**), but when comparing between different groups, the number and expression of DEGs are significantly different (**Figure 4A**, the volcano map and heat map of DEG expression between different groups are shown in **Supplementary Figures 1,2**). Among them, the number of DEGs, whether upregulated or downregulated, between the two groups, AC vs. AC and PVP, is the least (**Figure 4A**). Moreover, the Venn

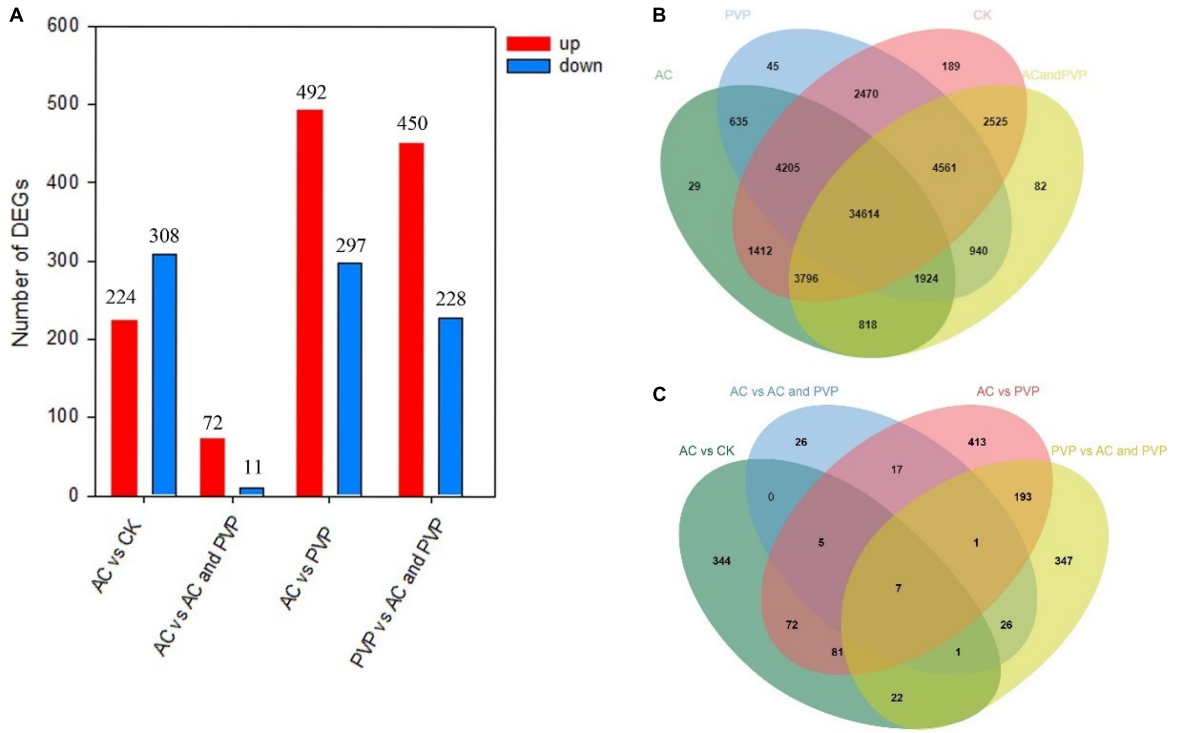


FIGURE 4 | (A) The histograms of DEGs between samples; **(B)** Venn diagrams for transcriptome analysis of the expressed genes detected in the four groups; **(C)** Venn diagrams for transcriptome analysis of the DEGs detected between different groups.

diagram shows that the number of DEGs only expressed between these two groups is also the least (**Figure 4C**), indicating that the difference in gene expression between these two groups is small, and the difference between the AC vs. AC and PVP groups and the other comparison groups is that they both added AC.

Gene Ontology Functional Classification and Kyoto Encyclopedia of Genes and Genomes Pathway Enrichment Analyses of Differentially Expressed Genes

The GO functional classification analysis shows that the DEGs between different groups were classified into 50 GO items, which were included in the biological process, the cellular component, and the molecular function, but the GO items compared between different groups were somewhat different [e.g., AC vs. CK group, **Figure 5**; the GO functional classification of other groups were shown in attached diagrams (**Supplementary Figures 3–5**)]. It is worth noting that the DEGs among the AC vs. CK, PVP vs. AC and PVP, and AC vs. PVP groups were mainly enriched in the "lipid transport" biological process (**Figure 5** and **Supplementary Figures 4,5**), and the DEGs among the AC vs. AC and PVP groups were mainly enriched in "photosynthesis, light harvesting," "protein-chromophore linkage," "nucleosome assembly," and so on (**Supplementary Figure 3**).

The KEGG pathway significant enrichment was used to determine the top 20 biochemical metabolic pathways and signal transduction pathways involved in the DEGs. The results were similar to GO functional classification. The metabolic pathways with the most significant enrichment of DEGs were the same among the AC vs. CK, PVP vs. AC and PVP, and AC vs. PVP groups, which were enriched in "phenylpropanoid biosynthesis" and "cutin, suberin, and wax biosynthesis" (**Figure 6** and **Supplementary Figures 6,7**). There are only two metabolic pathways with significant DEG enrichment in the AC vs. AC and PVP groups, namely, "cytochrome P450" and "phenylpropanoid biosynthesis" (**Figure 7**).

Real-Time Quantitative PCR to Verify the Expression of Differentially Expressed Genes

To verify the accuracy of the RNA-seq results, 19 DEGs were randomly selected for qRT-PCR. The materials used for RNA extraction are the same as those used for transcriptome sequencing. The results showed that the relative expression trend of these genes in different templates was consistent with the gene expression trend of transcriptome sequencing (**Figure 8**), indicating that the transcriptome sequencing data are reliable.

DISCUSSION

Previous studies have mostly used plant hormones and culture components to analyze the effects of peony embryo tissue culture, but the mechanism of anti-browning agents on the rapid seedling

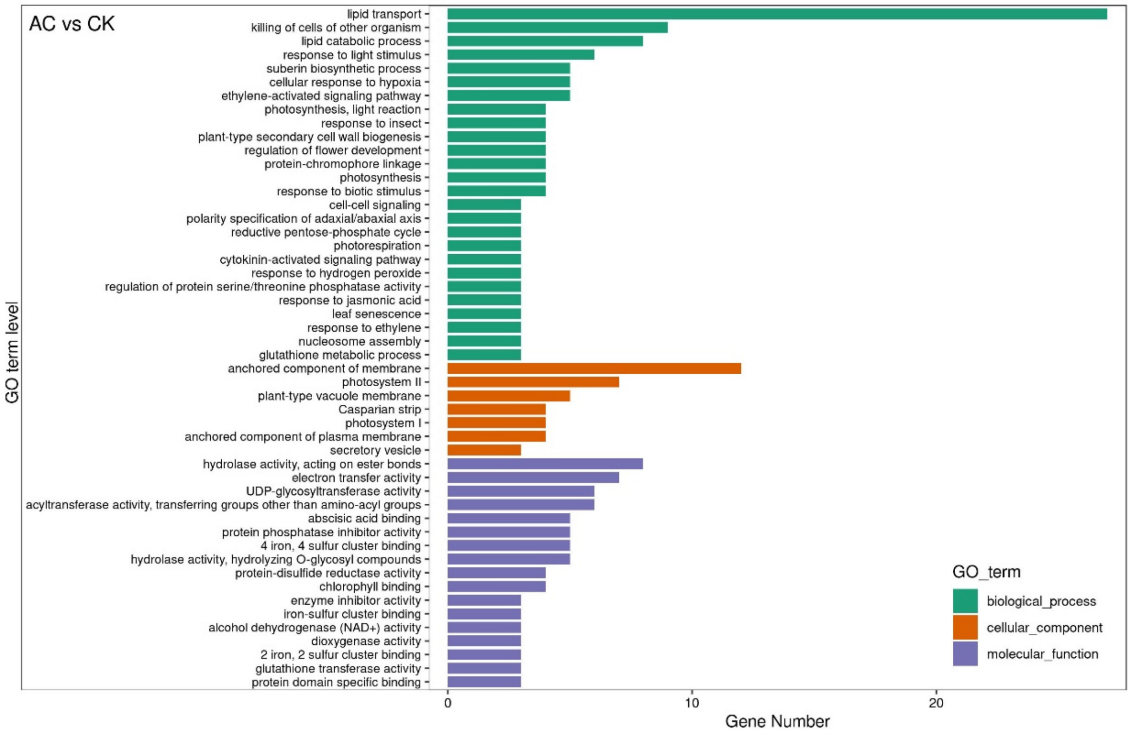


FIGURE 5 | The GO functional classification of DEGs between the activated carbon (AC) and control check (CK). The graph is drawn using the first 20 terms with the smallest *P*-value. The ordinate is GO term, and the abscissa is the number of genes with different numbers of GO term.

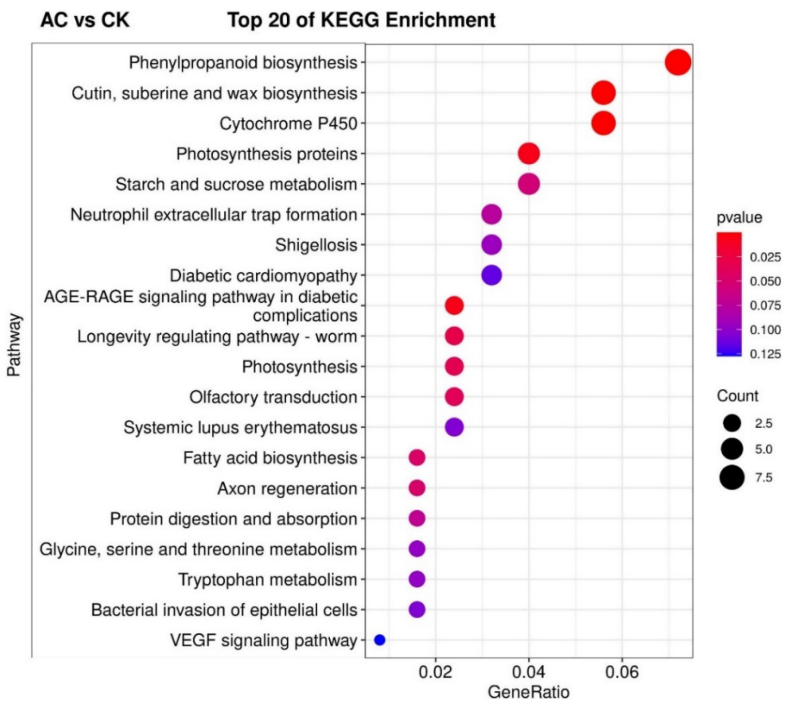


FIGURE 6 | The top 20 of the Kyoto Encyclopedia of Genes and Genomes (KEGG) pathway enrichment of DEGs between the AC and CK. The first 20 pathways with the smallest *P*-values were used to draw the map, with pathway as the ordinate and enrichment factors as the abscissa (the number of differences in this pathway divided by all the numbers). The size of the circle indicated the number. The redder the color was, the smaller the *P*-value was, and the pathway representing the redder bubbles had more DEGs.

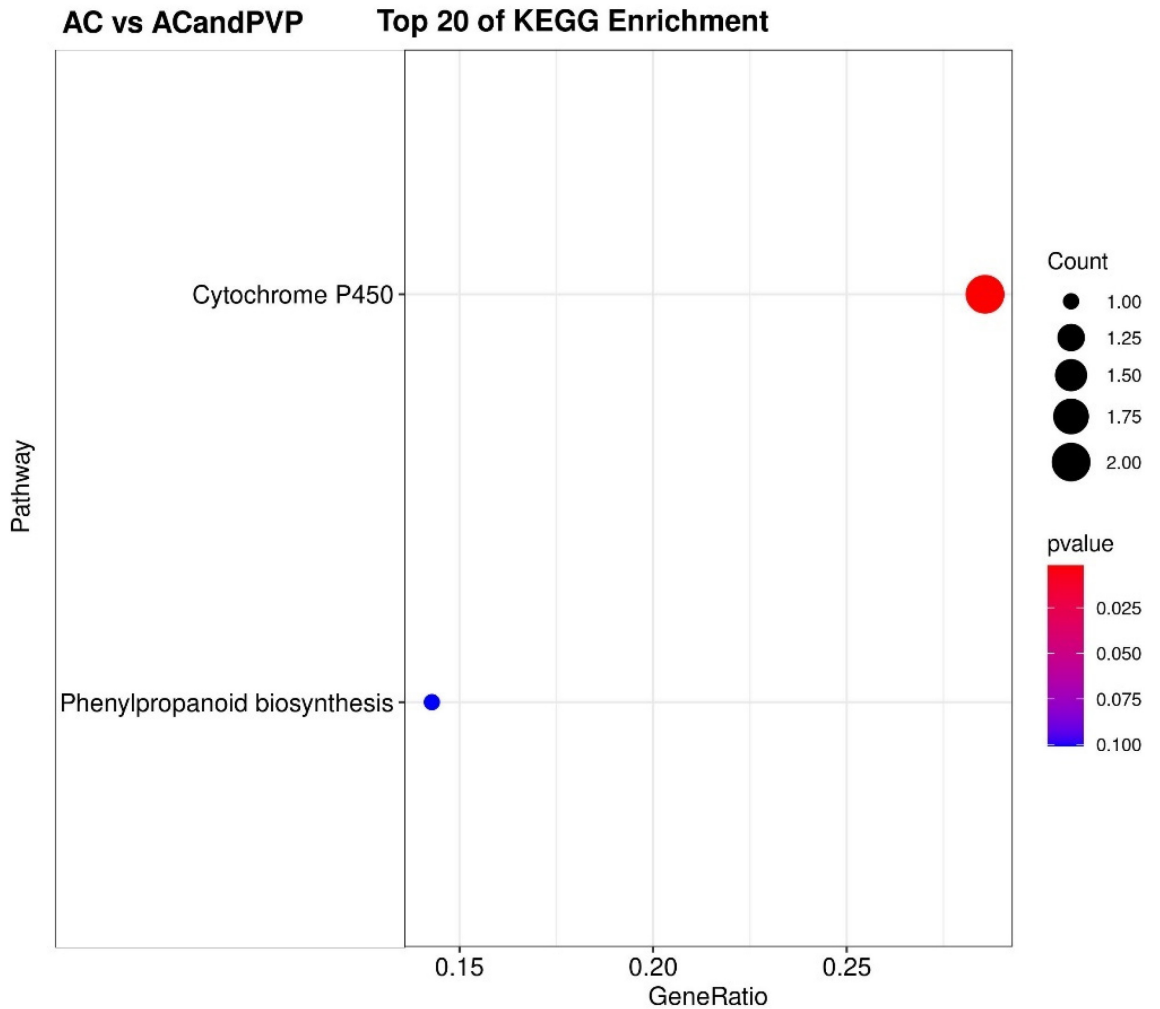


FIGURE 7 | The top 20 of the KEGG pathway enrichment of DEGs in the group of AC vs. AC and polyvinyl pyrrolidone (PVP). The first 20 pathways with the smallest *P*-values were used to draw the map, with pathway as the ordinate and enrichment factors as the abscissa (the number of differences in this pathway divided by all the numbers). The size of the circle indicated the number. The redder the color was, the smaller the *P*-value was, and the pathway representing the redder the bubbles had more DEGs.

formation of seed embryos is still unclear, and further research is needed (Liu et al., 2011). In this study, the effects of different anti-browning agents and their different combinations on the rapid seedling germination and rooting of the peony variety "FengDan" were analyzed. The results show that the addition of the two anti-browning agents, namely, AC and PVP, and their combination can effectively inhibit the browning phenomenon caused by damage during seed embryo peeling; compared with the CK group without adding any anti-browning agent, the germination rate of its seed embryos was significantly improved. In addition, the CK group and the PVP group can germinate but cannot take root at all. However, the AC and AC/PVP groups can not only increase the germination rate but also reach 100% rooting rate, and only the hypocotyls and roots of the plants in the AC/PVP group were thinner (**Figure 1**). It shows that both AC and PVP can prevent peony embryos from browning and increase the germination rate, while only the addition of AC and its combination with PVP can promote the further development of roots. To clarify its underlying mechanism, we conducted a transcriptome sequencing study.

Transcriptome sequencing data showed that there were 532,789, and 678 DEGs in the AC group compared with other groups (AC vs. CK; AC vs. PVP; AC and PVP vs. PVP), respectively; there were only 83 DEGs between the groups (AC vs. AC and PVP) that both have AC (**Figures 4A,C**). It shows that the gene expression of seed embryos has changed drastically after adding AC. These DEGs may be the key genes for AC to induce root development of peony seed embryos. At the same time, GO functional classification and KEGG pathway enrichment analysis showed that these DEGs were clustered in the same item between the AC vs. CK, AC vs. PVP, and AC and PVP vs. PVP groups, while the comparison between the AC and PVP vs. PVP groups was different from them (**Figures 5–7**). Among them, the DEGs of the AC vs. CK, AC vs. PVP, AC and

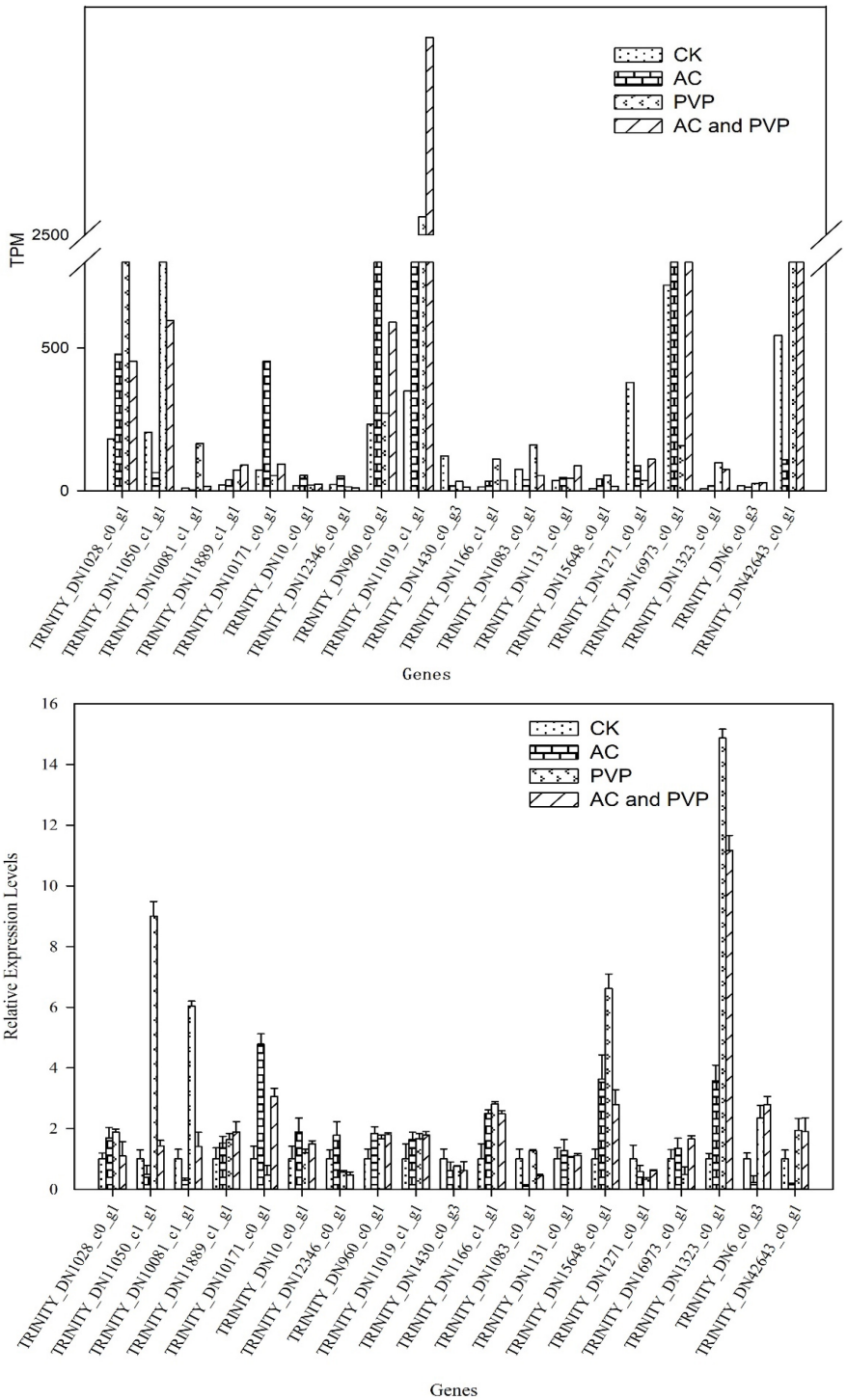


FIGURE 8 | Transcripts per million expression value and qRT-PCR relative expression of DEGs.

PVP vs. PVP groups were mainly enriched in "phenylpropanoid biosynthesis" in the KEGG pathway enrichment analysis. The phenylpropanoid biosynthesis pathway has high physiological significance in plants, because it directly or indirectly produces all the substances in the phenylpropane skeleton, which plays a vital role in the growth and development of plants (Min et al., 2011; Liu et al., 2019). For example, one of the physiological functions of the important phenylalanine ammonia lyase (*PAL*) gene family in the phenylpropane metabolic pathway is to promote cell differentiation and plant growth (Yun et al., 2015).

Through gene enrichment, phytohormone content determination, and metabonomic analysis, Wang et al. (2021) showed that the biosynthetic pathways of phenylpropanoids and flavonoids are related to root development, and flavonoid metabolism is accompanied by auxin biosynthesis and signal transduction to form the complex gene regulatory network in the process of main root development. Based on the results of this study, the gene families involved in this metabolic pathway are active, and most of them are upregulated, including peroxidase (*PER*), *PAL*, 4-coumarate: coenzyme A ligase (*4CL*), and caffeic acid 3-*O*-methyltransfease (*COMT*), especially the three peroxidase genes (*TRINITY_DN112784_c0_g1/TRINITY_DN649_c0_g1/TRINITY_DN9029_c0_g1*) among the three group comparisons showed upregulated expression (**Supplementary Tables 2,4,5**). It can be seen that AC can promote the development of roots by stimulating the expression of genes related to metabolic pathways of phenylpropanoid biosynthesis. The second enrichment pathway for these DEGs is "cutin, suberin, and wax biosynthesis." Studies have shown that cuticle, lignin, and so on can provide mechanical strength for plants and limit water loss and pathogen invasion (Xin and Herburger, 2021), and drought resistance is also involved in a variety of genetic backgrounds (Ma J. et al., 2019), which to a certain extent shows that AC can promote peony embryos to quickly adapt to the medium environment, resist microbial pollution, and further promote rooting and development of seedlings; it is also one of the important reasons for thicker cotyledons and thicker hypocotyls in plants (Ursache et al., 2021). However, in the comparison between the AC vs. AC and PVP groups, the DEGs of KEGG pathway enrichment analysis are mainly enriched in "cytochrome P450," and there are only two DEGs (*TRINITY_DN6_c0_g2/TRINITY_DN6_c0_g3*). Duan et al. (2017) found in the drought stress experiment of transgenic tobacco that overexpression of a spinach cytochrome p450 gene SoCYP85A1 can promote root development, enhance antioxidant enzyme activity, and regulate stress response. In our experiment, these two groups can promote rooting, but the root system development is obviously different. The roots of the group only added with AC is significantly stronger. It can be seen that these two DEGs are the key genes to promote the robust development of roots. It is worth mentioning that, in the comparison of the PVP vs. AC and PVP groups, only one gene (*TRINITY_DN112784_c0_g1*) was differentially expressed, and in the second enriched pathway "phenylpropanoid biosynthesis" of KEGG, it shows that, when both groups have AC, the effect of promoting root development through this metabolic pathway is minimal.

CONCLUSION

Peony seed embryo-forming technology can make peony seed embryos to quickly become seedlings, to shorten the breeding cycle, and to accelerate the process of hybrid breeding. This study investigated the effects of different anti-browning agents and their combinations on the embryo and rooting of tree peony seeds through transcriptome sequencing, aiming to illustrate their potential regulatory mechanisms. In general, both AC and PVP anti-browning agents can inhibit browning and increase the germination rate. The effect is best when the AC concentration is 0.9 g/L, but only AC and the combination of AC and PVP can promote further rooting development. Transcriptome data show that it may be related to AC, which can stimulate the expression of genes related to phenylpropanoid metabolism to promote root development. At the same time, it enhances the tissue structure by strengthening the biosynthesis of the cutin and suberin, resisting microbial contamination, and promoting plant development. This study can provide a theoretical basis for perfecting the technology of rapid seedling formation of peony embryo tissue culture.

DATA AVAILABILITY STATEMENT

The data presented in the study are deposited in the GEO database of NCBI repository, accession number GSE192345.

AUTHOR CONTRIBUTIONS

XZ, XC, and CY planned and designed the research. CY, GX, and HZ participated in the experiment of seed embryo tissue culture. XC, WJ, and SJ were responsible for the mapping of transcriptome data. XZ and SJ provided advice on transcriptome data analysis. XC and XZ were involved in manuscript editing. JN and HY participated in the revision of the manuscript. All authors read and approved the final manuscript.

FUNDING

This research was funded by the National Key R&D Program of China, Grant Number 2019YFD1001500; the Basic Public Welfare Research Project in Zhejiang Province, Grant Number LGN22C160006; and the Talent Project of Jiyang College of Zhejiang A&F University, Grant Number RQ2020B04/RQ1911B05.

SUPPLEMENTARY MATERIAL

The Supplementary Material for this article can be found online at: https://www.frontiersin.org/articles/10.3389/fpls.2022.832619/full#supplementary-material

REFERENCES

Bhatia, R., Dey, S. S., Sharma, K., Singh, S., and Kumar, R. (2021). Back-cross introgression of 'Tour' cytoplasm from *Brassica napus* through in vitro embryo rescue reveals partial restoration of sterility in B. oleracea. *Sci. Hortic.* 282:110014. doi: 10.1016/j.scienta.2021.110014

Bryant, D. M., Johnson, K., Ditommaso, T., Tickle, T., Couger, M. B., Payzin-Dogru, D., et al. (2017). A tissue-mapped axolotl de novo transcriptome enables identification of limb regeneration factors. *Cell Rep.* 18, 762–776. doi: 10.1016/j.celrep.2016.12.063

Chen, X., Lai, H. G., Li, R. M., Yao, Y., Liu, J., Yuan, S., et al. (2021). Character changes and Transcrip, tomic analysis of a cassava sexual Tetraploid. *BMC Plant Biol.* 21:188. doi: 10.1186/s12870-021-02963-1

Cheng, Y. F., Zhu, X. T., Ji, W., Hong, E. M., Li, X., Fan, Z., et al. (2019). Study on the proliferation and browning of peony callus. *Guangdong Agric. Sci.* 46, 30–36.

Dewey, C. N., and Li, B. (2011). RSEM: accurate transcript quantification from RNA-Seq data with or without a reference genome. *BMC Bioinformatics* 12:323. doi: 10.1186/1471-2105-12-323

Duan, F., Ding, J., Dongsun, L., Lu, X., Feng, Y., and Song, W. (2017). Overexpression of SoCYP85A1, a spinach cytochrome p450 gene in transgenic tobacco enhances root development and drought stress tolerance. *Front. Plant Sci.* 8:1909. doi: 10.3389/fpls.2017.01909

Fu, Z. Z. (2012). *Studies on the Relationship Between Phenolic Acids and Rooting and Browning of Peony Seedlings In Vitro.* Ph.D. thesis. Henan: Henan Agricultural University.

Haas, B. J., Papanicolaou, A., Yassour, M., Grabherr, M., Blood, P. D., Bowden, J., et al. (2013). transcript sequence reconstruction from RNA-seq using the trinity platform for reference generation and analysis. *Nat. Protocols* 8, 1494–1512. doi: 10.1038/nprot.2013.084

He, D. (2019). Study on embryo culture of peony and Paeonia lactiflora hybrids on different media. *J. Shandong Agric. Univ.* 50, 747–752.

Huang, S. J. (2020). *Research On In Vitro Rapid Propagation Technology Of Three Peony Varieties.* Ph.D. thesis. Beijing: Beijing Forestry University.

Jia, W., and Liu, H. (2014). Micropropagation of dwarf tree peony from lateral buds. *J. Appl. Sci.* 14, 2189–2193.

Langmead, B. (2009). Ultrafast and memory-efficient alignment of short DNA sequences to the human genome. *Genome Biol.* 10:R25. doi: 10.1186/gb-2009-10-3-r25

Li, P., Cheng, F. Y., and Zhang, Y. X. (2008). The effect of anti-browning agent on tissue culture browning, tissue culture seedling growth and proliferation of peony. *J. Beijing For. Univ.* 71–76.

Li, S. S., Yuan, R. Y., Chen, L. G., Wang, L. S., Hao, X. H., Wang, L. J., et al. (2015). Systematic qualitative and quantitative assessment of fatty acids in the seeds of 60 tree peony (Paeonia section Moutan DC.) cultivars by GC–MS. *Food Chem.* 173, 133–140. doi: 10.1016/j.foodchem.2014.10.017

Li, S., Liu, K., Yu, S., Jia, S., and Wang, Y. (2020). The process of embryo abortion of stenospermocarpic grape and it develops into plantlet in vitro using embryo rescue. *Plant Cell Tissue Organ Cult.* 143, 389–409.

Li, Y. Y., Guo, L. L., Lian, X. F., Guo, D. L., and Hou, X. G. (2018). Research progress of peony tissue culture technology. *Zhejiang Agric. Sci.* 59, 1646–1655.

Lian, X. F., Li, Y. Y., Zang, W. Q., Guo, L. L., Zang, Y. F., Hou, X. G., et al. (2020). Establishment of embryo culture system of fengdan tree paeonia and analysis of methylation variation of primary deformed seedlings. *Henan Agric. Sci.*49, 116–125.

Liu, F., Xie, L., Yao, Z., Zhou, Y., and Gong, C. (2019). Caragana korshinskii phenylalanine ammonialyase is up-regulated in the phenylpropanoid biosynthesis pathway in response to drought stress. *Biotechnol. Biotechnol. Equip.* 33, 842–854. doi: 10.1080/13102818.2019.1623718

Liu, L., Ji, C., Liu, H. C., and Jia, W. Q. (2011). Research on the rapid propagation of mature embryos of 'Fengdanbai' and the transplantation and domestication of tissue culture seedlings. *North. Hortic.* 99–101.

Love, M. I., Huber, W., and Anders, S. (2014). Moderated estimation of fold change and dispersion for RNA-seq data with DESeq2. *Genome Biol.* 15:550. doi: 10.1186/s13059-014-0550-8

Ma, J., Zhang, Y., Wang, H., Zhen, W., and Li, R. (2019). Differentially expressed genes and enriched pathways during drought-sensitive period under field conditions in bread wheat. *Plant Mol. Biol. Rep.* 37, 389–400. doi: 10.1007/s11105-019-01163-4

Ma, X. L., Wu, J. X., Liang, Y. X., Liu, S. H., and Wang, Y. M. (2019). Outdoor domestication cultivation and survival mechanism for tissue culture seedlings of Paeonia suffruticosa. *Asian Agric. Res.* 11, 64–67.

Min, W. H., Yun, Y. H., Kim, J. Y., and Kim, S. H. (2011). Fungal and plant phenylalanine ammonia-lyase. *Mycobiology* 39, 257–265.

Ongagna, A., Dzokouodzoyem, C. U., Youmbi, E., and Bakry, F. (2020). Positive effect of *in vitro* embryo rescue on breaking the dormancy of wild banana seeds compared to direct sowing in the greenhouse. *Fruits* 75, 194–203.

Patro, R., Duggal, G., Love, M. I., Irizarry, R. A., and Kingsford, C. (2017). Salmon provides fast and bias-aware quantification of transcript expression. *Nat. Methods* 14, 417–419. doi: 10.1038/nmeth.4197

Shang, W. Q., Wang, Z., He, S. L., He, D., Dong, N. L., Guo, Y., et al. (2020). Changes in endogenous IAA and related enzyme activities during the rooting of peony test-tube plantlets. *J. Northwest Sci. Tech. Univ. Agric. For.* 49, 129–136. doi: 10.13207/j.cnki.jnwafu

Shi, X. L., He, S. L., and Jia, W. Q. (2021). Preliminary study on tissue culture and rapid propagation technology of top bud of peony "Dahuhong". *J. Henan Inst. Sci. Technol.* 49:6.

Ursache, R., Teixeira, C., Tendon, V. D., Gully, K., and Vermeer, J. (2021). GDSL-domain proteins have key roles in suberin polymerization and degradation. *Nat. Plants* 7, 353–364. doi: 10.1038/s41477-021-00862-9

Wang, X. (2016). *'Fengdan' Peony in Vitro Rapid Propagation Technology Research.* Ph.D. thesis. Beijing: Beijing Forestry University.

Wang, Y. J., Dong, L., Zhang, C., and Wang, X. Q. (2012). Selection of internal reference genes in peony real-time quantitative PCR analysis. *J. Agric. Biotechnol.* 20, 521–528.

Wang, Y., Sun, H., Wang, H., Yang, X., Xu, Y., Yang, Z., et al. (2021). Integrating transcriptome, co-expression and QTL-seq analysis reveals that primary root growth in maize is regulated via flavonoid biosynthesis and auxin signal transduction. *J. Exp. Bot.* 13, doi: 10.1093/jxb/erab177

Xin, A., and Herburger, K. (2021). Precursor biosynthesis regulation of lignin, suberin and cutin. *Protoplasma* 258, 1171–1178. doi: 10.1007/s00709-021-01676-4

Xiu, Y., Wu, G. D., Chen, D. Z., Zhao, X. Q., Tang, W. S., Wang, H. F., et al. (2017). Breeding and cultivation techniques of peony varieties for greening oil. *J. Beijing For. Univ.* 39, 112–118.

Yang, Y. (2009). *Research on the Biological Characteristics of Peony Seed Germination and Dormancy Breaking Technology. Ph.D. thesis.* Harbin: Northeast Forestry University.

Yang, Z. J., Chu, P. F., Zhang, X. X., and Lv, F. T. (2015). Research progress of oil peony propagation technology in my country. *North. Hortic.* 201–204.

Yu, G., Wang, L. G., Han, Y., and He, Q. Y. (2012). clusterProfiler: an R package for comparing biological themes among gene clusters. *Omics J. Integr. Biol.* 16, 284–287. doi: 10.1089/omi.2011.0118

Yu, Q. Q., Du, J., Wang, J. M., and Yang, M. S. (2013). Hybrid embryo culture and plant regeneration of transgenic poplar 741. *J. Northeast For. Univ.* 65–68.

Yun, Y. H., Sun, K. J., Hwan, K. S., and Kong, W. S. (2015). Cloning and expression analysis of phenylalanine ammonia-lyase gene in the mycelium and fruit body of the edible mushroom *Flammulina velutipes*. *Mycobiology* 43, 327–332. doi: 10.5941/MYCO.2015.43.3.327

Zhang, R. L., Wang, X. B., Shao, L. M., Li, D. Q., Xia, Y. P., Zhang, J. P. (2021). Tissue culture and genetic transformation system construction of peony and peony. *Chinese J. Plant Physiol.* 57:13.

Zhang, Y., and Fan, J. A. (2008). Survey of research on Chinese medicinal material Moutan Cortex III Survey of chemical constituents of paeonol. Chongqing Res. *Chinese Herb. Med.* 24–31.

Zhu, X. T., Li, X. Q., Ding, W. J., Jin, S. H., and Wang, Y. (2018). Callus induction and plant regeneration from leaves of peony. *Hortic. Environ. Biotechnol.* 59, 575–582. doi: 10.1007/s13580-018-0065-4

Conflict of Interest: The authors declare that the research was conducted in the absence of any commercial or financial relationships that could be construed as a potential conflict of interest.

Publisher's Note: All claims expressed in this article are solely those of the authors and do not necessarily represent those of their affiliated organizations, or those of the publisher, the editors and the reviewers. Any product that may be evaluated in this article, or claim that may be made by its manufacturer, is not guaranteed or endorsed by the publisher.

Copyright © 2022 Chen, Yu, Nie, Yang, Ji, Xu, Zhu, Jin and Zhu. This is an open-access article distributed under the terms of the Creative Commons Attribution License (CC BY). The use, distribution or reproduction in other forums is permitted, provided the original author(s) and the copyright owner(s) are credited and that the original publication in this journal is cited, in accordance with accepted academic practice. No use, distribution or reproduction is permitted which does not comply with these terms.

frontiers | Frontiers in Plant Science

ORIGINAL RESEARCH
published: 05 April 2022
doi: 10.3389/fpls.2022.828287

Identification of Candidate Chromosome Region Related to Melon (*Cucumis melo* L.) Fruit Surface Groove Trait Through Biparental Genetic Mapping and Genome-Wide Association Study

Xin Du[1,2], Hongyu Liu[1,2], Zicheng Zhu[1,2], Shusen Liu[3], Zhengfeng Song[3], Lianqin Xia[3], Jingchao Zhao[4], Feishi Luan[1,2] and Shi Liu[1,2]**

[1]Key Laboratory of Biology and Genetic Improvement of Horticulture Crops (Northeast Region), Ministry of Agriculture and Rural Affairs, Northeast Agricultural University, Harbin, China, [2]Horticulture and Landscape Architecture College, Northeast Agricultural University, Harbin, China, [3]Shouguang Sanmu Seeding Co., Ltd., Shandong, China, [4]Qinggang Ruixue Agriculture Co., Ltd., Heilongjiang, China

The melon fruit surface groove (fsg) not only affects peel structure and causes stress-induced fruit cracking but also fits consumers' requirements in different regions. In this study, genetic inheritance analysis of three F_2 populations derived from six parental lines revealed that the fsg trait is controlled by a simple recessive inherited gene. Through bulked segregant analysis sequencing (BSA-seq), the *Cmfsg* locus was detected in an 8.96 Mb interval on chromosome 11 and then initially mapped to a region of approximately 1.15 Mb. Further fine mapping with a large F_2 population including 1,200 plants narrowed this region to 207 kb containing 11 genes. A genome-wide association study (GWAS) with 187 melon accessions also produced the same chromosome region for the *Cmfsg* locus. Due to the rare molecular markers and lack of mutations in the coding and promoter regions of the 11 candidate genes in the fine-mapped interval, we conducted *in silico* BSA to explore the natural melon panel to predict candidate genes for the *Cmfsg* locus. A 1.07 kb segment upstream of *MELO3C019694.2* (annotated as the AGAMOUS MADS-box transcription factor) exhibited a correlation with the grooved and non-grooved accessions among the F_2 individuals, and a natural panel consisted of 17 melon accessions. The expression level of *MELO3C019694.2* in the pericarp was higher in grooved lines than in non-grooved lines and was specifically expressed in fruit compared with other tissues (female flower, male flower, root, and leaf). This work provides fundamental information for further research on melon fsg trait formation and molecular markers for melon breeding.

Keywords: melon, fruit surface groove, BSA-seq, molecular marker, GWAS

OPEN ACCESS

Edited by:
Pei Xu,
China Jiliang University, China

Reviewed by:
Yong Xu,
Beijing Academy of Agriculture and Forestry Sciences, China
Chunhua Wei,
Northwest A&F University, China

****Correspondence:***
Feishi Luan
luanfeishi@neau.edu.cn
Shi Liu
shiliu@neau.edu.cn

Specialty section:
This article was submitted to Crop and Product Physiology, a section of the journal Frontiers in Plant Science

Received: *03 December 2021*
Accepted: *03 March 2022*
Published: *05 April 2022*

Citation:
Du X, Liu H, Zhu Z, Liu S, Song Z, Xia L, Zhao J, Luan F and Liu S (2022) Identification of Candidate Chromosome Region Related to Melon (Cucumis melo L.) Fruit Surface Groove Trait Through Biparental Genetic Mapping and Genome-Wide Association Study. Front. Plant Sci. 13:828287. doi: 10.3389/fpls.2022.828287

INTRODUCTION

Melon (*Cucumis melo* L.) is a worldwide economic cucurbit crop with multiple nutrients and delicious flavor. Uniform size and shape, high yield, and good quality are necessary conditions for elite varieties (Zalapa et al., 2007). Consumers have a high degree of melon acceptance, which is mainly affected by external characteristics (Pitrat, 2016). In recent years, a large number of genetic studies have focused on the external characteristics of melon, including peel color and fruit shape (Feder et al., 2015; Pereira et al., 2018; Oren et al., 2019). Diaz et al. (2011) and Monforte et al. (2014) reviewed the literature on QTL mapping in melon and inferred 9 meta-QTLs (five for fruit size and four for fruit weight) that could be detected in multiple melon mapping populations. Pan et al. (2020) sorted out the QTL analysis of fruit size, shape, and fruit weight of cucumber, melon, and watermelon, obtained approximately 150 consistent QTLs, and found that the homology of melon fruit shape gene is widely conservative in structure and function.

The melon fruit surface groove (fsg) is an important fruit morphological feature for consumer selection, which is mainly reflected in the fruits of some cucurbitaceae varieties and can be described as a suture from the flower end to the stem end (Zhao et al., 2019; Paris, 2000). The characteristics of fruit surface grooves affect the peel structure and fruit cracking of melon. Melon fsg can accelerate the browning of melon peel, and peel browning is the main factor leading to post harvest loss. Park and colleagues observed the area of melon fruit surface groove histologically and found that the volume and tightness of melon epidermal cells had changed during cold storage. The groove area on the fruit surface destroys the cuticle, reduces the protection of epidermal wax, and accelerates the browning of the pericarp (Park et al., 2020). The fruit surface groove also has a significant negative correlation with fruit cracking, and melon with fsg does not easily crack. The integrity of mature melon fruit without cracking is conducive to the transportation and storage of melon and increases the potential market value (Wang et al., 2018). Melon fruit groove width was negatively correlated with the edible part (Yousif et al., 2011). Since the reference genome of melon was published in 2012 (Garcia-Mas et al., 2012), some scholars have studied the genetics of melon fruit surface grooves. Zhao et al. (2019) predicted *MELO3C019694* as a melon fruit suture candidate gene by a GWAS strategy with a large number of melon germplasm resequencing data. Hu et al. (2019) also used a similar method to study the external characteristics of melon. Three SNP loci significantly related to the depth of the fruit surface groove were found on chromosomes 5, 7, and 11. Harel-Beja et al. (2010) identified a total of 44 fruit QTLs by constructing a genetic map, and among the three loci related to the melon fsg trait that were screened, two were located in linkage group 6, and one was in linkage group 11 and found that two loci were also colocalized with stripe traits. Ramamurthy and Waters (2015) studied the rib dept. of snake melon (*Cucumis melo* sub. *melo flexuosus*) and identified a QTL related to it at 0–16 cM on chromosome 11. Recently, Kishor et al. (2021) used 48 melon varieties to detect genome-wide SNPs by genotyping-by-sequencing (GBS) and then combined them with GWAS analysis, 18 important SNPs related to various morphological features were detected, and two SNPs related to fruit groove width were found on chromosomes 1 and 8. Based on the above research, we found that the melon fsg trait was an important trait in both melon fruit development and consumer choice. To date, some publications have shown that the candidate gene of fsg is located on chromosome 11, but fine mapping and candidate gene analysis are still lacking.

Previous studies have found that MADS-box family members have different regulatory functions in plant flowering time control, flower meristem maintenance, flower organ determination, wheel crack zone formation, fruit maturation, embryonic development, and vegetative organ development (Dreni and Zhang, 2016; Nakatsuka et al., 2016; Li et al., 2017). MADS boxes are expressed in the ovule, developing carpel, and developing fruit peel (Busi et al., 2003; Hileman et al., 2006). Floral organ development refers to the process of plant flower primordia developing into mature flower organs (Pelaz et al., 2000). In recent years, many studies have shown that the C-type functional gene AGAMOUS (AG) among the members of the MADS-box gene family plays an important role in the development of floral organs (Wei et al., 2020). The fruit of *A. thaliana* is a capsule with longitudinal cracking and persistent medial compound leaves, which are called siliques. The histogenesis and fragmentation of *A. thaliana* fruit are related to the action of specific transcription factors. In *A. thaliana*, several MADS-box transcription factors are necessary for different aspects of fruit development; these transcription factors include SHATTERPROOF1 (SHP1) and SHP2, which act redundantly to specify valve margin identity and the dehiscence zones in the fruit (Liljegren et al., 2000). The expression of SHP 1/2 in *Arabidopsis* is strictly located in the valve marginal region by inhibiting the expression of FUL in adjacent valve regions and inhibiting the expression of REPLUMLESS (RPL) in adjacent valve regions. SHP promotes the expression of two bHLH factors, INDEHISCENT (IND) and ALCATRAZ (ALC), which guide the production of the silique lignified layer and separation layer (Rajani and Sundaresan, 2001; Liljegren et al., 2004). Tomato AGAMOUS-LIKE 1 (TAGL1) is a MADS-box transcription factor gene belonging to the PLENA (PLE) lineage within the AGAMOUS (AG) branch. TAGL1 and FUL1/FUL2 are homologs of *Arabidopsis* SHATTERPROOF (SHP) and FUL, respectively, and their inhibition resulted in a mature defect phenotype that was partially similar to the *rin* mutant fruit (Shima et al., 2013). Mutation complementation and antisense gene expression analyses have demonstrated the function of MADS-RIN in regulating fruit ripening (Vrebalov et al., 2002). The MADS box has also been identified in several other fruits and is involved in early fruit development. A bilberry (*Vaccinium myrtillus*) FUL homolog, Vm-TDR4 (Jaakola et al., 2010), and a strawberry SHP homolog, Fa-SHP (Daminato et al., 2013), are associated with fruit development.

MATERIALS AND METHODS

Plant Materials

Three F_2 segregate populations were derived from three grooved ssp. *melo* inbred lines (M4-127, M4-120, and M4-133; **Figure 1**) and three non-grooved inbred lines (M4-12, M4-18, and M4-45; **Figure 1**) containing 187, 183, and 160 individuals, respectively. All the experimental materials were grown in a greenhouse at the Xiangyang Experimental Agricultural Farm of Northeast Agricultural University, Harbin, China in the spring of 2020. The three F_2 populations were used for genetic inheritance analysis in 2020. The F_2 populations derived from M4-12 and M4-127 were used for BSA-seq, initial mapping and fine mapping. In the spring of 2021, a total of 1,200 F_2 individuals derived from M4-127 and M4-12 were planted for recombinant selection. The selected recombinants were self-pollinated to obtain $F_{2:3}$ families for recombinant F_2 genotype identification.

Evaluation of fsg Trait

During the fruit maturity period (30 ~ 45 days after pollination, DAP), the fsg trait was investigated and photographed. The fsg trait data were investigated by direct observation. Due to the deep and shallow differences in the phenotype of fsg in F_2 fruit, cross-section should be observed along the fruit center axis to determine whether the fruit has fsg. The investigation traits were divided into two kinds of groove and non-groove (**Supplementary Figure S1**).

BSA-Seq and Initial Mapping

The young, disease-free leaves of the M4-12 and M4-127, F_1, and F_2 populations were collected 15 days after seeding for DNA extraction with the modified CTAB (cetyltrimethyl ammonium bromide) method (Murray and Thompson, 1980). All F_2 individuals from the M4-12 × M4-127-F_2 population were numbered. A total of two bulked samples were arranged by mixing an equal proportion of DNA extracted from 20 grooved and 20 non-grooved F_2 plants. The two gene pools and the genomic DNA of the parental lines were resequenced at the BGI Research Institute using the Illumina HiSeqXten platform (with at least 20× coverage genome sequencing depth for each sample) for BSA-seq analysis. The resequencing data analysis process was referenced by Takagi et al., 2013. Raw data obtained by sequencing were subjected to quality control to obtain clean data. The clean data were compared to the melon reference genome (DHL92 v3.6.1, http://cucurbitgenomics.org/ftp/genome/melon/v3.6.1/) through Burrows Wheeler Aligner (BWA) software (Li and Durbin, 2009). Different homozygous sites in the two gene pools were extracted to calculate the single-nucleotide polymorphism (SNP) or insertion–deletion (InDel) variation frequency and analyze the chromosome segment significantly associated with the fsg trait. To intuitively reflect the region of the difference between the two offspring pools, the difference between the two offspring SNP indices was calculated. One Mb was selected as the window with a 1 kb step size, and the average value of Δ (SNP index) in each window was calculated to reflect the distribution of Δ (SNP index). Combined with population

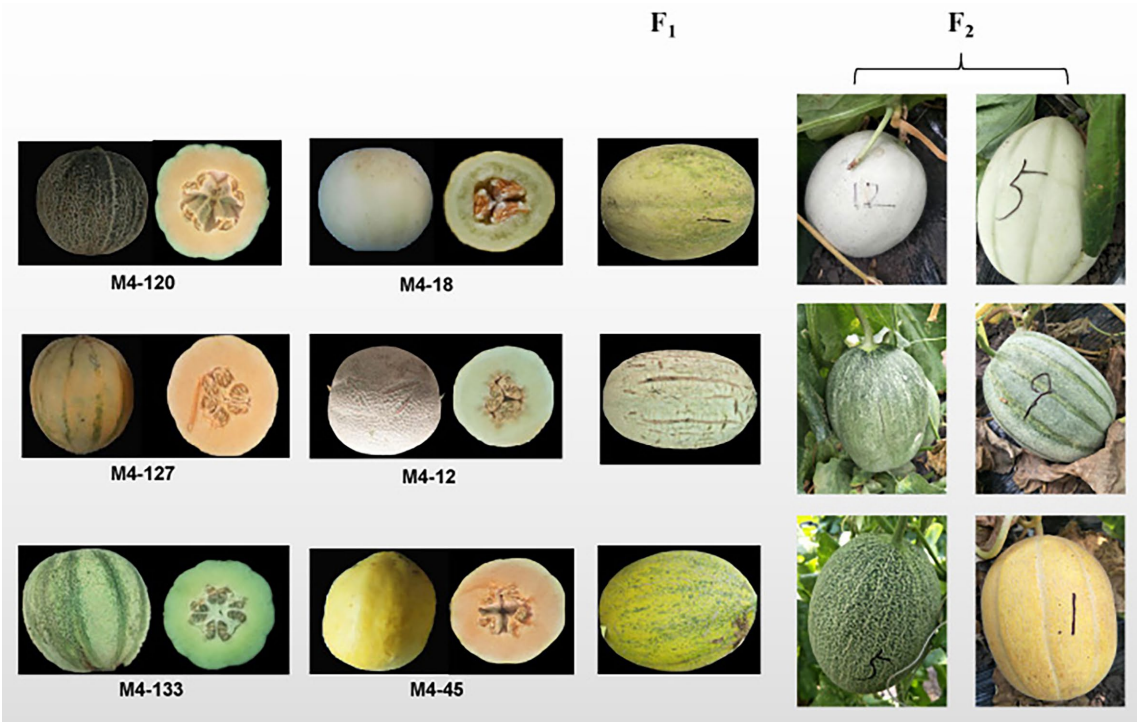


FIGURE 1 | Parental lines of the three genetic populations and the main phenotypes of the F_1 and F_2 populations.

type and offspring pool number, 1,000 permutation tests were performed, and 95 and 99% confidence levels were selected as threshold lines. The detected area above the threshold is designated as the chromosome segment primarily related to the fsg trait.

Subsequently, 500 bp before and after the InDel (Insertion and Deletion)/SNP-site sequences were extracted from the resequencing data for molecular marker exploitation. At least 6 bp InDel variation sites were selected for primer design. PCR products were separated by 8% denaturing polyacrylamide gel electrophoresis and silver staining for genotype data collection. SNPs in the restriction enzyme cutting sites were converted into CAPS (cleaved amplified polymorphic sequence) markers through SNP2CAPS software with 10 restriction enzymes (*Hin*dIII, *Bcl*I, *Xho*I, *Nde*I, *Eco*RI, *Eco*RV, *Alu*I, *Taq*I, *Xho*I, and *Dra*I). The PCR products and enzyme-digested products were detected by 1% agarose gel electrophoresis. Primers exhibiting codominant polymorphisms among the parental lines and the F_1 generation were selected for genotyping. InDel and CAPS markers were designed with Primer Premier v6.24 software based on the resequencing data from M4-12 and M4-127. SNPs that could not be converted into CAPS markers were designated Kompetitive Allele-Specific PCR (KASP) markers and genotyped at the Vegetable Research Center of the Beijing Academy of Agricultural and Forestry Sciences. Individuals with recessive trait in the F_2 population (M4-12 × M4-127-F_2) planted in 2020 were selected and genotyped to detect the recombination events for initial mapping.

Fine Mapping of the fsg Trait

A total of 1,200 F_2 individuals derived from M4-127 and M4-12 were sown in the greenhouse in the spring of 2021. Each individual in the F_2 population was numbered, and young leaves were collected 15 days after seeding for DNA extraction. The two flanking markers of the initial mapping region were used for recombinant selection. All recombinant plants were transplanted to the greenhouse of the Xiangyang Experimental Agricultural Station of Harbin Northeast Agricultural University and self-pollinated to obtain $F_{2:3}$ families. The fsg trait was investigated when the fruits were mature. $F_{2:3}$ families (at least 20 plants for each family) from the recombinant individuals with domain traits were planted in the autumn of 2021 to distinguish the genotypes of homozygotes and heterozygotes. New markers were also developed to detect recombination events in the initial mapping section to narrow down the initial mapping area.

Genome-Wide Association Study of the fsg Trait in Melon

A total of 187 out of 297 melon lines and their resequencing data from our previous publication (Liu et al., 2020) were selected for the GWAS analysis. The phenotype of the fsg trait was assessed from photographs of mature fruits taken in 2015 and 2016. A total of 2,045,412 high-quality SNPs (MAF > 0.05) were used for associated signal detection with a compressed mixed linear model (MLM). *p* values of association for each SNP and an individual trait were calculated with TASSEL 5.0.[1] The reference genome used for GWAS analysis was DHL 92 v3.5.1.[2] The Manhattan and Q-Q plots were graphed with TASSEL v5.0 and qqman v0.1.8[3] through R package 3.6.1.

Candidate Gene Prediction With *in silico* BSA and Expression Analysis

Candidate gene function annotation was performed according to a reference melon genome (DHL 92 v3.6.1). Nucleotide mutations and structural variations (in both the coding and promoter regions) in the candidate genes were first compared between M4-127 and M4-12 based on the resequencing data with Integrated Genomic Viewer (IGV) software.[4] We also selected genome resequencing data from other melon accessions (2 with the grooved: M4-120; M1-96 and 3 non-grooved: M4-12, M4-18, and M1-7) to compare genome sequences in the fine-mapping region for the variation polymorphisms between grooved and non-grooved melon accessions.

Ovaries and pericarp tissues with and without grooves (at the fruit mature stage) were collected from M4-127 and M4-12 for total RNA extraction and gene expression pattern analysis. RNA extraction was performed using a plant total RNA isolation kit (Sangon Biotech) according to the manufacturer's instructions. SYBR Green Master Mix was used as the fluorescent reagent. *MELO3C008032.2* was used as the actin gene. Primers for the actin gene and candidate gene are listed in **Table 1**. Specific transcript amplification was verified by the presence of a single peak in the melting curve obtained after the amplification reaction was complete. The expression levels of the potential genes were analyzed with the $2^{-\Delta\Delta Ct}$ method (Livak and Schmittgen, 2001).

Molecular Marker-Assisted Selection (MAS) for the *Cmfsg* Locus

A pair of primers (**Table 1**) was designed based on the sequences flanking the 1.07 kb deletion region (chr11: 24,149,100-24,150,171). This chromosome segment was amplified from 15 melon lines (9 with grooved traits and 6 non-grooved lines) and detected by 1% agarose gel electrophoresis to check the correlation between phenotype and genotype.

Statistical Analyses

A statistical field survey of the fsg trait data was carried out with Microsoft® Excel 2007. Genetic analyses and evaluations of differences in gene expression were performed using SPSS v.21.0 software (SPSS Inc., Chicago, IL, United States). Prism 7.0 software was used (GraphPad Inc., La Jolla, CA, United States) to prepare figures.

[1]https://tassel.bitbucket.io/
[2]http://cucurbitgenomics.org/ftp/genome/melon/v3.5.1/
[3]https://cran.r-project.org/web/packages/qqman/index.html
[4]http://www.igv.org/

TABLE 1 | Primers in this research.

Control gene primer	*MELO3C008032.2*	F:5′-GTGACAATGGAACTGGAATGG-3′ R:5′-AGACGGAGGATAGCGTGAGG-3′
qRT-PCR primer	*MELO3C019694.2*	F:5′-GGGAAGTGGAACTTCAGAGC-3′ R:5′-TCGTTTGCTGTTGTTGTTGC-3′
MAS PCR primer	PCR	F:5′-CATGCCTGCAAGTAAAGACA-3′ R:5′-ATGCGGAGGGTACAATAAGA-3′

TABLE 2 | Genetic analysis of the fsg trait among F_2 segregated populations.

Genetic population	Total	Groove	Nongroove	Expected	χ^2 value	*p* value
M4-12 × M4-127	187	51	136	1:3	0.515	0.47
M4-18 × M4-120	183	40	143	1:3	0.96	0.32
M4-45 × M4-133	160	36	124	1:3	0.53	0.46

TABLE 3 | Candidate genes in the fine mapping interval.

Gene ID	Physical location	Gene annotation
MELO3C019699.2	24,059,374. 24,062,605	Elongation factor 2
MELO3C019698.2	24,078,257. 24,093,312	Serine/threonine-protein kinase TNNI3K
MELO3C019697.2	24,109,474. 24,114,837	Elongation factor 2
MELO3C019696.2	24,119,712. 24,120,763	HVA22-like protein
MELO3C035125.2	24,127,294. 24,127,758	Transmembrane protein
MELO3C035126.2	24,129,470. 241,30,414	Myb/SANT-like DNA-binding domain protein
MELO3C034863.2	24,141,567. 24,141,728	Unknown protein
MELO3C019694.2	24,172,183. 24,177,539	AGAMOUS MADS box factor transcription factor
MELO3C019691.2	24,206,907. 24,211,844	Hexosyltransferase
MELO3C019692.2	24,211,247. 24,211,800	Unknown protein
MELO3C035128.2	24,234,163. 24,234,510	L10-interacting MYB domain-containing protein-like

RESULTS

The fsg Trait in Melon Is Regulated by a Single Recessive Gene, BSA-Seq, and Recombinant Events Delimiting the *Cmfsg* Locus Into a 207-kb Region

The F_1 generations from three hybridized combinations exhibited a smooth pericarp without fsg. In the three F_2 populations, the ratios of fsg to nonfsg populations were 51:136, 40:143, and 36:124, which was consistent with the 1:3 ratio (**Figure 1**; **Table 2**) indicating that the fsg trait in melon is controlled by a recessive gene. Genome resequencing produced a total of 22.738 Gb of raw data. After filtering low-quality and short reads, M4-12 produced 11.385 Gbp of clean data, and M4-127 produced 11.352 Gbp of clean data (Q30 ≥ 88.28%). The clean data were compared to the reference genome through BWA software with comparison rates of 94.88 and 97.24%. A total of 75,902,530 and 75,682,054 clean read pairs were generated from the non-grooved pool (24.54× depth coverage) and grooved pool (24.77× depth coverage), respectively. Finally, 2,588,595 SNPs and 544,356 InDels were used for BSA-seq analysis. The ΔSNP index was calculated and plotted against genome position. A ΔSNP-index signal (with a ΔSNP-index value >0.5) related to fsg was detected on chromosome 11 spanning approximately 8.96 Mb (from 20013001 to 28966000 bp; **Figure 2A**).

Thirty-six pairs of primers that were uniformly distributed on the region identified by BSA-seq were designed. After polymorphism detection, 8 markers (6 CAPS and 2 InDel markers) were used for initial mapping. Fifty-one individuals with a recessive phenotype (grooved) were selected from the F_2 generation in 2020 and genotyped with the 8 polymorphic markers. Ten out of the 51 plants that exhibited recombination events were used to reduce the BSA-seq region to approximately 1.71 Mb (from 2,300,980 to 24,713,146 bp) between the CAPS markers *Chr11_230070980* and *Chr11_24713146* and included 2 and 6 recombinants for each marker (**Figure 2B**).

To further narrow the initial mapping region, 1,200 F_2 plants derived from M4-12 × M4-127 were planted in the spring of 2021. *Chr11_23007980* and *Chr11_24713146* were used as flanking markers to screen recombinant individuals (**Figure 2B**). Seventy-seven recombinant plants were obtained and transplanted to the greenhouse. Another 13 polymorphic KASP markers in the initial region were developed to genotype the recombinant plants. The genotype of the dominant recombinants was confirmed based on phenotypic segregation in their $F_{2:3}$ families. Finally, the *Cmfsg* locus was delimited between the KASP markers *Chr11_24049463* and *Chr11_24256692* (approximately 207 kb of the physical distance, including 11 candidate genes) with two and two recombinants for each boundary marker, respectively (**Figure 2C** and **Table 3**).

GWAS Identified the *Cmfsg* Gene on Chromosome 11

According to the phenotype of plants grown in 2015 and 2016, the 187 melon lines consisted of 70 non-grooved lines and 117 grooved lines. The GWAS results revealed an obvious signal (approximately 1.23 Mb from 23,374,318 to 24,604,487 bp; reference genome: DHL 92 v3.5.1) associated with the fsg trait on chromosome 11 (**Figures 3A,B**). We also compared the 207-kb region to the genome reference DHL 92 v3.6.1, and this fine-mapping region was aligned from 24,049,540 to 24,256,769 bp, consistent with the biparental genetic mapping results.

In silico BSA With Genome Resequencing Data From Other Melon Accessions Revealed That a Deleted 1.07-kb Chromosome Segment Correlated With Melon fsg

The *Cmfsg* locus was finally mapped to a 207-kb region on chromosome 11 based on recombinant lines, but it was still a large interval. Although some recombinant plants were examined, no available markers were found in this segment according to the genome resequencing data from the parental lines. We also resequenced M4-120 and M4-18, and the results were the same as those obtained for M4-12 and M4-127; there were still no available markers in this region.

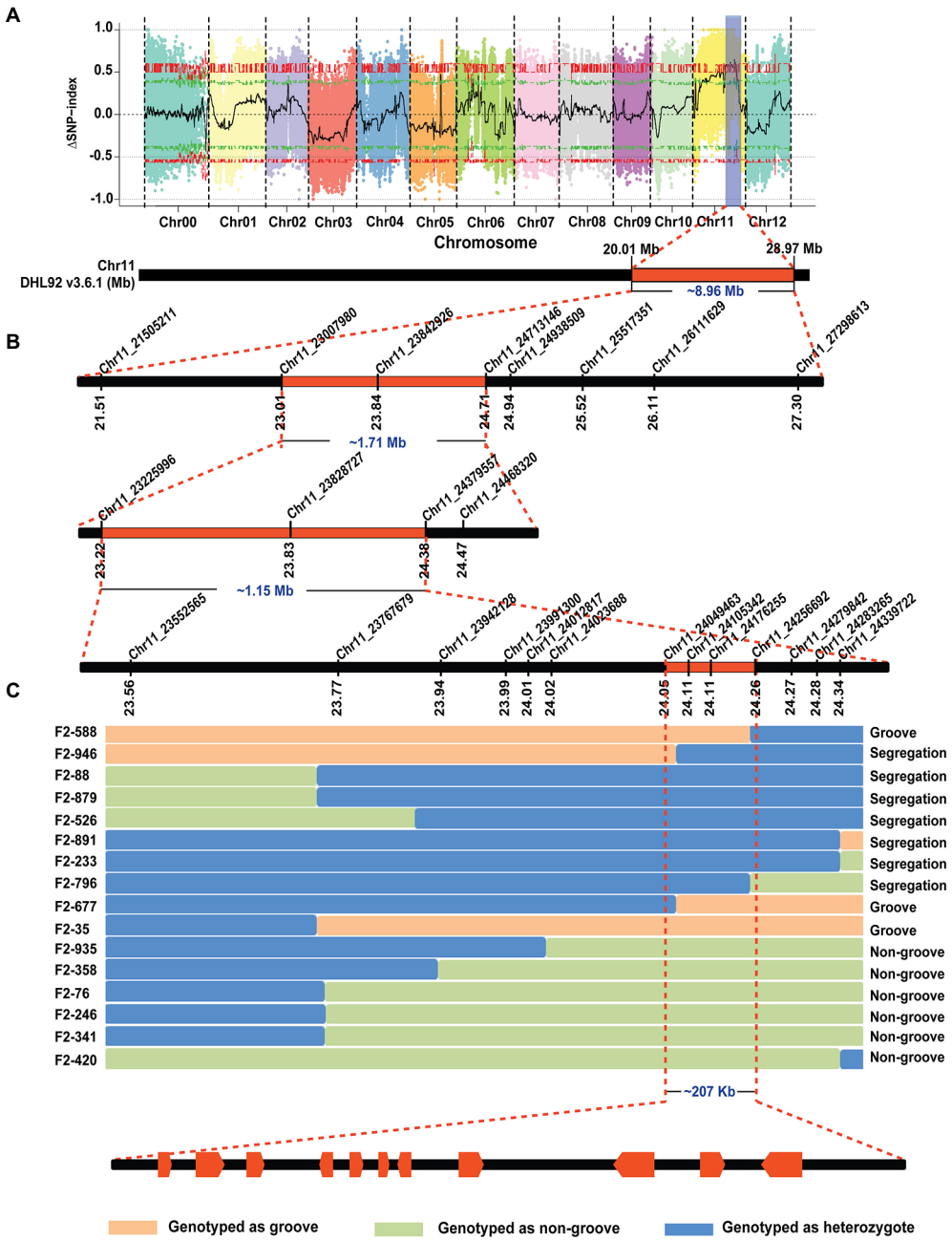


FIGURE 2 | BSA-seq analysis and fine mapping of the melon fsg trait. **(A)** BSA-seq results, the chromosome region related to the fsg trait, **(B)** initial mapping of the fsg trait. **(C)** Fine mapping of the fsg trait.

Additionally, many gaps in this interval existed according to the reference genome data. The association analysis results also showed that the GWAS interval contained only four SNPs associated with the fsg trait. For the above reasons, we planned to use *in silico* BSA to compare the genome resequencing data from other melon accessions to detect variations related to fsg. By scanning the genome region among the M4-127 melon accessions, a 1.07 kb chromosome segment (chr11: 24,149,096-24,150,171) deletion was found in grooved melon but existed in nonfsg melon (**Figure 4A**). Beyond this variation, we did not find any other mutations in either the coding or promoter region in the 207-kb interval of the 11 candidate genes that could distinguish grooved and non-grooved melon accessions. We designed a PCR marker (**Table 1**) according to the resequencing data containing this 1.07-kb variation and amplified this fragment from 17 melon accessions. The results showed that all the grooved lines produced a 101-bp PCR product, while a 1,171-bp

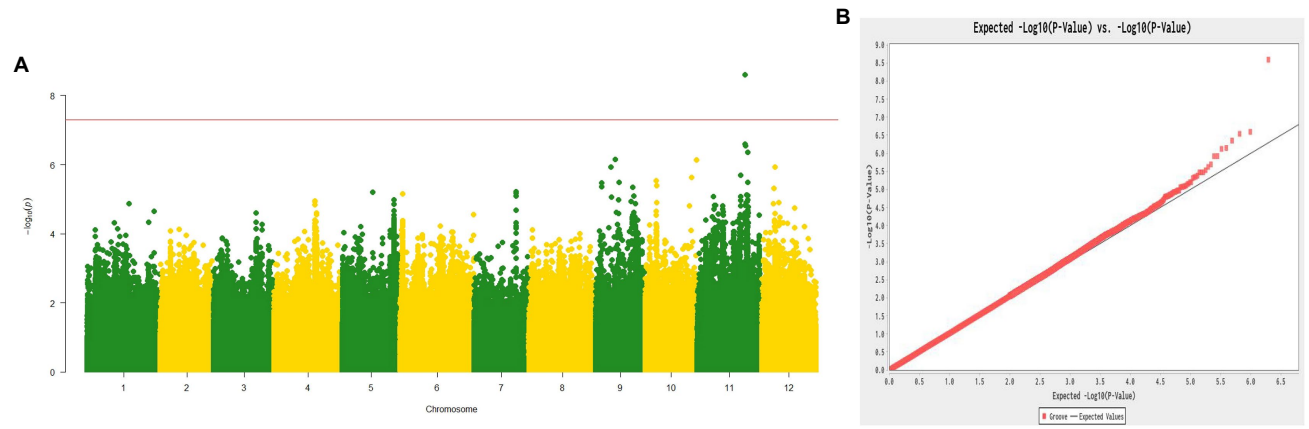


FIGURE 3 | Manhattan plot **(A)** and Q-Q plot **(B)** of the melon fsg trait through a genome-wide association study.

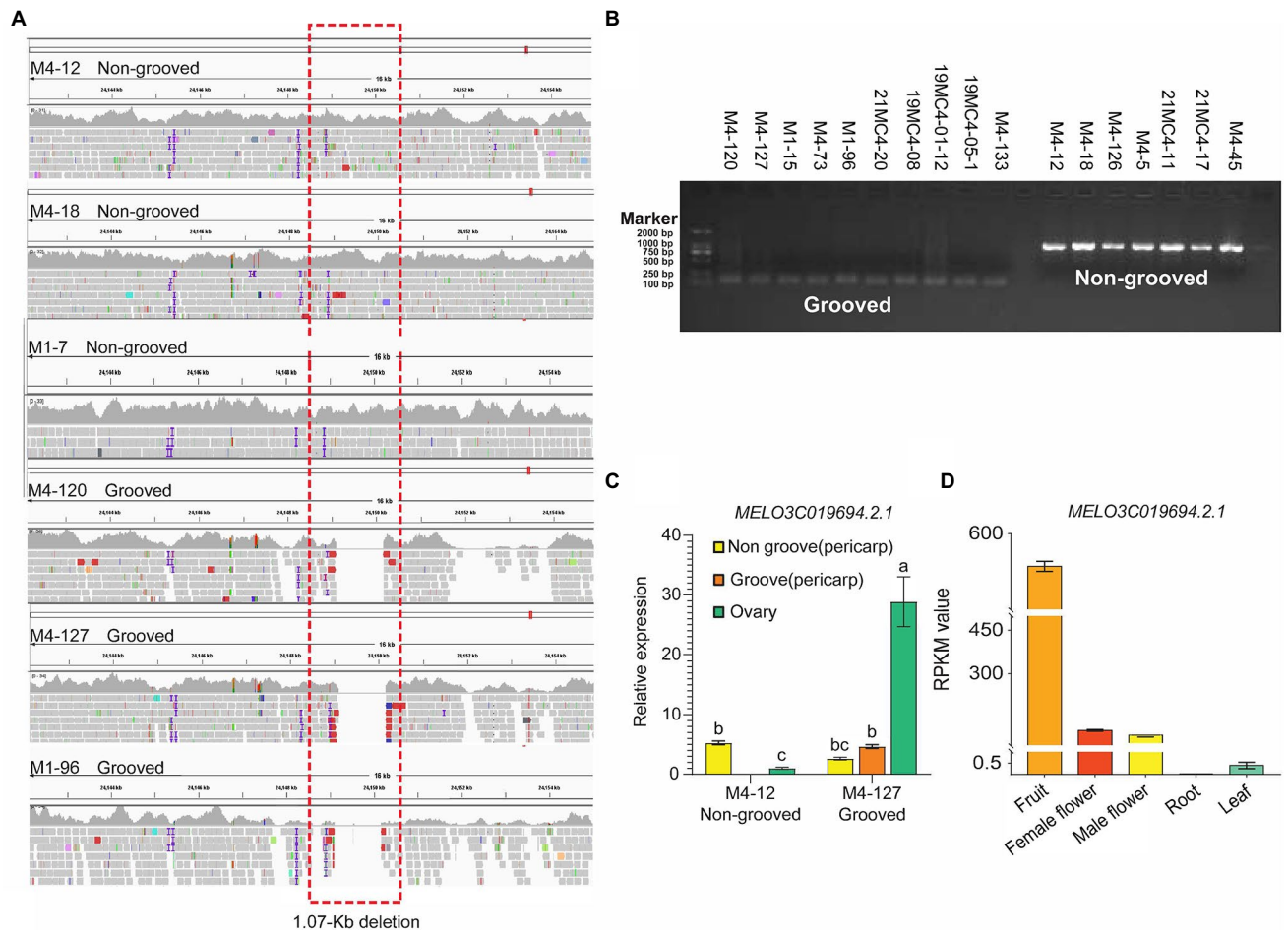


FIGURE 4 | Candidate gene analysis. **(A)** Sequence alignment of the 1,070-bp deletion region from different materials at 23.85 kb upstream of *MELO3C019694.2.1*. **(B)** Bands of amplified *Chr11_24149068* from 11 melon materials. **(C)** The expression level of the gene in the parental ovary and the grooved and non-grooved pericarp of the mature fruit. **(D)** Gene transcription data from fruit, female flowers, male flowers, roots, and leaves.

product was amplified from the non-grooved lines (**Figure 4B**). These results indicated that this 1.07-kb region is highly correlated with the fsg trait.

Gene Expression Analysis Revealed CmMADS-Box as a Candidate Gene for the Melon fsg Trait

To predict the candidate gene for melon fsg, we focused on the chromosome region containing the 1.07-kb segment. The 1.07-kb deletion was upstream (approximately 23.8 kb) of *MELO3C019694.2* (annotated as AGAMOUS MADS-box transcription factor). We then detected the expression pattern of *MELO3C019694.2* in the ovary and the grooved and non-grooved pericarp tissues in the mature fruit between M4-127 and M4-12. The results showed that *MELO3C019694.2* expression in the ovary of the M4-127 grooved line was 28.8 times higher than that of the M4-12 non-grooved line, with a significant difference. In mature fruit from the M4-127 line, *MELO3C019694.2* expression in the grooved part (4.65 ± 0.32b) was 1.77 times higher than that in the non-grooved part (2.62 ± 0.22bc). There was no difference in the *MELO3C019694.2* expression level in the non-grooved part of the mature fruit of the two parents (**Figure 4C**). Combined with the transcriptome data from the Cucurbitaceae database (BioProject: PRJNA383830; **Figure 4D**), *MELO3C019694.2* was more specifically expressed in fruit than in female flowers, male flowers, roots, and leaves, suggesting that this gene may be involved in the regulation of melon fsg trait formation.

DISCUSSION

The fruit surface groove is an important quality of fruit appearance that contributes to its commercial value. The external morphology of fruits also plays an important role in plant evolution. The diversity of fruit shapes, including variations such as stripes, may promote seed transmission and plant evolution by attracting fruit eaters (Encinas-Viso et al., 2014). In this study, six parental lines were used to configure three genetic populations, and these populations were used to analyze the genetic inheritance of melon fsg. The results showed that the fsg was controlled by a major effective gene, this is consistent with the research results of Harel-Beja et al. (2010), Wang et al. (2018), and Zhao et al. (2019). Zhao et al. (2019) identified the same gene and variation region in the study of melon fruit suture. But the 1.07 kb was not co-segregated with fruit groove among the melon nature panel. A 122 (15.18%) of 807 non grooves had a deletion of 1.07 kb, and 42 (16.34%) of 257 grooves had no deletion of 1.07 kb indicated that 1.07 kb deletion maybe not the only reason for groove trait formation. Previous studies also showed that there were multiple SNPs loci (not only on chromosome 11, but also on chromosome 5 and 7 related with the depth of fruit groove) related to fsg traits (Hu et al., 2019). It indicates that there may be other genes controlling fsg traits in melon. Based on our GWAS panel, we found that the 1.07 kb region was not associated with subspecies and geographic distribution. The 1.07 kb region could also associate with this trait, whether the accessions belonged to the *C. agrestis* or *C. melo* with different geographical distribution (In **Figures 4A,C**, M1-7, M1-96, and M1-15 belonged to *C. agrestis*, others belonged to *C. melo*).

Coincidentally, Harel-Beja et al. (2010) found that the stripes in the young ovary and the surface grooves in the mature fruit located in the same position indicated that the two traits had a high correlation. Pumpkins, cucumbers, and gourds usually display stripes of different colors and shapes prominently (Goldman, 2004). The formation of stripes is the irregular accumulation of some pigments, such as carotenoids, flavonoids, and chlorophyll (Feder et al., 2015). Therefore, peel stripes are also known as the second color of peel (Cohen et al., 2014). Fruit surface groove also called vein tracks (Zhao et al., 2019). Generally, strong or dark stripes appear between the main veins on the fruit surface, and light stripes are located above or near the main veins (Paris, 2002). The position of this external stripe is consistent with the position of the main subepidermal vascular system of the ovary and fruit (Paris, 2020). It seemed that the position of stripes was just located in the suture/groove. But many melon accessions without groove still have the strips. So, we speculated that the stripes and fruit groove are two phenotypic characters.

MELO3C019694.2 (annotated as AGAMOUS MADS-box transcription factor) was predicted as the most likely candidate gene for the melon fsg trait based on the expression patterns in the ovary, grooved, and non-grooved peel tissues in mature fruit from the parental lines in this study. The MADS-box family is an important transcription factor that plays an important role in plant growth and development and signal transduction (Zeng et al., 2018). In the process of evolution, the family experienced a series of gene duplication events, resulting in gene sub-functionalization or new functionalization and resulting in plant morphological diversity (Theissen et al., 2000). During plant growth and development, MADS-box genes may affect plant growth and development at different stages, parts, tissues, and organs (Hardenack et al., 1994). In addition to regulating flower development, the plant MADS box is also involved in the development of roots, leaves, fruits, seeds, and embryos (Garcia-maroto et al., 2003). Among the transcription factor networks that affect fruit ripening, MADS-box family transcription factors act as central regulators of ripening (Smaczniak et al., 2012; Gapper et al., 2013). In *Arabidopsis*, four genes, AG, SHATTERPROOF1 (SHP1), SHATTERPROOF2 (SHP2), and SEEDSTICK (STK), belong to the AG subfamily, of which SHP1 and SHP2 were previously called AGAMOUS-LIKE 1 and AGAMOUS-LIKE 5 (Li et al., 2016). Many studies have shown that the AGAMOUS (AG) gene, as a major regulator of floral organ differentiation and flowering decisions, can coordinate various cell fate decisions during flower development (Garceau et al., 2017). Studies on *Arabidopsis* found that the expression of SHP 1/2 is strictly localized in the marginal area of the valve by inhibiting FRUITFULL (FUL) expressed in the adjacent valve area and inhibiting REPLUMLESS (RPL) expressed in the adjacent valve area, which leads to silique cracking (Liljegren et al., 2000). FUL is responsible for the normal division and proliferation of cells in the valve, while

SHP1 and SHP2 control the differentiation of the split zone (Liljegren et al., 2004). SHP promotes the expression of INDEHISCENT (IND) and ALCATRAZ (ALC; Rajani and Sundaresan, 2001). Tomato AGAMOUS-LIKE 1 (*TAGL1*) is a MADS-box transcription factor gene. The study found that *TAGL1* is homologous to the repeat genes SHP1 and SHP2 of *Arabidopsis thaliana* (Wei et al., 2020). RNA interference (RNAi) inhibition of TAGL1 in tomato fruit resulted in inhibited fruit ripening and reduced pericarp thickness, suggesting the existence of a molecular bridge linking pulp pericarp development and fruit ripening (Fujisawa et al., 2014). However, there are large differences in the copy number of MADS-box genes in different species, resulting in the sub-functionalization of many parallel homologous genes (Smyth, 2018). Therefore, the most significant feature of the MADS-box gene family is that it is involved in the process of fruit development in different plants. The roles vary widely among family members. A comparative analysis of *Brassica* plants shows that changes in the expression of the MADS-box transcription factor can control the change from cracking to noncracking in fruits of related species (Muhlhausen et al., 2013; Carey et al., 2019). This may also be the reason why melons with the characteristics of fruit surface grooves do not easily crack, but the specific regulatory mechanism needs further research.

To identified if there existed some conserved domain in the 1.07 kb region, we extracted the sequences of the 1.07 kb and making a BLAST alignment. Unfortunately, we did not find any conserved domain. There were still 23.8 kb located between the 1.07 kb segment and the *MELO3C019694.2*, but still contain many gaps according to the reference genome. So there may exist some other gene in this 23.8 kb region regulate the groove trait formation. However, in addition to this mutation, we did not find any other mutations in the coding region or promoter region of 207 kb of 11 candidate genes. Much more information was needed in the further research, such as a comprehensive reference genome data, a more precise genetic mapping to confirm the candidate gene. Therefore, the mechanism of fsg trait formation will be the focus of future research.

DATA AVAILABILITY STATEMENT

The original contributions presented in the study are included in the article/**Supplementary Material**, further inquiries can be directed to the corresponding authors.

AUTHOR CONTRIBUTIONS

XD performed the major experiments. HL and ZZ serviced generations production. ShuL, ZS, LX, and JZ offered germplasm resources. ShiL designed the experiment and analyzed the data. FL and ShiL revised the manuscript and are the co-corresponding authors. All authors contributed to the article and approved the submitted version.

FUNDING

This work was supported by funding from the National Natural Science Foundation of China (grant no. 31972436 and 32030094) by the China Agriculture Research System of MOF and MARA (grant no. CARS-25), and by Taishan Industrial Leading Talents Project (grant no. LJNY202112).

SUPPLEMENTARY MATERIAL

The Supplementary Material for this article can be found online at: https://www.frontiersin.org/articles/10.3389/fpls.2022.828287/full#supplementary-material

Supplementary Figure S1 | Transverse sections of the groove and non-groove F_2 individuals.

REFERENCES

Busi, M. V., Bustamante, C., D'Angelo, C., Hidalgo-Cuevas, M., Boggio, S. B., Valle, E. M., et al. (2003). MADS-box genes expressed during tomato seed and fruit development. *Plant Mol. Biol.* 52, 801–815. doi: 10.1023/a:1025001402838

Carey, S., Mendler, K., and Hall, J. C. (2019). How to build a fruit: transcriptomics of a novel fruit type in the *Brassiceae*. *PLoS One* 14:e0209535. doi: 10.1371/journal.pone.0209535

Cohen, S., Itkin, M., Yeselson, Y., Tzuri, G., Portnoy, V., Harel-Baja, R., et al. (2014). The *PH* gene determines fruit acidity and contributes to the evolution of sweet melons. *Nat. Commun.* 5:4026. doi: 10.1038/ncomms5026

Daminato, M., Guzzo, F., and Casadoro, G. (2013). A SHATTERPROOF-like gene controls ripening in non-climacteric strawberries, and auxin and abscisic acid antagonistically affect its expression. *J. Exp. Bot.* 64, 3775–3786. doi: 10.1093/jxb/ert214

Diaz, A., Fergany, M., Formisano, G., Ziarsolo, P., Blanca, J., Fei, Z., et al. (2011). A consensus linkage map for molecular markers and quantitative trait loci associated with economically important traits in melon (*Cucumis melo* L.). *BMC Plant Biol.* 11, 1471–2229. doi: 10.1186/1471-2229-11-111

Dreni, L., and Zhang, D. (2016). Flower development: the evolutionary history and functions of the AGL6 subfamily MADS-box genes. *J. Exp. Bot.* 67, 1625–1638. doi: 10.1093/jxb/erw046

Encinas-Viso, F., Revilla, T. A., van Velzen, E., and Etienne, R. S. (2014). Frugivores and cheap fruits make fruiting fruitful. *J. Evol. Biol.* 27, 313–324. doi: 10.1111/jeb.12301

Feder, A., Burger, J., Gao, S., Lewinsohn, E., Katzir, N., Schaffer, A. A., et al. (2015). A Kelch domain-containing F-box coding gene negatively regulates flavonoid accumulation in muskmelon. *Plant Physiol.* 169, 1714–1726. doi: 10.1104/pp.15.01008

Fujisawa, M., Shima, Y., Nakagawa, H., Kitagawa, M., Kimbara, J., Nakano, T., et al. (2014). Transcriptional regulation of fruit ripening by tomato FRUITFULL homologs and associated MADS box proteins. *Plant Cell* 26, 89–101. doi: 10.1105/tpc.113.119453

Gapper, N. E., McQuinn, R. P., and Giovannoni, J. J. (2013). Molecular and genetic regulation of fruit ripening. *Plant Mol. Biol.* 82, 575–591. doi: 10.1007/s11103-013-0050-3

Garceau, D. C., Batson, M. K., and Pan, I. L. (2017). Variations on a theme in fruit development: the PLE lineage of MADS-box genes in tomato (TAGL1) and other species. *Planta* 246, 313–321. doi: 10.1007/s00425-017-2725-5

Garcia-Maroto, F., Carmona, M. J., Garrido, J. A., Vilches-Ferron, M., Rodriguez-Ruiz, J., and Alonso, D. L. (2003). New roles for MADS-box genes in higher plants. *Biol. Plant.* 46, 321–330. doi: 10.1023/A:1024353514081

Garcia-Mas, J., Benjak, A., Sanseverino, W., Bourgeois, M., Mir, G., Gonzalez, V. M., et al. (2012). The genome of melon (*Cucumis melo* L.). *Proc. Natl. Acad. Sci. U. S. A.* 109, 11872–11877. doi: 10.1073/pnas.1205415109

Goldman, A. (2004). *The Compleat Squash*. New York: Artisan Books.

Hardenack, S., Ye, D., Saedler, H., and Grant, S. (1994). Comparison of MADS box gene expression in developing male and female flowers of the dioecious plant white campion. *Plant Cell* 6, 1775–1787. doi: 10.1105/tpc.6.12.1775

Harel-Beja, R., Tzuri, G., Portnoy, V., Lotan-Pompan, M., Lev, S., Cohen, S., et al. (2010). A genetic map of melon highly enriched with fruit quality QTLs and EST markers, including sugar and carotenoid metabolism genes. *Theor. Appl. Genet.* 121, 511–533. doi: 10.1007/s00122-010-1327-4

Hileman, L. C., Sundstrom, J. F., Litt, A., Chen, M., Shumba, T., and Irish, V. F. (2006). Molecular and phylogenetic analyses of the MADS-box gene family in tomato. *Mol. Biol. Evol.* 23, 2245–2258. doi: 10.1093/molbev/msl095

Hu, Q. M., Yang, H. H., and Zhu, H. Y. (2019). Genome-wide association analysis of fruit fluff, fruit surface tumor and fruit surface ditch in melon. *Chin. Melon* 32, 7–12. doi: 10.16861/j.cnki.zggc.20190505.010 (in Chinese with English abstract).

Jaakola, L., Poole, M., Jones, M. O., Kämäräinen-Karppinen, T., Koskimäki, J. J., Hohtola, A., et al. (2010). A SQUAMOSA MADS box gene involved in the regulation of anthocyanin accumulation in bilberry fruits. *Plant Physiol.* 153, 1619–1629. doi: 10.1104/pp.110.158279

Kishor, D. S., Noh, Y., Song, W. H., Lee, G. P., Park, Y., Jung, J. K., et al. (2021). SNP marker assay and candidate gene identification for sex expression via genotyping-by-sequencing-based genome-wide associations (GWAS) analyses in oriental melon (*Cucumis melo* L. var. *makuwa*). *Sci. Hortic.* 2021:276. doi: 10.1016/j.scienta.2020.109711

Li, H., and Durbin, R. (2009). Fast and accurate short read alignment with burrows-wheeler transform. *Bioinformatics* 25, 1754–1760. doi: 10.1093/bioinformatics/btp324

Li, L. Y., Fang, Z. W., Li, X. F., and Liu, Z. X. (2017). Isolation and characterization of the C-class MADS-box gene from the distylous pseudocereal *Fagopyrum esculentum*. *Plant Biotechnol. J.* 60, 189–198. doi: 10.1007/s12374-016-0488-3

Li, B., Li, Q., Mao, X., Li, A., Wang, J., Chang, X., et al. (2016). Two novel AP2/EREBP transcription factor genes TaPARG have pleiotropic functions on plant architecture and yield-related traits in common wheat. *Front. Plant Sci.* 7:1191. doi: 10.3389/fpls.2016.01191

Liljegren, S. J., Ditta, G. S., Eshed, Y., Savidge, B., Bowman, J. L., and Yanofsky, M. F. (2000). SHATTERPROOF MADS-box genes control seed dispersal in *Arabidopsis*. *Nature* 404, 766–770. doi: 10.1038/35008089

Liljegren, S. J., Roeder, A. H., Kempin, S. A., Gremski, K., Østergaard, L., Guimil, S., et al. (2004). Control of fruit patterning in *Arabidopsis* by INDEHISCENT. *Cell* 116, 843–853. doi: 10.1016/s0092-8674(04)00217-x

Liu, S., Gao, P., Zhu, Q., Zhu, Z., Liu, H., Wang, X., et al. (2020). Resequencing of 297 melon accessions reveals the genomic history of improvement and loci related to fruit traits in melon. *Plant Biotechnol. J.* 18, 2545–2558. doi: 10.1111/pbi.13434

Livak, K. J., and Schmittgen, T. D. (2001). Analysis of relative gene expression data using real-time quantitative PCR and the $2^{-\Delta\Delta CT}$ method. *Methods* 25, 402–408. doi: 10.1006/meth.2001.1262

Monforte, A. J., Diaz, A., Caño-Delgado, A., and van der Knaap, E. (2014). The genetic basis of fruit morphology in horticultural crops: lessons from tomato and melon. *J. Exp. Bot.* 65, 4625–4637. doi: 10.1093/jxb/eru017

Muhlhausen, A., Lenser, T., Mummenhoff, K., and Theissen, G. (2013). Evidence that an evolutionary transition from dehiscent to indehiscent fruits in *Lepidium* (*Brassicaceae*) was caused by a change in the control of valve margin identity genes. *Plant J.* 73, 824–835. doi: 10.1111/tpj.12079

Murray, M. G., and Thompson, W. F. (1980). Rapid isolation of high molecular weight plant DNA. *Nucleic Acids Res.* 8, 4321–4326. doi: 10.1093/nar/8.19.4321

Nakatsuka, T., Saito, M., and Nishihara, M. (2016). Functional characterization of duplicated B-class MADS-box genes in Japanese gentian. *Plant Cell Rep.* 35, 895–904. doi: 10.1007/s00299-015-1930-6

Oren, E., Tzuri, G., Vexler, L., Dafna, A., Meir, A., Faigenboim, A., et al. (2019). The multi-allelic *APRR2* gene is associated with fruit pigment accumulation in melon and watermelon. *J. Exp. Bot.* 70, 3781–3794. doi: 10.1093/jxb/erz182

Pan, Y., Wang, Y., McGregor, C., Liu, S., Luan, F., Gao, M., et al. (2020). Genetic architecture of fruit size and shape variation in cucurbits: a comparative perspective. *Theor. Appl. Genet.* 133, 1–21. doi: 10.1007/s00122-019-03481-3

Paris, H. S. (2000). Genes for broad, contiguous dark stripes in cocozelle squash (*Cucurbita pepo*). *Euphytica* 115, 191–196. doi: 10.1023/A:1004074618717

Paris, H. S. (2002). "Characterization of reversed striping in Cucurbita pepo," in *Cucurbitaceae* ed. D. N. Maynard (Alexandria, VA: American Society for Horticultural Science) 2002, 36–40.

Paris, H. S. (2020). Dark-stem-dependent reverse fruit striping in *Cucurbita pepo* (pumpkin, squash, gourd: Cucurbitaceae): genes *l-2* and *W* are at the same locus. *Euphytica* 216:180. doi: 10.1007/s10681-020-02706-7

Park, M. H., Chang, E. H., Yang, H. J., Lee, J. S., Do, G. R., Song, H. J., et al. (2020). Modified atmosphere and humidity film reduces browning susceptibility of oriental melon suture tissue during cold storage. *Foods* 9:1329. doi: 10.3390/foods9091329

Pelaz, S., Ditta, G. S., Baumann, E., Wisman, E., and Yanofsky, M. F. (2000). B and C floral organ identity functions require SEPALLATA MADS-box genes. *Nature* 405, 200–203. doi: 10.1038/35012103

Pereira, L., Ruggieri, V., Pérez, S., Alexiou, K. G., Fernández, M., Jahrmann, T., et al. (2018). QTL mapping of melon fruit quality traits using a high-density GBS-based genetic map. *BMC Plant Biol.* 18:324. doi: 10.1186/s12870-018-1537-5

Pitrat, M. (2016). "Melon genetic resources: phenotypic diversity and horticultural taxonomy: genetics and genomics of *Cucurbitaceae*," in *Plant Genetics and Genomics: Crops and Models*. eds. R. Grumet, N. Katzir and J. Garcia-Mas (Cham: Springer), 25–60.

Rajani, S., and Sundaresan, V. (2001). The *Arabidopsis* myc/bHLH gene ALCATRAZ enables cell separation in fruit dehiscence. *Curr. Biol.* 11, 1914–1922. doi: 10.1016/s0960-9822(01)00593-0

Ramamurthy, R. K., and Waters, B. M. (2015). Identification of fruit quality and morphology QTLs in melon (*Cucumis melo*) using a population derived from *flexuosus* and *cantalupensis* botanical groups. *Euphytica* 204, 163–177. doi: 10.1007/s10681-015-1361-z

Shima, Y., Kitagawa, M., Fujisawa, M., Nakano, T., Kato, H., Kimbara, J., et al. (2013). Tomato FRUITFULL homologues act in fruit ripening via forming MADS-box transcription factor complexes with RIN. *Plant Mol. Biol.* 82, 427–438. doi: 10.1007/s11103-013-0071-y

Smaczniak, C., Immink, R. G., Angenent, G. C., and Kaufmann, K. (2012). Developmental and evolutionary diversity of plant MADS-domain factors: insights from recent studies. *Development* 139, 3081–3098. doi: 10.1242/dev.074674

Smyth, D. R. (2018). Evolution and genetic control of the floral ground plan. *New Phytol.* 220, 70–86. doi: 10.1111/nph.15282

Takagi, H., Abe, A., Yoshida, K., Kosugi, S., Natsume, S., Mitsuoka, C., et al. (2013). QTL-seq: rapid mapping of quantitative trait loci in rice by whole genome resequencing of DNA from two bulked populations. *Plant J.* 74, 174–183. doi: 10.1111/tpj.12105

Theissen, G., Becker, A., Di Rosa, A., Kanno, A., Kim, J. T., Münster, T., et al. (2000). A short history of MADS-box genes in plants. *Plant Mol. Biol.* 42, 115–149. doi: 10.1023/A:1006332105728

Vrebalov, J., Ruezinsky, D., Padmanabhan, V., White, R., Medrano, D., Drake, R., et al. (2002). A MADS-box gene necessary for fruit ripening at the tomato *ripening-inhibitor* (*rin*) locus. *Science* 296, 343–346. doi: 10.1126/science.1068181

Wang, X. Z., Qiu, G., and Chen, K. N. (2018). Study on develop CAPS markers to locate genes related to melon fruit sur-face groove based on BSA method. *J. Ne. Agric. Univ.* 49, 17–23. doi: 10.19720/j.cnki.issn.1005-9369.2018.05.003 (in Chinese with English abstract).

Wei, M. M., Zeng, X., An, Z. W., Hu, Y. S., Huang, X., and Li, W. G. (2020). Advances in the maintenance and termination of floral meristem regulated by C-type floral organ gene AGAMOUS (AG). *Biotechnol. Bull.* 36, 135–143. doi: 10.13560/j.cnki.biotech.bull.1985.2019-0877

Yousif, M. T., Elamin, T. M., Baraka, M., Jack, A. A., and Ahmed, E. A. (2011). Variability and correlation among morphological, vegetative, fruit and yield parameters of snake melon (*Cucumis melo* var. flexuosus). *Cucurbit Gene. Cooper. Rep.* 33–34:32–35.

Zalapa, J. E., Staub, J. E., McCreight, J. D., Chung, S. M., and Cuevas, H. (2007). Detection of QTL for yield-related traits using recombinant inbred lines derived from exotic and elite US Western shipping melon germplasm. *Theor. Appl. Genet.* 114, 1185–1201. doi: 10.1007/s00122-007-0510-8

Zeng, X., Liu, H., Du, H., Wang, S., Yang, W., Chi, Y., et al. (2018). Soybean MADS-box gene GmAGL1 promotes flowering via the photoperiod pathway. *BMC Genomics* 19:51. doi: 10.1186/s12864-017-4402-2

Zhao, G., Lian, Q., Zhang, Z., Fu, Q., He, Y., Ma, S., et al. (2019). A comprehensive genome variation map of melon identifies multiple domestication events and loci influencing agronomic traits. *Nat. Genet.* 51, 1607–1615. doi: 10.1038/s41588-019-0522-8

Conflict of Interest: JZ is employed by Qinggang Ruixue Agriculture Co., Ltd. ShuL, ZS, and LX are employed by Shouguang Sanmu Seeding Co., Ltd.

The remaining authors declare that the research was conducted in the absence of any commercial or financial relationships that could be construed as a potential conflict of interest.

Publisher's Note: All claims expressed in this article are solely those of the authors and do not necessarily represent those of their affiliated organizations, or those of the publisher, the editors and the reviewers. Any product that may be evaluated in this article, or claim that may be made by its manufacturer, is not guaranteed or endorsed by the publisher.

Copyright © 2022 Du, Liu, Zhu, Liu, Song, Xia, Zhao, Luan and Liu. This is an open-access article distributed under the terms of the Creative Commons Attribution License (CC BY). The use, distribution or reproduction in other forums is permitted, provided the original author(s) and the copyright owner(s) are credited and that the original publication in this journal is cited, in accordance with accepted academic practice. No use, distribution or reproduction is permitted which does not comply with these terms.

frontiers | Frontiers in Plant Science

ORIGINAL RESEARCH
published: 13 April 2022
doi: 10.3389/fpls.2022.859290

Quantitative Extraction and Evaluation of Tomato Fruit Phenotypes Based on Image Recognition

Yihang Zhu[1], Qing Gu[1], Yiying Zhao[1], Hongjian Wan[2], Rongqing Wang[2], Xiaobin Zhang[1] and Yuan Cheng[2]**

[1] Institute of Digital Agriculture, Zhejiang Academy of Agricultural Sciences, Hangzhou, China, [2] State Key Laboratory for Quality and Safety of Agro-Products, Institute of Vegetables, Zhejiang Academy of Agricultural Sciences, Hangzhou, China

Tomato fruit phenotypes are important agronomic traits in tomato breeding as a reference index. The traditional measurement methods based on manual observation, however, limit the high-throughput data collection of tomato fruit morphologies. In this study, fruits of 10 different tomato cultivars with considerable differences in fruit color, size, and other morphological characters were selected as samples. Constant illumination condition was applied to take images of the selected tomato fruit samples. Based on image recognition, automated methods for measuring color and size indicators of tomato fruit phenotypes were proposed. A deep learning model based on Mask Region-Convolutional Neural Network (R-CNN) was trained and tested to analyze the internal structure indicators of tomato fruit. The results revealed that the combined use of these methods can extract various important fruit phenotypes of tomato, including fruit color, horizontal and vertical diameters, top and navel angles, locule number, and pericarp thickness, automatically. Considering several corrections of missing and wrong segmentation cases in practice, the average precision of the deep learning model is more than 0.95 in practice. This suggests a promising locule segmentation and counting performance. Vertical/horizontal ratio (fruit shape index) and locule area proportion were also calculated based on the data collected here. The measurement precision was comparable to manual operation, and the measurement efficiency was highly improved. The results of this study will provide a new option for more accurate and efficient tomato fruit phenotyping, which can effectively avoid artificial error and increase the support efficiency of relevant data in the future breeding work of tomato and other fruit crops.

Keywords: quantitative, tomato fruit, phenotyping, image recognition, deep learning

OPEN ACCESS

Edited by:
Pei Xu,
China Jiliang University, China

Reviewed by:
Parvaiz Ahmad,
Government Degree College, Pulwama, India
Carlos Augusto Avila,
Texas A&M Research, United States

****Correspondence:***
Xiaobin Zhang
3504125@qq.com
Yuan Cheng
chengyuan1005@126.com

Specialty section:
This article was submitted to Crop and Product Physiology, a section of the journal Frontiers in Plant Science

Received: *21 January 2022*
Accepted: *28 February 2022*
Published: *13 April 2022*

Citation:
Zhu Y, Gu Q, Zhao Y, Wan H, Wang R, Zhang X and Cheng Y (2022) Quantitative Extraction and Evaluation of Tomato Fruit Phenotypes Based on Image Recognition. Front. Plant Sci. 13:859290. doi: 10.3389/fpls.2022.859290

INTRODUCTION

Tomato (*Solanum lycopersicum* L.) is one of the most widely consumed vegetables around the world (Kaya et al., 2020; Alam et al., 2021; Faizan et al., 2021). Tomatoes are used for food in a variety of forms and contain considerable vitamins A, C, and lycopene, which have been shown to reduce the risk of cancer and neurodegenerative disorder (Kinkade and Foolad, 2013;

Caseiro et al., 2020). Due to the genetic diversity and commercial value, tomato is also a model species for fruit development studies. Since tomato spread out through trade from South America and Mesoamerica where tomato domestication began, it was chosen for diverse fruit colors and sizes throughout breeding. Consequently, current tomato cultivars have various phenotypes including colors, sizes, and internal structure (Sierra-Orozco et al., 2021). For example, cultivated tomatoes have colors from green to orange, red, and black; sizes from 6 to 100 mm, and even larger; and internal shapes including diverse locule and pericarp traits. All these traits determine the market valuation and culinary consumption procedures of tomato fruits, including fresh, sliced, diced, or cooked (De Corato, 2020).

The growers' demand for lucrative tomatoes is associated with the color and size of the tomato fruits. Although all traits are crucial, consumers prefer to rate tomatoes initially on their sensory appearance and then on their flavor. For example, large-sized and flat tomatoes are preferred to be sliced or cooked because they are easier for manual processing. Thus, fruit size and vertical/horizontal ratio (fruit shape index) are important indicators of tomato traits. Fruit color is the most attractive attribute as commodities (Oltman et al., 2014). The pericarp is the circular outer part of the fruit fresh part developed from mesocarp. Locules are septum-enclosed independent spaces separated by the placenta which are filled with semiliquid tissue. Pericarp and locules determine the taste and malformation rate. Fruits with large locule area proportion tend to have higher moisture content and are suitable for fresh-eating, whereas fruits with small locules and thick pericarp are preferred for cooking (Tamasi et al., 2019). Because tomato fruit traits are so important to customers, tomato breeders are working hard to improve those qualities. A deeper knowledge of tomato fruit phenotypes can help in breeding attempts to enhance fruit quality.

Although the tomato genome has been sequenced for many years (The Tomato Genome Consortium, 2012) and many quantitative trait loci (QTLs) related to fruit morphology have been identified (Prudent et al., 2009; Celik et al., 2017), traditional breeding techniques are still dominant in tomato breeding, and the traits of parents for hybrid breeding are selected mainly depending on breeder's experience (Zhu et al., 2018). Such multidimensional screening of tomato phenotypes is not only time-consuming and labor-intensive but also limits the breeding accuracy and efficiency. Therefore, it is necessary to develop methods to quantitatively evaluate the tomato fruit phenotypes, including the fruit color, size, morphology, and locule structures (Bhatta et al., 2021). Moreover, as the concept of breeding 4.0 being raised, which seeks out the desirable traits combined with the aid of artificial intelligence based on fully comprehended bioinformatic and agronomic data (Wallace et al., 2018), high-throughput and quantitative phenotyping is more likely to promote crop breeding efficiency in a novel, data-driven way (Washburn et al., 2019).

Tomato fruit traits pertaining to morphological and structural aspects are used for fruit phenotyping (Darrigues et al., 2008), which is closely connected with genetic diversity analysis regarding the effects of breeding and crop genetic resources conservation and exploitation (Mata-Nicolás et al., 2020). With the progress of image recognition based on deep learning methods, quantitative and high-throughput plant phenotyping is becoming promising (Pereira et al., 2021). There are plenty of successful studies in most field crops (Li et al., 2020), but using high-throughput methods to assess quantitative phenotypes of vegetables is still at an earlier experimental stage (Tripodi et al., 2018; Boogaard et al., 2020). Most vegetable breeding initiatives appear to be hampered by a lack of affordable and accessible high-throughput techniques. Generally, manual fruit measurement, which is commonly utilized in traditional phenotypes evaluation and costs a lot of labor and time, is the main barrier in comprehensive tomato fruit phenotyping (Costa et al., 2018). A tool called *Tomato Analyzer* based on computer vision has shown to be quite effective in extracting tomato fruit morphometric and structural features automatically, yet the analysis of some fruit internal structures, such as locule number and area, still requires manual operations (Gonzalo et al., 2009). Another tool called *LocAnalyzer* attempts to count tomato fruit locule automatically with the help of computer vision recognition (Spetale et al., 2020), but it only processes one fruit in each image and requires image scanning of cut fruits.

In this study, a series of quantitative indicators (color, diameters, angles, locules, and pericarp) for tomato fruit phenotypes are proposed based on the quantitative requirements of tomato breeding. A combination of image recognition and Mask Region-Convolutional Neural Network (R-CNN) deep learning methods to extract these indicators is proposed. The findings are supposed to provide a useful tool for the high-throughput phenotyping of tomatoes. The tool also assists breeders to evaluate tomato fruit traits quantitatively and automatically and could be extended to other fruit crop breeding.

MATERIALS AND METHODS

Materials, Sampling, and Image Acquisition

The ripe fruits of all 591 tomato cultivars were applied for image acquisition and phenotyping. Ten cultivars with obvious differences in fruit size, fruit color, and other aspects were selected as samples for phenotyping comparison and verification (**Table 1** and **Figure 1A**). All tomato cultivars were cultivated in the tomato germplasm field of Zhejiang Academy of Agricultural Sciences, Yangdu, Haining City, Zhejiang, China (120.411°N, 30.441°E).

Three to four representative tomato fruit samples were placed on a white background at intervals. A black-white ruler card with accurate squares of 1 cm × 1 cm was attached next to the samples as reference (**Figure 1B**). Images of both the samples and the ruler card were acquired using a camera (Canon EOS 20D, 50 mm fixed-focus lens, Canon, Inc., Tokyo, Japan) in a photo box with a diffuse inner surface and a soft light (24 W, color temperature 6,000 K, WenaSelin Tec., Co. Ltd., Hangzhou, China) on the top. Due to the fixed focal length, the image with the ruler card was taken only once to calibrate the measurement before taking other images. After taking an image of the intact tomato fruits (**Figure 1B**), each fruit was sepal-removed and cut

vertically through the center. Then, another image of the vertical cut was taken (**Figure 1C**). Finally, both the vertical halves were cut horizontally, and the adjacent parts were put together to take a third image of the horizontal cut (**Figure 1D**).

Image Recognition and Phenotyping Indicators

To quantitatively extract tomato fruit phenotyping indicators from the images, OpenCV 4.5.3 computer vision library was applied to conduct image recognition tasks including background filtering, length measuring, and contour points locating. The tomato fruit locules were recognized using a deep learning instance segmentation model developed on PaddlePaddle 1.8.4 (Ma et al., 2019).

Intact Tomato Fruits

The image recognition process for the image of intact tomato fruits is shown in **Figure 1E**. The image was first transformed into Hue-Saturation-Value (HSV) color mode. Based on the saturation and value differences between the tomato fruits and the background, HSV filtering and binarization were then performed to remove the background. Pixels that had H between 0 and 180° (ranging 0–360°) and both S (ranging 0–255°) and V (ranging 0–255°) greater than a certain threshold were marked as tomato fruit area, and other pixels were background. According to our preliminary experiment, such a threshold would vary among cultivars. Still, for a certain fruit color type, the threshold stays the same. As background pixels were replaced with black color, the image was binarized, and only fruits were remained. Then, the fruit color in Red, Green, and Blue (RGB) color mode was extracted for each fruit in the image and taken the average R, G, and B value, respectively.

Vertical Cut

The image recognition process for the image of vertical cut is shown in **Figure 1F**. HSV filtering and binarization were performed first, as mentioned above. The fruit contours in the image and the corresponding minimum area rectangles enclosing the fruit contours were extracted. According to our preliminary experiment, the fruit horizontal diameters extracted from intact fruit and vertical cut image have no significant difference. Thus, the width and height of the rectangle were measured and recorded as the tomato fruit horizontal diameter and vertical diameter, respectively. Vertical/horizontal ratio (also called fruit shape index) is calculated as vertical diameter divided by horizontal diameter. Fruit navel angle and fruit top angle are the angles of the calyx indentation and top protrusion on the vertical section, respectively. They were measured as follows:

1. Find the fruit contour;
2. Use the Douglas-Peucker algorithm (Douglas and Peucker, 1973) to locate the approximate convex points;
3. Find the concave point on the contour that had the largest distance toward the line passing through its two adjacent convex points. This concave point is marked as the fruit navel point (red points in **Figure 1F**);
4. In rare cases, the abovementioned concave point is not the real fruit navel point. Crop the image region between each concave point and the center point of fruit contour. Under HSV color mode, find the concave point that has the lowest saturation in the cropped region. This concave point is the fruit navel point because the region near calyx on the vertical section is whiter than other fruit parts;
5. Find the farthest contour point on the opposite side of the contour. This is the fruit top point;
6. Find two adjacent convex points of both the fruit navel point and the fruit top point. Calculate the fruit navel angle and fruit top angle which are denoted in **Figure 1F**;
7. The top/navel ratio is calculated as fruit top angle divided by fruit navel angle.

Horizontal Cut

The image recognition process for the image of horizontal cut is shown in **Figure 1G**. The locules in tomato fruits were segmented using a deep learning instance segmentation model based on Mask R-CNN (He et al., 2018). The procedures are as follows.

Locules Labeling

Among all cultivars, 335 images of horizontal cut tomato fruits were selected to form a fruit locule image dataset. All locules in the images were manually labeled as polygons using an image annotation tool LabelMe (Russell et al., 2008).

Data Augmentation

Increasing the number of training images by transformation and enhancement techniques is useful to avoid the overfitting and non-convergence of R-CNN algorithms. Images rotating 90, 180, and 270° were appended into the dataset. Vertical and horizontal mirroring of images was also appended into the dataset. Images were resized into 0.1, 0.25, 0.5, 0.8, 2, and 4 times of the raw image size with bilinear interpolation. These images were appended into the dataset to augment image size levels. Besides the above transformation techniques, image blurry was applied as an enhancement technique to improve the model performance on blurred images. All the above mentioned transformed images were processed by Gaussian blurry with 5 × 5 kernel and

TABLE 1 | Tomato samples for image acquisition and phenotyping verification.

Cultivar no.	Fruit color[a]	First harvest/d[b]	Botanical name
No. 405	Green	112.8	*Solanum lycopersicum* L.
No. 459	Yellow	103.2	*Solanum lycopersicum* L. var. cerasiforme (Alef.) Voss
No. 106	Orange	118.0	*Solanum* spp.
No. 68	Orange	129.0	*Solanum lycopersicum* L.
No. 129	Orange	116.3	*Solanum lycopersicum* L.
No. 522	Red	111.2	*Solanum lycopersicum* L.
No. 80	Red	107.6	*Solanum lycopersicum* L.
No. 341	Red	126.2	*Solanum lycopersicum* L.
No. 123	Black	105.6	*Solanum* spp.
No. 113	Black	115.0	*Solanum* spp.

[a] *Fruit color is based on human eye sensory instead of accurate color types.*
[b] *The average number of days between planting and first harvest.*

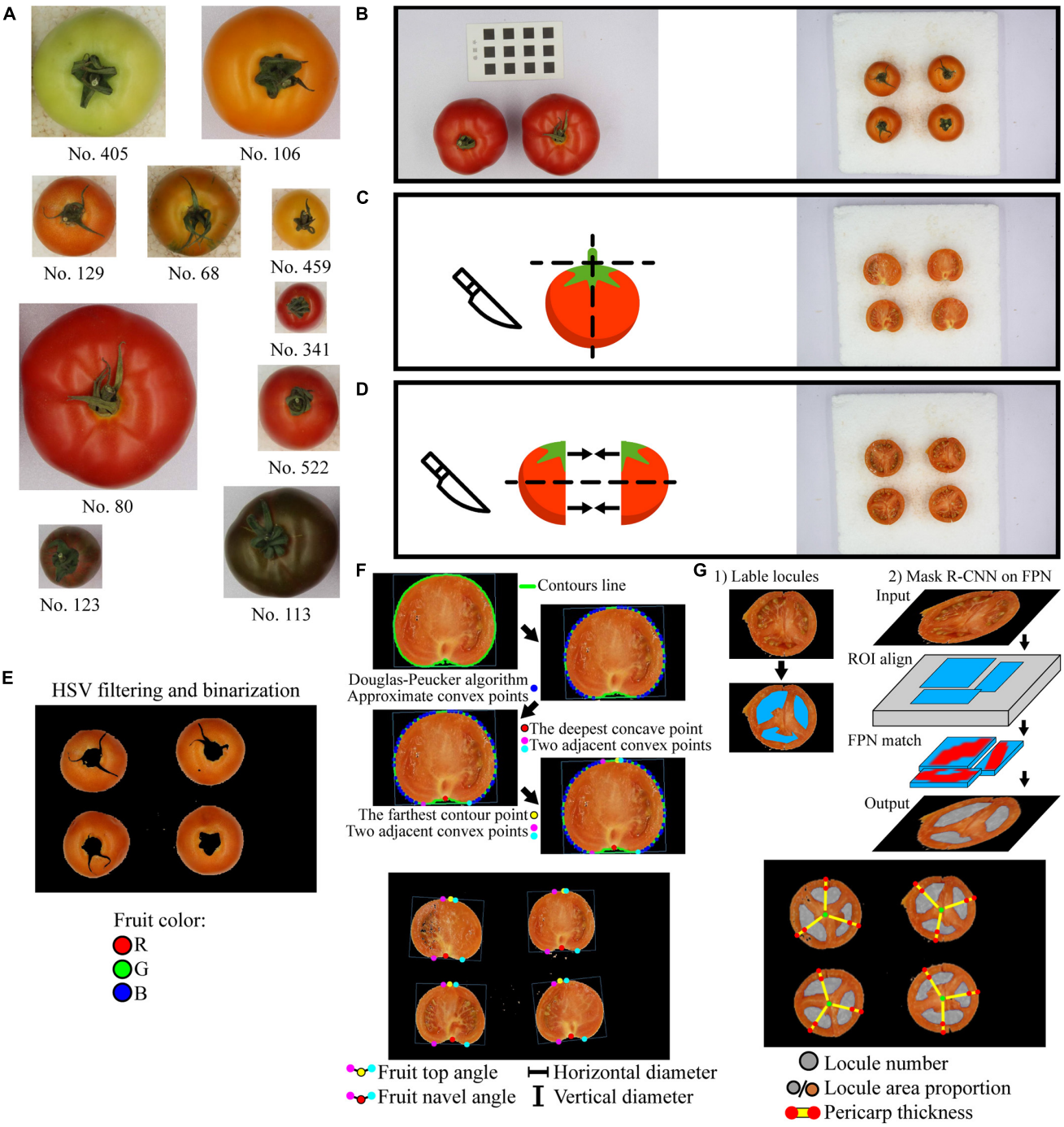


FIGURE 1 | Tomato samples and image acquisition process. **(A)** Tomato samples, images are proportional; **(B)** Image acquisition of ruler card and the intact fruit; **(C)** Image acquisition of the vertical cut; **(D)** Image acquisition of the horizontal cut; the same fruit of vertical cut is cut then joint the corresponding horizontal parts together. **(E)** The extraction of the fruit average color Red, Green, and Blue (R, G, B) values from the intact fruit images; **(F)** Fruit top angle, fruit navel angle, horizontal diameter, and vertical diameter extraction from the vertical cut images; the red, yellow, magenta, and cyan points are the navel point, the top point, the left, and the right adjacent convex points, respectively; **(G)** Fruit locule number, locule area proportion, and pericarp thickness extraction from the horizontal cut images; the gray and orange circles refer to the locule segmentation and the horizontal cut section, the green points are the center of the horizontal cut section, and the red points are the intersections of the lines and the edges.

appended into the dataset. The number of the image dataset was increased to 8,040 after the abovementioned augmentation methods. The dataset was then divided into training (5,628 images, 70%), validation (1,608 images, 20%), and testing (804 images, 10%) sets.

Deep Learning Model Training

Mask R-CNN has been wildly applied in fruit detecting (Gao et al., 2020) and segmentation (Liu et al., 2020), but the network model for tomato fruit locule segmentation still needs further training to improve the performance. Feature Pyramid Network (FPN) was implemented to fuse color and texture features into the model (Lin et al., 2017). Region Proposal Network (RPN) was applied to generate region proposals based on the features, which were aligned with the images through the Region of Interest (RoI) Align process (Tang et al., 2018). The model was then constructed by feeding the RoI Aligned features to the convolution layers for segmentation. During training, a positive segmentation was confirmed if Intersection over Union (IoU) is greater than 0.5. The loss function was defined as the sum of the bounding box regression loss. The termination condition is when the loss function value remained consistent or it hit 5,000 iterations.

Deep Learning Model Evaluation

To evaluate the segmentation results, all segmentation results were divided into four types, namely, true positive (TP), true negative (TN), false positive (FP, wrong segmentation), and false negative (FN, missing segmentation). Precision (***P***), recall (***R***), and *F*1-*score* (the harmonic average of ***P*** and ***R***) were defined as follows:

$$\mathbf{P} = \frac{\mathbf{T}P}{\mathbf{T}P+\mathbf{F}P}$$

$$\mathbf{R} = \frac{\mathbf{T}P}{\mathbf{T}P+\mathbf{F}N}$$

$$\mathbf{F1}-\mathbf{s}core = \frac{\mathbf{2}\times\mathbf{P}\times\mathbf{R}}{\mathbf{P}+\mathbf{R}}$$

Since there was only one segmentation class, average precision (***AP***) was defined as the area under the curve plotted with the ***P*** at the vertical axis and the ***R*** at the horizontal axis.

Phenotyping Indicators Extraction

The locule number was consequently the number of locule segmentations after the deep learning model recognition. The locule area proportion was the area proportion of all locule segmentations in one fruit over the corresponding fruit horizontal cut section. For each fruit, a line was drawn through the center of the horizontal cut section and each center of the locule segmentation. Each line intersects the edge of each locule segmentation and the horizontal cut section at a pair of points (red points in **Figure 1F**). Pericarp thickness was thus measured as the average of the lengths between these pairs of points.

Verification

Among all the phenotyping indicators, the tomato fruit horizontal diameter, vertical diameter, pericarp thickness, and locule number could be obtained by direct measurement. Thus, these indicators were manually counted or measured to make a comparison with the results obtained by image recognition. Unequal variance tests (Levene's test) and significance tests were conducted between the results of the manual measurement and the image recognition. The Root Mean Square Error (***RMSE***) was applied to evaluate the accuracy of the image recognition as follows:

$$\mathbf{R}MSE = \sqrt{\frac{\mathbf{1}}{\mathbf{n}}\sum_{\mathbf{i}=\mathbf{1}}^{\mathbf{n}}\left(\frac{\mathbf{R_i}-\mathbf{M_i}}{\mathbf{M_i}}\right)^{\mathbf{2}}}$$

where n represents the number of measurements, R_i represents the image recognition result, and M_i represents the manual result. All statistical calculations and analyses were conducted using the R programming language (version 4.0.5) (R Core Team, 2020). The C# code for the methods is presented in **Supplementary Material** "used_codes.cs."

RESULTS

Tomato Fruit Color

The threshold for HSV filtering and binarization is crucial to tomato fruit color recognition. For green, orange, red, and black tomato fruits, as sorted in colors in **Figure 2**, the H thresholds for HSV filtering keep the same while S and V thresholds change in a range of 30–130. However, the S threshold varies in a minimal range from 100 to 120, and the V threshold stays the same at 100 for most samples, except that the black tomatoes (No. 113, No. 123) need S and V thresholds of 30 and 130, and No. 68, which has mottle on the surface, needs S thresholds of 60. This suggests that there are certain S and V threshold combinations for the HSV filtering and binarization of pure color and black tomatoes. Since No. 68 is the only mottled tomatoes found among all cultivars, the S and V threshold combination (120, 60) should be considered as a simple case. Notably, the sepal and calyx are also marked as background and removed, and this is designed in the HSV filtering and binarization process so that the sepal and calyx do not influence the extraction of the fruit color R, G, and B values. As is shown in **Figure 2**, the fruit average color is objective and in accordance with the human eye sensory observation, suggesting that the fruit color obtained by image recognition is reliable and not subjected to human judgment. The detailed fruit color R, G, and B values are listed in **Supplementary Table 1**.

Performance of Phenotyping From Vertical Cut Images

The measurements of the tomato fruit vertical diameter and horizontal diameter were verified. The results are shown in **Figures 3A,B**. The results show that the measurements based on image recognition accord with the manual measurements. No. 80 has the largest horizontal and vertical diameter. No. 341 and No. 459 have the shortest horizontal and vertical diameter, respectively. The vertical diameter of No. 341 and No. 459 are quite close, which accord with the proportional images in **Figure 1A**. Significance tests suggest that there are no significant differences between the results of image recognition

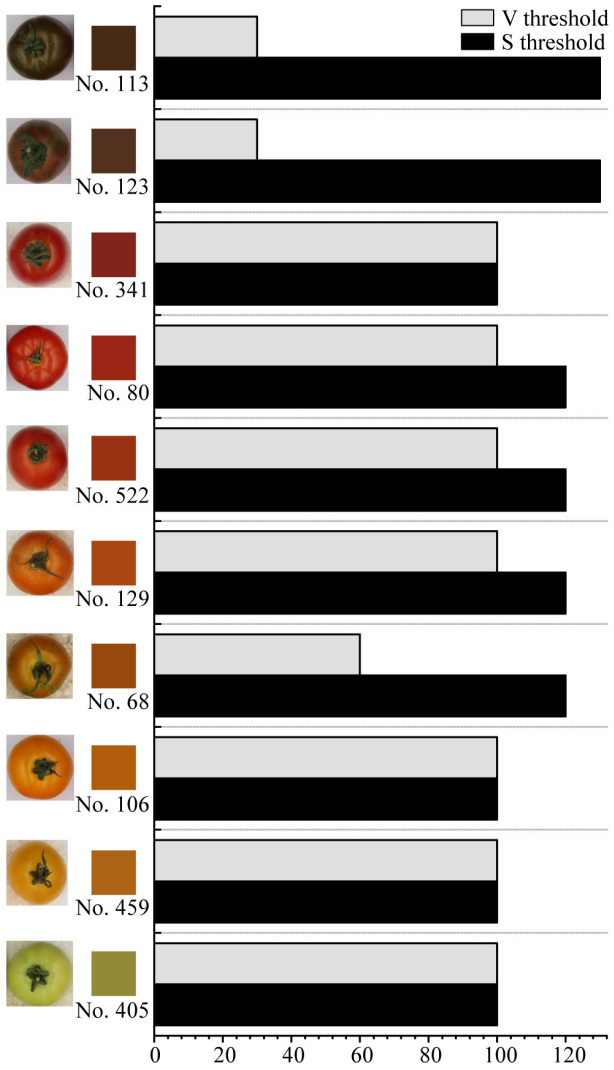


FIGURE 2 | Fruit average colors and thresholds for Hue-Saturation-Value (HSV) filtering and binarization of the intact fruit images. The square beside each tomato fruit image shows the fruit average color in RGB mode. Fruit images are not proportional.

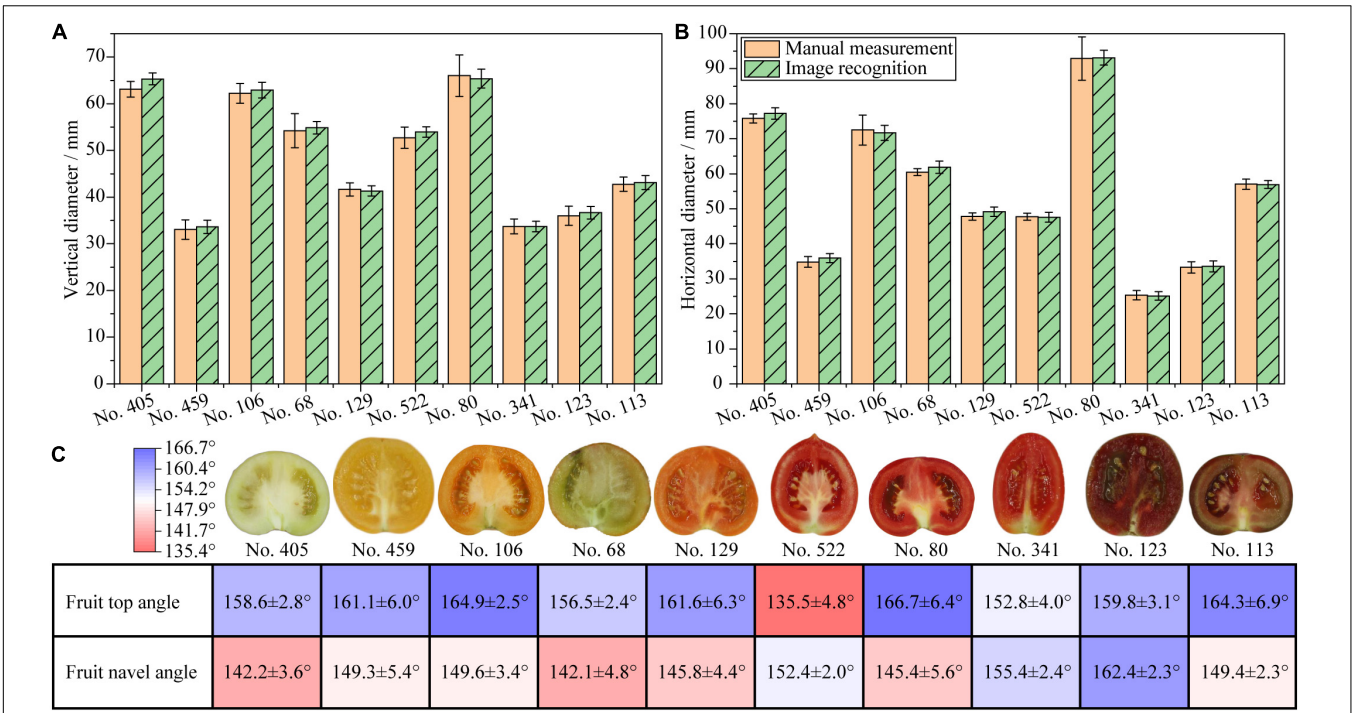
and manual measurements in the same sample. The RMSE values of the vertical and horizontal diameter measurements are 0.016 and 0.017, respectively, which are less than 0.100, an empirical threshold of RMSE determining the accuracy of measurement results. In addition, the Pearson's correlation R^2 between the image recognition and the manual measurements is greater than 0.99. These indicate that the accuracy of the image recognition measurement is equivalent to that of manual measurement. The unequal variance test indicates homogeneous variances between the results of the manual measurement and the image recognition (p = 0.265), indicating that the variances between image recognition and manual measurements are equal. This implies that the fruit vertical and horizontal diameter measurements by image recognition are as precise as manual measurements.

The results of fruit top and navel angles are shown in **Figure 3C**. Large fruit top angles indicate flat fruit top shape, whereas small fruit top angles indicate sharp protruding fruit top shape. Large fruit navel angles indicate flat fruit navel shape, whereas small fruit navel angles indicate deep indented or concave fruit navel shape. Among all samples, No. 522 has the smallest fruit top angle, which is due to the sharp protrusion on the fruit topside. No. 80 has the largest fruit top angle in accordance with the smooth and flat shape on the fruit topside. Fruit top angles of all samples except No. 522 are larger than 150°, which accord with the sensory judgment. No. 405 has the smallest fruit navel angle among all samples as the indentation on the fruit navel side is quite deep. No. 123 has the largest fruit navel angle as the indentation on the fruit navel side is quite shallow. For most samples, the fruit navel angles are smaller than the fruit top angles as expected, except that No. 522, 341, and 123 show the opposite pattern. Although the fruit top and navel angles are difficult to measure manually, the results accord quite close with the sensory judgment. Therefore, the fruit top and navel angles by image recognition are feasible to reflect the tomato fruit top and navel phenotypes quantitatively. Detailed fruit lengths and angles data are listed in **Supplementary Table 1**.

Performance of Phenotyping From Horizontal Cut Images

The number of iterations has an impact on the training results of deep learning models. The training and validation datasets had closely identical variation trends, indicating that the model was not overfitted with the parameters chosen during the validation procedure. The loss value reduces as the number of iterations increases, but it remains rather consistent as the number of iterations hits 4,000, and it progressively approaches the minimum value of 0.1505. The results show that the Mask R-CNN used in this model can learn the features efficiently and converge rapidly, indicating that it has the potential to accomplish the required objectives. The detailed loss curves of the training and validation sets for 5,000 iterations are shown in **Supplementary Figure 1A**.

When evaluating the performance of a model, both recall and precision are critical. As recall increases, the precision decreases, but the precision of an outperforming model keeps a high level as recall increases, implying the model will segment a large majority of TP before detecting FP. Thus, the *F1-score*, the harmonic average of precision and recall, is used to evaluate the model performance. Values between 0 and 1 are set as various thresholds. Segmentations having a prediction probability larger than the threshold are considered positive. The *F1-score* reaches the maximum of 0.8620 when the threshold is 0.6, implying that 0.6 is a trade-off that balances the precision and recall and maximizes the performance of the model. The AP is 0.8753, implying that the segmented locule areas match the true locule areas more than 87.53% of the circumstances. When the threshold is 0.9, the AP is 0.8107 (greater than 0.8). This indicates that the model based on Mask R-CNN has high accuracy. The trajectories of the *F1-score* at various thresholds are shown in **Supplementary Figure 1B**.



	No. 405	No. 459	No. 106	No. 68	No. 129	No. 522	No. 80	No. 341	No. 123	No. 113
Fruit top angle	158.6±2.8°	161.1±6.0°	164.9±2.5°	156.5±2.4°	161.6±6.3°	135.5±4.8°	166.7±6.4°	152.8±4.0°	159.8±3.1°	164.3±6.9°
Fruit navel angle	142.2±3.6°	149.3±5.4°	149.6±3.4°	142.1±4.8°	145.8±4.4°	152.4±2.0°	145.4±5.6°	155.4±2.4°	162.4±2.3°	149.4±2.3°

FIGURE 3 | Verification of phenotyping indicators from fruit vertical cut images. **(A)** Vertical diameters of tomato fruits; **(B)** Horizontal diameters of tomato fruits; **(C)** Fruit top and navel angles, fruit images are not proportional.

The measurements of tomato fruit locule number and pericarp thickness were verified and presented in **Figure 4**. Blue regions represent the locule segmentation by the deep learning segmentation model. The results suggest that the model can accurately segment locule areas from the fruit horizontal cut images after training. Color, fruit size, and seeds have barely influenced the model segmentation performance. No. 106 and No. 80 in **Figure 4A** indicate that small locules which are not fully formed in the fruit can also be segmented by the model. The locule counting results in **Table 2** show that locule counted by the deep learning segmentation model is promising, suggesting that the model can automatically count the fruit locule number with perfect accuracy. The only wrongly counted cultivar among all samples is No. 459, which is also difficult for manual counting due to its small fruit size and hazy septum.

The results in **Figure 4B** show that the pericarp thickness measurements based on image recognition accord with the manual measurements. No. 80 and No. 123 have the thickest and thinnest fruit pericarp, respectively. The thickness of No. 68 and No. 129 are quite close in accordance with the sensory judgment. Significance tests suggest that there are no significant differences between the pericarp thickness by image recognition and manual measurements in the same sample. The RMSE of the pericarp thickness measurement is 0.024, which is less than 0.100, indicating high accuracy of image recognition measurement. In addition, the Pearson's correlation R^2 between the image recognition and the manual measurements is greater than 0.99. This indicates that the accuracy of the pericarp thickness measurement by image recognition is equivalent to that of manual measurement. The unequal variance test indicates homogeneous variances between the results of the manual measurement and the image recognition (p = 0.303), indicating that the variances between image recognition and manual measurements are equal. This implies that the pericarp thickness measurements by image recognition are as precise as manual measurements.

The results of fruit locule area proportion are shown in **Figure 4C**. A larger locule area proportion indicates a larger locule volume proportion in the fruit. Among all samples, No. 459 and No. 68 have the largest and smallest locule area proportion, respectively. No. 129 has a larger locule area proportion than No. 106. The locule area proportions of No. 522 and No. 341 are quite close. These all accord with the sensory judgment from the fruit images. Although the fruit locule area proportions are difficult to measure manually, the results accord quite close with the sensory judgment. Therefore, the fruit locule area proportions measured by the deep learning segmentation model can quantitatively represent tomato fruit locule phenotypes. Detailed fruit locule number, locule area proportion, and pericarp thickness data are listed in **Supplementary Table 1**.

DISCUSSION

This study proposed a combination of image recognition and deep learning segmentation methods to extract several important tomato fruit phenotypes quantitatively. The manual measuring

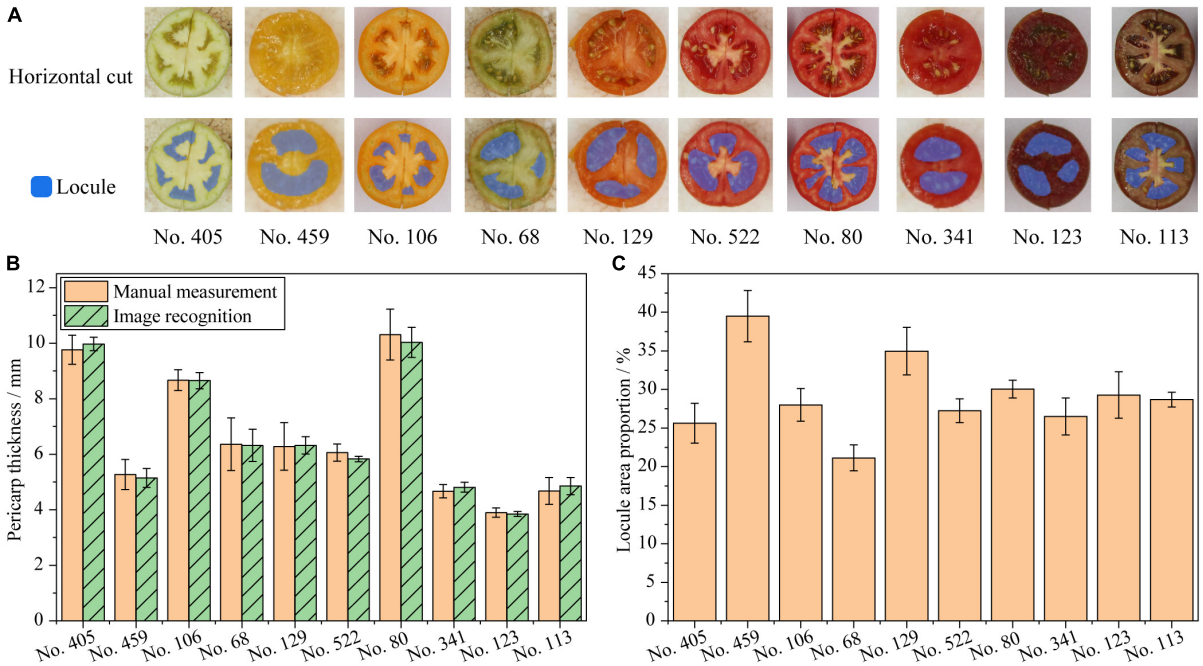


FIGURE 4 | Verification of phenotyping indicators from fruit horizontal cut images. **(A)** Fruit locule segmentation, fruit images are not proportional; **(B)** Pericarp thickness of tomato fruits; **(C)** Locule area proportions of tomato fruits.

of these phenotypes is essential for tomato breeding but is time-consuming. The proposed combination of methods can reduce the operating steps of tomato fruit phenotyping and increase the measurement accuracy, which greatly reduces the phenotyping time consumption. The HSV filtering and binarization process is applicable to isolate most pure color and black tomato fruits from the white background with a respective combination of S and V thresholds, which meets the requirement in most cases. Mottled tomato fruits use a different combination of S and V thresholds, but such cultivars are uncommon. Considering black tomato fruits do not fit the black background, blue might be a more general background color for tomato fruit phenotyping because blue or similar colored fruits are not found among all cultivars in this study or other studies (Merk et al., 2012). In addition, the images of intact tomato fruits are taken from the navel side instead of from the top side. This is because the shape, size, and other aspects of the sepals are also important phenotypes that require further analysis. The navel side images of intact tomato fruits include both extractable fruit and sepal phenotypes, which could investigate more phenotypes without increasing the number of images per tomato cultivar.

Based on the horizontal and vertical diameter and the navel and top angle, their corresponding ratios are also important fruit phenotypes, i.e., vertical/horizontal ratio and top/navel ratio. All cultivars are plotted with the top/navel ratio at the vertical axis and the vertical/horizontal ratio at the horizontal axis in **Figure 5A**. Most cultivars have a top/navel ratio between 0.9 and 1.3 and also a vertical/horizontal ratio between 0.7 and 1.0, indicating most tomato fruits have a longer horizontal diameter and a larger top angle. Although all samples have a linear trend

TABLE 2 | Tomato samples for image acquisition and phenotyping verification.

Cultivar no.	Average locule number per fruit[a]	
	Manual count	Deep learning segmentation
No. 405	4.25	4.25
No. 459	1.50	1.25
No. 106	3.50	3.50
No. 68	2.50	2.50
No. 129	3.00	3.00
No. 522	2.50	2.50
No. 80	4.50	4.50
No. 341	2.00	2.00
No. 123	2.50	2.50
No. 113	4.50	4.50

[a] *The averages are based on all tomato fruits in one horizontal cut image.*

in the plot (R^2 = 0.6995), all cultivars do not fit a specific trend, indicating that the top/navel ratio does not correlate with the vertical/horizontal ratio. Several cultivars are shown in **Figure 5A** to represent the sensory differences.

To increase locule segmentation performance, the deep learning model applied the feature mapping strategy (Gupta, 2014) to merge color and texture features in the FPN structure when training the Mask R-CNN. In this study, tomato fruits with different colors, sizes, and locule shapes were tested to evaluate the locule segmentation performance of the deep learning model. The tomato fruit locules are separately located on one surface in the images, thus overlapping and occluding do not occur in

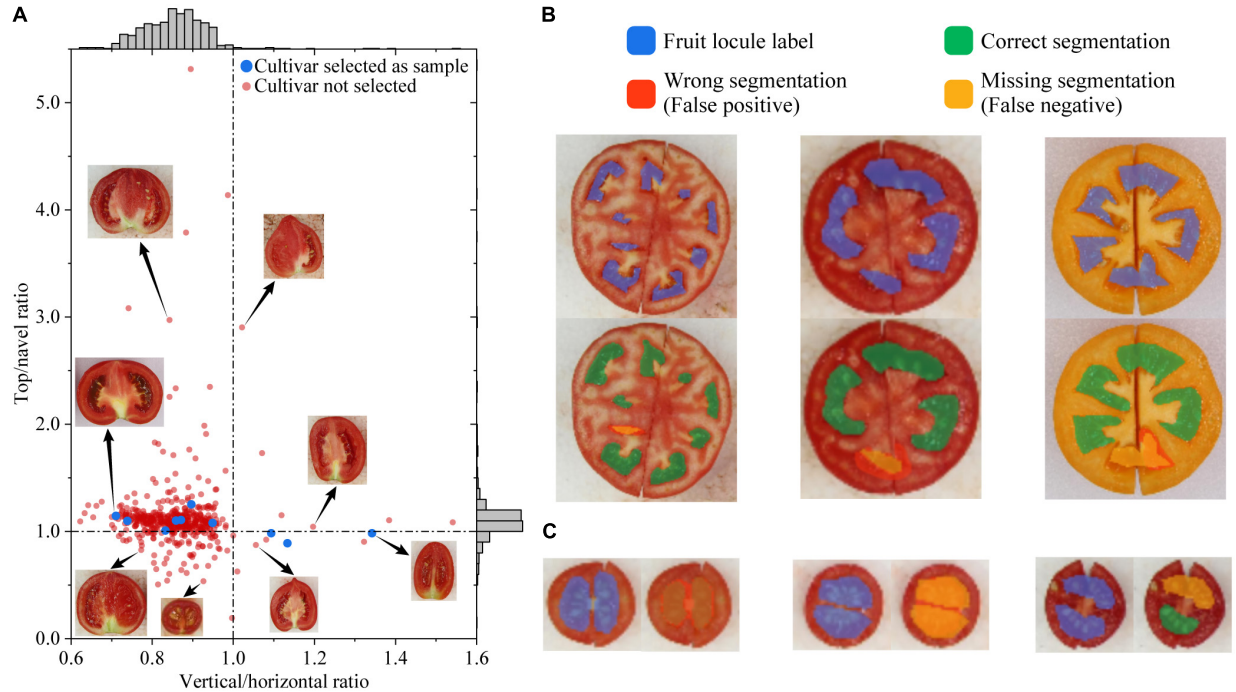


FIGURE 5 | Evaluation of tomato fruit phenotyping indicators and fruit locule segmentation. **(A)** Distribution of top/navel ratio against horizontal/vertical ratio among cultivars; the dashed line refers to the corresponding value equals one; **(B)** Incorrect segmentation cases that do the correct locule counting; **(C)** Incorrect segmentation cases caused by hazy septum. Fruit images are not proportional.

these scenarios. However, the deep learning model recognizes mainly two types of incorrect segmentations: ones that do the correct locule counting and ones that are caused by a hazy septum (**Figures 5B,C**). In the first type, one obstacle to locule segmentation is the slit between two joint parts of fruit cut. As shown in **Figure 4A**, although the fruit parts are joined together before taking the horizontal cut images, the slit between two joint parts does not influence the segmentation performance. Still, the only incorrect segmentation caused by the slit is shown on the right in **Figure 5B**, where the slit has passed through the locule. This implies that the fruit parts should be joined together closely or cut another fruit before taking the horizontal cut images. **Figure 5B** left and middle also shows representative incorrect segmentations that are partly correct and do the correct counting. Such cases do not miss any locules but still be recognized as missing segmentation due to the low IoU, yet they should be considered as correct in practice (Tripodi et al., 2018). In the second type, the most common incorrect segmentation cases are shown in **Figure 5C**. The tomato fruits in these cases all have small horizontal diameters and hazy septum. Manual labeling is difficult and unreliable for these cases, which could be the reason for wrong and missing segmentations. In practice, the locule number of such fruit is not essential and could be considered as one, whereas the recognition results of locule area proportion and pericarp thickness could be considered correct. With the abovementioned correct counting cases (except **Figure 5B** right) and hazy septum cases modified as correct, the AP is 0.9564 when the threshold is 0.6, indicating that the model is quite promising for tomato fruit locule segmentation and outperforms other image recognition methods. The results also indicate that the model is robust to segment fruit locules with different colors, sizes, and locule shapes. Compared with *Tomato Analyzer* (Gonzalo et al., 2009) and *LocAnalyzer* (Spetale et al., 2020), the advantage of the proposed methods is the ability to measure pericarp thickness, locule number, and area automatically. Moreover, the locule segmentation model increases the phenotyping efficiency by processing multi-fruit images instead of scanning one fruit each time, while still having a similar or even higher AP than *LocAnalyzer*.

The collection and analysis of phenotypes in a consistent manner is requisite for plant phenomics research (Song et al., 2021). Current crop phenotyping systems apply high-throughput techniques to capture numerous phenotypes automatically, and the accuracy of these procedures is steadily increasing (Zhang et al., 2021). The proposed combination of methods can automatically collect a group of tomato fruit phenotypes from a set of tomato fruit images. The results of the verification indicate that the locule number is reliably counted, and the locule area proportion is quantitatively defined. The fruit horizontal and vertical diameter, top and navel angle, and pericarp thickness are also accurately recognized. Furthermore, the proposed combination of methods may considerably minimize manual observation workloads and make cultivar investigation during tomato breeding more time-efficient. Operation mistakes during manual measurement can also be prevented. Besides, the efficiency and accuracy during the investigation of tomato fruit

phenotypes are greatly improved, particularly when assessing fruit locule number and area proportion.

In terms of the image acquisition method, all the fruit images are taken with a fixed focal length in a constant illumination condition, and the color space values are utilized to describe the fruit color, allowing the tomato fruit color to be shown quantitatively under the same standard. Nevertheless, the juice of the tomato fruit cut parts is likely to contaminate the background in practice, which requires cleaning up before taking each image. Based on the phenotyping demand and barriers in tomato breeding, this study proposed a quantitative and high-throughput phenotyping tool that integrates fruit processing, image acquisition, and phenotypes extraction. The tool is proved feasible and promising and has significant implications for the phenotypes evaluation of tomato fruit (Kim et al., 2021). Since tomato is the model species of fruit development studies, the methodology could also be extended to other fruit crops.

It is important for omics research to assess the tomato fruit phenotypes with a consistent and quantitative phenotyping tool based on image recognition and deep learning segmentation. Such consistent and quantitative phenotype data could also aid tomato genomic, metabolomic, and transcriptomic investigations. For example, studies have found several QTLs that control tomato fruit morphological shape and locule number (Illa-Berenguer et al., 2015; Barraj et al., 2021). Quantitative phenotyping tools also allow researchers to delve deeper into the mechanisms behind the formation of certain traits in tomato fruit at the genetic level (Marefatzadeh-Khameneh et al., 2021). Research on the association network analysis between tomato fruit color and metabolic pathways would possibly be accelerated further as well (Hu et al., 2020; Yuan et al., 2021).

CONCLUSION

In this study, a combination of image recognition and deep learning model is proposed to extract tomato fruit phenotypes quantitatively and automatically. First, images of intact tomatoes, vertical cut fruits, and horizontal cut fruits were acquired under a constant illumination condition. Second, the method based on image recognition isolated fruits from the background and extract fruit color, vertical/horizontal diameters, and top/navel angles from the images of intact tomatoes and vertical cut. Finally, the deep learning model based on Mask R-CNN was trained and tested to segment locules from the images of horizontal cut. The locule number, locule area proportion, and pericarp thickness were thus extracted automatically. The proposed combination of methods improves the efficiency and accuracy of tomato fruit phenotyping. The proposed deep learning model segments tomato fruit locules with high average precision, implying that the whole combination of methods is a promising tool to evaluate tomato fruit phenotypes thoroughly. In conclusion, the results of this study provide technical support for the quantitative analysis and evaluation of tomato fruit phenotyping, which is important for tomato breeding. Furthermore, the methodology could be extended to the phenotyping of other fruit crops.

DATA AVAILABILITY STATEMENT

The original contributions presented in the study are included in the article/**Supplementary Material**, further inquiries can be directed to the corresponding authors.

AUTHOR CONTRIBUTIONS

YZu and YC conceived and designed the concept and methodology. HW, RW, and YC prepared the tomato fruits and other materials. QG, YZa, and YC conducted the experiments. YZu and XZ realized the algorithms and methods, analyzed the data, and prepared the figures and tables. YZu wrote the manuscript. YC and XZ supervised the manuscript and made valuable inputs. All authors read and approved the submission of the manuscript.

FUNDING

This research was partially supported by the Key Research and Development Program of Zhejiang (2021C02052), National Natural Science Foundation of China (32172555), National Key Research and Development Program of China (2018YFD1000800), Zhejiang Provincial Agricultural (Vegetable) New Variety Breeding Project (2021C02065), State Key Laboratory Breeding Base for the Zhejiang Sustainable Pest and Disease Control (2010DS700124-ZZ1903), and China Agriculture Research System of MOF and MARA (CARS-23-G44).

ACKNOWLEDGMENTS

We are grateful for the help from Chen Zhang, Jerry Zhang, Baoliang Xie, and their colleagues in ZAAS for labeling the image datasets.

SUPPLEMENTARY MATERIAL

The Supplementary Material for this article can be found online at: https://www.frontiersin.org/articles/10.3389/fpls.2022.859290/full#supplementary-material

REFERENCES

Alam, P., Balawi, T. H., Altalayan, F. H., Hatamleh, A. A., Ashraf, M., et al. (2021). Silicon attenuates the negative effects of chromium stress in tomato plants by modifying antioxidant enzyme activities, ascorbate–glutathione cycle and glyoxalase system. *Acta Physiol. Plant.* 43:110. doi: 10.1007/s11738-021-03276-4

Barraj, B. R., Segado, P., Moreno-González, R., Heredia, A., Fernández-Muñoz, R., et al. (2021). Genome-wide qtl analysis of tomato fruit cuticle deposition and composition. *Horticulture Research* 8:113. doi: 10.1038/s41438-021-00548-5

Bhatta, M., Sandro, P., Smith, M. R., Delaney, O., Voss-Fels, K. P., Gutierrez, L., et al. (2021). Need for speed: manipulating plant growth to accelerate breeding cycles. *Curr. Opin. Plant Biol.* 60:101986. doi: 10.1016/j.pbi.2020.101986

Boogaard, F. P., Rongen, K. S. A. H., and Kootstra, G. W. (2020). Robust node detection and tracking in fruit-vegetable crops using deep learning and multi-view imaging. *Biosyst. Eng.* 192, 117–132. doi: 10.1016/j.biosystemseng.2020.01.023

Caseiro, M., Ascenso, A., Costa, A., Creagh-Flynn, J., Johnson, M., and Simões, S. (2020). Lycopene in human health. *LWT* 127:109323. doi: 10.1016/j.lwt.2020.109323

Celik, I., Gurbuz, N., Uncu, A. T., Frary, A., and Doganlar, S. (2017). Genome-wide snp discovery and qtl mapping for fruit quality traits in inbred backcross lines (ibls) of solanum pimpinellifolium using genotyping by sequencing. *BMC Genomics* 18:1. doi: 10.1186/s12864-016-3406-7

Costa, C., Schurr, U., Loreto, F., Menesatti, P., and Carpentier, S. (2018). Plant phenotyping research trends, a science mapping approach. *Front. Plant Sci.* 9:1933. doi: 10.3389/fpls.2018.01933

Darrigues, A., Hall, J., van der Knaap, E., Francis, D. M., and Dujmovic, N. (2008). Tomato analyzer-color test: a new tool for efficient digital phenotyping. *J. Amer. Soc. Hort. Sci.* 133, 579–586. doi: 10.21273/JASHS.133.4.579

De Corato, U. (2020). Improving the shelf-life and quality of fresh and minimally-processed fruits and vegetables for a modern food industry: a comprehensive critical review from the traditional technologies into the most promising advancements. *Crit. Rev. Food Sci.* 60, 940–975. doi: 10.1080/10408398.2018.1553025

Douglas, D. H., and Peucker, T. K. (1973). Algorithms for the reduction of the number of points required to represent a digitized line or its caricature. *Cartogr. Int. J. Geogr. Inform. Geovis.* 10, 112–122. doi: 10.3138/FM57-6770-U75U-7727

Faizan, M., Bhat, J. A., Noureldeen, A., Ahmad, P., and Yu, F. (2021). Zinc oxide nanoparticles and 24-epibrassinolide alleviates cu toxicity in tomato by regulating ros scavenging, stomatal movement and photosynthesis. *Ecotox. Environ. Safe* 218:112293. doi: 10.1016/j.ecoenv.2021.112293

Gao, F., Fu, L., Zhang, X., Majeed, Y., and Li, R. (2020). Multi-class fruit-on-plant detection for apple in snap system using faster r-cnn. *Comput. Electron. Agr.* 176:105634. doi: 10.1016/j.compag.2020.105634

Gonzalo, M. J., Brewer, M. T., Anderson, C., Sullivan, D., and Gray, S. (2009). Tomato fruit shape analysis using morphometric and morphology attributes implemented in tomato analyzer software program. *J. Am. Soc. Hortic. Sci.* 134, 77–87. doi: 10.21273/JASHS.134.1.77

Gupta, S. A. G. R. (2014). "Learning rich features from rgb-d images for object detection and segmentation," in *European conference on computer vision*, eds D. Fleet, T. Pajdla, B. Schiele, and T. Tuytelaars (Cham: Springer), 345–360. doi: 10.1007/978-3-319-10584-0_23

He, K., Gkioxari, G., Dollár, P., and Girshick, R. (2018). *Mask r-cnn*. Ithaca:NY: Cornell University, doi: arXiv:1703.06870v3

Hu, S., Liu, L., Li, S., Shao, Z., and Meng, F. (2020). Regulation of fruit ripening by the brassinosteroid biosynthetic gene slcyp90b3 via an ethylene-dependent pathway in tomato. *Hortic. Res.* 7:163. doi: 10.1038/s41438-020-00383-0

Illa-Berenguer, E., Van Houten, J., Huang, Z., and van der Knaap, E. (2015). Rapid and reliable identification of tomato fruit weight and locule number loci by qtl-seq. *Theor. Appl. Genet.* 128, 1329–1342. doi: 10.1007/s00122-015-2509-x

Kaya, C., Sarıoğlu, A., Ashraf, M., Alyemeni, M. N., and Ahmad, P. (2020). Gibberellic acid-induced generation of hydrogen sulfide alleviates boron toxicity in tomato (*Solanum lycopersicum* l.) Plants. *Plant Physiol. Bioch* 153, 53–63. doi: 10.1016/j.plaphy.2020.04.038

Kim, M., Jung, J., Shim, E., Chung, S., Park, Y., Lee, G. P., et al. (2021). Genome-wide snp discovery and core marker sets for dna barcoding and variety identification in commercial tomato cultivars. *Sci. Hortic. Amsterdam* 276:109734. doi: 10.1016/j.scienta.2020.109734

Kinkade, M. P., and Foolad, M. R. (2013). Validation and fine mapping of lyc12.1, a qtl for increased tomato fruit lycopene content. *Theor. Appl. Genet.* 126, 2163–2175. doi: 10.1007/s00122-013-2126-5

Li, Z., Guo, R., Li, M., Chen, Y., and Li, G. (2020). A review of computer vision technologies for plant phenotyping. *Comput. Electron. Agr.* 176, 105672. doi: 10.1016/j.compag.2020.105672

Lin, T., Dollár, P., Girshick, R., He, K., Hariharan, B., and Belongie, S. (2017). "Feature pyramid networks for object detection," in *Proceeding of the 2017 IEEE Conference on Computer Vision and Pattern Recognition (CVPR)*, (Honolulu, HI), 936–944. doi: 10.1109/CVPR.2017.106

Liu, X., Hu, C., and Li, P. (2020). Automatic segmentation of overlapped poplar seedling leaves combining mask r-cnn and dbscan. *Comput. Electron. Agr.* 178:105753. doi: 10.1016/j.compag.2020.105753

Ma, Y., Yu, D., Wu, T., and Wang, H. (2019). Paddlepaddle: an open-source deep learning platform from industrial practice. *Front. Data Comput.* 1, 105–115. doi: 10.11871/jfdc.issn.2096.742X.2019.01.011

Marefatzadeh-Khameneh, M., Fabriki-Ourang, S., Sorkhilalehloo, B., Abbasi-Kohpalekani, J., and Ahmadi, J. (2021). Genetic diversity in tomato (*Solanum lycopersicum* l.) Germplasm using fruit variation implemented by tomato analyzer software based on high throughput phenotyping. *Genet. Resour. Crop Ev.* 68, 2611–2625. doi: 10.1007/s10722-021-01153-0

Mata-Nicolás, E., Montero-Pau, J., Gimeno-Paez, E., Garcia-Carpintero, V., Ziarsolo, P., Menda, N., et al. (2020). Exploiting the diversity of tomato: the development of a phenotypically and genetically detailed germplasm collection. *Hortic. Res.* 7:66. doi: 10.1038/s41438-020-0291-7

Merk, H. L., Yarnes, S. C., Van Deynze, A., Tong, N., Menda, N., Lukas, A., et al. (2012). Trait diversity and potential for selection indices based on variation among regionally adapted processing tomato germplasm. *J. Am. Soc. Hortic. Sci.* 137, 427–437. doi: 10.21273/JASHS.137.6.427

Oltman, A. E., Jervis, S. M., and Drake, M. A. (2014). Consumer attitudes and preferences for fresh market tomatoes. *J. Food Sci.* 79, S2091–S2097. doi: 10.1111/1750-3841.12638

Pereira, L., Zhang, L., Sapkota, M., Ramos, A., Razifard, H., Caicedo, A. L., et al. (2021). Unraveling the genetics of tomato fruit weight during crop domestication and diversification. *Theor. Appl. Genet.* 134, 3363–3378. doi: 10.1007/s00122-021-03902-2

Prudent, M., Causse, M., Génard, M., Tripodi, P., Grandillo, S., Bertin, N., et al. (2009). Genetic and physiological analysis of tomato fruit weight and composition: influence of carbon availability on qtl detection. *J. Exp. Bot.* 60, 923–937. doi: 10.1093/jxb/ern338

R Core Team (2020). *R: A language and environment for statistical computing*. Vienna: R Core Team.

Russell, B. C., Torralba, A., Murphy, K. P., and Freeman, W. T. (2008). Labelme: a database and web-based tool for image annotation. *Int. J. Comput. Vision* 77, 157–173. doi: 10.1007/s11263-007-0090-8

Sierra-Orozco, E., Shekasteband, R., Illa-Berenguer, E., Snouffer, A., van der Knaap, E., Lee, T. G., et al. (2021). Identification and characterization of globe, a major gene controlling fruit shape and impacting fruit size and marketability in tomato. *Hortic. Res.* 8:138. doi: 10.1038/s41438-021-00574-3

Song, P., Wang, J., Guo, X., Yang, W., and Zhao, C. (2021). High-throughput phenotyping: breaking through the bottleneck in future crop breeding. *Crop J.* 9, 633–645. doi: 10.1016/j.cj.2021.03.015

Spetale, F. E., Murillo, J., Vazquez, D. V., Cacchiarelli, P., Rodríguez, G. R., Cacchiarelli, P., et al. (2020). Locanalyzer: a computer vision method to count locules in tomato fruits. *Comput. Electron. Agr.* 173:105382. doi: 10.1016/j.compag.2020.105382

Tamasi, G., Pardini, A., Bonechi, C., Donati, A., Pessina, F., Marcolongo, P., et al. (2019). Characterization of nutraceutical components in tomato pulp, skin and locular gel. *Eur. Food Res. Technol.* 245, 907–918. doi: 10.1007/s00217-019-03235-x

Tang, P., Wang, X., Wang, A., Yan, Y., Liu, W., et al. (2018). "Weakly supervised region proposal network and object detection," in *Proceedings of the European conference on computer vision (ECCV)*, (Munich), 352–368. doi: 10.1007/978-3-030-01252-6_22

The Tomato Genome Consortium (2012). The tomato genome sequence provides insights into fleshy fruit evolution. *Nature* 485, 635–641. doi: 10.1038/nature11119

Tripodi, P., Massa, D., Venezia, A., and Cardi, T. (2018). Sensing technologies for precision phenotyping in vegetable crops: current status and future challenges. *Agronomy* 8:57. doi: 10.3390/agronomy8040057

Wallace, J. G., Rodgers-Melnick, E., and Buckler, E. S. (2018). On the road to breeding 4.0: unraveling the good, the bad, and the boring of crop quantitative

genomics. *Annu. Rev. Genet.* 52, 421–444. doi: 10.1146/annurev-genet-120116-024846

Washburn, J. D., Mejia-Guerra, M. K., Ramstein, G., Kremling, K. A., Valluru, R., Buckler, E. S., et al. (2019). Evolutionarily informed deep learning methods for predicting relative transcript abundance from dna sequence. *Proc. Natl. Acad. Sci.* 116, 5542–5549. doi: 10.1073/pnas.1814551116

Yuan, J., Li, S., Cheng, J., Guo, C., Shen, C., He, J., et al. (2021). Potential role of methanogens in microbial reductive dechlorination of organic chlorinated pollutants *in situ*. *Environ. Sci. Technol.* 55, 5917–5928. doi: 10.1021/acs.est.0c08631

Zhang, X., Zhu, Y., Su, Y., Xie, B., Gu, Q., Zheng, K., et al. (2021). Quantitative extraction and analysis of pear fruit spot phenotypes based on image recognition. *Comput. Electron. Agr.* 190:106474. doi: 10.1016/j.compag.2021.106474

Zhu, G., Wang, S., Huang, Z., Zhang, S., Liao, Q., Zhang, C., et al. (2018). Rewiring of the fruit metabolome in tomato breeding. *Cell* 172, 249–261. doi: 10.1016/j.cell.2017.12.019

Conflict of Interest: The authors declare that the research was conducted in the absence of any commercial or financial relationships that could be construed as a potential conflict of interest.

Publisher's Note: All claims expressed in this article are solely those of the authors and do not necessarily represent those of their affiliated organizations, or those of the publisher, the editors and the reviewers. Any product that may be evaluated in this article, or claim that may be made by its manufacturer, is not guaranteed or endorsed by the publisher.

Copyright © 2022 Zhu, Gu, Zhao, Wan, Wang, Zhang and Cheng. This is an open-access article distributed under the terms of the Creative Commons Attribution License (CC BY). The use, distribution or reproduction in other forums is permitted, provided the original author(s) and the copyright owner(s) are credited and that the original publication in this journal is cited, in accordance with accepted academic practice. No use, distribution or reproduction is permitted which does not comply with these terms.

frontiers | Frontiers in Plant Science

ORIGINAL RESEARCH
published: 02 May 2022
doi: 10.3389/fpls.2022.860656

Deep Learning and Hyperspectral Images Based Tomato Soluble Solids Content and Firmness Estimation

*Yun Xiang[1], Qijun Chen[1], Zhongjing Su[1], Lu Zhang[1], Zuohui Chen[1], Guozhi Zhou[2], Zhuping Yao[2], Qi Xuan[1] and Yuan Cheng[2]**

[1] Institute of Cyberspace Security, Zhejiang University of Technology, Hangzhou, China, [2] Institute of Vegetables, Zhejiang Academy of Agricultural Sciences, Hangzhou, China

Cherry tomato (*Solanum lycopersicum*) is popular with consumers over the world due to its special flavor. Soluble solids content (SSC) and firmness are two key metrics for evaluating the product qualities. In this work, we develop non-destructive testing techniques for SSC and fruit firmness based on hyperspectral images and the corresponding deep learning regression model. Hyperspectral reflectance images of over 200 tomato fruits are derived with the spectrum ranging from 400 to 1,000 nm. The acquired hyperspectral images are corrected and the spectral information are extracted. A novel one-dimensional (1D) convolutional ResNet (Con1dResNet) based regression model is proposed and compared with the state of art techniques. Experimental results show that, with a relatively large number of samples our technique is 26.4% better than state of art technique for SSC and 33.7% for firmness. The results of this study indicate the application potential of hyperspectral imaging technique in the SSC and firmness detection, which provides a new option for non-destructive testing of cherry tomato fruit quality in the future.

Keywords: hyperspectral imaging, deep learning, cherry tomato, soluble solids content, firmness, one-dimensional convolutional neural networks

OPEN ACCESS

Edited by:
Pei Xu,
China Jiliang University, China

Reviewed by:
Ting Sun,
China Jiliang University, China
Wen-Feng Nie,
Yangzhou University, China

***Correspondence:**
Yuan Cheng
chengyuan1005@126.com

Specialty section:
This article was submitted to Crop and Product Physiology, a section of the journal Frontiers in Plant Science

Received: *23 January 2022*
Accepted: *24 March 2022*
Published: *02 May 2022*

Citation:
Xiang Y, Chen Q, Su Z, Zhang L, Chen Z, Zhou G, Yao Z, Xuan Q and Cheng Y (2022) Deep Learning and Hyperspectral Images Based Tomato Soluble Solids Content and Firmness Estimation. Front. Plant Sci. 13:860656. doi: 10.3389/fpls.2022.860656

1. INTRODUCTION

Tomato is a very popular fruit globally and its annual production reaches 186.82 million tons in 2020 (FAO, 2021). Tomatoes contain rich nutrients such as lycopene, β-carotene and vitamins (Sainju et al., 2003; Gao et al., 2020) etc. To facilitate the tomato production, processing, and marketing, its grade and maturity needs to be evaluated. In general, soluble solids and firmness are two key indicators (Beckles, 2012). SSC can be used to grade tomato quality and the firmness can be used to determine fruit maturity (Peng and Lu, 2008). The existing measuring techniques relying upon chemistry reactions can derive the SSC value accurately. However, the destructive methods can not be applied in high volume measurements. Moreover, there are significant variations so that sampling can be inefficient and inaccurate (Li et al., 2013). Therefore, in this work, we propose a hyperspectral imaging and deep learning based technique to measure tomato SSC and firmness nondestructively, accurately, and in high volume.

Spectroscopy is a widely used nondestructive testing method for fruit inspection. It includes various imaging techniques including visible, near infrared, terahertz spectroscopy, raman spectroscopy, and hyperspectral imaging etc. Visible and near infrared spectroscopy are rapid, convenient, and low cost. However, they are contrained by limited spectral band (Yin et al., 2019).

Terahertz (THz) radiation has microwave and infrared properties and is able to penetrate and interact with many common materials, its equipments are very expensive (Afsah-Hejri et al., 2019). Raman spectroscopy is easy to operate, quick to measure, and contains rich information. However, its performance is inferior in terms of stability and sensitivity (Weng et al., 2019). Hyperspectral imaging technology can simultaneously detect the two-dimensional spatial information and 1D spectral information, therefore combine image and spectral characteristics (Adão et al., 2017). It can derive the overall spatial spectral information of cherry tomato and thus, is selected as the imaging method.

Hyperspectral imaging has been widely used for non-destructive testing in various fields, such as detection of plant disease stress (Lowe et al., 2017), industrial food packaging (Medus et al., 2021), medical image classification (Jeyaraj and Nadar, 2019), and horticultural products (Huang et al., 2017). Hyperspectral images are also effective for quality analysis of fruits. Rahman et al. (2017) use hyperspectral imaging to estimate metrics such as water content and PH readings. Zhou et al. (2020) use it to classify the maize seeds. Fan et al. (2015) use it to predict SSC and firmness in pears. They combine the competitive adaptive reweighted sampling and successive projection algorithm to select the variables as in partial least squares regression (PLSR). Rahman et al. (2018) fit sweetness and firmness of tomato. Lu et al. (2017) gives a review of the application of recent hyperspectral techniques. Therefore, hyperspectral imaging techniques can effectively measure or classify fruit and vegetable products.

The existing spectral analysis techniques typically require a regression model to fit the spectral data (Jiang and Chen, 2015), which have been widely used in areas such as food, petrochemical, and pharmaceutical fields (Chen et al., 2018). In general, various machine learning based algorithms are employed to build classification and regression models for hyperspectral images. Li et al. (2016) use PLSR to build a hyperspectral regression model to predict the water status of grapevines. Guo C. et al. (2016) develop an SVM model to assess the maturity of strawberries. Abdulridha et al. (2019) combine hyperspectral imaging and KNN algorithm to differentiate ulcer-infected fruits. Ji et al. (2019) use the AdaBoost algorithm to recognize the rate of potato damage. The machine learning algorithms typically perform a filtering process on the spectral bands.

Deep learning models, e.g., convolutional neural network (CNN), can learn features automatically from a large amount of data (Guo Y. et al., 2016). It is widely used in medics (Esteva et al., 2019), industry (Hossain et al., 2018), agriculture (Kamilaris and Prenafeta-Boldú, 2018), object detection (Zou et al., 2019), and signal processing (Yu and Deng, 2010) etc. This technique is also used in building hyperspectral correction models for classification and prediction. Paoletti et al. (2019) summarize the application of deep learning for hyperspectral image classification and conclude that CNN based models are generally more effective due to their capacity to extract highly discriminatory features and leverage the spatial and spectral information. Qiu et al. (2018) demonstrate that CNN outperforms other machine learning methods for rice variety identification application. Kong et al. (2014) track activity of peroxidase in tomato hyperspectral images using genetic algorithm and extreme learning machine. Rahman et al. (2018) develop a regression model in 1,000–1,550 nm hyperspectral images using PLSR method to estimate sweetness and firmness with R^2 of 0.672 and 0.548, respectively.

In this work, we propose a deep learning and hyperspectral imaging based technique to estimate the metrics inside cherry tomato. Specifically, we have made the following contributions.

1. We demonstrate the effectiveness of deep learning based techniques and propose such a model to estimate fruit SSC and firmness.
2. We explore the tradeoff between sample number and model accuracy.
3. We collect real-world field data and evaluate the performance of our technique.

The experimental results show that our technique is 26.4% better than the state of art technique in SSC estimation and 33.4% in firmness estimation.

2. MATERIALS AND METHODS

In this section, we describe the sample preparation, hyperspectral image acquisition and calibration, and the ground truth measurements for SSC and firmness methods. Specifically, we develop Con1dResNet, a deep learning and hyperspectral image based SSC and firmness estimation technique. Meanwhile, four comparing baseline techniques are also introduced.

2.1. Sample Preparation

The sample plant is a local mainstream cherry tomato (cultivar: Zheyingfen-1), which is dominating in the local market more with 70% share. The seeds first grow in the lab with tight environment control for one month. Then the seedlings are transplanted to the greenhouse of the Zhejiang academy of agricultural sciences, Hangzhou, China (east longitude 120°2', north latitude 30°27') on April 2nd (early spring), 2021. Field management is implemented following the standard commercial procedures. Cherry tomato fruits are harvested in June 2021. Two-hundred fully mature fruits are collected from 50 different plants for hyperspectral image acquisition. Firmness and soluble solids content of each fruit is measured using portable firmness tester and hand-held refractometer after image acquisition, respectively. The fruits of "Zheyingfen-1" were ideal for our study due to its highly soluble solid content limit, which would help extending the modeling range in this study.

2.1.1. Hyperspectral Image Acquisition

A hyperspectral imaging system is used to derive the clear and unblurred hyperspectral images as shown in **Figure 1**. We use a push-broom hyperspectral camera (PIKA XC, Resonon Inc., Bozeman, MT, USA) mounted 20 cm above the tomato samples. The hyperspectral images are acquired with the spatial resolution of 50 pixels per mm^2 under artificial lighting (four 15 W 12 V light bulbs with two on either side of the lens). The main specifications of the hyperspectral camera were: interface, Firewire (IEEE 1394b), digital output (14 bit), and angular field

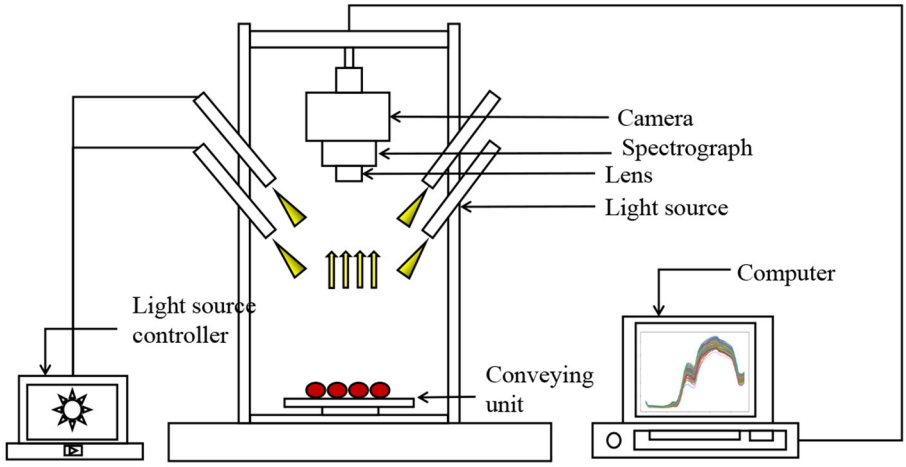


FIGURE 1 | Schematic of the hyperspectral imaging system for acquiring spectral scattering images from cherry tomatoes.

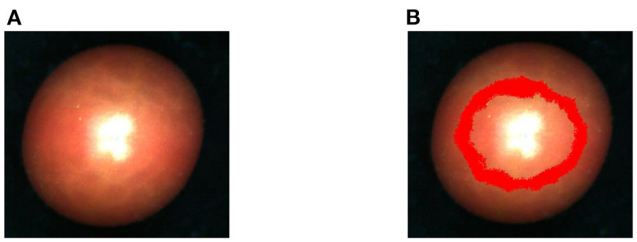


FIGURE 2 | (A) ENVI original hyperspectral image. **(B)** Area map of ROI acquired by ENVI.

of view of 7°. The objective lens had a 17 mm focal length (maximum aperture of F1.4), optimized for the hyperspectral. We acquire reflectance data in 462 spectral bands from 386 to 1,004 nm with a spectral resolution of 1.3 nm. Due to the convex surface of the samples, the uneven reflection creates a highlighted region near the vertical axial as shown in **Figure 2A**. Thus, we use ENVI5.3 (ITT, Visual Information Solutions, Boulder, CO, USA) (Su et al., 2021) to avoid the highlight region and extract the reflection value for each band from the region of interest (Xue, 2010; Fu et al., 2021; **Figure 2B**). The processed cherry tomato samples and the corresponding hyperspectral images are divided into training set, validation set, and test set with ratio of 7:1:2, respectively. We use varying dataset size, with a small set if 50 samples and a large set of 200 samples.

2.1.2. Hyperspectral Image Calibration

In reflectance calibration, the acquired hyperspectral image needs to be calibrated for the background spectral response of the instrument and the thermal dark current of the camera. The spectral data collected from the CCD device contains only the detector signal intensity value (Elmasry et al., 2012). Therefore, it is required to convert the raw data to reflectance or absorptivity values by comparing to the spectra of standard reference substances (Burger and Geladi, 2005) as shown in **Figure 3**. The reflectance can be derived using the following equation.

$$R_c = \frac{R_{ori} - R_{dark}}{R_{white} - R_{dark}},$$

where R_c is the corrected hyperspectral reflectance, R_{ori} is the original reflection value extracted from ENVI5.3, R_{dark} is the dark environment hyperspectral image reflection value, which is acquired using an opaque lens cap covering the hyperspectral lens, and R_{white} is the reflection value of a piece of white Teflon (100% reflectance, K-Mac Plastics, MI, USA).

2.1.3. Baseline Measurement

The baseline firmness and SSC of cherry tomatoes are measured in the lab. For the firmness measurement, the cherry tomatoes are fixed on a portable firmness measurement equipment (GY-4, Zhejiang Top Cloud-Agri Technology Co., Ltd, China). The equipment is zero-calibrated. Starting from the contact of the probe with the cherry tomato surface, the 10 mm downward pressure is considered as the firmness value.

SSC measurements follow the firmness measurements. Cherry tomatoes are cut along the vertical axis and wrapped using a gauze. Then they are squeezed manually to force out the solution. About one milliliter tomato solution is placed on the prism of a portable digital refractometer (PAL-1, ATAGO CHINA Guangzhou Co., Ltd, China) to derive the baseline SSC readings. Each cherry tomato sample solution is measured for three times and the results are averaged to reduce the effect of random environment events.

2.2. Hyperspectral Pre-processing

2.2.1. Multiple Scattering Correction

Multiple scattering correction (MSC) is a commonly used algorithm for hyperspectral data pre-processing (Zhang et al., 2012). MSC can effectively eliminate the spectral differences due to varying scattering levels, thus enhance the correlation

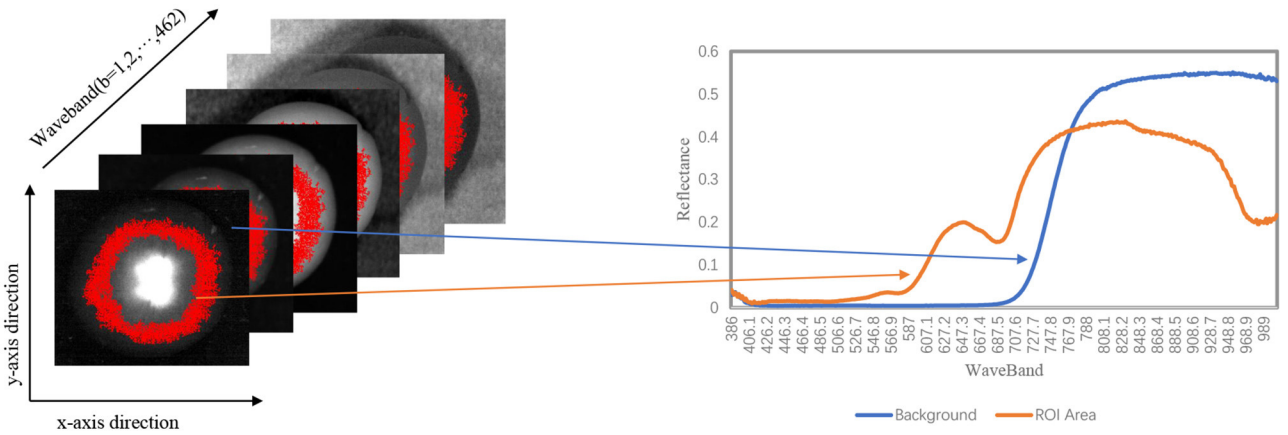


FIGURE 3 | Schematic diagram of the structure and data of the corrected hyperspectral image: spatial axis x, y, and wavebands.

between the spectrum and the data. This method can correct the baseline shifting and skewing using ideal spectra. The specific implementation is as follows:

1. assign the average of all hyperspectral data as "ideal spectrum;"
2. use one-dimensional linear regression and least square method to derive the baseline shifting and skewing values for each sample;
3. subtract the baseline shifting value and the divide the result using the skewing value to generate the corrected spectrum.

2.2.2. Spectral Differential Techniques

The spectral differentiation technique involves mathematical simulation of the reflectance spectrum and calculation of differential values of different orders to determine the spectral bending point and the wavelength for the maximum and minimum reflectance. The data processed using second-order differentiation can reflect the spectrum variation caused by the absorption of biochemical elements such as plant chlorophyll, water, and nitrogen (Liu, 2020).

2.3. Image Processing Models

2.3.1. Deep Learning Model

Deep learning models are widely used in medical image processings (Kiranyaz et al., 2015). However, in this work, it is required to build appropriate regression models. In general, we propose the Con1dResNet model to estimate the tomato SSC and firmness.

ResNet (He et al., 2016), a popular model for image classification, can solve the degradation problem of deep networks. Thus, ResNet34 is implemented as the baseline network structure, and the original convolutional layer is reconstructed to be one-dimensional, accordingly. We use the Adam optimizer and mean squared error loss function. We change the number of categories output by the last fully connected layer to one so that the network directly outputs the estimated values of SSC and firmness.

The specific network structure is shown in **Figure 4**. In the figure, the input is the reflectance values of the processed 462 spectral bands. There are five main blocks. The first block consists of a 1D convolution layer and a maximum pool layer, and then continues through a dropout layer with parameter 0.5. The second blockX contains three residuals module. The third blockX contains one downsampled module and three residuals module. The fourth blockX goes through one downsampled module and five residuals module before a dropout layer with parameter 0.5, and then continues through three residuals module. The fifth block consists of a mean pool layer and linear output layer. The number of convolution filters doubles as the block goes deeper (starting with 32 and ending with 128). All convolutional layers have a kernel size of 3 and a step size of 3. By connecting the convolutional layers together, deeper layers can be connected to a larger portion of the original input. Thus, different layers see the original input and learning ability at different levels. The last deeper layer outputs the SSC estimation, which converge to the ground truth value under the approximation of the MSE loss function.

2.3.2. Machine Learning Models

In this work, we select four widely-used machine learning models as references to our deep learning based technique.As described in **Table 1**, they are Support Vactor Regression (SVR) (Castro-Neto et al., 2009), K-Nearest Neighbors Regression (KNNR) (Yao and Ruzzo, 2006), Adaptive Boosting Regression (AdaBoostR) (Freund et al., 1999), and Partial Least Squares Regression(PLSR) (Wold et al., 2001).

2.3.3. Experimental Setup

The algorithms are trained and run on a platform with an I7-8750H CPU and a 1,060 GPU. They are programmed using python and tensorflow etc. The datasets are divided as described in **Table 2**. The processed spectral data are used in the machine learning models while the raw spectral data are used in the Con1dResNet network. Since our deep learning model Con1dResNet can extract low to high dimensional features automatically, we use the original spectral data instead. We set Relu as the activation function, Adam as the optimizer, MSE as the loss function, the number of iterations to 50, and the batch

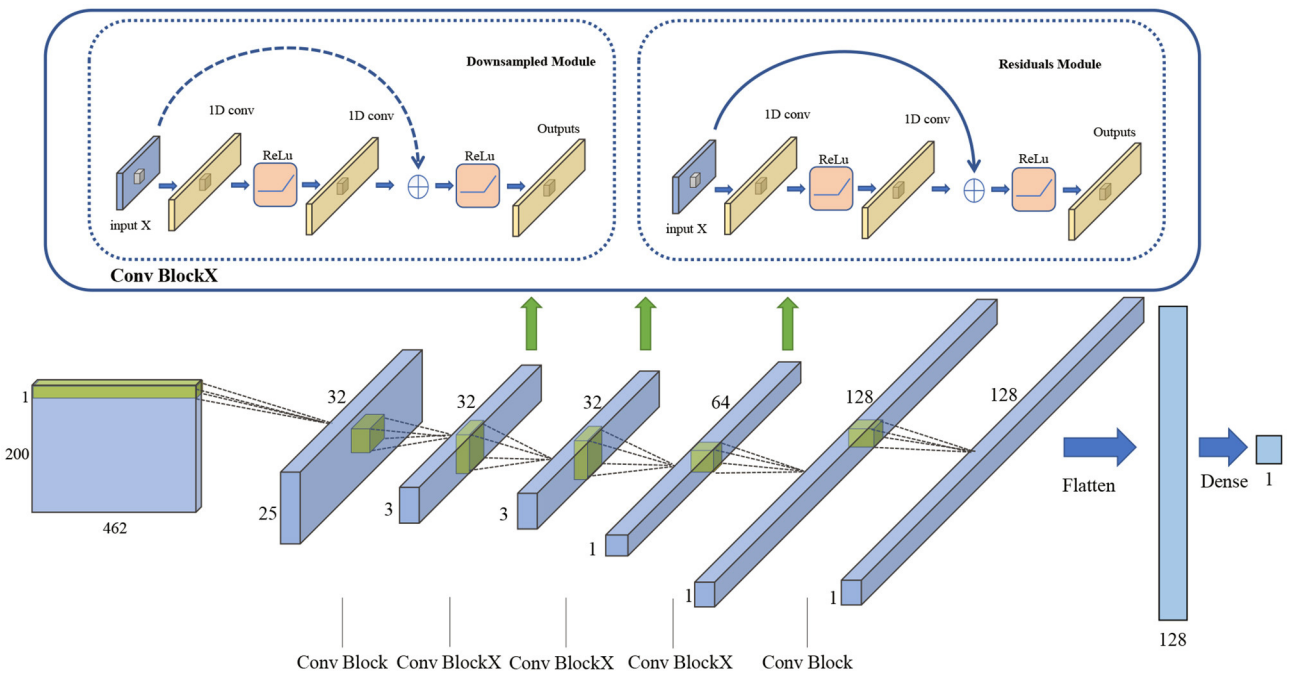


FIGURE 4 | Con1dResNet network structure schematic.

TABLE 1 | Advantages, disadvantages, and applications of machine learning models in hyperspectrum.

Machine learning models	Advantages	Disadvantages	Quality parameters
SVR	Fast data fitting	Prone to overfitting phenomenon	Rice moisture (Sun et al., 2017)
KNNR	Low training time complexity	Computationally intensive	biomass (Tian et al., 2021)
Adaboost	Weak learners can be constantly updated	Vulnerable to noise interference	Soil organic matter (Wei et al., 2020)
PLSR	Suitable for data with multiple features	Not suitable for data with few features	SSC (Li et al., 2016)

size t o 16. After 50 iterations of training, the loss decreases from 72.86 at the beginning to 0.01, indicating a convergence for the algorithm.

3. RESULTS

In this section, we evaluate our techniques in SSC and firmness estimation.

3.1. Hyperspectral Waveform Characteristics

Figure 5A shows the reflectance spectra of 200 cherry tomato samples at 386–1,004 nm. The spectral trends are similar for each sample since the reflection substances are the same. The cherry tomatoes have a strong absorption band at 400–550 nm due to the presence of carotenoids in ripe tomatoes (Ecarnot et al., 2013). The reflectance data are then processed using MSC. As shown in **Figure 5B**, it can effectively reduce the noise and hence, smooth the curve. Finally, we use second order differentiation method (Ichige et al., 2006) to process the smoothed reflectance data and discover clear peaks at locations of 580–590, 680–690, and 970–980 nm, as shown in **Figure 5C**. The three peaks are likely to be attributed to the combined effect of the second overtone of OH key, water, and tomato surface color (Li et al., 2013; Qiu et al., 2018). Therefore, by proper processing, the variations in the spectral curves can reveal certain hidden information, such as SSC and water.

3.2. Analysis

Table 2 summarizes the distribution characteristics of SSC and firmness in different stages. The SSC and firmness measurements for the 50 and 200 samples are close to normally distributed around the mean values of 9.11° Brix, 9.04 N/cm^2 and 8.72° Brix, 8.85 N/cm^2, standard deviations (SD) of 0.76, 1.35 and 0.66, 1.23, respectively.

3.3. SSC Estimation Result

Four machine learning models are implemented and compared with our proposed Con1dResNet network. We use R^2 and MSE as the evaluation metrics. They are calculated using the

TABLE 2 | Cherry tomato SSC and firmness dataset partitioning.

Sample size	Dataset	SSC (∘ Brix)				Firmness (N/cm^2)			
		Max	Min	Mean	STD	Max	Min	Mean	STD
Small	Total (50)	10.800	8.000	9.114	0.726	12.642	5.978	9.038	1.351
	Train set (35)	10.800	8.000	9.129	0.760	12.642	5.978	8.747	1.324
	Val set (5)	10.400	8.700	9.320	0.779	9.800	8.624	9.153	0.488
	Test set (10)	9.200	7.900	8.600	0.380	12.054	8.134	9.996	1.359
Large	Total(200)	11.100	7.200	8.719	0.662	12.936	5.978	8.853	1.229
	Train set (140)	11.100	7.200	8.790	0.726	12.936	5.978	9.140	1.266
	Val set (20)	9.200	7.800	8.500	0.407	9.996	7.305	8.345	0.708
	Test set (40)	9.000	7.200	8.455	0.478	10.192	7.056	8.102	0.858

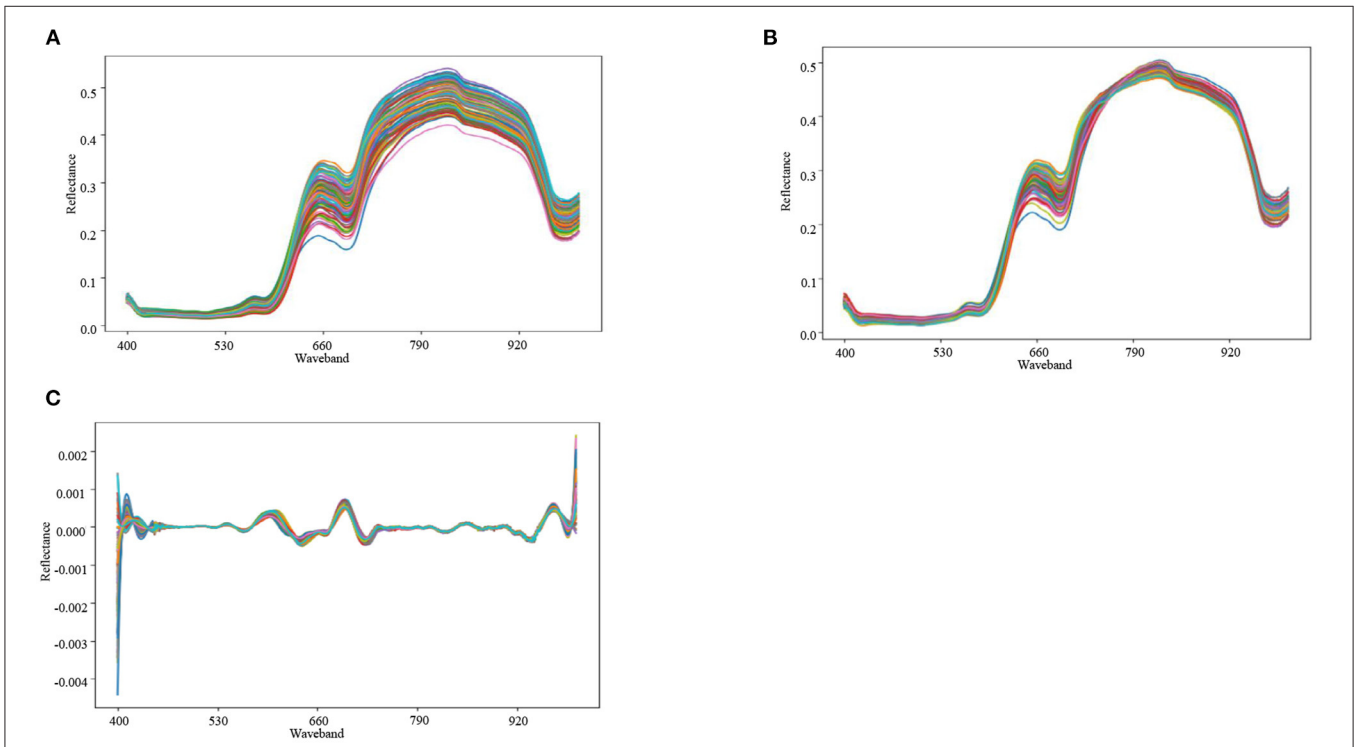


FIGURE 5 | (A) Corrected spectral reflectance map. **(B)** MSC preprocessing. **(C)** Second-order differential preprocessing.

following equations.

$$R^2 = 1 - \frac{\sum_i \left(\widehat{y_i} - y_i\right)^2}{\sum_i \left(\overline{y_i} - y_i\right)^2}$$

$$MSE = \frac{1}{m}\sum_{i=1}^{m}\left(y_i - \widehat{y_i}\right)^2$$

where $\widehat{y_i}$ is the estimated value, y_i is the ground true value, and $\overline{y_i}$ is the ground true mean value. The optimal R^2 and MSE values are 1 and 0, respectively.

The experimental results are shown in **Figure 6** and **Table 3**. In general, the second-order differential processing outperforms MSC. However, since the SVR and KNNR models lack the ability of data dimensionality reduction, the noise caused by unwanted reflectance cannot be removed. When the data size increases, the amount of interference also rises. Thus, the R^2 value decreases as the data size increases. As expected, they have the worst performance with $R^2 < 0.4$. For AdaBoostR, PLSR, and Con1dResNet models, R^2 values increase with increasing datasets size. For a relatively smaller data size, the PLSR model achieves the best performance, with R^2 of 0.577 and MSE of 0.055. As the data size increases, the performance of the Con1dResNet model is improved significantly, with R^2 increasing from 0.498 to 0.901 (26.4% better than the second best) and MSE decreasing from 0.065 to 0.018.

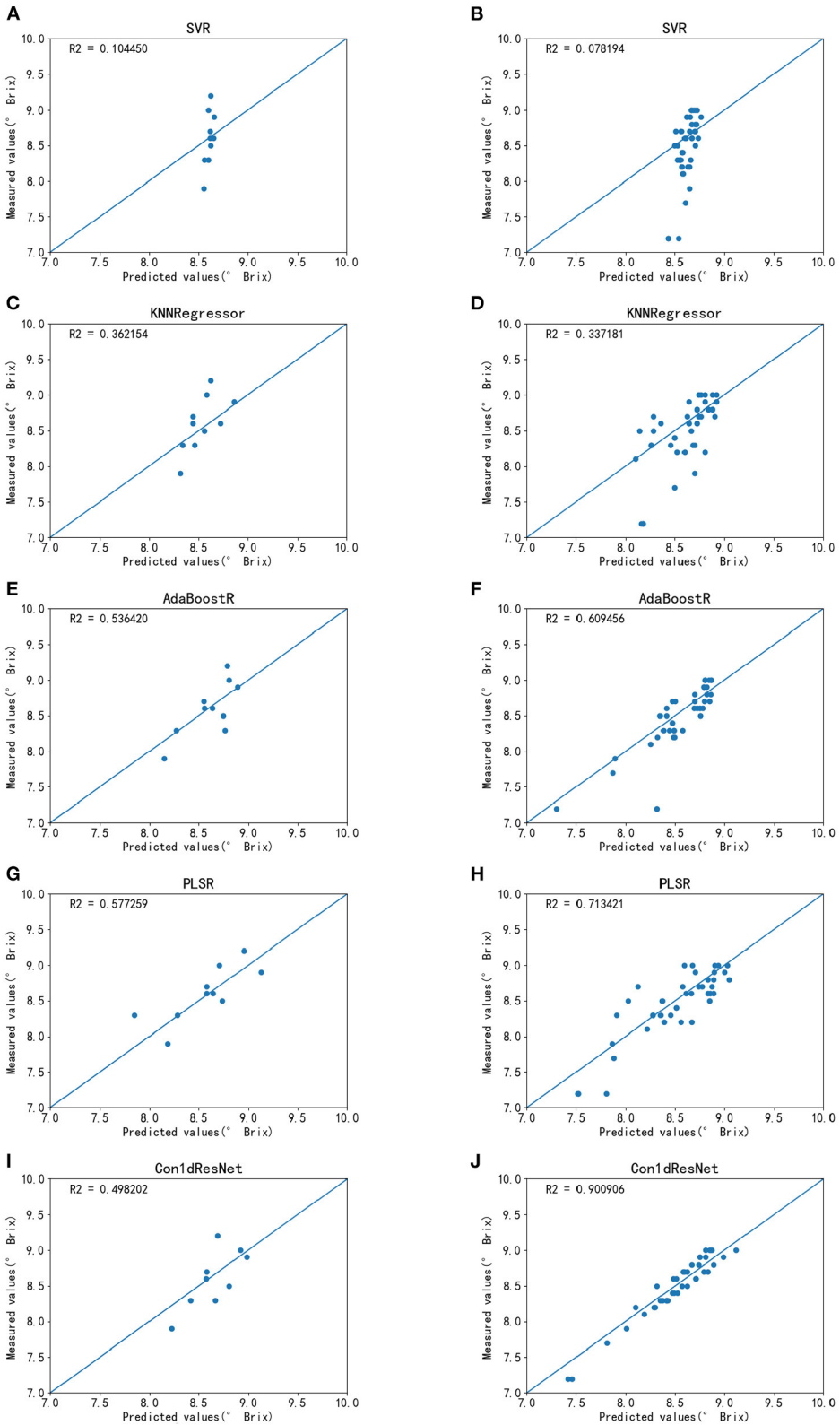


FIGURE 6 | SSC estimation results for each model. **(A)** SVR estimation results on small sample data. **(B)** SVR estimation results on large sample data. **(C)** KNNR estimation results on small sample data. **(D)** KNNR estimation results on large sample data. **(E)** AdaBoostR estimation results on small sample data. **(F)** AdaBoostR estimation results on large sample data. **(G)** PLSR estimation results on small sample data. **(H)** PLSR estimation results on large sample data. **(I)** Con1dResNet estimation results on small sample data. **(J)** Con1dResNet estimation results on large sample data.

TABLE 3 | R^2 and MSE of estimated SSC for each model.

Sample size	Model	Preprocessed	Second-order differential		MSC	
			R^2	MSE	R^2	MSE
Small (50)	SVR	✓	0.104	0.116	0.089	0.123
	KNNR	✓	0.362	0.083	0.289	0.096
	AdaBoost	✓	0.536	0.060	0.502	0.068
	PLSR	✓	0.557	0.055	0.528	0.062
	Con1dResNet	✗	R^2	0.498	MSE	0.065
Large (200)	SVR	✓	0.078	0.205	0.075	0.207
	KNNR	✓	0.337	0.147	0.316	0.152
	AdaBoost	✓	0.609	0.089	0.581	0.096
	PLSR	✓	0.713	0.064	0.710	0.067
	Con1dResNet	✗	R^2	0.901	MSE	0.018

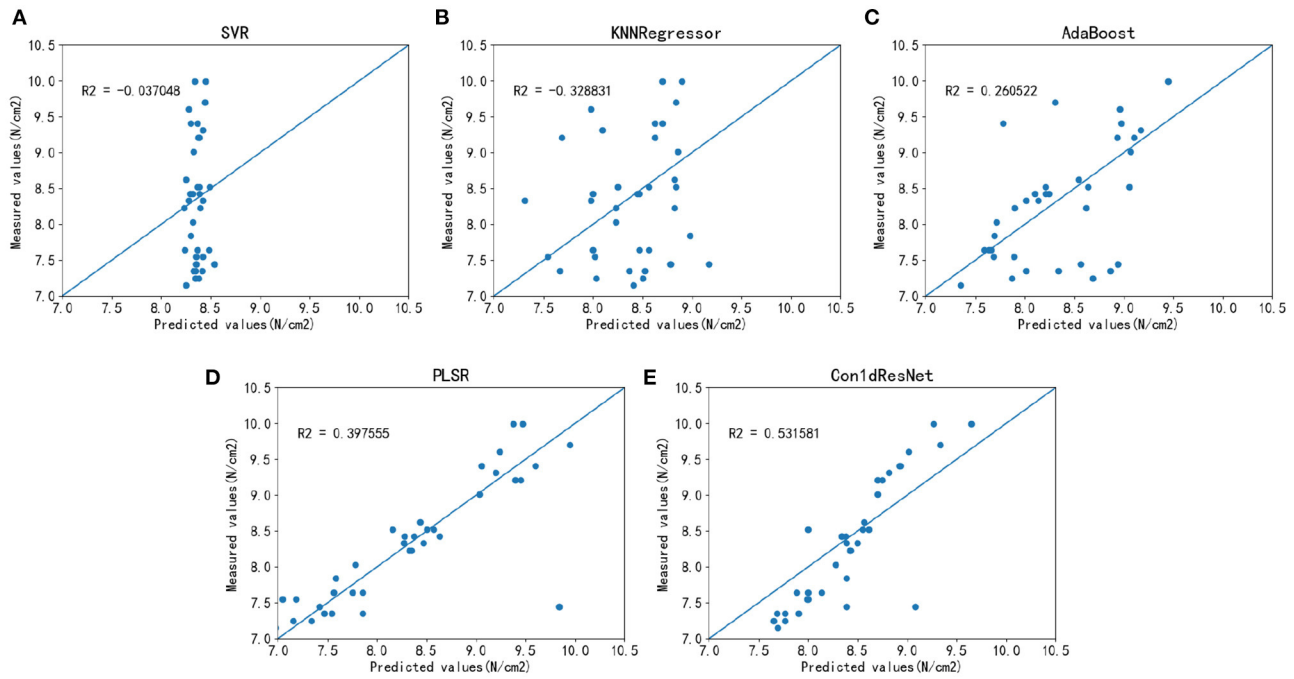


FIGURE 7 | Estimation results of firmness for each model on a large sample dataset. **(A)** SVR estimation results on large sample data. **(B)** KNNR estimation results on large sample data. **(C)** AdaBoostR estimation results on large sample data. **(D)** PLSR estimation results on large sample data. **(E)** Con1dResNet estimation results on large sample data.

3.4. Firmness Estimation Result

The same experimental setup is employed for firmness detection. As shown in **Figure 7** and **Table 4**, when MSC is employed for AdaBoost and PLSR, their R^2 values can be significantly improved (Wang et al., 2014). Therefore, we choose MSC as the preprocessing method for AdaBoost and PLSR, and second-order difference as the preprocessing method for SVR and KNNR. Although the method developed in this study has some advantages in data feature extraction compared with other methods, R^2 is still only 0.53, which does not achieve the accurate estimation standard. The R^2 of SVR and KNNR models is negative, which indicates the estimation accuracy is lower than the mean value.

4. DISCUSSION

The tomato flavor is important. SSC, which mainly consists of soluble sugars, can reflect the sweetness of cherry tomato. Hyperspectral imaging has been considered an effective technique for fruit SSC and firmness evaluation (Lu, 2004; Fan et al., 2015). In this work, we discover a great estimation result for SSC estimation, while an inferior result for firmness.

TABLE 4 | R^2 and MSE of estimated SSC for each model with all sample.

Model	Preprocessed	Second-order differential		MSC	
		R^2	MSE	R^2	MSE
SVR	✓	−0.037	1.108	−0.054	1.116
KNNR	✓	−0.329	1.251	−0.456	1.318
AdaBoost	✓	0.217	0.694	0.261	0.675
PLSR	✓	0.384	0.552	0.398	0.548
Con1dResNet	✗	R^2	0.532	MSE	0.416

As shown in **Table 3**, our proposed method does not fit as well as PLSR and AdaBoost on small sample datasets. This is because Con1dResNet requires a large amount of data for training. When the amount of data is small, many models, especially for the deep learning based models, tends to become overfitting, which can significantly reduce the performance. However, for the PLSR model, it includes a principal component analysis component, which screen the band contribution first, and then selects 5–20 feature bands with relatively large contribution rates for regression. In that case, it can have a relatively good fit for small dataset samples. Moreover, AdaBoost constantly corrects the data with large fitting errors, and thus, achieve self-evolution. Thus, AdaBoost can also derive decent results in small dataset samples.

The extracted spectral (Guo C. et al., 2016) features can derive excellent estimation results for large sample size. The experimental results show that SVR and KNNR does not fit well on both the small and large sample data set. The performance of SVR and KNNR decrease when the data increase since few new "learning material" is generated for these two models when the data increases. In that case, the learning ability of the models can be more easily affected by the interference bands, which demonstrates that these two models are not suitable for SSC estimation.

As the number of sample size increases, our Con1dResNet model gradually outperforms other models due to the improved feature extraction ability of deep learning models (Dara and Tumma, 2018). Our model includes 34 layers of neurons, which can effectively extract rich data features. The residual learning structure can also help increasing the overall performance. Therefore, the accuracy of our method outperforms all the other methods for large-scale data samples. For applications with less samples, it is demonstrated that the accuracy of our technique is still relatively high. Moreover, our model is insensitive to anomalous data. It can be trained using pre-trained models and thus, reducing the training cost. The experimental results demonstrate that Con1dResNet can significantly outperform the existing machine learning based techniques, with R^2 of 0.901 and MSE of 0.018. We believe that the experimental results of this work are also indicative for other horticultural crops.

For the hyperspectral images based tomato firmness, although it is reported that hyperspectral images can estimate fruit firmness (Lu, 2004; Fan et al., 2015), our experimental results suggest otherwise. Rahman et al. (2018) use PLSR to estimate tomato firmness using hyperspectral images in the 1,000–1,550 nm wavebands, and derive R^2 value of 0.6724. It is a little higher than our experiment due to the differences in the used hyperspectral wavebands and the experimental environments. Therefore, in future work, for the estimation of firmness, we should explore a wider range of hyperspectral image wavebands, optimize the parameters for the firmness experiments, and improve the overall estimation accuracy.

5. CONCLUSION

In this work, we propose Con1dResNet, a deep learning based technique, to estimate the SSC and firmness of cherry tomatoes using hyperspectral images. With sufficient sample size, it can achieve better results than traditional machine learning methods. For SSC estimation, its R^2 value is 0.901, which is 26.4% higher than PLSR, while its MSE is 0.018, which is 0.046 lower than PLSR. For Firmness estimation, its R^2 value is 0.532, which is still 33.7% better than PLSR. The results indicate that hyperspectral imaging combined with deep learning can significantly improve the cherry tomato SSC and firmness estimation accuracies.

DATA AVAILABILITY STATEMENT

The raw data supporting the conclusions of this article will be made available by the authors, without undue reservation.

AUTHOR CONTRIBUTIONS

YX, QC, YC, QX, and ZS performed a conceptual and formal analysis of the study. QC, YX, ZC, and YC wrote the manuscript. YX, YC, QC, LZ, GZ, ZY, and QX designed the experiment. QC, LZ, and ZS wrote the experimental code. YX and QX verified the experimental results. All authors contributed to the article and reviewed the manuscript. All authors contributed to the article and approved the submitted version.

FUNDING

This research was partially supported by National Key Research and Development Program of China (2018YFD1000800 and 2017YFE0114500), Key Research and Development Program of Zhejiang (2021C02052), National Natural Science Foundation of China (32172555), Zhejiang Provincial Agricultural (Vegetable) New Variety Breeding Project (2021C02065), China Agriculture Research System of MOF and MARA (CARS-23-G44), and State Key Laboratory Breeding Base for the Zhejiang Sustainable Pest and Disease Control (2010DS700124-ZZ1903).

REFERENCES

Abdulridha, J., Batuman, O., and Ampatzidis, Y. (2019). Uav-based remote sensing technique to detect citrus canker disease utilizing hyperspectral imaging and machine learning. *Remote Sens*. 11:1373. doi: 10.3390/rs11111373

Ad ao, T., Hruška, J., Pádua, L., Bessa, J., Peres, E., Morais, R., and Sousa, J. J. (2017). Hyperspectral imaging: a review on UAV-based sensors, data processing and applications for agriculture and forestry. *Remote Sens*. 9:1110. doi: 10.3390/rs9111110

Afsah-Hejri, L., Hajeb, P., Ara, P., and Ehsani, R. J. (2019). A comprehensive review on food applications of terahertz spectroscopy and imaging. *Comprehens. Rev. Food Sci. Food Saf*. 18, 1563–1621. doi: 10.1111/1541-4337.12490

Beckles, D. M. (2012). Factors affecting the postharvest soluble solids and sugar content of tomato (*Solanum lycopersicum* L.) fruit. *Posthar. Biol. Technol*. 63, 129–140. doi: 10.1016/j.postharvbio.2011.05.016

Burger, J., and Geladi, P. (2005). Hyperspectral NIR image regression part i: calibration and correction. *J. Chemometr*. 19, 355–363. doi: 10.1002/cem.938

Castro-Neto, M., Jeong, Y.-S., Jeong, M.-K., and Han, L. D. (2009). Online-svr for short-term traffic flow prediction under typical and atypical traffic conditions. *Expert Syst. Appl*. 36, 6164–6173. doi: 10.1016/j.eswa.2008.07.069

Chen, Q., Chen, M., Liu, Y., Wu, J., Wang, X., Ouyang, Q., et al. (2018). Application of ft-nir spectroscopy for simultaneous estimation of taste quality and taste-related compounds content of black tea. *J. Food Sci. Technol*. 55, 4363–4368. doi: 10.1007/s13197-018-3353-1

Dara, S., and Tumma, P. (2018). "Feature extraction by using deep learning: a survey," in *2018 Second International Conference on Electronics, Communication and Aerospace Technology (ICECA)* (Shanghai), 1795–1801. doi: 10.1109/ICECA.2018.8474912

Ecarnot, M., Bączyk, P., Tessarotto, L., and Chervin, C. (2013). Rapid phenotyping of the tomato fruit model, micro-tom, with a portable VIS-NIR spectrometer. *Plant Physiol. Biochem*. 70, 159–163. doi: 10.1016/j.plaphy.2013.05.019

Elmasry, G., Kamruzzaman, M., Sun, D.-W., and Allen, P. (2012). Principles and applications of hyperspectral imaging in quality evaluation of agro-food products: a review. *Crit. Rev. Food Sci. Nutr*. 52, 999–1023. doi: 10.1080/10408398.2010.543495

Esteva, A., Robicquet, A., Ramsundar, B., Kuleshov, V., DePristo, M., Chou, K., et al. (2019). A guide to deep learning in healthcare. *Nat. Med*. 25, 24–29. doi: 10.1038/s41591-018-0316-z

Fan, S., Huang, W., Guo, Z., Zhang, B., and Zhao, C. (2015). Prediction of soluble solids content and firmness of pears using hyperspectral reflectance imaging. *Food Anal. Methods* 8, 1936–1946. doi: 10.1007/s12161-014-0079-1

FAO (2021). *Tomato Growth Volume*. Available online at: https://www.fao.org/faostat/en/#data/QCL/visualize (accessed December 27, 2021).

Freund, Y., Schapire, R., and Abe, N. (1999). A short introduction to boosting. *J. Jpn. Soc. Artif. Intell*. 14:1612.

Fu, D., Zhou, J., Scaboo, A. M., and Niu, X. (2021). Nondestructive phenotyping fatty acid trait of single soybean seeds using reflective hyperspectral imagery. *J. Food Process Eng*. 2021:e13759. doi: 10.1111/jfpe.13759

Gao, Y.-F., Liu, J.-K., Yang, F.-M., Zhang, G.-Y., Wang, D., Zhang, L., et al. (2020). The wrky transcription factor WRKY8 promotes resistance to pathogen infection and mediates drought and salt stress tolerance in *Solanum lycopersicum*. *Physiol. Plant*. 168, 98–117. doi: 10.1111/ppl.12978

Guo, C., Liu, F., Kong, W., He, Y., Lou, B., et al. (2016). Hyperspectral imaging analysis for ripeness evaluation of strawberry with support vector machine. *J. Food Eng*. 179, 11–18. doi: 10.1016/j.jfoodeng.2016.01.002

Guo, Y., Liu, Y., Oerlemans, A., Lao, S., Wu, S., and Lew, M. S. (2016). Deep learning for visual understanding: a review. *Neurocomputing* 187, 27–48. doi: 10.1016/j.neucom.2015.09.116

He, K., Zhang, X., Ren, S., and Sun, J. (2016). "Identity mappings in deep residual networks," in *European Conference on Computer Vision* (Amsterdam: Springer), 630–645. doi: 10.1007/978-3-319-46493-0_38

Hossain, M. S., Al-Hammadi, M., and Muhammad, G. (2018). Automatic fruit classification using deep learning for industrial applications. *IEEE Trans. Indus. Informatics* 15, 1027–1034. doi: 10.1109/TII.2018.2875149

Huang, Y., Lu, R., and Chen, K. (2017). Development of a multichannel hyperspectral imaging probe for property and quality assessment of horticultural products. *Posthar. Biol. Technol*. 133, 88–97. doi: 10.1016/j.postharvbio.2017.07.009

Ichige, K., Ishikawa, Y., and Arai, H. (2006). "Accurate direction-of-arrival estimation using second-order differential of music spectrum," in *2006 International Symposium on Intelligent Signal Processing and Communications* (Tottori), 995–998. doi: 10.1109/ISPACS.2006.364805

Jeyaraj, P. R., and Nadar, E. R. S. (2019). Computer-assisted medical image classification for early diagnosis of oral cancer employing deep learning algorithm. *J. Cancer Res. Clin. Oncol*. 145, 829–837. doi: 10.1007/s00432-018-02834-7

Ji, Y., Sun, L., Li, Y., and Ye, D. (2019). Detection of bruised potatoes using hyperspectral imaging technique based on discrete wavelet transform. *Infrared Phys. Technol*. 103:103054. doi: 10.1016/j.infrared.2019.103054

Jiang, H., and Chen, Q. (2015). Chemometric models for the quantitative descriptive sensory properties of green tea (*Camellia sinensis* L.) using fourier transform near infrared (FT-NIR) spectroscopy. *Food Analyt. Methods* 8, 954–962. doi: 10.1007/s12161-014-9978-4

Kamilaris, A., and Prenafeta-Boldú, F. X. (2018). Deep learning in agriculture: a survey. *Comput. Electron. Agric*. 147, 70–90. doi: 10.1016/j.compag.2018.02.016

Kiranyaz, S., Ince, T., Hamila, R., and Gabbouj, M. (2015). "Convolutional neural networks for patient-specific ECG classification," in *2015 37th Annual International Conference of the IEEE Engineering in Medicine and Biology Society (EMBC)* (Shanghai), 2608–2611. doi: 10.1109/EMBC.2015.7318926

Kong, W., Liu, F., Zhang, C., Bao, Y., Yu, J., and He, Y. (2014). Fast detection of peroxidase (POD) activity in tomato leaves which infected with botrytis cinerea using hyperspectral imaging. *Spectrochim. Acta Part A* 118, 498–502. doi: 10.1016/j.saa.2013.09.009

Li, J., Huang, W., Zhao, C., and Zhang, B. (2013). A comparative study for the quantitative determination of soluble solids content, pH and firmness of pears by VIS/NIR spectroscopy. *J. Food Eng*. 116, 324–332. doi: 10.1016/j.jfoodeng.2012.11.007

Li, J., Tian, X., Huang, W., Zhang, B., and Fan, S. (2016). Application of long-wave near infrared hyperspectral imaging for measurement of soluble solid content (SSC) in pear. *Food Analyt. Methods* 9, 3087–3098. doi: 10.1007/s12161-016-0498-2

Liu, J. (2020). Quantitative study of hyperspectral chlorophyll content in crop canopy. *Front. Econ. Manage*. 1, 331–335. doi: 10.6981/FEM.202010_1(10).0050

Lowe, A., Harrison, N., and French, A. P. (2017). Hyperspectral image analysis techniques for the detection and classification of the early onset of plant disease and stress. *Plant Methods* 13, 1–12. doi: 10.1186/s13007-017-0233-z

Lu, R. (2004). Multispectral imaging for predicting firmness and soluble solids content of apple fruit. *Posthar. Biol. Technol*. 31, 147–157. doi: 10.1016/j.postharvbio.2003.08.006

Lu, Y., Huang, Y., and Lu, R. (2017). Innovative hyperspectral imaging-based techniques for quality evaluation of fruits and vegetables: a review. *Appl. Sci*. 7:189. doi: 10.3390/app7020189

Medus, L. D., Saban, M., Francés-Víllora, J. V., Bataller-Mompeán, M., and Rosado-Mu noz, A. (2021). Hyperspectral image classification using CNN: application to industrial food packaging. *Food Control* 125:107962. doi: 10.1016/j.foodcont.2021.107962

Paoletti, M., Haut, J., Plaza, J., and Plaza, A. (2019). Deep learning classifiers for hyperspectral imaging: a review. *ISPRS J. Photogr. Remote Sens*. 158, 279–317. doi: 10.1016/j.isprsjprs.2019.09.006

Peng, Y., and Lu, R. (2008). Analysis of spatially resolved hyperspectral scattering images for assessing apple fruit firmness and soluble solids content. *Posthar. Biol. Technol*. 48, 52–62. doi: 10.1016/j.postharvbio.2007.09.019

Qiu, Z., Chen, J., Zhao, Y., Zhu, S., He, Y., and Zhang, C. (2018). Variety identification of single rice seed using hyperspectral imaging combined with convolutional neural network. *Appl. Sci*. 8:212. doi: 10.3390/app8020212

Rahman, A., Kandpal, L. M., Lohumi, S., Kim, M. S., Lee, H., Mo, C., et al. (2017). Nondestructive estimation of moisture content, ph and soluble solid contents in intact tomatoes using hyperspectral imaging. *Appl. Sci*. 7:109. doi: 10.3390/app7010109

Rahman, A., Park, E., Bae, H., and Cho, B.-K. (2018). Hyperspectral imaging technique to evaluate the firmness and the sweetness index of tomatoes. *Korean J. Agric. Sci*. 45, 823–837. doi: 10.7744/kjoas.20180075

Sainju, U. M., Dris, R., and Singh, B. (2003). Mineral nutrition of tomato. *Food Agric. Environ*. 1, 176–183. doi: 10.1016/j.nima.2010.03.045

Su, Z., Zhang, C., Yan, T., Zhu, J., Zeng, Y., Lu, X., et al. (2021). Application of hyperspectral imaging for maturity and soluble solids content determination of strawberry with deep learning approaches. *Front. Plant Sci*. 12:736334. doi: 10.3389/fpls.2021.736334

Sun, J., Lu, X., Mao, H., Wu, X., and Gao, H. (2017). Quantitative determination of rice moisture based on hyperspectral imaging technology and BCC-LS-SVR algorithm. *J. Food Process Eng*. 40:e12446. doi: 10.1111/jfpe.12446

Tian, Y., Huang, H., Zhou, G., Zhang, Q., Tao, J., Zhang, Y., et al. (2021). Aboveground mangrove biomass estimation in Beibu gulf using machine learning and uav remote sensing. *Sci. Tot. Environ*. 781:146816. doi: 10.1016/j.scitotenv.2021.146816

Wang, D.-M., Ji, J.-M., and Gao, H.-Z. (2014). The effect of MSC spectral pretreatment regions on near infrared spectroscopy calibration results. *Guang Pu Xue Yu Guang Pu Fen Xi* 34, 2387–2390. doi: 10.3964/j.issn.1000-0593(2014)09-2387-04

Wei, L., Yuan, Z., Wang, Z., Zhao, L., Zhang, Y., Lu, X., et al. (2020). Hyperspectral inversion of soil organic matter content based on a combined spectral index model. *Sensors* 20:2777. doi: 10.3390/s20102777

Weng, S., Zhu, W., Zhang, X., Yuan, H., Zheng, L., Zhao, J., et al. (2019). Recent advances in Raman technology with applications in agriculture, food and biosystems: a review. *Artif. Intell. Agric*. 3, 1–10. doi: 10.1016/j.aiia.2019.11.001

Wold, S., Sjöström, M., and Eriksson, L. (2001). PLS-regression: a basic tool of chemometrics. *Chemometr. Intell. Lab. Syst*. 58, 109–130. doi: 10.1016/S0169-7439(01)00155-1

Xue, L. (2010). "Application of IDL and ENVI redevelopment in hyperspectral image preprocessing," in *International Conference on Computer and Computing Technologies in Agriculture* (Chengdu: Springer), 403–409. doi: 10.1007/978-3-642-18369-0_47

Yao, Z., and Ruzzo, W. L. (2006). A regression-based k nearest neighbor algorithm for gene function prediction from heterogeneous data. *BMC Bioinformatics* 7:S11. doi: 10.1186/1471-2105-7-S1-S11

Yin, L., Zhou, J., Chen, D., Han, T., Zheng, B., Younis, A., et al. (2019). A review of the application of near-infrared spectroscopy to rare traditional Chinese medicine. *Spectrochim. Acta Part A* 221:117208. doi: 10.1016/j.saa.2019.117208

Yu, D., and Deng, L. (2010). Deep learning and its applications to signal and information processing [exploratory DSP]. *IEEE Signal Process. Mag*. 28, 145–154. doi: 10.1109/MSP.2010.939038

Zhang, L., Li, Y., Peng, Y., Wang, W., Jiang, F., Tao, F., et al. (2012). Determination of pork freshness attributes by hyperspectral imaging technique. *Trans. Chinese Soc. Agric. Eng*. 28, 254–259. doi: 10.3969/j.issn.1002-6819.2012.07.042

Zhou, Q., Huang, W., Fan, S., Zhao, F., Liang, D., and Tian, X. (2020). Non-destructive discrimination of the variety of sweet maize seeds based on hyperspectral image coupled with wavelength selection algorithm. *Infrared Phys. Technol*. 109:103418. doi: 10.1016/j.infrared.2020.103418

Zou, Z., Shi, Z., Guo, Y., and Ye, J. (2019). Object detection in 20 years: a survey. *arXiv preprint arXiv:1905.05055*. doi: 10.48550/arXiv.1905.05055

Conflict of Interest: The authors declare that the research was conducted in the absence of any commercial or financial relationships that could be construed as a potential conflict of interest.

Publisher's Note: All claims expressed in this article are solely those of the authors and do not necessarily represent those of their affiliated organizations, or those of the publisher, the editors and the reviewers. Any product that may be evaluated in this article, or claim that may be made by its manufacturer, is not guaranteed or endorsed by the publisher.

Copyright © 2022 Xiang, Chen, Su, Zhang, Chen, Zhou, Yao, Xuan and Cheng. This is an open-access article distributed under the terms of the Creative Commons Attribution License (CC BY). The use, distribution or reproduction in other forums is permitted, provided the original author(s) and the copyright owner(s) are credited and that the original publication in this journal is cited, in accordance with accepted academic practice. No use, distribution or reproduction is permitted which does not comply with these terms.

frontiers | Frontiers in Plant Science

ORIGINAL RESEARCH
published: 09 May 2022
doi: 10.3389/fpls.2022.865082

Genetic Mapping and QTL Analysis of Stigma Color in Melon (*Cucumis melo* L.)

Yuanzuo Lv[1,2], *Peng Gao*[1,2], *Shi Liu*[1,2], *Xufeng Fang*[1,2], *Taifeng Zhang*[1,2], *Tai Liu*[1,2], *Sikandar Amanullah*[1,2], *Xinying Wang*[1,2] *and Feishi Luan*[1,2]*

[1] *Key Laboratory of Biology and Genetic Improvement of Horticulture Crops (Northeast Region), Ministry of Agriculture and Rural Affairs, Northeast Agricultural University, Harbin, China,* [2] *College of Horticulture and Landscape Architecture, Northeast Agricultural University, Harbin, China*

Melon is an important Cucurbitaceae crop. Field observations had shown that the green stigmas of melon are more attractive to pollinators than yellow stigmas. In this study, F_2 and $F_{2:3}$ populations obtained by crossing MR-1 (green stigma) and M4-7 (yellow stigma) were used for genetic analysis and mapping. A genetic map of 1,802.49 cm was constructed with 116 cleaved amplified polymorphism sequence (CAPS) markers. Two stable quantitative trait loci (QTLs) linked to the trait of stigma color were identified on chromosomes 2 (*SC2.1*) and 8 (*SC8.1*), respectively. An expanded F_2 population was used to narrow down the confidence regions of *SC2.1* and *SC8.1*. As a result, *SC2.1* was further mapped to a 3.6 cm region between CAPS markers S2M3 and S2B1-3, explaining 9.40% phenotypic variation. *SC8.1* was mapped to a 3.7-cm region between CAPS markers S8E7 and S8H-1, explaining 25.92% phenotypic variation. This study broadens our understanding of the mechanisms of stigma color regulation and will be of benefit to the breeding of melon.

Keywords: melon, stigma color, gene mapping, CAPS markers, chlorophyll

OPEN ACCESS

Edited by:
Pei Xu,
China Jiliang University, China

Reviewed by:
Jianbin Hu,
Henan Agricultural University, China
Kailiang Bo,
Insititute of Vegetables and Flowers (CAAS), China

***Correspondence:**
Feishi Luan
luanfeishi@neau.edu.cn

Specialty section:
This article was submitted to Crop and Product Physiology, a section of the journal Frontiers in Plant Science

Received: *29 January 2022*
Accepted: *28 March 2022*
Published: *09 May 2022*

Citation:
Lv Y, Gao P, Liu S, Fang X, Zhang T, Liu T, Amanullah S, Wang X and Luan F (2022) Genetic Mapping and QTL Analysis of Stigma Color in Melon (Cucumis melo L.). Front. Plant Sci. 13:865082. doi: 10.3389/fpls.2022.865082

INTRODUCTION

The economic benefits of pollination are the primary determinants for fruits, vegetables, and seed production, which influence at least 87 leading food crops around the world (Kevan and Viana, 2003; Klein et al., 2007). Pollination is crucial for reproduction in flowering plants whereby the male gamete (pollen grains) from the anther comes into contact with the female gamete (stigma). Likewise, successful reproduction is highly dependent on efficient pollinators (Blacquiere, 2010).

The trichromatic vision of bees is known to effectively handle different photoreceptor classes (blue, green, and UV ranges) (Peitsch et al., 1992). The floral pattern at the center of a flower can guide pollinators in finding the nectar (Lunau et al., 1996; Dafni and Giurfa, 1999; Lunau, 2005; Davies et al., 2012). Therefore, the center of a flower is easily recognizable by bees (Biesmeijer et al., 2005; Davies et al., 2012).

There is an important feature of distinct stigma color in each female flower, which directly provides a great support in plant reproduction. However, stigma color is a neglected trait in many cultivars of different fruit crops but it significantly possesses enormous benefits for desired crop production using different molecular breeding approaches. It has been reported that the level of carotenoid biosynthetic genes is associated with the accumulation of carotenoids and the resultant stigma color in *Crocus sativus* (Ahrazem et al., 2019). Similarly, during the transition from yellow

undeveloped to red fully developed stigmas, the accumulation of zeaxanthin occurred due to the expressions of *CsPSY* and *CsLcyb* (Castillo et al., 2005). In a stable inherited yellow stigma tomato mutant (*ys*) that was obtained using ethyl methane sulfonate, a single recessive gene was found to regulate the yellowing of stigma due to the accumulation of naringenin chalcone in *ys* (Zhao et al., 2017). In rice, two genes controlling the purple stigma were mapped on chromosomes 1 and 6 using 1,300 F_2 populations that are derived from XQZ (purple stigma and red lemma tip) and Kitaake (white stigma and colorless lemma tip) (Wang, 2016).

Melon (*Cucumis melo* L., 2n = 24) is an attractive fruit crop due to the extreme divergences in phenotypic diversity with a reported production of more than 42 million tons globally in 2020 (FAOSTAT; http://faostat.fao.org). Melon flowers bear yellow petals and yellow to green stigmas, which are mostly pollinated by bees under the natural field conditions (Rodrigo Gomez et al., 2016). Therefore, the green stigma can be favorable over the yellow stigma for the production of desired fruits and seeds, aimed at different breeding purposes, respectively.

Compared to the traditional breeding approaches, the marker-assisted selection (MAS) system has been proved as a more effective strategy that is used for genetic mapping of different crop traits. Until now, not all the genetic components of melon cultivars have been dissected, and there is a dire need to investigate the genetic patterns and molecular mechanisms associated with desirable traits, which should be an important part of breeding programs, aimed at genetic improvement of crops. Therefore, this study was aimed at identifying the stable quantitative trait loci (QTLs) regulating the stigma color, using the respective mapping population of F_2 and $F_{2:3}$ families that are derived from the crossing of MR-1 (green stigma) and M4-7 (yellow stigma) melon lines, respectively. The present novel outcomes would be beneficial to provide the fundamental basis for the genetic understanding of melon stigma color trait.

PLANT MATERIALS

Two different parent lines of melon MR-1 (P_1, female with green stigma) and M4-7 (P_2, male with yellow stigma) were selected as experimental material (**Figure 1**) and crossed to produce their F_1 progeny. The field experiments were performed in the plastic greenhouse at Xiang Yang Experiment Agricultural Station, Northeast Agricultural University, Harbin, China (lat. 44°04′N, long. 125°420′E) over 3 years (from 2019 to 2021). The plants were grown using a completely randomized design (CRD), and standard horticultural practices were adopted for successful germination.

In 2019, an F_2 mapping population comprising 133 plants was obtained from the parental lines crossing, and 55 plants with extremely divergent phenotypes were self-crossed to get the respective $F_{2:3}$ families. In 2020, all of the 55-$F_{2:3}$ families (20 plants for each family and a total of 1,100 individuals) were planted to detect the stable QTLs associated with stigma color. In 2021, an expanded population of 545-F_2 lines was also planted. In this study, fifteen (15) plants, each line for P_1, P_2, and F_1, generations, were grown along with all generations and subsequently utilized for genetic linkage analysis of melon stigma color.

OBSERVATION OF FLOWER-VISITING INSECTS

The observation site was located in Harbin, Heilongjiang Province, China. The numbers of flower-visiting insects on the stigmas of both parent lines "MR-1 and M4-7" were visually observed during the peak flowering. The flowers were observed on daily basis from 7:30 up to 9:30 am and photos were taken for 3 consecutive days using a Gopro7 camera in the time-lapse mode.

PHENOTYPIC DATA COLLECTION

The stigmas of respective flowers of F_2 and $F_{2:3}$ mapping populations were checked, three stigmas from each plant were chosen, and color phenotypes were collected from three flower repetitions using a 3NQ portable colorimeter (NR10QC). The respective color hues of "L," "A," and "B" were recorded, where "L" indicated lightness, "A" indicates red-green difference, "B" indicates yellow-blue difference, and "E" denoted the net color difference. The final three-dimensional orthogonal graph was plotted using the color phenotypes, and color difference "E" was calculated for each plant according to the following equation:

$$E = (L^2 + A^2 + B^2)\text{^}(1/2)$$

WHOLE GENOME RE-SEQUENCING AND MARKERS DEVELOPMENT

The leaf material (0.2 g) was taken from 2-week-old seedlings of P_1, P_2, F_1, and F_2 progeny, chilled in cryogenic liquid nitrogen, and freshly stored at −80°C. Then, high-quality DNA was isolated using the cetyl trimethyl ammonium bromide (CTAB) protocol with slight modifications. The quantified DNA was identified with 1% agarose gels electrophoresis fragmented with Bioruptor (Thermo Fisher Scientific, USA), and 200–300 bp fragments were prepared for the High-throughput Illumina™ X10 sequencing platform. The resultant clean end bases of paired-end sequencing of both parent lines were aligned to *de novo* assembled reference genome (DHL92, v3.5.1) of melon using the default algorithm of Burrows-Wheeler Aligner (BWA)-Maximal Exact Match (MEM) (https://sourceforge.net/projects/bio-bwa/files/). The Binary Alignment/Map (BAM) files were similarly used for the filtering and alignment of re-sequenced clean end bases. The major single-nucleotide polymorphisms (SNPs) were obtained and annotated using the SnpEff tool (v4.3), then 500 bp flanking sequences were extracted from each random SNP site.

The cleaved amplified polymorphism sequence (CAPS) markers were developed by identifying the suitable SNP-based restriction endonucleases (*Eco*RI, *Hin*dIII, *Pst*I, *Bam*HI, and *Bcl*I) using SNP2CAPS v0.6 and primer premier v6, respectively (Amanullah et al., 2020). The PCR products of each CAPS



FIGURE 1 | The primary phenotypes of MR-1 and M4-7.

marker were digested with restriction endonucleases to verify the codominant polymorphism of each marker. The PCR reaction mixture was prepared as follows: a pair of primers (8–10 pmol), deoxynucleotide triphosphates (dNTPs) (0.25 mM), Taq buffer (10×), and Taq polymerase (1 unit). A thermocycler PCR was performed by preheating the samples at 94°C for 7 min, followed by 30 cycles of 30 s at 94°C, 30 s at 60°C for the first cycle, and a stepwise down-gradient of 0.5°C per cycle, followed by 60 s at 72°C. Then, 10 cycles of 30 s at 94°C, 30 s at 45°C, and 60 s at 72°C were performed, followed by elongation for 5 min at 72°C. For enzyme digestion, a reaction mixture consisted of 4 μl of PCR product, 4.8 μl of ddH_2O, 1 μl of CutSmart buffer, and 0.2 μl of restriction enzymes and was incubated at 37°C for 4 h. The digested products were subsequently cleaved by 1% agarose gel electrophoresis.

LINKAGE MAPPING AND QTL ANALYSIS

A genetic linkage map was developed and QTLs were mapped by using the default parameter settings of the IciMapping (v4.2) tool as followed (Meng et al., 2015). All the genotyped CAPS markers were evenly scattered across the whole genome chromosomes. The coded genotypic data of respective F_2 mapping populations were grouped and anchored over the whole genome chromosomes according to their exact physical positions and maximum likelihood means. The default chi-squared method and Kosambi's mapping function were selected to determine the segregation ratio of genotypic markers and to estimate the genetic distances, intervals, and positions at p (>0.001). The significant QTLs were defined above the threshold level of the default logarithm of odd (LOD) score (3.00) and the genome-wide type I error at $\alpha = 0.05$.

qRT-PCR ANALYSIS

Total RNAs were extracted using DiNing DP230-01 Plant Total RNA Purification Kit following the manufacturer's protocol (DiNing Biotech, Beijing, China). The qRT-PCR was performed on RNA extracted from the stigma of MR-1 and M4-7 on the day the female flowers were opened using the *Actin* gene as *MELO03C023264.* For qRT-PCR, assays were prepared using 20 ng cDNA and 300 nM of each primer in a 10 μl of reaction mixture with the addition of SYBR Green I Master Mix. qRT-PCR was performed using three biological replicates for each tissue sample and at least three technical replicates of each biological replicate. After normalization of the transcript level of each gene with the most suitable internal control gene for each sample, fold change was calculated by a $2^{-\Delta\Delta CT}$ method.

RESULTS

Pollinator Observation

We observed that some flower-visiting insects generally fed on flowers for pollen and nectar, while some insects only stayed on

flowers with no further activity (**Figure 1**). The most frequent pollinators were *Apidae* (bees), followed by *Muscidae* (flies). The proportion of visiting pollinators for green stigma melon (MR-1) was three times more than that of yellow stigma melon (M4-7) (**Table 1**).

Genetic Analysis of Melon Stigma Color

"Lab" color space is based on the human eye's perception of color and could represent the colors observed by the human eye. The "E" values of MR-1 and M4-7 stigmas were measured for 3 consecutive years and the data obtained were stable, with the "E" value of M4-7 being consistently higher than that of MR-1 (**Supplementary Table S1**). According to **Figure 2**, the "E" value displays continuous variation among F_2 individuals and follows a normal distribution, suggesting that melon stigma color is controlled by quantitative loci. Besides, there is no color difference between the stigmas in one plant individual.

TABLE 1 | Visitation of flower visiting insects in melons with different stigma colors.

Sample	Time	Number of flower-visiting insects	Ratio of Hymenoptera	Ratio of Diptera
MR-1	2 h/d	22.1 ± 3.1	78.90%	10.06%
M4-7		6.80 ± 1.4	80.30%	11.50%

Linkage Map Construction and Primary Mapping

In 2019, a total of 116 CAPS markers were effectively developed and genotyped for linkage mapping, which spanned a total of 1802.49 cm length with an average of 15.54 cm over the whole genome chromosomes (**Figure 3**). The chromosome 8 showed the least number of CAPS markers and total of 8 polymorphic markers covered 183.88 cm length and separated with an average genetic distance of 8.32 cm; however, chromosome 12 exhibited more CAPS markers comprising 12 CAPS markers, which covered 174 cm length with an average distance of 14.06 cm between each marker.

Quantitative trait locus analysis exposed that three QTLs, *SC2.1*, *SC5.1*, and *SC8.1*, were mapped on chromosomes 2, 5, and 8, respectively (**Table 2**). *SC2.1* was mapped on the genetic position of chromosome 2 between flanking markers S2E1 and S2H19 with 5.92% phenotypic variance explained (PVE) and LOD value of 5.54, *SC5.1* was located on chromosome 5 between adjacent markers S5H10 and S5P3 with 12.30% PVE and LOD value of 3.90, and *SC8.1* was mapped on chromosome 8 between S8P19 and S8H9 with 23.18% PVE and LOD value of 14.29, respectively.

In 2020, the $F_{2:3}$ lines were generated from the same F_2 self-crosses and the genetic map was re-constructed to verify the stable QTLs. Then, two stable QTLs, *SC2.1* and *SC8.1*, were found to be consistent with the F_2 mapping population (**Table 2**); *SC2.1* explained somewhat lower phenotypic variation (9.71%) with an

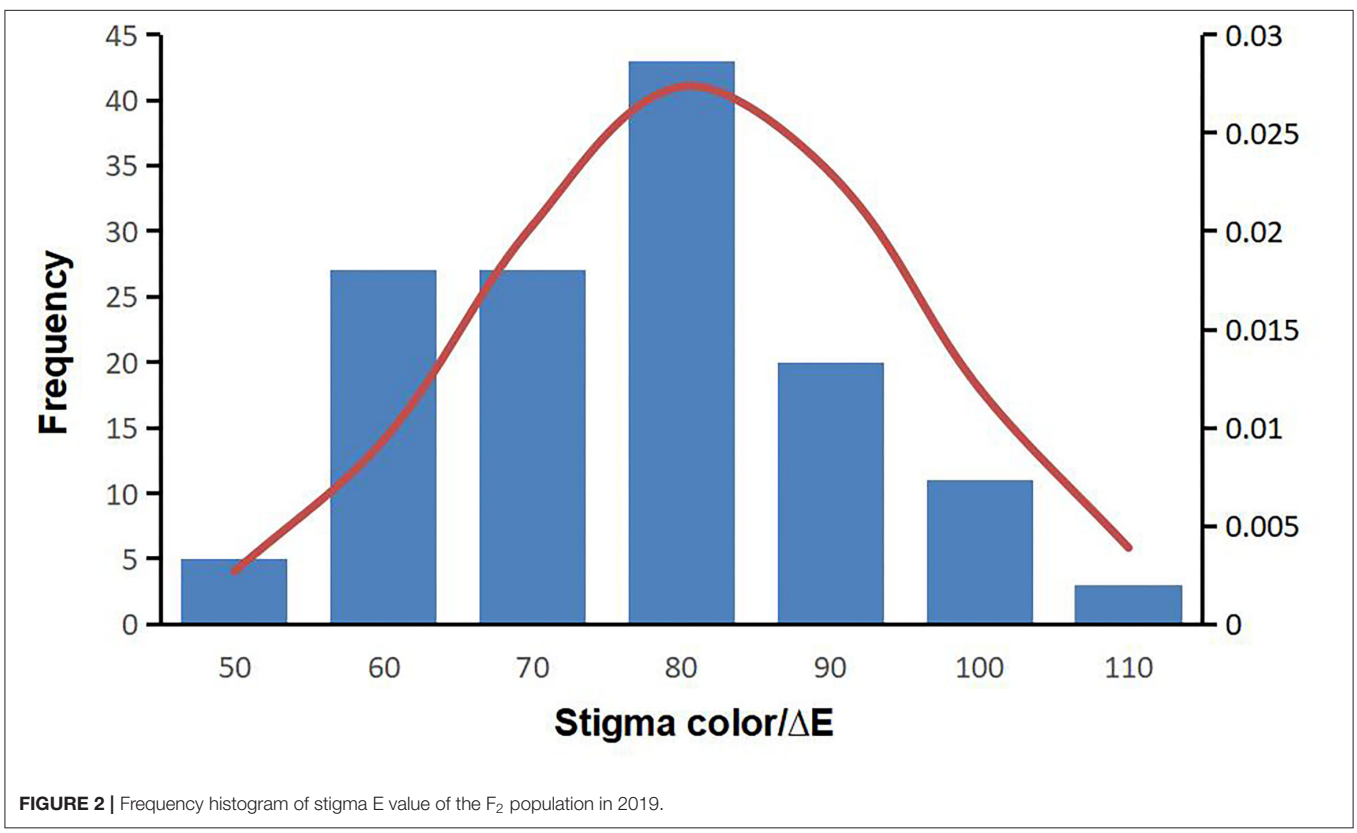


FIGURE 2 | Frequency histogram of stigma E value of the F_2 population in 2019.

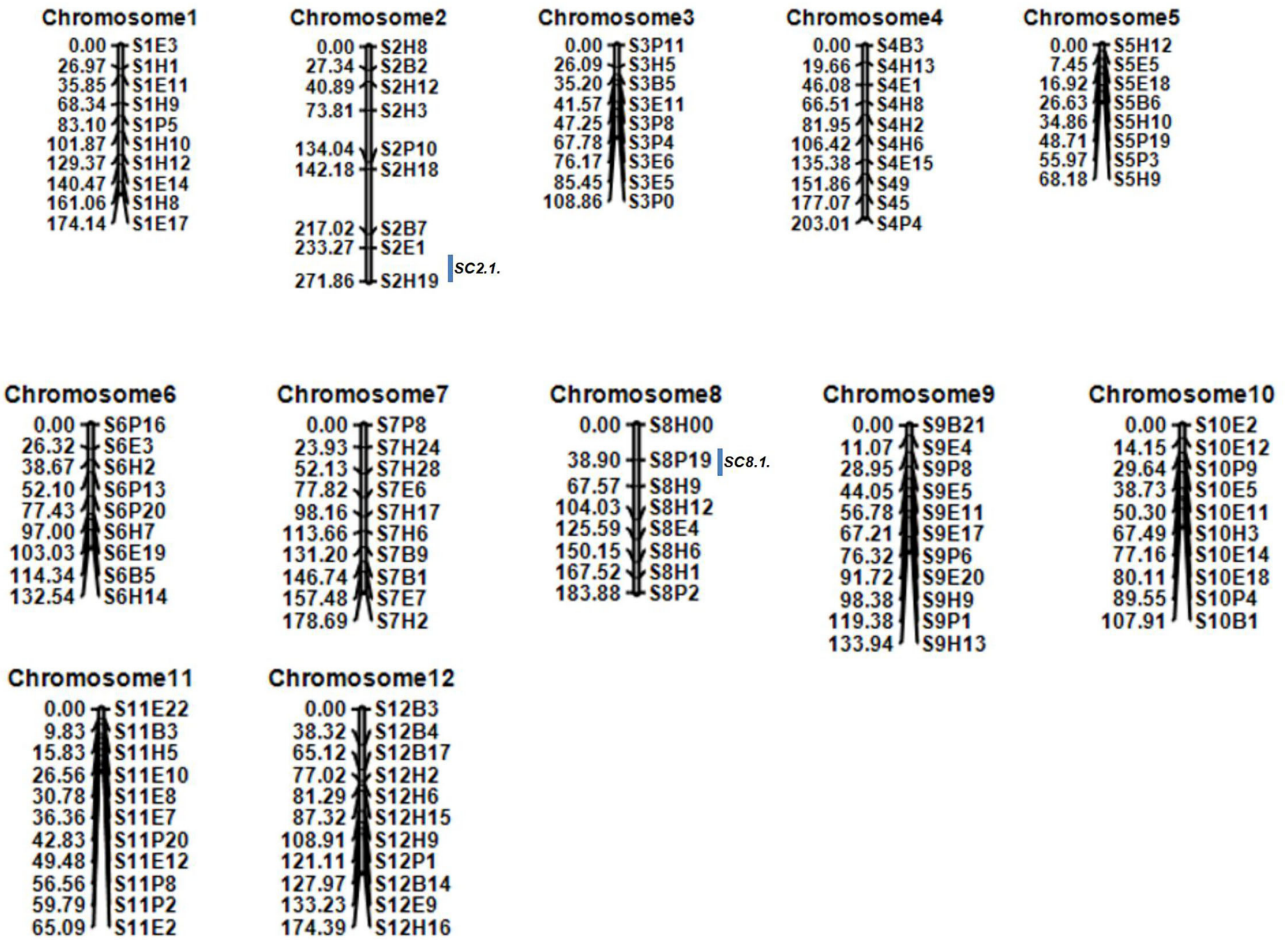


FIGURE 3 | A constructed linkage map of melon chromosomes based on the F_2 mapping population of a cross between parental lines "MR-1 and M4-7." The box to the right of the chromosomes indicates the stable quantitative trait loci (QTL) identified as associated with stigma color by 2 years of data.

TABLE 2 | Quantitative traits locus (QTL) analysis of melon stigma color using F_2 population and $F_{2:3}$ population, respectively.

Year	Population	QTL name	Trait	Adjacent marker	Chr.	LOD	R^2
2019	F_2	*SC2.1*	Stigma color/ΔE	S2E1∼S2H19	2	5.54	5.92%
		SC5.1		S5H10∼S5P3	5	3.91	12.30%
		SC8.1		S8P9∼S8H9	8	14.29	23.18%
2020	$F_{2:3}$	*SC2.1*		S2E1∼S2H19	2	3.62	9.71%
		SC8.1		S8P19∼S8H9	8	6.97	21.74%

LOD value of 3.6 and was positioned between markers S2E1 and S2H19. Meanwhile, *SC8.1* explained a high phenotypic variation (21.74%) with the LOD value of 6.97 between markers S8P19 and S8H9, respectively.

In 2021, we developed five new CAPS markers in the detected QTL regions (**Table 3**) and further validated that both candidate QTLs, *SC2.1* and *SC8.1,* were associated with stigma color. For this purpose, phenotypic data of an expanded mapping population comprising 545 F_2 individuals were incorporated for QTL analysis (**Table 4**). The confidence region of *SC2.1* explained 9.40% phenotypic variation and further delimited to 3.6 cm and physical position from 24,730,977 to 25,015,025 bp exhibited 180 kb interval between flanking markers S2M3 and S2B1-2 (**Figure 4**). The confidence interval (CI) of *SC8.1* explained 25.92% phenotypic variation in the enlarged mapping population, further narrowed down to a 3.7 cm region, which corresponded to a 138 kb interval (from 30,395,830 to 30,532,659 bp) between markers S8H-1 and S8E-7 (**Figure 5**), respectively.

A pairwise combination of the genotypes of *SC2.1* and *SC8.1* in the F_2 population was analyzed in 2019 and 2021 (**Figure 6A**).

The genotype of candidate QTLs *SC2.1* and *SC8.1* in MR-1 with green stigma was *AA* while for M4-7 with the yellow stigma it was *BB* (the genotypes of *SC2.1* and *SC8.1* being indicated by markers S2H9 and S8P19), respectively. The *AA* genotypes of *SC2.1*+*SC8.1* depicted that the "E" value was significantly lower as compared to *BB* genotypes, and the stigma color showed a natural tendency of green color. In contrast, the stigma color inclined to yellow when the genotype of *SC2.1*+*SC8.1* was *BB*; however, when the genotype of *SC2.1*+*SC8.1* was heterozygous, the "E" value was generally reported at the intermediate level. These findings support our claim that *SC2.1* and *SC8.1* jointly affected melon stigma color.

TABLE 3 | Detailed information of the new polymorphic cleaved amplified polymorphism sequence (CAPS) markers within *SC2.1* and *SC8.1*.

Marker	Sequence	Enzyme	Annealing temp
S2BC1	F:GCAACAACCAATATCACACCAT	BamI	55
	R:GCTCAGAGGCTAGAGATTATTCAA		
S2E-6	F:GTGTAAGTAAGAGATTGATGAGAGG	EcoRI	55
	R:TGGTTACCAACTCGAAGCTAA		
S2H-4	F:TGTACCTCTGTAATTCTTCGGATG	HindIII	55
	R:TGTAACAACCCACACAAACTCA		
S2M3	F:CTTCTTCTATGATGGCTACAGTCTT	PstI	55
	R:CGAGATGGTTGCTATCCTTGG		
S2B1-2	F:TGGACAACATGCACATTACACT	BclI	55
	R:AAGGTCGAAGATCATCTCCGTAT		
S8H9	F:TTTCAACCCACACTCTCATCTTC	HindIII	55
	R:CTCAATTATTTCCCTCTCCTACCC		
S8BC6	F:TGGTAAGAGTAGGACAACATATAGG	BclI	55
	R:GGAATATACGTTCACTCCATCAAC		
S8H-1	F:GCATGATAGTGATGTAGGTGAGAA	HindIII	55
	R:GTTCGGAATGGGAAAGAAGGTT		
S8E-1	F:AGAAGGAGATGAATCAAGTCTA	EcoRI	55
	R:TGTACCATACGCAATCGTTAGTCG		
S8S1	F:CCGTTCATCACACTCCACAAG	PstI	55
	R:GCGAAGTAATCCTATAACAGTCATC		

Analysis of Predicted Candidate Genes

A total of 10 and 26 genes with non-synonymous SNPs (nsSNPs) were identified as putative genes positioned on chromosomes 2 and 8 (**Tables 5**, **6**), and qRT-PCR was performed to identify the potential genes controlling stigma color, respectively (**Supplementary Figure S1**). A single gene (*MELO03C003165*) exhibited the significant differential expression profiling between parental lines at a 138 kb CI of *SC8.1* (**Figure 7**). In addition, a total of 6 genes exhibited significant differential expressions at a 180 kb CI of *SC2.1*.

The new marker 8B-13 used in 2021 is derived from the major effective QTL *GS8.1* obtained from another set of mapping populations used in a previous report from our lab (Qiao et al., 2021). Interestingly, QTLs representing the similar positions were obtained from two different populations, leading us to conclude that *SC8.1* is a stable QTL, which could have a major contribution to the regulation of stigma color. The gene *MELO03C003165* located in *GS8.1* also displayed the same

TABLE 4 | Quantitative traits locus (QTL) analysis of melon stigma color using expanded F_2 population.

QTL name	Trait	Adjacent marker	Marker interval position/cM	Chr.	LOD	R^2
SC2.1	stigma color/ΔE	S2M3∼S2B1-2	3.6	2	5.86	9.4%
SC8.1		S8E-7∼S8H-1	3.7	8	11.65	25.92%

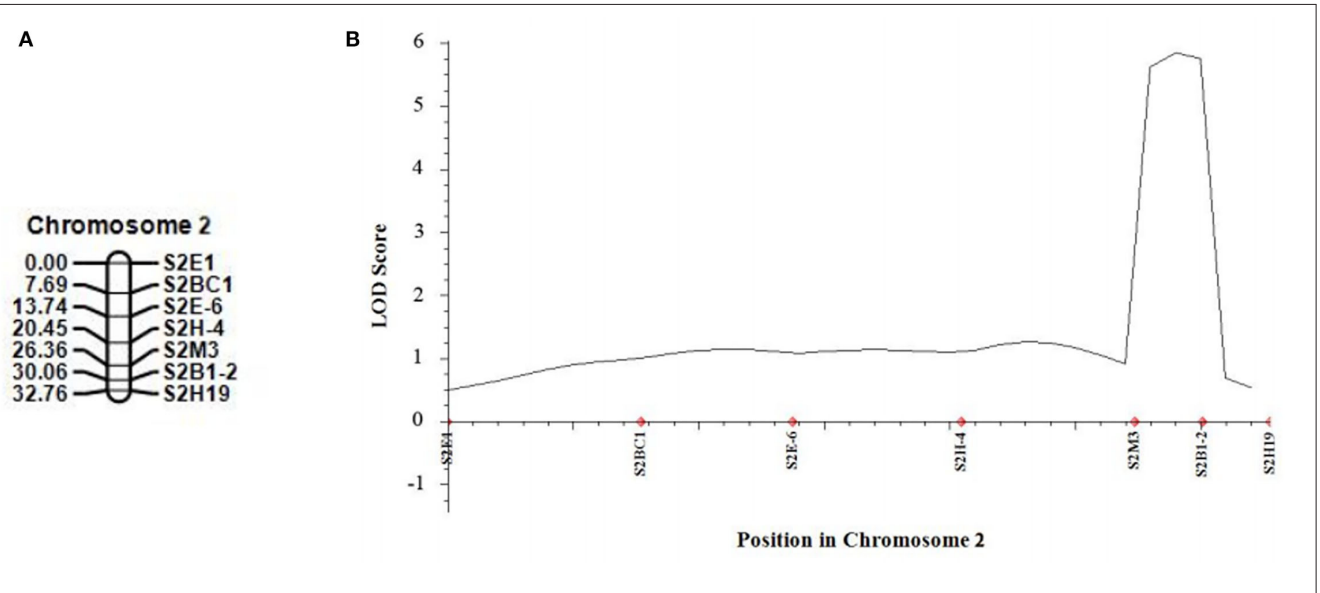


FIGURE 4 | Validation of the stigma color quantitative trait loci (QTL) in melon. **(A)** Linkage map of melon chromosome 2, based on 540 F_2 individuals derived from a cross between MR-1 and M4-7. **(B)** QTL curve for melon stigma color.

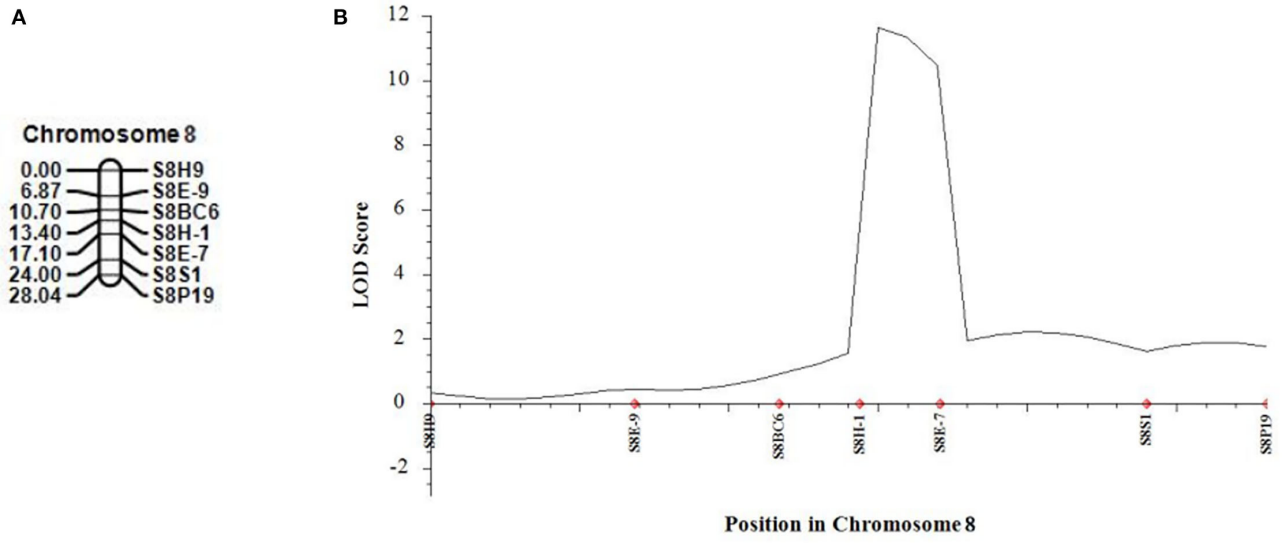


FIGURE 5 | Validation of the stigma color quantitative trait loci (QTLs) in melon. **(A)** Linkage map of melon chromosome 8 based on 540 F_2 individuals derived from parental lines crossing. **(B)** QTL curve for melon stigma color.

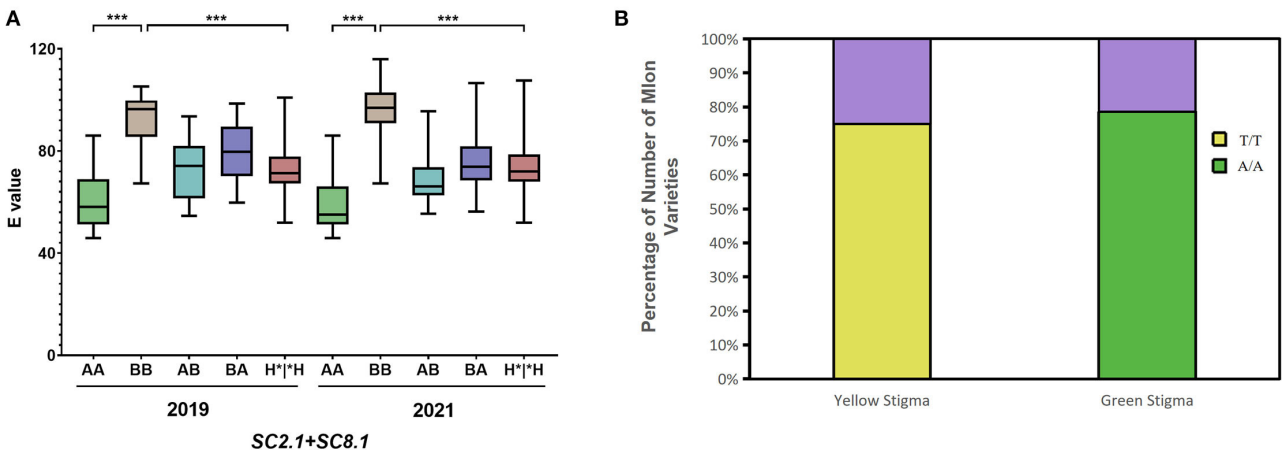


FIGURE 6 | Genotype analysis of quantitative trait locus (QTL) and candidate gene (*MELO03C003165*). **(A)** The combined genotype and phenotype of *SC2.1*+*SC8.1* in F_2 individuals were recorded in 2019 and 2021. In the horizontal coordinates, the former genotype belongs to *SC2.1*, the latter genotype belongs to *SC8.1*, and H*|*H represents the genotype containing H. **(B)** Relationship between genotype and stigma color of the *MELO03C003165* alleles in 110 melon varieties. The purple color shows the proportion of genotype and phenotype inconsistencies, Yellow and green show the proportion of genotype and phenotype concordance.

nsSNP mutation site ($SNP^{30,467,367}$), which was located in the exon region at 30,467,367th bp position. In MR-1, a base encodes leucine (Leu), whereas this base is mutated as T in the M4-7 line and significantly resulted in an amino acid change from Leu to histidine (His). Therefore, we analyzed *MELO03C003165* alleles across 110 melon varieties with different stigma colors (40 yellow stigmas and 70 green stigmas) and similarly checked the relationship between alleles and phenotype differences (**Supplementary Table S2**). The results showed that 78% of green stigma varieties had the same genotype with MR-1 and 75% of yellow stigma varieties had the same genotype with M4-7 (**Figure 6B**).

DISCUSSION

The stigma color phenotype is often considered as a communication signal for natural pollinators of flowers, and its differential diversity is driven by the natural selection process. At the physiological level, pigment content accumulation and chloroplast development are associated with differential coloration in higher plants (Yang et al., 2015). Different concentrations of chlorophyll and carotenoid components were known to cause a variety of colors in cucurbit fruits (Henderson et al., 1998; Burger et al., 2010; Zhang et al., 2016).

TABLE 5 | Predicted 26 genes with non-synonymous single-nucleotide polymorphisms (SNPs) between markers S2M3 and S2B1-2.

Gene ID	nsSNPs	Gene annotation
MELO3C017116	2	Kinesin-like protein
MELO3C017117	1	Calmodulin-binding protein 60 A-like isoform X1
MELO3C017120	2	Peroxidase 41-like
MELO3C017121	3	RING-type E3 ubiquitin transferase
MELO3C017123	6	Alpha-n-acetylglucosaminidase, putative
MELO3C017124	2	CDP-diacylglycerol-glycerol-3-phosphate 3-phosphatidyltransferase, putative
MELO3C017125	1	Betaine-aldehyde dehydrogenase
MELO3C017126	1	Mannose-1-phosphate guanyltransferase, putative
MELO3C017127	2	E2F transcription factor-like E2FE
MELO3C017128	1	Two-component response regulator ARR5-like
MELO3C017129	1	Chalcone synthase
MELO3C017130	3	Enhanced disease susceptibility 1
MELO3C017132	3	Microtubule-associated protein TORTIFOLIA1
MELO3C017134	1	Transcription factor MYB1R1
MELO3C017135	1	Serine/threonine-protein kinase AtPK2/AtPK19-like
MELO3C017136	1	Transportin-3
MELO3C017138	4	Germin-like protein subfamily T member 2
MELO3C017141	4	Dynein light chain
MELO3C017143	2	Transcription factor MYB35-like
MELO3C017144	1	DDT domain-containing protein DDR4
MELO3C017145	2	Protein NUCLEAR FUSION DEFECTIVE 4-like
MELO3C017146	2	Protein NUCLEAR FUSION DEFECTIVE 4
MELO3C017147	9	Zinc finger protein, putative
MELO3C017148	4	Ubiquitin carboxyl-terminal hydrolase-related protein
MELO3C017149	2	Pentatricopeptide repeat-containing protein
MELO3C017152	2	Protein NRT1/PTR FAMILY 2.10-like

TABLE 6 | Predicted 10 genes with non-synonymous single-nucleotide polymorphisms (SNPs) between markers S8P19 and S8H9.

Gene ID	nsSNPs	Gene annotation
MELO3C003159	2	Cysteine/Histidine-rich C1 domain family protein, putative
MELO3C003160	1	Cysteine/Histidine-rich C1 domain family protein, putative
MELO3C003161	4	Cysteine/Histidine-rich C1 domain family protein, putative
MELO3C003162	1	Early nodulin-75-like
MELO3C003163	1	Cysteine/Histidine-rich C1 domain family protein, putative
MELO3C003164	2	Cysteine/Histidine-rich C1 domain family protein, putative
MELO3C003165	1	Uracil phosphoribosyltransferase isoform X1
MELO3C003167	3	Glycine-rich cell wall structural protein 1.0-like
MELO3C003169	1	Ctenidin-1-like
MELO3C003172	1	Protein MIZU-KUSSEI 1

Development and usage of bi-parental F_2 population are known as a conventional and rapid method to identify the significant putative genes regulating the important traits. The size of F_2 mapping population can reduce the influence of environmental factors and reduce the biasness of accurate findings (Amanullah et al., 2021). In this study, we used fairly good mapping populations of F_2 and $F_{2:3}$ families and effectively identified two stable QTLs in chromosomes 2 and 8, harboring the potential genes associated with stigma color. Further, genetic mapping in the expanded F_2 population also signified the delimited target regions of *SC2.1* and *SC8.1*, respectively.

The QTL *SC8.1* was consistent with the genetic position of major QTL *GS8.1* that is reported in the previous report of our lab (Qiao et al., 2021), which similarly suggested the conservation of genetic mechanisms governing stigma color across distinct germplasms in melon. The gene *MELO03C003165* was the only gene with nsSNP mutation locus in both candidate QTLs (*SC8.1* and *GS8.1*) (**Table 6**). However, this gene exhibited to encode the uracil phosphoribosyl transferase (UPRT), triggered the plastid levels (Mainguet et al., 2009). The UK/UPRT has a dual role in coding both uridine kinase and uracil phosphoribosyltransferase that form uridine 5′-monophosphate (UMP) through the pyrimidine salvage pathway in *Arabidopsis* and regulates chlorophyll content in plants (Islam et al., 2007; Mainguet et al., 2009).

Further, our RT-qPCR analysis revealed 6 candidate genes harboring putative involvement in stigma color and similarly have explicit description, e.g., *MELO03C017116*, *MELO03C017120*, *MELO03C017121*, *MELO03C017130*, *MELO03C017134*, and *MELO03C017147* (**Table 5**). The gene *MELO03C017116* encodes kinesin-like protein (KAC), which is required for chloroplast dispersion within the cell under standard culture conditions (Suetsugu et al., 2012). In addition, KACs mediate the chloroplast light evasion response in an actin dependent (Shen et al., 2015). The gene *MELO03C017120* encodes peroxidase, which mediates chlorophyll degradation in the chloroplast or vacuole in the presence of phenolic compounds, such as apigenin (Yamauchi et al., 2004). The gene *MELO03C017121* encodes ring-type E3 ubiquitin transferase, which is homologous to the rice *GW2* gene encoding ring-type E3 ubiquitin transferase. The earlier studies have confirmed that *OsGW2* controlled the chlorophyll content with positive regulation of leaf senescence through genetic analysis of a knockout mutant (Shim et al., 2020). The gene *MELO03C017130* encodes enhanced disease susceptibility 1 (EDS1), which has been shown to affect many biological processes, such as chlorophyll content and reactive oxygen species (*ROS*) metabolism in annual plants (*Arabidopsis thaliana*) and woody plants (*Populus tremula* L. × *P. tremuloides*) (Su et al., 2014; Bernacki et al., 2018). The gene *MELO03C017134* encodes transcription factor *MYBR1*,

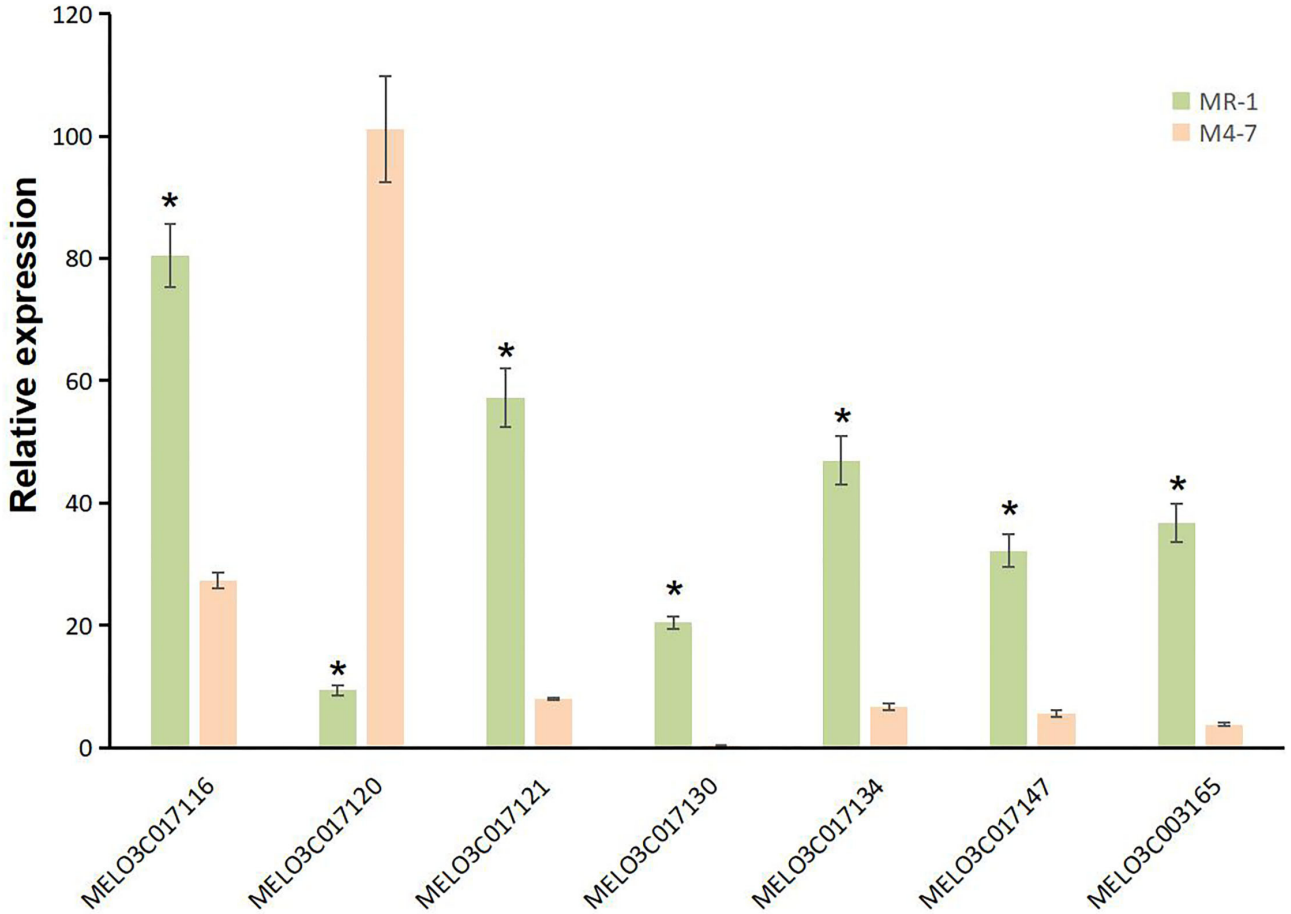


FIGURE 7 | Expression analysis for candidate genes with non-synonymous single-nucleotide polymorphisms (SNPs) on chromosome 2 (*MELO03C017116*, *MELO03C017120*, *MELO03C017121, MELO03C017130*, *MELO03C017134*, and *MELO03C017147*) and chromosome 8 (*MELO03C017165*). * represents the presence of significant differences.

and loss-of-function in *Arabidopsis* plants showed more rapid chlorophyll loss and senescence (Jaradat et al., 2013). The gene *MELO03C017147* encodes zinc finger protein, and it has been reported that overexpression of zinc-finger protein gene (such as *RHL41*, *AtZFP1*) resulted in an increase in chlorophyll content of *Arabidopsis* (Kazuoka et al., 2010; Han et al., 2014). *PSA2* is a member of the DnaJ-like zinc finger domain protein family that affects the light acclimation and chloroplast development (Wang et al., 2016). In conclusion, further screening of our candidate genes using more rigorous methodologies will provide more light in this direction.

At present, we infer that the difference in the stigma color of melon might be caused by the difference in total chlorophyll content in accordance with our results. There are other studies with similar results, chlorophyll deficiency in mutant tomato fruits triggered the yellowish skin color due to abnormal chloroplast development (Liu et al., 2021). At higher latitudes, some cucumbers are naturally subjected to a longer time for photosynthesis and chlorophyll synthesis, which results in green flesh color (Bo et al., 2019). However, the involvement of candidate genes in the synthesis and degradation of chlorophyll similarly indicate the specific biological pathway responsible for the differences in color of melon stigma, which need to be further investigated.

In addition, our field observations confirmed this favored behavior in bees feeding on melon flowers and showed a preference to visit the flowers with green stigma than flowers with yellow stigma. This confirms beyond the doubt that green stigmas are of greater value to melons both for farming and breeding programs. Thus, novel outcomes would be beneficial to provide the fundamental basis for the in-depth genetic understanding of the melon stigma color traits.

DATA AVAILABILITY STATEMENT

The original contributions presented in the study are included in the article/**Supplementary Material**, further inquiries can be directed to the corresponding author.

AUTHOR CONTRIBUTIONS

YL performed the experiment, data curation, formal analysis, manuscript draft, and reviewed and edited the manuscript. PG

and SL guided for the theoretical and practical experiments. XF, TZ, TL, and XW helped in formal analysis. SA reviewed and edited the manuscript language. FL supervised the research project and reviewed and edited the manuscript. All authors approved the final version of manuscript and disclosed no conflicts of interest.

FUNDING

This work was supported by the National Nature Science Foundation of China (31772331 and 32030094), the China Agriculture Research System of MOF and MARA (CARS-25), and Taishan Industrial Leading Talents Project [grant no. LJNY202112].

SUPPLEMENTARY MATERIAL

The Supplementary Material for this article can be found online at: https://www.frontiersin.org/articles/10.3389/fpls.2022.865082/full#supplementary-material

REFERENCES

Ahrazem, O., Diretto, G., Picazo, J. A., Fiore, A., Rubio-Moraga, A., Rial, C., et al. (2019). The specialized roles in carotenogenesis and apocarotenogenesis of the phytoene synthase gene family in saffron. *Front. Plant Sci.* 10, 249. doi: 10.3389/fpls.2019.00249

Amanullah, S., Gao, P., Osae, B. A., Saroj, A., Yang, T., Liu, S., et al. (2021). Genetic linkage mapping and QTLs identification for morphology and fruit quality related traits of melon by SNP based CAPS markers. *Sci. Hortic.* 278, 109849. doi: 10.1016/j.scienta.2020.109849

Amanullah, S., Saroj, A., Osae, B. A., Liu, S., Liu, H., Gao, P., et al. (2020). Detection of putative QTL regions associated with ovary traits in melon using SNP-CAPS markers. *Sci. Hortic.* 270, 109445. doi: 10.1016/j.scienta.2020.109445

Bernacki, M. J., Czarnocka, W., Witon, D., Rusaczonek, A., Szechynska-Hebda, M., Slesak, I., et al. (2018). Enhanced disease susceptibility 1 (EDS1) affects development, photosynthesis, and hormonal homeostasis in hybrid aspen (*Populus tremula* L. x *P. tremuloides*). *J. Plant Physiol.* 226, 91–102. doi: 10.1016/j.jplph.2018.04.014

Biesmeijer, J. C., Giurfa, M., Koedam, D., Potts, S. G., Joel, D. M., and Dafni, A. (2005). Convergent evolution: floral guides, stingless bee nest entrances, and insectivorous pitchers. *Sci. Nat.* 92, 444–450. doi: 10.1007/s00114-005-0017-6

Blacquiere, T. (2010). *Pesticide risk to wild pollinators: workshop report [Report]*. Wageningen University and Research Centre. Vol. 5. p. 17–20.

Bo, K., Wei, S., Wang, W., Miao, H., and Gu, X. (2019). Qtl mapping and genome-wide association study reveal two novel loci associated with green flesh color in cucumber. *BMC Plant Biol.* 19, 243. doi: 10.1186/s12870-019-1835-6

Burger, Y., Paris, H. S., Cohen, R., Katzir, N., Tadmor, Y., Lewinsohn, E., et al. (2010). Genetic diversity of *Cucumis melo*. *Hortic. Rev.* 36, 165–198. doi: 10.1002/9780470527238.ch3

Castillo, R., Fernandez, J. A., and Gomez-Gomez, L. (2005). Implications of carotenoid biosynthetic genes in apocarotenoid formation during the stigma development of crocus sativus and its closer relatives. *Plant Physiol.* 139, 674–689. doi: 10.1104/pp.105.067827

Dafni, A., and Giurfa, M. (1999). The functional ecology of floral guides in relation to insects behaviour and vision. *Evol. Theory Processes Mod. Perspect.* 363–383. doi: 10.1007/978-94-011-4830-6_23

Davies, K. M., Albert, N. W., and Schwinn, K. E. (2012). From landing lights to mimicry: the molecular regulation of flower colouration and mechanisms for pigmentation patterning. *Funct. Plant Biol.* 39, 619–638. doi: 10.1071/FP12195

Han, G. L., Wang, M. J., Yuan, F., Sui, N., Song, J., Wang, B. S., et al. (2014). The CCCH zinc finger protein gene AtZFP1 improves salt resistance in *Arabidopsis thaliana*. *Plant Mol. Biol.* 86, 237–253. doi: 10.1007/s11103-014-0226-5

Henderson, W. R., Scott, G. H., and Wehner, T. C. (1998). Interaction of flesh color genes in watermelon. *J. Hered* 89, 50–53. doi: 10.1093/jhered/89.1.50

Iida, A., Kazuoka, T., Torikai, S., Kikuchi, H., and Oeda, K. (2010). A zinc finger protein RHL41 mediates the light acclimatization response in Arabidopsis. *Plant J.* 24, 191–203. doi: 10.1046/j.1365-313x.2000.00864.x

Islam, M. R., Kim, H., Kang, S. W., Kim, J. S., Leong, Y. M., Hwang, H. J., et al. (2007). Functional characterization of a gene encoding a dual domain for uridine kinase and uracil phosphoribosyltransferase in *Arabidopsis thaliana*. *Plant Mol. Biol.* 63, 465–477. doi: 10.1007/s11103-006-9101-3

Jaradat, M. R., Feurtado, J. A., Huang, D., Lu, Y., and Cutler, A. J. (2013). Multiple roles of the transcription factor AtMYBR1/AtMYB44 in ABA signaling, stress responses, and leaf senescence. *BMC Plant Biol.* 13, 192. doi: 10.1186/1471-2229-13-192

Kevan, P. G., and Viana, B. F. (2003). The global decline of pollination services. *Biodiversity* 4, 3–8. doi: 10.1080/14888386.2003.9712703

Klein, A. M., Vaissiere, B. E., Cane, J. H., Steffan-Dewenter, I., Cunningham, S. A., Kremen, C., et al. (2007). Importance of pollinators in changing landscapes for world crops. *Proc. Biol. Sci.* 274, 303–313. doi: 10.1098/rspb.2006.3721

Liu, G. Z., Yu, H. Y., Yuan, L., Li, C., and Zhang, Y. (2021). SIRCM1, which encodes tomato Lytescent1, is required for chlorophyll synthesis and chloroplast development in fruits. *Hortic. Res.* 8, 14. doi: 10.1038/s41438-021-00563-6

Lunau, K. (2005). Stamens and mimic stamens as components of floral colour patterns. *Bot. Jahrb. Syst.* 127, 13–41. doi: 10.1127/0006-8152/2006/0127-0013

Lunau, K., Wacht, S., and Chittka, L. (1996). Colour choices of naive bumble bees and their implications for colour perception. *J. Comp. Physiol. A.* 178, 477–489. doi: 10.1007/BF00190178

Mainguet, S. E., Gakière, B., Majira, A., Pelletier, S., Bringel, F., Guérard, F., et al. (2009). Uracil salvage is necessary for early Arabidopsis development. *Plant J.* 60, 280–291. doi: 10.1111/j.1365-313X.2009.03963.x

Meng, L., Li, H., Zhang, L., and Wang, J. (2015). QTL Ici mapping: integrated software for genetic linkage map construction and quantitative trait locus mapping in biparental populations. *Crop J.* 3, 269–283. doi: 10.1016/j.cj.2015.01.001

Peitsch, D., Fietz, A., Hertel, H., Desouza, J., Ventura, D. F., and Menzel, R. (1992). The spectral input systems of hymenopteran insects and their receptor-based color-vision. *J. Compar. Physiol. Sensory Neural Behav. Physiol.* 170, 23–40. doi: 10.1007/BF00190398

Qiao, A. H., Fang, X. F., Liu, S., Liu, H. Y., Gao, P., et al. (2021). QTL-seq identifies major quantitative trait loci of stigma color in melon. *Hortic. Plant J.* 7, 318–326. doi: 10.1016/j.hpj.2021.01.004

Rodrigo Gomez, S., Ornosa, C., Selfa, J., Guara, M., and Polidori, C. (2016). Small sweat bees (hymenoptera: halictidae) as potential major pollinators of melon (*Cucumis melo*) in the mediterranean. *Entomol. Sci.* 19, 55–66. doi: 10.1111/ens.12168

Shen, Z. Y., Liu, Y. C., Bibeau, J. P., Lemoi, K. P., Tuzel, E., Vidali, L., et al. (2015). The kinesin-like proteins, KAC1/2, regulate actin dynamics underlying chloroplast light-avoidance in Physcomitrella patens. *J. Integr. Plant Biol.* 57, 106–119. doi: 10.1111/jipb.12303

Shim, K. C., Kim, S. H., Jeon, Y. A., Lee, H. S., Adeva, C., Kang, J. W., et al. (2020). A ring-type E3 ubiquitin ligase, *OsGW2*, controls chlorophyll content and dark-Induced senescence in rice. *Int. J. Mol. Sci.* 21, 1704. doi: 10.3390/ijms21051704

Su, X. F., Qi, X. L., and Cheng, H. M. (2014). Molecular cloning and characterization of enhanced disease susceptibility 1 (EDS1) from Gossypium barbadense. *Mol. Biol. Rep.* 41, 3821–3828. doi: 10.1007/s11033-014-3248-9

Suetsugu, N., Sato, Y., Tsuboi, H., Kasahara, M., Imaizumi, T., Kagawa, T., et al. (2012). The KAC family of kinesin-like proteins is essential for the association of chloroplasts with the plasma membrane in land plants. *Plant Cell Physiol.* 53, 1854–1865. doi: 10.1093/pcp/pcs133

Wang, C. H. (2016). *Fine mapping and Cloning of purple stigma gene in rice (Oryza sativa L.)* (master's thesis). Beijing: Chinese Academy of Agricultural Sciences.

Wang, Y. W., Chen, S. M., Wang, W. J., Huang, X. Q., Zhou, C. F., Zhuang, Z., et al. (2016). The dnaJ-like zinc finger domain protein PSA2 affects light acclimation and chloroplast development in *arabidopsis thaliana*. *Front. Plant Sci.* 7, 360. doi: 10.3389/fpls.2016.00360

Yamauchi, N., Funamoto, Y., and Shigyo, M. (2004). Peroxidase-mediated chlorophyll degradation in horticultural crops. *Phytoche. Rev*. 3, 221–228. doi: 10.1023/B:PHYT.0000047796.98784.06

Yang, Y. X., Chen, X. X., Xu, B., Li, Y. X., Ma, Y. H., and Wang, G. G. (2015). Phenotype and transcriptome analysis reveals chloroplast development and pigment biosynthesis together influenced the leaf color formation in mutants of *Anthurium andraeanum*'Sonate'. *Front. Plant Sci.* 6, 139. doi: 10.3389/fpls.2015.00139

Zhang, L., Zhang, Z. K., Zheng, T. T., Wei, W. L., Zhu, Y. M., Gao, Y. S., et al. (2016). Characterization of carotenoid accumulation and carotenogenic gene expression during fruit development in yellow and white loquat fruit. *Hortic. Plant J.* 2, 9–15. doi: 10.1016/j.hpj.2016.02.006

Zhao, G. Y., Qin, L., Tayeb, M., Zhang, Y., and Liang, Y. (2017). Inheritance and phenotypic analysis of yellow stigma (ys) mutent of tomato. *Acta Hortic. Sin.* 44, 2109–2116.

Conflict of Interest: The authors declare that the research was conducted in the absence of any commercial or financial relationships that could be construed as a potential conflict of interest.

Publisher's Note: All claims expressed in this article are solely those of the authors and do not necessarily represent those of their affiliated organizations, or those of the publisher, the editors and the reviewers. Any product that may be evaluated in this article, or claim that may be made by its manufacturer, is not guaranteed or endorsed by the publisher.

Copyright © 2022 Lv, Gao, Liu, Fang, Zhang, Liu, Amanullah, Wang and Luan. This is an open-access article distributed under the terms of the Creative Commons Attribution License (CC BY). The use, distribution or reproduction in other forums is permitted, provided the original author(s) and the copyright owner(s) are credited and that the original publication in this journal is cited, in accordance with accepted academic practice. No use, distribution or reproduction is permitted which does not comply with these terms.

frontiers | Frontiers in Plant Science

REVIEW
published: 19 May 2022
doi: 10.3389/fpls.2022.862486

Research Advances in Genetic Mechanisms of Major Cucumber Diseases Resistance

Yujin He[1†], Mingming Wei[2†], Yanyan Yan[1†], Chao Yu[1], Siqi Cheng[1], Yihan Sun[1], Xiangtao Zhu[3], Lingling Wei[4*], Huasen Wang[1,2*] and Li Miao[1*]*

[1] Key Laboratory for Quality and Safety Control of Subtropical Fruits and Vegetables, Collaborative Innovation Center for Efficient and Green Production of Agriculture in Mountainous Areas of Zhejiang Province, Ministry of Agriculture and Rural Affairs, College of Horticulture Science, Zhejiang Agriculture and Forestry University, Hangzhou, China, [2] Ministry of Agriculture Key Laboratory of Biology and Genetic Resource Utilization of Rubber Tree, State Key Laboratory Breeding Base of Cultivation and Physiology for Tropical Crops, Rubber Research Institute, Chinese Academy of Tropical Agricultural Sciences, Danzhou, China, [3] College of Jiyang, Zhejiang Agriculture and Forestry University, Zhuji, China, [4] Institute of Ecological Civilization, Zhejiang Agriculture and Forestry University, Hangzhou, China

OPEN ACCESS

Edited by:
Pei Xu,
China Jiliang University, China

Reviewed by:
Tianshu Sun,
University of Cambridge, United Kingdom
Changlong Wen,
Beijing Vegetable Research Center, China

***Correspondence:**
Xiangtao Zhu
zxt8202@163.com
Lingling Wei
wll@zafu.edu.cn
Huasen Wang
wanghs@zafu.edu.cn
Li Miao
happymml@163.com

[†] *These authors have contributed equally to this work*

Specialty section:
This article was submitted to Crop and Product Physiology, a section of the journal Frontiers in Plant Science

Received: *26 January 2022*
Accepted: *22 February 2022*
Published: *19 May 2022*

Citation:
He Y, Wei M, Yan Y, Yu C, Cheng S, Sun Y, Zhu X, Wei L, Wang H and Miao L (2022) Research Advances in Genetic Mechanisms of Major Cucumber Diseases Resistance. Front. Plant Sci. 13:862486. doi: 10.3389/fpls.2022.862486

Cucumber (*Cucumis sativus* L.) is an important economic vegetable crop worldwide that is susceptible to various common pathogens, including powdery mildew (PM), downy mildew (DM), and Fusarium wilt (FM). In cucumber breeding programs, identifying disease resistance and related molecular markers is generally a top priority. PM, DM, and FW are the major diseases of cucumber in China that cause severe yield losses and the genetic-based cucumber resistance against these diseases has been developed over the last decade. Still, the molecular mechanisms of cucumber disease resistance remain unclear. In this review, we summarize recent findings on the inheritance, molecular markers, and quantitative trait locus mapping of cucumber PM, DM, and FM resistance. In addition, several candidate genes, such as PM, DM, and FM resistance genes, with or without functional verification are reviewed. The data help to reveal the molecular mechanisms of cucumber disease resistance and provide exciting new opportunities for further resistance breeding.

Keywords: cucumber, powdery mildew, downy mildew, Fusarium wilt, genetic mechanism

INTRODUCTION

Cucumber (*Cucumis sativus* L.) is a popular vegetable grown on a large scale worldwide. It has an edible fruit with refreshing tastes and is enriched with vitamin E. In the recent years, with the increasing cultivation area of cucumber, it has gradually moved towards a large-scale planting model. However, because cucumber is susceptible to horticultural diseases, including powdery mildew (PM), downy mildew (DM), Fusarium wilt (FW), Verticillium wilt, *Cladosporium cucumerinum*, Corynespora leaf spot, green mottle mosaic virus, and bacterial soft rot, it does not help for industrialized production, which results in substantial economic losses to cucumber producers. Among the diseases, PM, DM, and FW are the serious main fungal diseases of cucumber that result in severe production and quality losses (Block and Reitsma, 2005; Zhang et al., 2016; Vakalounakis and Lamprou, 2018). Several effective approaches have been widely used to control these diseases, such as various fungicides, biofungicides, and grafting. However, the variable adaptability of pathogens, fungicides residues on plants and in the environment, and

higher production costs associated with these approaches indicate that better methods are required (Mahmood et al., 2016; Chen et al., 2021). Therefore, breeding more resistant cultivars is an efficient approach to control cucumber diseases and understanding the genetic and molecular mechanisms of cucumber disease resistance is a crucial focus of cucumber breeding programs.

There is no conclusive genetic data on cucumber disease resistance at present. Some studies have shown that PM, DM, and FW resistance are quantitative traits controlled by multiple genes, respectively. For instance, the resistance to PM is controlled by a recessive single gene, and susceptibility is controlled by partial dominant genes (Nie et al., 2015a). In cucumber, the DM resistance was controlled by multiple recessive genes and has the duplicate recessive epistasis and the additive effects data confirmed the detected 14 quantitative trait loci (QTLs) for DM resistance (Innark et al., 2020). Dong et al. (2019) found that the inheritance of FW resistance in cucumber is a quantitative resistance trait controlled by multiple genes, including two pairs of additive dominance-epistatic major genes and an additive-dominance polygene. However, resistance to PM, DM, and FW is also controlled by a single gene. For example, a single recessive gene, *pm*, for PM resistance in leaves, has been mapped to an approximately 468 kb region on chromosome 5 in IL52 (Zhang et al., 2018). A recessive resistance gene, *dm-1*, has been identified in many DM-resistant plant introduction (PI) lines, including PI 197087, Gy4, Chipper, and the Market more series (Barnes and Epps, 1954; Wehner and Shetty, 1997; Call et al., 2012a). *Foc* has been incorporated in the Dutch-type cucumber hybrids and has widely controlled FW of cucumber for 40 years (Vakalounakis and Fragkiadakis, 2003). Variety is a major factor in the inheritance of cucumber disease resistance. At present, the mapping population of cucumber PM-resistance genes has been mainly constructed using PI 197088, S06, WI 2757, H136, K8, and IL52. In the constructed segregation population, 19 possible PM resistance QTLs were identified (Wang et al., 2020). In the population generated using the high-resistance variety PI 197088, *pm1.1*, *pm1.3*, *pm4.3*, *pm5.1*, *pm5.3*, *pm5.4*, *pm6.2*, *pm6.3*, and *pm7.1* are the main resistance QTLs and *pm4.1* and *pm6.3* are two major QTLs in the population constructed using high-resistance variety S06. Additionally, *pm5.3* is the most important QTL for PM resistance in the population constructed using the high-resistance cultivar IL52 (Sakata et al., 2006; Liu et al., 2008; Fukino et al., 2013; Yoshioka et al., 2014; Zhang et al., 2018). Most PM-related genes are closely linked to DM-related genes; therefore, they may also play equally important roles in DM resistance (Wang et al., 2018; Zhang et al., 2018). The materials used for mapping genes associated with PM are also used for selecting genes associated with DM. At present, the DM-resistance gene mapping population has mainly been constructed using PI 197085, PI 197088, WI 7120 (PI 330628), WI 2757, S94, TH118FLM, IL52, and K8. In total, 16, 5, and 2 QTLs have been identified in PI 197085, PI 330628, and WI 2757, respectively (Wang et al., 2020). For example, Wang et al. (2018) developed 55 microsatellite markers and found that *dm5.1*, *dm5.2*, and *dm5.3* are the main resistance QTLs in the highly resistant variety PI 197088 and *dm1.1*, *dm2.1*, and *dm6.2* are the main sensitivity-related QTLs in the highly susceptible variety Coolgreen. Li et al. (2018) used 141 simple sequence repeat (SSR) markers to identify 5 QTLs, namely, *dm1.1*, *dm3.1*, *dm4.1*, and *dm5.1/dm5.2*, among which, *dm4.1* is a major resistance QTL in the cross-population derived from PI 197088 and Changchunmici. The development of resistance mechanisms against FW occurred more slowly than against PM and DM and few materials resistant to FW have been identified. Dong et al. (2019) detected a major effect QTL, *fw2.1*, in a 1.91-Mb region on chromosome 2 using F2 segregating populations derived from Superina (P1) and Rijiecheng (P2). Additionally, different identification and evaluation methods, mapping population, infection site, and pathogen races also influence the inheritance of cucumber disease resistance (Vakalounakis and Lamprou, 2018; Innark et al., 2020; Wang et al., 2020). The epigenetic variations also play important roles in crop disease resistance and are affected by environmental factors (Zhi and Chang, 2021), but the epigenetic regulation in cucumber disease resistance has not been found yet.

Many candidate genes for PM, DM, and FW disease resistance in cucumber have been identified using genetic mapping as well as transcriptomic and proteomic analyses and several genes have been cloned for functional verification. The candidate genes for these diseases are all involved in plant hormone signal transduction, cell redox homeostasis, and transcriptional regulation. In PM disease, the Mildew Resistance Locus O (*MLO*)-*like* genes, including *CsaMLO1–13*, but especially *CsMLO1*, *−8,* and *−11*, are the most studied PM genes in cucumber (Schouten et al., 2014; Nie et al., 2015b; Berg et al., 2017) and MLO-based PM resistance caused by the formation of cell wall depositions (papillae) by the plant cell directly beneath the site of PM penetration (Wolter et al., 1993), but the function is not yet unraveled. The candidate genes for DM resistance are involved in various metabolic pathways. For example, STAYGREEN (*CsSGR*), which is involved in the chlorophyll degradation pathway, plays important roles in DM disease resistance (Wang et al., 2019) and the transient expression of *CsLRK10L2*, which is a Damage-associated Molecular Pattern Molecule (DAMP) oligogalacturonan receptor and is involved in the breakdown of pectin, in *Nicotiana benthamiana* (*N. benthamiana*) leaves causes necrosis and results in high DM resistance (Berg et al., 2020). Several candidate genes of both DM and PM resistance have also been identified. The gene *Csa5M622830.1*, a GATA transcriptional factor gene, may prevent supplement nutrition from reaching DM and PM pathogens (Zhang et al., 2018). Compared with PM and DM, fewer candidate genes resist to FW have been identified. However, resistance to FW is enhanced in transgenic cucumber harboring Ginkbilobin2-1 (*GNK2-1*) (Liu et al., 2010). Additionally, a great number of candidate microRNAs (miRNAs), long non-coding RNAs (lncRNAs), proteins, and metabolites related to DM, PM, and FW in cucumber have also been identified (Li et al., 2011; Xu et al., 2019, 2021; Nie et al., 2021; Sun et al., 2021).

Although a number of molecular markers, QTLs, and candidate genes have been identified, the genetic mechanisms of cucumber disease resistance are not well understood. Here, we independently review the genetic mechanisms of cucumber resistance to PM, FW, and DM and also provide new insights into future management strategies.

INHERITANCE, QUANTITATIVE TRAIT LOCI MAPPING, AND CANDIDATE GENES OF CUCUMBER RESISTANCE TO POWDERY MILDEW

Powdery mildew mainly invades cotyledons, leaves, and stems, resulting in yellow, crisp dry leaves in which photosynthesis is seriously affected, thereby reducing cucumber yield. PM in cucumber is commonly caused by *Podosphaera xanthii* (*Sphaerotheca fuliginea*) and *Golovinomyces cichoracearum* (*Erysiphe cichoracearum*) (Block and Reitsma, 2005), which share the characteristics of frequent infection, short incubation period, and strong transmission. They also can occur annually during cucumber production.

Inheritance of Powdery Mildew Resistance in Cucumber

A classical genetic analysis demonstrated that cucumber PM resistance is a quantitative trait controlled by multiple recessive genes in different germplasms (Smith, 1948; Kooistra, 1968; Morishita et al., 2003; He et al., 2013). Early in 1948, Smith (1948) suggested that PM resistance in Puerto Rico 37 was controlled by recessive genes and then, associated recessive genes were identified in the PI 2008151 and Natsufushinari varieties (Kooistra, 1968). The two recessively inherited genes linked to the QTL in chromosome 5 are responsible for PM in WI2757 (He et al., 2013). Additionally, studies have shown that PM resistance in cucumber is controlled by a single recessive gene. A single recessive gene *pm* for PM resistance in leaves has been mapped to an approximately 468 kb region on chromosome 5 in IL52 (Zhang et al., 2018). The resistance to PM in the stem of NCG-12 is also controlled by a single recessive nuclear gene (*pm-s*) (Liu et al., 2017). The recessive inheritance of PM is not convenient to use in cucumber breeding (Xu X. et al., 2016). The temperature-dependent PM resistance in PI 197088-5 is due to one recessive gene and another incompletely dominant gene (Morishita et al., 2003). Shen et al. (2011) found that cucumber PM traits are determined by the interaction of major genes and polygenes in the JIN 5-508 variety and the inheritance of major genes dominates. Xu X. et al. (2016) first reported the dominantly inherited major-effect QTL (*Pm1.1*) for PM in the Jin5-508-derived SSSL0.7 line. However, quantitative resistance under polygenic control is generally more durable than that conferred by a single dominant gene (Kelly and Vallejo, 2006). The inheritance of cucumber disease resistance is dependent on the variety and material (Wang et al., 2020) and the genetic laws governing cucumber PM resistance are still not well understood.

Molecular Markers and Quantitative Trait Loci of Powdery Mildew Resistance in Cucumber

Effective molecular markers and QTLs controlling resistance to PM in cucumber have also been reported in recent years (de Ruiter et al., 2008; Fukino et al., 2013; He et al., 2013; Nie et al., 2015a; Wang et al., 2019). Various molecular markers have been used for mapping PM-associated loci in different cucumber species. In total, 140 PM-associated Specific-locus Amplified Fragment Sequencing (SLAFs) and two hot regions (*pm5.3* and *pm6.1*) have been identified on chromosomes 1 and 6 using an F2 segregating population derived from H136 as the susceptible parent and BK2 as the resistance donor (Zhang et al., 2015). In total, 17 SSR markers have been discovered to be linked to the *pm-s* gene, which maps to chromosome 5 between the pmSSR27 and pmSSR17 markers (Liu et al., 2017). The introgression of the 6.8-Mb segment that contains 3,016 single nucleotide polymorphisms (SNPs) causes the phenotypic variation in PM resistance between SSL508-28 and D8 (Xu et al., 2017) and this region, *pm5.1*, is consistent with major loci for PM resistance found in many studies (Nie et al., 2015a; Xu Q. et al., 2016; Wang et al., 2018). In total, 113 SNP and InDel markers significantly associated with PM resistance have been identified on chromosomes 4 and 5 using a genome-wide association analysis (GWAS) (Tan, 2021). Additionally, four QTLs (*pm1.1*, *pm2.1*, *pm5.1*, and *pm6.1*) have been identified on chromosomes 1, 2, 5, and 6 using the recombinant inbred line (RIL) population derived from a cross between PI 197088 and the susceptible line Coolgreen. Among them, *pm5.1* is the major-effect QTL, explaining 32.4% phenotypic variance, whereas the minor-effect QTL, *pm6.1*, contributed to disease susceptibility (Wang et al., 2018). Recently, *pm5.2* (30% R2 at LOD 11) and *pm6.1* (11% R2 at LOD 3.2) conferred PM resistance in an F2 population derived from a cross between PM-R (resistant) and PM-S (susceptible) (Zhang C. et al., 2021). After further studies on the segregation populations constructed from PI 197088, S06, WI 2757, H136, K8, and IL52, 19 possible QTLs for PM resistance were mapped (Wang et al., 2020). Moreover, PM resistance QTLs are also organ-dependent in cucumber. The disease indices of the hypocotyl, cotyledon, and true leaf of WI2757 were analyzed by multiple QTL mapping. *pm5.1* was the major QTL for cotyledon resistance, *pm5.2* controlled hypocotyl resistance, *pm1.1* and *pm1.2* controlled leaf resistance and both the minor QTLs, *pm3.1* and *pm4.1*, caused leaves or hypocotyls to have an increased PM susceptibility (He et al., 2013). Liu et al. (2017) showed that *pm-s*, located on chromosome 5, controls PM resistance in cucumber stem and the gene *Csa5G623470*, encoding an MLO protein, is closely related to the PM resistance of stem. Environmental factors also play important roles in the resistance to PM. Sakata et al. (2006) constructed a cucumber RIL using the PI197088-1 variety, resistant to PM, and the Santou variety, susceptible to PM, under both the high and low temperatures. Only one QTL played a role at high (26°C) and low (20°C) temperatures, which suggested that resistance was related to temperature. This was the first study on the QTL mapping of PM resistance genes at different temperatures. Like PM, DM is also an important disease in cucumber production. Many PM QTLs or genes are closely linked to DM QTLs or genes; consequently, they may also play equally important roles in DM resistance (Wang et al., 2018; Zhang et al., 2018). For example, *pm2.1*, *pm5.1*, and *pm6.1* associated with PM QTLs are colocalized with the DM QTLs *dm2.1*, *dm5.2*, and *dm6.1*, respectively (Wang et al., 2018). These studies showed inconsistent results regarding the number and

locations of QTLs underlying PM and this may be due to differences in the germplasms, genetic maps, analysis methods, and environmental conditions.

Candidate Genes or Proteins Involved in the Powdery Mildew Resistance of Cucumber

In the recent years, candidate genes or proteins associated with PM resistance have been identified using transcriptomic and proteomic analyses and genetic mapping. Differentially expressed genes (DEGs) have been identified between PM-resistant species and susceptible species, such as SSL508-28 and D8, XY09-118 and Q10, BK2 and H136, and NILs of S1003 and Near Iso-genic Lines (NIL) (*pm5.1*), using transcriptomes (Xu et al., 2017; Nie et al., 2021; Zhang P. et al., 2021; Zheng et al., 2021). These DEGs function in plant hormone signal transduction, phenylpropanoid biosynthesis, phenylalanine metabolism, ubiquinone and other terpenoid-quinone biosynthesis, endocytosis, plant–pathogen interaction, and Mitogen-activated Protein Kinases (MAPKS). In particular, genes encoding the transcriptome factors (WRKY, NAC, and TCP), peroxidase, nucleotide-binding site (NBS), glucanase, and chitinase have been analyzed (Zhang P. et al., 2021; Zheng et al., 2021). The miRNAs *Csa-miR172c-3p* and *Csa-miR395a-3p* are upregulated in PM-resistant D8 and *Csa-miR395d-3p* and *Csa-miR398b-3p* are downregulated in PM-susceptible SSSL508-28, suggesting that their target genes *AP2*, *bHLH*, *Dof*, *UGT*, and *LASPO* may play important roles in PM-inoculated cucumber leaves (Xu et al., 2020). Nie et al. (2021) showed that 49 differentially expressed lncRNAs may function as target mimics for 106 miRNAs during cucumber_PM interaction, including *miR156*, *miR159*, *miR164*, *miR166*, *miR169*, *miR171*, *miR172*, *miR6173, miR319*, *miR390, miR393*, *miR396*, and *miR5658*. Moreover, differentially regulated processes, proteins, and accumulated metabolites between different PM-resistant materials have also been detected, including flavonoid, hormones, fatty acid, diterpenoid metabolism, tetrapyrrole biosynthetic process, sulfur metabolic process, and cell redox homeostasis (Xu et al., 2019; Zhang P. et al., 2021).

A larger number of potential genes related to PM in cucumber have been identified using genetic mapping. Nie et al. (2015a) delimited the recessive major QTL *pm5.1* for PM resistance in an approximately 1.7-kb region between markers UW065021 and UW065094 and they identified an *MLO-like* gene *CsMLO1*, which encodes a cell membrane protein, as a candidate gene for PM resistance (Nie et al., 2015b). Schouten et al. (2014) obtained 13 *MLO* homologs, *CsaMLO1-13*, in cucumber. Among them, the ectopic expression of *CsMLO1* in the PM-resistant *Atmlo2-Atmlo12* double-mutant results in PM sensitivity recovery. The overexpression of *CsaMLO1* or *CsaMLO8* completely restores PM susceptibility in a tomato *mlo* mutant, whereas the overexpression of *CsaMLO11* only partially restores PM susceptibility (Nie et al., 2015b; Berg et al., 2017). To date, only *MLO* genes in cucumber have been functionally verified as being involved in PM resistance. In addition to *MLO* genes, other candidate PM resistance genes have been identified. *Csa1M064780* and *Csa1M064790*, encoding a cysteine-rich receptor-like protein kinase, are the most likely candidate PM resistance genes (Xu Q. et al., 2016). The single recessive gene *Csa5M622830*, which encodes a GATA transcriptional factor, is likely the gene for the complete PM resistance introgressed from *Cucumis hystrix* (Zhang et al., 2018). *CsGy5G015660*, which encodes a putative leucine-rich repeat receptor-like serine/threonine-protein kinase, is currently considered a strong candidate gene for PM resistance in cucumber (Liu et al., 2021; Zhang C. et al., 2021). Moreover, proteins related to PM resistance have also been identified and functionally verified. Two NBS-Leucine-rich Repeat (LRR) proteins (CsRSF1 and CsRSF2), closely correlated with Abscisic Acid (ABA) and Gibberellin (GA) signals in cucumber, are predicted to have a similar domain sequence with the *Arabidopsis* PM-resistance protein RESISTANCE TO POWDERY MILDEW8 (RPW8) (Xiao et al., 2001). The transient silencing of *CsRSF1* and *CsRSF2* reduces the resistance of cucumber to PM, whereas the transient overexpression of *CsRSF1* and *CsRSF2* improves the resistance of cucumber to PM (Wang et al., 2021). Transcription factors, such as GRAS, DNA-binding with One Finger (DoF), Eukaryotic Initiation Factor 2 (eIF2α), Polygalacturonase (PG), UDP-Glycosyltransferase (UGT), and Serine/threonine Protein Kinases (STPKs) and their target genes, are also differentially expressed after PM inoculation (Zhong, 2020). Translationally Controlled Tumor Protein (TCTP) is a highly conserved and multifunctional protein and CsTCTP1 may regulate the defense responses of cucumber or ABA signaling to control PM disease in cucumber. CsTCTP2 may regulate the Target of Rapamycin (TOR) signal in response to PM stress (Meng et al., 2018). These studies provide new insights into cucumber responses to PM and the potential genes related to PM will be highly helpful in breeding cucumber varieties with enhanced PM resistance.

INHERITANCE, QUANTITATIVE TRAIT LOCI MAPPING, AND CANDIDATE GENES OF CUCUMBER RESISTANCE TO DOWNY MILDEW

Downy mildew of cucumber is caused by the obligate biotrophic oomycete *Pseudoperonospora cubensis*. It mainly infects leaves, but can also harm stems and inflorescences. It can occur from seedling to adult stage, but is particularly prevalent when cucumber enters the harvest stage. During the period of seedling infection, irregular chlorotic and withered yellow spots are produced on the reverse sides of cotyledons. A gray-black mold layer is produced when the plant becomes wet and cotyledons die when the infection is serious. During the adult stage, the disease gradually spreads upward from the lower leaves. At the beginning of the disease, light green water-immersion spots appear on the backs of the leaves. At the middle stage of the disease, the leaf spots fade from green to light yellow and the leaf backs become yellowish-brown. At the later stage, the disease spots converge and shrink upward from the leaf edges and finally, the whole leaf withers. In serious cases, all the leaves on the plant die (Zhang et al., 2016).

Inheritance of Downy Mildew Resistance in Cucumber

Researchers have studied the inheritance of cucumber DM resistance. However, due to different resistance germplasms and inconsistent identification methods, there is no consensus on the genetic laws governing cucumber DM resistance. As early as 1942, DM-resistant lines were screened and DM resistance is controlled by a recessive resistance gene, *dm-1*, in many resistant PI lines, including PI 197087, Gy4, Chipper, and the Marketmore series (Jenkins, 1942; Barnes and Epps, 1954; Wehner and Shetty, 1997; Call et al., 2012a). Simultaneously, multiple recessive genes are also involved in the regulation of cucumber DM resistance in resistant germplasms, including cucumber varieties WI4783, Wisconsin SMR18, K8 and K18, PI19708, CSL0067, and CSL0139 (Doruchowski and Lakowska-Ryk, 1992; Zhang et al., 2013; Szczechura et al., 2015; Wang et al., 2016). Call et al. (2012b) identified three highly DM-resistant materials, PI 197088, PI 330628, and PI 605996, from 1,300 cucumber collections. Among them, PI 197088 is the most studied for DM resistance, with multiple genes being controlled in breeding programs (Li et al., 2018; Liu et al., 2021). PI 197088 also has high resistance to PM. There are different genetic bases of DM-resistant germplasms. Therefore, the identification of DM-associated molecular markers and QTLs in various resistant materials may help to increase the inheritance of DM through breeding programs.

Molecular Markers and Quantitative Trait Loci of Downy Mildew Resistance in Cucumber

A variety of DM-associated QTLs has been identified in different varieties using Sequence Characterized Amplified Regions (SCAR), SSR, and SNP markers in recent years. The genetic linkage map was constructed using 66 polymorphic SSR markers and using this linkage map, 14 QTLs have been detected by evaluating DM in cotyledons as well as first and second true leaves after inoculation. LG5.1, located between the SSR03943 and SSR19172 markers, was detected at all the leaf stages (Innark et al., 2020). Based on the linkage map having 328 SSR and SNP markers, *dm4.1,* and *dm5.1*, compared with *dm2.1* and *dm6.1*, were determined to be the major effect of QTL (R^2 = 15–30%) with additive effects and this has been reproducibly detected in four environments (US2013, US2014, IT2013, and NL2013) (Wang et al., 2016). In total, five QTLs associated with DM resistance have been identified on chromosomes 1, 3, 4, and 5 in seven independent experiments and *dm4.1*, explaining 27% of the phenotypic variance, has been reliably detected in all the indoor experiments (Li et al., 2018). The DM candidate QTLs related to DM have been detected using diverse evaluation methods that consist of different plant organs (cotyledons and true leaves), developmental stages (seedlings and adult plants), and evaluation criteria (lesion expansion and sporulation extent) and the *dm1.1* QTL has the largest effect on resistance among the nine QTLs detected (Yoshioka et al., 2014). In addition to QTL mapping methods, bulked segregant analyses (BSAs), next-generation sequencing (NGS), and GWASs have been the most rapid and effective ways of studying the genetic inheritance of DM resistant in cucumber. In total, five QTLs (*dm2.2*, *dm4.1*, *dm5.1*, *dm5.2*, and *dm6.1*) have been identified and *dm2.2* has the largest effect on DM resistance as assessed by combining BSA and NGS methods based on SNP markers (Win et al., 2017). Additionally, 18 QTLs have been detected through the GWAS of a core database of 97 cucumber lines, but only six QTLs (*dmG1.4*, *dmG4.1*, *dmG4.3*, *dmG5.2*, *dmG7.1*, and *dmG7.2*) are associated with stable DM resistance (Liu et al., 2021). To date, PI 197085, PI 197088, WI 7120 (PI 330628), WI 2757, S94, TH118FLM, IL52, and K8 have been used for mapping QTLs associated with DM resistance. Different cucumber germplasm resources may show stable genetic bases and QTLs for DM. For example, *dm5.1* and *dm5.2* have been detected in five resistance sources (Wang et al., 2020). New QTLs have also been detected in commonly used disease-resistant materials. In PI 197087, Berg et al. (2020) focused on a QTL on chromosome *4-DM4.1* in the NILs produced by PI 197087 and a susceptible cucumber line (HS279) and this contained three sub-QTLs: *DM4.1.1* that affects pathogen-induced necrosis, *DM4.1.2* that has additive effects on sporulation, and *DM4.1.3* that has recessive effects on chlorosis and sporulation. In general, the DM-associated QTLs varied depending on the germplasm and plant tissue as well as the developmental stage used in these analyses.

Candidate Genes or Proteins Involved in the Downy Mildew Resistance of Cucumber

A series of candidate genes or proteins related to DM resistance have been identified in cucumber through transcriptome profiling, proteomic analysis, and fine mapping. A large number of DEGs between DM-resistant and susceptible materials were identified by transcriptome analyses and these DEGs are involved in multiple defense response-related functions, including response: hormone signaling, regulation of nutrient supply, pathogen-associated molecular pattern recognition, signal transduction, reactive oxygen species and lignin accumulation, cell cycle, protein binding and metabolism, and transcriptional regulation (Li et al., 2011; Burkhardt and Day, 2016; Gao et al., 2021). For example, five genes play important roles in the cucumber DM defense pathway: *Csa5G139760* encodes an acidic chitin endonuclease, *Csa6G080320* encodes a kinase having an LRR domain and transmembrane domain, *Csa5G471600* is a retroviral receptor-like protein, and *Csa5G544050* and *Csa5G564290* encode the RNA-dependent RNA polymerase gene (Gao et al., 2021). Consistently, differentially expressed proteins between the resistant and susceptible cucumber lines have also been identified and most of these proteins focus on cell rescue, defense, and energy metabolism (Sun et al., 2021). Zinc finger-homeodomain (ZHD) proteins encode a family of plant-specific transcription factors that are responsive to DM in cucumber, such as *CsZHD1–3*, *CsZHD6*, *CsZHD8*, and *CsZHD10* (Lai et al., 2021). Many novel QTLs for DM resistance in different cucumber species have been detected, such as *dm2.1*, *dm4.1*, *dm4.1.2*, *dm4.1.3*, *dmG2.1*, and *dmG7.1* (Win et al., 2017; Berg et al., 2020; Liu et al., 2021), and these

precise molecular markers and QTLs for DM resistance are helpful for the consequent fine mapping and positional cloning of QTLs. Liu et al. (2021) identified seven DM-resistance candidate genes using GWAS, including *Csa1G575030* for *dmG1.4*, *Csa2G060360* for *dmG2.1*, *Csa4G064680* for *dmG4.1*, *Csa5G606470* for *dmG5.2*, and *Csa7G004020* for *dmG7.1*. Among them, *Csa5G606470* is a WRKY transcription factor and it was also identified within the DM-associated QTL *dm5.2* using a Bulked Sergeant Analysis with Whole-genome Resequencing (BSA-seq) analysis (Zhang et al., 2018). Cucumber *CsSGR* encodes a magnesium dechelatase and plays critical regulatory roles in the chlorophyll degradation pathway and a loss-of-susceptibility mutation of *CsSGR* results in durable broad-spectrum DM disease resistance (Wang et al., 2019). *CsLRK10L2* acts as a DAMP oligogalacturonan receptor and is involved in the breakdown of pectin, which is involved in the production of plant cell walls. This gene has been identified as a likely candidate for the sub-QTL *DM4.1.2* because the transient expression of its loss-of-function mutation *CsLRK10L2* from the DM-susceptible parent HS279 in *N. benthamiana* leaves causes necrosis (Berg et al., 2020). A series of DM- and PM-associated QTLs were also colocalized in typical Northern Chinese type cucumber K8, PI 197088, and PI 197088-derived line CS-PMR1. For example, *dm2.1/pm2.1*, *dm5.3/pm5.1*, and *dm6.2/pm6.1* have been colocated in PI 197088 (Wang et al., 2018). Several candidate genes for both the DM and PM resistance have also been identified, including *Csa5M622800.1*, *Csa5M622830.1*, and *Csa5M623490.1*. The gene *Csa5M622830.1* is a GATA transcriptional factor gene and it may prevent the nutrition from reaching DM and PM pathogens (Zhang et al., 2018). In addition, Cucumis sativus Irregular Vasculature Patterning (*CsIVP*)-RNA interference (*RNAi*) plants having higher salicylic acid levels show higher resistance to DM than wild type (WT) and it was proposed that *CsIVP* may interact with *CsNIMIN1*, which is a negative regulator in the salicylic acid-signaling pathway, to improve DM resistance in cucumber (Yan et al., 2020). At present, the candidate genes for DM resistance in cucumber identified by forward genetic analysis methods need to be verified by overexpression or knockout experiments in cucumber.

INHERITANCE, QUANTITATIVE TRAIT LOCI MAPPING, AND CANDIDATE GENES OF CUCUMBER RESISTANCE TO FUSARIUM WILT

Cucumber FW, caused by *Fusarium oxysporum* f. sp. *cucumerinum* Owen (FOC), is a systemic soil-borne fungal disease and the hyphae of this pathogen penetrate cucumber roots, which causes vascular wilt. The disease causes necrotic lesions on the stem bases, foliar wilting, and eventually whole-plant wilt and even death and it occurs throughout cucumber development (Vakalounakis and Lamprou, 2018). The main factor affecting the incidence of FW is the number of FOC in the soil, which is positively correlated.

Inheritance of Fusarium Wilt Resistance in Cucumber

To understand the genetic inheritance of FW resistance, it is important to develop resistance breeding resources and breed-resistant varieties. The inheritance of FW resistance in cucumber has been studied for a long time, but with different conclusions (Toshimitsu and Noguchi, 1975; Netzer et al., 1977; Vakalounakis, 1993, 1995; Zhang et al., 2014; Vakalounakis and Lamprou, 2018; Dong et al., 2019; Jaber et al., 2020). Dong et al. (2019) found that the inheritance of FW resistance in cucumber is a quantitative trait controlled by multiple genes using an F2 population derived from a cross between the susceptible line Superina and the resistant line Rijiecheng and several studies agreed with this inheritance of FW resistance in cucumber (Toshimitsu and Noguchi, 1975; Zhang et al., 2014). Other researchers have reported that the FW resistance in cucumber is a qualitative trait controlled by a single *Foc* gene (Netzer et al., 1977; Vakalounakis, 1993, 1995; Vakalounakis and Lamprou, 2018; Jaber et al., 2020). The *Foc* gene has been incorporated in the Dutch-type cucumber hybrids and has widely controlled FW in cucumber for 40 years (Vakalounakis and Fragkiadakis, 2003). The different patterns of FW inheritance in cucumber are also influenced by pathogen races, including races 1–3 from America, Israel, and Japan, respectively, and race 4 from China (Zhang et al., 2014). Vakalounakis and Lamprou (2018) found that *Foc* (syn.*Fcu*-1), which has been identified as a dominant FW resistance gene in the cultivars SMR-18 and WIS2757, controls FW resistance to races 1, 2, and 3, which indicates that FW resistance is not related to different pathogen races. Additionally, the *Foc* gene was found to be linked to the *Ccu* gene, which controls resistance to scab in cucumber inbred line 9110Gt, possible due to the FW and scab resistance in cucumber both being controlled by an NBS-type *R* gene (Vakalounakis, 1993; Mao et al., 2008). In the future, the availability of more natural FW-resistant resources aids in revealing the inheritance pattern of FW resistance in cucumber.

Molecular Markers and Quantitative Trait Loci of Fusarium Wilt Resistance in Cucumber

Compared with PM and DM, there are limited reports on molecular linkage markers and QTL mapping related to the inheritance of FW resistance in cucumber. Wang (2005) identified an Amplified Fragment Length Polymorphisms (AFLP) marker E25M70 and an SSR marker CSWCT06A linked to cucumber *Foc2.1* at genetic distances of 8.12 and 5.98 cM, respectively. One major QTL, *Foc2.1*, has been screened from the F9 RILs derived from the cross between 9110Gt and 9930 and it is located between SSR03084 and SSR17631 on chromosome 2. The marker SSR17631 has been validated with an 87.88% accuracy among 46 cucumber germplasms (Zhang et al., 2014). Moreover, Zhou et al. (2015) mapped the QTL of *Foc4* resistance to FW in the region of SSR17631 and SSR00684 on chromosome 2. Another major QTL, *fw2.1*, located on chromosome 2, has also been detected and fine-mapped, with a physical distance of 0.60 Mb (InDel1248093–InDel1817308) and it contains 80

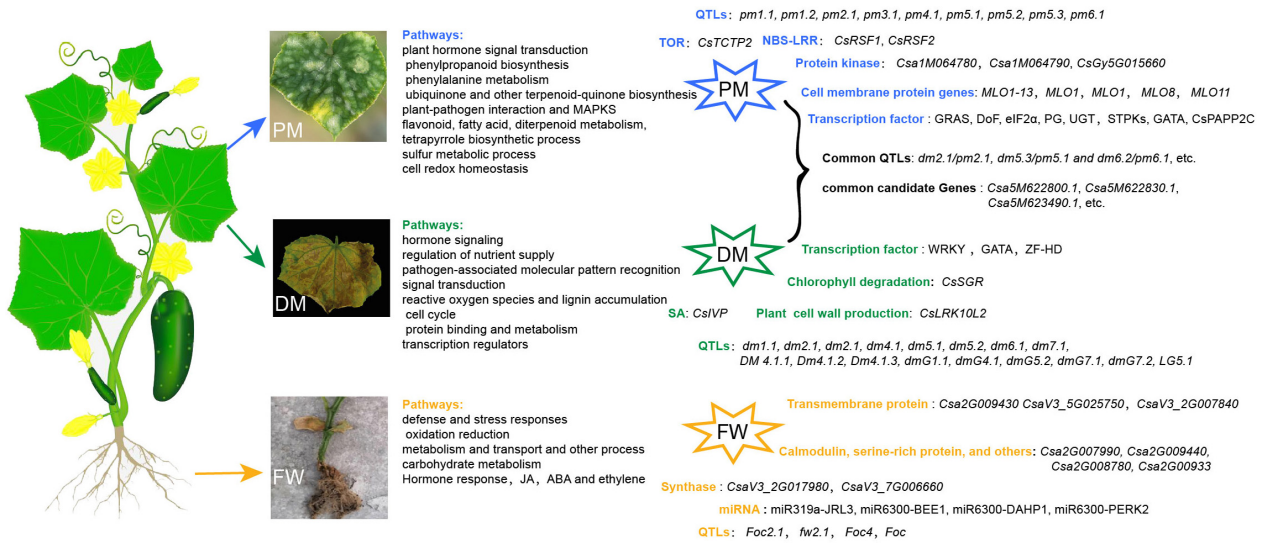


FIGURE 1 | The symptoms, QTL mapping and candidate genes or proteins related to cucumber PM, DM, and FW, respectively.

candidate genes (Dong et al., 2019). One AFLP marker of FW resistance in cucumber has been identified at a distance of 6.0 cm from the *Foc* gene and it was converted into SCE12M50$_B$ and SCE12M50$_A$ codominant markers (Jaber et al., 2020). The SCE12M50$_B$ marker is located 7.0 cm away from SSR03084 and is linked to the *Ccu* locus that controls resistance to scab in cultivar SMR-18 (Mao et al., 2008; Jaber et al., 2020). Owing to the complexity of FW symptoms and the defects of related research techniques, the mechanisms and functions of these loci have not been determined and require further exploration.

Candidate Genes or Proteins Involved in the Fusarium Wilt Resistance of Cucumber

Some FW candidate proteins and genes in cucumber have been identified using proteomic and transcriptomic analyses in different FW-resistant varieties. A comparative proteomic analysis of root proteins isolated from infected highly susceptible 995 and highly resistant F9 revealed that 15 overaccumulated proteins are mainly involved in defense and stress responses, oxidation-reduction, metabolism, transport and other processes, and jasmonic acid and redox signaling components. LRR family- and stress-related proteins may be crucial in the defense responses to FW in cucumber (Zhang et al., 2016). Moreover, defense mechanisms against oxidation and detoxification as well as carbohydrate metabolism may also be necessary for FW resistance in cucumber (Du et al., 2016). Xu et al. (2021) identified 210 and 243 differentially regulated proteins in the FW resistance Rijiecheng and high-susceptibility Superina after Foc infection. Additionally, four genes, *TMEM115* (*CsaV3_5G025750*), which encodes a transmembrane protein, *TET8* (*CsaV3_2G007840*), which functions as a tetraspanin, *TPS10* (*CsaV3_2G017980*), which encodes a terpene synthase, and *MGT2* (*CsaV3_7G006660*), which encodes a glycosyltransferase, are remarkably upregulated in both the cultivars after Foc inoculation, but with higher expression levels in Superina. In total, 14 chitinase defense-related genes have higher expression levels in FW susceptible and resistant lines and *CsChi23* may play an important role in activating a rapid immune reaction against FW (Bartholomew et al., 2019). Furthermore, other defense-related genes are activated to regulate the defense responses of cucumber to a Foc inoculation, including several genes related to ABA and ethylene (Zhou and Wu, 2009; Dong et al., 2020). *miR319a-JRL3*, *miR6300-BEE1*, *miR6300-DAHP1*, and *miR6300-PERK2* also regulate cucumber defenses against FW (Xu et al., 2021). Dong et al. (2019) identified five candidate FW-resistance genes in *fw2.1* by combining genetic mapping and a transcriptome analysis, *Csa2G007990*, which encodes calmodulin, *Csa2G009430*, which encodes a transmembrane protein, *Csa2G009440*, which encodes a serine-rich protein, and *Csa2G008780* and *Csa2G009330*, which are novel genes. This is the only report of mapping FW candidate genes in cucumber, but the functions of the candidate genes have not been verified.

FUTURE PROSPECTS FOR ENHANCING CUCUMBER DISEASE RESISTANCE

In summary, the inheritance of PM, DM, and FW resistance in cucumber has been widely investigated and cucumber resistance traits are generally considered as quantitative traits controlled by more one gene. Because of the complicated inheritance of resistance to cucumber diseases, the results are not unified. Simultaneously, several molecular markers and QTLs for PM, DM, and FW resistance in cucumber have been identified (**Figure 1** and **Supplementary Table 1**). Many factors affect cucumber resistance to these three diseases, including pathogen species, plant materials, pathogen invasion site, environment,

and genetic linkage, resulting in a variety of effective molecular markers and QTLs for cucumber disease. Large numbers of candidate genes and immune proteins associated with DM, PM, and FW have been identified using mapping, GWAS, RNA sequencing (RNA-seq), and proteomic assay technology, but only a few have been functionally verified (**Figure 1** and **Supplementary Table 1**). For example, only the functions of *MLO-like* genes that are important in PM resistance have been verified in cucumber. The transient silencing of the two NBS-LRR genes (*CsRSF1* and *CsRSF2*) reduces cucumber resistance to PM. Among the DM-resistant candidate genes, *CsSGR*, *CsLRK10L2*, and *CsIVP* have been functionally verified through mutation, transient expression, or RNAi. Additionally, the resistance of *GNK2-1* transgenic cucumber to FW is enhanced compared with WT (Liu et al., 2010). Because of a lack of cucumber FW-resistant germplasms in China, the susceptibility of most cultivars, and the relatively narrow genetic variation among cucumber FW, the breeding of cucumber FW-resistant cultivars has been restricted to a certain extent and research on the molecular mechanisms of FW has not progressed as far as research on PM and DW.

To better effectively prevent cucumber diseases and explore the genetic and molecular mechanisms of cucumber resistance to PM, DM, and FW, respectively, we propose five aspects of work that need to be performed in the future: (1) collect more disease-resistant cucumber germplasms, especially materials that are resistant to multiple pathogens, including wild germplasm resources, cultivars, and mutants; (2) identify more effective molecular markers and QTLs associated with PM, DM, and FW to be used in selecting germplasms and accelerating resistance breeding; (3) analyze more differently expressed DNA, RNA, miRNAs, lncRNAs, or metabolic related to PM, DM, or FW, respectively, through omics or multiomics and bioinformatics tools would provide considerable experimental information for mechanistic investigations and understand the regulatory network for cucumber diseases, such as transcriptomics, proteomics, metabolomics, epigenomics, and interactomics. Additionally, the data-driven interface through a user-friendly web interface would also be helpful for the mechanism of cucumber diseases, such as plant regulomics (Ran et al., 2020); (4) improve the efficiency and stability of genetic transformation in cucumber. There are now effective methods for gene functional verification that use biotechnology, such as transgenes, RNAi, Transcription Activator-like Effector Nucleases (TALENs), and CRISPR-Cas; (5) develop persistent and safe preventive measures, including chemical, biological, and physical controls. For example, maintaining an optimization of blue light in the growth light before nighttime UV is important for the management of PW in cucumber (Palma et al., 2021). A balance between effective defense and crops yield should be established through these preventive measures. The plant immunity engineering toolbox that integrates genetics, technology, and engineering is required for enhancing disease resistance in crops in the future and the molecular mechanisms of cucumber resistance to PM, DM, and FW need to be further studied.

AUTHOR CONTRIBUTIONS

YH, MW, and YY drafted the manuscript. CY, SC, and YS modified the manuscript. LM, HW, XZ, and LW designed the project and gave suggestions on the revision of the manuscript. All the authors approved the final version of the manuscript.

FUNDING

This study was supported by "Pioneer" and "Leading Goose" R&D Program of Zhejiang (No. 2022C02051), the Zhejiang Natural Science Foundation of China (Grant No. LY19C150008), Opening Project Fund of Key Laboratory of Biology and Genetic Resources of Rubber Tree, Ministry of Agriculture and Rural Affairs, PR China/State Key Laboratory Breeding Base of Cultivation and Physiology for Tropical Crops/Danzhou Investigation and Experiment Station of Tropical Crops, Ministry of Agriculture and Rural Affairs, PR China (No. RRI-KLOF202102), the Natural Science Foundation of Zhejiang province (Grant Nos. LY21C150002 and LQY19C150001), the National Natural Science Foundation of China (Grant Nos. 31872105, 31972221, 32002048, 31801862, and 32172595), the National College Students Innovation and Entrepreneurship Training Program in 2019 and 2021 (Nos. 202110341043 and 201910341005), and the Student Scientific research training program of Zhejiang Agriculture and Forestry University (Nos. 2021KX0196 and 2021KX019), Ministry of Agriculture, and the National Key Research and Development Program of China (Nos. 2018YFD1000800 and 2019YFD1000300).

SUPPLEMENTARY MATERIAL

The Supplementary Material for this article can be found online at: https://www.frontiersin.org/articles/10.3389/fpls.2022.862486/full#supplementary-material

REFERENCES

Barnes, W. C., and Epps, W. M. (1954). An unreported type of resistance to cucumber downy mildew. *Plant Dis.* Rep. 38:620.

Bartholomew, E. S., Black, K., Feng, Z., Wan, L., Nan, S., Xiao, Z., et al. (2019). Comprehensive analysis of the chitinase gene family in cucumber (*Cucumis sativus* L.): from gene identification and evolution to expression in response to Fusarium oxysporum. *Int. J. Mol. Sci.* 20:5309. doi: 10.3390/ijms20215309

Berg, J. A., Appiano, M., Bijsterbosch, G., Richard, G. F. V., Henk, J. S., and Yuling, B. (2017). Functional characterization of cucumber (*Cucumis sativus* L.) Clade V MLO genes. *BMC Plant Biol.* 17:80. doi: 10.1186/s12870-017-1029-z

Berg, J. A., Hermans, F. W., Beenders, F., Lou, L., Vriezen, W. H., Visser, R. G., et al. (2020). Analysis of QTL DM4. 1 for downy mildew resistance in cucumber reveals multiple subQTL: a novel *RLK* as candidate gene for the most important subQTL. *Front. Plant Sci.* 11:1601. doi: 10.3389/fpls.2020.569876

Block, C. C., and Reitsma, K. R. (2005). Powdery mildew resistance in the US national plant germplasm system cucumber collection. *HortScience* 40, 416–420. doi: 10.21273/hortsci.40.2.416

Burkhardt, A., and Day, B. (2016). Transcriptome and small RNAome dynamics during a resistant and susceptible interaction between cucumber and downy mildew. *Plant Genome* 9:plantgenome2015.08.0069. doi: 10.3835/plantgenome2015.08.0069

Call, A. D., Criswell, A. D., Wehner, T. C., Ando, K., and Grumet, R. (2012a). Resistance of cucumber cultivars to a new strain of cucurbit downy mildew. *HortScience* 47, 171–178. doi: 10.21273/hortsci.47.2.171

Call, A. D., Criswell, A. D., Wehner, T. C., Klosinska, U., and Kozik, E. U. (2012b). Screening cucumber for resistance to downy mildew caused by *Pseudoperonospora cubensis* (Berk. and Curt.) Rostov. *Crop Sci*. 52, 577–592. doi: 10.2135/cropsci2011.06.0296

Chen, Q., Yu, G., Wang, X., Meng, X., and Lv, C. (2021). Genetics and resistance mechanism of the cucumber (*Cucumis sativus* L.) against powdery mildew. *J. Plant Growth Regul.* 40, 147–153. doi: 10.1007/s00344-020-10075-7

Dong, J., Wang, Y., Xian, Q., Chen, X., and Xu, J. (2020). Transcriptome analysis reveals ethylene-mediated defense responses to *Fusarium oxysporum* f. sp. *cucumerinum* infection in *Cucumis sativus* L. *BMC Plant Biol*. 20:334. doi: 10.1186/s12870-020-02537-7

Dong, J., Xu, J., Xu, X., Xu, Q., and Chen, X. (2019). Inheritance and quantitative trait locus mapping of Fusarium wilt resistance in cucumber. *Front. Plant Sci*. 10:1425. doi: 10.3389/fpls.2019.01425

Doruchowski, R. W., and Lakowska-Ryk, E. (1992). "Inheritance of resistance to downy mildew (*Pseudoperonospora cubensis* Berk & Curt) in *Cucumis sativus*," in *Proceedings of the 5th EUCARPIA Cucurbitaceae Symposiyum*, 66–69. doi: 10.1007/BF00035865

Du, N., Shi, L., Yuan, Y., Li, B., Shu, S., Sun, J., et al. (2016). Proteomic analysis reveals the positive roles of the plant-growth-promoting rhizobacterium NSY50 in the response of cucumber roots to *Fusarium oxysporum* f. sp. *cucumerinum* inoculation. *Front. Plant Sci*. 7:1859. doi: 10.3389/fpls.2016.01859

Fukino, N., Yoshioka, Y., Sugiyama, M., Sakata, Y., and Matsumoto, S. (2013). Identification and validation of powdery mildew (*Podosphaera xanthii*)-resistant loci in recombinant inbred lines of cucumber (*Cucumis sativus* L.). *Mol. Breed*. 32, 267–277. doi: 10.1007/s11032-013-9867-3

Gao, X., Guo, P., Wang, Z., Chen, C., and Ren, Z. (2021). Transcriptome profiling reveals response genes for downy mildew resistance in cucumber. *Planta* 253:112. doi: 10.1007/s00425-021-03603-6

He, X., Li, Y., Pandey, S., Yandell, B. S., Pathak, M., and Weng, Y. (2013). QTL mapping of powdery mildew resistance in WI 2757 cucumber (*Cucumis sativus* L.). *Theor. Appl. Genet*. 126, 2149–2161. doi: 10.1007/s00122-013-2125-6

Innark, P., Panyanitikoon, H., Khanobdee, C., Samipak, S., and Jantasuriyarat, C. (2020). QTL identification for downy mildew resistance in cucumber using genetic linkage map based on SSR markers. *J. Genet. Genomics* 99:81. doi: 10.1007/s12041-020-01242-6

Jaber, E. H. A., Srour, A. Y., Zambounis, A. G., Vakalounakis, D. J., and Doulis, A. G. (2020). Identification of SCAR markers linked to the Foc gene governing resistance to *Fusarium oxysporum* f. sp. *cucumerinum* in cucumber cv. SMR-18. *Eur. J. Plant Pathol*. 157, 845–855. doi: 10.1007/s10658-020-02045-2

Jenkins, J. M. Jr. (1942). Downy mildew resistance in cucumbers. *J. Hered*. 33, 35–38. doi: 10.1093/oxfordjournals.jhered.a105122

Kelly, J. D., and Vallejo, V. (2006). "QTL analysis of multigenic disease resistance in plant breeding," in *Multigenic and Induced Systemic Resistance in Plants*, eds S. Tuzan and E. Bent (Boston, MA: Springer), 21–48. doi: 10.1007/0-387-23266-4_3

Kooistra, E. (1968). Powdery mildew resistance in cucumber. *Euphytica* 17, 236–244. doi: 10.1007/BF00021216

Lai, W., Zhu, C., Hu, Z., Liu, S., Wu, H., and Zhou, Y. (2021). Identification and transcriptional analysis of Zinc Finger-Homeodomain (ZF-HD) family genes in cucumber. *Biochem. Genet*. 59, 884–901. doi: 10.1007/s10528-021-10036-z

Li, J. W., Liu, J., Zhang, H., and Xie, C. H. (2011). Identification and transcriptional profiling of differentially expressed genes associated with resistance to *Pseudoperonospora cubensis* in cucumber. *Plant Cell Rep*. 30, 345–357. doi: 10.1007/s00299-010-0959-9

Li, L., He, H., Zou, Z., and Li, Y. (2018). QTL analysis for downy mildew resistance in cucumber inbred line PI 197088. *Plant Dis*. 102, 1240–1245. doi: 10.1094/PDIS-04-17-0491-RE

Liu, J., Tian, H., Wang, Y., and Guo, A. (2010). Overexpression of a novel antifungal protein gene *GNK2-1* results in elevated resistance of transgenic cucumber to *Fusarium oxysporum*. *Chin. Bull. Bot*. 45:411. doi: 10.3969/j.issn.1674-3466.2010.04.003

Liu, L., Cai, R., Yuan, X., He, H., and Pan, J. (2008). QTL molecular marker location of powdery mildew resistance in cucumber (*Cucumis sativus* L.). *Sci. China Life Sci*. 51, 1003–1008. doi: 10.1007/s11427-008-0110-0

Liu, P., Miao, H., Lu, H., Cui, J., Tian, G., Wehner, T. C., et al. (2017). Molecular mapping and candidate gene analysis for resistance to powdery mildew in *Cucumis sativus* stem. *Genet. Mol. Res*. 16:gmr16039680. doi: 10.4238/gmr16039680

Liu, X., Gu, X., Lu, H., Liu, P., Miao, H., Bai, Y., et al. (2021). Identification of novel loci and candidate genes for resistance to powdery mildew in a resequenced cucumber germplasm. *Genes* 12:584. doi: 10.3390/genes12040584

Mahmood, I., Imadi, S. R., Shazadi, K., Gul, A., and Hakeem, K. R. (2016). "Effects of pesticides on environment," in *Plant, Soil and Microbes*, eds K. Hakeem, M. Akhtar, and S. Abdullah (Cham: Springer), 253–269. doi: 10.1007/978-3-319-27455-3_13

Mao, A., Zhang, Z., and Zhang, L. (2008). Analysis on the inheritance of resistance to fusarium wilt race 4 and cucumber scab and their linkage in cucumber WLS2757. *Zhongguo Nong Ye Ke Xue* 41, 3382–3388. doi: 10.3864/j.issn.0578-1752.2008.10.062

Meng, X., Yu, Y., Zhao, J., Cui, N., Song, T., Yang, Y., et al. (2018). The two translationally controlled tumor protein genes, *CsTCTP1* and *CsTCTP2*, are negative modulators in the *Cucumis sativus* defense response to *Sphaerotheca fuliginea*. *Front. Plant Sci*. 9:544. doi: 10.3389/fpls.2018.00544

Morishita, M., Sugiyama, K., Saito, T., and Sakata, Y. (2003). Powdery mildew resistance in cucumber. *Jpn. Agric. Res. Q*. 37, 7–14. doi: 10.6090/jarq.37.7

Netzer, D., Niego, S., and Galun, E. (1977). A dominant gene conferring resistance to *Fusarium* wilt in cucumber. *Phytopathology* 67, 525–527. doi: 10.1094/Phyto-67-525

Nie, J., He, H., Peng, J., Yang, X., Bie, B., Zhao, J., et al. (2015a). Identification and fine mapping of *pm5. 1*: a recessive gene for powdery mildew resistance in cucumber (*Cucumis sativus* L.). *Mol. Breed*. 35:7. doi: 10.1007/s11032-015-0206-8

Nie, J., Wang, Y., He, H., Guo, C., Zhu, W., Pan, J., et al. (2015b). Loss-of-function mutations in CsMLO1 confer durable powdery mildew resistance in cucumber (*Cucumis sativus* L.). *Front. Plant Sci*. 6:1155. doi: 10.3389/fpls.2015.01155

Nie, J., Wang, H., Zhang, W., Teng, X., Yu, C., Cai, R., et al. (2021). Characterization of lncRNAs and mRNAs involved in powdery mildew resistance in cucumber. *Phytopathology®* 111, 1613–1624. doi: 10.1094/PHYTO-11-20-0521-R

Palma, C. F. F., Castro-Alves, V., Morales, L. O., Rosenqvist, E., Ottosen, C. O., and Strid, Å (2021). Spectral composition of light affects sensitivity to UV-B and photoinhibition in cucumber. *Front. Plant Sci*. 11:610011. doi: 10.3389/fpls.2020.610011

Ran, X., Zhao, F., Wang, Y., Liu, J., Zhuang, Y., Ye, L., et al. (2020). Plant regulomics: a data-driven interface for retrieving upstream regulators from plant multi-omics data. *Plant J*. 101, 237–248. doi: 10.1111/tpj.14526

Ruiter, W. D., Hofstede, R., Vries, J. D., and Heuvel, H. (2008). "Combining QTLs for resistance to CYSDV and powdery mildew in a single cucumber line. In Cucurbitaceae 2008," in *Proceedings of the IXth EUCARPIA Meeting on Genetics and Breeding of Cucurbitaceae, Avignon, France, 21-24 May 2008*, (Paris: Institut National de la Recherche Agronomique (INRA)), 181–188.

Sakata, Y., Kubo, N., Morishita, M., Kitadani, E., Sugiyama, M., and Hirai, M. (2006). QTL analysis of powdery mildew resistance in cucumber (*Cucumis sativus* L.). *Theor. Appl. Genet*. 112, 243–250. doi: 10.1007/s00122-005-0121-1

Schouten, H. J., Krauskopf, J., Visser, R. G., and Bai, Y. (2014). Identification of candidate genes required for susceptibility to powdery or downy mildew in cucumber. *Euphytica* 200, 475–486. doi: 10.1007/s10681-014-1216-z

Shen, L., Xu, Q., Qi, X., and Chen, X. (2011). Genetic model analysis of cucumber powdery mildew resistance. *J. Jiangsu Agric.* 27, 361–365.

Smith, P. G. (1948). Powdery mildew resistance in cucumber. *Phytopathology* 38, 1027–1028.

Sun, C., Song, X., Zheng, J., Li, X., Feng, Z., and Yan, L. (2021). Comparative proteomic profiles of resistant/susceptible cucumber leaves in response to downy mildew infection. *Hortic. Plant J.* 7, 327–340. doi: 10.1016/j.hpj.2021.01.008

Szczechura, W., Staniaszek, M., Klosinska, U., and Kozik, E. U. (2015). Molecular analysis of new sources of resistance to *Pseudoperonospora cubensis* (Berk. et Curt.) Rostovzev in cucumber. *Russ. J. Genet.* 51, 974–979. doi: 10.7868/s0016675815090118

Tan, M. (2021). *Cucumber Powdery Mildew Resistance Key Genes Identification Based on Genome-Wide Association Analysis.* Yangzhou: Yangzhou University. doi: 10.27441/d.cnki.gyzdu.2021.001588

Toshimitsu, Y., and Noguchi, T. (1975). "Inheritance of resistance to *Fusarium* wilt in cucumber," in *Proceedings of the Meeting of the Japanese Horticultural Society*, 150–151.

Vakalounakis, D. J. (1993). Inheritance and genetic linkage of fusarium wilt {*Fusarium oxysporum* f. sp. *cucumerinum* race 1) and scab {*Cladosporium cucumerinum*) resistance genes in cucumber (*Cucumis sativus*). *Ann. Appl. Biol.* 123, 359–365. doi: 10.1111/j.1744-7348.1993.tb04098.x

Vakalounakis, D. J. (1995). Inheritance and linkage of resistance in cucumber line SMR-18 to races 1 and 2 of *Fusarium oxysporum* f. sp. *cucumerinum*. *Plant Pathol.* 44, 169–172.

Vakalounakis, D. J., and Fragkiadakis, G. A. (2003). *Plant Pathobreeding with Emphasis in Tomato and Cucurbits*, ed. D. J. Vakalounakis (Heraklio).

Vakalounakis, D. J., and Lamprou, K. (2018). The Foc gene governs resistance to race 3 of *Fusarium oxysporum* f. sp. *cucumerinum* in the cucumber cv. SMR-18. *Eur. J. Plant Pathol.* 152, 653–656. doi: 10.1007/s10658-018-1508-6

Wang, X., Chen, Q., Huang, J., Meng, X., Cui, N., Yu, Y., et al. (2021). Nucleotide-binding leucine-rich repeat genes *CsRSF1* and *CsRSF2*are positive modulators in the *Cucumis sativus*defense response to *Sphaerotheca fuliginea*. *Int. J. Mol. Sci.* 22:3986. doi: 10.3390/ijms22083986

Wang, Y. (2005). *Molecular Markers of Fusarium Wilt Resistance-Related Genes in Cucumber (Cucumis sativus L.).* Yangling: Northwest A & F University.

Wang, Y., Bo, K., Gu, X., Pan, J., Li, Y., Chen, J., et al. (2020). Molecularly tagged genes and quantitative trait loci in cucumber with recommendations for QTL nomenclature. *Hort. Res.* 7:3. doi: 10.1038/s41438-019-0226-3

Wang, Y., Tan, J., Wu, Z., VandenLangenberg, K., Wehner, T. C., Wen, C., et al. (2019). STAYGREEN, STAY HEALTHY: a loss-of-susceptibility mutation in the STAYGREEN gene provides durable, broad-spectrum disease resistances for over 50 years of US cucumber production. *New Phytol.* 221, 415–430. doi: 10.1111/nph.15353

Wang, Y., VandenLangenberg, K., Wehner, T. C., Kraan, P. A., Suelmann, J., Zheng, X., et al. (2016). QTL mapping for downy mildew resistance in cucumber inbred line WI7120 (PI 330628). *Theor. Appl. Genet.* 129, 1493–1505. doi: 10.1007/s00122-016-2719-x

Wang, Y., VandenLangenberg, K., Wen, C., Wehner, T. C., and Weng, Y. (2018). QTL mapping of downy and powdery mildew resistances in PI 197088 cucumber with genotyping-by-sequencing in RIL population. *Theor. Appl. Genet.* 131, 597–611. doi: 10.1007/s00122-017-3022-1

Wehner, T. C., and Shetty, N. V. (1997). Downy mildew resistance of the cucumber germplasm collection in North Carolina field tests. *HortScience* 32:450. doi: 10.2135/cropsci1997.0011183X003700040050x

Win, K. T., Vegas, J., Zhang, C., Song, K., and Lee, S. (2017). QTL mapping for downy mildew resistance in cucumber via bulked segregant analysis using next-generation sequencing and conventional methods. *Theor. Appl. Genet.* 130, 199–211. doi: 10.1007/s00122-016-2806-z

Wolter, M., Hollricher, K., Salamini, F., and Schulze-Lefert, P. (1993). The mlo resistance alleles to powdery mildew infection in barley trigger a developmentally controlled defence mimic phenotype. *Mol Gen Genet.* 239, 122–128. doi: 10.1007/BF00281610

Xiao, S., Ellwood, S., Calis, O., Patrick, E., Li, T., Coleman, M., et al. (2001). Broad spectrum mildew resistance in *Arabidopsis thaliana* mediated by RPW8. *Science* 291, 118–120. doi: 10.1126/science.291.5501.118

Xu, J., Wang, K., Xian, Q., Zhang, N., Dong, J., and Chen, X. (2021). Identification of susceptibility genes for *Fusarium oxysporum* in cucumber via comparative proteomic analysis. *Genes* 12:1781. doi: 10.3390/genes12111781

Xu, Q., Shi, Y., Yu, T., Xu, X., Yan, Y., Qi, X., et al. (2016). Whole-genome resequencing of a cucumber chromosome segment substitution line and its recurrent parent to identify candidate genes governing powdery mildew resistance. *PLoS One* 11:e0164469. doi: 10.1371/journal.pone.0164469

Xu, Q., Xu, X., Shi, Y., Qi, X., and Chen, X. (2017). Elucidation of the molecular responses of a cucumber segment substitution line carrying Pm5.1 and its recurrent parent triggered by powdery mildew by comparative transcriptome profiling. *BMC Genom.* 18:21. doi: 10.1186/s12864-016-3438-z

Xu, X., Liu, X., Yan, Y., Wang, W., Gebretsadik, K., Qi, X., et al. (2019). Comparative proteomic analysis of cucumber powdery mildew resistance between a single-segment substitution line and its recurrent parent. *Hort. Res.* 6:115. doi: 10.1038/s41438-019-0198-3

Xu, X., Yu, T., Xu, R., Shi, Y., Lin, X., Xu, Q., et al. (2016). Fine mapping of a dominantly inherited powdery mildew resistance major-effect QTL, Pm1.1, in cucumber identifies a 41.1 kb region containing two tandemly arrayed cysteine-rich receptor-like protein kinase genes. *Theor. Appl. Genet.* 129, 507–516. doi: 10.1007/s00122-015-2644-4

Xu, X., Zhong, C., Tan, M., Song, Y., Qi, X., Xu, Q., et al. (2020). Identification of MicroRNAs and their targets that respond to powdery mildew infection in cucumber by small RNA and degradome sequencing. *Front. Genet.* 11:246. doi: 10.3389/fgene.2020.00246

Yan, S., Ning, K., Wang, Z., Liu, X., Zhong, Y., Ding, L., et al. (2020). CsIVP functions in vasculature development and downy mildew resistance in cucumber. *PLoS Biol.* 18:e3000671. doi: 10.1371/journal.pbio.3000671

Yoshioka, Y., Sakata, Y., Sugiyama, M., and Fukino, N. (2014). Identification of quantitative trait loci for downy mildew resistance in cucumber (*Cucumis sativus* L.). *Euphytica* 198, 265–276. doi: 10.1007/s10681-014-1102-8

Zhang, C., Anarjan, M. B., Win, K. T., Begum, S., and Lee, S. (2021). QTL-seq analysis of powdery mildew resistance in a Korean cucumber inbred line. *Theor. Appl. Genet.* 134, 435–451. doi: 10.1007/s00122-020-03705-x

Zhang, D., Meng, K., Hao, Y., Fan, H., Cui, N., Wang, S., et al. (2016). Comparative proteomic analysis of cucumber roots infected by *Fusarium oxysporum* f. sp. *cucumerium* Owen. *Physiol. Mol. Plant Pathol.* 96, 77–84. doi: 10.1016/j.pmpp.2016.09.002

Zhang, K., Wang, X., Zhu, W., Qin, X., Xu, J., Cheng, C., et al. (2018). Complete resistance to powdery mildew and partial resistance to downy mildew in a *Cucumis hystrix* introgression line of cucumber were controlled by a co-localized locus. *Theor. Appl. Genet.* 131, 2229–2243. doi: 10.1007/s00122-018-3150-2

Zhang, P., Zhu, Y., and Zhou, S. (2021). Comparative analysis of powdery mildew resistant and susceptible cultivated cucumber (*Cucumis sativus* L.) varieties to reveal the metabolic responses to *Sphaerotheca fuliginea* infection. *BMC Plant Biol.* 21:24. doi: 10.1186/s12870-020-02797-3

Zhang, S., Liu, M., Miao, H., Zhang, S., Yang, Y., Xie, B., et al. (2013). Chromosomal mapping and QTL analysis of resistance to downy mildew in *Cucumis sativus*. *Plant Dis.* 97, 245–251. doi: 10.1094/PDIS-11-11-0941-RE

Zhang, S., Miao, H., Yang, Y., Xie, B., Wang, Y., and Gu, X. (2014). A major quantitative trait locus conferring resistance to Fusarium wilt was detected in cucumber by using recombinant inbred lines. *Mol. Breed.* 34, 1805–1815. doi: 10.1007/s11032-014-0140-1

Zhang, Z., Mao, L., Chen, H., Bu, F., Li, G., and Sun, J. (2015). Genome-wide mapping of structural variations reveals a copy number variant that determines reproductive morphology in cucumber. *Plant Cell* 27, 1595–1604. doi: 10.1105/tpc.114.135848

Zheng, L., Zhang, M., Zhuo, Z., Wang, Y., Gao, X., and Li, Y. (2021). Transcriptome profiling analysis reveals distinct resistance response of cucumber leaves infected with powdery mildew. *Plant Biol.* 23, 327–340. doi: 10.1111/plb.13213

Zhi, P., and Chang, C. (2021). Exploiting epigenetic variations for crop disease resistance improvement. *Front. Plant Sci.* 12:953. doi: 10.3389/fpls.2021.692328

Zhong, C. (2020). *Identification and Functional Analysis of miRNAs Against Powdery Mildew in Cucumber*. Yangzhou: Yangzhou University. doi: 10.27441/d.cnki.gyzdu.2020.001914

Zhou, H., Dong, C., Zhang, H., Ren, Y., Guo, S., and Yang, W. (2015). SSR molecular markers and location of the gene Foc-4 linked to the resistance to *Fusarium* wilt of cucumber. *Mol. Plant Breed.* 13, 1980–1986. doi: 10.13271/j.mpb.013.001980

Zhou, X., and Wu, F. (2009). Differentially expressed transcripts from cucumber (*Cucumis sativus* L.) root upon inoculation with *Fusarium oxysporum* f. sp.

cucumerinum Owen. *Physiol. Mol. Plant Pathol.* 74, 142–150. doi: 10.1016/j.pmpp.2009.10.005

Conflict of Interest: The authors declare that the research was conducted in the absence of any commercial or financial relationships that could be construed as a potential conflict of interest.

Publisher's Note: All claims expressed in this article are solely those of the authors and do not necessarily represent those of their affiliated organizations, or those of the publisher, the editors and the reviewers. Any product that may be evaluated in this article, or claim that may be made by its manufacturer, is not guaranteed or endorsed by the publisher.

Copyright © 2022 He, Wei, Yan, Yu, Cheng, Sun, Zhu, Wei, Wang and Miao. This is an open-access article distributed under the terms of the Creative Commons Attribution License (CC BY). The use, distribution or reproduction in other forums is permitted, provided the original author(s) and the copyright owner(s) are credited and that the original publication in this journal is cited, in accordance with accepted academic practice. No use, distribution or reproduction is permitted which does not comply with these terms.

Advantages of publishing in Frontiers

OPEN ACCESS
Articles are free to read for greatest visibility and readership

FAST PUBLICATION
Around 90 days from submission to decision

HIGH QUALITY PEER-REVIEW
Rigorous, collaborative, and constructive peer-review

TRANSPARENT PEER-REVIEW
Editors and reviewers acknowledged by name on published articles

Frontiers
Avenue du Tribunal-Fédéral 34
1005 Lausanne | Switzerland

Visit us: www.frontiersin.org
Contact us: frontiersin.org/about/contact

REPRODUCIBILITY OF RESEARCH
Support open data and methods to enhance research reproducibility

DIGITAL PUBLISHING
Articles designed for optimal readership across devices

FOLLOW US
@frontiersin

IMPACT METRICS
Advanced article metrics track visibility across digital media

EXTENSIVE PROMOTION
Marketing and promotion of impactful research

LOOP RESEARCH NETWORK
Our network increases your article's readership